WILEY

Edited by
Gyorgy Szekely and Dan Zhao

Sustainable Separation Engineering

Materials, Techniques and Process Development

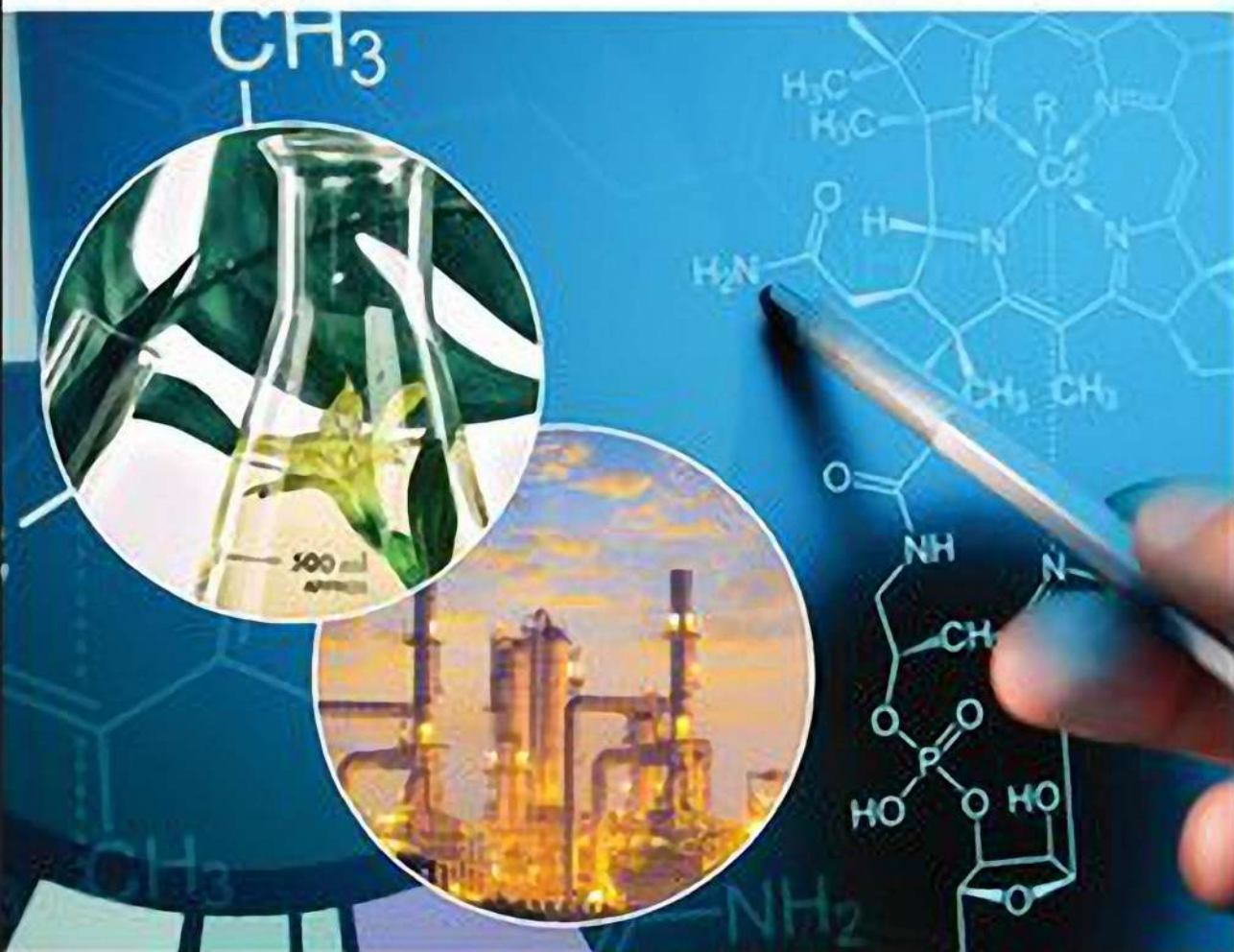

Sustainable Separation Engineering

Sustainable Separation Engineering

Materials, Techniques and Process Development

Volume 1

Edited by

Gyorgy Szekely
KAUST
Advanced Membranes and Porous Materials Center
Thuwal, Saudi Arabia

Dan Zhao
National University of Singapore
Chemical and Biomolecular Engineering
Singapore, Singapore

WILEY

This edition first published 2022
© 2022 by John Wiley & Sons Ltd. All rights reserved.

All rights reserved. No part of this publication may be reproduced, stored in a retrieval system, or transmitted, in any form or by any means, electronic, mechanical, photocopying, recording or otherwise, except as permitted by law. Advice on how to obtain permission to reuse material from this title is available at http://www.wiley.com/go/permissions.

The right of Gyorgy Szekely and Dan Zhao to be identified as the authors of this work has been asserted in accordance with law.

Registered Offices
John Wiley & Sons, Inc., 111 River Street, Hoboken, NJ 07030, USA
John Wiley & Sons Ltd, The Atrium, Southern Gate, Chichester, West Sussex, PO19 8SQ, UK

Editorial Office
The Atrium, Southern Gate, Chichester, West Sussex, PO19 8SQ, UK

For details of our global editorial offices, customer services, and more information about Wiley products visit us at www.wiley.com. Wiley also publishes its books in a variety of electronic formats and by print-on-demand. Some content that appears in standard print versions of this book may not be available in other formats.

Limit of Liability/Disclaimer of Warranty
In view of ongoing research, equipment modifications, changes in governmental regulations, and the constant flow of information relating to the use of experimental reagents, equipment, and devices, the reader is urged to review and evaluate the information provided in the package insert or instructions for each chemical, piece of equipment, reagent, or device for, among other things, any changes in the instructions or indication of usage and for added warnings and precautions. While the publisher and authors have used their best efforts in preparing this work, they make no representations or warranties with respect to the accuracy or completeness of the contents of this work and specifically disclaim all warranties, including without limitation any implied warranties of merchantability or fitness for a particular purpose. No warranty may be created or extended by sales representatives, written sales materials or promotional statements for this work. The fact that an organization, website, or product is referred to in this work as a citation and/or potential source of further information does not mean that the publisher and authors endorse the information or services the organization, website, or product may provide or recommendations it may make. This work is sold with the understanding that the publisher is not engaged in rendering professional services. The advice and strategies contained herein may not be suitable for your situation. You should consult with a specialist where appropriate. Further, readers should be aware that websites listed in this work may have changed or disappeared between when this work was written and when it is read. Neither the publisher nor authors shall be liable for any loss of profit or any other commercial damages, including but not limited to special, incidental, consequential, or other damages.

For general information on our other products and services or for technical support, please contact our Customer Care Department within the United States at (800) 762-2974, outside the United States at (317) 572-3993 or fax (317) 572-4002.

Wiley also publishes its books in a variety of electronic formats. Some content that appears in print may not be available in electronic formats. For more information about Wiley products, visit our web site at ww.wiley.com.

Library of Congress Cataloging-in-Publication Data applied for:
ISBN: 9781119740087

Cover Design: Wiley
Cover Images: © nicolas_/Getty Image RonFullHD/Getty Images Artfully79/Getty Images

Set in 9.5/12.5pt STIXTwoText by Straive, Pondicherry, India

10 9 8 7 6 5 4 3 2 1

Contents

About the Editors

Gyorgy Szekely

Gyorgy Szekely received his MSc degree in Chemical Engineering from the Technical University of Budapest, Hungary. He subsequently earned his PhD degree in Chemistry from the Technical University of Dortmund, Germany, under Marie Curie Actions. Gyorgy worked as an Early Stage Researcher in the Pharmaceutical Research and Development Centre of Hovione PharmaScience Ltd. in Portugal and as an IAESTE Fellow at the University of Tokyo, Japan. He was a visiting researcher at Biotage MIP Technologies AB in Sweden. Gyorgy was a Postdoctoral Research Associate working with Prof. Andrew Livingston in Imperial College London, UK. He was appointed as a Lecturer in Chemical Engineering at The University of Manchester, UK, between 2014 and 2019, where he received the Distinguished Visiting Fellowship of the Royal Academy of Engineering. Gyorgy also served as an Adjunct Faculty Member at Saveetha University between 2016 and 2018. He is currently an Assistant Professor in Chemical Engineering at the Advanced Membranes & Porous Materials Center at King Abdullah University of Science and Technology (KAUST), Saudi Arabia, and has been a Visiting Academic at The University of Manchester, 2019–2022. His multidisciplinary professional background covers green process engineering, green solvents and materials, continuous reactions, and membrane separations. He serves as an Academic Editor for the journals *Advances in Polymer Technology, Advanced Materials Letters*; as an Associate Editor for the Separation Processes section of *Frontiers in Chemical Engineering*; he is a member of the Editorial Advisory Board for *ACS Applied Polymer Materials*, and a member of the Early Career Editorial Board of the *Journal of Membrane Science*. He is a Member of the Royal Society of Chemistry and a Fellow of the Higher Education Academy in the UK. Gyorgy has been designing

novel materials and processes for molecular level separations, which has resulted in several articles, industrial collaborations and consultancy works, books, patents, and invited keynote lectures. To learn more about Gyorgy, follow him on Twitter @SzekelyGroup and through his group's website at www.szekelygroup.com.

Dan Zhao

Dan Zhao received his MS degree in Polymer Chemistry and Physics from Zhejiang University, China. He went on to obtain his PhD degree in Chemistry (Inorganic Division) from Texas A&M University, USA, under Prof. Hong-Cai Zhou in 2010. Following this, he worked with Dr. Di-Jia Liu at Argonne National Laboratory as a Postdoctoral Fellow between 2010 and 2012. Dan was appointed as an Assistant Professor in Chemical Engineering at the National University of Singapore between 2012 and 2018, where he received multiple local and global accolades for his outstanding academic contributions and commendable teaching dedications. He has been an Associate Professor in Chemical Engineering at the National University of Singapore since 2019. Dan is highly interested in interdisciplinary research in advanced porous materials and hybrid membranes for applications in clean energy and environmental sustainability. His work has generated multiple highly cited papers, industrial collaboration and translation, patents, book chapters, and invited presentations. He is the Clarivate Analytics' Highly Cited Researcher (Cross-Field) for 2019–2020 and was appointed as the Dean's Chair of the Faculty of Engineering at the National University of Singapore in 2021. Dan served as a Member of the Editorial Advisory Board for *Inorganic Chemistry* from 2018 to 2020. He is currently serving as the Associate Editor for *Industrial & Engineering Chemistry Research*, an Advisory Board Member of *Aggregate*, and an Early Career Advisory Board Member of *ACS Sustainable Chemistry & Engineering* and *Chemistry – An Asian Journal*. He is an Executive Committee Member of the Materials Research Society of Singapore and a Membrane of the Membrane Society of Singapore. To learn more about Dan, follow him on Twitter @ZhaoGroupNUS and through his group's website at https://blog.nus.edu.sg/dzhao/.

List of Contributors

Andrea Adamo
Zaiput Flow Technologies
Waltham, MA, USA

Elaf A. Ahmed
Research & Development Center
Saudi Aramco
Dhahran, Saudi Arabia

Faheem Hassan Akhtar
Biological and Environmental Science and Engineering Division (BESE)
Water Desalination and Reuse Center (WDRC)
King Abdullah University of Science and Technology (KAUST)
Thuwal, Saudi Arabia

Hasan A. Al Abdulgader
Research & Development Center
Saudi Aramco, Dhahran, Saudi Arabia

T. Alan Hatton
Department of Chemical Engineering
Massachusetts Institute of Technology
Cambridge, MA, USA

Sajad Razavi Bazaz
School of Biomedical Engineering
University of Technology Sydney
Sydney, Australia

Muhammad Burhan
Biological and Environmental Science and Engineering Division (BESE)
Water Desalination and Reuse Center (WDRC)
King Abdullah University of Science and Technology (KAUST)
Thuwal, Saudi Arabia

Yus Donald Chaniago
Ulsan National Institute of Science and Technology
Ulsan, South Korea

Farid Chemat
GREEN Extraction Team, INRAE
Avignon University
Avignon, France

Qian Chen
Biological and Environmental Science and Engineering Division (BESE)
Water Desalination and Reuse Center (WDRC)
King Abdullah University of Science and Technology (KAUST)
Thuwal, Saudi Arabia

Young Chul Choi
Research & Development Center
Saudi Aramco
Dhahran, Saudi Arabia

Mariana C. da Costa
School of Chemical Engineering (FEQ)
University of Campinas (UNICAMP)
Campinas, São Paulo, Brazil

André M. da Costa Lopes
CICECO – Aveiro Institute of Materials
Department of Chemistry
University of Aveiro
Aveiro, Portugal
CECOLAB – Collaborative Laboratory
Towards Circular Economy
R. Nossa Senhora da Conceição
Oliveira do Hospital
Coimbra, Portugal

Gergő Dargó
RotaChrom Technologies LLC
Dabas, Hungary

Gaurav G. Dastane
Department of Chemical Engineering
Institute of Chemical Technology
Mumbai, India

Jing Deng
School of Chemical, Biological, and
Materials Engineering
University of Oklahoma
Norman, OK, USA

Ketan S. Desai
Department of Chemical Engineering
Institute of Chemical Technology
Mumbai, India

Francesco Donsi
Department of Industrial Engineering
University of Salerno
Fisciano, Italy

Eric Falascino
William G. Lowrie Department of
Chemical and Biomolecular Engineering
The Ohio State University
Columbus, OH, USA

Liang-Shih Fan
William G. Lowrie Department of
Chemical and Biomolecular
Engineering
The Ohio State University
Columbus, OH, USA

Michele Galizia
School of Chemical, Biological, and
Materials Engineering
University of Oklahoma
Norman, OK, USA

María González-Miquel
Department of Chemical Engineering
and Analytical Sciences
The University of Manchester
Manchester, UK
Departamento de Ingeniería Química
Industrial y del Medioambiente
ETS Ingenieros Industriales
Universidad Politécnica de Madrid
Madrid, Spain

Patricia Gorgojo
Department of Chemical Engineering
and Analytical Sciences
The University of Manchester
Manchester, UK

Nanoscience and Materials Institute of
Aragón (INMA)
CSIC-Universidad de Zaragoza
Zaragoza, Spain

Chemical and Environmental Engineering
Department
Universidad de Zaragoza
Zaragoza, Spain

Benjamin S. Hsiao
Department of Chemistry
Stony Brook University
Stony Brook, NY, USA

Xiangyu Huang
Department of Chemistry
Stony Brook University
Stony Brook, NY, USA

Ananda J. Jadhav
Department of Chemical Engineering
Institute of Chemical Technology
Mumbai, India

Anet Režek Jambrak
Faculty of Food Technology and Biotechnology
University of Zagreb
Zagreb, Croatia

Muhammad Ahmad Jamil
Mechanical & Construction Engineering Department
Northumbria University
Newcastle Upon Tyne, UK

Kalyani Jangam
William G. Lowrie Department of Chemical and Biomolecular Engineering
The Ohio State University
Columbus, OH, USA

Anuj Joshi
William G. Lowrie Department of Chemical and Biomolecular Engineering
The Ohio State University
Columbus, OH, USA

Shankar B. Kausley
TCS Research
Physical Sciences Research Area
Tata Consultancy Services
Pune, India

Chetsada Khositanon
Department of Chemical Engineering
Burapha University
Muang, Chonburi, Thailand

Árpád Könczöl
RotaChrom Technologies LLC
Dabas, Hungary

Kai Fabian Kruber
Institute of Process Systems Engineering
Hamburg University of Technology
Hamburg, Germany

Ramesh Kumar
Department of Earth Resources & Environmental Engineering
Hanyang University
Seoul, Republic of Korea

M. Kumja
Biological and Environmental Science and Engineering Division (BESE)
Water Desalination and Reuse Center (WDRC)
King Abdullah University of Science and Technology (KAUST)
Thuwal, Saudi Arabia

Moonyong Lee
Yeungnam University
Gyeongsan, South Korea

Ki Min Lim
School of Chemical and Energy Engineering
Universiti Teknologi Malaysia
Johor Bahru, Malaysia

Pablo López-Porfiri
Department of Chemical Engineering and Analytical Sciences
The University of Manchester
Manchester, UK

Ali Abouei Mehrizi
Department of Life Sciences Engineering
University of Tehran, Tehran, Iran

Francesco Meneguzzo
Istituto per la Bioeconomia
CNR, Sesto Fiorentino, FI, Italy

Fateme Mirakhorli
School of Biomedical Engineering
University of Technology Sydney
Sydney, Australia
Climate Change Cluster
University of Technology Sydney
Australia

Pinak Mohapatra
William G. Lowrie Department of
Chemical and Biomolecular
Engineering
The Ohio State University
Columbus, OH, USA

Seyed Sepehr Mohseni
Department of Life Sciences
Engineering
University of Tehran
Tehran, Iran

Rattana Muangrat
Faculty of Agro-Industry
Chiang Mai University
Chiang Mai, Thailand

Trevor Murray
Zaiput Flow Technologies
Waltham, MA, USA

Kim Choon Ng
Biological and Environmental Science
and Engineering Division (BESE)
Water Desalination and Reuse
Center (WDRC)
King Abdullah University of Science and
Technology (KAUST)
Thuwal, Saudi Arabia

Marinela Nutrizio
Faculty of Food Technology and
Biotechnology
University of Zagreb
Zagreb, Croatia

Lanre M. Oshinowo
Research & Development Center
Saudi Aramco
Dhahran, Saudi Arabia

Parimal Pal
Chemical Engineering Department
National Institute of Technology
Durgapur, India

Mario Pagliaro
Istituto per lo Studio dei Materiali
Nanostrutturati
CNR, Palermo, Italy

Aniruddha B. Pandit
Department of Chemical Engineering
Institute of Chemical Technology
Mumbai, India

Rajshree A. Patil
Department of Chemical Engineering
Institute of Chemical Technology
Mumbai, India

Yuthana Phimolsiripol
Faculty of Agro-Industry
Chiang Mai University
Chiang Mai, Thailand

Peter J. Ralph
Climate Change Cluster
University of Technology Sydney
Australia

Sepideh Razavi
School of Chemical, Biological, and
Materials Engineering
University of Oklahoma
Norman, OK, USA

Thomas Rodgers
Department of Chemical Engineering
and Analytical Science
The University of Manchester
Manchester, UK

Phisit Seesuriyachan
Faculty of Agro-Industry
Chiang Mai University
Chiang Mai, Thailand

Mateus Lodi Segatto
Department of Chemistry
Federal University of São Carlos
São Paulo, Brazil

Vedant Shah
William G. Lowrie Department of
Chemical and Biomolecular Engineering
The Ohio State University
Columbus, OH, USA

Muhammad Wakil Shahzad
Mechanical & Construction Engineering
Department
Northumbria University
Newcastle Upon Tyne, UK

Priyanka R. Sharma
Department of Chemistry
Stony Brook University
Stony Brook, NY, USA

Sunil K. Sharma
Department of Chemistry
Stony Brook University
Stony Brook, NY, USA

Armando J. D. Silvestre
CICECO – Aveiro Institute of Materials
Department of Chemistry
University of Aveiro
Aveiro, Portugal

Mirko Skiborowski
Institute of Process Systems Engineering
Hamburg University of Technology
Hamburg, Germany

Filipe H. B. Sosa
School of Chemical Engineering (FEQ)
University of Campinas (UNICAMP)
Campinas, São Paulo, Brazil
CICECO – Aveiro Institute of Materials
Department of Chemistry
University of Aveiro
Aveiro, Portugal

Aylon Matheus Stahl
Department of Chemistry
Federal University of São Carlos
São Paulo, Brazil

Kai-Jher Tan
Department of Chemical Engineering
Massachusetts Institute of Technology
Cambridge, MA, USA

Thomas Waltermann
Covestro Deutschland AG
Process Technology – Digital Process
Leverkusen, Germany

Majid Ebrahimi Warkiani
School of Biomedical Engineering
University of Technology Sydney
Sydney, Australia
Institute of Molecular Medicine
Sechenov University
Moscow, Russia

Nazlee Faisal Ghazali
School of Chemical and Energy Engineering
Universiti Teknologi Malaysia
Johor Bahru, Malaysia

Nopphon Weeranoppanant
Department of Chemical Engineering
Burapha University
Muang, Chonburi, Thailand
School of Biomolecular Science and
Engineering (BSE)
Vidyasirimedhi Institute of Science and
Technology (VISTEC)
Wangchan, Rayong, Thailand

Mengying Yang
Department of Chemistry
Stony Brook University
Stony Brook, NY, USA

Doskhan Ybyraiymkul
Biological and Environmental Science and Engineering Division (BESE)
Water Desalination and Reuse Center (WDRC)
King Abdullah University of Science and Technology (KAUST)
Thuwal, Saudi Arabia

Karine Zanotti
Department of Chemistry
Federal University of São Carlos
São Paulo, Brazil

Vânia Gomes Zuin
Department of Chemistry
Federal University of São Carlos
São Paulo, Brazil
Green Chemistry Centre of Excellence
University of York, York, UK
Institute of Sustainable and Environmental Chemistry, Leuphana University
Lüneburg, Germany

Preface

Welcome to the first edition of our book *Sustainable Separation Engineering*. This is the brainchild of our academic and industrial research, as well as our university teachings on advanced separations and green engineering. You will find this two-volume book both as an engaging and exciting reference guide on the latest materials, techniques, and processes related to sustainable separations and as a textbook that builds a solid theoretical foundation for sustainable separations. Our main objective is to present an overview of the fundamentals underlying the conventional and emerging separation processes, with an emphasis on sustainability. Gone are the days when separation engineering was the exclusive domain of chemical engineers. Modern sustainable separation engineering is highly interdisciplinary, with significant contributions ranging from chemical engineering to materials and polymer sciences to renewable energy sciences. Therefore, this book is intended for a broad audience to provide a bird's-eye view of the interplay among these disciplinaries to design sustainable solutions. An up-to-date reference index is also provided for easy lookup of the most relevant literature for a more detailed description of each topic.

One of the aims of sustainability is to manufacture products in the most environmentally benign, economic, and socially beneficial way through the optimization of resource utilization and the conservation of materials, energy, and natural resources. The Sustainable Development Goals set by the United Nations crafted a blueprint through which a thriving and more sustainable future can be achieved for all. These goals target the global challenges we face, and most of them are directly or indirectly linked to material separations. During the manufacturing of products, separation steps are undesired yet unavoidable. Owing to the high energy demand and considerable waste produced during separation processes, there is a need to develop advanced materials and processes that minimize the associated environmental burden. Academic and industrial researchers are making great efforts to design greener processes and products. The authors of the 21 chapters in this book aimed to develop a holistic view of various types of separations covering microscale (chemistry, materials), mesoscale (unit operations), and macroscale (processes). Discussion is also extended to the role of sustainable separations in the chemical engineering curriculum.

This book gives a contemporary and inclusive account of the sustainability aspects of separation engineering. It will be a useful resource for students of separation engineering and experts alike, as well as prospective learners who wish to broaden their horizons and discover other topics related to their core discipline.

Gyorgy Szekely
Jeddah, Saudi Arabia
Advanced Membranes and Porous Materials Center
King Abdullah University of Science and Technology (KAUST)

Dan Zhao
Singapore
Chemical and Biomolecular Engineering
National University of Singapore (NUS)

1

Electrochemically Mediated Sustainable Separations in Water

Kai-Jher Tan and T. Alan Hatton

Department of Chemical Engineering, Massachusetts Institute of Technology, Cambridge, MA, USA

1.1 Introduction

With the continuing growth of economic development and resource requirements by the expanding world population, separation processes continue to be critical and ubiquitously present in every aspect of human society [1, 2], and are effectively applied in areas ranging from chemical production to environmental remediation. The latter is especially important as it directly pertains to human livelihood, with the pressing issue of insufficient water availability affecting billions of people around the world [3]. Rising constraints on freshwater resulting from increasing water demand and decreasing water supply have been identified as a crucial challenge for the twenty-first century, necessitating improvements in aspects such as water policy, as well as technologies for water use and treatment [4–6].

Electrochemically mediated processes have emerged as promising tools for water-based separations due to their high potential for compact design [7, 8], low-energy operations [9–11], and molecularly selective removal [12–14]. These attractive features are well-suited to tackle challenges associated with the current state of separation science, which include the needs for improving the removal of species at dilute concentrations, and furthering understanding of interfacial phenomena [15]. The innate tunability of electrochemical frameworks renders them suitable for targeting desirable aqueous species in industrial purification processes, and a myriad of contaminants arising from other anthropogenic sources such as pharmaceutical and personal care products (PPCPs) [16], and agricultural and manufacturing activities. Judiciously designed electrochemically mediated systems can potentially take on a pivotal role in water purification trains as an individual treatment step, or even as a plug-and-play portable unit for remote use on-site, providing a strong alternative in the future for efficient and high-throughput new-generation water-phase separations. While cheaper and less energy-intensive water purification technologies will undoubtedly assist in attenuating the impact of water scarcity, their development may also enable the extension of the aqueous phase for use as a medium to facilitate separations of other compounds like carbon dioxide.

Sustainable Separation Engineering: Materials, Techniques and Process Development, Volume 1, First Edition. Edited by Gyorgy Szekely and Dan Zhao.
© 2022 John Wiley & Sons Ltd. Published 2022 by John Wiley & Sons Ltd.

This chapter will provide a brief introduction to some applicable electrochemical theory and a general overview of aqueous electrochemical separation methods, followed by a more detailed discussion of recent advances in the area of electrochemically mediated sustainable separations in water using heterogeneous redox-active materials.

1.2 Separation Processes

Separation processes are unit operations that distinguish materials based on their molecular, thermodynamic, or transport properties. A separation process can be conducted via addition of mass or energy separating agents, and can be operated under equilibrium or rate-limiting conditions. To quantify the efficacy of a separation process, a variety of performance indicators can be used. One of the most important is analyte selectivity, which can be evaluated through the separation factor (Eq. 1.1) [17, 18]:

$$S_{A/B} = \frac{(C_{A\_initial} / C_A) - 1}{(C_{B\_initial} / C_B) - 1} \tag{1.1}$$

where $S_{A/B}$ is the separation factor of species A relative to B (or the selectivity for species A relative to B), C_A is the concentration of species A, C_B is the concentration of species B, $C_{A\_initial}$ is the initial concentration of species A, and $C_{B\_initial}$ is the initial concentration of species B. A separation factor of unity would indicate that the process has no selectivity for either of the two species. Other useful metrics for separation processes include efficiency, capacity, and throughput [15]. Common separation techniques found in chemical industries include distillation, crystallization, and adsorption, and are employed to perform tasks such as species purification and recovery, gas production, product drying, and contaminant removal [19, 20]. However, one of the greatest drawbacks of these processes is their high energy requirement, which has been estimated to make up as much as 15% of energy usage around the world [21, 22]. To address this, key areas for improvement have been highlighted within current separation technologies and frameworks, which include reducing energetic footprints, boosting key performance indicators (i.e. selectivity, capacity, and throughput), as well as targeted development in many water-related applications such as uranium recovery from seawater and other trace contaminant removal from dilute streams [2, 15].

1.3 Electrochemical Theory

1.3.1 Thermodynamics

Electrochemical processes operate by means of electron transfer and a chemical change and can be expressed via the generic half-cell equation for a redox reaction (Eq. 1.2): [23, 24]

$$\mathrm{Ox} + n\mathrm{e}^- \underset{k_b}{\overset{k_f}{\leftrightarrow}} \mathrm{Red} \tag{1.2}$$

where Ox is the oxidized species, n is the number of electrons, Red is the reduced species, k_f is the rate constant of the forward reaction, and k_b is the rate constant of the backward reaction. Applying thermodynamic relationships to Eq. 1.2 results in the derivation of the Nernst equation, which describes the properties of a redox half-cell reaction at equilibrium (Eq. 1.3): [23, 24]

$$E = E^{0'} - \frac{RT}{nF} \ln \frac{C_{\text{Red}}}{C_{\text{Ox}}} \tag{1.3}$$

where E is the half-cell potential of the redox reaction, $E^{0'}$ is the formal potential of the redox reaction, R is the gas constant, T is the temperature, n is the number of electrons transferred, F is Faraday's constant, C_{Red} and C_{Ox} are the concentrations of the reduced and oxidized species, respectively, at equilibrium [24]. Redox couples can be activated homogeneously in solution, or heterogeneously with a surface-immobilized species, but both cases require the presence of an electrode at which the species converts electrochemically. The thermodynamic propensity for a half-cell reaction to occur is directly related to its standard reduction potential, which is readily accessible in tabulated form, known as the electrochemical series, for common homogeneous redox reactions [25]. Applying an electrochemical potential less than the standard reduction potential will favor the generation of the reduced species in the half-cell reaction.

At the electrode-solution interface, a phenomenon known as the electrical double layer manifests as a result of the accumulation of oppositely charged ions at the charged surface, allowing for the storage of charge (Figure 1.1). The earliest mathematical representation of this structure was given by the Helmholtz model for a parallel-plate capacitor (Eq. 1.4): [24]

$$C_{\text{d}} = \frac{\varepsilon \varepsilon_0}{d} \tag{1.4}$$

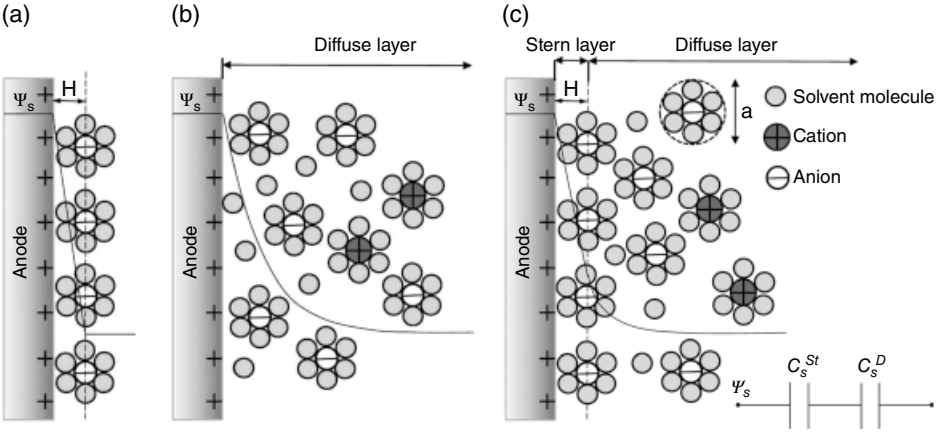

Figure 1.1 Visual representations of the (a) Helmholtz, (b) Gouy-Chapman, and (c) Gouy-Chapman-Stern models of the electrical double layer. *Source:* Reprinted with permission from [26]. Copyright 2011, American Chemical Society.

where C_d is the differential capacitance, ε is the dielectric constant of the fluid, ε_0 is the permittivity of free space, and d is the distance between the two electrodes. The Gouy-Chapman theory proposed the notion of a diffuse layer of charge in the solution with its average distance of charge separation dependent on factors such as electrode potential and electrolyte concentration. The Stern modification was later added to the Gouy-Chapman model to account for the finite sizes of ions and set a limit on the proximity with which they can approach the electrode surface. The resulting Gouy-Chapman-Stern model comprises a compact layer at the surface in series with the diffuse layer separated by the outer Helmholtz plane, providing a more realistic differential capacitance profile. Larger polarizations and electrolyte concentrations compress the charge to a greater extent so that the overall EDL structure approaches the initial Helmholtz model [23, 24, 26].

1.3.2 Kinetics

The rate of an electrochemical reaction is directly proportional to the current passed through the electrode at which it occurs (Eq. 1.5): [24]

$$\nu = \frac{i}{nFA} \tag{1.5}$$

where ν is the rate of reaction, i is the current passed through the electrode, n is the stoichiometric number of electrons transferred in the reaction, F is Faraday's constant, and A is the surface area of the electrode. The reaction rate can also be written directly in terms of the general redox half-cell reaction in Eq. 1.2, resulting in a kinetic expression (Eq. 1.6): [24]

$$\nu = k_f C_{Ox} - k_b C_{Red} \tag{1.6}$$

The rate constant of a chemical reaction can be denoted as a function of temperature. Using the Arrhenius equation, which describes the surmounting of an activation energy along a reaction coordinate, an empirical exponential correlation can be developed (Eq. 1.7): [23, 24]

$$k = A' e^{-\Delta G_{act}/RT} \tag{1.7}$$

where k is the rate constant, A' is a constant, ΔG_{act} is the standard free energy of activation, R is the gas constant, and T is the temperature. Using the more rigorous transition state theory framework in which the reactants form an activated complex before the products, an equation of a similar form to the Arrhenius relation in Eq. (1.7) is obtained (Eq. 1.8): [23, 24]

$$k = \kappa \frac{KT}{h} e^{-\Delta G_{act}/RT} \tag{1.8}$$

where κ is the transmission coefficient, K is the Boltzmann constant, and h is the Planck constant.

The kinetics of an electrochemical reaction depend strongly on the electrode potential. As seen in Eq. (1.5), since the reaction rate varies linearly with current, this

relationship can be formally described through the current-potential characteristic (Eq. 1.9): [23, 24]

$$i = FAk^0\left[C_{\mathrm{Ox}}(0,t)\mathrm{e}^{-\alpha\frac{F}{RT}\left(E-E^{0'}\right)} - C_{\mathrm{Red}}(0,t)\mathrm{e}^{(1-\alpha)\frac{F}{RT}\left(E-E^{0'}\right)}\right] \tag{1.9}$$

where k^0 is the standard rate constant, $C_{\mathrm{Ox}}(0,t)$ is the concentration of the oxidized species at the electrode surface at time t, $C_{\mathrm{Red}}(0,t)$ is the concentration of the reduced species at the electrode surface at time t, and α is the transfer coefficient. As expected, the reaction rate of a redox couple can also be affected by other variables. Specifically, in the absence of mass-transfer limitations, Eq. (1.9) simplifies to the Butler-Volmer equation (Eq. 1.10): [23, 24]

$$i = i_0\left[\mathrm{e}^{-\alpha\frac{F}{RT}\eta} - \mathrm{e}^{(1-\alpha)\frac{F}{RT}\eta}\right] \tag{1.10}$$

where i_0 is the exchange current (equivalent to FAk^0C, where $C = C_{\mathrm{Ox}} = C_{\mathrm{Red}}$), and η is the overpotential (equivalent to $E-E_{\mathrm{eq}}$, where E_{eq} is the equilibrium potential). At large overpotentials, the Butler-Volmer equation further simplifies to an expression of the Tafel form (Eq. 1.11): [23, 24]

$$i = i_0\mathrm{e}^{-\alpha\frac{F}{RT}\eta} \tag{1.11}$$

An exponential Tafel response suggests an irreversible redox-active couple because the sluggish kinetics produce current only at high overpotentials in one reaction direction. Contrastingly, reversible redox-active couples have facile kinetics that are always at equilibrium and exhibit a Nernstian response independent of current (Eq. 1.3). The aforementioned expressions are developed from a single step, one-electron transfer process, and the kinetics would vary for multistep mechanisms, which may include other events such as chemical reactions or surface reactions [23, 24].

1.4 Electrochemical Separation Methods

Electrochemical separation methods use redox reactions to enable or facilitate species removal and can be broadly grouped into categories based on their separation mechanism (Table 1.1). Conventional techniques commonly utilize indirect effects of electrochemical processes to separate solid analytes, as well as charged or neutral dissolved species, but approaches involving a redox event that directly results in the separation of the target analyte also exist (Figure 1.2). In fact, recent developments in the field have leveraged such direct approaches in the development of new electrochemical separation systems to achieve selective analyte removal, as well as process reversibility.

Table 1.1 Electrochemical separation methods.

	Electrochemical separation method	Mechanism description	Nature of mechanism	Analyte type
Irreversible	Electrochemical electrolyte/ electrode conversion	Repurposes the effects of certain electrolytic processes: • Water electrolysis: – pH changes: switches the sorbent state between active and inactive via protonation – Gas evolution: removes the analyte via flotation – Potential difference: removes the analyte via electromigration • Electrode dissolution: Releases metal ions into the solution that coagulate the analyte for subsequent removal	Indirect	Solid, Charged, Neutral
Reversible	Electrochemical analyte conversion	Converts the analyte into a new form: • Metal reduction: alters the analyte oxidation state • Heterogeneous reaction: reacts the analyte with the electrode material to form a new chemical species • Reactive separations: couples electrochemical separation processes with simultaneous or subsequent conversion of the separated analytes to a more desirable form	Direct	Charged
	Electrical double layer	Leverages the ion-storing electrical double layer structure that is formed when an electrode is held under electric potential	Direct	Charged
	Electrochemically mediated binding	Uses an electrochemical stimulus to convert a redox-active species to a different oxidation state to facilitate targeted binding between the altered redox-active species and an analyte	Direct	Charged
	Electrochemically mediated hydrophilicity tuning	Varies the oxidation state of a redox-active species in order to modulate the overall hydrophilicity of a sorbent material	Indirect	Charged, Neutral

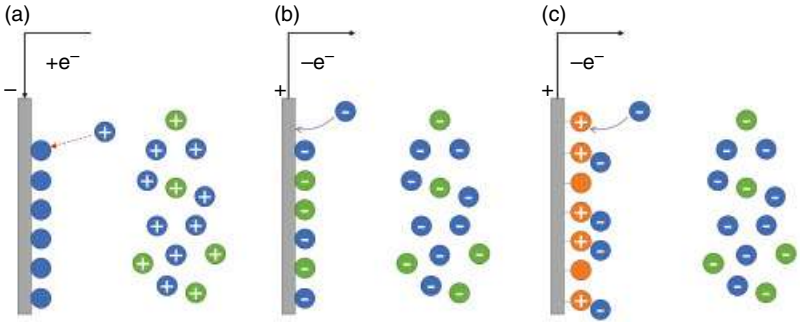

Figure 1.2 Examples of direct approaches for electrochemical separation: (a) metal reduction to a neutral state (electrochemical analyte conversion), (b) ion adsorption (electrical double layer), and (c) selective interactions between electrochemically activated redox-active groups and specific ions (electrochemically mediated binding). Blue and green represent different types of ions, and orange represents a redox-active species.

1.5 Conventional Electrochemical Separation Methods

Traditional electrochemical separations often involve electrolytic reactions that convert water, the electrode, or the target analyte species itself to a new form in order to extract it from solution. Electrolytic processes operate by using an applied current or potential to drive a homogeneous electrochemical reaction at an electrode. Electrochemical technologies for wastewater processing are numerous and can be very effective for targeted remediation, but may also require higher energy usage [27].

1.5.1 Water Electrolysis

Water electrolysis separation methods utilize electrochemical cells that perform either water oxidation at the anode (Eq. 1.12), water reduction at the cathode (Eq. 1.13), or both:

$$H_2O \rightarrow 2e^- + \frac{1}{2}O_2 + 2H^+ \tag{1.12}$$

$$2H_2O + 2e^- \rightarrow 2OH^- + H_2 \tag{1.13}$$

The volumetric rate of gas production from water electrolysis at standard temperature and pressure can be expressed using Faraday's laws (Eq. 1.14): [23, 24, 28, 29]

$$Q_g = Q_H + Q_O = \frac{I_{cell} V_o}{F}\left(\frac{1}{n_H} + \frac{1}{n_O}\right) \tag{1.14}$$

where Q_g is the total gas production rate, Q_H is the hydrogen gas production rate, Q_O is the oxygen gas production rate, I_{cell} is the applied water electrolysis current, V_o is the molar volume of gases at standard temperature and pressure, F is Faraday's constant, n_H is the number of electrons transferred per mole of hydrogen, and n_O is the number of electrons transferred per mole of oxygen.

1.5.1.1 Electrodialysis

Electrodialysis combines the migration of ions via an applied potential difference with membrane separation. Specifically, an electrodialysis cell undergoes water splitting reactions to move ions toward the resulting oppositely charged electrodes, with ion exchange membranes placed in the ion trajectories to either screen them or allow them through, thus generating concentrated and dilute electrolyte streams. If chloride is present in the solution, it can also oxidize to chlorine gas at the anode. Electrodialysis stacks include alternating anion and cation exchange membranes placed between and in parallel with the electrodes, with the aqueous feed stream flowing through the channels (Figure 1.3) [17, 31–34]. The energetic requirements of electrodialysis can be determined in terms of a single-stack electrochemical cell (Eq. 1.15): [31]

$$W_{\mathrm{EDI}} = R_{\mathrm{avg,st}} t \left(\frac{Q_{\mathrm{d,st}} F \left(C_{\mathrm{f}} - C_{\mathrm{d}} \right)}{\xi} \right)^2 \tag{1.15}$$

where W_{EDI} is the energy consumption of electrodialysis, $R_{\mathrm{avg,st}}$ is the average resistance of the stack, t is the operating duration, $Q_{\mathrm{d,st}}$ is the diluate flow through the stack, F is Faraday's constant, C_{f} is the equivalent feed concentration, C_{d} is the equivalent diluate concentration, and ξ is the current utilization.

The ability of electrodialysis to separate ionic species from nonionic species allows for its utilization in product purification and recovery in a variety of areas (Table 1.2), with a key application being desalination [31, 32, 34, 63, 64]. Electrodialysis can be further combined

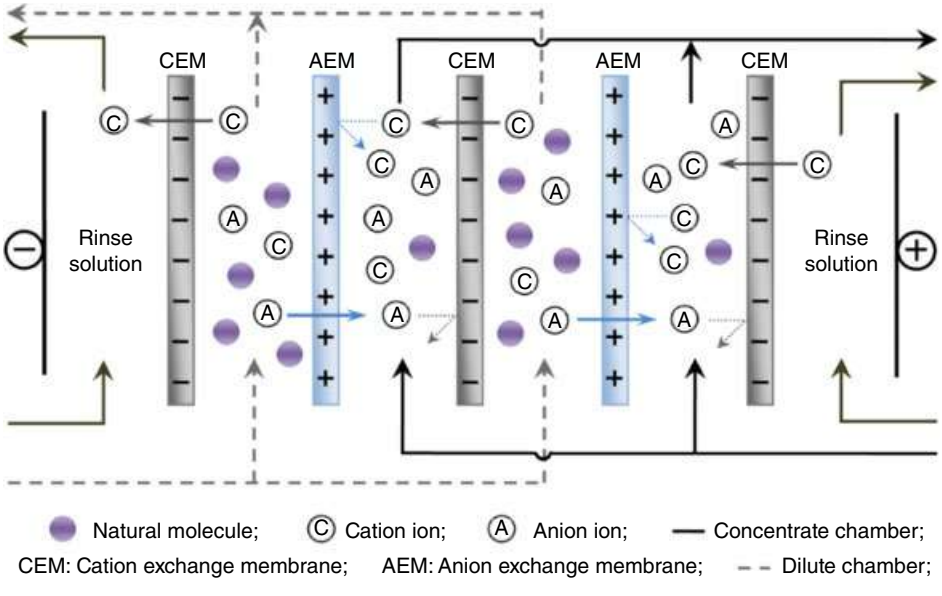

Figure 1.3 A conventional electrodialysis stack setup. *Source:* Reprinted from [30]. Copyright 2017, with permission from Elsevier.

Table 1.2 Applications of traditional and augmented electrodialysis processes.

Traditional electrodialysis	**Application**	**Examples of specific use**
	Desalination	• Brackish and process water [31, 32] • Seawater [35, 36] • Reverse osmosis brine solution discharge [37] • Drinking water treatment: Removal of nitrates [38, 39] and hardness [40, 41] • Defluoridation of brackish water [42] • Wastewater treatment: removal of phosphate [43], lead [44], cadmium [45]
	Metal recovery	• Copper [46], iron and water from synthetic copper electrowinning solutions [47]
	Nutrient recovery	• NH_4-N concentrate [48]
	Food industry	• Table salt production [31, 49] • Citrus juice deacidification [32, 49] • Demineralization of products such as whey [31, 32, 49]
	Bioprocessing	• Protein purification and amino acid recovery [32]
Augmented electrodialysis	**Addition**	**Examples of specific use**
	Permselective membranes	• Capture of specific ions [50]
	Bipolar membranes [51]	• Generation of acids and bases from their associated salts [31, 32, 52] • Production of soy protein isolates [52] • Recovery of organic acids [53] from fermentation broths or other streams: [31, 32] – Citric acid [54] – Acetic acid [55] – Lactic acid [56–58] • Separation of carbon dioxide [59–61]
	Ion exchange resins	• Separation of carbon dioxide via in situ electrochemical pH control in resin-wafer electrodeionization [62] • Generation of ultrapure highly deionized water [31]

with other separation materials to enable the performance of specialized tasks such as acid production and carbon dioxide removal.

A related method to electrodialysis is shock electrodialysis, a recently developed electrochemical technique that enhances the removal of charged species from water. In this process, water flows through a porous medium placed in between two ion exchange elements that have an ionic current passed between them, resulting in the removal of salt as the formed ion depletion zone is propagated through the pores as a shock wave (Figure 1.4a and b). The sharp boundary between the depleted and nondepleted zones arises from the role of the porous medium's charged surfaces in allowing the ions to move faster than with only diffusion; this enhanced transport allows for an "over-limiting current" and provides

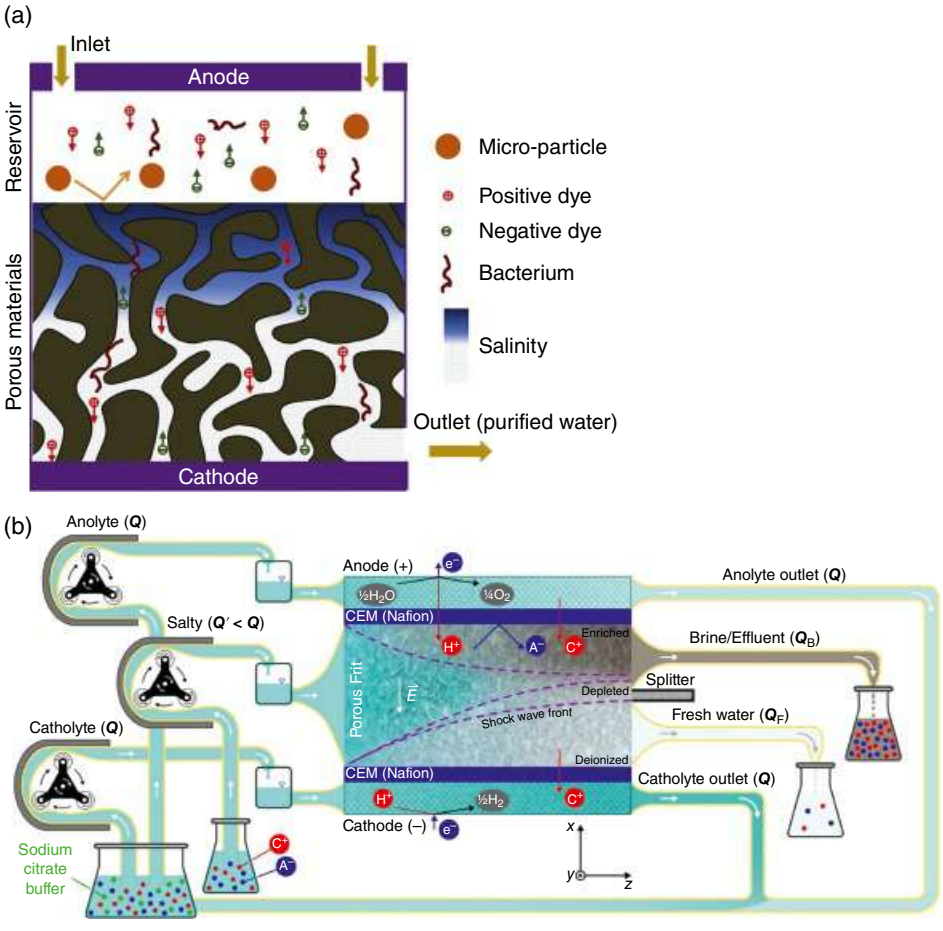

Figure 1.4 The shock electrodialysis process as depicted in two different flow device setups for (a) a synthetic water matrix, *Source:* Reprinted from [65]. Copyright 2015, with permission from Elsevier. and (b) seawater. *Source:* Reprinted from [66]. Copyright 2020, with permission from Elsevier.

this scheme with high scalability for continuous desalination [65, 67, 68]. In addition, shock electrodialysis possesses the capabilities of performing disinfection and filtration functions during operation [65], and removing radionuclides [69], as well as selectively separating ions like Mg^{2+} in the presence of a ninefold excess of Na^{+} with a scaled retention selectivity on the order of magnitude of 10^{1} [66, 70].

1.5.1.2 Electrochemical Ion Exchange

A subset of water electrolysis-based separation methods is the electrochemical ion exchange (EIX) process, which employs water electrolysis reactions to activate or regenerate the ion exchange electrodes through localized pH changes at their surfaces. A typical cation EIX scheme consists of three steps, starting first with the reduction of water (Eq. 1.13), followed

by the deprotonation of the acidic exchange material (e.g. −COOH carboxyl groups) with the generated hydroxide anions (Eq. 1.16): [71, 72]

$$R-COOH + OH^- \rightarrow R-COO^- + H_2O \tag{1.16}$$

Finally, the negatively charged active sites adsorb the desired cation (Eq. 1.17): [71, 72]

$$R\text{-}COO^- + I_{Cation}{}^+ \rightarrow R\text{-}COO^-I_{Cation}{}^+ \tag{1.17}$$

where R is the non-active portion of the ion exchange material, and $I_{cation}{}^+$ is a cation. Changing the electrode potential to facilitate proton generation from water oxidation enables release of the previously bound cation. Conversely, anion EIX schemes use basic exchangers activated to their positively charged states via protonation from water oxidation [71–73]. EIX systems have been used to separate chromate [74], various inorganic ions such as Cl^-, $SO_4{}^{2-}$, $PO_4{}^{3-}$, Ca^{2+}, Fe^{2+}, and Mg^{2+} [75], and cobalt via the alkaline hydrolysis of the non-ion-exchanging α-zirconium hydrogen phosphate to the ion-exchanging zirconium oxide [76], as well as copper cations using sulfonated resin [77], poly(4-vinylpyridine) [78], and poly(acrylic acid) [79, 80]. The latter cases of copper removal with poly(4-vinylpyridine) and poly(acrylic acid) were accomplished using a two-step methodology whereby the as-made carboxyl and pyridine moieties were first used to capture copper cations through physisorption and were then protonated to their pyridinium and carboxylic acid forms with protons created locally from water oxidation to release the adsorbed copper (Figure 1.5a and b) [78, 79].

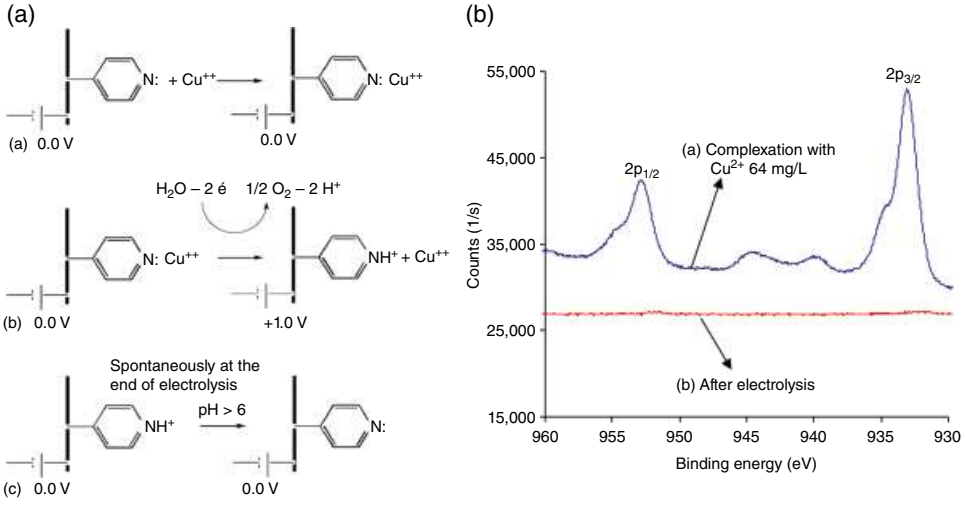

Figure 1.5 (a) A cationic EIX process for reversible copper anion removal via pH-mediated binding with pyridine/pyridinium. *Source:* Reprinted from [78]. Copyright 2007, with permission from Elsevier. (b) X-ray photoelectron spectra illustrating the presence and absence of copper within a poly(acrylic acid) film before and after electrolysis, respectively. *Source:* Reprinted from [79]. Copyright 2008, with permission from Elsevier.

Electrochemical techniques have also been applied in other ways to ion exchange processes. For example, after removing vanadium and molybdenum from solution with an anion exchange resin, a current was used to reduce only the pentavalent vanadium anion species to a tetravalent cation for selective electrochemical elution of vanadium over molybdenum [81]. Other methods have leveraged electrochemistry in ways such as creating acidic and basic aqueous solutions via bipolar membrane electrodialysis for subsequent regeneration of anion and cation exchange membranes used in a closed-loop water-softening process [82], and the electrochemical regeneration of metal aluminosilicate hydrate zeolites after being used for ammonia removal [83].

1.5.1.3 Electroflotation

The process of electroflotation utilizes the bubbles produced from electrochemical water splitting (oxygen from anodic water oxidation in Eq. (1.12) and/or hydrogen from cathodic water reduction in Eq. (1.13)) to physically separate undissolved material from the aqueous phase. The energetic requirements of electroflotation can be determined for an electrochemical cell (Eq. 1.18): [28, 29]

$$W_{\mathrm{EF}} = \frac{I_{\mathrm{cell}} E_{\mathrm{cell}}}{Q_{\mathrm{w}}} \tag{1.18}$$

where W_{EF} is the energy consumption for electroflotation, I_{cell} is the applied electrolysis current, E_{cell} is the cell potential, and Q_{w} is the water flow rate. In addition to current density for bubble production, electroflotation performance depends on other variables such as hydraulic retention time, species concentration, solution conductivity, solution pH, cell design, and electrode materials [28, 29, 84–86].

Electrolytically generated bubbles are small compared with bubbles produced from methods like dissolved air flotation and electrostatic spraying [87], can be easily controlled in terms of production, and provide a higher surface area-to-volume ratio for enhanced contact with the material to be removed [28, 29, 84, 85]. Froth flotation is an established and widely used industrial technique in mineral processing for beneficiation [84–86, 88], and electroflotation processes have similarly been used for the removal of fine particles like quartz [89], pyrite [90], chalcopyrite [91], and silica [92]. Like conventional flotation, electroflotation has also been employed to leverage density and hydrophobic differences to separate oil–water emulsions [28, 29, 84–86, 93, 94] from oil field [95] and palm oil mill [96] effluents, as well as to remediate turbidity in textile wastewater [97]. In flotation processes, other additives known as flotation reagents may also be introduced to the system to assist with material removal by increasing hydrophobicity, adjusting selectivity, improving recovery, and changing separation kinetics. These compounds include collectors/promoters to render the solids hydrophobic, frothers to improve collection and form a frothing layer at the solution surface, and auxiliary reagents such as activators/depressants for enhancing or hindering collection [88].

Bubble generation for electroflotation necessitates the selection of proper materials for the electrodes within the electroflotation cell. Cathode materials are usually selected to be inert metal and alloy materials which facilitate hydrogen production, such as nickel, titanium, stainless steel, and aluminum. The other end of the cell often suffers from stability

problems due to electrochemical corrosion, and as such, development has resulted in the use of graphite, lead oxide, platinum, and various titanium-containing species as common inert anodic materials [28, 29, 85, 98]. Alternatively, active anodes can also be used as sacrificial materials to release metal ions upon oxidation, which then form species that aggregate unwanted compounds for electroflotation to the solution surface. This latter technique is termed electrocoagulation and is often used in conjunction with electroflotation in a single process to remove the flocculated particles via electroflocculation [28, 29, 84–86, 99]. These electrochemical processes have been used to treat aqueous streams from the textile [100], dairy, paper [101], laundry [102, 103], tannery [104], mining [105], semiconductor [106], oil [107, 108], maritime, restaurant [109], and food industries [110], as well as for purification of drinking water [111], surface waters [112] and other streams containing industrial effluents, heavy metals [113–117], and biological wastes [28, 29, 84–86].

1.5.2 Electrocoagulation

In electrocoagulation, coagulating agents for the aqueous media to be treated are generated in situ via electrolytic electrode dissolution (Figure 1.6). Similar to a chemical coagulation process, the dissolved reagents destabilize the target species by precipitation and/or the breaking of emulsions and suspensions to separate them from the water phase and are extracted through another method like filtration or electroflotation. In a conventional electrocoagulation cell, iron and aluminum are typically used as sacrificial anode materials for generating charged cations upon oxidation to form subsequent coagulating agents such as polyhydroxides that facilitate a three-stage aggregation process comprising double layer compression of the charged species, charge neutralization of ionic species by the released

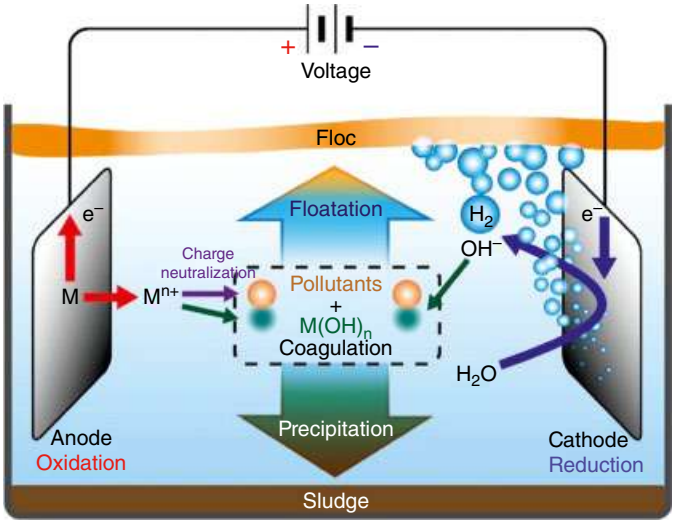

Figure 1.6 Setup and operation of a typical two-electrode electrocoagulation cell. *Source:* Reprinted from [118]. Copyright 2017, with permission from Elsevier.

anodic counter-ions, and floc formation [99, 119–123]. Like water electrolysis, the metal dissolution rate during electrocoagulation can be expressed using Faraday's Laws (Eq. 1.19): [23, 24, 99, 119, 120, 122, 123]

$$Q_{\mathrm{m}} = \frac{I_{\mathrm{cell}} M_{\mathrm{m}}}{nF} \tag{1.19}$$

where Q_{m} is the metal dissolution rate, I_{cell} is the applied electrolytic current, M_{m} is the molar mass of the metal, n is the number of electrons transferred per mole of the metal, and F is Faraday's constant. During cell operation, oxygen and hydrogen bubbles are also generated (oxygen from anodic water oxidation in Eq. (1.12) and/or hydrogen from cathodic water reduction in Eq. (1.13)), rendering electroflotation intrinsically suitable for use alongside electrocoagulation to fully separate the solid materials from the solutions. Furthermore, electrocoagulation processes are generally easy to operate, do not require the addition of chemicals, and produce flocs and sludge with tractable properties for separation [85, 99, 117, 119–123]. Electrocoagulation has been used to remove a variety of different pollutants from aqueous solution (Table 1.3) [146] and also has potential as a localized water treatment technology [147].

1.5.3 Electrodeposition

Electrodeposition refers to electrolytic processes that facilitate the electrochemical reduction of dissolved metal ions to their solid forms at cathode surfaces (Eq. 1.20): [23, 24, 85, 148–151]

$$M^{n+}{}_{(\mathrm{aq})} + n\mathrm{e}^{-} \leftrightarrow M_{(\mathrm{s})} \tag{1.20}$$

Table 1.3 Applications of electrocoagulation processes.

Water sources	Contaminants
• Wastewater: – Tanneries [124] – Petroleum refineries [125] – Paint manufacturing [126] – Olive mills [127, 128] – Potato chip manufacturing [129] – Baker's yeast production [130] – Electroplating [131] – Textile industry [132–134] – Black liquor from the paper industry [135] – Dairy effluents [136] • Tap water [144] • Potable water [145]	• Oil [118] • Dyes [137, 138] such as orange II [139] • *Escherichia coli* cells for disinfection [140] • Trivalent chromium [141] • Nitrate [142] • Arsenic [143] • Copper, zinc, and hexavalent chromium [131] • Iron [144]

where $M^{n+}_{(aq)}$ is the metal ion to be extracted, n is its valence, and $M_{(s)}$ is the reduced neutral metal in its solid state. The energetic requirements of electrodeposition can be determined for an electrochemical cell (Eq. 1.21): [149, 150]

$$W_{EDP} = \frac{nFE_{cell}}{M_m(CE)} \tag{1.21}$$

where W_{EDP} is the energy consumption for electrodeposition, F is Faraday's constant, E_{cell} is the applied cell potential, M_m is the molar mass of the metal, and CE is the current efficiency. Historically, electrochemical deposition has been utilized notably for the electrowinning of metals in metallurgy (i.e. the extraction of metal species from solution by reducing them electrochemically) [149–151] and electroplating applications to generate coatings [148, 150, 152], but can also be applied to the extraction of metals from aqueous waste streams [117, 153]. Electrochemistry is employed in the field of electrometallurgy for the electrowinning of metals from leaching solutions after isolation from their ores, as well as for the subsequent electrorefining of an electrowon metal via further dissolution and deposition to remove co-deposited impurities. In aqueous electrowinning, lead is often used as the anode, and titanium or stainless steel as the cathode. The anode can also be modified or selected in a way to catalytically promote oxygen evolution to reduce its overpotential and lower energy consumption. Similarly, metals with relatively lower reduction potentials may be difficult or impossible to electrowin in aqueous media due to competition from hydrogen evolution, hence the common application of aqueous electrowinning to the production of metals such as copper [154] and zinc [155], as well as for cadmium [156] and nickel [157] recovery [149–151]. However, electrodeposition has also been utilized for the separation of various other metals (Table 1.4).

Selective separation processes can be carried out before the electrodeposition step to enable individual metal ion extraction, but in theory, electrodeposition can also be performed with specificity from a mixture of metal ions based on differences in metal reduction potentials. For example, this has been accomplished experimentally with the removal of copper and nickel by electrodeposition from electronic and galvanic industrial waste solutions [178, 179], as well as the recovery of copper, lead, cadmium, and zinc from chloride solution [180]. Selective electrodeposition has also been used in the targeted reduction of uranyl cations to urania onto an anionic conducting polymer over competing lanthanide cations for radioactive waste applications [181], as well as onto amidoxime-functionalized carbon over competing ions from seawater using a half-wave-rectified alternating current electrochemical method [182]. In another study, cadmium was recovered from binary mixtures containing either cobalt or nickel without co-deposition of the latter cation through the use of nucleation potential measurements obtained from the addition of counter-anions at different cation concentrations to influence deposition potentials [183]. In a final example, a direct/alternating current electrochemical method with tunable alternating current amplitude, frequency, and offset was utilized to separately recover copper, cadmium, and lead from the same solution [184].

The concept of electrochemically recovering metals from metal–organic complexes through electrodeposition has been further extended to carbon dioxide separation in

Table 1.4 Applications of electrodeposition processes.

Number of metals removed in application	Metal(s)	Recovery application/solution
One	Copper	• Cathodic reduction in a microbial fuel cell [158] • Photoelectrocatalytic oxidation cell for copper–ethylenediaminetetraacetic acid complexes [159] • Ultrafiltration cell for copper–poly(acrylic acid) complexes [160] • Electrowinning from spent electroplating electrolyte [161] • From printed circuit boards after acid leaching [162–164]
	Gold	• From thiourea solution [165]
	Iron	• From sulfate solution [166]
	Lead	• From smelting fly ash of waste lead-acid batteries [167]
	Selenium	• Cyclone electrowinning [168]
	Palladium	• From nitric acid [169]
	Cobalt	• From sulfate solution [170]
	Zinc	• From electric arc furnace dust leach liquor [171]
	Cadmium	• From spent batteries subject to an acid leaching process [172]
Two	Zinc and cadmium	• From spent batteries subject to an acid leaching process [173]
	Zinc and manganese	• From household alkaline batteries [174]
	Copper and lead	• From printed circuit boards after acid leaching [175]
Three	Copper, nickel, and cadmium	• Cyclic electrowinning and precipitation system [176]
	Copper, nickel, and cobalt	• From chelated complexes using a two-chamber cell fitted with a cation exchange membrane [177]

aqueous media. An example of this is the electrochemically mediated amine regeneration (EMAR) process (Figure 1.7a and b), which makes use of the electrochemical conversion of copper between its ionic and solid states to mediate reversible CO_2 capture and release (Eqs. 1.22–1.24): [186, 187]

$$\mathrm{Am}_{(\mathrm{aq})} + m\mathrm{CO}_{2(\mathrm{g})} \leftrightarrow \mathrm{Am}\left(\mathrm{CO}_2\right)_{m(\mathrm{aq})} \tag{1.22}$$

$$\frac{2}{m}\mathrm{Am}\left(\mathrm{CO}_2\right)_{m(\mathrm{aq})} + \mathrm{Cu}_{(\mathrm{s})} \leftrightarrow \mathrm{CuAm}^{2+}{}_{\frac{2}{m}(\mathrm{aq})} + 2\mathrm{CO}_{2(\mathrm{g})} + 2\mathrm{e}^- \tag{1.23}$$

$$\mathrm{CuAm}^{2+}{}_{\frac{2}{m}(\mathrm{aq})} + 2\mathrm{e}^- \leftrightarrow \mathrm{Cu}_{(\mathrm{s})} + \frac{2}{m}\mathrm{Am}_{(\mathrm{aq})} \tag{1.24}$$

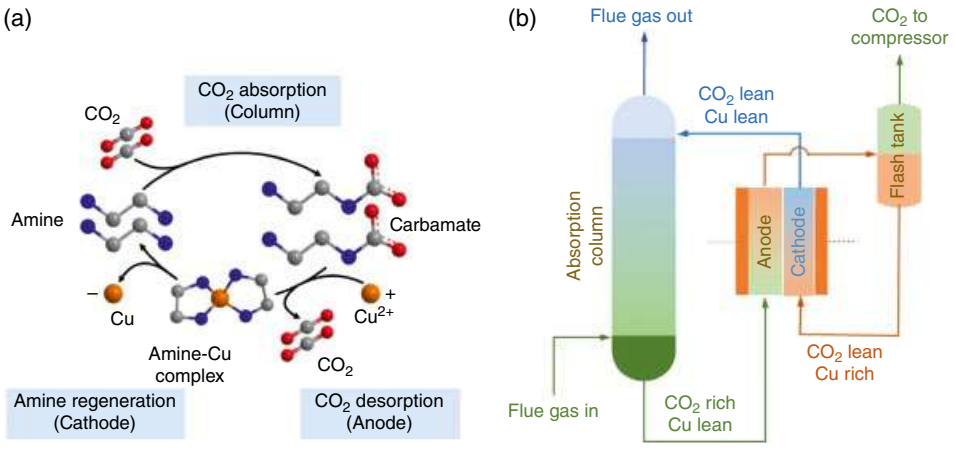

Figure 1.7 (a) EMAR cycle for the reversible complexation of copper and CO_2 with homogeneous amines and (b) EMAR process schematic illustrating the generation of an amine stream loaded with CO_2 in an absorber for subsequent CO_2 desorption in an electrochemical cell. *Source:* Reprinted from [185]. Copyright 2019, with permission from Elsevier.

where Cu is copper, Am is an amine, and *m* is a stoichiometric coefficient. The EMAR system has been extensively studied and developed through multiple bench-scale experimental setups [185, 186, 188–190], detailed modeling [187, 189], and technoeconomic analyses [191], and can be applied to post-combustion capture with projected energy consumptions of 50 kJ/mol CO_2 with potential for further reduction to 40–45 kJ/mol CO_2, stability after 200 hours of continuous operation with electrode switching, and estimated carbon capture costs of below \$50/ton CO_2 [192].

Similar aqueous electrochemically modulated complexation processes leveraging the Cu(I)/Cu(II) redox couple have been applied for the capture and release of carbon dioxide [193] via a binuclear copper complex to reversibly bind carbonate with the ability of concentrating CO_2 content from 10 to 75% in nitrogen [194], the selective extraction of other gaseous species such as carbon monoxide from nitrogen [195], and ethylene from ethane [196] using copper chlorides, as well as various alkenes using a copper triflate vinyl sulfonate complex [197].

1.6 Electrochemically Mediated Sustainable Separation Methods

While many conventional electrochemical separation processes have been very successful in commercial and industrial applications, electrochemical processes for water treatment can often require high energetic inputs [7], especially since a majority of them rely on water electrolysis to enable removal of the desired material. Contrastingly, electrochemically mediated sustainable separation systems offer strong potential for enhanced separation efficiency, specifically in areas such as heightened selectivity for specific target analytes, reduction in energetic requirements, and process reversibility. In general, these methods utilize heterogeneous electrochemical phenomena at bare or

functionalized electrodes to nondestructively remove target species in their initial state, such as ions [198], but can also be combined with electrochemical reactions for enhanced remediation.

1.6.1 Electrochemical Conversion Processes

Electrochemical conversion involves the direct reaction of an electrode material with the target analyte to create a new phase through the formation of chemical bonds. An interesting example is the specific electrochemical reaction of bismuth with chloride, which has been expressed as the following anodic half-reactions (Eqs. 1.25 and 1.26): [199, 200]

$$Bi + Bi_2O_3 + 3Cl^- \leftrightarrow 3BiOCl + 3e^- \tag{1.25}$$

$$Bi + Cl^- + H_2O \leftrightarrow BiOCl + 2H^+ + 3e^- \tag{1.26}$$

This reversible phenomenon is highly pertinent to water desalination and facilitates the targeted uptake and release of chloride anions from seawater. The bismuth electrode can then be coupled with a sodium-selective redox species at the other electrode to form a desalination battery (Figure 1.8a). Chloride extraction via electrochemical conversion for desalination has also been accomplished using the Ag/AgCl redox couple [202], in both asymmetric and symmetric configurations. A hybrid battery comprised of a silver electrode and the sodium-intercalating $Na_{2-x}Mn_5O_{10}$ species yielded high selectivity for sodium and chloride ion removal from seawater with coulombic efficiencies of 57 and 76%, respectively, with less than 10% efficiency for each of the other competing ions after 50% of the total salt was removed [203]. The Ag/AgCl system has also been incorporated into a "rocking-chair" battery framework comprised of silver and silver-chloride electrodes (Figure 1.8b) that produced a salt removal capacity of 115 mg/g at a concentration of

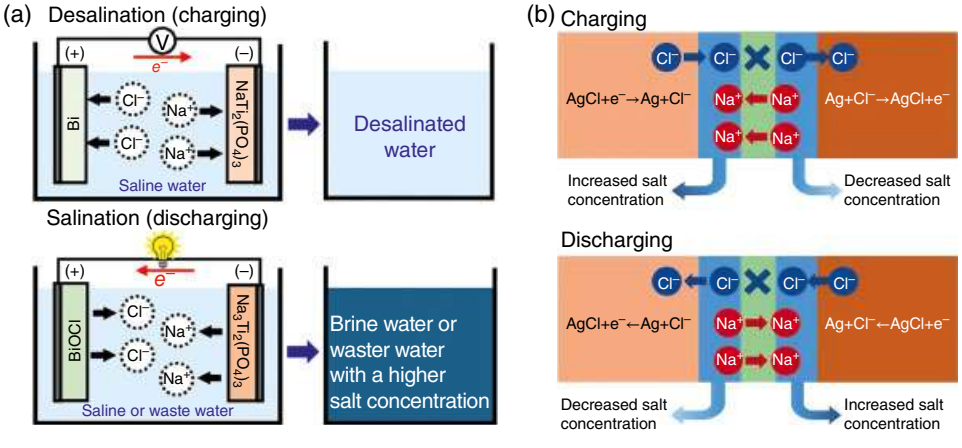

Figure 1.8 A desalination battery framework for chloride anion removal via the reversible electrochemical reactions of chloride with (a) bismuth. *Source:* Reprinted with permission from [200]. Copyright 2017, American Chemical Society and (b) silver [201]. License under CC BY 3.0.

600 mM NaCl with a cell voltage of only 0.2 V [201]. In the same vein, aqueous battery chemistries utilizing metal-halide bond formation for energy storage may also be potentially applicable for reversible water-based ion separations in the future [204, 205], with a noteworthy case study being an aqueous lithium-ion battery containing a composite cathode made up of graphite and LiBr and LiCl salts, which was reversibly oxidized to yield Br^- and Cl^- anions for subsequent intercalation into the graphite [206].

1.6.2 Electrical Double Layer Processes

The main electrochemical separation technique that leverages the ability of the electrical double layer to store ions is capacitive deionization (CDI). CDI operates through the activation of an electrochemical potential difference between porous electrodes to form electrical double layers at their surfaces for ion removal by electrosorption (Figure 1.9a) and is primarily applied for water desalination and softening with high potential for use as an energy-efficient separation process in the brackish salinity range [9, 10, 202, 207, 210–213], but has also been used for carbon dioxide removal through a supercapacitive swing adsorption process [214]. The CDI process is reversible with charging (salt uptake) and discharging (salt release) voltages usually around 1.2 and 0 V, respectively, which can

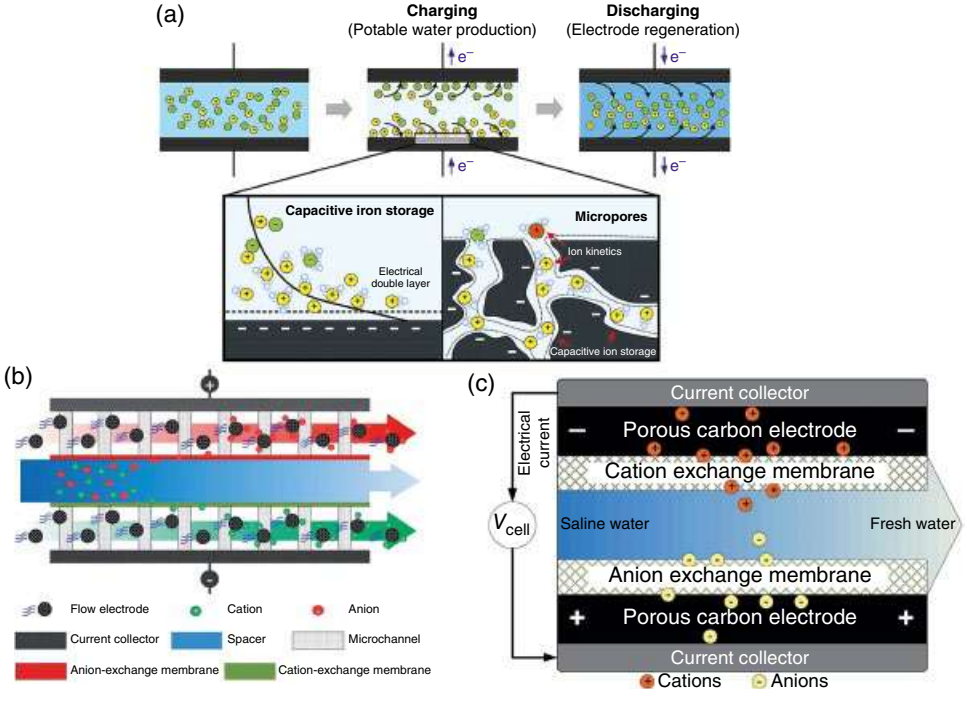

Figure 1.9 The electrochemical ion separation processes of (a) CDI, *Source:* Reprinted from [207]. Copyright 2018, with permission from Elsevier. (b) FCDI, *Source:* Republished with permission from [208], and (c) MCDI, *Source:* Republished with permission from [209].

subsequently lead to salt adsorption capacities of nearly 15 mg/g and over 20 mg/g under batch and flow operation conditions, respectively [9, 211]. During CDI, both non-Faradaic and Faradaic phenomena can occur. Non-Faradaic effects include the main capacitive ion storage mechanism in the formed electrical double layers, and transport of ions within the porous electrodes, and can also include interactions between ions and chemical charges present on the electrode surface. Faradaic changes may also occur at the anode and cathode, such as oxidation and reduction of the carbon material, and water chemistry half-reactions like chloride oxidation and oxygen reduction, as well as water splitting from water oxidation and water reduction, respectively. Parasitic side reactions can lower performance and are the dominant cause of energy losses at low charging currents due to the longer durations that the electrodes operate at higher voltages [215]. Additionally, unwanted Faradaic reactions may affect water quality by causing changes in solution pH, as well as the formation of chemical byproducts. Leakage current from water electrolysis also causes the charging potential to be constrained by the water stability window of 1.23 V [9, 10, 207, 211].

Selective ion adsorption with CDI can be accomplished through a variety of methods [10, 211, 216]. Examples exploiting ion characteristics include the leveraging of hydrated ion properties using an ultramicroporous electrode with narrow pores less than 1 nm to allow for targeted adsorption of the planar weakly hydrated nitrate over chloride and sulfate with selectivities of over 6 and 17 at a one- and half fold excess, respectively [217], hydration ratios (ratio of the hydrated ion radius to the bare ion radius) for favored uptake of low hydration ratio ions like ammonium and nitrate over sodium and fluoride, respectively [218], hydrated ionic radii for better separation of the smaller potassium over sodium [212, 213, 219], ionic charges for enhanced extraction of the divalent calcium over the monovalent sodium attributed to surface charge screening [212, 213], ion diffusion rates to attain selectivities of up to ca. 10 for perchlorate (higher diffusion coefficient) over an eightfold excess of chloride at 0.6 V [220], and ion electronegativities for the preferential removal of the more electronegative perrhenate over chloride [221]. In addition to ion effects, selectivity has been imparted through modification of the electrode surfaces with additions such as chemical charges from chemical oxidation, which almost doubled the hydrated radius size-based selectivity of smaller potassium over lithium [222], nitrogen groups in N-functionalized graphene for highly selective extraction of heavy metals over alkali/alkaline earth metals due to short-range interactions [223], anion exchange resin-coated carbon electrodes for targeted separation of sulfate [224] and nitrate [225, 226], sulfonic [227] and amine functional groups on graphene [228], and cetyl trimethyl ammonium bromide (CTAB) that enabled a 6.5-fold selective physisorption of nitrate over chloride followed by electrochemical desorption [229].

CDI has been employed in a variety of additional different configurations [230]. Examples include inverted CDI (i-CDI), where desorption instead of adsorption occurs during charging [231–234], flow CDI (FCDI) (Figure 1.9b), where a flowing suspension of carbon particles is used in lieu of the fixed carbon electrodes [208, 235–239], and membrane CDI (MCDI) (Figure 1.9c), [9, 10, 207–209, 211, 216, 240–243] where ion exchange membranes are placed in front of the carbon electrodes to offer enhanced ion selectivity, salt removal capacity, and energetic performance by virtue of the exchange membrane's ion specificity,

retention of co-ions (ion with same charge as the electrode) during charging, and ability to provide efficient counter-ion flushing during regeneration. Additionally, the ion-exchange membrane layer in MCDI can mitigate detrimental phenomena such as anode oxidation from parasitic side reactions by restricting the contact of the electrode with the bulk solution [207, 244, 245]. MCDI has been used for targeted ion removal of fluoride over sulfate [246], nitrate over chloride [247], lead over calcium and magnesium [248], lithium over magnesium [249], monovalent cations over divalent cations [250], calcium over sodium [251, 252], and even carbon dioxide [253, 254]. Another electrical double layer method similar to CDI is ion concentration polarization [255, 256], a technique that makes use of the charge mismatch in nanochannels to facilitate a concentration gradient for ion enrichment that can be used for desalination.

1.6.3 Heterogeneously Functionalized Redox-Active Species Processes

The addition of redox-active species to a conductive heterogeneous framework can allow them to be used as electrodes with pre-mediated selectivity as a result of designed electrochemical interactions between the redox material and specific analytes [12–14]. Faradaic compounds can provide additional pseudocapacitance to enhance the performance of electrochemical capacitors [257–260]. Compared to traditional CDI operations, electrochemical separation processes developed with Faradaic redox-active species can also provide significantly enhanced ion adsorption capacities [207, 216], as observed from both experiments [211, 261] and modeling [262].

1.6.3.1 Electrochemically Mediated Binding

Electrochemically mediated binding processes operate by utilizing a direct interaction between heterogeneous redox-active species and specific analytes to achieve targeted separation. An electrochemical stimulus is used to alter the oxidation state of a redox-active material to allow it to attract particular molecules. Since this affinity is imparted through electrochemical activation, the process is fundamentally reversible, and previously captured species can be subsequently released by simply altering the electrochemical potential or direction of current flow (Figure 1.10) [12–14].

1.6.3.1.1 Redox-Active Polymers

A powerful class of redox-active species for ion separation is the metallocene. As the classic example of a facile and reversible redox couple, ferrocene (charge of 0) is able to capture anions by undergoing a one-electron oxidation reaction to the ferrocenium cation (charge of +1) [264] (Eq. 1.27): [265–267]

$$\mathrm{Fc} + \mathrm{I_{Anion}}^{-} \leftrightarrow \mathrm{Fc^{+}I_{Anion}}^{-} + \mathrm{e}^{-} \tag{1.27}$$

where Fc is ferrocene, Fc^{+} is ferrocenium, and $\mathrm{I_{Anion}}^{-}$ is an anion. The nature of the anion interacting with ferrocenium affects its electrochemical response, and, in general, it has been observed that inorganic electrolyte anions that are more hydrophobic promote ferrocene oxidation and the formation of ferrocenium-anion ion pairs [265–271].

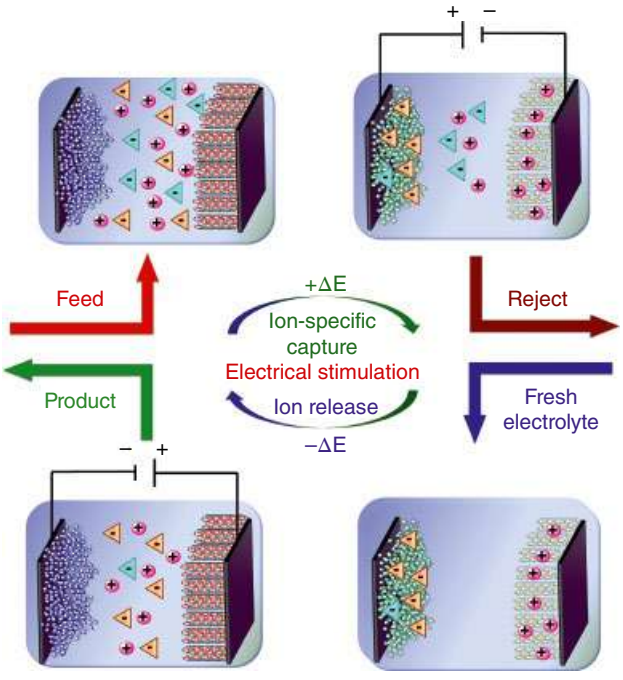

Figure 1.10 An electrochemically mediated binding process for the reversible selective capture and release of anions and cations. *Source:* Reprinted with permission from [263]. Copyright 2016, American Chemical Society.

The electrochemically mediated anion-dependent interaction of ferrocene has resulted in its ubiquitous use as a redox probe in applications such as sensing [272–274] and catalysis (Figure 1.11) [275–277].

In its neutral state, ferrocene is hydrophobic and is thus well-posed to extract anions from aqueous media heterogeneously. To further improve its immobility as a solid electrode, ferrocene can be prepared as a vinyl homopolymer, poly(vinylferrocene) (PVFc) [278], allowing it to be tethered to carbon nanotubes to form a nanostructured material (PVFc-CNT) through non-covalent pi-pi stacking interactions. In a conductive framework, the ferrocene moieties are quickly activated and better utilized, resulting in a higher redox-enhanced pseudocapacitance (Figure 1.12a) [279, 281]. PVFc composites have been used to perform targeted separation of simple organic anions (i.e. carboxylates, [263, 282] sulfonates, phosphonates) [283], more complex organic micropollutants [284], proteins [285], inorganic heavy metal oxyanions (HMOAs) from wastewater [280, 286–289], and nuclear waste [73, 290]. As the separation process occurs only in the presence of ferrocenium, it follows that the amount of analyte electrosorbed by PVFc composites is dependent on the extent of oxidation of the ferrocene units, and thus the applied electrochemical potential (Figure 1.12b). Furthermore, due to the reversible nature of the ferrocene redox couple, the ferrocenium moieties can be electrochemically regenerated via reduction back to ferrocene, desorbing the previously adsorbed analyte for successive separation cycles with unchanged capacity (Figure 1.12c).

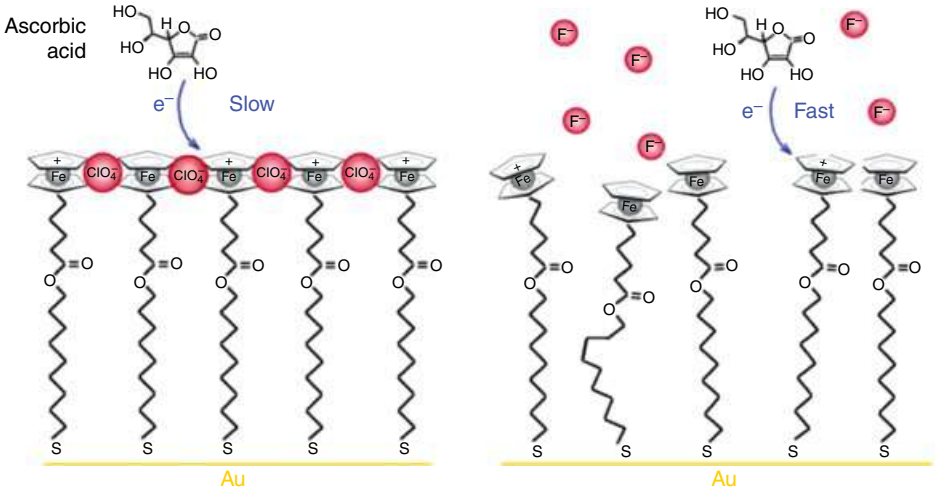

Figure 1.11 Proposed structural changes for describing the variation in electrocatalytic behavior of ferrocene self-assembled monolayers (SAMs) for ascorbic acid oxidation in the presence of different supporting electrolyte anions. *Source:* Reprinted with permission from [270]. Copyright 2004, American Chemical Society.

Density functional theory (DFT) electronic structure calculations have revealed high binding energies for certain ferrocenium ion pairs (Figure 1.13a and b) that have been ascribed to redox-enhanced hydrogen bonding [283], as well as the lower ionization potentials and electronegativities for certain transition metal-containing oxyanions compared to halide electrolyte species [280]. These results have been supported by the experimentally observed separation selectivity of organic anions such as formate [283] and benzoate [282], and inorganic HMOAs of chromium [280], arsenic [280, 286, 289], and vanadium [288], over competing inorganic anions such as perchlorate. The targeted nature of the ferrocenium–anion interactions was clearly seen through the removal of vanadium from a 40-fold excess of background electrolyte with an ion selectivity greater than 10 after 3 hours adsorption at 0.8 V vs Ag/AgCl (Figure 1.13c) [288], as well as the continuous flow removal of benzoate from a 50-fold excess of supporting anions with an ion selectivity of 3 after 2 minutes adsorption at 0.35 V vs Ag/AgCl at a flow rate of 1 mL/min [282]. Ferrocene moieties have also been incorporated into cation exchange polymers as a means of electrochemically releasing species that were previously adsorbed by the ion exchange component (Figure 1.13d). Specifically, an electroactive ion exchange polymer containing vinyl ferrocene (VFc), styrene (STY), and styrene sulfonate (SS^-) groups, (STY)-(SS^-)-(VFc), was used to reversibly separate the redox-active methyl viologen cation (Figure 1.13e and f) [291].

Other cobalt-containing metallocene counterparts to ferrocene have also been used in electrochemically mediated redox-active separation processes. Cobaltocene is a cobalt-containing chemical analogue to ferrocene, and both the cobaltocenium cation and ferrocene share a stable 18-electron configuration [292]. The stability of cobaltocene (charge of 0) in its oxidized cobaltocenium state (charge of +1) allows for its use as a reducing redox-active species. Cobaltocenium can be synthesized as a metallopolymer, poly(2-(methacryloyloxy)ethyl cobaltocenium) ($PMAECoCp_2$) [284, 293, 294], which has been used as a cathodic electron

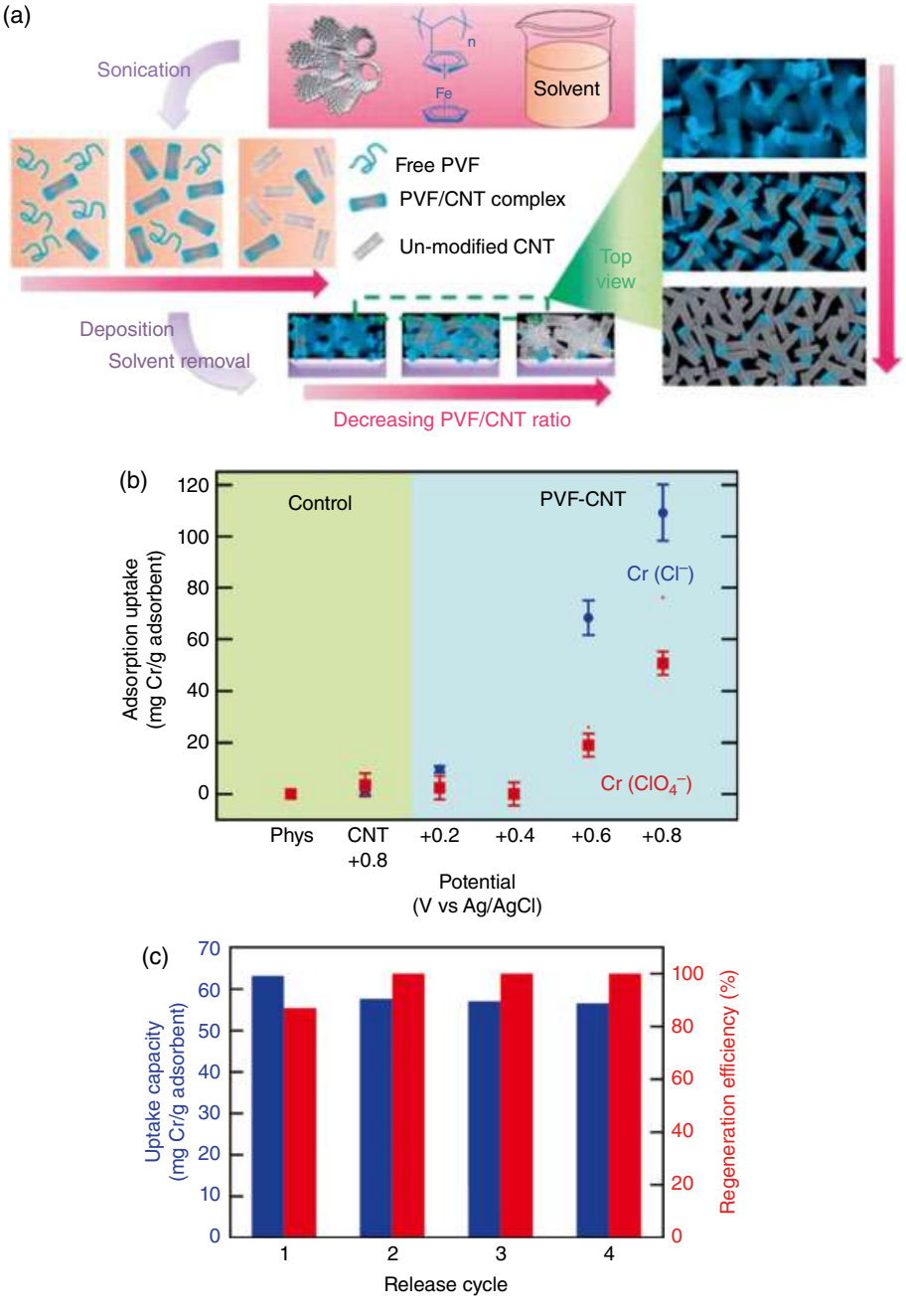

Figure 1.12 (a) A solution process for the preparation of conductive PVFc-CNT composites via dispersion and subsequent solvent removal. *Source:* Republished with permission from [279]. (b) Variation of PVFc-CNT electrosorption capacity for chromium HMOAs with electrochemical potential, and (c) electrochemical reversibility of chromium HMOA electrosorption and electrodesorption by PVFc-CNT [280]. Licensed under CC BY 4.0.

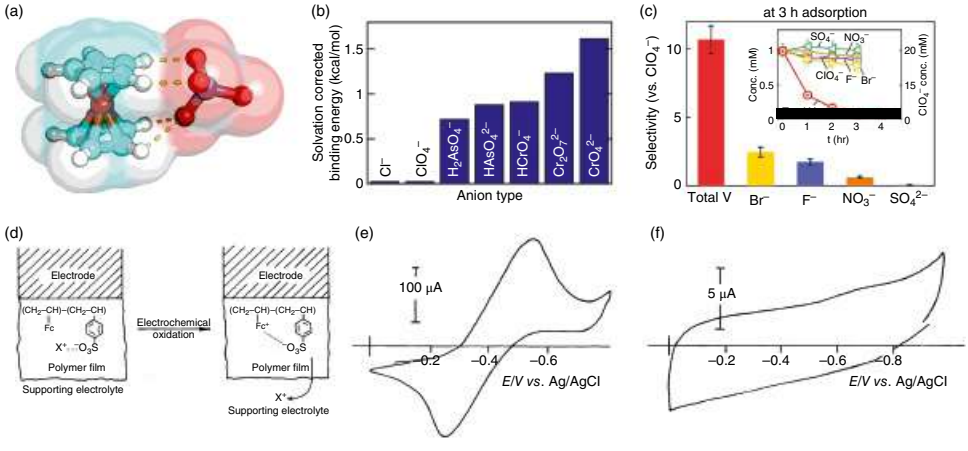

Figure 1.13 (a) DFT-optimized structure of the ferrocenium-chromate ion pair and (b) zero-temperature solvation-corrected binding energies of various ferrocenium-HMOA complexes from DFT calculations [280]. Licensed under CC BY 4.0. (c) Experimentally determined selectivities of PVFc-CNT for vanadium HMOAs over competing electrolyte anions. *Source:* Used with permission from [288]. Copyright 2020, John Wiley & Sons. (d) Proposed scheme for the adsorption and subsequent release of cations into an electroactive ion exchange polymer as mediated by the electrochemical oxidation of ferrocene groups, and cyclic voltammograms of (STY)-(SS^-)-(VFc) (e) after exposure to a solution containing the redox-active methyl viologen cation, and (f) after electrorelease of methyl viologen by applying an electrochemical potential to oxidize the ferrocene groups. *Source:* Republished with permission from [291].

sink to suppress parasitic water splitting reactions during electrochemical separations [284]. A cobalt-containing organometallic variant of cobaltocene, [η^5-(1-oxo-4-methacryloyloxybutyl)-cyclo-pentadienyl]cobalt(η^4-tetraphenylcyclobutadiene) (CpCoCbMA), has also been prepared in its metallopolymer form, PCpCoCbMA [295], and subsequently applied for electrochemical separation. Contrary to cobaltocene, the redox-active portion of PCpCoCbMA, η^5-cyclopentadienyl-cobalt-η^4-cyclobutadiene (CpCoCb), has a stable 18-electron configuration in its neutral state (charge of 0) [296], and upon electrochemical reduction becomes a negative anion (charge of −1) [297], and is thus able to separate cationic species [284].

The redox-active quinone species has been utilized for reversible carbon dioxide separation in aqueous media [298]. The electrochemical interaction of quinones and other compounds [299] with carbon dioxide has previously been observed in aprotic organic media [300–302], and the extension of its operation to a water phase removes concerns with solvent safety and toxicity. Anthraquinone can reversibly bind with carbon dioxide (Figure 1.14a) and has been heterogeneously functionalized on an electrode in the form of a heterogeneous poly(1,4-anthraquinone) (PAQ) conductive composite for use in an electrochemical cell (Figure 1.14b) with near-stoichiometric CO_2 uptake and release over multiple cycles (Figure 1.14c) in a water-in-salt electrolyte at a competitive energy consumption of ca. 56 kJ/mol CO_2 [298]. Electrochemically mediated separation of carbon dioxide in water has also been accomplished with an organic semiconductor electrode comprising a naphthalene bisimide derivative at a capture efficiency of ca. 2.3 mmol/g [303]. In addition, quinones [304, 305] and other species like phenazines [306, 307] and a biological proton carrier [308] have been employed homogeneously in aqueous solution to electrochemically separate carbon dioxide at reasonable energy consumption values via pH gradients from proton-coupled electron transfer reactions.

1.6.3.1.2 Conducting Polymers

Conducting polymers have also been used for electrochemically mediated separations. In general, many conducting polymers are conjugated pi polymers and are conductive because they contain delocalized pi electrons that can move through unsaturated backbones (Figure 1.15a) [309, 313, 314], a property which has resulted in their application to sensing [315], energy storage [316, 317], and environmental remediation [318]. Their conductivities can be varied through the addition of a dopant, which can create positive (p-doping) or negative (n-doping) polarons or bipolarons through a charge transfer redox process [309, 313, 314, 319]. Redox conversion of the conducting polymer can also be performed electrochemically and leveraged for ion binding. This reversible process is known as electrochemical doping and allows for precise control of the uptake of various dopant ions. A common example of a conducting polymer is poly(pyrrole) (PPy), which can be electrochemically oxidized to create positively charged species (Figure 1.15b), and has subsequently been applied for the separation of anions such as perchlorate [320], hexavalent chromium [321], and chloride via chloride-ion [322] and desalination batteries [323]. PPy has been used in electrochemical solid-phase microextraction (SP-ME) techniques [324, 325] for the enhanced removal of species such as fluoroquinolones [326] and inorganic anions [327], as well as in the electrochemical chromatography [328] of dansyl amino acids; the latter application is particularly interesting due to the ability of the process to vary the capacity factors of the amino acids by at least an order of magnitude and reducing

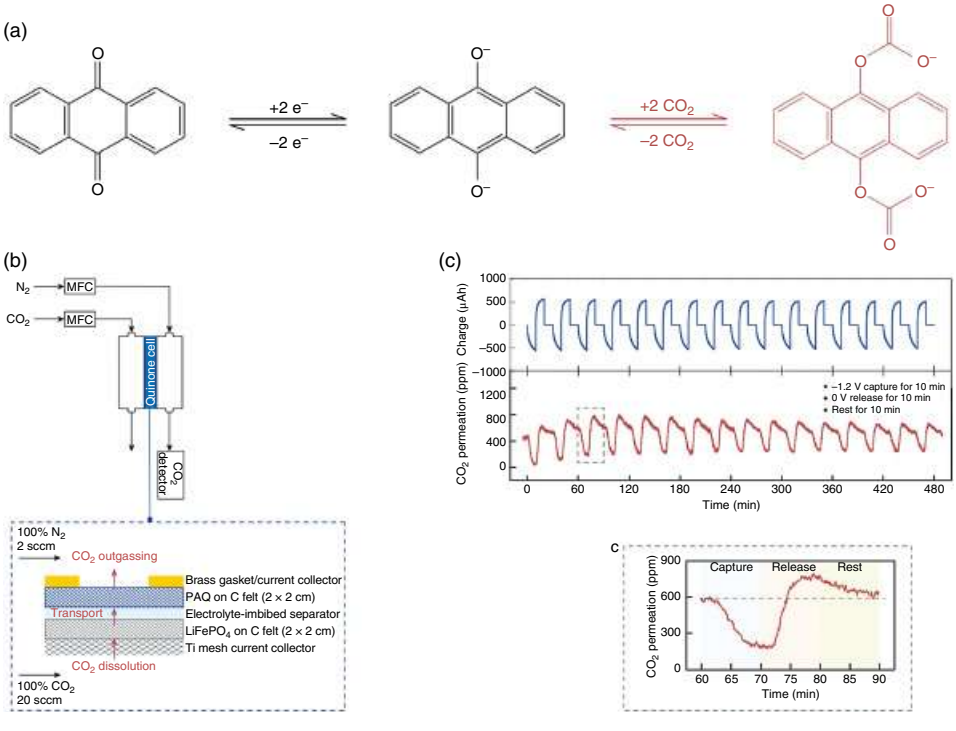

Figure 1.14 (a) Electrochemically mediated reversible reaction between anthraquinone and carbon dioxide and (b) implementation of conductive PAQ composite into an electrochemical cell for (c) CO_2 uptake and release over multiple cycles [298]. Licensed under CC BY 4.0.

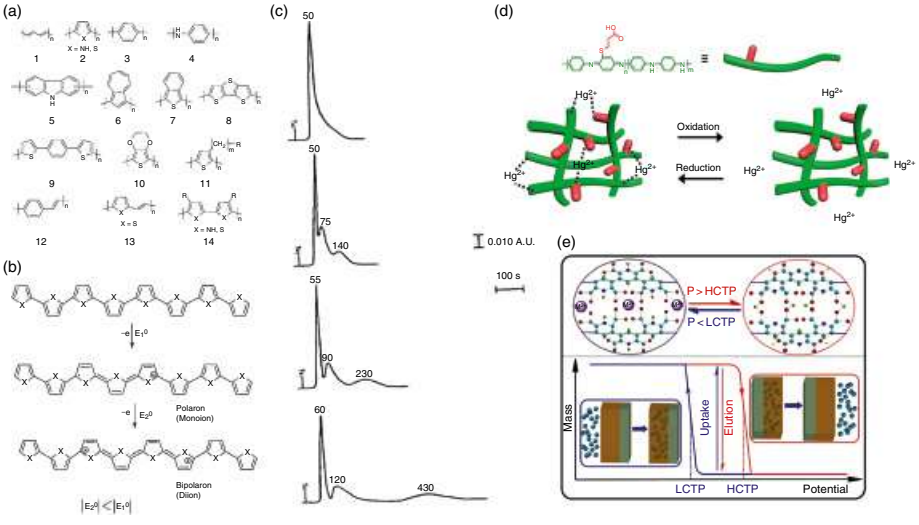

Figure 1.15 (a) Examples of conducting polymers and (b) the electrochemical oxidation mechanism of PPy and poly(thiophene). *Source:* Reprinted with permission from [309]. Copyright 2010, American Chemical Society. (c) Chromatographs illustrating the variation in the separation of a mixture of three dansyl amino acids with electrochemical modulation of the PPy stationary phase. *Source:* Reprinted from [310]. Copyright 1995, with permission from Elsevier. (d) Mercaptopropionic acid-grafted PANI for the reversible electrochemical separation of mercury. *Source:* Reprinted with permission from [311]. Copyright 2018, American Chemical Society. (e) Electrochemical scheme for copper removal with PPDA via potential-triggered proton self-exchange. *Source:* Reprinted from [312]. Copyright 2014, with permission from Elsevier.

elution band half-widths and retention times for the optimized separation of a mixture containing three different amino acids (Figure 1.15c) [310]. Other conducting polymers have also been used for electrochemical ion separation, including poly(aniline) (PANI) for fluoride [329] and heavy metal cations (Figure 1.15d) [311, 330], poly(3-methylthiophene) (P3MT) for arsenate anions [331], and poly(2,6-pyridinedicarboxylic acid) (PPDA) for copper anions [312]. The latter polymer leverages a three-way interaction between Cu^{2+}, the PPDA carboxyl group, and the PPDA pyridine group, whereby potentials below the lowest critical transfer potential (LCTP) and above the highest critical transfer potential (HCTP) result in the formation of intermolecular hydrogen bonds between the copper cations and the carboxyl groups, and the pyridine and carboxyl groups, respectively, resulting in high selectivities for Cu^{2+} uptake over co-existing cations in solution (Figure 1.15e) [312].

1.6.3.1.3 Electroactive Crystalline Species

Like the aforementioned organic macromolecules, inorganic species can also possess redox-active properties. The quintessential archetype is the Prussian Blue analog (PBA) class of compounds, which contain electrochemically active transition metals that enable the redox-mediated selective intercalation of cations into its open framework [332–334]. This reversible phenomenon has been applied to the uptake of ammonium ions [335], divalent alkaline earth metal cations like magnesium and calcium (Figure 1.16a) [336], and trivalent cations like aluminum and yttrium [340], as well as in electrochemically switched ion exchange (ESIX) processes for alkali metal cations such as sodium and cesium (Figure 1.16b), the latter of which have found fitting applications in both nuclear waste remediation due to the radioactive ^{137}Cs isotope (Figure 1.16c) [337, 338, 341, 342], and desalination [343]. The nickel hexacyanoferrate (NiHCF) PBA has been observed to exhibit selectivities for both Cs^+ and K^+ over Na^+, at experimentally quantified separation factors of around 360 and 5 in solutions with an 80-fold and a 10-fold excess of Na^+, respectively, measured at steady-state conditions after voltammetric cycling [342]. It has been previously observed that it is easier for alkali metal cations with smaller hydrated ionic radii to electrochemically intercalate into NiHCF, hence its affinity for cesium over sodium [344–347]. Electrode materials for aqueous batteries (especially of the near-neutral class) such as graphite, oxides, and polyanionic compounds may potentially also be repurposed for ion extraction in water, due to their ability to reversibly store charge carriers like metal cations (e.g. lithium, potassium, sodium, magnesium, calcium, zinc, and aluminum) and non-metal ions (e.g. hydroxide, halides, protons, ammonium, and even nitrate [348]) [204]. Specifically, some possible candidates include hexacyanomanganate compounds [349], iron-based polyanionic compounds (e.g. $FePO_4$), vanadium-based oxides (e.g. VO_2), and manganese-based oxides (e.g. MnO_2). The proton-intercalating ability of MnO_2 has also been leveraged to control the pH of aqueous media to facilitate electrochemically mediated proton concentration for carbon dioxide capture and release [350, 351]. Some of these crystalline species are already being used interchangeably between energy storage and separations, with the most notable examples being PBAs and lithium-intercalating compounds for the extraction of lithium from brine (Figure 1.16d) [339, 352], and the recovery of ammonium from wastewater [353]. Metal-organic frameworks (MOFs) with engineered electrochemical properties are a rapidly growing field [354–357] and may also prove to be

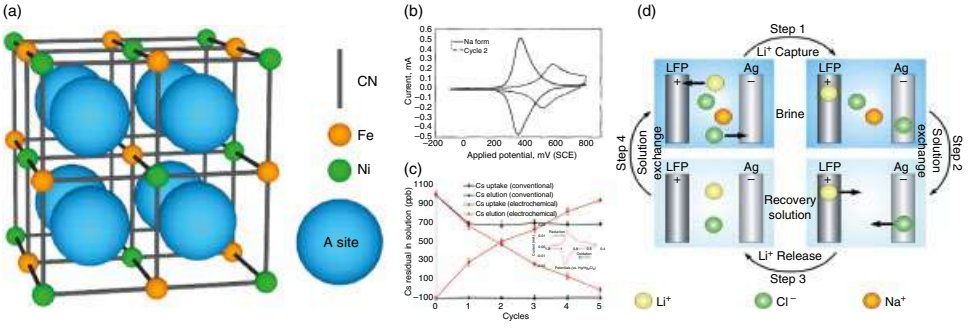

Figure 1.16 (a) Crystalline structure of NiHCF with vacant A sites for cation intercalation. *Source:* Reprinted with permission from [336]. Copyright 2013, American Chemical Society. (b) Variation of cation intercalation into NiHCF as illustrated by a shift in the cyclic voltammogram to a higher redox potential in the presence of cesium as opposed to sodium. *Source:* Reprinted from [337]. Copyright 1997, with permission from Elsevier. (c) Electrochemically enhanced removal of cesium using the copper hexacyanoferrate PBA. *Source:* Reprinted with permission from [338]. Copyright 2013, American Chemical Society. (d) Electrochemical battery system for the recovery of lithium from brine using a $FePO_4$ electrode for selective lithium removal. *Source:* Republished with permission from [339].

possible options for future use in separation processes, with some species already exhibiting promising performance in aqueous supercapacitor applications [358–360].

1.6.3.1.4 Hybrid Organic–Inorganic Composites

Hybrid systems leveraging both organic and inorganic redox-active materials have also been developed for electrochemically mediated separation. One framework involved a layered α-zirconium phosphate (α-ZrP) nanosheet intercalated with a poly(aniline) chain for the reversible capture and release of heavy metals via a proton-pumping mechanism (Figure 1.17a). Specifically, heavy metal cations enter the α-ZrP reservoir under reducing potential and are expelled in the oxidizing step by the protons released from PANI oxidation. In its reduced state, the composite had an adsorption capacity of ca. 100 mg Ni^{2+}/g in the presence of various other heavy metal cations at the same concentration of 100 mM, revealing a roughly 10-fold selectivity for Ni^{2+} (Figure 1.17b) [361]. The technique of ion imprinting has also been leveraged to impart selectivity in electrochemical separations. Molecular imprinting involves the preparation of a material with tailor-made templated sites with memory recognition for preferential species binding [363]. Imprinted ferricyanide-embedded poly(pyrrole) (FCN/PPy) synthesized through unipolar pulse electropolymerization (UPEP) of pyrrole doped with ferricyanide in the presence of Ni^{2+} and Y^{3+} allowed for the selective removal of those cations during electrochemical reduction of the $Fe(CN)_6^{3-}$ groups to $Fe(CN)_6^{4-}$ followed by their subsequent release during oxidation (Figure 1.17c and d) [362, 364].

1.6.3.1.5 Asymmetric Electrochemical Cells

The concept of an asymmetric electrode system in charge storage applications can also be utilized for electrochemically mediated separation processes. In this context, the anode and cathode of the electrochemical cell are each functionalized with a different redox-active species for the purpose of providing enhanced separation performance and additional functionality.

One such example of a dual-functionalized redox-active framework is a heterogeneous system comprising poly(vinylferrocene) at its anode and a transition metal hexacyanoferrate at its cathode (Figure 1.18a). This combination has an innately low energetic requirement due to the tunability of the crystalline material (Figure 1.18b), which is used to impart a high initial extent of oxidation for the cathodic material (Figure 1.18c), as well as achieve a close proximity between the redox potentials of the two species (Figure 1.18d). The presence of the Faradaic hexacyanoferrate species allows not only for the removal of sodium cations at the cathode in tandem with anions at the anode but also for the diversion of current away from the parasitic water reduction side reaction. The latter provides multiple benefits, namely, boosting anion recovery amounts (Figure 1.18e), reducing separation energy requirements by fourfold compared with a nonfunctionalized inert cathode (Figure 1.18f), suppressing pH increases in the solution, and undesirable changes in oxidation state to redox-active analytes like phosphomolybdate at the cathode-solution interface [287].

Contrary to water electrolysis and electrical double layer methods, the electrochemical current results from the pseudocapacitance of the functionalized electroactive species. In water, PVFc and nickel hexacyanoferrate have oxidation and reduction potentials at ca. 0.6

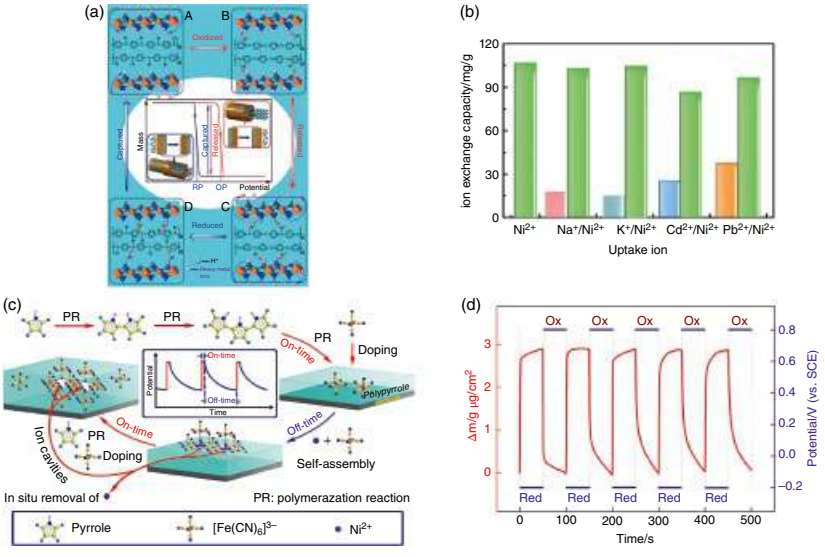

Figure 1.17 (a) A hybrid organic–inorganic α-ZrP/PANI redox-active composite material for the reversible uptake and release of heavy metal cations via a proton-pumping mechanism and (b) selectivity of the α-ZrP/PANI material for nickel cations over other heavy metal cations. *Source:* Republished with permission from [361]. (c) An ion-imprinting scheme to generate FCN/PPy for selective nickel removal and (d) mass variation of the FCN/PPy film with electrochemical switching between its reduced and oxidized states in the presence of nickel cations. *Source:* Reprinted with permission from [362]. Copyright 2014, American Chemical Society.

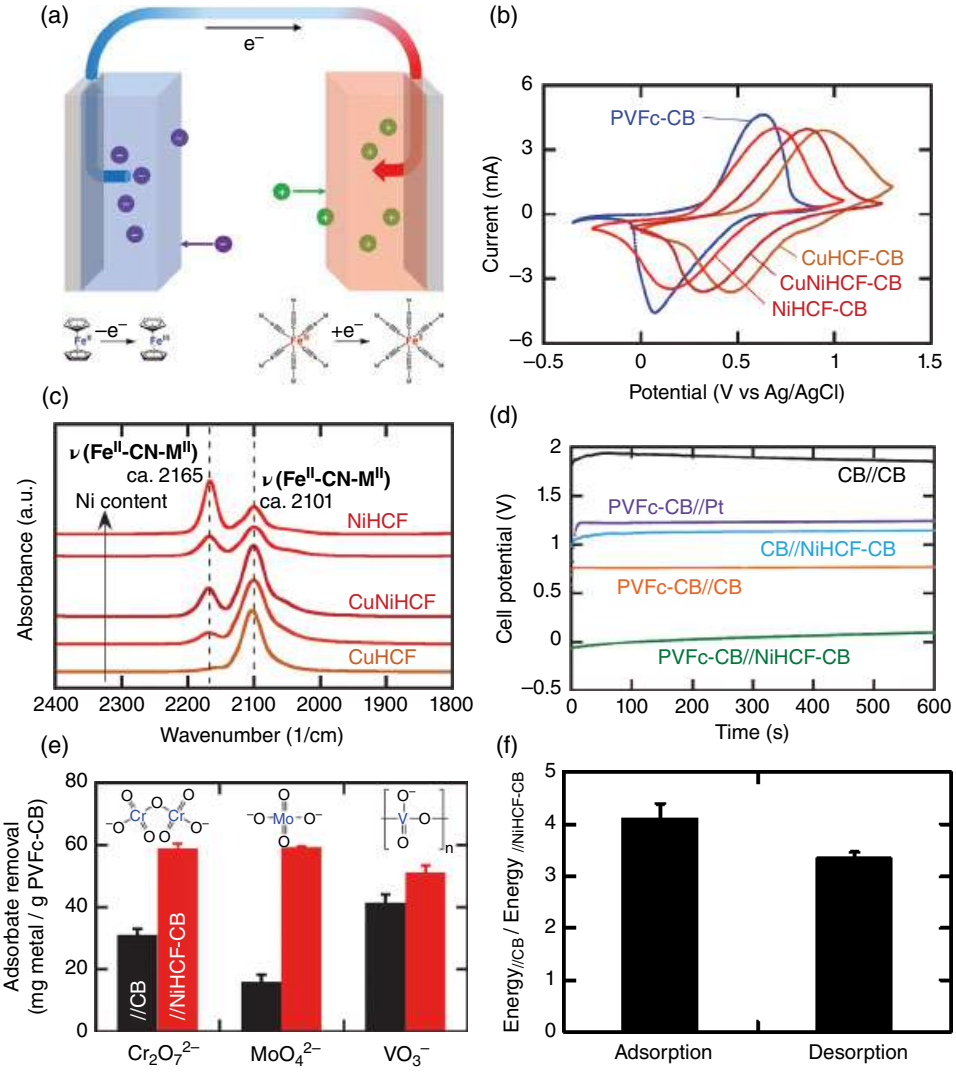

Figure 1.18 (a) An asymmetric PVFc//NiHCF scheme that leverages dual redox-active iron centers for enhanced electrochemical separation, (b) tunable cathode redox potentials arising from the changing of the high-spin PBA metal center, (c) variation in initial extent of oxidation of the cathode material with different metal center compositions, (d) comparison of cell potentials required for operation at ca. 0.1 A/m^2 in 100 mM $NaClO_4$ for different electrode configurations, (e) enhancement of HMOA removal via the cation-intercalating cathode, and (f) four- and threefold reductions in energy for adsorption and desorption operations, respectively, with the use of a NiHCF cathode as opposed to an inert carbon black electrode. *Source:* Used with permission from [287]. Copyright 2020, Wiley.

and 0.2 V vs Ag/AgCl (ca. 0.83 and 0.43 V vs SHE), respectively [287], compared to those of water oxidation and reduction at 0.81 and −0.41 V vs SHE at pH 7, respectively. As such, the operation of the electrochemical cell at redox potentials well within the water stability window offers both significant energy savings, as well as the prevention of rises in water

pH. Basification of solution chemistry can hinder the adsorption capacity of PVFc via the fouling or destruction of the ferrocene moieties by nucleophilic species such as hydroxide anions, with one hypothesized mechanism for ferrocene deactivation being the substitution of the cyclopentadiene ring with the nucleophile [284, 365–367].

An additional asymmetric design for electrochemically mediated ion separation in a constant pH environment leverages redox-active polymers at both the anode and cathode [284]. As reducing analogues to ferrocene, the use of the cobalt-containing metallopolymers PMAECoCp$_2$ and PCpCoCbMA at the cathode are able to both prevent pH excursions (Figure 1.19a) by accepting electrons, but achieve electroneutrality differently due to the nature of their redox-mediated oxidation state changes. Specifically, PMAECoCp$_2$ starts in an oxidized state (charge of +1) as PMAECoCp$_2^+$PF$_6^-$ and reduces to PMAECoCp$_2$ (charge of 0) by releasing the PF_6^- anion into the solution (Figure 1.19b and c) [284, 293, 294], whereas PCpCoCbMA begins in a neutral state (charge of 0) and reduces to a negatively charged form that allows it to subsequently remove cations in the solution in a similar fashion as NiHCF (Figure 1.19d) [295–297].

Other asymmetric electrochemical separation systems have also been developed, such as a dual-functionalized poly(pyrrole) and NiHCF cell for the simultaneous selective separation of iodide and cesium from a 100-fold excess of sodium chloride with separation factors of 90 and ca. 450, respectively, after 200 minutes adsorption at 2V [368], as well as a continuous flow process using PVFc anodes coupled with poly(pyrrole)-dodecylbenzenesulfonate (PPy-DBS) cathodes (Figure 1.19e and f) [282, 288]. These various asymmetric systems have been successfully applied for the separation of inorganic species like heavy metal oxyanions, phosphomolybdate, alkali metal cations, and iodide, as well as organic compounds such as benzoate and micropollutant species including butyl pyridinium and methyl viologen [282, 284, 287, 288, 368].

1.6.3.2 Electrochemically Mediated Hydrophilicity Tuning

The electrochemical modulation of the redox state of heterogeneous redox-active materials can also be used to alter their hydrophilicity, allowing them to then be used for the selective targeting of neutral organic compounds. This indirect separation approach has previously been referred to as electrochemically tunable affinity separation (ETAS) [369].

ETAS has previously been explored using a hybrid adsorbent consisting of electropolymerized poly(pyrrole) and electroprecipitated PVFc (Figure 1.20a) [369, 371]. Electrochemical oxidation of the ferrocene units in the co-deposited PVFc/PPy composite increased its hydrophilicity for the subsequent physisorption of organic pollutants, and subsequent reduction of the ferrocene moieties released the adsorbed species to complete the electrochemical cycle. Changes in the level of hydrophilicity of the adsorbent through precise electrochemical modulation of the ratio of hydrophobic ferrocene to hydrophilic ferrocenium yielded starkly different removal amounts (Figure 1.20b), demonstrating the ability of ETAS to optimize selectivity and thus, adsorption capacity, based on the nature of the target organic species (Figure 1.20c), as well as balance separation degree versus energetic efficiency [369]. In general, ETAS required energy consumption on the order of 10^2 to 10^3 J/g organic compound removed (and even reached as low as ca. 20 J/g in the case of the separation of Sudan Orange G with a 0.30–0.35 V potential swing), compared to that of 10^4 J/g usually required by a thermal swing approach. The technique of ferrocene-mediated

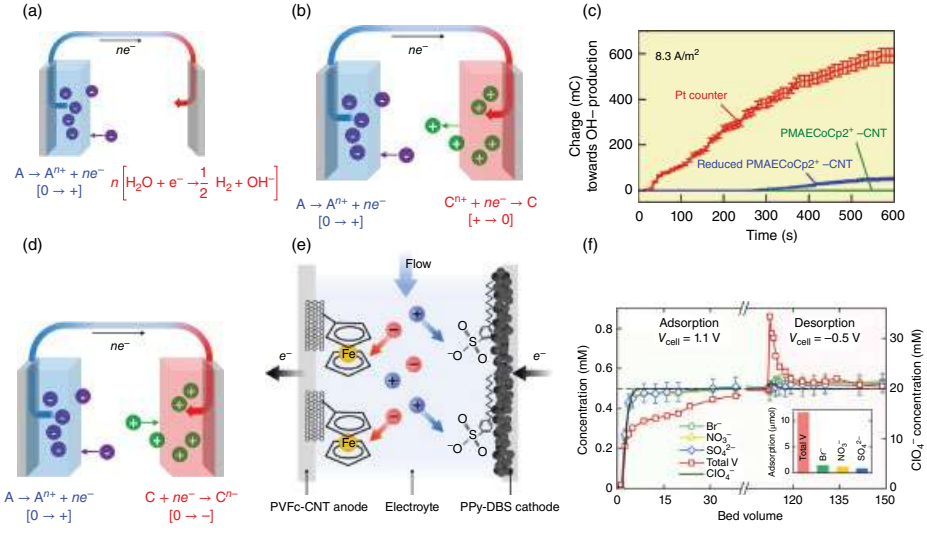

Figure 1.19 Electrochemically mediated binding schemes for heterogeneous separation involving (a) a single redox-active species for anion capture with parasitic water reduction, and (b) two redox-active species for anion capture without parasitic water reduction. (c) Changes in solution pH with different cathodes used during electrochemical separation. *Source:* Republished with permission from [284]. (d) Electrochemically mediated binding scheme with two redox-active species for concurrent anion and cation removal. (e) An asymmetric flow system leveraging PVFc and PPy-DBS for tandem ion separation and (f) selective, continuous, and reversible separation of vanadium using the PVFc//PPy-DBS framework under flow conditions. *Source:* Used with permission from [288]. Copyright 2020, Wiley.

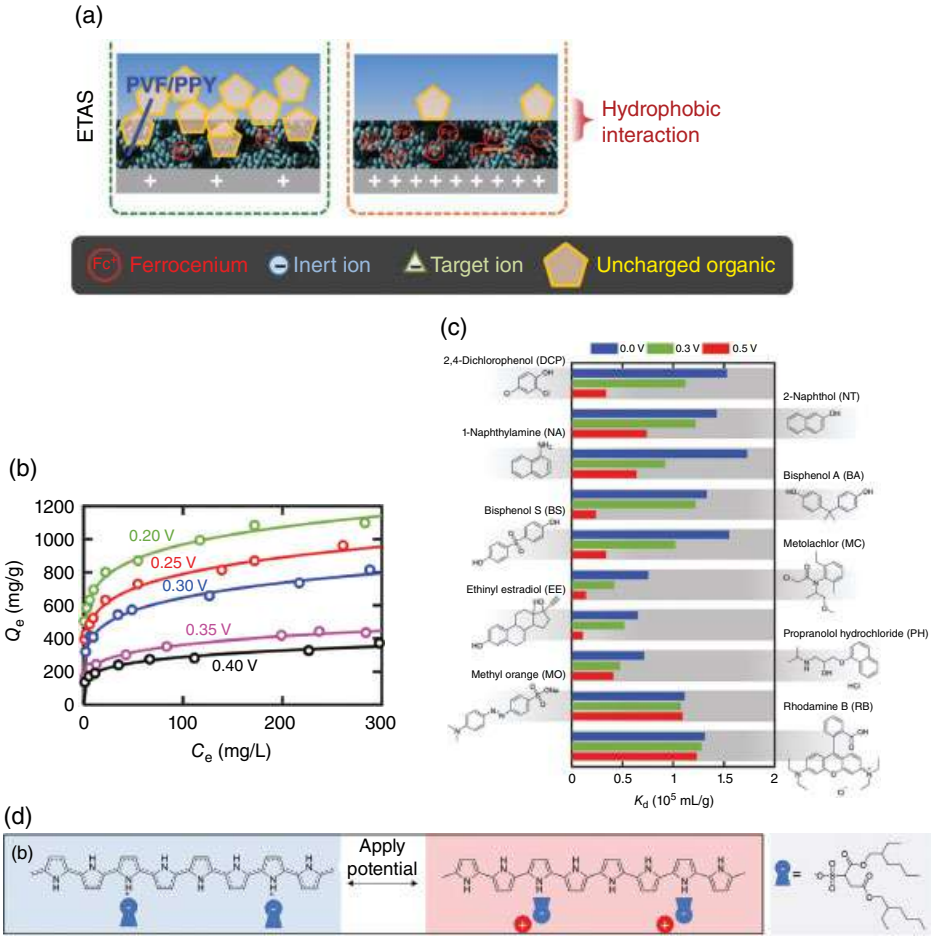

Figure 1.20 (a) Hybrid PVFc/PPy material for ETAS via the redox activity of PVFc, (b) variation in the adsorption isotherms of Sudan Orange G with the activation potential of the PVFc/PPy carbon nanotube composite sorbent, and (c) variation of contaminant distribution coefficients with different PVFc/PPy activation potentials [369]. Licensed under CC BY 3.0. (d) AOT-doped PPy material for ETAS via the change in orientation of AOT. *Source:* Used with permission from [370]. Copyright 2018, Wiley.

hydrophilicity switching has also been previously shown with poly(vinylferrocene-co-hydroxybutylmethacrylate) hydrogels, which selectively extracted butanol with a separation factor of ca. 6 at ca. 1% butanol by mass in water when the ferrocene moieties were in their neutral state, and then released the captured butanol upon chemical oxidation of the ferrocene groups to ferrocenium [372].

PPy has also been separately studied for its ability to vary its hydrophilicity through electrochemically controlled modulation of its dopant anion configuration (Figure 1.20d). Specifically, when PPy doped with dioctyl sulfosuccinate (AOT) surfactant anions was oxidized to PPy^+, DFT calculations revealed that the AOT anions were oriented with their negatively charged

sulfonate groups electrostatically bound to PPy^+, leaving their hydrophobic alkyl chains facing the aqueous solution. This configuration allowed AOT-doped PPy^+ to adsorb neutral hydrogen bond donor species such as Sudan Orange G with a capacity of more than 570 mg/g polymer through pi-pi stacking, as well as moderate to strong hydrogen bonding arising from strong electrostatic, polarization, and charge-transfer interactions. Upon reduction from PPy^+ to PPy, the AOT rotated such that its alkyl chains were facing toward PPy, rendering the polymer surface hydrophilic and allowing for the release of the previously bound molecules. It was also observed that the addition of bipyrrole during the synthesis of PPy increased polymer porosity and imparted superhydrophobic properties that aided in its ability to separate oils [373], as well as other neutral organic pollutants. The AOT-doped PPy has also been combined with PVFc/PPy to form a complementary electrochemical cell that can be modulated between hydrophilic and hydrophobic states for the selective and reversible separation of organic contaminants such as 1-napthol from a 10-fold excess of propranolol hydrochloride with a separation factor of ca. 7. This system was observed to yield a lower specific energy consumption (1258 J/g contaminant) when regenerated and reactivated at 0.9 and 0.3 V, respectively, compared to activated carbons regenerated via thermal desorption (1474 J/g contaminant) [370, 374].

1.6.3.3 Electrochemically Mediated Reactive Separations

A promising new direction and application for redox-active species is in the design of novel electrochemically mediated reactive separation methods. Traditional reactive separations aim to improve process efficiency by integrating both the reaction and separation steps into one unit for concurrent generation and removal of products, and find industrial application in techniques such as reactive distillation [375, 376]. The innate two-electrode setup of an electrochemical cell inherently provides a favorably suitable framework for reactive separations. In fact, combined electrocoagulation–electroflotation systems reflect this concept [122], although the electrodes used in the process are not necessarily comprised of heterogeneously tethered redox-active species.

To this end, a hybrid electrochemical system for synchronized desalination and oxidation has previously been developed using a redox-active species as the cathode and an oxidant-generating material as the anode. In this cell, a sodium manganese oxide cathode was used to selectively intercalate sodium cations, with the chloride counter-anions diffusing across an anion exchange membrane for electrochemical oxidation at a titanium oxide nanotube anode, allowing for simultaneous ion separation and generation of reactive chlorine and oxygen species. The anodic oxidation process was used as a technique to effectively overcome the capacity limitations of electrochemical desalination systems with poor anion removal, as observed from the desalination coulombic efficiency of over 96% at a specific capacity of ca. 33 mAh/g cation-selective material (Figure 1.21a) [377].

Two additional reactive separation schemes using a single electrochemical cell employing heterogeneous redox-active polymers have also been developed for the capture and subsequent transformation of heavy metal oxyanions (HMOAs). In both designs, the target HMOA analyte is first electrochemically removed from aqueous solution by poly(vinylferrocenium) ($PVFc^+$) via an adsorption stage and then subsequently released and altered in a combined desorption and conversion stage. The switch between the two steps in this staggered approach is easily facilitated by modulating the polarity and

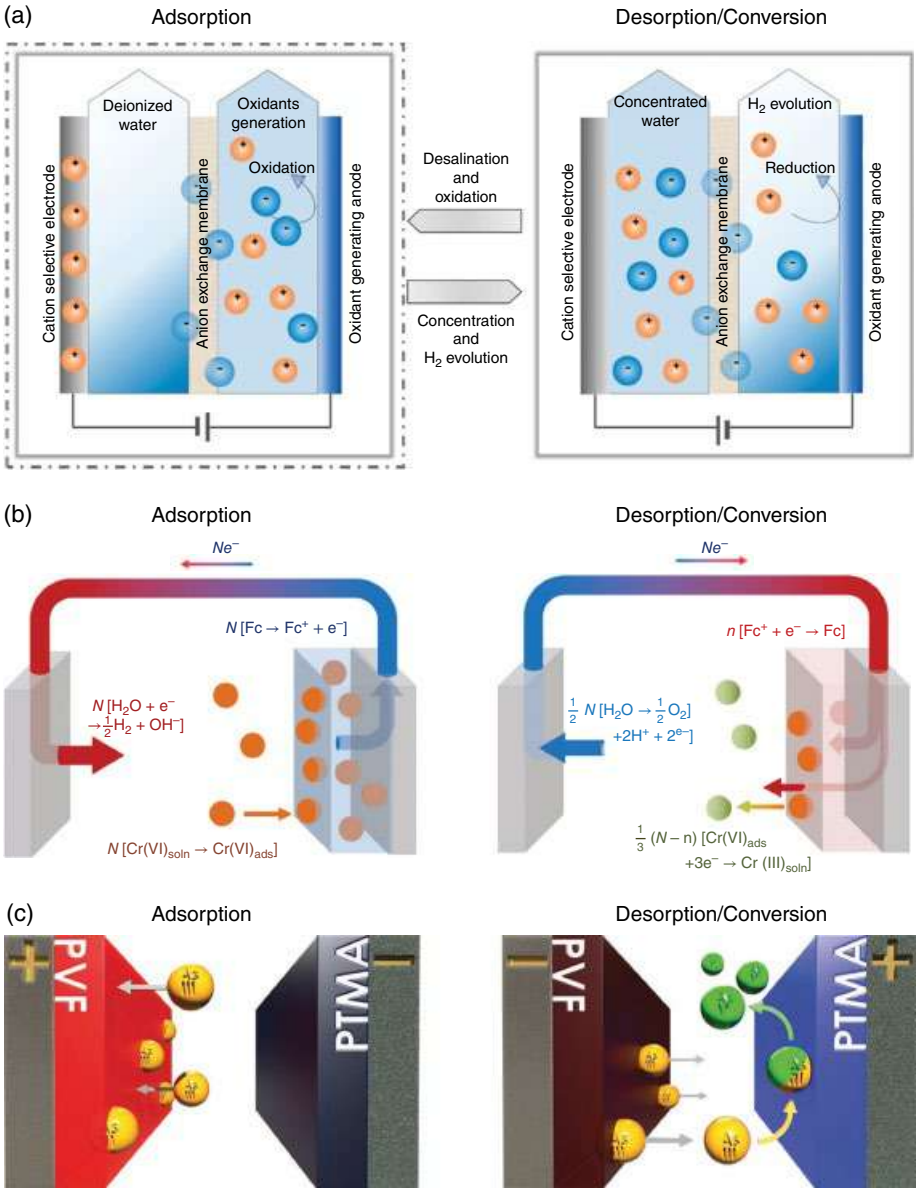

Figure 1.21 Electrochemical reactive separation processes for (a) simultaneous desalination and reactive chlorine and oxygen species generation via electrochemical oxidation, *Source:* Adapted with permission from [377]. Copyright 2018, American Chemical Society. The separation and conversion of (b) chromium [280] Licensed under CC BY 4.0., and (c) arsenic. *Source:* Used with permission from [286]. Copyright 2020, Wiley.

magnitude of the cell potential. In the first reactive separation system, chromium is first adsorbed at the $PVFc^+$ anode in the hexavalent state as either $Cr_2O_7^{2-}$, CrO_4^{2-}, or $HCrO_4^-$, and then converted to its trivalent state as the less toxic Cr^{3+} upon its release from the $PVFc^+$ electrode (Figure 1.21b). During electrodesorption, the $PVFc^+$ electrode accepts

electrons in order to return back to its neutral PVFc form, with a portion of the electrons also reducing the oxidation state of the released chromium species from +6 to +3. At the same time, water oxidation occurs at the opposite inert electrode to complete the circuit, acidifying the solution for even more conducive conversion of Cr(VI) to Cr(III). The process can be performed by changing the potential of the PVFc electrode from 0.8 to 0 V vs Ag/AgCl for chromium uptake and discharge/conversion, respectively [280]. In the second reactive separation system, arsenic is first removed through binding with $PVFc^+$ in the trivalent state, and then converted to its pentavalent state at the opposite electrode after its release from the $PVFc^+$ electrode (Figure 1.21c). The complementary electrode is functionalized with a redox-active polymer (PTMA) containing (2,2,6,6-tetramethylpiperidin-1-yl)oxyl (TEMPO) radical moieties which are strong oxidants in their oxoammonium cationic form ($TEMPO^+$). The TEMPO moieties oxidize to $TEMPO^+$ while As(III) re-enters the solution as a result of $PVFc^+$ reverting to PVFc and are then used to enhance the electrocatalytic oxidation of As(III) to the less harmful As(V). Arsenic electrosorption and conversion can be achieved using electrode potentials of 0.8 V vs Ag/AgCl for both the PVFc and PTMA electrodes, respectively. Under an energy integration approach with the asymmetric framework, the overall process was observed to consume a total of 0.45 kWh/mol arsenic for arsenic separation and conversion. The well-defined nature of the second framework allows for the compartmentalization of the separation and reaction processes to two specialized individual electrodes for electrosorption and electrocatalysis, respectively [286]. In both cases, capturing an as-made HMOA and converting it to a less harmful state upon or right after its release avoids the need to implement a separate purification step for toxicity mitigation.

1.7 Conclusions and Future Outlook

Electrochemical techniques have been extensively studied and engineered for use in aqueous separations to address areas ranging from water remediation to the recovery of valuable bioproducts. Traditional electrochemical processes leverage electrolytic phenomena such as electrodeposition and water splitting, with many of them having well-established applications in sectors like the mining, food, and bioprocess industries. The burgeoning field of electrochemically mediated sustainable separations is developing quickly, with the aim of further increasing separation efficiency by reducing electrochemical energy requirements and improving separation selectivity through novel concepts to meet growing global resource demand, as well as other critical and persistent challenges like water security. Heterogeneous electrochemically mediated systems hold great promise as a next-generation water-based separation technology, by virtue of their innate potential to be compactly designed, reversibly operated, precisely controlled, and easily scaled. Current frameworks employ redox-active moieties in the form of polymers and/or crystalline species to capture a variety of water-soluble species via electrochemical conversion, direct electrochemical binding or sorbent hydrophilicity modulation, and can provide specificity in molecular recognition in addition to amplifying uptake capacity through Faradaic pseudocapacitance. In particular, asymmetric systems comprised of two complementary electroactive materials have been shown to effectively enhance separation performance by increasing the overall amount of species removed, preventing

parasitic water splitting reactions from raising cell potentials and generating excursions in solution pH, minimizing energy requirements by tuning the redox potentials of the anode and cathode, and either mitigating undesirable analyte conversion or facilitating beneficial reactive separation.

Electrochemically mediated sustainable separations have already been investigated for use in desalination, charged and neutral contaminant removal, valuable product recovery, and aqueous carbon dioxide capture, and may continue to find prospective future application in fields such as sensing, catalysis [378, 379], contaminant remediation [380, 381], drug delivery, and energy storage [279, 371], as well as in organic phase separations [263, 382]. Moving forward, the format and efficacy of these electrochemical systems will undoubtedly depend greatly on the advancement of redox-active materials. Environmentally friendly materials made through simpler synthesis strategies or from sustainable sources can further improve the sustainability of electrochemical processes such as CDI [234, 383, 384], water electrolysis [385], and even energy storage [386]. Repurposing energy storage materials for separation, as well as synthesizing more complex structures such as new redox-active metal-organic frameworks and macrocycles may also broaden the research space by imparting further functionality to heterogeneous electrosorbents. From an engineering perspective, the continuation of the extensive development in flow and stack layout design within areas like capacitive deionization is also crucial in order to achieve scalable continuous electrochemical separation processes. Other points of consideration may include the planning of batch or in-line regeneration steps to ensure cyclic separation, as well as stream recycling. The separation performance of a finalized system at scale can then offer insight regarding its optimal application suitability, either as a small portable device, integrated within separation process trains as a standalone module, or as a larger and more comprehensive unit operation.

References

1 Anastas, P.T. and Zimmerman, J.B. (2003). Peer reviewed: design through the 12 principles of green engineering. *Environmental Science & Technology* 37 (5): 94A–101A.

2 Sholl, D.S. and Lively, R.P. (2016). Seven chemical separations to change the world. *Nature* 532 (7600): 435–437.

3 Mekonnen, M.M. and Hoekstra, A.Y. (2016). Four billion people facing severe water scarcity. *Science Advances* 2 (2): e1500323.

4 Boretti, A. and Rosa, L. (2019). Reassessing the projections of the world water development report. *npj Clean Water* 2 (1): 15.

5 Jury, W.A. and Vaux, H. (2005). The role of science in solving the world's emerging water problems. *Proceedings of the National Academy of Sciences of the United States of America* 102 (44): 15715.

6 Shannon, M.A., Bohn, P.W., Elimelech, M. et al. (2008). Science and technology for water purification in the coming decades. *Nature* 452 (7185): 301–310.

7 Radjenovic, J. and Sedlak, D.L. (2015). Challenges and opportunities for electrochemical processes as next-generation technologies for the treatment of contaminated water. *Environmental Science & Technology* 49 (19): 11292–11302.

8 Chaplin, B.P. (2019). The prospect of electrochemical technologies advancing worldwide water treatment. *Accounts of Chemical Research* 52 (3): 596–604.

9 Porada, S., Zhao, R., van der Wal, A. et al. (2013). Review on the science and technology of water desalination by capacitive deionization. *Progress in Materials Science* 58 (8): 1388–1442.

10 Choi, J., Dorji, P., Shon, H.K., and Hong, S. (2019). Applications of capacitive deionization: desalination, softening, selective removal, and energy efficiency. *Desalination* 449: 118–130.

11 Subramani, A., Badruzzaman, M., Oppenheimer, J., and Jacangelo, J.G. (2011). Energy minimization strategies and renewable energy utilization for desalination: a review. *Water Research* 45 (5): 1907–1920.

12 Su, X. and Hatton, T.A. (2017). Electrosorption at functional interfaces: from molecular-level interactions to electrochemical cell design. *Physical Chemistry Chemical Physics* 19 (35): 23570–23584.

13 Su, X. and Hatton, T.A. (2016). Electrosorption. Kirk-Othmer Encyclopedia of Chemical Technology. p. 1–11.

14 Su, X. and Hatton, T.A. (2017). Redox-electrodes for selective electrochemical separations. *Advances in Colloid and Interface Science* 244: 6–20.

15 National Academies of Sciences Engineering and Medicine (2019). *A Research Agenda for Transforming Separation Science*, 114. Washington, DC: The National Academies Press.

16 Daughton, C.G. and Ternes, T.A. (1999). Pharmaceuticals and personal care products in the environment: agents of subtle change? *Environmental Health Perspectives* 107 (Suppl 6): 907–938.

17 Seader, J.D., Henley, E.J., and Roper, D.K. (2010). *Separation Process Principles*, 3e. Wiley.

18 Richardson, J.F., Harker, J.H., and Backhurst, J.R. (2002). In: *Chemical Engineering*, 5e (eds. J.F. Richardson, J.H. Harker and J.R. Backhurst), 1076. Oxford: Butterworth-Heinemann.

19 Humphrey, J.L. (1995). Separation processes: playing a critical role. *Chemical Engineering Progress* 91 (10): 31–41.

20 National Research Council (1998). *Separation Technologies for the Industries of the Future*, 128. Washington, DC: The National Academies Press.

21 Humphrey, J.L. and Keller, G.E. (1997). *Separation Process Technology*. McGraw-Hill.

22 Oak Ridge National Laboratory (2005). Materials for Separation Technologies: Energy and Emission Reduction Opportunities.

23 Bagotsky, V.S. (2005). *Fundamentals of Electrochemistry*, 2e, 33–50. Wiley.

24 Bard, A.J. and Faulkner, L.R. (2000). *Electrochemical Methods: Fundamentals and Applications*. Wiley.

25 Vanysek, P. (2000). Electrochemical series. In: *CRC Handbook of Chemistry and Physics*, 8. 81e (ed. D.R. Lide), 2556. Boca Raton, FL: CRC Press.

26 Wang, H. and Pilon, L. (2011). Accurate simulations of electric double layer capacitance of ultramicroelectrodes. *The Journal of Physical Chemistry C* 115 (33): 16711–16719.

27 Feng, Y., Yang, L., Liu, J., and Logan, B.E. (2016). Electrochemical technologies for wastewater treatment and resource reclamation. *Environmental Science: Water Research & Technology* 2 (5): 800–831.

28 Chen, X. and Chen, G. (2010). Electroflotation. In: *Electrochemistry for the Environment* (eds. C. Comninellis and G. Chen), 263–277. New York, NY: Springer.

29 Mohtashami, R. and Shang, J.Q. (2019). Electroflotation for treatment of industrial wastewaters: a focused review. *Environmental Processes* 6 (2): 325–353.

30 Ran, J., Wu, L., He, Y. et al. (2017). Ion exchange membranes: new developments and applications. *Journal of Membrane Science* 522: 267–291.

31 Strathmann, H. (2010). Electrodialysis, a mature technology with a multitude of new applications. *Desalination* 264 (3): 268–288.

32 Davis, T.A. and Glassner, D.A. (1997). Electrodialysis. In: *Handbook of Downstream Processing* (ed. E. Goldberg), 140–166. Dordrecht, Netherlands: Springer.

33 Mani, K.N. (1991). Electrodialysis water splitting technology. *Journal of Membrane Science* 58 (2): 117–138.

34 Xu, T. and Huang, C. (2008). Electrodialysis-based separation technologies: a critical review. *AIChE Journal* 54 (12): 3147–3159.

35 Galama, A.H., Saakes, M., Bruning, H. et al. (2014). Seawater predesalination with electrodialysis. *Desalination* 342: 61–69.

36 Sadrzadeh, M. and Mohammadi, T. (2008). Sea water desalination using electrodialysis. *Desalination* 221 (1): 440–447.

37 Korngold, E., Aronov, L., and Daltrophe, N. (2009). Electrodialysis of brine solutions discharged from an RO plant. *Desalination* 242 (1): 215–227.

38 Elmidaoui, A., Elhannouni, F., Menkouchi Sahli, M.A. et al. (2001). Pollution of nitrate in Moroccan ground water: removal by electrodialysis. *Desalination* 136 (1): 325–332.

39 El Midaoui, A., Elhannouni, F., Taky, M. et al. (2002). Optimization of nitrate removal operation from ground water by electrodialysis. *Separation and Purification Technology* 29 (3): 235–244.

40 Hell, F., Lahnsteiner, J., Frischherz, H., and Baumgartner, G. (1998). Experience with full-scale electrodialysis for nitrate and hardness removal. *Desalination* 117 (1): 173–180.

41 Hell, F. and Lahnsteiner, J. (2002). The application of electrodialysis for drinking water treatment. In: *Water Resources Quality: Preserving the Quality of our Water Resources* (eds. H. Rubin, U. Shamir, P. Nachtnebel and J. Fürst), 315–327. Berlin, Heidelberg: Springer.

42 Adhikary, S.K., Tipnis, U.K., Harkare, W.P., and Govindan, K.P. (1989). Defluoridation during desalination of brackish water by electrodialysis. *Desalination* 71 (3): 301–312.

43 Zhang, Y., Desmidt, E., Van Looveren, A. et al. (2013). Phosphate separation and recovery from wastewater by novel electrodialysis. *Environmental Science & Technology* 47 (11): 5888–5895.

44 Mohammadi, T., Razmi, A., and Sadrzadeh, M. (2004). Effect of operating parameters on Pb^{2+} separation from wastewater using electrodialysis. *Desalination* 167: 379–385.

45 Marder, L., Bernardes, A.M., and Zoppas, F.J. (2004). Cadmium electroplating wastewater treatment using a laboratory-scale electrodialysis system. *Separation and Purification Technology* 37 (3): 247–255.

46 Mohammadi, T., Moheb, A., Sadrzadeh, M., and Razmi, A. (2004). Separation of copper ions by electrodialysis using Taguchi experimental design. *Desalination* 169 (1): 21–31.

47 Cifuentes, L., García, I., Arriagada, P., and Casas, J.M. (2009). The use of electrodialysis for metal separation and water recovery from $CuSO_4$–H_2SO_4–Fe solutions. *Separation and Purification Technology* 68 (1): 105–108.

48 Ward, A.J., Arola, K., Thompson Brewster, E. et al. (2018). Nutrient recovery from wastewater through pilot scale electrodialysis. *Water Research* 135: 57–65.

49 Fidaleo, M. and Moresi, M. (2006). Electrodialysis applications in the food industry. *Advances in Food and Nutrition Research* 51: Academic Press: 265–360.

50 Sata, T. (1994). Studies on ion exchange membranes with permselectivity for specific ions in electrodialysis. *Journal of Membrane Science* 93 (2): 117–135.

51 Huang, C. and Xu, T. (2006). Electrodialysis with bipolar membranes for sustainable development. *Environmental Science & Technology* 40 (17): 5233–5243.

52 Bazinet, L., Lamarche, F., and Ippersiel, D. (1998). Bipolar-membrane electrodialysis: applications of electrodialysis in the food industry. *Trends in Food Science & Technology* 9 (3): 107–113.

53 Huang, C., Xu, T., Zhang, Y. et al. (2007). Application of electrodialysis to the production of organic acids: state-of-the-art and recent developments. *Journal of Membrane Science* 288 (1): 1–12.

54 Tongwen, X. and Weihua, Y. (2002). Citric acid production by electrodialysis with bipolar membranes. *Chemical Engineering and Processing: Process Intensification* 41 (6): 519–524.

55 Yu, L., Guo, Q., Hao, J., and Jiang, W. (2000). Recovery of acetic acid from dilute wastewater by means of bipolar membrane electrodialysis. *Desalination* 129 (3): 283–288.

56 Gyo Lee, E., Moon, S.-H., Keun Chang, Y. et al. (1998). Lactic acid recovery using two-stage electrodialysis and its modelling. *Journal of Membrane Science* 145 (1): 53–66.

57 Madzingaidzo, L., Danner, H., and Braun, R. (2002). Process development and optimisation of lactic acid purification using electrodialysis. *Journal of Biotechnology* 96 (3): 223–239.

58 Hábová, V., Melzoch, K., Rychtera, M., and Sekavová, B. (2004). Electrodialysis as a useful technique for lactic acid separation from a model solution and a fermentation broth. *Desalination* 162: 361–372.

59 Bandi, A., Specht, M., Weimer, T., and Schaber, K. (1995). CO_2 recycling for hydrogen storage and transportation —electrochemical CO_2 removal and fixation. *Energy Conversion and Management* 36 (6): 899–902.

60 Eisaman, M.D., Parajuly, K., Tuganov, A. et al. (2012). CO_2 extraction from seawater using bipolar membrane electrodialysis. *Energy & Environmental Science* 5 (6): 7346–7352.

61 Eisaman, M.D., Alvarado, L., Larner, D. et al. (2011). CO_2 separation using bipolar membrane electrodialysis. *Energy & Environmental Science* 4 (4): 1319–1328.

62 Datta, S., Henry, M.P., Lin, Y.J. et al. (2013). Electrochemical CO_2 capture using resin-wafer electrodeionization. *Industrial & Engineering Chemistry Research* 52 (43): 15177–15186.

63 Campione, A., Gurreri, L., Ciofalo, M. et al. (2018). Electrodialysis for water desalination: a critical assessment of recent developments on process fundamentals, models and applications. *Desalination* 434: 121–160.

64 Pilat, B. (2001). Practice of water desalination by electrodialysis. *Desalination* 139 (1): 385–392.

65 Deng, D., Aouad, W., Braff, W.A. et al. (2015). Water purification by shock electrodialysis: deionization, filtration, separation, and disinfection. *Desalination* 357: 77–83.

66 Alkhadra, M.A., Gao, T., Conforti, K.M. et al. (2020). Small-scale desalination of seawater by shock electrodialysis. *Desalination* 476: 114219.

67 Deng, D., Dydek, E.V., Han, J.-H. et al. (2013). Overlimiting current and shock electrodialysis in porous media. *Langmuir* 29 (52): 16167–16177.

68 Schlumpberger, S., Lu, N.B., Suss, M.E., and Bazant, M.Z. (2015). Scalable and continuous water deionization by shock electrodialysis. *Environmental Science & Technology Letters* 2 (12): 367–372.

69 Alkhadra, M.A., Conforti, K.M., Gao, T. et al. (2020). Continuous separation of radionuclides from contaminated water by shock electrodialysis. *Environmental Science & Technology* 54 (1): 527–536.

70 Conforti, K.M. and Bazant, M.Z. (2020). Continuous ion-selective separations by shock electrodialysis. *AIChE Journal* 66 (1): e16751.

71 Allen, P.M., Bridger, N.J., Jones, C.P. et al. (1990). Electrochemical ion exchange. In: *Recent Developments in Ion Exchange, 2* (eds. P.A. Williams and M.J. Hudson), 213–218. Dordrecht, Netherlands: Springer.

72 Bridger, N.J., Jones, C.P., and Neville, M.D. (1991). Electrochemical ion exchange. *Journal of Chemical Technology & Biotechnology* 50 (4): 469–481.

73 Sukamto, J.P.H., Rassat, S.D., Orth, R.J., and Lilga, M.A. (2000). Electrochemical ion exchange. In: *Encyclopedia of Separation Science* (ed. I.D. Wilson). Academic Press.

74 Basha, C.A., Ramanathan, K., Rajkumar, R. et al. (2008). Management of chromium plating rinsewater using electrochemical ion exchange. *Industrial & Engineering Chemistry Research* 47 (7): 2279–2286.

75 Basha, C.A., Ghosh, P.K., and Gajalakshmi, G. (2008). Total dissolved solids removal by electrochemical ion exchange (EIX) process. *Electrochimica Acta* 54 (2): 474–483.

76 Adams, R.J.W. and Hudson, M.J. (1991). Reversible extraction of ionic species using electrochemically assisted ion exchange part 1: cobalt(II) using alpha-zirconium hydrogen phosphate. *Solvent Extraction and Ion Exchange* 9 (3): 497–513.

77 Wu, W.S., Uddin, M.S., Chi, H., and Hidajat, K. (1994). Electrochemically assisted metal uptake by cation exchange based chemically modified electrodes. *Journal of Applied Electrochemistry* 24 (6): 548–553.

78 Pascal, V., Laetitia, D., Joël, L. et al. (2007). New concept to remove heavy metals from liquid waste based on electrochemical pH-switchable immobilized ligands. *Applied Surface Science* 253 (6): 3263–3269.

79 Le, X.T., Jégou, P., Viel, P., and Palacin, S. (2008). Electro-switchable surfaces for heavy metal waste treatment: study of polyacrylic acid films grafted on gold surfaces. *Electrochemistry Communications* 10 (5): 699–703.

80 Le, X.T., Viel, P., Jégou, P. et al. (2009). Electrochemical-switchable polymer film: an emerging technique for treatment of metallic ion aqueous waste. *Separation and Purification Technology* 69 (2): 135–140.

81 Henry, P. and Van Lierde, A. (1998). Selective separation of vanadium from molybdenum by electrochemical ion exchange. *Hydrometallurgy* 48 (1): 73–81.

82 Chen, Y., Davis, J.R., Nguyen, C.H. et al. (2016). Electrochemical ion-exchange regeneration and fluidized bed crystallization for zero-liquid-discharge water softening. *Environmental Science & Technology* 50 (11): 5900–5907.

83 Li, M., Feng, C., Zhang, Z. et al. (2009). Application of an electrochemical-ion exchange reactor for ammonia removal. *Electrochimica Acta* 55 (1): 159–164.

84 Matis, K.A. and Peleka, E.N. (2010). Alternative flotation techniques for wastewater treatment: focus on electroflotation. *Separation Science and Technology* 45 (16): 2465–2474.

85 Chen, G. (2004). Electrochemical technologies in wastewater treatment. *Separation and Purification Technology* 38 (1): 11–41.

86 Kyzas, G.Z. and Matis, K.A. (2016). Electroflotation process: a review. *Journal of Molecular Liquids* 220: 657–664.

87 Burns, S.E., Yiacoumi, S., and Tsouris, C. (1997). Microbubble generation for environmental and industrial separations. *Separation and Purification Technology* 11 (3): 221–232.

88 Yarar, B. (2000). Flotation. Kirk-Othmer Encyclopedia of Chemical Technology.

89 Ketkar, D.R., Mallikarjunan, R., and Venkatachalam, S. (1991). Electroflotation of quartz fines. *International Journal of Mineral Processing* 31 (1): 127–138.

90 Kydros, K.A., Gallios, G.P., and Matis, K.A. (1994). Electrolytic flotation of pyrite. *Journal of Chemical Technology & Biotechnology* 59 (3): 223–232.

91 Bhaskar Raju, G. and Khangaonkar, P.R. (1982). Electro-flotation of chalcopyrite fines. *International Journal of Mineral Processing* 9 (2): 133–143.

92 Sarkar, M.S.K.A., Donne, S.W., and Evans, G.M. (2010). Hydrogen bubble flotation of silica. *Advanced Powder Technology* 21 (4): 412–418.

93 Mráz, R. and Krýsa, J. (1994). Long service life IrO_2/Ta_2O_5 electrodes for electroflotation. *Journal of Applied Electrochemistry* 24 (12): 1262–1266.

94 Hosny, A.Y. (1996). Separating oil from oil-water emulsions by electroflotation technique. *Separations Technology* 6 (1): 9–17.

95 Bande, R.M., Prasad, B., Mishra, I.M., and Wasewar, K.L. (2008). Oil field effluent water treatment for safe disposal by electroflotation. *Chemical Engineering Journal* 137 (3): 503–509.

96 Ho, C.C. and Chan, C.Y. (1986). The application of lead dioxide-coated titanium anode in the electroflotation of palm oil mill effluent. *Water Research* 20 (12): 1523–1527.

97 Belkacem, M., Khodir, M., and Abdelkrim, S. (2008). Treatment characteristics of textile wastewater and removal of heavy metals using the electroflotation technique. *Desalination* 228 (1): 245–254.

98 Chen, X., Chen, G., and Yue, P.L. (2002). Novel electrode system for electroflotation of wastewater. *Environmental Science & Technology* 36 (4): 778–783.

99 Liu, H., Zhao, X., and Qu, J. (2010). Electrocoagulation in water treatment. In: *Electrochemistry for the Environment* (eds. C. Comninellis and G. Chen), 245–262. New York, NY: Springer.

100 Essadki, A.H., Bennajah, M., Gourich, B. et al. (2008). Electrocoagulation/electroflotation in an external-loop airlift reactor—Application to the decolorization of textile dye wastewater: a case study. *Chemical Engineering and Processing: Process Intensification* 47 (8): 1211–1223.

101 Mansour, L.B., Ksentini, I., and Elleuch, B. (2007). Treatment of wastewaters of paper industry by coagulation–electroflotation. *Desalination* 208 (1): 34–41.

102 Ge, J., Qu, J., Lei, P., and Liu, H. (2004). New bipolar electrocoagulation–electroflotation process for the treatment of laundry wastewater. *Separation and Purification Technology* 36 (1): 33–39.

103 Wang, C.-T., Chou, W.-L., and Kuo, Y.-M. (2009). Removal of COD from laundry wastewater by electrocoagulation/electroflotation. *Journal of Hazardous Materials* 164 (1): 81–86.

104 Murugananthan, M., Bhaskar Raju, G., and Prabhakar, S. (2004). Separation of pollutants from tannery effluents by electro flotation. *Separation and Purification Technology* 40 (1): 69–75.

105 Alexandrova, L., Nedialkova, T., and Nishkov, I. (1994). Electroflotation of metal ions in waste water. *International Journal of Mineral Processing* 41 (3): 285–294.

106 Aoudj, S., Khelifa, A., Drouiche, N. et al. (2015). Simultaneous removal of chromium(VI) and fluoride by electrocoagulation–electroflotation: application of a hybrid Fe-Al anode. *Chemical Engineering Journal* 267: 153–162.

107 Ibrahim, M.Y., Mostafa, S.R., Fahmy, M.F.M., and Hafez, A.I. (2001). Utilization of electroflotation in remediation of oily wastewater. *Separation Science and Technology* 36 (16): 3749–3762.

108 Mansour, L.B. and Chalbi, S. (2006). Removal of oil from oil/water emulsions using electroflotation process. *Journal of Applied Electrochemistry* 36 (5): 577–581.

109 Chen, G., Chen, X., and Yue, P.L. (2000). Electrocoagulation and electroflotation of restaurant wastewater. *Journal of Environmental Engineering* 126 (9): 858–863.

110 Hernlem, B.J. and Tsai, L.S. (2000). Chlorine generation and disinfection by electroflotation. *Journal of Food Science* 65 (5): 834–837.

111 Zuo, Q., Chen, X., Li, W., and Chen, G. (2008). Combined electrocoagulation and electroflotation for removal of fluoride from drinking water. *Journal of Hazardous Materials* 159 (2): 452–457.

112 Ricordel, C., Darchen, A., and Hadjiev, D. (2010). Electrocoagulation–electroflotation as a surface water treatment for industrial uses. *Separation and Purification Technology* 74 (3): 342–347.

113 Poon, C.P.C. (1997). Electroflotation for groundwater decontamination. *Journal of Hazardous Materials* 55 (1): 159–170.

114 Khelifa, A., Moulay, S., and Naceur, A.W. (2005). Treatment of metal finishing effluents by the electroflotation technique. *Desalination* 181 (1): 27–33.

115 Merzouk, B., Gourich, B., Sekki, A. et al. (2009). Removal turbidity and separation of heavy metals using electrocoagulation–electroflotation technique: a case study. *Journal of Hazardous Materials* 164 (1): 215–222.

116 Gao, P., Chen, X., Shen, F., and Chen, G. (2005). Removal of chromium(VI) from wastewater by combined electrocoagulation–electroflotation without a filter. *Separation and Purification Technology* 43 (2): 117–123.

117 Fu, F. and Wang, Q. (2011). Removal of heavy metal ions from wastewaters: a review. *Journal of Environmental Management* 92 (3): 407–418.

118 An, C., Huang, G., Yao, Y., and Zhao, S. (2017). Emerging usage of electrocoagulation technology for oil removal from wastewater: a review. *Science of The Total Environment* 579: 537–556.

119 Sahu, O., Mazumdar, B., and Chaudhari, P.K. (2014). Treatment of wastewater by electrocoagulation: a review. *Environmental Science and Pollution Research* 21 (4): 2397–2413.

120 Moussa, D.T., El-Naas, M.H., Nasser, M., and Al-Marri, M.J. (2017). A comprehensive review of electrocoagulation for water treatment: potentials and challenges. *Journal of Environmental Management* 186: 24–41.

121 Mollah, M.Y.A., Schennach, R., Parga, J.R., and Cocke, D.L. (2001). Electrocoagulation (EC) — science and applications. *Journal of Hazardous Materials* 84 (1): 29–41.

122 Mollah, M.Y.A., Morkovsky, P., Gomes, J.A.G. et al. (2004). Fundamentals, present and future perspectives of electrocoagulation. *Journal of Hazardous Materials* 114 (1): 199–210.

123 Garcia-Segura, S., Eiband, M.M.S.G., de Melo, J.V., and Martínez-Huitle, C.A. (2017). Electrocoagulation and advanced electrocoagulation processes: a general review about the fundamentals, emerging applications and its association with other technologies. *Journal of Electroanalytical Chemistry* 801: 267–299.

124 Feng, J.-w., Sun, Y.-b., Zheng, Z. et al. (2007). Treatment of tannery wastewater by electrocoagulation. *Journal of Environmental Sciences* 19 (12): 1409–1415.

125 El-Naas, M.H., Al-Zuhair, S., Al-Lobaney, A., and Makhlouf, S. (2009). Assessment of electrocoagulation for the treatment of petroleum refinery wastewater. *Journal of Environmental Management* 91 (1): 180–185.

126 Akyol, A. (2012). Treatment of paint manufacturing wastewater by electrocoagulation. *Desalination* 285: 91–99.

127 Adhoum, N. and Monser, L. (2004). Decolourization and removal of phenolic compounds from olive mill wastewater by electrocoagulation. *Chemical Engineering and Processing: Process Intensification* 43 (10): 1281–1287.

128 Tezcan Ün, Ü., Uğur, S., Koparal, A.S., and Bakır Öğütveren, Ü. (2006). Electrocoagulation of olive mill wastewaters. *Separation and Purification Technology* 52 (1): 136–141.

129 Kobya, M., Hiz, H., Senturk, E. et al. (2006). Treatment of potato chips manufacturing wastewater by electrocoagulation. *Desalination* 190 (1): 201–211.

130 Kobya, M. and Delipinar, S. (2008). Treatment of the baker's yeast wastewater by electrocoagulation. *Journal of Hazardous Materials* 154 (1): 1133–1140.

131 Adhoum, N., Monser, L., Bellakhal, N., and Belgaied, J.-E. (2004). Treatment of electroplating wastewater containing Cu^{2+}, Zn^{2+} and Cr(VI) by electrocoagulation. *Journal of Hazardous Materials* 112 (3): 207–213.

132 Kobya, M., Can, O.T., and Bayramoglu, M. (2003). Treatment of textile wastewaters by electrocoagulation using iron and aluminum electrodes. *Journal of Hazardous Materials* 100 (1): 163–178.

133 Can, O.T., Kobya, M., Demirbas, E., and Bayramoglu, M. (2006). Treatment of the textile wastewater by combined electrocoagulation. *Chemosphere* 62 (2): 181–187.

134 Bayramoglu, M., Eyvaz, M., and Kobya, M. (2007). Treatment of the textile wastewater by electrocoagulation: economical evaluation. *Chemical Engineering Journal* 128 (2): 155–161.

135 Zaied, M. and Bellakhal, N. (2009). Electrocoagulation treatment of black liquor from paper industry. *Journal of Hazardous Materials* 163 (2): 995–1000.

136 Tchamango, S., Nanseu-Njiki, C.P., Ngameni, E. et al. (2010). Treatment of dairy effluents by electrocoagulation using aluminium electrodes. *Science of The Total Environment* 408 (4): 947–952.

137 Gürses, A., Yalçin, M., and Doğar, C. (2002). Electrocoagulation of some reactive dyes: a statistical investigation of some electrochemical variables. *Waste Management* 22 (5): 491–499.

138 Do, J.S. and Chen, M.L. (1994). Decolourization of dye-containing solutions by electrocoagulation. *Journal of Applied Electrochemistry* 24 (8): 785–790.

139 Daneshvar, N., Ashassi-Sorkhabi, H., and Tizpar, A. (2003). Decolorization of orange II by electrocoagulation method. *Separation and Purification Technology* 31 (2): 153–162.

140 Ghernaout, D., Badis, A., Kellil, A., and Ghernaout, B. (2008). Application of electrocoagulation in *Escherichia coli* culture and two surface waters. *Desalination* 219 (1): 118–125.

141 Golder, A.K., Samanta, A.N., and Ray, S. (2007). Removal of trivalent chromium by electrocoagulation. *Separation and Purification Technology* 53 (1): 33–41.

142 Lacasa, E., Cañizares, P., Sáez, C. et al. (2011). Removal of nitrates from groundwater by electrocoagulation. *Chemical Engineering Journal* 171 (3): 1012–1017.

143 Ratna Kumar, P., Chaudhari, S., Khilar, K.C., and Mahajan, S.P. (2004). Removal of arsenic from water by electrocoagulation. *Chemosphere* 55 (9): 1245–1252.

144 Ghosh, D., Solanki, H., and Purkait, M.K. (2008). Removal of Fe(II) from tap water by electrocoagulation technique. *Journal of Hazardous Materials* 155 (1): 135–143.

145 Vik, E.A., Carlson, D.A., Eikum, A.S., and Gjessing, E.T. (1984). Electrocoagulation of potable water. *Water Research* 18 (11): 1355–1360.

146 Emamjomeh, M.M. and Sivakumar, M. (2009). Review of pollutants removed by electrocoagulation and electrocoagulation/flotation processes. *Journal of Environmental Management* 90 (5): 1663–1679.

147 Holt, P.K., Barton, G.W., and Mitchell, C.A. (2005). The future for electrocoagulation as a localised water treatment technology. *Chemosphere* 59 (3): 355–367.

148 Paunovic, M. (2007). Electrochemical deposition. Encyclopedia of Electrochemistry.

149 Free, M.L. and Moats, M. (2014). Chapter 2.7 - Hydrometallurgical processing. In: *Treatise on Process Metallurgy* (ed. S. Seetharaman), 949–982. Boston: Elsevier.

150 Perez, N. (ed.) (2004). Electrometallurgy. In: *Electrochemistry and Corrosion Science*, 189–246. Boston, MA, US: Springer.

151 Pletcher, D. (1984). Metal extraction and refining. In: *Industrial Electrochemistry* (ed. D. Pletcher), 114–131. Dordrecht, Netherlands: Springer.

152 Landolt, D. (2002). Electrodeposition science and technology in the last quarter of the twentieth century. *Journal of The Electrochemical Society* 149 (3): S9.

153 Dean, J.G., Bosqui, F.L., and Lanouette, K.H. (1972). Removing heavy metals from waste water. *Environmental Science & Technology* 6 (6): 518–522.

154 Cooper, W.C. (1985). Advances and future prospects in copper electrowinning. *Journal of Applied Electrochemistry* 15 (6): 789–805.

155 Jha, M.K., Kumar, V., and Singh, R.J. (2001). Review of hydrometallurgical recovery of zinc from industrial wastes. *Resources, Conservation and Recycling* 33 (1): 1–22.

156 Sadegh Safarzadeh, M., Bafghi, M.S., Moradkhani, D., and Ojaghi Ilkhchi, M. (2007). A review on hydrometallurgical extraction and recovery of cadmium from various resources. *Minerals Engineering* 20 (3): 211–220.

157 Moskalyk, R.R. and Alfantazi, A.M. (2002). Nickel laterite processing and electrowinning practice. *Minerals Engineering* 15 (8): 593–605.

158 Tao, H.-C., Liang, M., Li, W. et al. (2011). Removal of copper from aqueous solution by electrodeposition in cathode chamber of microbial fuel cell. *Journal of Hazardous Materials* 189 (1): 186–192.

159 Zhao, X., Guo, L., Zhang, B. et al. (2013). Photoelectrocatalytic oxidation of Cu(II)–EDTA at the TiO_2 electrode and simultaneous recovery of Cu(II) by electrodeposition. *Environmental Science & Technology* 47 (9): 4480–4488.

160 Camarillo, R., Llanos, J., García-Fernández, L. et al. (2010). Treatment of copper (II)-loaded aqueous nitrate solutions by polymer enhanced ultrafiltration and electrodeposition. *Separation and Purification Technology* 70 (3): 320–328.

161 Dutra, A.J.B., Rocha, G.P., and Pombo, F.R. (2008). Copper recovery and cyanide oxidation by electrowinning from a spent copper-cyanide electroplating electrolyte. *Journal of Hazardous Materials* 152 (2): 648–655.

162 Guimarães, Y.F., Santos, I.D., and Dutra, A.J.B. (2014). Direct recovery of copper from printed circuit boards (PCBs) powder concentrate by a simultaneous electroleaching–electrodeposition process. *Hydrometallurgy* 149: 63–70.

163 Alam, M.S., Tanaka, M., Koyama, K. et al. (2007). Electrolyte purification in energy-saving monovalent copper electrowinning processes. *Hydrometallurgy* 87 (1): 36–44.

164 Veit, H.M., Bernardes, A.M., Ferreira, J.Z. et al. (2006). Recovery of copper from printed circuit boards scraps by mechanical processing and electrometallurgy. *Journal of Hazardous Materials* 137 (3): 1704–1709.

165 Juarez, C.M. and Dutra, A.J.B. (2000). Gold electrowinning from thiourea solutions. *Minerals Engineering* 13 (10): 1083–1096.

166 Mostad, E., Rolseth, S., and Thonstad, J. (2008). Electrowinning of iron from sulphate solutions. *Hydrometallurgy* 90 (2): 213–220.

167 Chen, C.-S., Shih, Y.-J., and Huang, Y.-H. (2016). Recovery of lead from smelting fly ash of waste lead-acid battery by leaching and electrowinning. *Waste Management* 52: 212–220.

168 Wang, Y., Xue, Y., Su, J. et al. (2018). Efficient electrochemical recovery of dilute selenium by cyclone electrowinning. *Hydrometallurgy* 179: 232–237.

169 Jayakumar, M., Venkatesan, K.A., Sudha, R. et al. (2011). Electrodeposition of ruthenium, rhodium and palladium from nitric acid and ionic liquid media: recovery and surface morphology of the deposits. *Materials Chemistry and Physics* 128 (1): 141–150.

170 Sharma, I.G., Alex, P., Bidaye, A.C., and Suri, A.K. (2005). Electrowinning of cobalt from sulphate solutions. *Hydrometallurgy* 80 (1): 132–138.

171 Tsakiridis, P.E., Oustadakis, P., Katsiapi, A., and Agatzini-Leonardou, S. (2010). Hydrometallurgical process for zinc recovery from electric arc furnace dust (EAFD). Part II: downstream processing and zinc recovery by electrowinning. *Journal of Hazardous Materials* 179 (1): 8–14.

172 Yang, C.-C. (2003). Recovery of heavy metals from spent Ni–Cd batteries by a potentiostatic electrodeposition technique. *Journal of Power Sources* 115 (2): 352–359.

173 Tanong, K., Tran, L.-H., Mercier, G., and Blais, J.-F. (2017). Recovery of Zn (II), Mn (II), Cd (II) and Ni (II) from the unsorted spent batteries using solvent extraction, electrodeposition and precipitation methods. *Journal of Cleaner Production* 148: 233–244.

174 de Souza, C.C.B.M. and Tenório, J.A.S. (2004). Simultaneous recovery of zinc and manganese dioxide from household alkaline batteries through hydrometallurgical processing. *Journal of Power Sources* 136 (1): 191–196.

175 Mecucci, A. and Scott, K. (2002). Leaching and electrochemical recovery of copper, lead and tin from scrap printed circuit boards. *Journal of Chemical Technology & Biotechnology* 77 (4): 449–457.

176 Grimshaw, P., Calo, J.M., and Hradil, G. (2011). Cyclic electrowinning/precipitation (CEP) system for the removal of heavy metal mixtures from aqueous solutions. *Chemical Engineering Journal* 175: 103–109.

177 Oztekin, Y. and Yazicigil, Z. (2006). Recovery of metals from complexed solutions by electrodeposition. *Desalination* 190 (1): 79–88.

178 Vegliò, F., Quaresima, R., Fornari, P., and Ubaldini, S. (2003). Recovery of valuable metals from electronic and galvanic industrial wastes by leaching and electrowinning. *Waste Management* 23 (3): 245–252.

179 Fornari, P. and Abbruzzese, C. (1999). Copper and nickel selective recovery by electrowinning from electronic and galvanic industrial solutions. *Hydrometallurgy* 52 (3): 209–222.

180 Doulakas, L., Novy, K., Stucki, S., and Comninellis, C. (2000). Recovery of Cu, Pb, Cd and Zn from synthetic mixture by selective electrodeposition in chloride solution. *Electrochimica Acta* 46 (2): 349–356.

181 Agarwal, R. and Sharma, M.K. (2018). Selective electrochemical separation and recovery of uranium from mixture of uranium(VI) and lanthanide(III) ions in aqueous medium. *Inorganic Chemistry* 57 (17): 10984–10992.

182 Liu, C., Hsu, P.-C., Xie, J. et al. (2017). A half-wave rectified alternating current electrochemical method for uranium extraction from seawater. *Nature Energy* 2 (4): 17007.

183 Armstrong, R.D., Todd, M., Atkinson, J.W., and Scott, K. (1996). Selective electrodeposition of metals from simulated waste solutions. *Journal of Applied Electrochemistry* 26 (4): 379–384.

184 Liu, C., Wu, T., Hsu, P.-C. et al. (2019). Direct/alternating current electrochemical method for removing and recovering heavy metal from water using graphene oxide electrode. *ACS Nano* 13 (6): 6431–6437.

185 Wang, M., Rahimi, M., Kumar, A. et al. (2019). Flue gas CO_2 capture via electrochemically mediated amine regeneration: system design and performance. *Applied Energy* 255: 113879.

186 Stern, M.C., Simeon, F., Herzog, H., and Hatton, T.A. (2013). Post-combustion carbon dioxide capture using electrochemically mediated amine regeneration. *Energy & Environmental Science* 6 (8): 2505–2517.

187 Wang, M. and Hatton, T.A. (2020). Flue gas CO_2 capture via electrochemically mediated amine regeneration: desorption unit design and analysis. *Industrial & Engineering Chemistry Research* 59 (21): 10120–10129.

188 Stern, M.C. and Hatton, T.A. (2014). Bench-scale demonstration of CO_2 capture with electrochemically-mediated amine regeneration. *RSC Advances* 4 (12): 5906–5914.

189 Wang, M., Hariharan, S., Shaw, R.A., and Hatton, T.A. (2019). Energetics of electrochemically mediated amine regeneration process for flue gas CO_2 capture. *International Journal of Greenhouse Gas Control* 82: 48–58.

190 Rahimi, M., Diederichsen, K.M., Ozbek, N. et al. (2020). An electrochemically mediated amine regeneration process with a mixed absorbent for postcombustion CO_2 capture. *Environmental Science & Technology* 54 (14): 8999–9007.

191 Wang, M., Shaw, R., Gencer, E., and Hatton, T.A. (2020). Technoeconomic analysis of the electrochemically mediated amine regeneration CO_2 capture process. *Industrial & Engineering Chemistry Research* 59 (31): 14085–14095.

192 Wang, M., Herzog, H.J., and Hatton, T.A. (2020). CO_2 capture using electrochemically mediated amine regeneration. *Industrial & Engineering Chemistry Research* 59 (15): 7087–7096.

193 Renfrew, S.E., Starr, D.E., and Strasser, P. (2020). Electrochemical approaches toward CO_2 capture and concentration. *ACS Catalysis* 10 (21): 13058–13074.

194 Appel, A.M., Newell, R., DuBois, D.L., and Rakowski DuBois, M. (2005). Concentration of carbon dioxide by electrochemically modulated complexation with a binuclear copper complex. *Inorganic Chemistry* 44 (9): 3046–3056.

195 Terry, P.A., Walis, H.J., Noble, R.D., and Koval, C.A. (1995). Electrochemically modulated complexation process for gas removal and concentration. *AIChE Journal* 41 (12): 2556–2564.

196 Terry, P.A., Noble, R.D., Swanson, D., and Koval, C.A. (1997). Electrochemically modulated complexation process for ethylene/ethane separation. *AIChE Journal* 43 (7): 1709–1716.

197 Suzuki, T., Noble, R.D., and Koval, C.A. (1997). Electrochemistry, stability, and alkene complexation chemistry of copper(I) triflate in aqueous solution. Potential for use in electrochemically modulated complexation-based separation processes. *Inorganic Chemistry* 36 (2): 136–140.

198 Yoon, H., Lee, J., Kim, S., and Yoon, J. (2019). Review of concepts and applications of electrochemical ion separation (EIONS) process. *Separation and Purification Technology* 215: 190–207.

199 Chen, F., Leong, Z.Y., and Yang, H.Y. (2017). An aqueous rechargeable chloride ion battery. *Energy Storage Materials* 7: 189–194.

200 Nam, D.-H. and Choi, K.-S. (2017). Bismuth as a new chloride-storage electrode enabling the construction of a practical high capacity desalination battery. *Journal of the American Chemical Society* 139 (32): 11055–11063.

201 Srimuk, P., Husmann, S., and Presser, V. (2019). Low voltage operation of a silver/silver chloride battery with high desalination capacity in seawater. *RSC Advances* 9 (26): 14849–14858.

202 Blair, J.W. and Murphy, G.W. (1960). Electrochemical demineralization of water with porous electrodes of large surface area. Saline Water Conversion. *Advances in Chemistry* 27: American Chemical Society: 206–223.

203 Pasta, M., Wessells, C.D., Cui, Y., and La Mantia, F. (2012). A desalination battery. *Nano Letters* 12 (2): 839–843.

204 Chao, D., Zhou, W., Xie, F. et al. (2020). Roadmap for advanced aqueous batteries: from design of materials to applications. *Science Advances* 6 (21): eaba4098.

205 Zhao, X., Zhao-Karger, Z., Fichtner, M., and Shen, X. (2020). Halide-based materials and chemistry for rechargeable batteries. *Angewandte Chemie International Edition* 59 (15): 5902–5949.

206 Yang, C., Chen, J., Ji, X. et al. (2019). Aqueous Li-ion battery enabled by halogen conversion–intercalation chemistry in graphite. *Nature* 569 (7755): 245–250.

207 Zhang, C., He, D., Ma, J. et al. (2018). Faradaic reactions in capacitive deionization (CDI) – problems and possibilities: a review. *Water Research* 128: 314–330.

208 Jeon, S.-i., Park, H.-r., Yeo, J.-g. et al. (2013). Desalination via a new membrane capacitive deionization process utilizing flow-electrodes. *Energy & Environmental Science* 6 (5): 1471–1475.

209 Zhao, R., Biesheuvel, P.M., and van der Wal, A. (2012). Energy consumption and constant current operation in membrane capacitive deionization. *Energy & Environmental Science* 5 (11): 9520–9527.

210 Oren, Y. (2008). Capacitive deionization (CDI) for desalination and water treatment — past, present and future (a review). *Desalination* 228 (1): 10–29.

211 Suss, M.E., Porada, S., Sun, X. et al. (2015). Water desalination via capacitive deionization: what is it and what can we expect from it? *Energy & Environmental Science* 8 (8): 2296–2319.

212 Hou, C.-H. and Huang, C.-Y. (2013). A comparative study of electrosorption selectivity of ions by activated carbon electrodes in capacitive deionization. *Desalination* 314: 124–129.

213 Seo, S.-J., Jeon, H., Lee, J.K. et al. (2010). Investigation on removal of hardness ions by capacitive deionization (CDI) for water softening applications. *Water Research* 44 (7): 2267–2275.

214 Kokoszka, B., Jarrah, N.K., Liu, C. et al. (2014). Supercapacitive swing adsorption of carbon dioxide. *Angewandte Chemie International Edition* 53 (14): 3698–3701.

215 Hemmatifar, A., Palko, J.W., Stadermann, M., and Santiago, J.G. (2016). Energy breakdown in capacitive deionization. *Water Research* 104: 303–311.

216 Zhang, X., Zuo, K., Zhang, X. et al. (2020). Selective ion separation by capacitive deionization (CDI) based technologies: a state-of-the-art review. *Environmental Science: Water Research & Technology* 6 (2): 243–257.

217 Hawks, S.A., Cerón, M.R., Oyarzun, D.I. et al. (2019). Using ultramicroporous carbon for the selective removal of nitrate with capacitive deionization. *Environmental Science & Technology* 53 (18): 10863–10870.

218 Li, Y., Zhang, C., Jiang, Y. et al. (2016). Effects of the hydration ratio on the electrosorption selectivity of ions during capacitive deionization. *Desalination* 399: 171–177.

219 Suss, M.E. (2017). Size-based ion selectivity of micropore electric double layers in capacitive deionization electrodes. *Journal of The Electrochemical Society* 164 (9): E270.

220 Xing, W., Liang, J., Tang, W. et al. (2019). Perchlorate removal from brackish water by capacitive deionization: experimental and theoretical investigations. *Chemical Engineering Journal* 361: 209–218.

221 Sun, Z., Chai, L., Liu, M. et al. (2018). Effect of the electronegativity on the electrosorption selectivity of anions during capacitive deionization. *Chemosphere* 195: 282–290.

222 Guyes, E.N., Malka, T., and Suss, M.E. (2019). Enhancing the ion-size-based selectivity of capacitive deionization electrodes. *Environmental Science & Technology* 53 (14): 8447–8454.

223 Ji, Q., An, X., Liu, H. et al. (2015). Electric double-layer effects induce separation of aqueous metal ions. *ACS Nano* 9 (11): 10922–10930.

224 Zuo, K., Kim, J., Jain, A. et al. (2018). Novel composite electrodes for selective removal of sulfate by the capacitive deionization process. *Environmental Science & Technology* 52 (16): 9486–9494.

225 Kim, Y.-J. and Choi, J.-H. (2012). Selective removal of nitrate ion using a novel composite carbon electrode in capacitive deionization. *Water Research* 46 (18): 6033–6039.

226 Gan, L., Wu, Y., Song, H. et al. (2019). Selective removal of nitrate ion using a novel activated carbon composite carbon electrode in capacitive deionization. *Separation and Purification Technology* 212: 728–736.

227 Qian, B., Wang, G., Ling, Z. et al. (2015). Sulfonated graphene as cation-selective coating: a new strategy for high-performance membrane capacitive deionization. *Advanced Materials Interfaces* 2 (16): 1500372.

228 Liu, P., Wang, H., Yan, T. et al. (2016). Grafting sulfonic and amine functional groups on 3D graphene for improved capacitive deionization. *Journal of Materials Chemistry A* 4 (14): 5303–5313.

229 Oyarzun, D.I., Hemmatifar, A., Palko, J.W. et al. (2018). Ion selectivity in capacitive deionization with functionalized electrode: theory and experimental validation. *Water Research X* 1: 100008.

230 Tang, W., Liang, J., He, D. et al. (2019). Various cell architectures of capacitive deionization: recent advances and future trends. *Water Research* 150: 225–251.

231 Gao, X., Omosebi, A., Landon, J., and Liu, K. (2015). Enhanced salt removal in an inverted capacitive deionization cell using amine modified microporous carbon cathodes. *Environmental Science & Technology* 49 (18): 10920–10926.

232 Gao, X., Omosebi, A., Landon, J., and Liu, K. (2015). Surface charge enhanced carbon electrodes for stable and efficient capacitive deionization using inverted adsorption–desorption behavior. *Energy & Environmental Science* 8 (3): 897–909.

233 Wu, T., Wang, G., Zhan, F. et al. (2016). Surface-treated carbon electrodes with modified potential of zero charge for capacitive deionization. *Water Research* 93: 30–37.

234 Kang, J.S., Kim, S., Chung, D.Y. et al. (2020). Rapid inversion of surface charges in heteroatom-doped porous carbon: a route to robust electrochemical desalination. *Advanced Functional Materials* 30 (9): 1909387.

235 Yang, S., Choi, J., Yeo, J.-g. et al. (2016). Flow-electrode capacitive deionization using an aqueous electrolyte with a high salt concentration. *Environmental Science & Technology* 50 (11): 5892–5899.

236 Jeon, S.-i., Yeo, J.-g., Yang, S. et al. (2014). Ion storage and energy recovery of a flow-electrode capacitive deionization process. *Journal of Materials Chemistry A* 2 (18): 6378–6383.

237 Hatzell, K.B., Hatzell, M.C., Cook, K.M. et al. (2015). Effect of oxidation of carbon material on suspension electrodes for flow electrode capacitive deionization. *Environmental Science & Technology* 49 (5): 3040–3047.

238 Rommerskirchen, A., Gendel, Y., and Wessling, M. (2015). Single module flow-electrode capacitive deionization for continuous water desalination. *Electrochemistry Communications* 60: 34–37.

239 Porada, S., Weingarth, D., Hamelers, H.V.M. et al. (2014). Carbon flow electrodes for continuous operation of capacitive deionization and capacitive mixing energy generation. *Journal of Materials Chemistry A* 2 (24): 9313–9321.

240 Biesheuvel, P.M. and van der Wal, A. (2010). Membrane capacitive deionization. *Journal of Membrane Science* 346 (2): 256–262.

241 Zhao, Y., Wang, Y., Wang, R. et al. (2013). Performance comparison and energy consumption analysis of capacitive deionization and membrane capacitive deionization processes. *Desalination* 324: 127–133.

242 Li, H. and Zou, L. (2011). Ion-exchange membrane capacitive deionization: a new strategy for brackish water desalination. *Desalination* 275 (1): 62–66.

243 Lee, J.-B., Park, K.-K., Eum, H.-M., and Lee, C.-W. (2006). Desalination of a thermal power plant wastewater by membrane capacitive deionization. *Desalination* 196 (1): 125–134.

244 Chang, J., Tang, K., Cao, H. et al. (2018). Application of anion exchange membrane and the effect of its properties on asymmetric membrane capacitive deionization. *Separation and Purification Technology* 207: 387–395.

245 McNair, R., Cseri, L., Szekely, G., and Dryfe, R. (2020). Asymmetric membrane capacitive deionization using anion-exchange membranes based on quaternized polymer blends. *ACS Applied Polymer Materials* 2 (7): 2946–2956.

246 Pan, J., Zheng, Y., Ding, J. et al. (2018). Fluoride removal from water by membrane capacitive deionization with a monovalent anion selective membrane. *Industrial & Engineering Chemistry Research* 57 (20): 7048–7053.

247 Kim, Y.-J., Kim, J.-H., and Choi, J.-H. (2013). Selective removal of nitrate ions by controlling the applied current in membrane capacitive deionization (MCDI). *Journal of Membrane Science* 429: 52–57.

248 Dong, Q., Guo, X., Huang, X. et al. (2019). Selective removal of lead ions through capacitive deionization: role of ion-exchange membrane. *Chemical Engineering Journal* 361: 1535–1542.

249 Shi, W., Liu, X., Ye, C. et al. (2019). Efficient lithium extraction by membrane capacitive deionization incorporated with monovalent selective cation exchange membrane. *Separation and Purification Technology* 210: 885–890.

250 Choi, J., Lee, H., and Hong, S. (2016). Capacitive deionization (CDI) integrated with monovalent cation selective membrane for producing divalent cation-rich solution. *Desalination* 400: 38–46.

251 Wang, L. and Lin, S. (2019). Mechanism of selective ion removal in membrane capacitive deionization for water softening. *Environmental Science & Technology* 53 (10): 5797–5804.

252 Kim, J., Jain, A., Zuo, K. et al. (2019). Removal of calcium ions from water by selective electrosorption using target-ion specific nanocomposite electrode. *Water Research* 160: 445–453.

253 Legrand, L., Schaetzle, O., de Kler, R.C.F., and Hamelers, H.V.M. (2018). Solvent-free CO_2 capture using membrane capacitive deionization. *Environmental Science & Technology* 52 (16): 9478–9485.

254 Legrand, L., Shu, Q., Tedesco, M. et al. (2020). Role of ion exchange membranes and capacitive electrodes in membrane capacitive deionization (MCDI) for CO_2 capture. *Journal of Colloid and Interface Science* 564: 478–490.

255 Li, M. and Anand, R.K. (2016). Recent advancements in ion concentration polarization. *Analyst* 141 (12): 3496–3510.

256 Kim, S.J., Ko, S.H., Kang, K.H., and Han, J. (2010). Direct seawater desalination by ion concentration polarization. *Nature Nanotechnology* 5 (4): 297–301.

257 Achilleos, D.S. and Hatton, T.A. (2015). Surface design and engineering of hierarchical hybrid nanostructures for asymmetric supercapacitors with improved electrochemical performance. *Journal of Colloid and Interface Science* 447: 282–301.

258 Miller, J.R. and Simon, P. (2008). Electrochemical capacitors for energy management. *Science* 321 (5889): 651.

259 Kötz, R. and Carlen, M. (2000). Principles and applications of electrochemical capacitors. *Electrochimica Acta* 45 (15): 2483–2498.

260 Wang, G., Zhang, L., and Zhang, J. (2012). A review of electrode materials for electrochemical supercapacitors. *Chemical Society Reviews* 41 (2): 797–828.

261 Suss, M.E. and Presser, V. (2018). Water desalination with energy storage electrode materials. *Joule* 2 (1): 10–15.

262 He, F., Biesheuvel, P.M., Bazant, M.Z., and Hatton, T.A. (2018). Theory of water treatment by capacitive deionization with redox active porous electrodes. *Water Research* 132: 282–291.

263 Achilleos, D.S. and Hatton, T.A. (2016). Selective molecularly mediated pseudocapacitive separation of ionic species in solution. *ACS Applied Materials & Interfaces* 8 (48): 32743–32753.

264 Connelly, N.G. and Geiger, W.E. (1996). Chemical redox agents for organometallic chemistry. *Chemical Reviews* 96 (2): 877–910.

265 Ju, H. and Leech, D. (1999). Effect of electrolytes on the electrochemical behaviour of 11-(ferrocenylcarbonyloxy)undecanethiol SAMs on gold disk electrodes. *Physical Chemistry Chemical Physics* 1 (7): 1549–1554.

266 Norman, L.L. and Badia, A. (2011). Microcantilevers modified with ferrocene-terminated self-assembled monolayers: effect of molecular structure and electrolyte anion on the redox-induced surface stress. *The Journal of Physical Chemistry C* 115 (5): 1985–1995.

267 Rowe, G.K. and Creager, S.E. (1991). Redox and ion-pairing thermodynamics in self-assembled monolayers. *Langmuir* 7 (10): 2307–2312.

268 Rowe, G.K. and Creager, S.E. (1994). Interfacial solvation and double-layer effects on redox reactions in organized assemblies. *The Journal of Physical Chemistry* 98 (21): 5500–5507.

269 Rudnev, A.V., Zhumaev, U., Utsunomiya, T. et al. (2013). Ferrocene-terminated alkanethiol self-assembled monolayers: an electrochemical and in situ surface-enhanced infra-red absorption spectroscopy study. *Electrochimica Acta* 107: 33–44.

270 Valincius, G., Niaura, G., Kazakevičienė, B. et al. (2004). Anion effect on mediated electron transfer through ferrocene-terminated self-assembled monolayers. *Langmuir* 20 (16): 6631–6638.

271 Wong, R.A., Yokota, Y., Wakisaka, M. et al. (2020). Probing consequences of anion-dictated electrochemistry on the electrode/monolayer/electrolyte interfacial properties. *Nature Communications* 11 (1): 4194.

272 Larik, F.A., Saeed, A., Fattah, T.A. et al. (2017). Recent advances in the synthesis, biological activities and various applications of ferrocene derivatives. *Applied Organometallic Chemistry* 31 (8): e3664.

273 Saleem, M., Yu, H., Wang, L. et al. (2015). Review on synthesis of ferrocene-based redox polymers and derivatives and their application in glucose sensing. *Analytica Chimica Acta* 876: 9–25.

274 Sun, R., Wang, L., Yu, H. et al. (2014). Molecular recognition and sensing based on ferrocene derivatives and ferrocene-based polymers. *Organometallics* 33 (18): 4560–4573.

275 Atkinson, R.C.J., Gibson, V.C., and Long, N.J. (2004). The syntheses and catalytic applications of unsymmetrical ferrocene ligands. *Chemical Society Reviews* 33 (5): 313–328.

276 Gómez Arrayás, R., Adrio, J., and Carretero, J.C. (2006). Recent applications of chiral ferrocene ligands in asymmetric catalysis. *Angewandte Chemie International Edition* 45 (46): 7674–7715.

277 Tong, R., Zhao, Y., Wang, L. et al. (2014). Recent research progress in the synthesis and properties of burning rate catalysts based on ferrocene-containing polymers and derivatives. *Journal of Organometallic Chemistry* 755: 16–32.

278 Arimoto, F.S. and Haven, A.C. (1955). Derivatives of Dicyclopentadienyliron[1]. *Journal of the American Chemical Society* 77 (23): 6295–6297.

279 Mao, X., Simeon, F., Achilleos, D.S. et al. (2013). Metallocene/carbon hybrids prepared by a solution process for supercapacitor applications. *Journal of Materials Chemistry A* 1 (42): 13120–13127.

280 Su, X., Kushima, A., Halliday, C. et al. (2018). Electrochemically-mediated selective capture of heavy metal chromium and arsenic oxyanions from water. *Nature Communications* 9 (1): 4701.

281 Akhoury, A., Bromberg, L., and Hatton, T.A. (2013). Interplay of electron hopping and bounded diffusion during charge transport in redox polymer electrodes. *The Journal of Physical Chemistry B* 117 (1): 333–342.

282 He, F., Hemmatifar, A., Bazant, M.Z., and Hatton, T.A. (2020). Selective adsorption of organic anions in a flow cell with asymmetric redox active electrodes. *Water Research* 182: 115963.

283 Su, X., Kulik, H.J., Jamison, T.F., and Hatton, T.A. (2016). Anion-selective redox electrodes: electrochemically mediated separation with heterogeneous organometallic interfaces. *Advanced Functional Materials* 26 (20): 3394–3404.

284 Su, X., Tan, K.-J., Elbert, J. et al. (2017). Asymmetric Faradaic systems for selective electrochemical separations. *Energy & Environmental Science* 10: 1272–1283.

285 Su, X., Hübner, J., Kauke, M.J. et al. (2017). Redox interfaces for electrochemically controlled protein–surface interactions: bioseparations and heterogeneous enzyme catalysis. *Chemistry of Materials* 29 (13): 5702–5712.

286 Kim, K., Cotty, S., Elbert, J. et al. (2020). Asymmetric redox-polymer interfaces for electrochemical reactive separations: synergistic capture and conversion of arsenic. *Advanced Materials* 32 (6): 1906877.

287 Tan, K.-J., Su, X., and Hatton, T.A. (2020). An asymmetric iron-based redox-active system for electrochemical separation of ions in aqueous media. *Advanced Functional Materials* 30 (15): 1910363.

288 Hemmatifar, A., Ozbek, N., Halliday, C., and Hatton, T.A. (2020). Electrochemical selective recovery of heavy metal vanadium oxyanion from continuously flowing aqueous streams. *ChemSusChem* 13 (15): 3865–3874.

289 Song, Z., Garg, S., Ma, J., and Waite, T.D. (2020). Selective arsenic removal from groundwaters using redox-active polyvinylferrocene-functionalized electrodes: role of oxygen. *Environmental Science & Technology* 54 (19): 12081–12091.

290 Balasubramanian, M., Giacomini, M.T., Lee, H.S. et al. (2002). X-ray absorption studies of poly(vinylferrocene) polymers for anion separation. *Journal of The Electrochemical Society* 149 (9): D137.

291 Espenscheid, M.W., Ghatak-Roy, A.R., Moore, R.B. et al. (1986). Sensors from polymer modified electrodes. *Journal of the Chemical Society, Faraday Transactions 1: Physical Chemistry in Condensed Phases* 82 (4): 1051–1070.

292 Stojanovic, R.S. and Bond, A.M. (1993). Examination of conditions under which the reduction of the cobaltocenium cation can be used as a standard voltammetric reference process in organic and aqueous solvents. *Analytical Chemistry* 65 (1): 56–64.

293 Ren, L., Hardy, C.G., and Tang, C. (2010). Synthesis and solution self-assembly of side-chain cobaltocenium-containing block copolymers. *Journal of the American Chemical Society* 132 (26): 8874–8875.

294 Ren, L., Hardy, C.G., Tang, S. et al. (2010). Preparation of side-chain 18-e cobaltocenium-containing acrylate monomers and polymers. *Macromolecules* 43 (22): 9304–9310.

295 Rüttiger, C., Pfeifer, V., Rittscher, V. et al. (2016). One for all: cobalt-containing polymethacrylates for magnetic ceramics, block copolymerization, unexpected electrochemistry, and stimuli-responsiveness. *Polymer Chemistry* 7 (5): 1129–1137.

296 Chadha, P. and Ragogna, P.J. (2011). Side chain Co(I) polymers featuring acrylate functionalized neutral 18 electron $CpCo(C_4R_4)$ (R = Ph, Me) units. *Chemical Communications* 47 (18): 5301–5303.

297 Brotin, T., Pospíšil, L., Fiedler, J. et al. (1998). Toward a square grid polymer: electrochemistry of tentacled tetragonal star connectors, $C_4R_4{-}Co{-}C_5(HgY)_5$, on mercury. *The Journal of Physical Chemistry B* 102 (49): 10062–10070.

298 Liu, Y., Ye, H.-Z., Diederichsen, K.M. et al. (2020). Electrochemically mediated carbon dioxide separation with quinone chemistry in salt-concentrated aqueous media. *Nature Communications* 11 (1): 2278.

299 Rheinhardt, J.H., Singh, P., Tarakeshwar, P., and Buttry, D.A. (2017). Electrochemical capture and release of carbon dioxide. *ACS Energy Letters* 2 (2): 454–461.

300 Bell, W.L., Miedaner, A., Smart, J.C. et al. (1988). Synthesis and evaluation of electroactive CO_2 carriers. *18th Intersociety Conference on Environmental Systems*, San Francisco, CA (11–13 July 1988). SAE International.

301 De Sousa Bulhões, L.O. and Zara, A.J. (1988). The effect of carbon dioxide on the electroreduction of 1,4-benzoquinone. *Journal of Electroanalytical Chemistry and Interfacial Electrochemistry* 248 (1): 159–165.

302 Mizen, M.B. and Wrighton, M.S. (1989). Reductive addition of CO_2 to 9,10-phenanthrenequinone. *Journal of The Electrochemical Society* 136 (4): 941–946.

303 Apaydin, D.H., Gora, M., Portenkirchner, E. et al. (2017). Electrochemical capture and release of CO_2 in aqueous electrolytes using an organic semiconductor electrode. *ACS Applied Materials & Interfaces* 9 (15): 12919–12923.

304 Huang, C., Liu, C., Wu, K. et al. (2019). CO_2 capture from flue gas using an electrochemically reversible hydroquinone/quinone solution. *Energy & Fuels* 33 (4): 3380–3389.

305 Watkins, J.D., Siefert, N.S., Zhou, X. et al. (2015). Redox-mediated separation of carbon dioxide from flue gas. *Energy & Fuels* 29 (11): 7508–7515.

306 Jin, S., Wu, M., Gordon, R.G. et al. (2020). pH swing cycle for CO_2 capture electrochemically driven through proton-coupled electron transfer. *Energy & Environmental Science* 13 (10): 3706–3722.

307 Xie, H., Wu, Y., Liu, T. et al. (2020). Low-energy-consumption electrochemical CO_2 capture driven by biomimetic phenazine derivatives redox medium. *Applied Energy* 259: 114119.

308 Xie, H., Jiang, W., Liu, T. et al. (2020). Low-energy electrochemical carbon dioxide capture based on a biological redox proton carrier. *Cell Reports Physical Science* 1 (5): 100046.

309 Heinze, J., Frontana-Uribe, B.A., and Ludwigs, S. (2010). Electrochemistry of conducting polymers—persistent models and new concepts. *Chemical Reviews* 110 (8): 4724–4771.

310 Deinhammer, R.S., Porter, M.D., and Shimazu, K. (1995). Retention characteristics of polypyrrole as a stationary phase for the electrochemically modulated liquid chromatographic (EMLC) separations of dansyl amino acids. *Journal of Electroanalytical Chemistry* 387 (1): 35–46.

311 Kim, Y., Lin, Z., Jeon, I. et al. (2018). Polyaniline nanofiber electrodes for reversible capture and release of mercury(II) from water. *Journal of the American Chemical Society* 140 (43): 14413–14420.

312 Wang, Z., Ma, Y., Hao, X. et al. (2014). Enhancement of heavy metals removal efficiency from liquid wastes by using potential-triggered proton self-exchange effects. *Electrochimica Acta* 130: 40–45.

313 Inzelt, G. (2012). *Conducting Polymers: A New Era in Electrochemistry*. Berlin, Heidelberg: Springer.

314 Le, T.-H., Kim, Y., and Yoon, H. (2017). Electrical and electrochemical properties of conducting polymers. *Polymers* 9 (4): 150.

315 Janata, J. and Josowicz, M. (2003). Conducting polymers in electronic chemical sensors. *Nature Materials* 2 (1): 19–24.

316 Bryan, A.M., Santino, L.M., Lu, Y. et al. (2016). Conducting polymers for pseudocapacitive energy storage. *Chemistry of Materials* 28 (17): 5989–5998.

317 Rudge, A., Davey, J., Raistrick, I. et al. (1994). Conducting polymers as active materials in electrochemical capacitors. *Journal of Power Sources* 47 (1): 89–107.

318 Ibanez, J.G., Rincón, M.E., Gutierrez-Granados, S. et al. (2018). Conducting polymers in the fields of energy, environmental remediation, and chemical–chiral sensors. *Chemical Reviews* 118 (9): 4731–4816.

319 Bredas, J.L. and Street, G.B. (1985). Polarons, bipolarons, and solitons in conducting polymers. *Accounts of Chemical Research* 18 (10): 309–315.

320 Lin, Y., Cui, X., and Bontha, J. (2006). Electrically controlled anion exchange based on polypyrrole and carbon nanotubes nanocomposite for perchlorate removal. *Environmental Science & Technology* 40 (12): 4004–4009.

321 Xing, J., Zhu, C., Chowdhury, I. et al. (2018). Electrically switched Ion exchange based on polypyrrole and carbon nanotube nanocomposite for the removal of chromium(VI) from aqueous solution. *Industrial & Engineering Chemistry Research* 57 (2): 768–774.

322 Zhao, X., Zhao, Z., Yang, M. et al. (2017). Developing polymer cathode material for the chloride ion battery. *ACS Applied Materials & Interfaces* 9 (3): 2535–2540.

323 Kong, H., Yang, M., Miao, Y., and Zhao, X. (2019). Polypyrrole as a novel chloride-storage electrode for seawater desalination. *Energy Technology* 7 (11): 1900835.

324 Bagheri, H., Ayazi, Z., and Naderi, M. (2013). Conductive polymer-based microextraction methods: a review. *Analytica Chimica Acta* 767: 1–13.

325 Wu, J., Mullett, W.M., and Pawliszyn, J. (2002). Electrochemically controlled solid-phase microextraction based on conductive polypyrrole films. *Analytical Chemistry* 74 (18): 4855–4859.

326 Liu, X., Wang, X., Tan, F. et al. (2012). An electrochemically enhanced solid-phase microextraction approach based on molecularly imprinted polypyrrole/multi-walled carbon nanotubes composite coating for selective extraction of fluoroquinolones in aqueous samples. *Analytica Chimica Acta* 727: 26–33.

327 Şahin, Y., Ercan, B., and Şahin, M. (2008). Solid-phase microextraction and ion chromatographic analysis of anions based on polypyrrole electrode. *Journal of Applied Polymer Science* 108 (5): 3298–3304.

328 Ge, H. and Wallace, G.G. (1990). Electrochemically controlled liquid chromatography on conducting polymer stationary phases. *Journal of Liquid Chromatography* 13 (16): 3245–3260.

329 Cui, H., Li, Q., Qian, Y. et al. (2011). Defluoridation of water via electrically controlled anion exchange by polyaniline modified electrode reactor. *Water Research* 45 (17): 5736–5744.

330 Zhang, B., Du, X., Hao, X. et al. (2018). A novel potential-triggered SBA-15/PANI/PSS composite film for selective removal of lead ions from wastewater. *Journal of Solid State Electrochemistry* 22 (8): 2473–2483.

331 Gbatu, T.P., Ceylan, O., Sutton, K.L. et al. (1999). Electrochemical control of solid phase micro-extraction using unique conducting polymer coated fibers. *Analytical Communications* 36 (5): 203–205.

332 Scholz, F.K. and Kahlert, H. (2007). Electrochemistry of polycyanometalates. Encyclopedia of Electrochemistry.

333 Hurlbutt, K., Wheeler, S., Capone, I., and Pasta, M. (2018). Prussian blue analogs as battery materials. *Joule* 2 (10): 1950–1960.

334 Neff, V.D. (1978). Electrochemical oxidation and reduction of thin films of prussian blue. *Journal of The Electrochemical Society* 125 (6): 886–887.

335 Wu, X., Qi, Y., Hong, J.J. et al. (2017). Rocking-chair ammonium-ion battery: a highly reversible aqueous energy storage system. *Angewandte Chemie International Edition* 56 (42): 13026–13030.

336 Wang, R.Y., Wessells, C.D., Huggins, R.A., and Cui, Y. (2013). Highly reversible open framework nanoscale electrodes for divalent ion batteries. *Nano Letters* 13 (11): 5748–5752.

337 Lilga, M.A., Orth, R.J., Sukamto, J.P.H. et al. (1997). Metal ion separations using electrically switched ion exchange. *Separation and Purification Technology* 11 (3): 147–158.

338 Chen, R., Tanaka, H., Kawamoto, T. et al. (2013). Thermodynamics and mechanism studies on electrochemical removal of cesium ions from aqueous solution using a nanoparticle film of copper hexacyanoferrate. *ACS Applied Materials & Interfaces* 5 (24): 12984–12990.

339 Pasta, M., Battistel, A., and La Mantia, F. (2012). Batteries for lithium recovery from brines. *Energy & Environmental Science* 5 (11): 9487–9491.

340 Wang, R.Y., Shyam, B., Stone, K.H. et al. (2015). Reversible multivalent (monovalent, divalent, trivalent) ion insertion in open framework materials. *Advanced Energy Materials* 5 (12): 1401869.

341 Chen, W. and Xia, X.H. (2007). Highly stable nickel hexacyanoferrate nanotubes for electrically switched ion exchange. *Advanced Functional Materials* 17 (15): 2943–2948.

342 Rassat, S.D., Sukamto, J.H., Orth, R.J. et al. (1999). Development of an electrically switched ion exchange process for selective ion separations. *Separation and Purification Technology* 15 (3): 207–222.

343 Porada, S., Shrivastava, A., Bukowska, P. et al. (2017). Nickel hexacyanoferrate electrodes for continuous cation intercalation desalination of brackish water. *Electrochimica Acta* 255: 369–378.

344 Bocarsly, A.B. and Sinha, S. (1982). Effects of surface structure on electrode charge transfer properties: induction of ion selectivity at the chemically derivatized interface. *Journal of Electroanalytical Chemistry and Interfacial Electrochemistry* 140 (1): 167–172.

345 Joseph, J., Gomathi, H., and Prabhakara Rao, G. (1991). Electrochemical characteristics of thin films of nickel hexacyanoferrate formed on carbon substrates. *Electrochimica Acta* 36 (10): 1537–1541.

346 Schneemeyer, L.F., Spengler, S.E., and Murphy, D.W. (1985). Ion selectivity in nickel hexacyanoferrate films on electrode surfaces. *Inorganic Chemistry* 24 (19): 3044–3046.

347 Sinha, S., Humphrey, B.D., and Bocarsly, A.B. (1984). Reaction of nickel electrode surfaces with anionic metal-cyanide complexes: formation of precipitated surfaces. *Inorganic Chemistry* 23 (2): 203–212.

348 Jiang, H., Wei, Z., Ma, L. et al. (2019). An aqueous dual-ion battery cathode of Mn_3O_4 via reversible insertion of nitrate. *Angewandte Chemie International Edition* 58 (16): 5286–5291.

349 Pasta, M., Wessells, C.D., Liu, N. et al. (2014). Full open-framework batteries for stationary energy storage. *Nature Communications* 5 (1): 3007.

350 Rahimi, M., Catalini, G., Puccini, M., and Hatton, T.A. (2020). Bench-scale demonstration of CO_2 capture with an electrochemically driven proton concentration process. *RSC Advances* 10 (29): 16832–16843.

351 Rahimi, M., Catalini, G., Hariharan, S. et al. (2020). Carbon dioxide capture using an electrochemically driven proton concentration process. *Cell Reports Physical Science* 1 (4): 100033.

352 Kanoh, H., Ooi, K., Miyai, Y., and Katoh, S. (1993). Electrochemical recovery of lithium ions in the aqueous phase. *Separation Science and Technology* 28 (1–3): 643–651.

353 Kim, T., Gorski, C.A., and Logan, B.E. (2018). Ammonium removal from domestic wastewater using selective battery electrodes. *Environmental Science & Technology Letters* 5 (9): 578–583.

354 Morozan, A. and Jaouen, F. (2012). Metal organic frameworks for electrochemical applications. *Energy & Environmental Science* 5 (11): 9269–9290.

355 Wu, H.B. and Lou, X.W. (2017). Metal-organic frameworks and their derived materials for electrochemical energy storage and conversion: promises and challenges. *Science Advances* 3 (12): eaap9252.

356 Xia, W., Mahmood, A., Zou, R., and Xu, Q. (2015). Metal–organic frameworks and their derived nanostructures for electrochemical energy storage and conversion. *Energy & Environmental Science* 8 (7): 1837–1866.

357 Zheng, S., Li, X., Yan, B. et al. (2017). Transition-metal (Fe, Co, Ni) based metal-organic frameworks for electrochemical energy storage. *Advanced Energy Materials* 7 (18): 1602733.

358 Lee, D.Y., Yoon, S.J., Shrestha, N.K. et al. (2012). Unusual energy storage and charge retention in Co-based metal–organic-frameworks. *Microporous and Mesoporous Materials* 153: 163–165.

359 Li, Y., Xu, Y., Liu, Y., and Pang, H. (2019). Exposing {001} crystal plane on hexagonal Ni-MOF with surface-grown cross-linked mesh-structures for electrochemical energy storage. *Small* 15 (36): 1902463.

360 Xu, J., Wang, Y., Cao, S. et al. (2018). Ultrathin Cu-MOF@δ-MnO_2 nanosheets for aqueous electrolyte-based high-voltage electrochemical capacitors. *Journal of Materials Chemistry A* 6 (36): 17329–17336.

361 Wang, Z., Feng, Y., Hao, X. et al. (2014). A novel potential-responsive ion exchange film system for heavy metal removal. *Journal of Materials Chemistry A* 2 (26): 10263–10272.

362 Du, X., Zhang, H., Hao, X. et al. (2014). Facile preparation of ion-imprinted composite film for selective electrochemical removal of nickel(II) ions. *ACS Applied Materials & Interfaces* 6 (12): 9543–9549.

363 Chen, L., Xu, S., and Li, J. (2011). Recent advances in molecular imprinting technology: current status, challenges and highlighted applications. *Chemical Society Reviews* 40 (5): 2922–2942.

364 Du, X., Sun, X., Zhang, H. et al. (2015). A facile potential-induced in situ ion removal trick: fabrication of high-selective ion-imprinted film for trivalent yttrium ion separation. *Electrochimica Acta* 176: 1313–1323.

365 Holeček, J., Handlíř, K., Klikorka, J., and Bang, N.D. (1979). Decomposition of ferricenium cation in alkaline medium. *Collection of Czechoslovak Chemical Communications* 44 (5): 1379–1387.

366 Karpinski, Z.J., Nanjundiah, C., and Osteryoung, R.A. (1984). Electrochemical studies of ferrocene and ferrocenium ion in aluminum chloride-N-(1-butyl)pyridinium chloride ionic liquid. *Inorganic Chemistry* 23 (21): 3358–3364.

367 Prins, R., Korswagen, A.R., and Kortbeek, A.G.T.G. (1972). Decomposition of the ferricenium cation by nucleophilic reagents. *Journal of Organometallic Chemistry* 39 (2): 335–344.

368 Liao, S., Xue, C., Wang, Y. et al. (2015). Simultaneous separation of iodide and cesium ions from dilute wastewater based on PPy/PTCF and NiHCF/PTCF electrodes using electrochemically switched ion exchange method. *Separation and Purification Technology* 139: 63–69.

369 Mao, X., Tian, W., Ren, Y. et al. (2018). Energetically efficient electrochemically tunable affinity separation using multicomponent polymeric nanostructures for water treatment. *Energy & Environmental Science* 11 (10): 2954–2963.

370 Ren, Y., Lin, Z., Mao, X. et al. (2018). Superhydrophobic, surfactant-doped, conducting polymers for electrochemically reversible adsorption of organic contaminants. *Advanced Functional Materials* 28 (32): 1801466.

371 Tian, W., Mao, X., Brown, P. et al. (2015). Electrochemically nanostructured polyvinylferrocene/polypyrrole hybrids with synergy for energy storage. *Advanced Functional Materials* 25 (30): 4803–4813.

372 Akhoury, A., Bromberg, L., and Hatton, T.A. (2011). Redox-responsive gels with tunable hydrophobicity for controlled solubilization and release of organics. *ACS Applied Materials & Interfaces* 3 (4): 1167–1174.

373 Tan, X., Hu, C., Li, X. et al. (2020). Reversible superwettability switching of a conductive polymer membrane for oil-water separation and self-cleaning. *Journal of Membrane Science* 605: 118088.

374 Ren, Y., Mao, X., and Hatton, T.A. (2019). An asymmetric electrochemical system with complementary tunability in hydrophobicity for selective separations of organics. *ACS Central Science* 5 (8): 1396–1406.

375 Kiss, A.A. (2014). *Reactive Separation Processes. Process Intensification Technologies for Biodiesel Production: Reactive Separation Processes*, 25–33. Cham: Springer International Publishing.

376 Stankiewicz, A. (2003). Reactive separations for process intensification: an industrial perspective. *Chemical Engineering and Processing: Process Intensification* 42 (3): 137–144.

377 Kim, S., Kim, C., Lee, J. et al. (2018). Hybrid electrochemical desalination system combined with an oxidation process. *ACS Sustainable Chemistry & Engineering* 6 (2): 1620–1626.

378 Mao, X., Yan, E.H., Rutledge, G.C., and Hatton, T.A. (2016). Enhanced redox transformation efficiency in unconjugated electroactive polymer/carbon nanotube hybrids. *Chemistry of Materials* 28 (2): 543–548.

379 Mao, X., Tian, W., Wu, J. et al. (2015). Electrochemically responsive heterogeneous catalysis for controlling reaction kinetics. *Journal of the American Chemical Society* 137 (3): 1348–1355.

380 Su, X., Bromberg, L., Tan, K.-J. et al. (2017). Electrochemically mediated reduction of nitrosamines by hemin-functionalized redox electrodes. *Environmental Science & Technology Letters* 4 (4): 161–167.

381 Bromberg, L., Ozbek, N., Tan, K.-J. et al. (2020). Iron phosphomolybdate complexes in electrocatalytic reduction of aqueous disinfection byproducts. *Chemical Engineering Journal* 408: 127354.

382 Wang, K. and Stiefel, E.I. (2001). Toward separation and purification of olefins using dithiolene complexes: an electrochemical approach. *Science* 291 (5501): 106.

383 Chaleawlert-umpon, S. and Pimpha, N. (2020). Sustainable lignin-derived hierarchically porous carbon for capacitive deionization applications. *New Journal of Chemistry* 44 (28): 12058–12067.

384 Wu, Q., Liang, D., Ma, X. et al. (2019). Chitosan-based activated carbon as economic and efficient sustainable material for capacitive deionization of low salinity water. *RSC Advances* 9 (46): 26676–26684.

385 Miller, H.A., Bouzek, K., Hnat, J. et al. (2020). Green hydrogen from anion exchange membrane water electrolysis: a review of recent developments in critical materials and operating conditions. *Sustainable Energy & Fuels* 4 (5): 2114–2133.

386 Hernández, G., Işik, M., Mantione, D. et al. (2017). Redox-active poly(ionic liquid)s as active materials for energy storage applications. *Journal of Materials Chemistry A* 5 (31): 16231–16240.

2

Green and Sustainable Extraction of High-Value Compounds: Protein from Food Supply Chain Waste

Karine Zanotti[1], Aylon Matheus Stahl[1], Mateus Lodi Segatto[1], and Vânia Gomes Zuin[1,2,3]

[1] *Department of Chemistry, Federal University of São Carlos, São Paulo, Brazil*
[2] *Green Chemistry Centre of Excellence, University of York, York, UK*
[3] *Institute of Sustainable and Environmental Chemistry, Leuphana University, Lüneburg, Germany*

2.1 Introduction

Global challenges have often been discussed within different environments in recent years and the COVID-19 outbreak has clearly shown how such issues must be dealt with through cooperation among countries. This is no different when addressing food security, access, and distribution, for instance, where global relations interplay and require complex solutions. Better distribution and pricing should be one of the primary responses to improve food access in poorer countries as changes in politics and economic dynamics may help enhance distribution. Long-distance transport contributes significantly to greenhouse gas emissions. Thus, local or regional solutions must be prioritized, and social and political factors have to be addressed and could help in enhancing the emancipation of deeply dependent economies. Another major cause of poor food access across the globe is the amount of waste and losses throughout the food supply chain (FSC), which comprises all steps related to food production for human consumption.

It is estimated that nearly one-third of the total food mass-produced is discarded as waste, totalling 1.3 billion tons yearly [1]. The level of the chain in which most of the Food Supply Chain Waste (FSCW) is generated varies among developed and developing countries. While in developed countries, waste is generated mostly at retailer and consumer levels of the FSC, developing countries show a higher loss during harvest and postharvest steps (e.g. transport and storage logistics) [2]. This large volume of FSCW can also be translated into a financial loss to agro-industrial and food companies (U$750 bi/year) [3] and a high environmental burden (4.4 bi tons of CO_2 equiv./year) [4], not to mention the high social and health impacts of the lack of accessibility to food with high nutritional quality. The environmental impact of food waste is mostly, but not uniquely, related to landfill disposal. Other factors include the embedded carbon footprint of the supply chain, land-use

Sustainable Separation Engineering: Materials, Techniques and Process Development, Volume 1, First Edition. Edited by Gyorgy Szekely and Dan Zhao.
© 2022 John Wiley & Sons Ltd. Published 2022 by John Wiley & Sons Ltd.

change, depletion of natural resources, and the use of mineral fertilizers and pesticides [5]. Whilst a large sum of this waste can be dealt with through improved logistics practices and better consumer behavior, most of it is considered to be unavoidable. The unavoidable FSCW (uFSCW) is defined as the nonedible waste from the chain, consisting mainly of fruit skin, cores, and other parts of food-related plants, as well as bones from meat industries [5]. This waste stream is responsible for most of the plant-based residues generated by humankind.

The European Green Deal (2020) [6], the recent effort made by the European Union (EU) to boost sustainable development on the continent, has at its core the "Farm to Fork" strategy, a set of policies aimed toward developing a fairer and more sustainable FSC [7]. Indeed, food is frequently at the centre of discussions regarding the future of our planet. The second of the United Nation's 17 Sustainable Development Goals (SDGs) [8], "Zero Hunger" aims at developing a better food network to increase security and access, strengthen small scale food producers to be resilient to climate change impacts, increase productivity, and develop sustainable food production systems. Besides that, the UN highlights the access to healthy, nutritionally enhanced food – a shift from current market practices that offer cheap, industrialized, and nutritionally poor food. Minimizing food waste is addressed in SDG 12, "Responsible Consumption and Production," as one of the key components to reduce the environmental impact of the FSC and to enhance food security and nutrition [8].

Another point regarding the steps necessary for humankind to achieve more sustainable use of its resources is the shift of current economic and industrial practices. Old linear-based economy, in which a product is manufactured from a limited resource, shipped, consumed, and discarded at the end of the chain, would have to be changed to a circular economy, where minimum waste is generated between the process of fabricating and consuming a good [9]. Encompassed within this change is the use of green and sustainable processes, which inherently generates less waste, but also have better energy and material efficiency. This point is currently addressed by the Green and Sustainable Chemistry movement, which aims at improving such efficiencies, as well as enhancing process security and looking into the environmental impacts of the whole process and its products. Its purpose is to have a more holistic view regarding chemistry and its systems, considering environmental, economic, and social factors [10]. A push toward an economy based on biological feedstocks, processes, and products (bioeconomy) has also been part of the discussions within this context, aiming at reducing or removing the use of nonrenewable resources and developing synergetic and energetically efficient processes [11]. Lastly, ethical factors should be considered in this new industrial environment as a way to protect local communities and ensure that no human rights are being violated in the process of making a product.

Industrial systematization based on recently developed ideas in the context of sustainable development, as presented above, culminated in the concept of biorefineries. By definition, biorefineries are chemical or biochemical platforms that convert biomass into value-added products, from biofuels to specialty chemical products [12]. Different to petrol refineries, biorefineries use natural renewable feedstock, and using high-end separation and isolation processes, are developed to obtain several compounds from the same starting material or a mixture of feedstocks. This model has been discussed as a financially viable project to incorporate FSCWs back into the economy as these are complex materials that have the potential to offer multiple products that could be used in the food, pharmaceutical, and materials

sectors [13]. It is important to notice the importance of developing green and sustainable processes and products to be applied in such biorefinery schemes, fulfilling the gaps for a sustainable industry and integrating concepts of a circular and bio-based economy [14].

All these factors combined have been naturally – and also promoted by prominent sustainable development policies – stimulating various studies that use natural products from agro-industrial and food waste in order to extract valuable compounds and create new sorts of products and ingredients that meet the requirements of a sustainable future [15]. Maina et al. (2017) have listed some of the current practices on the valorization of waste in the context of bioeconomy [16]. In this case, it is important to study and develop new methodologies to extract, isolate, determine, and process valuable compounds. Green and sustainable extractions are chemical, biochemical, or physical methodologies to extract target compounds that, by determining sustainability factors and metrics, are intrinsically less harmful to the environment and are aware of social and economic spheres. In academic production, works related to sample preparation in analytical studies are considered guidelines for future industrial processes that can be used to efficiently extract such compounds from agro-industrial residues.

Waste materials can be recycled back to the FSC and be used in a wide range of applications, either as low-cost substitutes for food ingredients, adding financial value to the FSC, as well as to enhance the nutritional value of food products [17]. Therefore, it would be possible to reduce costs and improve food quality overall, fulfilling the needs of a more sustainable FSC. Sustainability and efficiency metrics play an important role in the consolidation of food waste biorefineries, which can help highlight its importance within sustainable development practices [18]. A scheme on how circular economy is applied in FSC is shown in Figure 2.1.

In light of the facts presented above, the concepts that circulate current discussions on sustainable development and food security, including the circular economy, bioeconomy, green and sustainable chemistry, and biorefineries, are well intertwined and present interesting opportunities for research. In this context, a recent action launched in 2019 in Brazil and known as the Field & Food Tech Hub – UFSCar encompasses and materializes these objectives, aiming at bringing together initiatives regarding the design, production, distribution, consumption, and management of biomass or agro-industrial food chain residues and other appropriate materials.[1] Considering that the humanitarian goals for the reduction of avoidable food waste will be achieved, as well as to preserve new developments from competing with food growth and production, the unavoidable part of the FSC has been studied as a good candidate for valorizing residues in the FSC. The characteristics of these materials and the main challenges of implementing these industrial frameworks will be discussed next.

2.1.1 High-Value Compounds from Food Supply Chain Waste (FSCW)

The FSCW consists of a wide range of materials mostly generated upstream the FSC, i.e. at harvest, postharvest, storage, transport, and processing of agricultural and meat goods. Besides being a natural and renewable feedstock to explore, it is produced in high volumes and the cost of disposing it off has been increasing every year [13], which has recently been pressing for applications for its valorization. Since it is mostly disposed off into landfills,

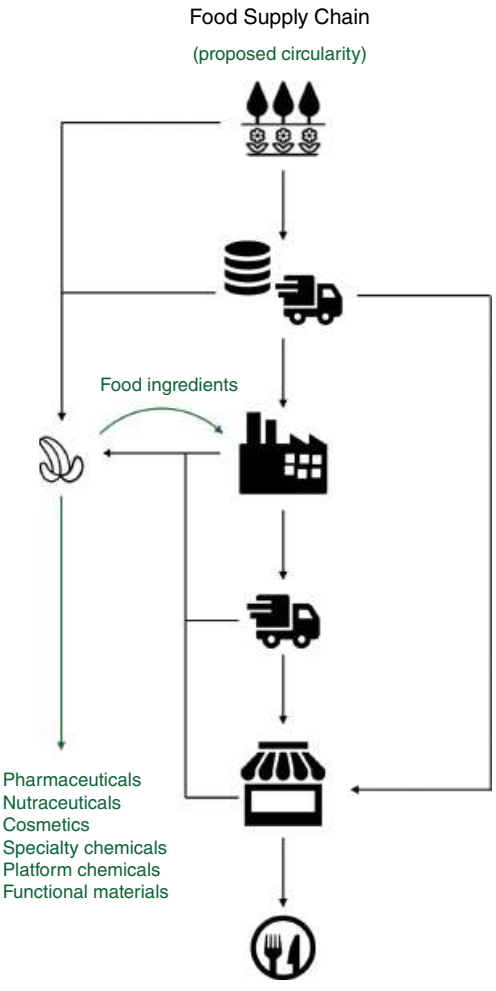

Figure 2.1 Scheme of proposed circularity in FSC applying biorefinery concepts.

the option to use it as feedstock for other processes is a good opportunity to reduce the pollutant loading of the FSC as these materials have high COD and BOD levels [19]. Additionally, as most of the uFSCW is generated between harvest and processing levels, it has improved traceability and a more homogeneous composition, when compared to end-of-chain domestic and commercial organic wastes [20], increasing its potential for valorization. The fact that it is mostly produced in agricultural and industrial complexes is also an advantage for creating integrated food-waste biorefinery industrial networks, a more economically feasible scenario due to the high costs of transportation of these often highly moisturized materials [13].

In fact, as illustrated by Cecilia et al. (2019) [19], the classification of different streams of food waste shows that organic crop residues and animal by-products (including processing wastes) demonstrate a higher potential for valorization. The main applications that develop most of the potential of such fractions are valuable component extraction and biofuel production. These applications are considered by Imbert (2017) [21] as highly valorized

practices along with the production of biogas through anaerobic digestion. This hierarchy of value for FSCW applications is shown in numbers by Tuck et al. (2012) [22], exemplifying that an average bulk chemical production has a valorization of US$1000/tonne of biomass, followed by transportation fuel (200–400), cattle feed (70–200), electricity generation (60–150), and disposal in a landfill, which has a cost of US$400/tonne of biomass. The current practice for most global FSC waste streams, although more frequent in countries with more expensive landfills, is to add some value to the waste, whether using it for generating electricity, land spreading, or animal feed.

Developing new processes and products for extraction, separation, and chemical or biochemical conversion of biomass is, therefore, the main strategy to valorize waste streams in the FSC. The seasonal fluctuation of feedstock volumes and the chemical composition of agricultural streams poses one of the main challenges for valorizing uFSCWs. Developing flexible processes and equipment, which receive and treat different feedstocks throughout the year, is a promising approach to solve this issue. As mentioned above, the high amount of moisture content in these materials increases the cost of transportation and usually concludes that on-site processing is more financially feasible than transporting the residue to other locations. Technological constraints also limit the progress of uFSCW-processing factories that require high-end technologies to separate valuable compounds from complex materials. Legislation and market acceptance of new products may also impose barriers and must be dealt with by having in-depth discussions and market development.

Plant and animal metabolites are the main focus of studies regarding the use of uFSCW as they are compounds that are biosynthesized by the living organisms where they are found, consequently found in the unused fraction of the food chain that is discarded. Primary metabolites are the substances that are essential to an organism's growth, development, and reproduction, accounting for the major fraction of the total mass. The main compounds encompassed in this class are proteins, lipids, carbohydrates, and other biopolymers, such as lignin. Since this is a broad classification, the different groups of materials encompassed in primary metabolites will be discussed separately, according to the current interest in their valorization within the FSC residues. Secondary metabolites, instead, are substances found in much lower concentrations in organisms, and are responsible for defence, color, smell, and other natural mechanisms. Although found in small fractions, they represent a very wide number of compounds, and their bioactivity and other special features make them a valuable asset that can increase financial feasibility in FSCW biorefineries.

Figure 2.2 shows metabolite classes that could be obtained from FSCW and its applications. As can be seen, the possibilities of extracting high-value compounds are complementary, thus reinforcing the role of biorefinery. The main groups of substances that are considered to increase value in the FSC will be discussed in the next section, including their concepts, singularities, and examples.

2.1.1.1 Secondary Metabolites

Secondary metabolites are a diverse class of organic chemical compounds of low molecular weight synthesized by plants that present biological activity (or bioactivity). While primary metabolites have structural and energy storage functions, secondary metabolites play a very important role in plants' ecological functions. Different from what the term "secondary" may suggest, these compounds are not secondary in chemical grounds as all-natural

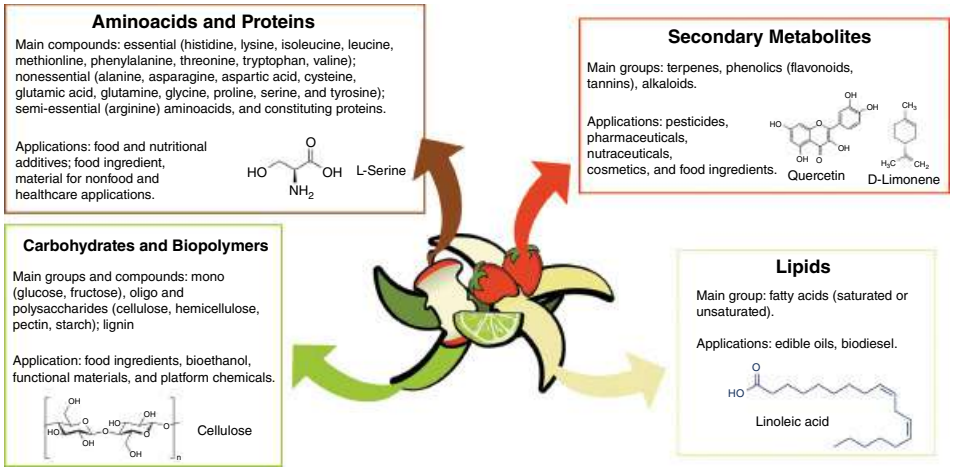

Figure 2.2 The main groups of compounds obtainable from FSCW, its applications, and a few examples.

products produced by plants have some survival value to the plant. They are key components of active and potent defence mechanisms of plants and are essential for plant survival in stressful environments, protecting plants against herbivores, pests, and pathogens through deterrence, toxicity, or acting as precursors of physical defence systems, besides making a major contribution to the smell, taste, and color of plants, serving as an attraction for pollinators. Secondary metabolites can be divided into three chemically distinct groups: terpenes, phenolic compounds, and nitrogen compounds.

Terpenes are a large group of compounds and, despite their diversity, they have a simple unifying feature referred to as the isoprene rule, which describes that all terpenes have fundamental repeating five-carbon isoprene units. The function of terpenes in plants is generally considered to be both ecological and physiological. Many of them are known because of their resistance to various insect pests and pathogens, containing insecticidal action and inhibiting the growth of competing plants. The insecticidal activity of terpenes is due to their deterrent action, in the release of toxins, or as modifiers of insect development. Others are known to attract insect pollinators. Both in attraction (limonene and menthol, for example) and repulsion of insects (pyrethroids and natural insecticides), the smell is an important feature for terpenes, and they have been valued for their presence in essential oils and their use as fragrances. Moreover, they are a source of rubber and medicines to treat cancer [23].

Phenolic compounds represent a structurally diverse group of secondary metabolites, including metabolites derived from the condensation of acetate units; produced by the modification of aromatic amino acids; flavonoids; isoflavonoids; and tannins [24]. Among the main functions that phenolics play in plants are their action as a deterrent for herbivores (insects and birds) and enzyme inhibitors. They also play an important role in resistance against fungal infection, bacteria, and nematodes by direct toxic effects or active and rapid deposition of barriers, in addition to providing defence against freeze/thaw, nutrient deprivation, and dehydration. In the case of flavonoids,

they also act as a defence against oxygen radicals generated during photosynthesis and ultraviolet (UV)-B light and are also recognized due to health-enhancing effects such as antioxidant, anti-inflammatory, antiallergic, hepatoprotective, antithrombotic, antiviral, and anticarcinogenic ones [23]. Berries are an example of an excellent source of flavonoids among fruits – blueberries, bilberries, huckleberries, cranberries, and lingonberries.

Nitrogen compounds or alkaloids are basic compounds synthesized from plants of different groups, pharmacologically active and derived from amino acids that contain one or more heterocyclic nitrogen atoms. This class of compounds is known for the presence of substances that have a marked effect on the nervous system and its main uses are in the form of plant extracts for poisons, narcotics, stimulants, and medicines. Therefore, many of the drugs taken today are based on alkaloids. Some examples are caffeine, nicotine, cocaine, and morphine.

Human interest in secondary metabolites is mainly due to their potential use for medicinal purposes. The ecological self-defence functions of plants reflect these same effects on humans. For example, the secondary metabolites that act in the defence of microbial pathogens through cytotoxicity can be useful as antimicrobial medicines in humans (if they are not too toxic); those involved in defence against herbivores through neurotoxic activity may have antidepressants, sedatives, muscle relaxants, or anaesthetic effects through their action on our central nervous system; flavonoids protect humans against oxygen radicals and destructive agents and processes the same way they act in plants [23]. The extraction of bioactive secondary metabolites from FSCW has been extensively explored over the last decade, either targeting their potential use by pharmaceutical and nutraceutical use or as part of the composition of cosmetics and processed food products [17, 25–30]. New markets such as cosmeceuticals, i.e. cosmetics that use natural compounds with active properties, have boosted the demand for natural ingredients in the cosmetic and beauty industries. Biodegradable packaging films embedded with bioactive compounds can use food waste-derived secondary metabolites in order to have better storage for fresh food and help avoid food waste downstream of the FSC [31]. The development of methodologies to the efficient and sustainable separation of these fractions from FSCW [32–35] has been seen as a viable approach to biorefineries and may help achieve more sustainable production, either to manufacture specialty chemicals for other industries or to use such compounds incorporated in the same food chain [15].

2.1.1.2 Lipids

Lipids are generally defined as biomolecules insoluble in water and soluble in nonpolar solvents. Fatty acids are the simplest lipids – made up of a polar hydrophilic head region connected to a long hydrophobic tail – and their derivatives can be acylglycerol esters, wax esters, or alcohols such as sterols. Up to 99% of lipids in plant and animal material consist of such esters, also referred to as fats and oils [36]. Many lipids are used for plants for energy storage in fruits and seeds, as in fats and oils found in avocados, olives, soybeans, sunflower seeds, and peanuts.

Some fats, such as linoleic acid and α-linolenic acid have protective properties and are the second main cardioprotective nutrient. These are referred to as essential fatty acids and, as the name implies, they play an essential role in human nutrition. Their main functions

in human physiology are the formation of healthy cell membranes and their importance in the proper development and functioning of the brain and the nervous system – studies suggest that a diet with an ideal balance of these fats can delay the onset of neurodegenerative diseases, such as Parkinson's and Alzheimer's disease [23]. Good examples of where to find linoleic acid are seeds, nuts, grains, and legumes, while α-linolenic acid can be found in the green leaves of plants, including phytoplankton and algae, and in flax and canola seeds, nuts, and soybeans.

Considering food and agricultural wastes, the main use of lipids involves the conversion of fatty acids into biodiesel through transesterification, especially using used cooking oils [37]. Besides that, oil extracted from fruit and vegetable seeds contained in food-processing wastes often contain a higher phenolic content and can be used as nutritionally enhanced ingredients for food and cosmetic applications [29]. Promising examples include mango seed fats [38], which can even be used as an alternative to cocoa butter, citrus seed oil [39], coconut solid fats [40], passion fruit seed oil [41], and many others [42].

2.1.1.3 Carbohydrates

This is the most abundant class of organic compounds found in plants. Carbohydrates, popularly known as sugars, are primary sources of energy for plants. They are produced from photosynthesis – a process in which carbon dioxide is reduced in the presence of light and chlorophyll. The energy that carbohydrates provide is stored as starch or fructan, used as sucrose and polymerized to form cellulose. Carbohydrates also combine to form glycosides of many fundamental groups of natural products, including terpenes, phenols, and alkaloids. Depending on the size of their chain, carbohydrates can be divided into three groups: monosaccharides, oligosaccharides, and polysaccharides.

Monosaccharides are the simplest carbohydrate group, and glucose and fructose are part of it. Corn syrup consisting mainly of glucose – obtained from the hydrolysis of corn starch – is widely used in many commercial products. Fructose is also used for this purpose, especially in the food industry. It is largely present, for example, in the manufacturing of soft drinks, through an enzymatic process that converts about half of the glucose in corn syrup into fructose, forming a very sweet corn sweetener [23]. Oligosaccharides or disaccharides are formed by the condensation of a pair of monosaccharides and one of the best known is sucrose. It is the sweetest of the disaccharides and is extensively used for commercial purposes. Polysaccharides are compounds of high molecular weight and it is the carbohydrate class that is mostly found in plants. The most abundant organic material on the planet is cellulose, a polysaccharide that has a structural function in the cell walls of plants and is the major component of wood. Its main use is in papermaking from the chemical treatment of wood pulp.

While cellulose is mostly derived from glucose, hemicellulose, another abundant polysaccharide, is composed of many different sugar monomers. A branched polymeric structure allows hemicellulose to bind in cell walls between cellulose and pectin, another structural polysaccharide that constitutes the composition of plants. Although not a carbohydrate, lignin is a biopolymer often found in association with cellulose and hemicellulose, and it is commonly discussed together with the polysaccharides as the main materials found in plants, and, consequently, in agro-industrial residues.

The main feedstocks for biotechnological conversion to alcohols, carbohydrates found in FSCW are often used to produce bioethanol, especially fractions that are rich in glucose and edible sugars [43]. Polysaccharides with higher complexity, such as starch, cellulose, and lignin, are required to have extensive pretreatments prior to fermentation, and residues richer in those fractions have been extensively explored in second-generation bioethanol production [44]. Carbohydrates can be isolated from food residues to serve a wide range of applications, from ingredients for food to specialty chemicals, passing through functional materials and building blocks to produce a series of chemical compounds [13, 20].

2.1.1.4 Proteins

Proteins are the primary constituents of living things. Much of the genetic information that each plant and animal cell has is expressed in the form of proteins – not just one type, but several thousand. Proteins are compounds that often have high molecular weight and are made individually from large chains of amino acids – the sequence of amino acids and their content determines the biological activity of a specific protein. Smaller proteins (made up of short chains of amino acids) are called peptides. Amino acids, as the name suggests, are organic compounds that contain both carboxyl and amino functional groups. They play an important role in living cells, not only as building blocks of proteins, but also as intermediates in the metabolism.

Human bodies can use all the amino acids obtained from food to synthesize new proteins. There are nine amino acids considered essential for living beings that are not produced by their organism but must be present in their diet. They are: histidine, lysine, isoleucine, leucine, methionine, phenylalanine, threonine, tryptophan, and valine [23, 45]. On the other hand, there are amino acids that do not need to be provided by the diet as they can be synthesized from other amino acids in the body. They are: alanine, asparagine, aspartic acid, cysteine, glutamic acid, glutamine, glycine, proline, serine, and tyrosine [45]. In addition, there are amino acids that are considered semi-essential, such as arginine, because it is essential for babies, who are unable to synthesize it, but are not essential for adults, as they are able to synthesize it in other ways. The same occurs with glutamine, which is fundamental only in very stressful conditions, such as very intense exercise, infectious diseases, surgery, burns, or any other acute trauma.

Due to the flexible nature of proteins, they can change between several different structures in the performance of their biological function. These structures are called conformational changes and are classified as primary, secondary, tertiary, and quaternary structures. The primary one is the simplest structure, consisting of the sequence of amino acids. The secondary one considers the folding of the protein, which may result in structures that resemble leaves or helices. The tertiary structure corresponds to the general shape of a single protein molecule and is the result of the previous conformations. The quaternary refers to the shape or structure that results from the union of more than one protein molecule. A simplified version of these structures is represented in Figure 2.3. In addition, there is a fifth form, called post-translational modification, which corresponds to the addition of other chemical groups to the protein, varying according to their interactions with other molecules within the cell that leads many proteins to their final cellular function.

Proteins perform several fundamental functions in living organisms. They form a large part of the structure of cells and tissues. Some proteins channel a huge variety of reactions

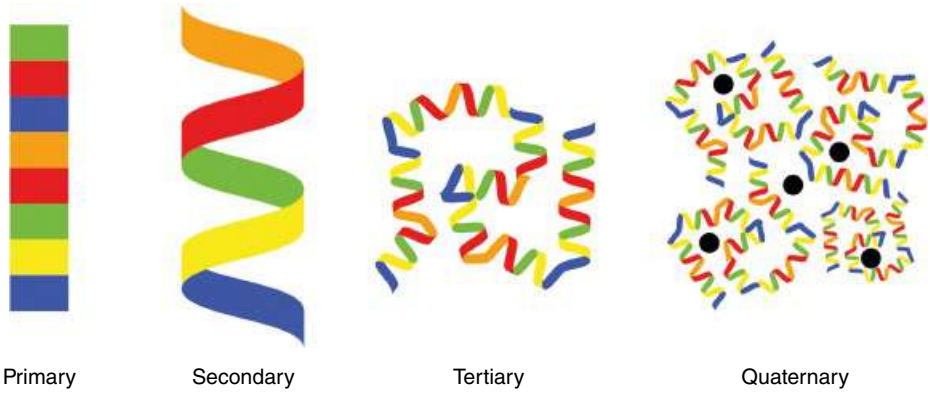

Figure 2.3 The four protein structures.

in metabolism into essential pathways through enzymes, the natural catalysts – to make compounds as those discussed earlier, such as sugars, waxes, lignin, starch, pigments, or alkaloids, plants use specific enzymes for each reaction. Other proteins act as receptors for molecules, changing their conformation when they come into contact with these specific molecules. Some proteins, referred to as seed storage protein, act as an energy reserve for the cell, and are synthesized and stored in seed and fruit cells during fruit ripening – the main storage proteins in soybeans are glycolines and in rice are prolamine, albumin, globulin, and glutelin [23].

Proteins have immense importance for the proper functioning of all living organisms. Their role in human health and nutrition and in the economy will be presented in the next section, considering the problems related to their deficiency, their significance in the food chain and the current state of the global protein market. Further on, ways to obtain proteins from the uFSCW will also be discussed as a way of adding value to them, redirecting the linearity of the food production and consumption chain.

2.1.2 Proteins: Importance, Market, and Alternative Sources

As mentioned earlier, proteins play a central role in sustaining structural and regulatory functions in the body and are necessary for its growth and development. Muscles and organs are largely made of proteins; they are an essential constituent of certain hormones; fundamental for body maintenance and the repair and replacement of worn-out or damaged tissues; and also important to produce metabolic and digestive enzymes [45].

As they are essential nutrients for a healthy metabolism, the interest in protein consumption has been consistently growing in recent years. Proteins are conventionally found in animals (meat and milk) and plant-based foods, but as the world's population increases at a fast pace, food, water, and land resources are becoming scarce due to an unbalanced relationship with natural resources [46]. Considering the food challenge, together with our obligation to find new ways to survive in a sustainable way, it is of great interest to find alternative ways to provide the protein required to meet human nutritional needs. Therefore, the market of proteins from different sources, including waste, could be an

alternative and has a huge potential to meet this need, and is advantageous to extract proteins from residues that already exist instead of increasing crops and livestock to do so, as the problem we face today is not necessarily a lack of food, but a matter of efficiency – as mentioned before when discussing the food waste scenario.

Despite the wastage that has accompanied our food consumption chain model, in 2008, the World Bank estimated that there were 967 million malnourished people in the world and most of them lived on a monocarbohydrate diet (e.g. maize or rice) and lacked the required protein consumption, as well as fat, vitamin A, iodine, zinc, and iron [46]. Studies have reported that most of the weaning foods consumed by children from developing countries are deficient in essential macronutrients and micronutrients [45]. More recently, in 2015, hunger began to rise in the world and malnutrition emerged as a growing concern [47].

Food insecurity is largely responsible for this scenario. Millions of people worldwide, especially children and those from developing countries, suffer the effects of the disruption of food intake or eating patterns due to a lack of financial resources. All these cases lead to an energy-protein deficiency owing to the non-ingestion in adequate amounts of the smaller molecules which constitute proteins and amino acids. Consequences range in severity from fatigue, insulin resistance, hair loss, and loss of hair pigment, cracking of the skin, loss of muscle mass, low body temperature, low immunity, growth failure – resulting in low weight and short stature –, hormonal irregularities, weakening of the heart, respiratory system problems, and even death [23, 46].

The characteristics of even a small and relatively simple protein are a composite of the properties of the amino acids which comprise the protein. That is why each amino acid within a protein is unique and irreplaceable. The nutritional quality of food proteins is determined largely by their composition of amino acids, ratios of essential amino acids, and susceptibility to hydrolysis during digestion. Once the failure to obtain enough of one of the nine essential amino acids has serious health implications, an adequate diet must contain all of them [45]. Among the ways of obtaining essential amino acids, in the first place is the intake of meat, and occupying a secondary position is the consumption of cereal grains and legumes as an alternative source of protein.

It is clear that the match between dietary supply and human protein needs is vital to support the health and well-being of human populations. Equally important is how this protein gets from the field to the table considering sustainable socio-environmental aspects, resulting in an expandable protein market, in which alternative sources have been growing considerably. Without these concerns and constant innovations, the world risks failing to meet the United Nations' SDGs, especially number 2 "Zero Hunger," and today's children will have to deal with a planet where much of the population will suffer from malnutrition and preventable diseases.

2.1.2.1 Plant-based Protein Market

The scenario of alternative proteins says a lot about current consumption models, as well as future challenges and aspirations. Paralleling to the conventional animal protein market, the growth rate of alternative proteins from plants in contrast to meat is completely secondary as the market base for alternative protein is approximately US$2.2 billion compared to a global meat market of approximately US$1.7 trillion [48]. Considering that the current protein demand for the 7.3 billion inhabitants of the world is approximately

202 million tonnes globally [49] and that the global demand for protein ingredients is expected to reach approximately 6.8 million tons by 2025, which corresponds to US$50 billion [50], alternative proteins have room to grow in the market and in people's awareness. However, it still competes mildly with a conventional model that needs to be rethought considering socio-environmental issues.

The challenge will be to feed a future population of 10 billion people in 2050 [51] with a healthy and sustainable diet within planetary boundaries. Reaching this goal means reconceiving the current supply system to an equally sustainable food system. This transformation to healthy and sustainable diets by 2050 will require substantial dietary changes: the overall consumption of fruits, vegetables, nuts, and legumes will have to double, and the consumption of foods such as red meat and sugar will have to be reduced by more than 50% [51]. These strategies are at the top of the list published by the Eat-Lancet Commission to achieve the sustainable food system goal as a diet rich in plant-based foods and with fewer animal source foods confers both improved health and environmental benefits, achieving not only many of the United Nations' SDGs, but also contributing to the Paris Agreement as the world has been severely degraded by the current practices used in the FSC.

High expectations fall on alternative sources of protein. As part of these sources, plant-based proteins are derived from plants such as soybean, wheat, nuts, pea, lentil, peanuts, seeds, potato, rice, and others. They are a highly nutritive source, containing fiber, vitamins, minerals, and essential amino acids. These products tend to be lower in calories and fat than animal proteins and higher in fiber and essential nutrients [46].

The interest in plant-based proteins grew gradually until 2007 and accelerated over the past decade [48]. Increasing consumers' preference for plant-based food and beverages and for the adoption of a vegan diet is one of the major factors expected to drive the growth of the plant-based protein market across the globe, besides concerns about lactose intolerance and glutamic disorders. The number of consumers who self-declare themselves as vegan has increased in many industrialized countries, such as the United States, where it grew from 1 to 6% between 2014 and 2017, a very significant increase [48, 49]. These preferences are due to health concerns, including the risks of type 2 diabetes and cardiovascular diseases related to the consumption of meat products; animal protein allergies – 90% of food allergy is caused by eggs, milk, fish, red meat, soy, and nuts [49] –; environmental concerns, and animal welfare.

North America is expected to dominate the global plant-based protein market owing to the increasing awareness of healthy food ingredients and the trend of weight management among consumers. Europe is the second-largest region in the global plant-based protein market due to the increasing demand for healthy and nutritional products, as well as health and wellness trends. The global alternative protein market was valued at US$16.45 billion in 2018, the same year that sales of plant-based foods increased by 17%, and it is expected to reach US$40.53 billion by 2025 [49].

However, the inconsistent plant raw material price is a factor that may hamper the growth of the alternative protein market. Although the commercialization of soy protein dominates sales, remarkable growth in the consumption of proteins is already being observed from different plant sources. Proteins from pulses (peas, chickpeas, lentils, and beans), potatoes, rice, corn, oats, algae, and ancient grains are gaining traction [50,

52] – while concerns over allergenic and estrogenic effects from the soybean reduced its consumption slightly, the interest in pea protein, for example, grew at a compound annual growth rate of 30% from 2004 to 2019 [48]. These new sources linked to the global increase in consumer interest in nonmeat-based products can provide various opportunities for the further spread of the plant-based protein market.

The diversity of feedstock options of this market shows its versatility, demonstrating the vastness of the plant-based protein marketplace. However, the question is: how many new possibilities can arise by obtaining proteins from other sources, more specifically the alternative sources discussed above? Considering the uFSCW, there is a potential extensive source of proteins with no significant use that can be very well utilized considering its reintroduction into the FSC in a circular way. There are many challenges that should be faced, such as motivation to achieve a more sustainable future in the FSC toward what addresses SDG 12, "Responsible Consumption and Production," such as replacing chemical ingredients with functional proteins, enhancing the nutritional value of food products; making these novel products more affordable; and finding a unique and competitive place in the market. Therefore, proteins from uFSCW can become potential substitutes for current sources [17]. The different sources of residues from food-processing streams will be discussed next, exploring their potential uses as a protein source, availability, and possibilities.

2.1.2.2 Unavoidable Food Supply Chain Waste (FSCW) as a Protein Source

Many of the products offered by the chemical industry are still derived from petroleum. However, the increasing financial and environmental costs of oil have led to alternative routes for manufacturing chemicals, fuels, and solvents, for example. The key point of this route is to use residual biomass. Several studies have focused on the insertion of this residual biomass – uFSCW, by-products of current agro-industrial, and food-processing flows – as a raw material for obtaining various classes of chemicals [22]. The interest in recovering proteins from these residues has grown for different purposes in several areas of the industry [53] – protein-containing by-products have become increasingly abundant due to the growth of the biodiesel and bioethanol markets, for example. Among the varied uses for extracted proteins from agro-industrial and food-processing stream residues, they could be reutilized not only as nutrients for food and dietary supplements, but also as techno-functional food ingredients due to their emulsifying, gelling, foaming, and water-binding properties; as a biopolymer development material for a variety of food, nonfood, and healthcare products; and for other biorefinery purposes [54].

Some products have been on the market for a long time, such as whey and soy protein, which will be explained next. After being extracted, they are commercialized as proteins in different types: isolated, concentrated, hydrolyzed, and flour. The usual classification occurs through the percentage of protein that each one contains: protein flours contain up to 65% of proteins, protein concentrates contain up to 65–90%, isolates contain more than 90%, and hydrolyzed proteins can contain 95% of proteins, which may be more digestible than native proteins due to the unfolding of the protein structure [54]. Among this categorization, proteins could be derived from animals or plants.

Regarding animal proteins, the main source of hydrolyzed, isolated, or concentrated commercialized protein is whey – the most well-established product of separated protein from

animal sources on the market. Whey protein is a by-product of cheese manufacturing. In rural dairies, milk is taken to a manufacturing and processing centre. During the process of making cheese, enzymes are added to the milk, separating it into its constituent parts: the solid part, called curd, that consists of casein and lipids – used in the production of the cheese, and the liquid fraction that contains whey proteins, carbohydrates (lactose), and fats [55]. Then, the whey is pasteurized and dried, resulting in a powder with several purposes.

Among the main uses of whey protein are the improvement in physical and mental quality, nutritional supplementation, the prevention of hypersensitivity conditions in newborn children, weight reduction in individuals with HIV, and prevention of cancer agents, besides the advantages such as lactose intolerance, gluten-free, and simplicity of conveying. It is also used in novel aesthetics and beauty items such as face care rest patches, eye cover gel, against wrinkle whey protein patches, hostile to maturing facial veil, whey protein brow veil, and hair fall and hair development cleanser. An increase in livestock has also attracted interest in terms of animal protein, as well as interest in human nutrition and health. In addition to the interest in nutrition and human health, the increase in livestock is also driving the interest in animal protein [56]. The size of the global whey protein market has been estimated at US$7.4 billion and the development of awareness about the advantages of consuming this product is expected to boost the market even more from 2020 to 2025 [56].

Another residue from animal sources used for protein production comes from the production of shrimp meat, as a considerable amount of protein contained in this residue is used in animal feed. However, this waste could be used to a more valuable end as a raw material to produce basic organic compounds. For example, essential amino acids could be used for animal feed purposes and nonessential amino acids, such as chemical feedstocks [22]. The main coproduct in poultry production is feathers, another feedstock that could be considered to produce protein, generated mainly in poultry slaughterhouses. About 15 billion tonnes of chicken feathers are produced per year globally [57]. Similarly to the residues generated in shrimp meat production, feathers have been used as animal feed, although in small quantities. The problem is that most of them go to landfills, causing problematic environmental issues of waste disposal. The feathers are composed of more than 90% of keratin [53] – rigid and fibrous protein also found in hair, skin, hooves, and nails. Globally, chicken feather residues are the most abundant and sustainable keratinous material in nature that have not yet been used properly [57] and may have the potential to be used in a more valuable way. Some specific properties that keratin has, its availability and low cost, make chicken feathers an excellent option for several applications for materials that require good tensile strength and elasticity, as they can be used to produce film, fibers, hydrogels, blinders, particles for cosmetics, medicines, textiles, composites, and other industrial uses [57, 58].

Despite this scenario that shows great whey adhesion by consumers and several opportunities for new products from residues from animal protein sources, consumers' opinions about protein sources are gradually changing. A study carried out in 2018 revealed that 74% of the people interviewed classified proteins from animal sources as healthy, whereas for proteins from plant sources, the percentage was 82% [48].

Regarding plant-based proteins, only those originating from soybean and rapeseed or canola are commercialized as isolated or concentrated, unlike the different types of protein

flours which are widely marketed [54], which means that soybean still dominates this market. Soybean protein is produced from the remaining solid obtained through soy oil extraction, which is dried and cooled to be commercialized later. However, only 2% of waste from soy grain processing is destined for human consumption, while the main use is for feeding cattle and other livestock [59]. Although most soybean protein is not used for human consumption, many studies have begun to emerge showing other alternatives to extract protein from biomass. The food and beverage industry, for example, generates a large amount of protein-containing by-products, such as distiller's grains (from maize or wheat), vinasse (from sugar, beet, or sugarcane), fish silage, cakes (from oil seeds like rapeseed or palm), materials from coffee and tea processing, by-products from the production of biofuels, among other agricultural residues from various crops [22, 53].

These examples are just some of the possibilities for recovery and reinsertion of the huge amounts of animal and vegetable waste that the planet receives each year. Their uses are the most diverse, and especially among those that are already on the market, range from alternatives to conventional food – processed meat, poultry, seafood, bakery products, dairy alternatives, protein beverages –, new products aimed at aesthetics, and primarily for sports nutrition and nutritional supplements. There are two target audiences very focused on these last uses, respectively: athletes who have difficulty in reaching their daily protein goals as they need more than the recommended daily protein dose; and the elderly, although supplements are not yet expressively used by this age group, because a greater amount of protein to maintain muscle mass is needed as these people age, while consuming it naturally, as food, is reduced because this population´s taste buds start developing a taste for sweet food [60].

The growing availability of agro-industrial by-products paves the way for developing novel sustainable extraction technologies. Since biomass waste is a complex and variable mixture of molecules, separation becomes a key issue, fundamental for the conversion of biomass into new biomaterials. Following the sustainability line, more than reuse waste in a circular way, the techniques applied to deal with these residues must also be consistent with sustainability factors. The extraction methods must present efficiency, low energy consumption, nontoxic reagents, among other variables that ensure an environmentally friendly model from the beginning to the end.

2.2 Protein Extraction Methods from Waste: Current Trends and Perspectives

A crucial step for efficient protein extraction from most biomasses is cell lysis. It consists of cell disruption caused by chemical, physical, or biochemical processes, that results in the release of intracellular content to the extraction media. Any of the procedures for the concentration and isolation of proteins depends on successful cell lysis [61]. Although there are many different methods, most conditions for protein extraction vary according to cell structures, protein location, solubility, target protein denaturation parameters, if this is the case and using the protein after obtaining it. This means an extraction procedure must be specific for each type of biomass [53].

Generally, two classifications of extraction techniques are used: wet basis or dry basis, according to the physical state of the media; or chemical, physical, or biochemical,

according to the cell disruption methodology [62]. Recently, novel technologies have been used for protein extraction, overall, for their improved efficiency compared with traditional extraction methods. Therefore, a new way of categorizing these methodologies consists of observing whether the techniques are conventional or are new technologies for the purpose discussed. These classes can outline differences and similarities among extraction methods and help green and sustainable chemistry discussions based on detailed comparisons between the options, in order to provide guidance for a more environmentally aware decision. A scheme of this classification is shown in Figure 2.4.

Some additional examples of technologies – novel and traditional ones – and their mechanisms for cell disruption are discussed in the next sections.

2.2.1 Conventional Extraction Technologies

2.2.1.1 pH Extraction – Alkaline or Acid Extractions

Alkaline or acid extractions are cell lysis techniques that are commonly followed by a recovery step, both accomplished by pH shift of the media. One example of it is the isoelectric precipitation procedure that consists of adding an alkaline aqueous solution to biomass samples, which helps the solubilization of cell membranes due to interactions between them and OH- ions, hence weakening the intermolecular interactions and resulting in a higher permeability of the cells. The basic media also increases the net charge of the amino acids by favoring the deprotonated form of carboxylic acid groups, thus intensifying their interaction with water. Acid solutions, following an analogous rationalization, could also be used for the lysis step [62]. Afterward, the liquid phase is separated from the mixture and then pH is shifted to the proteins' isoelectric point – in which the net charge of amino acids is zero, or both amino and carboxylic groups are in ionic form –, thus reducing the

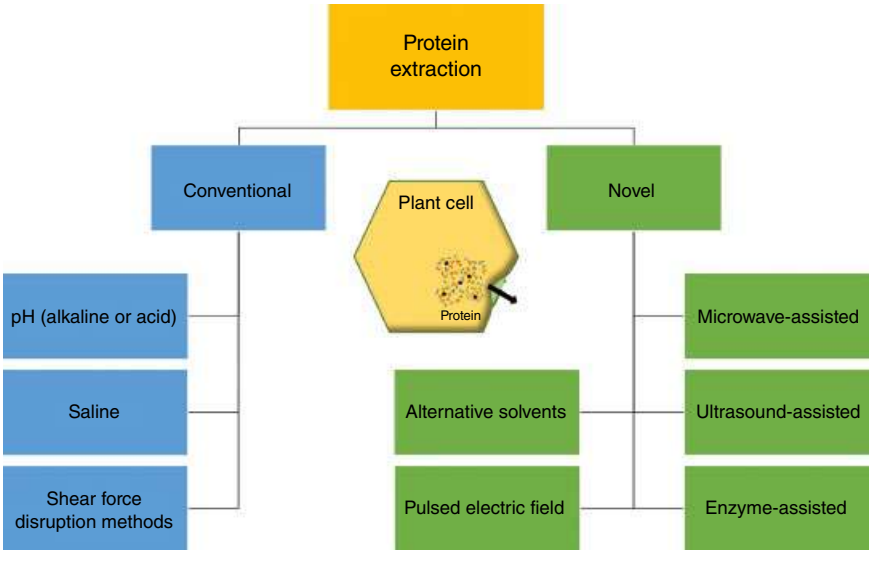

Figure 2.4 Cell disruption method classification: conventional and novel technologies.

water solubility and causing precipitation of these compounds, and recovering them from the solid phase [63]. The efficiency of cell lysis depends on the interaction between cell and extraction media, a slow process that takes about 6–12 hours to be completed [62]. To accelerate this event, it is common to combine the procedure with temperatures above RT. As a downside, proteins may lose their structure due to the same interactions occurring for cell solubilization, and also some amino acids can be converted into others, therefore changing the protein structure entirely which can alter their quality and safety for human uses. For isoelectric precipitation, bases such as NaOH and KOH and acids such as HCl are used as pH shift agents, all of which are considered green substances [64], although, in the context, they are not recoverable by simple processes. A large number of reactants and solvents used in this technique is also a point for improvement. Proteins were extracted from *Ulva lactuca* algae [65], grass pea [66], and Yellowfin tuna [67] using the isoelectric precipitation procedure with some modifications.

2.2.1.2 Saline Extraction

This method relates to the inner osmotic pressure of cells to cause cell lysis by quick changes in the ionic strength of the extraction media. Adding salt to a pure water and biomass mixture may cause cell rupture due to rapid water movement into the cell to reach osmotic equilibrium. This phenomenon can also happen in the reverse direction, starting from a high ionic strength biomass solution followed by dilution of the media [68]. Cell walls and other mechanisms of natural resistance to this event lead to low efficiency of cell lysis. Therefore, the procedure is not likely to be applied alone but in combination with others [69]. Low ionic strength media raises the solubility of the proteins in water by interacting with their polar surface, consequently increasing water–protein interaction, an event called salting-in. For further recovery of the protein, more salt is added to the mixture, and water–ion interactions cause proteins to be removed from the solution by favoring the protein–protein interactions, which results in their precipitation, a procedure named salting-out [70, 71]. Although it is inexpensive, easily scalable and of green chemistry interest, salt-based procedures, as described, demand salt recovery/clean-up steps in subsequent downstream processes. This method has been recently applied to algae protein [72, 73] and larvae protein [74] recovery, combined with other techniques.

2.2.1.3 Shear Force Disruption – Bead Mills and High-pressure Homogenizer

Shear force disruption consists of a mechanical method of destroying cell membranes and walls through collision forces, high pressure, or liquid flow. Despite the existence of innovative technologies that are based on similar concepts, in this topic, we focus on two of the most used laboratory and industrial scales techniques, bead milling and high-pressure homogenization [62]. In the first, a sample suspension is submitted to rapid agitation with metal, glass, or ceramic beads. The impact of the beads is sufficient for breaking the cells and dispersing their content to the media. Some parameters such as size, density, and sample–to–liquid ratio are relevant. In spite of being very effective on cell lysis, the method ends up generating heat, which could denature the proteins being studied [75]. Due to the heat generation, energy efficiency is low and extraction time is affected by equipment-cooling down periods. Another downside is the fact that a harsh cell break leads to much more complex mixtures, implicating separation and recovery issues [76]. One recent

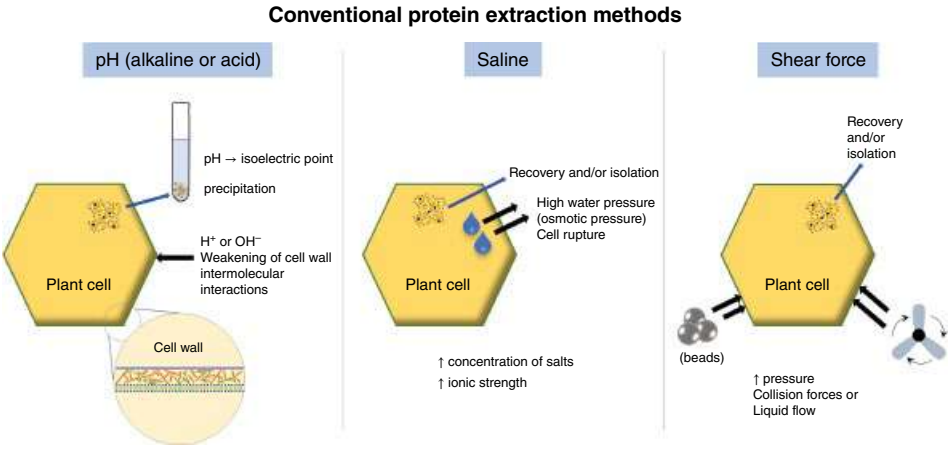

Figure 2.5 Conventional extraction method mechanisms.

example of its use is protein extraction from invertebrates [77]. The other method, high-pressure homogenization, is a technique that relies on pressure variance. Sample biomass suspension is forced to pass through a small orifice in the high-pressure homogenizer, which results in high turbulence and strong shear forces, due to depressurization that occurs when the sample passes through. It is a technique that has similar issues to bead milling, such as generating complex mixtures and residual heat [62, 76]. It is also less replicable and more costly due to specific equipment requirements. The protein structure may also change due to high pressure on cells, affecting its activity. Peanut [78] and cyanobacteria [79] protein extraction are examples of using the high-pressure homogenization method.

Figure 2.5 summarizes the mechanism of the techniques discussed in this section.

2.2.2 Novel Extraction Technologies

2.2.2.1 Microwave-assisted Extraction

Microwave-assisted extraction is a physical method of cell disruption that consists of submitting samples to microwaves, electromagnetic radiation with wavelengths ranging from 1 mm to 1 m. The energy contained in these waves is absorbed by polar molecules inside the cells, which lead to an increase in temperature and water evaporation, therefore raising internal pressure and causing cell disruption. Accompanied with this phenomenon, microwaves also weaken the cell wall and membranes by bond disruption, favoring solvent penetration [80]. Irradiation power plays a significant role in proteins and other biomolecule extraction yields. Even being considered energetically efficient for compound extraction due to uniform heating (heat flow from inside to outside of sample cells), the high amount of energy generated by the process may cause degradation in proteins [81]. From a green chemistry perspective, less solvent consumption and time are needed for microwave-assisted extraction than for some of the conventional methods, which are indicators of a cleaner extraction. From a sustainable chemistry view, it should be mentioned that it is relatively expensive if compared with chemical-based lysis processes, alongside the fact

that it is a scalable method for industrial production [80]. Despite this fact, the referred extraction technique is widely studied in protein extraction of different biological matrices, such as soy [82], coffee silverskin [83], and algae [84].

2.2.2.2 Ultrasound-assisted Extraction

Consisting of another physical radiation technique, the ultrasound-assisted extraction principle occurs by submitting sample cells to ultrasonic waves – mechanical waves with frequencies ranging from 20 kHz to 10 MHz. It is a versatile method considering its application as it could be used in low ultrasonic frequency and high-power input or high frequency and low power; the first presents a cell-destructive condition, and thus fits an extraction end, and the latter presents mild conditions for protein and other labile-compound extraction [85]. Ultrasonic waves travel through the extraction media, inducing regions of alternating compression and rarefaction on medium molecules. The rarefaction cycle eventually surpasses the attractive forces of the liquid and forms cavitation bubbles, which become larger as more cycles occur, until a critical size when they collapse and produce shock waves in small local spots that raise both temperature and pressure to extreme levels (5000 K and 1000 atm). Medium molecules near the implosion are sent at high speed to cell surfaces, finally causing cell disruption and release of their inner content [85, 86]. The technique is considered to be of high reproducibility, cheap, low-solvent consuming, industrially scalable and time-efficient, and is suitable for sustainable and green chemistry guidelines [87, 88]. Some recent applications of ultrasound technology for protein extraction are for rice bran [89], algae [90], and plant roots [91].

2.2.2.3 Enzyme-assisted Extraction

Enzyme-assisted extraction includes a vast number of procedures of biochemically based disruption of cell membranes and walls. Enzymes are mostly protein molecules that organisms produce for metabolism purposes as they function similar to catalysts for reactions occurring within the cell. Normally, each enzyme can assist only a limited number of reactions; therefore, extraction procedures using biocatalysts are specific to the sample, as enzymes must be unique to cell membranes and wall composition. The method consists of the contact between the sample cells and the enzymes, which results in cell disruption by the enzymatic activity that is responsible for degrading specific bonds in the cellular membranes and walls [92]. Due to the proteic nature of these catalysts, the experimental conditions must be controlled. It is considered a clean method as a result of its specificity, neither generating cell debris as mechanical methods or undesired side reactions, as chemical ones [93]. Moreover, the mild conditions (pH, temperature, and pressure) bring more sustainability to the process. In industrial practices, laccase, lipase, phospholipase, pectinases, cellulases, and hemicellulases are applied in plant bioactive compound extraction, also demonstrating the feasibility for protein extraction processes [92, 93]. A concern of using this technology is the consumption of resources for the production of enzymes (water, energy, and chemicals), which must be taken into account for a green and sustainable process to be planned [94]. Applying enzyme-assisted extraction as a pretreatment combined with other techniques leads to higher yields [92]. Proteins were extracted from algae [95], almond press cake [96], and sesame bran [97] using the enzymatic process.

2.2.2.4 Pulsed Electric Field

This technique consists of submitting cells to high-voltage electric field pulses in a short period of time. These pulses can charge the cell lipid bilayer, which forms pores over its structure. Due to this phenomenon, the method is also called electroporation. These small pores allow mass transference between the medium and the cells, easing the solvation process of proteins and other bioactive compounds. Electroporation may be reversible or irreversible depending on experimental conditions, the latter being important for further cell disruption [98, 99]. Due to their composition, some studies hypothesize that cell walls are affected differently to cell membranes, and suppose that age, function, and constituents need to be taken into account for electroporation to perform properly [100]. As for green and sustainable chemistry, it is a technique that does not add any reactants to the process except the solvent, also being a scalable method for industrial processes. The energy consumption is considered low and the technique is, overall, cheap [101]. Protein extraction by a pulsed electric field method has not yet been fully investigated in protein extraction and is generally combined with another method, which is considered a pretreatment procedure. Algae [102, 103] and sesame cake [104] protein extractions are examples of applications of this technology.

Figure 2.6 demonstrates the mechanisms of the discussed extraction techniques on this topic.

2.2.3 Alternative Solvents

While in the topics above, procedures for extraction and sample disruption were discussed, in this section, alternatives for solvents that can be used in all solid–liquid protein extractions will be presented. It should be implicit that all of the techniques are dependent on protein solubility and solvent properties. Organic solvents can help cell disruption by permeating cell barriers and causing a loss in their functionality. These solvents need to be replaced due to their environmental and human toxicity, considering green and sustainable guidelines. This topic will cover some extraction methods with the potential of turning into

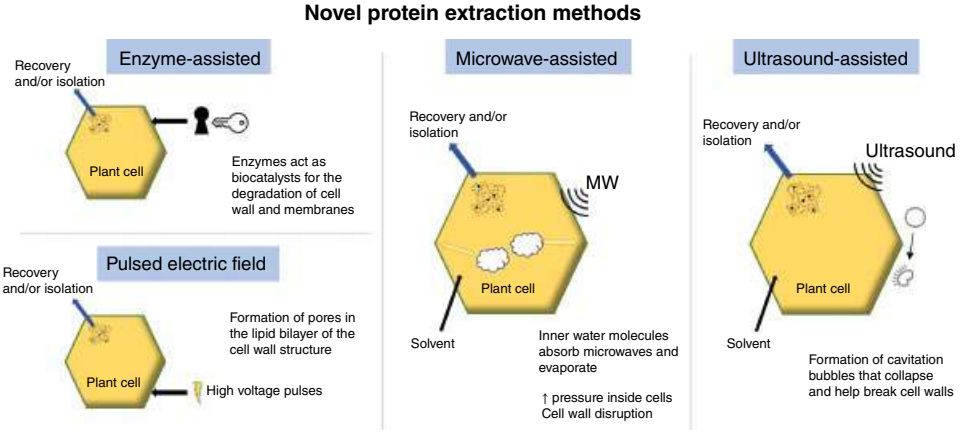

Figure 2.6 Mechanisms behind novel protein extraction techniques.

more green and sustainable processes. Conventional and new technologies for protein extraction are equally important for FSCW biorefineries, and studies on this specific niche reveal how researchers are tackling the subject. Two alternative solvents that can meet sustainable aspects for extraction could serve as surrogates: subcritical fluids and deep eutectic solvents (DESs).

2.2.3.1 Subcritical Water

Subcritical fluids are solvents submitted to temperatures above their boiling point but maintained at the liquid phase by compression. The properties of these solvents, such as dielectric constants, diffusion, surface tension, and, consequently, their polarity and solubility parameters are different from those at room temperature [105]. These properties can be tuned by altering the conditions of subcritical fluid production and maintenance, which broadens the range of application of substances such as water and carbon dioxide, allowing them to be cleaner and safer replacements of organic solvents such as hexane and dimethyl sulfoxide [106]. The protein structure is not maintained due to high pressures and temperatures. Therefore, subcritical water can cause hydrolysis of these biopolymers [107]. Extractions done with subcritical fluids are also known as pressurized liquid extraction. Low solvent consumption and extraction time are the main advantages of these techniques, and high energy cost and the need for optimization of the experimental conditions to obtain efficiency are its major drawbacks [107]. Some examples of samples used in protein extraction using subcritical water are flaxseed meal [108], soybean [109], and black rice bran [110].

2.2.3.2 Deep Eutectic Solvents (DESs)

Considered a hot topic for bioactive compound extraction, DESs are ionic liquids formed by the mixture of two or more substances capable of donating or receiving hydrogen bonds. Organic acids, amino acids, sugars, alcohols, cholinium derivatives (such as cholinium chloride, ChCl), and quaternary ammonium salts are some naturally occurring species that can compose DES [111, 112]. They are nonvolatile, nonflammable, they have low toxicity, are biodegradable, cheap to manufacture, and their production does not need purification steps or generate by-products, important characteristics for an organic solvent substitute [111]. Due to both polar and nonpolar interactions, DES can solubilize a large pool of compounds, fitting protein variability regarding water solubility [112]. These solvents have high viscosity, properties that directly affect mass transfer phenomena, and are also not chemically inert, which is a downside for extraction applications [113]. Separation of extracted substances and DES recovery is not easy due to requiring energy and/or large volumes of other solvents, and thus it is an obstacle for industrial applications [114]. As for protein extraction, DES was recently used for oats [115], pomegranates [116], and brewer's spent grain [117] studies.

2.2.4 Current Practices on Green and Sustainable Protein Extraction

This topic aims to present a brief overview of some FSCW protein extraction methods. For this purpose, a search on the Web of Science platform was conducted to investigate what extraction methods are currently being used for protein extraction of plant residue in food

processing. To do this, "protein extraction" and "green" or "sustainable" were used as search words. All retrieved results were carefully classified and only those studies of food-processing plant-related residues were selected. A table of the results of this search informing the sample, extraction method, conditions, and year of the study is shown next (Table 2.1). The purpose of the table is not to exhaustively present the studies on the topic, but to discuss some aspects of conditions through a green and sustainable view – from the choice of the sample to the methods of extracting proteins from it.

Moreno-Nájera et al. discuss using jackfruit leaves (1st entry of the table), which are residues from pruning jackfruit trees, as a sustainable source of protein extraction. Only in India, approximately 10 tons of pruning waste are generated per year [118]. Such residues, however, can have several uses of high added value, such as forage material and food source for livestock and human health, as they are essential amino acid sources and have properties as palliative methods to treat anemia, diarrhea, and coughing. To extract proteins, the authors analyze four extraction methods, most of which are emerging and environmentally friendly technologies.

First, the extraction of jackfruit leaves using the conventional alkaline extraction (or isoelectric precipitation) method is described. The extraction is performed in an alkaline medium, with NaOH aqueous solution as the solvent used. The stirring time is the longest among the four methods analyzed, corresponding to 30 minutes. From these conditions, the content of proteins found in the jackfruit leaf was 84.1 mg/g in a dry base. The three techniques that follow are emerging extraction technologies, considered as potential sustainable methods, especially since the extraction solvent is a saline solution, a nontoxic solvent. In ultrasound-assisted extraction, the extraction time is reduced to 20 minutes and the optimal value for protein extraction was 96.3 mg/g. In microwave-assisted extraction, the solvent concentration is reduced by half and the extraction time is 4 minutes, the shortest of all methods. The extraction yield considering the best condition for this method (0.5 M NaCl as a solvent) is not shown in the article, but it is known that it presented the best results. However, using methanol as the solvent in the microwave extraction, the estimated value was 95.6 mg/g, which represents the lowest percentage of protein obtained by the other three emerging methods. The latest extraction technique of jackfruit leaves compared by the authors is high hydrostatic pressure-assisted extraction. The extraction time is 20 minutes, and it has the highest extraction yield, 147.3 mg/g of protein, which can be attributed to the ionic strength in combination with the contact surface at high hydrostatic pressure.

It is important to note that the three new methods have shorter extraction times compared to the conventional method, use a saline solution as an extractor solvent, and were the techniques that showed the highest yields. These methods are therefore effective and have proved to be potentially sustainable.

Further down Table 2.1, Boyle et al. introduce a novel source of vegetable protein, *Camelina sativa* seeds (12th entry of the table), as a new plant-based protein ingredient that has great potential to be introduced to the market as the demand for protein is expected to increase significantly in the coming years, as discussed in Section 2.2.1. *Camelina sativa* is an oilseed with a high fat content (30–38%) and protein (25–30%), and is attractive for the production of both oil and protein ingredients, and *Camelina* flour could be produced from the waste generated in the oil production [50]. The authors discuss that it is a sustainable

Table 2.1 Overview of FSCW of plants in recent (2010–2020) studies, according to the year of publication, sample, extraction method, and conditions.

Entry #	Year	Sample	Extraction method	Conditions and general procedures	Reference
1	2020	Jackfruit leaves	Alkaline extraction	Sample powder mass: 5 g Solvent: 1 M NaOH and H_2O pH: 12.5 Stirring time: 30 min Liquid phase separation pH: 2 (adding HCl)	[118]
			Ultrasound-assisted extraction	Sample powder/Solvent ratio: 1:5 m/v Solvent: 1 M NaCl Sonication frequency: 42 kHz Sonication time: 20 min. Solid phase resuspension Solvent: EtOH 70% +1% CH_3COONa Sonication conditions repeat	
			Microwave-assisted extraction	Sample powder/Solvent ratio: 1:5 m/v Solvent: 0.5 M NaCl Microwave power: 1200 W Extraction time: 4 min	
			High hydrostatic pressure-assisted extraction	Sample powder/Solvent ratio: 1:5 m/v Solvent: 0.5 M NaCl Mixture vacuum packing w/ high-density polyethylene. Pressure: 300 Mpa Extraction time: 20 min	
2	2020	Dehulled rapeseeds	Twin screw-press combined with alkaline extraction	Sample powder mass: 150 g Solvent: H_2O Sample powder/Solvent ratio: 1:8 (w/w) Temperature: Room temperature Stirring time: 4 h pH: 9 (adding few drops 0.5 M NaOH) Blending processing at maximum speed Blending time: 2 min Twin-screw press processing Liquid phase separation pH: 9	[119]

(*Continued*)

Table 2.1 (Continued)

Entry #	Year	Sample	Extraction method	Conditions and general procedures	Reference
3	2020	Tip of bamboo shoot	Deep eutectic solvent (DES) extraction	DES composition: ChCl and levulinic acid Levulinic acid – ChCl ratio: 6 Added Water: 40% (v/v) Sample powder/Solvent ratio: 30 mg/mL Water bath temperature: 80 °C Extraction time: 50 min	[120]
		Basal bamboo shoot		Same as tip of bamboo shoot, except for sample powder/ solvent ratio: 70 mg/mL	
		Bamboo sheath		Same as tip of basal bamboo shoot	
4	2020	Brewer's spent grain and pasture grass	Alkaline extraction	Sample/Solvent ratio: 1:10 (w/w) Solvent: 0.1 M NaOH and H_2O pH: >11 Stirring time: 2 h Temperature: 40 °C Liquid phase separation pH: 3.0 (adding 1.0 M CCl_3COOH)	[121]
			Aqueous extraction	Sample/ solvent ratio: 1:10 (w/w) Stirring time: 2 h Temperature: 40 °C Liquid phase separation pH: 3.0 (adding 1.0 M CCl_3COOH)	
			Subcritical water extraction	Temperature: 200 °C Pressure: 4 Mpa Flowrate: 6 mL/min Extraction time: 20 min; Liquid phase separation pH: 3.0 (adding 1.0 M CCl_3COOH)	
5	2020	Hazelnut meal	Alkaline extraction	Sample powder/Solvent ratio: 1:12 (w/w) Solvent: 5 M NaOH and H_2O Temperature: Room temperature Stirring time: 1 h Liquid phase separation pH 4.5 (adding 2 M HCl)	[122]

Table 2.1 (Continued)

Entry #	Year	Sample	Extraction method	Conditions and general procedures	Reference
6	2019	Viz. ryegrass, red clover, Ryegrass-white clover mixture and spinach	Twin-screw press extraction	Sample Mass: 2 g Coarse screen hole sizes: 1 mm Liquid phase separation Sample volume: 30 mL Lignosulfonate mass: ≤6 g pH: 2–3 (adding 6 M HCl)	[123]
7	2019	Brewer's spent grain	Alkaline extraction	Sample mass: 70 g Solvent: 0.1 M NaOH and H_2O Volume: 700 mL pH: >11 Stirring time: 2 h Temperature: 40 °C Liquid phase separation pH: 3.0 (adding 1.0 M CCl_3COOH)	[124]
8	2019	Hemp press-cakes	Alkaline extraction	Solvent: water Press-cake powder/water mass ratio: 5–10% Temperature: Room temperature Extraction time: overnight (>12 h) pH: >9 (adding 2 M NaOH)	[125]
9	2019	Tall fescue	Twin-screw press extraction	Sample mass: 200 g Solvent: H_2O Solvent volume: 200 mL Coarse screen hole sizes: 1 mm Heat precipitation step Sample juice volume: 500 mL Water bath temperature: 95 °C Extraction time: 31 min	[126]
10	2019	Palm kernel meal	Alkaline extraction	Sample powder mass: 75 g Solvent: 0.03 M NaOH Volume: 750 mL pH: 12 Temperature: 80 °C Stirring time: 4 h Stirring speed: 150 rpm Liquid phase separation Sample volume 50 mL Solvent: 80% EtOH Temperature: 0 °C	[127]

(*Continued*)

Table 2.1 (Continued)

Entry #	Year	Sample	Extraction method	Conditions and general procedures	Reference
11	2018	Rapeseed cake Evening primrose cake	DES extraction	DES composition: ChCl and Glycerin ChCl – Glycerol ratio: 1:2 Sample powder mass: 5 g DES mass: 45 g Stirring speed: 500 rpm Extraction time: 2 h Temperature: 60 and 100 °C Liquid phase separation Solvent: H_2O Volume: 250 mL Temperature: 4 °C Time: 12 h	[128]
12	2018	Camelina sativa seeds	Alkaline extraction	Solvent: H_2O Sample powder/Solvent ratio: 5% (w/v) pH: 12 (adding 2 N of NaOH) Stirring time: 1 h Liquid phase separation pH: 5 (adding 2 N HCl)	[50]
			Saline extraction	Solvent: 0.05 M K_3PO_4 buffer + 1 M NaCl pH: 8 Stirring time: 1 h Temperature: 50 °C Liquid phase separation Addition of $(NH_4)_2SO_4$ Salt saturation: 85% Stirring time: 3 h	
13	2018	Pomegranate seed	Enzyme-assisted extraction	Sample powder mass: 10 g Solvent: 50 mM Na_3SO_4 buffer Volume: 79 mL pH: 7.2 Protease enzyme addition Enzyme/Sample ratio: 50 (U/g) Temperature: 45 °C Extraction time: 14 h Stirring speed: 110 rpm	[129]

Table 2.1 (Continued)

Entry #	Year	Sample	Extraction method	Conditions and general procedures	Reference
14	2017	Coriander fruit and seeds	Alkaline extraction	Sample powder mass: 100 g Solvent: H_2O Temperature: 50 °C pH: 10.0 (adding 1 M NaOH) Rotation speed: 250 rpm Extraction time: 90 min Liquid phase separation pH: 3.5 (adding 1 M HCl)	[130]
15	2016	Tomato peels and seeds	Alkaline extraction	Sample powder mass: 10 g Solvent: 0.05 M NaOH Volume: 200 mL Temperature: 90 °C Stirring speed: 700 rpm Liquid phase separation pH: 4 (adding 0.5 M citric acid)	[131]
16	2016	Green tea residue	Alkaline extraction combined w/ EtOH enzymatic-treatment	Pre-treatment Sample mass: 200 mg Solvent: 0.02 CH_3COONa + CH_3COOH buffer Solvent volume 4 pH: 4.5 Enzyme: Viscozyme® L Enzymatic loading: 120 FBGU*/g sample Incubation time: 20 h Temperature: 30 °C Rotation speed: 1000 rpm Adding 4 mL 50% EtOH Solid phase separation for protein extraction Solvent: 0.1 M NaOH Volume: 7 mL Extraction temperature: 95 °C Rotation speed: 1000 rpm Extraction time: 2 h	[132]
17	2016	Sugar beet leaves	Screw-press extraction	Dried leaves pressing Liquid phase separation Temperature: 50 °C Extraction time: 30 min	[133]

(*Continued*)

Table 2.1 (Continued)

Entry #	Year	Sample	Extraction method	Conditions and general procedures	Reference
18	2015	Green tea residue	Alkaline extraction	Sample mass: 0.5 g Solvent: 0.1 M NaOH Temperature: 25–95 °C Extraction time: 2 h	[134]
19	2015	Screw-pressed *Jatropha curcas* L. residue and aqueous de-oiled *Jatropha curcas* L. residue	Alkaline extraction	Sample mass: 50 g Solvent: H_2O Solid–to–liquid ratio: 1:11 (m/m) Temperature: 60 °C Stirring speed: 200 rpm pH: 11 (adding 2 M NaOH) Extraction time: 30 min Liquid phase separation Mass: 250 g pH: 4 Stirring speed: 200 rpm Decantation time: 2 h	[135]
			Enzyme-assisted extraction	Sample mass: 50 g Solvent: H_2O Solid–to–liquid ratio: 1:12 (m/m) pH: 8 Temperature: 55 °C Enzyme: Protease A01 Enzymatic loading: 0.5% (w/w) Extraction time: 60 min	
20	2014	Green tea residue	Alkaline extraction	Sample mass: 0.5 g Solvent: 4 mM NaOH Solvent/Sample ratio: 40 mL/g Temperature: 95 °C Extraction time: 2 h Liquid phase separation Sample volume: 10 mL pH: 3.5 (adding 1 M HCl)	[136]
21	2012	*C. korshinskii Kom.*	Alkaline extraction	Milled sample mass: 100 g Solvent: 0.12 NaOH Volume: 2 L Stirring time: 1 h Temperature: 37 °C Liquid phase separation pH: 4 (adding 0.1 N HCl)	[137]

Table 2.1 (Continued)

Entry #	Year	Sample	Extraction method	Conditions and general procedures	Reference
			Solvent-based extraction	Milled sample mass: 100 g Solvent: 62.5 mmol/L Tris-HCl, 0.5% sodium dodecyl sulfate 10% glycerol, and 5% 2-Mercaptoethanol pH: 6.8 Volume: 2 L Extraction time: 7 h Temperature: 4 °C Liquid phase separation Cooled acetone addition and incubation overnight	
			Solvent-based extraction	Milled sample mass: 100 g Solvent: Cold acetone containing 10% CCl_3COOH (w/v) and 0.07% 2-Mercaptoethanol (v/v) pH: 6.8 Volume: 2 L Temperature: 4 °C Incubation overnight	
22	2010	Sunflower seeds	Saline extraction	Sample meal/Solvent ratio: 0.05 g/mL Solvent: 1.3 M NaCl solution pH: 6 Stirring time: 15 min Extraction time: 1 h	[138]

oilseed, as its culture contributes to reducing soil and water erosion and soil nitrate leaching, increases carbon sequestration, and reduces inputs of energy and pesticide. In addition to the environmental benefits, the amino acid composition of the *Camelina* protein is comparable to that of the soy protein. Therefore, it presents excellent nutritional quality. Thus, justifying being a sustainable source to extract proteins, the authors evaluated two different approaches, alkaline and saline extraction.

First, the extraction of *Camelina sativa* seeds using the alkaline technique is described. The extraction occurs by adding the strong NaOH base in an aqueous solution and then stirring for 1 hour. The highest yield of extractions using this method was 38% (it represents the amount of protein extracted relative to the total amount of protein in the *Camelina sativa* seeds). The second method analyzed was saline extraction. In this technique, a buffer solution of K_3PO_4 with NaCl was used as the solvent and the stirring time was also 1 hour. The best extraction yielded 42%.

Unlike the four methods analyzed by Moreno-Nájera et al., in this case, both alkaline and saline extraction have the same time. Therefore, extraction is governed by the solvent used. The saline solution, in addition to being a more sustainable way of conducting extractions, presented the highest yield of protein, resulting in a protein concentration of 82.2%. Besides that, Boyle et al. also analyzed the structural differences in proteins extracted following both methods and the data showed that saline extraction produces less denatured and more functional *Camelina* protein concentrates. Again, the most environmentally friendly method proved to be more efficient and a better option when considering green aspects.

Gofferjé et al. discuss the protein extraction from *Jatropha curcas L.* (19th entry of the table) as a great alternative to avoid the "tank or table" discussion as it is a nonedible oil plant and can be used for biodiesel production. However, in the oil extraction process, high amounts of *Jatropha* meals are obtained. This oil plant waste presents high protein content (up to 40%). So, it can be used as raw material for further applications, not just as a by-product of oil extraction. Such applications include organic fertilizer, rodent repellent or for biogas production and technical applications (e.g. glues, film coatings, and emulsifiers) [135]. Due to the presence of several toxic and anti-nutritional substances, such as phorbol esters, lectin, and phytate, it is not suitable for feed or food applications. Then, the authors analyzed different techniques to extract proteins from two samples of *Jatropha curcas L.*, the screw-pressed *Jatropha curcas L.* residue (SPJR) and the aqueous de-oiled *Jatropha curcas L.* residue (ADJR).

First, *Jatropha* extraction is described using the conventional alkaline extraction method. The extraction occurred with the addition of the strong base NaOH in an aqueous solution at 60 °C and the extraction time was 30 minutes. Considering this technique, the protein yields obtained in the ADJR extraction were 76% and in the SPJR were 79%. The other method, considered a novel technology, is enzyme-assisted extraction. The extraction took place in an aqueous medium with the presence of the protease A01 enzyme at 50 °C, with the extraction time corresponding to 1 hour. The protein yields obtained in both ADJR and SPJR enzyme-assisted extractions were 75%. The results show that the yields obtained were similar for both raw materials and both extraction methods applied, making the enzyme-assisted extraction competitive to the conventional approach and a clean option when considering sustainable aspects due to its mild conditions as pH and temperature, in this case.

When planning a sustainable process, researchers should be alert not only to improve extraction yields, but also to the quantity and quality of the resources used – including toxicity, production impact, and other factors. Therefore, the conditions applied to the techniques could be used as a comparative parameter of greenness; once through them, it is possible to verify the integrity of the method, considering whether there are dangerous substances, large quantities of compounds, and high energy consumption. An analysis of Table 2.1 could also be made considering this aspect, bringing two different points of view for the comparison of studies, one centered on the techniques and the other on the samples.

Starting from extraction techniques, most of the works applied conventional alkaline extraction. The conditions informed on the articles for this technique are sample mass, sample–to–solvent ratio, solvent volume, pH, temperature, stirring time, and stirring speed. Those conditions could be grouped in four, regarding their related resource: solvent volume, time, energy, and feedstock.

As for solvents, all the studies used aqueous sodium hydroxide solutions, which is considered a green base according to GSK's guide for acid and base selection [64], though the pH varies from 10 to 12.5. Considering that a pH shift must be performed for the precipitation of proteins, a lower pH of the alkaline extraction could imply the use of less volume of base. Of course, this reasoning is valid if considering acid solutions with the same concentrations, as low as possible for safe managing. Thus, if feasible and consistent with the sample used, the table's 14th entry shows a more sustainable use of the pH on the alkaline extraction of proteins, using pH 10 to perform an alkaline extraction in coriander fruits and seeds [130].

A similar comparison can be performed on the alkaline extraction considering time, represented in the table as extraction time or stirring time, according to the method applied. This variable shows a significant variance from 30 minutes up to 4 hours, and even overnight (more than 12 hours). From an industrial scale point of view, quicker processes are favorable over time-consuming processes. Besides that, time efficiency could also affect positively labor conditions, which are highly connected with sustainability. Overall, the data demonstrate that time efficiency is achievable as in the 1st and 19th entries, with 30 minutes of total extraction time [118, 135].

The energy employed on the alkaline protein extraction could be apprehended by the analysis of extraction time and stirring time (accounted above), stirring speed (that is not present in all methods), and temperature, which varied from room temperature to 95 °C. Processes energy efficiency is closely related to their costs. These expenses are dependent on the type of combustible source used to provide energy to the extraction procedure, and in this context, the techniques performed at room temperature are preferable. The table's 5th, 8th, and 18th are examples of sustainable processes considering temperature, which had extractions running at room temperature [122, 125, 134].

The mass of feedstock is a condition that meets the best sustainability scenario when the process employed extracts all of its protein content. Even though the authors seek to optimize the extraction, it must be noted that a simple comparison of mass values cannot serve to select more sustainable conditions due to different experimental proportions taken in the studies. Therefore, the sample–to–solvent ratio must be assessed. This variable also relates to solvent volume efficiency, as expected. This condition is presented as more sustainable when the ratio is higher, and thus less solvent is needed and more plant residue (which is largely available in the context) is better used. Regarding the sample–to–solvent ratio, the analysis of the table shows values ranging from approximately 0.025 to 0.1, where the most sustainable ratio encountered is used in the 4th, 7th, 8th, and 10th entries [121, 124, 125, 127].

This analysis could be repeated for the other protein extraction methods, following the same reasoning presented for alkaline extraction, respecting their own specificities. For instance, for DES extraction described in the 11th entry, one should [128] be aware of the substances that compose the DES regarding their greenness and the cost involved in the production of the DES. As for enzyme-assisted extraction, the enzyme load must be minimized in order to fit sustainable aspects.

The authors note that the extraction scale and sample type (regarding species and pretreatment conditions) are relevant and decisive. Therefore, a generalist method of protein extraction following green and sustainable aspects is not possible. This means that the

comparisons made in this text serve more as an example of how to move toward more sustainable processes, as these comparisons must be guided by researchers' knowledge within the limits and potential of each technique used. Therefore, the community must also invest efforts in improving them, whether they are conventional or innovative.

The second point of view, centered on sample similarities, can be performed to analyze qualitatively the techniques that are more sustainable in terms of method of extraction chosen, the solvent used, temperature, and pH, in a way of suggesting that it is possible to hold sustainable conditions for different plant species. The authors grouped the sample similarities into five groups: seeds, meals, grains, leaves, and other plant parts (kernel, fruit, shoot, and grass).

Regarding the extractions of seeds as samples, five out of seven methods are conventional (alkaline or saline extraction). Ntone et al. (2nd entry) use milder conditions on alkaline extraction, employing water as solvent and room temperatures in the extraction process [119]. The DES extraction, despite using a promisor solvent, used higher temperatures (60 and 100 °C). The same occurs with enzyme-assisted extraction, which applies high temperatures and has a high energy consumption in the process (14 hours of extraction) [129]. It is essential that the choice of a considered green and sustainable method must be accompanied by milder conditions whenever possible.

In relation to the extractions of parts of plants as samples, alkaline extraction is also the most used method. While the temperature selected for the extractions is between 80 and 90 °C, the time varies greatly, ranging from a few minutes to more than 12 hours. DES is used as a green solvent option in two papers [120, 128], and both twin-screw press extraction [123, 126] and alkaline extractions [125, 127, 130] use water as a solvent, showing other possible sustainable conditions for the extraction of proteins from plant parts.

Regarding the extractions of meals as samples, it is interesting to note that, as mentioned previously in the discussion by Gofferjé et al. [135] – which compares alkaline extraction with enzyme-assisted extraction –, the enzyme-assisted extraction proved to be a promising option, with milder conditions for temperature, time, and pH. However, when making this comparison by sample type, it could be observed that there is the possibility of making the conditions even more sustainable in alkaline extraction, using water as a solvent and room temperature, as shown in the table's 5th entry [122].

For extractions using grains as samples, it is interesting to note that alkaline extraction presents exactly the same solvent, temperature, and pH conditions for the different grains. It can also be noted that the novel subcritical water extraction method is employed, which reduces the extraction time from 2 hours to 20 minutes, but uses extremely high temperatures (200 °C) to achieve the adequate properties to act as a subcritical fluid [121, 124].

Regarding the extractions of leaves as samples, again the alkaline extraction stands out in a greater number [118, 132, 134, 136]. Promising techniques such as ultrasound and microwave are tested [118] and present shorter extraction times, reducing from hours to minutes, also employing saline solution as an extractor solvent instead of a strong base. Including screw-press extraction [133], such techniques are potentially greener for extracting proteins from leaves.

Through these comparisons, it can be observed that the conditions vary considerably in the same group of samples, from milder methods using water and room temperature, to methods with high temperatures and extraction times. The main objective of this

comparison is to show that, potentially, protein extraction from similar samples in a more sustainable way is feasible, not only considering the extraction technique itself but all that it encompasses. It is important to note that the extraction yields were not considered – once the quantity extracted is not the only key point when considering green and sustainable aspects. This comparison is a good strategy to instigate critical and holistic thinking when choosing an extraction method based on sample type, although it must be stressed again that a general method is not possible due to structural variance between plant species.

As sustainability gains more relevance for research, another objective must be included, without neglecting yield optimization, which is thinking about the lab-scale experiments to sketch industrial processes. To do this, researchers must assess their experiments based on green metrics such as life cycle assessment. In the extraction context, a simple-to-use metric is Sustainable Factors [139], which is based on ratios of the mass of the substance extracted per unit of resource used to perform the extraction (such as time, energy, solvent volume, etc.). This metric is presented as the first step toward the optimization of efficiency beyond the extraction yield, therefore following the steps shared by the authors in this section of the text.

The scientific community should always be aware that green and sustainable chemistry targets global and local problems full of dilemmas, paradigms, and different valid solutions. For instance, here we discuss one way of helping to solve the human hunger/food poverty problem. For proteins, a wide range of extraction methods have been shown, but that is not the end of the matter. Separation, concentration, isolation, and other processes are just as decisive for developing environmentally friendly products. These processes are highly dependent on each other, as the choice of using microwaves instead of bead milling will have a ripple effect in the decisions in the following steps for example. The same is true when transposing a method from laboratory to industrial scale, therefore considering the broader implications of a study is mandatory and should be considered an interdisciplinary objective.

2.3 Final Considerations

In this chapter, we discussed the role of FSCW and how to address it. The biorefinery and green and sustainable chemistry concepts are a basis for rethinking waste as a resource to tackle global nutrition problems and implement innovative guidelines for circularity. Considering the volume of FSCW, we considered some of the compounds and materials that could be extracted from them and reintegrated into the industrial food chain production for human and animal applications. Among the many substances, proteins were taken into account since they are essential macronutrients for all living beings. In fact, there is currently a lack of daily intake of this nutrient by the population – either by eating ultra-processed foods or by not eating any source of protein. In a scenario in which malnutrition caused by low protein consumption, poverty, and the increase in the world population are combined, new sources for this macronutrient are emerging. FSCWs from plants are nutrient-rich biomasses that could serve this purpose. To reach this objective, protein extraction methods with high efficiency need to be designed. Thus, we exposed some of the most promising extractive methods regarding green and sustainable aspects, untangling

their mechanisms as we highlighted advantages and disadvantages. A brief overview of current tendencies in the research field demonstrated that considering scaling up and optimizing the methods, conditions for resource efficiency are the next important steps to be investigated. At the same time, an effort to rethink the FSC to increase processing efficiency toward maximum integration of proteins and other important nutrients from the raw material must be made to reduce generating waste, thus dealing with the problem at its origin. Thus, green and sustainable techniques can be applied to promote good health by producing safe and healthy protein-based food in an ethical, fair, inclusive way for all human beings.

This work was financially supported by the São Paulo Research Foundation (FAPESP) Brazil (2017/05712-0, 2018/11409-0, and 2017/25015-1), the National Council for Scientific and Technological Development (CNPq), and by the Coordination for the Improvement of Higher Education Personnel (CAPES), Brazil (001/1622968).

Note

1 More details on: http://fieldfoodtechhub.ufscar.br.

References

1 Gustavsson, J., Cederberg, C., and Sonesson, U. (2011). Global food losses and food waste. https://www.madr.ro/docs/ind-alimentara/risipa_alimentara/presentation_food_waste.pdf.
2 Parfitt, J., Barthel, M., and Macnaughton, S. (2010). Food waste within food supply chains: quantification and potential for change to 2050. *Philos Trans R Soc B Biol Sci* 365 (1554): 3065–3081. http://rstb.royalsocietypublishing.org/cgi/doi/10.1098/rstb.2010.0126.
3 FAO (2013). Food wastage footprint – Summary Report. http://www.fao.org/publications/card/en/c/000d4a32-7304-5785-a2f1-f64c6de8e7a2/.
4 FAO (2015). Food wastage footprint & climate change, 1–4. http://www.fao.org/nr/sustainability/food-loss-and-waste.
5 Papargyropoulou, E., Lozano, R., Steinberger, J.K. et al. (2014). The food waste hierarchy as a framework for the management of food surplus and food waste. *J Clean Prod* 76: 106–115.
6 EU (2020). A European Green Deal – striving to be the first climate-neutral continent. https://ec.europa.eu/info/strategy/priorities-2019-2024/european-green-deal_en.
7 European Commission (2020). Farm to Fork Strategy – for a fair, healthy and environmentally-friendly food system. https://ec.europa.eu/food/farm2fork_en.
8 United Nations (2018). Sustainable development goals. https://sustainabledevelopment.un.org/sdgs.
9 Zuin, V.G. (2016). Circularity in green chemical products, processes and services: innovative routes based on integrated eco-design and solution systems. *Curr Opin Green Sustain Chem* 2: 40–44. https://linkinghub.elsevier.com/retrieve/pii/S2452223616300190.

10 Kümmerer, K., Clark, J.H., and Zuin, V.G. (2020). Rethinking chemistry for a circular economy. *Science* 367 (6476): 369–370. https://www.sciencemag.org/lookup/doi/10.1126/science.aba4979.

11 Schmid, O., Padel, S., and Levidow, L. (2012). The bio-economy concept and knowledge base in a public goods and farmer perspective. *Bio-based Appl Econ* 1 (1): 47–63.

12 Cherubini, F. (2010). The biorefinery concept: using biomass instead of oil for producing energy and chemicals. *Energy Convers Manag* 51 (7): 1412–1421. http://dx.doi.org/10.1016/j.enconman.2010.01.015.

13 Pfaltzgraff, L.A., De Bruyn, M., Cooper, E.C. et al. (2013). Food waste biomass: a resource for high-value chemicals. *Green Chem* 15 (2): 307. http://xlink.rsc.org/?DOI=c2gc36978h.

14 Clark, J.H., Pfaltzgraff, L.A., Budarin, V.L. et al. (2013). From waste to wealth using green chemistry. *Pure Appl Chem* 85 (8): 1625–1631. http://www.degruyter.com/view/j/pac.2013.85.issue-8/pac-con-12-09-01/pac-con-12-09-01.xml.

15 Matharu, A.S., de Melo, E.M., and Houghton, J.A. (2016). Opportunity for high value-added chemicals from food supply chain wastes. *Bioresour Technol* 215: 123–130.

16 Maina, S., Kachrimanidou, V., and Koutinas, A. (2017). A roadmap towards a circular and sustainable bioeconomy through waste valorization. *Curr Opin Green Sustain Chem* 8: 18–23. http://dx.doi.org/10.1016/j.cogsc.2017.07.007.

17 Kumar, K., Yadav, A.N., Kumar, V. et al. (2017). Food waste: a potential bioresource for extraction of nutraceuticals and bioactive compounds. *Bioresour Bioprocess* 4 (1): 18.

18 Vandermeersch, T., Alvarenga, R.A.F., Ragaert, P., and Dewulf, J. (2014). Environmental sustainability assessment of food waste valorization options. *Resour Conserv Recycl* 87: 57–64. http://dx.doi.org/10.1016/j.resconrec.2014.03.008.

19 Cecilia, J.A., García-Sancho, C., Maireles-Torres, P.J., and Luque, R. (2019). Industrial food waste valorization: a general overview. In: *Biorefinery*, 253–277. Cham: Springer International Publishing http://link.springer.com/10.1007/978-3-030-10961-5_11.

20 CSK, L., Pfaltzgraff, L.A., Herrero-Davila, L. et al. (2013). Food waste as a valuable resource for the production of chemicals, materials and fuels. Current situation and global perspective. *Energy Environ Sci* 6 (2): 426. http://xlink.rsc.org/?DOI=c2ee23440h.

21 Imbert, E. (2017). Food waste valorization options: opportunities from the bioeconomy. *Open Agric* 2 (1): 195–204. https://www.degruyter.com/doi/10.1515/opag-2017-0020.

22 Tuck, C.O., Perez, E., Horvath, I.T. et al. (2012). Valorization of biomass: deriving more value from waste. *Science* 337 (6095): 695–699. https://www.sciencemag.org/lookup/doi/10.1126/science.338.6107.604-b.

23 Cseke, J.L., Kirakosyan, A., Kaufman, B.P. et al. (2006). *Natural Producs from Plants*, 2e, 551. CRC Press.

24 Bennett, R.N. and Wallsgrove, R.M. (1994). Secondary metabolites in plant defence mechanisms. *New Phytol* 127 (4): 617–633. http://doi.wiley.com/10.1111/j.1469-8137.1994.tb02968.x.

25 Schieber, A. (2017). Side streams of plant food processing as a source of valuable compounds: selected examples. *Annu Rev Food Sci Technol* 8 (1): 97–112. http://www.annualreviews.org/doi/10.1146/annurev-food-030216-030135.

26 Banerjee, J., Singh, R., Vijayaraghavan, R. et al. (2017). Bioactives from fruit processing wastes: green approaches to valuable chemicals. *Food Chem* 225: 10–22. http://dx.doi.org/10.1016/j.foodchem.2016.12.093.

27 Vuong, Q.V. (2017). *Utilisation of Bioactive Compounds from Agricultural and Food Waste*. Boca Raton: CRC Press https://doi.org/10.1201/9781315151540.

28 Deng, G.-F., Shen, C., Xu, X.-R. et al. (2012). Potential of fruit wastes as natural resources of bioactive compounds. *Int J Mol Sci* 13 (7): 8308–8323. http://www.mdpi.com/1422-0067/13/7/8308.

29 Sagar, N.A., Pareek, S., Sharma, S. et al. (2018). Fruit and vegetable waste: bioactive compounds, their extraction, and possible utilization. *Compr Rev Food Sci Food Saf* 17 (3): 512–531. http://doi.wiley.com/10.1111/1541-4337.12330.

30 Ain, H.B.U., Saeed, F., Barrow, C.J. et al. (2020). Food processing waste: a potential source for bioactive compounds. In: *Bioactiv Compounds in Underutilized Fruits and Nuts* (eds. H.N. Murthy and V.A. Bapat), 625–649. Cham: Springer Nature Switzerland http://link.springer.com/10.1007/978-3-030-30182-8_45.

31 Bhargava, N., Sharanagat, V.S., Mor, R.S., and Kumar, K. (2020). Active and intelligent biodegradable packaging films using food and food waste-derived bioactive compounds: a review. *Trends Food Sci Technol* 105 (September): 385–401. https://doi.org/10.1016/j.tifs.2020.09.015.

32 Zuin, V.G., Segatto, M.L., and Ramin, L.Z. (2018). Plants as resources for organic molecules: facing the green and sustainable future today. *Curr Opin Green Sustain Chem* 9: 1–7. http://linkinghub.elsevier.com/retrieve/pii/S2452223617300810.

33 Panzella, L., Moccia, F., Nasti, R. et al. (2020). Bioactive phenolic compounds from agri-food wastes: an update on green and sustainable extraction methodologies. *Front Nutr* 7 (May): 1–27.

34 Rombaut, N., Tixier, A.-S., Bily, A., and Chemat, F. (2014). Green extraction processes of natural products as tools for biorefinery. *Biofuels Bioprod Biorefin* 8 (4): 530–544. http://doi.wiley.com/10.1002/bbb.1486.

35 Curiel, J.A. (2021). Application of biotechnological techniques aimed to obtain bioactive compounds from food industry by-products. *Biomolecules* 11 (1): 88. https://www.mdpi.com/2218-273X/11/1/88.

36 Finley, J.W. and deMan, J.M. (2018). Lipids. In: *Principles of Food Chemistry*, 39–116. Cham: Springer International Publishing.

37 Karmee, S.K., Linardi, D., Lee, J., and Lin, C.S.K. (2015). Conversion of lipid from food waste to biodiesel. *Waste Manag* 41: 169–173. http://dx.doi.org/10.1016/j.wasman.2015.03.025.

38 Jahurul, M.H.A., Zaidul, I.S.M., Ghafoor, K. et al. (2015). Mango (Mangifera indica L.) by-products and their valuable components: a review. *Food Chem* 183: 173–180. http://dx.doi.org/10.1016/j.foodchem.2015.03.046.

39 Matthaus, B. and Özcan, M.M. (2012). Chemical evaluation of citrus seeds, an agro-industrial waste, as a new potential source of vegetable oils. *Grasas Aceites* 63 (3): 313–320. http://grasasyaceites.revistas.csic.es/index.php/grasasyaceites/article/view/1384/1381.

40 Sulaiman, S., Abdul Aziz, A.R., and Kheireddine, A.M. (2013). Optimization and modeling of extraction of solid coconut waste oil. *J Food Eng* 114 (2): 228–234. https://www.sciencedirect.com/science/article/pii/S0260877412004086.

41 Malacrida, C.R. and Jorge, N. (2012). Yellow passion fruit seed oil (Passiflora edulis f. flavicarpa): physical and chemical characteristics. *Braz Arch Biol Technol* 55: 127–134.

http://www.scielo.br/scielo.php?script=sci_arttext&pid=S1516-89132012000100016&nrm=iso.

42 Wadhwa, M., Bakshi, M., and Makkar, H. (2015). Wastes to worth: value added products from fruit and vegetable wastes. *CAB Rev Perspect Agri Vet Sci Nutr Nat Resour* 10 (043): 1–25. http://www.cabi.org/cabreviews/review/20163022692.

43 Karmee, S.K. (2016). Liquid biofuels from food waste: current trends, prospect and limitation. *Renew Sust Energ Rev* 53: 945–953. https://linkinghub.elsevier.com/retrieve/pii/S1364032115010114.

44 Aditiya, H.B., Mahlia, T.M.I., Chong, W.T. et al. (2016). Second generation bioethanol production: a critical review. *Renew Sust Energ Rev* 66: 631–653. https://linkinghub.elsevier.com/retrieve/pii/S1364032116303434.

45 LML, N. and Toldra, F. (eds.) (2012). *Handbook of Analysis of Active Compounds in Functional Foods*, 1–905. CRC Press.

46 FAO (2020). The State of Food Security and Nutrition in the World. http://www.fao.org/3/ca9692en/online/ca9692en.html.

47 UNEP (2020). How to feed 10 billion people. https://www.unep.org/news-and-stories/story/how-feed-10-billion-people.

48 Bashi, Z., McCullough, R., Ong, L., and Ramirez, M. (2019). Alternative proteins: the race for market share is on. https://www.mckinsey.com/industries/agriculture/our-insights/alternative-proteins-the-race-for-market-share-is-on.

49 Medgadget (2020). At 13.75% CAGR, Plant-Based Protein Market Size 2020 Global Industry Analysis, Growth, Trends and Research Development Report, 2025.

50 Boyle, C., Hansen, L., Hinnenkamp, C., and Ismail, B.P. (2018). Emerging camelina protein: extraction, modification, and structural/functional characterization. *J Am Oil Chem Soc* 95 (8): 1049–1062.

51 EAT-Lancet Commission (2019). Healthy diets from sustainable food systems. https://eatforum.org/content/uploads/2019/01/EAT-Lancet_Commission_Summary_Report.pdf.

52 Boye, J., Zare, F., and Pletch, A. (2010). Pulse proteins: processing, characterization, functional properties and applications in food and feed. *Food Res Int* 43 (2): 414–431.

53 Di Domenico, Z.H., Buller, L.S., Mudhoo, A. et al. (2020). An overview of subcritical and supercritical water treatment of different biomasses for protein and amino acids production and recovery. *J Environ Chem Eng* 8 (5): 104406.

54 Pojić, M., Mišan, A., and Tiwari, B. (2018). Eco-innovative technologies for extraction of proteins for human consumption from renewable protein sources of plant origin. *Trends Food Sci Technol* 75: 93–104.

55 Aldalur, A., Bustamante, M.Á., and Barron, L.J.R. (2019). Effects of technological settings on yield, curd, whey, and cheese composition during the cheese-making process from raw sheep milk in small rural dairies: emphasis on cutting and cooking conditions. *J Dairy Sci* 102 (9): 7813–7825.

56 Market Data Forecast (2020). Europe whey protein market. https://www.marketdataforecast.com/market-reports/europe-whey-protein-market.

57 Fagbemi, O.D., Sithole, B., and Tesfaye, T. (2020). Optimization of keratin protein extraction from waste chicken feathers using hybrid pre-treatment techniques. *Sustain Chem Pharm* 17: 100267.

58 Muhammad, A. and Khosa, A.U. (2013). A sustainable role of keratin biopolymer in green chemistry: a review. *Invit Innov J Food Process Beverages* 1 (1): 1–8.

59 De Pretto, C., Giordano, R.L.C., Tardioli, P.W., and Costa, C.B.B. (2018). Possibilities for producing energy, fuels, and chemicals from soybean: a biorefinery concept. *Waste Biomass Valorization* 9 (10): 1703–1730.

60 ASBRAN (2018). Proteína, suplementos, nutrição e muita discussão. https://www.asbran.org.br/noticias/proteina-suplementos-nutricao-e-muita-discussao.

61 Ahmed, H. (2004). Protein extraction. In: *Principles and Reactions of Protein Extraction, Purification, and Characterization*, 1e, 1–33. CRC Press LLC.

62 Islam, S.M., Aryasomayajula, A., and Selvaganapathy, P.R. (2017). A review on macroscale and microscale cell lysis methods. *Micromachines* 8 (3): 83.

63 Burgess, R.R. (2009). Protein precipitation techniques. In: *Guide to Protein Purification*, 2e (eds. R.R. Burgess and M.P. Deutscher), 331–342. Academic Press (Methods in Enzymology; vol. 463).

64 Henderson, R.K., Hill, A.P., Redman, A.M., and Sneddon, H.F. (2015). Development of GSK{'}s acid and base selection guides. *Green Chem* 17 (2): 945–949.

65 Harrysson, H., Konasani, V.R., Toth, G.B. et al. (2019). Strategies for improving the protein yield in pH-shift processing of ulva lactuca linnaeus: effects of ulvan lyases, pH-exposure time, and temperature. *ACS Sustain Chem Eng* 7 (15): 12688–12691.

66 Hayati Zeidanloo, M., Ahmadzadeh Ghavidel, R., Ghiafeh Davoodi, M., and Arianfar, A. (2019). Functional properties of Grass pea protein concentrates prepared using various precipitation methods. *J Food Sci Technol* 56 (11): 4799–4808.

67 Shen, K., Mu, W., Xia, S. et al. (2021). Preparation of protein powder from the liver of Yellowfin tuna (Thunnus albacores): a comparison of acid- and alkali-aided pH-shifting. *Food Sci Technol* https://doi.org/10.1590/fst.40120.

68 Boye, J.I. and Barbana, C. (2012). *Protein Processing in Food and Bioproduct Manufacturing and Techniques for Analysis*, 85–113. Food and Industrial Bioproducts and Bioprocessing (Wiley Online Books).

69 Lee, S.Y., Cho, J.M., Chang, Y.K., and Oh, Y.-K. (2017). Cell disruption and lipid extraction for microalgal biorefineries: a review. *Bioresour Technol* 244: 1317–1328.

70 Amorim, M.L., Soares, J., dos Reis Coimbra, J.S. et al. (2020). Microalgae proteins: production, separation, isolation, quantification, and application in food and feed. *Crit Rev Food Sci Nutr* 0 (0): 1–27.

71 Novák, P. and Havlicek, V. (2016). Protein extraction and precipitation. In: *Proteomic Profiling and Analytical Chemistry*, 52–62. Elsevier.

72 Krishna Koyande, A., Tanzil, V., Murraly Dharan, H. et al. (2020). Integration of osmotic shock assisted liquid biphasic system for protein extraction from microalgae Chlorella vulgaris. *Biochem Eng J* 157: 107532.

73 Halim, R., Papachristou, I., Kubisch, C. et al. (2021). Hypotonic osmotic shock treatment to enhance lipid and protein recoveries from concentrated saltwater Nannochloropsis slurries. *Fuel* 287: 119442.

74 Jiang, Y., Zhu, Y., Zheng, Y. et al. (2021). Effects of salting-in/out-assisted extractions on structural, physicochemical and functional properties of Tenebrio molitor larvae protein isolates. *Food Chem* 338: 128158.

75 Goldberg, S. (2008). Mechanical/physical methods of cell disruption and tissue homogenization. *Methods Mol Biol* 424: 3–22.

76 Hu, Y. and Bassi, A. (2020). Extraction of biomolecules from microalgae. In: *Handbook of Microalgae-Based Processes and Products* (eds. E. Jacob-Lopes, M.M. Maroneze, M.I. Queiroz and L.Q. Zepka), 283–308. Academic Press.

77 Cuff, J.P., Wilder, S.M., Tercel, M.P.T.G. et al. (2021). MEDI: macronutrient extraction and determination from invertebrates, a rapid, cheap and streamlined protocol. *Methods Ecol Evol* n/a (n/a) https://doi.org/10.1111/2041-210X.13551.

78 Dong, X., Zhao, M., Shi, J. et al. (2011). Effects of combined high-pressure homogenization and enzymatic treatment on extraction yield, hydrolysis and function properties of peanut proteins. *Innov Food Sci Emerg Technol* 12 (4): 478–483.

79 Parimi, N.S., Singh, M., Kastner, J.R. et al. (2015). Optimization of protein extraction from spirulina platensis to generate a potential co-product and a biofuel feedstock with reduced nitrogen content. *Front Energy Res* 3: 30.

80 Kumar, M., Tomar, M., Potkule, J. et al. (2021). Advances in the plant protein extraction: mechanism and recommendations. *Food Hydrocoll* 115: 106595.

81 Lefebvre, T., Destandau, E., and Lesellier, E. (1635). Selective extraction of bioactive compounds from plants using recent extraction techniques: a review. *J Chromatogr A* 2021: 461770.

82 Amponsah, A. and Nayak, B. (2016). Effects of microwave and ultrasound assisted extraction on the recovery of soy proteins for soy allergen detection. *J Food Sci* 81 (11): T2876–T2885.

83 Wen, L., Álvarez, C., Zhang, Z. et al. (2020). Optimisation and characterisation of protein extraction from coffee silverskin assisted by ultrasound or microwave techniques. *Biomass Convers Biorefinery* 11 (5): 1575–1585.

84 Chew, K.W., Chia, S.R., Lee, S.Y. et al. (2019). Enhanced microalgal protein extraction and purification using sustainable microwave-assisted multiphase partitioning technique. *Chem Eng J* 367: 1–8.

85 Soria, A.C. and Villamiel, M. (2010). Effect of ultrasound on the technological properties and bioactivity of food: a review. *Trends Food Sci Technol* 21 (7): 323–331.

86 Picó, Y. (2013). Ultrasound-assisted extraction for food and environmental samples. *TrAC Trends Anal Chem* 43: 84–99.

87 Chemat, F., Rombaut, N., Sicaire, A.-G. et al. (2017). Ultrasound assisted extraction of food and natural products. Mechanisms, techniques, combinations, protocols and applications. A review. *Ultrason Sonochem* 34: 540–560. http://linkinghub.elsevier.com/retrieve/pii/S1350417716302358.

88 Vilkhu, K., Mawson, R., Simons, L., and Bates, D. (2008). Applications and opportunities for ultrasound assisted extraction in the food industry – a review. *Innov Food Sci Emerg Technol* 9 (2): 161–169.

89 Hayta, M., Benli, B., İşçimen, E.M., and Kaya, A. (2020). Optimization of antihypertensive and antioxidant hydrolysate extraction from rice bran proteins using ultrasound assisted enzymatic hydrolysis. *J Food Meas Charact* 14 (5): 2578–2589.

90 Hildebrand, G., Poojary, M.M., O'Donnell, C. et al. (2020). Ultrasound-assisted processing of Chlorella vulgaris for enhanced protein extraction. *J Appl Phycol* 32 (3): 1709–1718.

91 Abugabr Elhag, H.E.E., Naila, A., Nour, A.H. et al. (2019). Optimization of protein yields by ultrasound assisted extraction from Eurycoma longifolia roots and effect of agitation speed. *J King Saud Univ Sci* 31 (4): 913–930.

92 Puri, M., Sharma, D., and Barrow, C.J. (2012). Enzyme-assisted extraction of bioactives from plants. *Trends Biotechnol* 30 (1): 37–44. https://linkinghub.elsevier.com/retrieve/pii/S0167779911001181.

93 Demuez, M., Mahdy, A., Tomás-Pejó, E. et al. (2015). Enzymatic cell disruption of microalgae biomass in biorefinery processes. *Biotechnol Bioeng* 112 (10): 1955–1966.

94 Becker, M., Lütz, S., and Rosenthal, K. (2021). Environmental assessment of enzyme production and purification. *Molecules* 26 (3): 573.

95 Bjarnadóttir, M., Aðalbjörnsson, B.V., Nilsson, A. et al. (2018). Palmaria palmata as an alternative protein source: enzymatic protein extraction, amino acid composition, and nitrogen-to-protein conversion factor. *J Appl Phycol* 30 (3): 2061–2070.

96 Souza, T.S.P., Dias, F.F.G., Koblitz, M.G.B., and Juliana, M.L.N.M.B. (2019). Aqueous and enzymatic extraction of oil and protein from almond cake: a comparative study. *Processes* 7 (7): 472.

97 Görgüç, A., Bircan, C., and Yılmaz, F.M. (2019). Sesame bran as an unexploited by-product: effect of enzyme and ultrasound-assisted extraction on the recovery of protein and antioxidant compounds. *Food Chem* 283: 637–645.

98 Zeng, X. and Zhang, Z. (2019). Pulsed electric field assisted extraction of bioactive compounds. In: *Advances in Food Processing Technology* (eds. J. Jia, D. Liu and H. Ma), 125–135. Springer.

99 Thulasidas, J.S., Varadarajan, G.S., and Sundararajan, R. (2019). Pulsed electric field for enhanced extraction of intracellular bioactive compounds from plant products: an overview. *Nov Appro Drug Des Dev* 5 (2): 555657.

100 Delsart, C. (2017). Plant cell wall: description, role in transport, and effect of electroporation. In: *Handbook of Electroporation* (ed. D. Miklavčič), 489–509. Cham: Springer International Publishing.

101 Yan, L.-G., He, L., and Xi, J. (2017). High intensity pulsed electric field as an innovative technique for extraction of bioactive compounds – a review. *Crit Rev Food Sci Nutr* 57 (13): 2877–2888.

102 Gateau, H., Blanckaert, V., Veidl, B. et al. (2021). Application of pulsed electric fields for the biocompatible extraction of proteins from the microalga Haematococcus pluvialis. *Bioelectrochemistry* 137: 107588.

103 Elersek, T., Flisar, K., Likozar, B. et al. (2020). Electroporation as a solvent-free green technique for non-destructive extraction of proteins and lipids from Chlorella vulgaris. *Front Bioeng Biotechnol* 8: 443.

104 Sarkis, J.R., Boussetta, N., Blouet, C. et al. (2015). Effect of pulsed electric fields and high voltage electrical discharges on polyphenol and protein extraction from sesame cake. *Innov Food Sci Emerg Technol* 29 (SI): 170–177.

105 Chaves, J.O., de Souza, M.C., da Silva, L.C. et al. (2020). Extraction of flavonoids from natural sources using modern techniques. *Front Chem* 8: 864.

106 Marcet, I., Álvarez, C., Paredes, B., and Díaz, M. (2016). The use of sub-critical water hydrolysis for the recovery of peptides and free amino acids from food processing wastes. Review of sources and main parameters. *Waste Manag* 49: 364–371.

107 Álvarez-Viñas, M., Rodríguez-Seoane, P., Flórez-Fernández, N. et al. (2021). Subcritical water for the extraction and hydrolysis of protein and other fractions in biorefineries from agro-food wastes and algae: a review. *Food Bioprocess Technol* 14 (3): 373–387.

108 Ho, C.H.L., Cacace, J.E., and Mazza, G. (2007). Extraction of lignans, proteins and carbohydrates from flaxseed meal with pressurized low polarity water. *LWT Food Sci Technol* 40 (9): 1637–1647.

109 Ndlela, S.C., de Moura, J.M.L.N., Olson, N.K., and Johnson, L.A. (2012). Aqueous extraction of oil and protein from soybeans with subcritical water. *J Am Oil Chem Soc* 89 (6): 1145–1153.

110 Wiboonsirikul, J., Hata, S., Tsuno, T. et al. (2007). Production of functional substances from black rice bran by its treatment in subcritical water. *LWT Food Sci Technol* 40 (10): 1732–1740.

111 Aly, A.A. and Górecki, T. (2020). Green approaches to sample preparation based on extraction techniques. *Molecules* 25: 1719.

112 Yucui, H., Congfei, Y., and Weize, W. (2018). Deep eutectic solvents: green solvents for separation applications. *Acta Phys Chim Sin* 34 (8): 873–885.

113 Chen, Y. and Mu, T. (2021). Revisiting greenness of ionic liquids and deep eutectic solvents. *Green Chem Eng* 2 (2): 174–186.

114 Vilková, M., Płotka-Wasylka, J., and Andruch, V. (2020). The role of water in deep eutectic solvent-base extraction. *J Mol Liq* 304: 112747.

115 Yue, J., Zhu, Z., Yi, J. et al. (2021). Structure and functionality of oat protein extracted by choline chloride–dihydric alcohol deep eutectic solvent and its water binary mixtures. *Food Hydrocoll* 112: 106330.

116 Hernández-Corroto, E., Plaza, M., Marina, M.L., and García, M.C. (2020). Sustainable extraction of proteins and bioactive substances from pomegranate peel (Punica granatum L.) using pressurized liquids and deep eutectic solvents. *Innov Food Sci Emerg Technol* 60: 102314.

117 Wahlström, R., Rommi, K., Willberg-Keyriläinen, P. et al. (2017). High yield protein extraction from Brewer's spent grain with novel carboxylate salt – urea aqueous deep eutectic solvents. *ChemistrySelect* 2 (29): 9355–9363.

118 Moreno-Nájera, L.C., Ragazzo-Sánchez, J.A., Gastón-Peña, C.R., and Calderón-Santoyo, M. (2020). Green technologies for the extraction of proteins from jackfruit leaves (Artocarpus heterophyllus Lam). *Food Sci Biotechnol* 29 (12): 1675–1684.

119 Ntone, E., Bitter, J.H., and Nikiforidis, C.V. (2020). Not sequentially but simultaneously: facile extraction of proteins and oleosomes from oilseeds. *Food Hydrocoll* 102: 105598.

120 Lin, Z., Jiao, G., Zhang, J. et al. (2020). Optimization of protein extraction from bamboo shoots and processing wastes using deep eutectic solvents in a biorefinery approach. *Biomass Convers Biorefinery* https://doi.org/10.1007/s13399-020-00614-3.

121 Du, L., Arauzo, P.J., Zavala, M.F.M. et al. (2020). Towards the properties of different biomass-derived proteins via various extraction methods. *Molecules* 25 (3): 488.

122 Sen, D. and Kahveci, D. (2020). Production of a protein concentrate from hazelnut meal obtained as a hazelnut oil industry by-product and its application in a functional beverage. *Waste Biomass Valorization* 11 (10, SI): 5099–5107.

123 Ia Cour, R., Schjoerring, J.K., and Jorgensen, H. (2019). Enhancing Protein Recovery in Green Biorefineries by Lignosulfonate-Assisted Precipitation. *Front Sustain Food Syst* 3.

124 Arauzo, P.J., Du, L., Olszewski, M.P. et al. (2019). Effect of protein during hydrothermal carbonization of brewer's spent grain. *Bioresour Technol* 293: 122117.

125 Potin, F., Lubbers, S., Husson, F., and Saurel, R. (2019). Hemp (Cannabis sativa L.) protein extraction conditions affect extraction yield and protein quality. *J Food Sci* 84 (12): 3682–3690.

126 Larsen, S.U., Jorgensen, H., Bukh, C., and Schjoerring, J.K. (2019). Green biorefining: effect of nitrogen fertilization on protein yield, protein extractability and amino acid composition of tall fescue biomass. *Ind Crop Prod* 130: 642–652.

127 Choi, W.C., Hon, W.M., Mohamad, M. et al. (2019). Antioxidant properties of crude and cold ethanol precipitated protein from palm kernel cake (pkc) as potential cosmeceutical agent. *J Oil Palm Res* 31 (1): 159–164.

128 Grudniewska, A., de Melo, E.M., Chan, A. et al. (2018). Enhanced protein extraction from oilseed cakes using glycerol-choline chloride-deep eutectic solvents: a biorefinery approach. *ACS Sustain Chem Eng* 6 (11): 15791–15800.

129 Talekar, S., Patti, A.F., Singh, R. et al. (2018). From waste to wealth: high recovery of nutraceuticals from pomegranate seed waste using a green extraction process. *Ind Crop Prod* 112: 790–802.

130 Hojilla-Evangelista, M.P. and Evangelista, R.L. (2017). Effects of steam distillation and screw-pressing on extraction, composition and functional properties of protein in dehulled coriander (Coriandrum sativum L.). *J Am Oil Chem Soc* 94 (2): 315–324.

131 Kehili, M., Schmidt, L.M., Reynolds, W. et al. (2016). Biorefinery cascade processing for creating added value on tomato industrial by-products from Tunisia. *Biotechnol Biofuels* 9 (1): 261. http://biotechnologyforbiofuels.biomedcentral.com/articles/10.1186/s13068-016-0676-x.

132 Zhang, C., van Krimpen, M.M., Sanders, J.P.M., and Bruins, M.E. (2016). Improving yield and composition of protein concentrates from green tea residue in an agri-food supply chain: effect of pre-treatment. *Food Bioprod Process* 100: 92–101.

133 Tamayo Tenorio, A., Gieteling, J., de Jong, G.A.H. et al. (2016). Recovery of protein from green leaves: overview of crucial steps for utilisation. *Food Chem* 203: 402–408.

134 Zhang, C., Sanders, J.P.M., Xiao, T.T., and Bruins, M.E. (2015). How does alkali aid protein extraction in green tea leaf residue: a basis for integrated biorefinery of leaves. *PLoS One* 10 (7): 1–14.

135 Gofferje, G., Zoettl, A., Staebler, A. et al. (2015). Influence of protein extraction techniques of different de-oiled residues from Jatropha curcas L. on protein recovery and techno-functional properties. *Waste Biomass Valorization* 6 (2): 225–235.

136 Zhang, C., Sanders, J.P.M., and Bruins, M.E. (2014). Critical parameters in cost-effective alkaline extraction for high protein yield from leaves. *Biomass Bioenergy* 67: 466–472.

137 Zhong, C., Wang, R., Zhou, Z. et al. (2012). Functional properties of protein isolates from Caragana korshinskii Kom. Extracted by three different methods. *J Agric Food Chem* 60 (41): 10337–10342.

138 Weisz, G.M., Schneider, L., Schweiggert, U. et al. (2010). Sustainable sunflower processing – I. Development of a process for the adsorptive decolorization of sunflower [Helianthus annuus L.] protein extracts. *Innov Food Sci Emerg Technol* 11 (4): 733–741.

139 da Silva, F.D., Lopes, A.P., Segatto, M.L. et al. (2020). Development and application of green and sustainable analytical methods for flavonoid extraction from Passiflora waste. *BMC Chem* 14 (1): 56. https://bmcchem.biomedcentral.com/articles/10.1186/s13065-020-00710-5.

3

Separation Processes for Sustainable Produced Water Treatment and Management

Lanre M. Oshinowo, Young Chul Choi, Elaf A. Ahmed, and Hasan A. Al Abdulgader

Research & Development Center, Saudi Aramco, Dhahran, Saudi Arabia

3.1 Introduction

Produced water is the water found in the same formations as oil and gas and is a by-product of hydrocarbon production operations that is brought to the surface along with oil and gas from onshore and offshore wells. It is the single largest by-product stream by volume from onshore and offshore oil and gas production facilities.

Produced water primarily consists of the naturally occurring formation or connate water trapped for millions of years associated with the oil and gas in the underground hydrocarbon reservoirs of porous sedimentary rock between layers of impermeable strata with the earth's crust, water that has been injected into the formation for the purposes of enhancing oil recovery, chemicals used to facilitate production, and possible reaction by-products formed through abiotic or biotic processes [1–3].

Produced water is reused for oil and gas production, recycled for use in the operations, disposed off to underground reservoirs or discharged into the environment, and used for beneficial purposes in non-oil and gas industry applications. Reuse and recycling of produced water is possible through a range of current separation processes to reduce the organic (mostly oil) and inorganic (mostly salt) components to levels acceptable for the intended usage.

The sustainability of produced water treatment and management within the context of hydrocarbon resource recovery considers the direct, indirect, and cumulative impacts across the project life cycle. The reuse and recycling of produced water in a sustainable way requires an assessment of the origin of produced water and its constituents, the current produced water management practices, and the current technology for treating and removing the dispersed or suspended components in the produced water. Technologies to treat produced water for the removal of dissolved components, primarily dissolved salts, for reuse in other operations or for beneficial reuse can enhance the sustainability of produced water treatment and reduce the reliance on freshwater consumption. The objective of this

Sustainable Separation Engineering: Materials, Techniques and Process Development, Volume 1, First Edition. Edited by Gyorgy Szekely and Dan Zhao.
© 2022 John Wiley & Sons Ltd. Published 2022 by John Wiley & Sons Ltd.

chapter is to review the current technologies and present new directions for produced water treatment with a focus on sustainability, energy efficiency, and produced water reuse.

3.1.1 Origins and Sources of Produced Water

The oil and gas industry globally produced approximately 159 billion barrels of water in 2020 from current onshore and offshore production of oil and gas from conventional and unconventional reservoirs [4]. Considering the global production of approximately 34.4 billion barrels of oil in 2020 [5], the current ratio of daily produced water production to oil production is about five barrels of produced water per barrel of oil. When reservoirs reach a stage of maturity, they experience an increase in the water–to–oil ratios.

Produced water is a complex mixture of dissolved and particulate organic and inorganic chemicals in the water that ranges from essentially freshwater to concentrated saline brine [1]. The components of produced water can be broadly classified into organic and inorganic compounds, including dissolved and dispersed oils, grease, heavy metals, suspended solids, radionuclides, treating chemicals, formation solids, dissolved solids, dissolved gases, scale products, waxes, microorganisms, and oilfield chemicals (polymers) [6, 7]. Oil and gas production additionally consumes large volumes of surface water, freshwater or marine, and aquifer water that become commingled with the produced water [6–9].

Decades of oil and gas production have developed many solutions to managing this waste stream from using produced water to sustain the pressure of underground reservoirs to enable continued extraction of oil and gas to the potential beneficial uses for produced water including agricultural uses. Most produced water is either reinjected or disposed of. In the United States, about two-fifths of the produced water is reinjected while about half is disposed of using saltwater disposal (SWD) wells with the remainder recycled for reuse in fracturing operations.

During oil and gas production, managing the produced water is an essential aspect of the process. The volume of produced water varies by the reservoir, the type of production operations, and changes over time during the life of the production operations [10]. In conventional oil and gas production, oil and/or gas exist in relatively permeable geologic formations, and the natural pressures in the formation conditions, often facilitated by pumping, pushing, or lifting the oil, gas, and formation water toward a well for surface extraction [11, 12]. Figure 3.1 illustrates the well types in conventional and unconventional oil and gas production. The amount of produced water created by a conventional oil and gas well can increase over time as the hydrocarbon reservoir depletes, resulting in greater water–to–hydrocarbon ratios over time [13]. When oil and/or gas have low mobility or are found in geological formations with low permeability, such as shale beds or "tight" sands, unconventional production occurs.

Most wells in unconventional oil and gas formations (e.g. shale, coal bed methane, and tight gas sands) are stimulated using hydraulic fracturing where water, typically freshwater from lakes and rivers or groundwater from underground wells, is injected under pressure into the formation to create pathways allowing the oil or gas to be recovered in a cost-effective manner [14].

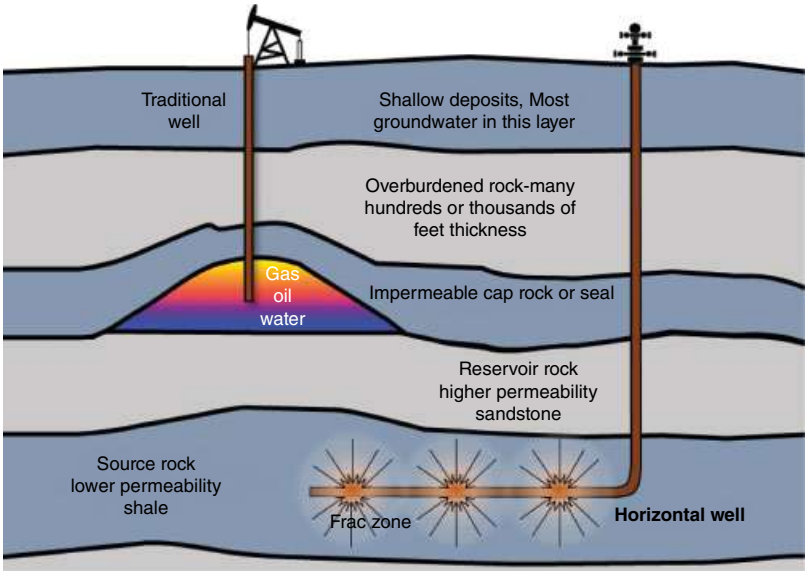

Figure 3.1 Conventional and unconventional oil and gas wells. Not to scale. *Source:* Courtesy of Lanre Oshinowo.

Immediately following hydraulic fracturing in the well, the injected water returns to the surface and is known as flowback water. The quantity of this flowback water decreases over the next weeks or months until any produced water coming from the well to the surface along with hydrocarbons is mostly formation water [15]. As such, the produced water flow rate from an unconventional well decreases over time as the return of flowback water decreases and the well produces relatively lower volumes of formation water.

The produced water from unconventional reservoirs cannot typically be reinjected into the shale reservoir for enhanced recovery but requires disposal to non-oil-producing geologic intervals (e.g. salt water disposal wells) or reuse for hydraulic fracturing [16]. In 2020, the main water issues associated with unconventional oil and gas extraction include rising water demand for hydraulic fracturing, managing high water volumes that are coproduced with oil and gas (produced water, including flowback water from hydraulic fracturing, and water from subsurface formations) [11].

A sustainable water life cycle for unconventional oil and gas wells is illustrated in Figure 3.2 showing the principal water streams including a recycle of the flowback and produced water after treatment and the application of treated produced water for beneficial uses. Evaporation that occurs during transportation and storage contributes to produced water losses that could alternatively be contained and reused in the produced water life cycle. The life cycle freshwater consumption, e.g. makeup water, for tight oil is less than that of conventional onshore oil production [17]. Additional considerations for greenhouse gas emissions in the life cycle analysis can provide a holistic view of the environmental impact associated with drilling and production.

Approximately, 55% of produced water generated from conventional and unconventional activities in the United States is handled as wastewater for disposal [18]. However, large

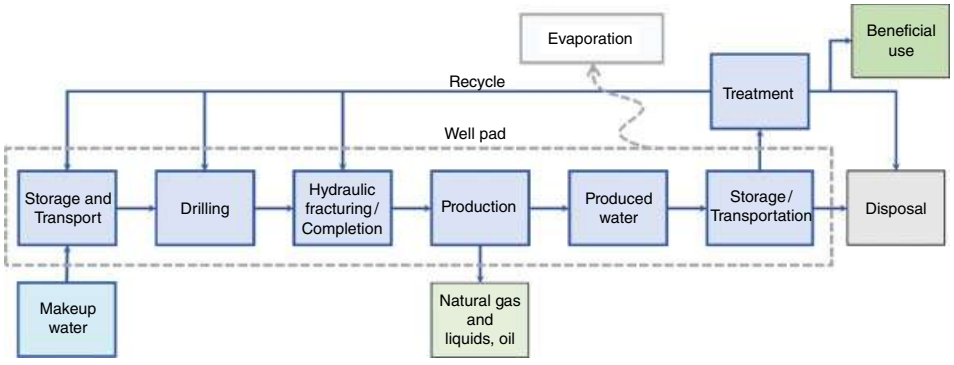

Figure 3.2 Water life cycle for unconventional oil and gas production. *Source:* Adapted from [18].

quantities of produced water are being reused for new drilling fluids, hydraulic fracturing operations, and in conventional activities for waterfloods conducted to enhance oil recovery (EOR). With increasing produced water volumes from increasing unconventional production, produced water disposal in saltwater disposal wells has raised concerns over surface water and groundwater contamination and also the risk of increasing seismic events [19, 20].

In the offshore oil and gas industry, approximately 75% of the produced water is treated and discharged into the ocean with the balance being reinjected [21]. In offshore oil and gas production, most of the produced water is discharged directly to the ocean after meeting the environmental regulations and standards through the application of effective and economical treatment technologies. The disposal of untreated produced water containing many hazardous materials will not be environmentally sustainable.

In onshore oil and gas production, approximately 90% of the produced water is reinjected with the remainder being discharged, reused for other purposes, or evaporated [10]. There are differences between onshore and offshore produced water handling in the applicable environmental regulations and standards, produced water volumes generated, and the differences in targeted pollutants that lead to different produced water management approaches. While onshore operations are mostly targeted at decreasing the salt content, in offshore operations, oil and grease content are the primary concern [21–23].

Increasing produced water production has the potential to make available a substantial volume of water that could potentially offset, or supplement, freshwater demands in geographic locations that are semiarid [18]. Water usage for oil and gas operations competes with other beneficiaries like agriculture, industry, and municipalities for access to freshwater resources. Produced water reuse is beneficial to oil and gas producers as an alternative to disposal in underground wells, which can be costly, locally unavailable, or subject to volume restrictions.

In 2014, the global freshwater usage in oil and gas conventional and unconventional production was 10 billion cubic meters (63 billion barrels) increasing to 11 billion cubic meters (69 billion barrels) by 2040 representing 2% of the total groundwater and surface water withdrawals for energy production and just 0.2% of the global water withdrawal demand [24].

Opportunities to use produced water in applications outside the oil and gas industry are not as readily available but may make sense in certain circumstances. Most produced water contains large amounts of salt (often expressed as total dissolved solids or TDS) and cannot be used for applications requiring freshwater without some degree of treatment. Further, produced water may contain many other chemical components. Knowing the components of produced water and the type of treatment required to make the treated water fit for its end use are important steps in evaluating reuse projects [14].

Excessive production of water is the main criterion to abandon oil and gas wells, leaving large volumes of hydrocarbons behind [25]. By implementing economically viable water management schemes during field development, the production of additional recoverable reserves is enabled. When the volume of produced water increases, the handling costs increase and there is a potential environmental impact. With oil and gas production continuing to provide wealth for society, the water must be managed responsibly in an environmentally responsible manner and at an economically viable cost.

3.1.2 Characteristics of Produced Water

The chemical and physical properties of produced water are complex and vary considerably based on the geographic formation, the type of hydrocarbon produced, and variations in chemicals used during drilling and production [6]. Produced water contains a high level of mineral salts including cations and anions dissolved in water (often expressed as salinity, conductivity, or TDS), and organic compounds including volatile and semi-volatile organics, hydrocarbons, organic acids, waxes, grease, and oils in dispersed/free/suspended form and in dissolved form. Other contaminants include suspended solids, inorganic metals, and other inorganic components including compounds such as sulfate and ammonia, naturally occurring radioactive material (NORM), chemical additives to improve drilling, and production chemicals such as biocides, scale and corrosion inhibitors, and emulsion and reverse-emulsion breakers, transformational by-products formed from the interaction between added chemicals and formation water, dissolved gases, and bacteria. Fluids used in hydraulic fracturing for unconventional oil and gas production or "fracking" fluids contain a mix of hundreds of organic and inorganic additives in aqueous media that are produced with the flowback water discussed previously and with significant implications for disposal and reuse [26].

In produced water management, discharge into the environment is done with the consideration of the necessary treatment steps required to eliminate impactful components in the produced water to meet the environmental regulations and minimize the impact on the environment in a sustainable manner. The produced water characterization illustrated in Figure 3.3 highlights the need to deploy different treatment and technology solutions to treat produced water to desired quality. The components in produced water may be considered dissolved if the mean size passes through a 0.45-micron filter. Any larger particulate or droplet is considered dispersed or suspended.

The characteristics are described by the concentrations of undissolved and dissolved oil components and organics, like BTEX (benzene, toluene ethylbenzene, and xylene), PAH (polycyclic aromatic hydrocarbons), organic acids, NPD (naphthalenes, phenanthrenes, and dibenzothiophenes), organic acids, alkylated phenols, and inorganics (e.g. major cations and anions, formation solids, and proppants), as well as NORM as determined from various analytical methods [27].

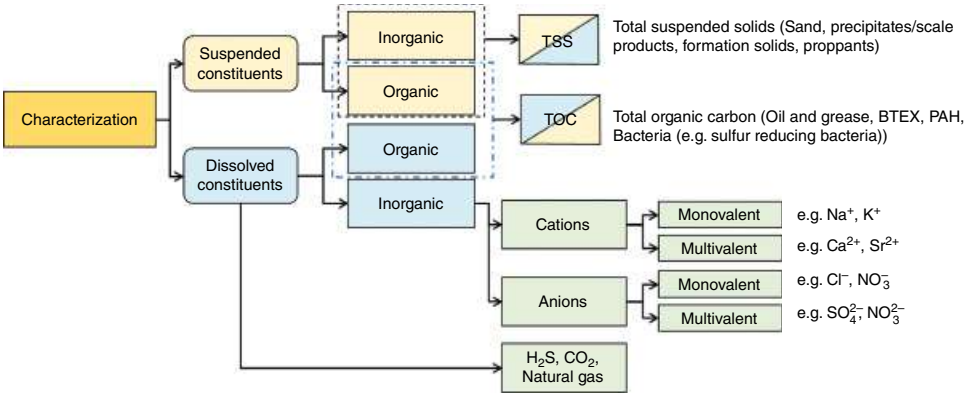

Figure 3.3 Characterization of produced water. *Source:* Adapted from [28].

The characteristic properties of produced water around the world are detailed in these references [1, 8, 16, 29–33]. The main physical and chemical properties of produced water are summarized here in Table 3.1. Table 3.2 summarizes the typical inorganic ions in produced water. The divalent cations (Ba^{2+}, Sr^{2+}, Ca^{2+}, and Mg^{2+}) in produced water form scales and must be partially decreased to reduce the scale-formation potential of the treated produced water for reuse in oil production with minimal additional treatment [34, 35].

3.1.3 Current Produced Water Management Practice

A number of factors impact the cost magnitude for the amount of treatment needed to address the water chemistry for reuse and recycle, and the regulatory requirements for handling and disposal [9]. Produced water management has been the focus of oil and gas industry in view of the stringent legislations on the discharge of oil and gas produced water into the environment and the potential of produced water as a source of freshwater, which hitherto comes from surface water, groundwater, or municipal water, for water-deficient oil-producing regions or countries.

During oil and gas production, produced water is managed by one or more of the methods illustrated in Figure 3.4. Reusing, treating, and recycling produced water in oil and gas operations, as well as meeting discharge regulations and exploring potentially beneficial uses such as aquifer regeneration, agricultural water uses, livestock and animal drinking water, and even human consumption water, are all goals of oil and gas produced water management [37]. Regulatory requirements, environmental effects, water risk, and the technological and economic viability of alternatives are just a few of the factors that influence decisions about produced water management activities [38].

The following options and costs for oil and gas produced water management are listed as follows [22, 39–41]:

1) **Injection into oil wells:** The produced water is injected into the same oil well from where it is produced or transported to the disposal well at another location. The cost associated with this process can reach up to $6.00 per barrel depending primarily on the

Table 3.1 Typical physical and chemical properties of oil and gas field produced water [9, 22, 29, 31, 36].

Parameter	Units	Oilfield produced water	Gas field produced water
Total dissolved solids (TDS)	mg/L	1000–400,000	2600–360,000
Total suspended solids (TSS)	mg/L	1.2–21,820	8–5484
Density	kg/m^3	1014–1140	
pH		4.3–10	3.1–7
Total organic carbon (TOC)	mg/L	3.4–5960	67–38,000
Chemical oxygen demand (COD)	mg/L	1200	2600–120,000
Biological oxygen demand (BOD)	mg/L	NA	75–2870
Total petroleum hydrocarbons (TPH)	mg/L	2–565	
BTEX (benzene, toluene, ethylbenzene, and xylene)	mg/L	0.39–35	
Surface tension	dyne/cm	43–78	
Conductivity	μS/cm	4200–58,600	
Alkalinity ($CaCO_3$)	mg/L	6.1–200	
Phenol	mg/L	Up to 23	
Volatile fatty acids	mg/L	2–4900	
Oil and grease	mg/L	6.9–210	2.3–60
m-xylene	mg/L	0.015–0.611	
Methylene chloride	mg/L	1.41–1.71	0.02
Methylene blue active substances (anionic surfactants)	mg/L	0.01–54	
Hexane extractable materials	mg/L	0.6–2000	

transportation and storage costs, the level of treatment required for injection, and compliance with environmental regulations.

2) **Reuse in oil and gas operations:** The produced water could be treated and used in oil and gas processing operations. The usual cost associated with this process varies from $0.04 to $0.07 per barrel.
3) **Direct discharge:** The produced water is discharged directly as per regulation norms with usual cost associated to this process varying from $0.01 to $0.05 per barrel.
4) **Consumed for different applications:** The produced water can be treated to convert it into an asset with a cost range from $0.25 per barrel and up.

3.2 Produced Water Treatment Technologies

Produced water must be treated prior to disposal, reuse, or recycle for use in oil and gas production. This includes produced water disposal offshore or onshore in disposal wells or for reservoir pressure maintenance. Treatment is generally accomplished in stages for the

Table 3.2 Typical concentrations of inorganic ions in oil and gas field produced water, in mg/L [9, 22, 29, 31, 36].

Component	Oilfield produced water	Gas field produced water	Component	Oilfield produced water	Gas field produced water
Cl	80–310,561	1400–190,000	Cd	<0.005–0.2	<0.02–1.21
Br	0–12,000	150–1149	Cr	0.02–1.1	Up to 0.03
I	0–500		Cu	<0.002–1.5	Up to 5
HCO_3	1.9–7355		Li	3–50	4.6–572
CO_3	0–800		Mn	<0.004–175	Up to 63
SO_4	0.5–7851	<0.1–47	Ni	NA	<1–9.2
SO_3	~10		Pb	0.002–8.8	<0.2–10.2
PO_4	0–0.10		Sr	0.02–1000	Up to 6200
NO_3	0–3.5		Ti	<0.01–0.7	
NO_2	0.05		Zn	0.01–35	<0.02–5
NH_3–N	10–300		As	<0.005–0.3	Up to 151
Ca	18–132,687	Up to 51,300	Hg	<0.001–0.002	NA
Na	316–134,652	520–120,000	Ag	<0.001–0.15	0.047–7.0
K	8.6–14,649	149–3870	Be	<0.001–0.004	
Mg	4–18,145	0.9–4300	Total Ra ^{238}U	0.008–2.7	
Fe	<0.1–100	Up to 1100	^{232}Th	0.008–0.027	
Al	310–410	<0.5–83	^{210}Pb	1.35–5130	
B	5–95	Up to 56	^{210}Po	0.005–0.17	
Ba	0–22,400	<1–1740	NORM	0.054–32,400	

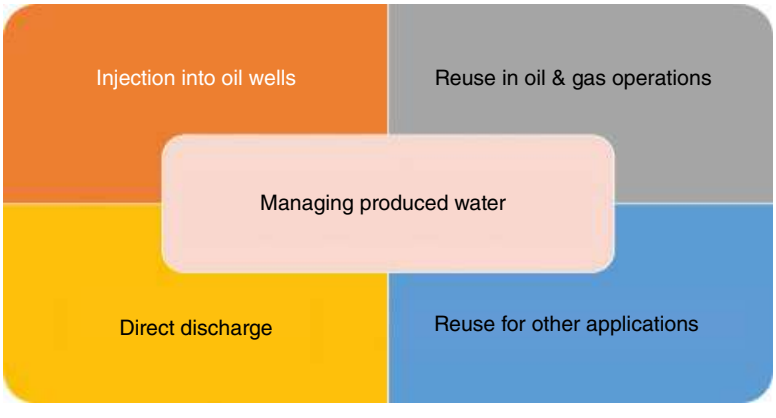

Figure 3.4 Current strategies for produced water management. *Source:* Courtesy of Elaf Ahmed.

removal of dispersed, insoluble, or free oil and suspended solids, and the reduction of the dissolved components as illustrated by the schematic in Figure 3.5.

The free or dispersed oil typically occurs in concentrations up to 10,000 ppm and typically will require multiple treatment steps to reduce the concentration to an acceptable level appropriate for reinjection, reuse in operations, or offshore disposal. These treatment steps are commonly classified as primary, secondary, and tertiary stages. However, there is no common delineation for each classification.

Generally, each treatment stage in a produced water treatment process is defined by the influent and effluent oil in water concentrations and particle sizes of the suspended/dispersed/free oil and suspended solids in each stage. Each treatment stage reduces the oil and solids concentration and increases the cost, complexity, and energy requirements for produced water treatment. The separation of the dispersed oil and solids occurs through normal or enhanced gravity separation or filtration technologies. The separated solids must be removed from the produced water treatment system to avoid solids buildup and accumulation of "schmoo," which is a sticky material that is a combination of solids and oil field treatment chemicals used for corrosion inhibition, emulsion demulsifiers, and scale inhibitors, which builds up on every surface exposed to the produced water [9].

The process schematic for a typical onshore oil and gas production facility with two stages for produced water treatment for reinjection is illustrated in Figure 3.6. The production fluids – oil, water, and gas – are received by the production separators to separate gas and produced water from the wet crude. Following an optional crude-heating step, the wet crude is dehydrated in an electrostatic coalescer vessel [42]. The produced water is processed to remove the dispersed oil in two processing stages. The first is a water–oil separator (WOSEP) followed by a flotation unit or de-oiling hydrocyclones. Figure 3.7 illustrates the process schematic for a typical offshore oil and gas production facility with three stages for produced water treatment for disposal overboard. The dispersed or suspended components in the produced water are removed through a sequence of stages including hydrocyclones for de-oiling and for de-sanding, a de-gasser, or a flotation unit, and finally, filtration with membrane filtration or media filters.

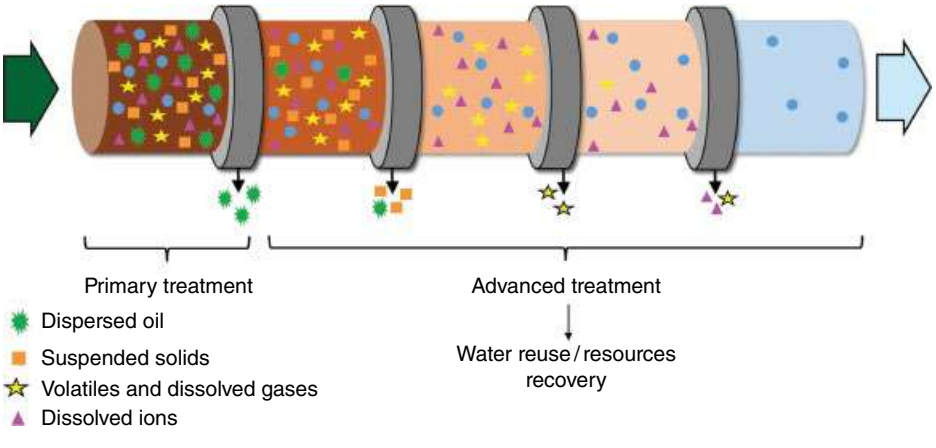

Figure 3.5 Process for produced water treatment by removal of dispersed/suspended and dissolved components. *Source:* Courtesy of Young Chul Choi.

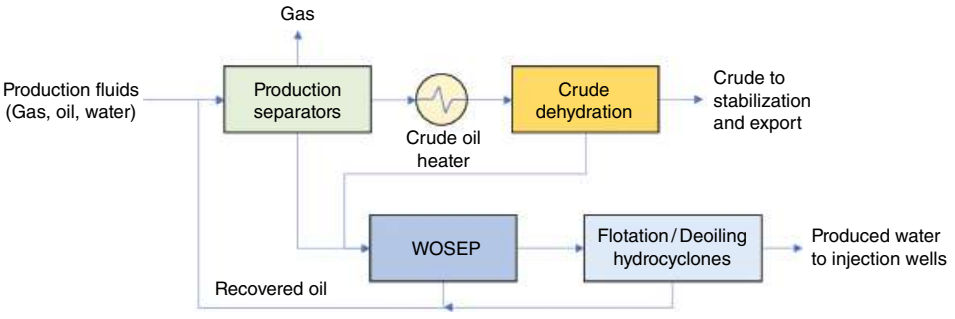

Figure 3.6 Typical onshore oil and gas production facility with two stages (primary and secondary) for produced water treatment for reinjection. *Source:* Courtesy of Lanre Oshinowo.

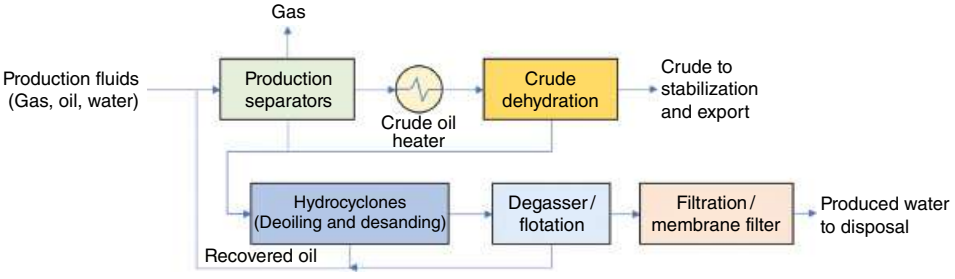

Figure 3.7 Typical offshore oil and gas production facility with three stages (primary, secondary, and tertiary) for produced water treatment for disposal overboard. *Source:* Courtesy of Lanre Oshinowo.

The dissolved or soluble components in produced water can be reduced using technologies for desalination and mineral extraction only after the dispersed/suspended components and some dissolved components, e.g. dissolved gases (H_2S), and volatile organics. The following sections will review the technologies for the removal of dispersed and dissolved components in produced water.

3.2.1 Removal of Oil, Particles, and Gaseous Components

During pipeline transportation from the reservoir, crude oil, produced water, and associated gas flow in complex multiphase flow patterns where dispersions of emulsions and foams are formed. The gas-phase generally separates quickly due to density differences, but the liquid phase emulsions are typically stable or "tight" and difficult to separate and chemical additives called demulsifiers are injected into the production header at the inlet of the production facility to "break" the emulsions and improve separation [43]. Emulsion stability is a consequence of the amphiphilic species that are indigenously present in the crude oil, such as asphaltenes, resins, and acids [44]. Some exogenous factors increase the emulsion stability, like fine solids or chemical additives applied in the production network for flow assurance purposes like corrosion inhibition, scale formation, biocides, and hydrate inhibitors. These oil field chemicals act as surfactants that stabilize the oil–water

Table 3.3 Injection water quality characterization.

Parameter	Injection
Particle size (micron)	<5
Dispersed oil (mg/L)	<20
Suspended solids and oil (mg/L)	<50

Source: Courtesy of Mohammed Soliman.

interface forming oil–water emulsions or reducing oil droplet coalescence in the produced water [45, 46]. This phenomenon increases the difficulty of removing dispersed oil droplets from the produced water stream without an engineered system or resolving the chemical applicability or compatibility issues between different oilfield chemicals [47].

The current practice of produced water treatment has a twofold objective. The first objective is to remove oil and suspended solids so that the reinjection or deep well disposal can be conducted without serious plugging or frequent cleaning [48]. Typically, oil and gas wells decrease in injectivity as they age and new wells need to be drilled every few years to maintain production, which is a high cost and requires a significant amount of chemicals and energy. If the treatment of the oil and suspended solids can be successfully implemented, the oil and gas recovery can be achieved with lower environmental impact since there will be less need to drill new wells and to inject chemicals for periodic cleaning of the wells. Table 3.3 shows a typical example of produced water contaminants and their target concentrations for reinjection. Most of the oil and gas fields currently use some form of oil–water separation as well as solids removal. These mechanisms rely on gravity-based separation and flotation which use minimal energy.

The second objective is to treat the produced water with more advanced technologies to remove dissolved species, such as ions and dissolved organics, for reuse. Produced water typically has high concentrations of TDS and it requires higher levels of pressure, temperature, or other energy input for separation from water. Such a high level of treatment for produced water has not been widely implemented due to the lack of economical technologies suitable for the oil and gas industries.

Oil and suspended solids removal generally start with low energy methods, such as gravity-based water–oil separation, that can remove large droplets and particles. This is followed by higher energy processes, such as hydrocyclones, flotation, and filtration, are used to remove progressively smaller oil droplets and particles.

3.2.1.1 De-oiling and Filtration

One of the most important factors for the removal of oil is droplet size. Specific technologies are designed to handle specific size ranges of the influent oil droplet size and removing the oil droplets greater than a specific minimum. Within each process, oil separation from produced water is promoted by increasing the oil droplet size through droplet coalescence.

The coalescence process in fluid-particle systems can be described by three prevailing theories: film drainage model, energetic collision mechanism, and the critical approach velocity model [49] and rely on collision and contact between fluid particles (droplets) as

Table 3.4 Particle size removal capabilities.

Technology	Removes particles greater than size indicated (in microns)
API gravity separator	150
Corrugated plate separator	40
Hydrocyclones	10–15
Induced gas flotation without chemical addition	25
Induced gas flotation with chemical addition	3–5
Fiber or mesh coalesce	5
Media filter	5
Centrifuge	2
Membrane filter	0.01

Source: Adapted from [51].

the fundamental basis for coalescence. The relative velocity between droplets is responsible for collisions and the external flow dictates the frequency, force, and duration of collisions that, in turn, is dependent on fluctuations or velocity gradients in the continuous phase or by differences in droplet rising or settling velocities caused by body forces or buoyancy. In the film drainage model, droplets deform and a thin liquid film between the droplets delays coalescence until the film thins and drains to a critical thickness. This is followed by film rupture and, consequently, coalescence. The film thickness is critical to the efficiency of the coalescence process and needs to be sufficiently small for the electrostatic attraction to break the film and multiple small droplets merge to form a larger droplet. Coalescence is controlled by factors, such as fluid velocity, turbulence, pressure, droplet size, interfacial tension, and interfacial curvature [50].

Produced water from upstream multiphase separators may contain droplets larger than 200 μm (free oil). It may be necessary depending on the produced water end use to remove oil droplets down to 0.1 μm or smaller. The initial concentration of the oil may be 1000 ppm or higher, and the effluent concentration can be as low as 1 ppm with advanced treatment, such as ceramic membranes. In general, there is not a single technology that can treat all droplet sizes and multiple steps are necessary to remove progressively smaller droplets. Table 3.4 shows the nominal cut-off point for oil droplet sizes that can be removed in different treatment technologies.

3.2.1.1.1 API Separator

The first step for oil removal typically uses gravity separation, such as American Petroleum Institute (API) and WOSEPs [52]. The API design criteria are set by the API and use the difference in the specific gravity between water and oil and between water and suspended solids. These separators are used to remove the largest sizes of oil droplets, generally exceeding 150 μm. The API separator, as shown in Figure 3.8, provides a laminar condition where oil droplets will rise to the surface (gas/air–liquid interface) where they are removed by a mechanical skimmer in the case of the API separator or by an overflow weir into an oil

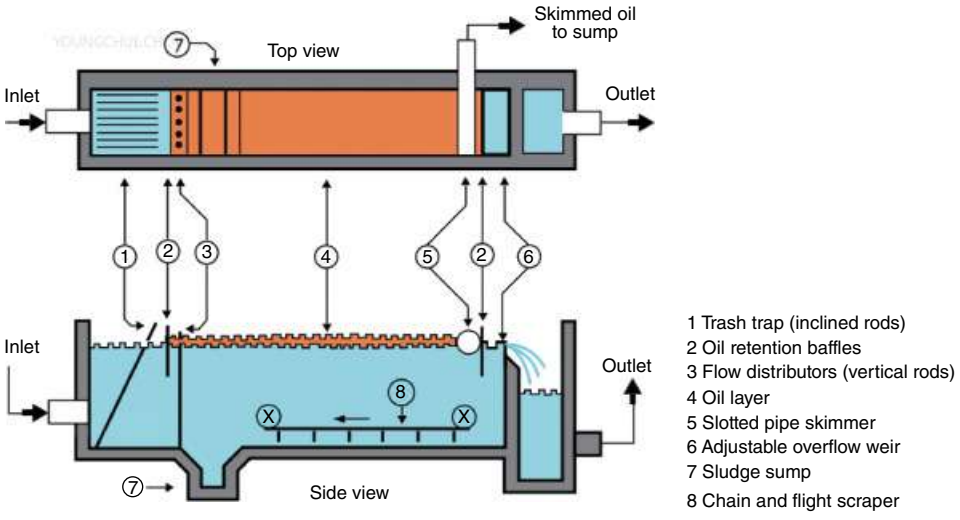

Figure 3.8 API separator. *Source:* Reproduced with permission from [51].

collection bucket. The solids settle to the bottom as sludge [53]. Figure 3.8 illustrates the mechanisms of the API separator. The rate of the oil droplet rise or the solid particle settling is described by the Stokes' law that determines the rise or settling velocity v (m/s) of an unhindered sphere in a quiescent liquid and is given by [54]:

$$v = \frac{1}{18}\frac{|\rho_o - \rho_w|}{\mu} gD^2$$

where, g is the gravitational acceleration (m/s^2), D is the diameter of the oil droplet (m), ρ_o is the mass density of the oil (kg/m^3), ρ_w is the mass density of water (kg/m^3), and μ is the dynamic viscosity of water (Pa.s). Turbulence in the system needs to be low for this equation to be valid. The oil and light fractions that have lower densities than water are removed. The settled sludge particles at the bottom of the separator will then be transferred to desanding hydrocyclones for further treatment by gravity separation. The mean horizontal velocity in the API separator is to be less than 3 feet per minute [55–57].

The polymeric flocculants can be added to facilitate the coalescence of particles by sedimentation. However, the use of synthetic organic polymers, such as polyacrylamides and polyamines, for produced water treatment has been discouraged due to their toxicity under certain conditions [58]. These limitations have led to the considerations for biodegradable coagulants, such as bentonite (coagulant aid) and chitosan (coagulants/flocculants), as eco-friendly and cost-effective improvements for API separators [9].

3.2.1.1.2 Water–Oil Separator (WOSEP)

The WOSEP is a horizontal gravity separator pressure vessel with a central inlet and two outlets for de-oiled produced water on either end of the vessel. Figure 3.9 shows the components and flow inside WOSEP. The feed mixture of oil and water enters the split-flow WOSEP vessel in the central compartment (A), where internal weirs separate water and oil (B). The oil

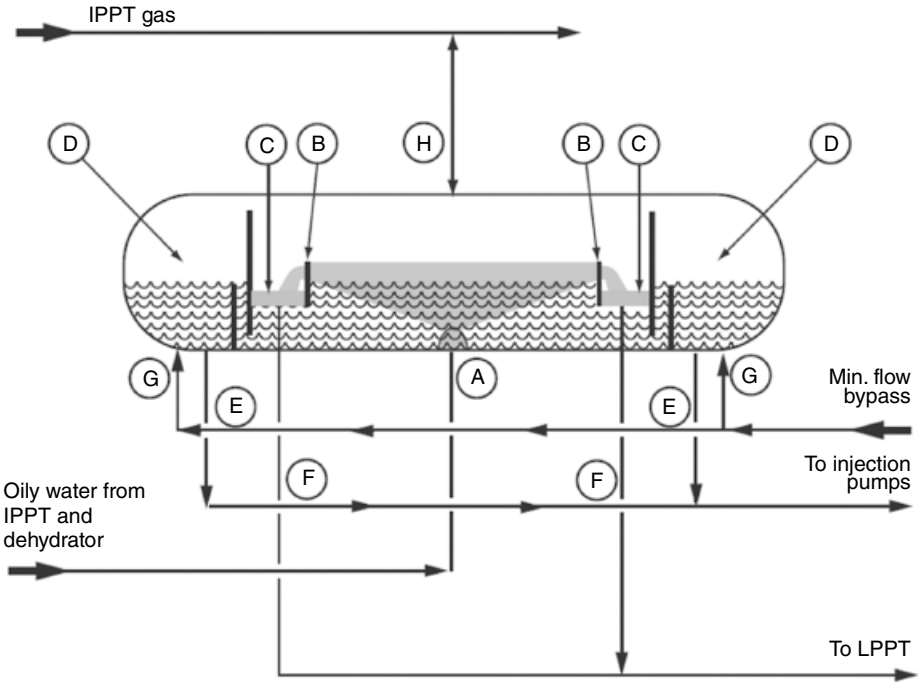

Figure 3.9 Water–oil separator (WOSEP) vessel. IPPT – intermediate pressure production trap/separator. LPPT - low pressure production trap/separator. *Source:* Courtesy of Saudi Aramco.

floats to the top and flows into two identical skimmers or oil buckets located on each end of the central separation compartment C. Separated water underflows each oil draw-off compartment, then overflows the water weir into water compartments at both ends of the vessel (D). Water from the vessel end compartments is combined in external piping and sent to the injection pumps, which boosts the pressure for reinjection into the reservoir. The total pump discharge flow rate is controlled by the WOSEP level controllers in compartment D. The injection pumps are protected against low-low discharge flow by minimum flow recycle to the WOSEP (G). The freeboard is filled with blanket gas at pressure.

A computational fluid dynamics (CFD) simulation of produced water flow in a WOSEP is shown in Figure 3.10 [59]. The streamlines colored by the time show the general flow pattern of flow in the vessel which is of importance to the overall separation performance of the vessel. CFD is typically used to quantify the deviation from idealized uniform plug flow through the separator and support the assumptions of the zero-order sizing and design tools [60]. Here, CFD is used to determine the flow patterns and de-oiling effectiveness at different produced water flow rates during the life of the field.

The WOSEP is designed to receive an inlet water quality of 1000 ppm oil-in-water. The produced water at the WOSEP outlet contains less than 100 ppm oil-in-water, and oil droplets greater than 150 μm are removed.

3.2.1.1.3 Corrugated Plate Interceptors (CPI)

The corrugated plate interceptor (CPI) was developed to overcome the limitations of API, which required a large footprint and the removal efficiency was low. The basic principle of

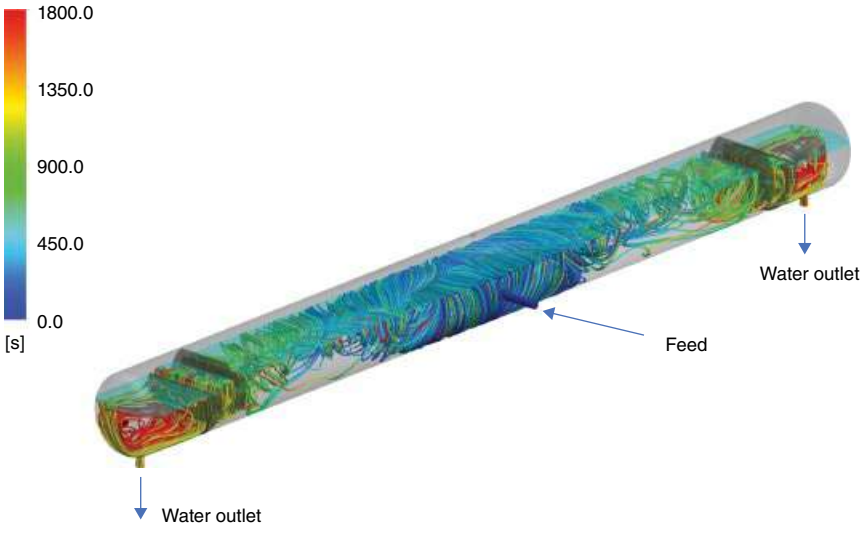

Figure 3.10 CFD simulation of produced water flow in a WOSEP illustrated by streamlines colored by time. CFD is used to determine the flow patterns and de-oiling effectiveness at different flow rates during the life of the field. The oil outlets are at the bottom of each oil bucket. *Source:* [59]. Courtesy of Lanre Oshinowo and Maher Sharif.

difference in gravity between liquids is employed in a CPI oil–water separation. This is defined as gravity separation. It is, therefore, apparent that the phase with high density (water) will settle and with lower density (oil) float to the surface. In the plate pack of the CPI separator, the oil droplets are intercepted and coalesce into large droplets. The droplets leave the plate pack rapidly countercurrent upward against the bulk liquid flow to the free surface. The clear water or treated effluent from the CPI separator leaves the plate pack at the bottom and is discharged over a weir arrangement to the outlet nozzle. Because separation in the CPI does not require chemical addition or applied pressure, it is generally considered to be environmentally friendly while providing higher performance. Figure 3.11 illustrates the working principle of the CPI.

The CPI is shown in Figure 3.12 where the produced water enters through the inlet nozzle (center right), the oily water overflows the perforated weir and flows into the parallel plate assembly. There is an opening for blanket gas, exits for primary and secondary solids, and jetting water injection to clear solids accumulation. The packing consists of stacks of angled corrugated surfaces where oil droplets can coalesce and become larger, which makes it easier to rise to the water surface due to the reduced settling distance for solids and rise distance for free oil. Also, because of such tight packing, the CPI is prone to plugging in high solids/scaling applications.

The performance of CPI is generally dependent on physical capacity, operating conditions, and material types of the corrugated plate coalescer [62]. It was reported that the lipophilicity of the plate surface was an important factor and the contact angle of oil less than 70° against the material surface was considered optimal [61].

The CPI separator can remove smaller oil droplets compared to the API separator, typically 40 μm or larger, requires less space, and its treatment efficiency is better than that of

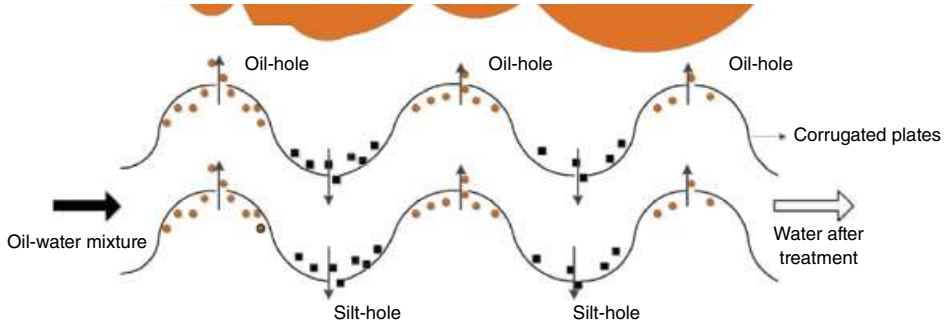

Figure 3.11 Schematic diagram of the process of oil removal and silt removal. *Source:* Reproduced with permission from [61].

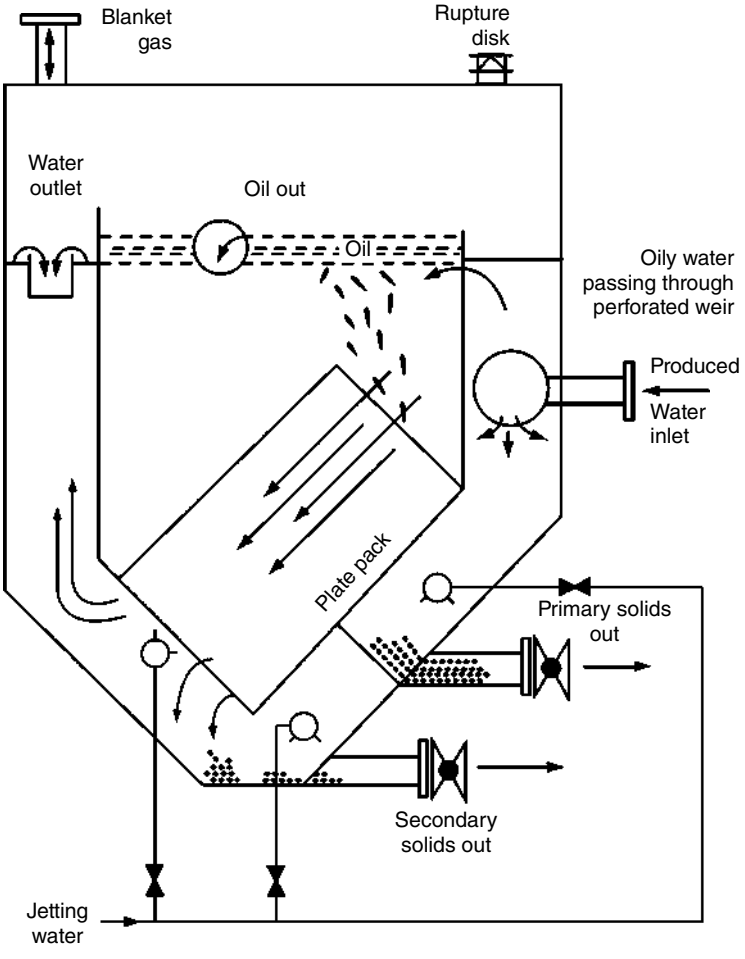

Figure 3.12 Corrugated plate impactor (CPI) oil–water separator. *Source:* Courtesy of Saudi Aramco.

the API separator [61]. However, smaller oil droplet removal is difficult with the CPI due to the physical limitations in the oil–water separation area that can be achieved with packing.

3.2.1.1.4 Gunbarrel Settling Tank Separator

A Gunbarrel settling tank is a three-phase separator commonly used for onshore separation of oil, produced water, and some gas at or close to atmospheric pressure. The Gunbarrel tank receives the well production fluids or the oily water from an upstream primary gas–oil–water separator as shown in Figure 3.13. Gas is initially disengaged in a central vertically oriented pipe and the oily water enters through a spreader below to oil–water interface to decelerate and spread the oil to improve buoyancy separation. After several hours of residence time, the oil overflows a weir at the top of the tank. The liquid level in the tank is maintained by an adjustable water leg on the water outlet. Typical oil recovery achieved in the Gunbarrel separator is 100–500 ppm oil-in-water if emulsions are not present. Gas bubbles can be injected into the water layer to increase oil recovery separation efficiency or to

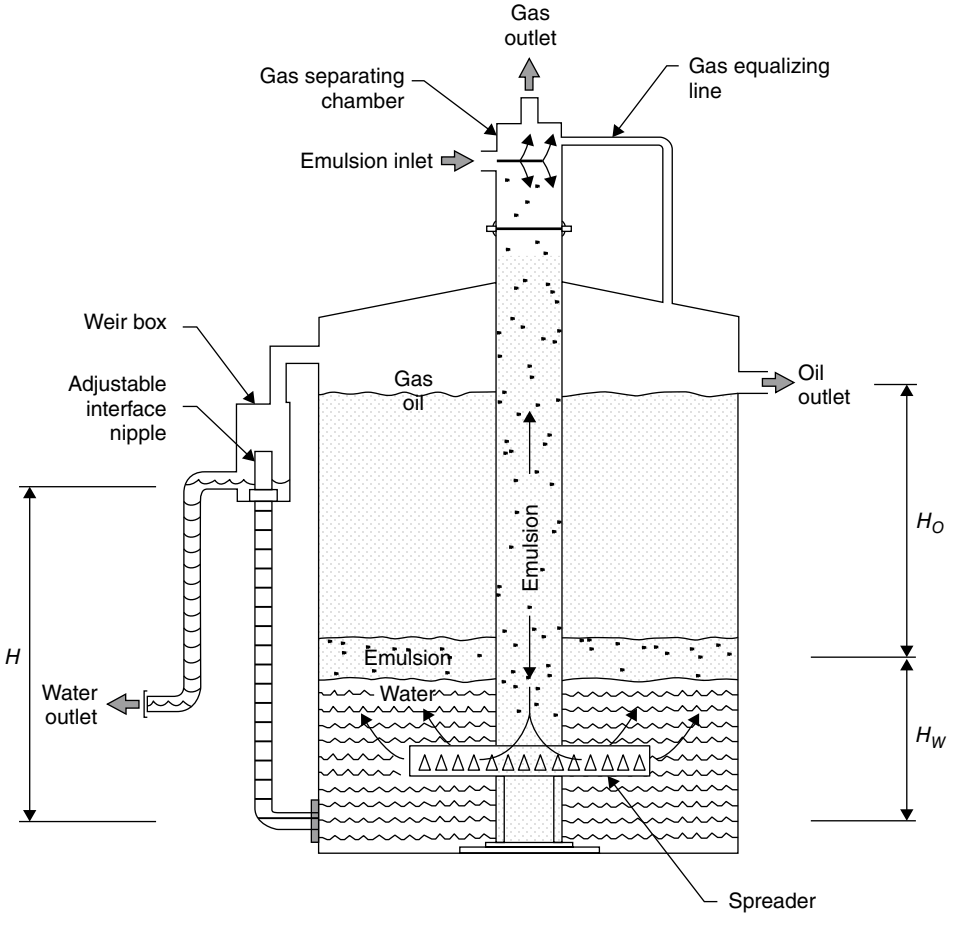

Figure 3.13 Typical Gunbarrel settling tank. *Source:* Reproduced with permission from [64].

reduce the tank size. The Gunbarrel separator is designed to remove oil droplets 100 μm and larger from the water phase, and water droplets 500 μm or greater from the oil phase [63].

3.2.1.1.5 Hydrocyclones

Hydrocyclones can be used to separate oil from water, water from oil, and sand from water, oil, or other fluid. After the gravity-based treatment, such as API and CPI, the produced water can be treated with de-sanding hydrocyclones to remove solids from the bottom and de-oiling hydrocyclones to remove oil from the skimmed top layer. The resulting treated water will have much smaller dispersed or suspended particles or oil droplets. Hydrocyclones have the advantage of being highly compact when compared with gravity-based settlers, and being simple in design, relatively inexpensive to manufacture, while requiring little maintenance, containing no moving parts, and having the ability to operate at high temperatures and pressures [65]. Hydrocyclones are mostly used in offshore applications because of their compact size relative to API and CPI separators and space-saving advantage.

The operating principle of hydrocyclones is to induce a spiral or helical rotation on the fluid-enhancing radial acceleration and centrifugal forces on a suspended secondary phase. Referring to Figure 3.14, the inlet flow containing both the dense and light phases are introduced tangentially into the involute section, an upper cylindrical section that narrows to form a conical base. There are two outlets: the underflow (situated at the apex of the cone) and the overflow (an axial tube, also called vortex finder). The denser phase migrates quickly toward the cone wall where the flow is directed downward. The lighter phase migrates more slowly and is captured in the counter-rotating upward spiral flow, exiting through the vortex finder. The performance of the hydrocyclone is sensitive to the geometrical shape and vortex core stability, as well as phase concentrations and dispersed droplet or particle sizes.

Although hydrocyclones require more energy to generate the centrifugal force, it generally has higher performance for water–solid separation. However, the treatment efficiency of liquid–liquid hydrocyclones is significantly less compared to liquid–solid because of the

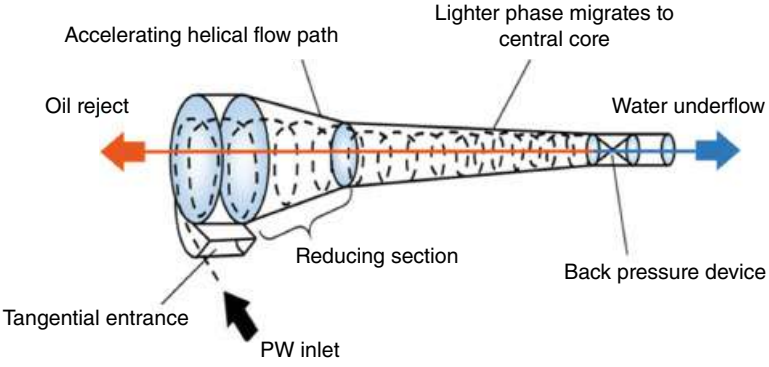

Figure 3.14 Operating principle of the de-oiling hydrocyclone represented in a single liner. *Source:* Reproduced with permission from [29].

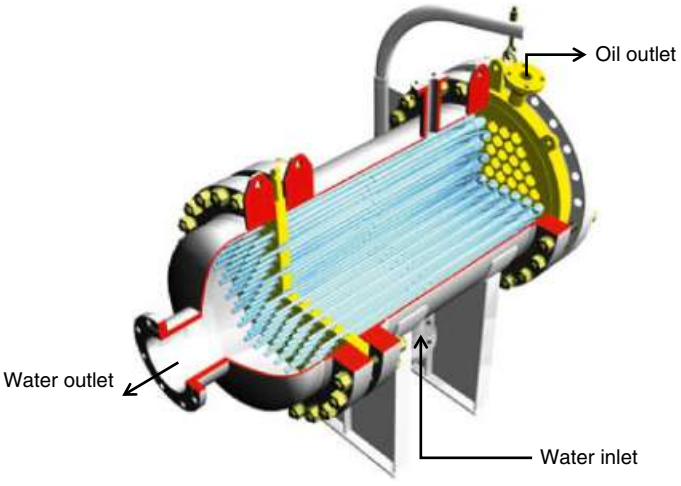

Figure 3.15 De-oiling hydrocyclone unit with multiple liners. *Source:* Courtesy of Suez environment.

high viscosity, relatively low-density difference, and small oil droplet sizes. The liquid–liquid or de-oiling hydrocyclone must be much longer to accommodate the relatively slower separation. The performance parameters affecting the de-oiling hydrocyclone operation include the inlet oil concentration and drop size distribution, the turndown ratio, the pressure drop ratio, the flow split, and the geometrical parameters [66]. The oil droplet size that can be removed from hydrocyclone is typically 10–15 μm and greater.

To improve throughput and separation efficiency, multiple hydrocyclones or liners are packed within a single vessel as shown in Figure 3.15. If a single liner performs well, all 100 or so liners will perform at the same efficiency. The number of liners selected will depend on the feed throughput, range of operating throughput, and separation required. This configuration minimizes the space requirements for the application on offshore platforms. Some improvements have been made to conventional hydrocyclones, such as the double-cone air-sparged hydrocyclone, which can shorten the settling time [67].

3.2.1.1.6 Induced Gas Flotation (IGF) and Dissolved Gas Flotation (DGF)

Induced gas flotation (IGF) and dissolved gas flotation (DGF) both use small bubbles in the range of 100–1000 μm that attach to oil and particles and move them to the surface of the water. Skimmers can be used to remove the sludge from the surface or hydraulic methods can be used to overflow the top layer [68, 69].

There are two types of IGF: mechanical and hydraulic. In mechanical IGF, impellers rotating at high speed generate a vortex that induces and mixes gas into the liquid phase as shown in Figure 3.16.

The hydraulic IGF uses an eductor/venturi to entrain gas bubbles. A portion of the effluent is recycled back to the flotation chamber and the eductor/venture, which draws and mixes gas bubbles into the wastewater to form bubbles that capture the oily contaminants and help rise to the surface of the water. Figure 3.17 illustrates the flow schemes of hydraulic-type IGF.

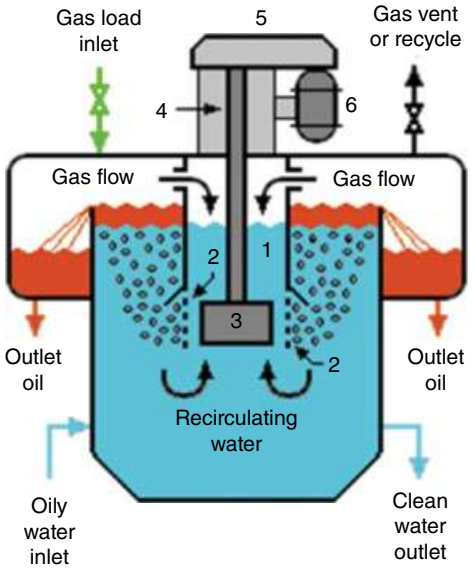

1 Standpipe and hood
2 Bubble dispensers
3 Rotating impeller
4 Rotating shaft
5 Belt drive
6 Electric motor

Figure 3.16 Schematic diagram of a mechanical-type IGF cell. *Source:* Milton Beychok, Mechanical IGF. Retrieved from: https://en.citizendium.org/wiki/File:Mechanical_IGF.png. Licensed under CC0 1.0 Universal License.

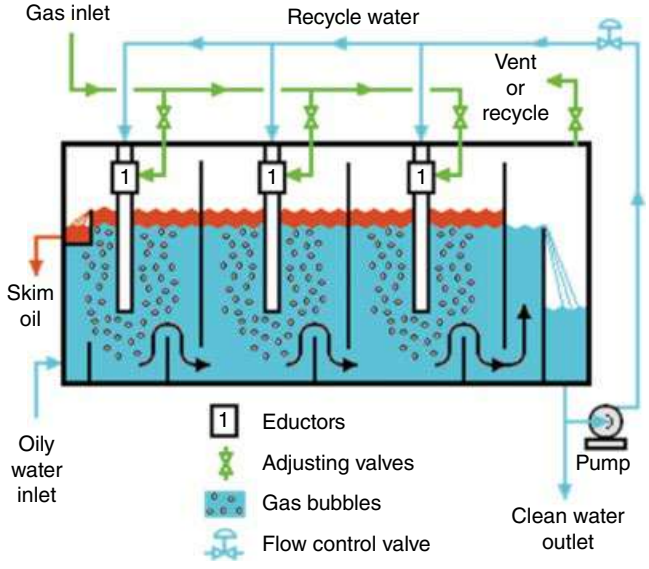

Figure 3.17 Schematic diagram of a hydraulic-type IGF unit. *Source:* Milton Beychok, Hydraulic IGF. Retrieved from https://en.citizendium.org/wiki/File:Hydraulic_IGF.png. Licensed under CC0 1.0 Universal License.

The hydraulic-type IGF is generally lower in capital and operating costs requiring less downtime for maintenance compared to the mechanical-type IGF. Most IGF units are operated in horizontal vessels, but vertical arrangements are also possible [70]. Since oxygen can cause explosion or corrosion issues, natural gas is typically used in IGF since it is readily available at oil and gas sites. Carbon dioxide (CO_2) can also be used.

DGF systems use similar mechanisms for the removal of oil droplets as IGF but produce gas bubbles by pressurizing the water. Gas is dissolved under pressure and much smaller bubbles in the range of 10–100 μm are formed. Figure 3.18 shows the mechanism of vertical DGF and Figure 3.19 illustrates the horizontal DGF.

Both IGF and DGF are used to remove oil droplets greater than 25 μm. When flocculants are used, droplets as small as 3–5 μm can be removed. Adding coagulants helps aggregate the oil droplets and promote movement to the surface of the water [72]. A comparison of the IGF and DGF is presented in Table 3.5. The IGF and DGF performance can be improved by increasing the collision of bubbles with oil droplets by generating greater amounts of smaller bubbles. Also, slow mixing and coalescing plates can help increase the collision rate and thus the overall removal efficiency of IGF and DGF.

3.2.1.1.7 Compact Flotation Unit (CFU)

The compact flotation unit (CFU) utilizes both dissolved and induced gas flotation to remove oil droplets from produced water. The CFU, as illustrated in Figure 3.20, is a vertical vessel with internals, that combines centrifugation and swirling or cyclonic flow

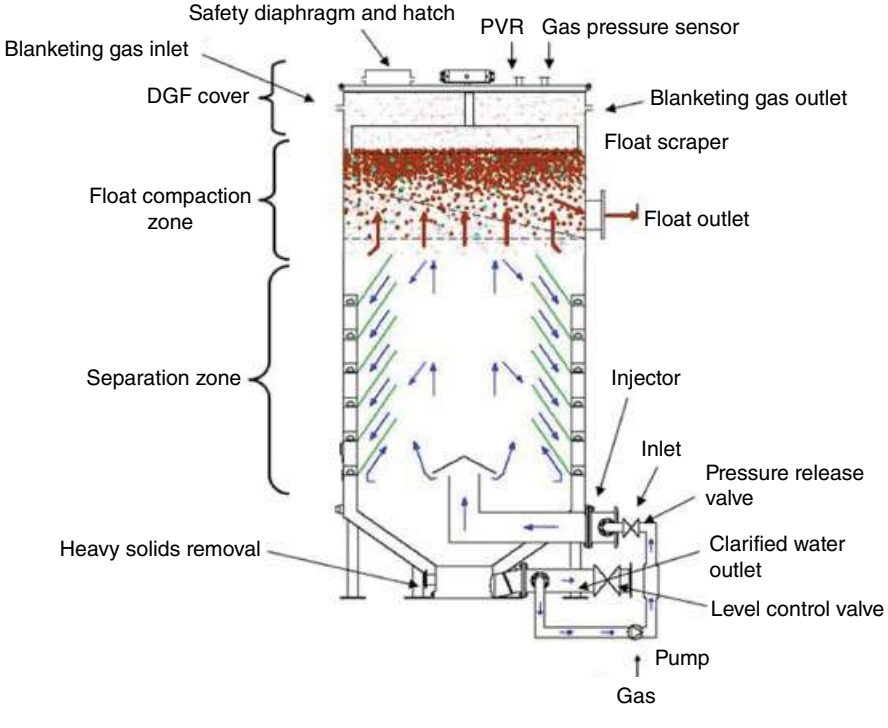

Figure 3.18 Vertical dissolved gas flotation system [71].

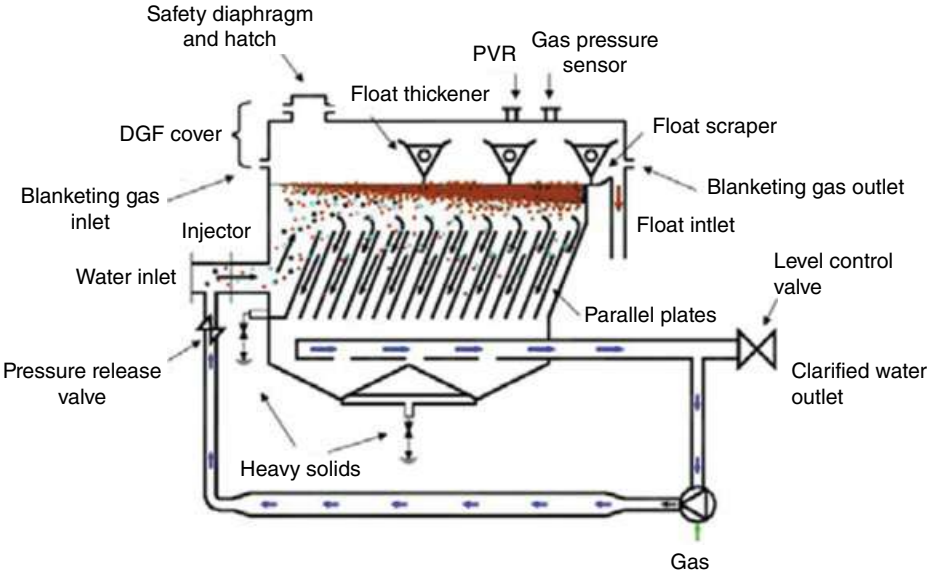

Figure 3.19 Horizontal dissolved gas flotation system [71].

Table 3.5 Comparison of IGF and DGF.

Parameters	IGF	DGF
Bubble size	100–1000 μm	10–100 μm
Bubble generation method	Velocity based; Entrainment and dispersion	Pressure based; Saturation and depressurization
Bubble generation quantity	High	Low (limited by saturation)
Operating conditions	Turbulent and less quiescent; multicell configuration	Quiescent; usually single-cell configuration
Retention time	<5 min	5–15 min
Footprint	Compact (due to short residence time)	Large (due to high residence time)
Capital cost	Low	High (large tank and saturator system)
Maintenance	Significant	Low (no moving parts)

Adapted from [73].

with flotation. The produced water is introduced into the vessel through a swirling device that imparts tangential motion. The gas is injected with the inlet water stream or a portion of the de-oiled water is recycled and reinjected along with gas into the vessel. The CFU is designed with floating offshore production platforms in mind featuring minimal space requirements, resilience to wave-induced motion, and reduced weight.

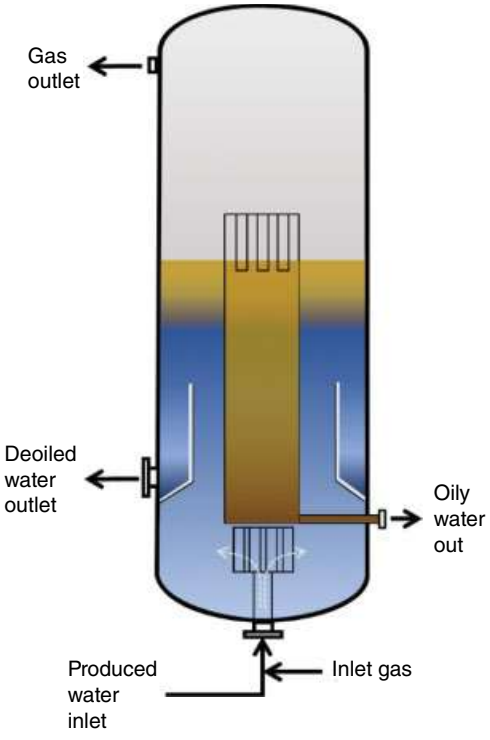

Figure 3.20 Compact flotation column. *Source:* Courtesy of Lanre Oshinowo.

CFUs have a low residence time compared to IGF and DGF and are typically more difficult to operate [74]. Small gas bubbles are generated and induced into the inlet produced water stream. CFUs typically remove oil down to below 10–20 ppm and oil droplets greater than 20 μm.

3.2.1.1.8 Fiber, Mesh, or Particle Media Bed Coalescer

After all the suspended particles and large oil droplets are removed by gravity or flotation, smaller droplets can be removed by coalescers [50]. Coalescers facilitate the coalescence and merging multiple oil droplets and making them into larger droplets to promote separation. The common types of coalescers applied in the industry include fibrous cartridge filters, fiber bed, and particle bed coalescers.

Figure 3.21 shows a schematic of a particle bed coalescer that treats a produced water stream with dispersed oil and uses a polymeric resin particle media bed [75–77]. The oil removal ability increases with increasing oil wettability of bed material. In this example, the vessel is divided into an upper and lower chamber. The produced water flows into the lower chamber flowing downward through the particle media bed to coalesce the oil droplets, the water and larger oil droplets flow up through the central riser into the upper chamber where the oil separates from the water. The interface between the decanted oil layer and the water is maintained.

Compared with gravity separation, coalescers generally have a more compact structure, higher separation efficiency, and longer service life of coalescence materials. However, in some cases, coalescence may be impeded by organic or inorganic particles remaining in the

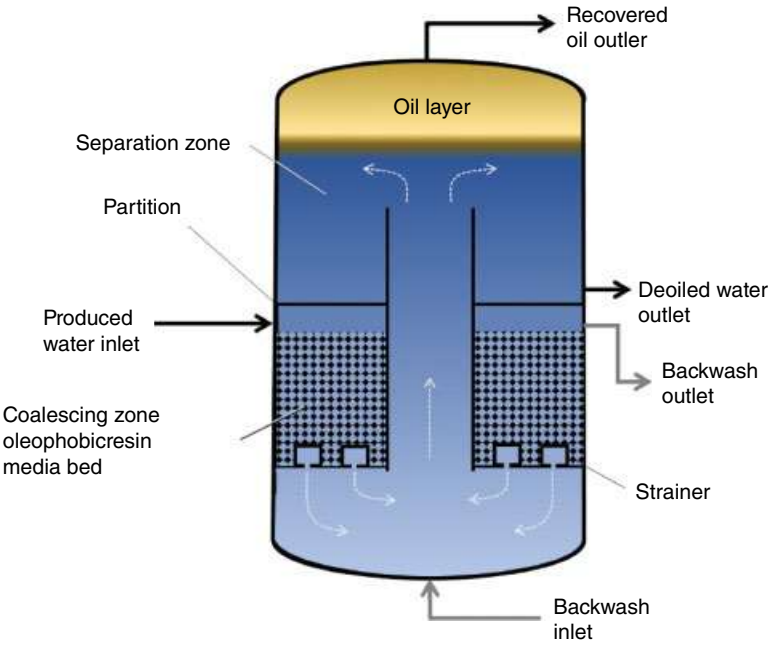

Figure 3.21 Coalescer with resin media bed for produced water treatment. *Source:* Courtesy of Lanre Oshinowo.

produced water [78]. The coalescing media must be periodically backwashed by flowing at high velocities in the reverse direction for a short period of time. Coalescers can separate emulsified oil droplets smaller than 10 μm and reduce oil-in-water concentration from 100 to 300 ppm to below 15–20 ppm [50].

3.2.1.1.9 Media Filters

Another technology that can remove smaller oil droplets compared to hydrocyclones or flotation are media filters. Media filters use a packed column of granular media that captures oil and suspended particles in the intergranular space. They can remove oil droplets to below 5 μm and can be used as a polishing step following a DGF or IGF. Small oil droplets and suspended particles can be adsorbed onto the surface or simply captured where they cannot pass through the pores. The media can act as a coalescing surface where small oil droplets can be adsorbed onto the surface and then become larger droplets by merging with other droplets.

Common types include a dual media filter, such as anthracite and sand, and a nutshell filter, such as walnut shell filters. In the oil and gas industry, nutshell filters are commonly used due to their removal efficiencies for oil droplets and the ease of backwashing.

Nutshell filters usually have two operating modes: filtration and backwash. An example of a nutshell filter operation is shown in Figure 3.22. During the filtration mode, oil and particles are accumulated within the bed of the media. Pressure will increase over time, and backwash is performed to remove the oil and particles and restore the pressure and contaminants holding capacity. Smaller media (granule size) will help with the effluent

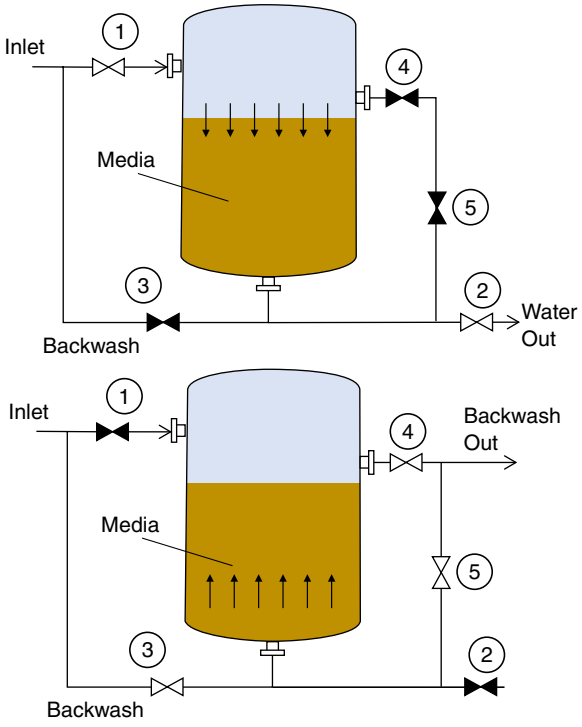

Figure 3.22 Nutshell filter operation (top) and backwash cycle (bottom). *Source:* Courtesy of Lanre Oshinowo.

quality but the pressure drop will be greater and faster. In filtration mode, valves 1 and 2 are open, allowing continuous downflow of the water through the media bed. When the pressure drop reaches a preset condition (e.g. 15 psi), backwash mode will start. During backwash, valves 1 and 2 are closed to take the filter offline and valves 3, 4, and 5 are opened. A parallel filter can be brought online to allow continuous treatment.

3.2.1.1.10 Membranes

Gravity-based or centrifugation-based separation is not applicable when the contaminant in the water stream is dissolved. Membranes offer the highest degree of treatment for oil and suspended solids, and they can be used even when dissolved organics and very small suspended solids need to be removed.

For produced water filtration, microfiltration (MF) and ultrafiltration (UF) are commonly used. When combined with coagulants and flocculants, membrane processes can remove droplets and particles down to 0.01 μm. Compared to the technologies discussed so far, membranes generally have the highest consistency in removal efficiency. Also, the effluent quality is less influenced by the raw water quality [79]. Membranes can remove droplets that are smaller than their pore size by increasing the coalescence of oil droplets and achieve higher removal efficiency. If desalination or the removal of dissolved ions are necessary for produced water treatment, membranes offer the best pretreatment option.

All membranes suffer from fouling where a layer of oil, solids, and other components accumulates on the membrane surface decreasing flux and consequently increasing operating costs [45].

For typical water treatment, MF/UF are operated in dead-end mode by passing the feed solution directly through the membrane without any flow parallel to the membrane to maximize the water recovery. In produced water treatment, cross-flow mode is generally used to maintain the flux across the membrane and minimize the buildup of the foulant layer. As in the media filters, MF/UF have filtration and backwash modes [80]. Membrane cleaning in produced water applications requires extra chemicals or energy, and the downtime of the treatment system. In case of severe fouling, chemically enhanced backwash (CEB) can be performed daily or weekly. For more thorough restoration of filtration flux, clean-in-place (CIP) is performed monthly or quarterly.

The most common material for MF/UF includes PVDF, PTFE, PES, and PS. These polymers are used because of their low cost and ease of manufacturing. But they may be vulnerable to temperatures higher than 35 °C and some chemical species in produced water may damage the membrane. Ceramic MF/UF membranes can withstand higher temperatures and organics, such as BTEX, do not affect their performance. Also, the flux is generally higher than in the polymeric counterparts [81]. Figure 3.23 shows an example of a full-size ceramic membrane element.

Membranes are the newest addition in the treatment technology for oil removal in produced water and it is still an active area of research and development. There are significant opportunities for improving the membrane processes for produced water treatment, such as new material for membrane construction, the addition of chemicals like coagulants to aid the performance, and in combination with biological processes, such as membrane bioreactors (MBRs).

Figure 3.24 shows a result from CFD simulation of membrane filtration and illustrates the concentration distribution of water (red) and solute (blue) with vector arrows showing the movement of fluid in the system [83]. With CFD simulations, the load loss along a membrane fiber can be predicted and then optimized by varying the influence of solute

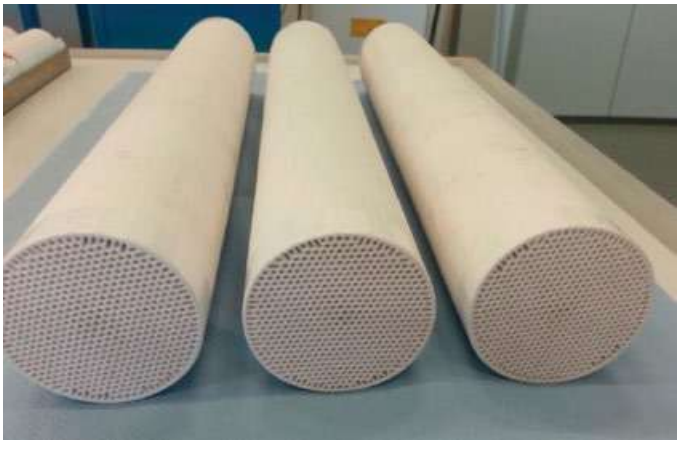

Figure 3.23 Ceramic nanofiltration (NF) membrane elements with 559 channels and 4.5 m^2 element, used with permission. *Source:* Reproduced with permission from [82].

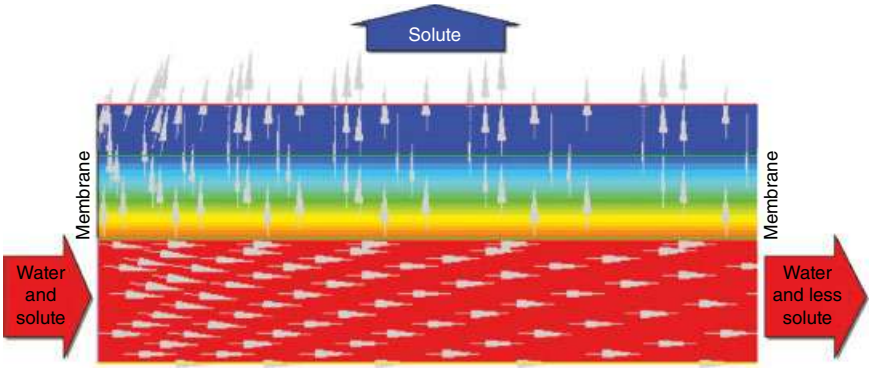

Figure 3.24 CFD simulation of a membrane filtration process illustrating the solute pathways in the device [83].

concentration, flow rate, pressure differential, and the geometric attributes of the filtration device to obtain uniform filtration and efficient membrane cleaning [84–86].

3.2.1.1.11 Oil Concentrations and Removal Efficiencies

In general, technologies that can remove a larger size of droplets and suspended solids can handle higher concentrations of those contents. For example, API separators and hydrocyclones can remove greater quantities of oil compared to membranes that can remove smaller droplets but cannot handle high concentrations of oil in the feed stream. Membranes are better suited as a polishing step where the larger size contaminants have already been removed by gravity-based technologies, such as API and flotation.

Figure 3.25 summarizes the technologies discussed so far and the range of oil-in-water concentrations in the feed and effluent streams. As a convention, the API, WOSEP,

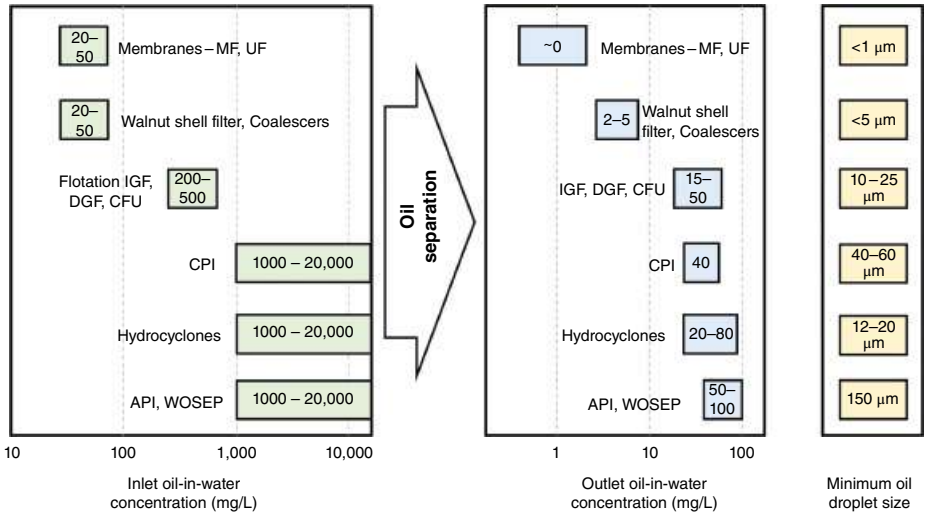

Figure 3.25 Technologies for oil and suspended solids removal and the oil removal performance as a function of the inlet and outlet oil-in-water concentration, and the minimum oil droplet size in the produced water effluent. *Source:* Courtesy of Lanre Oshinowo and Young Chul Choi.

hydrocyclones, and CPI can be classified as primary treatment methods, while IGF, DGF, and coalescers can be classified as secondary treatment. Tertiary treatment can include walnut shell filters and membranes. In general, hydrocyclones have the highest treatment capacity (m^3/h) per footprint (m^2) or volume of the system (m^3) but do not have the capability of removing small oil droplets with high efficiency [55]. Membranes are recommended when complete removal of oil is needed.

3.2.1.2 Dissolved Gas Removal

In addition to oil droplets and suspended solids, produced water may also contain significant concentrations of dissolved gases and volatile organics. They include H_2S, BTEX, and other volatile organic carbon (VOC) species. In addition to being health hazards, these compounds can also cause problems in the downstream processes like reverse osmosis (RO) or thermal evaporators. Hence, degassing (or stripping) treatment is an important pretreatment step for advanced produced water treatment though the processes discussed so far have little effect on the gaseous contaminants. It is necessary to utilize the technologies specifically designed for the removal of gaseous compounds.

3.2.1.2.1 Degasser

The degasser, also called a degassing vessel or flash drum, may receive the effluent from de-oiling hydrocyclones or any other process that has been used for oil and suspended solids removal [27]. A degasser vessel can be used as a final polishing stage in different configurations of produced water treatment. The primary function of the degasser is to release dissolved gas prior to discharge of the produced water, including H_2S and dissolved volatile organics, such as BTEX and phenol. Since the discharge of these pollutants directly to the atmosphere may not be allowed in many regions, the stripped gaseous compounds need to be transferred to another liquid phase using a scrubber. This creates a secondary stream requiring additional treatment. Where feasible, the off-gas from the degasser/stripper may be sent to flares where they can be oxidized.

The secondary function of the degasser/stripper is the flotation and skimming of any remaining oil. The degasser is operated close to atmospheric pressure, and when the pressurized stream enters, small bubbles are formed that assist in the upward movement of remaining oil droplets to the surface.

3.2.1.2.2 Adsorption

Adsorbent material with high surface area, such as activated carbon, can be used to capture dissolved gases. When the capacity is exhausted, the carbon media can be regenerated onsite or can be sent off-site for regeneration. Zeolite has been used to remove BTEX and it can be regenerated using air sparging [87]. But this will have the same issue with air stripping where the off-gas needs further treatment.

3.2.1.2.3 Membrane Contactor

Gas transfer membranes can be used to remove gaseous compounds from produced water. With hollow fiber polypropylene membranes, the removal efficiency of higher than 98% for H_2S and CH_4 has been reported [88, 89].

3.2.1.2.4 Summary of De-Oiling, Degassing, and Filtration Technologies

Table 3.6 summarizes the oil removal technologies for produced water treatment compiled from multiple references [7, 90–95]. Technologies in the same box can be considered alternative choices and the recent improvement for each size class is presented.

3.2.2 Desalination and Demineralization Processes

The oil and gas industry consumes substantial quantities of freshwater for its operation. The source of this water is usually either groundwater or surface water. Many of these resources are limited and unrenewable. To ensure sustainable operations for oil and gas companies, there is a need for a reliable and sustainable supply of freshwater. A potential and promising option source is produced water. As presented earlier, produced water contains an elevated level of dissolved salts and other contaminants that must be reduced or removed completely as a requirement for reuse as industrial water. The desalination of saline water can be performed by a single technology or by an integration of multiple technologies [96–101]. In this section, selected promising desalination technologies are described.

Table 3.6 Summary of de-oiling/degassing/filtration technologies for each contaminant [7, 90–95].

Contaminant	Current technologies	Tech under R&D	Direction of development
Oil (>150 μm)	API, oil–water separator (WOSEP), CPI (>60 μm)	WOSEP with coalescer plate packs; Hybrid WOSEP with flotation; Centrifugal separator	Smaller footprint Smaller droplet removal
Oil (>20 μm)	DGF, IGF, hydrocyclones	Compact flotation unit; Hydrocyclones with diffused gas	Higher removal efficiency
Oil (<5 μm)	Coalescer, media filters, nutshell filters	Oleophobic media filters	Ease of backwash, less maintenance
Oil (<1 μm)	Polymeric MF/UF membranes, Ceramic MF/UF membranes	Ceramic nanofiltration (NF)	Removal of smaller organic compounds
Dissolved organics	Coagulation/ flocculation	Electrocoagulation with PV; Advanced oxidation; Membrane bioreactors (MBRs)	Higher removal efficiency, reduced energy, and chemical usage
Suspended solids	Desander, sedimentation	Ceramic membranes	Smaller footprint, higher removal efficiency
H_2S	Degasser, air stripper, scrubber	Liquid scavengers and fixed-bed adsorbent media; Membrane contactor	Compact system, targeted removal of H_2S
Volatile organics (BTEX)	Degasser, air stripper	Biofilm reactors; Biofilters	Complete destruction of the BTEX molecules

Source: Courtesy of Young-Chul Choi.

3.2.2.1 Desalination Technologies

3.2.2.1.1 Vapor Compression

Vapor compression (VC) is a thermal technology that has been demonstrated to treat and desalinate produced water [102–106]. Compared with other desalination technologies, it requires less pretreatment and tolerates a higher level of contaminants in the feed. VC can desalinate the ultra-saline produced water in one step from a TDS of 100,000–250,000 ppm to <100 ppm [107]. Compared with other thermal-based technologies, VC is usually more energy efficient and compact, making it suitable to be used in remote areas [34, 103, 108].

The technology utilizes heat produced from compressed steam. The compression can be done through a mechanical compressor or a steam ejector. If the compression is done mechanically, the system is often referred to as mechanical vapor compression (MVC). The key advantage of MVC over thermal vapor compression (TVC) is that the MVC does not require multiple stages to improve its thermal efficiency, making it suitable for small energy-efficient installations. The main components of MVC include a mechanical vapor compressor, a preheater heat exchanger, and an evaporator/condenser unit, as shown schematically in Figure 3.26.

The feed water is sprayed inside the evaporation/condenser unit through distributed nozzles. The sprayed feed saline water is directed toward the hot tubes placed inside the unit. Superheated compressed vapor is flowing inside these hot tubes. Evaporation occurs because of latent heat transfer from the steam inside the hot tubes to the sprayed feed that is in contact with the hot tubes. The vapor generated leaves the evaporation/condenser unit and is mechanically compressed to reach a superheated state to be used as a heating stream.

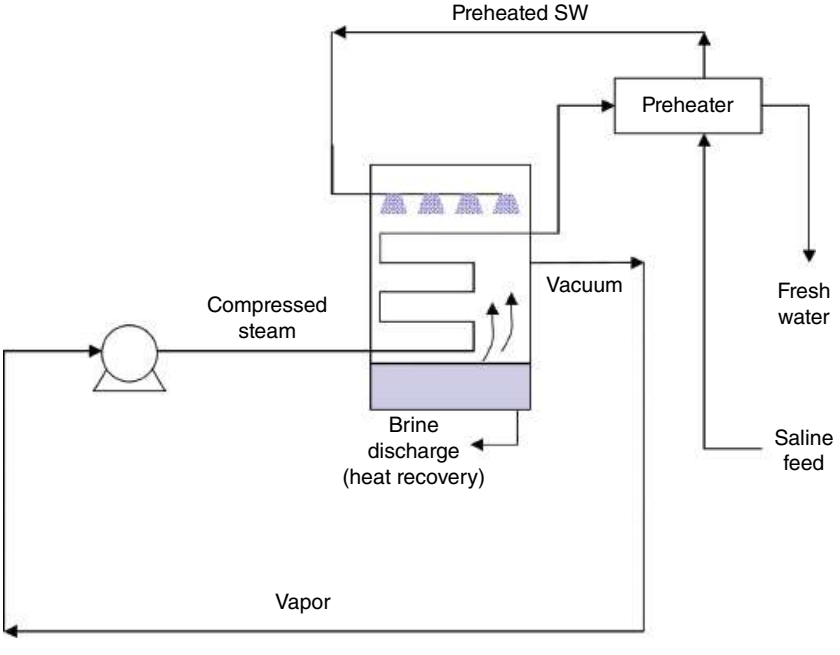

Figure 3.26 Mechanical vapor compression (MVC) process for desalination. *Source:* Miller [111]. Public domain.

During the heat exchange inside the unit, vapor condensation inside the tubes occurs because of heat transfer to the sprayed feed water. To minimize the energy consumption of the MVC process, heat is recovered from the rejected brine and condensed vapor through heat exchangers used to preheat the incoming feed saline water [109].

Although MVC is a proven reliable technology, its use is still limited due to its relatively high capital and operating costs [110–112]. The high capital cost comes mainly from the material selection and the compressor. The energy consumption in MVC is the major contributor to the elevated operating cost of MVC. Also, most of the energy required to operate MVC is in the form of high-grade electrical energy, which is not always available in remote locations or where energy costs are high [113]. Recent advancements in the compressor and heat exchanger design have reduced the cost of MVC to ~\$0.51/m^3 for seawater.

3.2.2.1.2 Membrane Distillation

Membrane distillation (MD) is a desalination technology that utilizes both thermal energy and membranes to desalinate saline water. Although the technology was first introduced more than fifty years ago, in the last twenty years, the technology has received increased attention and research [114, 115]. An MD system simply comprises a heating source, feed zone, a membrane, and a permeate zone. The heat source creates a temperature difference between the feed and permeate zones, which generates a vapor pressure difference across hydrophobic, microporous membrane. The vapor pressure difference is the driving force instigating water vapor to pass through the membrane.

A prominent feature of MD technology is the operation at atmospheric pressure and at temperatures lower than the boiling points. This provides the opportunity to utilize low-grade waste heat sources. Another compelling feature of the MD technology is the capacity to desalinate highly saline water. On the other hand, the MD system design and membrane materials are two of the biggest challenges in an MD process [116].

In general, suitable MD membrane characteristics include high hydrophobicity and porosity, low thermal conductivity, and low membrane thickness. MD membranes should have high liquid entry pressure (LEP) to avoid being wetted by the liquid feed. LEP is the pressure needed to force the liquid to penetrate the pores of the membrane to pass through to the other side. An optimized MD system design can have a significant impact on the system efficiency and permeate flux.

Various MD systems have been proposed and evaluated in the past years. The most common system designs are illustrated in Figure 3.27: direct contact membrane distillation (DCMD), air gap membrane distillation (AGMD), sweeping gas membrane distillation (SGMD), and vacuum membrane distillation (VMD) [117–127].

DCMD is the most basic design where the water vapor passes from the feed side through the membrane and condenses directly on the permeate stream on the other side of the membrane. The main limitation of DCMD is its low energy efficiency due to high heat losses. In AGMD, the water vapor condenses on a cold surface, usually glass, on the permeate side. There is a gap filled with air between the cold surface and the membrane. Although this system entails higher energy efficiency, the permeate flux is low due to low mass transport rates. In SGMD, there is a flowing gas on the permeate side that is used to carry the water vapor outside the membrane module to an external condenser. Though system design provides good mass transport rates, it is more complex and more expensive due to

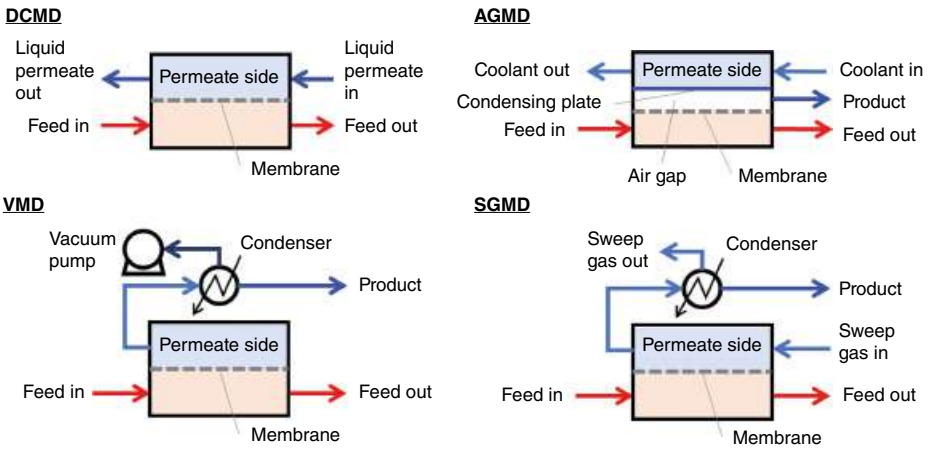

Figure 3.27 The most common membrane distillation (MD) system designs. *Source:* Courtesy of Lanre Oshinowo and Hasan Al Abdulgader.

the need for an external condenser and air blower. In VMD, the permeate side is a vacuum that will allow water vapor to pass through the membrane and condense in an external condenser. This design offers good permeate flux and is suitable to treat feed that contains volatiles. However, the system is more complex and more expensive than other designs.

3.2.2.2 Membrane Reverse Osmosis

The Reverse Osmosis (RO) process involves a simple migration of a solute species across a semipermeable membrane because of a concentration difference on the two sides of the membrane. The application of a pressure difference can accelerate the diffusion process. Dissolved solutes and suspended solids are retained in the concentrate (brine), while water passes through the membrane. RO is an important membrane filtration process for the desalination of produced water utilizing selective barriers that allow water through but not the dissolved ionic compounds. As shown in Figure 3.28, RO has the highest degree of rejection for all the contaminants in produced water.

RO membranes can be made of zeolite, cellulose acetate, polyvinylidene fluoride, polyethersulfone, and polyamide [81]. Polyamide-based RO membranes are the most common and are widely used in the desalination industry. RO is generally of the lowest cost and consumes the least amount of energy compared to other desalination technologies. However, these membranes have an upper limit on the feed water TDS or salinity at about 60,000 ppm. Produced water often exceeds this level of salinity, which limits RO from wider acceptability as experienced in seawater desalination. It was shown that RO membranes made of zeolite undergo 55 bars to reduce the TDS in produced water from over 180,000 ppm to about 110,000 ppm [128].

Other issues with RO for adoption by the oil and gas industry include its limited tolerance to temperature (up to about 38 °C), susceptibility to attacks from BTEX and other organics in the water, and H_2S compatibility. RO for the oil and gas industry would require thorough pretreatment compared to seawater desalination and the life span of the RO membranes is expected to be shorter. RO is often used downstream of oil and suspended

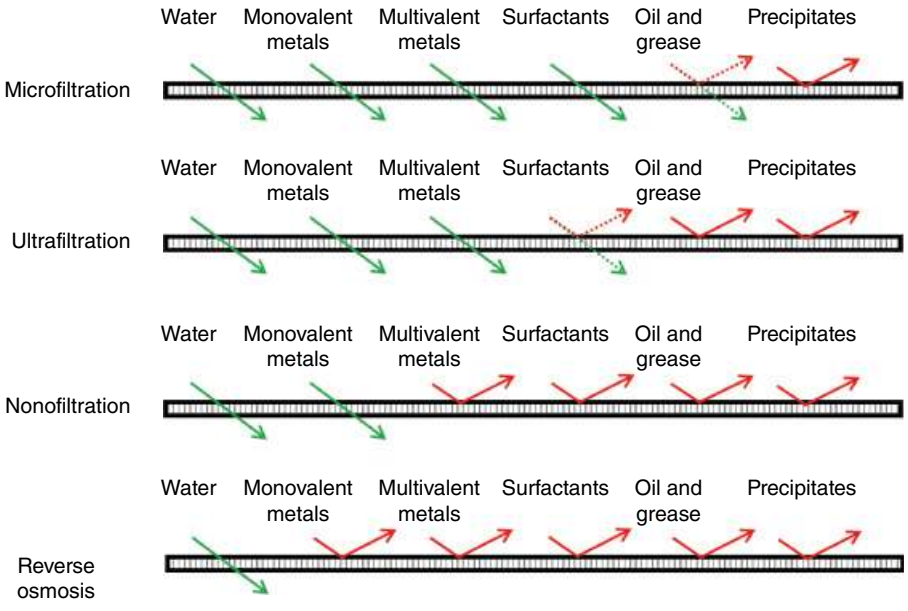

Figure 3.28 Different membrane types and their separation characteristics. *Source:* Courtesy of IFMWater Cycle Technologies.

particle removal pretreatment, such as API/WOSEP, coagulation/flocculation, settling/flotation, and UF/MF membranes.

3.2.2.3 Nanofiltration

Nanofiltration (NF) is a membrane technology with a high diffusion velocity that blocks divalent ions while allowing monovalent ions to pass through. The physical appearance of the NF membrane is the same as the RO membrane and requires similar pretreatment. NF membranes will also block the passage of organics or oil. In the oil and gas industry, NF is used primarily to remove sulfate anions from seawater.

NF membranes are constructed with polyamide as in RO and have similar issues and limitations with the constituents of produced water – TDS or salinity, temperature, organics, and H_2S in produced water. Unlike RO, it is possible to build NF membranes with ceramic material, such as TiO_2/ZrO_2, that are not affected by these conditions. But this is a new area of research and more innovations are required particularly to address fouling before ceramic membranes are suitable for industrial-scale produced water treatment.

3.2.2.4 Forward Osmosis

Forward Osmosis (FO) is an emerging technology with potential to be deployed in various water treatment applications including the desalination of produced water [129–132]. The technology is based on the natural osmosis phenomenon where the water is driven through a semipermeable membrane from the high chemical potential region to the low chemical potential region.

For FO technology to be applied to desalinate saline water, a concentrated "draw" solution with a higher chemical potential is placed on the other side of the membrane

[133, 134]. The water is drawn from the saline water side to the other side. Then, the water gets separated from the draw solution to become a freshwater produce stream, and the draw solution is used again to recover more water from the saline side.

Few studies have investigated the use of FO technology to desalinate highly saline produced water [135–140]. The utilization of FO technology for desalinating produced water is motivated by the fact that the FO process fundamentally does not require high pressures or temperatures to operate. This means the technology has the potential to consume less energy than conventional technologies, such as MVC and RO. Also, unlike RO membranes, the FO membranes are relatively cheap and can tolerate more suspended contaminants in the feed without getting extremely fouled [141]. Despite these advantages, FO technology still faces challenges that impact a large-scale deployment of the technology in the water desalination industry. One of these challenges is the limited availability of cost-effective and efficient draw solutions. Favorable characteristics of a draw solution include high osmotic pressure, nontoxic, easily recoverable, low cost, and compatibility with the FO membrane [142–144].

3.3 New Directions for Produced Water Treatment – Toward Sustainable Produced Water Management

According to the United Nations, sustainability is "meeting the needs of the present without compromising the ability of future generations to meet their own needs." Of the 17 UN Sustainable Development Goals, there are 11 priority SDGs that have an impact on the oil and gas extraction and production industry. The SDG with the most relevance to produced water management is SDG 6, which is to ensure the availability and sustainable management of water and sanitation for all.

Sustainable produced water management involves a holistic approach to environmental management that takes into consideration the direct, indirect, and cumulative impacts across the project life cycle. This includes the coordinated development and management of water to maximize the resultant economic and social welfare in an equitable manner without compromising the sustainability of vital ecosystems. Produced water management is a framework which follows the following principle tenets:

- Reuse and recycling of produced water for the purposes of sustaining and stimulating oil and gas reservoirs to increase production.
- Reduce and replace freshwater (groundwater and surface water) consumption in oil and gas production, agriculture, and industrial and domestic use.
- Elimination of groundwater contamination.

In the management of produced water, there must be a consideration of all aspects of the oil and gas production over the entire life cycle. Sustainability can be achieved with the improvement in all aspects of higher efficiency, lower energy consumption, lower footprint requirements, and fewer consumables. Water management and cost control typically selects an economical disposal option or finds an appropriate beneficial usage for the produced water.

Treatment of produced water may be required for disposal to meet or exceed the regulatory limit for certain components that may be toxic to flora and fauna. On-site reuse for produced water is a common practice in conventional and unconventional oil and gas production and is subject to the specific technical and economic considerations for a given oil and gas field [39].

The reuse and recycling of produced water include enhanced oil recovery (EOR) or waterflooding for produced water utilization. Disposal pump energy costs should be minimized and included in the life cycle assessment of the operations. Other reuse initiatives like Greening the Desert that reuse produced water in arid areas around desert oil fields to stimulate forestry, agriculture, and wetlands, to the treating of low-quality water using power generated from associated gas in remote oilfields aligns with the tenets of sustainable development [25, 145–147]. For aquifer water use to be completely sustainable, the water levels in subsurface groundwater cannot decrease.

In arid regions like Saudi Arabia, groundwater use is predominated by agriculture and to a much lesser extent by oil and gas extraction [148]. The accessibility to freshwater for operations and the large quantities of produced water requiring treatment and disposal could constrain future energy production in certain regions, including semiarid regions [11]. The demands for the freshwater used in many hydraulic fracturing operations are placing pressure on water sources in some regions of the United States [149].

Effective produced water management considers the total costs of water from a life cycle perspective from acquisition to disposal. This includes the availability of freshwater, acquisition, transportation costs, transfer to the well site, transfer from well to disposal, water treatment, and disposal. A principal water life cycle process can be generated for the unconventional gas well to give a holistic view of the sources and fate of all water utilized during hydrocarbon extraction [150]. The major stages in the process contain multiple sublevel processes and a supply chain production of fuels, electricity, and materials that cause indirect water consumption and water quality pollution impacts [149]. A cost–benefit analysis for the produced water treatment technology selection is critical with a review of the pros and cons, advantages, and disadvantages [8, 9, 14, 29].

The increased demand for and natural variability of water resources in the United States has led to interest from policymakers, regulators, and society in the potential for produced water reuse [39]. An example is treating and reducing the salinity of produced water making it available for reuse in hydraulic fracturing operations and irrigation activities reducing the demand for freshwater in stimulation operations and well injection and disposal. There are challenges with having the water available for reuse at the location the water is needed. Information on the volume and quality of the produced water for reuse will be needed by the end user and must be made available as a component of the produced water management.

With an understanding of the produced water composition, the environmental, health, and regulatory concerns can be evaluated for produced water reuse outside of oil and gas operations [39]. The challenges for reuse are illustrated in Figure 3.29. There are regulatory challenges to reuse produced water that involve storage and transportation, water quality, permits, and approvals from governing bodies. On water ownership, where the water may belong to the government, landowners or other entities will require authorization for water

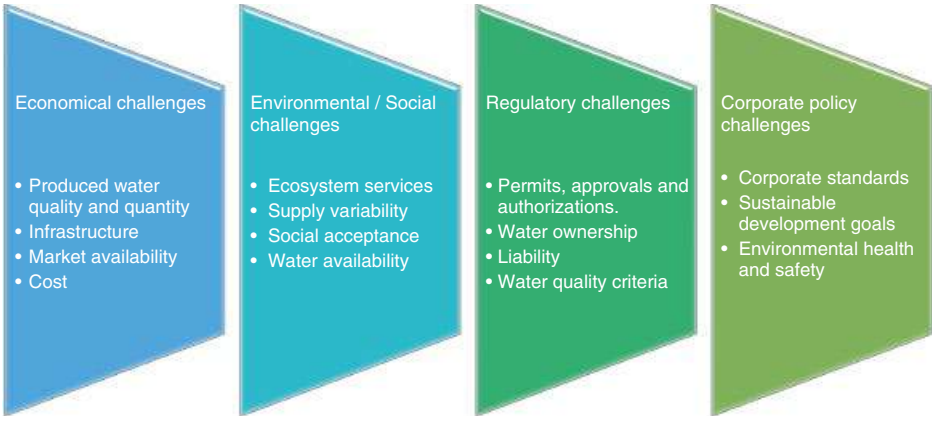

Figure 3.29 Produced water management challenges for reuse outside the oil and gas industry. *Source:* Courtesy of Elaf Ahmed.

management [151]. For disposal purposes, produced water needs to undergo effective treatments to satisfy the current legislation when considering the destination of the treated water. Hence, the treatment technology must meet the regulatory standard before discharging into the environment.

For produced water management to be sustainable, the methods and processes to handle and treat produced water must utilize the best available, cost-effective technology while simultaneously seeking to develop new, cost-effective, produced water separation processes based on sustainable design principles. The design principles are lower energy intensity, less waste, more reuse, and more beneficial uses [152].

3.3.1 Energy Efficiency and Green Energy

The use of green power sources and reducing chemical consumption can lower the greenhouse gas (GHG) emissions in oil and gas production. Using more compact and more efficient systems to reduce the footprint and energy consumption is the general direction preferred by the oil and gas facilities' operators. In addition to the low-pressure membranes, such as MF and UF, CFU can significantly reduce the footprint of produced water treatment systems [153]. The CFU also improves on the issues with DGF where oil droplets larger than 100 μm cannot be floated because the volume of the gas bubbles is not large enough and IGF systems where oil droplets much smaller than 100 μm may escape flotation, as small oil droplets do not attach well to large gas bubbles [74].

Energy reduction in auxiliary equipment, like low-speed, high-efficiency pumps, can also have a double benefit by reducing both energy requirements and the turbulent shearing that breaks up dispersed oil droplets making them smaller and more difficult to separate in downstream separation units. An example of low-energy process for produced water treatment is nature-based treatment, such as wetlands. Multiple contaminants can be removed in a single process without the use of chemicals, high pressure, or high temperature, which makes it an ideal candidate in certain cases [154, 155].

Electrocoagulation can be used to remove heavy metals, suspended and colloidal particles, and chemical oxygen demand (COD) of oilfield produced water could be rapidly reduced [156]. Produced water containing organic pollutants and bacteria can be coagulated without the requirement for transportation of chemicals to the production site [157]. Further improvement of electrocoagulation with electricity generation from solar or other green sources reduces both the need for nongreen electricity and chemicals [158]. Superhydrophobic materials that improve performance and reduce cleaning needs can also help with the reduction of chemical usage [159].

The indirect solar desalination of produced water may be done by solar assisted multi-effect desalination (MED) in a system comprised of a solar subsystem that converts solar energy into either heat or electricity and a MED subsystem that compresses the steam needed to heat the process using vapor compressors [160].

3.3.2 Focus on Reuse of Produced Water – Higher Degree of Treatment

Using membranes and other desalination technologies for the removal of salinity will enable the reuse of the treated produced water for industrial purposes. Membranes based on novel material, such as graphene oxide (GO) with polybenzimidazole (PBI) base, has been shown to improve the removal rate of oil emulsion [161]. The use of biological methods can reduce the risk of harmful dissolved organic contaminants being discharged. Ultrahigh pressure (UHP) RO can be used for salinity, where the maximum pressure rating is improved to 1800 psi compared to regular RO membrane's 1200 psi. Increased pressure means higher salinity water can be treated [162].

Biological treatments, such as biofilters and MBRs, can remove dissolved organics. Biological treatments can be a low energy option to remove small, dissolved organics that will pass through the MF/UF membranes [79]. Biological treatments use the biodegradation of the organics by bacteria in the reactor. But it may also require a significant footprint, consumes oxygen, and generates sludge that needs to be further handled.

Advanced oxidation with photocatalytic, ultrasonic, and chemical enhancements can also be used for dissolved organics removal [163, 164]. In general, lower molecule size organics and higher salinity in produced water are the focus of recent developments.

There are examples of successful reuse applications at specific locations in oil and gas operations including reuse for drilling and completion, reuse for hydraulic fracturing, and reuse for mining oil sands. In the following examples, produced water can be treated to remove hydrocarbons and suspended solids before being reused in drilling and completion operations. Recycling a significant portion of produced water in drilling operations can lead to substantial operating cost reductions associated with water management and disposal. Flowback water can be processed for reuse in hydraulic fracturing operations by using large-scale containment ponds and additional treatment to remove suspended solids. Produced water can be de-oiled and reused for steam generation in steam-assisted gravity drainage (SAGD) for in situ oil sands production enabling the recycling of 90% of the water returned from recovering the oil sands [165].

The reuse of produced water for non-oil and gas operations will involve technical, regulatory, economic, environmental, and social considerations and falls under the category of beneficial uses for produced water. The beneficial reuse of produced water will require

energy-intensive treatment systems that operators will be unwilling to deploy without the necessary incentives while regulators will seek ways to craft legislation to guide the industry toward achieving sustainability while seeking more economical and energy-efficient treatment alternatives.

To the degree feasible at each location, oil and gas operators recognize the benefits of reusing produced water in their own operations to minimize the use of other water resources, such as groundwater. And, where geologic conditions are appropriate for reinjection, underground disposal of produced water is often selected as the most practical management option [39]. Customized technology packages suited to fit a specific production site will maximize the benefits for produced water reuse.

3.3.2.1 Beneficial Reuse of Produced Water

Social factors impact the beneficial reuse of produced water. Even when produced water is treated to meet applicable water quality standards, the public may have reservations about its reuse in some cases. Some examples of successful reuse of produced water outside the oil and gas industry are irrigation use, agriculture and energy reduction, livestock and wildlife watering, usage in other processes (electrical power plants), and other industrial and commercial uses [39, 166]:

1) Treated produced water from oil and gas formations with extremely low salinity can be used as irrigation water, particularly for salt-tolerant crops. Produced water with low salinity (TDS of 750 mg/L) is mixed with other freshwater sources and used as irrigation water by local water districts in Kern County, California [167]. Produced water with a moderate salinity (TDS of 7000–8000 mg/L) introduced to constructed wetlands to undergo natural treatment and improve wildlife habitat after oil–water separation.
2) Reed beds in constructed wetlands remove pollutants from produced water and have the potential to make water available for local use. Since 2010, Petroleum Development Oman and Shell has been operating a commercial water treatment plant in Nimr, Oman, that uses salt-tolerant reed beds to treat residual oil in produced water [168]. This project has allowed produced water to be reused for agriculture in an area where freshwater is scarce, while also lowering the power consumption and CO_2 emissions associated with deep-well disposal equipment.
3) Depending on the water quality requirements of each plant, treated produced water can be used to supplement cooling water feed or other power industry uses. A power station in Chinchilla, Queensland, Australia, draws and treats raw produced water from coal seam gas operations for cooling and steam processing [169]. Produced water can be used for different purposes, such as vehicles washing, firefighting, and road dust control.

Produced water that meets quality standards can be used in several applications, including crop irrigation, wildlife and livestock use, aquifer storage and recharge, and power generation, both within and outside the oilfield. And with the world's population increasing, the drinking water supply is under threat. Agriculture and energy production use an increasing amount of freshwater, contaminating an already scarce freshwater resource.

The large volumes of produced water provided by oil and gas industries around the world could be used for a variety of purposes, including potable water. Produced water has similar problems to other forms of wastewater in terms of potable reuse. High treatment costs,

the potential for chronic toxicity of the treated produced water, and public acceptance are among the challenges. Moreover, the characteristics and properties of produced water change with time, which make the "one-size-fits-all" approach impossible.

The treatment cost of oil and gas produced water is heavily influenced by the physical and chemical characteristics of the water, which can differ greatly between fields and change over time within a field as well as the regulatory climate. For example, TDS, oil, and grease content in produced water from gas production, and especially coalbed methane production, typically is lower than that from oil production making the treatment more economically attractive compared to other wastewater sources. Consequently, technology strategies for potable reuse of produced water must be tailored to the properties of the produced water, as well as the volume of water to be treated. RO would most likely be used for potable reuse applications due to the need for desalination and the removal of a significant number of organic compounds.

Advanced oxidation can be used as a polishing unit to remove dissolved organics before sending the produced water to RO [163]. While RO is capable of efficiently removing a wide range of organic compounds, the cumulative chronic toxicity of the organic compounds found in the RO permeate must be carefully assessed before direct reuse.

3.3.3 Resource Recovery from Produced Water

The presence and recovery of valuable resources that exist as solutes in produced water can improve the sustainability and economics for treatment. These include lithium, rare earth elements, vanadium, uranium, or even Ba, Br, and other common salts. Lithium recovery could potentially address the rising demand for lithium due to an increased production of electric vehicles and energy storage devices [36, 170]. Lithium concentrations up to 600 mg/L have been found in produced water and different technologies are being applied to recover lithium from produced water including solvent extraction, adsorbents, membranes, and electrochemical processes [36]. Vanadium has been widely used in many industries in particular in a wide range of metal alloys including with iron, aluminum, chromium, and other metals [171]. Uranium is a critical resource for nuclear power generation. The uranium concentration in the flowback produced water is ~3 μg/L in the Marcellus shale gas in northeastern United States while Barium can be selectively extracted from hydraulic fracturing wastewater in the form of barium sulfate that can be used in drilling mud used to protect the wellbore during drilling [172].

3.3.4 Overall Improvement of Sustainability

The sustainability of produced water generated by oil and gas production is increased by reuse, elimination of freshwater usage, and the maximization of green energy generation. Sustainability can be achieved generally with improvements to the overall efficiency of all aspects of production including higher process efficiency, lower energy consumption, lower footprint requirement, and lower material consumption.

Improving separation efficiency typically comes at a cost. Any potential gains in efficiency should be assessed against what is reasonably practical and the impact on the environment, including the carbon footprint, emissions, energy impacts, and society. The energy

requirements include supply and transportation, distribution, recycled and wastewater collection, treatment and discharge, and treatment for beneficial uses. The various options for produced water treatment can be evaluated based on both monetary and nonmonetary considerations. Nonmonetary considerations include protecting the resources and preserving or bequeathing the resource to future generations.

Acknowledgments

The authors acknowledge the support and permission from Saudi Aramco management for publishing this work.

References

1 Neff, J., Lee, K., and DeBlois, E.M. (2011). Produced water: overview of composition, fates, and effects. In: *Produced Water: Environmental Risks and Advances in Mitigation Technologies* (eds. K. Lee and J. Neff), 3–54. Springer.
2 Igunnu, E.T. and Chen, G.Z. (2014). Produced water treatment technologies. *International Journal of Low Carbon Technologies* 9 (3): 157–177.
3 Danforth, C., McPartland, J., Blotevogel, J. et al. (2019). Alternative management of oil and gas produced water requires more research on its hazards and risks. *Integrated Environmental Assessment and Management* 15 (5): 677–682.
4 Produced Water Society (2020). Global produced water volumes (Annual production data from US Energy Information Administration, surveys conducted by Oil & Gas Journal, and research conducted by Global Water Intelligence). Produced Water Society. https://www.producedwatersociety.com/resources/chart-data/global-produced-water-volumes.
5 U.S. Energy Information Administration (2021). Annual petroleum and other liquids production. U.S. Energy Information Administration. https://www.eia.gov/international/data/world/petroleum-and-other-liquids/annual-petroleum-and-other-liquids-production.
6 Fakhru'l-Razi, A., Pendashteh, A., Abdullah, L.C. et al. (2009). Review of technologies for oil and gas produced water treatment. *Journal of Hazardous Materials* 170 (2–3): 530–551.
7 Jiménez, S., Micó, M., Arnaldos, M. et al. (2018). State of the art of produced water treatment. *Chemosphere* 192: 186–208.
8 Al-Ghouti, M.A., Al-Kaabi, M.A., Ashfaq, M.Y., and Da'na, D.A. (2019). Produced water characteristics, treatment and reuse: a review. *Journal of Water Process Engineering* 28: 222–239.
9 Olajire, A.A. (2020). Recent advances on the treatment technology of oil and gas produced water for sustainable energy industry-Mechanistic aspects and process chemistry perspectives. *Chemical Engineering Journal Advances* 4: 100049.
10 Clark, C.E. and Veil, J.A. (2009). *Produced Water Volumes and Management Practices in the United States*. Argonne, IL (United States): Argonne National Lab.(ANL).
11 Scanlon, B.R., Ikonnikova, S., Yang, Q., and Reedy, R.C. (2020). Will water issues constrain oil and gas production in the United States? *Environmental Science and Technology* 54 (6): 3510–3519.

12 Scanlon, B.R., Reedy, R.C., and Nicot, J.-P. (2014). Comparison of water use for hydraulic fracturing for unconventional oil and gas versus conventional oil. *Environmental Science and Technology* 48 (20): 12386–12393.

13 McIntosh, J.C. and Ferguson, G. (2019). Conventional oil – the forgotten part of the water-energy nexus. *Groundwater* 57 (5): 669–677.

14 Veil, J. (2015). *US Produced Water Volumes and Management Practices in 2012*. Oklahoma, USA: Groundwater Protection Council.

15 Kondash, A.J., Albright, E., and Vengosh, A. (2017). Quantity of flowback and produced waters from unconventional oil and gas exploration. *The Science of the Total Environment* 574: 314–321.

16 Jiang, W., Lin, L., Xu, X. et al. (2021). A critical review of analytical methods for comprehensive characterization of produced water. *Water* 13 (2): 183.

17 Laurenzi, I.J., Bergerson, J.A., and Motazedi, K. (2016). Life cycle greenhouse gas emissions and freshwater consumption associated with Bakken tight oil. *Proceedings of the National Academy of Sciences* 113 (48): E7672–E7680.

18 Ground Water Protection Council (2019). Produced water report: regulations, current practices, and research needs. Oklahoma City, Oklahoma, USA; 2019.

19 Hincks, T., Aspinall, W., Cooke, R., and Gernon, T. (2018). Oklahoma's induced seismicity strongly linked to wastewater injection depth. *Science* 359 (6381): 1251–1255.

20 Hildenbrand, Z.L., Carlton, D.D. Jr., Fontenot, B.E. et al. (2015). A comprehensive analysis of groundwater quality in the Barnett Shale region. *Environmental Science and Technology* 49 (13): 8254–8262.

21 Bakke, T., Klungsøyr, J., and Sanni, S. (2013). Environmental impacts of produced water and drilling waste discharges from the Norwegian offshore petroleum industry. *Marine Environmental Research* 92: 154–169.

22 Kabyl, A., Yang, M., Abbassi, R., and Li, S.J. (2020). A risk-based approach to produced water management in offshore oil and gas operations. *Process Safety and Environment Protection* 139: 341–361.

23 Danforth, C., Chiu, W.A., Rusyn, I. et al. (2020). An integrative method for identification and prioritization of constituents of concern in produced water from onshore oil and gas extraction. *Environment International* 134: 105280.

24 International Energy Agency (2017). Special Report: Water-Energy Nexus, Paris, France.

25 Khatib, Z. and Verbeek, P. (eds.). (2002). Water to value-produced water management for sustainable field development of mature and green fields. SPE International Conference on Health, Safety and Environment in Oil and Gas Exploration and Production. Society of Petroleum Engineers.

26 Ferrer, I. and Thurman, E.M. (2015). Chemical constituents and analytical approaches for hydraulic fracturing waters. *Trends in Environmental Analytical Chemistry* 5: 18–25.

27 Hansen, B. and Davies, S. (1994). Review of potential technologies for the removal of dissolved components from produced water. *Chemical Engineering Research and Design* 72 (2): 176–188.

28 Mohammad-Pajooh, E., Weichgrebe, D., Cuff, G. et al. (2018). On-site treatment of flowback and produced water from shale gas hydraulic fracturing: a review and economic evaluation. *Chemosphere* 212: 898–914.

29 Liu, Y., Lu, H., Li, Y. et al. (2021). A review of treatment technologies for produced water in offshore oil and gas fields. *Science of the Total Environment* 775: 145485.

30 Alley, B., Beebe, A., Rodgers, J. Jr., and Castle, J.W. (2011). Chemical and physical characterization of produced waters from conventional and unconventional fossil fuel resources. *Chemosphere* 85 (1): 74–82.

31 Engle, M.A., Saraswathula, V., Thordsen, J.J. et al. (2019). U.S. Geological Survey National Produced Waters Geochemical Database v2.3. United States Geological Survey.

32 Røe Utvik, T.I. and Hasle, J.R. (eds.). (2002). Recent knowledge about produced water composition, and the contribution from different chemicals to risk of harmful environmental effects. SPE International Conference on Health, Safety and Environment in Oil and Gas Exploration and Production. Society of Petroleum Engineers.

33 Tibbetts, P., Buchanan, I., Gawel, L., and Large, R. (1992). *A Comprehensive Determination of Produced Water Composition. Produced Water*, 97–112. Springer.

34 Wenzlick, M. and Siefert, N. (2020). Techno-economic analysis of converting oil & gas produced water into valuable resources. *Desalination* 481: 114381.

35 Shafer-Peltier, K., Kenner, C., Albertson, E. et al. (2020). Removing scale-forming cations from produced waters. *Environmental Science: Water Research & Technology* 6 (1): 132–143.

36 Kumar, A., Fukuda, H., Hatton, T.A., and Lienhard, J.H. (2019). Lithium recovery from oil and gas produced water: a need for a growing energy industry. *ACS Energy Letters* 4 (6): 1471–1474.

37 Pichtel, J. (2016). Oil and gas production wastewater: soil contamination and pollution prevention. *Applied and Environmental Soil Science* 2016: 1–24.

38 Shpiner, R., Vathi, S., and Stuckey, D. (2009). Treatment of oil well "produced water" by waste stabilization ponds: removal of heavy metals. *Water Research* 43 (17): 4258–4468.

39 Gray, M. (ed.). (2020). Reuse of produced water in the oil and gas industry. SPE International Conference and Exhibition on Health, Safety, Environment, and Sustainability. Society of Petroleum Engineers.

40 Macedonio, F., Ali, A., Poerio, T. et al. (2014). Direct contact membrane distillation for treatment of oilfield produced water. *Separation and Purification Technology* 126: 69–81.

41 Myers, J.E. (ed.). (2014). Chevron San Ardo Facility Unit (SAFU) beneficial produced water reuse for irrigation. SPE International Conference on Health, Safety, and Environment. Society of Petroleum Engineers.

42 Mhatre, S., Vivacqua, V., Ghadiri, M. et al. (2015). Electrostatic phase separation: a review. *Chemical Engineering Research and Design* 96: 177–195.

43 Kokal, S. (2005). Crude-oil emulsions: a state of the art review. *SPE Production & Facilities* 20 (1): 5–13.

44 Sjöblom, J., Aske, N., Auflem, I.H. et al. (2003). Our current understanding of water-in-crude oil emulsions. Recent characterization techniques and high pressure performance. *Advances in Colloid and Interface Science* 100–102: 399–473.

45 Dickhout, J.M., Moreno, J., Biesheuvel, P.M. et al. (2017). Produced water treatment by membranes: a review from a colloidal perspective. *Journal of Colloid and Interface Science* 487: 523–534.

46 Kelland, M.A. (2019). Challenges with gas hydrate formation. *IOP Conference Series: Materials Science and Engineering* 700 (1): 012057.

47 Kelland, M.A. (2014). *Production Chemicals for the Oil and Gas Industry*, 2e. CRC Press.

48 Soliman, M.A., Al-Zahrani, T., Al-Qallaf, M. et al. (eds.). (2016). Innovative approach to treat produced water for re-use in Saudi Aramco reservoirs pressure maintenance. Abu Dhabi International Petroleum Exhibition & Conference. Society of Petroleum Engineers.

49 Liao, Y. and Lucas, D. (2010). A literature review on mechanisms and models for the coalescence process of fluid particles. *Chemical Engineering Science* 65: 2851–2864.

50 da Silva Almeida, F.B.P., Esquerre, K.P.S.O.R., Soletti, J.I., and Silva, C.E.D.F. (2019). Coalescence process to treat produced water: an updated overview and environmental outlook. *Environmental Science and Pollution Research* 26 (28): 28668–28688.

51 Robinson, D. (2013). Oil and gas: treatment and discharge of produced waters onshore. *Filtration & Separation* 50 (3): 40–46.

52 White, R. and Alhamoud, A. (eds.). (2019). Best practices and technologies for enhancing produced water quality. Abu Dhabi International Petroleum Exhibition & Conference. Society of Petroleum Engineers.

53 Schultz, T.E. (2005). Get the most out of API separators: the keys to maximizing performance include a realistic, educated awareness of the separator's capabilities, an understanding of how the device functions, and an appreciation of what it should have in the way of support equipment. *Chemical Engineering* 112 (7): 38–43.

54 Arnold, K. and Stewart, M. (2008). *Surface Production Operations: Design of Oil Handling Systems and Facilities*. Amsterdam: Elsevier.

55 Judd, S., Qiblawey, H., Al-Marri, M. et al. (2014). The size and performance of offshore produced water oil-removal technologies for reinjection. *Separation and Purification Technology* 134: 241–246.

56 Veil, J.A., Puder, M.G., Elcock, D., and Redweik, R.J. Jr. (2004). A white paper describing produced water from production of crude oil, natural gas, and coal bed methane. Argonne National Lab., IL (US).

57 American Petroleum Institute (1990). Monographs on refinery environmental control, management of water discharges, design and operation of water separators. Publication 421, American Petroleum Institute.

58 Mallevialle, J., Bruchet, A., and Fiessinger, F. (1984). How safe are organic polymers in water treatment? *Journal American Water Works Association* 76 (6): 87–93.

59 Shariff, M. and Oshinowo, L. (2017). Debottlenecking water-oil separation with increasing water flow rates in mature oil fields. 5th Water Arabia 2017 Conference and Exhibition, Khobar, Saudi Arabia (17–19 October 2017).

60 Oshinowo, L.M. and Vilagines, R.D. (2020). Modeling of oil–water separation efficiency in three-phase separators: effect of emulsion rheology and droplet size distribution. *Chemical Engineering Research and Design* 159: 278–290.

61 Han, Y., He, L., Luo, X. et al. (2017). A review of the recent advances in design of corrugated plate packs applied for oil–water separation. *Journal of Industrial and Engineering Chemistry* 53: 37–50.

62 Boraey, M.A. (2018). A hydro-kinematic approach for the design of compact corrugated plate interceptors for the de-oiling of produced water. *Chemical Engineering and Processing Process Intensification* 130: 127–133.

63 Arnold, K. and Stewart, M. (1999). *Surface Production Operations*, Design of Gas-Handling Systems and Facilities, vol. 2. Elsevier.

64 Stewart, M. and Arnold, K. (2008). *Emulsions and Oil Treating Equipment: Selection, Sizing and Troubleshooting*. Elsevier.

65 Husveg, T., Rambeau, O., Drengstig, T., and Bilstad, T. (2007). Performance of a deoiling hydrocyclone during variable flow rates. *Minerals Engineering* 20 (4): 368–379.

66 Kharoua, N., Khezzar, L., and Nemouchi, Z. (2010). Hydrocyclones for de-oiling applications – a review. *Petroleum Science and Technology* 28 (7): 738–755.

67 Liu, S., Zhao, X., Dong, X. et al. (eds.). (2005). Treatment of produced water from polymer flooding process using a new type of air sparged hydrocyclone. SPE Asia Pacific Health, Safety and Environment Conference and Exhibition. Society of Petroleum Engineers.

68 Piccioli, M., Aanesen, S.V., Zhao, H. et al. (2020). Gas flotation of petroleum produced water: a review on status, fundamental aspects, and perspectives. *Energy and Fuels* 34 (12): 15579–15592.

69 Saththasivam, J., Loganathan, K., and Sarp, S. (2016). An overview of oil–water separation using gas flotation systems. *Chemosphere* 144: 671–680.

70 Environmental Protection Agency (1996). Development document for final effluent limitations guidelines and standards for the coastal subcategory of the oil and gas extraction point source category. Environmental Protection Agency, Washington, DC (United States). Office of Science and Technology. Report No.: PB-97-127559/XAB; EPA-821/R-96/023; TRN: 70341258 United States TRN: 70341258 NTIS GRA English Contract No.: EPA-821-R-96-023.

71 Bradford, M. and Santharam, S. (2015). Removal of emulsified O&G and TSS from wastewater. 2015 International Water Conference, Orlando, Florida, USA (15–19 November 2015).

72 Al-Shamrani, A., James, A., and Xiao, H. (2002). Destabilisation of oil–water emulsions and separation by dissolved air flotation. *Water Research* 36 (6): 1503–1512.

73 Rubio, J., Souza, M., and Smith, R. (2002). Overview of flotation as a wastewater treatment technique. *Minerals Engineering* 15 (3): 139–155.

74 Das, T. and Jäschke, J. (2018). Simplified first-principles model of a compact flotation unit for use in optimization and control. *Industrial and Engineering Chemistry Research* 58 (3): 1273–1285.

75 Madia, J.R., Fruh, S.M., Miller, C.A., and Beerbower, A. (1976). Granular packed bed coalescer: influence of packing wettability on coalescence. *Environmental Science and Technology* 10 (10): 1044–1046.

76 Motta, A., Borges, C., Esquerre, K., and Kiperstok, A. (2014). Oil produced water treatment for oil removal by an integration of coalescer bed and microfiltration membrane processes. *Journal of Membrane Science* 469: 371–378.

77 Spielman, L.A. and Su, Y.-P. (1977). Coalescence of oil-in-water suspensions by flow through porous media. *Industrial and Engineering Chemistry Fundamentals* 16 (2): 272–282.

78 Li, C., Li, J., Wang, N. et al. (2021). Status of the treatment of produced water containing polymer in oilfields: a review. *Journal of Environmental Chemical Engineering* 9: 105303.

79 Adham, S., Hussain, A., Minier-Matar, J. et al. (2018). Membrane applications and opportunities for water management in the oil & gas industry. *Desalination* 440: 2–17.

80 Jepsen, K.L., Bram, M.V., Pedersen, S., and Yang, Z. (2018). Membrane fouling for produced water treatment: a review study from a process control perspective. *Water* 10 (7): 847.

81 Alzahrani, S. and Mohammad, A.W. (2014). Challenges and trends in membrane technology implementation for produced water treatment: a review. *Journal of Water Process Engineering* 4: 107–133.

82 Voigt, I., Richter, H., Stahn, M. et al. (2019). Scale-up of ceramic nanofiltration membranes to meet large scale applications. *Separation and Purification Technology* 215: 329–334.

83 Oshinowo, L. and Schowalter, D. (2008). Produced water unit operation optimization through simulation. 18th Annual Produced Water Seminar (January 2008). Nassau Bay, TX: Produced Water Society.

84 Keir, G. and Jegatheesan, V. (2014). A review of computational fluid dynamics applications in pressure-driven membrane filtration. *Reviews in Environmental Science and Biotechnology* 13: 183–201.

85 Echakouri, M., Salama, A., and Henni, A. (2021). Experimental and computational fluid dynamics investigation of the deterioration of the rejection capacity of the membranes used in the filtration of oily water systems. *ACS EST Water* 1 (3): 728–744.

86 Gruber, M.F., Aslak, U., and Hélix-Nielsen, C. (2016). Open-source CFD model for optimization of forward osmosis and reverse osmosis membrane modules. *Separation and Purification Technology* 158: 183–192.

87 Ranck, J.M., Weeber, J.L., Tan, G. et al. (eds.) (2002). Removal of BTEX from produced waters using surfactant-modified zeolite. Conference proceedings.

88 Agrahari, G.K., Rawat, A., Verma, N., and Bhattacharya, P.K. (2013). Removal of dissolved H_2S from wastewater using hollow fiber membrane contactor: experimental and mathematical analysis. *Desalination* 314: 34–42.

89 Rehm, B., Haghshenas, A., Paknejad, A.S. et al. (2013). *Underbalanced Drilling: Limits and Extremes*. Elsevier.

90 White, R., Mulas, S., and Al-Jughayman, A. (eds.) (2020). Enhanced produced water deoiling using a centrifugal separator. Abu Dhabi International Petroleum Exhibition & Conference. Society of Petroleum Engineers.

91 Rawlins, C.H. and Sadeghi, F. (2018). Experimental study on oil removal in nutshell filters for produced-water treatment. *SPE Production & Operations* 33 (01): 145–153.

92 Cabrera, S.M., Winnubst, L., Richter, H. et al. (2021). Industrial application of ceramic nanofiltration membranes for water treatment in oil sands mines. *Separation and Purification Technology* 256: 117821.

93 Shams Ashaghi, K., Ebrahimi, M., and Czermak, P. (2007). Ceramic ultra-and nanofiltration membranes for oilfield produced water treatment: a mini review. *Open Environmental Sciences* 1 (1) https://doi.org/10.2174/187423350701011053.

94 Xu, Y., Lin, Y., Chew, N.G.P. et al. (2019). Biocatalytic PVDF composite hollow fiber membranes for CO2 removal in gas-liquid membrane contactor. *Journal of Membrane Science* 572: 532–544.

95 Freedman, D.E., Riley, S.M., Jones, Z.L. et al. (2017). Biologically active filtration for fracturing flowback and produced water treatment. *Journal of Water Process Engineering* 18: 29–40.

96 Hilal, N., Kochkodan, V., Al Abdulgader, H. et al. (2015). A combined ion exchange–nanofiltration process for water desalination: I. Sulphate–chloride ion-exchange in saline solutions. *Desalination* 363: 44–50.

97 Hamed, O.A. (2005). Overview of hybrid desalination systems – current status and future prospects. *Desalination* 186 (1–3): 207–214.

98 Hilal, N., Kochkodan, V., Al Abdulgader, H., and Johnson, D. (2015). A combined ion exchange–nanofiltration process for water desalination: II. Membrane selection. *Desalination* 363: 51–57.

99 Choi, S., Chang, B., Kang, J.H. et al. (2017). Energy-efficient hybrid FCDI-NF desalination process with tunable salt rejection and high water recovery. *Journal of Membrane Science* 541: 580–586.

100 Hilal, N., Kochkodan, V., Al Abdulgader, H. et al. (2015). A combined ion exchange–nanofiltration process for water desalination: III. Pilot scale studies. *Desalination* 363: 58–63.

101 Al Abdulgader, H., Kochkodan, V., and Hilal, N. (2013). Hybrid ion exchange–pressure driven membrane processes in water treatment: a review. *Separation and Purification Technology* 116: 253–264.

102 El-Dessouky, H.T. and Ettouney, H.M. (2002). *Fundamentals of Salt Water Desalination*. Elsevier.

103 Aly, N.H. and El-Figi, A.K. (2003). Mechanical vapor compression desalination systems – a case study. *Desalination* 158 (1–3): 143–150.

104 Koren, A. and Nadav, N. (1994). Mechanical vapour compression to treat oil field produced water. *Desalination* 98 (1–3): 41–48.

105 Han, D. (2015). Study on zero-emission desalination system based on mechanical vapor recompression technology. *Energy Procedia* 75: 1436–1444.

106 Dahmardeh, H., Amiri, H.A., and Nowee, S. (2019). Evaluation of mechanical vapor recompression crystallization process for treatment of high salinity wastewater. *Chemical Engineering and Processing Process Intensification* 145: 107682.

107 Liang, L., Han, D., Ma, R., and Peng, T. (2013). Treatment of high-concentration wastewater using double-effect mechanical vapor recompression. *Desalination* 314: 139–146.

108 Matz, R. and Fisher, U. (1981). A comparison of the relative economics of sea water desalination by vapour compression and reverse osmosis for small to medium capacity plants. *Desalination* 36 (2): 137–151.

109 Ettouney, H. (2006). Design of single-effect mechanical vapor compression. *Desalination* 190 (1–3): 1–15.

110 Bahar, R., Hawlader, M., and Woei, L.S. (2004). Performance evaluation of a mechanical vapor compression desalination system. *Desalination* 166: 123–127.

111 Miller, J.E. (2003). *Review of Water Resources and Desalination Technologies*. Albuquerque, NM: Sandia National Laboratories Report No.: SAND2003-0800.

112 Ettouney, H.M., El-Dessouky, H.T., Faibish, R.S., and Gowin, P.J. (2002). Evaluating the economics of desalination. *Chemical Engineering Progress* 98 (12): 32–39.

113 Chen, L., Xu, Q., Gossage, J.L., and Lou, H.H. (2016). Simulation and economic evaluation of a coupled thermal vapor compression desalination process for produced water management. *Journal of Natural Gas Science and Engineering* 36: 442–453.

114 Weyl, P.K. (1967). InventorRecovery of demineralized water from saline waters. US Patent 3,340,186A.

115 Findley, M. (1967). Vaporization through porous membranes. *Industrial and Engineering Chemistry Process Design and Development* 6 (2): 226–230.

116 Hanbury, W. and Hodgkiess, T. (1985). Membrane distillation-an assessment. *Desalination* 56: 287–297.

117 Martinez, L. and Florido-Diaz, F. (2001). Theoretical and experimental studies on desalination using membrane distillation. *Desalination* 139 (1–3): 373–379.

118 Phattaranawik, J. and Jiraratananon, R. (2001). Direct contact membrane distillation: effect of mass transfer on heat transfer. *Journal of Membrane Science* 188 (1): 137–143.

119 Lawson, K.W. and Lloyd, D.R. (1996). Membrane distillation. I. Module design and performance evaluation using vacuum membrane distillation. *Journal of Membrane Science* 120 (1): 111–121.

120 Bandini, S., Gostoli, C., and Sarti, G. (1992). Separation efficiency in vacuum membrane distillation. *Journal of Membrane Science* 73 (2–3): 217–229.

121 Basini, L., D'Angelo, G., Gobbi, M. et al. (1987). A desalination process through sweeping gas membrane distillation. *Desalination* 64: 245–257.

122 Khayet, M., Godino, P., and Mengual, J.I. (2000). Theory and experiments on sweeping gas membrane distillation. *Journal of Membrane Science* 165 (2): 261–272.

123 Chernyshov, M., Meindersma, G., and De Haan, A. (2005). Comparison of spacers for temperature polarization reduction in air gap membrane distillation. *Desalination* 183 (1–3): 363–374.

124 Shirazi, M.M.A., Kargari, A., and Shirazi, M.J.A. (2012). Direct contact membrane distillation for seawater desalination. *Desalination and Water Treatment* 49 (1–3): 368–375.

125 Xu, Y., Zhu, B.-K., and Xu, Y.-Y. (2006). Pilot test of vacuum membrane distillation for seawater desalination on a ship. *Desalination* 189 (1–3): 165–169.

126 Shirazi, M.M.A., Kargari, A., Bastani, D., and Fatehi, L. (2014). Production of drinking water from seawater using membrane distillation (MD) alternative: direct contact MD and sweeping gas MD approaches. *Desalination and Water Treatment* 52 (13–15): 2372–2381.

127 Khayet, M. and Cojocaru, C. (2012). Air gap membrane distillation: desalination, modeling and optimization. *Desalination* 287: 138–145.

128 Lee, R.L. and Dong, J. (2004). Modified reverse osmosis system for treatment of produced waters. New Mexico Institute of Mining and Technology (US).

129 Akther, N., Sodiq, A., Giwa, A. et al. (2015). Recent advancements in forward osmosis desalination: a review. *Chemical Engineering Journal* 281: 502–522.

130 Zhao, S., Zou, L., Tang, C.Y., and Mulcahy, D. (2012). Recent developments in forward osmosis: opportunities and challenges. *Journal of Membrane Science* 396: 1–21.

131 Qasim, M., Darwish, N.A., Sarp, S., and Hilal, N. (2015). Water desalination by forward (direct) osmosis phenomenon: a comprehensive review. *Desalination* 374: 47–69.

132 Al Abdulgader, H. and Rushd, S. (2020). *Advancements in Unconventional Seawater Desalination Technologies. Corrosion and Fouling Control in Desalination Industry*, 71–95. Springer.

133 Kim, Y., Elimelech, M., Shon, H.K., and Hong, S. (2014). Combined organic and colloidal fouling in forward osmosis: fouling reversibility and the role of applied pressure. *Journal of Membrane Science* 460: 206–212.

134 Kravath, R.E. and Davis, J.A. (1975). Desalination of sea water by direct osmosis. *Desalination* 16 (2): 151–155.

135 Shaffer, D.L., Arias Chavez, L.H., Ben-Sasson, M. et al. (2013). Desalination and reuse of high-salinity shale gas produced water: drivers, technologies, and future directions. *Environmental Science and Technology* 47 (17): 9569–9583.

136 McCutcheon, J.R., McGinnis, R.L., and Elimelech, M. (2006). Desalination by ammonia–carbon dioxide forward osmosis: influence of draw and feed solution concentrations on process performance. *Journal of Membrane Science* 278 (1–2): 114–123.

137 McGinnis, R.L., Hancock, N.T., Nowosielski-Slepowron, M.S., and McGurgan, G.D. (2013). Pilot demonstration of the NH3/CO2 forward osmosis desalination process on high salinity brines. *Desalination* 312: 67–74.

138 Coday, B.D., Xu, P., Beaudry, E.G. et al. (2014). The sweet spot of forward osmosis: treatment of produced water, drilling wastewater, and other complex and difficult liquid streams. *Desalination* 333 (1): 23–35.

139 Liden, T., Carlton, D.D. Jr., Miyazaki, S. et al. (2019). Forward osmosis remediation of high salinity Permian Basin produced water from unconventional oil and gas development. *Science of the Total Environment* 653: 82–90.

140 Al-Furaiji, M.H., Arena, J.T., Maqsud, C. et al. (2018). Use of forward osmosis in treatment of hyper-saline water. *Desalination and Water Treatment* 133: 1–9.

141 Lee, S., Boo, C., Elimelech, M., and Hong, S. (2010). Comparison of fouling behavior in forward osmosis (FO) and reverse osmosis (RO). *Journal of Membrane Science* 365 (1–2): 34–39.

142 Chung, T.-S., Li, X., Ong, R.C. et al. (2012). Emerging forward osmosis (FO) technologies and challenges ahead for clean water and clean energy applications. *Current Opinion in Chemical Engineering* 1 (3): 246–257.

143 Ge, Q., Ling, M., and Chung, T.-S. (2013). Draw solutions for forward osmosis processes: developments, challenges, and prospects for the future. *Journal of Membrane Science* 442: 225–237.

144 Chekli, L., Phuntsho, S., Shon, H.K. et al. (2012). A review of draw solutes in forward osmosis process and their use in modern applications. *Desalination and Water Treatment* 43 (1–3): 167–184.

145 Stefanakis, A.I. (2018). Constructed Wetlands case studies for the treatment of water polluted with fuel and oil hydrocarbons. In: *Phytoremediation*, 151–167. Springer.

146 Sluijterman, A., Al-Lawati, Y., Al-Asmi, S. et al. (eds.) (2004). Opportunities for re-use of produced water around desert oil fields. Abu Dhabi International Conference and Exhibition. Society of Petroleum Engineers.

147 Breuer, R., Al Sharji, B., Thaker, Y.I., and Headley, T.R. (eds.) (2012). The first year operation of the Nimr Water Treatment Plant in Oman-sustainable produced water management using wetlands. International Conference on Health, Safety and Environment in Oil and Gas Exploration and Production. Society of Petroleum Engineers.

148 Sultan, M., Sturchio, N.C., Alsefry, S. et al. (2019). Assessment of age, origin, and sustainability of fossil aquifers: a geochemical and remote sensing-based approach. *Journal of Hydrology* 576: 325–341.

149 Boschee, P. (2014). Produced and flowback water recycling and reuse: economics, limitations, and technology. *Oil and Gas Facilities* 3 (01): 16–21.

150 Jiang, M., Hendrickson, C.T., and Van Briesen, J.M. (2014). Life cycle water consumption and wastewater generation impacts of a Marcellus shale gas well. *Environmental Science and Technology* 48 (3): 1911–1920.

151 Li, Q., Du, J., Qiao, F., and Yu, L. (2017). Challenges and opportunities in produced water and drilling waste treatment techniques to mitigate the adverse environmental impacts. *Environment Pollution and Climate Change* 1 (143) https://doi.org/10.4172/2573-458X.1000143.

152 Ceschin, F. and Gaziulusoy, I. (2016). Evolution of design for sustainability: from product design to design for system innovations and transitions. *Design Studies* 47: 118–163.

153 Maelum, M. and Rabe, K. (eds.) (2015). Improving oil separation from produced water using new compact flotation unit design. SPE Production and Operations Symposium. SPE-173589-MS.

154 Clay, L. and Pichtel, J. (2019). Treatment of simulated oil and gas produced water via pilot-scale rhizofiltration and constructed wetlands. *International Journal of Environmental Research* 13 (1): 185–198.

155 Rehman, K., Imran, A., Amin, I., and Afzal, M. (2019). Enhancement of oil field-produced wastewater remediation by bacterially-augmented floating treatment wetlands. *Chemosphere* 217: 576–583.

156 Shamaei, L., Khorshidi, B., Perdicakis, B., and Sadrzadeh, M. (2018). Treatment of oil sands produced water using combined electrocoagulation and chemical coagulation techniques. *The Science of the Total Environment* 645: 560–572.

157 Szép, A. and Kohlheb, R. (2010). Water treatment technology for produced water. *Water Science and Technology* 62 (10): 2372–2380.

158 Ighilahriz, K., Ahmed, M.T., Djelal, H., and Maachi, R. (2018). Efficiency of an electrocoagulation treatment of water contaminated by hydrocarbons in a continuous mode powered by photovoltaic solar modules. *Environmental Engineering and Management Journal* 17 (7): 1521–1529.

159 Zhu, X., Zhang, Z., Ge, B. et al. (2014). A versatile approach to produce superhydrophobic materials used for oil–water separation. *Journal of Colloid and Interface Science* 432: 105–108.

160 Milow, B. and Zarza, E. (1997). Advanced MED solar desalination plants. Configurations, costs, future – seven years of experience at the Plataforma Solar de Almeria (Spain). *Desalination* 108 (1–3): 51–58.

161 Alammar, A., Park, S.H., Williams, C.J. et al. (2020). Oil-in-water separation with graphene-based nanocomposite membranes for produced water treatment. *Journal of Membrane Science* 603: 118007.

162 Davenport, D.M., Ritt, C.L., Verbeke, R. et al. (2020). Thin film composite membrane compaction in high-pressure reverse osmosis. *Journal of Membrane Science* 610: 118268.

163 Jiménez, S., Andreozzi, M., Micó, M.M. et al. (2019). Produced water treatment by advanced oxidation processes. *Science of the Total Environment* 666: 12–21.

164 Coha, M., Farinelli, G., Tiraferri, A. et al. (2021). Advanced oxidation processes in the removal of organic substances from produced water: potential, configurations, and research needs. *Chemical Engineering Journal* 414: 128668.

165 Heins, W.F. (2010). Is a paradigm shift in produced water treatment technology occurring at SAGD facilities? *Journal of Canadian Petroleum Technology* 49 (01): 10–15.

166 Echchelh, A., Hess, T., and Sakrabani, R. (2018). Reusing oil and gas produced water for irrigation of food crops in drylands. *Agricultural Water Management* 206: 124–134.

167 Mallants, D., Šimůnek, J., and Torkzaban, S. (2017). Determining water quality requirements of coal seam gas produced water for sustainable irrigation. *Agricultural Water Management* 189: 52–69.

168 Mathew, B.P. (ed.) (2014). Produced Water Management – Nimr Water Treatment project. SPE Middle East Health, Safety, Environment & Sustainable Development Conference and Exhibition. SPE-170335-MS.

169 National Water Commission (2011). Onshore co-produced water: extent and management. Bioregional Assessment Source Dataset.

170 Sujanani, R., Landsman, M.R., Jiao, S. et al. (2020). Designing solute-tailored selectivity in membranes: perspectives for water reuse and resource recovery. *ACS Macro Letters* 9 (11): 1709–1717.

171 Moskalyk, R. and Alfantazi, A. (2003). Processing of vanadium: a review. *Minerals Engineering* 16 (9): 793–805.

172 Chang, H., Liu, B., Crittenden, J.C., and Vidic, R.D. (2019). Resource recovery and reuse for hydraulic fracturing wastewater in unconventional shale gas and oil extraction. *Environmental Science and Technology* 53 (23): 13547–13548.

4

Applications of Ultrasound in Separation Processes

Shankar B. Kausley[1], Gaurav G. Dastane[2], Rajshree A. Patil[2], Ananda J. Jadhav[2], Ketan S. Desai[2], and Aniruddha B. Pandit[2]

[1] *TCS Research, Physical Sciences Research Area, Tata Consultancy Services, Pune, India*
[2] *Department of Chemical Engineering, Institute of Chemical Technology, Mumbai, India*

4.1 Introduction

Separation is a technique for isolating specific constituents, either desired products or impurities, from the mixture based on the difference in their physical and chemical properties. This includes various physical and chemical processes like distillation, absorption, crystallization, adsorption, extraction, and so on. The separation is achieved by supplying external energy and material to the system. Usually, these processes are energy-intensive and many times use toxic chemicals, which are not environmentally friendly. Hence, there is a need for the development of more sustainable processes which need minimum energy and are environmentally friendly.

Several efforts have been made to improve the efficiency of these separation processes in an economically attractive way. Ultrasound (US) is one such option that can be effectively utilized to intensify these processes in terms of better yield and selectivity with lower energy consumption without using any toxic chemical that adversely affects the environment [1].

US refers to sound waves with frequencies ranging from 16 kHz to 500 MHz (higher than the human hearing threshold) that can be transmitted in the form of mechanical energy through any elastomeric media such as water, aqueous particle suspension, and gas-saturated water. US waves, when transmitted in an aqueous solution, cause acoustic cavitation leading to various physical effects and chemical reactions. The adiabatic collapse of cavity bubbles generates high-temperature (several thousand K) and high-pressure conditions (a few hundred bars) for a small time interval of few microseconds [2]. The high-temperature conditions initiate different chain reactions. These extreme conditions also cause the splitting of water into hydrogen and hydroxyl radicals. The generated hydroxyl radicals help in oxidizing different organic compounds in their vicinity. The collapse of cavitation bubbles also produces liquid jets of high velocities (100 m/s). Although the

Sustainable Separation Engineering: Materials, Techniques and Process Development, Volume 1, First Edition. Edited by Gyorgy Szekely and Dan Zhao.
© 2022 John Wiley & Sons Ltd. Published 2022 by John Wiley & Sons Ltd.

impact of cavitating jets is harmful to hydraulic parts, the impact produced by microjets is found to be utilized for different applications, such as surface cleaning, surface treatments, and peening of metallic materials. The acoustic streaming is found to improve the mass transfer in a multiphase system. The shock waves generated during cavitation result in high-velocity interparticle collisions in liquid–solid systems. The acoustic waves produce vortices in the pores of suspended solids in aqueous solution as well as at the interface of solid and liquid [3–5]. Acoustic waves are also found to break the boundary layer between solid and liquid interfaces and help in mass transfer enhancement. Additionally, all these effects can be achieved in a noninvasive manner, i.e. without keeping ultrasonic wave-generating probe into the reactor through the reactor walls. Hence, in a process reactor, US is mounted outside the reactor and waves are transmitted in the reactor. This avoids the design complexities and cross-contamination due to contact of process fluid with external accessories and makes the process safe.

In this chapter, we have discussed the application of US in different separation processes, such as crystallization, extraction, emulsion breaking, desorption, distillation, and cleaning of membranes and delicate articles such as jewellery, watches, electronic parts, and lenses. The main objective is to understand the basic principle of US utilized during the intensification of these processes, the level of understanding achieved in the field and future perspectives. Figure 4.1 summarizes the different applications of US, the operating parameters, and the basic principles of US utilized in each of these processes.

4.2 Sonocrystallization

Crystallization is one of the most crucial separation techniques in the chemical industry. In crystallization, the dissolved solute precipitates from the liquid solvent in the form of solid crystals. The most important applications of crystallization are in the field of pharmaceuticals, polymers, the food industry, and speciality chemicals, where it is essential to control the crystal size, shape, and polymorphism, as they have a direct impact on the product quality. Compliance with the product quality criteria necessitates a crystallization technique that can produce consistent results. Reported techniques to control the crystallization process include the addition of polymers, surfactants, or amphiphilic molecules to control crystallization kinetics, controlling the crystal size by controlling initial seeding in the solution, milling, using supercritical fluids as a solvent or anti-solvent, using static mixers, or application of US. Prasad and Dalvi [6] have provided a good comparison of key features of all these processes in their review.

The application of US during crystallization is referred to as sonocrystallization. Researchers have been aware of the use of US in the crystallization process for almost a century now. The earliest reference of the application of US in crystallization was made by Richards and Loomis in 1927 [7]. US has been widely used to obtain fine crystals since the 1960s [8]. However, these early applications were primarily at a small scale. The use of sonocrystallization at an industrial scale has only gained interest in the last couple of decades. The physical effects of acoustic cavitation are primarily utilized in sonocrystallization process. The effects of US on various stages of crystallization process are discussed in this section.

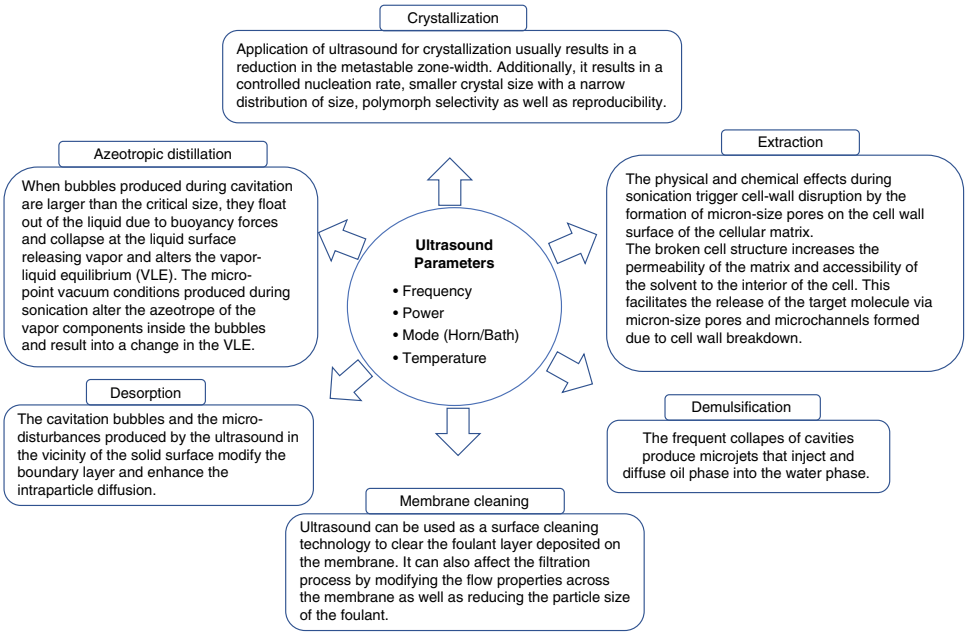

Figure 4.1 Application of US in different separation processes, operating parameters, and basic principles utilized in each separation process.

4.2.1 Crystallization Process

In the crystallization process, the solute particles precipitate from the solvent phase, thus creating a two-phase system consisting of solid and liquid phases. For this process to take place, the solution needs to be supersaturated, and, subsequently, nucleation and growth of the crystals also need to take place [9]. The solute's solubility is the primary governing factor in this process. Figure 4.2 shows a typical solubility diagram marked with the areas of supersaturation and saturation. The thermodynamic limit of solute in the solution is represented by the solubility line, while the limit beyond which spontaneous precipitation of crystal nuclei takes place is shown by the spontaneous nucleation line. The metastable zone (MSZ) is the zone between the solubility and the spontaneous nucleation curves.

For crystallization of the solute from the solution at point A, it is necessary to first destabilize the system equilibrium. This can be attained by reducing the solubility by decreasing the temperature till it reaches the critical solubility by intersecting the solubility line, represented by point B. However, crystallization does not begin until the temperature is reduced further to point C, where it crosses the nucleation line. At this point, instantaneous nucleation takes place, resulting in crystal formation. Alternatively, crystallization can also be achieved by increasing the solute concentration from point A to point B* by evaporating the solvent or adding an anti-solvent to reduce solubility [9].

4.2.2 Effect of US on Crystallization

Application of US for crystallization usually results in a reduction in the metastable zone-width (MSZW) indicated by the region between solubility line and nucleation line in Figure 4.2. Additionally, sonocrystallization also results in a controlled nucleation rate, smaller crystal size with a narrow distribution of size, polymorph selectivity as well as reproducibility. However, few exceptions have also been reported by some researchers [10, 11].

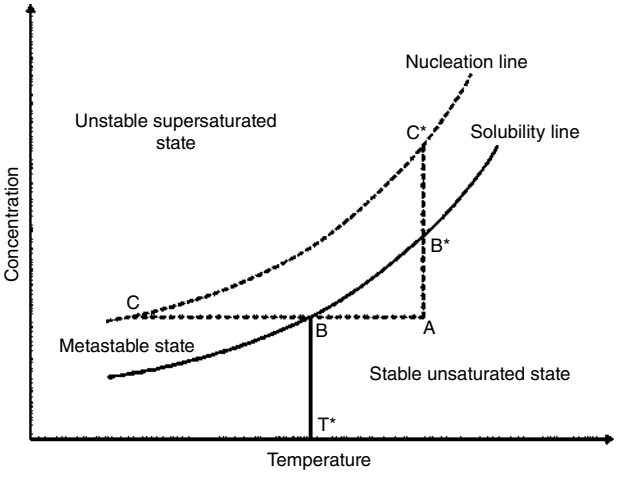

Figure 4.2 Typical solubility diagram showing solubility as a function of temperature. *Source:* Adapted from [9].

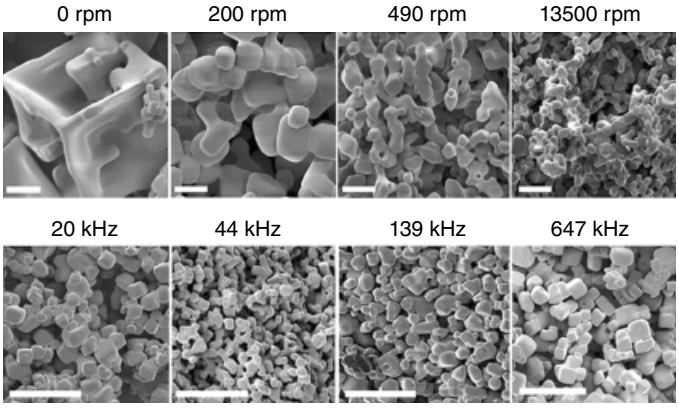

Figure 4.3 NaCl crystals made in anti-solvent crystallization using mixing (top row) and US (bottom). The white scale in the image corresponds to 20 µm. *Source:* Adapted from [13].

However, most often, the crystals produced under sonication are found to be more uniform in size and shape as compared to simple mixing [8, 12, 13]. It can be seen from Figure 4.3 that the crystals produced with US irradiation are more regular, and do not have any agglomerates.

4.2.3 Effect of US on Nucleation

Nucleation is the most important step in initiating the crystallization process. There are several theories on how ultrasonic cavitation may affect primary nucleation.

- *Cooling:* Evaporation of liquid from bulk to the cavity takes place during the cavity expansion phase, which results in the cooling of the cavity surface. Hickling Theory suggests that this lowering of temperature causes local supersaturation in the layer adjacent to the cavity surface, which can result in nucleation [14]. The drop in temperature for a bubble size of 100 µm is estimated to be about 1 °C [8, 15]. However, such a change in temperature is not sufficient to bring about any significant nucleation, and it is believed that the surface-cooling effect does not have a major impact on nucleation [8].
- *Pressure:* It is well known that the collapse of a cavity results in the generation of high pressure in the surrounding region. At these elevated pressures, most solutes have reduced solubility. This results in an increase in supersaturation as well as the nucleation rate. This hypothesis has been validated by researchers experimentally as well as numerically [8, 16, 17]. However, some conflicting results have also been reported [15, 18]. The conflict arises when the solubility of the solute is not affected by the pressure. Further research needs to be conducted to determine the components for which this theory holds true.
- *Evaporation:* As stated earlier, the liquid evaporates from bulk into the bubble during the growth of the cavity. This also induces a depletion layer of the solvent close to the wall of the cavity, resulting in local supersaturation which triggers nucleation [18]. However, there is not enough experimental evidence to suggest if this has a significant effect on nucleation [19].

- *Segregation:* When a cavitation bubble collapses, a high-velocity microjet is generated which accelerates the molecules around it. This acceleration is different for different molecules of varying densities. Hence, the solute clusters denser than other molecules will be accelerated slower than other molecules and get segregated. These clusters create supersaturation conditions near the liquid–bubble interface for a brief period of time and may collide with each other, resulting in nucleation. This hypothesis has been tested numerically [20]. However, attempts of experimental validation are inconclusive and need further efforts [21].
- *Convection:* The high-velocity microjets produced due to acoustic streaming generate micro-turbulence in the system, which increases the nucleation rate. However, there are different opinions about the exact mechanism. One hypothesis states that the flow induced by cavitation promotes collision of solute molecules which results in enhancement of nucleation rate [12, 22]. Nalajala and Moholkar found that the shockwaves generated during cavity collapse result in a higher nucleation rate, whereas the micro-turbulence results in enhancement of crystal growth. The pressure shockwaves accelerate the solute molecules resulting in collisions that form larger clusters, which form nuclei for crystallization [23]. Another theory suggests that micro-turbulence enhances the heat and mass transfer via diffusion [23–28]. In the case of evaporative crystallization, this means the enhanced rate of evaporation of the solvent [27]. The anti-solvent crystallization leads to rapid and uniform mixing of the solvent and anti-solvent, thus reducing the solubility and increasing the rate of nucleation [28, 29].
- *Heterogeneous Nucleation:* The presence of foreign particles in a solution acts as nucleation sites that enhance the nucleation rate. A cavitation bubble generated due to US also acts as a site for nucleation [30–33]. This hypothesis has been tested experimentally by Wohlgemuth et al. [19, 34]. Additionally, a mathematical model for heterogeneous nucleation using US has also been proposed in the literature [33]. It was found that the contact angle between the foreign particle and the crystal plays a crucial role in determining the energy necessary for heterogeneous nucleation. The force generated by the cavitation bubble can alter this angle, irrespective of whether nucleation takes place at the solution–foreign solid particle interface, the solution–bubble wall interface or the solution–bubble wall–solid particle interface [26, 35].
- *Secondary Nucleation:* In sonocrystallization, secondary nucleation takes place due to the fragmentation of the crystals resulting from the implosion of the cavity. The fragments of crystals thus formed act as sites for secondary nucleation [36, 37]. This process can be assumed to work similar to the sono-defragmentation process. However, the detailed mechanism of secondary nucleation has not been reported in the literature and there is a scope for such a study.

4.2.4 Effect of US on the Growth of Crystals

The impact of sonication on crystal growth is not very substantial. Hence, these effects are less understood than the effects of ultrasonic cavitation on the process of nucleation [38–40]. Most of the available literature on the effect of ultrasonic cavitation on the growth of crystals is associated with the shape and size of the crystals.

- *Effect on Particle Size:* In sonocrystallization, the US effect on the growth of the crystals is usually negated by its effect on nucleation and crystal breakage. The crystal breakage due to US results in the reduction of particle size, whereas the enhanced nucleation rate results in a large number of nuclei which are converted to a large number of smaller crystals. Both these effects hinder the possibility of crystal growth into large crystals. Generally, US has a more significant effect on nucleation than that on crystal breakage, and hence smaller crystal sizes with narrow crystal size distribution are obtained. However, few studies report an increase in crystal growth rates with the application of US. This effect can be attributed to the enhanced heat and mass transfer rates achieved due to acoustic streaming. These effects are most prominent at a high frequency of US (>1 MHz) and also at a very low frequency (~20 kHz), where transient cavitation takes place. However, at low frequency, the crystal breakage rates are also high, while at a high frequency, they are relatively lower [11, 27, 41, 42]. This effect on growth rate kinetics was also studied using a mathematical model and it was found that enhancement of up to 20% in crystal growth rate is possible by using US, when compared to crystallization without US [23].

US also results in narrow crystal size distribution, which is usually attributed to good levels of micro-mixing achieved due to acoustic streaming [13, 33, 40, 43]. Micro-mixing ensures that the anti-solvent and/or temperature distribution is uniform everywhere and no local supersaturation zone is created. This results in uniform growth of all the crystals, and thus a narrow crystal size distribution [23, 42, 44].

- *Effect on Particle Shape:* Several studies in the literature report the formation of more sphere-like crystals due to sonocrystallization [45–49]. Although the exact mechanism is not completely understood, there are two leading arguments made in this regard. The first argument theorizes that the uniformity in crystal shape arises due to uniformly enhanced mass transfer rates all around the crystal. This leads to crystal growth in all directions rather than favoring a particular crystal face, which results in increased sphericity of the final crystals [45, 47, 48, 50]. The second argument attributes this effect to the melting of the crystal particles due to cavity collapse in its vicinity [47, 51–53]. High temperatures resulting from cavity collapse can melt the particles and fuse them together. Such agglomerates with smooth surfaces have been reported when slurries of Sn. Zn, Cu, Ni, Cr, and Fe were sonicated [25, 54].

4.2.5 Effect of US on Crystal Breakage/Deagglomeration

Most of the available literature on sonofragmentation or crystal breakage reports the results for inorganic crystals in water [13, 55–57]. It is reported that sonofragmentation is mostly affected by the temperature of the system, the type of the cavity, and the properties of the material such as the Vickers hardness and Young's modulus.

Sonofragmentation takes place due to the high shear forces generated during cavity collapse. As discussed earlier, the number of cavitational events increase with temperature. However, the intensity of these events decreases. Hence, there is an optimum temperature at which maximum sonofragmentation is observed [58]. It is also reported that the type of cavitation bubbles, whether stable or transient cavities, also affect the extent of sonofragmentation. Stable cavities generated at higher US frequency can break the crystals only to a coarser size, while the transient cavities generated with lower US frequency can break the

crystals to a much smaller size [41, 59, 60]. Additionally, researchers have also reported that crystals with higher Vickers hardness and Young's modulus require extended sonication to break the crystals to a smaller size. The rate of fragmentation is linearly proportional to Vickers hardness or Young's modulus [61].

Additionally, US is also responsible for the deagglomeration of crystal aggregates. The effectiveness of US in deagglomeration is largely dependent on the time of application of US during the sonocrystallization process. US enhances the extent of micro-mixing, which increases the number of suspended particles as well as the frequency of their collisions. Thus, any aggregates formed during crystallization can be effectively disordered before they are set into agglomerates. If US is used at the end of the crystallization process to deagglomerate the aggregates, it results in surface erosion and very little deagglomeration is observed. However, if the US is used during the initial stages of crystallization, it is very effective in inhibiting the formation of agglomerates. It is recommended that to get maximum deagglomeration, the US should be applied until a complete de-supersaturation of the solute takes place [62–64].

4.2.6 Effect of US on Polymorphism

Polymorphs are crystals of the same chemical compound with different crystal structures. Most of the crystalline compounds display polymorphism. Polymorphism results in different material properties such as density, rate of dissolution, crystal shape, etc. In certain applications, such as in pharmaceutical industries, this may have a crucial role, and it becomes important to control the polymorphism during crystallization. During sonocrystallization, the polymorphic behavior is different than that observed without using US. It is observed that the probability of generation of energetically less stable polymorph is higher in the case of sonocrystallization. This observation is more common in the case of highly supersaturated solutions. At higher supersaturation levels, there is less time available for clusters of solute molecules to rearrange and reorient themselves during the nucleation phase. Hence, it is more likely that the crystals are stuck at a structure with a local minimum energy level. This can result in the formation of the polymorphic form with lower stability. Sonication also increases the rate of supersaturation, which further increases the chances of the formation of the less stable polymorphic form. If the solution has a low supersaturation level, the molecules can reorient themselves into the more stable polymorphic form. Additionally, the high mass transfer rates due to acoustic streaming at high frequency (>1 MHz) are also considered to increase the supersaturation level, thus resulting in a higher concentration of less stable polymorphic form [40, 65–67].

4.2.7 Effect of US on Chirality

Similar to polymorphism, US has also been reported to have an impact on the chirality of the crystals. This is very important in the pharmaceutical industry, as many times, only one of the enantiomers is desired. While researchers agree that US does not affect chiral crystallization and chirality directly, the process may get significantly influenced by the secondary effects of cavitation. The chiral symmetry is thought to be disrupted during a sonocrystallization process, predominantly through the secondary nucleation enhanced by US.

The secondary nuclei preserve the chirality of the parent crystal. This phenomenon is also observed in systems with high levels of turbulence and mixing. If the sonocrystallization system has a slight surplus of one enantiomer, and/or the system is undergoing racemization, it may create chiral amplification [68–70].

The combined effect of all the processes discussed in this section is quite complex. Several mathematical models have been reported in the literature that tries to incorporate various simultaneous effects of US on crystallization using the population balance method [23, 59, 71, 72]. There are several factors which need to be considered to find the optimum conditions for sonocrystallization. These factors include US frequency, power, temperature, duration of US irradiation, the phase of crystallization when US is used, and so on. Detailed literature reviews are available on possible mechanisms of sonocrystallization, which discuss these factors in detail [6, 8, 21, 73, 74].

4.3 Application of US in Extraction

Extraction is one of the most important unit operations in processing industries for the separation of a specific constituent from a complex matrix comprising different constituents for chemical analytics or the production of active ingredients. Extraction can be of a type of liquid–liquid extraction where an active component is extracted by combining two immiscible liquids which leads to the migration of the active component into one of the liquids according to its solubility preference. The solid–liquid extraction involved bringing in contact a solid matrix and a solvent in which the target molecule is soluble, and the other constituents are insoluble. Different methods of extraction include solvent extraction, applying pressure to the matrix, and distillation of mixture to compound. Among these, solvent extraction is the most widely used method due to its effectiveness, ease, and comparatively low cost to that of others [75–77]. Extraction of bioactive molecules from natural sources and mineral extraction from their ores are examples of commonly used extraction processes for commercial applications [78].

The solvent extraction process uses a specific solvent to extract a target compound from its source material. The conventional extraction techniques include maceration, heat reflux, and Soxhlet extraction. Extraction in all the above-mentioned processes is by diffusion of active components into the solvent where some method like Soxhlet extraction is facilitated by heat. As such, no shear pressure is involved in this method which results in low yield even after consumption of a large volume of solvent. The US-assisted solvent extraction technology is one of the emerging technologies widely used to intensify the solvent-based extraction process for extracting a broad range of commercially important active ingredients from a variety of raw materials [79–81]. In this section, the application of US in the extraction of different biomolecules is discussed in more detail.

Biomolecules are any of the countless compounds created by cells of living organisms, including animal, plant, and bacterial cells. They played a significant role in structural integrity, adhesion, and cell-to-cell communication. Polysaccharides, vitamins, antioxidants, essential oils, proteins, peptides, amino acids, enzymes, steroids, and collagen are few examples of commercially important biomolecules [82]. Recently, biomolecules and bioactive compounds are gaining tremendous demands in therapeutic application. Several

studies have been reported to prove their effectiveness and specificity in the treatment of various diseases with considerably fewer side effects. Increased demand for such molecules opens a new sector in the pharmaceutical, food, and nutraceutical-based industries to commercialize products comprising a bioactive molecule.

The major process during the manufacturing of these compounds is their extraction from a complex cellular matrix in a suitable solvent, usually a buffer solution. These molecules are frequently entrenched inside the cells which makes their removal challenging. The conventional process many times involves the use of solvents toxic in nature leading to environmental and health risks. For few decades, newer technologies are employed to intensify the biomolecule extraction process to make them economical, safe, and environmentally friendly by using a relatively safe solvent. The extraction process with US-assisted method has shown to increase in yield and safety of the product even after using a green solvent with less extraction capacity [83].

The US-assisted extraction process is initiated by breaking the cell wall of the cellular matrix as an effect of applied sonication with a frequency in the range of 20–40 kHz. The energy generated during the process transfers in the form of heat to the biomatrix and solvent mixture. The amount of heat generated depends on intensity, power, and exposure time. US exerts a mechanical effect on the reaction mixture due to vibration of the content, cavitation effect, and shear force. All these effects trigger cell-wall disruption by the formation of micron-size pores on the cell wall surface [84]. The broken cell structure, in turn, increases the permeability of the matrix and accessibility of the solvent to the interior of the cell. This facilitates the release of the target molecule via micron-sized pores and microchannels formed due to cell wall breakdown. Pretreatment of the cellular matrix, such as grinding, chopping, and enzymatic treatment, to reduced particle size, further increases the penetration of the solvent to the interior of the matrix and dissolution of the target compound into the solvent. The dilution of the microchannel may also improve the transport of the extractant as well as the target molecule.

US-assisted extraction of the desired component from its raw material is a complicated process involving mass transfer and reaction with a range of oxidative radicals that influences the final quantity and quality of the product. Several factors are responsible for the yield and quality of the extracted bioactive components. The major factors include frequency, type of reactor, exposure time, temperature, type of solvent, and source material.

The frequency of propagated US waves plays a significant role in the yield of bioactive material [85]. Higher extraction yield is observed at low frequency as it generates greater mechanical and cavitation stress. Most of the ultrasonic extraction equipment have a set of frequencies to carry out the operation. Frequency in the range of 20–40 kHz is the most suitable range used for the extraction of bioactive components. In general, the amount of sound energy delivered into the extraction system and the ultrasonic frequency has a direct link with the effect of sonication on mass transfer.

The US extraction process can be carried out in an ultrasonic probe or bath-based system. Both the systems differ significantly in efficiency and capabilities. In the probe-based ultrasonic system, the probe is inserted in the reaction vessel and thus energy is directly transmitted into the extraction medium at extremely high intensity. Since the probe is in direct contact with the sample, the mass transfer rate is high due to no interference in the path of US propagation. The volume of the sample that can be processed is determined by the diameter of the probe tip. Smaller tip diameter leads to high intensity and concentration of

cavitation in a small area. Whereas larger tip diameter produces less intense cavitation due to lower surface energy density but can process a larger volume of sample. However, the probe-based system suffers due to probe erosion which may leave residues in the extract and thus cause deterioration of product quality. The processes requiring high energy input need to be performed in a probe-based system as acceleration required for the overall reaction is not possible to achieve in the bath-based system. In the bath-based system, the sample is not in direct contact with the sound wave generator. The wave energy is transmitted from the transducer, in an upward direction into the bath containing the reaction mixture in a fairly attenuated form. This indirect way of sonication is effective for small volume samples. A bath-based system is easy, safe, and economical to extract a small amount of bioactive material. As discussed above, the chemical reaction requiring high energy input cannot be carried out in a bath-based system.

Generally, US-based extraction takes time between 20 and 45 minutes. Long extraction time increases yield. However, it can also induce undesirable changes in the final product. However, depending on the matrix, a longer extraction time may be necessary.

The generation of US waves causes an increase in temperature. The high temperature helps in the interaction of solvent and the material matrix and enhances the solvent diffusion rate, while low temperature enhances cavitation. Cavitation is minimized at higher extraction temperatures because voids are filled with solvent vapors. Depending on ultrasonic intensity and solvent, extraction temperatures can range from 10 to 80 °C. This increase in temperature is however detrimental to some bioactive compounds and thus in such a process, cooling water is circulated to stabilize the reaction temperature [76].

The extraction efficiency of the ultrasonically assisted process varies with the type and complex nature of the source material. This is mainly due to the difference in cellular structure, their internal component, and composition. The particle size of the matrix (surface area–to–volume ratio), its interaction with solvent, and affinity of the matrix with solvent determines the concentration of molecules in the extract. The selection of solvent for extraction of target compound depends on the solubility of the target molecules in the specific solvent**.** Ultrasonic extraction enhances the efficiency of solvent to extract the target compounds and therefore the amount of solvent consumed during the process is less. This, in turn, leads to a reduction in the cost and release of toxic chemicals into the environment. Since ultrasonication can enhance the efficiency of solvent, an environmentally safe solvent but with poor extraction capability can also be used during the process.

The application of US extraction for the extraction of the bioactive compound is widely explored in different industries and is well documented in the literature [80, 86–88]. The high-end biomolecules like dietary supplements, lipids, essential oils, ginseng, and saponin are typically extracted by employing the US-aided technique. Few examples of the US-assisted extraction of biomolecules are summarized in Table 4.1.

4.4 Membrane Cleaning and Filtration

Fouling is one of the largest issues hindering the application of membrane-based separation technology. The use of US irradiation is an unconventional, yet effective, method of cleaning the fouled membranes, as well as control further fouling. US can be used as a surface-cleaning technology to clear the foulant layer deposited on the membrane. It can

Table 4.1 US-assisted extraction of commercially important biomolecules.

Biomolecules/Compound and matrix source	Solvent	US process parameters	Performance/Result
Polyphenols (flavanones) Matrix source: Orange (Citrus sinensis) peel [89]	Ethanol: Water 4:1 (v/v)	• Bath-based system with cooling arrangement • Frequency: 25 kHz • Power: 60–150 W • Temperature: 40 °C • Time: 15 min	• Extraction of total phenolic content was found 3 times faster under US as compared to conventional procedure (Time decreased from 60 min to 15 min) • 35–40% increase in total phenolic content with US-assisted extraction as compared to solvent extraction • The free radical-scavenging activity (FRSA) of the phenolic compound was found to be higher (54%) in US-assisted extract as compared to solvent extracted compound (42%)
Polysaccharides Matrix source: Typha domingensis stem [90]	NaOH solution (1.5 M)	• Bath-based system with cooling arrangement • Frequency: 50 kHz • Temperature: 70 °C • Time: 40 min	• Enhancement in antioxidant activity • Low processing time as compared to conventional hot water
Kefiran biomaterial (prebiotic exopolysaccharide) Matrix source: kefir grains [91]	Hot water	• Bath-based system • Frequency: 34 kHz • Power: 100 W • Temperature: 25–50 °C • Time: 10 min.	• Increase protein content value of the sample in US-assisted extraction, i.e. hot water extract shows protein content of 0.12%, whereas ultrasonic-assisted extraction with hot water shows an increase in protein content up to 1.22% • Increase in antioxidant activity from measures as FRSA from 35 µmol/L to 55 µmol/L. • The sample extracted in hot water assisted with US shows high antimicrobial activity against bacterial strain as compared to only hot water extract due to high protein content • Better color retainment of the product

Carotenoids Orange peel [92]	Cyclohexane, olive oil, non-refined oil	Bath-based system Frequency: 40 kHz Power: 150 W Time: 35 min Temperature: 42 °C	• Reduction in consumption of energy and solvent • High-quality product • Use of vegetable oil for extraction process
Collagen Matrix source: Calipash tissue of soft-shelled turtle (Pelodiscus sinensis) [93]	Acetic acid (0.5 M, w/v)	Probe-based system Frequency: 24 kHz Power: 200 W Time: 24 min Temperature: 20 °C	• US-assisted extraction leads to an increase in collagen content by 16.3% over the collagen from the conventional extraction method • The product obtained is of higher thermal stability and elasticity • Superior functionality
Ergosterol Matrix source: Agaricus bisporus L. (Mushrooms) [94]	n-Hexane, ethanol and limonene	Probe-based system Frequency: 20 kHz Power: 375 W Time: 15 min Temperature:Ambient	US-assisted extraction required 15 min to yield 671.5 ± 0.5 mg ergosterol/100 g dry weight where a similar yield required 4 h with Soxhlet extraction
Anthocyanins and other phenolic compounds Matrix source: Fresh purple eggplant [95]	Ethanol: Water	Probe-based system Frequency: 12 kHz Power: 400 W Time: 30 min Temperature: 25 °C	• The maximum polyphenols were obtained by using supplementary extraction (SE) after every ultrasonic (US) treatment. • It was found to increase from 0.19 mg to 29.011 GAE/g DM (Gallic acid equivalents/g dried matter). • Reduction in process time Enhancement in quality of product

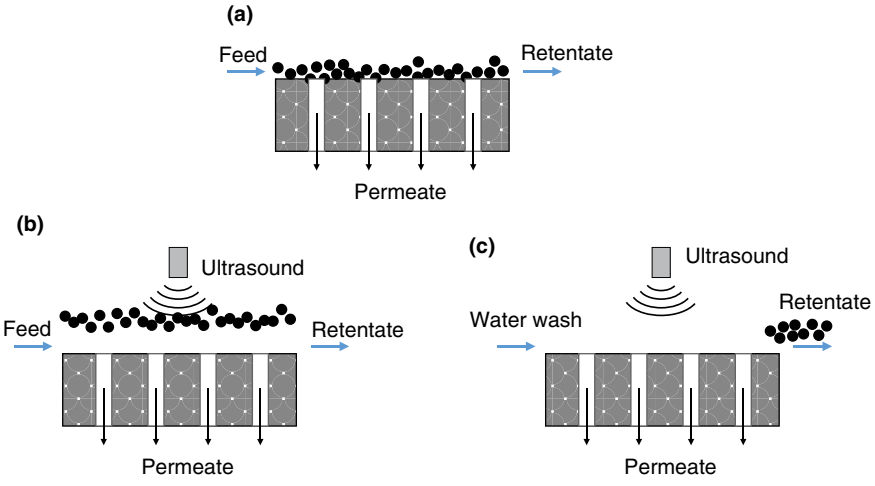

Figure 4.4 US-assisted membrane filtration and cleaning (a) membrane filtration without US; (b) membrane filtration with US; (c) membrane cleaning with US. *Source:* Modified from [96].

also affect the filtration process by modifying the flow properties across the membrane as well as reducing the particle size of the foulant. Figure 4.4 shows a schematic representation of the effect of US on membrane filtration. Figure 4.4a shows the conventional filtration where a layer of foulant particles builds up on the membrane surface, which reduces the permeate flow over time. Figure 4.4b shows the filtration process carried out under US irradiation, where the foulant particles are cleared due to US, during the filtration process. Alternatively, US can be used during washing of the membrane for enhanced surface cleaning as shown in Figure 4.4c.

This section provides an overview of the effects of key operating parameters of US on membrane filtration.

4.4.1 Frequency

The energy dissipated from the cavity collapse and the maximum cavity size before collapse are strongly dependent on the US frequency [96, 97]. A reduction in cavity size is observed with an increase in frequency, while the number of cavities increases. Generally, smaller cavities result in relatively lower energy release. This results in more hot spots which are less energized, while fewer but larger cavities generated at lower frequencies result in a smaller number of high-energy hot spots [98]. The selection of optimal frequency is thus crucial for membrane cleaning since there is a trade-off between the size and the number density of cavities. A summary of some of the studies on the influence of US frequency on membrane cleaning and fouling control has been listed in Table 4.2.

From the reports in the literature, it can be established that the recovery of the flux can be improved using a low US frequency, which reduces the membrane's filtration resistances due to the removal of the cake layer. The use of high frequency generates more cavities but they result in lower energy release on collapse. However, at higher frequencies, the solid particles that cause fouling are also likely to get degraded. This reduces the chances of

Table 4.2 Effect of US frequency on membrane filtration.

Study details	Process parameters	Results
Effect of US on filtration membrane with fouling [101]	Cross-flow filtration; Foulant: Inorganic Frequency: 40 to 23 kHz.	• An increase in the filtration flow rate was observed with a reduction in frequency. This was because the particulate matter adsorbs the sound differently.
Use of US in ultrafiltration of dextran solution [102]	Cross-flow filtration Foulant: Dextran Frequency: 28, 45, 100 kHz Power: 2.5–3.3 W/cm^2	• Permeate flow reduced by increasing the frequency • No improvement in permeation due to US at a frequency of 100 kHz
Treatment of peptone and milk using US-assisted UF and MF [96]	Cross-flow filtration Foulant: Peptone and milk Frequency: 28, 45, 100 kHz Power: 23 W/cm^2	• Permeate flow reduced by increasing the frequency • Only slight improvement in permeation was observed at a frequency of 100 kHz
US-assisted cleaning of fouled ceramic membranes [103]	Dead-end microfiltration Foulant: Sulfate polystyrene latex Frequency: 70–1062 kHz Power: 0.21–2.1 W/cm^2	• Lower frequencies resulted in better cleaning. • Higher frequencies generate smaller cavitation bubbles which release less energy on collapse; this is not sufficient to easily detach particles on the membrane surface
US-enhanced membrane filtration of industrial effluent [104]	Cross-flow filtration Foulant: Industrial wastewater from the paper industry Frequency: 27, 40, 200 kHz Power: 120–400 W	• Low-frequency US irradiated for a short time is a gentle, yet efficient, method of membrane cleaning
US cleaning of membranes with BSA as a foulant [105]	Cross-flow ultrafiltration Foulant: Bovine serum albumin (BSA) Frequency: 20, 25, 30, 38 kHz Power: 300 W	• Flow enhancement observed at low frequencies • Higher frequencies did not affect filtration rate
US cleaning of membranes with multiple frequencies [106]	Hollow fiber membrane filtration Foulant: Bentonite Frequency: Alternating between 220 kHz for 8 s, and 28 kHz for 2 s	• The use of two US frequencies was found to be more efficient in removing fouling from the membrane wall. • A large number of small cavities were generated using high frequency, which acted as nuclei for cavitation on the application of low frequency
Effect of US power on membrane cleaning [107]	Flat sheet membrane filtration Foulant: Milk Frequency: Alternating between 80 kHz for 60 s, and 37 kHz for 60 s Power: 375, 750, and 1125 W	• Low frequency and tandem frequencies showed similar enhancement in flux, though the use of tandem frequencies resulted in slightly more flux

(*Continued*)

Table 4.2 (Continued)

Study details	Process parameters	Results
Desalination using US-assisted direct contact membrane distillation [108]	PVDF hollow fiber membrane Foulant: Salt Frequency: 20–68 kHz Power: 110–260 W	• Up to 60% increase in permeation flux was observed by using lower ultrasonic frequency
US irradiation for cleaning of membrane bioreactors [109]	Hollow-fiber ultrafiltration membrane Foulant: Biomass Frequency: 20–40 kHz Power: 15 W	• Low frequencies inhibit the formation of cake on the membrane surface, which favors the membrane transmembrane pressure control while reducing the quality of the effluent • Significant biomass fragmentation is observed at lower frequencies which also affects the effluent quality.

these particles fouling the membrane. The selection of an optimum frequency can depend on the membrane characteristics and the foulant material, and needs to be adjusted considering operating conditions, like required transmembrane pressure (TMP) [99] and feed temperature [100].

4.4.2 US Intensity

The power dissipated by US irradiation per unit area is also referred to as ultrasonic intensity. Ultrasonic intensity can have a crucial effect on the effectiveness of US-assisted membrane cleaning [110]. In practical applications, adjusting the power of US is easier as compared to changing the frequency. This is one of the reasons why this parameter is used regularly as an optimizing parameter in US applications. A summary of selected literature on the influence of US intensity on membrane cleaning is listed in Table 4.3.

It can be summarized that higher ultrasonic power induces more violent cavity collapse. This results in releasing more energy at higher intensity, which generally results in increasing the cleaning efficiency and the fluxes. However, the use of very high power may result in structural damage or the loss of integrity of the membrane and also may induce additional physicochemical effects of cavitation that may be undesirable. Hence, the filtration performance of the membrane as a function of the change in ultrasonic power needs to be evaluated to determine an optimum level that can satisfy the objective of US-assisted cleaning of the membrane without damaging its structure.

4.4.3 Filtration Pressure

The pressure affects the US-assisted filtration in two ways:

a) It affects the adhesion of deposited foulant particles on the surface of the membrane, and
b) It influences the number and the size of cavities generated [117].

Table 4.3 Effect of US intensity on membrane filtration.

Study details	Process parameters	Results
Enhancement of membrane permeation by US microfiltration [111]	Cross-flow microfiltration Foulant: Bovine serum albumin and Baker's Yeast Frequency: 28 kHz Power: 120–240 W	• Five ceramic membranes with varying pore sizes were studied • It was found that the effect of an increase in the US power was less prominent for larger pore sizes
US -assisted dead-end ultrafiltration [112]	Dead end ultrafiltration Foulant: Dextran Frequency: 20 kHz Power: 8–20 W	• It was observed that US induces an effect similar to stirring • An increase in permeate fluxes was observed by increasing ultrasonic power
US-assisted cleaning of fouled ceramic membranes [103]	Dead-end microfiltration Foulant: Sulfate polystyrene latex Frequency: 70–1062 kHz Power: 0.21–2.1 W/cm^2	• An increase in power increased the flux ratio as the number of cavities and the acoustic energy dispersed in the system increased
US-enhanced ultrafiltration of suspended solutions [113]	Cross-flow ultrafiltration Foulant: Cu^{2+} polyethylenimine, W/O emulsion Frequency: 20 kHz Power: 0–150 W	• Permeate flux was directly proportional to the ultrasonic power • Flux was highest at stronger intensities, whereas no significant improvement in flux was observed at lower intensities
Effect of US power on membrane cleaning [107]	Flat sheet membrane filtration Foulant: Milk Frequency: Alternating between 80 kHz for 60 s, and 37 kHz for 60 s Power: 375, 750 and 1125 W	• Permeate flux was directly proportional to the ultrasonic power
US cleaning of UF membranes fouled with dairy solutions [114]	Cross-flow ultrafiltration Foulant: Whey solution Frequency: 50 kHz Power: 0–55 W	• Membrane cleaning efficiency was directly proportional to the ultrasonic power
Effect of US on polymeric MF membranes [115]	Dead-end microfiltration Foulant: Soy bean protein Frequency: 40 kHz Power: 0, 1.43, 2.13, 3.57 W/cm^2	• Permeate flux was affected by US intensity for all membranes except the PVDF membrane. • Higher power intensity resulted in better cleaning efficiency, but it also resulted in higher membrane damage, particularly in case of membranes having sensitive selective layers

(*Continued*)

Table 4.3 (Continued)

Study details	Process parameters	Results
US-assisted cleaning of inorganic scales on nanofiltration membranes [99]	Cross-flow nanofiltration Foulant: Arsenic Frequency: 40 kHz Power: 1–4.5 W/cm^2	• Power intensities above 1 W/cm^2 resulted in permanent damage to the membrane • 1 W/cm^2 of power enhanced the permeation flux with no substantial difference in rejection rate
Continuous and intermittent US with UF for treatment of water containing emulsion [116]	Hollow-fiber and flat-sheet membranes Foulant: Paraffin in water emulsion Frequency: 40 kHz Power: 150–450 W	• A power threshold is observed below which the mean emulsion oil droplet size is proportional to the ultrasonic power. Hence, for oily wastewater, lower power intensity was found to be better • Above the threshold, the droplet sizes reduced due to acoustic streaming and oil rejection was decreased • Higher power also resulted in the emulsification of oily wastewater, which affected the filtration negatively

Increasing the filtration pressure increases the cavitation threshold, resulting in the formation of fewer cavities [118, 119]. Cavities formed under such conditions may not only increase the intensity of cavity collapse, which results in stronger physical effects that can help in improving the membrane-cleaning efficiency, [120] but may also affect the membrane integrity. Fewer bubbles also mean a lower shielding effect, which allows the US waves to reach the membrane surface more effectively [121]. Higher intensity of the microturbulence at the membrane surface along with intense acoustic streaming leads to higher shear stresses and improved cleaning of the membranes [117]. Alternatively, a higher pressure may also increase the probability of the particle detachment from the cake layer to flow back to the membrane surface and get redeposited [117]. Higher pressure may also result in a higher density of the cake layer if the cake is compressible [122]. Additionally, it could also push the foulant particles into the membrane pores [123]. In both cases, the resistance for permeation increases and the flux decreases. The literature pertaining to the effect of filtration pressure is summarized in Table 4.4. It can be concluded that although increasing the filtration pressure may increase the intensity of cavitation, very high filtration pressure could be less effective as it tends to compact the cake layer. Usually, an optimum filtration pressure exists that provides the most enhancement in permeate flux [124].

4.4.4 Temperature

A significant effect of temperature on US-assisted membrane filtration has been reported. In the filtration process, an increase in the temperature leads to increased solubility, better

Table 4.4 Effect of filtration pressure on US-assisted membrane filtration.

Study details	Process parameters	Results
Use of US in ultrafiltration of dextran solution [102]	Cross-flow filtration Foulant: Dextran Frequency: 28, 45, 100 kHz Pressure: 0–150 kPa	• The effectiveness of US on the membrane flux improved with an increase in TMP
Effect of US on membrane permeation performance in microfiltration [111]	Dead-end microfiltration Foulant: Carrot juice Frequency: 20 kHz, 400–1000 W Pressure: 0.2, 0.5 bar	• Permeate flow rate obtained at 0.5 bar pressure was more than that at 0.2 bar
US-assisted cleaning of UF ceramic membrane [125]	Cross-flow ultrafiltration Foulant: Reactive Black 5 dye particles Frequency: 37 and 80 kHz, 88–220 W Pressure: 0.5, 1.5, 2.5 bar	• Peak cleaning efficiency was obtained at 1.1 bar • This was found to be due to the simultaneous processes of particles detaching from the surface because of cavitation and the TMP pushing the detached particles back into the membrane pores
Effect of US on membrane filtration of industrial effluent [104]	Cross-flow ultrafiltration Foulant: Paper industry wastewater Frequency: 27–200 kHz, 120–400 W Pressure: 0–3 bar	• Membrane cleaning was found to be more difficult at higher pressures
Particle fouling control in ceramic membranes using US [117]	Cross-flow ultrafiltration Foulant: Silica particles Frequency: 20 kHz, 3.8 W/cm^2 Pressure: 1–8 psi	• An increase in pressure resulted in decrease in permeate flux by ~41% • Higher pressures resulted in greater permeation drag force on the foulant toward the surface of the membrane
Application of US in dairy whey ultrafiltration [100]	Cross-flow ultrafiltration Foulant: Dairy whey Frequency: 50 kHz, 105 W Pressure: 55, 150, 225, 300 kPa	• An increase in TMP decreased the permeate flow as the cake layer was subjected to higher compressive forces
Enhancement of membrane permeation performance in US-assisted microfiltration [111]	Cross-flow microfiltration Foulant: Bovine serum albumin and Baker's Yeast Frequency: 28 kHz, 120–240 W Pressure: 20–120 kPa	• Flux was unaffected by the pressure in absence of US • In presence of US, an optimum pressure with the highest permeate flux was obtained, beyond which the flux reduced

diffusion, lower viscosity, and, thus, a higher Reynolds number. All these effects result in improved cleaning efficiency and higher flux [114, 126]. Additionally, US cavitation is also affected by temperature, which, in turn, affects its cleaning efficiency [127]. At elevated temperatures, the vapor pressure of the solvent increases, which causes rapid cavity formation. Such a condition reduces the intensity of shock waves generated due to cavity collapse, which are responsible for the cleaning of the membrane surface [128, 129]. Generally, lowering the temperature leads to an increase in cavitation threshold as a combined effect of change in surface tension, increased viscosity and/or lower liquid vapor pressure [99]. Hence, it is proposed that an optimum temperature could exist, where the cavitation effect is highest while the liquid transport properties are also beneficial [128]. A summary of few studies on the effect of temperature on the US-assisted membrane filtration in literature is given in Table 4.5 below.

Table 4.5 Effect of temperature on US-assisted membrane filtration.

Study details	Process parameters	Results
US cleaning of polymeric membranes for water treatment [130]	Cross-flow ultra and microfiltration Foulant: Peptone Frequency: 45 kHz, 2.73 W/cm^2 Temperature: 20–40 °C	• Permeate flux increased with an increase in temperature • At higher temperature, increased solubility resulted in faster recovery of permeate flux
Application of US in dairy whey ultrafiltration [100]	Cross-flow ultrafiltration Foulant: Dairy whey Frequency: 50 kHz, 105 W Temperature: 10–55 °C	• Improved cleaning efficiency at a higher temperatures due to reduction of solution viscosity
Desalination using US-assisted direct contact membrane distillation [108]	PVDF hollow fiber membrane Foulant: Salt Frequency: 20 kHz, 110–260 W Temperature: 40–70 °C	• Permeate flux increased at higher temperatures due to reduction in viscosity of the feed and the reduced boundary layer thickness • However, the effect of US on the flux was more at a lower temperature
Modeling of membrane distillation enhancement due to US [127]	Air gap membrane distillation Foulant: Common salt Frequency: 10–65 kHz, 0.5–6.5 W/cm^2 Temperature: 40–65 °C	• At a higher temperature, the enhancement in permeate flux decreased, possibly due to an increase in the saturation vapor pressure
US cleaning of nylon MF membranes [129]	Cross-flow microfiltration Foulant: Paper mill wastewater Frequency: 20 kHz, 82.9 W/cm^2 Temperature: 20–40 °C	• Membrane permeate flux increased with a decrease in cleaning temperature

Table 4.5 (Continued)

Study details	Process parameters	Results
US-assisted cleaning of inorganic scales on nano-filtration membranes [99]	Cross-flow nanofiltration Foulant: Arsenic Frequency: 40 kHz, 1–4.5 W/cm^2 Temperature: 15–60 °C	• The efficiency of the US-assisted cleaning method improved with temperature because of improvement in transport processes • However, this effect was countered by the effect of temperature on cavitation • An optimum level was found at 30 °C, where the two effects can get balanced

4.4.5 Effect of US Application Mode

Some researchers have also studied the effect of the mode of application of US (i.e. pulsed or continuous) on membrane cleaning. The mode of application has a direct energy cost implication and also can affect the membrane structure. Simon et al. [131] reported that both the application modes result in improvement in permeate flux. However, it was found that this improvement is observed only when US is ON. Hence, the continuous application of US was reported to be more effective than the pulsed mode. Similar observations have been described by Naddeo et al. and Lamminen et al. [132, 133]. However, they also reported that continuous sonication can cause damage to the membrane surface, especially when operated at higher power. Lamminen et al. reported that although the improvement in permeate flux is less with pulsed sonication, continuous sonication at higher power resulted in damage to the membrane. The pulsed mode did not result in such damage [132]. It was theorized that during pulsed sonication, a thin layer of foulant deposits on the membrane whenever US is turned off. This layer of foulant material acts as a barrier and helps in protecting the membrane surface from any damage. Chen et al. [117] also reported that the flux recovery was highest for continuous sonication and reduces as the time interval between the US pulses increases. However, they reported that the pulsed sonication mode resulted in significantly higher energy efficiency. Agi et al. [116] have reported that pulsed sonication can even enhance the permeate flux more than that with continuous sonication during ultrafiltration of an oil-in-water emulsion.

Thus, it can be concluded that although pulsed sonication may result in lower enhancement of permeate flux, it should still be preferred over continuous sonication because of its higher energy efficiency and lower tendency to cause membrane surface damage. However, the pulse period and frequency need to be optimized for different applications. The use of US in the enhancement of membrane filtration is indeed quite beneficial. US can help in cleaning the foulant material from the membrane surface, and can greatly enhance the membrane performance. Literature reviews on the use of US in membrane filtration are also available for a further detailed study on the topic [126, 128, 134]. The influence of various operating parameters has been discussed in this section and is broadly summarized in Table 4.6 below.

Table 4.6 Summary of effect of US parameters on membrane filtration and cleaning.

Parameter	Influence on membrane filtration
US frequency	• Lower frequency is more effective in cleaning the membrane surface • Higher frequencies may result in the degradation of foulant material due to cavitation • Optimum frequency should be chosen based on foulant material and membrane characteristics
US power	• Higher power results in more enhancement of permeate flux • Very high power may damage the membrane
filtration pressure	• Permeate flux increases with the filtration pressure till an optimum threshold is reached • However, beyond this optimum pressure, the flux reduces due to compacting of the filtration cake
Temperature	• At lower temperatures, the cavitation effects are more prominent • At higher temperatures, cavitation is less prominent but enhancement in flux may take place due to improved solubility and a higher Reynolds number • Usually, an optimum temperature exists where the enhancement is the highest
Sonication mode	• Continuous sonication results in enhancement of permeate flux • However, pulsed sonication is more energy-efficient and causes less membrane damage and, hence, is usually recommended

4.5 Emulsion Breaking

The separation of the continuous phase and dispersed phase of the emulsions is called demulsification. In the demulsification process, the emulsion goes through several steps, such as creaming and sedimentation, flocculation, Ostwald ripening, and coalescence [135], before being separated into two different phases. There are various methods available for demulsification of the emulsion, such as chemical, mechanical, and biological [136]. Each method has its own advantages and limitations. Hence, the choice is dependent on the type of emulsion, composition of emulsion, quantity, and cost. The thermal and mechanical effects produced by ultrasonic waves are mainly responsible for the demulsification of emulsions. The factors that cause the separation efficiency are principally categorized as acoustic operating parameters, physicochemical properties of the dispersed and continuous phase, and experimental process conditions (for example, temperature). The acoustic operating parameters that affect the efficiency of oil–water separation mainly contain the intensity of cavitation, sonication time, and operating frequency. The lower operating frequency is favorable to achieve the higher demulsification efficiency of crude oil because lower operating frequency increases the intensity of cavitation. Very high operating frequency or extreme acoustic intensity lessens separation efficiency as well as causes tiny oil droplets to separate in water. This is because the frequent collapse of cavities produces microjets that inject and diffuse the oil phase into the water phase. The demulsification efficiency is directly proportional to the sonication time. The experimental properties that

control the separation efficiency are mainly water content, interfacial tension, and viscosity of the oil phase. The high viscosity of the oil phase reduces the cavitation effect as well as the droplet vibration. So, the separation efficiency reduces if the oil phase is highly viscous. In this case, the combinations of cavitation and chemical demulsifiers are effective. Since the cavitation can be equally performed in a low interfacial tension system, it can be used to treat the low interfacial tension emulsions. The high water reduces the separation efficiency due to the unnecessary dissipation of acoustic energy. The US-assisted demulsification of emulsion primarily utilizes the viscosity-reducing effect and the agglomeration effect along with increasing droplet collision frequency due to acoustic streaming, which accelerates the separation of two phases [137]. In case of water-in-heavy crude oil emulsion, US enables/accelerates the clumping of the dispersed water phase in the form of big droplets in the continuous crude oil phase, thereby facilitating the separation of two phases. The density and compressibility differences of the dispersed droplets and the continuous phase are the reason for the acoustic waves to transfer homogeneously through the suspended droplets [138]. The simplicity and efficiency of US-assisted demulsification of water-in-crude oil emulsions have attracted research attention. The demulsification efficiency is defined as the volume of the separated dispersed phase divided by the initial volume of the dispersed phase. The various literature works related to cavitation-assisted demulsification are summarized in Table 4.7.

The main advantages of US-assisted demulsification over the other methods are low time and energy requirement, high efficiency, no degradation of either or both the phases. The efficacy of US-assisted demulsification principally depends on the optimization of the process parameters (irradiation frequency, operating power and time, and operating temperature) based on the destabilization of emulsion are summarized in Table 4.7. It is reported that for a high concentration of dispersed phase, the high operating time and power are suitable to achieve the high efficiency of emulsion separation. For the highly viscous dispersed phase, a high operating temperature is recommended.

The idea to use acoustic cavitation energy for the separation of phases in emulsions has been circulating decades ago. However, acoustic cavitation has not yet been fully explored at the industrial scale in the industries. Similarly, the use of hydrodynamic cavitation for the demulsification of emulsions has not been explored yet. Hence, there is an urgent need to bring all the relevant researchers on a single platform for the progression of the demulsification process through acoustic as well as hydrodynamic cavitation at the lab as well as industrial scale.

4.6 Desorption of Resins

Adsorption is one of the important processes which is utilized for different applications such as the removal of pollutants in the water in small concentrations and purification of essential constituents from fruits and plants. The regeneration of the adsorbent is a key step in the adsorption process since it affects the adsorption–desorption cycle, as well as the operating cost and, hence, decides the feasibility of the adsorption process for specific applications. The two different desorption processes include thermal regeneration (direct heating and application of hot air) and chemical regeneration using desorption chemicals (organic solvents or inorganic chemicals).

Table 4.7 Cavitation-assisted demulsification.

Type of emulsion	Process parameters	Demulsification efficiency (%)
Water-in-crude oil emulsion [139]	Power: 57.7 W Irradiation time: 6.2 min Temperature: 100 °C	99.8
Water-in-crude oil emulsion [140]	Two-stage ultrasonic irradiation Primary stage power: 75 W Secondary stage power: 50 W Irradiation time: 45 s (for each stage)	96
Water-in-crude oil emulsion [141]	Power: 160 W Irradiation time: 15 min Temperature: 45 °C	65
Synthetic water-in-oil emulsions [142]	In ultrasonic bath Operating frequency: 45 kHz Irradiation time: 15 min	65
Water-in-crude oil emulsion [143]	In ultrasonic bath Operating amplitude: 100% Irradiation time: 15 min	93
Refinery oil sludge [144]	Power: 66 W Irradiation time: 10 min	80
Water-in-Gachsaran crude oil [145]	Power density: 1 W/cm^3 Operating frequency: 20 kHz Irradiation time: 5 min	95
Water-in-Lu-Ning crude oil [146]	Power: 90 W Operating frequency: 10 kHz Irradiation time: 6 min	75
Water-in- Iranian crude oil [140]	Power: 75 W Operating frequency: 28 kHz Irradiation time: 45 s	96
Water-in-SAGD heavy oil [147]	Power: 200 W Operating frequency: 20 kHz Irradiation time: 4 min	70
Water-in-Brazilian heavy crude oil [141]	Power: 160 W Operating frequency: 35 kHz Irradiation time: 30 min	52

The method based on thermal regeneration has limitations such as the need for a high temperature in the hundreds of degrees and adsorbent loss after extreme burnout. The method based on the use of desorption chemicals uses specific chemicals which form complexes with the adsorbate molecule and bring them in the bulk phase. Then a secondary separation process is used to remove the desorbed molecule from the desorption chemical.

However, the secondary separation is very difficult and incur high investment and operating cost [148, 149]. Many times the desorption chemicals are not environmentally friendly.

In acoustic cavitation, when cavity bubbles reach a critical size, they collapse under adiabatic conditions with the release of a tremendous amount of energy. Since desorption is an endothermic process, it utilizes the energy released during the cavitation for the desorption of adsorbed molecules. The physical and chemical effects produced during acoustic cavitation help in enhancing the desorption process. The cavitation bubbles, and the microdisturbances in the vicinity of the solid surface, modify the boundary layer, and enhance the intraparticle diffusion. Different parameters affecting the desorption performance include US frequency, acoustic intensity, reactor geometry, and process conditions (pH and temperature). The increase in frequency and intensity was found to increase the desorption process. However, the increase in intensity over the threshold limit results in damage of adsorbents specifically in the case of polymeric resin. Lower frequencies show more deterioration because cavitation bubbles are larger at lower frequencies, resulting in stronger cavitational collapses and generated microjets, putting more mechanical stress on the adsorbent surface. The various literature works related to cavitation-assisted adsorption are summarized in Table 4.8.

Hamdaoui et al. studied the US-assisted desorption of p-chlorophenol from the activated carbon at an US frequency of 21 kHz [3]. The US intensity and temperature have shown a positive effect on desorption. The use of chemicals (ethanol or sodium hydroxide) have shown synergistic enhancement of the US-assisted desorption of p-chlorophenol.

Tao et al. has studied the mass transfer enhancement during the adsorption and desorption of anthocyanin on the microporous resin [150]. The US has shown no negative effect on the surface area, pore diameter, and volume but has affected the size of the resin. Compared to agitation, the US has shown an enhancement in external mass transfer coefficient (kL) and diffusion coefficient (Ds) by 2 and 140%, respectively.

Zhang et al. reported the feasibility of employing US for the desorption of chloramphenicol (CAP) from powdered activated carbon (PAC) [151]. Different cavitation effects, such as high-speed microjets, high-pressure shock waves, and hydroxyl radicals, were found to impact the functionality and the pores of the adsorbent, allowing effective CAP desorption from the PAC.

The study revealed that different cavitation effects, such as high-pressure shock waves, high-speed microjets and hydroxyl radical oxidation, affected the pores and functionality of the adsorbent surface (PAC) which has enhanced the desorption of CAP from the PAC. However, the efficiency (capacity and selectivity) of the regenerated PAC is found to be reduced when the study was conducted with real water samples. To increase the efficiency of desorption of refractory organic pollutants from PAC, authors have suggested using the combination of US with other advanced oxidation processes such as the use of peroxysulfate.

4.7 Separation of Azeotropic Mixtures

An azeotropic mixture is a mixture of two or more constituents having the same concentration of vapor and fluid phases. It has constant or same boiling points and its vapor will also have the same composition as that of liquid. Usually, distillation is used to separate

Table 4.8 Cavitation-assisted desorption.

Study details	Process parameters	Results
Reduction of TOC and pyrogens [149]	Adsorbate: Fructose (surrogate to pyrogens) Adsorbent: Microporous polymeric resin Amberlite CR 1320 Ca framework Reactor: 0.6 L Glass vessel US frequencies: 40.6 and 350.5 kHz	• US aids in the desorption of molecules from the surface of the adsorbent and increases the pore diffusion during the adsorption process • Increased efficiency with increase in frequency and intensity • Suitable for small-scale applications like mobile ultrapure stations where online regeneration of adsorbent can be made possible • Suitable for offline regeneration of exhausted polymeric resin in bulk quantity • To avoid the damage of resin, one needs to operate at the required frequency and at optimum intensity • The geometry of the reactor and mode of operation were found to influence the effectiveness • Need to evaluate field distribution and penetration depth
Desorption of p-chlorophenol adsorbed on the granular activated carbon (GAC) [3]	Adsorbate: p-chlorophenol Adsorbent: GAC. Reactor: 0.1 L glass reactor with cooling arrangement US frequency: 21 kHz	• The micro disturbance produced due to cavitation bubbles modifies the boundary layer and enhances intraparticle diffusion • The US intensity and temperature have a positive effect on the desorption rate • The use of ethanol with US has shown synergistic enhancement in the desorption of p-chlorophenol
Desorption of metal ions from activated carbon [152]	Adsorbate: Metal ions Adsorbent: Activated carbon Reactor: 0.1 L US frequency:22.15 kHz	• The thermal and nonthermal effects have improved the surface diffusivity • US irradiation improved the rate of desorption and desorbed amount • Temperature and US intensity show a positive effect • The desorption of copper ions was improved by adding ethanol during US treatment and keeping the pH of the regenerating solution at pH 1
Activation of peanut husk and subsequent adsorption of copper [153]	Adsorbate: Copper Adsorbent: Peanut husk US frequency: 20 kHz	• The application of US during activation of peanut husk has enhanced the peanut husk's copper adsorption capability • The US has reduced the requirement of acid during chemical activation • The use of US and phosphoric acid has shown synergy, where the adsorption capacity is increased by 10% compared to usual chemical activation and 30% compared to peanut husk

Table 4.8 (Continued)

Study details	Process parameters	Results
Purification of polyphenols from asparagus [154]	Adsorbate: polyphenols Adsobent: D101 Resin US frequency: 20 kHz	• The increase in diffusion and mass transfer reduces the equilibrium time • The use of high-intensity US causes the degradation of the resin
Adsorption of CAP onto PAC and its desorption [151]	Adsobate: CAP Adsorbent: PAC, US frequency: 40 kHz Acoustic density: 0.09–0.36 W/mL	The cavitation effects enhance the surface functionalities of the adsorbent
Regeneration of desiccant (zeolite 13X) A porous material made of crystalline alumina silicate [155]	Adsorbate: Moisture Adsorbent: Zeolite 13X Reactor: US frequencies: ~ 28, 40, 80 kHz	• At the same power consumption, the US improves zeolite 13X regeneration • The maximum reduction observed in energy and time was 24 and 23.8%, respectively • Lower ultrasonic frequencies resulted in higher efficiency • The exact mechanism needs to be understood

constituents when one constituent is more volatile than the others. However, in an azeotropic mixture, the separation using distillation is challenging as the vapor and liquid concentration is the same. Different methods explored for the separation of an azeotropic mixture are azeotropic distillation, extractive distillation, pervaporation and dividing-wall distillation column [156–158]. Considering the different limitations of conventional methods, there is still a need to develop a more efficient and safe method having an attractive fixed cost and operating cost.

US is found to enhance the azeotropic distillation by positively affecting the vapor–liquid equilibrium [158]. Even though the exact mechanism is still unknown, researchers have proposed different possible mechanisms. When an ultrasonic wave passes through a liquid medium, the growth, formation, and collapse of bubbles take place. Depending on the operating condition, bubbles either collapse inside the liquid generating high-temperature conditions at the local point or collapse at the surface of liquid releasing vapors. When bubble size is small than the critical size, bubbles collapse inside the liquid generating high-temperature conditions locally which causes the formation of radicals and highly reactive intermediates initiating different chemical pathways [159]. When bubble size is larger than the critical size, they float out of the liquid due to buoyancy forces and collapse at the liquid surface releasing vapor [160]. Suzuki et al. reported similar behavior in ethanol/water mixture, where bubbles collapse at the surface releasing the alcohol vapor in the bubble to the vapor phase [161]. This has a significant effect on vapor–liquid separation processes and cleaning applications. The ultrasonic wave also creates micro-point vacuum conditions, which alter the azeotrope of the vapor components inside the bubbles and result in a change in the vapor–liquid equilibrium. The rapid enhancement in heat and mass transfer alters the thermodynamics of the process and change the vapor–liquid equilibrium of the system.

Sonication is a transient process that occurs for microseconds, which causes the effect locally but doesn't significantly affect the global operating conditions of the distillation process. Unlike other conventional processes, such as extractive distillation, US-assisted distillation doesn't need any separating agent and separation can be achieved in a single column. This helps in reducing the equipment size and safety issues related to the addition, recovery, and recycling of separating agents through multiple equipments.

Different factors affecting the US-assisted distillation other than the parameters affecting conventional distillation (location of the feed stage, the effect of reflux ratio, etc.) are the intensity and frequency of US. The increase in intensity causes an increase in bubble population which ultimately results in a number of local vacuum-points and ultimately affects the thermodynamics of the vapor–liquid equilibrium of the system. However, the ultrasonic frequency has a negative effect on the performance of ultrasonic-assisted distillation. With a reduction in US frequency, the size of the bubble increases which affects the mass transfer of vapor phase into the bubble and their movement toward the surface, where they collapse and release the vapor, which is required for the vapor–liquid separation process. The application of US-assisted distillation for the separation of different azeotropic mixtures is given in Table 4.9.

The US-assisted distillation provides numerous advantages over conventional distillation. However, it also adds additional energy for operating ultrasonic transducers and needs a thorough cost comparison of the additional energy required for the US system vs. the cost savings due to a reduction in the number of distillation columns and its operating cost and cost of separating material management system. More study is required to make the system efficient, economically attractive, simple in operation, and environmentally friendly.

Micro-point vacuum conditions' generation during sonication helps maintain low-pressure operating conditions which are preferred for low boiling point azeotrope. However, for high boiling azeotropes (nitric acid/water and acetone/chloroform mixtures), high-pressure conditions are required to shift the azeotropic point. This is one of the limitations of using US for the distillation of azeotropic mixtures.

4.8 Ultrasonic Cleaning of Delicate Articles (Jewellery, Watches, Electronic Parts, and Optical Lenses)

Ultrasonic cleaning has been used over decades to clean delicate items such as jewellery, watches, microelectronics, hard disc drives, medical devices, automotive components, and optical lens elements. Different conventional methods used to clean such items are brush scrubbing by hand, passing water vapors, stirring in a liquid solution, and spraying the liquid through a nozzle. However, these methods are unable to remove fine dust of micron and submicron size, oily or greasy materials, or any sort of biological contamination trapped between the minute components or built inside the small crevice or holes that are difficult to access [165]. Such items can be cleaned very efficiently by the shear force generated due to ultrasonic waves which eliminate tightly adhered or embedded fine particles on or inside of an object that are inaccessible [166, 167].

Table 4.9 Application of US in the separation of different azeotropic mixtures.

System	Process conditions	Performance
Ethanol/Ethyl acetate (55 mol% ETAC) at minimum boiling point of 71.8 °C [162]	Feed: 65 mol% of ETAC entered at the bottom of the column at 100 kmol/h US intensity: 500 W/cm^2 US frequency: 25 kHz.	• Number of stages for the desired separation: 27 • US intensity has shown a positive effect on the separation. A required separation (99 mol% ETAC) was achieved at the ultrasonic intensity of 500 W/cm^2 • Frequency has shown a negative effect on the separation. The required purity (99 mol% ETAC) was obtained at a frequency of 25 kHz • System has shown good separation (99 mol% purity of the top product) for other azeotropic mixtures (ethanol–water, butanol–water and methyl acetate–methanol)
Mixture of methyl tert-butyl ether (MTBE) and methanol (MeOH) (70 mol% MTBE) [163]	System I: US Horn Amplitude 22 W/cm^2 Frequency 24 kHz System II: US bath Amplitude 22 W/cm^2 Frequency 35 kHz	• Theoretical plates decreased from three to two • Marginal change in the azeotropic point
Ethyl acetate and ethanol mixture [164]	Feed: 65% of ethyl acetate at 333.15 K and 1 bar (Azeotrope formation occurs for ethyl acetate-ethanol system at 55 mol % of ethyl acetate) Minimum boiling point: 71.8 °C Ultrasonic Distillation (UD): Distillation column with the addition of an ultrasonic transducer in the equilibrium stages. Sonication stages start from the feed stage to the top column (rectifying section), US intensity: 500 W/cm^2 US frequency: 25 kHz Reflux ratio: 8 Number of stages: 35	• A top product with 99% purity was produced from a feed containing 65% ethyl acetate • Effect of operating parameters was observed for purity of the top product and heat duty • Proposed system based on ultrasonic distillation offers 14.6% savings in operating cost compared to extractive distillation • The proposed system is limited to minimum boiling point azeotropic mixtures

The US cleaning technique involves placing the objects to be cleaned in a chamber containing a suitable cleaning solution and agitating the liquid with ultrasonic waves at a set frequency. Ultrasonic cleaning equipment comes in an array of capacities and features, making it an alternative for numerous cleaning operations. The cleaning solution used

throughout the process is either aqueous or organic, based on the type of impurity. Plain water, water blended with a surfactant, or any detergent could be used as the aqueous solution. To improve US-aided cleaning for specific applications, commercial formulations incorporating surface-active agents, enzymes, and wetting agents are now available. Organic solvents are frequently used to remove soils that are hydrophobic in nature and thus not soluble in water.

The essential components of ultrasonic-assisted cleaning equipment are an US wave generator and ultrasonic transducers. A variety of US systems are available in the market, with tanks ranging in size from 10 to 2500 L depending on the scope of the application. A standard low-intensity laboratory ultrasonic cleaning equipment will have a hollow tank with one or more transducers attached to the tank's bottom or sidewall to activate and transmit vibrational energy into the liquid through a diaphragm. The ultrasonic generator creates electrical energy at the desired frequency, which is translated by the transducer into mechanical vibrations [168]. During the process, the transducer vibrates, producing ultrasonic waves at a frequency of 20–40 kHz. Vibrations produced by the ultrasonic-assisted cleaning technique generate tiny cavitation bubbles to oscillate in the solution as the wave travels through it. The bubbles become exceedingly unstable and finally collapse causing implosions and shockwaves across the entire solution. This cavitation is created in a fraction of a second with a pressure predicted to be roughly 35–70 MPa at the 20 kHz frequency, and the transient localized temperatures are around 5000 °C, with a micro-streaming velocity of roughly 400 km/h. The implosions formed with such a high force displace and remove securely attached contaminants from the objects, either by dissolution or displacement of soluble contaminants. As a result, the contaminants embedded in microscopic fissures and crevices are therefore eliminated.

Sound wave frequency, exposure time, volume of items placed, level of contamination, system power, cleaning agent, solvent type, system setup, and bath temperature are all aspects that influence cavitation and its cleaning power [169]. The cleaning solution's viscosity has an impact on cavitation. The impact of cavitation is larger when the viscosity of the solution is lower. Because high viscosity solutions move slowly in the system, they do not quickly respond enough to build cavitation bubbles, which eventually implode.

The frequency of US waves affects the cleaning effectiveness. Low frequency leads to the formation of larger vapor bubbles which turn powerful when collapsing. When the frequency increases, the vapor bubbles that emerge grow smaller and release less energy. Different frequencies can be employed for cleaning applications depending on the type of items to be cleaned. The frequency in the range of 20–40 kHz is used to remove greasy soil from heavy-duty items like engine blocks and heavy metal parts; frequency in the range of 40–70 kHz is applied for cleaning jewellery, some components of optics; frequency in the range of 70–190 kHz is used for disk drive components and other sensitive items and frequency in the range of 190–500 kHz is used for ultrafine cleaning of semiconductor chips, thin ceramic optics, and reflecting items like a mirror [170].

Temperature is one of the most significant factors in US-assisted cleaning procedures. This is because several factors listed are affected by temperature. The viscosity of the fluid lowers as the temperature rises, as does the amount of dissolved gas in the solution. In most circumstances, raising the temperature improves performance [171–173].

The use of ultrasonic cleaning technology offers several benefits when compared with manually cleaning. It is feasible to clean more objects in less time, resulting in reduced labor costs. Cleaning of objects using the ultrasonic machine is easy and safe for the worker as it merely needs to place the items in the tank, addition of cleaning agent and switching on the machine. Thus, users are not exposed to hazardous chemical agents. Moreover, since the process does not require any manual handling of the objects, getting injured by skin puncture with sharp objects, such as scalpels and drill bits, is likely to be less. Ultrasonic cleaning reduces the amount of harmful material emitted into the atmosphere because it takes place in a confined tank. Furthermore, ultrasonic cleaning consumes less energy and cleaning agent, thus resulting in less pollution. Similarly, hand-cleaning and strong chemicals are not recommended for delicate items like jewellery or precision instruments. These artefacts necessitate a thorough cleaning as well as a careful procedure. An ultrasonic cleaner's cavitation effect allows a solution of water and detergent to penetrate tiny crevices and removes undesired residue while keeping the piece intact.

Ultrasonic cleaners can be utilized in a variety of settings, for example, cleaning jewellery and collectible coins to remove dust, grime, and skin oils; cleaning of automotive parts and tools to remove used lubricants, metal burrs, and other residues that can prevent a car from performing at its best and biological soils from surgical instruments. To eliminate specific impurities, some cleaners utilize specialized detergents, while others merely need tap water and a small bit of detergent or degreaser.

Ultrasonic cleaners are far more efficient than hand-cleaning or other machine-based cleaning methods as they can reach inaccessible parts readily. It utilizes less water and electricity, and are thus more energy-efficient, as well as working considerably faster and more efficiently. However, ultrasonic cleaning also suffers from few limitations. The blasting action of cavitation bubbles can produce high pressures that lead to distortion and cracks on the surface of brittle materials and thus must need to handle with caution. Similarly, ultrasonic vibration has been demonstrated to produce particles by eroding the surface over a long time of exposure, resulting in device damage. Figure 4.5 shows the US-based cleaning of delicate items such as jewellery, geared parts, optical lenses, and timepieces. The ultrasonic treatment, as shown in the figure, completely removes the dirt and regains the original luster of the items.

4.9 Summary and Future Perspectives

US has been found to be effective in several separation processes. In this study, the application of US is discussed for different applications such as crystallization, extraction, emulsion breaking, desorption, azeotropic distillation, and cleaning of membranes and delicate articles. US can be used as a stand-alone technique, or it could even be used as a complementary technique for intensification of another existing separation process. The extent of the application of US in separation processes varies for each of the processes and less spatial control. However, one of the key issues limiting the application of US in large-scale operations is the poor scalability of the process. Some continuous flow reactors have been developed and studied in recent years. However, more research on these methods is necessary before the technology can be applied and accepted at an industrial scale.

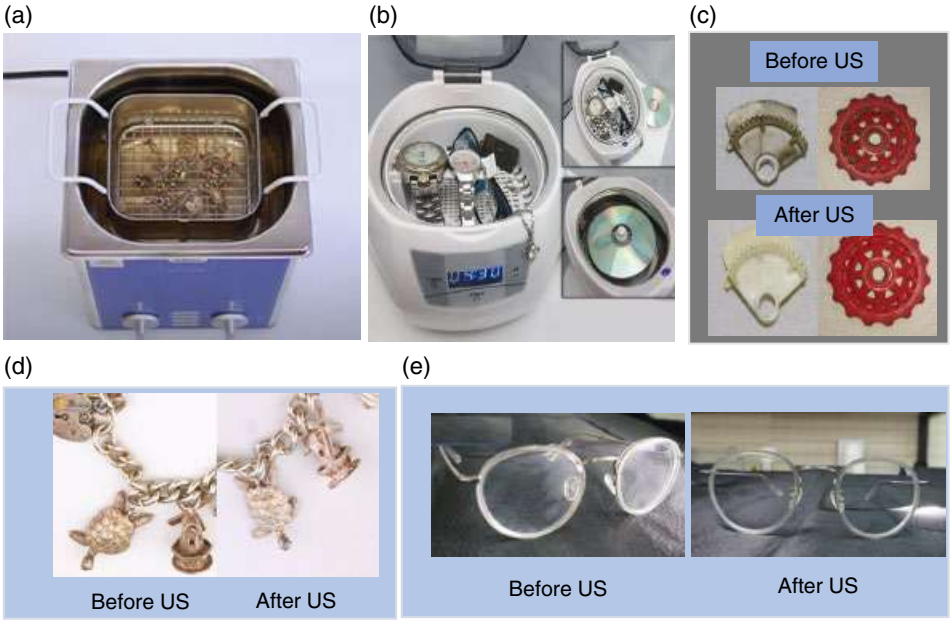

Figure 4.5 Application of US in the cleaning of delicate articles (a) US bath [174], (b) ultrasonic cleaner [175], (c) geared parts cleaned using US [176], (d) jewellery cleaned using US [174], (e) glass and lenses cleaned using US [177].

The use of US in the case of sonocrystallization is relatively more common as compared to some of the other separation processes. Although this process also faces the issue with large-scale applications, it can be used in some industries for the manufacturing of specialty chemicals and pharmaceuticals that are usually produced in smaller volumes. However, there is a necessity of exploring the possible ways to scale up the process for its application in most industries. Also, despite a large amount of research on sonocrystallization, some aspects of the process are still not completely understood, which makes the scale-up even more challenging. Developing mathematical models to accurately predict the crystal size and crystal size distribution can help in overcoming these difficulties in scale-up.

US acts as a process intensification tool in case of membrane filtration and cleaning. Although the effectiveness of US in enhancing the filtration rates and cleaning the membrane surfaces has been well documented, most of the reported literature is for lab-scale studies. These studies have been carried out using US probes, horns, or baths which are effective at lab scale but are difficult to scale up to industrial scales. Additionally, there is also a concern of membrane damage due to US in certain cases. There is a lot of scope for research in the scale-up of this process at an industrial scale, under real-life scenarios.

US has shown great potential for the extraction of biomolecules and the demulsification process. However, it is still not explored at an industrial scale to exploit its full potential. For successful scale-up, there is a need to study the performance using both acoustic and hydrodynamic cavitation and use the best combination of them at an industrial scale.

US has shown great potential in separating the azeotropic mixtures. However, it is at a preliminary level and needs more research on the development of an efficient, economically attractive, simple, safe, and environmentally friendly process with proper scientific reasoning.

US has shown several benefits for the cleaning of delicate articles, such as jewellery, optical lenses, and electronic parts, compared to manual cleaning. It has shown significant savings in terms of time, labor cost, and is simple and safe to use.

Even though adequate literature is available on the performance of US for different applications, the information about the energy requirement, specifically the total energy supplied vs. the actual energy utilized for the application is not reported uniformly. Hence, there is a need to create specific guidelines to report the specific energy consumption of US along with its efficiency for the specific application. This information will help researchers focus on energy minimization which is required for effective scale-up of the process.

Acknowledgments

The author Shankar B. Kausley acknowledges the support extended by Dr. Beena Rai, Head, Physical Sciences Research Area, TCS Research, Tata Research Development and Design Centre (TRDDC), Tata Consultancy Services Ltd., Pune, India.

References

1 Chatel, G. (2018). How sonochemistry contributes to green chemistry? *Ultrason. Sonochem.* 40: 117–122.
2 Franc, J.-P. and Michel, J.-M. (2006). *Fundamentals of Cavitation*, vol. 76. Springer Science & Business Media.
3 Hamdaoui, O., Naffrechoux, E., Tifouti, L., and Pétrier, C. (2003). Effects of ultrasound on adsorption--desorption of p-chlorophenol on granular activated carbon. *Ultrason. Sonochem.* 10 (2): 109–114.
4 Suslick, K.S., Casadonte, D.J., and Doktycz, S.J. (1989). Ultrasonic irradiation of copper powder. *Chem. Mater.* 1 (1): 6–8.
5 Yao, Y. (2016). Enhancement of mass transfer by ultrasound: application to adsorbent regeneration and food drying/dehydration. *Ultrason. Sonochem.* 31: 512–531.
6 Prasad, R. and Dalvi, S.V. (2020). Sonocrystallization: monitoring and controlling crystallization using ultrasound. *Chem. Eng. Sci.* 226: 115911.
7 Richards, W.T. and Loomis, A.L. (1927). The chemical effects of high frequency sound waves I. A preliminary survey. *J. Am. Chem. Soc.* 49 (12): 3086–3100.
8 Hem, S.L. (1967). The effect of ultrasonic vibrations on crystallization processes. *Ultrasonics* 5 (4): 202–207.
9 Mullin, J.W. (2001). *Crystallization*, 4e. Oxford, USA: Elsevier.
10 Kurotani, M., Miyasaka, E., Ebihara, S., and Hirasawa, I. (2009). Effect of ultrasonic irradiation on the behavior of primary nucleation of amino acids in supersaturated solutions. *J. Cryst. Growth* 311 (9): 2714–2721.

11 Nii, S. and Takayanagi, S. (2014). Growth and size control in anti-solvent crystallization of glycine with high frequency ultrasound. *Ultrason. Sonochem.* 21 (3): 1182–1186.

12 Nalajala, V.S. and Moholkar, V.S. (2011). Investigations in the physical mechanism of sonocrystallization. *Ultrason. Sonochem.* 18 (1): 345–355.

13 Lee, J., Ashokkumar, M., and Kentish, S.E. (2014). Influence of mixing and ultrasound frequency on antisolvent crystallisation of sodium chloride. *Ultrason. Sonochem.* 21 (1): 60–68.

14 Cheng, X., Zhang, M., Xu, B. et al. (2015). The principles of ultrasound and its application in freezing related processes of food materials: a review. *Ultrason. Sonochem.* 27: 576–585.

15 Brotchie, A., Grieser, F., and Ashokkumar, M. (2009). Effect of power and frequency on bubble-size distributions in acoustic cavitation. *Phys. Rev. Lett.* 102 (8): 084302.

16 Cogné, C., Labouret, S., Peczalski, R. et al. (2016). Theoretical model of ice nucleation induced by acoustic cavitation. Part 1: pressure and temperature profiles around a single bubble. *Ultrason. Sonochem.* 29: 447–454.

17 Cogné, C., Labouret, S., Peczalski, R. et al. (2016). Theoretical model of ice nucleation induced by inertial acoustic cavitation. Part 2: number of ice nuclei generated by a single bubble. *Ultrason. Sonochem.* 28: 185–191.

18 Harzali, H., Baillon, F., Louisnard, O. et al. (2011). Experimental study of sono-crystallisation of $ZnSO_4.7H_2O$, and interpretation by the segregation theory. *Ultrason. Sonochem.* 18 (5): 1097–1106.

19 Wohlgemuth, K., Kordylla, A., Ruether, F., and Schembecker, G. (2009). Experimental study of the effect of bubbles on nucleation during batch cooling crystallization. *Chem. Eng. Sci.* 64 (19): 4155–4163.

20 Louisnard, O., Gomez, F.J., and Grossier, R. (2007). Segregation of a liquid mixture by a radially oscillating bubble. *J. Fluid Mech.* 577: 385–415.

21 Jordens, J., Gielen, B., Xiouras, C. et al. (2019). Sonocrystallisation: observations, theories and guidelines. *Chem. Eng. Process. Process Intensif.* 139: 130–154.

22 Kiani, H., Zhang, Z., Delgado, A., and Sun, D.-W. (2011). Ultrasound assisted nucleation of some liquid and solid model foods during freezing. *Food Res. Int.* 44 (9): 2915–2921.

23 Bari, A.H., Chawla, A., and Pandit, A.B. (2017). Sono-crystallization kinetics of K_2SO_4: estimation of nucleation, growth, breakage and agglomeration kinetics. *Ultrason. Sonochem.* 35: 196–203.

24 Zhang, X., Inada, T., and Tezuka, A. (2003). Ultrasonic-induced nucleation of ice in water containing air bubbles. *Ultrason. Sonochem.* 10 (2): 71–76.

25 Zhang, Z., Sun, D.-W., Zhu, Z., and Cheng, L. (2015). Enhancement of crystallization processes by power ultrasound: current state-of-the-art and research advances. *Compr. Rev. Food Sci. Food Saf.* 14 (4): 303–316.

26 Guo, Z., Jones, A.G., and Li, N. (2006). The effect of ultrasound on the homogeneous nucleation of $BaSO_4$ during reactive crystallization. *Chem. Eng. Sci.* 61 (5): 1617–1626.

27 Cao, H.-L., Yin, D.-C., Guo, Y.-Z. et al. (2012). Rapid crystallization from acoustically levitated droplets. *J. Acoust. Soc. Am.* 131 (4): 3164–3172.

28 Patel, S.R. and Murthy, Z.V.P. (2011). Effect of process parameters on crystal size and morphology of lactose in ultrasound-assisted crystallization. *Cryst. Res. Technol.* 46 (3): 243–248.

29 Patel, S.R. and Murthy, Z. (2011). Anti-solvent sonocrystallisation of lactose. *Chem. Process. Eng.* 32 (4): 379–389.

30 Bari, A.H. and Pandit, A.B. (2018). Sequential crystallization parameter estimation method for determination of nucleation, growth, breakage, and agglomeration kinetics. *Ind. Eng. Chem. Res.* 57 (5): 1370–1379.

31 Cacciuto, A., Auer, S., and Frenkel, D. (2004). Onset of heterogeneous crystal nucleation in colloidal suspensions. *Nature* 428 (6981): 404–406.

32 Kirwan, D.J. and Orella, C.J. (2002). Crystallization in the pharmaceutical and bioprocessing industries. In: *Handbook of Industrial Crystallization* (ed. A.S. Myerson), 249–266. Elsevier.

33 Kordylla, A., Krawczyk, T., Tumakaka, F., and Schembecker, G. (2009). Modeling ultrasound-induced nucleation during cooling crystallization. *Chem. Eng. Sci.* 64 (8): 1635–1642.

34 Wohlgemuth, K., Ruether, F., and Schembecker, G. (2010). Sonocrystallization and crystallization with gassing of adipic acid. *Chem. Eng. Sci.* 65 (2): 1016–1027.

35 Horst, C., Gogate, P.R., and Pandit, A.B. (2007). Ultrasound reactors. In: *Modeling of Process Intensification* (ed. F.J. Keil), 193–277. Weinheim: Wiley-VCH Verlag GmbH & Co. KGaA.

36 Chow, R., Blindt, R., Chivers, R., and Povey, M. (2003). The sonocrystallisation of ice in sucrose solutions: primary and secondary nucleation. *Ultrasonics* 41 (8): 595–604.

37 Chow, R., Blindt, R., Chivers, R., and Povey, M. (2005). A study on the primary and secondary nucleation of ice by power ultrasound. *Ultrasonics* 43 (4): 227–230.

38 Ruecroft, G., Hipkiss, D., Ly, T. et al. (2005). Sonocrystallization: the use of ultrasound for improved industrial crystallization. *Org. Process. Res. Dev.* 9 (6): 923–932.

39 Ramisetty, K.A., Pandit, A.B., and Gogate, P.R. (2013). Ultrasound-assisted antisolvent crystallization of benzoic acid: effect of process variables supported by theoretical simulations. *Ind. Eng. Chem. Res.* 52 (49): 17573–17582.

40 Bhangu, S.K., Ashokkumar, M., and Lee, J. (2016). Ultrasound assisted crystallization of paracetamol: crystal size distribution and polymorph control. *Cryst. Growth Des.* 16 (4): 1934–1941.

41 Jordens, J., Appermont, T., Gielen, B. et al. (2016). Sonofragmentation: effect of ultrasound frequency and power on particle breakage. *Cryst. Growth Des.* 16 (11): 6167–6177.

42 Jordens, J., Bamps, B., Gielen, B. et al. (2016). The effects of ultrasound on micromixing. *Ultrason. Sonochem.* 32: 68–78.

43 Vishwakarma, R.S. and Gogate, P.R. (2017). Intensified oxalic acid crystallization using ultrasonic reactors: understanding effect of operating parameters and type of ultrasonic reactor. *Ultrason. Sonochem.* 39: 111–119.

44 Kougoulos, E., Marziano, I., and Miller, P.R. (2010). Lactose particle engineering: influence of ultrasound and anti-solvent on crystal habit and particle size. *J. Cryst. Growth* 312 (23): 3509–3520.

45 Belkacem, N., Sheikh Salem, M.A., and AlKhatib, H.S. (2015). Effect of ultrasound on the physico-chemical properties of poorly soluble drugs: antisolvent sonocrystallization of ketoprofen. *Powder Technol.* 285: 16–24.

46 Guo, Z., Zhang, M., Li, H. et al. (2005). Effect of ultrasound on anti-solvent crystallization process. *J. Cryst. Growth* 273 (3–4): 555–563.

47 Li, H., Wang, J., Bao, Y. et al. (2003). Rapid sonocrystallization in the salting-out process. *J. Cryst. Growth* 247 (1–2): 192–198.

48 Moghtada, A., Shahrouzianfar, A., and Ashiri, R. (2017). Low-temperature ultrasound synthesis of nanocrystals $CoTiO_3$ without a calcination step: effect of ultrasonic waves on formation of the crystal growth mechanism. *Adv. Powder Technol.* 28 (4): 1109–1117.

49 Pohl, B., Jamshidi, R., Brenner, G., and Peuker, U.A. (2012). Experimental study of continuous ultrasonic reactors for mixing and precipitation of nanoparticles. *Chem. Eng. Sci.* 69 (1): 365–372.

50 Li, H., Li, H., Guo, Z., and Liu, Y. (2006). The application of power ultrasound to reaction crystallization. *Ultrason. Sonochem.* 13 (4): 359–363.

51 Yang, L.-X., Zhu, Y.-J., Tong, H., and Wang, W.-W. (2007). Submicrocubes and highly oriented assemblies of $MnCO_3$ synthesized by ultrasound agitation method and their thermal transformation to nanoporous Mn_2O_3. *Ultrason. Sonochem.* 14 (2): 259–265.

52 Suslick, K.S., Doktycz, S.J., and Flint, E.B. (1990). On the origin of sonoluminescence and sonochemistry. *Ultrasonics* 28 (5): 280–290.

53 Prozorov, T., Prozorov, R., and Suslick, K.S. (2004). High velocity interparticle collisions driven by ultrasound. *J. Am. Chem. Soc.* 126 (43): 13890–13891.

54 Ambrus, R., Amirzadi, N.N., Sipos, P., and Szabó-Révész, P. (2010). Effect of sonocrystallization on the habit and structure of gemfibrozil crystals. *Chem. Eng. Technol.* 33 (5): 827–832.

55 Zeiger, B.W. and Suslick, K.S. (2011). Sonofragmentation of molecular crystals. *J. Am. Chem. Soc.* 133 (37): 14530–14533.

56 Sander, J.R.G., Zeiger, B.W., and Suslick, K.S. (2014). Sonocrystallization and sonofragmentation. *Ultrason. Sonochem.* 21 (6): 1908–1915.

57 Gao, J.X., Huang, H.Q., Li, X.X. et al. (2015). Breakage and particle size redistribution in an ultrasound-intensified leaching process. *Chem. Eng. Technol.* 38 (9): 1665–1670.

58 Raman, V. and Abbas, A. (2008). Experimental investigations on ultrasound mediated particle breakage. *Ultrason. Sonochem.* 15 (1): 55–64.

59 Bari, A.H. and Pandit, A.B. (2014). Ultrasound-facilitated particle breakage: estimation of kinetic parameters using population balance modelling. *Can. J. Chem. Eng.* 92 (12): 2046–2052.

60 Xiouras, C., Fytopoulos, A.A., Ter Horst, J.H. et al. (2018). Particle breakage kinetics and mechanisms in attrition-enhanced deracemization. *Cryst. Growth Des.* 18 (5): 3051–3061.

61 Kim, H.N. and Suslick, K.S. (2017). Sonofragmentation of ionic crystals. *Chem - A Eur. J.* 23 (12): 2778–2782.

62 Ivanov, A.N. (2012). Ultrasonic dispersion of Al–AlN and Al_2O_3 nanopowder agglomerates and of nanostructured AlOOH particles. *Russ. Phys. J.* 54 (12): 1413–1417.

63 Kudryashova, O. and Vorozhtsov, S. (2016). On the mechanism of ultrasound-driven deagglomeration of nanoparticle agglomerates in aluminum melt. *JOM* 68 (5): 1307–1311.

64 Gielen, B., Jordens, J., Thomassen, L. et al. (2017). Agglomeration control during ultrasonic crystallization of an active pharmaceutical ingredient. *Crystals* 7 (2): 40.

65 Bai, C., Wang, C., Zheng, T., and Hu, Q. (2018). Growth of β-glycine crystals promoted by standing surface acoustic waves (SSAWs). *CrystEngComm* 20 (9): 1245–1251.

66 Louhi-Kultanen, M., Karjalainen, M., Rantanen, J. et al. (2006). Crystallization of glycine with ultrasound. *Int. J. Pharm.* 320 (1–2): 23–29.

67 Ike, Y. and Hirasawa, I. (2017). Polymorph control of *L* -ArgHCl on antisolvent crystallization by ultrasonic irradiation. *Chem. Eng. Technol.* 40 (7): 1318–1322.

68 Medina, D.D., Gedanken, A., and Mastai, Y. (2011). Chiral amplification in crystallization under ultrasound radiation. *Chem - A Eur. J.* 17 (40): 11139–11142.

69 Zhou, X., Wang, H., and Zeng, Q. (2017). Chiral separation of DL-glutamic acid by ultrasonic field. *CrystEngComm* 19 (5): 762–766.

70 Xiouras, C., Fytopoulos, A., Jordens, J. et al. (2018). Applications of ultrasound to chiral crystallization, resolution and deracemization. *Ultrason. Sonochem.* 43: 184–192.

71 Patruno, L.E., Dorao, C.A., Svendsen, H.F., and Jakobsen, H.A. (2009). Analysis of breakage kernels for population balance modelling. *Chem. Eng. Sci.* 64 (3): 501–508.

72 Kusters, K.A., Pratsinis, S.E., Thoma, S.G., and Smith, D.M. (1993). Ultrasonic fragmentation of agglomerate powders. *Chem. Eng. Sci.* 48 (24): 4119–4127.

73 Nalesso, S., Bussemaker, M.J., Sear, R.P. et al. (2019). A review on possible mechanisms of sonocrystallisation in solution. *Ultrason. Sonochem.* 57: 125–138.

74 de Castillo-Peinado, L., L.S. and Luque de Castro, M.D. (2016). The role of ultrasound in pharmaceutical production: sonocrystallization. *J. Pharm. Pharmacol.* 68: 1249–1267.

75 Breil, C., Abert Vian, M., Zemb, T. et al. (2017). "Bligh and Dyer" and Folch methods for solid--liquid--liquid extraction of lipids from microorganisms. Comprehension of solvatation mechanisms and towards substitution with alternative solvents. *Int. J. Mol. Sci.* 18 (4): 708.

76 Rodrigues, S. and FAN, F. (2017). Extraction processes assisted by ultrasound. In: *Ultrasound: Advances in Food Processing and Preservation* (ed. D. Bermudez-Aguirre), 351–368. Elsevier.

77 Slabi, S.A., Mathé, C., Basselin, M. et al. (2020). Multi-objective optimization of solid/liquid extraction of total sunflower proteins from cold press meal. *Food Chem.* 317: 126423.

78 Xu, D., Shah, Z., Cui, Y. et al. (2018). Recovery of rare earths from nitric acid leach solutions of phosphate ores using solvent extraction with a new amide extractant (TODGA). *Hydrometallurgy* 180: 132–138.

79 Liang, Y., Pan, Z., Chen, Z. et al. (2020). Ultrasound-assisted natural deep eutectic solvents as separation-free extraction media for hydroxytyrosol from olives. *ChemistrySelect* 5 (35): 10939–10944.

80 Chemat, F., Rombaut, N., Sicaire, A.-G. et al. (2017). Ultrasound assisted extraction of food and natural products. Mechanisms, techniques, combinations, protocols and applications. A review. *Ultrason. Sonochem.* 34: 540–560.

81 Boukroufa, M., Boutekedjiret, C., Petigny, L. et al. (2015). Bio-refinery of orange peels waste: a new concept based on integrated green and solvent free extraction processes using ultrasound and microwave techniques to obtain essential oil, polyphenols and pectin. *Ultrason. Sonochem.* 24: 72–79.

82 Singh, M., Kumar, A., Singh, R., and Pandey, K.D. (2017). Endophytic bacteria: a new source of bioactive compounds. *3 Biotech.* 7 (5): 1–14.

83 Zhang, Z., Poojary, M.M., Choudhary, A. et al. (2018). Comparison of selected clean and green extraction technologies for biomolecules from apple pomace. *Electrophoresis* 39 (15): 1934–1945.

84 Nowacka, M., Tylewicz, U., Laghi, L. et al. (2014). Effect of ultrasound treatment on the water state in kiwifruit during osmotic dehydration. *Food Chem.* 144: 18–25. https://www.sciencedirect.com/science/article/pii/S0308814613007358.

85 Ojha, K.S., Aznar, R., O'Donnell, C., and Tiwari, B.K. (2020). Ultrasound technology for the extraction of biologically active molecules from plant, animal and marine sources. *TrAC Trends Anal. Chem.* 122: 115663.

86 Montero-Calderon, A., Cortes, C., Zulueta, A. et al. (2019). Green solvents and ultrasound-assisted extraction of bioactive orange (citrus sinensis) peel compounds. *Sci. Rep.* 9 (1): 1–8.

87 Bimakr, M., Ganjloo, A., Zarringhalami, S., and Ansarian, E. (2017). Ultrasound-assisted extraction of bioactive compounds from Malva sylvestris leaves and its comparison with agitated bed extraction technique. *Food Sci. Biotechnol.* 26 (6): 1481–1490.

88 Ghitescu, R.-E., Volf, I., Carausu, C. et al. (2015). Optimization of ultrasound-assisted extraction of polyphenols from spruce wood bark. *Ultrason. Sonochem.* 22: 535–541.

89 Khan, M.K., Abert-Vian, M., Fabiano-Tixier, A.-S. et al. (2010). Ultrasound-assisted extraction of polyphenols (flavanone glycosides) from orange (Citrus sinensis L.) peel. *Food Chem.* 119 (2): 851–858.

90 Sorourian, R., Khajehrahimi, A.E., Tadayoni, M. et al. (2020). Ultrasound-assisted extraction of polysaccharides from Typha domingensis: structural characterization and functional properties. *Int. J. Biol. Macromol.* 160: 758–768.

91 Hasheminya, S.-M. and Dehghannya, J. (2020). Novel ultrasound-assisted extraction of kefiran biomaterial, a prebiotic exopolysaccharide, and investigation of its physicochemical, antioxidant and antimicrobial properties. *Mater. Chem. Phys.* 243: 122645.

92 Savic Gajic, I.M., Savic, I.M., Gajic, D.G., and Dosic, A. (2021). Ultrasound-assisted extraction of carotenoids from orange peel using olive oil and its encapsulation in ca-alginate beads. *Biomol. Ther.* 11 (2): 225.

93 Zou, Y., Wang, L., Cai, P. et al. (2017). Effect of ultrasound assisted extraction on the physicochemical and functional properties of collagen from soft-shelled turtle calipash. *Int. J. Biol. Macromol.* 105: 1602–1610.

94 Heleno, S.A., Diz, P., Prieto, M.A. et al. (2016). Optimization of ultrasound-assisted extraction to obtain mycosterols from Agaricus bisporus L. by response surface methodology and comparison with conventional Soxhlet extraction. *Food Chem.* 197: 1054–10563.

95 Ferarsa, S., Zhang, W., Moulai-Mostefa, N. et al. (2018). Recovery of anthocyanins and other phenolic compounds from purple eggplant peels and pulps using ultrasonic-assisted extraction. *Food Bioprod. Process.* 109: 19–28.

96 Kobayashi, T., Kobayashi, T., Hosaka, Y., and Fujii, N. (2003). Ultrasound-enhanced membrane-cleaning processes applied water treatments: influence of sonic frequency on filtration treatments. *Ultrasonics* 41 (3): 185–190.

97 Naddeo, V., Borea, L., and Belgiorno, V. (2015). Sonochemical control of fouling formation in membrane ultrafiltration of wastewater: effect of ultrasonic frequency. *J. Water Process Eng.* 8: e92–e97.

98 Crum, L.A. (1995). Comments on the evolving field of sonochemistry by a cavitation physicist. *Ultrason. Sonochem.* 2 (2): S147–S152.

99 Wang, J., Gao, X., Xu, Y. et al. (2016). Ultrasonic-assisted acid cleaning of nanofiltration membranes fouled by inorganic scales in arsenic-rich brackish water. *Desalination* 377: 172–177.

100 Muthukumaran, S., Kentish, S., Ashokkumar, M., and STEVENS, G. (2005). Mechanisms for the ultrasonic enhancement of dairy whey ultrafiltration. *J. Membr. Sci.* 258 (1–2): 106–114.

101 Tarleton, E.S. and Wakeman, R.J. (1992). Electro-acoustic crossflow microfiltration. *Filtr. Sep.* 29 (5): 425–432.

102 Kobayashi, T., Chai, X., and Fujii, N. (1999). Ultrasound enhanced cross-flow membrane filtration. *Sep. Purif. Technol.* 17 (1): 31–40.

103 Lamminen, M., Walker, H.W., and Weavers, L.K. (2004). Mechanisms and factors influencing the ultrasonic cleaning of particle-fouled ceramic membranes. *J. Membr. Sci.* 237 (1–2): 213–223.

104 Kyllönen, H., Pirkonen, P., Nyström, M. et al. (2006). Experimental aspects of ultrasonically enhanced cross-flow membrane filtration of industrial wastewater. *Ultrason. Sonochem.* 13 (4): 295–302.

105 Luján-Facundo, M.J., Mendoza-Roca, J.A., Cuartas-Uribe, B., and Álvarez-Blanco, S. (2013). Ultrasonic cleaning of ultrafiltration membranes fouled with BSA solution. *Sep. Purif. Technol.* 120: 275–281.

106 Gonzalez-Avila, S.R., Prabowo, F., Kumar, A., and Ohl, C.-D. (2012). Improved ultrasonic cleaning of membranes with tandem frequency excitation. *J. Membr. Sci.* 415–416: 776–783.

107 Maskooki, A., Shahraki, M.H., and Mohamadi, M. (2016). Effects of various frequencies and powers of ultrasound on cleaning of flat sheet membrane during and after microfiltration. *Desalin. Water Treat.* 57 (12): 5376–5384.

108 Hou, D., Dai, G., Fan, H. et al. (2015). An ultrasonic assisted direct contact membrane distillation hybrid process for desalination. *J. Membr. Sci.* 476: 59–67.

109 Ruiz, L.M., Perez, J.I., Gómez, A. et al. (2017). Ultrasonic irradiation for ultrafiltration membrane cleaning in MBR systems: operational conditions and consequences. *Water Sci. Technol.* 75 (4): 802–812.

110 Zhang, R., Ning, D., Qiu, L. et al. (2016). The research of procyanidins extracting and membrane concentration efficiency based on ultrasonic -assisted filtration. *Open Biotechnol. J.* 10 (1): 239–247.

111 Matsumoto, Y., Miwa, T., Nakao, S., and Kimura, S. (1996). Improvement of membrane permeation performance by ultrasonic microfiltration. *J. Chem. Eng. Japan* 29 (4): 561–567.

112 Simon, A., Penpenic, L., Gondrexon, N. et al. (2000). A comparative study between classical stirred and ultrasonically-assisted dead-end ultrafiltration. *Ultrason. Sonochem.* 7 (4): 183–186.

113 Juang, R.-S. and Lin, K.-H. (2004). Flux recovery in the ultrafiltration of suspended solutions with ultrasound. *J. Membr. Sci.* 243 (1–2): 115–124.

114 Muthukumaran, S., Kentish, S., Lalchandani, S. et al. (2005). The optimisation of ultrasonic cleaning procedures for dairy fouled ultrafiltration membranes. *Ultrason. Sonochem.* 12 (1–2): 29–35.

115 Wang, X., Li, X., Fu, X. et al. (2005). Effect of ultrasound irradiation on polymeric microfiltration membranes. *Desalination* 175 (2): 187–196.

116 Agi, A., Junin, R., Yahya, A. et al. (2018). Comparative study of continuous and intermittent ultrasonic ultrafiltration membrane for treatment of synthetic produced water containing emulsion. *Chem. Eng. Process. Process Intensif.* 132: 137–147.

117 Chen, D., Weavers, L.K., and Walker, H.W. (2006). Ultrasonic control of ceramic membrane fouling by particles: effect of ultrasonic factors. *Ultrason. Sonochem.* 13 (5): 379–387.

118 Henglein, A. and Gutierrez, M. (1993). Sonochemistry and sonoluminescence: effects of external pressure. *J. Phys. Chem.* 97 (1): 158–162.

119 Chendke, P.K. and Fogler, H.S. (1983). Sonoluminescence and sonochemical reactions of aqueous carbon tetrachloride solutions. *J. Phys. Chem.* 87 (8): 1362–1369.

120 Lorimer, J.P. and Mason, T.J. (1987). Sonochemistry. Part 1—the physical aspects. *Chem. Soc. Rev.* 16: 239–274.

121 Roy, R.A. (1999). Cavitation sonophysics. In: *Sonochemistry and Sonoluminescence* (eds. L.A. Crum, T.J. Mason, J.L. Reisse and K.S. Suslick), 25–38. Dordrecht: Springer Netherlands.

122 Jönsson, A.-S. and Jönsson, B. (1996). Ultrafiltration of colloidal dispersions—a theoretical model of the concentration polarization phenomena. *J. Colloid Interface Sci.* 180 (2): 504–518.

123 Zhu, X. and Elimelech, M. (1995). Fouling of reverse osmosis membranes by aluminum oxide colloids. *J. Environ. Eng.* 121 (12): 884–892.

124 Ahmad, A.L., Che Lah, N.F., Ismail, S., and Ooi, B.S. (2012). Membrane antifouling methods and alternatives: ultrasound approach. *Sep. Purif. Rev.* 41 (4): 318–346.

125 Alventosa-deLara, E., Barredo-Damas, S., Alcaina-Miranda, M.I., and Iborra-Clar, M.I. (2014). Study and optimization of the ultrasound-enhanced cleaning of an ultrafiltration ceramic membrane through a combined experimental–statistical approach. *Ultrason. Sonochem.* 21 (3): 1222–1234.

126 Kyllönen, H.M., Pirkonen, P., and Nyström, M. (2005). Membrane filtration enhanced by ultrasound: a review. *Desalination* 181 (1–3): 319–335.

127 Zhu, C. and Liu, G. (2000). Modeling of ultrasonic enhancement on membrane distillation. *J. Membr. Sci.* 176 (1): 31–41.

128 Muthukumaran, S., Kentish, S.E., Stevens, G.W., and Ashokkumar, M. (2006). Application of ultrasound in membrane separation processes: a review. *Rev. Chem. Eng.* 22 (3): 155–194. https://doi.org/10.1515/REVCE.2006.22.3.155.

129 Li, J., Sanderson, R.D., and Jacobs, E.P. (2002). Ultrasonic cleaning of nylon microfiltration membranes fouled by Kraft paper mill effluent. *J. Membr. Sci.* 205 (1–2): 247–257.

130 Chai, X., Kobayashi, T., and Fujii, N. (1999). Ultrasound-associated cleaning of polymeric membranes for water treatment. *Sep. Purif. Technol.* 15 (2): 139–146.

131 Simon, A., Gonderxon, N., Taha, S. et al. (2000). Low-frequency ultrasound to improve dead-end ultrafiltration performance. *Sep. Sci. Technol.* 35 (16): 2619–2637.

132 Lamminen, M.O., Walker, H.W., and Weavers, L.K. (2006). Cleaning of particle-fouled membranes during cross-flow filtration using an embedded ultrasonic transducer system. *J. Membr. Sci.* 283 (1–2): 225–232.

133 Naddeo, V., Belgiorno, V., Borea, L. et al. (2015). Control of fouling formation in membrane ultrafiltration by ultrasound irradiation. *Environ. Technol.* 36 (10): 1299–1307.

134 Aghapour Aktij, S., Taghipour, A., Rahimpour, A. et al. (2020). A critical review on ultrasonic-assisted fouling control and cleaning of fouled membranes. *Ultrasonics* 108: 106228.

135 Saad, M.A., Kamil, M., Abdurahman, N.H. et al. (2019). An overview of recent advances in state-of-the-art techniques in the demulsification of crude oil emulsions. *Processes* 7 (7): 470.

136 Raya, S.A., Saaid, I.M., Ahmed, A.A., and Umar, A.A. (2020). A critical review of development and demulsification mechanisms of crude oil emulsion in the petroleum industry. *J. Pet. Explor. Prod. Technol.* 10 (4): 1711–1728.

137 Wang, Z., Wang, Y., and Liu, G. (2016). Rapid and efficient separation of oil from oil-in-water emulsions using a Janus cotton fabric. *Angew. Chem.* 128 (4): 1313–1316.

138 Bauer, W.-A.C., Fischlechner, M., Abell, C., and Huck, W.T.S. (2010). Hydrophilic PDMS microchannels for high-throughput formation of oil-in-water microdroplets and water-in-oil-in-water double emulsions. *Lab Chip* 10 (14): 1814–1819.

139 Check, G.R. and Mowla, D. (2013). Theoretical and experimental investigation of desalting and dehydration of crude oil by assistance of ultrasonic irradiation. *Ultrason. Sonochem.* 20 (1): 378–385.

140 Check, G.R. (2014). Two-stage ultrasonic irradiation for dehydration and desalting of crude oil: a novel method. *Chem. Eng. Process. Process Intensif.* 81: 72–78.

141 Antes, F.G., Diehl, L.O., Pereira, J.S.F. et al. (2015). Feasibility of low frequency ultrasound for water removal from crude oil emulsions. *Ultrason. Sonochem.* 25: 70–75.

142 Antes, F.G., Diehl, L.O., Pereira, J.S.F. et al. (2017). Effect of ultrasonic frequency on separation of water from heavy crude oil emulsion using ultrasonic baths. *Ultrason. Sonochem.* 35: 541–546.

143 Pedrotti, M.F., Enders, M.S.P., Pereira, L.S.F. et al. (2018). Intensification of ultrasonic-assisted crude oil demulsification based on acoustic field distribution data. *Ultrason. Sonochem.* 40: 53–59.

144 Zhang, J., Li, J., Thring, R.W. et al. (2012). Oil recovery from refinery oily sludge via ultrasound and freeze/thaw. *J. Hazard. Mater.* 203: 195–203.

145 Khajehesamedini, A., Sadatshojaie, A., Parvasi, P. et al. (2018). Experimental and theoretical study of crude oil pretreatment using low-frequency ultrasonic waves. *Ultrason. Sonochem.* 48: 383–395.

146 Xie, W., Li, R., and Lu, X. (2015). Pulsed ultrasound assisted dehydration of waste oil. *Ultrason. Sonochem.* 26: 136–141.

147 Wang, Z., Gu, S., and Zhou, L. (2018). Research on the static experiment of super heavy crude oil demulsification and dehydration using ultrasonic wave and audible sound wave at high temperatures. *Ultrason. Sonochem.* 40: 1014–1020.

148 Breitbach, M., Bathen, D., and Schmidt-Traub, H. (2003). Effect of ultrasound on adsorption and desorption processes. *Ind. Eng. Chem. Res.* 42 (22): 5635–5646.

149 Breitbach, M. and Bathen, D. (2001). Influence of ultrasound on adsorption processes. *Ultrason. Sonochem.* 8 (3): 277–283.

150 Tao, Y., Wu, Y., Han, Y. et al. (2020). Insight into mass transfer during ultrasound-enhanced adsorption/desorption of blueberry anthocyanins on macroporous resins by numerical simulation considering ultrasonic influence on resin properties. *Chem. Eng. J.* 380: 122530.

151 Zhang, T., Yang, Y., Li, X. et al. (2021). Adsorption characteristics of chloramphenicol onto powdered activated carbon and its desorption performance by ultrasound. *Environ. Technol.* 42 (4): 571–583.

152 Hamdaoui, O., Djeribi, R., and Naffrechoux, E. (2005). Desorption of metal ions from activated carbon in the presence of ultrasound. *Ind. Eng. Chem. Res.* 44 (13): 4737–4744.
153 Ingle, P.K., Attarkar, K., and Rathod, V.K. (2019). Ultrasound assisted chemical activation of peanut husk for copper removal. *Green Process Synth.* 8 (1): 46–53.
154 Yu, Q., Fan, L., and Li, J. (2020). A novel process for asparagus polyphenols utilization by ultrasound assisted adsorption and desorption using resins. *Ultrason. Sonochem.* 63: 104920.
155 Daghooghi-Mobarakeh, H., Campbell, N., Bertrand, W.K. et al. (2020). Ultrasound-assisted regeneration of zeolite/water adsorption pair. *Ultrason. Sonochem.* 64: 105042.
156 Mahdi, T., Ahmad, A., Nasef, M.M., and Ripin, A. (2015). State-of-the-art technologies for separation of azeotropic mixtures. *Sep. Purif. Rev.* 44 (4): 308–330.
157 Alkhudhiri, A., Darwish, N., and Hilal, N. (2012). Membrane distillation: a comprehensive review. *Desalination* 287: 2–18.
158 Liang, S., Cao, Y., Liu, X. et al. (2017). Insight into pressure-swing distillation from azeotropic phenomenon to dynamic control. *Chem. Eng. Res. Des.* 117: 318–335.
159 Ashokkumar, M. and Mason, T.J. (2000). Sonochemistry. In: *Encyclopedia of Chemical Technology* (eds. R.E. Kirk and D.F. Othmer), 1–34. Wiley https://doi.org/10.1002/0471238961.1915141519211912.a01.pub2.
160 Louisnard, O. and González-Garcia, J. (2011). Acoustic cavitation. In: *Ultrasound Technologies for Food and Bioprocessing* (eds. H. Feng, G.V. Barbosa-Cánovas and J. Weiss), 13–64. Springer.
161 Suzuki, K., Arashi, K., and Nii, S. (2012). Determination of droplet and vapor ratio of ultrasonically-atomized aqueous ethanol solution. *J. Chem. Eng. Japan* 45 (5): 337–342.
162 Mahdi, T., Ahmad, A., Ripin, A., and Nasef, M.M. (2015). Separation of azeotropic mixture using multi-stage ultrasound-assisted flash distillation. *Chem. Prod. Process. Model.* 10 (4): 237–242.
163 Anschuetz, F., Franke, M., Braeutigam, P., and Ondruschka, B. (2012). The separation of azeotropic mixtures by ultrasound-assisted distillation.
164 Mahdi, T. and Al-Kawaz, A.E. (2018). A simulation study of enhanced distillation using ultrasound waves for the separation of azeotropic mixtures. *Am. J. Eng. Appl. Sci.* 11 (1): 97–107.
165 Fuchs FJ. Ultrasonic cleaning and washing of surfaces. In: Juan Gallego-Juarez Power Ultrasonics. Elsevier; 2015. p. 577–609.
166 Nagarajan, R. (1997). Survey of cleaning and cleanliness measurement in disk drive manufacture. *Precis Clean.* 13–22. https://p2infohouse.org/ref/01/00930.pdf (accessed 15 June 2021).
167 Nagarajan, R. (2006). Use of ultrasonic cavitation in surface cleaning: a mathematical model to relate cleaning efficiency and surface erosion rate. *J. IEST* 49 (2): 40–50.
168 Yao, Y., Pan, Y., and Liu, S. (2020). Power ultrasound and its applications: a state-of-the-art review. *Ultrason. Sonochem.* 62: 104722.
169 Halbert, J. (1988). Surface cleaning: using ultrasonic techniques for wet process cleaning. *Microcontamination* 6: 36.
170 Awad, S.B. and Nagarajan, R. (2010). Ultrasonic cleaning. In: *Developments in Surface Contamination and Cleaning*, 225–280. Elsevier.

171 Ibisi, M. and Brown, B. (1967). Variation of the relative intensity of cavitation with temperature. *J. Acoust. Soc. Am.* 41 (3): 568–572.

172 Mason, T.J. (2016). Ultrasonic cleaning: an historical perspective. *Ultrason. Sonochem.* 29: 519–523.

173 Niemczewski, B. (1980). A comparison of ultrasonic cavitation intensity in liquids. *Ultrasonics* 18 (3): 107–110.

174 Cooksongold (2018). How to clean jewellery using elma ultrasonics. [cited 27 June 2021]. https://www.cooksongold.com/blog/learn/how-to-clean-jewellery-using-elma-ultrasonics/ (accessed 15 June 2021).

175 Ultrasonic Cleaner (2013). High performance digital household 50W ultrasonic cleaner for jewelries/glasses/watches/CDs w/750ml capacity. [cited 27 June 2021]. http://www.ankaka.com/high-performance-digital-household-50w-ultrasonic-cleaner-for-jewelriesglasseswatchescds-w750ml-capacity_p49289.html (accessed 15 June 2021).

176 Duran, F. and Teke, M. (2018). Design and implementation of an intelligent ultrasonic cleaning device. *Intell. Autom. Soft Comput.* 25 (3): 441–450.

177 Smartclean (2018). Smartclean Vision.5: a portable ultrasonic cleaner. [cited 27 June 2021]. https://www.medgadget.com/2018/05/smartclean-vision-5-a-portable-ultrasonic-cleaner.html (accessed 15 June 2021).

5

The Role of Chemical Looping in Industrial Gas Separation

Vedant Shah, Kalyani Jangam, Anuj Joshi, Pinak Mohapatra, Eric Falascino, and Liang-Shih Fan

William G. Lowrie Department of Chemical and Biomolecular Engineering, The Ohio State University, Columbus, OH, USA

5.1 Introduction

5.1.1 Relevance of Separation to Chemical Industry

The origin of the chemical industry can be traced back to the start of the industrial revolution in the late eighteenth century [1]. Extensive research and innovation coupled with factors such as consumer demand, industrial consolidation, and globalization have led to an exponential growth of the chemical industry over the years. In 2017, the net sale from the chemical industry in the United States exceeded $765 billion and is projected to further increase [2]. Production of chemicals such as methanol, ammonia, and other high-value petrochemicals provides the impetus for the growth of the chemical industry. As seen from Figure 5.1, in 2018, the chemical industry comprising the industries producing bulk chemicals, the refining sector, and the mining industry accounted for about 58% of the total energy consumed by the industrial sector [3]. A large amount of the energy consumed by the chemical industry is used for carrying out separation processes. For example, distillation, a commonly used separation process in the chemical industry consumed roughly 15% of the total energy consumption in the United States as per a report published by Oak Ridge National Laboratory [4]. A common problem that has been persistent in the chemical industry is the separation of different constituents from product streams to separate the desirable component from byproducts.

This is because a chemical reaction always encounters issues due to incomplete reactant conversion and occurrence of parallel reactions leading to the formation of undesirable products and other thermodynamic constraints arising from the operating parameters that inhibit the product yield. As a result, separation processes are heavily used by chemical industries to separate unwanted components from product streams. Some of the commonly used separation techniques include distillation, absorption, adsorption, and membrane separation. Efficiently designed separation processes allow an improvement in

Sustainable Separation Engineering: Materials, Techniques and Process Development, Volume 1, First Edition. Edited by Gyorgy Szekely and Dan Zhao.
© 2022 John Wiley & Sons Ltd. Published 2022 by John Wiley & Sons Ltd.

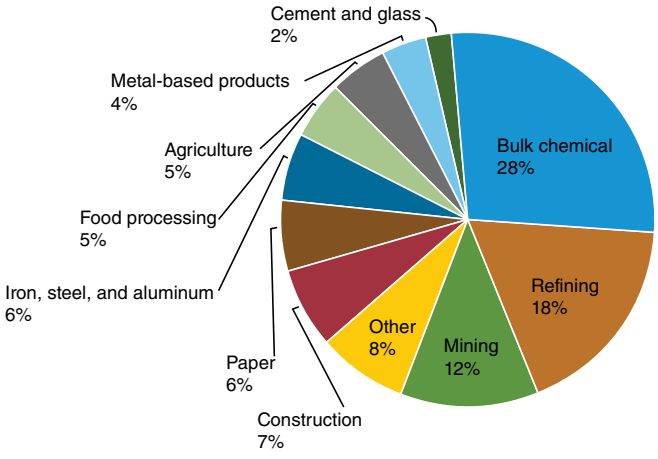

Figure 5.1 Sector-wise industrial energy consumption in the United States in 2018.

the overall economics of a plant by reducing the energy and material input requirement [5]. As environmental regulations become more stringent, the separation processes can be leveraged for the selective removal of unwanted components from the product streams. This selective removal allows careful storage and disposal which otherwise would not have been possible. Two problems have been identified with the conventional separation systems – low separation efficiency and an increased operational cost [5]. Efforts are being made to address these issues while opening new avenues to develop more sustainable and efficient separation processes. Although single-phase and multiphase separations are both used in the industry, the separation of components from a gas mixture is exclusively presented in this chapter.

This chapter solely focuses on the use of chemical looping-assisted gas separation techniques, where chemical looping can be employed to carry out either in situ separation of gases or reactive separation through gas–solid reactions. The advantages of utilizing chemical looping for industrial gas separation manifest in the form of high efficiency, operational simplicity, and relatively low cost of operation as opposed to the conventional processes. A detailed description of the chemical looping process along with various milestones achieved by the technology over the years since its inception has been briefly described. As CO_2 capture has gained immense interest in both academia as well as the industry, the use of redox looping and calcium looping schemes has been elaborately discussed here. Various aspects of these technologies including the selection of looping media, reactor design, and reaction schemes have been extensively described in this chapter. Apart from this, the role of chemical looping in separating N_2 and O_2 from the air using a highly specialized class of metal oxides is discussed in detail. The criteria for the selection of these metal oxides along with the underlying thermodynamics and selection of operating conditions to maximize the product yield has also been reported. The use of chemical looping technology for air separation provides a viable alternative to the conventionally used cryogenic separation. Similarly, a discussion on the metal sulfide-based chemical looping process for selective H_2S separation is presented in this chapter. The chemical looping approach allows conversion of H_2S into H_2 and elemental sulfur, where both the commercially

desired products are obtained through different streams. Lastly, various challenges faced by the chemical looping technology have been discussed while proposing new ways of process intensification to make the prospect of gas separation using chemical looping more economically attractive and sustainable in the long run.

5.1.2 Introduction to Chemical Looping

Out of the 4.12 trillion kWh of electricity generated in the United States in 2019, 63% was generated using fossil fuels comprising coal and natural gas [6]. The processing of fossil fuels is responsible for the generation of pollutants that take a severe toll on human health as well as the environment. Several strategies have been devised for tackling these pollutants comprising oxides of nitrogen, sulfur, and carbon, mercury, ash, fine particulates, etc. Amongst all these, CO_2 capture has gained prime importance due to its unprecedented release into the earth's atmosphere [7]. CO_2 is a known greenhouse gas and contributes significantly toward global warming [8]. Strategies for controlling CO_2 emissions from power plants are being developed to produce electricity at the expense of minimum environmental damage. Carbon capture, utilization, and storage (CCUS) strategies are being implemented for CO_2 removal from flue gas streams and direct-air CO_2 capture [9, 10]. As the cost of CO_2 capture is significantly higher than that of transportation and storage, developing a cost-effective CO_2 capture technology is the key to achieving affordable emission control [11]. Various technologies developed for CO_2 capture can be categorized as post-combustion, precombustion, and oxy-combustion capture [12]. In post-combustion capture, CO_2 is separated from the flue gas stream by means of separation processes such as amine-based separation, membrane separation, etc. In precombustion capture, carbon-derivatives such as CO and CO_2 are completely removed while converting fossil fuel into hydrogen (clean-burning fuel) through a combination of gasification/reforming and water–gas shift (WGS) reactions. In oxy-combustion capture, pure O_2 stream obtained using cryogenic distillation of air is used for combusting fossil fuel. The advantages and limitations pertaining to the three approaches are described in Table 5.1. Based on the merits and limitations of several carbon capture technologies, the United States Department of Energy (US DOE) estimated the amount of time required for technology commercialization and the cost-reduction benefit achieved through its implementation as shown in Figure 5.2. It lists various technologies that are currently being developed for decarbonization of various processes through CO_2 capture, where the listing of these technologies is based on the amount of time required for their commercial implementation. Technologies such as amine-based CO_2 separation and cryogenic distillation of air to obtain O_2 for oxy-combustion have been actively used in the industry for a long time, and hence do not require any major upgrade for their deployment on a large scale in the industry. On the other hand, processes such as chemical looping, biological separation, and membrane separation are relatively new, thereby needing more time for commercialization as they need to be tested extensively at various scales to ensure economically and environmentally sustainable CO_2 capture. As seen from Figure 5.2, chemical looping is at the forefront of CO_2 capture strategies. Although chemical looping has been anticipated to have a long wait time before it can be practiced in the industry, it is projected to be the most economical option for CO_2 separation due to its operational simplicity, high capture efficiency, and low parasitic energy demands.

Table 5.1 Advantages and limitations of the three carbon capture approaches.

Approach	Advantages	Limitations
Post-combustion capture	• Can be retrofitted • Compatible with existing plants	• Low per-pass capture efficiency • CO_2 captured at low pressure
Precombustion capture	• CO_2 capture at high pressure possible	• Capital-intensive • Requires extensive auxiliary support
Oxy-combustion capture	• Retrofit-compatible • Concentrated CO_2 stream in flue gas	• Capital-intensive due to cryogenic air separation requirement • Low process efficiency

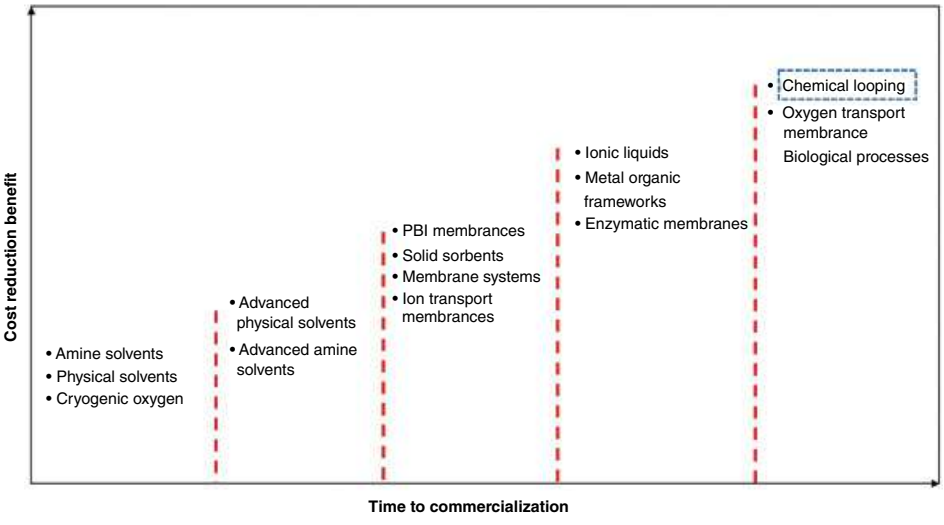

Figure 5.2 Cost-effectiveness and preparedness of the different CO_2 capture technologies.

The term "chemical looping" can be used to describe a process in which one fundamental chemical reaction is broken into multiple sub-reactions by using a chemical intermediate that undergoes reaction and regeneration cyclically [13]. Although the term "chemical looping" was first used by Ishida et al. in 1987 to describe such a process, the concept has been in use for more than 100 years [14]. Table 5.2 describes various chemical looping processes developed since the early twentieth century until recently. Chemical looping gained importance over the years due to the requirement of an efficient process for converting the abundantly available fossil fuels into value-added products while preventing CO_2 emission into the atmosphere [15]. Although initially developed with this objective, many more novel applications have been developed since as reported in subsequent sections. A chemical looping system possesses three prime benefits as compared to other technologies: (i) As a

Table 5.2 Major developments in chemical looping technology.

Processes/Developers	First reported	Looping media	Reactor design	References
Lane process and Messerschmitt process	1910s	Fe_3O_4-FeO-Fe	Fixed bed	[17, 18]
Lewis and Gilliland process	1950s	CuO-Cu_2O	Fluidized bed	[19, 20]
IGT HYGAS process	1970s	Fe_3O_4-FeO	Staged fluidized bed	[16, 21]
CO_2 acceptor process	1970s	CaO-$CaCO_3$	Fluidized bed	[22]
Atlantic Richfield Company	1980s	Mn oxides	Fluidized bed	[23, 24]
DuPont: Butane to maleic anhydride	1990s	VPO	Circulating fluidized bed	[25, 26]
Chalmers University of Technology	2000s	Ni, Fe, Mn, and Cu oxides	Circulating fluidized bed	[27]
The Ohio State University (H_2 generation)	2000s	Fe_2O-Fe_3O_4-FeO-Fe	Moving bed	[28]
Darmstadt University	2010	$FeTiO_3/Fe_2O_3$	Circulating fluidized bed	[29]
The Ohio State University (CO_2 capture)	2016	Fe_2O-Fe_3O_4-FeO-Fe	Moving bed	[30]

single reaction is split into multiple reactions occurring independently, the energy loss arising from irreversibility of the process is minimized, (ii) various products formed during the reaction are separated easily and efficiently, and (iii) the overall parasitic energy requirement of the process is reduced, thereby rendering it more efficient [16].

Figure 5.3 depicts a generic configuration of two types of chemical looping process schemes: one that involves the occurrence of multiple oxidation states of the looping medium (Redox looping) and the other one where the looping media does not undergo a

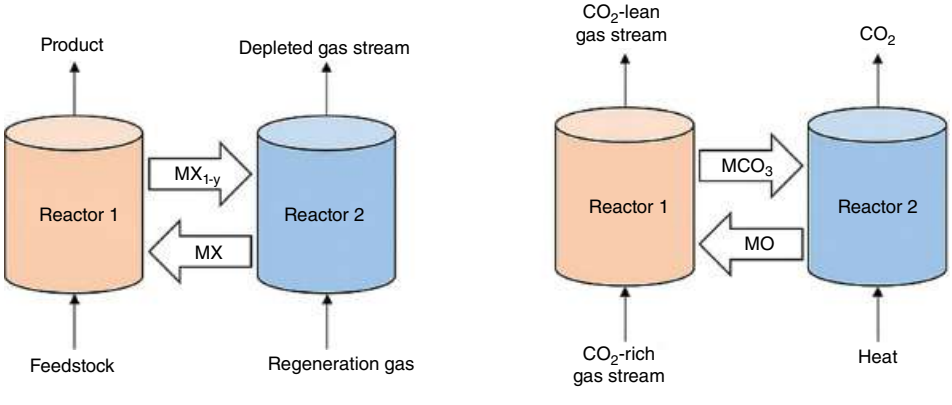

Figure 5.3 Generic configuration of (a) Redox chemical looping and (b) Calcium looping schemes for reactive/selective gas separation.

change in its oxidation state (Calcium looping). In a redox chemical looping scheme, the feed going into Reactor 1 reacts with the looping media and forms the reaction products, while the looping media undergoes change (lowering) in its oxidation state. Regeneration of the looping media is carried out in Reactor 2 using a suitable regenerating agent to complete the loop. The looping media in this type of scheme can be an oxide, sulfide, nitride, or carbide derivative of a metal whose existence across multiple oxidation states is governed thermodynamically. Few examples of redox chemical looping include syngas production, CO_2 capture from fossil fuel combustion, and hydrogen generation [14]. The calcium looping scheme is a unique process specifically developed for selective removal of CO_2 from flue gas streams. CO_2-rich entering Reactor R1 reacts with either a metal oxide of alkali or alkaline earth elements (predominantly CaO) and is converted into its corresponding carbonate phase, thus capturing CO_2 in the process. The metal carbonate is transported to another reactor (Reactor R2) where it is decomposed thermally to recover the metal oxide and remove pure, sequestration ready CO_2 [29]. Various chemical looping processes can be tailored by using different combinations of inlet feeds, looping media, and process configurations to carry out the gas separation in a sustainable and efficient manner as described in later sections.

5.1.3 Role of the Looping Media in Chemical Looping

The looping media used in a chemical looping system typically comprises metal oxide; however, the use of metal sulfides, nitrides, and carbides has also been explored [31]. Using the looping media as an elemental carrier in chemical looping systems allows the splitting of a single chemical reaction into multiple independent reactions. This imparts additional degrees of freedom to the system as parameters such as temperature, pressure, and feedstock flowrates can be independently controlled for a different set of reactions [32]. The looping media or elemental carriers (based on the transferrable element such as oxygen/sulfur/nitrogen), as commonly known, possess the unique ability to react with the feedstock in one reactor to form products, while undergoing regeneration in another reactor. In a chemical looping system, the elemental carriers serve a dual purpose – they provide the necessary active sites for feedstock conversion to products and they allow the transfer of heat across the reactors [33–35]. Thus, the elemental carrier can be tuned such that it provides superior thermodynamic performance for product generation and possesses optimum heat transfer capability. Based on the immense experience gained over the years, the following properties are deemed suitable for the looping media used in various chemical looping applications:

a) The looping media needs to possess a high element-carrying capacity. For example, a metal oxide can be selected such that the maximum amount of its lattice oxygen can contribute toward the chemical reaction [36, 37]. The element-carrying capacity of a metal-based carrier is defined as the total amount of elements that can be transferred during the reaction, thereby being subjected to solid conversion during the process.
b) As the carrier undergoes two sets of reactions – reduction and oxidation (with respect to the change in its oxidation state and electron transfer), it is expected that the carrier exhibits good kinetics for both the reactions to ensure maximum feed conversion and

high product yields [38, 39]. These materials for the carriers can be selected such that they aptly provide specific surface area and tolerance to sintering through appropriate material synthesis [40].

c) The selection of looping media can be conducted in accordance with the reactor configuration and gas–solid contact mode to ensure maximum gas and solid conversions during the process. The underlying thermodynamics and reaction kinetics need to be explored to achieve desirable results.
d) It is important that the looping media possesses long-term recyclability. In the long term, this helps reduce the amount of solids inventory that needs to be replenished during the process [40].
e) The looping media needs to possess a high mechanical strength as well as resistance to attrition and fragmentation over the course of operation. An increase in mechanical strength is often accompanied by a decrease in reaction rates. It is therefore important to optimize the composition of the elemental carrier such that it maintains its strength across extended cycles without compromising its reactivity.
f) As stated earlier, the looping media is responsible for heat transfer across the reactors and is expected to have a high heat capacity. Thus, the selection of the metal oxide ingredients is also important from the heat transfer point of view [41]. As chemical looping applications typically involve high temperature, the carriers need to have a high melting point while ensuring that it is significantly higher than the operating temperature.
g) The size of the looping media can be decided based on the reactor design and type employed. If used in a fluidized bed-type reactor, the particle size can be small to reduce the gas flow requirement. Similarly, if used in a packed bed or moving bed-type configuration, the particle size can be large enough to ensure minimization of pressure drop across the reactor [42].
h) Various types of feedstocks are used in a chemical looping system. To minimize the operational cost, the use of as-obtained feedstock is desirable. However, it may contain certain impurities with varying proportions that might react with the looping media and cause poisoning or disintegration of the carrier particle. Therefore, the selected elemental carrier needs to have a high degree of tolerance toward contaminants.
i) Careful and cost-effective disposal of the looping media while abiding by all the environmental regulations is important. The materials used for synthesizing the looping media need to be selected such that the preparation as well as disposal does not cause any harm to human health or the environment.

A chemical looping system can be designed to process different types of feedstocks and selection of the looping media is done accordingly. Figure 5.4 shows different configurations of the chemical looping systems reported in the literature. Figure 5.4a shows metal oxide-assisted chemical looping for full or partial oxidation of hydrocarbons like coal, biomass, natural gas, petroleum coke, and biogas [14, 16, 43]. This process can be used for electricity generation in power plants while ensuring almost complete carbon capture or it can be utilized for the generation of syngas, an extremely versatile industrial commodity. Figure 5.4b represents the thermochemical splitting of CO_2/H_2O wherein the metal oxide-based elemental carrier loses molecular oxygen at elevated temperatures and is regenerated

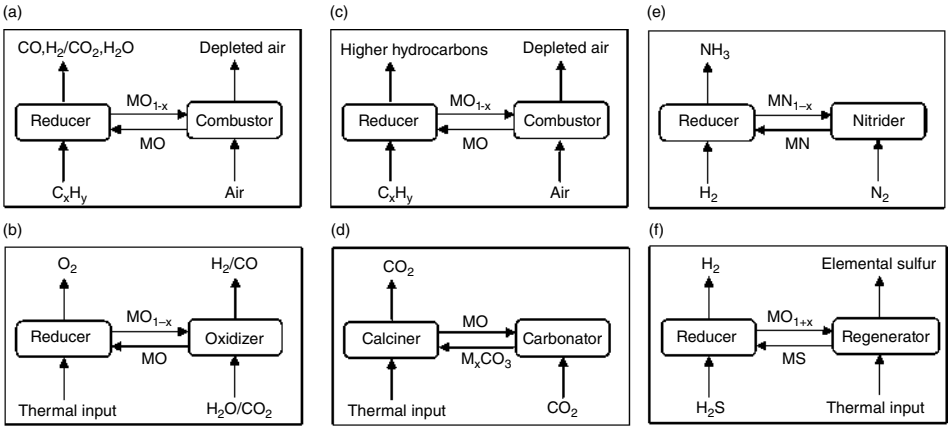

Figure 5.4 Different chemical looping schemes using varied looping media for inherent gas separation (a) full/partial oxidation of carbonaceous feedstock, (b) thermochemical water/CO_2 splitting with oxygen uncoupling, (c) higher hydrocarbon synthesis through oxidative coupling, (d) calcium looping for CO_2 capture, (e) ammonia synthesis, and (f) H_2S utilization for H_2 and sulfur recovery.

in either steam or CO_2 while producing H_2 or CO, respectively [44]. Selective oxidation of feedstocks like CH_4 to form higher hydrocarbons is shown in Figure 5.4c. This chemical looping configuration allows single-step upgradation of hydrocarbon feed to form >C2+ derivatives, for example, chemical looping oxidative coupling of methane [45]. Chemical looping for post-combustion CO_2 capture is depicted in Figure 5.4d, wherein the looping media oscillates between a metal oxide and carbonate phase [46]. Figure 5.4e and f show ammonia and hydrogen production using a metal nitride and a metal sulfide carrier, respectively [47, 48].

Although used conventionally for processing fossil fuels and the associated energy conversion, chemical looping systems can also be used for gas separation processes. Reactor configuration, gas–solid contact mode, operating temperature and pressure, and the looping media selection are critical parameters that decide the nature and type of gas separation. Separation of gases such as CO_2 and SO_2 from flue gas streams, O_2 and N_2 present in air, and selective removal of H_2S using chemical looping approach are some of the processes that are described in this chapter.

5.2 Case Studies

5.2.1 CO_2 Capture Using Redox Looping Scheme

5.2.1.1 Process Description

Achieving fossil energy conversion with CO_2 capture has provided the necessary driving force to find alternatives to the existing technologies. The major source of CO_2 emission are the fossil fuel-based power plants and other industrial units where fuel is burnt to produce process heat [3]. As air is typically used for combusting the fossil fuel to produce heat, the exiting flue gas stream is laden with the unconverted N_2 from the air along with CO_2, which

form the two major components of the gas stream. Other components such as NO_x, SO_x, CO, and H_2S are found in smaller amounts [49]. Conventionally, this flue gas stream was released directly into the atmosphere due to relaxed environmental laws and regulations. However, increased threats of climate change arising from the alarming CO_2 levels in the atmosphere led to restrictions on CO_2 emission. As a result, post-combustion CO_2 capture technologies were developed and retrofitted in power plants to selectively remove CO_2 from flue gas streams. Common CO_2 separation strategies involve the use of solvents/absorbents for carrying out chemical/physical absorption, low-temperature adsorption, separation membranes, metal-organic frameworks, ionic liquids, molecular filtration, and enzyme-based systems [12]. Out of all the available technologies, monoethanolamine (MEA)-based CO_2 absorption is used widespread commercially and Figure 5.5 shows the process flow diagram of the MEA scrubbing system designed for post-combustion CO_2 capture [16]. Despite extensive research in this area, deploying an MEA-based separation process remains highly capital-intensive, which is because of an exceptionally high energy requirement for the MEA solvent regeneration. This energy is provided by utilizing steam, which reduces the overall power output, and thereby reduces the power plant efficiency [50]. Chemical looping combustion (CLC) serves as an alternate technology wherein fossil fuels can be combusted fully with inherent CO_2 separation.

Figure 5.6a illustrates a schematic of the chemical looping combustion (CLC) process for in situ CO_2 separation. The aim of this technology is to provide a viable substitute for the existing power plants to produce electricity more efficiently in an environmentally benign way. In this process, hydrocarbon sources like natural gas, biomass, coal, biogas, and petroleum coke are allowed to undergo combustion using metal oxide-based oxygen carriers as opposed to molecular oxygen from air as practiced in a conventional combustion process. The CLC process utilizes two reactors – reducer (fuel reactor) and combustor (air reactor). The fuel entering the reducer reacts with the oxygen carriers at high temperature, which allows the transfer of lattice oxygen from the solids to the gas/solid reactant. This transfer enables the combustion of fuel to produce full combustion products (CO_2 and H_2O), while the oxygen carriers are reduced due to the loss of lattice oxygen as shown in Reaction 5.1.

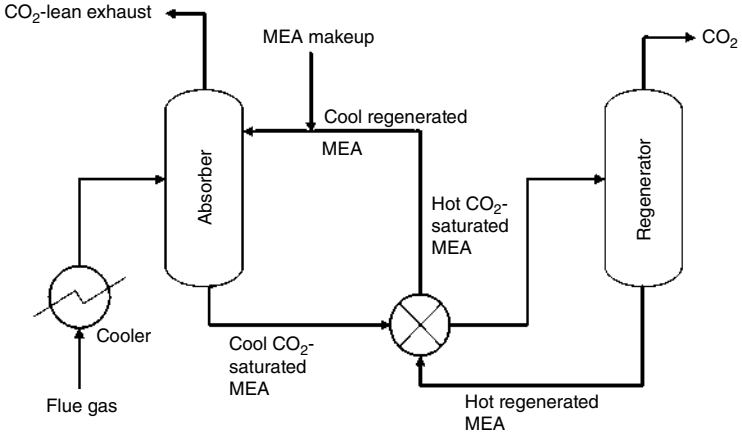

Figure 5.5 Post-combustion CO_2 capture using monoethanolamine (MEA)-based absorption.

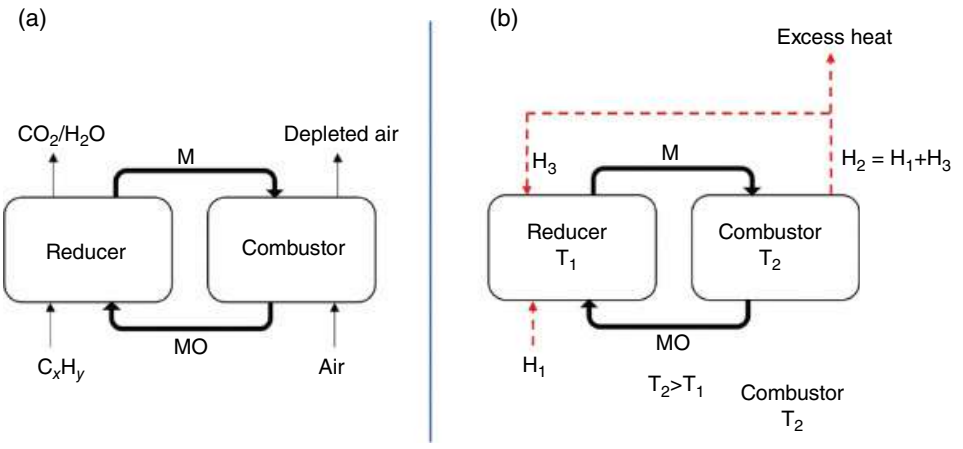

Figure 5.6 (a) Schematic representation of a CLC process and (b) heat integration in a CLC process for selective CO_2 separation.

An almost pure, sequestration-ready CO_2 stream is obtained at the reducer outlet through condensation of steam. The reduced oxygen carriers are transferred to the oxidizer where they are regenerated fully in the air as displayed in Reaction 5.2. As combustion of fuel and regeneration of the oxygen carriers is done in two separate reactors, no mixing between N_2 (from the air) and CO_2 takes place, thus allowing in situ separation. As a result, highly capital and energy-intensive downstream CO_2 separation can be avoided.

$$\left(2x+\frac{y}{2}\right)\mathrm{MO}+C_xH_y \rightarrow \left(2x+\frac{y}{2}\right)\mathrm{M}+x\mathrm{CO_2}+\frac{y}{2}\mathrm{H_2O} \tag{5.1}$$

$$\mathrm{M}+\frac{1}{2}\mathrm{O_2}+\mathrm{N_2} \rightarrow \mathrm{MO}+\mathrm{N_2} \tag{5.2}$$

Fuel conversion in the reducer can be either exothermic or endothermic depending on the type of metal oxide oxygen carrier used in the process, while the regeneration of the reduced oxygen carrier is highly exothermic. Based on the heat requirement of the process, heat integration can be carried out between the two reactors such that the net process is thermoneutral and excess heat can be used for converting water to steam for electricity generation. Figure 5.6b shows the generic heat integration scheme that can be employed in a CLC process. As seen from Figure 5.6b, the amount of heat generated from the combustor (operating at a higher temperature than the reducer) is in excess and some portion can be transferred to the reducer while the remaining can be used for power generation.

The CLC process offers an economic advantage over the conventional combustion process as it does not require an air separation unit (ASU) or energy-intensive downstream CO_2 separation. The capital cost can be further reduced by optimizing the reactor size such that maximum fuel conversion with high selectivity toward complete combustion can be achieved through faster reaction kinetics. As the reactions are thermodynamically governed, faster kinetics ensure that the equilibrium is reached quickly, thereby reducing the residence time requirement and subsequently reducing the reactor volume [51]. Thus, the selection of oxygen carrier, gas-solid contact pattern, and reactor configuration needs to be done carefully.

5.2.1.2 Oxygen Carrier Selection

The success of a CLC process depends on the performance of the oxygen carrier used. For a CLC process, oxygen carriers made using the oxides of transition metals such as Fe, Ni, Cu, Mn, and Co are typically employed [16] as the metal oxides of these elements have multiple oxidation states, wherein a phase with higher oxidation state can lose its lattice oxygen to form another phase with a lower oxidation state, thereby undergoing reduction. For example, Fe-oxide and Ni-oxide show a transition from $Fe_2O_3 \rightarrow Fe_3O_4 \rightarrow FeO \rightarrow Fe$ and $NiO \rightarrow Ni$, respectively. The oxidation-reduction potential of different metal oxides that can be used as oxygen carriers is studied using a modified Ellingham diagram, where the change in Gibbs free energy of the metal oxides is plotted against temperature and selection/screening of the oxygen carrier material can be done based on the region in which it lies on the plot. Metal oxides such as Fe_2O_3, NiO, CuO, CoO, and Fe_3O_4 are used for CLC applications due to their high oxidative potential. An interesting trait is observed where the metal oxides do not undergo a reduction in presence of a reducing agent and thus cannot be used as oxygen carriers. However, they can be mixed with the active metal oxide (redox capable) as an inert support. The addition of support has multiple benefits such as enhanced rates of ionic diffusion, higher tolerance toward sintering and better dispersion of the active material with increased active surface area [40, 52]. As the CLC process involves continuous reduction-oxidation of the oxygen carriers, the addition of support helps increase their integrity so that they can sustain long-term operations.

5.2.1.3 Reactor Design for CLC Processes

Along with oxygen carrier selection, the reactor design affects the performance of a CLC process. A fundamental understanding of gas–solid reaction engineering, multiphase flow hydrodynamics, and the intervening kinetic and thermodynamic interaction is needed to design and develop a chemical looping reactor. This is due to the occurrence of multiple reactions in two different reactors along with the continuous circulation of solids (oxygen carriers) across them. Optimization of each individual reactor needs to be done while maintaining an efficient performance of the overall system. As the primary objective of a CLC system is generating power with in situ CO_2 capture, the combustor is typically designed as a fluidized bed [51]. This type of design serves two objectives: regeneration of the reduced oxygen carrier and pneumatic conveying of the regenerated oxygen carriers to the reducer. As air is provided in stoichiometric excess, enough oxygen is made available to overcome the mass transfer limitations in a fluidized bed, thereby allowing rapid regeneration of the oxygen carriers. Designing the reducer is crucial to the success of a CLC system as complex kinetic and thermodynamic factors need to be taken into consideration. Two designs as shown in Figure 5.7 have been widely proposed for the reducer.

Design 1 represents a fluidized bed reactor, where it is typically operated in a bubbling or turbulent fluidization regime [53]. Most of the CLC processes use this type of design. With a combustor as a fluidized bed, the overall system represents an interconnected dual circulating fluidized bed (CFB). Important parameters that need to be considered while using this type of design include oxygen carrier reaction kinetics and physical properties such as particle size and density. As particles undergo continuous circulation, they need to be sufficiently attrition-resistant. Attrition needs to be minimized as the particle fines can agglomerate, which can eventually lead to defluidization of the bed. As both the reactors

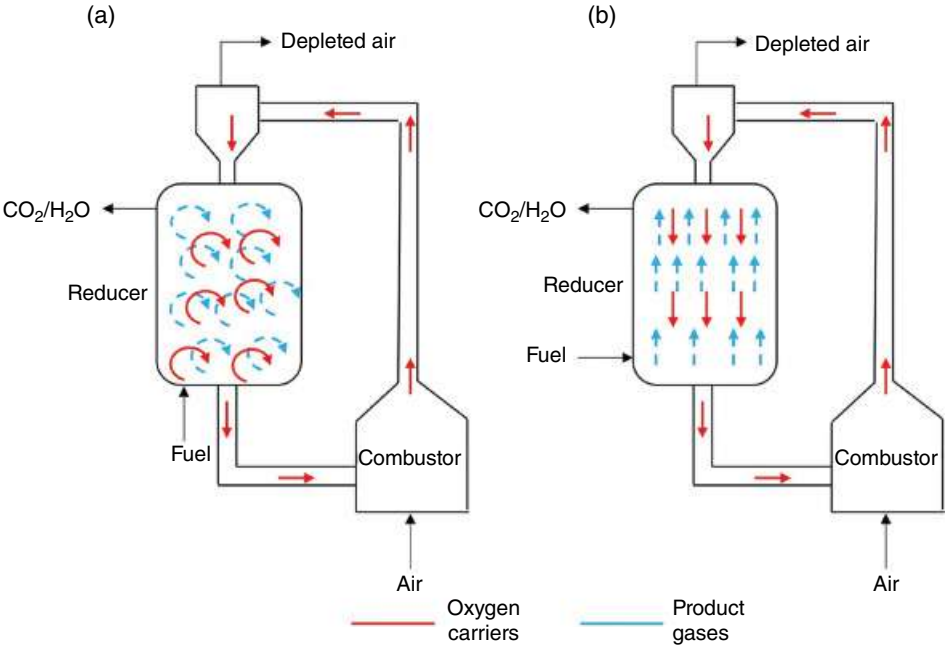

Figure 5.7 (a) Design 1 (fluidized bed) and (b) Design 2 (packed moving bed) for a reducer in the CLC process.

operate as fluidized beds, the oxygen carrier particle size is typically kept between 75 and 250 microns. The flow pattern in Design 1 is mixed or like that observed in commercial risers, where the solids and gases flow in the same direction. Design 1 is characterized by back mixing of solids, which is an inherent property of a fluidized bed, which leads to uneven solid conversion of the oxygen carrier and thereby poor fuel conversion.

Design 2, contrarily, adopts a countercurrent gas–solid contact pattern through the utilization of a moving-bed reactor setup. In this type of design, the solids move down along the length of the reactor in the form of a continuously moving packed bed whereas gas flows in the opposite direction. Having this type of configuration enables maximum fuel conversion along with a high CO_2 yield. As the fuel is injected at the reactor bottom, it is converted to CO/CO_2 and H_2/H_2O as the gases move toward the reducer outlet. As CO and H_2 encounter the fully oxidized oxygen carriers flowing from the top, these gases are oxidized to form CO_2 and H_2O, thereby allowing CO_2 production close to the thermodynamic limit. This can be realized through an example of Fe_2O_3 as the oxygen carrier. In Design 1, as carbon from the fuel is converted to CO and CO_2, the solid conversion of Fe_2O_3 is restricted to Fe_3O_4 due to higher partial pressure of CO_2 over CO. However, when switched to Design 2, as CO_2/CO partial pressure is high at the reactor top, Fe_2O_3 is just slightly reduced and its solid conversion keeps on increasing as it moves downward. A decrease in the CO_2/CO partial pressure along the length of the reducer allows the formation of Fe/FeO mixture at the reducer exit. As higher solid conversion can be obtained in this mode of operation, the solid circulation rate can be decreased, which translates to the lowering of parasitic energy requirements. The significant differences between the two CLC designs are summarized in Table 5.3.

Table 5.3 Comparing the two modes of reducer operation in a CLC process.

Design	1	2
reactor type	Fluidized bed	Moving bed
Gas–solid contact pattern	Mixed	Countercurrent
Fuel conversion	Poor	High
Solid conversion (for Fe_2O_3)	Restricted to 11.1% (Fe_3O_4)	>50% (Fe/FeO mixture)
Process intensification	No	Yes
Particle size	75–250 microns	1000–2000 microns
Relative reactor size	Large	Small
Hydrodynamic effects	Large	Small

Deeper reduction of the oxygen carrier using Design 2 enables process flexibility which can be explored for further process intensification as described in Section 5.2.1.4. It is noted that the selection of mode of operation dictates solid circulation, which, in turn, affects the scalability and economics of the overall process.

5.2.1.4 CLC System with Enhanced Capabilities

One of the advantages of a CLC process is that it not only allows in situ CO_2 separation, but can be further modified for process intensification. One such modification to a conventional CLC system with countercurrent gas–solid contact pattern can yield high-purity hydrogen. Hydrogen production has become essential due to a gradual shift toward "hydrogen economy," owing to its virtue of being a clean fuel [54]. H_2 is also used as an important industrial feedstock for producing liquid hydrocarbons through the Fischer–Tropsch synthesis and chemicals like ammonia, one of the chemical industry's most important products [55]. H_2 production is commercially carried out through reforming of natural gas to first produce syngas, which is further subjected to WGS reaction to produce H_2. This approach involves limitations such as burning large quantities of natural gas to sustain high operating temperatures, frequent replenishment of catalyst inventory due to coking, and usage of highly energy-intensive acid gas removal (AGR) or pressure swing adsorption (PSA) process for separating H_2 from CO_2 [14]. If the CO_2 exiting the furnaces is captured, it reduces the overall efficiency of the process by up to 24% [13]. As a result, a modified CLC process can be utilized for H_2 production where high-purity H_2 and CO_2 streams are obtained through two different reactors, thereby rendering the downstream gas separation redundant.

Figure 5.8a shows H_2 production using a CLC process that utilizes an Fe_2O_3-based oxygen carrier. Any metal oxide that is thermodynamically capable of reducing steam to generate H_2 can be used for this process. This H_2 production scheme utilizes a three-reactor chemical looping system. Fully oxidized oxygen carriers react with the carbonaceous fuel in the countercurrently operated reducer while producing a pure CO_2 stream at the gas outlet. The solids exiting this reactor are reduced beyond 33% to form Fe/FeO phase. A deeper reduction of the oxygen carrier helps achieve higher thermodynamic steam conversion and therefore a higher H_2 yield. The reduced oxygen carrier then enters the oxidizer

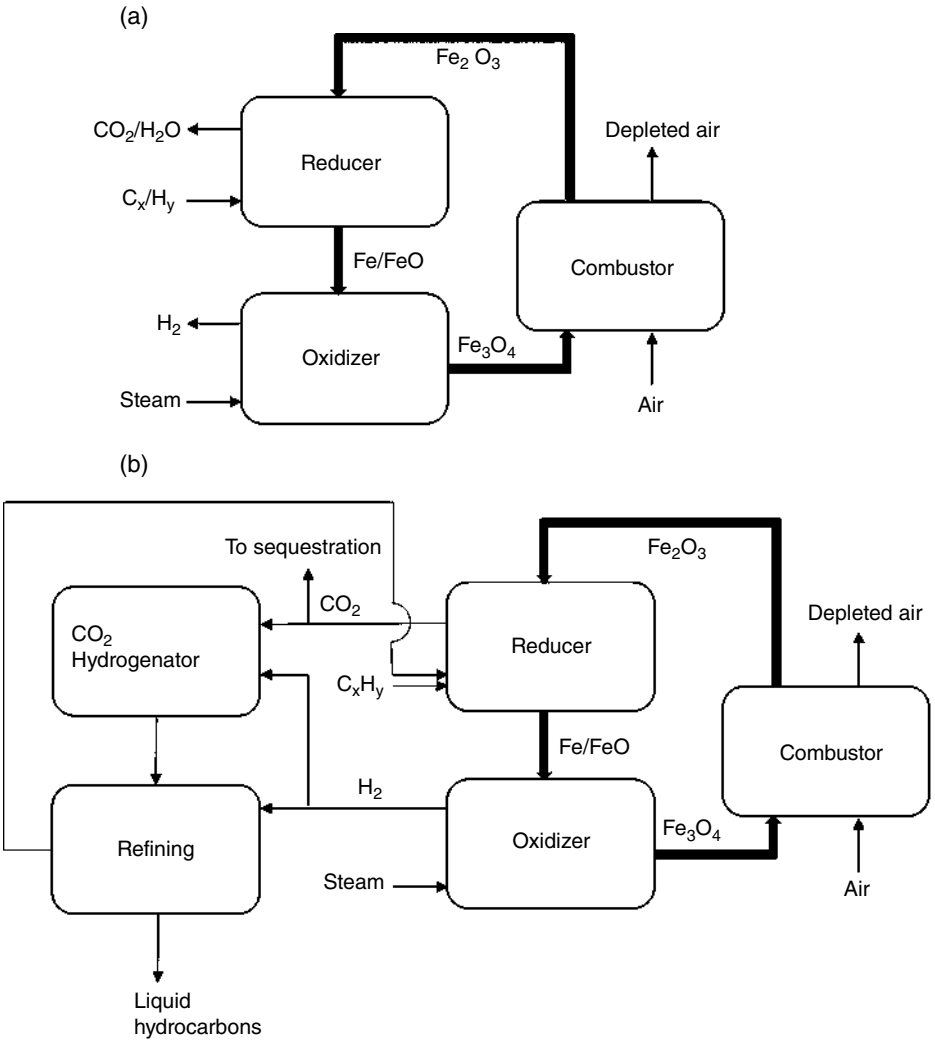

Figure 5.8 CLC process enhancement for (a) hydrogen production and (b) liquid fuels production.

where it is oxidized in steam to produce H_2, where the steam oxidation of Fe/FeO phases is thermodynamically limited to Fe_3O_4 [16]. This reaction is exothermic and needs to be performed at low temperatures to increase the thermodynamic feasibility. However, lower operating temperatures lead to slow oxidation kinetics. The operating temperature, therefore, needs to be carefully optimized to ensure fast kinetics with optimum steam conversion. The partially oxidized oxygen carriers are then sent to the combustor where they are regenerated in air. The reaction occurring in the reducer is endothermic whereas the ones occurring in the oxidizer and combustor are mildly and strongly exothermic, respectively. The heat generated during Fe_3O_4 oxidation provides the necessary endothermic heat to make the overall process thermoneutral. It is important to note that most of the hydrocarbons used as fuel in this process tend to deposit carbon on the oxygen carrier surface

through coking. If this carbon is carried over to the oxidizer, it can reduce the hydrogen purity due to CO formation. Thus, oxygen carriers employed for this process need to be designed such that they inhibit carbon deposition. CLC-assisted H_2 production allows inherent separation of H_2, CO_2, and N_2 without the requirement of any energy and capital-intensive auxiliary separation device.

The three-reactor CLC system can also be used for producing liquid hydrocarbons through catalytic CO_2 hydrogenation as shown in Figure 5.8b. This process combines the reverse WGS process along with the Fischer–Tropsch (F–T) process and allows a single-step synthesis of liquid fuels as shown in Reaction 5.3, thereby allowing effective utilization of the CO_2 produced during the process. A schematic of the F–T process for liquid fuel synthesis is depicted in Figure 5.9. In a typical F–T process, feed gases including CO, H_2, and CO_2 are fed into a reactor embedded with catalysts, where the operating temperature and pressure are controlled to synthesize the desired product [56]. Liquid fuel production by this approach allows reducing the work input by 28% as compared to the conventional hydrocarbons-to-liquid fuels process scheme [13]. This reduction is achieved due to the minimization of exergy loss owing to better heat integration across reactors along with a relatively low operating temperature.

$$x\mathrm{CO_2} + 3x\mathrm{H_2} \rightarrow x - \left(\mathrm{CH_2}\right) - + 2x\mathrm{H_2O} \tag{5.3}$$

5.2.2 CO_2 Capture Using Calcium Looping Scheme

5.2.2.1 Introduction to Post-Combustion CO_2 Capture

One of the problems linked to carbon capture and sequestration (CCS) is the high cost and energy requirement associated with obtaining a pure CO_2 stream from a mixture of product gases. The current technology that addresses the issue of selective CO_2 capture involves the use of amine-based sorbents such as MEA for scrubbing of CO_2 from the vent gases post-combustion. This technology is being improved over issues such as the cost, the risk of

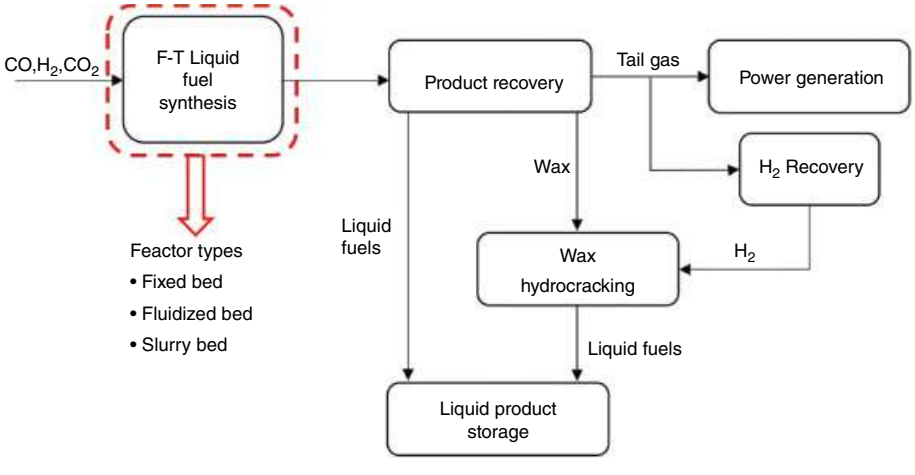

Figure 5.9 A schematic illustrating the process flow in the Fischer–Tropsch (F–T) synthesis for liquid fuel production.

reactions amongst gas components, and temperature-dependent degradation of the solvent [50]. Oxyfuel combustion is another evolving technology where coal is combusted in presence of a flue gas–oxygen mixture and the temperature of the flame is maintained by recycling a part of flue gases into the combustor [57]. As the quantity of oxygen required is substantial, a cryogenic air separator with a large volume needs to be installed, which can supply the required amount of O_2. Multiple drawbacks of these processes have provided the necessary impetus to develop an alternate process that can address the shortcomings of existing technologies and has a high scale-up potential. One such process that is being actively investigated is calcium looping.

5.2.2.2 Calcium Looping Process Description

Calcium looping is a cyclic redox process where calcium oxide (sorbent) and CO_2 from the flue gas react to form $CaCO_3$ (calcium carbonate) in the carbonator reactor and the $CaCO_3$ formed is then transported and decomposed back into its constituents (CaO and CO_2) in another reactor known as calciner, thereby producing a pure, sequestration-ready CO_2 stream. The process is continued by sending the regenerated sorbent back into the carbonator to complete the calcium loop [58]. The sorbent is also capable of capturing other pollutants such as H_2S, COS, and halides from the feed gas. However, this leads to an increased rate of sorbent deactivation and thus necessitates an increased purge and makeup rate to maintain an efficient continuity of the overall process. This concept of using CaO as the looping media to capture CO_2 (sorbent) has gained significant interest and has been researched thoroughly for carbon capture by numerous corporations and academic institutions for the last three decades [16]. Although Shimizu et al. introduced this concept for the post-combustion CO_2 capture, it was initially used in H_2 production using enhanced WGS reaction following the precombustion pathway [59]. The CaO sorbent can be procured economically from naturally occurring sources like limestone or dolomite (comprising about 50% MgO). Experimental investigation revealed that dolomite shows higher resistance to deactivation as compared to limestone. However, this translates to an increased solid loading due to the inert nature of MgO [60]. The carbonation reaction is exothermic in nature and the heat evolved can be captured for its use in the form of process heat. For example, water can be converted into steam, which can then be used to run steam turbines to economize energy and promote efficient heat integration across the overall process. A balance is needed between the increased reaction rate in the carbonator at elevated temperatures and the higher thermodynamic equilibrium conversions at lower temperatures. The efficiency of the process can be further improved significantly if the used sorbent can be utilized in other industries to offset the operating costs.

Some of the key advantages of the calcium looping technology for CO_2 separation are:

a) The fresh sorbent (CaO) is inexpensive, and it can be easily sourced while the spent sorbent can be incorporated into various industries, for example, the cement industry [61].
b) A more efficient and cost-effective option is available using circulating fluidized beds (CFBs) in contrast to large solvent scrubbing towers required for amine scrubbing.
c) MEA scrubbing is incompatible with coal combustion flue gas streams and requires SO_2 concentration ≤ 10 ppm to prevent solvent deactivation. This prevents the use of MEA

technology for the use of low-grade coals that contain high sulfur. Calcium looping can effectively separate both CO_2 as well as SO_2.

d) The oxy-combustion technology suffers from air infiltration issues that can lead to dilution of flue gas stream. Also, the ASU units for air separation can be very energy-intensive.

e) Other separation technologies such as membrane separation face durability issues at high temperatures in addition to the challenges pertaining to product selectivity. For the membrane to be effective, high-pressure flue gas is required. Calcium looping does not have this requirement.

The challenge currently restricting the commercial deployment of calcium looping is the sorbent deactivation across multiple cycles. The CaO derived from natural limestone progressively loses its reaction capabilities after several cycles of reaction with CO_2. Academic researchers along with support from the industry are working to address this issue by using different sorbent sources for CO_2 capture [62]. For instance, one strategy involves combining natural limestone with several other chemicals or heating it beforehand to produce a tailored sorbent to impede the deactivation rate. Hydration of the used sorbent prior to the calcination step has yielded a promising solution to the issue [63]. Nevertheless, some of the techniques used to increase the limestone reactivity can cause deterioration of its strength. Pelletizing the active material has shown to reduce this issue to a certain extent but not complete elimination. Like any other chemical looping technology, the performance of different CaO-based sorbents has been demonstrated in large pilot-scale reactors for an extended time to assess their mechanical and thermal stability [64].

5.2.2.3 Calcium Looping Reaction Scheme

There are two aspects critical to the success of calcium looping availability of a CaO-based sorbent that can sustain CO_2 capture and release across a large number of cycles without deactivation and testing of an integrated calcium looping unit to assess the overall performance of the system. Naturally occurring CaO derivatives such as limestone and dolomite as well as synthetic CaO-based sorbents are supported with an inert metal oxide to prevent agglomeration of the CaO grains and assure retention of the porous structure. The use of supports like Al_2O_3, TiO_2, SiO_2, Y_2O_3, CeO_2, and WO_3 has been reported in the literature with two types of sorbent design schemes – (i) homogenous distribution of sorbent and the support, and (ii) core-shell-type structure [65]. Huang et al. have reported the use of an alkali-doped CaO sorbent for selective CO_2 separation using calcium looping. Dopants such as Li, Na, and K were tested, where incorporating Li into the sorbent increased the CO_2 uptake by ~3.5 times as compared to the undoped sample [66]. The use of a hollow, spherical sorbent particle has been reported by Anthony et al. where the high surface area in the sorbent is shown to provide more active sites for carbonation, thus allowing higher CO_2 uptake. Moreover, this sorbent is also reported to be more resistant to reaction-induced volumetric changes and therefore capable of undergoing multiple CO_2 capture cycles without deactivation [67]. Although a significant amount of work has been done on developing CaO-based sorbents on a lab scale, they also need to be tested in fixed beds and fluidized beds in a continuous manner under the conditions expected in the industry. The operational data collected through these test campaigns can be used for developing a robust

process model coupled with a detailed techno-economic assessment, which can be used for identifying various technological gaps and gathering scale-up data for the potential commercialization of the technology [68]. Table 5.4 summarizes the design and performance of various bench- and pilot-scale calcium looping units that have been designed and tested by different academic and industrial research institutions across the globe. It can be seen that various types of reactor configurations and operating parameters have been employed by different groups, while collectively achieving a CO_2 capture efficiency of >90%.

This section discusses the overall calcium looping process including reaction schemes, the rationale behind reactor design, and the prevalent operating conditions. The carbonation and calcination reaction steps outlined previously are reversible in nature. Calcium looping leverages the reversibility of these two reactions, which constitutes the core chemistry of this process. The recyclability analyses of the sorbent have been mostly conducted using a thermogravimetric analyzer (TGA). The carbonation reaction (CO_2 capture) is exothermic in nature, and it occurs in the carbonator which is maintained at temperatures between 600 and 800 °C to ensure high thermodynamic equilibrium conversions and a good reaction rate. The range of carbonation temperature is chosen such that the equilibrium partial pressure (EPP) of CO_2 at those temperatures is less than the actual partial pressure (APP) of CO_2 to provide the driving force for its removal. In the carbonator,

Table 5.4 Summary of different scaled-up calcium looping processes for selective CO_2 capture from flue gas streams.

	Carbonator			Calciner			
Developers	Capacity (kW_{th})	Type[a]	Operating temperature (°C)	Type[a]	Operating temperature (°C)	CO_2 capture efficiency (%)	Reference
Industrial Technology Research Institute	1900	BFB	650	MB	800–900	99	[69]
Consejo Superior de Investigaciones Cientificas	1700	CFB	600–715	CFB	820–950	90	[70]
Darmstadt University of Technology	1000	CFB	~650	CFB	<1000	~90	[71]
IFK at University of Stuttgart	200	CFB	~650	CFB	875–930	~93	[72]
Ohio State University	120	EB	450–650	RK	850–1300	>90	[73]
Vienna University of Technology	100	BFB	650	CFB	850	—	[74]
CANMET Energy	75	BFB/MB	600–700	CFB	900–950	97	[75]
Tsinghua University	10	BFB	~600	BFB	850	95	[76]

[a] BFB: Bubbling fluidized bed, CFB: Circulating fluidized bed, EB: Entrained bed, MB: Moving bed, RK: Rotary kiln.

CO_2-rich gas is contacted with CaO where these two react to form $CaCO_3$. The gaseous exit stream from the carbonator is CO_2-lean whereas the solid stream exiting is carbon-rich. The solid products are further sent to a calciner operating at higher temperatures (850–1000 °C) where $CaCO_3$ is thermally cracked to separate CaO and CO_2. The rates and efficiency of these two reactions vary widely due to the fundamental difference in their mechanism. Out of these two, the carbonation reaction has been often reported to be more challenging owing to the loss of sorbent reactivity across extended redox cycles. This necessitates the replacement of spent sorbent, which can be done in such a way that the makeup can sustain the process over longer time periods while maintaining the economic prospects of the process.

The most common approach adopted by researchers to tackle the issue of reactivity loss in CaO-based sorbents is sorbent modification through the incorporation of inert supports and dopants. Loss of reactivity in the sorbents takes place due to sintering, which is caused because of high-temperature regeneration of the sorbent in the calciner. To overcome this issue, The Ohio State University (OSU) has successfully developed a patented three-step calcium looping process that integrates an intermediate sorbent reactivation step with the conventional two-step process [77]. This process has been termed the carbonation–calcination reaction (CCR) process, where a hydrator is placed between the calciner and carbonator as shown in Figure 5.10. The incoming CaO from the calciner is reacted with steam at temperatures >350 °C in the hydrator to form $Ca(OH)_2$, which is then sent into the carbonator for CO_2 capture. Transitioning from CaO to $Ca(OH)_2$ minimizes the temperature swing between the three reaction steps, thereby impeding the effect of sintering and allowing retention of sorbent reactivity across several CO_2 capture cycles [63]. The CCR process thus combines superior reactivity of $Ca(OH)_2$ compared to CaO with the optimum operating conditions to allow effective separation of CO_2 from a flue gas stream [78]. This allows lowering of solid circulation rate, less sorbent consumption, and a low solid disposal rate as compared to the conventional two-step calcium looping process. Reactivity of the CaO sorbent using the CCR process has been evaluated across multiple cycles, which suggests that high-temperature steam-assisted regeneration of the sorbent helps maintain the reactivity of CaO toward CO_2 over an extended number of cycles [79].

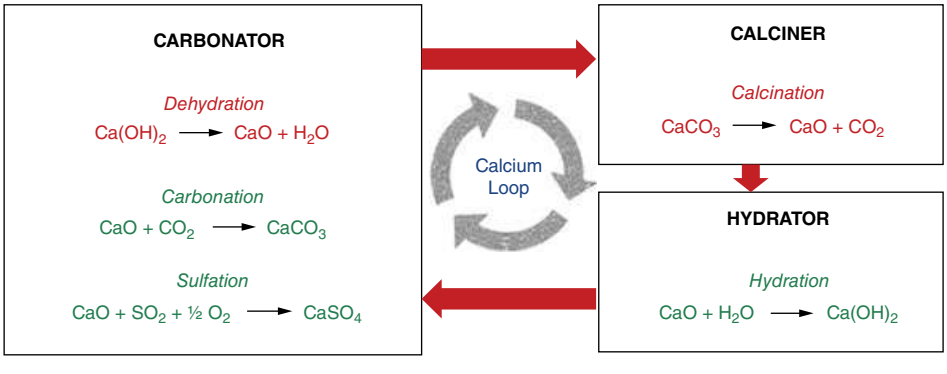

Figure 5.10 Schematic of the 3-step carbonation–calcination reaction (CCR) process developed at The Ohio State University.

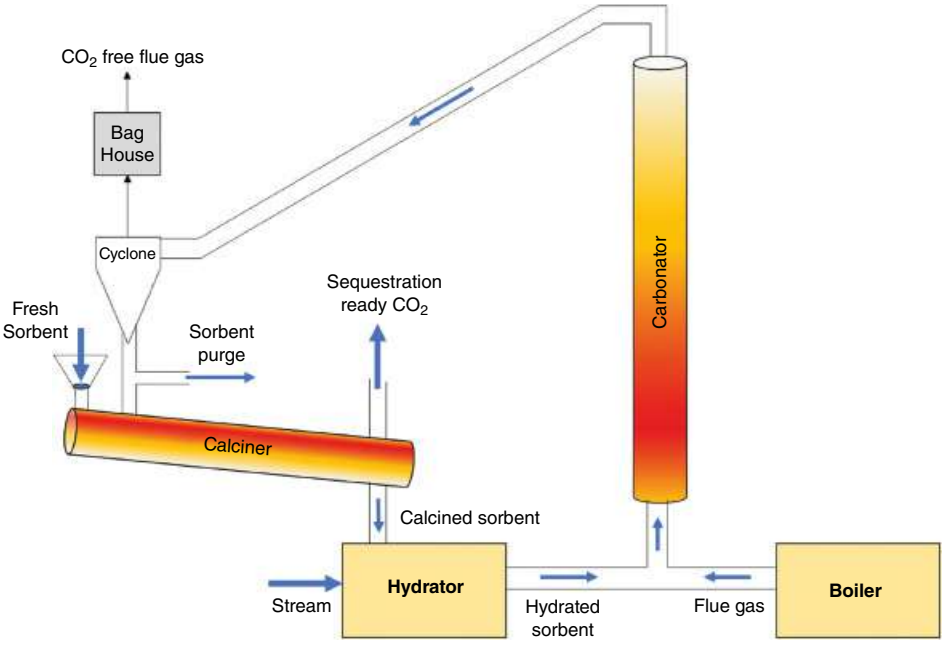

Figure 5.11 Reaction scheme of the CCR process depicting the hydration-assisted calcium looping for CO_2 capture.

The 120 kW_{th} unit built and demonstrated at the OSU is capable of capturing CO_2 and SO_2 from the flue gas obtained through a stoker boiler using a regenerable sorbent through the carbonation–calcination–hydration cycle as illustrated in Figure 5.11 [63, 73]. Morphological studies of the hydrated sorbent reveal higher surface area and pore volume resulting in higher CO_2 removal [63]. The CCR process has stemmed from two other processes developed at the OSU, OSCAR (Ohio State Carbonation Ash Reactivation) and CaRS–CO_2 (calcium-based reaction separation for CO_2), where both the processes use calcium-based sorbents. In particular, the OSCAR process allows the removal of sulfur, arsenic, selenium, and mercury from flue gas whereas the CaRS–CO_2 process specifically targets CO_2 and SO_2 separation using a highly reactive and regenerable sorbent. The carbonator is designed as an entrained bed reactor. The flue gas is stripped of CO_2 and SO_2 in the forms of $CaCO_3$ and $CaSO_4$, respectively in a temperature range of 450–650 °C. The spent sorbent is then sent to a rotary kiln-type calciner (operating between 850 and 1300 °C) where it is regenerated and a pure, sequestration-ready CO_2 stream is generated. The calcined sorbent is finally fed to the hydrator where it is reactivated using steam. The reactivated sorbent is circulated back to the carbonator to complete the calcium loop. The pure CO_2 stream from the calciner is compressed and sent for subsequent sequestration. Considering the mild operating conditions of calciner for $CaSO_4$ decomposition (requiring temperature >1450 °C), a small amount (2–10%) of spent solids is purged out depending on the sulfur content of flue gas. Furthermore, this process can be integrated with fuel sources not limited to natural gas, coal, and biomass. In addition, a negligible effect of the fly ash content is observed on the removal efficiency considering an adequate sorbent purge is

employed. With an efficient heat integration system in place, the process achieved >90 and ~100% CO_2 and SO_2 capture, respectively, thus rendering more economically attractive than other CO_2 capture technologies.

5.2.3 Chemical Looping Air Separation (CLAS)

5.2.3.1 Background and Process Description

Oxygen is one of the most sought-after chemicals in the world with ~30% share in the global industrial gas market [80–82]. Molecular O_2 has found its use in varied applications like metallurgy, chemical synthesis, glass manufacturing, pulp and paper industry, and the health sector. As oxygen is present in abundance in the earth's atmosphere along with N_2, air separation is the predominant approach for oxygen production [83]. Currently, the market revenue of ASUs exceeds $4 billion per year and is expected to grow to $5.8 billion by 2022 [84, 85].

O_2 is conventionally produced using a process known as cryogenic separation, which was developed in the early twentieth century [86] and involves the distillation of liquid air based on relative volatilities. In a typical cryogenic air separation plant, ambient air is compressed and treated to make it devoid of any moisture, hydrocarbons, and CO_2. The treated air is then passed through a series of heat exchangers to cool it down to cryogenic temperatures. The cooled air is then expanded and fed to the distillation column where it is separated into N_2 and O_2 streams. These streams also contain noble gases that can be further separated by distillation. Thus, O_2 with purity >99% can be produced using this process [83]. However, cryogenic separation is a highly complex and expensive process and has low thermodynamic efficiency (<25%) [87–89]. As a result, other non-cryogenic routes have been explored for air separation. PSA is another matured technology that has been developed for air separation. It employs the use of selective adsorbents which leverage the difference of polarizability between N_2 and O_2 for separation [90, 91]. However, PSA has limitations pertaining to the product gas purity and the overall processing capacity. It can only produce O_2 with purity as high as 95% and renders uneconomical as compared to cryogenic separation when O_2 production > 150 short tons per day (STPD) is required [83, 88, 92]. With recent advancement in ceramics-based technology, membrane separation is also being heavily researched for its use as a potential technology to produce high-purity O_2. Conductive oxygen membranes and mixed ionic–electronic conducting membranes can produce O_2 with purity >99% [83]. However, there are a lot of challenges with the practical employment of this technology and it is still in the development stage. Table 5.5 showcases the comparison between various air separation technologies.

Table 5.5 Comparison amongst different air separation technologies.

Process	Economic production range (STPD)	Purity limit (vol. %)
Cryogenic	>20	>99
PSA	<150	~95
Ionic membranes	Undetermined	>99

Chemical looping air separation (CLAS) has the potential to replace cryogenic air separation because it addresses various limitations of the conventional process [84]. CLAS is based on the principle of oxygen uncoupling, which involves the spontaneous release of oxygen by a solid metal oxide at high temperatures [93]. The metal oxide-based oxygen carriers used in the chemical looping process act as the oxygen source. In CLC, as described in Section 5.2.1.1, a reducing gas is required to abstract lattice oxygen from the oxygen carrier. However, an oxygen uncoupling material can release its lattice oxygen in the form of molecular O_2 even in the absence of a reducing gas. An example of such a material is CuO, which loses its oxygen as shown in Reaction 5.4.

$$2CuO \rightarrow Cu_2O + \frac{1}{2}O_2 \tag{5.4}$$

This essentially signifies that no chemical reaction with the oxygen carrier is necessary for its reduction to obtain molecular O_2. The amount of O_2 released, which can also be defined as the extent of reduction in the oxygen carrier is a function of the oxygen partial pressure. In other words, when an oxygen uncoupling-based carrier is subjected to high temperatures in the presence of an inert gas stream, O_2 release can be achieved.

A typical CLAS schematic is depicted in Figure 5.12, where the process utilizes two reactors – a reducer and an oxidizer. Air enters the oxidizer where it reacts with reduced oxygen carriers as shown in Reaction 5.5. As oxygen transfer occurs from air to the reduced carriers, an oxygen-depleted air stream is obtained at the oxidizer outlet. Fully oxidized particles are then transferred to the reducer, where they lose molecular O_2 through the uncoupling process in presence of an inert gas as shown in Reaction 5.6. Steam has been considered as an ideal inert gas as it does not react with the reduced oxygen carriers and can be condensed easily to recover molecular O_2 from the reducer exit gas stream.

$$MO_{x-y} + \frac{y}{2}O_2 \rightarrow MO_x \tag{5.5}$$

$$MO_x \rightarrow MO_{x-y} + \frac{y}{2}O_2 \tag{5.6}$$

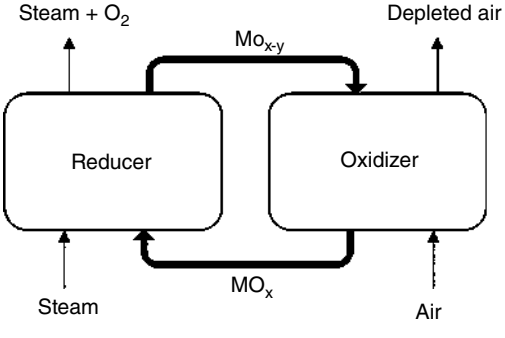

Figure 5.12 Schematic of the chemical looping air separation (CLAS) process for selective separation of O_2 from the air.

One of the biggest advantages of using CLAS is that it offers significant economic benefits because of its low energy demand coupled with the relative simplicity of operation [89]. The low energy demand stems from the fact that the heat required in Reaction 5.5 is the same as the heat released in Reaction 5.6. Thermodynamic calculations reveal that the specific power required for operating a CLAS unit is just 26% of that of a cryogenic separation unit [84]. The process can be designed such that the stoichiometric amount of O_2 required to fully

Table 5.6 Minimum decomposition temperature and oxygen transport capacity (OTC) of oxygen uncoupling materials.

Metal oxide system	Minimum decomposition temperature (°C)	Oxygen transport capacity (OTC) (%)
CuO/Cu_2O	830	10.06
Co_3O_4/CoO	793	6.64
Mn_2O_3/Mn_3O_4	653	3.07

regenerate the oxygen carrier can be supplied in the form of air, thus allowing selective separation of N_2 and O_2 from the air stream.

Like other chemical looping applications, the CLAS process also depends on the oxygen carrier selection, gas–solid contact pattern, and reactor configuration where the latter two are like the CLC process. The reducer can be designed as a fluidized bed or a moving bed reactor, where each design configuration has its own advantages and disadvantages. The oxidizer is typically designed as a fluidized bed reactor because it not only assists in oxygen carrier regeneration but also in pneumatically conveying regenerated solids to the reducer. Consequently, the selection of oxygen carrier is critical in CLAS as the inherent thermodynamic and material properties of the oxygen carrier constituents decide the overall O_2 yield of the system.

The selection of different metal oxides capable of losing molecular O_2 can be carried out through thermodynamic screening. However, this approach ignores the stability issues related to the metal oxides. For example, the temperature at which the oxygen carrier loses molecular O_2 can be lowered through the incorporation of a certain dopant or promoter. Similarly, metal oxides can be mixed with inert supports which make the carrier more tolerant toward sintering and hence less prone to deactivation [94, 95]. Moreover, extensive research is being conducted to develop mixed metal oxides that can utilize the synergistic effects of multiple components and bring down the overall energy requirement of the process [96, 97].

5.2.3.2 Selection of Oxygen Carrier with Uncoupling Behavior

The success of any chemical looping system depends on the performance of the oxygen carriers, where their ability to reversibly react with oxygen dictates the overall performance of the system [84]. The oxides of Cu, Co, and Mn show excellent oxygen uncoupling behavior and hence are the most popular choices for CLAS application. Other metal oxides such as Fe_3O_4 and ZnO also tend to lose molecular O_2 but at significantly high temperatures, which can be economically utilized only with the assistance of nonconventional heat sources like solar, geothermal, or nuclear energy [14]. However, loss of reactivity due to sintering caused by high temperature and melting/agglomeration of the oxygen carriers remains a big hurdle. Oxygen carrier selection for CLAS process is often based on the following criteria:

Oxygen transport capacity (OTC): The OTC of an oxygen carrier is defined as the maximum amount of oxygen that can be transferred between the reduced and oxidized phases per unit mass of the fully oxidized carrier [89]. In the CLAS process, the amount of oxygen carrier required in a fully operational system is inversely proportional to the transport

capacity. As a result, oxygen carriers with high OTC are desired to the process more economical.

Oxygen uncoupling temperature: Oxygen uncoupling temperature is the minimum temperature required for the decomposition of the oxidized phase. In other words, the uncoupling temperature is the minimum operating temperature of the reducer reactor. A low uncoupling temperature is favorable as it decreases the energy requirement of heating. Table 5.6 shows the minimum decomposition temperature for some metal oxides along with their OTC.

Equilibrium partial pressure (EPP) and steam demand: As stated in Section 5.2.3.1, steam has been identified as the ideal inert gas in the reducer reactor of the CLAS process due to its ease of separation from molecular O_2. The system is to be optimized and operated in such a way that maximum oxygen throughput can be obtained while maintaining a low steam requirement. Steam demand in the CLAS process is closely related to the EPP of oxygen in the reducer.

EPP for each oxygen carrier is calculated based on the change in Gibbs free energy (ΔG) for Reaction 5.5 or 5.6 [61]. As ΔG is a function of temperature, the EPP also becomes a function of temperature as depicted in Figure 5.13. As the input to the oxidizer reactor is air, the maximum oxygen partial pressure in the oxidizer is fixed at 21%. Thus, for any metal oxide system, the maximum operating temperature is the point at which EPP reaches 21%. With O_2 concentration restricted to 21%, operating at temperatures higher than the EPP value is not feasible as air cannot oxidize the reduced carriers. As an example, Figure 5.13 shows that the EPP of CuO/Cu_2O system reaches 0.21 at approximately 1020 °C. Thus, the temperature of the oxidizer is to be maintained below 1020 °C.

Deciding the reducer operating temperature is not as straightforward as the oxidizer. Steam (or any other inert gas) can be used as a gaseous medium in the reducer where the reduction of metal oxides takes place to release O_2. The presence of steam ensures that the oxygen carrier does not lose O_2 unless the APP of oxygen is ≤EPP. It is theoretically possible to operate the reducer at a temperature where EPP is equal to 100%. At this point, no external steam input is required (APP = EPP) but operating at such high temperatures leads to a higher energy footprint and oxygen carrier degradation. As seen from Figure 5.13, the EPP remains low at temperatures just above the uncoupling temperature and, as a result, a

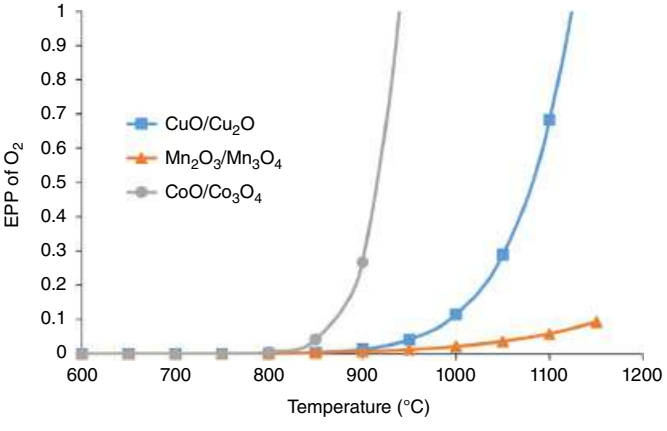

Figure 5.13 EPP of O_2 as a function of temperature.

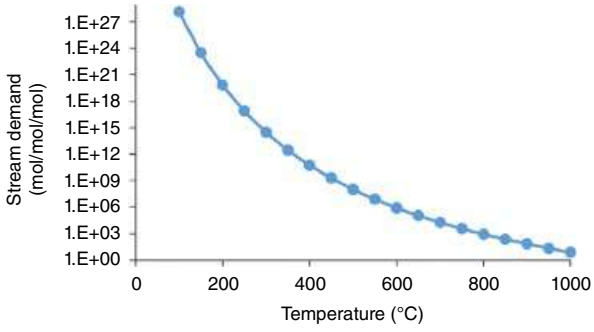

Figure 5.14 Reducer steam demand as a function of temperature.

large amount of steam is required. Consequently, a decrease in steam demand is observed as the operating temperature increases, which can be seen in Figure 5.14 that provides an illustration of the CuO/Cu_2O system. Hence, the operating temperature of the reducer is decided based on the balance between the energy required for heating the reducer and steam generation. It is important to note that although these temperatures are typically obtained from the analysis of reaction thermodynamics, reaction kinetics also dictate the operating temperature.

5.2.4 Selective Separation of H_2S

5.2.4.1 Description of H_2S Removal

Hydrogen sulfide (H_2S) is a highly toxic and corrosive pollutant gas, inherently present in fossil fuels (e.g. natural gas, crude oil) and generated through industrial processes like fuel extraction and refining, coal gasification, petrochemical production, and wastewater treatments [98]. It has been recognized as a hazardous waste for the environment, human health and particularly damaging to many industrial processes, where H_2S is mainly produced during hydrodesulfurization of fuels (natural gas, crude oil, and coal). According to International Energy Agency, about 43% of the world's natural gas reserves are currently contaminated with acidic gases – H_2S and CO_2, with the Middle East containing the most of them [99–101]. This contaminated natural gas, also known as sour gas, is cleaned using AGR processes before its processing. Likewise, more than 50% of crude oil reserves contain sour oil due to the presence of a high level of sulfur compounds (e.g. thiophene, mercaptans, and sulfides) in them. The sulfur present in crude oil and solid fuels like coal is converted into H_2S when they are processed in the refining, petrochemical, or energy industries. These processes emit large amounts of H_2S, resulting from either emission during the routine operation phases or from releases related to near-misses and accidental events. H_2S emission has thus become a concern as more and more fossil fuels are being consumed to meet the ever-increasing global energy demand, where fossil fuels contribute to nearly 80% of global primary energy production [102]. Apart from being used as an energy source, they are also used as feedstock for value-added chemical production through catalytic processes (e.g. the Fischer–Tropsch process, steam methane reforming). Even low-concentration H_2S (>30 ppmv) can cause material corrosion and catalyst deactivation, thereby limiting their usage as feedstock [103]. H_2S has a deleterious effect on human health and its overexposure can lead to acute and chronic poisoning or can even prove to be fatal [104]. It is also an

environmental pollutant if directly released to the atmosphere or, indirectly, after oxidation to SO_2 as it enters the biosphere in the form of acid rain [105]. All these harmful effects impose the need for fuel desulfurization/separation prior to its use in any industrial process and further treatment in a safe manner to avoid environmental degradation through H_2S emission.

5.2.4.2 Conventional H_2S Processing Scheme

The organosulfur compounds emitted during the refining of fuels like natural gas and crude oil are first converted into H_2S gas in a hydrodesulfurization step. The H_2S formed is then selectively scrubbed off using an amine-absorption process, also known as the AGR process. Absorption units generally operate in the temperature range of 25–40 °C, and use solvents such as methyl diethanolamine (MDEA), selexol, or rectisol (operating temperature between −40 and −60 °C) to selectively absorb H_2S (and, in some cases, CO_2) from the gas mixture containing other hydrocarbon gases. At the end of this process, the used solvents are regenerated using steam and the stream containing a high concentration of H_2S and CO_2 is stripped off. It usually contains varying concentrations of H_2S and CO_2 (typically in the range of 10–40% CO_2 and 50–90% H_2S for refining off gases), is saturated with water, and frequently has small amounts of hydrocarbons and other impurities (e.g. NH_3) in addition to the primary components [106]. This stream serves as the feed for the Claus process where it is oxidatively decomposed for elemental sulfur recovery. First patented in 1883, the Claus process is still utilized commercially for H_2S treatment in oil refineries, gas reservoirs, and gasifiers. The oxidative decomposition route followed in the Claus process can be represented using Reactions 5.7 and 5.8 [48].

$$H_2S + 1.5O_2 \rightarrow H_2O + SO_2 \tag{5.7}$$

$$2H_2S + SO_2 \rightarrow 2H_2O + 3S \tag{5.8}$$

Reaction 5.7 is a highly exothermic, non-catalytic partial combustion reaction to produce SO_2, carried out in blast furnaces at high temperatures ~1000 °C. On the other hand, Reaction 5.8 is an exothermic catalytic reaction operating at a temperature around 300 °C and carried out in a series of catalytic reactors using alumina/titania catalyst [107]. The outlet gas from the furnace is cooled in a waste heat boiler before feeding it to a catalytic reactor. Condenser and preheater are required in between the two catalytic reactors for removal of liquid sulfur and heating the stream to prevent catalyst deactivation, respectively. The process achieves up to 97% H_2S conversion into elemental sulfur with a series of three catalytic reactors [108]. Multiple catalytic reactors are used as the reaction is exothermic in nature and thus H_2S conversion is favored at low temperature, which impedes the reaction rate. Thus, using multiple reactors operating at varying temperatures allows high H_2S conversion. The tail gas coming from the last stage of the sulfur condenser typically contains unconverted H_2S, SO_2, and COS. The presence of sulfurous gases in the tail gas prevents its direct atmospheric emission due to the stringent governmental regulations for the discharge of such compounds. Therefore, very often a tail gas treatment unit is coupled with Claus sulfur recovery units for reducing the content of sulfurous gases to meet permissible limits before tail gas disposal [109].

The effectiveness of each step in the conventional desulfurization scheme is limited due to certain factors. The solvents used in the absorption process are rendered unusable even if there is a minor change in the feed gas composition. The overall process efficiency remains low due to factors such as high cooling load caused by lower operating temperatures, the energy requirement for regeneration of the used solvent, foaming of solution in contactor or regenerator, and corrosion of the pipes carrying solvent [110, 111]. On the other hand, the use of multiple catalytic reactors in the Claus process is essential to achieve high H_2S conversion. The overall configuration of heat exchangers required not only increases the process complexity but also makes the process highly cost- and energy-intensive. The oxidative decomposition chemistry of the process prevents recovery of H_2 selectively. The direct reactive separation of H_2S in presence of other gases such as hydrocarbons, CO, H_2, and CO_2 has been primarily investigated using regenerable and non-regenerable sorbents. For such adsorption processes, Zn- and/or Fe-based adsorbents have shown to have a good selectivity toward H_2S adsorption [112]. These adsorbents are regenerated using air while producing SO_2 or stream washing method, and both methods lead to loss of sorbent reactivity after several cycles, thus making the process cost-intensive.

5.2.4.3 Chemical Looping for H_2S Removal and H_2 Recovery

The conventional H_2S separation scheme only allows recovery of elemental sulfur through the oxidative decomposition route followed in the Claus process, thus inhibiting H_2 recovery due to steam formation. This issue can be effectively targeted using the H_2S splitting process as shown in Reaction 5.9 [113].

$$H_2S \leftrightarrow H_2 + 0.5S_2 \; \Delta_r H^0 = 20.6\,\text{kJ/mol} \tag{5.9}$$

Different approaches such as thermolysis, thermocatalysis, photocatalysis, and multistep thermochemical decomposition have been reported in the literature to carry out H_2S splitting [114]. These approaches allow selective separation of H_2S using a smaller number of unit operations and processes while generating a value-added product – H_2. However, H_2S splitting is endothermic and the occurrence of the reverse reaction limits its conversion to H_2. H_2S conversion is improved by continuously removing the decomposed products to shift the reaction equilibrium in the forward direction. Numerous research studies have been performed to improve the H_2S conversion by integrating membrane separation, sulfur condensation, thermal diffusion, or closed circulating system with intermittent removal of H_2 or chemical adsorption of sulfur [114]. The chemical looping scheme offers a promising way for carrying out selective H_2S separation efficiently in two sub-steps with minimal complexity.

Figure 5.15 shows a schematic of the chemical looping process consisting of two reactors, viz. sulfidation and regeneration connected to each other to form a loop. The sulfidation reactor enables desulfurization of the gaseous stream, where metal sulfide-based carrier (M_xS_y) selectively decomposes H_2S into H_2 and elemental sulfur, with the latter captured within M_xS_y to produce a sulfur-rich phase – M_xS_{y+z}. The H_2-rich gas stream is obtained at the reactor outlet with H_2S concentrations <1% (represented as Reaction 5.10). The captured sulfur is desorbed in the regeneration reactor by thermally decomposing M_xS_{y+z} into M_xS_y in an inert atmosphere (e.g. N_2, Ar) operating at a higher temperature

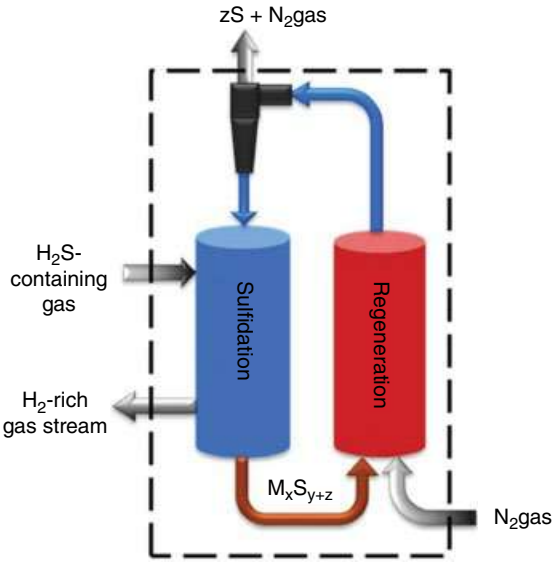

Figure 5.15 Simplified flow diagram for chemical looping-assisted H_2S splitting.

and/or lower pressure than the sulfidation reactor (represented as Reaction 5.11). The elemental sulfur is then condensed and separated from the exit gas stream.

$$\text{Sulfidation reaction}: M_xS_y + H_2S \rightarrow M_xS_{y+z} + H_2 \tag{5.10}$$

$$\text{Regeneration reaction}: M_xS_{y+z} \rightarrow M_xS_y + zS \tag{5.11}$$

The chemical looping scheme for H_2S splitting was first introduced in 1961 through Weiner et al. where a cyclic process was operated using a sulfur-lean metal sulfide of iron, nickel, and cobalt to capture sulfur from H_2S while forming a sulfur-rich metal sulfide [115]. Various patents have been issued since then for this scheme using various materials. However, very few of these processes and technologies discuss selective separation of H_2S using the H_2S splitting approach from a gas mixture containing hydrocarbons (e.g. CH_4), CO, and CO_2 which are commonly found in feed-streams undergoing desulfurization. A process for reactive separation of H_2S while producing H_2 from a mixture of gases containing CO, CH_4, and hydrocarbons (C_1-C_4) was demonstrated over a wide temperature range with H_2S conversion >99% [116]. This process allows conversion of H_2S into H_2 and S, two value-added products while also separating hydrocarbons and other gases from H_2S, thus rendering the process highly economical and less energy-intensive. The use of this process also prevents the requirement of a multi-reactor setup for H_2S removal, thus leading to a considerable drop in the capital cost requirement. A study done by Reddy et al. shows that the use of Fe_7S_8–FeS_2 system for H_2S capture has overall energy and exergy efficiency higher by 14.74 and 21.54% points, respectively than the Claus process. H_2 recovery of ~99.31% has also been reported with 6.52 MW lower exergy destruction as compared to the Claus process due to the removal of the high-temperature thermal oxidation and heat recovery step in the chemical looping process [48]. Although H_2S separation has been

actively investigated over many years, it has not been yet commercialized. Some of the limitations that need to be overcome are low H_2S conversion at the given operating condition, the reactivity of solids with other gas components present in the stream, and sustained reactivity and recyclability of solids over multiple cycles. The design and composition of the metal sulfide-based solids need to be investigated for possible commercialization of H_2S separation using the chemical looping route.

5.3 Potential for Process Intensification, Sustainability, and Challenges

The chemical looping technology is poised to become more mature and to progress toward its commercialization through extensive research on materials, process design, and new schemes that help achieve efficient gas separation with minimal energy requirement. As the profit margins on chemicals/electricity production with an efficient product/flue gas separation remain narrow, chemical looping schemes can be combined with other emerging technologies such as membrane separation, microwave heating, and modularization of reactors to carry out process intensification [117–119]. The use of ceramic membranes to carry out in situ chemical looping-assisted gas separation has generated a significant research interest recently due to its potential of generating higher product yields. This stems from the fact that the membrane placed in the reactor allows selective separation of the product, thus breaking the thermodynamic equilibrium and therefore providing the necessary driving force to push the equilibrium in the forward direction to produce more products [120]. Even though the use of membranes in a chemical looping setting is highly attractive, more fundamental research is required to understand various phenomena associated with the process including cost, ionic transport across membranes, microstructural optimization in membranes, and their performance at high temperatures for an extended time period. Apart from integrating chemical looping with another technology to achieve process intensification, it can also be carried out by leveraging the nonlinearity of thermodynamics in the process scheme. For example, Kathe et al. has reported the use of a modular-reactor chemical looping scheme for syngas generation where multiple reactors operating in parallel allows ~23% reduction in the natural gas consumption as compared to autothermal reforming [119]. Such a significant reduction in the natural gas requirement translates to a lower operating cost, thereby realizing the aim of process intensification and optimization.

Apart from process intensification, the commercial readiness of chemical looping technology heavily depends on the successful design and development of the looping media, which should sustain extreme reaction conditions for a long duration without any loss in performance. Research is being actively conducted to design such materials that maintain their physical and chemical integrity for thousands of cycles [40]. The use of nanoparticles in chemical looping is gaining considerable interest due to their unique properties, where the small average coordination number of the metal atoms in the looping media allows faster adsorption and activation of the reacting gas molecule [121]. This enables fast reaction kinetics even at relatively low temperatures, thus expanding the operating range of the process [122].

There are two important aspects of the commercial preparedness of chemical looping technology for gas separation and product generation – process efficiency and cost, and sustainability. The chemical looping processes can be optimized to increase product yield while controlling the performance of the looping media carriers to render the overall process more efficient and economically viable [123]. Apart from it, the chemical looping process can be more sustainable in operation as it offers the additional flexibility of being conjointly used with the other technologies. For example, a pure CO_2 stream exiting the chemical looping combustion process can be used as a feedstock for algal cultivation, where the algae can be used for biodiesel synthesis [124]. This strategy allows the minimization of CO_2 emissions while increasing the profitability of the process from biofuel production. Another approach that can be employed is the incorporation of CO_2 within the chemical looping process itself. CO_2 and coal can be co-injected into the reducer reactor for syngas generation, where the integration of this chemical looping-assisted syngas generation plant with a commercial acetic acid plant can be operated as a CO_2-negative process, thereby yielding a higher CO_2 consumption as compared to its generation [125]. Equivalently, the steam-CO_2 mixture can be used to oxidize the reduced oxygen carriers to produce additional syngas, thereby increasing the product yield per mol of fuel input while making the overall process more sustainable [126]. The reduction of looping media (especially in combustion/gasification/reforming applications) is typically highly endothermic in nature and external heat needs to be provided to sustain the reaction (if not operated adiabatically). Providing endothermic heat requires the burning of fossil fuels in furnaces, which requires an additional CO_2 capture mechanism. This renders the system less environmentally sustainable. The use of alternate heat forms such as solar and microwave heating can be explored, which help reduce the dependence on conventional heat sources. The use of renewable energy sources such as biomass, biogas, and landfill gases should also be encouraged for power generation and chemicals production through chemical looping as it gives higher efficiencies at relatively low-cost requirement [127]. It is important to realize that to achieve the desired sustainability goals using chemical looping, the looping media must be developed along with process development. One of the major challenges in chemical looping is particle attrition and the loss of reactivity of the looping media, which if occurs, a makeup of particles in the reactor is needed [128, 129]. It is thus important to understand the intrinsic reaction mechanism and its effect on the physical integrity of the looping particles to allow their long life, which, in turn, benefits the overall process economics.

The challenge for the chemical looping applications is also on their adoption in the industry. Chemical looping is a new technology as compared to other means of gas separation currently available. However, the challenge is not in the technology's ability to reshape the chemical processing industry, but rather in conducting adequate sub-pilot and pilot scale testing to substantiate the technology's enhanced capability to separate gases with certainty. The process analyses and optimal process system configurations for various chemical looping reaction applications remain to be further probed.

The challenges associated with CO_2 capture using chemical looping are based mainly on the ease with which the technology can be applied in industry. As such, the plan for retrofitting to the existing industrial facility, for example, chemical or electricity production, can be considered. However, even within the same class of plants, factors such as age,

geographical location, available space, governmental regulations, and climate may make retrofitting difficult. For a new facility built using chemical looping for complete CO_2 capture, the challenge can be the handling of the large quantity of CO_2 for end usage or storage. In the case of calcium looping, trends in using novel sorbents instead of limestone-based sorbents do not exhibit strong economic incentives owing to the lack of scale-up activities after successful lab-scale experiments. Some testing does not fully parallel operating conditions that are consistent with industrial practice such as flue gas contaminant conditions and calcination environments. Nevertheless, calcium looping is a simple and efficient technology, and is known to be more energy-efficient and cost-effective than the existing post-combustion amine scrubbing technologies and membrane-based separation. In calcium looping, the loss of reactivity in sorbents is commonly encountered, which is typically evolved after a few CO_2 capture cycles. Integrating calcium looping with existing processes such as cement manufacturing can provide synergy for the calcium looping process operation.

CLAS is a promising approach for oxygen production. The reduction of operating costs can be made if the system is optimized. The challenges that need to be addressed include how to maintain the correct partial pressure of oxygen in each reactor to increase the throughput and hence reducing the energy waste. The further the partial pressures drift from equilibrium, the more expensive the operation becomes as the efficiency declines. Also, the production of an O_2 stream with high yields is a challenge that needs to be investigated further as the current O_2 yield levels remain low. If the use of recycled CO_2 is used as part of the purge gas in the reducer reactor, the downstream equipment needs to be sized accordingly, which may make the footprint too large to have CLAS as a feasible option without a complete plant overhaul.

The application of a chemical looping scheme for H_2S separation needs to be economically feasible, which is directly related to the conversion and selectivity of H_2S in the incoming stream. Further advancements in the looping media required for selectively separating H_2S and converting it to H_2 are needed to ensure the attractiveness of the technology for industrial use.

5.4 Conclusion

An increase in the demand for energy, various chemicals, and petrochemical products have led to significant growth in the development of new gas separation technologies. The aim of these technologies is to produce pure product streams with minimum energy utilization and maximum benefit–cost ratio while operating under the constraint of environmental regulations. This is being achieved by means of discovering new processes and materials, and their synergy being explored to allow large-scale gas separation. Technologies such as amine scrubbing, membrane separation, adsorption-assisted separation, and cryogenic distillation have been developed to separate gas components in streams originating from different sources and containing varied components. Compared to these technologies, gas separation using chemical looping offers a different perspective while achieving attractive separation efficiency. It makes use of a multi-reactor system where pure gas streams are generated in each reactor, thereby leading to in situ separation. The efficiency of separation is achieved through the synergy of multiple factors including operating temperature,

pressure, the ratio of feed gas to the looping media flowrate in the system, and co-injection of supplementary gas feed to further enhance thermodynamic conversion. Apart from these factors, the design and performance of the reactor system play an important role in rendering a high efficiency of the process operation. Separation of gases like CO_2, air separation, H_2S removal, and post-combustion CO_2 capture has been demonstrated using the chemical looping technology along with extensive process analysis based on industrial operating condition requirement. Active research is in progress toward developing looping media for various chemical looping-assisted separation processes that are of high reactivity and recyclability with good physical strength, inexpensive in materials used and synthesis methods, and disposable in an environmentally friendly manner. The advantage offered by novel looping materials coupled with novel reactor design strategies for chemical looping technology can provide an economically and technologically attractive alternative to conventional approaches for industrial gas separation.

References

1 Derry, T.K. and Williams, T. (1960). *A Short History of Technology from the Earliest Times to A.D. 1900*. New York: Dover Publications, Inc.

2 Chemical Industry Spotlight | SelectUSA.gov https://www.selectusa.gov/chemical-industry-united-states

3 Outlook EIAAE (2019). Technical report, US Energy Information Administration. https://www.eia.gov/outlooks/aeo/pdf/aeo2019.pdf.

4 Ritter, S.K. (2017). Putting distillation out of business in the chemical industry. *Chemical and Engineering News* 95 (25): 18–21.

5 Council NR, others (1999). *Separation Technologies for the Industries of the Future*, vol. 487. National Academies Press.

6 US Department of Energy (2019). Frequently Asked Questions (FAQs) – U.S. Energy Information Administration (EIA) EIA. https://www.eia.gov/tools/faqs/faq.php?id=427&t=3

7 NASA (2019). Graphic: the relentless rise of carbon dioxide – climate change: vital signs of the planet. National Oceanic and Atmospheric Administration. https://climate.nasa.gov/climate_resources/24/graphic-the-relentless-rise-of-carbon-dioxide/.

8 Yang, S., Lei, L., Zeng, Z. et al. (2019). An assessment of anthropogenic CO_2 emissions by satellite-based observations in China. *Sensors* 19 (5): 1118.

9 Aiche (2019). What is CCUS? | AIChE, 1–2. https://www.aiche.org/ccusnetwork/what-ccus.

10 Koytsoumpa, E.I., Bergins, C., and Kakaras, E. (2018). The CO_2 economy: review of CO_2 capture and reuse technologies. *Journal of Supercritical Fluids* 132: 3–16.

11 Metz, B., Davidson, O., de Coninck, H. et al. (2005). Carbon Dioxide Capture and Storage: Summary for Policymakers. IPCC Special Report.

12 Figueroa, J.D., Fout, T., Plasynski, S. et al. (2008). Advances in CO_2 capture technology-the U.S. Department of Energy's Carbon Sequestration Program. *International Journal of Greenhouse Gas Control* 2 (1): 9–20.

13 Fan, L.-S., Zeng, L., Wang, W., and Luo, S. (2012). Chemical looping processes for CO_2 capture and carbonaceous fuel conversion-prospect and opportunity. *Energy and Environmental Science* 5 (6): 7254–7280.

14 Fan, L.-S. (2017). *Chemical Looping Partial Oxidation: Gasification, Reforming, and Chemical Syntheses*. Cambridge University Press.

15 Zhao, X., Zhou, H., Sikarwar, V.S. et al. (2017). Biomass-based chemical looping technologies: the good, the bad and the future. *Energy and Environmental Science* 10 (9): 1885–1910.

16 Fan, L.-S. (2011). *Chemical Looping Systems for Fossil Energy Conversions*. Wiley.

17 Lane, H. (1913). Process for the production of hydrogen. US Patent 1,078,686.

18 Messerschmitt, A. (1910) Process of producing hydrogen. US Patent 971,206.

19 Lewis, W.K. and Gilliland, E.R. (1950). Conversion of hydrocarbons with suspended catalyst. US Patent 2,498,088.

20 Lewis, W.K. and Gilliland, E.R. (1954). Production of pure carbon dioxide. US Patent 2,665,972.

21 Tarman, P.B. and Biljetina, R. (1978). *Steam – Iron Process for Hydrogen Production*. Chicago, IL, USA: Institute of Gas Technology.

22 Dobbyn, R.C., Ondik, H.M., Willard, W.A. et al. (1978). Evaluation of the Performance of Materials and Components Used in the CO/Sub 2/Acceptor Process Gasification Pilot Plant. Final Report. Continental Oil Co., Liberty, PA, USA.

23 Keller, G.E. and Bhasin, M.M. (1982). Synthesis of ethylene via oxidative coupling of methane. I. Determination of active catalysts. *Journal of Catalysis* 73 (1): 9–19.

24 Neal, L.M., Yusuf, S., Sofranko, J.A., and Li, F. (2016). Oxidative dehydrogenation of ethane: a chemical looping approach. *Energy Technology* 4 (10): 1200–1208.

25 Contractor, R.M. (1999). Dupont's CFB technology for maleic anhydride. *Chemical Engineering Science* 54 (22): 5627–5632.

26 Patience, G.S. and Bockrath, R.E. (2010). Butane oxidation process development in a circulating fluidized bed. *Applied Catalysis A: General* 376 (1–2): 4–12.

27 Zeng, L., Cheng, Z., Fan, J.A. et al. (2018). Metal oxide redox chemistry for chemical looping processes. *Nature Reviews Chemistry* 2 (11): 349–364.

28 Sridhar, D., Tong, A., Kim, H. et al. (2012). Syngas chemical looping process: design and construction of a 25 kW th subpilot unit. *Energy and Fuels* 26 (4): 2292–2302.

29 Fan, L.-S., Zeng, L., and Luo, S. (2015). Chemical-looping technology platform. *AICHE Journal* 61 (1): 2–22.

30 Velazques-Vargas, L.G., Devault, D.J., Flynn, T.J. et al. (2014). Techno-economic analysis of a 550 MWe atmospheric iron-based coal-direct chemical looping process. 3rd International Conference on Chemical Looping.

31 Sandvik, P., Wang, W., Kathe, M. et al. (2019). Operating strategy of chemical looping systems with varied reducer and combustor pressures. *Industrial & Engineering Chemistry Research* 58 (13): 5228–5235.

32 Zhu, X., Imtiaz, Q., Donat, F. et al. (2020). Chemical looping beyond combustion-a perspective. *Energy and Environmental Science* 13 (3): 772–804.

33 Cheng, Z., Qin, L., Guo, M. et al. (2016). Oxygen vacancy promoted methane partial oxidation over iron oxide oxygen carriers in the chemical looping process. *Physical Chemistry Chemical Physics* 18 (47): 32418–32428.

34 Kathe, M.V., Empfield, A., Na, J. et al. (2016). Hydrogen production from natural gas using an iron-based chemical looping technology: thermodynamic simulations and process system analysis. *Applied Energy* 165: 183–201.

35 Shah, V., Mohapatra, P., and Fan, L.-S. (2020). Thermodynamic and process analyses of syngas production using chemical looping reforming assisted by flexible dicalcium ferrite-based oxygen carrier regeneration. *Energy and Fuels* 34 (5): 6490–6500.

36 Luo, S., Zeng, L., Xu, D. et al. (2014). Shale gas-to-syngas chemical looping process for stable shale gas conversion to high purity syngas with a H_2: CO ratio of 2:1. *Energy & Environmental Science* 7 (12): 4104–4117.

37 Shah, V., Joshi, R., and Fan, L.-S. (2020). Thermodynamic investigation of process enhancement in chemical looping reforming of methane through modified Ca–Fe oxygen carrier utilization. *Industrial & Engineering Chemistry Research* 59 (35): 15531–15541.

38 Qin, L., Cheng, Z., Guo, M. et al. (2017). Impact of 1% lanthanum dopant on carbonaceous fuel redox reactions with an iron-based oxygen carrier in chemical looping processes. *ACS Energy Letters* 2 (1): 70–74.

39 Qin, L., Guo, M., Liu, Y. et al. (2018). Enhanced methane conversion in chemical looping partial oxidation systems using a copper doping modification. *Applied Catalysis B: Environmental* 235: 143–149.

40 Chung, C., Qin, L., Shah, V., and Fan, L.-S. (2017). Chemically and physically robust, commercially-viable iron-based composite oxygen carriers sustainable over 3000 redox cycles at high temperatures for chemical looping applications. *Energy & Environmental Science* 10 (11): 2318–2323.

41 Kong, F., Li, C., Zhang, Y. et al. (2020). Hydrogen production from natural gas using an iron-based chemical looping technology: process modeling, heat integration, and exergy analysis. *Energy Technology* 8 (8): 1900377.

42 Zeng, L., Kathe, M.V., Chung, E.Y., and Fan, L.-S. (2012). Some remarks on direct solid fuel combustion using chemical looping processes. *Current Opinion in Chemical Engineering* 1 (3): 290–295.

43 Joshi, R.K., Shah, V., and Fan, L.-S. (2020). Acetic acid production using calcium ferrite-assisted chemical looping gasification of petroleum coke with in situ sulfur capture. *Energy & Fuels* 34 (12): 16560–16571.

44 Abanades, S. and Le Gal, A. (2012). CO_2 splitting by thermo-chemical looping based on $Zr_xCe_{1-x}O_2$ oxygen carriers for synthetic fuel generation. *Fuel* 102: 180–186.

45 Cheng, Z., Baser, D.S., Nadgouda, S.G. et al. (2018). C2 selectivity enhancement in chemical looping oxidative coupling of methane over a Mg-Mn composite oxygen carrier by Li-doping-induced oxygen vacancies. *ACS Energy Letters* 3 (7): 1730–1736.

46 Phalak, N., Ramkumar, S., Deshpande, N. et al. (2012). Calcium looping process for clean coal conversion: design and operation of the subpilot-scale carbonator. *Industrial & Engineering Chemistry Research* 51 (30): 9938–9944.

47 Michalsky, R., Avram, A.M., Peterson, B.A. et al. (2015). Chemical looping of metal nitride catalysts: low-pressure ammonia synthesis for energy storage. *Chemical Science* 6 (7): 3965–3974.

48 Reddy, S., Nadgouda, S.G., Tong, A., and Fan, L.-S. (2019). Metal sulfide-based process analysis for hydrogen generation from hydrogen sulfide conversion. *International Journal of Hydrogen Energy* 44 (39): 21336–21350.

49 Speight, J.G. (2018). *Natural Gas: A Basic Handbook*. Gulf Professional Publishing.

50 Rao, A.B. and Rubin, E.S. (2002). A technical, economic, and environmental assessment of amine-based CO_2 capture technology for power plant greenhouse gas control. *Environmental Science & Technology* 36 (20): 4467–4475.

51 Park, C., Hsieh, T.L., Pottimurthy, Y. et al. (2019). Design and operations of a 15 kW_{th} subpilot unit for the methane-to-syngas chemical looping process with CO_2 utilization. *Industrial & Engineering Chemistry Research* 59 (15): 6886–6899.

52 Chen, Y.Y., Nadgouda, S., Shah, V. et al. (2020). Oxidation kinetic modelling of Fe-based oxygen carriers for chemical looping applications: impact of the topochemical effect. *Applied Energy* 279: 115701.

53 Luis, F., Garci, F., Gayán, P. et al. (2007). Operation of a 10kWth chemical-looping combustor during 200h with a $CuO–Al_2O_3$ oxygen carrier. *Fuel* 86 (7–8): 1036–1045.

54 Crabtree, G.W., Dresselhaus, M.S., and Buchanan, M.V. (2004). The hydrogen economy. *Physics Today* 57 (12): 39–44.

55 Industrial ammonia production emits more CO_2 than any other chemical-making reaction. https://cen.acs.org/environment/green-chemistry/Industrial-ammonia-production-emits-CO2/97/i24.

56 Schulz, H. (1999). Short history and present trends of Fischer–Tropsch synthesis. *Applied Catalysis A: General* 186 (1–2): 3–12.

57 Hou, S.-S., Chiang, C.-Y., and Lin, T.-H. (2020). Oxy-fuel combustion characteristics of pulverized coal under O_2/recirculated flue gas atmospheres. *Applied Sciences* 10 (4): 1362.

58 Blamey, J., Anthony, E.J., Wang, J., and Fennell, P.S. (2010). The calcium looping cycle for large-scale CO_2 capture. *Progress in Energy and Combustion Science* 36 (2): 260–279.

59 Shimizu, T., Hirama, T., Hosoda, H. et al. (1999). A twin fluid-bed reactor for removal of CO_2 from combustion processes. *Chemical Engineering Research and Design* 77 (1): 62–68.

60 Curran, G.P., Fink, C.E., and Gorin, E. (1967). *CO2 Acceptor Gasification Process: Studies of Acceptor Properties*. ACS Publications.

61 Dean, C.C., Blamey, J., Florin, N.H. et al. (2011). The calcium looping cycle for CO_2 capture from power generation, cement manufacture and hydrogen production. *Chemical Engineering Research and Design* 89 (6): 836–855.

62 Liu, W., An, H., Qin, C. et al. (2012). Performance enhancement of calcium oxide sorbents for cyclic CO_2 capture: a review. *Energy & Fuels* 26 (5): 2751–2767.

63 Yu, F.-C., Phalak, N., Sun, Z., and Fan, L.-S. (2012). Activation strategies for calcium-based sorbents for CO_2 capture: a perspective. *Industrial & Engineering Chemistry Research* 51 (4): 2133–2142.

64 Ortiz, C., Valverde, J.M., Chacartegui, R. et al. (2019). The calcium-looping ($CaCO_3$/CaO) process for thermochemical energy storage in concentrating solar power plants. *Renewable and Sustainable Energy Reviews* 113: 109252.

65 Chen, J., Duan, L., and Sun, Z. (2020). Review on the development of sorbents for calcium looping. *Energy & Fuels* 34 (7): 7806–7836.

66 Huang, L., Zhang, Y., Gao, W. et al. (2017). Alkali carbonate molten salt coated calcium oxide with highly improved carbon dioxide capture capacity. *Energy Technology* 5 (8): 1328–1336.

67 Chen, J., Duan, L., Shi, T. et al. (2019). A facile one-pot synthesis of CaO/CuO hollow microspheres featuring highly porous shells for enhanced CO_2 capture in a combined Ca–Cu looping process via a template-free synthesis approach. *Journal of Materials Chemistry A* 7 (37): 21096–21105.

68 Yan, Y., Wang, K., Clough, P.T., and Anthony, E.J. (2020). Developments in calcium/chemical looping and metal oxide redox cycles for high-temperature thermochemical energy storage: a review. *Fuel Processing Technology* 199: 106280.

69 Chang, M.H., Huang, C.M., Liu, W.H. et al. (2013). Design and experimental investigation of calcium looping process for 3-kWth and 1.9-MWth facilities. *Chemical Engineering & Technology* 36 (9): 1525–1532.

70 Cordero, J.M., Alonso, M., Arias, B., and Abanades, J.C. (2014). Sulfation performance of CaO purges derived from calcium looping CO_2 capture systems. *Energy & Fuels* 28 (2): 1325–1330.

71 Plötz, S., Bayrak, A., Galloy, A. et al. (2012). First carbonate looping experiments with a 1 MWth test facility consisting of two interconnected CFBs. In 21st International Conference on Fluidized Bed Combustion, 421–428.

72 Dieter, H., Hawthorne, C., Zieba, M., and Scheffknecht, G. (2013). Progress in calcium looping post combustion CO_2 capture: successful pilot scale demonstration. *Energy Procedia* 37: 48–56.

73 Wang, W., Ramkumar, S., Li, S. et al. (2010). Subpilot demonstration of the carbonation–calcination reaction (CCR) process: high-temperature CO_2 and sulfur capture from coal-fired power plants. *Industrial & Engineering Chemistry Research* 49 (11): 5094–5101.

74 Hanak, D.P., Anthony, E.J., and Manovic, V. (2015). A review of developments in pilot-plant testing and modelling of calcium looping process for CO_2 capture from power generation systems. *Energy & Environmental Science* 8 (8): 2199–2249.

75 Lu, D.Y., Hughes, R.W., and Anthony, E.J. (2008). Ca-based sorbent looping combustion for CO_2 capture in pilot-scale dual fluidized beds. *Fuel Processing Technology* 89 (12): 1386–1395.

76 Hanak, D., Manovic, V., and Anthony, E.J. (2014). The future of Ca looping–a review of developments. Combustion and CCS Center, Cranfield University, Bedford, United Kingdom.

77 Phalak, N., Wang, W., and Fan, L.-S. (2013). Ca $(OH)_2$-based calcium looping process development at The Ohio State University. *Chemical Engineering & Technology* 36 (9): 1451–1459.

78 Wang, W., Ramkumar, S., and Fan, L.-S. (2013). Energy penalty of CO_2 capture for the carbonation–calcination reaction (CCR) process: parametric effects and comparisons with alternative processes. *Fuel* 104: 561–574.

79 Phalak, N., Deshpande, N., and Fan, L.-S. (2012). Investigation of high-temperature steam hydration of naturally derived calcium oxide for improved carbon dioxide capture capacity over multiple cycles. *Energy & Fuels* 26 (6): 3903–3909.

80 Kerry, F.G. (2007). *Industrial Gas Handbook: Gas Separation and Purification*. CRC Press.

81 Belloni, A. (2008). *Industrial Gases Processing*. Wiley.

82 Castle, W.F. (2002). Air separation and liquefaction: recent developments and prospects for the beginning of the new millennium. *International Journal of Refrigeration* 25 (1): 158–172.

83 Smith, A.R. and Klosek, J. (2001). A review of air separation technologies and their integration with energy conversion processes. *Fuel Processing Technology* 70 (2): 115–134.

84 Moghtaderi, B. (2010). Application of chemical looping concept for air separation at high temperatures. *Energy & Fuels* 24 (1): 190–198.

85 Air Separation Plant Market 2018 Is Estimated to Reach US 58527 Million by 2022 – MarketWatch. https://www.marketwatch.com/amp/story/guid/173f345a-2a0e-41c8-ab43-3a6f8a1823d9.

86 Wilcox, J. (2012). *Carbon Capture*. Springer Science & Business Media.

87 Pfaff, I. and Kather, A. (2009). Comparative thermodynamic analysis and integration issues of CCS steam power plants based on oxy-combustion with cryogenic or membrane based air separation. *Energy Procedia* 1 (1): 495–502.

88 Banaszkiewicz, T., Chorowski, M., and Gizicki, W. (2014). Comparative analysis of cryogenic and PTSA technologies for systems of oxygen production. AIP Conference Proceedings, vol. 1573, No. 1, pp. 1373–1378. American Institutre of Physics.

89 Wang, K., Yu, Q., and Qin, Q. (2013). The thermodynamic method for selecting oxygen carriers used for chemical looping air separation. *Journal of Thermal Analysis and Calorimetry* 112 (2): 747–753.

90 Fu, Y., Liu, Y., Yang, X. et al. (2019). Thermodynamic analysis of molecular simulations of N_2 and O_2 adsorption on zeolites under plateau special conditions. *Applied Surface Science* 480: 868–875.

91 Yang, X., Epiepang, F.E., Li, J. et al. (2019). Sr-LSX zeolite for air separation. *Chemical Engineering Journal* 362: 482–486.

92 Ding, Z., Han, Z., Fu, Q. et al. (2018). Optimization and analysis of the VPSA process for industrial-scale oxygen production. *Adsorption* 24 (5): 499–516.

93 Lewis, W.K., Gilliland, E.R., and Sweeney, M.P. (1951). Gasification of carbon-metal oxides in a fluidized powder bed. *Chemical Engineering Progress* 47 (5): 251–256.

94 Song, H., Shah, K., Doroodchi, E., and Moghtaderi, B. (2014). Development of a Cu–Mg-based oxygen carrier with SiO_2 as a support for chemical looping air separation. *Energy & Fuels* 28 (1): 163–172.

95 Song, H., Shah, K., Doroodchi, E. et al. (2014). Reactivity of Al_2O_3- or SiO_2-supported Cu-, Mn-, and Co-based oxygen carriers for chemical looping air separation. *Energy and Fuels* 28 (2): 1284–1294.

96 Dou, J., Krzystowczyk, E., Mishra, A. et al. (2018). Perovskite promoted mixed cobalt – iron oxides for enhanced chemical looping air separation. *ACS Sustainable Chemistry & Engineering* 6 (11): 15528–15540.

97 Dou, J., Krzystowczyk, E., Wang, X. et al. (2020). A- and B-site codoped $SrFeO_3$ oxygen sorbents for enhanced chemical looping air separation. *ChemSusChem* 13 (2): 385–393.

98 ATSDR – public health statement: hydrogen sulfide carbonyl sulfide. https://www.atsdr.cdc.gov/phs/phs.asp?id=387&tid=67.

99 Huo, D. (2012). The global sour gas problem. Stanford Energy Club.

100 Alkatheri, M., Grandas, R., Betancourt-Torcat, A., and Almansoori, A. (2016). Ultra-sour natural gas sweetening using membranes/amines hybrid systems for recurrent middle east conditions. Abu Dhabi International Petroleum Exhibition & Conference. Society of Petroleum Engineers.

101 https://www.nsenergybusiness.com/features/largest-natural-gas-reserves-middle-east/ (accessed 25 November 2020).

102 Global CCS Institute (2019). The Global Status of CCS: 2019. Australia. https://www.globalccsinstitute.com/wpcontent/uploads/2019/12/GCC_GLOBAL_STATUS_REPORT_2019.pdf.

103 Carter, D.R., Adams, N.J., and others (1979). Hydrogen sulfide in the drilling industry. SPE Deep Drilling and Production Symposium. Society of Petroleum engineers.

104 Guidotti, T.L. (1996). Hydrogen sulphide. *Occupational Medicine* 46 (5): 367–371.

105 Miner, S. (1969). *Air Pollution Aspects of Barium and Its Compounds*. Bethesda, MD: Litton Systems.

106 Linde process plants I. Sulfur process technology. https://www.linde-engineering.com/en/images/Sulfur Process Technology_tcm19-111155.pdf

107 Eow, J.S. (2002). Recovery of sulfur from sour acid gas: a review of the technology. *Environmental Progress* 21 (3): 143–162.

108 Stewart, M.I. (2014). Gas sweetening. In: *Surface Production Operations*, 433–539. Elsevier.

109 Schmidt, R., Cross, J.B., and Latimer, E.G. (2009). Tail-gas cleanup by simultaneous SO_2 and H_2S removal. *Energy and Fuels* 23 (7): 3612–3616.

110 Tavan, Y., Gholami, H., and Shahhosseini, S. (2016). Some notes on process intensification of amine based gas sweetening process for better temperature distribution in contactor to reduce the amount of amine as a result of corrosion and foaming. *Journal of Loss Prevention in the Process Industries* 41: 169–177.

111 Jassim, M.S. (2016). Sensitivity analyses and optimization of a gas sweetening plant for hydrogen sulfide and carbon dioxide capture using methyldiethanolamine solutions. *Journal of Natural Gas Science and Engineering* 36: 175–183.

112 Liu, D., Wang, Q., Wu, J., and Liu, Y. (2019). A review of sorbents for high-temperature hydrogen sulfide removal from hot coal gas. *Environmental Chemistry Letters* 17 (1): 259–276.

113 Moghiman, M., Javadi, S.M., Moghiman, A.R., and Hosseini, S.B. (2010). A numerical study on thermal dissociation of H_2S. *World Academy of Science, Engineering and Technology, International Journal of Mechanical, Aerospace, Industrial, Mechatronic and Manufacturing Engineering* 4 (2): 244–249.

114 Pietro, R.A., Klemeš, J.J., Varbanov, P.S., and Fabiano, B. (2016). A review on hydrogen production from hydrogen sulphide by chemical and photochemical methods. *Journal of Cleaner Production* 136: 72–80.

115 Weiner, J.G. and William, L.C. (1961). Process for production of hydrogen and sulfur. US Patent 2,979,384.

116 Fan, L.-S., Nadgouda, S.G., and Jangam K. Systems, methods and materials for hydrogen sulfide conversion. US Patent US WO2020033500A1.

117 Thursfield, A., Murugan, A., Franca, R., and Metcalfe, I.S. (2012). Chemical looping and oxygen permeable ceramic membranes for hydrogen production–a review. *Energy & Environmental Science* 5 (6): 7421–7459.

118 Zhang, B., Zhang, J., Zhong, Z. et al. (2019). Syngas production and trace element emissions from microwave-assisted chemical looping gasification of heavy metal hyperaccumulators. *Science of the Total Environment* 659: 612–620.

119 Kathe, M., Fryer, C., Sandvik, P. et al. (2017). Modularization strategy for syngas generation in chemical looping methane reforming systems with CO_2 as feedstock. *AICHE Journal* 63 (8): 3343–3360.

120 Medrano, J.A., Potdar, I., Melendez, J. et al. (2018). The membrane-assisted chemical looping reforming concept for efficient H2 production with inherent CO_2 capture: experimental demonstration and model validation. *Applied Energy* 215: 75–86.

121 Liu, Y., Qin, L., Cheng, Z. et al. (2019). Near 100% CO selectivity in nanoscaled iron-based oxygen carriers for chemical looping methane partial oxidation. *Nature Communications* 10 (1): 1–6.

122 Qin, L., Chen, Y.Y., Guo, M. et al. (2021). Driving towards highly selective and coking-resistant natural gas reforming through a hybrid oxygen carrier design. *ChemCatChem* 13 (2): 617–626.

123 Fan, J., Hong, H., and Jin, H. (2018). Power generation based on chemical looping combustion: will it qualify to reduce greenhouse gas emissions from life-cycle assessment? *ACS Sustainable Chemistry & Engineering* 6 (5): 6730–6737.

124 Munguía-López, A.D., Rico-Ramírez, V., and Ponce-Ortega, J.M. (2018). Analysis of carbon policies in the optimal integration of power plants involving chemical looping combustion with algal cultivation systems. *ACS Sustainable Chemistry & Engineering* 6 (4): 5248–5264.

125 Kathe, M., Sandvik, P., Fryer, C. et al. (2018). Coal refining chemical looping systems with CO_2 as a co-feedstock for chemical syntheses. *Energy & Fuels* 32 (2): 1139–1154.

126 Shah, V., Cheng, Z., Baser, D.S. et al. Highly selective production of syngas from chemical looping reforming of methane with CO_2 utilization on MgO-supported calcium ferrite redox materials. *Applied Energy* 282: 116111.

127 Mohamed, U., Zhao, Y., Huang, Y. et al. (2020). Sustainability evaluation of biomass direct gasification using chemical looping technology for power generation w/o CO_2 capture. *Energy* 21: 117904.

128 Kang, Y., Tian, M., Wang, Y. et al. (2018). Silica modified alumina as supports of Fe_2O_3 with high performance in chemical looping combustion of methane. *ACS Sustainable Chemistry & Engineering* 6 (10): 12884–12892.

129 Galinsky, N.L., Huang, Y., Shafiefarhood, A., and Li, F. (2013). Iron oxide with facilitated O^{2-} transport for facile fuel oxidation and CO_2 capture in a chemical looping scheme. *ACS Sustainable Chemistry & Engineering* 1 (3): 364–373.

6

Flow Technologies for Efficient Separations

Nopphon Weeranoppanant[1,2], Chetsada Khositanon[1], Trevor Murray[3], and Andrea Adamo[3]

[1] *Department of Chemical Engineering, Burapha University, Muang, Chonburi, Thailand*
[2] *School of Biomolecular Science and Engineering (BSE), Vidyasirimedhi Institute of Science and Technology (VISTEC), Wangchan, Rayong, Thailand*
[3] *Zaiput Flow Technologies, Waltham, MA, USA*

6.1 Introduction

Flow chemistry is an approach to chemical synthesis and processing that has been rapidly growing in the last two decades because of the many advantages it provides to its practitioners. In this chapter, we review key technologies leveraged for separation in the context of flow chemistry. More specifically, after providing background information about flow chemistry, we then describe the most common separation methods used for the removal of a solute from a process solution: adsorption/scavenger and liquid–liquid extraction (LLE). They are both used either for downstream purification or for in-line purification. There are other flow separation technologies such as nanofiltration (covered in another chapter of this book), evaporator, and distillation (covered elsewhere in the literature) [1, 2].

6.2 Background on Flow Chemistry

Flow chemistry usually refers to an approach where chemicals are reacted as they flow through a reactor. In this context, chemical reactors essentially have a channel-like geometry. A flow chemistry setup typically involves equipment such as pumps, flow meters, reactors, heating or cooling units, separators, mixers, valves, sampling valves, and chemical analysis equipment. The early development of flow chemistry was mostly carried out in microreactors that were made in materials, such as glass, ceramic, silicon, and steel, with advanced fabrication techniques. Later on, mesoscale flow reactors, made of polymer and stainless steel tubing [3], have taken the stage as they are less expensive, simpler to operate, and retain the key advantages brought by the flow-based approach.

Sustainable Separation Engineering: Materials, Techniques and Process Development, Volume 1, First Edition. Edited by Gyorgy Szekely and Dan Zhao.
© 2022 John Wiley & Sons Ltd. Published 2022 by John Wiley & Sons Ltd.

Flow chemistry provides several advantages. Due to the microscale or milli-scale dimension of a reactor channel with a high area–to–volume ratio, reagent mixing and heat transfer are enhanced and more repeatable [4–6]. Therefore, the temperature can be well-controlled due to fast heat absorption or dissipation. Additionally, the small volume typically involved in flow reactors allows for the easy handling of hazardous reactions. As an example, reactions such as nitration, halogenation, and organometallic reactions produce highly reactive or unstable compounds that provide challenges when carried out in traditional glassware. This problem can be solved by performing the reaction in a flow reactor [7, 8]. Additionally, flow chemistry also benefits multistep synthesis as several process steps can be cascaded or "telescoped" with minimal or no exposure of intermediates to air. Flow chemistry facilitates the pressurization of reactors and also the implementation of the automated setup, which can be used for screening reaction conditions [9]. Finally, the flow-based operation is more amenable to scaling than existing batch-based approaches. Most of the commercially available equipment is designed with scale-up being a key characteristic. Thus, similarly performing solutions are available from bench through production scale providing a critical reduction of time and cost to take a new molecule to market. In many scenarios, flow chemistry provides an avenue to intensify processes, and the reduced footprint of the equipment enables new paradigms of portable chemical manufacturing.

Due to the several advantages described above, applications of flow chemistry are rapidly growing and are being deployed in different contexts, to name a few, multiphase reactions (gas–liquid, liquid–liquid, solid–liquid, or solid–gas–liquid) [10–13], flash reactions, biocatalytic reactions [14], and photochemical reactions [15]. The pharmaceutical industry has been one of the key players in the adoption of flow chemistry and flow technologies to address critical process steps where flow provides a compelling technical advantage. In this industry, more generally, flow chemistry is the technical answer to continuous chemical manufacturing that is believed to be a paradigm that offers significant advantages in terms of process robustness, quality, and cost.

Devices for flow separation have been particularly useful for flow chemistry as they allow for in-line purification of a flow stream [1]. In most cases, they enable simple telescoping or integration of a multistep continuous synthesis as impurities, excess reagents, and undesired byproducts can be removed continuously while the remaining stream is delivered to a subsequent flow reaction. They can also permit in situ solvent or catalyst recovery, which thereby enhances the sustainability of a flow reaction. Examples of flow technologies for separation include adsorption/scavenger, LLE, cross-flow microfiltration [16], nanofiltration [17–19], and distillation/evaporation [2, 20, 21]. This chapter will offer an overview of the most common techniques: adsorption/scavenger and LLE.

6.3 Typical Methods for Flow Separation

6.3.1 Adsorption and Scavenger in Flow

A post-synthesis liquid may contain both impurities/reagents and desired products in the same phase. In batch, these components are separated from one another via methods of

crystallization, chromatography, and adsorption. Among these methods, adsorption is the most common one in flow due to its simple and low-cost operation. Different adsorbents can be used such as silica, activated carbons, biochars, chitosan, natural wastes, and metal–organic frameworks. Adsorbents and molecules can have either physical or chemical interaction. These interactions occur at the surface of adsorbents. The physical interaction is a weak attraction such as Van der Waals force while chemical interaction refers to the formation of covalent or ionic bonds between the molecules and adsorbents. The bonds can be reversible or irreversible. Adsorption is suitable for a flow setup since solid adsorbents can be packed into a flow-through column and the liquid is flowed through when separation is needed. Depending on the thermodynamic equilibrium, either desired molecules or impurities will selectively be adsorbed onto the surface. The properties of the adsorbent and carrier solvents are key to selectivity. An efficient adsorbent should also be strong enough to withstand mechanical agitation or shear flow and provide a high interfacial area for a high adsorption capacity.

Silica gel-based cartridges often serve as an in-line flow purification method, particularly in flow-based organic synthesis and biocatalysis. For example [22], the flow synthesis of a natural product O-methylsiphonazole required the preparation of oxazole carboxylic acid, which served as an intermediate as shown in Figure 6.1a. The preparation with 90% yield

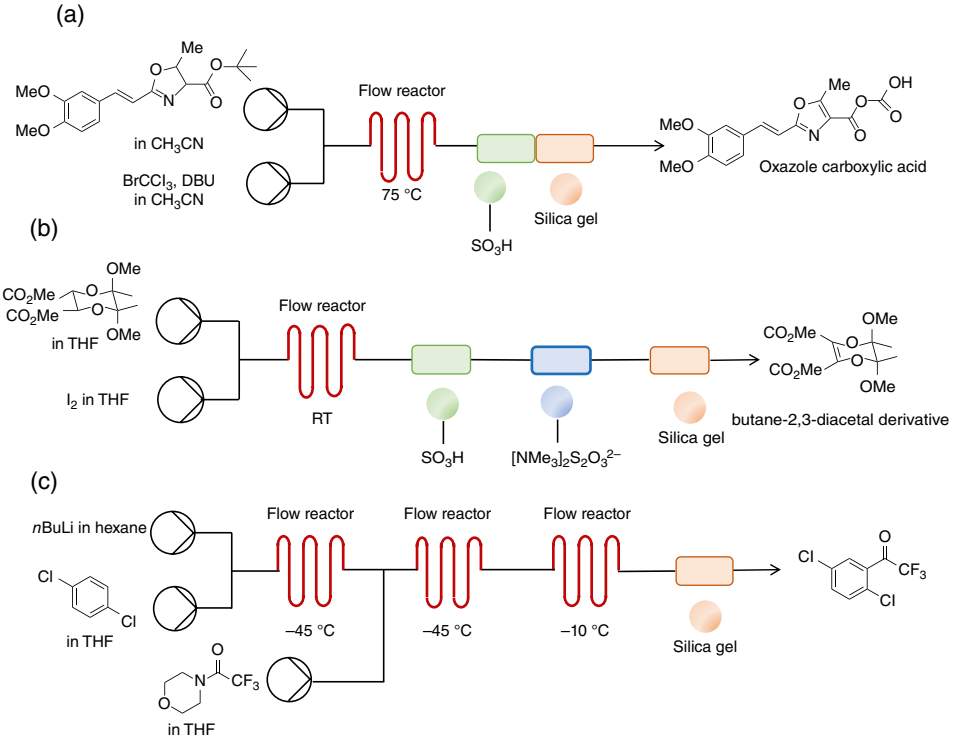

Figure 6.1 Flow adsorption using silica cartridge in different flow synthesis examples: (a) oxazole carboxylic acid synthesis, *Source:* Modified from [22], (b) butane-2,3-diacetal derivative synthesis, *Source:* Modified from [23], (c) trifluoromethyl ketone synthesis, *Source:* Modified from [24].

and high purity was achieved with a silica gel to trap one of the remaining reagents and the byproduct – hydrofluoric acid. In the same group, a silica gel cartridge was used to remove inorganic lithium salts during the synthesis of the butane-2,3-diacetal derivative [23] (Figure 6.1b). Silica is found to be effective and mild enough to prevent side reactions. For instance, it is used to trap morpholine by-product in a telescoped continuous-flow synthesis of trifluoromethyl ketone, an intermediate in Efavirenz preparation [24] (Figure 6.1c).

Silica gel cartridges have been used also in flow biocatalysis. Flow biocatalysis has recently received a lot of attention as a flow setup allows for a higher performance of the biocatalysts as well as enabling cofactor fixation and recycling. Jamison and colleagues implemented a silica gel cartridge for catching amines during the continuous-flow amination of ketones into chiral amines using a packed bed reactor containing the *immobilized E. coli* expressing (R)-selective transaminase and the immobilized cofactor PLP [25] as shown in Figure 6.2. However, silica gels are hydrophilic and can adsorb a wide range of molecules via Van der Waals forces and hydrogen bonds. To increase their adsorption selectivity and capacity, they can be functionalized or modified with clusters and nanoparticles [26, 27].

In addition to silica, functionalized supports can be based on different materials such as polystyrene, carbon, clay, alumina, zeolite, and polymer [28]. Functionalized supports can be packed into a column and used in two main purification strategies: scavenging or catch-and-release. Polymers bound with functional groups or scavenger resins are commonly employed. [29]. Scavenger resins serve to catch specific by-products or excess reagents. In batch, they are added to a mixture and separated by means of filtration. In flow, a flow stream passes through a packed column, eliminating the solid–liquid separation step. For the catch-and-release purification, the desired component, mostly products from the synthesis, binds to the resins. To recover the products, another reactant is added to substitute or release the desired bound product. Scavenger and catch-and-release purifications have been demonstrated in flow, often integrated with a flow synthesis step [30]. Selected examples are shown in Figure 6.3. The Ley group reported the continuous-flow cycloaddition of acetylenes with azides to substituted triazoles [31] (Figure 6.3a). The reaction was based on copper (I)-mediated click chemistry. In this flow synthesis, copper was immobilized onto a support through a weak coordination with amine. Therefore, some leaching of copper was observed. To prevent copper contamination in the product stream, a column of

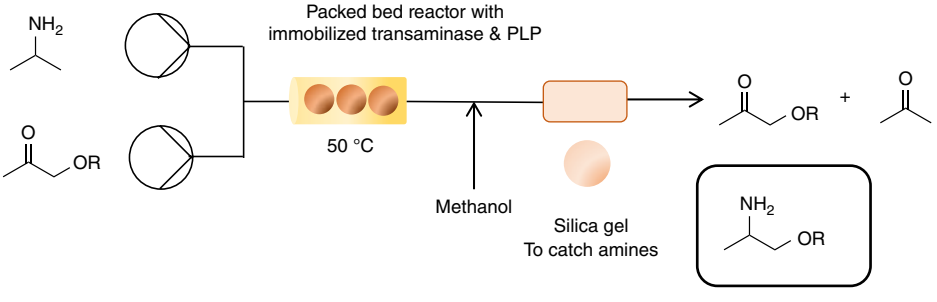

Figure 6.2 Silica gel cartridge was used to catch amine products during the continuous-flow amination of ketones into chiral amines, *Source:* Modified from [25].

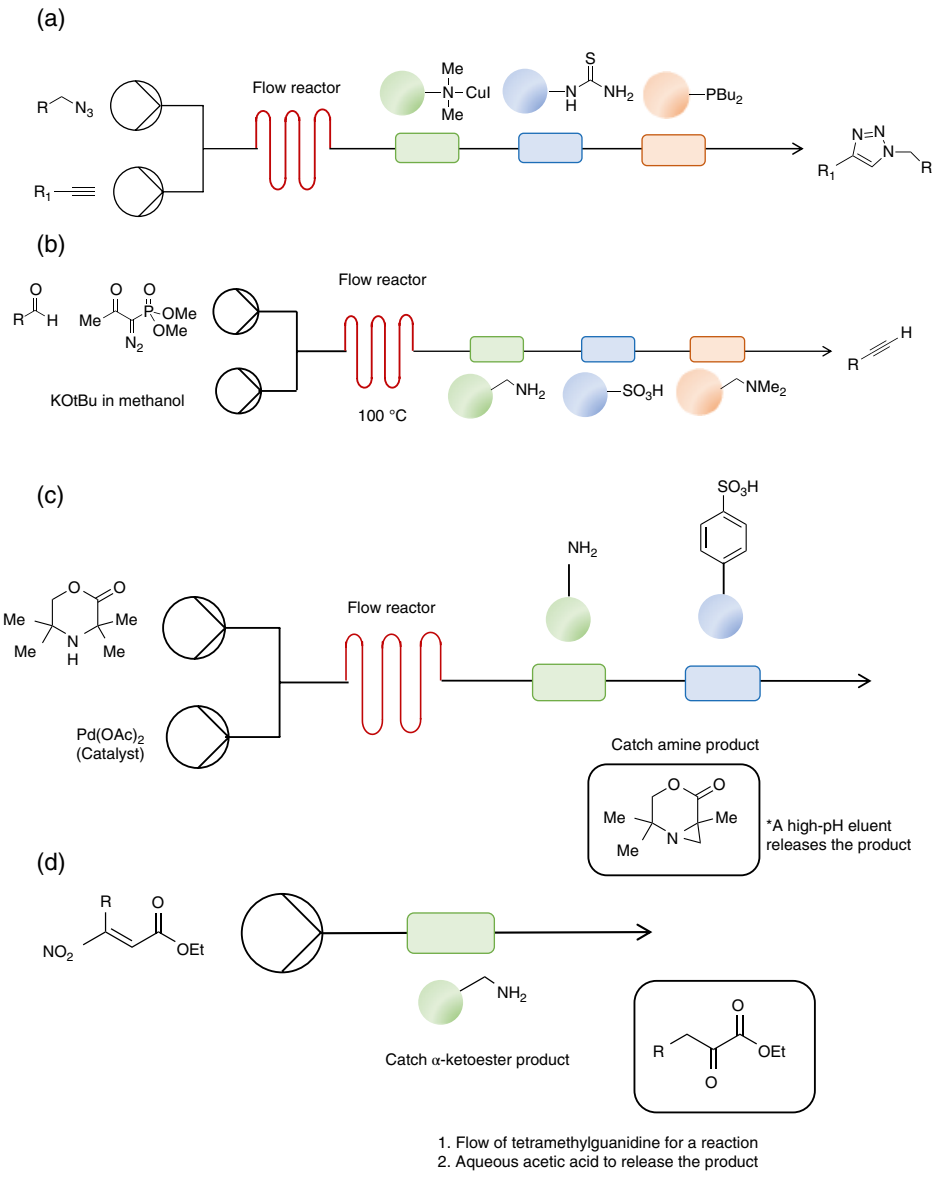

Figure 6.3 Two main flow purification strategies via the use of functionalized supports, along with selected examples: (a) resins to scavenge leached coppers and residual azides, *Source:* Modified from [31], (b) resins to scavenge excess reagents and base/acids, *Source:* Modified from [32], (c) resins to catch the amine product, *Source:* Modified from [33], (d) resins to catch α-ketoester product, *Source:* Modified from [34].

Quadrapure-TU with functionalized thiourea was added to capture the leached copper. Another column with immobilized phosphine on supports was also used to remove any remaining azide. The product stream was found with high purity (>95%). In another work, the same group also reported a series of scavenging columns to remove excess reagents during the flow synthesis of terminal alkynes [32] (Figure 6.3b). The three columns are

Quadrapure-benzylamine resin (QP-BZA) (QP-BZA), Amberlyst-15 with functionalized sulfonic acid (A-15), Amberlyst-21 with functionalized dimethyl amine (A-21) to remove excess aldehydes, bases, and acids, respectively, which eventually gave a pure stream of alkyne products. A similar scheme was used for further synthesis of triazoles to aldehydes and alcohols.

Catch-and-release purification has been used in many organic syntheses. For instance, as shown in Figure 6.3c, a continuous-flow synthesis of aziridines by palladium-catalyzed C-H activation required in-line separation of catalysts and products from other excess reagents [33]. The first column was packed with metal scavengers QuadraSil AP functionalized with a primary amine to capture palladium catalysts. Then, the second column was used to catch the amine product. The product was recovered with an eluent at high pH. Nucleophiles such as carboxylic acids and azides could be added together with the eluent to achieve aziridine ring-opening to obtain functionalized morpholinones. As another example, continuous-flow preparation of α-ketoesters was achieved with a catch-and-release strategy [34] (Figure 6.3d). The column packed with a benzylamine polymer (QP-BZA) was flowed first with the main substrate, nitroolefinic ester, as captured on the polymer. Then, tetramethylguanidine was flowed in a second cycle to produce enamino acid esters. In the following cycle, a washing stream was flowed into a column, and, finally, by an aqueous acetic acid to hydrolyze and release α-ketoester product. This example was shown with a simplified flow scheme without tedious workup.

6.3.2 Continuous Liquid–Liquid Extraction

6.3.2.1 Introduction

A powerful and quite common separation technique in both flow and batch applications is LLE. LLE leverages differences in solubility to separate compounds of interest. It is a common workup strategy in a variety of chemical processes due to its high selectivity and large capacity at relatively small energy consumption. Further, LLE can be performed under ambient temperature conditions, enabling the separation of molecules with similar boiling points, reducing the probability that temperature-sensitive components degrade or react further and allowing for the easy separation of azeotropes [35].

In a general sense, LLE can be regarded as a green separation method based on the typically low energy requirement for mass transfer at large capacities, LLE also is a cost-effective separation technique compared to other techniques such as distillation and crystallization.

For the remainder of the chapter, after providing background theory for LLE, we focus on technologies available for its implementation in a flow chemistry context. Specifically, we'll elucidate first "membrane-based phase separation" which is the technique that has been specifically developed for the implementation of LLE in flow chemistry. We will then review existing continuous technologies which have been implemented or adapted to flow chemistry.

6.3.2.2 Theory of Liquid–Liquid Extraction

LLE requires two separate phases and comprises two fundamental actions: mass transfer and phase separation. For each of a variety of extraction technologies, these functions are

carried out in different manners. However, the overarching goal remains the same. Mass transfer is carried out by mixing the two phases together to enable the diffusion of compounds of interest between the phases.

The mass transfer ends at an equilibrium point which is determined by the capability of each phase to selectively dissolve the compound being extracted. Following the completion of mass transfer, the phases are allowed to separate, bringing with them some portion of the extracted compound. This phase separation is usually reliant on the driving force being gravity (columns and mixer settlers) or density difference (centrifuges). However, new technologies are opening up the possibility for new methods of phase separation for extractions (membranes).

The composition following the extraction must be determined experimentally as thermodynamic models can only approximate the outcomes of the extraction [35] and are unavailable or inaccurate for new molecules. How much of a certain compound moves from the raffinate phase to the extract phase can be represented by the partition (or distribution) coefficient K as indicated in Eq. (6.1) [36]. A partition coefficient is a dimensionless number calculated by dividing the concentration of the solute in the extract phase by that remaining in the raffinate phase. It is important to note that since K is based upon concentration, it is independent of how much of each solvent is used.

$$K = \frac{\text{Concentration of a species in Extract}\left(\frac{\text{g}}{\text{mL}}\right)}{\text{Concentration of a species in Raffinate}\left(\frac{\text{g}}{\text{mL}}\right)} \tag{6.1}$$

The magnitude of K relies upon the relative solubility of the solute of interest in each phase, which is based on intramolecular interactions such as hydrogen bonding, ionic interactions and Van der Waals forces. Hydrogen bonding (H-bonding) appears to have a large effect on deviations from Raoult's law. Solvents are classified into H-donor, H-acceptor, non-H-bonding groups, which provide a quick guide for extraction solvent selection [37]. In many cases, a choice of solvent for extractions is based around maximizing the partition coefficient for the desired compound, which, in turn, minimizes the amount of solvent needed in the extraction (for greenness, cost savings, or concentration for further steps) and/or reduce the number of extractions necessary for removal (for capital cost and system complexity). The degree to which an extract phase can solvate the desired compound is called the capacity of the solvent and is another important factor when determining which solvent is best for a given system.

Similarly, for systems in which the goal is to separate one compound from another, a separation factor α is calculated to determine the effectiveness in the separation of the two compounds as shown in Eq. (6.2). The separation factor (α) is the ratio of the distribution coefficient for each of the two compounds and provides a basis for determining how many extractive steps will be needed to separate the two compounds.

$$\alpha = K_A / K_B \tag{6.2}$$

Where K_A and K_B are the partition coefficients of species A and B in the extraction system, respectively. Similar compounds will have similar partition coefficients and thus a

Table 6.1 Theoretical estimations of the extraction efficiency for different partition coefficients.

Partition coefficient (K)	Extraction efficiency (%*E*)
1	50%
5	83%
10	90%
25	96%
100	99%

separation factor near 1 between them, e.g. enantiomers, alkanes with similar length, or two polar ketone bodies. In order to separate these molecules, multiple extractive steps (e.g. cascading in countercurrent) are necessary. In some cases, extractants are added to form a complex preferentially with one compound than the other [38, 39].

The percentage to which a compound is extracted from its original phase, often termed extraction efficiency, is a key metric when determining the effectiveness of extraction. Under ideal conditions, and when the aqueous and organic phases have an even ratio, the percentage of the compound of interest remaining in the raffinate (%*E*) can be calculated by Eq. (6.3), and when there is a difference in phase ratio, it can be calculated by Eq. (6.4) [40].

$$\%E = \frac{K}{1+K} \tag{6.3}$$

$$\%E = \frac{KV_{\text{Ext}}}{V_{\text{Raf}} + KV_{\text{ext}}} \tag{6.4}$$

Where V_{Ext} and V_{Raf} are volumes of extract and raffinate phases, respectively. Equations (6.3) and (6.4) then lead to the extraction efficiency or %*E*. Low partition coefficients can lead to dramatically reduced product recovery or impurity removal, oftentimes, as seen in Table 6.1. Partition coefficients below 10–20 can leave large amounts of unrecovered product.

In order to hit purity or yield requirements for a given product, many processes will require multiple extractive steps to remove impurities from the product phase. This can be carried out by multiple extractions with the same solvent (i.e. three aqueous washes) or washes with different solvents (i.e. washes of different organics or at different pH). When carrying out *n* extractions with the same solvent in batch, they are often repeated in the same vessel and the amount removed for each extraction is found by compounding the extraction efficiency of a single extraction. Thus, the total amount removed becomes (Eq. 6.5):

$$\text{A ratio of species being extracted} = 1 - \frac{1}{\left(1+\%E\right)^N} \tag{6.5}$$

This repeated extraction can dramatically improve yields for low partition coefficient extractions. However, it brings the downside of introducing excess solvent and diluting the

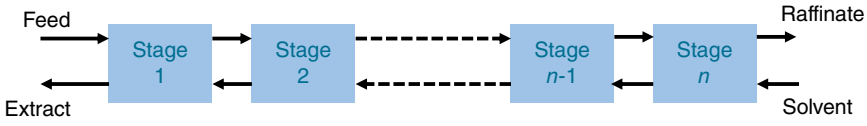

Figure 6.4 A diagram of countercurrent multistage extraction.

product. To overcome this shortcoming of repeated (crosscurrent) extractions, countercurrent extraction is used. Countercurrent extraction uses the same amount of solvent as a single-stage extraction, yet leveraging concentration gradients at each of the stages, can remove significantly more product than in a single-stage extraction. A diagram of this setup is shown in Figure 6.4.

In countercurrent, each stage can be approximated by full phase separation after reaching an extractive equilibrium, although this is not always the case, for example, in extraction columns. The total product extracted for a countercurrent can be derived, but for simplicity, the final formula for an n-stage countercurrent extraction is given below.

$$\text{A ratio of species being extracted} = 1 - \frac{1}{\sum_{n=0}^{N} \%E^n} \tag{6.6}$$

Because of the significantly reduced solvent use in countercurrent extraction, it is a much greener process than crosscurrent extraction. It is favored by many practitioners in the industry for this reason, and is even more important when the solvent cost is taken into consideration.

6.3.2.3 Membrane Separation/Extraction

As discussed in the previous section, LLE is carried out by a first mass transfer step where two immiscible phases are mixed together and a subsequent phase separation step. Mass transfer in flow chemistry applications is typically achieved with passive in-line devices such as micro static mixers [41, 42] or in small diameter tubes, phase segmentation naturally takes place (Taylor flow) increasing the mass transfer rate [43]. Despite their absence of active agitation, the static mixer and microchannels can provide larger interfacial areas (100–1000 m^2/m^3 and 3400–9000 m^2/m^3, respectively) than that of stirred tanks (100–2000 m^2/m^3) [44]. Membrane-based separation offers a way to continuously separate the two immiscible phases as soon as the mass transfer is completed. Membrane-based separation relies on the difference in wetting properties the two phases exhibit onto a porous surface (membrane) [45–48].

As depicted in Figure 6.5, when the two phases enter the device, one preferentially wets the membrane and the other is naturally repelled. Wetting is a natural phenomenon that refers to the ability of a liquid to maintain contact with a solid surface, most typically by spreading over it because of the affinity the liquid has for the solid surface. A common example of wetting is provided by oil that spreads easily on a nonstick-coated frying pan; an example of a non-wetting surface is provided by rainwater that beads up and slides off a winter jacket. In both cases, specific coatings are engineered to provide the desired effect.

This same phenomenon occurs inside the membrane separator. Now, by establishing a small and adequate pressure difference across the membrane (transmembrane pressure),

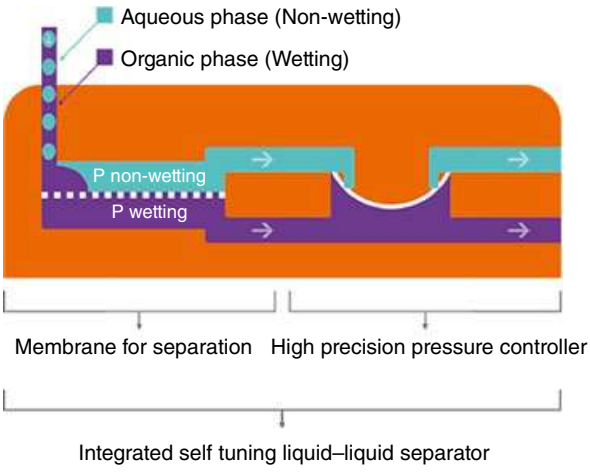

Figure 6.5 A drawing of a membrane separator with an integrated mechanical controller to ensure desired pressure difference across a hydrophobic membrane ($P_{non\text{-}wetting}$ and $P_{wetting}$ refer to fluidic pressure of non-wetting and wetting phases, respectively).

the wetting phase can flow through the membrane thus being separated from the non-wetting phase. In other words, successful and selective phase separation is the result of adequate control of the transmembrane pressure at all times [49]. This accurate control is achieved inside the separator by an integrated mechanical differential pressure controller [47]. The importance of the controller is that separation can be achieved even when flow conditions change (i.e. change of flow rate, change of boundary conditions, etc.), something that is particularly important in flow chemistry.

There are two main failure modes for membrane-based separation: (i) retention, (ii) breakthrough. Retention means that the wetting phase is retained with the non-wetting one. This typically happens if the transmembrane pressure is too low. In other words, there is not enough driving force to push through the membrane all the wetting phase. Breakthrough means that the non-wetting phase also permeates through the membrane with the non-wetting one; this is typically obtained if the transmembrane pressure is too large.

Membrane separation technology began as a lab-scale technology [47, 50]. It was then commercialized by Zaiput Flow Technologies. Zaiput® has also demonstrated a scale-up of the technology across several orders of magnitude, thus providing a full technological solution from lab to production (Figure 6.6).

A key feature of the membrane-based phase separation is the fact that it relies neither on gravity nor on density differences to achieve separation. As a result, the separation of liquid with identical densities can be readily accomplished as well as separation in a gravity-free environment, such as experimentation in space [51]. An important consequence of this gravity-independent separation is the ability to separate emulsions. Following Figure 6.7, emulsions can be of two main types: “water in oil” and “oil in water.” The first type can be effectively separated by leveraging a hydrophobic membrane. In this scenario, the continuous phase is oil or an organic solvent, which can be readily removed by the membrane to result in coalescence of the dispersed (water) phase. For the “oil in water,” conversely the

Figure 6.6 Zaiput® membrane separators for different flow capacities. *Source:* Zaiput.

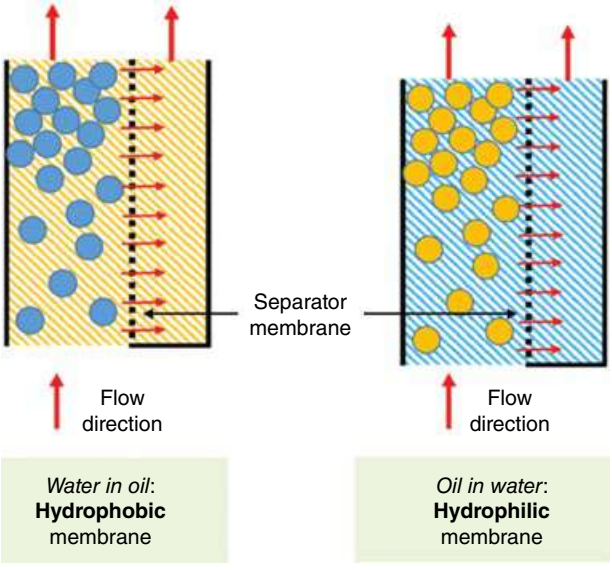

Figure 6.7 Sketch of how a membrane-based separator deals with emulsions. Proper selection of the wetting properties of the membrane ensures removal of the continuous phase and hence high separation efficiency (blue: aqueous phase, yellow: oil phase).

utilization of a hydrophilic membrane provides an avenue to remove water (the dispersing medium), thus forcing the coalescence of the dispersed organic phase.

The ability to break emulsion continuously is an important feature in the context of industrial chemical processing. As a matter of fact, emulsified two-phase systems can waste hours or days and a great deal of effort is spent in trying to optimize LLE in a way that is fast to separate by gravity.

Another important feature of membrane-based separation is its rather small internal volume, typically by one or two orders of magnitude than any other existing approach. This feature carries important consequences from a process chemistry standpoint in flow systems. First, the smaller the internal volume, the smaller is the time needed for the chemical process to reach a steady state. This is important when processing expensive materials or in a laboratory setting. Small internal volume has also a positive advantage on residence time distribution and is of great aid to the chemist in cases where fast quench and separation is needed to address unstable compounds. Finally, a small internal volume, without headspace, provides advantages for all chemical processes that have associated safety concerns (i.e. explosive materials and aggressive chemicals). In this context, several examples of dangerous chemistries have been published in the literature leveraging membrane-based phase separation [52, 53].

An additional feature of membrane-based separators is their modularity. Each unit is a standalone device and several units can be used together to achieve specific purposes. The first consequence of modularity is the fact that a separator provides a theoretical stage of extraction. This means that an LLE carried out with a membrane separator provides practically theoretical efficiency. The reason for this high performance is that mass transfer in flow is effective to reach equilibrium and the separator then readily separates the mixture.

When one extraction step is not sufficient to achieve the desired product removal, several devices can be deployed for a multistage operation, which can be done in both cross-current or countercurrent setups.

Figure 6.8 shows a process diagram of a five-stage countercurrent extraction arranged with the membrane separators. All the advantages of the device are retained. Hence, this setup is scalable and because of the small internal volume of the separators, it provides a minimal holdup volume (one to two orders of magnitude less than any other technology). This latter feature together with the scalability down to a small scale provides a powerful platform to collect real data in the lab with a rather complex extraction system.

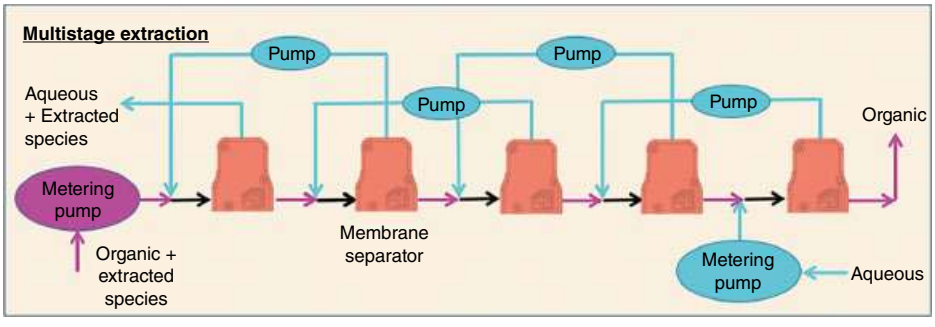

Figure 6.8 A platform of countercurrent extraction (five-stage) enabled by membrane separators.

Characterization of the countercurrent-current multistage extraction platform shows the device provide theoretical efficiency [40]. In this work, model extraction systems (e.g. extraction of acetic acid from water using ethyl acetate) were used to validate that each physical stage of the platform reaches an equilibrium stage. The experimental data matched well with the data assuming equilibrium in all stages (i.e. extraction efficiency = 100%), verifying a high-extraction efficiency of the platform.

Membrane-based separation technology has been utilized in many papers that cover a rather wide range of chemistries such as pharmaceutical ingredient production [50, 54–56], organic reactions [57–59], and nanomaterial synthesis [60–62]. The scalability of the technology is a critical feature for industrial applications, together with the ability to separate emulsions. As an example, [63] provide an example where a 3-stage countercurrent extraction was carried out to both purify the product of a biphasic alcohol oxidation reaction and recover the phase transfer catalyst used. A scale-up of the developed process showed a 650x from low flow rates used the lab-scale devices to the pilot plant size. Importantly, in this separation, the gravity separation of the two phases (water and benzaldehyde) with the presence of a phase transfer catalyst was a very slow gravity separation (1.04 g/mL vs. 1.01 g/mL) taking 19 hours to gravity separate. The membrane-based technology was able to easily separate these two phases before extraction, enabling a quick, continuous process.

6.3.2.4 Mixer Settlers

Mixer settlers are one of the more traditional methods of extraction for both single and multistage extraction. Each extractive stage consists of a mixing section followed by a settling tank to allow for phase separation. In the mixing section, an impeller is used to promote mass transfer between the two phases and, if designed properly, should enable the two phases to come to an extractive equilibrium, making this an efficient extraction technology. As depicted in Figure 6.9, following the mass transfer, the two phases flow into a

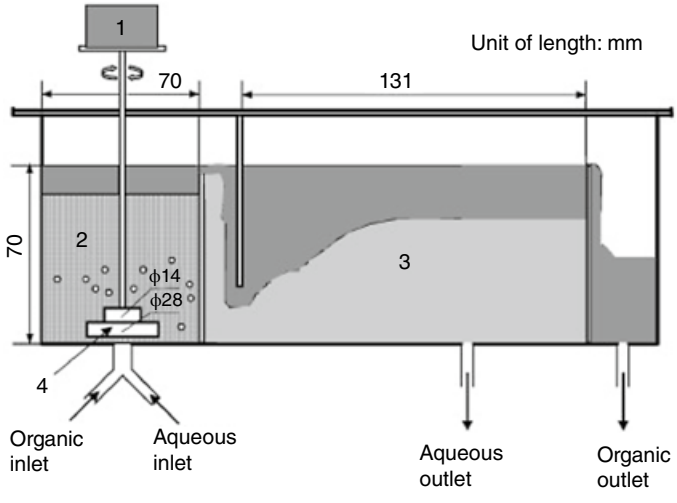

Figure 6.9 An example of mixer-settler (1) agitation motor, (2) mixing chamber, (3) settling chamber, (4) mixing turbine, *Source:* Reprinted from [65]. Copyright 2008, with permission from Elsevier.

large settling tank where they are allowed to gravity separate based on their density differences [64]. The settling tank must be designed to give enough time for the two phases to coalesce and separate before the denser phase passes under a weir to exit the tank while the lighter phase passes over the weir.

Mixer settlers can be set up in countercurrent to improve extraction efficiency as previously described. They are widely used for their simplicity, low cost, and ability to handle solids. Because of the simplicity, the equipment requires minimal instrumentation or maintenance and is easily cleaned. On the other hand, they are not an easily scalable technology as settling times can greatly increase at larger scales and can lead to large setting tanks, taking up large portions of precious plant space. This technology is reliant on significant density differences between the two phases and high interfacial tension to prevent emulsification, otherwise the settling tank size can become unrealistic.

While they are a continuous technology, they do not lend themselves well to flow chemistry because their large internal volume leads to long residence times. This problem is especially compounded when a multistage operation is used. Despite this, a team at Eli-Lilly [66] successfully demonstrated the use of continuous mixer settlers for purification following flow hydrogenation of an API, as shown in Figure 6.10.

The team demonstrated the successful scale-up of the extraction to 22 L vessels each close to 100% stage efficiency for up to 12 kg/day of production. The residence time in the mixers was 60–90 minutes and in the settlers was 90–96 minutes, which points to the need for excess volume to enable clean phase separation.

6.3.2.5 Extraction Columns

Extraction columns are another extremely common countercurrent extraction technology used in industry. In an extraction column, the denser of the two phases enters at the top

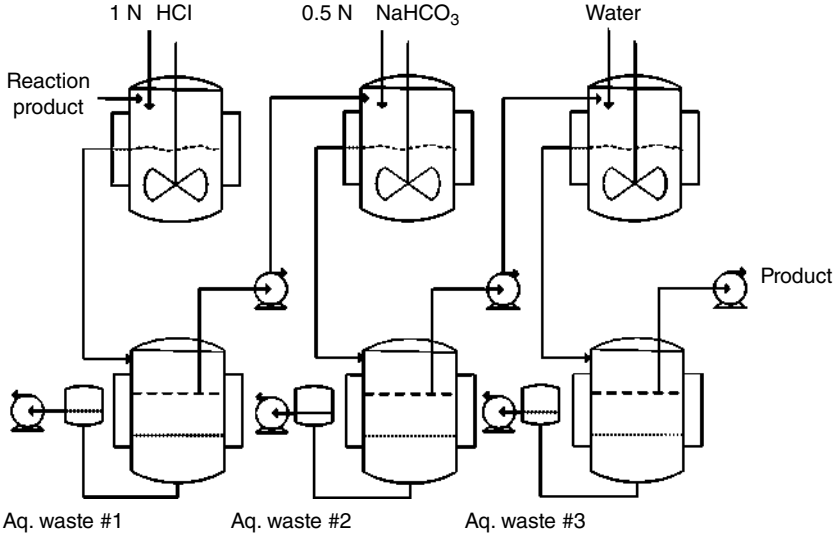

Figure 6.10 A cascade of mixer-settlers for multistage purification. *Source:* Reprinted with permission from [66]. Copyright 2012 American Chemical Society.

and mixes with the less dense phase which flows up through the column. Since an extraction column does not have a distinct number of extractive stages like a mixer settler, the number of stages achieved is back-calculated after an extraction experiment has taken place. Columns also rely on gravity as their driving force of separation and require settling tanks (decanters) at both ends of the column. There are many different styles of extraction columns. However, they can essentially be broken down into two categories: active and passive columns [67]. Each column type takes a different route to promote mass transfer to reduce the height of the column required to achieve a theoretical stage of extraction.

Passive columns, or packed columns, have either free-floating packing material inside or a rigid structure designed to create droplet breakup and promote mass transfer. The lack of moving parts makes these columns easy to use and maintain. However, the lack of active mixing makes them much less efficient than active columns. This simplicity also trickles down to a lower price tag than their more active counterparts.

Active columns use agitation to create droplet breakup and increase mass transfer. This can take one of a few forms, pulsed columns, reciprocating plate columns, and rotating disk contactors [36]. Pulsed columns use piston pumps to vary the inlet flow rate and force two phases through perforated plates in the column, forcing droplet breakup and increasing mass transfer. There are many variations on this design, but they all rely on the principle of a pulsating flow to promote mass transfer. Similar to this, reciprocating plate columns rely not on pulsating the liquid, but instead rapid movement of the plates inside the column. Reciprocating plate columns are advantageous in that they often have much higher throughputs than pulsed columns. Finally, rotating disc columns use an impeller like rotating shaft with discs that are designed to break the dispersed axially into baffles on the side of the column.

Extraction columns are appreciated for their large capacity and suitability for many stages of extraction, which is particularly advantageous when compounds with similar partition coefficients need to be separated. Their capability for large throughputs lends to their use in bulk and commodity chemical manufacturing as designing larger columns can be done relatively easily by increasing the height or diameter of the column. The solvent choice is particularly important for extraction columns since the mixing methods can lead to high amounts of emulsification which greatly reduces the capacity of the column. While columns can be extremely effective for large-scale extractions, they do not scale down well and their large internal volume makes it very challenging to use at laboratory and even pilot scales. As with mixer settlers, the technology is necessarily continuous, but is not commonly used by flow chemistry practitioners because of the large internal volume and the resulting long residence times.

Recent efforts have pushed to miniaturize this technology to make it more amenable to flow systems. As shown in Figure 6.11, Kockmann's group [68] has demonstrated that a 2-meter column with just a 15-mm internal diameter (1.4-liter internal volume) can produce 15 stages of theoretical extraction for flow rates between 5 and 40 mL/min. While the multi-liter internal volume and 2-meter height are still prohibitive for lab-scale chemistry, this work provides an avenue for small pilot extraction development in columns for batch and flow chemists.

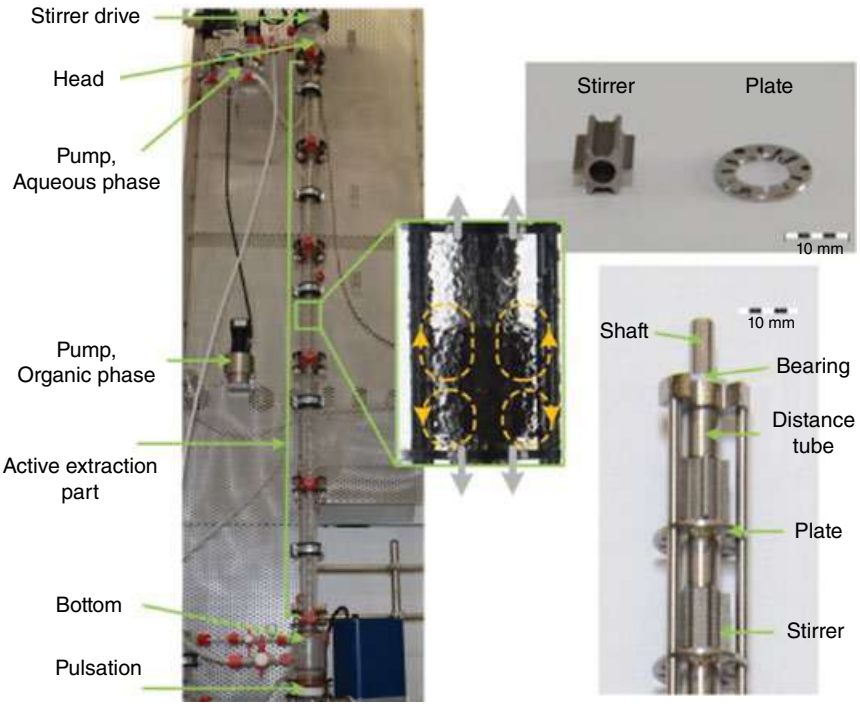

Figure 6.11 A milli-structured, stirred-pulsed column for intensified continuous countercurrent extraction, *Source:* Reprinted with permission from [68].

6.3.3 Extraction Technology Selection for Flow Chemistry

When determining which of the previously mentioned technologies will be best to use for a given process, a flow chemist must consider a variety of factors. The physical properties of the solvent system are important as they can rule out certain technologies. For instance, mixer-settlers are ineffective for systems with small density differences. Beyond this, the flow chemist must consider how many stages of extraction are required for the process and the cost associated with building many stages. Extraction columns are very amenable to large numbers of stages and especially for stage numbers > 10, and they are cost-efficient on a per stage basis. Conversely, centrifugal extractors can be expensive for > 10 stages of operation. Another key consideration examined by flow chemists is the internal volume of the technology as reducing residence time is an important target in designing a continuous process. For this reason, many flow chemists use the membrane separators such as those commercialized by Zaiput® because they are characterized with an internal volume that has orders of magnitude lower than that of other extractive technologies. A mechanically agitated system may be required for highly viscous fluids. The solvent systems containing solids may be best handled by mixer-style extractors while those with emulsions may suit better to the membrane-based extractors. In addition, the extractive technology with discrete physical stages (e.g. centrifugal extractors, Zaiput® membrane separators) can be simpler for scale-up as each of the physical stages can be characterized with percent efficiency

(i.e. its relative performance to the equilibrium extraction). It is also essential to consider the chemical compatibility of the equipment parts as many examples of flow chemistry involve the use of aggressive reagents. Lastly, the size (e.g. dimension and footprint area) of the extractors is also another important design factor. All in all, the selection criteria for the extractive technology can be summarized as follows:

- Physical properties of the fluids
  - Density differences
  - Viscosity
  - Presence of solids
  - Presence of emulsions
- Number of stages required
- Chemical compatibility of the equipment parts
- Internal volume of the extractive equipment
- Scale-up strategies
- Size of the extractive equipment

6.4 Conclusion

This chapter provides an overview of current flow technologies for separation. Although there have been many flow-based techniques, the most common ones are adsorption/scavenger and extraction. Adsorption and scavenger are closely related concepts as they rely on different interactions of different compounds to solid materials. On the other hand, in solvent extraction, different compounds have different solubilities in solvent (liquid). So, they are partitioned in different ratios in immiscible liquid–liquid systems. The solvent extraction consists of two steps: mass transfer (mixing) and phase separation. There are a number of extractive technologies discussed in this chapter including membrane separators/extractors, continuous mixer-settlers, and continuous extraction columns. Users must consider different aspects, such as the physical properties of fluids, the required number of stages, and the internal volume of the extractors, when selecting which types of extractors to use.

References

1 Weeranoppanant, N. and Adamo, A. (2019). In-line purification: a key component to facilitate drug synthesis and process development in medicinal chemistry. *ACS Medicinal Chemistry Letters* 11 (1): 9–15.

2 Bittorf, L., Reichmann, F., Schmalenberg, M. et al. (2019). Equipment and separation units for flow chemistry applications and process development. *Chemical Engineering & Technology* 42 (10): 1985–1995.

3 Jensen, K.F. (2017). Flow chemistry – microreaction technology comes of age. *AIChE Journal* 63 (3): 858–869.

4 Halder, R., Lawal, A., and Damavarapu, R. (2007). Nitration of toluene in a microreactor. *Catalysis Today* 125 (1–2): 74–80.

5 Inoue, T., Schmidt, M.A., and Jensen, K.F. (2007). Microfabricated multiphase reactors for the direct synthesis of hydrogen peroxide from hydrogen and oxygen. *Industrial and Engineering Chemistry Research* 46 (4): 1153–1160.

6 de Mas, N., Günther, A., Schmidt, M.A., and Jensen, K.F. (2009). Increasing productivity of microreactors for fast gas– liquid reactions: the case of direct fluorination of toluene. *Industrial and Engineering Chemistry Research* 48 (3): 1428–1434.

7 Movsisyan, M., Delbeke, E., Berton, J. et al. (2016). Taming hazardous chemistry by continuous flow technology. *Chemical Society Reviews* 45 (18): 4892–4928.

8 Gutmann, B. and Kappe, C.O. (2017). Forbidden chemistries – paths to a sustainable future engaging continuous processing. *Journal of Flow Chemistry.* 7 (3–4): 65–71.

9 Boros, Z., Nagy-Győr, L., Kátai-Fadgyas, K. et al. (2019). Continuous flow production in the final step of vortioxetine synthesis. Piperazine ring formation on a flow platform with a focus on productivity and scalability. *Journal of Flow Chemistry* 9 (2): 101–113.

10 Brzozowski, M., O'Brien, M., Ley, S.V., and Polyzos, A. (2015). Flow chemistry: intelligent processing of gas–liquid transformations using a tube-in-tube reactor. *Accounts of Chemical Research* 48 (2): 349–362.

11 Ramezani, M., Kashfipour, M.A., and Abolhasani, M. (2020). Minireview: flow chemistry studies of high-pressure gas-liquid reactions with carbon monoxide and hydrogen. *Journal of Flow Chemistry* 10 (1): 93–101.

12 Weeranoppanant, N. (2019). Enabling tools for continuous-flow biphasic liquid–liquid reaction. *Reaction Chemistry & Engineering* 4 (2): 235–243.

13 Yang, C., Teixeira, A.R., Shi, Y. et al. (2018). Catalytic hydrogenation of N-4-nitrophenyl nicotinamide in a micro-packed bed reactor. *Green Chemistry* 20 (4): 886–893.

14 Britton, J., Majumdar, S., and Weiss, G.A. (2018). Continuous flow biocatalysis. *Chemical Society Reviews* 47 (15): 5891–5918.

15 Gilmore, K. and Seeberger, P.H. (2014). Continuous flow photochemistry. *The Chemical Record* 14 (3): 410–418.

16 Weeranoppanant, N., Amar, L.I., Tong, E. et al. (2019). Modeling of fouling in cross-flow microfiltration of suspensions. *AIChE Journal* 65 (1): 207–213.

17 Kisszekelyi, P., Alammar, A., Kupai, J. et al. (2019). Asymmetric synthesis with cinchona-decorated cyclodextrin in a continuous-flow membrane reactor. *Journal of Catalysis* 371: 255–261.

18 Fodi, T., Didaskalou, C., Kupai, J. et al. (2017). Nanofiltration-enabled in situ solvent and reagent recycle for sustainable continuous-flow synthesis. *ChemSusChem* 10 (17): 3435.

19 O'Neal, E.J. and Jensen, K.F. (2014). Continuous nanofiltration and recycle of a metathesis catalyst in a microflow system. *ChemCatChem* 6 (10): 3004–3011.

20 Hartman, R.L., Naber, J.R., Buchwald, S.L., and Jensen, K.F. (2010). Multistep microchemical synthesis enabled by microfluidic distillation. *Angewandte Chemie International Edition* 49 (5): 899–903.

21 Deadman, B.J., Battilocchio, C., Sliwinski, E., and Ley, S.V. (2013). A prototype device for evaporation in batch and flow chemical processes. *Green Chemistry* 15 (8): 2050–2055.

22 Pastre, J.C., Browne, D.L., and Ley, S.V. (2013). Flow chemistry syntheses of natural products. *Chemical Society Reviews* 42 (23): 8849–8869.

23 Carter, C.F., Baxendale, I.R., O'Brien, M. et al. (2009). Synthesis of acetal protected building blocks using flow chemistry with flow IR analysis: preparation of butane-2, 3-diacetal tartrates. *Organic and Biomolecular Chemistry* 7 (22): 4594–4597.

24 Correia, C.A., Gilmore, K., McQuade, D.T., and Seeberger, P.H. (2015). A concise flow synthesis of efavirenz. *Angewandte Chemie International Edition* 54 (16): 4945–4948.

25 Andrade, L.H., Kroutil, W., and Jamison, T.F. (2014). Continuous flow synthesis of chiral amines in organic solvents: immobilization of E. coli cells containing both ω-transaminase and PLP. *Organic Letters* 16 (23): 6092–6095.

26 Legrand, A.P. (1998). *The Surface Properties of Silicas*. Wiley.

27 Leboda, R. (1980). The chemical nature of adsorption centers in modified carbon-silica adsorbents prepared by the pyrolysis of alcohols. *Chromatographia* 13 (11): 703–708.

28 Ley, S.V., Baxendale, I.R., Bream, R.N. et al. (2000). Multi-step organic synthesis using solid-supported reagents and scavengers: a new paradigm in chemical library generation. *Journal of the Chemical Society, Perkin Transactions* 1 (23): 3815–4195.

29 Thompson, L.A. (2000). Recent applications of polymer-supported reagents and scavengers in combinatorial, parallel, or multistep synthesis. *Current Opinion in Chemical Biology* 4 (3): 324–337.

30 Seeberger, P.H. (2009). Organic synthesis: scavengers in full flow. *Nature Chemistry* 1 (4): 258.

31 Smith, C.D., Baxendale, I.R., Lanners, S. et al. (2007). [3+2] Cycloaddition of acetylenes with azides to give 1, 4-disubstituted 1, 2, 3-triazoles in a modular flow reactor. *Organic and Biomolecular Chemistry* 5 (10): 1559–1561.

32 Baxendale, I.R., Ley, S.V., Mansfield, A.C., and Smith, C.D. (2009). Multistep synthesis using modular flow reactors: Bestmann–Ohira reagent for the formation of alkynes and triazoles. *Angewandte Chemie International Edition* 121 (22): 4077–4081.

33 Zakrzewski, J., Smalley, A.P., Kabeshov, M.A. et al. (2016). Continuous-flow synthesis and derivatization of aziridines through palladium-catalyzed C (sp3)– H activation. *Angewandte Chemie International Edition* 55 (31): 8878–8883.

34 Palmieri, A., Ley, S.V., Polyzos, A. et al. (2009). Continuous flow based catch and release protocol for the synthesis of α-ketoesters. *Beilstein Journal of Organic Chemistry* 5 (1): 23.

35 Mersmann, A., Kind, M., and Stichlmair, J. (2005). *Thermische Verfahrenstechnik: Grundlagen und Methoden*. Springer.

36 Seader, J.D., Henley, E.J., and Roper, D.K. (1998). *Separation Process Principles*. New York: Wiley.

37 Green, D.W. and Southard, M.Z. (2019). *Perry's Chemical Engineers' Handbook*. McGraw-Hill Education.

38 Kuang, S. and Liao, W. (2018). Progress in the extraction and separation of rare earths and related metals with novel extractants: a review. *Science China Technological Sciences* 61 (9): 1319–1328.

39 Tang, K., Yi, J., Huang, K., and Zhang, G. (2009). Biphasic recognition chiral extraction: a novel method for separation of mandelic acid enantiomers. *Chirality* 21 (3): 390–395.

40 Weeranoppanant, N., Adamo, A., Saparbaiuly, G. et al. (2017). Design of multistage counter-current liquid–liquid extraction for small-scale applications. *Industrial and Engineering Chemistry Research* 56 (14): 4095–4103.

41 Bertsch, A., Heimgartner, S., Cousseau, P., and Renaud, P. (2001). Static micromixers based on large-scale industrial mixer geometry. *Lab on a Chip* 1 (1): 56–60.

42 Schönfeld, F., Hessel, V., and Hofmann, C. (2004). An optimised split-and-recombine micro-mixer with uniform 'chaotic'mixing. *Lab on a Chip* 4 (1): 65–69.

43 Hohmann, L., Kurt, S.K., Soboll, S., and Kockmann, N. (2016). Separation units and equipment for lab-scale process development. *Journal of Flow Chemistry* 6 (3): 181–190.

44 Su, Y., Straathof, N.J., Hessel, V., and Noël, T. (2014). Photochemical transformations accelerated in continuous-flow reactors: basic concepts and applications. *Chemistry – A European Journal* 20 (34): 10562–10589.

45 Kralj, J.G., Sahoo, H.R., and Jensen, K.F. (2007). Integrated continuous microfluidic liquid–liquid extraction. *Lab on a Chip* 7 (2): 256–263.

46 Cervera-Padrell, A.E., Morthensen, S.T., Lewandowski, D.J. et al. (2012). Continuous hydrolysis and liquid–liquid phase separation of an active pharmaceutical ingredient intermediate using a miniscale hydrophobic membrane separator. *Organic Process Research and Development* 16 (5): 888–900.

47 Adamo, A., Heider, P.L., Weeranoppanant, N., and Jensen, K.F. (2013). Membrane-based, liquid–liquid separator with integrated pressure control. *Industrial and Engineering Chemistry Research* 52 (31): 10802–10808.

48 Imbrogno, J., Rogers, L., Thomas, D.A., and Jensen, K.F. (2018). Continuous purification of active pharmaceutical ingredients utilizing polymer membrane surface wettability. *Chemical Communications* 54 (1): 70–73.

49 Yang, L., Weeranoppanant, N., and Jensen, K.F. (2017). Characterization and modeling of the operating curves of membrane microseparators. *Industrial and Engineering Chemistry Research* 56 (42): 12184–12191.

50 Adamo, A., Beingessner, R.L., Behnam, M. et al. (2016). On-demand continuous-flow production of pharmaceuticals in a compact, reconfigurable system. *Science* 352 (6281): 61–67.

51 Adamo, A. (ed.) (2018). Establishing the basis for continuous liquid-liquid separation and extraction in space. Abstracts of Papers of The American Chemical Society. Amer Chemical Soc 1155 16th St, NW, Washington, DC 20036 USA.

52 Glotz, G., Lebl, R., Dallinger, D., and Kappe, C.O. (2017). Integration of bromine and cyanogen bromide generators for the continuous-flow synthesis of cyclic guanidines. *Angewandte Chemie International Edition* 56 (44): 13786–13789.

53 Lehmann, H. (2017). A scalable and safe continuous flow procedure for in-line generation of diazomethane and its precursor MNU. *Green Chemistry* 19 (6): 1449–1453.

54 Zhang, P., Weeranoppanant, N., Thomas, D.A. et al. (2018). Advanced continuous flow platform for on-demand pharmaceutical manufacturing. *Chemistry – A European Journal* 24 (11): 2776–2784.

55 Monbaliu, J.-C.M., Stelzer, T., Revalor, E. et al. (2016). Compact and integrated approach for advanced end-to-end production, purification, and aqueous formulation of lidocaine hydrochloride. *Organic Process Research and Development* 20 (7): 1347–1353.

56 Dai, C., Snead, D.R., Zhang, P., and Jamison, T.F. (2015). Continuous-flow synthesis and purification of atropine with sequential in-line separations of structurally similar impurities. *Journal of Flow Chemistry* 5 (3): 133–138.

57 Govaerts, S., Nyuchev, A., and Noel, T. (2020). Pushing the boundaries of C–H bond functionalization chemistry using flow technology. *Journal of Flow Chemistry* 10 (1): 13–71.

58 Sheeran, J.W., Campbell, K., Breen, C.P. et al. (2020). Scalable on-demand production of purified diazomethane suitable for sensitive catalytic reactions. *Organic Process Research and Development* 25: 522–528.

59 Miller, S.J., Ishitani, H., Furiya, Y., and Kobayashi, S. (2021). High-throughput synthesis of (S)-α-phellandrene through three-step sequential continuous-flow reactions. *Organic Process Research and Development* 25 (2): 192–198.

60 Shen, Y., Weeranoppanant, N., Xie, L. et al. (2017). Multistage extraction platform for highly efficient and fully continuous purification of nanoparticles. *Nanoscale* 9 (23): 7703–7707.

61 Khositanon, C., Adpakpang, K., Bureekaew, S., and Weeranoppanant, N. (2020). Continuous-flow purification of silver nanoparticles and its integration with flow synthesis. *Journal of Flow Chemistry* 10 (1): 353–362.

62 Chow, E., Raguse, B., Della Gaspera, E. et al. (2020). Flow-controlled synthesis of gold nanoparticles in a biphasic system with inline liquid–liquid separation. *Reaction Chemistry & Engineering* 5 (2): 356–366.

63 Peer, M., Weeranoppanant, N., Adamo, A. et al. (2016). Biphasic catalytic hydrogen peroxide oxidation of alcohols in flow: scale-up and extraction. *Organic Process Research and Development* 20 (9): 1677–1685.

64 Law, J.D. and Todd, T.A. (2008). *Liquid-Liquid Extraction Equipment*. Idaho National Laboratory (INL).

65 Tanaka, M., Huang, Y., Yahagi, T. et al. (2008). Solvent extraction recovery of nickel from spent electroless nickel plating baths by a mixer-settler extractor. *Separation and Purification Technology* 62 (1): 97–102.

66 Johnson, M.D., May, S.A., Calvin, J.R. et al. (2012). Development and scale-up of a continuous, high-pressure, asymmetric hydrogenation reaction, workup, and isolation. *Organic Process Research and Development* 16 (5): 1017–1038.

67 McCabe, W.L., Smith, J.C., and Harriott, P. (1993). *Unit Operations of Chemical Engineering*. New York: McGraw-Hill.

68 Holbach, A., Çalışkan, E., Lee, H.-S., and Kockmann, N. (2014). Process intensification in small scale extraction columns for counter-current operations. *Chemical Engineering and Processing Process Intensification* 80: 21–28.

7

Sustainable Features of Centrifugal Partition Chromatography

Gergő Dargó and Árpád Könczöl

RotaChrom Technologies LLC, Dabas, Hungary

7.1 Introduction

Over the past two decades, there has been an emerging trend for the implementation of the principles of green chemistry and for the application of sustainable technologies in various areas of the chemical and biotechnology industries [1, 2]. Although a great deal of original research has been done so far in diverse fields of green chemistry and the utilization of these results to establish improved industrial processes is already ongoing, there is still tremendous work to be done if we desire to build a more healthful, constantly renewing, and rejuvenating world for future generations [2]. In 2007, the members of the ACS Green Chemistry Institute® Pharmaceutical Roundtable assembled the key research areas the in the aspect of pharmaceutical manufacturing [3], which was then extended to the perspectives of both pharmaceuticals and fine chemicals [4]. In this later review, the Roundtable collected and prioritized some key green engineering research areas where separation and reaction technologies and solvent selection, recycling, and optimization were designated as the second and third most important fields of research besides continuous processing, bioprocesses, and process intensification in the top five areas [4]. Separation operations are present in almost every manufacturing process within the chemical industry: the removal of impurities from raw materials and feed mixtures, the recirculation of solvents and unconverted reactants, the isolation of products for subsequent processing, the purification of final products and recycle streams, the recovery of by-products, and post-treatment of effluent streams all require some kind of separation techniques [5]. As the energy and time requirements for separation steps often substantially exceed those required for chemical reactions, they are the predominant contributor to processing energy and costs (they can be responsible for as much as 70% of the plant cost) [6], which requires novel, intensified, integrated, and more energy-efficient separation methods for a greener and more sustainable manufacturing process [4].

Chromatography is one of the most widely used separation techniques in the chemical industry which can be used for analysis, isolation, and purification purposes on a scale from

Sustainable Separation Engineering: Materials, Techniques and Process Development, Volume 1, First Edition. Edited by Gyorgy Szekely and Dan Zhao.
© 2022 John Wiley & Sons Ltd. Published 2022 by John Wiley & Sons Ltd.

the minuscule quantities needed for the identification of compounds to the hundreds of kilograms of material processed to final products [7]. Although the term "sustainable chromatography" has been called to be an oxymoron and avoidance of chromatography by turning to crystallization, classical resolution, biotransformation, asymmetric syntheses, etc., is preferred if applicable [8], the steadily increasing number of scientific publications in the field of chromatography (over a total of 2,200,000 hits in February 2021) (see top of Figure 7.1) suggests that chromatography still is and will probably remain a fundamental part of separation processes. To reduce the high solvent consumption of conventional preparative-scale chromatographic purification methods, by cautious solvent selection, reuse, and recycling, the waste impact (i.e. the tons of used silica gel) of flash chromatography is sought to be

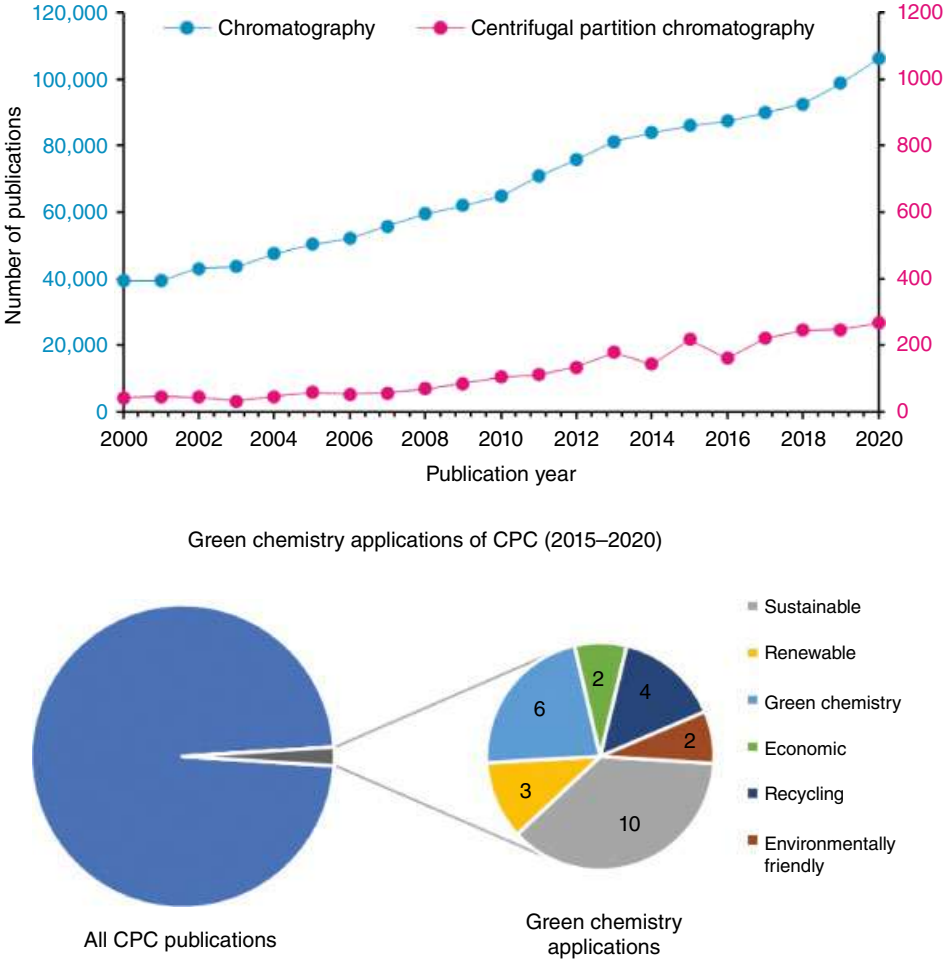

Figure 7.1 Number of publications by year for the search terms "chromatography" (left axis) and "centrifugal partition chromatography" (right axis) (top). Number of hits containing "centrifugal partition chromatography" + keywords (sustainable [9–18], renewable [11, 19, 20], green chemistry [13, 21–25], economic [13, 26], recycling [10, 27–29], environmentally friendly [30, 31] (bottom) (February 2021, Scopus™)).

minimized or more sustainable alternative methods (i.e. supercritical fluid chromatography [SFC], ion exchange resins, reverse-phase high-pressure or medium-pressure liquid chromatography [HPLC/MPLC], etc.) can be used [8]. To this avail, another promising but less widespread alternative is the group of support-free liquid–liquid chromatographic techniques, such as hydrodynamic and hydrostatic countercurrent chromatography (CCC) [32]. In this chapter, we focus on how green chemistry principles and sustainable thinking can be implemented in practice during separations carried out by hydrostatic CCC or more commonly known as centrifugal partition chromatography (CPC). This topic is also well represented in recent publications focusing on the sustainable features of CPC (see bottom of Figure 7.1 and references therein). Although a trend toward greener methods in separation techniques is present in the chemical industry, the number of articles focusing on green chemistry applications of CPC is yet quite low compared with all CPC-related publications (around only 2% between 2015 and 2020). Therefore, further research is needed in this area to make CPC a widely known, green and sustainable separation technique.

7.2 Centrifugal Partition Chromatography

7.2.1 Introduction

CPC is a liquid–liquid chromatographic technique, where in contrast to conventional chromatographic techniques, both the stationary and the mobile phases are liquids. Its categorization into countercurrent chromatographic (CCC) techniques is somewhat unfortunate as only the original demonstration and some later CCC models used actual countercurrent flow of the two liquid phases [33]. Since the first paper describing the first CPC prototypes manufactured by Sanki Engineering, Ltd. in the 1980s [34], the development and industrial applications of CPC were somewhat suppressed by the spread of solid/liquid chromatography as main purification techniques and also by the unreliability and poor engineering of early instruments [32]. Fortunately, as the technique has been becoming more commonly known and newer designs and more reliable instruments are manufactured (Table 7.1), and due to the advantages of the technology and its capabilities for sustainable development, the rapidly increasing number of publications in the past decades confirms a renewed interest in the research area and the possible industrial applications of the technique (Figure 7.1) [41].

7.2.2 Theory

In CPC, the support-free stationary phase is held stagnant by a strong centrifugal force inside the column (rotor) while the mobile phase is pumped through it by force (using typically an LC pump) [42]. The purification process in liquid–liquid chromatography is governed by the partitioning of solutes between the two immiscible liquid phases. During the chromatographic runs, the retention of the solutes depends on the time they spend in the stationary phase during the consecutive exchanges occurring between stationary and mobile phases. This mechanism can be described by the following equation:

$$V_R = V_M + K_D \cdot V_S \tag{7.1}$$

Table 7.1 Comprehensive summary of commercially available CPC instruments.

Vendor	Model/ column name	Column volume (mL)	Max rotation speed (rpm)	Max flow rate (mL/min)	Max backpressure (bar)	Typical sample size per injection (g)
AECS-Quickprep Ltd. Quattro CCC + Quattro CPC.(St Columb Major, UK) [35]	QuickPrep CPC	250	800	20	35	0.3–10
		500	800	40	35	0.5–20
	LabPrep CPC	1000	800	70	35	1–40
		2000	800	150	35	2–80
	PilotPrep CPC	4800	800	200	35	10–200
	ProcessPrep CPC	12,000	800	1000	35	25–480
ETS Couturier(Clairegoutte, France) [36]	Partitron 25	25,000	1500	500	150	n.d.
Ever Seiko Corp(Tokyo, Japan) [37]	CPC80	80	2000	10	~58.8	1
	CPC240	240	2000	20	~58.8	5
	CPC1400	1400	1500	80	~58.8	20
Gilson Inc.(Middleton, USA) [38]	CPC 100	100	3000	15	100	1
	CPC 250	250	3000	15	100	6
	CPC 1000	1000	1500	50	80	30
	CPC 250 PRO	250	3000	80	100	30
	CPC 1000 PRO	1000	2000	350	80	100
	CPC 5000 PRO	5000	1800	3000	80	350
Kromaton Sarl	FCPC 25	25	3000	10	80	0.01–0.5
Groupe Rousselet-Robatel(Annonay, France) [39]	FCPC 50	50	3000	10	80	0.01–1
	FCPC 200	200	2000	20	80	0.1–5
	FCPC 1000	1000	2000	50	80	1–30
	FCPC 5000	5000	1000	150	~62.1	150
RotaChrom Technologies LLC(Budapest, Hungary) [40]	rCPC	2100	1000	300	100	150
	iCPC	23,000	1000	5000	100	1500

where V_R is the retention volume, V_M and V_S are the mobile and stationary phases inside the CPC column, and K_D is the partition coefficient or distribution constant of the solute, which can be obtained as:

$$K_D = \frac{c_S}{c_M} \tag{7.2}$$

where c_S and c_M represent the total concentration of all forms (neutral, ionized, dimers, etc.) of solutes in the stationary and mobile phases.

The column volume can be described as:

$$V_C = V_M + V_S \tag{7.3}$$

And the stationary phase retention ratio can be given as:

$$S_f = \frac{V_S}{V_C} \tag{7.4}$$

By substituting Eqs. (7.3) and (7.4) into Eq. (7.1), it can be rewritten as:

$$V_R = V_C + \left(K_D - 1\right) \cdot V_S = Vc \cdot \left[1 + \left(K_D - 1\right) \cdot S_f\right] \tag{7.5}$$

Based on Eq. (7.5) it is easy to see that since the V_C and the S_f values are known or easy to be measured, if we know the partition coefficient of a solute, then its retention volume, therefore its position on the chromatogram can be unambiguously predicted and vice versa.

Provided that we have the measured K_D values in a series of possible biphasic solvent systems, the most adequate solvent system and the role of its two phases (mobile phase or stationary phase) during the chromatographic run can be determined so that the target compounds could elute in the "sweet spot" of the polarity range where separation is optimal [43]. When choosing between descending (the denser phase being the mobile phase, the lighter phase being the stationary phase) and ascending (the lighter phase being the mobile phase and the denser phase being the stationary phase) modes for a given separation task, we must also consider other aspects: if descending mode is chosen, the stationary phase retention is usually better and no air bubbles formation and trapping of the bubbles in the detector flow cell is expected; however, in the case of choosing of ascending mode, the collected, usually organic solvent-rich fractions with lower boiling point are much easier to dry compared with the aqueous fractions of descending runs, which reduces expenses and facilitates the recycling of solvents [44].

7.2.3 Instrumentation

Since the first prototypes of CPC instruments in the 1980s, with the development of engineering tools, several companies have joined the market of manufacturing CPC instruments providing columns with different cell geometry and capacity (Figure 7.2) [45]. As can be seen in Table 7.1, CPC instruments with different size of columns ranging from some 10 mLs to some 10 L volume are now commercially

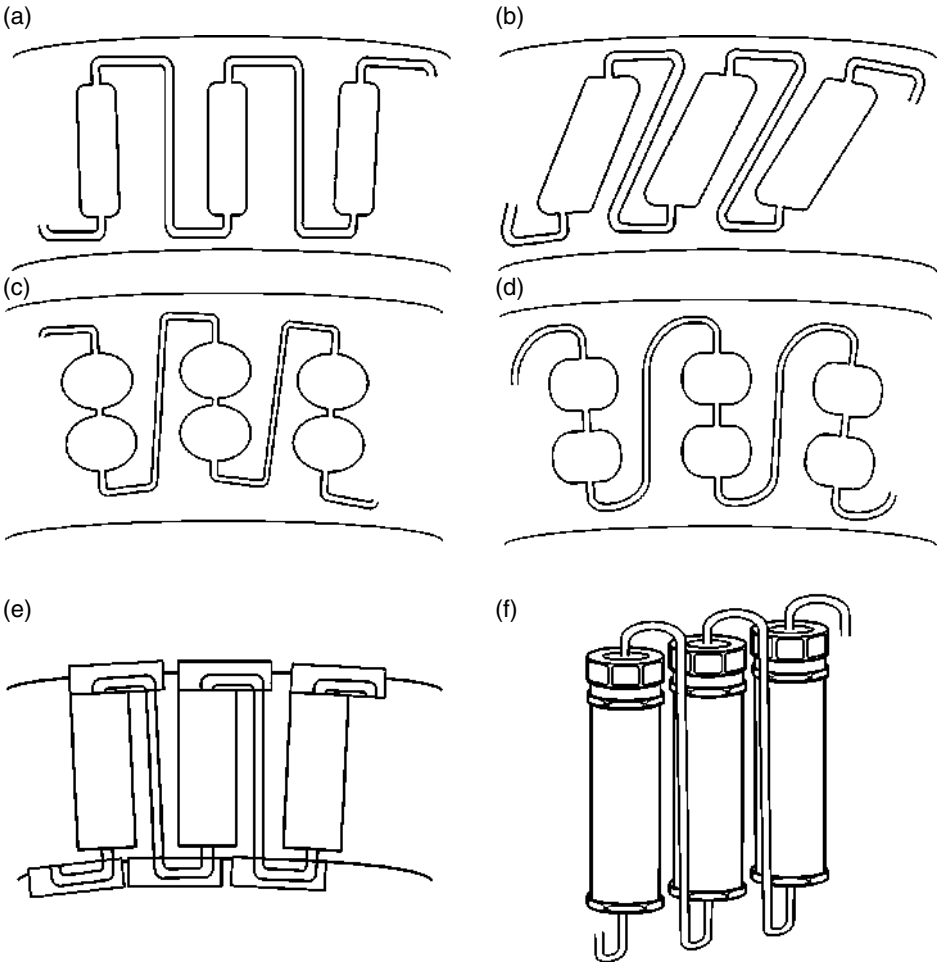

Figure 7.2 Different commercially available cell types utilized in CPC instruments. (a) radial cell; (b) FCPC®-chamber (Kromaton Sarl Groupe Rousselet-Robatel); (c and d) twin cells (Gilson Inc.); (e) small cylindrical cell (radially drilled in a cylindrical rotor wall, ETS Couturier); (f) large cylindrical cell (radially mounted on a rotor, RotaChrom Technologies LLC).

available for laboratory-, pilot-, and industrial-scale separations. It must be also emphasized that data given here are collected from websites, application notes, and brochures and should be considered as indicative only, as different companies are detailing information in specifications on different levels. Also, the maximum rotor speed, mobile phase flow rate, and sample loads are strongly dependent on the chosen biphasic system and the solubility of the compound of interest and matrix components of crude samples; therefore, it can change from separation task to separation task. Operational costs of the CPC instruments will also change according to rotor size and further task-specific parameters (rotor speed, flow rates, the price of the solvents of the biphasic system, etc.).

7.3 Strategies for Making CPC-Based Separation Processes Sustainable

By changing from the conventional solid–liquid phase separation techniques to a liquid–liquid system, a significant cost from purchasing the expensive silica gel and a substantial amount of solvents can be spared, meanwhile the generation of solid waste and its disposal costs can also be avoided [46]. However, the expensive instrumentation of CPC, the fear of switching from a traditional technology to one not yet widely known and the costs of acquiring regulatory approval for the new technology have hindered the spread of CPC, even though the integration of CPC to the chromatography workflow would save money for companies on the long run [46].

From the aspect of green chemistry and sustainable development, four main steps of the separation workflow can be appointed as key areas where significant reduction of costs and footprint may be achieved: (i) the selection of green solvent solvents as components of the biphasic solvent system, (ii) recycling of solvent waste to the start of the separation process, (iii) coupling and integration of CPC with downstream processes, and (iv) the valorization of waste as input materials of CPC (Figure 7.3).

7.3.1 Solvent-system Selection Strategies: Green Alternatives

While in solid/liquid chromatography we can choose from only a limited number of stationary phases (mostly some kind of silica-based solid packing) which can be changed only by the replacement of the whole column and the separation can be mostly fine-tuned by changing the composition of the mobile phase, in CPC, numerous possible biphasic liquid–liquid systems can be chosen using the same column [32]. The versatility of the system is further increased by the possibility of interchangeability of the phases by switching between ascending mode and descending mode [42]. These properties of the CPC system make possible the easy optimization of the chromatographic run depending on solely the polarity of the sample, its solubility in the biphasic system, and the type of the separation task to be carried out [47]. When choosing the solvent for a biphasic system, it is important to remember that for ideal use in CPC, the system must have a low viscosity, should be UV transparent for easy detection, must cover a wide polarity range, strong interfacial tension must be present between the aqueous and organic phases for fast equilibration upon mixing, while from the aspect of the post-separation work-up processes of the fraction, low boiling point of the solvents is preferred.

For finding the appropriate biphasic system for the separation task ahead, starting from the least polar systems with no water content (e.g. alkane/methanol [MeOH], alkane/dimethyl sulfoxide [DMSO]) to the most polar systems containing water in both phases (called aqueous two-phase systems, ATPS) (e.g. phosphate/polyethylene glycol [PEG]/water, dextran/PEG/water) [32] there are numerous possibilities, which makes the selection process laborious and time-consuming by the trial and error method as the polarity range to cover can be quite wide. To remedy this, several attempts have been made to establish simplified solvent selection strategies [47–49], and there is also an increasing trend for using computer-aided methods for screening purposes [50–53], like the conductor-like screening model for real solvents (COSMO-RS) [49, 54, 55].

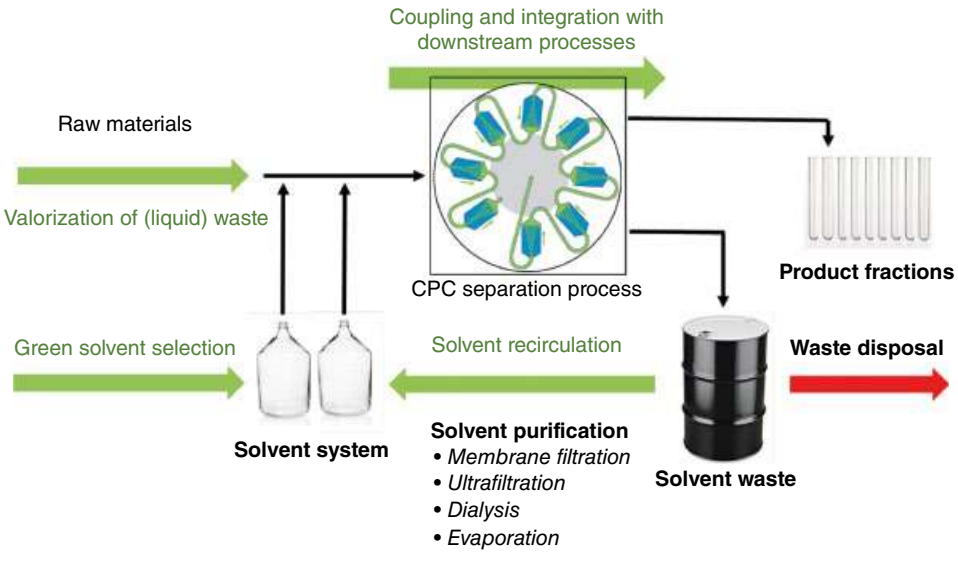

Figure 7.3 Typical workflow of a CPC separation process presenting possible approaches for the implementation of green chemistry aspects: (i) green solvent selection (Subchapter 7.3.1); (ii) solvent recirculation (Subchapter 7.3.2); (iii) coupling and integration with downstream processes (Subchapter 7.3.3); (iv) waste valorization (Subchapter 7.3.4).

Among the classical biphasic solvent systems most widely used in CCC that can cover a large polarity range are the ChMWat (chloroform/MeOH/water) and HEMWat (hexane/ethyl acetate/MeOH/water) systems [43, 48], and the refined version of the HEMWat system (with the less toxic heptane, instead of hexane), called the Arizona system [56] (Table 7.2). The Arizona system consists of biphasic mixtures where the volume ratio of heptane/ethyl acetate and MeOH/water is kept 1:1 with identical, systematically changing MeOH over water ratio and heptane over ethyl acetate ratio resulting in more polar (Arizona A-M) and less polar (Arizona P-Z) compositions with solvent proportions in symmetrically inverse order toward the central liquid system (Arizona N, 1/1/1/1 ratio) [56]. Several other solvent systems can be used such as the methyl isobutyl ketone (MIBK)/acetone/water solvent system families, *tert*-butylmethyl ether (MTBE)/1-butanol/acetonitrile (MeCN)/water system, MTBE/water systems with triethylamine (TEA) and HCl for pH-zone refining [60], the WDT system (water/DMSO/THF) for highly insoluble solutes [61], the ethyl acetate/1-butanol/water system, ideal for gradient runs [57]. An extensive list of further examples for solvent systems formerly used in high-speed CCC which could be also used in CPC has been collected previously [44].

From the aspect of green chemistry, the ecological footprint of a purification process can be reduced by rigorous management of work-up solvents [67] or choosing renewable, green solvents instead of halogenated and petroleum-based ones [63]. A solvent can be considered as green, if it possesses reduced health and environmental absorption and toxicity and displays a reduced life cycle impact [46, 68–70]. To facilitate the choice, certain guides can be found in the literature [71] made by pharmaceutical companies, like Pfizer's solvent selection guide which categorizes solvents as Preferred, Usable, and Undesirable based on

Table 7.2 Commonly used classical solvent systems and green alternatives in CPC.

Solvent systems	Components	Applications in CPC
Classical ones		
ChMWat	Chloroform/MeOH/Water	Dinitrophenyl amino acids [48]
HEMWat	Hexane/Ethyl acetate/MeOH/Water	Dinitrophenyl amino acids [48]
Arizona	Heptane/Ethyl acetate/MeOH/Water	Natural extracts (*Piper longum, Polygonum cuspidatum*) [56]
EtOAc/1-BuOH/Water	Ethyl acetate/1-Butanol/Water	Anthocyanins [57]
MIBK/Acetone/Water	Methyl isobutyl ketone/Acetone/Water	10-Deacetyl-baccatin (docetaxel starting material) [58]
MTBE/1-BuOH/MeCN/Water	*tert*-butylmethyl ether (MTBE)/1-Butanol/Acetonitrile/Water system	Gangliosides (amphiphilic glycolipids) [59]
MTBE/Water with TEA and HCl		Antioxidant recovery and alkaloid isolation [60]
WDT	Water/DMSO/THF	Amphotericin B [61]
Green alternatives		
ATPS	Polymers (PEG, polyacrylate)/phosphate buffer/NaCl	Monoclonal antibodies (mAb) [62]
Limonene/MeOH/Water and Limonene/EtOAc/EtOH/Water		Methylparahydroxybenzoate and diethyl phtalate (model mixture) [63]; occine red, aspirin, and coumarin (model mixture) [64]
Natural deep eutectic solvents (NaDES)	Choline chloride (ChCl), urea, carboxylic acids, and polyols	Naringenin, retinol, β-ionone, and α-tocopherol [65]
CPME	Cyclopentyl methyl ether	Peptide intermediate of bivalirudin synthesis [66]

worker safety, process safety, and environmental and regulatory considerations [72]; GlaxoSmithKline's (GSK) solvent sustainability guide (last updated in 2016), which categorizes solvents into Green, Amber, and Red classes based on their inherent waste disposal, environmental, health, and safety issues [73]; Sanofi's guide which ranked solvents into four categories: Recommended, Substitution advisable, Substitution requested, and Banned based on their IHC limit, Occupational Health, Safety and Environmental Hazard Bands, and other industrial or legal constraints [74].

As the different guides ranked solvents based on different criteria, conflicting classifications have emerged in several cases. To remedy this, the Innovative Medicines Initiative (IMI)-CHEM21 consortium compiled and combined these previous data to create the CHEM21 selection guide of classical- and less classical-solvents which allows a better ranking comparison of solvents [75]. The combined guide ranked solvents into Recommended, Problematic, Hazardous, and Highly Hazardous classes (Table 7.3). Also, for further help in solvent selection, an interactive online selection tool created by the ACS GCI Pharmaceutical Roundtable is available [76], which is an approximate duplicate of the original tool built by AstraZeneca [77]. In addition to the classification of a solvent in these guides, when looking for an alternative solvent that is appropriate for CPC separations, density, viscosity, and boiling point are also key factors to be considered.

Applicability of the most prominent green solvents and additives utilized in CPC separations will be discussed in detail in the following four sections (see Figure 7.4).

7.3.1.1 Substitution of Alkanes

Since recent regulations banned several hazardous solvents like *n*-hexane which was most commonly used for extractions of natural products, another alternative had to be found. 2-Methyl-Tetrahydrofuran (2-Me-THF) (Figure 7.4) is often considered as a green alternative to THF in syntheses as 2-Me-THF is nontoxic, it has low miscibility with water, and its stability compared with other heterocycles is remarkable. 2-Me-THF is a biomass-derived chemical and this in accordance with several of the green chemistry principles. 2-Me-THF can be produced from renewable raw materials, it is biodegradable, easy to recycle, possesses a promising environmental footprint, and a good preliminary toxicology [78]. Compared

Table 7.3 The CHEM21 selection guide, combining previous ranking guides for better comparison of solvents.

Recommended	Water, MeOH, ethanol (EtOH), 2-propanol, 1-butanol, tert-butanol, acetone, ethylene glycol, ethyl, isopropyl, isobutyl and isoamyl acetate, dimethyl carbonate (DMC), ethyl methyl ketone (MEK), isobutyl methyl ketone (MIBK), tert-amyl-methyl ether (TAME), etc.
Problematic	Methyl acetate, THF, methyl-THF, toluene, heptane, cyclohexane, MeCN, DMSO, etc.
Hazardous	Diisopropyl ether, MTBE, 1,4-dioxane, pentane, hexane, dichloromethane (DCM), methoxy-ethanol, etc.
Highly Hazardous	Diethyl ether, benzene, chloroform, CCl_4, 1,2-dichloroethane, nitromethane, CS_2, etc.

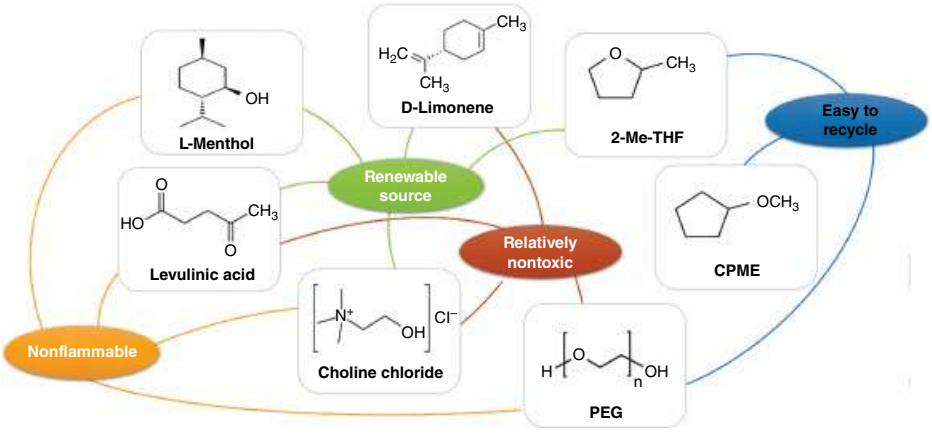

Figure 7.4 Chemical structures of green solvents and additives utilized in CPC separations. 2-Me-THF, CPME, and D-limonene are used for alkane substitution (Subchapter 7.3.1.1); CPME is also extensively studied for the replacement of DCM (Subchapter 7.3.1.2); PEGs are inevitable polymer components of ATPS used for protein purifications (Subchapter 7.3.1.3); while L-menthol, choline chloride, and levulinic acid are representing the emerging class of CPC-compatible natural deep eutectic solvents (Subchapter 7.3.1.4).

with *n*-hexane, it has almost the same molecular weight (86.1 Da), a higher boiling point (80.2 °C), and flashpoint (–1.9 °C), which makes it less flammable and hazardous. Its higher density (0.854 g/cm^3) and viscosity (0.46 cP) might be a drawback during CPC runs compared with *n*-hexane but is well within the operational range of CPC as by using decreased rotor speed and flow rate, systems with much higher viscosity, like the octanol-water system [79], polymer-rich ATPS, and even natural deep eutectic solvents (NaDES) [65] can also be used without reaching the maximum pressure drop of the CPC instrument.

Limonene is an apolar solvent, a natural cyclic monoterpene (Figure 7.4), with a pleasant fruity odor, and its D-isomer is the major component in the essential oils of citrus fruits (59–90%) [80]. The world production of citrus fruits is over 120 million tons per year [81], 40–50% of which is destined for industrial processing, where the resulting citrus peel waste is about 50–70% (w/w) of the processed fruits resulting in an annual world production close to 10 million tons [82]. The biomass generated this way typically contains 5.4 kg of oil per a ton of raw biomass, of which approximately 90–98% is D-limonene; therefore, it can be considered as an easily available and renewable solvent [82]. From the regulatory aspect, the legal status of limonene is clear, it has been listed by the Food and Drug Administration (FDA) agency as a "Generally Recognized As Safe" (GRAS) food additive, flavoring and fragrance additive [83]. Also, in a Reregistration Evaluation Decision, the US Environmental Protection Agency (US EPA) stated that limonene can be used without resulting in unreasonable adverse effects to humans and the environment and that it is granted an exemption from the requirement of a tolerance when, as an inert ingredient, it is used as a solvent or fragrance in pesticide formulations [84]. On the other hand, limonene is ranked as a problematic solvent by the CHEM21 guide due to its relatively high boiling point and aquatic toxicity [75]. However, its natural origin still makes it a better, greener alternative to the alkanes hexane and heptane in the HEMWat and Arizona systems, which solvents are

ranked as problematic/hazardous due to their flammability, aquatic toxicity, and the neurotoxic human metabolite of hexane. Previous studies have already investigated the impact of the substitution of heptane with limonene in the biphasic systems [63] and also proposed an even greener alternative by changing MeOH to EtOH [64, 85]. It is also noteworthy that D-limonene might be considered as a selector for enantiomer separations by CPC in the future due to its chirality [63], which enables enantioselective interactions with other chiral compounds.

Limonene and heptane are very close in polarity (dielectric constants [ε]: 2.37 and 1.92, respectively) [85] and they also show quite similar solvation capability toward water and MeOH (Table 7.4). The overlapping ternary plots of limonene, hexane, and heptane with water/MeOH mixtures share strong similarity in the biphasic systems (Figure 7.5).

The most notable difference in their properties is the density difference between the alkanes and limonene (Table 7.4), which will affect their position in the biphasic systems: in the case of a system with heptane/methanol/water 10/9/1 (v/v) ratio, heptane is the upper phase due to its lower density and therefore it can be used as a mobile phase in ascending mode, while it is the opposite in the case of limonene, where in the case of a system limonene/methanol/water 10/9/1 (v/v) ratio, limonene is the lower phase due to its higher density, making it useful as a mobile phase in descending mode [63]. At this composition, the low difference between the densities of the phases is also an advantage for CPC runs that allowed the use of high rotation speed with reduced pressure drop compared with the system containing heptane [63]. However, as the stationary phase retention (S_f) was significantly lower and more sensitive to a change in flow rate in the case of limonene as compared with heptane, only a lower flow rate (3 mL/min) could be applied to reach a moderate S_f (43%) that was enough for baseline separation of the model mixture of methyl parahydroxybenzoate and diethyl phtalate [28].

Table 7.4 Physicochemical properties of *n*-heptane, methanol, and their green alternatives, limonene and ethanol [63, 85].

	n-Heptane	Limonene	MeOH	EtOH
Molar weight (Da)	100	136	32	46
Boiling point (°C)	98.4	178	64.6	78.4
Density (g/cm^3)	0.679	0.841	0.791	0.789
Viscosity, 25 °C (cP)	0.389	0.923	0.544	1.0740
Surface tension (mN/m)	20.8	28.5	22.6	22.4
Dielectric constant, ε (-)	1.92	2.37	32.7	24.3
Water solubility (w%)	0.00024	0.08	Miscible	Miscible
MeOH/EtOH solubility (w%)	29.7/miscible	32/miscible	Miscible	Miscible
log$P_{o/w}$	4.50	4.58	−0.74	−0.31
UV cutoff (nm)	200	250	205	210

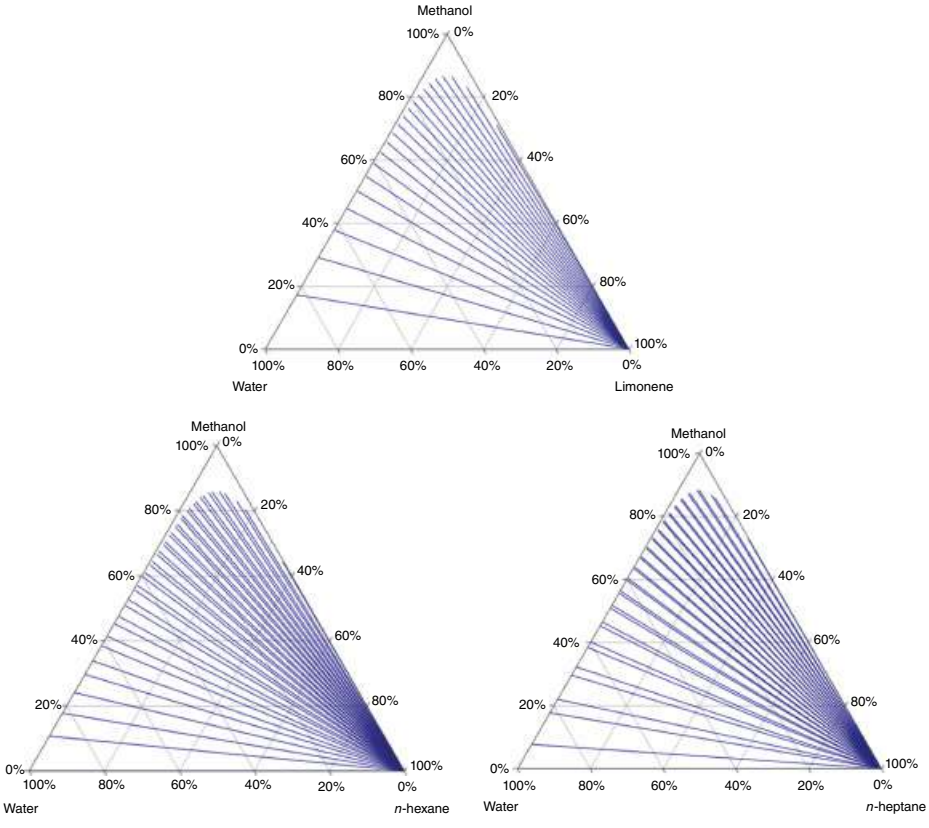

Figure 7.5 Demonstrating high similarity between ternary plots of Limonene/MeOH/Water, *n*-Hexane/MeOH/Water, and *n*-Heptane/MeOH/Water systems (diagrams were simulated by vle-calc.com ver. 11/55/2020).

If besides the heptane–limonene change, MeOH is also replaced with the less toxic EtOH in the Arizona system, similar ternary plots can be acquired for the heptane/EtOH/water and limonene/EtOH/water systems (Figure 7.5), which further supports previous observations suggesting similar solving properties of limonene and heptane [29]. However, as in the Arizona system, EtOAc is also present, and we must investigate its solubility in MeOH and EtOH, where significant difference can be found in favor of EtOH, which has significantly higher solving ability toward water-immiscible compounds (see Table 7.3) [85]. Also, a major difference between the classical and green Arizona systems is that limonene and EtOH are fully miscible, while heptane and MeOH form a biphasic system at room temperature. As a consequence, proportions Arizona Y and Z form monophasic solutions and Arizona W and X are milky biphases with settling times of several minutes, rendering these four compositions inappropriate for use in CPC [85]. Moreover, the seemingly small difference between the polarity of MeOH ($\log P_{o/w} = -0.74$) and EtOH ($\log P_{o/w} = -0.31$) will have significant consequence in the four-component Arizona system. The distribution of EtOH will be much better between the upper and lower phases in the green Arizona solvent family, than the distribution of MeOH is in the original one, resulting in more

EtOH in the upper phases, raising their polarity. For the same solutes, this will induce different distribution; therefore, separation differences between when using classical and green Arizona systems with the same proportions [85].

Another advantageous property of the green Arizona system was the low density differences (<0.06 g/cm^3) for half of the green system compositions, which allows working with maximum centrifugal fields to result in high S_f values; therefore, better resolution [64]. Similarities have also been found between the original and the green Arizona systems: the relationship between the logarithm of solute partition coefficients and the system composition (upper phase alcohol content % [v/v]) remained linear, however, with a much steeper slope in the case of the green Arizona system, which can be explained by better distribution of EtOH between the phases. Based on the measured data, we can assume that the green Arizona systems are one- or two-letter more polar than their corresponding pairs in the original system [64]. The results of these investigations confirm that limonene and also EtOH are possible green alternative solvents for use in CPC if the changes they induce in the systems are kept in mind during method development.

7.3.1.2 Replacement of Chlorinated Solvents

The substitution of chlorinated solvents is a long-desired goal of the chemical industry; solvent selection guidelines mark almost all of them as hazardous or highly hazardous [75]. For example, the substitution of DCM has not yet been fully implemented in organic synthesis or in chromatography. To replace DCM in the widely used MeOH-DCM system, several investigations have been carried out, besides DMC, MTBE, and 2-Me-THF, cyclopentyl methyl ether (CPME) was found to be a possible direct alternative of DCM in those systems [86]. CPME has low toxicity, high boiling point (106 °C), hydrophobicity, low heat of vaporization, moderate density (0.86 g/cm^3, 20 °C) and viscosity (0.57 cP, 20 °C), and high surface tension (25.17 mN/m) making it an ideal choice for CPC separations as well [87–89]. CPME has also already been successfully used as a substitute for chloroform in high-performance liquid chromatography [90], and its application in CPC has also been reported as an alternative choice to replace MTBE, THF, 2-Me-THF, and dioxane in a new type I biphasic solvent system using CPME/DMF/Water (CDW) [66]. By means of the CDW system, a peptide intermediate of bivalirudin synthesis was successfully purified using a pH-zone refining CPC method with TEA as an organic retainer (to induce analytes to retain in the stationary phase). Using a solvent ratio of CPME/DMF/W=49/40/11 (v/v) with TEA (28 mM) in the upper phase and methanesulfonic acid (18 mM) in the lower phase, 66.4% stationary phase retention could be achieved at a rotation speed of 1400 rpm and a flow rate of 6 mL/min. An excellent recovery (94%) and high purity (HPLC purity 99.05%) of the target peptide could be realized by CPC [66].

7.3.1.3 The Greenest Systems Possible: Toward Biotechnological Applications Using Aqueous Two-Phase Systems

Water, as the first choice of green solvent, is the safest and the most environmentally friendly solvent widely employed in various kinds of green separation processes [91]. It is also the most polar solvent that we can chose, being one of the endpoints of the relative polarity scale [92]. A special group of biphasic systems often used in liquid–liquid extractions is called ATPS, where phase-forming components like two incompatible polymers or

a salt and a polymer are dissolved in water and upon reaching a certain concentration, the biphasic system is spontaneously formed [93, 94]. Typical ATPS are the PEG/Phosphate, PEG/Sulphate, PEG/Dextran, or the PEG/Ionic liquid (IL) systems [95]. Due to their high water content (>85%), these systems provide ideal environment for cells, organelles, peptides, and other macromolecules [93]. Partitioning of the protein will be mainly dependent on the size, hydrophobicity, and surface net charge of the protein and the composition, pH, ionic strength, and the presence of additional salt in the ATPS [96]. Also, as a rule of thumb, negatively charged proteins tend to partition to the PEG-rich phase; therefore, by adjusting the pH above the pI value of the protein, this behavior can be strengthened [97]. By adding NaCl to the system, the polarity difference between the lower and upper phases can be increased, which often drives the proteins, especially hydrophobic ones, to the polymer phase [98]. On the other hand, the anion of $NaClO_4$ is relatively hydrophobic, which tends to partition into the upper, PEG-rich phase, attracting positively charged proteins to partition into the upper phase. At a pH higher than the pI, the presence of the ClO_4^- anion repels negatively charged proteins from the upper phase [96].

It has been shown in several cases that the ATPS containing PEG-1000/K_2HPO_4/Water can be used for CPC separation of proteins (e.g. myoglobin and lysozyme) [95, 99]. The major problem in the case of ATPSs is the increase of the flow rate which decreased the stationary phase retention significantly and thus separation became more difficult. However, compared with hydrodynamic CCC columns, which are working inefficiently with ATPS, CPC can still provide acceptable resolutions. Moreover, in the case of the hydrostatic CPC instrument, the scale-up step from a lab-scale instrument (with a 500 mL column) to a preparative-scale column (with 6.25 L volume) could be easily handled even with a relatively low $S_f = 0.3$ value [95]. For a better separation of the two proteins, addition of IL can be suggested, as low as 1.5% 1-Ethyl-3-methylimidazolium chloride ([EMIM]Cl) could move the partition coefficients of myoglobin and lysozyme closer to the sweet-spot ($0.5 < K_D < 2$), while high S_f values and reasonable flow rates could be maintained. Also, 20% of the total column volume could be injected into the system, which theoretically could be increased to even further to raise productivity [100].

ATPSs also provide gentle conditions for the separation of enzymes; however, the question has arisen whether the shear forces inside the CPC instrument during the chromatographic run would damage the enzymes causing loss of activity. To investigate this, supernatant containing active laccases was used for separation by CPC at 1000 rpm rotational speed, 5 mL/min flow rate in an ATPS consisting of PEG-3000 (13% w/w)/Phosphate (6% w/w)/NaCl (2.2 or 2.5% w/w) [101]. The results of the study showed that the shear and interfacial forces inside the instrument did not lower the activity of the laccases significantly. Also, it was found that as opposed to previous observations, S_f values higher than 70% could be achieved in this system, which might be explained by the higher molecular weight of PEG in this particular study.

Another promising area for the application of ATPSs in CPC is the purification of biopharmaceuticals. Year by year the number of biologics among the top 200 drugs worldwide increase [102], the current landscape of this research area promises continuous growth. Without doubt the research in the field of separation processes of biotherapeutics will be of major importance in the forthcoming decades to decrease the significant cost of downstream processes. The first studies in this area for the applicability of CPC have already

been carried out [62, 103, 104]. For the purification of three monoclonal antibodies (mAb) from host cell protein (HCP) precipitation and redissolving, batch partitioning in PEG 400/citrate-systems, CPC separation (single and dual mode) in the same type of ATPS and the combinations of these process steps were investigated [62]. It was found that although mAb recovery was >96% in all cases, neither batch partitioning nor CPC could reduce HCP content satisfactorily. The best results were observed in the case of precipitation and re-solubilization (96.4%). However, when the techniques were combined, the different process steps seemingly removed different population of HCP, resulting in a >98% reduction, while mAb recovery only slightly decreased (~93%). The authors also pointed out that the implementation of the combined process containing a CPC step might yet be problematic in GMP surroundings [62]. To further increase the chromatographic performance of the separation of mAbs, the abovementioned addition of ILs was proposed [100].

The same research group has also investigated the possibility of CPC separation in the case of virus-like particles (VLPs) [104]. Based on the chromatograms and measured S_f values, the applicability of CPC has once again proven to be possible also for this group of biomolecules. It could be observed that for a high stationary phase retention, a high-density difference between top and bottom phase was needed, which is mostly determined by the salt concentration in the bottom phase; choosing system compositions of longer tie-lines will lead to higher S_f values. However, in the case of VLPs, resolution was not satisfactory due to the extreme distribution constant originating from low solubility of VLPs in PEG and salt solutions, which is the main issue hampering the development of robust and selective ATPSs. Also, it was found that upon addition of NaCl into the ATPS, about 20% of the VLP precipitated and partitioned to the interphase; however, by increasing the salt concentration, no further effect could be observed. Moreover, there were no changes measured in the partitioning coefficients of neither HCPs nor VLPs upon addition of NaCl. Thus, the observed separation can be only explained by a change in physical properties of the ATPS. A possible explanation can be the size-dependent adsorption of HCP and VLP on the interphase of the PEG-salt ATPS.

7.3.1.4 Natural Deep Eutectic Solvents

Within the confines of green chemistry, another group of compounds with suddenly growing interest is the group of so-called deep eutectic solvents (DES) or when their components are of natural origin, NaDES [105]. These solvents are characterized by a large depression of freezing point, which is usually higher than 150 °C (Figure 7.6) [107].

DESs originate from the desire after greener, metal-free ILs; however, they cannot be considered as ILs, because they are not composed of ionic species solely and can be even formed from nonionic species. DESs can be acquired by simply mixing together two safe, cheap, renewable and biodegradable components which are capable of forming an eutectic mixture. They can be described by the general formula Cat^+X^-zY, where Cat^+ can be any ammonium, phosphonium, or sulfonium cation; X is a Lewis base, generally a halide anion; Y is either a Lewis or Bronsted acid [106]. Hydrogen-bonding interactions between the components are suggested to be the main cause for the freezing point depression. The melting points of the DESs are generally lower than 100 °C [65]. One of the most widely used components of DESs is choline chloride (ChCl), which meets the requirements of being cheap, biodegradable and nontoxic [107], and is most widely used as hydrogen-bond

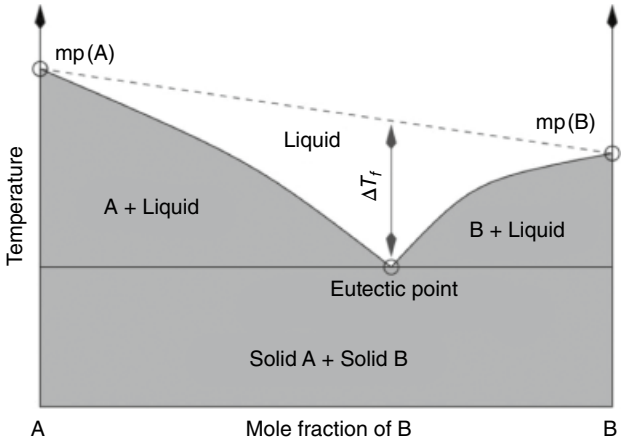

Figure 7.6 Typical phase diagram of eutectic solvents. Mp stands for melting point [106].

acceptor (HBA). Possible hydrogen-bond donors (HBD) can be urea, carboxylic acids, and polyols, such as glycerol [107]. As several poorly water-soluble drugs demonstrated the solvation power of DESs, they might act as substitutes for water and biphasic solvent systems used in CPC [65].

It has been shown that using heptane/EtOH/DES systems (30/40/30, v/v/v), biphases with similar density and density difference between the upper and lower phases can be created as compared with the classical HEMWat (7/3/6/5, v/v/v/v) system. However, the viscosities of the phases will be significantly higher in the lower (DES-rich) phases, and much closer to the PEG-rich upper phase of the PEG-1000/Phosphate/Water ATPS [65]. As opposed to classical systems, varying DESs in the system, the partition coefficients of solutes can be adjusted to the preferred range for CPC without changing the ratios of components in the biphasic system due to the different HBD and HBA affinity of different DESs. Using this new type of biphasic system, the successful separation of hydrophobic model compounds naringenin, retinol, β-ionone, and α-tocopherol were carried out using a centrifugal partition extractor (CPE) [65].

To find further alternative DESs that can be used in CCC as water-free systems, the liquid–liquid equilibria of the biphasic systems comprised of heptane, MeOH, and three NaDESs (levulinic acid/L-menthol; levulinic acid/thymol; levulinic acid/carvacrol) were experimentally determined [108, 109]. Potential application of the heptane/MeOH/levulinic acid/ L-Menthol biphasic solvent system as stationary and mobile phase in CPC was investigated. Stationary phase retention of the system containing 5 wt% NaDES could be kept above 60% even in the case of high flow rates (40 mL/min). However, if the system contained 15 wt% NaDES, the decrease of S_f with increasing flow rate was much steeper (Sf = 0.4 at 40 mL/min). Pulse injections of model compounds (coumarin, β-ionone, and α-tocopherol in descending mode; β-carotene, β-ionone, and α-tocopherol in ascending mode) were carried out. In the case of injection into the biphasic system with higher (15 wt%) L-menthol and levulinic acid content, stationary phase loss was observed; however, this could be reduced when a biphasic system with only 5 wt% of the NaDES was used.

It can be concluded that NaDESs can provide a promising alternative of water-free solvent systems with a polarity range facilitating mostly the separation of less polar and hydrophobic compounds. However, before they can be considered as truly green solvents, solute recovery and recycling of the DES-constituents need to be developed first. This might be carried out using either extraction, diafiltration, or precipitation after the removal of the volatile components [109].

7.3.2 Recirculation of Solvent Systems

When designing a separation process to be sustainable, it is desired to recycle most of the solvents used whenever it is possible. To this avail, several solutions have been developed such as membrane filtration, ultrafiltration, dialysis, and density-based recirculation (by a mixer-settler).

In 2012, GSK combined a lab-scale CCC method with organic solvent nanofiltration (OSN) for a more cost-effective purification of an API with ~600 Da molecular weight (Figure 7.7) [110]. After testing several types of membranes, the authors found that rejection of membranes is highly dependent on the composition of the solvent mixture used and that even though API rejection remained >99% throughout the whole process, the overall API loss added up to 2.3%; therefore, there is a growing need for development of membranes with 100% rejection. By means of recycling the mobile phase solvent using OSN, a 56% mass-intensity improvement was observed indicating that this process has a significant potential for improving overall CCC mass-efficiency.

Other potential solutions for the recycling of CPC solvents have been reported by Santos et al. [10, 111]. Dialysis has been successfully used for isolation of the separated phenolic compounds and the recycling of sodium polyacrylate and PEG-rich phases of the ATPS used for CPC purification (Figure 7.8). Comparing the process utilizing recirculation of the solvent system with the one without reuse of solvents, the carbon footprint could be reduced by 36% using dialysis [111].

In another case, the continuous separation of PEGylated and non-PEGylated Cytochrome-c (Cyt-c) as model proteins using CPC has been modeled (Figure 7.9) [10]. By the means of ultrafiltration, the PEGylated product and the unreacted protein could be isolated with high recoveries (88–100%) and purities (~100%), while the PEG-rich ATPS used in the CPC separation could be recycled and reused in a consecutive cycle of purification. Comparing the process with and without recycling, it was found that nearly a 100% decrease in the E-factor and a 67% reduction of carbon footprint can be achieved using ultrafiltration.

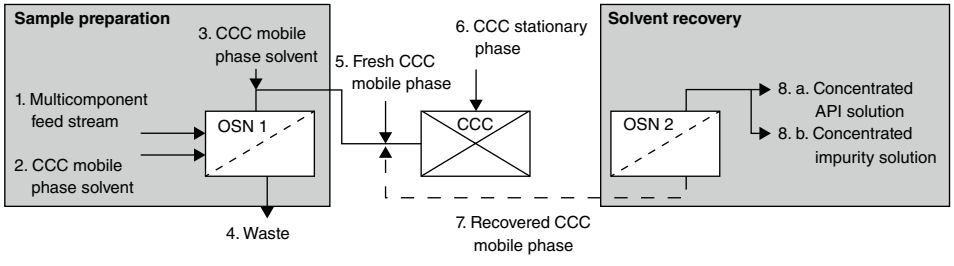

Figure 7.7 Process diagram of the recirculation of CCC mobile phases using OSN [110].

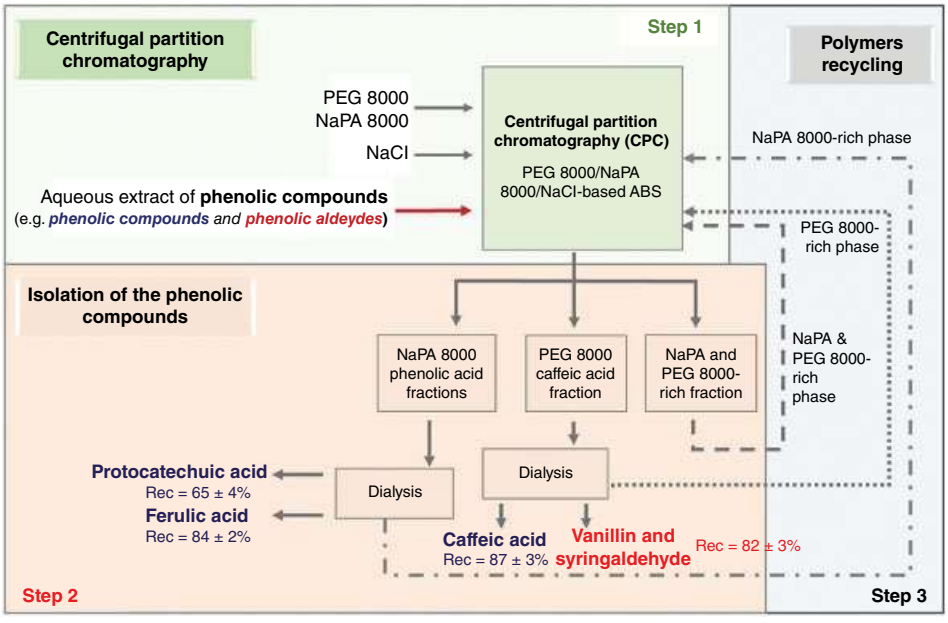

Figure 7.8 Schematic representation of the purification of five phenolic compounds by CPC and recycling of solvents [111].

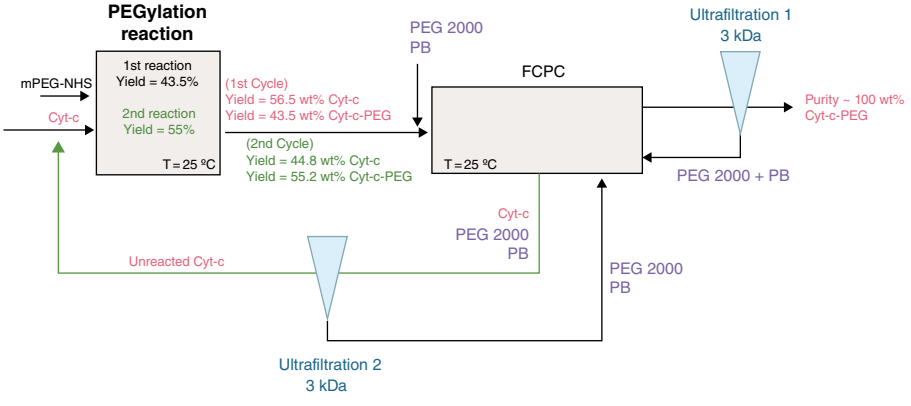

Figure 7.9 Schematic representation of the solvent system recirculation process by ultrafiltration in the PEGylation model reaction of Cytochrom-c (Cyt-c). FCPC stands for fast centrifugal partition chromatography; PB stands for phosphate buffer [10].

Another novel strategy for the continuous in-line recycling of CPC solvents and density measurement-based readjustment of ternary solvent system has been reported recently (Figure 7.10) [27]. In this automated system, pure solvents are fed into the mixer-settler unit where the solvent system with the desired ratio of solvents is prepared and then its composition is checked by density measurements. The prepared phases are stored in buffer tanks from where they are pumped into the CPC during the chromatographic run. After

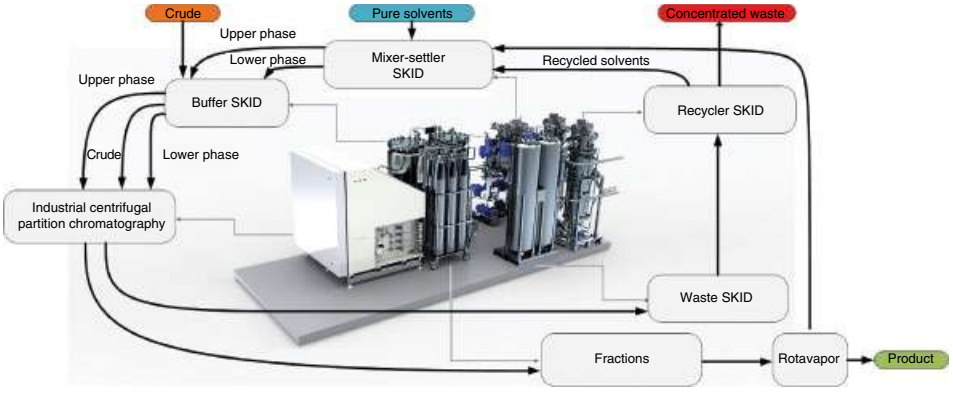

Figure 7.10 General scheme of the industrial-scale implementation of the designed continuous process with streams and automatic solvent system handling units [27].

the CPC run is completed, the waste solvents are separated from the impurities in the recycler skid and then they are fed back into the mixer-settler unit together with evaporated solvents from product fractions. After the density-based readjustment of the solvent system, the phases can be reused in the subsequent CPC cycle. Based on the purification project carried out within confines of this work, 14.865 kg of crude steroid API purified, with an average purity of 98.74%. By means of the skid system, more than 90% of the MIBK and acetone content of each run of the 153 cycles was successfully recycled and reused.

7.3.3 Coupling and Integration of CPC with Downstream Processes

7.3.3.1 CPC as a Bioreactor

What could be a more sustainable way for the reduction of solvent cost and energy than the possibility to shorten the manufacturing process by merging the chemical reaction and the separation process into one step instead of two consecutive ones? This question has already captured the interest of researchers before and to this avail, the "CPC reactor" as a possible solution has been contemplated.

In the late 1990s, the equilibrium-limited hydrolysis of N-acetyl-L-methionine has been extensively studied by den Hollander et al. [112, 113]. They found that lower equilibrium conversions could be achieved at high initial substrate concentrations due to the reverse reaction, which made the production of large amounts of optically pure amino acids inefficient by conventional processes. As a possible alternative to suppress the reverse reaction, the applicability of CPC was investigated. The prerequisite for this is that the reaction must be faster than the residence time of the reactants in the column, without mass transfer resistance and dispersion being rate limiting. Based on experimentally determined partition coefficients, S_f values, volumetric mass transfer coefficients, and kinetic parameters, they could predict experimental peak shapes, conversion, and resolution values as the function of enzyme and PEG concentration in the selected PEG600/potassium phosphate/water ATPSs to find optimal settings where both the conversion of the hydrolysis and separation of the products and reactants were satisfactory.

Another research group investigated the kinetics of lipase-catalyzed esterification of oleic acid by *n*-butanol to find the optimal enzyme and substrate concentrations, rotational speed, and flow rate in a *n*-heptane/*n*-butanol/phosphate buffer (pH 5.6) system [114]. The productivity using the optimal conditions was two-fold higher than the one achieved in the batch reactor and a continuous 72-hour-long experiment in the CPC showed that reaction performance could be maintained through 24 hours after which a gradual diminution could be observed, most likely due to low enzyme stability at room temperatures. In a follow-up study, the kinetic parameters and the specific interfacial area during continuous operation was determined [115]. They found that in contrast to dynamic mixing intensified reactors, the achievable high specific interfacial area was not depending on flow rate; therefore, the CPC reactor can be compared rather with the tubular flow microreactors, where the pulsation is the main factor on diphasic hydrodynamics inside the reactor [116, 117].

In another example, the procedure for the selection of aqueous organic two-phase systems for the conversion of hydrophobic substrates and optimal operation conditions in CPC were studied through the lipase-catalyzed hydrolysis of 4-nitrophenyl palmitate [118]. The buffer type and concentration and the pH of the system were optimized, then an appropriate organic solvent has been chosen keeping in mind that it must be compatible not only with the enzyme (and cofactors, co-substrates, energy carriers for the reaction, etc.) but also must be able to form adequate biphasic system for CPC separations with appropriate partition coefficient of substrate, enzyme, and products. After all these requirements were fulfilled, the operation conditions of the CPC (rotational speed, flow rate) were studied, then the optimal method was compared with results of experiments in stirred tank reactor (STR). Using the CPC reactor, two times higher conversion could be achieved which makes CPC a promising apparatus concept for multiphase reaction systems.

In another article, the reaction performance of STR was compared with the operation of the CPC reactor, where CPC showed competitive mixing conditions and could handle low volumes of aqueous phases more efficiently than the STR [119]. However, at higher enzyme amounts, CPC runs into limitations faster and was not easily scalable due to complex effects of the flow pattern. The results demonstrated that the development of CPC rotors or chamber geometries is still needed for CPC to offer a better alternative to STR as an easily scalable continuous system.

7.3.3.2 Coupling CPC with Traditional Methods to Achieve Industrial Scale Sustainability

CPC also carries the possibility for coupling with conventional separation and isolation techniques to develop an alternative methodology for a more sustainable and economic production process. A fine example of this has been reported in a methodology for the sustainable production of functionalized taxanoids [13]. Following the microbial upcycling of low-value feedstocks, CPC was integrated for the economic isolation of taxadiene allowing subsequent continuous chemo-enzymatic functionalization. This new downstream processing strategy displayed a greener alternative to conventional biphasic, in situ extraction and purification using reversed-phase HPLC (RP-HPLC) by combining a rapid and easy two-step extraction procedure with a subsequent CPC purification step. By means of CPC, the admixing and adsorption issues observed during RP-HPLC could be avoided, providing

taxadiene with 95% purity and a throughput of ~250 mg/L. This increased diterpene mass load of taxadiene in CPC purification significantly raised process efficiency, resulting in improved recovery from high cell density fermentation broth. The developed methodology opened a path for industrial-scale biology-oriented synthesis of *ad hoc* designed bioactive taxanoids.

Another recent example shows a pilot-scale continuous process for recovery of bioactive components (hydroxytyrosol [HT], oleocanthal, oleacein, the monoaldehydic form of oleuropein aglycone [MFOA] and of ligstroside aglycone [MFLA]) from extra virgin olive oil. In this application, CPC has been integrated into the purification process for the enrichment of the total phenolic fractions after antecedent fractionation using liquid–liquid extractors [120]. Using a step-gradient elution extrusion method in biphasic systems composed of *n*-heptane, EtOAc, EtOH, and water, oleocanthal, oleacein, MFOA, and MFLA could be recovered on the gram-scale with purities >80%, which could be further purified to >95% purity using preparative HPLC. By the integration of these three industrial-scale techniques, a highly productive methodology was developed, where the large amount of recovered pure compounds enabled the possibility of *in vivo* experiments for the first time.

7.3.3.3 Integration with Continuous Processes

In the past two decades, the efforts for process intensification and the switch from batch to continuous manufacturing have started the rapid evolution of production processes, which is encouraged and strongly supported by the authorities and the scientific communities alike, especially in the pharmaceutical and chemical industries [4, 121–123]. Although this transition poses many challenges to overcome in the short run, the expected long-term benefits, such as improved automation, better quality control, simpler scale-up, and higher throughput and an all-in-all more sustainable and green end-to-end manufacturing process, make it an attractive alternative for profit-oriented companies [123, 124].

In this perspective, the possibility of the integration of CPC-based quasi-continuous purification step into the multistep continuous synthesis of the key intermediate of bioactive carbazoles has been investigated previously [28]. Following the two-step continuous-flow synthesis of the target molecule, a multiple dual-mode (MDM) CPC purification was coupled to the end of the synthesis resulting in a 59% overall yield, >99.9 purity, and 2.24 g/h/L productivity when using one-phase intake of the sample solution into the CPC purification step. Another advantage of this setup that from the aspect of industrial scale-up, the throughput of a system of this kind can be easily increased by scaling up the column capacity, which makes it a promising alternative for continuous purification when designing future manufacturing processes of APIs and intermediates.

As can be seen from these examples, in line with the expectations, some initial research has been carried out on the key areas declared by the ACS Roundtable regarding the possibility of implementation of CPC in the manufacturing process as a continuous/quasi-continuous solution for purification. However, without further examples to show, we can conclude that not enough work has yet been invested in this area, which might impede the widespread use of CPC in the industry. Therefore, further studies are needed to be reported in the future that showcase the advantages and opportunities of implementing CPC into the production line to facilitate the switch from batch to continuous processes using sustainable and green technologies.

7.3.4 Waste Valorization by Means of CPC

Every year, millions of tons of agricultural, industrial, municipal, and forest waste are generated worldwide, the waste treatment of which poses a huge challenge for both companies and governments [125, 126]. Besides the conventional, physical, and chemical treatments, another alternative strategy is the recycling, recovery, and reuse of waste in the name of sustainable development (Figure 7.11). As a result of an environmentally sound management of waste, the use of raw materials in manufacturing processes and the environmental impact of waste accumulation can be reduced and valuable compounds can be recovered for use in nutraceuticals, cosmetics, and pharmaceutics [125–127].

A prime example of this is the recovery of HT from table olive processing wastewater [16]. HT is one of the main phenolic compounds in virgin olive oil and table olive possessing a naturally derived antioxidative and remarkable free radical scavenging activity which can help in prevention of reactive oxygen species-mediated degenerative diseases [128, 129]. After isolation of the phenolic compounds using nonionic adsorption resin, 1.81 g/h/Vc productivity could be achieved for efficient and low-cost recovery of HT using pilot-scale CPC runs in a cyclohexane/EtOAc/EtOH/Water (1:9:2:8, v/v/v/v) solvent system [16].

In another publication, the optimization and scale-up of monosaccharide fractionation from hydrolyzed sugar beet pulp using a CPC separation step instead of multiple resin chromatography steps have been reported [14]. Sugar beet pulp primarily consists of cellulose and pectin, the poor gelling properties of which prevent its use as gelling agent. Instead, it is generally dried and pelleted for sale as low-value animal feed [130]. However, due to its cheapness, abundance, and high carbohydrate content, after thermo-chemical pretreatment, it can also be used as a source for bioethanol fermentation [131] or hydrolyzed into monosaccharides which can be fractionated by CPC. The scale-up of this monosaccharide isolation to preparative-scale CPC using an ethanol/ammonium sulphate-based solvent system has already been optimized, resulting in a final monosaccharide throughput of 1.9 g/L/h, normalized by column volume [14]. Furthermore, integration of CPC purification into the workflow of a biorefinery allows the conversion of purified arabinose into the top commodity biochemical, arabitol, or to other higher added value compounds, such as L-gluco-heptulose, which is used in cancer therapy and hypoglycemia [26].

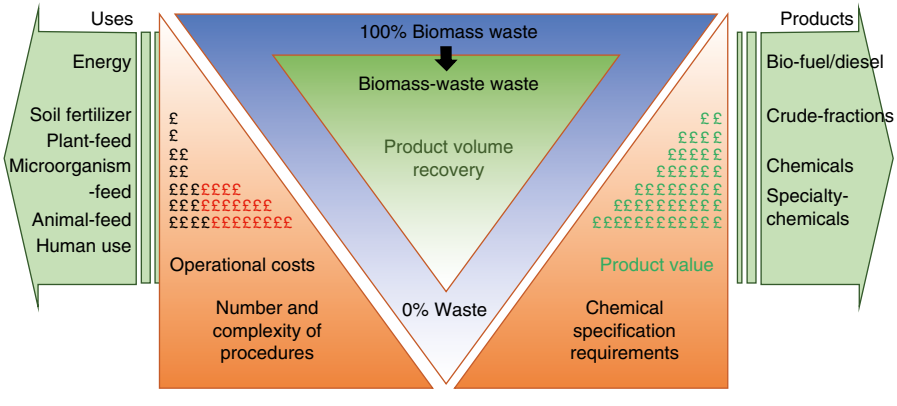

Figure 7.11 Biomass waste transformation into its different uses and products [127].

7.4 Conclusions and Future Trends

CPC is a constantly evolving technique, trying to keep up with continuously changing requirements of the chemical industry. Due to the versatility of the technique and the wide range of possible application areas where isolation, fractionation, and purification might be carried out using CPC, it can become an attractive green and sustainable alternative to conventional separation processes.

Besides the already mentioned improvements of the CPC instrument, other possible application fields are also worth mentioning where future developments may be expected. One of these areas could be the establishment of a CPC instrument capable of handling supercritical fluids (SF). Supercritical extraction (SCE) is often favored for the separation and purification of natural products, medicines, etc., as the extraction solvent needed for it eliminates the presence of toxic residues of organic solvents. The first attempts for its integration with CPC have been carried out to reduce the solvent consumption and cost of the production of cannabinoids [132]. Comparing the conventional methods for the production of Δ^9-tetrahydrocannabinol (Δ^9-THC) [133, 134], several advantages of the alternative green process have been found. The number of process steps could be reduced by 65%, the cost of the production of Δ^9-THC was calculated to be decreased by 57% in the case of a 5 kg per year production capacity and by 36% in the case of a 500 kg per year scale. Besides the highest yields and the reduction of waste production, no sweet water consumption was needed using the alternative SF-CPC process [132]. However, it must be noted that engineering efforts are still necessary to further develop this technology for the successful applications of the SF-CPC process, as due to instrumentational restrictions, the current systems are yet to be capable of fulfilling the requirements of an industrial-scale system.

Further developments in the field of on-line coupling CPC to analytical techniques such as mass spectrometry (MS), nuclear magnetic resonance (NMR) spectrometry, and high performance liquid chromatography (HPLC) are also expected to improve detection potential [135, 136]. Also, as multidimensional separation techniques are becoming more and more implemented, CPC can be used as the first-dimension or even as first- and second-dimension separation method on a preparative scale [137–142].

As the sudden development of available computational tools and artificial intelligence transpired in the past decade, the prediction of the logarithm of partition coefficients in the octanol–water system (log*P* values), the most widely used lipophilicity descriptor in the pharmaceutical industry has been already reported using machine learning/deep learning methods as a part of the SAMPL6 log*P* Challenge [143–145]. We can hope that these methods will become available for various biphasic systems in the future, which might facilitate method development for CPC.

Abbreviations

2-Methyltetrahydrofuran	2-Me-THF
Acetonitrile	MeCN
American Chemical Society	ACS
Active pharmaceutical ingredient	API

Aqueous two-phase systems	ATPS
Centrifugal partition chromatography	CPC
Chloroform/MeOH/water solvent system	ChMWat
Conductor-like screening model for real solvents	COSMO-RS
Countercurrent chromatography	CCC
Cyclopentyl methyl ether	CPME
Deep eutectic solvent	DES
Dichloromethane	DCM
Dimethyl carbonate	DMC
Dimethyl sulfoxide	DMSO
1-Ethyl-3-methylimidazolium chloride	(EMIM)Cl
Ethyl methyl ketone	MEK
Good Manufacturing Practice	GMP
GlaxoSmithKline	GSK
Heptane/ethyl acetate/methanol/water solvent system	Arizona
Hexane/ethyl acetate/MeOH/water solvent system	HEMWat
High-performance liquid chromatography	HPLC
High-pressure/medium-pressure chromatography	HPLC/MPLC
Host cell protein	HCP
Hydroxytyrosol	HT
Ionic liquid	IL
Mass spectrometry	MS
Methyl isobutyl ketone	MIBK
Monoaldehydic form of oleuropein aglycone	MFOA
Monoaldehydic form of ligstroside aglycone	MFLA
Monoclonal antibody	mAb
Multiple dual-mode	MDM
Natural deep eutectic solvents	NaDES
Nuclear magnetic resonance (spectroscopy)	NMR
Organic solvent nanofiltration	OSN
Polyethylene glycol	PEG
Reversed-phase high-performance liquid chromatography	RP-HPLC
Stirred tank reactor	STR
Supercritical fluid chromatography	SFC
Supercritical fluid extraction	SFE
Tert-butylmethyl ether	MTBE
Ultra-violet	UV
Virus-like particle	VLP
Water/dimethyl sulfoxide/tetrahydrofuran solvent system	WDT

References

1 Hearn, M.T.W. (2017). Recent progress toward more sustainable biomanufacturing. In: *Preparative Chromatography for Separation of Proteins* (eds. A. Staby, A.S. Rathore and S. Ahuja), 537–582. Wiley https://doi.org/10.1002/9781119031116.ch18.

2 Erythropel, H.C., Zimmerman, J.B., De Winter, T.M. et al. (2018). The Green ChemisTREE: 20 years after taking root with the 12 principles. *Green Chem* 20 (9): 1929–1961.

3 Constable, D.J.C., Dunn, P.J., Hayler, J.D. et al. (2007). Key green chemistry research areas – a perspective from pharmaceutical manufacturers. *Green Chem* 9 (5): 411–442. https://pubs.rsc.org/en/content/articlehtml/2007/gc/b703488c.

4 Jiménez-González, C., Poechlauer, P., Broxterman, Q.B. et al. (2011). Key green engineering research areas for sustainable manufacturing: a perspective from pharmaceutical and fine chemicals manufacturers. *Org Process Res Dev* 15 (4): 900–911. https://pubs.acs.org/doi/10.1021/op100327d.

5 Haan, A.B., Eral, H.B., and Schuur, B. (2020). Chapter 1. Characteristics of separation processes. In: *Industrial Separation Processes*, 1–16. De Gruyter https://www.degruyter.com/view/book/9783110654806/10.1515/9783110654806-001.xml.

6 Matlack, A.S. (2010). Chemical separations. In: *Introduction to Green Chemistry*, 187–214. CRC Press, Taylor and Francis Group, LLC https://www.taylorfrancis.com/books/introduction-green-chemistry-albert-matlack/10.1201/9781439882115.

7 Poole, C.F. (2000). Chromatography. In: *Encyclopedia of Separation Science*, 40–64. Elsevier https://linkinghub.elsevier.com/retrieve/pii/B0122267702000211.

8 Peterson, E.A., Dillon, B., Raheem, I. et al. (2014). Sustainable chromatography (an oxymoron?). *Green Chem* 16 (9): 4060–4075.

9 Dias, M.K.H.M., Madusanka, D.M.D., Han, E.J. et al. (2020). (−)-loliolide isolated from sargassum horneri protects against fine dust-induced oxidative stress in human keratinocytes. *Antioxidants* 9 (6): 474.

10 Santos, J.H.P.M., Ferreira, A.M., Almeida, M.R. et al. (2019). Continuous separation of cytochrome-c PEGylated conjugates by fast centrifugal partition chromatography. *Green Chem* 21 (20): 5501–5506.

11 Charon, N., Le Masle, A., and Chahen, L. (2018). Analyse des espèces oxygénées présentes dans les produits issus de la valorisation de la biomasse. *Actual Chim* 427–428: 80–83.

12 Mischko, W., Hirte, M., Roehrer, S. et al. (2018). Modular biomanufacturing for a sustainable production of terpenoid-based insect deterrents. *Green Chem* 20 (11): 2637–2650.

13 Hirte, M., Mischko, W., Kemper, K. et al. (2018). From microbial upcycling to biology-oriented synthesis: combining whole-cell production and chemo-enzymatic functionalization for sustainable taxanoid delivery. *Green Chem* 20 (23): 5374–5384.

14 Ward, D.P., Hewitson, P., Cárdenas-Fernández, M. et al. (2017). Centrifugal partition chromatography in a biorefinery context: optimisation and scale-up of monosaccharide fractionation from hydrolysed sugar beet pulp. *J Chromatogr A* 1497: 56–63. https://linkinghub.elsevier.com/retrieve/pii/S0021967317303370.

15 Destandau, E., Charpentier, J.P., Bostyn, S. et al. (2016). Gram-scale purification of dihydrorobinetin from Robinia pseudoacacia L. Wood by centrifugal partition chromatography. *Separations* 3 (3): 23.

16 Xynos, N., Abatis, D., Argyropoulou, A. et al. (2015). Development of a sustainable procedure for the recovery of hydroxytyrosol from table olive processing wastewater using adsorption resin technology and centrifugal partition chromatography. *Planta Med* 81 (17): 1621–1627. http://www.thieme-connect.de/DOI/DOI?10.1055/s-0035-1558111.

17 Bunnell, K., Lau, C.S., Lay, J.O. et al. (2015). Production and fractionation of xylose oligomers from switchgrass hemicelluloses using centrifugal partition chromatography. *J Liq Chromatogr Relat Technol* 38 (7): 801–809.

18 Ward, D.P., Cárdenas-Fernández, M., Hewitson, P. et al. (2015). Centrifugal partition chromatography in a biorefinery context: separation of monosaccharides from hydrolysed sugar beet pulp. *J Chromatogr A* 1411: 84–91.

19 Cottet, K., Fromentin, Y., Kritsanida, M. et al. (2015). Isolation of guttiferones from renewable parts of symphonia globulifera by centrifugal partition chromatography. *Planta Med* 81 (17): 1604–1608.

20 Kulakowski, D., Leme-Kraus, A.A., Nam, J.W. et al. (2017). Oligomeric proanthocyanidins released from dentin induce regenerative dental pulp cell response. *Acta Biomater* 55: 262–270.

21 Duval, J., Destandau, E., Pecher, V. et al. (2016). Selective enrichment in bioactive compound from Kniphofia uvaria by super/subcritical fluid extraction and centrifugal partition chromatography. *J Chromatogr A* 1447: 26–38.

22 Boonloed, A., Weber, G.L., Ramzy, K.M. et al. (2016). Centrifugal partition chromatography: a preparative tool for isolation and purification of xylindein from Chlorociboria aeruginosa. *J Chromatogr A* 1478: 19–25.

23 Kouka, P., Priftis, A., Stagos, D. et al. (2017). Assessment of the antioxidant activity of an olive oil total polyphenolic fraction and hydroxytyrosol from a Greek Olea europea variety in endothelial cells and myoblasts. *Int J Mol Med* 40 (3): 703–712.

24 Marié, T., Willig, G., Teixeira, A.R.S. et al. (2018). Enzymatic synthesis of resveratrol α-glycosides from β-cyclodextrin-resveratrol complex in water. *ACS Sustain Chem Eng* 6 (4): 5370–5380.

25 Marlot, L., Batteau, M., and Faure, K. (2020). Classification of biphasic solvent systems according to Abraham descriptors for countercurrent chromatography. *J Chromatogr A* 26: 1617.

26 Cárdenas-Fernández, M., Bawn, M., Hamley-Bennett, C. et al. (2017). An integrated biorefinery concept for conversion of sugar beet pulp into value-added chemicals and pharmaceutical intermediates. *Faraday Discuss* 202: 415–431.

27 Lorántfy, L., Rutterschmid, D., Örkényi, R. et al. (2020). Continuous industrial-scale centrifugal partition chromatography with automatic solvent system handling: concept and instrumentation. *Org Process Res Dev* 24 (11): 2676–2688. https://pubs.acs.org/doi/10.1021/acs.oprd.0c00338.

28 Örkényi, R., Éles, J., Faigl, F. et al. (2017). Continuous synthesis and purification by coupling a multistep flow reaction with centrifugal partition chromatography. *Angew Chem Int Ed* 56 (30): 8742–8745.

29 Huang, X.Y., Pei, D., Liu, J.F., and Di, D.L. (2018). A review on chiral separation by counter-current chromatography: development, applications and future outlook. *J Chromatogr A* 1531: 1–12.

30 Karkoula, E., Angelis, A., Koulakiotis, N.S. et al. (2018). Rapid isolation and characterization of crocins, picrocrocin, and crocetin from saffron using centrifugal partition chromatography and LC–MS. *J Sep Sci* 41 (22): 4105–4114.

31 Azevedo, L., Faqueti, L., Kritsanida, M. et al. (2016). Three new trixane glycosides obtained from the leaves of Jungia sellowii Less. using centrifugal partition chromatography. *Beilstein J Org Chem* 12: 674–683.

32 Faure, K., Mekaoui, N., and Berthod, A. (2014). Saving solvents in chromatographic purifications: the counter-current chromatography technique. In: *Green Chromatographic Techniques: Separation and Purification of Organic and Inorganic Analytes*, 1–18. Dordrecht: Springer https://doi.org/10.1007/978-94-007-7735-4_1.

33 Conway, W.D. (2011). Counter-current chromatography: simple process and confusing terminology. *J Chromatogr A* 1218 (36): 6015–6023. http://dx.doi.org/10.1016/j.chroma.2011.03.056.

34 Murayama, W., Kobayashi, T., Kosuge, Y. et al. (1982). A new centrifugal counter-current chromatograph and its application. *J Chromatogr A* 239 (C): 643–649. https://linkinghub.elsevier.com/retrieve/pii/S0021967300820221.

35 AECS-Quickprep Ltd. http://www.quattroprep.com/.

36 Partitron 25. https://partus.ets-couturier.com/en/welcome/.

37 Ever Seiko Corporation. http://everseiko.co.jp/scientific/hpcpc.html.

38 Gilson | Home | Liquid Handling, Purification and Extraction Solutions USA. https://www.gilson.com/default/.

39 KROMATON, Expert in Centrifugal Partition Chromatography – Kromaton. http://www.kromaton.com/en/.

40 Rotachrom Technologies LLC. | Industrial scale centrifugal partition chromatography. https://rotachrom.com/.

41 Berthod, A., Ruiz-Ángel, M.J., and Carda-Broch, S. (2009). Countercurrent chromatography: people and applications. *J Chromatogr A* 1216 (19): 4206–4217.

42 Berthod, A. (2002). Chapter 1 Fundamentals of countercurrent chromatography. In: *Comprehensive Analytical Chemistry*, 1–20. Elsevier https://linkinghub.elsevier.com/retrieve/pii/S0166526X02800046.

43 Brent Friesen, J. and Pauli, G.F. (2005). G.U.E.S.S. – A generally useful estimate of solvent systems for CCC. *J Liq Chromatogr Relat Technol* 28 (17): 2777–2806. https://www.tandfonline.com/doi/abs/10.1080/10826070500225234.

44 Ito, Y. (2005). Golden rules and pitfalls in selecting optimum conditions for high-speed counter-current chromatography. *J Chromatogr A* 1065 (2): 145–168. https://linkinghub.elsevier.com/retrieve/pii/S0021967304023374.

45 Schwienheer, C., Merz, J., and Schembecker, G. (2015). Investigation, comparison and design of chambers used in centrifugal partition chromatography on the basis of flow pattern and separation experiments. *J Chromatogr A* 1390: 39–49. https://linkinghub.elsevier.com/retrieve/pii/S0021967315001818.

46 Audo, G. (2018). Centrifugal partition chromatography: the key to green preparative chromatography. https://www.labcompare.com/10-Featured-Articles/348383-Centrifugal-Partition-Chromatography-The-Key-to-Green-Preparative-Chromatography/

47 Foucault, A. and Chevolot, L. (1998). Counter-current chromatography: instrumentation, solvent selection and some recent applications to natural product purification. *J Chromatogr A* 808 (1–2): 3–22. http://linkinghub.elsevier.com/retrieve/pii/S0021967398001216.

48 Oka, F., Oka, H., and Ito, Y. (1991). Systematic search for suitable two-phase solvent systems for high-speed counter-current chromatography. *J Chromatogr A* 538 (1): 99–108.

49 Liu, Y., Friesen, J., McAlpine, J., and Pauli, G. (2015). Solvent system selection strategies in countercurrent separation. *Planta Med* 81 (17): 1582–1591.

50 Liang, J., Meng, J., Wu, D. et al. (2015). A novel 9×9 map-based solvent selection strategy for targeted counter-current chromatography isolation of natural products. *J Chromatogr A* 1400: 27–39.

51 Dubant, S., Mathews, B., Higginson, P. et al. (2008). Practical solvent system selection for counter-current separation of pharmaceutical compounds. *J Chromatogr A* 1207 (1–2): 190–192.

52 Han, Q.-B., Wong, L., Yang, N.-Y. et al. (2008). A simple method to optimize the HSCCC two-phase solvent system by predicting the partition coefficient for target compound. *J Sep Sci* 31 (6–7): 1189–1194. http://doi.wiley.com/10.1002/jssc.200700582.

53 Wang, X., Liu, C., Ma, Q.Y. et al. (2020). A rapid and practical prediction method for the Arizona solvent system family used in high speed countercurrent chromatography. *J Chromatogr A* 1629: 461426.

54 Hopmann, E., Arlt, W., and Minceva, M. (2011). Solvent system selection in counter-current chromatography using conductor-like screening model for real solvents. *J Chromatogr A* 1218 (2): 242–250. https://linkinghub.elsevier.com/retrieve/pii/S0021967310015840.

55 Frey, A., Hopmann, E., and Minceva, M. (2014). Selection of biphasic liquid systems in liquid-liquid chromatography using predictive thermodynamic models. *Chem Eng Technol* 37 (10): 1663–1674.

56 Lu, Y., Berthod, A., Hu, R. et al. (2009). Screening of complex natural extracts by countercurrent chromatography using a parallel protocol. *Anal Chem* 81 (10): 4048–4059. https://pubs.acs.org/sharingguidelines.

57 Renault, J.-H., Thépenier, P., Zéches-Hanrot, M. et al. (1997). Preparative separation of anthocyanins by gradient elution centrifugal partition chromatography. *J Chromatogr A* 763 (1–2): 345–352. https://linkinghub.elsevier.com/retrieve/pii/S0021967396008801.

58 Margraff, R. (1995). Preparative centrifugal partition chromatography. In: *Centrifugal Partition Chromatography* (ed. A.P. Foucault), 331–350. Marcel Dekker, Inc.

59 Kato, T. and Hatanaka, K. (2008). Purification of gangliosides by liquid-liquid partition chromatography. *J Lipid Res* 49 (11): 2474–2478.

60 Kukula-Koch, W., Koch, W., Angelis, A. et al. (2016). Application of pH-zone refining hydrostatic countercurrent chromatography (hCCC) for the recovery of antioxidant phenolics and the isolation of alkaloids from Siberian barberry herb. *Food Chem* 203: 394–401.

61 Foucault, A.P., Durand, P., Frias, E.C., and Le Goffic, F. (1993). Biphasic mixture of water, dimethyl sulfoxide, and tetrahydrofuran for use in centrifugal partition chromatography. *Anal Chem* 65 (15): 2150–2154. https://pubs.acs.org/sharingguidelines.

62 Oelmeier, S.A., Ladd-Effio, C., and Hubbuch, J. (2013). Alternative separation steps for monoclonal antibody purification: combination of centrifugal partitioning chromatography and precipitation. *J Chromatogr A* 1319: 118–126. http://dx.doi.org/10.1016/j.chroma.2013.10.043.

63 Faure, K., Bouju, E., Suchet, P., and Berthod, A. (2013). Use of limonene in countercurrent chromatography: a green alkane substitute. *Anal Chem* 85 (9): 4644–4650.

64 Faure, K., Bouju, E., Doby, J., and Berthod, A. (2014). Limonene in Arizona liquid systems used in countercurrent chromatography. II Polarity and stationary-phase retention. *Anal Bioanal Chem* 406 (24): 5919–5926.

65 Roehrer, S., Bezold, F., García, E.M., and Minceva, M. (2016). Deep eutectic solvents in countercurrent and centrifugal partition chromatography. *J Chromatogr A* 1434: 102–110. http://dx.doi.org/10.1016/j.chroma.2016.01.024.

66 Amarouche, N., Boudesocque, L., Borie, N. et al. (2014). New biphasic solvent system based on cyclopentyl methyl ether for the purification of a non-polar synthetic peptide by pH-zone refining centrifugal partition chromatography. *J Sep Sci* 37 (11): 1222–1228. http://doi.wiley.com/10.1002/jssc.201300971.

67 Curzons, A.D., Constable, D.J.C., Mortimer, D.N., and Cunningham, V.L. (2001). So you think your process is green, how do you know? Using principles of sustainability to determine what is green – a corporate perspective. In: *Green Chemistry*, 1–6. Royal Society of Chemistry https://pubs.rsc.org/en/content/articlehtml/2001/gc/b007871i.

68 Nelson, W.M. (2003). Green solvents in green chemistry. In: *Green Solvents for Chemistry: Perspectives and Practice*, 91–115. Oxford University Press, Inc.

69 Capello, C., Fischer, U., and Hungerbühler, K. (2007). What is a green solvent? A comprehensive framework for the environmental assessment of solvents. *Green Chem* 9 (9): 927. https://pubs.rsc.org/en/content/articlehtml/2007/gc/b617536h.

70 Pena-Pereira, F. and Tobiszewski, M. (2017). Initial considerations. In: *The Application of Green Solvents in Separation Processes* (eds. F. Pena-Pereira and M. Tobiszewski), 3–16. Elsevier Inc.

71 Byrne, F.P., Jin, S., Paggiola, G. et al. (2016). Tools and techniques for solvent selection: green solvent selection guides. *Sustain Chem Process* 4 (1): 7. http://sustainablechemicalprocesses.springeropen.com/articles/10.1186/s40508-016-0051-z.

72 Alfonsi, K., Colberg, J., Dunn, P.J. et al. (2008). Green chemistry tools to influence a medicinal chemistry and research chemistry based organisation. *Green Chem* 10 (1): 31–36. www.rsc.org/greenchem.

73 Alder, C.M., Hayler, J.D., Henderson, R.K. et al. (2016). Updating and further expanding GSK's solvent sustainability guide. *Green Chem* 18 (13): 3879–3890.

74 Prat, D., Pardigon, O., Flemming, H.W. et al. (2013). Sanofi's solvent selection guide: a step toward more sustainable processes. *Org Process Res Dev* 17 (12): 1517–1525. https://pubs.acs.org/doi/abs/10.1021/op4002565.

75 Prat, D., Wells, A., Hayler, J. et al. (2015). CHEM21 selection guide of classical- and less classical-solvents. *Green Chem* 18 (1): 288–296. www.rsc.org/greenchem.

76 ACS GCI Pharmaceutical Roundtable Portal (2019). Solvent tool. https://www.acsgcipr.org/tools-for-innovation-in-chemistry/solvent-tool/.

77 Diorazio, L.J., Hose, D.R.J., and Adlington, N.K. (2016). Toward a more holistic framework for solvent selection. *Org Process Res Dev* 20 (4): 760–773. https://pubs.acs.org/sharingguidelines.

78 Sicaire, A.-G., Vian, M.A., Filly, A. et al. (2014). 2-Methyltetrahydrofuran: main properties, production processes, and application in extraction of natural products, 253–268. http://link.springer.com/10.1007/978-3-662-43628-8_12.

79 Berthod, A. and Armstrong, D.W. (1988). Centrifugal partition chromatography. I. General features. *J Liq Chromatogr* 11 (3): 547–566. http://www.tandfonline.com/doi/abs/10.1080/01483918808068331.

80 Zema, D.A., Calabrò, P.S., Folino, A. et al. (2018). Valorisation of citrus processing waste: a review. *Waste Manage* 80: 252–273.

81 Citrus fruit, fresh and processed. Food and agriculture organisation of the United Nations, 2016.

82 Chavan, P., Singh, A.K., and Kaur, G. (2018). Recent progress in the utilization of industrial waste and by-products of citrus fruits: a review. *J Food Process Eng* 41 (8): e12895. https://onlinelibrary.wiley.com/doi/abs/10.1111/jfpe.12895.

83 Code of Federal Regulations, Title 21, § 182.60. https://ecfr.federalregister.gov/current/title-21/chapter-I/subchapter-B/part-182/subpart-A/section-182.60.

84 United Stated Environmental Protection Agency (1994). Reregistration Eligibility Decision (RED) Limonene, EPA 738-R-94-034.

85 Faure, K., Bouju, E., Suchet, P., and Berthod, A. (2014). Limonene in Arizona liquid systems used in countercurrent chromatography. I physicochemical properties. *Anal Bioanal Chem* 406 (24): 5909–5917.

86 MacMillan, D.S., Murray, J., Sneddon, H.F. et al. (2012). Replacement of dichloromethane within chromatographic purification: a guide to alternative solvents. *Green Chem* 14 (11): 3016–3019. https://pubs.rsc.org/en/content/articlehtml/2012/gc/c2gc36378j.

87 Azzena, U., Carraro, M., Pisano, L. et al. (2019). Cyclopentyl methyl ether: an elective ecofriendly ethereal solvent in classical and modern organic chemistry. *ChemSusChem* 12 (1): 40–70.

88 Specialty chemicals – cyclopentyl methyl ether (CPME) – products:ZEON CORPORATION. http://www.zeon.co.jp/business_e/enterprise/spechemi/spechemi5-13.html#h2-3.

89 de Gonzalo, G., Alcántara, A.R., and Domínguez de María, P. (2019). Cyclopentyl methyl ether (CPME): a versatile eco-friendly solvent for applications in biotechnology and biorefineries. *ChemSusChem* 12 (10): 2083–2097. https://onlinelibrary.wiley.com/doi/abs/10.1002/cssc.201900079.

90 Prache, N., Abreu, S., Sassiat, P. et al. (2016). Alternative solvents for improving the greenness of normal phase liquid chromatography of lipid classes. *J Chromatogr A* 1464: 55–63.

91 Hartonen, K. and Riekkola, M.L. (2017). Water as the first choice green solvent. In: *The Application of Green Solvents in Separation Processes*, 19–55. Elsevier https://reader.elsevier.com/reader/sd/pii/B9780128052976000024?token=33A2FB4236D7CDC344028321D95EE413584F4DB131ED7CE4BA20690A34CCF65E3828E8DA77E099D69BC373FCF262338E.

92 Reichardt, C. and Welton, T. (2010). Empirical parameters of solvent polarity. In: *Solvents and Solvent Effects in Organic Chemistry*, 425–508. Weinheim: Wiley-VCH Verlag GmbH & Co. KGaA.

93 Magri, M.L., Cabrera, R.B., Miranda, M.V. et al. (2003). Performance of an aqueous two-phase-based countercurrent chromatographic system for horseradish peroxidase purification. *J Sep Sci* 26 (18): 1701–1706.

94 Faria, D.F., Silva, T.P., Aires-Barros, M.R., and Azevedo, A.M. (2019). A chronology of the development of aqueous two-phase systems as a viable liquid-liquid extraction for biological products. In: *Reference Module in Chemistry, Molecular Sciences and Chemical Engineering*, 1–12. Elsevier Inc. http://dx.doi.org/10.1016/B978-0-12-409547-2.14393-8.

95 Mekaoui, N., Faure, K., and Berthod, A. (2012). Advances in countercurrent chromatography for protein separations. *Bioanalysis* 4 (7): 833–844.

96 Grudzień, Ł., Madeira, L., Fisher, D. et al. (2013). Phase system selection with fractional factorial design for purification of recombinant cyanovirin-N from a hydroponic culture medium using centrifugal partition chromatography. *J Chromatogr A* 1285: 57–68.

97 Asenjo, J.A. and Andrews, B.A. (2011). Aqueous two-phase systems for protein separation: a perspective. *J Chromatogr A* 1218: 8826–8835.

98 Harris, D.P., Andrews, A.T., Wright, G. et al. (1998). The application of aqueous two-phase systems to the purification of pharmaceutical proteins from transgenic sheep milk. *Bioseparation* 7 (1): 31–37. https://pubmed.ncbi.nlm.nih.gov/9615611/.

99 Goll, J., Audo, G., and Minceva, M. (2015). Comparison of twin-cell centrifugal partition chromatographic columns with different cell volume. *J Chromatogr A* 1406: 129–135.

100 Bezold, F., Roehrer, S., and Minceva, M. (2019). Ionic liquids as modifying agents for protein separation in centrifugal partition chromatography. *Chem Eng Technol* 42 (2): 474–482.

101 Schwienheer, C., Prinz, A., Zeiner, T., and Merz, J. (2015). Separation of active laccases from Pleurotus sapidus culture supernatant using aqueous two-phase systems in centrifugal partition chromatography. *J Chromatogr B: Anal Technol Biomed Life Sci* 1002: 1–7. http://dx.doi.org/10.1016/j.jchromb.2015.07.050.

102 Top 15 Best-Selling Drugs Launched in 2020. https://www.genengnews.com/a-lists/top-15-best-selling-drugs-launched-in-2020/.

103 Ladd Effio, C. (2016). *Novel Development Tools for Processing of Recombinant Virus-Like Particles*. Karlsruher Instituts f¨ur Technologie (KIT).

104 Ladd Effio, C., Wenger, L., Ötes, O. et al. (2015). Downstream processing of virus-like particles: single-stage and multi-stage aqueous two-phase extraction. *J Chromatogr A* 1383: 35–46. http://dx.doi.org/10.1016/j.chroma.2015.01.007.

105 Zullaikah, S., Rachmaniah, O., Utomo, A.T. et al. (2018). Green separation of bioactive natural products using liquefied mixture of solids. In: *Green Chemistry*. InTech http://www.intechopen.com/books/green-chemistry/green-separation-of-bioactive-natural-products-using-liquefied-mixture-of-solids.

106 Smith, E.L., Abbott, A.P., and Ryder, K.S. (2014). Deep eutectic solvents (DESs) and their applications. *Chem Rev* 114 (21): 11060–11082.

107 Zhang, Q., De Oliveira, V.K., Royer, S., and Jérôme, F. (2012). Deep eutectic solvents: syntheses, properties and applications. *Chem Soc Rev* 41 (21): 7108–7146.

108 Bezold, F. and Minceva, M. (2018). Liquid-liquid equilibria of n-heptane, methanol and deep eutectic solvents composed of carboxylic acid and monocyclic terpenes. *Fluid Phase Equilib* 477: 98–106. https://doi.org/10.1016/j.fluid.2018.08.020.

109 Bezold, F. and Minceva, M. (2019). A water-free solvent system containing an L-menthol-based deep eutectic solvent for centrifugal partition chromatography applications. *J Chromatogr A* 1587: 166–171. https://doi.org/10.1016/j.chroma.2018.11.083.

110 Rundquist, E., Pink, C., Vilminot, E., and Livingston, A. (2012). Facilitating the use of counter-current chromatography in pharmaceutical purification through use of organic solvent nanofiltration. *J Chromatogr A* 1229: 156–163.

111 Santos, J.H.P.M.P.M., Almeida, M.R., Martins, C.I.R.R. et al. (2018). Separation of phenolic compounds by centrifugal partition chromatography. *Green Chem* 20 (8): 1906–1916. http://dx.doi.org/10.1039/c8gc00179k.

112 den Hollander, J.L., Stribos, B.I., van Buel, M.J. et al. (1998). Centrifugal partition chromatographic reaction for the production of chiral amino acids. *J Chromatogr B: Biomed Sci Appl* 711 (1–2): 223–235. https://linkinghub.elsevier.com/retrieve/pii/S0378434798000127.

113 Den Hollander, J.L., Wai Wong, Y., Luyben, K.C.A.M. et al. (1999). Non-separating effects in a centrifugal partition chromatographic reactor for the enzymatic production of L-amino acids. *Chem Eng Sci* 54 (15–16): 3207–3215. https://linkinghub.elsevier.com/retrieve/pii/S0009250998003479.

114 Nioi, C., Riboul, D., Destrac, P. et al. (2015). The centrifugal partition reactor, a novel intensified continuous reactor for liquid-liquid enzymatic reactions. *Biochem Eng J* 103: 227–233. http://dx.doi.org/10.1016/j.bej.2015.07.018.

115 Nioi, C., Destrac, P., and Condoret, J.S. (2019). Lipase esterification in the Centrifugal Partition Reactor: modelling and determination of the specific interfacial area. *Biochem Eng J* 143 (December 2018): 179–184.

116 Mazubert, A., Poux, M., and Aubin, J. (2013). Intensified processes for FAME production from waste cooking oil: a technological review. *Chem Eng J* 233: 201–223.

117 Rashid, W.N.W.A., Uemura, Y., Kusakabe, K. et al. (2014). Synthesis of biodiesel from palm oil in capillary millichannel reactor: effect of temperature, methanol to oil molar ratio, and KOH concentration on FAME yield. *Procedia Chem* 9: 165–171. www.sciencedirect.com.

118 Krause, J., Oeldorf, T., Schembecker, G., and Merz, J. (2015). Enzymatic hydrolysis in an aqueous organic two-phase system using centrifugal partition chromatography. *J Chromatogr A* 1391 (1): 72–79. http://dx.doi.org/10.1016/j.chroma.2015.02.071.

119 Krause, J. and Merz, J. (2017). Comparison of enzymatic hydrolysis in a centrifugal partition chromatograph and stirred tank reactor. *J Chromatogr A* 1504: 64–70. http://dx.doi.org/10.1016/j.chroma.2017.05.006.

120 Angelis, A., Michailidis, D., Antoniadi, L. et al. (2021). Pilot continuous centrifugal liquid-liquid extraction of extra virgin olive oil biophenols and gram-scale recovery of pure oleocanthal, oleacein, MFOA, MFLA and hydroxytyrosol. *Sep Purif Technol* 255: 117692.

121 US Food and Drug Administration (2021). Advanced manufacturing. https://www.fda.gov/emergency-preparedness-and-response/mcm-issues/advanced-manufacturing.

122 Tian, Y., Demirel, S.E., Hasan, M.M.F., and Pistikopoulos, E.N. (2018). An overview of process systems engineering approaches for process intensification: state of the art. *Chem Eng Process: Process Intensif* 133: 160–210. https://doi.org/10.1016/j.cep.2018.07.014.

123 Rogers, L. and Jensen, K.F. (2019). Continuous manufacturing-the Green Chemistry promise? *Green Chem* 21 (13): 3481–3498. https://pubs.rsc.org/en/content/articlehtml/2019/gc/c9gc00773c.

124 Costandy, J.G., Edgar, T.F., and Baldea, M. (2019). Switching from batch to continuous reactors is a trajectory optimization problem. *Ind Eng Chem Res* 58 (30): 13718–13736. https://pubs.acs.org/doi/pdf/10.1021/acs.iecr.9b01126.

125 Arockiam JeyaSundar, P.G.S., Ali, A., Guo, d., and Zhang, Z. (2020). Waste treatment approaches for environmental sustainability. In: *Microorganisms for Sustainable Environment and Health*, 119–135. Elsevier.

126 Millati, R., Cahyono, R.B., Ariyanto, T. et al. (2019). Agricultural, industrial, municipal, and forest wastes: an overview. In: *Sustainable Resource Recovery and Zero Waste Approaches*, 1–22. Elsevier https://linkinghub.elsevier.com/retrieve/pii/B9780444642004000013.

127 Quirino, J.P., Alejandro, F.M., and Bissember, A.C. (2020). Towards cleaner downstream processing of biomass waste chemical products by liquid chromatography: a review and recommendations. *J Clean Prod* 253: 119937. https://doi.org/10.1016/j.jclepro.2019.119937.

128 Andreadou, I., Iliodromitis, E.K., Mikros, E. et al. (2006). The olive constituent oleuropein exhibits anti-ischemic, antioxidative, and hypolipidemic effects in anesthetized rabbits. *J Nutr* 136 (8): 2213–2219. https://pubmed.ncbi.nlm.nih.gov/16857843/.

129 Deiana, M., Rosa, A., Corona, G. et al. (2007). Protective effect of olive oil minor polar components against oxidative damage in rats treated with ferric-nitrilotriacetate. *Food Chem Toxicol* 45 (12): 2434–2440. https://pubmed.ncbi.nlm.nih.gov/17686562/.

130 Zheng, Y., Yu, C., Cheng, Y.S. et al. (2012). Integrating sugar beet pulp storage, hydrolysis and fermentation for fuel ethanol production. *Appl Energy* 93: 168–175.

131 Hamley-Bennett, C., Lye, G.J., and Leak, D.J. (2016). Selective fractionation of Sugar Beet Pulp for release of fermentation and chemical feedstocks; optimisation of thermo-chemical pre-treatment. *Bioresour Technol* 209: 259–264.

132 Perrotin-Brunel, H. (2011). *Sustainable Production of Cannabinoids with Supercritical Carbon Dioxide Technologies*. Technische Universiteit Delft.

133 Goodwin, N.J., Archer, N.J., Murray, C. et al. (2003). Production of delta 9 tetrahydrocannabinol. United States Patent Application Publication, US 2005/0171361 A1.

134 Bhatarah, P., Mchattie, D., and Greenwood, A.K. (2009). Production of delta 9 tetrahydrocannabinol. World Intellectual Property Organization, WO 2009/133376 A1.

135 Michel, T., Destandau, E., and Elfakir, C. (2014). New advances in countercurrent chromatography and centrifugal partition chromatography: focus on coupling strategy. *Anal Bioanal Chem* 406 (4): 957–969.

136 Dubuis, A., Le Masle, A., Chahen, L. et al. (2019). Centrifugal partition chromatography as a fractionation tool for the analysis of lignocellulosic biomass products by liquid chromatography coupled to mass spectrometry. *J Chromatogr A* 1597: 159–166.

137 Marlot, L., Batteau, M., and Faure, K. (2018). Comparison between centrifugal partition chromatography and preparative liquid chromatography as first dimensions in off-line two-dimensional separation: application to the isolation of multi-targeted compounds from Edelweiss plant. *Electrophoresis* 39 (15): 2011–2019. http://doi.wiley.com/10.1002/elps.201800032.

138 Reymond, C., Le Masle, A., Colas, C., and Charon, N. (2020). Input of an off-line, comprehensive, three-dimensional method (CPC×SFC/HRMS) to quantify polycyclic aromatic hydrocarbons in vacuum gas oils. *Anal Chem* 92 (9): 6684–6692.

139 Pompermaier, L., Schwaiger, S., Mawunu, M. et al. (2020). Purification of thonningianins A and B and four further derivatives from Thonningia sanguinea by one- and two-dimensional centrifugal partition chromatography. *J Sep Sci* 43 (2): 524–530.

140 Marlot, L., Batteau, M., De Beer, D., and Faure, K. (2018). In silico screening of comprehensive two-dimensional centrifugal partition chromatography × liquid chromatography for multiple compound isolation. *Anal Chem* 90 (24): 14279–14286.

141 Le Masle, A., Santin, S., Marlot, L. et al. (2018). Centrifugal partition chromatography a first dimension for biomass fast pyrolysis oil analysis. *Anal Chim Acta* 1029: 116–124.

142 Marlot, L., Batteau, M., Escofet, M.C. et al. (2017). Two-dimensional multi-heart cutting centrifugal partition chromatography–liquid chromatography for the preparative isolation of antioxidants from Edelweiss plant. *J Chromatogr A* 1504: 55–63.

143 Prasad, S. and Brooks, B.R. (2020). A deep learning approach for the blind logP prediction in SAMPL6 challenge. *J Comput Aided Mol Des* 34 (5): 535–542. https://link.springer.com/article/10.1007/s10822-020-00292-3.

144 Xie, L., Xu, L., Kong, R. et al. (2020). Improvement of prediction performance with conjoint molecular fingerprint in deep learning. *Front Pharmacol* 11: 2148. https://www.frontiersin.org/articles/10.3389/fphar.2020.606668/full.

145 Işık, M., Bergazin, T.D., Fox, T. et al. (2020). Assessing the accuracy of octanol–water partition coefficient predictions in the SAMPL6 Part II log P challenge. *J Comput Aided Mol Des* 34 (4): 335–370. https://link.springer.com/article/10.1007/s10822-020-00295-0.

8

Liquid Membrane Technology for Sustainable Separations

Pablo López-Porfiri[1], María González-Miquel[1,2], and Patricia Gorgojo[1,3,4]

[1] *Department of Chemical Engineering and Analytical Sciences, The University of Manchester, Manchester, UK*
[2] *Departamento de Ingeniería Química Industrial y del Medioambiente, ETS Ingenieros Industriales, Universidad Politécnica de Madrid, Madrid, Spain*
[3] *Nanoscience and Materials Institute of Aragón (INMA) CSIC-Universidad de Zaragoza, Zaragoza, Spain*
[4] *Chemical and Environmental Engineering Department, Universidad de Zaragoza, Zaragoza, Spain*

8.1 Introduction to Liquid Membrane (LM) Technology

Chemical engineering is continuously evolving to improve process efficiencies, considering not only economic aspects but also major global social concerns. In order to enhance competitiveness and sustainability, chemical industries must advance toward green practices, reducing energy consumption, using renewable fuels and raw materials, and looking at sustainable synergies with the environment. Separation operations, the core stage of chemical processes, are often the bottleneck in process development, due to their high energy demand and use of toxic substances. Among several avenues of separation engineering research, membrane technology has gained great interest over the past few decades. Membrane-based separation methods can be an order of magnitude more energy-efficient than heat-driven separations as they do not involve phase change [1].

A membrane is a semipermeable barrier that allows the selective transport of substances between two streams. Membranes are typically thin polymer films fabricated on highly porous substrates, although other materials such as inorganic ceramics, zeolites, metal–organic frameworks (MOFs), and metals are often used. Novel materials such as polymer/graphene nanocomposite membranes are currently being investigated with promising results [2–4]. It is worth noting the extended use of membranes in the following processes: micro-/ultrafiltration (MF/UF), water treatment, desalination, gas purification, pervaporation (PV), and dialysis. Membranes can be classified according to the operational pressures they work at or pore size [5]. Reverse osmosis (RO) has been widely implemented for water desalinization with extremely dense membranes (equivalent pore size of 1–5 Å), at pressures ranging from 20 to 100 bar, which are required to overcome the osmotic pressure.

Sustainable Separation Engineering: Materials, Techniques and Process Development, Volume 1, First Edition. Edited by Gyorgy Szekely and Dan Zhao.
© 2022 John Wiley & Sons Ltd. Published 2022 by John Wiley & Sons Ltd.

Nanofiltration (NF) membranes, on the other hand, work at lower pressures of 5–15 bar with pores below 1 nm, for the separation of species larger than monovalent ions. Filtration of larger bodies, e.g. micro-organics, lipids, and proteins, can be done by UF with membranes of 2–100 nm pore size, as well as MF for suspended solids and bacteria bigger than 0.1 μm at a pressure below 1 bar. Amongst other membrane techniques, electro-membranes are used for ion separation; in gas separation (GS) membranes, the permeating species are gases, while PV and membrane distillation (MD) allow for volatile components separation.

A noteworthy membrane type is the so-called liquid membrane (LM), where the semi-permeable barrier is composed of a liquid instead of a solid medium. Taking advantage of the liquid immiscibility, LMs can still separate two streams and transfer target solutes in a diffusional process. Thus, they combine two processes in one stage: liquid–liquid extraction (LLX) and stripping altogether. LMs do not need pressure or temperature gradient to accomplish the separation, which translates into low energy consumption. The reduction in solvents' requirements as compared to other processes such as LLX, simplicity of operation, and energy-efficiency, make LM technology stand as a competitive alternative to traditional separation operations [6]. As discussed in detail further in this chapter, LMs have been applied in biorefinery, GS, wastewater treatment processes, the recovery of amino acids, metal ions, and rare earths (REs), as well as the removal of nuclear waste and heavy metals, as illustrated in Figure 8.1.

This chapter gives a comprehensive overview of the LM technology applied for sustainable separations. The basic concepts and definitions of LMs are presented, along with a selection of the most relevant applications for the development of sustainable processes. Fundamental aspects inherent to the liquid membrane operation are given as well to help the reader understand the scope of the technology and its current limitations.

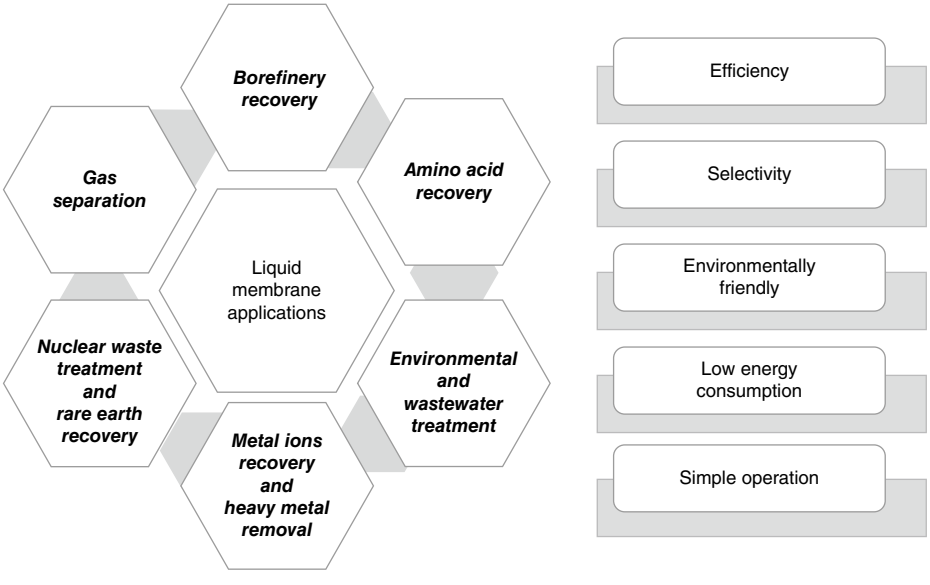

Figure 8.1 Fields where liquid membranes (LMs) are applied and main features.

8.1.1 Components of a Liquid Membrane

An LM is an immiscible liquid that acts as a barrier, allowing compounds to move from one stream to another while keeping them separated. The target solute to be recovered or removed is extracted from a concentrated feed stream, and transferred into a receiving stream, the stripping phase, as represented in Figure 8.2. Both streams can be in a gaseous or liquid phase, according to the nature of the process. The diffusional pathways that compounds follow across the membrane depend on thermodynamic affinities and hydrodynamic parameters, which contribute to the overall transport rate. The selectivity of an LM is related to the difference in velocity at which different compounds move through the membrane. In comparison to polymer matrices, diffusion coefficients are higher in liquids, within a range of 10^{-6}–10^{-5} cm^2/s, which translates into larger solute flux [7]. For the membranes process, this transport velocity is known as solute permeation. Still, other operational variables, such as temperature, and pressure or electric field gradients, can be tailored to improve the membrane performance [6].

From a phenomenological perspective, LMs share more similarities with LLX than filtration processes. Solutes permeate from the feed to the receiving side of the membrane (the stripping phase) following a concentration gradient. Nevertheless, in LM, the permeation ratio is not governed by thermodynamics equilibrium, but by the chemical potential gradient in a constant diffusional phenomenon. Thus, extraction against the concentration gradient could be achieved given the appropriate conditions. LMs allow for accomplishing reactive extraction and its back extractions comprising the extraction and stripping in a sole process stage, continuously recycling the extractant agent. Furthermore, LM can attain a larger mass transfer area per unit volume in comparison to LLX columns [8]. This process simplification, in both step number and solvent requirements, leads to a reduction of operational costs. Since LMs can accomplish the separation by solute-phase affinity gradients, operation conditions found in the literature are often atmospheric pressure and room temperature, which represent no extra energy requirements. On the other hand, both parameters become critical in gas stream separations.

The simplest LMs are conformed of a single solvent to separate the phases, transporting the target solute by diffusion. This solvent can be a pure compound, though mixtures of solvents plus modifiers are often adopted to tailor the membrane properties, e.g. the viscosity. Nonetheless, mixtures composed of a diluent solvent and a carrier or extractant agent

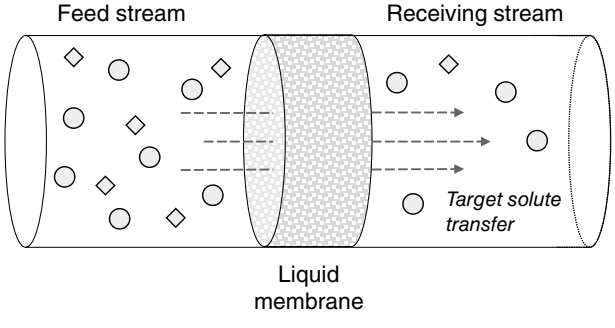

Figure 8.2 Liquid membrane system scheme.

are the most promising alternative. While in membranes without a carrier, the solute transport is just driven by intermolecular affinities; in those where a carrier is present, there is a reversible reaction that leads to a carrier-solute complex that enhances the solubility and diffusivity. The presence of carriers enhances not only the mass transfer but the selectivity as well. Moreover, carriers can accomplish high chiral resolution for enantiomer separations with LMs [9, 10]. However, carrier selection and its reaction kinetics must be carefully considered for the process design in order to find a suitable candidate. Acid carriers, di(2-ethylhaxyl)phosphoric acid (D2EHPA), for example, and basic carriers, such as trioctylamine (TOA), tributylphosphate (TBP), and Aliquat® 336, are widely found in the literature, yet neutral carriers might be employed as well [11]. Water-immiscible solvents are required to extract compounds from aqueous matrices, and aqueous solutions are required to extract substances from organic solutions. Kerosene and n-heptane are highly hydrophobic solvents used as a diluent on LM for the extraction of organic compounds, phenol, REs, and metal ions from aqueous solutions. Novel solvents such as ionic liquids (ILs) are escalating in popularity for LM, the so-called IL-membranes [12–16], which find their use in organic acids recovery [17–19], removal of phenols [20–23], and heavy metals [24], as well as bio-alcohol PV separations [25]. Moreover, hydrophobic deep eutectic solvents (DESs) have been recently investigated for the preparation of LM and applied in biorefinery [26] and amino acid recovery [27], and bio-based vegetable oils can be found in LM to enhance their performance; coconut oil [28], sunflower oil [29, 30], rice oil [31, 32], corn oil [33], palm oil [34–36], and even waste vegetable oil [37] have been incorporated as a diluent for LMs using TOA or D2EHPA as the carriers. Vegetable oils are mainly mixtures of tri-, di-, and monoglycerides, with a nonpolar nature. However, due to their natural sources, vegetable oils can vary in their composition, which compromises the reproducibility of LMs.

8.1.2 Liquid Membrane Configurations

LMs are classified into three main configurations as shown in Figure 8.3: (i) bulk liquid membrane (BLM), which uses relatively large amounts of extraction solvent within the membrane; (ii) emulsion liquid membrane (ELM), also called double emulsion membrane, where the membrane is emulsified as globules in the feed, thus maximizing the exchange area; and (iii) supported liquid membrane (SLM), where a small amount of liquid is used to impregnate a thin porous layer, reducing the mass transfer resistance from the feed to the product stream.

There are advantages and limitations for each membrane configuration, as summarized in Table 8.1, and its selection depends on the specific applications and the whole process design. Further details on operational aspects will be presented in Section 8.2.

8.1.2.1 Bulk Liquid Membranes

BLM configurations contain three bulk liquid phases, where the feed and the striping streams are kept separated by an immiscible solvent. Specific arrangements have been proposed to avoid the mixture of the feed and the receiving phases, often by physical barriers and profiting from density differences, at the same time they are continuously stirring [38]. In more elaborate designs, semipermeable barriers have been used in layered BLM to hold the membrane phase between streams. BLM stands out by its easy setup at a laboratory

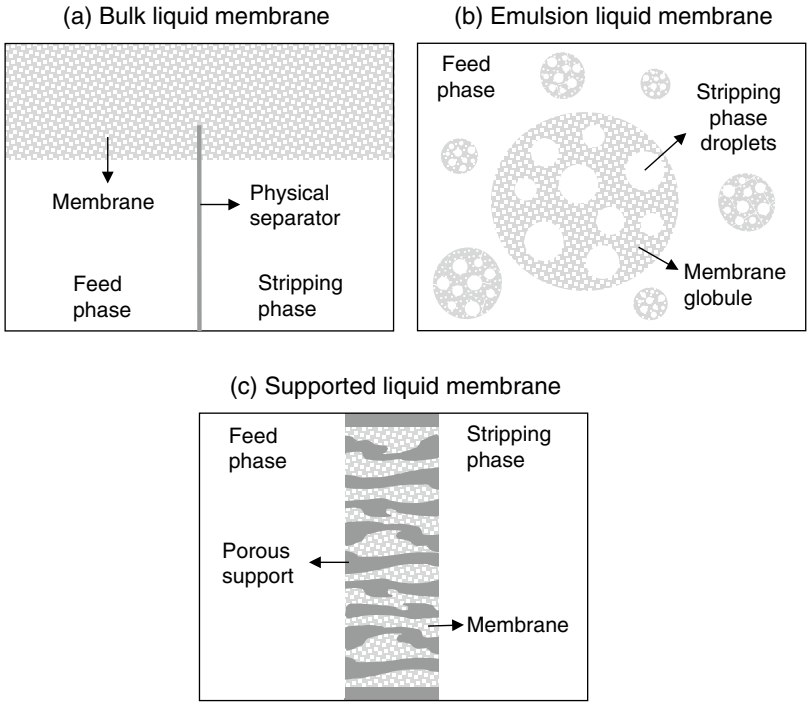

Figure 8.3 Main liquid membrane configurations. (a) Bulk liquid membrane; (b) Emulsion liquid membrane; (c) Supported liquid membrane.

Table 8.1 Strengths and limitations of the three main liquid membrane configurations.

	Strengths	Limitations
BLM	• Simple construction and operation • High membrane stability • Allows to determine mass transfer and kinetic parameters at laboratory scale	• Low mass transfer surface area and flux • A large amount of solvent requirement • Not feasible on an industrial scale
ELM	• Simple equipment • Largest surface–to–volume area ratio • High concentration factors (i.e. stripping phase results in more concentrate than the feed phase) • Can be broadly applied	• The addition of surfactants required • Requires extra emulsification and de-emulsification stages • Numerous operational variables • Emulsion stability issue by breakage and swelling phenomena • Risk of feed and stripping mix
SLM	• Low solvent requirement • Thin layers reduce mass transfer resistance • Large surface area per unit volume may be obtained using hollow fiber or spiral wound arrays • No loading and floating issues • Simple to scale up	• Support capacity to retain the solvent determines its stability, operational life, and overall performance • The support matrix adds extra mass resistance • Membrane instability leads to low mass flux or poor selectivity

scale, allowing determining mass transfer and kinetic parameters. Nonetheless, this configuration is not particularly attractive for industrial applications due to the low mass transfer area–to–bulk volume ratio. Another important limitation is the difficulty in ensuring liquid immiscibility with both the feed and the receiving phases, and carrier leaching throughout the extraction process.

8.1.2.2 Emulsion Liquid Membranes

While in BLMs, phase mixing must be completely prevented, EMLs use surfactants to emulsify the stripping phase within the LM and then disperse the emulsion inward the feed phase. Although it may be the other way around: the feed phase inward the membrane globule and the stripping phase outside. First proposed by Li in 1968 [39], depending on the streams and the membrane nature, ELMs are typically classified as water in oil in water (W/O/W) for aqueous feed/stripping phases and an organic membrane process, or oil in water in oil (O/W/O) when the membrane is an aqueous solution. Besides the diluent and extracting solvents, the procedure requires a surfactant to form the membrane globules. Kumar et al. have published comprehensive reviews on ELM developments [40] and on sustainable solvents to form them [41]. ELMs take advantage of the different component permeation rates through the membrane globules, separating the target solute into a stripping immiscible solvent. The resulting double emulsion configuration provides a large total surface area–to–volume ratio of 1000–3000 m^2/m^3, and small membrane average thickness, favoring the mass flux [7].

The process involves stages of emulsification, extraction, separation, and, finally, a de-emulsification to recover the stripping phase together with the target solute. The emulsification may be done by mechanical agitation or ultrasounds. Among the de-emulsification mechanisms, heat or an electrostatic field are applied to the mixtures to achieve the internal phase coalescence, and, lastly, the membrane-stripping phase separation by density difference [42]. The simplicity of each stage offers simple operation with low equipment investment, up to 40% less, plus the possibility to regenerate the membrane phase. The opportunity to recover the extracting solvent reduces waste production, as well as improving the energy efficiency, turning the ELM into a highly sustainable separation process. Nonetheless, despite the simple operational procedures of ELMs, the degrees of freedom during process design increase due to the growth in operating variable numbers.

Due to the above reason, most of the ELM studies are focused on statistical analyses of the operating variable effect contributions, in order to find an optimum recovery point. Stream concentrations and emulsion composition affect directly not only in the process hydrodynamics but also in the overall extraction performance. Moreover, due to its heterogeneous mixture nature, its stability becomes another crucial factor in its optimization. The more stable mixtures are harder to break in the downstream process, requiring more energy-demanding processes that hinder the final solute back-extraction stage.

8.1.2.3 Supported Liquid Membranes

In SLMs, the solvent media is immobilized within a nano- or microporous matrix, which together composes the semipermeable barrier between the phases. Common supports are polymeric matrix, among them: polypropylene (PP), polyethylene sulfurize (PES),

polyvinylidene fluoride (PVDF), and polytetrafluoroethylene (PTFE), as well as inorganic materials, such as ceramics and metal matrices.

SLM dated from the late 1960s. Since then, continuous developments in both membrane phase and supporting materials have been researched and their applications at an industrial scale broadened [43]. Due to their high selectivity, as well as the low investment and operational costs, SLMs have captured the attention of several separation processes. Depending on the nature of the process extraction from an aqueous or organic stream, hydrophobic and hydrophilic matrix alternatives may be adopted, respectively. The LM impregnation on the support for the SLM preparation may be done by simple immersion or application of pressure/vacuum methods. Although they provide similar outcomes, the proper procedure is chosen according to the supporting material and the liquid properties, viscosity being one of the most relevant.

The matrix parameters that characterize a porous membrane are its thickness, pore size, porosity, and pore tortuosity. Typical SLM supports present high porosity and low thickness, usually of 100 and 200–300 μm for flat sheet and hollow fiber (HF), respectively [44]. This allows a significant reduction of solvent requirement and improves the solute flux. Nevertheless, it is important to consider the reduction in mechanical stability as well as its loss of LM retention capacity. Contrary to conventional membrane filtration processes, SLM separation is not carried out by the solute size relative to the pore diameter, but by the solute-membrane phase affinity. Nonetheless, the pore size helps retain the LM inside them by capillary forces. For viscous solvents such as ILs, the suitable pore size in polymer supports is within 100–200 nm [12]. SLMs are commonly studied as flat sheet configurations, allowing to determine their transport properties and stabilities. However, to ensure their feasibility at an industrial scale, other configurations with better surface area–to–volume ratios, such as HF or spiral wound, must be adopted. HF geometry, solution physicochemical properties, stream velocity, and solute diffusion coefficients affect the mass transfer rate. Dimensionless correlations for mass transfer coefficient in specific HF geometries can be found in the work published by Gabelmana and Hwang [45].

8.1.2.4 Other Liquid Membrane Configurations

More complex configuration designs can be found in the literature. In an attempt to increase the mass transfer rate on BLM, arrangements as a continuous liquid membrane (CLM) have been adopted, where the membrane phase is bubbled into the feed and stripping phases, mixed, and then recirculated [37]. In a bulk flow liquid membrane (BFLM), the carrier solution is fed into a pressurized feed side which is kept separated from the stripping side by means of a UF membrane, permeates through the porous barrier, releases the solute, and is recirculated back to the feed chamber [46].

Using an electric field, electrostatic pseudo-liquid membranes (ESPLIM) aim at stabilizing and dispersing the ELM [47]. Instead of common surfactants, pickering ELM (PELM) uses magnetic nanoparticles, chitin nanocrystals, cellulose microfibers, polymer particles, or starch to form the emulsion globules. This improves membrane stability and aids in the de-emulsification stage [42]. Pérez and Fontalvo [48] developed an ELM in a Taylor flow liquid membrane (TFLM), where the aqueous phases (feed and stripping) are injected at specific intervals as droplets into a membrane phase flowing through a pipe. As shown in Figure 8.4a, the continuous flow causes toroidal vortexes within the droplets and in the LM

filling the space within them. The design allows natural stirring in each phase due to the turbulent regime and increases the interfacial area, increasing mass transfer. The Taylor–Couette flow was previously proposed in a similar arrangement, using a rotary vertical cylinder to create the vortexes within the feed phase and the emulsion [49]. ELM can also be carried out as a spray column, dispersing the membrane globules into the feed solution at countercurrent flow, as represented in Figure 8.4b [50]. In order to reduce the organic membrane required, a similar arrangement called bubbling organic liquid membrane (BOLM) was proposed [51]. A gas stream is fed altogether with the organic phase forming bubbles that support a layer of organic LM. An aqueous-to-oil ratio greater than 600:1 can be reached maintaining the surface area and the solute mass flux. Afterward, the loaded LM is treated in a stripping tank to recover the solute.

In an attempt to avoid solvent losses from the pores in the SLM configuration, gelled and polymer inclusion membranes (PIMs), also known as plasticized polymer membranes (PPMs) or fixed site membranes (FSMs) have been developed. They are produced by adding a gelator agent into the extraction solution or polymerizing it into a dense matrix, to ensure adherence to the support. This allows reducing the extracting agent required, giving it an eco-friendly feature [15, 16, 52].

New materials are currently being developed which benefit from novel solvent features in membrane separations. Porous IL polymers are a porous matrix composed of the IL itself [53]. The fluidic IL is solidified forming a polymer with tunable physicochemical properties, high porosity, and high surface area. Thanks to the electrostatic field and ionic density inside the pores, the material is expected to improve separation processes.

At an industrial scale, HF [54], Figure 8.4c, and spiral-wound modules [55] have been adopted to build SLM and increase the effective exchange surface up to 104 m^2/m^3 [56]. Hollow fiber renewal liquid membrane (HFRLM), shown in Figure 8.4d, is based on the surface renewal theory; the feed circulates outside the fibers, whose pores are previously filled with the solvent, while a mixture of the stripping phase with low solvent content is pumped into the lumen side of the fiber [57, 58]. The arrangement creates a thin LM layer that covers the inside of the fiber, being continually renewed by the stripping-membrane stream that flows through it. A combination of ELM with a hollow fiber contactor allows for the separation of the emulsion from the feed, reducing its breakage [59, 60]. Furthermore, pseudo-emulsion hollow fiber strip dispersion (PEHFSD), Figure 8.4e, has been developed, having the feed flowing inside the HFs impregnated with LM while a mixture of LM and the stripping phase flows from the outside. It is called "pseudo-emulsion" since the LM is supported into the HF matrix as well as dispersed into the stripping phase. The arrangement overcomes the SLM stability issues, as the LM losses become part of the pseudo-emulsion [61–63].

8.2 Fundamental Aspects of Liquid Membranes

8.2.1 Theoretical Background

A range of mathematical transport models for LMs can be found in the literature. Although the derivation of transport models depends strongly on the specific system constituents and LM configuration, i.e. physical phases and contactor arrangement, the solute-diffusion

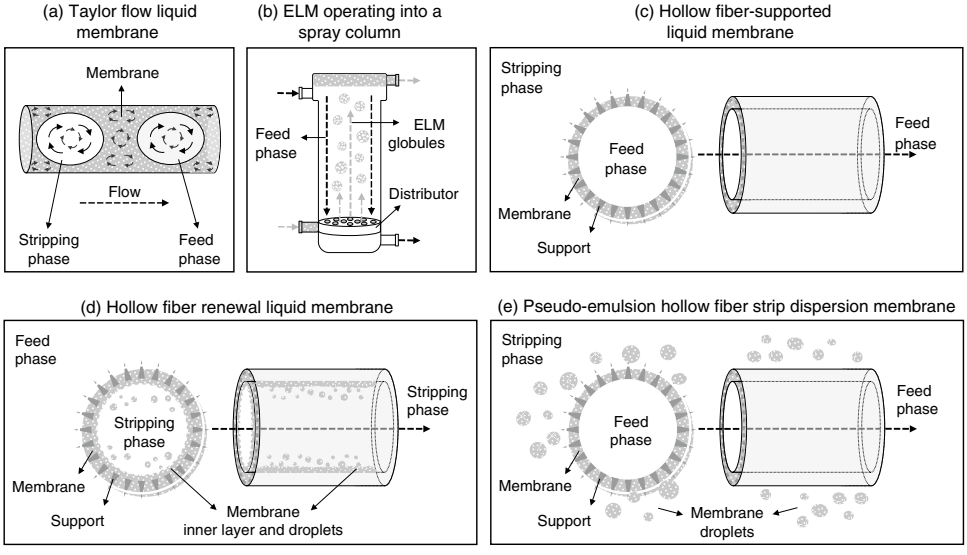

Figure 8.4 Other liquid membrane arrangement schemes: (a) Taylor flow LM; (b) ELM operating into a spray column; (c) Hollow fiber SLM; (d) Hollow fiber renewal liquid membrane; (e) Pseudo-emulsion hollow fiber strip dispersion membrane.

approach is their common starting point [6]. These models can be divided into two main groups according to their transport mechanism: simple transport and facilitated transport. In the simple transport model, the solute mass transfer rate is governed only by its respective phase affinity, which can be quantified by the species chemical potential in the solution. In the facilitated transport, also known as reactive extraction, the solute undergoes a chemical reaction to enhance the molecule movement toward the stripping phase.

As with other spontaneous phenomena, the movement of solutes in LMs occurs when the Gibb's free energy of the system is minimized. In this case, the system is a set of different components and the free energy is the summation of all the chemical potentials for each component in the mixture. In LM, the solute moves across the solvent (membrane phase), from a high to a low chemical potential. In traditional LLX, the solute chemical potential in each phase converges to an equilibrium state, at which point the mass transfer ceases. Contrariwise, in an LM process, the difference of chemical potential between the feed and the membrane, and the membrane and the stripping phase is maintained, for both simple and reactive extraction modes. This enhances the mass transfer, allowing solute movement even against concentration gradients.

The chemical potential of a solution containing solute "i", μ_i (J/mol) is given by its chemical potential as a pure component, μ_i^p, and its activity, a_i (mol_i/mol), which is defined as the solute concentration, c_i (mol_i/mol) times its activity coefficient, γ_i (–). Both μ_i^p and γ_i can be lumped together into a standard chemical potential term (μ_i^{std}). Therefore, the solute chemical potential contribution can be expressed by Eq. (8.1):

$$\mu_i = \mu_i^p + \mathrm{RTln}\left(a_i\right) = \mu_i^p + \mathrm{RTln}\left(\gamma_i c_i\right) = \mu_i^{\mathrm{std}} + \mathrm{RTln}\left(c_i\right) \tag{8.1}$$

In a one-dimensional frame, considering the mass transfer occurs in only one dimension through the x-axis, the driving force corresponds to the chemical potential gradient, $-d\mu_i/dx$. The solute chemical potential across an LM barrier is represented in Figure 8.5; the solute movement can be divided into seven steps from the feed down to the stripping stream:

i) from the bulk feed solution to the proximity of the membrane;
ii) transport to the surface of LM;
iii) interface adsorption into the LM;

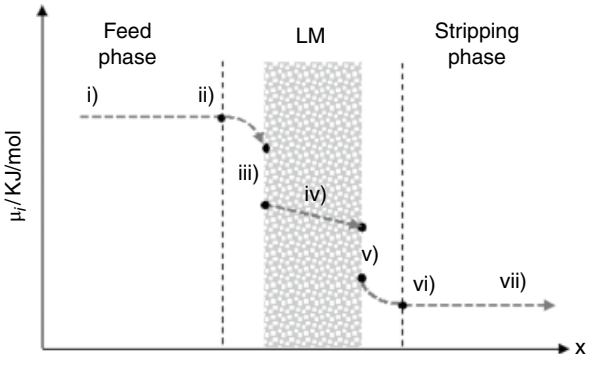

Figure 8.5 Solute chemical potential, μ_i/kJ/mol, profile through a liquid membrane.

iv) inner movement within LM;
v) desorption from LM interface;
vi) transport in the proximity of the LM on the stripping side;
vii) transport to the bulk stripping phase.

At the feed and stripping phases, i.e. steps (i), (ii), (vi), and (vii), the mass transfer resistance is increased due to a concentration polarization effect, reducing the solute movement at the bulk streams and widening the interface film thickness at both membrane sides. The aforementioned effect may be minimized by increasing turbulent mixing at the membrane surface.

If a negligible influence of activity coefficient and molar density variations along the x-axis is assumed, i.e. they are constant values, the chemical potential gradient results in Eq. (8.2), as a function only of the concentration profile, C_i (mol_i/m^3). According to the Nernst–Planck equation, without considering an electrostatic potential, the solute mass flow per unit area, J_i ($mol_i/m^2/s$), can be determined by the solute concentration times the molecular mobility, u_i, and the driving force [11]. The result resembled Fick's law of diffusion as shown in Eq. (8.3), where D (m^2/s) is the solute diffusion coefficient.

$$\frac{d\mu_i}{dx} = \frac{RT}{c_i}\frac{dc_i}{dx} = \frac{RT}{C_i}\frac{dC_i}{dx} \tag{8.2}$$

$$J_i = C_i u_i\left(-\frac{d\mu_i}{dx}\right) = -u_i RT\frac{dC_i}{dx} = -D\frac{dC_i}{dx} \tag{8.3}$$

In the bulk phases, the diffusion coefficient is given by the Stokes–Einstein correlation, Eq. (8.4), based on the Boltzmann constant, $k_{Boltzmann} = 1.38{\cdot}10^{-23}$ (J/K), temperature, T (K), phase dynamic viscosity, η (Pa·s), and molecule radius, r (m), [64].

$$D = \frac{k_{Boltzmann}T}{6\pi\eta r} \tag{8.4}$$

Considering a steady-state mass transfer without chemical reaction and a membrane phase totally immiscible, the concentration profile may be simplified as shown in Figure 8.6, and Eq. (8.3) simplified into Eq. (8.5), where the solute flux, $J_{i,}$ depends only on the membrane thickness L (m), the diffusion coefficient D (lamped together into a new mass transfer coefficient, k_{phase} [m/s]), and the difference in solute concentration (ΔC_i). In this approach, the films and solvent diffusion resistances are included as a whole membrane resistance, as well as the pore diffusion resistance for the supported membrane cases. C_{Fi}* and C_{Si}* are hypothetical solute concentrations at their respective "whole-barrier" side in the feed and the stripping phases, respectively. The overall process results in three stages: (i) feed to membrane extraction, also called pertraction; (ii) membrane diffusion; and (iii) membrane to stripping recovery, as shown in Eq. (8.6).

$$J_i = \frac{D}{L}\Delta C_i = k_{phase}\Delta C_i \tag{8.5}$$

$$J_i = k_F\left(C_{BF} - C_{Fi}\right) = k_{LM}\left(C_{Fi} - C_{Si}\right) = k_S\left(C_{Si} - C_{SB}\right) \tag{8.6}$$

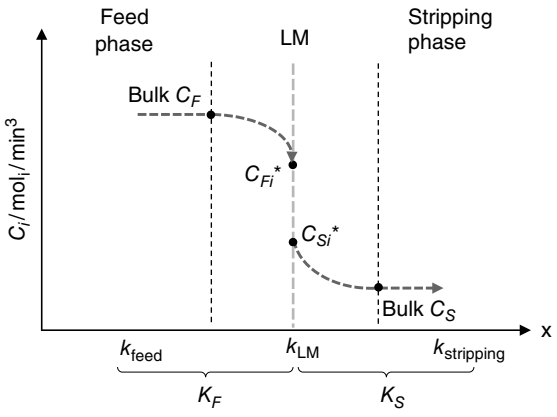

Figure 8.6 Solute concentration, C_i/mol/m^3, profile through a liquid membrane.

The global mass transfer coefficient at the feed and stripping phase, K_F and K_S, is obtained by Eqs. (8.7) and (8.8), respectively, where the solute distribution coefficient, m, assumed constant over the concentration range, is expressed by Eq. (8.9) [56].

$$\frac{1}{K_F} = \frac{1}{k_F} + \frac{1}{mk_{LM}} + \frac{1}{mk_S} \tag{8.7}$$

$$\frac{1}{K_S} = \frac{m}{k_F} + \frac{1}{k_{LM}} + \frac{1}{k_S} \tag{8.8}$$

$$m = \frac{C_{Si}^*}{C_{FB}} = \frac{C_{Si}}{C_{Fi}} = \frac{C_{SB}}{C_{Fi}^*} \tag{8.9}$$

If no solute accumulation in the film is assumed, i.e. when a steady state is reached, the total mass flux is defined by the membrane permeability, P (m/s), resulting in Eq. (8.10).

$$J_i = K_F \cdot \left(C_{FB} - C_{Fi}^*\right) = K_S \cdot \left(C_{Si}^* - C_{SB}\right) = -P \cdot \left(C_{SB} - C_{FB}\right) \tag{8.10}$$

For multicomponent mixture separation, where two or more solutes are present, the membrane selectivity for an a-component with respect to a b-component, $S_{a,b}$, is determined by the ratio of their respective permeabilities, as shown in Eq. (8.11):

$$S_{a,b} = \frac{P_a}{P_b} \tag{8.11}$$

Since temperature affects the solute chemical potential in each phase, the membrane permeability is sensible to temperature changes. Permeability temperature dependence, $P_i = P_i(T)$, can be described according to an Arrhenius-form equation, Eq. (8.12), where $R = 8.314$ (J/mol.K) is the gas constant and E_i (J/mol) the activation energy, which is a fitting parameter usually obtained using experimental data [12].

$$\frac{P_i\left(T_2\right)}{P_i\left(T_1\right)} = \exp\left[-\frac{E_i}{R}\left(\frac{1}{T_2} - \frac{1}{T_1}\right)\right] \tag{8.12}$$

8.2.2 Transport Mechanisms in Liquid Membranes

The commonly accepted solute transport mechanism in an LM is solution-diffusion, where transport is governed by the chemical potential gradient as explained in Section 8.2.1. This corresponds to the so-called simple transport model (Figure 8.7a); the solute diffusion depends only on the intermolecular interactions, such as van der Waals forces, electrostatics, and hydrogen bonding.

However, in order to overcome the trade-off behavior in solution-diffusion membranes, reaction-activated transport mechanisms can be found, where the mechanism grows in complexity and variable number, yet the mass transfer rate is increased due to a resistance reduction either at the interfaces or within the LM. The stripping phase reaction-facilitated transport, Figure 8.7b, allows compensating for the lack of spontaneity on the solute back-extraction from the LM. Since a high solute solubility in the membrane phase improves the extraction from the feed solution, desorption into the stripping phase may be an important resistance. Solute saturation in the membrane reduces, even to an endpoint, the solute flow rate. To diminish this effect, an agent (B) dissolved in the stripping stream continuously reacts with the solute (A) to decrease the concentration at the interface, promoting the

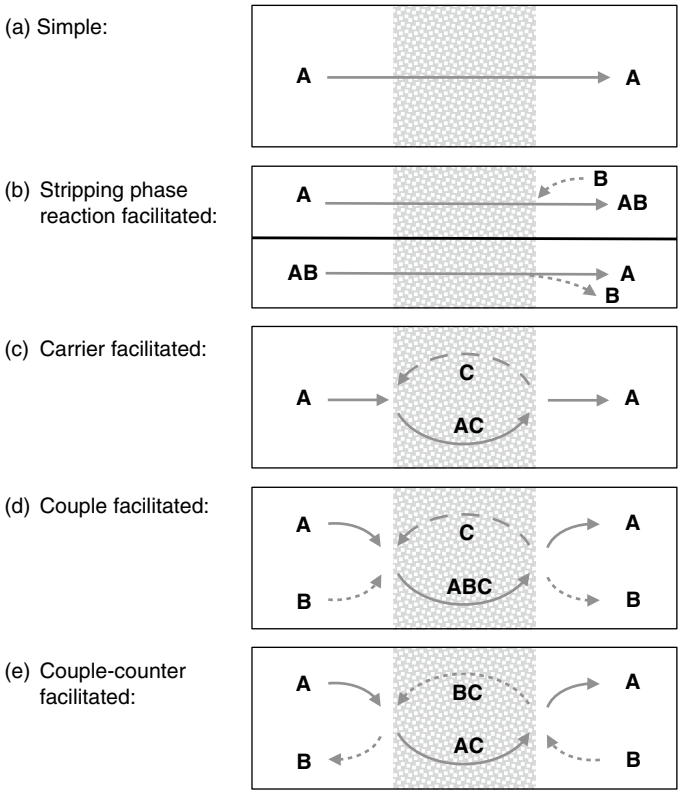

Figure 8.7 Transport mechanisms in liquid membrane: (a) simple transport; (b) stripping phase reaction reaction-facilitated transport; (c) carrier-facilitated transport; (d) couple-facilitated transport; (e) couple-counter-facilitated transport.

solute desorption and the overall solute flux. Likewise, buffers, strong acid or base solutions, are used to reach an optimum extraction yield by controlling the pH.

If the main resistance is at the membrane phase, a third agent may be included to reinforce its internal movement, and this is known as a carrier-facilitated transport mechanism, see Figure 8.7c. The carrier, a complexing agent, must be soluble only in the LM to ensure membrane stability without leaching to the other streams. Solute (A) reacts with the carrier (C) at the feed-membrane interface to form the complex (AC) that diffuses through the LM. Then the reaction is reverted at the membrane-stripping interface, allowing the solute desorption and recycling of the carrier. The flow rate increases with the complexing agent concentration in the diluent, which acts as a barrier with no significant extraction role.

The formation of complexes may also involve more compounds from the feed or stripping phases. In couple-facilitated transport, Figure 8.7d, two or more substances are transported through the membrane along with the target solute as a sole complex molecule. A couple-counter-facilitated transport, Figure 8.7e, can be used to maintain the osmotic pressure or the solution electroneutrality, exchanging substances between the feed and stripping phases. Carrier selection thoroughly depended on the complexation and decomplexation rates balance. On one hand, weak carriers do not reach suitable fluxes due to the slow extraction rate at the feed-membrane interface but offer a spontaneity decomplexation to release the solutes toward the stripping phase. On the other hand, strong carriers result in a high initial solute flux at the feed-membrane interface, but they quickly saturate the membrane phase, reducing the concentration gradient within the membrane and thereby the flux rate. The carrier strength is determined by its bond energy, where a suggested range is $1{\cdot}10^4$–$5{\cdot}10^4$ kJ/mol [64].

8.2.3 Extraction and Recovery Efficiencies

Despite LMs being described as single-step processes, they effectively work in two stages: (i) solute extraction from feed to membrane, and (ii) solute recovery from the membrane to the stripping stream. Figure 8.8a schematized the typical phase concentration behavior observed in LM processes. As the extraction progresses, the solute concentration decreases in the feed phase and increases in both membrane and stripping phases, surpassing the concentration in the feed under favorable conditions. If the membrane phase volume is enlarged with respect to the other phases, a greater solute extraction occurs, but this does not imply a greater recovery to the stripping phase. In the first stage, the larger membrane volume enhances the flux due to a lower solute concentration in the LM, but flux gets reduced at the stripping stage due to solute accumulation halfway through the process.

The performance of an LM is typically described by the capacity to transport the target solute in terms of extracting percentage or permeation ratios. Although, the terminology used to report it varies among works. The overall extraction, recovery, or yield (Ex) is expressed by the total solute recovery in the stripping phase with respect to the initial feed, according to Eq. (8.13), where $C_{i,S}$ and $C_{i,Fo}$ are the solute concentration in the stripping phase and the solute initial concentration in the feed phase, respectively.

$$Ex = \frac{C_{i,S}}{C_{i,Fo}} \tag{8.13}$$

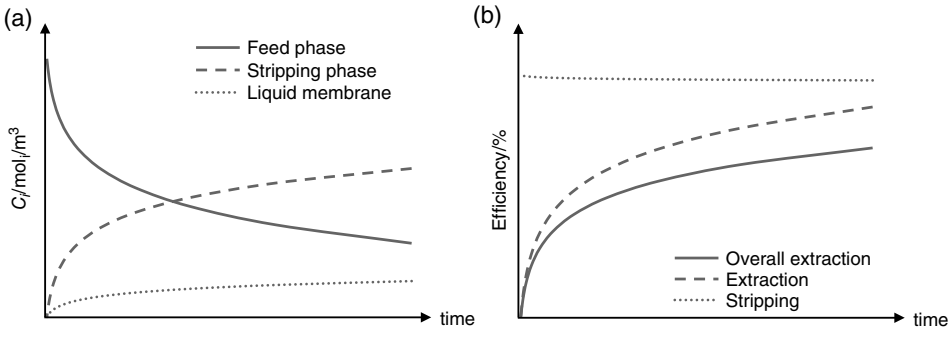

Figure 8.8 Schematic typical behavior in the LM extraction process: (a) phase concentration profile; (b) extraction efficiency parameters.

Generally, there are two extraction efficiencies to consider in the process, the extraction of solute from the feed stream (Ex_F) and the solute recovery to the strip stream, the so-called stripping efficiency (Ex_S). The extraction efficiency (Eq. 8.14) is defined as the membrane capacity to extract the solute from the feed phase, while the stripping efficiency (Eq. 8.15) represents the membrane capacity to release the solute into the stripping phase [20]. Note that these definitions assume a feed-stripping volume ratio equal to 1. Otherwise, a mass-based relationship must be adopted to properly describe the extraction performance.

$$Ex_F = 1 - \frac{C_{i,F}}{C_{i,Fo}} \tag{8.14}$$

$$Ex_S = \frac{C_{i,S}}{C_{i,Fo} - C_{i,F}} \tag{8.15}$$

Typical Ex (solute recovery), Ex_F, and Ex_S profiles are illustrated in Figure 8.8b. Due to membrane solute retention, the expected recovery is lower than the extraction from the feed phase. On the other hand, Ex_S depends on the membrane-stripping capacity to accomplish the solute back-extraction.

8.2.4 Liquid Membrane Stability

As aforementioned, the main limitation of LMs is membrane stability, i.e. their capacity to stay as a separate phase, avoiding leaching of one or more components from it. Membrane losses within the feed and stripping phases may occur by dispersion (or evaporation in the case of gaseous streams). Losses also imply contamination of the feed and/or stripping streams with the leached LM components, which can negatively affect the separation process such as when toxic diluents or carriers are used [8]. Therefore, phase immiscibility is crucial in order to guarantee stability, although the nature and amount of the potential leached components and operational conditions have a great influence as well. For instance, the limited contact area of BLMs results in lower membrane losses and, hence, higher stability.

ELM stability may be expressed by two distinct terms: (i) the membrane breakage rate (%), which represents the percentage of internal phase losses toward the external phase, and (ii) the emulsion swelling rate (%), which measures the increment in the emulsion volume. Usually, high osmotic pressures between the feed and the stripping phase might cause reverse micelles (aqueous solution pockets) transporting water to the internal phase, which leads to globule swelling. Being able to homogenize speed and emulsification time is crucial in the formation of a stable emulsion. Although higher stirring speed contributes to increasing the mass transfer rate, it may cause breakage. Emulsion size, composition, and operational conditions, such as temperature, pH, concentrations, and stirring rate, as well as retention time, might affect the swelling phenomenon [42]. Both effects are correlated and determine the overall LM extraction performance: high swelling rates may lead to emulsion breakage.

Droplet size and rheological properties are the main factors in ELM stability. Both emulsion globule and droplet sizes depend on the phase ratios, composition, solvent properties, and emulsification process conditions. Bigger globules that contain more droplets can reach a large internal mass transfer, around 10^6 m^2/m^3. To ensure good ELM stability without jeopardizing its performance, the inner droplets, usually the stripping phase, should have a small diameter of about 1–3 μm. The whole membrane globule has an average size of less than 2 mm [56]. As the diluent is the major component in an LM, its immiscibility ability greatly contributes to better ELM stability. Also, it is worth noting that as discussed in Section 8.2.1, the diffusion coefficient is inversely proportional to the membrane viscosity (see Eq. 8.4); so, the use of common nontoxic diluents with low water solubility and high viscosity, results in greater mass transfer resistance [36].

Phase ratios, i.e. emulsion–to–feed and stripping–to–membrane ratios, play other fundamental roles in ELM stability. The relation between emulsion globule (membrane and stripping phase heterogeneous mixture) and feed phase volume is defined as the treat ratio, V_{ELM}/V_F. At a larger treat ratio or large emulsion volume, the total interface area is increased by the number and dispersibility of membrane globules in the global mixture [34]. On the other hand, the internal–to–membrane phase ratio corresponds to the stripping (internal phase) to the membrane phase volume proportion, V_{int}/V_{LM}. Increasing this ratio causes a reduction of the LM requirements for the process, although the emulsion globules become unstable, leading to breakage or emulsion inversion, i.e. the emulsion might turn from W/O to O/W. When the internal–to–membrane phase ratio is increased, an improvement can be observed, but this might also lead to the internal droplet coalescence. Contrariwise, low internal–to–membrane phase ratios lead to poor inner droplets dispersion and high surface tension, which reduces the overall membrane performance and stability. Since the internal surface area at the membrane-stripping interface is typically several orders of magnitude larger than at the feed-emulsion interface, the major mass transfer resistance is found at the membrane adsorption stage. Therefore, the treat ratio has a larger influence on the overall process performance. On the contrary, the internal–to–membrane phase ratio has a less significant effect on the performance, and it should be optimized aiming for membrane stability rather than high extraction yields.

In SLMs, the lack of membrane phase within the pores reduces solute flux and its selectivity. Thus, the stability of SLMs, defined as the capacity of the support to hold the membrane phase, becomes their main limitation. As for all the LMs, the stability of the SLM

depends on the membrane phase immiscibility with the other streams, although the affinity LM-support and the capillary forces also favor retention. Despite the increase of mass transfer resistance, viscous membranes show higher stabilities due to larger van der Waals forces. Hydrophobic supports retain organic solvents more strongly by strong molecular interactions. Pore size and tortuosity of the support porosity must be tailored to ensure a high solute flux and avoid LM losses. Generally, bigger pore sizes increase the effective surface area but reduce the capillary forces, while higher porosities enhance the mass transfer rate and stability due to hydrostatic pressure [12].

When several extraction cycles are carried out, the membrane performance may be affected by stability issues, leading to partial compound or total LM losses, and thus changing its physicochemical properties. During the ELM de-emulsification stage, losses of volatile modifiers alter its viscosity and thereby the overall mass transfer coefficient [34]. Although PIMs show high stability, a minor drop in solute transport can be observed when reused. PIMs' losses can be evidenced by changes in membrane mass or morphological variations on the surface observed in scanning probe microscopy images [52]. However, some works on membrane setup improvements have reported a reduction in losses over the cycles, preserving an extraction yield near to the original one [27, 65].

8.2.5 Compounds' Interaction within Liquid Membranes

In a steady-state process, the overall mass transfer from the feed to the stripping phases is controlled by the step with greater resistance. As stressed in Section 8.2.1, the extraction in LM can be subdivided into internal streams, surface interface films, and interface transport steps. By implementing proper stirring at each phase, the concentration polarization effect and thereby the film resistances can be minimized. Including a carrier to the membrane phase and a stripping agent to the receiving phase, i.e. adopting facilitated transport, the inner LM movement is considerably improved. The above arrangements leave the major resistance at the interface mass transfer. Nevertheless, complexation kinetics become dominant. The mass transfer is not limited by the bulk feed to membrane resistance, but by the interface transport. Likewise, solute desorption is limited by decomplexation. Higher carrier concentrations increase chances for complex formation, while higher stripping agent concentrations favors carrier regeneration, both improving the mass flux within the membrane phase. Nevertheless, this increment has a limit; when the ionic strength of the stripping solution becomes a significant resistance to the solute mass transfer, complex carrier-solute accumulates at the membrane-stripping interface.

Emulsion surfactants have an important effect on the membrane performance as well as the carrier. To form the emulsion globules, ionized or nonionic surfactants must be included either in W/O/W or O/W/O systems, although the selection depends on the respective phase solubility. The hydrophilic–lipophilic balance value (HLB) is used to represent the surfactant molecule percentage of hydrophilic functional groups. At higher HLB (>8), i.e. more hydrophilic surfactant, the mixture tends to form an O/W/O system, and vice versa, when HLB <6, W/O/W emulsions take place. A common environmentally friendly surfactant found in the literature is sorbitan monooleate, Span® 80, (HLB = 4.3) [40]. Nevertheless, under certain conditions, Span 80 have been reported to permit water transport, causing swelling, and being susceptible to hydrolysis reactions [66]. Besides

contributing to the emulsion drop formation and its stability, surfactants influence the membrane–solute interactions. Better extraction efficiency can be observed at lower surfactant concentrations. The improvement is maintained as far as it is kept at a minimum concentration, above which point the extraction performance suddenly drops due to the membrane instability [29]. Furthermore, surfactant agents may act as a carrier as well, forming complexes with the solute. Separations of similar components require careful system optimization. In multicomponent systems, such as fermentation broths, membrane selectivity becomes a paramount factor. For instance, the proper surfactant agent choice has shown to be determinant on the selective separation of acetic acid from succinic acid in an aqueous solution [67].

The extraction performance depends on the specific mechanisms resulting from the solute– membrane interaction. This effect is particularly evident in dissociable solutes, where adjusting the solution pH, the molecular acid form, i.e. dissociated, undissociated, mono- or di-anionic forms, can be controlled. Pratiwi et al. [17] compared the extraction of succinic acid with an IL-based SLM and PIM. For the first case, the solute permeability improves at a feed pH of 6.5, coincident with the fermentation broth pH range [68]. At such pH, the dissociated form of the acid reacts by an ion-exchange mechanism with the LM and diffuses as an IL-solute complex. On the other hand, for the PIM tests, better permeability was found at pH lower than the acid dissociation constant (pKa) of succinic acid, suggesting less membrane-succinic anion interactions, and the solute was extracted by simple transport mechanisms (see Figure 8.7a). The same dependence was observed in an amino acid extraction study, where authors found an increase in the extraction efficiency directly proportional to the stripping phase pH and inversely proportional to feed acidity. Results identify pH as one of the most important variables in the extraction operation [27].

8.3 Sustainable Separations with Liquid Membranes

LM technology has proved to be a sustainable separation method at a laboratory scale, which could potentially replace commercial LLX systems for several applications. As observed in Figure 8.9, throughout the last decades, there has been a sustained increase in LM research.

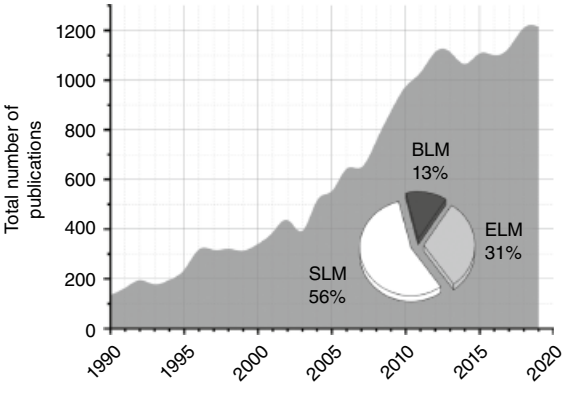

Figure 8.9 Total liquid membrane publications' number per year given by the search engine Google Scholar using the keywords "bulk liquid membranes," "emulsion liquid membranes," and "supported liquid membranes."

This section presents a comprehensive recompilation of recent studies published on the topic, focusing on liquid stream separations. In the last decade, good progress has been made on LM technology for the recovery of value-added substances. Organic LMs have been extensively studied for the recovery of organic compounds from aqueous solutions in the biorefinery industry. ELMs have been successfully used for the recovery of metal ions, such as copper, lithium, bismuth, cadmium, silver, vanadium, palladium, and high-value RE elements. LMs have also proved useful for wastewater remediation. For instance, removal of pullulans such as by-product organic compounds, pharmaceutic residues, lignin from pulping waste, heavy metals, and nuclear radioactive waste have been accomplished. Extracted solutes reported in the last 10 years using LMs are discussed in detail in this review.

For more specific details on LMs and their applications, readers are referred to the textbook by Kislik et al. [6] where LM model derivations and their progress in separation processes are discussed, and chapters of other books regarding LM basic concepts [56, 64], industrial developments [7, 11], and novel IL-based membranes [16, 69]. Likewise, literature offers LM chapters dedicated to specific applications, such as pharmaceutical and biotechnology [9], GS [70, 71], radioactive waste and metal separation [72], organic acids recovery [17], and dyes removal [73].

8.3.1 Recovery of Biomolecules in Biorefinery

Biorefineries are an emerging industry conceived for the conversion of biomass into a range of valuable bio-based compounds as alternatives to conventional commodities such as polymers, organic acids, alcohols, composites, surfactants, paintings and coatings, lubricants; binders; plasticizers; and solvents. It is well known that the production of biomolecules by fermentation routes often presents challenges in the downstream purification stages. Fermentation broths contain mainly water and a small concentration of valuable biomolecules, which often involves very high energy consumption for their extraction. For instance, nonvolatile organic acids, high-value building blocks for a wide variety of industrial sectors [74], require separation processes such as precipitation or liquid extraction using volatile organic compounds (VOCs). Moreover, throughout the bio-organic acid production process, the separation cost can represent more than two-thirds of the total production cost [75, 76]. In order to overcome the high energy requirement and the use of toxic compounds, LMs have been extensively investigated. They have been successful in the extraction of organic acids exploiting the properties of novel solvents such as ILs [17]. In this section, recent research on LM application for bio-based organic acids and other essential biomolecules is presented and summarized in Table 8.2.

Lactic acid is one of the smallest organic acids and a high-value building block used for chemical, food, cosmetic, textile, biomedical, and bioplastic industries. It can be produced from renewable sources, such as biomass and food wastes and a range of separation technologies have been thoroughly researched for its extraction [84]. The extraction of lactic acid by ELM was studied using a membrane composed of TOA as a carrier diluted in n-heptane and a solution of sodium carbonate as a stripping phase [77]. The membrane interchanged the lactate–amine complex with carbonate–amine complex from one phase to another in a couple-counter-facilitated transport regimen (see Figure 8.7e). The authors

Table 8.2 Summary of recent liquid membrane studies for the recovery of compounds in biorefinery.

Solute	Membrane	Results	Ref.
Lactic acid	TOA in n-heptane ELM	95% extraction and 80% stripping efficiencies	[77]
	Aliquat 336 in sunflower oil ELM	99% extraction efficiency	[29]
	Aliquat 336 in rice oil ELM	96% extraction efficiency	[31]
	Aliquat 336 in rice oil ELM	95% extraction efficiency	[32]
	TOA in dodecanol and dodecane TFLM	27% in productivity increase	[48, 78]
Succinic acid	TOA or Amberlite LA-2 in kerosene ELM	98% extraction efficiency	[79]
	Palm oil ELM	Complete recovery	[34]
Levulinic acid	TBP in imidazolium-based ILs BLM	99% extraction and 95% stripping	[18]
Benzoic acid	Isooctane or dodecane BLM	Diffusive transport model	[80]
Gibberellic acid	Aliquat 336 in n-heptane ELM	Recovery of 88% for model solution and for broths 68% for real solution with a concentration factor of 2.2	[81]
Acetic acid	C9232, TOA or Amberlite LA-2 in kerosene ELM	>92% extraction efficiency	[67]
	TBP in ($[C_4min][Tf_2N]$, $[C_4min][PF_6]$, $[C_6min][Tf_2N]$, and $[C_6min][PF_6]$) BLM	92% extraction and 81% stripping efficiencies	[19]
	TBA in oleyl alcohol BLM	>75% extraction efficiency	[82]
Formic acid	TBA in oleyl alcohol BLM	>57% extraction efficiency	[82]
Propionic acid	TBA in oleyl alcohol BLM	>75% extraction efficiency	[82]
Butyric acid	TBA in oleyl alcohol BLM	>75% extraction efficiency	[82]
Ethanol	n-Hexane ELM	95% extraction efficiency	[83]
ABE	Gelled $[C_4min][PF_6]$ in PTFE hollow fibers–supported liquid membrane (HF-SLM)	Trans-membrane fluxes and selectivity	[25]
Penicillin G	HFRLM	Concentration factor of 4.4	[57]
Catechin (±C)	TBP in vegetable-based solvent BLM	70% extraction and 40% stripping efficiencies	[30]
Furfural	DES-based in polymeric SLM	Permeability > $3.3{\cdot}10^{-4}$ m/s	[26]
Hydroxymethylfurfural	DES-based in polymeric SLM	Permeability > $0.2{\cdot}10^{-4}$ m/s	[26]

evaluated the effect of Na_2CO_3 concentration, phase ratios (strip–to–membrane and feed–to–emulsion), and contact time into the lactic acid pertraction (extraction from feed to membrane), and recovery (extraction from membrane to strip) efficiencies. The study determined an optimal operation zone where pertraction efficiency is above 95% and the

recovery efficiencies over 80%. Vegetable diluents were also studied for the recovery of lactic acid with green ELMs. Under optimal operation conditions, ELMs based on sunflower oil [29] and rice oil [31, 32], using Aliquat 336 as a carrier, proved to reach as high lactic acid recovery values as those obtained in petrochemical-derived solvents-based ELM. As a way to improve extraction yields of lactic acid from fermentation broths, Pérez et al. [48, 78] proposed a novel LM configuration (TFLM shown in Figure 8.4a) using a membrane composed of dodecanol and dodecane as diluent plus TOA as the carrier, and sodium carbonate solution as the stripping phase. Feed and stripping droplets were injected into the membrane phase, which improved the phase internal agitation due to the turbulent flow created inside the droplets as well as in the LM within them. Lactic acid removal was done in situ to minimize acidification, thus increasing the fermentation yield. The hybrid fermentation–extractor operation reached a lactic acid productivity 27% greater than that obtained in a conventional fermenter.

Succinic acid is used as a starting material in the production of a wide range of commodities, including 1–4-butanediol, γ-butyrolactone, tetrahydrofuran, and bio-based polymers such as butylene succinic acid. It can be obtained through the fermentation of sugars (e.g. lactose, xylose, arabinose, and cellobiose) from various biomass sources such as whey, cane molasses, straw, corn fiber, crop stalk, wheat, and duckweed [68]. Succinic acid extraction yields up to 98% were obtained using TOA or Amberlite® LA-2 (a secondary amine) as extracting agents, in kerosene-based ELM [79]. Succinic acid recovery in multiples cycle was assessed using palm oil-based ELM, reaching a complete recovery in the first cycle, dropping to 62% in the second cycle, and lastly, to 43% in the third cycle [34].

Levulinic acid is widely used as a starting material for solvents, biofuels, chemical intermediates, resins, and other products. It can be produced using monosaccharides, HMF, furfural, polysaccharides or starch, and lignocellulosic biomass as raw materials [85]. Hydrophobic ILs ($[C_4min][Tf_2N]$, $[C_4min][PF_6]$, $[C_6min][Tf_2N]$, and $[C_6min][PF_6]$) were studied for the extraction of levulinic acid using a BLM with TBP and NaOH solution as carrier and stripping phase, respectively [18]. Since the ILs employed are denser than the aqueous feed and stripping solutions, the extractions were carried out into a U-tube arrangement. The effect of several operational variables was investigated, although all tested imidazolium-based ILs exhibited similar extraction and stripping efficiencies of up to 99 and 95%, respectively.

Similarly, LMs have been proposed for the recovery of large carboxyl acids. Koter and Szczepański [80] developed a diffusive transport model for aqueous benzoic acid, a food preservative, and precursor of several high-value chemicals, through isooctane or dodecane-based BLM. Considering molecular dissociation and dimerization effects, the authors achieved a successful prediction of the acid concentration profile as a function of time for all three phases. The carrier-surfactant composition of ELMs containing n-heptane, Aliquat 336, and Span 80 was optimized to maximize the recovery from fermentation broths of gibberellic acid, a vegetable growth promoter [81]. The optimization conditions for model solutions resulted in a recovery of 88% and for broths 68% with a concentration factor of 2.2.

Moreover, LMs can be used for the separation of volatile compounds. In carboxylic acid fermentation processes, for instance, acetic acid is a common by-product which leads to product inhibition. C9232-based ELMs showed good performance and high selective acetic acid separation over succinic acid fermentation broth [67]. ILs ($[C_4min][Tf_2N]$, $[C_4min][PF_6]$, $[C_6min][Tf_2N]$, and $[C_6min][PF_6]$) were studied in BLM for acetic acid removal from

aqueous solution using TBP and NaOH solution as the carrier and stripping medium, respectively [19]. As a result, extraction and stripping efficiencies of 92 and 81%, respectively, were obtained. In this work, it was found a significant effect of carrier and stripping concentrations on the efficiencies, while the initial feed concentration was not relevant under the operational range. Several other volatile carboxylic acids have been recovered via BLMs from aqueous solutions. Mixtures of oleyl alcohol and tributylamine (TBA) were successfully used for the extraction of acetic, propionic, and butyric acids, with yields over 75%, and yields above 57% for the extraction of formic acid [82]. An n-hexane-based ELM was used for ethanol extraction from aqueous matrices [83]. The work studied the effect of different salt concentrations in the stripping phase and found a drastic reduction in ethanol extraction when salts were present, which was attributed to ions and water cotransport due to osmotic pressure.

LMs have also been used for liquid–gas separations in PV mode. Bio-butanol is a sustainable fuel that is produced via the fermentation of biomass. The resulting broth is an aqueous mixture of acetone, butanol, and ethanol (ABE) that is typically separated via conventional distillation, although research is now geared toward the use of PV membranes, including LMs [86]. Hydrophobic HF-SLMs based on PTFE filled with [C_4min][PF_6] were prepared and tested for the recovery of butanol from ABE mixtures in aqueous solutions [25]. To improve the solvent retention in the pores, the IL was gelled with 12-hydroxystearic acid, and the authors compared the performance of the SLM in sweep gas PV mode to a membrane evaporation process, using the PTFE HF membrane without IL. Results showed a slight increase in butanol selectivity over the other organic compounds for the SLM with the main mass transfer resistance being the solute diffusion inside the membrane.

Penicillin G is a natural antibiotic and precursor of other semisynthetic ones. Although its recovery from fermentation broths has been industrialized for massive production, gaps remain to improve efficiency and avoid product losses. In this context, the feasibility to recover Penicillin G utilizing HFRLM in a cascade process was studied [57]. In this work, hydrophobic PP-based HF supports were filled with di-n-octylamine in iso-octanol and kerosene, and a K_2CO_3 aqueous solution was selected as the stripping phase. The proposed arrangement reached a concentration in the stripping phase of up to 4.4 times higher than that of the feed.

The development of novel green solvents opens an avenue to improve LM technology for sustainable separations [87]. In this regard, BLMs containing vegetable-based solvents (sunflower, soybean, and coconut oil) were compared to analogous conventional petrochemical-derived solvents (iso-octane, n-decane, and n-heptane) for the extraction of catechin, a natural substance retrieved from tea leaves with pharmacological applications, from an aqueous solution [30]. The selected carrier was TBP, and better extraction performance was obtained when using the bio-based solvents; the BLM with sunflower oil extracted around 70% of catechin and the recovery to the stripping phase was up to 40%.

Alongside ILs, SLM impregnated with DESs have been tested. DESs share many of the features that positioned ILs as promising alternative solvents for several industrial processes. While ILs are composed of a pair of cation–anion, DESs are formed by hydrogen bond donor (HBD) and acceptor (HBA) compounds [88]. Recovery of bio-based furfural and hydroxymethylfurfural from model aqueous solutions, starting raw materials in the

production of bioplastic monomers, were studied with different polymeric SLMs [26]. Several DESs, based on decanoic acid and thymol as the HBD-component and tetraoctylammonium bromide, thymol, menthol, and lidocaine as the HBA-component, were used as the membrane phases. In such work, authors found larger furfural permeability than hydroxymethylfurfural, attributed to the solute hydrophobicity difference. Moreover, the study showed that bigger pores and lower viscosity improve the permeability but increased solvent losses, pointing out the extraction method limitations besides the importance of its proper optimization.

8.3.2 Amino Acid Recovery

Amino acids are the fundamental constituents of proteins. Their primary exponents are L-cysteine, L-histidine, L-isoleucine, L-leucine, L-lysine, L-methionine, L-phenylalanine, L-threonine, L-tryptophan, and L-valine. They have an important place in the chemical industry, and proof of this is their rising sustained commercialization, projected to surpass $35 billons in the coming years [89]. They are used as a starting material for the synthesis of chiral-active ingredients and bioplastics, as well as food, agricultural, and pharmaceutical products' manufacturing. Sustainable amino acid production is mainly carried out by aerobic microbial conversion, attaining growing interest in their synthesis from renewable feedstock, such as lipids, cellulose, hemicellulose, lignin, and chitin. Table 8.3 collects the studies developed for amino acid recovery with LMs.

Proteins and amino acids are complex molecules, which are susceptible to be denatured by organic solvents [92]. To avoid compounds' denaturalization, biocompatible solvents, such as hydrophobic ILs, have been proposed for amino acid extraction [93]. Likewise, DESs have shown high biocompatibility. Several polymeric porous supports were impregnated with quaternary ammonium salt-based DESs for amino acid recovery from aqueous solutions [27]. Among other common amino acids, the best extraction yield (86%) was achieved for tryptophan, followed by glycine and DL-aspartic acid with yields for both greater than 60%. The optimal SLM, in terms of solute flux, was found for mixed cellulose support impregnated with DESs composed of choline chloride and *p*-toluene sulfonic acid, at a molar ratio of 1:2. This membrane was reused in extraction cycles up to seven times, with an extraction efficiency drop of less than 20%. The observed decrease was attributed to solvent losses due to membrane instability. L-cysteine extraction from a KCl solution was

Table 8.3 Summary of recent liquid membrane studies for the recovery of amino acids.

Solute	Membrane	Results	Ref.
L-tryptophan	Quaternary ammonium salt-based DESs in polymeric SLM	86% extraction efficiency	[27]
L-cysteine	Dicyclohexyl-18-crown-6 in toluene ELM	>96% extraction efficiency	[90]
L-phenylalanine	Paraffin, sulfonated kerosene, D2EHPA ELM	>94% extraction efficiency	[91]

achieved using a dicyclohexyl-18-crown-6 in toluene [90]. The observed transport mechanism was based on the extraction agent and the potassium ion complexation, which acted as the actual carrier for amino acid extraction. Furthermore, the proposed ELM gave a high L-cysteine selectivity over other amino acids. Through a backpropagation neural network combined with a genetic algorithm, the extracting of L-phenylalanine using ELM was successfully simulated in real-time [91]. Training the simulation with experimental data, the authors found the optimal operational conditions. An extraction efficiency greater than 94% was reached with an ELM composed of paraffin, sulfonated kerosene, D2EHPA, and Span 80.

As with bio-based products, the downstream separation in the amino acid production is a critical stage due to their complexity and energy consumption. Moreover, amino acid production requires a specific chiral orientation. Therefore, the selective separation of amino acid enantiomers from racemic mixtures becomes one of the key concerns. Enantioseparation achieved through LMs has been reported to be comparable to traditional techniques, such as chiral chromatography and diastereoisomeric crystallization. In this regard, high enantioselectivity of amino acid was reported for HF-SLM containing specific chiral carriers, such as N-3,5-dinitrobenzoyl-L-alanine octyl ester, copper(II) N-dodecyl-L-hydroxyproline, and quinidine or quinine derivatives [10]. Selective extraction of stereoisomers can also be improved by a previous enzymatic reaction, which converts the target enantiomer into a complex transportable by the LM.

8.3.3 Environmental and Wastewater Treatment

Water streams from industrial processes contaminated with organic compounds are a growing hazard to population health and aquatic ecosystems. Their treatment is of paramount concern, prompting stricter government regulations. Luckily, many of these pollutants can be removed to meet the discharge requirements while valuable chemicals are recovered. Studies on wastewater remediation with LMs are compiled in Table 8.4.

Phenolic compounds are commonly generated as waste in several industries; however, they are extendedly used as raw material for chemical derivatives' production. Thus, there is substantial research toward the development of sustainable extraction processes. Treatment of olive oil plant wastewater for the removal of phenol and two of its derivatives, tyrosol, and *p*-coumaric acid, was carried out with an ELM, with a recovery of up to 97–99% [94]. Several carriers including Hostarex® A327, Alamine® 336, Aliquat 336, and Cyanex® 923 were tested in isoparaffinic hydrocarbon. The effect of adding iso-decanol as a membrane modifier was also studied showing an enhancement in the extraction efficiency. Removal of *p*-nitrophenol (starting compound for several pesticides) and aniline (pharmaceutical and dye waste) was studied using organic solvent-based ELM [65]. Operational variables and membrane composition, such as diluent type, n-hexane, n-heptane, and kerosene, and surfactant (Span 80) concentration were optimized. The work showed a nearly complete *p*-nitrophenol and aniline removal.

In order to reduce the organic solvent requirement in the ELM conformation, the use of vegetable oils was proposed. The effect of the diluent composition ratio, palm oil–kerosene mixture, on the phenol removal efficiency was studied [35]. With a considerable solvent decrease, a palm oil-to-kerosene ratio of 70:30 showed good emulsion stability. Under

Table 8.4 Summary of recent liquid membrane studies for wastewater treatment.

Solute	Membrane	Results	Ref.
Phenol, tyrosol, and p-coumaric acid	Hostarex A327, Alamine 336, Aliquat 336, and Cyanex 923 in isoparaffinic hydrocarbon ELM	97–99% recovery efficiency	[94]
p-Nitrophenol	n-Hexane, n-heptane, and kerosene ELM	Complete removal	[65]
Aniline	n-Hexane, n-heptane, and kerosene ELM	Complete removal	[65]
Phenol	Palm oil:kerosene ELM	83% extraction efficiency	[35]
	($[C_4min][Tf_2N]$, $[C_4min][PF_6]$, and $[C_4min][FAP]$) BLM	96% extraction and 98% stripping efficiencies	[20]
	$[C_4min][PF_6]$ BLM	99% removal	[21]
Phenol and chlorophenol compounds	$[C_4min][PF_6]$ + TBP kerosene ELM	>99% phenol removal >90% chlorophenol removal	[22]
Bisphenol A	ILs supported in PVDF SLM	44% of solute permeation within 24 hours	[23]
	n-Heptane in PP HF-SLM	96% extraction efficiency	[95]
Diclofenac	Tetrabutylammonium bromide dichloromethane in ELM	99% removal	[96]
Ibuprofen	TOA in Parleam 4 ELM	Complete removal	[97]
Tetracycline	TBP and Fe_2O_3 nanoparticles in n-heptane PELM	97% removal	[98]
(S)-amlodipine	O,O'-dibenzoyl-(2S,3S)-tartaric acid diluted in organic solvents in PP HF-SLM	78% extraction and 75% recovery efficiencies. Enantiomeric excess of 58%	[99]
Ethylparaben	TOA in n-heptane ELM	90% removal	[100]
Propylparaben	TOPO in hexane ELM	Complete removal	[101]
Kraft lignin	Aliquat 336 in kerosene and 2-ethyl-1-hexanol ELM	98% recovery efficiency	[102]
Lignosulfonate	TOA in dichloroethane in Nylon 6,6 SLM	50% removal	[103]

optimal conditions, phenol extraction using the pure diluents reached 97 and 82% for kerosene and palm oil, respectively, while at 70:30 diluent composition ratio, the removal was nearly 83%. Since no carrier was used, the phenol transport was achieved by simple diffusion through the membrane, reacting with an NaOH solution that constituted the stripping phase (see Figure 8.7b). This suggests that the membrane viscosity, related to the solute diffusivity by Eq. (8.4), is the main factor in the membrane performance.

IL-based LMs have also been investigated for the removal of phenol. Hydrophobic imidazolium-ILs ($[C_4min][Tf_2N]$, $[C_4min][PF_6]$, and $[C_4min][FAP]$) were used for the preparation of BLM for phenol removal from aqueous effluents [20]. Maximum extraction

and stripping efficiencies of 96 and 98%, respectively, were obtained. This work also compared the performance of LMs containing $[C_4min][Tf_2N]$ with analogs made of conventional organic solvents such as dichloromethane. Due to the low viscosity of the organic solvent, higher phenol diffusivity values were expected. However, similar extraction and stripping efficiencies were obtained for both types of solvents. It is worth noting that ILs can be considered for the preparation of facilitated-transport LMs as well. For example, phenol migration was studied in $[C_4min][PF_6]$ in BLMs, where the complex solute-IL was formed and was transported across the membrane by hydrogen bonding interactions [21]. Likewise, $[C_4min][PF_6]$ was added to TBP and used as the carrier in the removal of phenolic compounds using kerosene-based ELMs [22]. In comparison to pure TBP carrier, the use of the IL mixture improved the emulsion stability as well as the removal efficiency. Given the high viscosity of ILs, they are also suitable candidates for the preparation of SLMs. A range of ILs supported in a PVDF matrix was tested for the removal of bisphenol A, an endocrine disruptor used in plastic production, from aqueous effluents [23]. Flat sheet SLMs of 12 cm^2 were tested and reached a maximum of 44% of solute permeation within 24 hours, and it was suggested that performance could be improved by phase pH control. Moreover, in another work, a maximum bisphenol A extraction of 96% was achieved in a 9-hour cycle using an HF-SLM module [95]. The membrane was PP fibers impregnated with n-heptane, with a total surface area of 1.4 m^2. Although a conventional organic solvent was used in the aforementioned study, the results highlight the feasibility of scaling up SLM for industrial processes.

Looking at other types of contaminants in water bodies, the presence of prescribed and unprescribed drugs, such as painkillers and nonsteroidal anti-inflammatories, is a growing field of concern in domestic wastewater treatment plants. Human and animal excretions may carry several substances discharged in feces and urine in unchanged form or metabolized into secondary compounds. Nevertheless, due to their toxicity and bioaccumulation, the presence of pharmaceutical waste in household and hospital waste effluents means a risk to aquatic ecosystems with potential hazards to human health. For instance, around 15% of the administered anti-inflammatory drug diclofenac is excreted without chemical changes [96], while 70% of antibiotics are not metabolized [98]. As an alternative to conventional separation processes, the removal of pharmaceuticals from wastewater has been carried out with LMs. In a 6-minute process, over 99% removal of diclofenac ions was reached with ELMs [96]. The membrane was composed of tetrabutylammonium bromide, Span 80, and dichloromethane as the carrier, surfactant, and diluent, respectively. Similarly, almost complete ibuprofen removal was reached using an ELM prepared with organic solvent Parleam® 4 as a diluent, surfactant Abil® EM90, and extracting agent TOA [97]. Another work reported an efficiency of 97% for the removal of tetracycline, an antibiotic drug, using nano-fluid emulsion [98]. The PELM was composed of Fe_2O_3 nanoparticles in n-heptane and stabilized with oleic acid, and TBP was used as the extracting agent. The work compared the PELM performance against the ELM technique and results showed that the stability of the membrane was substantially improved by nanoparticle inclusion. In the case of racemic mixtures, the separation process must offer a high chiral resolution to accomplish the recovery target [9, 10]. Enantioseparation of (R)- and (S)-amlodipine from pharmaceutical wastewater was studied using PP-based HF-SLM [99]. (S)-amlodipine is a high-value compound used to treat hypertension and as an antianginal agent, while

(R)-amlodipine is inactive; hence, the process selectivity becomes essential. The membrane was prepared with the chiral extractant O,O'-dibenzoyl-(2S,3S)-tartaric acid diluted in organic solvents. For the release of (S)-amlodipine into the stripping solution, b-cyclodextrin was added. The process attained a maximum extraction and stripping efficiency of 78 and 75%, respectively, and reached an (S)-amlodipine enantiomeric excess of 58%.

Other dangerous pollutants from plants and urban wastewater have been found in water bodies, becoming a major environmental hazard. Alkyl esters of p-hydroxybenzoic acid, better known as paraben compounds, are used as preservatives in cosmetics, pharmaceutics, and food products. However, they are also known as endocrine-disrupting chemicals and related to other health issues. Therefore, ELMs have also been proposed for the removal of parabens from aqueous solutions. In a comprehensive emulsion characterization study, 90% of ethylparaben was removed using an n-heptane-based ELM, with TOA as the carrier [100]. Similarly, trioctylphosphine oxide (TOPO) in hexane was used for complete propylparaben removal from aqueous solutions [101].

Pulp and paper industries generate millions of metric tons of lignin waste annually. Beyond its enormous impact on the ecosystems, lignin offers the opportunity to be used as a renewable feedstock in the production of high-value compounds. Recovery of up to 98% of kraft lignin from pulping wastewater was reported using Aliquat 336 as the carrier in a kerosene-based ELM and 2-ethyl-1-hexanol as a modifier [102]. Moreover, the treatment proved to be as feasible in actual pulp wastewater as the model solution.

8.3.4 Metal Ion Recovery and Heavy Metal Removal

Metal-contaminated wastewaters are commonly found in industrial processes as well as in natural reservoirs, where groundwater sources can be heavily polluted. Although some metals such as lithium, iron, gold, and bismuth have low toxicity, other heavy metal elements are an undeniable health threat due to their bioaccumulation, toxicity, and carcinogenic effects. Their removal in contaminated waters for human consumption and prior to the discharge of wastewater industrial streams is thus necessary. Copper, silver, vanadium, and palladium are among the highly toxic heavy metals. Yet, arsenic, cadmium, chromium, lead, and mercury are major hazards to both humans and the environment. It is important to note that the development of separation technologies of metal solutions has hoarded a great interest for not only environmental and health reasons but also economic reasons since some metal ion solutions have great added value potential. Nowadays, their extraction is carried by physicochemical treatments, such as solvent extraction, absorption, precipitation, membrane filtration, and electrocoagulation. And, alternatively, biosorption, phytoremediation, and sulfate reducing are other biological remediation techniques [104]. Likewise, LM technology has been investigated for this purpose, as Table 8.5 summarizes.

Organic solvent-based BLMs, with carbon tetrachloride, chloroform, and dichloromethane, were studied for mercury removal [105]. In this work, extraction and recovery kinetic parameters of Hg (II) using calix[4]arene thioalkyl derivative carriers were determinate. An SLM, composed of TOA in dichloroethane supported in Nylon 6,6, was studied for mercury (II) removal [103]. Under optimal conditions, the membrane showed a removal efficiency of 81–88%. In the same work, the SLM was tested for mercury removal from a complex mixture. The model solution, containing mercury chloride and sodium

Table 8.5 Summary of recent liquid membrane studies for the removal of heavy metals and recovery of metal ions.

Solute	Membrane	Results	Ref.
Mercury	Calix[4]arene thioalkyl derivative in CCl_4, $CHCl_3$, and CH_2Cl_2 BLM	Extraction and recovery kinetic parameters	[105]
	TOA in dichloroethane in Nylon 6,6 SLM	81–88% removal	[103]
	Aliquat 336 in toluene PP HF-SLM	Nearly complete removal	[106]
	TOA in coconut oil supported in PVDF SLM	95% removal	[28]
Lithium	TBP in $[Tf_2N]$-based ILs supported in PVDF SLM	Permeability of $1.2{\cdot}10^{-6}$ m/s	[107]
Copper and lithium	Cyanex 272 diluted in kerosene HF-SLM and SLM	Cu(II) over Li(I) separation factor of 18 and 178 for HF-SLM and SLM, respectively	[108]
Copper	D2EHPA in kerosene HFRLM	60% removal	[58]
	Acorga M5640 in aliphatic diluent PEHFSD LM	96–97% removal	[61]
	LIX 984N in kerosene ELM	>99% removal	[109]
	D2EHPA in waste vegetable oil CLM	96% removal	[37]
Bismuth	D2EHPA in n-pentanol ELM	Complete removal	[110]
Rhodium	Polyisobutylene and TOA in kerosene ELM	46% removal	[111]
Silver	Cyanex 302 in paraffinic and naphthenic hydrocarbon-diluent ELM	95–99% extraction efficiency	[112]
Vanadium	D2EHPA in paraffin ELM	91% recovery efficiency	[113]
Platinum	$[P_{88812}][Cl]$ IL in PVDF-co-hexafluoropropyle and 2-nitrophenyloctyl ether PIM	96% recovery efficiency	[52]
Palladium	$[P_{88812}][Cl]$ IL in PVDF-co-hexafluoropropyle and 2-nitrophenyloctyl ether PIM	96% recovery efficiency	[52]
	Cyanex 302 in kerosene ELM	97% recovery efficiency	[114]
Arsenic	Aliquat 336 and 2-ethyl hexanol in kerosene ELM	78 and 88% removal, respectively	[115]
Chromium	Aliquat 336 in kerosene and decanol ELM, spray column	Volumetric mass transfer coefficient of 0.036–0.074/s	[50]
	TOMAC in $[C_4min][Tf_2N]$ and kerosene ELM	97% removal	[24]
Lead	Fe_2O_3 magnetic particles and D2EHPA in kerosene PELM	97% removal	[116]
Cadmium	Aliquat 336 in corn oil ELM	>98% removal	[33]

lignosulfonate, emulated wastewater from pulp and paper industries. The extraction efficiency was 53 and 50% for mercury and lignosulfonate, respectively, which demonstrated the need for testing real mixtures. Treatment of petroleum-produced water using a PP-based HF-SLM impregnated with Aliquat 336 in toluene showed a nearly complete mercury extraction [106].

Since the IL trioctyl(dodecyl) phosphonium chloride, $[P_{88812}][Cl]$, has shown high platinum-group metal extraction, their ions recovery with a reduced amount of $[P_{88812}][Cl]$ polymerized as PIM was proposed as a greener alternative [52]. The membrane was prepared with the polymer PVDF-co-hexafluoropropyle and 2-nitrophenyloctyl ether as the plasticizer. In a two-stage sequential transport cycle, the authors aimed to the selective separation of an aqueous mixture of platinum, palladium, and rhodium. For each sequence, a proper stripping solution was used to enhance the permeation of a single metal, each following a specific transport mechanism. The optimum stripping solutions were 0.1 M $NaClO_4$ in 1 M HCl and 0.1 M KSCN in 1 M HCl for platinum and palladium, respectively, and the experiments reached 96% of recovery efficiency for Pt(IV) in the first transport and 96% of Pd(II) in the second. In neither of both sequences Rd(III) was transported. The high selectivity attained by tuning the stripping solution highlights the versatility of LM technology to be tailored in order to efficaciously perform the extraction process.

The recovery of lithium ions from complex aqueous mixtures was studied using SLMs impregnated with TBP in ILs [107]. Several $[Tf_2N]$-based ILs were tested supporting them in PVDF matrices varying the support thickness and pore size. Faster Li(II) permeation than Mg(II), one of the main impurities in lithium brines, was observed. Likewise, the study tested the lithium permeation in the presence of Co(II) and Ni(II), by-products obtained from recycle lithium-ion batteries, also showing good selectivity, but reducing the Li(II) permeation coefficient. In a comparative study, separation of copper and lithium ions was carried out using an HF-SLM via nondispersive solvent extraction and compared with the use of the membranes in flat sheet configuration and also against the use of a dispersive solvent extraction process [108]. LMs in this work were composed of Cyanex 272 diluted in kerosene, and although results showed similar performance for the three methods, the authors outstripped the advantages that HF membranes offer when scaling up the process. Other HF-based configurations have also been used for the extraction of copper. HFRLMs (see Figure 8.4d) containing D2EHPA in kerosene were used to remove copper from sulfate solutions [58]. A complete model to describe the mass transfer coefficients and flux rate, which fit the experimental data, was reported. Similarly, a PEHFSD arrangement (see Figure 8.4e) was proposed for this system [61]; the copper mass transfer coefficients and the effect of having Fe and Zn ions were studied. Comparing the extraction performance, the authors obtained a Cu removal efficiency of 96–97% for PEHFSD versus 91–97% for an equivalent ELM. Besides the lower overall extraction yields, ELMs showed poor copper/iron selectivity, attributed to swelling issues.

Nonetheless, other works have reported effective metal recovery throughout ELMs. A kerosene-based ELM obtained more than 99% of copper removal using LIX® 984N as the carrier [109]. Bismuth extraction from nitric solutions was achieved using an ELM based on D2EHPA in n-pentanol and biodegradable surfactant Triton® X-100 [110]. Emulsion membranes containing polyisobutylene, TOA, and Span 80 in kerosene were used to reduce the toxicity of rhodium-contaminated wastewater [111]. Using an ELM based on Cyanex

302 in paraffinic and naphthenic hydrocarbon diluent, silver extractions of 95–99% were obtained within 15 minutes of treatment [112]. ELM composed of D2EHPA in paraffin reached 91% of vanadium recovery from a stone coal leaching solution [113]. High palladium recovery from electroplating wastewater was attained using a Cyanex 302 in kerosene ELM [114]. The membrane also showed good Pd over Cr selectivity. Kerosene-based ELMs were used for arsenic (V) removal, with Aliquat 336 and 2-ethyl hexanol as carriers, obtaining a maximum removal of 78 and 88%, respectively [115].

Other LMs have been proposed as well for the removal of highly toxic heavy metals from wastewater. In order to improve the ELM dispersibility in chromium (VI) removal, a spray column (see Figure 8.4b) was modified to include a rotator that produced centrifugal acceleration [50]. The work showed that the addition of the rotor resulted in an approximately ten times higher mass transfer coefficient for chromium using an emulsion conformed of Aliquat 336 in kerosene and decanol. To improve membrane stability, a stabilizer compound can also be included to avoid globule breakage. In a chromium removal study, IL $[C_4min][Tf_2N]$ was added to a kerosene membrane also containing extracting agent tri-n-octylmethylammonium chloride (TOMAC) [24]. Despite the slight reduction in the extraction efficiency, high stability was obtained with 3% (w/w) of the IL, reaching 97% of Cr removal. In another work, α-Fe_2O_3 magnetic particles were used as co-stabilizer in a PELM composed of D2EHPA in kerosene, resulting in 97% lead removal, and a significant increase in membrane stability [116].

Aiming to develop more sustainable metal extraction LM technologies, sustainable green-based LMs have been proposed. A waste-vegetable oil membrane was used for copper recovery in a CLM configuration with D2EHPA as the carrier and reached 96% of Cu removal [37]. The work compared the effect of replacing the diluent with fresh-vegetable oil or kerosene, and separation performance followed the trend kerosene > fresh oil > waste oil, which was attributed to an improved ion diffusivity due to the reduction in diluent viscosity. More than 98% of cadmium removal was obtained with a corn oil-based ELM which contained extracting agent Aliquat 336 and surfactant Span 80 [33]. Using palm oil as the diluent in an ELM, 97–99% of chromium (Vl) removal was reached with TOMAC as the carrier [36]. Vegetable oils can be used in SLM configurations as well. A PVDF support was impregnated with TOA in coconut oil for mercury removal [28]. The membrane showed great performance, in terms of extraction efficiency and stability, with only slight improvements when the carrier was added, from 91% with no carrier to 95% at a carrier concentration of 4% (v/v). The vegetable-based membrane exhibited similar performance to SLMs with organic solvents, such as dichloroethane or n-heptane, which highlights the sustainability of LM technology as an extraction alternative.

Further applications of ELMs based on organic solvents, such as kerosene or n-heptane, and their operational effects on the removal of heavy metals (copper, nickel, chromium, cobalt, zinc, silver, lead, mercury, cadmium, gold, molybdenum, platinum, and palladium) have been reviewed by Ahmad et al. [117].

8.3.5 Nuclear Waste Treatment

Nuclear waste treatment is another field of application of LM technology. Nuclear waste is produced at resource extraction, nuclear facilities, and power plants, as well as in nuclear fuel conversion, fabrication, and reprocessing of spent fuel. It can contain: (i) actinides, the

main source of fissile fuels uranium and plutonium, (ii) americium, (iii) lanthanides such as cerium, a radioactive poison, which hinders the waste transmutation into short-lived radionuclides, (iv) isotopes of molybdenum-99 (^{99}Mo), used in medical imaging procedures, cesium-137 (^{137}Cs), an irradiation source, cobalt-60 (^{60}Co), widely used for sterilization, radiography, and density measurements, and strontium-90 (^{90}Sr), administered for cancer radiotherapy. The traditional technique to recover plutonium and uranium from used nuclear fuels is the PUREX (plutonium uranium reduction extraction) process [118]. It is based on dissolving the spent fuel in nitric acid and separation by LLX using a mixture of 20–30% (v/v) of TBP diluted in an organic paraffinic hydrocarbon solvent. The process results in two high-purity uranium and plutonium nitric solutions, which can be further converted into metal oxides, along with solid wastes and a remaining radiative stream, classified into high, intermediated, and low-level waste, that are derivate to further treatments. Several LM systems have been proposed for radioactive waste remediation. Table 8.6 presents a summary of the works discussed in this section.

Ambashta and Sillanpää [120] published a review on liquid nuclear waste treatment using membrane technology, where advances on the use of RO, MF, MD, and PV techniques are discussed for low-level waste decontamination. However, these methods are unable to treat high-level waste due to their acid nature which compromises the stability of the polymer-based membranes. Several NF membranes have been studied for cobalt species removal. Colloidal solutions of ^{239}Pu, ^{240}Pu, and ^{214}Am were pretreated by seeded UF and flocculation MF, where a suspension solution was formed by "seed particles" that absorbed the solutes or flocculated them to increase its size, respectively. Inorganic membranes, such as ceramic and zeolite-based, are an alternative to polymer-based membranes as they can be operated under a wide pH range. A zeolite NaA membrane in RO mode showed complete rejection of Cs^{+}, Sr^{+2}, and MoO_4^{-2} from low-concentration solutions.

As an alternative to membrane filtration processes, the above review also presents the LMs as an emergent approach to radioactive waste remediation. BLM using D2EHPA as the carrier was applied to ^{90}Sr extraction from an alkaline solution to an acid stripping phase, where it was precipitated as $SrSO_4$. An Aliquat 336-based ELM was used for ^{99}Mo removal. PIMs composed of plasticized cellulose triacetate and different crown ethers or TBP as the carrier and SLM composed by calix(4)-bis-2,3-naphtho-crown-6 dissolved in 2-nitrophenyl octyl ether and dodecane in a PTFE support showed effective ^{137}Cs transport. Remediation of model low-level waste containing cerium was studied using SLMs. The membrane phases were composed of octyl (phenyl)-*N,N*-diisobutyl carbamoyl methyl phosphine oxide, and TBP as carriers, dissolved in dodecane. Cellulose triacetate plasticized-PIM using octyl-(phenyl)–N,N-diisobutyl carbamoyl methyl phosphine oxide (CMPO) or *N,N,N*-tetraoctyl-3-oxapentane diamine carriers in 2-nitrophenyl *n*-octyl ether shows efficient Ce^{+3} transport. TBP in dodecane-based BLM had reached 90% of cerium transport after its electro-oxidation to Ce^{+4}. HF-SLMs were developed using mixtures of CMPO in dodecane and TBP in kerosene for the removal of neodymium and uranium, respectively, from nitric acid solutions.

ELMs for waste uranium extraction have been studied since the 1980s. TBP used as a carrier has been shown to improve the distribution ratio on benzoyl acetone and dibenzoyl methane membranes [119]. The use of TOPO carriers leads to a uranium extraction above 90%, and Aliquat 336-based membranes surpass conventional process efficiency, reaching

Table 8.6 Summary of recent liquid membrane studies for nuclear waste treatment.

Solute	Membrane	Results	Ref.
Uranium	2-Thenoyltrifluoroacetone in kerosene ELM	>99% removal	[119]
	TBP in kerosene PE HF-SLM	67% extraction and 40% recovery efficiencies	[120]
	Alamine 336 in heavy paraffin ELM	Concentration factor of 6.9	[121]
	D2EHPA and cellulose triacetate PIM	Nearly complete extraction	[121]
	D2EHPA, TBP, Cyanex 272, Alamine 336, and Aliquat 336 in polyvinylchloride PIM	Nearly complete extraction with D2EHPA carrier	[121]
	TBP in paraffin hydrocarbon PEHFSD LM	>84% recovery efficiency	[121]
Plutonium	TBP in dodecane PP HF-SLM	>80% extraction efficiency	[121]
Americium	Cyanex 301 in cellulose triacetate-TBP PIM	Unirradiated and irradiated (194.4 kGy) permeability greater than $5.1 \cdot 10^{-4}$ and $1.1 \cdot 10^{-4}$ m/s, respectively	[121]
	2-Ethylhexyl phosphonic acid mono-2-ethylhexyl ester in dodecane ELM	93% extraction efficiency	[121]
Yttrium	Two-stage PTFE SLMs using 2-ethyl hexyl phosphoric acid-mono-2-ethyl hexyl ester and CMPO in dodecane, respectively	95% removal	[121]
Strontium	D2EHPA BLM	98% removal	[120]
Molybdenum	Aliquat 336-based ELM	85% removal	[120]
Cesium	Crown ethers or TBP in calix(4)-bis-2,3-naphtho-crown-6, 2-nitrophenyl octyl ether and dodecane supported in cellulose triacetate-PTFE PIM	Permeability of $8.5 \cdot 10^{-5}$ cm/s	[120]
	TBP and octyl (phenyl)-*N,N*-diisobutyl carbamoyl methyl phosphine oxide in dodecane supported in PP SLM	>99% removal	[120]
	CMPO or *N,N,N*,-tetraoctyl-3-oxapentane diamine in 2-nitrophenyl *n*-octyl ether supported in cellulose triacetate-PIM	Permeation rates	[120]
	TBP in dodecane BLM	90% removal	[120]
	Cobalt dicabollide on phenyl trifluoromethyl sulphone in PTFE SLM	>95% extraction efficiency	[121]
	TBP or crown ether carriers in cellulose triacetate PIM	Permeability of $0.2 \cdot 10^{-5}$–$8.1 \cdot 10^{-5}$ cm/s	[121]
Neodymium	CMPO in dodecane PVDF SLM	95% extraction efficiency	[120]
	CMPO, N,N-dihexyl octanamide, and N,N,N',N'-tetraoctyl diglycolamide paraffinic hydrocarbon PP HF-SLM	Nearly complete extraction	[121]

a complete uranium extraction. In a recent study, hexavalent uranium extraction from aqueous acid solutions using kerosene-based ELM was evaluated. The membrane included 2-thenoyltrifluoroacetone as the carrier and surfactant Span 80, and an HCl solution was used as the stripping phase. Under optimal conditions, the authors were able to quickly extract the uranyl ions, within 1 minute, which was explained by the pH differences between the feed and stripping phases.

Likewise, another comprehensive review of nuclear waste remediation with LMs was published by Rathore et al. [121]. For instance, high selective uranyl ion permeation was reported using an Alamine 336-based ELM. The study found a uranium (VI) concentration factor of 6.9, with remarkable selectivity removal from the leach liquor containing Fe^{+3}, Mg^{+2}, Ca^{+2}, and Mn. Americium (III) transport with Cyanex 301 in a cellulose triacetate-based PIM was researched using TBP as the plasticizer. In a Stripping phase reaction-facilitated transport regime (see Figure 8.7b), alpha-hydroxy iso-butyric acid was added as a stripping extracting agent to drive the Am^{+3} back extraction. Several radionuclides could be removed from PUREX waste employing ELM with 2-ethylhexyl phosphonic acid mono-2-ethylhexyl ester as the carrier in dodecane. More than 93% of the Am(III), Ce(III), Nb(III), and Zr(IV) were extracted from the feed waste stream. In a two-stage process, SLMs using 2-ethyl hexyl phosphoric acid-mono-2-ethyl hexyl ester and CMPO for the first and second stages, respectively, 95% of Yttrium-90 (^{90}Y) removal has been archived. The system also has been able to retain ^{90}Sr, a common second impurity, between the stage membranes, giving a high-purity final product. Cesium (I) removal from nitric acid solutions by cobalt dicabollide in phenyl trifluoromethyl sulphone and PTFE as the support, showing a strong permeability dependence with the feed phase acidity and carrier concentration. To ensure SLM stability in high-level waste treatments for selective Cs extraction, PIMs have been studied. Likewise, PIM-based on di-tert-butylbenzo-18-crown-6, TBP, and cellulose triacetate as the plasticizer was effectively used for Cs transport from acidic solutions. PIMs were used for uranium removal as well. Through the addition of different plasticizers and scintillants to a D2EHPA and cellulose triacetate PIM, high uranium extraction from nitrate solutions was achieved. Several carriers, such as D2EHPA, TBP, Cyanex 272, Alamine 336, and Aliquat 336, were tested for dioxouranium (II) extraction from acidic sulfate solutions with polyvinylchloride-based PIM. The study showed D2EHPA as the best extracting agent, through an intricate complexation kinetic. Each UO_2^{+2} ion is bonded to two carrier molecules and two carrier conjugated bases. HF-SLM had also been used for the removal of trivalent lanthanides and actinide from nitric solutions using CMPO, N,N-dihexyl octanamide, and N,N,N',N'-tetraoctyl diglycolamide as carriers in paraffinic hydrocarbon. Lastly, plutonium (IV) and uranium (IV) removal have been achieved by PEHFSD-based membranes and TBP as the extracting agent.

8.3.6 Rare-Earth Recovery

REs are a group of elements that comprises scandium, yttrium, and lanthanides. They are used in the production of technological devices, electronic components, rechargeable batteries' manufacturing, as well as on metallurgy, medical, optical, magnets, and catalysis chemistry applications. REs are commonly purified by solvent extraction techniques, such as cation or anion exchangers, solvation–chelating extractants, and synergistic solvent

Table 8.7 Summary of recent liquid membrane studies for the recovery of RE elements.

Solute	Membrane	Results	Ref.
RE oxides	$(RO)_2P(O)OPh$-COOH in sulfonated kerosene ELM	83% recovery efficiency	[66]
	Primary amine N1923 in sec-Caprylic alcohol and kerosene BOLM	RE over Al separation factor of 45	[51]
Gadolinium	D2EHPA in kerosene ELM	99% extraction and 79% stripping efficiencies	[123]
Dysprosium	D2EHPA in kerosene ELM	>99% recovery efficiency	[124]
	Cyanex 572 in kerosene ELM	99% recovery efficiency	[125]
	2-Ethyl hexyl phosphoric acid-mono-2-ethyl hexyl ester in kerosene PEHFSD LM	96% extraction efficiency	[63]
Yttrium	D2EHPA in kerosene PEHFSD LM	99% extraction and 98% recovery efficiencies	[62]
RE radioactive nuclides	Bis(2-ethylhexyl) hydrogen phosphate-decal supported in PTFE SLM	Permeation of 95% cerium, 95% promethium, 80% gadolinium, and 10% ytterbium	[120]
Samarium	D2EHPA in cyclohexane ELM	Permeation rates	[120]
Neodymium	Thenoyltrifluoroacetone and TOPO in cyclohexane ELM	Permeation rates	[120]

extraction [122]. Nonetheless, LMs have been investigated as an alternative to the highly complex solvent extraction processes needed for RE recovery. Recent studies on the RE extraction with LMs are presented in Table 8.7.

The production of phosphoric acid by a wet process often carries lanthanide oxides from the phosphate ore. ELMs were used to compare the extraction efficiency of RE oxides: La_2O_3, Ce_2O_3, Y_2O_3, and Nd_2O_3, from a model HNO_3 solution [66]. The emulsions were composed of sulfonated kerosene and polyisocrotyl succinimide as the diluent and surfactant, respectively, and an H_3PO_4 solution was used for the stripping phase. In this work, different carriers: D2EHPA, $(RO)_2P(O)OPh$-COOH, and $(RO)_2P(O)OPh$, were tested, and results showed a feed phase acidic dependence of the extraction yield; increasing the pH significantly improved the RE oxides' recovery, $(RO)_2P(O)OPh$-COOH being the carrier with the best performance (83%), attributed to its carboxyl group. The observed trend agreed with previous works, where at greater pH solutions, more RE complexes are formed at the feed-globule interface, enhancing the mass transfer [124, 126]. Likewise, extraction and stripping yields of 99% and 79%, respectively, were achieved for gadolinium (III) recovery, which is typically used as a contrast in medical procedures and the production of alloys, using an ELM of D2EHPA in kerosene [123]. Recovery of dysprosium (III), mainly used in permanent magnets' manufacturing, was also studied with D2EHPA in kerosene-based ELMs with a stripping efficiency above 99% [124]. Likewise, a Cyanex 572 in

kerosene-based ELM shows an extraction efficiency of 99% with a high Dy (III) selectivity with respect to Nd (III) [125]. BOLM composed of primary amine N1923 in sec-Caprylic alcohol and kerosene has been proposed as an environmentally friendly alternative to the RE separation from aluminum oxide impurity in leaching solutions [51]. The process gives a highly RE to Al selectivity, reaching a separation coefficient of 45.

Successful dysprosium (III) extraction from acidic solution was also carried out using a PEHFSD (see Figure 8.4e), a variation of HF-SLM to improve the SLM stability [63]. The system resembled a tube and shell exchanger, where the feed phase was pumped into the fibers, while the stripping phase with LM droplets remained in the shell. The composition of the LM was 2-ethyl hexyl phosphoric acid-mono-2-ethyl hexyl ester dissolved in kerosene, and within 170 minutes, the authors reached a transport efficiency of 96%. The recovery of yttrium (III) from mixed oxide ores was also achieved using PEHFSDs in facilitated transport mode, using D2EHPA (carrier) in kerosene [62]. The authors reached an extraction yield of 99% and a stripping recovery of 98%, which represents a substantial improvement with respect to HF-SLM systems.

During nuclear waste treatments, several lanthanide radioisotopes are removed as a part of the remediation process. Separation of RE radioactive nuclides in acidic solution using a PTFE-based SLM impregnated with bis(2-ethylhexyl) hydrogen phosphate-decalin showed a selective preference for light RE elements [120]. The mixture composed of cerium, promethium, gadolinium, and ytterbium in a 0.5 N HCl solution reached a permeation of 95%, 95%, 80%, and 10% for each element, respectively, while no transport was observed for other components. In another work, ELMs composed of cyclohexane and Span 80 were studied for RE recovery from nitrate solutions using HNO_3 as a stripping phase. The carriers used for the recovery of samarium (III) and neodymium (III) were D2EHPA and a mixture of thenoyltrifluoroacetone and TOPO, respectively.

8.4 Conclusions

Since liquid membranes were first proposed, advances in the field have geared toward improving their scope and suitability as a sustainable alternative to traditional solvent extraction and membrane filtration. Liquid membranes have been successfully applied at laboratory scale in the recovery of compounds in biorefinery, amino acids, metal ions, and RE elements, as well as for the removal of heavy metals, and wastewater, and nuclear waste treatment. Throughout this chapter, recent advances in liquid membranes' research and their fundamental basis have been overviewed. Different liquid membrane configurations have been discussed highlighting their pros and cons. For example, despite their low flux, bulk liquid membranes have proved to be useful to determine membrane performance in terms of extraction kinetics and transport coefficients. ELMs are broadly studied due to the likelihood of being implemented at an industrial scale. However, most studies mainly focus on statistical models of effects contribution and significance due to the larger operational variables involved in this arrangement. Finally, a third category which involves the use of porous supports, i.e. SLMs, can improve the separation performance of bulk and ELMs, minimizing the solvent requirements while avoiding contamination into the feed and stripping phases due to membrane leakage. Furthermore, other novel membrane arrangements,

often based on these three main configurations, can help overcome specific limitations, and the most relevant ones have been presented in this chapter.

It is important to note that several aspects of liquid membranes related to their potential as commercial technology remain a challenge. Based on the results found in the literature, future work should focus on improving the mass transfer resistance, membrane stability, and solvent-process compatibility. Moreover, there is a clear need to adopt standard terminology to allow proper evaluation and comparison. Great efforts on process design and integration are also required to understand the feasibility of the new technology for each particular separation. Liquid membranes have been widely presented as an eco-friendly alternative, stressing their environmental applications. Nevertheless, some of the reported membranes discussed in this chapter still use less environmentally friendly compounds where waste membrane management is poorly discussed. Variable optimization, operational costs, and membrane lifecycle should be evaluated by both, simulation and pilot-scale experiments.

The possibility of replacing toxic conventional solvents with greener alternatives such as novel ILs or vegetable-based oils is promising, allowing an enhancement in the sustainability and efficiency of the process. In the near future, industrial applications ranging from the recovery of high-value components to high-risk waste remediation will undoubtedly benefit from current research on liquid membrane technology as a sustainable alternative to conventional processes.

References

1 Sholl, D.S. and Lively, R.P. (2016). Seven chemical separations to change the world. *Nature* 532 (7600): 435–437. http://www.nature.com/articles/532435a.

2 Abdel-Karim, A., Leaper, S., Alberto, M. et al. (2018). High flux and fouling resistant flat sheet polyethersulfone membranes incorporated with graphene oxide for ultrafiltration applications. *Chem Eng J* 334 (October 2017): 789–799.

3 Paseta, L., Luque-Alled, J.M., Malankowska, M. et al. (2020). Functionalized graphene-based polyamide thin film nanocomposite membranes for organic solvent nanofiltration. *Sep Purif Technol* 247 (December 2019): 116995. https://doi.org/10.1016/j.seppur.2020.116995.

4 Leaper, S., Abdel-Karim, A., Faki, B. et al. (2018). Flux-enhanced PVDF mixed matrix membranes incorporating APTS-functionalized graphene oxide for membrane distillation. *J Membr Sci* 554 (March): 309–323. https://doi.org/10.1016/j.memsci.2018.03.013.

5 Baker, R.W. (2012). *Membrane Technology and Applications*, 3e. Chichester: Wiley.

6 Kislik, V.S. (2010). *Liquid Membranes: Principles and Applications in Chemical Separations and Wastewater Treatment*, *1*e. Elsevier B.V.

7 Scott, K. and Hughes, R. (1996). *Industrial Membrane Separation Technology*, *1*e. London: Blackie Academic & Professional.

8 Parhi, P.K. (2013). Supported liquid membrane principle and its practices: a short review. *J Chem* 2013: 1–11. http://www.hindawi.com/journals/jchem/2013/618236/.

9 Charcosset, C. (2012). Other membrane processes. In: *Membrane Processes in Biotechnology and Pharmaceutics*, 253–293. Elsevier https://linkinghub.elsevier.com/retrieve/pii/B9780444563347000071.

10 Dżygiel, P. and Wieczorek, P.P. (2010). Supported liquid membranes and their modifications. In: *Liquid Membranes* (ed. V.S. Kislik), 73–140. Elsevier https://linkinghub.elsevier.com/retrieve/pii/B9780444532183000039.

11 Ghoshal, A.K. and Saha, P. (2015). Liquid – membrane filters. In: *Progress in Filtration and Separation*, 155–205. Elsevier http://dx.doi.org/10.1016/B978-0-12-384746-1.00005-7.

12 Wang, J., Luo, J., Feng, S. et al. (2016). Recent development of ionic liquid membranes. *Green Energy Environ* 1 (1): 43–61. http://dx.doi.org/10.1016/j.gee.2016.05.002.

13 Noble, R.D. and Gin, D.L. (2011). Perspective on ionic liquids and ionic liquid membranes. *J Membr Sci* 369 (1–2): 1–4. http://dx.doi.org/10.1016/j.memsci.2010.11.075.

14 Malik, M.A., Hashim, M.A., and Nabi, F. (2011). Ionic liquids in supported liquid membrane technology. *Chem Eng J* 171 (1): 242–254. http://dx.doi.org/10.1016/j.cej.2011.03.041.

15 Lozano, L.J., Godínez, C., de los Ríos, A.P. et al. (2011). Recent advances in supported ionic liquid membrane technology. *J Membr Sci* 376 (1–2): 1–14. http://dx.doi.org/10.1016/j.memsci.2011.03.036.

16 Crespo, J.G. and Noble, R.D. (2014). Ionic liquid membrane technology. In: *Ionic Liquids Further UnCOILed*, 87–116. Hoboken, NJ: Wiley http://doi.wiley.com/10.1002/9781118839706.ch4.

17 Pratiwi, A.I. and Matsumoto, M. (2014). Separation of organic acids through liquid membranes containing ionic liquids. In: *Ionic Liquids in Separation Technology*, 189–206. Elsevier http://dx.doi.org/10.1016/B978-0-444-63257-9.00005-5.

18 Baylan, N. and Çehreli, S. (2018). Ionic liquids as bulk liquid membranes on levulinic acid removal: a design study. *J Mol Liq* 266: 299–308. https://doi.org/10.1016/j.molliq.2018.06.075.

19 Baylan, N. and Çehreli, S. (2019). Removal of acetic acid from aqueous solutions using bulk ionic liquid membranes: a transport and experimental design study. *Sep Purif Technol* 224 (April): 51–61. https://doi.org/10.1016/j.seppur.2019.05.001.

20 Ng, Y.S., Jayakumar, N.S., and Hashim, M.A. (2011). Behavior of hydrophobic ionic liquids as liquid membranes on phenol removal: experimental study and optimization. *Desalination* 278 (1–3): 250–258. https://linkinghub.elsevier.com/retrieve/pii/S0011916411004607.

21 Lu, S. and Pei, L. (2016). A study on phenol migration by coupling the liquid membrane in the ionic liquid. *Int J Hydrog Energy* 41 (35): 15724–15732. http://dx.doi.org/10.1016/j.ijhydene.2016.05.008.

22 Balasubramanian, A. and Venkatesan, S. (2012). Removal of phenolic compounds from aqueous solutions by emulsion liquid membrane containing Ionic Liquid [BMIM]+[PF6]− in Tributyl phosphate. *Desalination* 289: 27–34. http://dx.doi.org/10.1016/j.desal.2011.12.027.

23 Panigrahi, A., Pilli, S.R., and Mohanty, K. (2013). Selective separation of Bisphenol A from aqueous solution using supported ionic liquid membrane. *Sep Purif Technol* 107: 70–78. https://linkinghub.elsevier.com/retrieve/pii/S138358661300035X.

24 Goyal, R.K., Jayakumar, N.S., and Hashim, M.A. (2011). Chromium removal by emulsion liquid membrane using [BMIM]+[NTf2]− as stabilizer and TOMAC as extractant. *Desalination* 278 (1–3): 50–56. http://dx.doi.org/10.1016/j.desal.2011.05.001.

25 Plaza, A., Merlet, G., Hasanoglu, A. et al. (2013). Separation of butanol from ABE mixtures by sweep gas pervaporation using a supported gelled ionic liquid membrane: analysis of

transport phenomena and selectivity. *J Membr Sci* 444: 201–212. http://dx.doi.org/10.1016/j.memsci.2013.04.034.

26 Dietz, C.H.J.T., Kroon, M.C., Di Stefano, M. et al. (2018). Selective separation of furfural and hydroxymethylfurfural from an aqueous solution using a supported hydrophobic deep eutectic solvent liquid membrane. *Faraday Discuss* 206: 77–92. http://xlink.rsc.org/?DOI=C7FD00152E.

27 Li, Z., Cui, Y., Shen, Y., and Li, C. (2018). Extraction process of amino acids with deep eutectic solvents-based supported liquid membranes. *Ind Eng Chem Res* 57 (12): 4407–4419. https://pubs.acs.org/doi/10.1021/acs.iecr.7b05221.

28 Chakrabarty, K., Saha, P., and Ghoshal, A.K. (2010). Separation of mercury from its aqueous solution through supported liquid membrane using environmentally benign diluent. *J Membr Sci* 350 (1–2): 395–401.

29 Garavand, F., Razavi, S.H., and Cacciotti, I. (2018). Synchronized extraction and purification of L-lactic acid from fermentation broth by emulsion liquid membrane technique. *J Dispers Sci Technol* 39 (9): 1291–1299. https://doi.org/10.1080/01932691.2017.1396225.

30 Manna, M.S., Bhatluri, K.K., Saha, P., and Ghoshal, A.K. (2012). Transportation of catechin (±C) using physiologically benign vegetable oil as liquid membrane. *Ind Eng Chem Res* 51 (46): 15207–15216. https://pubs.acs.org/doi/10.1021/ie3017863.

31 Kumar, A., Thakur, A., and Panesar, P.S. (2019). A comparative study on experimental and response surface optimization of lactic acid synergistic extraction using green emulsion liquid membrane. *Sep Purif Technol* 211 (May 2018): 54–62. https://doi.org/10.1016/j.seppur.2018.09.048.

32 Kumar, A., Thakur, A., and Panesar, P.S. (2018). Statistical optimization of lactic acid extraction using green emulsion ionic liquid membrane (GEILM). *J Environ Chem Eng* 6 (2): 1855–1864. https://doi.org/10.1016/j.jece.2018.01.037.

33 Ahmad, A.L., Shah Buddin, M.M.H., Ooi, B.S., and Kusumastuti, A. (2017). Utilization of environmentally benign emulsion liquid membrane (ELM) for cadmium extraction from aqueous solution. *J Water Process Eng* 15: 26–30. http://dx.doi.org/10.1016/j.jwpe.2016.05.010.

34 Jusoh, N., Sulaiman, R.N.R., Othman, N. et al. (2020). Development of vegetable oil-based emulsion liquid membrane for downstream processing of bio-succinic acid. *Food Bioprod Process* 119: 161–169. https://doi.org/10.1016/j.fbp.2019.11.003.

35 Othman, N., Noah, N.F.M., Shu, L.Y. et al. (2017). Easy removing of phenol from wastewater using vegetable oil-based organic solvent in emulsion liquid membrane process. *Chin J Chem Eng* 25 (1): 45–52. http://dx.doi.org/10.1016/j.cjche.2016.06.002.

36 Björkegren, S., Karimi, R., Martinelli, A. et al. (2015). A new emulsion liquid membrane based on a palm oil for the extraction of heavy metals. *Membranes (Basel)* 5 (2): 168–179. http://www.mdpi.com/2077-0375/5/2/168.

37 Chang, S.H. (2017). Parametric studies on an innovative waste vegetable oil-based continuous liquid membrane (WVCLM) for Cu(II) ion separation from aqueous solutions. *J Ind Eng Chem* 50: 102–110. http://dx.doi.org/10.1016/j.jiec.2017.01.037.

38 Diaconu, I., Ruse, E., Aboul-Enein, H.Y., and Bunaciu, A.A. (2016). Analytical applications of transport through bulk liquid membranes. *Crit Rev Anal Chem* 46 (4): 332–341. http://dx.doi.org/10.1080/10408347.2015.1064759.

39 Li, N.N. (1968). Separating hydrocarbons with liquid membranes. US Patent 3,410,794.

40 Kumar, A., Thakur, A., and Panesar, P.S. (2019). A review on emulsion liquid membrane (ELM) for the treatment of various industrial effluent streams. *Rev Environ Sci Biotechnol* 18 (1): 153–182. https://doi.org/10.1007/s11157-019-09492-2.

41 Kumar, A., Thakur, A., and Panesar, P.S. (2019). Recent developments on sustainable solvents for emulsion liquid membrane processes. *J Clean Prod* 240: 118250. https://doi.org/10.1016/j.jclepro.2019.118250.

42 Hussein, M.A., Mohammed, A.A., and Atiya, M.A. (2019). Application of emulsion and pickering emulsion liquid membrane technique for wastewater treatment: an overview. *Environ Sci Pollut Res* 26 (36): 36184–36204. http://link.springer.com/10.1007/s11356-019-06652-3.

43 San Román, M.F., Bringas, E., Ibáñez, R., and Ortiz, I. (2010). Liquid membrane technology: fundamentals and review of its applications. *J Chem Technol Biotechnol* 85 (1): 2–10. http://doi.wiley.com/10.1002/jctb.2252.

44 Ryšavá, L., Dvořák, M., and Kubáň, P. (2019). The effect of membrane thickness on supported liquid membrane extractions in-line coupled to capillary electrophoresis for analyses of complex samples. *J Chromatogr A* 1596: 226–232. https://linkinghub.elsevier.com/retrieve/pii/S0021967319302225.

45 Gabelman, A. and Hwang, S.-T. (1999). Hollow fiber membrane contactors. *J Membr Sci* 159 (1–2): 61–106. https://linkinghub.elsevier.com/retrieve/pii/S037673889900040X.

46 Teramoto, M., Takeuchi, N., Maki, T., and Matsuyama, H. (2002). Ethylene/ethane separation by facilitated transport membrane accompanied by permeation of aqueous silver nitrate solution. *Sep Purif Technol* 28 (2): 117–124. https://linkinghub.elsevier.com/retrieve/pii/S138358660200045X.

47 Gu, Z., Wu, Q., Zheng, Z. et al. (1994). Laboratory and pilot plant test of yttrium recovery from wastewater by electrostatic pseudo liquid membrane. *J Membr Sci* 93 (2): 137–147.

48 Pérez, A.D. and Fontalvo, J. (2019). A new concept of liquid membranes in Taylor flow: performance for lactic acid removal. *Chem Eng Process Process Intensif* 139 (March): 95–102. https://doi.org/10.1016/j.cep.2019.03.015.

49 Park, Y., Forney, L.J., Kim, J.H., and Skelland, A.H.P. (2004). Optimum emulsion liquid membranes stabilized by non-Newtonian conversion in Taylor–Couette flow. *Chem Eng Sci* 59 (24): 5725–5734. https://linkinghub.elsevier.com/retrieve/pii/S0009250904003859.

50 Bhowal, A., Bhattacharyya, G., Inturu, B., and Datta, S. (2012). Continuous removal of hexavalent chromium by emulsion liquid membrane in a modified spray column. *Sep Purif Technol* 99: 69–76. http://dx.doi.org/10.1016/j.seppur.2012.08.026.

51 Liu, J., Huang, K., Wu, X.H., and Liu, H. (2017). Enrichment of low concentration rare earths from leach solutions of ion-adsorption ores by bubbling organic liquid membrane extraction using N1923. *ACS Sustain Chem Eng* 5 (9): 8070–8078.

52 Fajar, A.T.N., Hanada, T., Firmansyah, M.L. et al. (2020). Selective separation of platinum group metals via sequential transport through polymer inclusion membranes containing an ionic liquid carrier. *ACS Sustain Chem Eng* 8 (30): 11283–11291.

53 Zhang, S., Dokko, K., and Watanabe, M. (2015). Porous ionic liquids: synthesis and application. *Chem Sci* 6 (7): 3684–3691.

54 Pabby, A.K. and Sastre, A.M. (2013). State-of-the-art review on hollow fibre contactor technology and membrane-based extraction processes. *J Membr Sci* 430: 263–303. http://dx.doi.org/10.1016/j.memsci.2012.11.060.

55 Offeman, R.D. and Robertson, G.H. (2008). Spiral-wound liquid membrane module for separation of fluids and gases. US Patent US7341663B2.

56 Ho Winston, S.W. and Sirkar, K.K. (1992). *Membrane Handbook*. New York: Van Nostrand Reinhold.

57 He, L., Li, L., Sun, W. et al. (2016). Extraction and recovery of penicillin G from solution by cascade process of hollow fiber renewal liquid membrane. *Biochem Eng J* 110: 8–16. http://dx.doi.org/10.1016/j.bej.2016.02.002.

58 Ren, Z., Zhang, W., Dai, Y. et al. (2008). Modeling of effect of pH on mass transfer of copper(II) extraction by hollow fiber renewal liquid membrane. *Ind Eng Chem Res* 47 (12): 4256–4262. https://pubs.acs.org/doi/10.1021/ie0714798.

59 Hu, S.B. and Wiencek, J.M. (1998). Emulsion-liquid-membrane extraction of copper using a hollow-fiber contactor. *AIChE J* 44 (3): 570–581.

60 Fouad, E.A. and Bart, H.-J. (2008). Emulsion liquid membrane extraction of zinc by a hollow-fiber contactor. *J Membr Sci* 307 (2): 156–168. https://linkinghub.elsevier.com/retrieve/pii/S0376738807006801.

61 Agarwal, S., Reis, M.T.A., Ismael, M.R.C. et al. (2013). Application of pseudo-emulsion based hollow fibre strip dispersion (PEHFSD) for the recovery of copper from sulphate solutions. *Sep Purif Technol* 102: 103–110. http://dx.doi.org/10.1016/j.seppur.2012.09.026.

62 Pirom, T., Arponwichanop, A., Pancharoen, U. et al. (2018). Yttrium (III) recovery with D2EHPA in pseudo-emulsion hollow fiber strip dispersion system. *Sci Rep* 8 (1): 7627. http://www.nature.com/articles/s41598-018-25771-4.

63 Pei, L., Wang, L., Guo, W., and Zhao, N. (2011). Stripping dispersion hollow fiber liquid membrane containing PC-88A as carrier and HCl for transport behavior of trivalent dysprosium. *J Membr Sci* 378 (1–2): 520–530. http://dx.doi.org/10.1016/j.memsci.2011.05.037.

64 Mulder, M. (1991). *Basic Principles of Membrane Technology*. Dordrecht: Kluwer Academic Publishers.

65 Chaouchi, S. and Hamdaoui, O. (2014). Extraction of priority pollutant 4-nitrophenol from water by emulsion liquid membrane: emulsion stability, effect of operational conditions and membrane reuse. *J Dispers Sci Technol* 35 (9): 1278–1288. http://www.tandfonline.com/doi/abs/10.1080/01932691.2013.844704.

66 Chen, Q., Ma, X., Zhang, X. et al. (2018). Extraction of rare earth ions from phosphate leach solution using emulsion liquid membrane in concentrated nitric acid medium. *J Rare Earths* 36 (11): 1190–1197. https://doi.org/10.1016/j.jre.2018.05.006.

67 Lee, S.C. and Hyun, K.-S. (2010). Development of an emulsion liquid membrane system for separation of acetic acid from succinic acid. *J Membr Sci* 350 (1–2): 333–339. https://linkinghub.elsevier.com/retrieve/pii/S0376738810000177.

68 Jiang, M., Ma, J., Wu, M. et al. (2017). Progress of succinic acid production from renewable resources: metabolic and fermentative strategies. *Bioresour Technol* 245 (30): 1710–1717. https://doi.org/10.1016/j.biortech.2017.05.209.

69 Gubicza, L., Nemestóthy, N., Bélafi-Bakó, K., and Findrik, Z. (2014). The role of ionic liquids in enzyme-membrane integrated systems. In: *Ionic Liquids in Separation*

Technology, 235–259. Elsevier https://linkinghub.elsevier.com/retrieve/pii/B9780444632579000079.

70 Bélafi-Bakó, K., Nemestóthy, N., and Bakonyi, P. (2014). Separation of gases using membranes containing ionic liquids. In: *Ionic Liquids in Separation Technology*, 261–273. Elsevier https://linkinghub.elsevier.com/retrieve/pii/B9780444632579000080.

71 Luis, P. (2018). Gas permeation and supported liquid membranes. In: *Fundamental Modelling of Membrane Systems*, 103–151. Elsevier http://dx.doi.org/10.1016/B978-0-12-813483-2.00004-6.

72 Sastre, A.M. (2015). Handbook of membrane separations. In: *Handbook of Membrane Separations*, *2*e (eds. A.K. Pabby, R. SSH and R. AMS). CRC Press https://www.taylorfrancis.com/books/9781466555587.

73 Othman, N., Mili, N., Idris, A., and Zailani, S.N. (2012). Removal of dyes from liquid waste solution: study on liquid membrane component selection and stability. In: *Sustainable Membrane Technology for Energy, Water, and Environment*, 221–229. Hoboken, NJ: Wiley http://doi.wiley.com/10.1002/9781118190180.ch19.

74 Werpy, T.A., Holladay, J.E., and White, J.F. (2004). Top value added chemicals from biomass: I. Results of screening for potential candidates from sugars and synthesis gas. United States 2004. https://www.osti.gov/servlets/purl/926125.

75 Song, H. and Lee, S.Y. (2006). Production of succinic acid by bacterial fermentation. *Enzym Microb Technol* 39 (3): 352–361. https://linkinghub.elsevier.com/retrieve/pii/S0141022906001190.

76 Inci, I. (2007). Linear solvation energy relationship modeling and kinetic studies on reactive extraction of succinic acid by tridodecylamine dissolved in MIBK. *Biotechnol Prog* 23 (5): 1171–1179.

77 Chanukya, B.S., Kumar, M., and Rastogi, N.K. (2013). Optimization of lactic acid pertraction using liquid emulsion membranes by response surface methodology. *Sep Purif Technol* 111: 1–8. http://dx.doi.org/10.1016/j.seppur.2013.03.026.

78 Pérez, A.D., Rodríguez-Barona, S., and Fontalvo, J. (2019). Integration of a liquid membrane in Taylor flow regime with a fermentation by Lactobacillus casei ATCC 393 for in-situ lactic acid removal. *Chem Eng Process Process Intensif* 140 (April): 85–90. https://doi.org/10.1016/j.cep.2019.05.002.

79 Lee, S.C. (2011). Extraction of succinic acid from simulated media by emulsion liquid membranes. *J Membr Sci* 381 (1–2): 237–243. http://dx.doi.org/10.1016/j.memsci.2011.07.039.

80 Koter, S. and Szczepański, P. (2011). Modeling of diffusive transport of benzoic acid through a liquid membrane. *Chem Pap* 65 (5): 584–595. http://www.degruyter.com/view/j/chempap.2011.65.issue-5/s11696-011-0010-9/s11696-011-0010-9.xml.

81 Berrios, J., Pyle, D.L., and Aroca, G. (2010). Gibberellic acid extraction from aqueous solutions and fermentation broths by using emulsion liquid membranes. *J Membr Sci* 348 (1–2): 91–98. https://linkinghub.elsevier.com/retrieve/pii/S0376738809007820.

82 Baylan, N., Çehreli, S., and Özparlak, N. (2017). Transport and separation of carboxylic acids through bulk liquid membranes containing tributylamine. *J Dispers Sci Technol* 38 (6): 895–900. http://dx.doi.org/10.1080/01932691.2016.1214841.

83 Bouranene, S., Soualmia, A., Fievet, P. et al. (2017). Extraction of ethanol from aqueous solutions by emulsion liquid membrane: optimization of operating conditions and

influence of salts in the feed phase. *Desalin Water Treat* 88 (November): 106–115. http://www.deswater.com/DWT_abstracts/vol_88/88_2017_106.pdf.

84 Kumar, A., Thakur, A., and Panesar, P.S. (2019). Lactic acid and its separation and purification techniques: a review. *Rev Environ Sci Biotechnol* 18 (4): 823–853. https://doi.org/10.1007/s11157-019-09517-w.

85 Morone, A., Apte, M., and Pandey, R.A. (2015). Levulinic acid production from renewable waste resources: bottlenecks, potential remedies, advancements and applications. *Renew Sust Energ Rev* 51: 548–565.

86 Alberto, M., Bhavsar, R., Luque-Alled, J.M. et al. (2018). Study on the formation of thin film nanocomposite (TFN) membranes of polymers of intrinsic microporosity and graphene-like fillers: effect of lateral flake size and chemical functionalization. *J Membr Sci* 565 (August): 390–401.

87 López-Porfiri, P., Gorgojo, P., and Gonzalez-Miquel, M. (2020). Green solvent selection guide for biobased organic acid recovery. *ACS Sustain Chem Eng* 8 (24): 8958–8969. https://pubs.acs.org/doi/10.1021/acssuschemeng.0c01456.

88 Smith, E.L., Abbott, A.P., and Ryder, K.S. (2014). Deep eutectic solvents (DESs) and their applications. *Chem Rev* 114 (21): 11060–11082. https://pubs.acs.org/doi/10.1021/cr300162p.

89 Yan, N. and Wang, Y. (2019). Catalyst: is the amino acid a new frontier for biorefineries? *Chem* 5 (4): 739–741. https://doi.org/10.1016/j.chempr.2019.03.016.

90 Fathi, S.A.M., Yaftian, M.R., and Kargari, A. (2013). Water-in-oil emulsion liquid membrane transport of L-cysteine. *Sep Sci Technol* 48 (1): 105–112. http://www.tandfonline.com/doi/abs/10.1080/01496395.2012.675001.

91 Fang, Z., Liu, X., Zhang, M. et al. (2016). A neural network approach to simulating the dynamic extraction process of l-phenylalanine from sodium chloride aqueous solutions by emulsion liquid membrane. *Chem Eng Res Des* 105: 188–199. http://dx.doi.org/10.1016/j.cherd.2015.11.012.

92 Gonzalez-Miquel, M. and Esteban, J. (2019). Novel solvents for biotechnology applications. In: *Comprehensive Biotechnology*, *3*e (ed. M. Moo-Young), 790–806. Pergamon: Elsevier.

93 Tomé, L.I.N., Catambas, V.R., Teles, A.R.R. et al. (2010). Tryptophan extraction using hydrophobic ionic liquids. *Sep Purif Technol* 72 (2): 167–173. https://linkinghub.elsevier.com/retrieve/pii/S1383586610000584.

94 Reis, M.T.A., Freitas, O.M.F., Agarwal, S. et al. (2011). Removal of phenols from aqueous solutions by emulsion liquid membranes. *J Hazard Mater* 192 (3): 986–994. http://dx.doi.org/10.1016/j.jhazmat.2011.05.092.

95 Gupta, S., Chakraborty, M., and Murthy, Z.V.P. (2014). Performance study of hollow fiber supported liquid membrane system for the separation of bisphenol A from aqueous solutions. *J Ind Eng Chem* 20 (4): 2138–2145. http://dx.doi.org/10.1016/j.jiec.2013.09.043.

96 Seifollahi, Z. and Rahbar-Kelishami, A. (2017). Diclofenac extraction from aqueous solution by an emulsion liquid membrane: parameter study and optimization using the response surface methodology. *J Mol Liq* 231: 1–10. http://dx.doi.org/10.1016/j.molliq.2017.01.081.

97 Razo-Lazcano, T.A., Stambouli, M., González-Muñoz, P. et al. (2014). Emulsion liquid membranes for recovery of ibuprofen from aqueous solutions. *J Chem Technol Biotechnol* 89 (6): 890–898. http://doi.wiley.com/10.1002/jctb.4329.

98 Mohammed, A.A., Atiya, M.A., and Hussein, M.A. (2020). Removal of antibiotic tetracycline using nano-fluid emulsion liquid membrane: breakage, extraction and stripping studies. *Colloids Surf A Physicochem Eng Asp* 595 (December 2019): 124680. https://doi.org/10.1016/j.colsurfa.2020.124680.

99 Sunsandee, N., Ramakul, P., Pancharoen, U., and Leepipatpiboon, N. (2013). Enantioseparation of (S)-amlodipine from pharmaceutical industry wastewater by stripping phase recovery via HFSLM: polarity of diluent and membrane stability investigation. *Sep Purif Technol* 116: 405–414. https://doi.org/10.1016/j.seppur.2013.06.014.

100 Kohli, H.P., Gupta, S., and Chakraborty, M. (2018). Extraction of ethylparaben by emulsion liquid membrane: statistical analysis of operating parameters. *Colloids Surf A Physicochem Eng Asp* 539 (November 2017): 371–381. https://doi.org/10.1016/j.colsurfa.2017.12.002.

101 Chaouchi, S. and Hamdaoui, O. (2015). Extraction of endocrine disrupting compound propylparaben from water by emulsion liquid membrane using trioctylphosphine oxide as carrier. *J Ind Eng Chem* 22: 296–305. http://dx.doi.org/10.1016/j.jiec.2014.07.023.

102 Ooi, Z.-Y., Harruddin, N., and Othman, N. (2015). Recovery of kraft lignin from pulping wastewater via emulsion liquid membrane process. *Biotechnol Prog* 31 (5): 1305–1314. http://doi.wiley.com/10.1002/btpr.2129.

103 Chakrabarty, K., Saha, P., and Ghoshal, A.K. (2010). Simultaneous separation of mercury and lignosulfonate from aqueous solution using supported liquid membrane. *J Membr Sci* 346 (1): 37–44. https://linkinghub.elsevier.com/retrieve/pii/S0376738809006541.

104 Rene, E.R., Sahinkaya, E., Lewis, A., and Lens, P.N.L. (2017). *Sustainable Heavy Metal Remediation* (eds. E.R. Rene, E. Sahinkaya, A. Lewis and L. PNL). Cham: Springer International Publishing (Environmental Chemistry for a Sustainable World; vol. 8). http://link.springer.com/10.1007/978-3-319-58622-9.

105 Minhas, F.T., Memon, S., and Bhanger, M.I. (2010). Transport of Hg(II) through bulk liquid membrane containing calix[4]arene thioalkyl derivative as a carrier. *Desalination* 262 (1–3): 215–220. http://dx.doi.org/10.1016/j.desal.2010.06.014.

106 Chaturabul, S., Srirachat, W., Wannachod, T. et al. (2015). Separation of mercury(II) from petroleum produced water via hollow fiber supported liquid membrane and mass transfer modeling. *Chem Eng J* 265: 34–46. http://dx.doi.org/10.1016/j.cej.2014.12.034.

107 Zante, G., Boltoeva, M., Masmoudi, A. et al. (2019). Lithium extraction from complex aqueous solutions using supported ionic liquid membranes. *J Membr Sci* 580 (March): 62–76. https://doi.org/10.1016/j.memsci.2019.03.013.

108 Swain, B., Mishra, C., Jeong, J. et al. (2015). Separation of Co(II) and Li(I) with Cyanex 272 using hollow fiber supported liquid membrane: a comparison with flat sheet supported liquid membrane and dispersive solvent extraction process. *Chem Eng J* 271: 61–70. http://dx.doi.org/10.1016/j.cej.2015.02.040.

109 Ma, H., Kökkılıç, O., and Waters, K.E. (2017). The use of the emulsion liquid membrane technique to remove copper ions from aqueous systems using statistical experimental design. *Miner Eng* 107: 88–99. http://dx.doi.org/10.1016/j.mineng.2016.10.014.

110 Mokhtari, B. and Pourabdollah, K. (2015). Emulsion liquid membrane for selective extraction of Bi(III). *Chin J Chem Eng* 23 (4): 641–645. http://dx.doi.org/10.1016/j.cjche.2014.06.035.

111 Moyo, F. and Tandlich, R. (2014). Daphnia pulex toxicity testing of ethylenediaminetetraacetic acid tetrasodium salt dihydrate and the wastewater effluent from extraction of rhodium using emulsion liquid membranes. *Int J Environ Res* 8 (4): 1019–1026.

112 Laki, S. and Kargari, A. (2016). Extraction of silver ions from aqueous solutions by emulsion liquid membrane. *J Membr Sci Res* 2 (1): 33–40.

113 Liu, H., Zhang, Y., Huang, J. et al. (2017). Optimization of vanadium (IV) extraction from stone coal leaching solution by emulsion liquid membrane using response surface methodology. *Chem Eng Res Des* 123: 111–119. http://dx.doi.org/10.1016/j.cherd.2017.05.001.

114 Noah, N.F.M., Othman, N., and Jusoh, N. (2016). Highly selective transport of palladium from electroplating wastewater using emulsion liquid membrane process. *J Taiwan Inst Chem Eng* 64: 134–141. https://linkinghub.elsevier.com/retrieve/pii/S1876107016300293.

115 Srivastava, A., Bhagat, A., Sharma, U. et al. (2017). Comparative study of arsenic(V) removal from aqueous solution using Aliquat-336 and 2-ethyl hexanol through emulsion liquid membrane. *J Water Process Eng* 16: 64–68. http://dx.doi.org/10.1016/j.jwpe.2016.12.007.

116 Salman, H.M. and Mohammed, A.A. (2019). Extraction of lead ions from aqueous solution by co-stabilization mechanisms of magnetic Fe2O3 particles and nonionic surfactants in emulsion liquid membrane. *Colloids Surf A Physicochem Eng Asp* 568 (February): 301–310. https://doi.org/10.1016/j.colsurfa.2019.02.018.

117 Ahmad, A.L., Kusumastuti, A., Derek, C.J.C., and Ooi, B.S. (2011). Emulsion liquid membrane for heavy metal removal: an overview on emulsion stabilization and destabilization. *Chem Eng J* 171 (3): 870–882. http://dx.doi.org/10.1016/j.cej.2011.05.102.

118 Herbst, R.S., Baron, P., and Nilsson, M. (2011). Standard and advanced separation: PUREX processes for nuclear fuel reprocessing. In: *Advanced Separation Techniques for Nuclear Fuel Reprocessing and Radioactive Waste Treatment*, 141–175. Elsevier http://dx.doi.org/10.1533/9780857092274.2.141.

119 Zaheri, P. and Davarkhah, R. (2017). Rapid removal of uranium from aqueous solution by emulsion liquid membrane containing thenoyltrifluoroacetone. *J Environ Chem Eng* 5 (4): 4064–4068. http://dx.doi.org/10.1016/j.jece.2017.07.076.

120 Ambashta, R.D. and Sillanpää, M.E.T. (2012). Membrane purification in radioactive waste management: a short review. *J Environ Radioact* 105: 76–84. http://dx.doi.org/10.1016/j.jenvrad.2011.12.002.

121 Rathore, N.S., Sastre, A.M., and Pabby, A.K. (2016). Membrane assisted liquid extraction of actinides and remediation of nuclear waste: a review. *J Membr Sci Res* 2 (1): 2–13.

122 Xie, F., Zhang, T.A., Dreisinger, D., and Doyle, F. (2014). A critical review on solvent extraction of rare earths from aqueous solutions. *Miner Eng* 56: 10–28. http://dx.doi.org/10.1016/j.mineng.2013.10.021.

123 Davoodi-Nasab, P., Rahbar-Kelishami, A., Safdari, J., and Abolghasemi, H. (2018). Evaluation of the emulsion liquid membrane performance on the removal of gadolinium from acidic solutions. *J Mol Liq* 262: 97–103. https://doi.org/10.1016/j.molliq.2018.04.062.

124 Raji, M., Abolghasemi, H., Safdari, J., and Kargari, A. (2017). Pertraction of dysprosium from nitrate medium by emulsion liquid membrane containing mixed surfactant system.

Chem Eng Process Process Intensif 120 (January): 184–194. http://dx.doi.org/10.1016/j.cep.2017.06.010.

125 Raji, M., Abolghasemi, H., Safdari, J., and Kargari, A. (2018). Selective extraction of dysprosium from acidic solutions containing dysprosium and neodymium through emulsion liquid membrane by Cyanex 572 as carrier. *J Mol Liq* 254: 108–119. https://doi.org/10.1016/j.molliq.2017.11.058.

126 Hasan, M.A., Aglan, R.F., and El-Reefy, S.A. (2009). Modeling of gadolinium recovery from nitrate medium with 8-hydroxyquinoline by emulsion liquid membrane. *J Hazard Mater* 166 (2–3): 1076–1081.

9

Membrane-Enabled Sustainable Biofuel Production

Parimal Pal[1] *and Ramesh Kumar*[2]

[1] *Chemical Engineering Department, National Institute of Technology, Durgapur, India*
[2] *Department of Earth Resources & Environmental Engineering, Hanyang University, Seoul, Republic of Korea*

9.1 Introduction

The emergence of alternative fuels can mitigate various environmental issues arising from the large-scale burning of fossil fuels. Biomass may be an alternative eco-friendly source that can be transformed into fuels and other valuable chemicals through bio/chemical and/or thermochemical processes [1]. Alternative sources of clean energy need to be explored in the present scenario to reduce the overdependence on conventional fast dwindling sources of petroleum fuels and for a meaningful reduction in emission of greenhouse gas (GHG). Several renewable resources as feedstocks have been utilized for the production of biofuels that may be categorized as the first-, second-, third-, and fourth-generation of biofuels based upon the nature of feedstocks. For example, the first-generation biofuels are produced from edible oil (*viz.* sunflower, soybean, rice bran, coconut, and safflower oil in biodiesel production) and edible or ready-to-use carbon sources (*viz.* sugarcane juice, corn, sweet sorghum, beetroot, fruits, wheat, and barley for bioethanol production). Lignocellulosic biomass such as lignin, cellulose, hemicellulose, and nonedible plant oil (karanja seed, jatropha, rubber tree, salmon, jojoba, and tobacco seed) are categorized as the feedstocks used for the production of the second-generation biofuels. In the case of the third- and fourth-generation biofuels, microalgal biomass and genetically modified microorganisms like microalgae, yeast, fungi, and cyanobacteria with improved growth rate, better oil content, and lower structural complexity are used as feedstocks [2]. The fourth-generation biofuels are still in the initial stage of an application having high-risk potential for the environment as well as human health [3]. The first-generation biofuels are derived from agricultural and forestry residues which need an adequate amount of water, fertilizer, and a large area of cropland. Such feedstocks may directly and/or indirectly compete with food security to human beings. There is a necessity to give more attention to the

Sustainable Separation Engineering: Materials, Techniques and Process Development, Volume 1, First Edition. Edited by Gyorgy Szekely and Dan Zhao.
© 2022 John Wiley & Sons Ltd. Published 2022 by John Wiley & Sons Ltd.

development of advanced technologies and devices for efficient and effective utilization of nonconsumable parts of plant sources such as plant residues, wheat straw, rice straw, and corn stover, sugarcane bagasse, beet bagasse for producing EtOH, and nonedible plant oil for biodiesel.

Besides EtOH, another important transportation fuel is biodiesel which may be a good substitute for petroleum diesel due to the same calorific value while being cleaner in terms of sulfur content and better in other burning and flow characteristics like flash point, lubricity, cetane number, and ease of handling [4]. Feedstocks from animal fats and plant oil contain saturated and unsaturated fatty acids which are converted into fatty acid alkyl esters through transesterification processes [5]. A molar ratio of 3:1 or more of alcohol with triglycerides is required for transesterification reaction in presence of suitable catalysts. After completion of the reaction, the product esters, being of low viscosity (due to lower molecular weight), are bestowed in the upper region during gravity settling. For economical production of biodiesel, selection of cheap and potential feedstocks such as nonedible plant oil, algal oil, and waste animal fats/oil is of utmost importance, being a major cost component in biodiesel production [6]. The cost may be lowered by immobilizing the catalysts for long and repeated use, better resistance to thermal and solvent exposure (especially for biocatalysts) and easy separation. Different support materials like carbonaceous support, graphene oxide (GO), silica-based carriers, and synthetic polymers are very useful for immobilizing catalysts [7]. MeOH is used widely as the alcohol source due to better yield and efficient removal of unreacted part of MeOH after transesterification reaction. Bio-EtOH, fuels derived from renewable resources for eco-friendly production of biodiesel [8], may be a good substitute for petroleum-based fuel.

Conventionally, centrifugation, filtration, decantation, gravity settling, sedimentation, and distillation are used to separate biodiesel from the reaction mixture [2]. The crude biodiesel may undergo wet and/or dry washing for the removal of impurities like free glycerol, catalysts, unreacted alcohol, and oil. Wet washing is the most commonly used process for the removal of impurities. However, the process generates a huge quantity of wastewater in addition to an increase in the cost and time of purification [9]. For dry washing, magnesol powder (cellulose-based Mg-silicate powder) and ion exchange are normally applied for the downstream purification (DSP) of crude biodiesel. However, the high cost and unknown chemistry of dry washing make the process unattractive [2]. For EtOH purification by a conventional process like distillation, problems emanating from issues of high energy consumption and azeotropism affect the final product purification and economic viability of the process [10, 11]. Approximately, 40% of the total energy is consumed in dehydration of EtOH due to the formation of water-EtOH azeotrope during the refining process.

A viable alternative to the costly and energy-intensive conventional unit operations is membrane-based separation technology, which, being compact and modular in design, is more efficient, energy-saving as well as flexible [12]. Many of the limitations of the traditional processes may be overcome through the adoption of such membrane-integrated technologies which are not only more economical but also sustainable from an environmental point of view.

9.2 Novel Approaches for Biomass Selection, Pretreatment, and Utilization

The use of edible oil as a biofuel ingredient is not a wise option in developing countries where this puts additional strain on the food sources [13]. Animal fats are difficult to process and are mostly consumed in skincare products because of their long shelf-life. However, oils from nonedible plant sources like *Pongamia pinnata* (karanja), *Croton megalocarpus*, *Jatropha curcas* (physic nut), *Hevea brasiliensis* (rubber seed), *Madhuca indica* (mahua), *Ricinus communis* (castor), etc., can be used as feedstocks. Moreover, these plants are easily grown in relatively harsh climatic conditions as well as in areas that are unsuitable for the cultivation of edible food crops. Globally, 350 plant varieties have been identified with oil-bearing seeds as the potential sources of feedstocks may be converted into biodiesel [14]. Feedstocks that can be produced on a large scale from a low cost of cultivation are naturally desired in this context [13]. The high viscosity of oil is due to the high content of glycerides (mono-, di-, and tri-). Alcohol is used to convert these glycerides into alkyl esters by transesterification reaction to convert oil into a diesel-like property [2]. Pretreatment of feedstocks (plant oils) is used to remove the free fatty acid (FFA) content as well as traces of water. The water content in oil causes hydrolysis of triglycerides into FFAs and causes saponification during transesterification using base catalysts [13].

The purity, as well as yield of biodiesel, depends on the FFAs' content of the selected oil which should be preferably low (<0.5%). For higher content of FFAs in oil, acid esterification followed by base catalyst transesterification must be done to neutralize the effect of FFAs [15]. Oils from feedstocks like sunflower, rapeseed, soybean, and mustard contain unsaturated fatty acids which produce biodiesel of good cold flow properties. However, biodiesel produced from highly unsaturated fatty acids may not be stable for longer periods, whereas, in reverse, highly saturated fatty acids containing oil would not be suitable for cold climate [16]. Thus, for the production of a better quality of biodiesel like its stability as well as better flow characteristics at low temperature (20 °C) could be possible by proper mixing of unsaturated fatty acids in the oil, oil fractionation, and by mixing of some additives in alkyl esters. The algal oil is obtained from microalgal biomass which requires less arable land and having no impact on either human food or animal fodder supply chain, removing any chances of food crisis. Microalgae could be grown in the environment that are not suitable to other crops such as brackish water or nonarable wasteland [12]. Microalgal biomass usually contains 20–50% of algal oils on dry weight biomass but could be enhanced more with genetic modification or selection of appropriate algal species [17]. The algal oil, being a high degree of saturation, remains in its neutral nature, but commercial production of biofuels from microalgae faces several hurdles like mass cultivation, low yields, adaptation to growing in waste effluents, separation, dying, and oil separation. These hurdles could be overcome by biotechnological approaches either by isolation of high-yielding and robust strain or genetic modification for obtaining the desired strain [13].

Selecting appropriate techniques during the extraction of oil from plant sources is a key step for the production of biodiesel. Different types of physical-chemical and enzymatic pretreatment methods such as steam distillation, mechanical extraction, solvent extraction,

and enzymatic extraction are applied. In steam distillation, the oil-containing plant material is charged in the distillation apparatus and exposed to steam after maceration. The steam passes through the pores of the raw material and takes the oil contained in it, which can be later collected after evaporating the vapor [18]. This method has advantages like lesser chances of oil degradation as the temperature hardly exceeds 100 °C and amount and treatment duration can be efficiently controlled. However, few limitations are associated like raw materials should be evenly distributed, homogeneous in size, strongly packed to sustain the pressure created by the steam, and high initial capital cost making the process unattractive.

The mechanical method of extraction of oil involves a manual ram press or an engine-driven press which could enable extraction of 60–65% of crude oil. The crude oil needs further treatment like filtration and degumming to produce pure oil. Cooking raw seeds before mechanical press would increase the oil yield up to 89% after the first press and 91% after the second press [19]. Another method is solvent extraction which involves chemical leaching and soxhlet extraction. In chemical leaching, a liquid reagent is used to extract the oil from the raw material which could be affected by the particle size, nature of extracting reagent used, temperature, and rate of agitation of biomass along with solvent [19]. The small particle size of raw materials, as well as the low viscous reagent, facilitates a larger interfacial area between the raw material and the solvent and free circulation of the reagent. Agitation speed and temperature play a crucial role in increasing the diffusion rate (thus increasing the transferral of oil through and from the raw material) and solubility of the oil, respectively [13]. The Soxhlet extractor is laboratory equipment invented by Franz von Soxhlet which is used for the extraction of oil from raw material. A small quantity of solvent is mixed in a large quantity of the desired compound which is suspended into the reflux solvent to extract the oil. The coffee oil has been extracted using a Soxhlet extractor from spent coffee grounds [20]. However, due to the longer operation process (up to several hours to days) under high temperature, the distillation flask is heated for a higher period which may result in degradation of the solvent.

The enzymatic oil extraction procedure is proved to be promising as well as eco-friendly. In the absence of any volatile organic compounds, utilization of these methods permits recovery of the oil under ambient conditions. However, high cost, longer incubation period, and requirement post-treatment such as de-emulsification, affinity, and perfusion chromatography during DSP make the process costly [21].

Other recent innovative techniques used for the recovery of oil from biomass include supercritical fluid extraction, microwave-assisted extraction (MAE), and ultrasound-assisted extraction. The MAE method which is regulated by the principle of ionic conduction and dipole rotation has been implemented successfully [22]. The MAE process is blessed with a high rate and yield of extraction using a lesser amount of solvent, with low CO_2 emissions and low consumption of energy as compared to the conventional processes [23]. Few limitations are associated with MAE, like the presence of solid materials that hinder heat and mass transfer. The process is also affected by volatile or nonpolar substances.

In ultrasonic-assisted extraction (UAE), oil-containing biomass is submerged with a polar solvent (water) or nonpolar solvent (alcohol or other solvents) and then treated with ultrasonic vibrations [24]. The ultrasonic vibration of 18 kHz to 118 MHz has been introduced in the target source to irradiate as well as create acoustic pressure. This leads to the formation of cavitation bubbles whose size is increased with the number of acoustic cycles and finally

collapse into smaller bubbles to enhance the overall chemical reactivity. This enables UAE to release the oil from the source material (like seeds, flowers, leaves, etc.) when mixed with a solvent [25]. The pros and cons associated with UAE like a low initial investment and fast oil extraction but the requirement of large solvent volume and the deleterious effects on the chemical nature of oil by ultrasound wave may limit the applications.

9.3 Traditional Routes for the Production of Biofuels (Biodiesel)

Edible and nonedible plant oil with different fatty acid profiles may be potential ingredients in biodiesel production. In addition to the edible and nonedible oils, new sources like microalgae (*viz. Spirulina platensis* and *Chlorella protothecoides*), animal fats, fish oils, beef tallow, poultry fats, and waste cooking oils have also been investigated over the recent years for biodiesel production. The chemical nature, fatty acid contents, technical aspects in the pretreatment of these oils, molar ratio, types, and amount of catalysts have been investigated in the context of biofuel production [26]. The operating conditions like temperature (50–60 °C), the molar ratio of alcohol-to-oil (6–12:1), transesterification reaction time (2 hours), and concentration of catalysts (1% w/w) are suggested as optimum values in biodiesel production [27]. The technical challenges in biodiesel production lie in controlling these parameters like quality of feedstock (molecular weight, fatty acid profiles, and unsaturated FFA structure), types of catalysts (homogeneous or heterogeneous) and alcohol (C1, C2, or higher alcohol) that have strong influences on the quality as well as the yield of biodiesel [28]. In the commercial production of biodiesel, edible oil is used as a feedstock that has the potential to produce 95% of the total biodiesel worldwide and these edible oils include rapeseed oil (80%), sunflower oil (12%), palm oil (1%), and other edible oils (2%) [28]. However, nonedible oil should be used as future feedstock subject to the availability and chemical nature suitable to biodiesel production.

9.3.1 Selection of Catalysts for Biodiesel Production

Homogeneous and/or heterogeneous catalysts like acids, bases, and enzymes have been used for the transesterification of triglycerides during biodiesel production [29]. The homogeneous alkaline catalysts such as Na/K hydroxide or Na/K acetate are cheap, easily available, and the most efficient [29]. In industry, Na/K hydroxides are the most widely used catalysts due to their low price but Na-acetate has been reported as the most active catalyst among other homogeneous catalysts yielding >98% of biodiesel in a short time of 30 minutes. However, for oil, containing ≥3% of FFAs, transesterification reaction should be conducted under anhydrous conditions to avoid soap formation as water may react with oils and fats to form FFAs which later form soap in presence of sodium. Low-quality oil or feedstocks containing a high amount of FFAs and water can be converted into biodiesel by acid-based esterification and transesterification simultaneously. The major drawback in homogeneous catalysis lies in recovery and reuse. Besides, such processes are not eco-friendly as a huge amount of wastewater is generated during the DSP of the final product, i.e. alkyl esters [30].

To easily recover and reuse the catalysts, solid catalysts like CaO, MgO, ZrO_2, and Raney-Ni and catalyst-supported (*viz.* biomass-derived carbonaceous support) solid material have been used for transesterification reaction [31, 32]. Solid catalysts have shown better stability in acid–base medium, high water tolerance, nontoxic in nature, and simple product recovery as well as ease of separation, regeneration, and reuse as these are neither dissolved nor consumed [33]. Moreover, the catalytic activity of the solid catalysts could also be enhanced by increasing their surface area. For example, the nano-form of the CaO was found very effective in the transesterification reaction. Being cheap, easily available, simple, and safe to use, the nano-CaO catalyst has been used as neat, doped, loaded CaO, as well as waste CaO to get high-yielding and economical biodiesel [34]. Few limitations like the requirement of the high molar ratio of alcohol-to-oil, high catalyst dose, high temperature, and leaching effect are associated with heterogeneous solid catalysts, though these have high yield [35].

An alternative route needs to be searched for, which should be operated at ambient temperature with improved yield and purity, and generate minimum wastewater. The enzymatic catalysts can be operated in mild conditions with no side reaction, easy DSP, low waste generation, and less energy requirement without any pretreatment of feedstocks that ensures better yield, purity, and economic product [36]. Thus, the enzymatic route of transesterification leads to a high quality of biodiesel in the absence of saponification and resistance to FFAs, making it a suitable candidate for a wide variety of oils even if higher FFA content [1]. One of the most widely used eco-friendly biocatalysts employed in transesterification reaction is lipase which is a hydrophobic protein that acts on the glyceride lipids at the interface of water and oil, leading to high conversion to alkyl ester [37]. Despite several advantages, enzymes are hardly competitive with chemical ones in the industrial scale of application due to high cost, stability factors in harsh solvent as well as high temperature, and the difficulty of enzyme recovery [38]. However, entrapment or immobilization of free enzyme into suitable support materials or matrix has shown better stability against the exposure of thermal and harsh chemical conditions, easily separable, and reduced operational cost due to prolonged operation [39]. Various types of support materials like carbonaceous supports, silica-based supports, GO, and synthetic polymers have been used as carriers for enzymes during the transesterification reaction [1, 7]. Novel magnetic responsive nanoparticle support materials like poly(styrene-methacrylic acid) microspheres [40], ionic liquid (IL)-functionalized magnetic silica [41], and Fe_3O_4-poly (glycidyl methacrylate-co-methacrylic acid) [42] have been used recently for covalent entrapment as well as easy recovery of biocatalysts under external magnetic field. Lipase immobilized in silica aerogel had yielded 93% of biodiesel and repeatedly used up to 10 cycles with a minimum loss of 11% in the yield [43]. However, magnetic nanoparticles due to strong dipole–dipole interaction undergo aggregation and the large surface energy could hamper the catalytic activity of an enzyme [44]. Recently, GO has been successfully utilized as a support material for various biologically active agents like biocatalysts, biosensors, and as a drug delivery agent, which appears to be cheap and attractive [45].

9.3.2 Green Solvent/Catalysts

Another eco-friendly and sustainable alternative to the chemical catalysts is the use of green solvents like deep eutectic solvents (DESs) and ILs which have a very high potential

as extracting solvents, cosolvents, and catalysts with high chances of reuse and recycling as reported in recent studies. During most of the chemical reactions, excessive use of solvents is required for proper mixing of the reactants, and extraction and washing of the products. Thus, green solvents are very useful as well as emerging solvents due to being less corrosive that can stabilize the catalysts, enhance catalytic activity as well as improve productivity and easy separation of product in comparison to replace the conventional solvents and catalysts. However, most of the widely used ILs have petroleum sources as well as are persistent in nature due to high aqueous solubility and poor biodegradables like imidazolium and pyridinium salts which have shown a toxic effect on microorganisms, vertebrates, and invertebrates when disposed of untreated. Due to low vapor pressure, ILs have lesser chances of air pollution as compared to most of the volatile chemical catalysts but they may increase the water pollution. Moreover, the high cost of ILs, complex synthesis methods, and persistent nature influence its recyclability. Thus, toxicity, long-term stability, and nonbiodegradability have been evaluated from the life cycle assessment which limits the wide applications at industrial scale [46].

Another green solvent of similar physiochemical properties that of ILs is DESs which have a less toxic effect and are eco-friendly. DES is composed of a mixture of hydrogen bond acceptor (HBA) compounds like choline chloride, and a hydrogen bond donor (HBD) such as urea, glycerol, and carboxylic acids. The mixture of two solid compounds of HBD and HBA results in a liquid mixture whose freezing point is much lower than that of individual mixing compounds due to the eutectic effect. DESs are much cheaper, eco-friendly, biodegradable, do not produce toxic compounds and are formed from readily accessible compounds. The properties of DESs depend upon the ratio of HBD and HBA salts as well as their chemical nature, which are formed by hydrogen bonding, van der Waals forces, and electrostatic interaction. Being polar, the poor ionic conductivity has been shown by DESs due to viscosity. Cholorometallate anions are also known as ILs such as $Al_2Cl_7^-$. However, these are cheap and more eco-friendly than the Lewis acid ILs that are composed of imidazole cation. Different ratios of choline chloride and $ZnCl_2$ have attracted many applications like an electrolytic deposition, regiospecific Fischer indole reaction and Diels–Alder reaction due to being easy to prepare and accessible, easy to handle, having stable moisture, and relatively cheap [47]. Low viscous DESs are preferred to act as a catalyst during transesterification reaction. For example, soybean oil and MeOH were used for biodiesel production using DESs formed by choline chloride-to-zinc chloride ratio of 1:2 as a Lewis acid catalyst [47]. Initially, Lewis acid catalysts were dissolved in MeOH using a magnetic stirrer at 70 °C, then feedstock (soyabean oil) was added slowly. Increasing the amount of $ZnCl_2$ in Lewis acid catalysts enhanced the biodiesel yield, but increasing the amount of choline chloride hardly affects the yield. Besides, increasing the molar ratio of MeOH:oil (up to 16), the biodiesel content rapidly increased due to a change in the reaction equilibrium in the forward direction and better catalytic activity of choline chloride:$2ZnCl_2$ in high MeOH. Two-step transesterification has also been used like solubilization of oil and alcohol in DESs followed by catalysis by CaO to give the enhancement in the yield of esters from 87.3 to 95% [48]. DESs from renewable resources like choline chloride, urea, and glycerol along with enzymes (lipase and Novozyme 35) have been used to achieve a sustainable and eco-friendly yield of esters up to 99% purity in a two-step transesterification reaction [49].

9.3.3 Conventional Reactors Used for Biodiesel Production

Different reactors have been used for transesterification reaction such as plug flow reactor [50], continuous stirred tank reactor (CSTR) [51], fixed-bed reactor [52], helical reactor [53], transport riser reactor [54], and oscillatory flow reactor [33]. Behzadi and Farid [55] have used a gas–liquid reactor with the provision of the spray of heated oil in the chamber of a reactor filled with vapors of MeOH for transesterification reaction in presence of Na-methoxide as a catalyst. Recently, some microreactors have been reported [56] with improved performance in terms of better heat and mass transfer, better mixing due to short diffusion distance with large area per unit volume, resulting in higher yield. Batch reactors have shown several limitations for commercial-scale production due to the high-cost tedious mode of operation. These limitations of conventional batch reactors have led to the application of plug-flow reactors, CSTRs, and fixed-bed reactors to carry out the transesterification reaction. Still, there is scope for an increase in efficiency, conversion rate, mass transfer, and yield through the development of novel systems and/or modifications of the existing reactors. For example, the temperature almost equivalent to the boiling point of alcohol (MeOH) has been used in CSTRs or plug flow reactors along with high shearing mixing to avoid the mass transfer limitations in industrial applications. Similarly, immobilized enzyme-assisted transesterification of waste cooking oil in a packed-bed micro-flow (porous channel) tubular reactor was designed for the cost-effective production of biodiesel [57]. However, these limitations can be largely overcome by the application of membrane-based systems that can overcome the difficulties of the conventional systems such as immiscibility of alcohol to oil as well as reversibility [58].

9.3.4 Supercritical Methanol/Ethanol-Based Transesterification

Several novel approaches have been attempted to develop alternative processes for biodiesel production by reducing the number of unit operations to overcome the key challenges of suboptimal net energy ratio. Supercritical transesterification (SCT) is one such process in which reactants are put under supercritical conditions for biodiesel production through direct or non-catalytic transesterification [59, 60]. Recently, SCT has become the method of choice due to several advantages like microalgal feedstock with high moisture content, takes less reaction time than the conventional process, catalyst-free process, high yield, and easy DSP [59]. The moisture-containing biomass like microalgal biomass could be easily transesterified using the SCT method. Thus, SCT is simple as well as advantageous which attributes eco-friendly process, no need for acid or base catalysts, moisture-containing feedstocks, the high conversion rate in a short time with no post-treatment. Different process conditions like temperature (257 °C), time (32 minutes), MeOH:dry weight of microalgae ratio (8 mL/g), and moisture content (39%) were optimized toward a high yield of biodiesel of 99.32% [61]. Microwave-treated dried microalgal species *Chlamydomonas sp. JSC4* was converted 100% to biodiesel using direct SCT [62]. In another research, fatty acid methyl ester (FAME) yield of 96.9% using lipid content of 52% (w/w), the water content in biomass of 5.57 mL, and MeOH-loading rate of 115 mL/g have been used [59]. Hegel et al. [60] got a higher yield of 15.9 wt.% of biodiesel with respect to dried microalgal biomass using a temperature of 305 °C in a short reaction time of 40 minutes.

9.4 Traditional Downstream Purification (DSP) of Biodiesel

9.4.1 Dry Wasing and Wet Washing

Approximately, 60–80% of the total production cost is contributed in DSP of the biodiesel to satisfy the international standards (*viz.* EN 14214 and ASTM D6751). Dry washing and wet washing are used during conventional purification of the biodiesel to remove the impurities like residual oil, alcohol, glycerides, soap, etc., from the alkyl ester mixture [57]. During wet washing, hot water (~80 °C) is used 2–3 times to separate the impurities from the crude biodiesel mixture. However, separation of alcohol (EtOH/MeOH) cannot be possible during wet washing due to the higher miscibility of alcohol with water. The residual alcohol could be removed conventionally by a high energy-consuming distillation process, whereas final esters are separated from soap by dry adsorbent [58]. A large amount of water, i.e. 3 L of water is consumed for the partial purification of 1 kg of biodiesel for the removal of catalysts and soap till neutrality [58]. Organic solvents from petroleum sources like ether, n-hexane, and tetrahydrofuran have also been used for purification as well as dehydration of biodiesel during wet washing.

In dry washing, absorbents like Mg-silicate, Al-silicate, and other metal oxides are used in place of water. However, to make the process cost-effective, recovery and reuse of spent adsorbent should be optimized. Few commercial absorbents such as Magnesol, Amberlite BD10DRY, Purolite PD206, and silica have been popularly used as dry washing agents for the large-scale production of biodiesels [58]. For quick and one-step recovery of biodiesel, a commercial adsorbent like silica (Trysil 3000) is used which has the adsorbing capacity of 235% of its weight when operated under 0.2 bar of vacuum pressure and temperature range of 65–90 °C [63]. Silica adsorbed non-selectively the impurities like 100% MeOH, water, and glycerine, FFAs, under optimized conditions of 1.1 w/w% of silica, the operating pressure of 0.2 bar, and temperature of 90 °C in 45 minutes [63]. However, a few challenges and issues like high cost, complex process, and generation of wastewater remain a major concern for scale-up at industrial scale.

9.4.2 Natural Adsorbents

Natural adsorbents like rice husk ash (RHA), sugarcane bagasse, waste biomass (cellulose fibers), starch, etc., have been investigated for DSP of biodiesel as reported in the literature [63, 64]. RHA contains mesopores and macropores along with a high quantity of silica which enables it to be a good adsorbent. For example, only 4% of RHA could remove more than 95% of impurities from the alkyl ester mixture [63]. Further, naturally obtained cellulose and starch from different sources like corn, potato, cassava, and rice were also used for DSP of biodiesel at ambient temperature in 10 minutes only [64]. However, recycling, reuse, and disposal of natural adsorbents remain a problem.

In a recent study, pressurized CO_2 was used for water as well as solvent-free washing of alkyl ester mixture to remove the impurities. When CO_2 of 20–50 mass% with the pressure of 6–12 bar at temperature 25–50 °C injected in the reaction cell containing the product (alkyl esters), residual alcohol, catalysts, glycerol and triglycerides, two distinct phases are separated due to liquid–liquid equilibrium. The lighter or upper phase of alkyl esters is collected by opening the one-way valve with a relatively very low concentration of

impurities [65]. It is used as the water-free washing of crude biodiesel mixture without any use of a solvent. Here, pressure and concentration of CO_2 play a minor role, whereas temperature (ambient) is the most affected in the separation of impurities during biodiesel purification. It is a successful as well as an environmentally efficient purification process, which would generate the least of effluents and waste. It acts as a dry nonpolar solvent which could separate the polar impurities like residual MeOH and glycerol from the reaction mixture. However, industrial application of supercritical fluids needs further research such as process simulations and economic analysis, and knowledge of thermodynamic and transport properties of the reactants in presence of CO_2 flow.

9.4.3 Ion-Exchange Resin

Another method of the dry purification reaction mixture can be done by salt precipitation and ion-exchange resins. Ferrero et al. [66] have used ion-exchange resin of 6 w/w% and/or 0.1 μm ceramic membranes along with precipitation with sodium carbonate. In this process, the catalyst Ca was precipitated out as $CaCO_3$, whereas sodium soap was separated by either filtration or adsorption by resin.

The international standard of quality of biodiesel is given in Table 9.1 [67].

9.5 Membrane-Based Technologies for Biodiesel Production

The capacity of the unit process, cost of feedstocks, and DSP are the most vital factors for the economical production of biodiesel at a large scale in an era of emaciated profit margin. As the DSP of biodiesel has shared most of the production cost, so this section needs to be

Table 9.1 The properties of biodiesel as international standards as suggested by ASTM (Biodiesel Standard D 6751) (adapted from 67).

Properties	ASTM limits
Flash point (°C)	130 minimum
Water and sediment (%, volume)	0.05
Specific gravity at 25 °C	0.875–0.9 (15 °C)
Kinematic viscosity (mm^2/s) at 60 °C	5–6
Acid number (mg KOH/g)	0.5
Cetane number	47 min
Calorific value (MJ/kg)	37.27
Sulfated ash (%, mass)	0.02
Sulfur (%, mass)	0.0015
Carbon residue (%, mass)	0.05
Free glycerine (%, mass)	0.02
Total glycerine (%, mass)	0.24

explored more to find out the economic as well as the eco-friendly process. This is where the membrane system stepped in for the development of economically viable and eco-friendly process technology for the DSP of biodiesel. The comparative study of the membrane-based system with conventional one has been mentioned in Table 9.2.

9.5.1 Membrane-Based Operation

The membrane-based separation process may be pressure-driven, osmotic pressure-driven, and temperature gradient-driven. The membrane-based processes are used for the separation, purification, and concentration of the desired product from the reaction mixture. The operation of the membrane-based process may be continuous, batch, semicontinuous, cross-flow, dead-end types [68]. The high degree of product purity, eco-friendly nature, operation in ambient conditions, modular design, and compact plant are few attractive features of the membrane-based system. Being selective, it acts as a barrier to control the

Table 9.2 Advantages of membrane-based DSP during biodiesel production in comparison to traditional processes (adapted from [2]).

Parameters	Membrane-integrated system	Traditional process
Commercial capability		
Size of the plant	Compact and occupies less space	Bigger in size and occupies large space
Operational viability	Modular and highly flexible	Fixed and less flexible
Duration of research to market	It takes less time to implement	It takes more time to implement
Responsive process	Highly responsive	Less responsive
Process		
Nature of product	Gets high purity of the product	Chances of impurity in the finally purified product
Rates of operation	Relatively fast	Slow process
Process safety	Safety is high	Relatively less safe
Product properties	Enhanced	Not so improved
Continuous processing	Yes, possible	Not possible every time
Processing condition	Broader	Not like that, limited
Environment		
Energy consumption	Less energy consumption	Highly energy-extensive process
Waste generation	Relatively low solid or liquid waste generation	A considerable amount of waste generated
Scope of recycling	Unused/residual substrates recycle back for further use	Not possible
Blockade of landscape	Relatively less blockade	High blockade
Overall process	Faster, safer, greener, and highly sustainable process	Slow and unsustainable process

transport of molecules/solutes (liquid, gas, or vapor) based on membrane permeability [69]. Membranes are categorized based on – (i) pore size-like microfiltration (MF), ultrafiltration (UF), nanofiltration (NF), and reverse osmosis (RO); (ii) based on types of materials used for fabrication like hydrophobic and hydrophilic membranes. The membranes may be polymeric or ceramic (based on the materials); packing elements are of different geometry like flat tubular, hollow-fiber, multi-tubular capillaries, or spiral wounds [70]. The pore size ranges from 50 nm to 5 μm for MF membranes and 2 to 50 nm for UF membranes. The operating pressure ranges from 1 to 3 bars for MF membranes and 4 to 8 bars for UF membranes. The separation of solute by MF and UF is based on the sieving mechanism, i.e. size-exclusion and molecular weight cutoff (MWCO) [71]. It means that the solutes or molecules of higher size or molecular weight than that of pore size or MWCO value of membrane are rejected, whereas lower ones are permeated [72]. The smaller solutes, molecules, or ions are separated by NF and RO which have the pore size <1 nm and operated at a higher pressure range of 10–40 bar with the working principle of the Donnan effect [73]. The Donnan effect is the electrostatic interaction among the charged ions present in the feed solution with the polyelectrolytes present in the surface of the membrane [74, 75]. Different fabricating materials such as polyacrylonitrile (PAN), polyvinylidene difluoride (PVDF), polyethersulfone (PES), polytetrafluoroethylene (PTFE), polyethylene terephthalate (PET), polyethersulfone polyvinyl-pyrrolidone (PES-PVP), polypropylene (PP), and polyvinyl chloride (PVC) are used as the functional layer over the surface of the base material of nonwoven polyester [76]. The ceramic membranes are fabricated by zirconia, alumina, and silica with porous support layers such as ceramic-ceramic, i.e. Al_2O_3 or ZrO_2, and metal-ceramic like TiO_2 and Zr-O_2-TiO_2.

9.5.2 Novel Membrane Reactor

The membrane separation technology can be applied for upstream and downstream separation and purification during the transesterification reaction. It can perform a dual role, i.e. transesterification of triglycerides in presence of alcohol and catalysts as well as DSP of alkyl esters from impurities present in the reaction mixture without any use of water, acids, solvents, and absorbent/adsorbent. The reaction could take place efficiently in a membrane reactor as it reduces the contact time between reactants and catalysts and simultaneously adds the reactants for transesterification reaction. Also, it avoids the equilibrium by continuous separation product which results in maximum yield/conversion of triglycerides. Moreover, plug-flow membrane reactors are very useful for reversible or general reactions for better yield and productivity with higher selectivity, environmental benign process, and reduced waste generation [77]. The challenges of the immiscibility of canola oil in MeOH were overcome by the use of a membrane reactor as reported by Dubé et al. [78]. A two-phase membrane reactor of 300 mL capacity was used for transesterification reaction as well as product separation to move the reaction in the forward direction to get more yield. A carbon membrane of 1.2 m of the length of a tube-like structure having internal and external diameters of 6 to 8 mm and pore size of 0.05 μm with the total surface area of 2.2×10^{-2} m^2 was used as a vessel for transesterification reaction between oil and MeOH (1:2) as shown in Figure 9.1 [78]. The two-phase system of the carbon membrane tube which was resistant to acid–base medium permeated the product (fatty acid methyl esters)

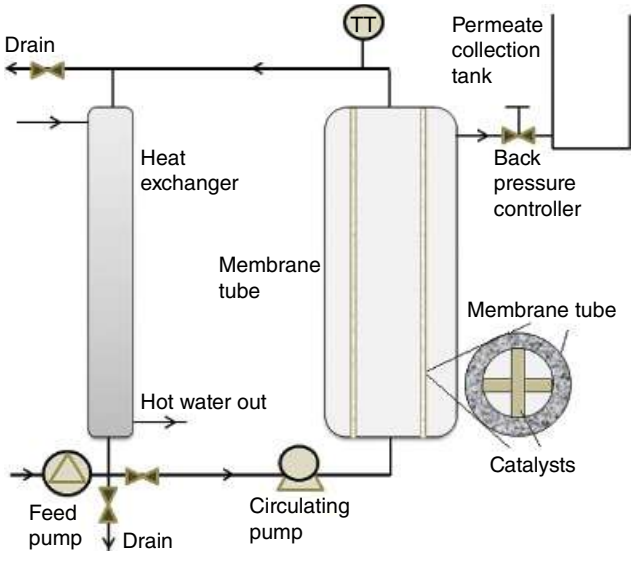

Figure 9.1 Schematic diagram of two-phase membrane reactor [78].

successfully inhibiting the transfer of unreacted oil, glycerol, etc. However, sometimes permeation of highly hydrophobic molecules is becoming difficult in the two-phase barrier, thereby limiting biodiesel production [78]. The ceramic membrane of the honeycomb structure was also used as a membrane reactor using a monolithic catalyst (like KF/ca-Mg-Al) concentration of 1.5 w/w% and feed velocity of 4.8 mL/min at 67 °C to achieve a 94.9% conversion rate in 3 hours of reaction time [79]. Higher resilience toward solvents, harsh pH conditions, and high temperature are few advantages of ceramic membranes over polymeric membranes due to macroporous support of alumina, titania, and zirconia.

9.5.3 Membrane Systems Used in DSP of Biodiesel

9.5.3.1 Hollow Fiber Membrane Extraction

The hollow fiber membrane module has been characterized as a compact device with a high surface area per unit volume for efficient separation and effectiveness compared with conventional DSP of biodiesel. With the modular design, a hollow fiber membrane enables better purity of alkyl esters without any post-treatment like emulsification and density differences [78]. Hollow fiber membrane-based refining of biodiesel was reported by He et al. [80] using polysulphone membrane to get 99% of pure biodiesel in comparison to 97% through the conventional system without any loss of alkyl esters. In a novel refining method of biodiesel, the hollow fiber membrane was immersed in a reactor initially filled with pure water at 20 °C and, subsequently, biodiesel was pumped through cartridge at a flow rate of 0.5 mL/min and 0.1 MPa pressure followed by dehydration by Na_2SO_4 to get highly pure biodiesel as shown in Figure 9.2 [80].

Membrane contractors with the facility of liquid–liquid extraction toward the purification of biodiesel up to 99.6% as reported by Atadashi et al. [81] by eliminating the number of traditional distillation steps. As illustrated in Figure 9.3 [82], the crude biodiesel as feed and

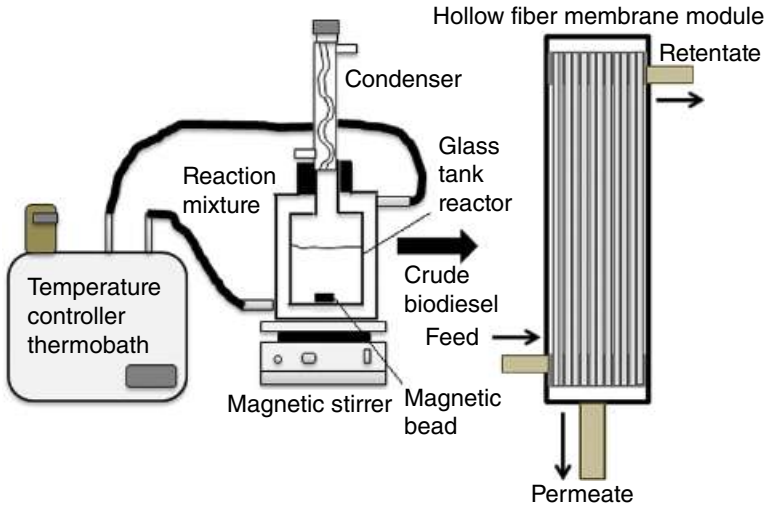

Figure 9.2 Schematic diagram of the experimental set-up of hollow fiber membrane extraction using polysulfone membrane [80].

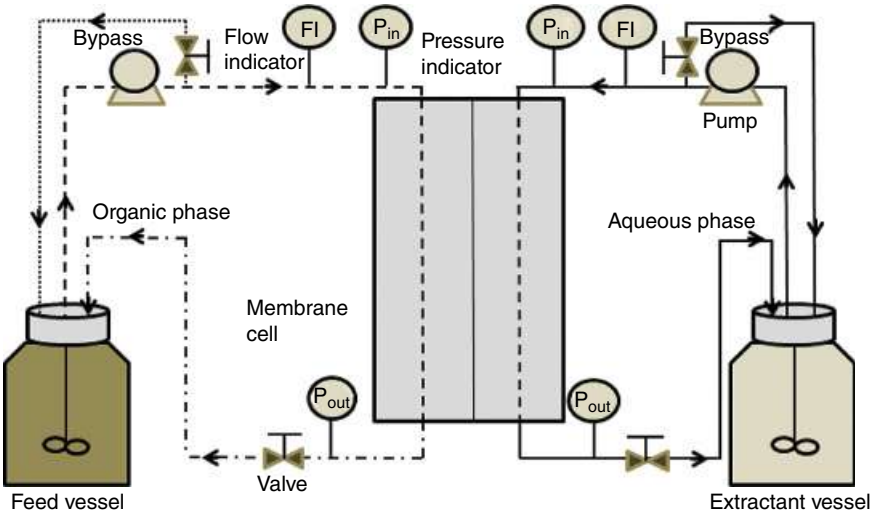

Figure 9.3 Experimental set-up of rectangular configuration membrane cell in which feed and extractant are flowing in cocurrent mode of operation [82].

water as an extractant is pumped to the membrane module of rectangular shape concurrently at the desired pressure difference in between the membrane module. The retentates of both phases are recycled back to their respective tanks/reservoirs. Here the membrane such as hydrophobic membrane (PTFE) is fixed over the stainless steel spacer to avoid any flow obstruction due to pressure. The membrane-based liquid–liquid extraction has the upper hand in comparison to the conventional one. However, membrane fouling, high mass transfer-resistance, and short life span of the membrane are few limitations [83].

9.5.3.2 Ceramic and Polymeric Membranes

For the refining of biodiesel, the ceramic membranes have been found quite stable and durable due to better chemical, mechanical, and thermal resistances. The ceramic membrane made up of Al_2O_3/TiO_2 material of pore size 0.2 μm in multichannel tubular shape was used to purify the crude biodiesel in cross-flow module meeting specifications of ASTMD and EN as illustrated in Figure 9.4 [81]. Atadashi et al. [81] optimized the flow rate, temperature, and operating pressure using a tool from design expert software, i.e. response surface methodology. The maximum flux of 9.08 kg/m^2·hour and 98.3% of glycerol rejection was achieved under the optimized conditions of 2 bar transmembrane pressure, 150 L/min cross-flow rate at 40 °C temperature. In another study, tubular ceramic UF membrane made up of Al_2O_3/TiO_2 of average pore size of 0.05 μm and 20 kDa used for glycerol separation has also been investigated for glycerol separation from the reaction mixture [84]. The UF ceramic membrane enables better retention of impurities due to the formation of dispersed phase between oil and methanol in the highly acidic condition under stable fluxes at a high flow rate.

Polymeric MF membranes fabricated by cellulose ester with pore sizes 0.22 and 0.3 μm as well as UF membrane of 10 and 30 kDa of MWCO (GE Osmonics, USA) with a disc-shaped diameter of 45 mm were investigated for the purification of crude biodiesel [85]. The UF membrane of 10 kDa MWCO was found most suitable to reduce the glycerol level below 0.02% by adding 0.2 mass% water in the crude biodiesel by applying 1 bar pressure using N_2 gas cylinder as shown in Figure 9.5 [85]. However, the flux was declined seriously within 5 minutes due to the dead-end mode of operation. In another report, a hydrophobic UF membrane, resistant to solvent, was used for the separation of by-product glycerol and EtOH [86]. It was observed that the UF membrane made up of PVDF material could reject 67% of glycerol, whereas polysulfone-based UF could reject only 48% after adding 0.5% v/v of water at 30 °C and transmembrane pressure of 5 bar while yielding flux of 9.5 L/m^2·hour. The PVDF material was found more resistant toward solvents and temperature during DSP

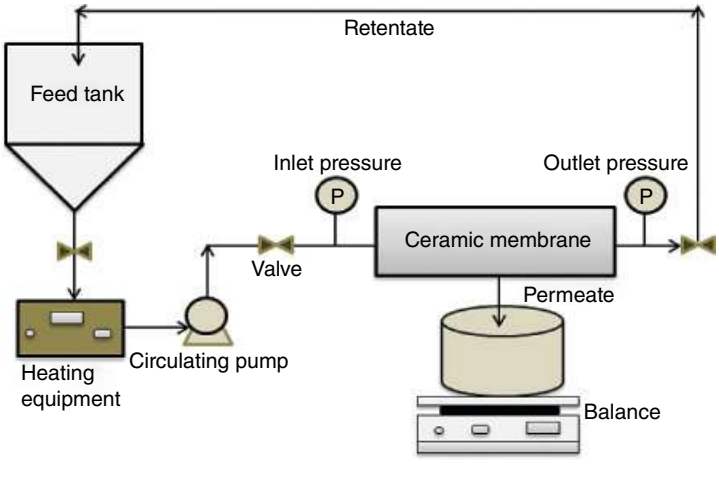

Figure 9.4 Schematic diagram of a multichannel tubular type ceramic membrane-based separation unit for purification of crude biodiesel [81].

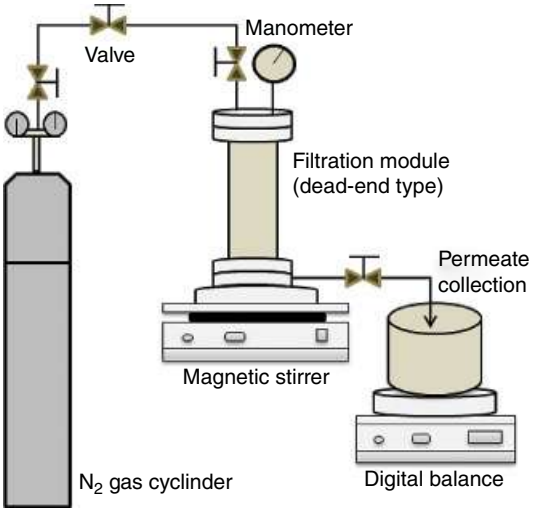

Figure 9.5 Experimental set-up of semi-batch filtration of the dead-end-type module containing flat sheet UF membrane for DSP of biodiesel [85].

of biodiesel. Commercial UF membrane made up of PAN with 100 kDa MWCO could be able to reject 63–70% of glycerol when circulating the pretreated feed (MeOH-free crude biodiesel but added 0.02 mass% water) and the flux declined from 13 to 7 L/m^2·hour within 3 hours [87].

9.5.3.3 Multi-Staged Membrane System for DSP of Crude Biodiesel: Membrane Distillation (MD) Followed by UF

To get a pure and economically viable product amidst tough global competition, a paradigm shift is now imminent which can be done by selecting membrane-based emerging technologies. To get the pure biodiesel of international standards, the impurities such as residual alcohol, free as well as bound glycerol (TG, DG, and MG), catalysts and water should be removed up to the permissible limit. If these impurities remain in the biodiesel above the permissible limit, it may affect the engine performance due to lower flash point, increased viscosity, and oxidation stability, and form ice crystals and damage the rubber seal, and gaskets [88]. One of the major impurities is glycerol. If it presents > 0.02% in biodiesel, then it may create problems during storage and decantation due to gum-like deposits around the injector tips and valve heads. These impurities can be separated by membrane-based separation technology which can successfully replace the conventional production plant into a compact, modular, energy-saving, and flexible system [1]. Different forms of the membrane-like cross-flow membrane module, membrane contractor, membrane adsorption, MD, and PV can be used at different stages in production as well as DSP of biodiesel.

In a novel approach, membrane systems have been used to separate the alcohol and glycerol to match the international standards such as alcohol ≤0.2% and free glycerol ≤0.02%. Traditionally, wet washing (water) and distillation processes are used to separate glycerol and alcohol, respectively. However, waste-effluent generation and a huge amount of energy consumption make the process environmentally polluting as well as costly, which is

equivalent to half of the total production cost. However, recovery and reuse of residual alcohol as well as by-product glycerol during the production of alkyl esters make the overall process eco-friendly and cost-effective. MD/PV may be used to recover the MeOH/EtOH at a temperature much below their boiling points, i.e. 50–60 °C. On the other hand, glycerol purification by membrane depends upon the presence of water as well as glycerol in the feed solution. The presence of residual EtOH/MeOH in the crude biodiesel has adversely affected the UF membrane system to separate the free glycerol as the residual alcohol and glycerol are mutually soluble and permeate through the UF membrane. Moreover, the addition of a small amount of water in the feed solution forms large particles with the glycerol which later dispersed from alkyl esters and rejected during UF separation. This indicates that the separation of glycerol could not be possible in presence of alcohol as the glycerol-alcohol-dispersed phase could not be feasible but solubilizes the glycerol in biodiesel [87]. Thus, two-steps membrane-based system, i.e., recovery of residual alcohol by MD followed by glycerol separation by UF membrane could be an economical feasible downstream purification of biodiesel. The application of different hydrophobic membranes (PTFE/PET, PP, and PTFE/PP) in solar-driven membrane distillation (MD) and UF of PES have been applied for stepwise DSP of crude biodiesel. The novel system could separate ~77% glycerol and recover the EtOH which left the final concentration of EtOH and glycerol of permissible limit of international standards [1].

9.6 Conclusion

In the recent past, several improvements in the production and DSP of biodiesel have taken place. A wide variety of feedstocks, pretreatment options, and avenues of oil extraction with a high yield of oil are emerging with the progress of time. The green catalysts such as ILs, DESs, or biocatalysts can now replace the chemical types for the eco-friendly production of biodiesel. This is now apparent that the membrane-based separation unit integrated with a conventional reactor has the potential to bring about extensive process intensification (PI) in biodiesel production. The logical sequence of operations coupled with proper selection of membrane as well as a module (cross-flow mode) may result in a sustainable system for continuous production and purification of biofuel. The membrane system can ensure an environmentally benign production regime in terms of operational flexibility, compactness, energy consumption, and space intensity. Thus, green catalyst-assisted transesterification of nonedible oil and, finally, DSP using MD followed by UF can yield the target alkyl esters at a relatively lower cost and with a reduced environmental footprint.

Abbreviations

CSTR Continuous stirred tank reactor
DESs Deep eutectic solvents
DSP Downstream purification

FFA	Free fatty acids
GO	Graphene oxide
HBA	Hydrogen bond acceptor
HBD	Hydrogen bond donor
ILs	Ionic liquids
MAE	Microwave-assisted extraction
MWCO	Molecular weight cutoff
PAN	Polyacrylonitrile
PES	Polyethersulfone
PES-PVP	Polyethersulfone polyvinyl-pyrrolidone
PET	Polyethylene terephthalate
PP	Polypropylene
PTFE	Polytetrafluoroethylene
PVC	Polyvinyl chloride
PVDF	Polyvinylidene difluoride
RHA	Rice husk ash
SCT	Supercritical transesterification

References

1 Kumar, R. and Pal, P. (2021). Lipase immobilized graphene oxide biocatalyst assisted enzymatic transesterification of Pongamia pinnata (Karanja) oil and downstream enrichment of biodiesel by solar-driven direct contact membrane distillation followed by ultrafiltration. *Fuel Process. Technol.* 211: 106577.

2 Kumar, R., Ghosh, A.K., and Pal, P. (2020). Sustainable production of biofuels through membrane-integrated systems. *Sep. Purif. Rev.* 49 (3): 207–228.

3 Abdullah, B., Muhammad, S.A.F.S., Shokravi, Z. et al. (2019). Fourth generation biofuel: a review on risks and mitigation strategies. *Renew. Sust. Energ. Rev.* 107: 37–50.

4 Kapor, N.Z.A., Maniam, G.P., Rahim, M.H.A., and Yusoff, M.M. (2017). Palm fatty acid distillate as a potential source for biodiesel production-a review. *J. Clean. Prod.* 143: 1–9.

5 Savaliya, M.L., Dhorajiya, B.D., and Dholakiya, B.Z. (2015). Current trends in separation and purification of fatty acid methyl ester. *Sep. Purif. Rev.* 44: 28–40.

6 Giwa, A., Adeyemi, I., Dindi, A. et al. (2018). Techno-economic assessment of the sustainability of an integrated biorefinery from microalgae and Jatropha: a review and case study. *Renew. Sust. Energ. Rev.* 88: 239–257.

7 Edmond, L. and Luong, J.H.T. (2014). Carbon materials as catalyst supports and catalysts in the transformation of biomass to fuels and chemicals. *ACS Catal.* 4: 3393–3310.

8 Uthman, H. and Abdulkareem, A.S. (2014). The production and characterization of ethyl ester (biodiesel) from waste vegetable oil as alternative to petro-diesel. *Energ. Source. Part A* 36: 2135–2141.

9 Berrios, M. and Skelton, R.L. (2008). Comparison of purification methods for biodiesel. *Chem. Eng. J.* 144: 459–465.

10 Leuchtenberger, W., Huthmacher, K., and Drauz, K. (2005). Biotechnological production of amino acids and derivatives: current status and prospects. *Appl. Microbiol. Biotechnol.* 69: 1–8.

11 Pal, P., Kumar, R., and Ghosh, A.K. (2018). Analysis of process intensification and performance assessment for fermentative continuous production of bioethanol in a multi-staged membrane-integrated bioreactor system. *Energy Convers. Manag.* 171: 371–383.

12 Kumar, R., Ghosh, A.K., and Pal, P. (2020). Synergy of biofuel production with waste remediation along with value added co-products recovery through microalgae cultivation: a review of membrane-integrated green approach. *Sci. Total Environ.* 698: 134169.

13 Karmakar, B. and Halder, G. (2019). Progress and future of biodiesel synthesis: advancements in oil extraction and conversion technologies. *Energy Convers. Manag.* 182: 307–339.

14 Karmakar, B., Samanta, S., and Halder, G. (2020). *Delonix regia* heterogeneous catalyzed two-step biodiesel production from Pongamia pinnata oil using methanol and 2-propanol. *J. Clean. Prod.* 255: 120313.

15 Issariyakul, T. and Dalai, A.K. (2014). Biodiesel from vegetable oils. *Renew. Sust. Energ. Rev.* 31: 446–471.

16 Verma, P., Sharma, M.P., and Dwivedi, G. (2016). Evaluation and enhancement of cold flow properties of palm oil and its biodiesel. *Energy Rep.* 2: 8–13.

17 Mata, T.M., Martins, A.A., and Caetano, N.S. (2010). Microalgae for biodiesel production and other applications: a review. *Renew. Sust. Energ. Rev.* 14 (1): 217–232.

18 Hesham, H., Rassem, A., Nour, A.H., and Yunus, R.M. (2016). Techniques for extraction of essential oils from plants: a review. *Aus. J. Basic Appl. Sci.* 10 (16): 117–127.

19 Achten, W.M.J., Verchit, L., Mathijs Franken, Y.J. et al. (2008). Jatropha bio-diesel production and use. *Biomass Bioenerg.* 32 (12): 1063–1084.

20 Al-Hamamre, Z., Foerster, S., Hartmann, F. et al. (2012). Oil extracted from spent coffee grounds as a renewable source for fatty acid methyl ester manufacturing. *Fuel* 96: 70–76.

21 Lamsal, B.P. and Johnson, L.A. (2007). Separating oil from aqueous extraction fractions of soybean. *J. Am. Oil Chem. Soc.* 84: 785–792.

22 Letellier, M., Budzinski, H., Charrier, L. et al. (1999). Optimization by factorial design of focused microwave-assisted extraction of polycyclic aromatic hydrocarbons from marine sediment. *J. Anal. Chem.* 364: 228–237.

23 Golmakani, M.T. and Rezaei, K. (2008). Comparison of microwave-assisted hydrodistillation with the traditional hydrodistillation method in the extraction of essential oils from Thymus vulgaris L. *Food Chem.* 109: 925–930.

24 Karim Assami, D.P. (2012). Ultrasound-induced intensification and selective extraction of essential oil from Carum carvi L. seeds. *Chem. Eng. Process. Process Intensif.* 62: 99–105.

25 Bhaskaracharya, R.K., Kentish, S., and Ashokkumar, M. (2009). Selected applications of ultrasonics in food processing. *Food Eng. Rev.* 1: 31–49.

26 Verma, P. and Sharma, M.P. (2016). Review of process parameters for biodiesel production from different feedstocks. *Renew. Sust. Energ. Rev.* 62: 1063–1071.

27 Salam, K.A., Velasquez-Orta, S.B., and Harvey, A.P. (2016). A sustainable integrated in situ transesterification of microalgae for biodiesel production and associated co-product - a review. *Renew. Sust. Energ. Rev.* 65: 1179–1198.

28 Sajjadi, B., Raman, A.A.A., and Arandiyan, H. (2016). A comprehensive review on properties of edible and non-edible vegetable oil-based biodiesel: composition, specifications and prediction models. *Renew. Sust. Energ. Rev.* 63: 62–92.

29 Tariq, M., Ali, S., and Khalid, N. (2012). Activity of homogeneous and heterogeneous catalysts, spectroscopic and chromatographic characterization of biodiesel: a review. *Renew. Sust. Energ. Rev.* 16: 6303–6316.

30 Atadashi, I.M., Aroua, M.K., Aziz, A.R.A., and Sulaiman, N.M.N. (2013). The effects of catalysts in biodiesel production: a review. *J. Ind. Eng. Chem.* 19: 14–26.

31 Wei, G., Liu, Z., Zhang, L., and Li, Z. (2018). Catalytic upgrading of Jatropha oil biodiesel by partial hydrogenation using Raney-Ni as catalyst under microwave heating. *Energy Convers. Manag.* 163: 208–218.

32 Dhawane, S.H., Kumar, T., and Halder, G. (2018). Recent advancement and prospective of heterogeneous carbonaceous catalysts in chemical and enzymatic transformation of biodiesel. *Energy Convers. Manag.* 167: 176–202.

33 Lam, M.K., Keat, T.L., and Abdul Rahman, M. (2010). Homogeneous, heterogeneous and enzymatic catalysis for transesterification of high free fatty acid oil (waste cooking oil) to biodiesel: a review. *Biotechnol. Adv.* 28: 500–518.

34 IB, B.–.I., Miladinović, M.R., Stamenković, O.S., and Veljković, V.B. (2017). Application of nano CaO–based catalysts in biodiesel synthesis. *Renew. Sust. Energ. Rev.* 72: 746–760.

35 Zabeti, M., Daud, W.M.A.W., and Aroua, M.K. (2009). Activity of solid catalysts for biodiesel production: a review. *Fuel Process. Technol.* 90: 770–777.

36 Moazeni, F., Chen, Y.-C., and Zhang, G. (2019). Enzymatic transesterification for biodiesel production from used cooking oil, a review. *J. Clean. Prod.* 216: 117–128.

37 Zhong, L., Feng, Y., Wang, G. et al. (2020). Production and use of immobilized lipases in/on nanomaterials: a review from the waste to biodiesel production. *Int. J. Biol. Macromol.* 152: 207–222.

38 Quayson, E., Amoah, J., Rachmadona, N. et al. (2020). Biodiesel-mediated biodiesel production: a recombinant Fusarium heterosporum lipase-catalyzed transesterification of crude plant oils. *Fuel Process. Technol.* 199: 106278.

39 Hermanová, S., Zarevúcká, M., Bouša, D. et al. (2015). Graphene oxide immobilized enzymes show high thermal and solvent stability. *Nanoscale* 7: 5852–5858.

40 Xie, W. and Wang, J. (2014). Enzymatic production of biodiesel from soybean oil by using Immobilized lipase on Fe_3O_4/Poly(styrene-methacrylic acid) magnetic microsphere as a biocatalyst. *Energy Fuel* 28 (4): 2624–2631.

41 Xie, W. and Zang, X. (2018). Lipase immobilized on ionic liquid-functionalized magnetic silica composites as a magnetic biocatalyst for production of trans -free plastic fats. *Food Chem.* 257: 15–22.

42 Xie, W. and Huang, M. (2020). Fabrication of immobilized Candida rugosa lipase on magnetic Fe_3O_4-poly(glycidyl methacrylate-co-methacrylic acid) composite as an efficient and recyclable biocatalyst for enzymatic production of biodiesel. *Renew. Energy* 158: 474–486.

43 Arumugam, A., Thulasidharan, D., and Jegadeesan, G.B. (2018). Process optimization of biodiesel production from Hevea brasiliensis oil using lipase immobilized on spherical silica aerogel. *Renew. Energy* 116: 755–761.

44 Xie, W. and Zang, X. (2016). Immobilized lipase on core–shell structured Fe_3O_4-MCM-41 nanocomposites as a magnetically recyclable biocatalyst for interesterification of soybean oil and lard. *Food Chem.* 194: 160–166.

45 Kuila, T., Bose, S., Khanra, P. et al. (2011). Recent advances in graphene-based biosensors. *Biosens. Bioelectron.* 26: 4637–4648.

46 Stark, A. (2015). Ionic liquid-based processes in the biorefinery: a SWOT analysis. In: *Ionic Liquids in the Biorefinery Concept: Challenges and Perspectives*, 1e (ed. R. Bogel-Lukasik), 281–289. Cambridge; UK: Royal Society of Chemistry.

47 Long, T., Deng, Y., Gan, S., and Chen, J. (2010). Application of choline chloride $ZnCl_2$ ionic liquids for preparation of biodiesel. *Chin. J. Chem. Eng.* 18: 322–327.

48 Huang, W., Tang, S., Zhao, H., and Tian, S. (2013). Activation of commercial CaO for biodiesel production from rapeseed oil using a novel deep eutectic solvent. *Ind. Eng. Chem. Res.* 52: 11943–11947.

49 Zhao, H., Baker, G.A., and Holmes, S. (2011). New eutectic ionic liquids for lipase activation and enzymatic preparation of biodiesel. *Org. Biomol. Chem.* 6: 908–916.

50 Lu, P., Yuan, Z., Li, L. et al. (2010). Biodiesel from different oil using fixed-bed and plug-flow reactors. *Renew. Energy* 35 (1): 283–287.

51 Harding, K.G., Dennis, J.S., von Blottnitz, H., and Harrison, S.T.L. (2007). A life-cycle comparison between inorganic and biological catalysis for the production of biodiesel. *J. Clean. Prod.* 16: 1368–1378.

52 Li, X., Lu, G., Guo, Y. et al. (2007). A novel solid superbase of Eu_2O_3/Al_2O_3 and its catalytic performance for the transesterification of soybean oil to biodiesel. *Catal. Commun.* 8: 1969–1972.

53 Avellaneda, F. and Salvado, J. (2011). Continuous transesterification of biodiesel in a helicoidal reactor using recycled oil. *Fuel Process. Technol.* 92: 83–91.

54 Chew, T.L. and Bhatia, S. (2009). Effect of catalyst additives on the production of biofuels from palm oil cracking in a transport riser reactor. *Bioresour. Technol.* 100: 2540–2545.

55 Behzadi, S. and Farid, M.M. (2009). Production of biodiesel using a continuous gas–liquid reactor. *Bioresour. Technol.* 100: 683–689.

56 Tiwari, A., Rajesh, V.M., and Yadav, S. (2018). Biodiesel production in micro-reactors: a review. *Energy Sustain. Dev.* 43: 143–161.

57 Budžaki, S., Sundaram, S., Tišma, M., and Hessel, V. (2019). Cost analysis of oil cake-to-biodiesel production in packed-bed micro-flow reactors with immobilized lipases. *J. Biosci. Bioeng.* 128 (1): 98–102.

58 Cao, P., Dubé, M.A., and Tremblay, A.Y. (2008). High-purity fatty acid methyl ester production from canola, soybean, palm, and yellow grease lipids by means of a membrane reactor. *Biomass Bioenerg.* 32: 1028–1036.

59 Chauhan, D.S., Goswami, G., Dineshbabu, G. et al. (2020). Evaluation and optimization of feedstock quality for direct conversion of microalga Chlorella sp. FC2 IITG into biodiesel via supercritical methanol transesterification. *Biomass Conv. Bioref.* 10: 339–349.

60 Hegel, P.E., Martín, L.A., Popovich, C.A. et al. (2019). Biodiesel production from Halamphora coffeaeformis microalga oil by supercritical ethanol transesterification. *Chem. Eng. Process. Process Intensif.* 145: 107670.

61 Shirazi, H.M., Karimi-Sabet, J., and Ghotbi, C. (2017). Biodiesel production from Spirulina microalgae feedstock using direct transesterification near supercritical methanol condition. *Bioresour. Technol.* 239: 378–386.

62 Chen, C.-L., Huang, C.-C., Ho, K.-C. et al. (2015). Biodiesel production from wet microalgae feedstock using sequential wet extraction/transesterification and direct transesterification processes. *Bioresour. Technol.* 194: 179–186.

63 Faccini, C.S., Da Cunha, M.E., Moraes, M.S.A. et al. (2010). Dry washing in biodiesel purification: a comparative study of adsorbents. *J. Braz. Chem. Soc.* 22: 1–6.

64 Manique, M.C., Faccini, C.S., Onorevoli, B. et al. (2012). Rice husk ash as an adsorbent for purifying biodiesel from waste frying oil. *Fuel* 92: 56–61.

65 Escorsim, A.M., Cordeiro, C.S., Ramos, L.P. et al. (2015). Assessment of biodiesel purification using CO_2 at high pressures. *J. Supercrit. Fluids* 96: 68–76.

66 Ferrero, G.O., Almeida, M.F., Alvim-Ferraz, M.C.M., and Dias, J.M. (2014). Water-free process for eco-friendly purification of biodiesel obtained using a heterogeneous Ca-based catalyst. *Fuel Process. Technol.* 121: 114–118.

67 Knothe, G. (2006). Analyzing biodiesel: standards and other methods. *J. Amer. Oil Chem. Soc.* 83: 823–833.

68 Kumar, R., Ghosh, A.K., and Pal, P. (2017). Fermentative energy conversion: renewable carbon source to biofuels (ethanol) using Saccharomyces cerevisiae and downstream purification through solar driven membrane distillation and nanofiltration. *Energy Convers. Manag.* 150: 545–557.

69 Pal, P., Kumar, R., and Banerjee, S. (2019). Purification and concentration of gluconic acid from an integrated fermentation and membrane process using response surface optimized conditions. *Front. Chem. Sci. Eng.* 13 (1): 152–163.

70 Kumar, R., Ghosh, A.K., and Pal, P. (2019). Fermentative ethanol production from Madhuca indica flowers using immobilized yeast cells coupled with solar driven direct contact membrane distillation with commercial hydrophobic membranes. *Energ. Convers. Manage.* 181: 593–607.

71 Kumar, R. and Pal, P. (2015). A novel forward osmosis-nano filtration integrated system for coke-oven wastewater reclamation. *Chem. Eng. Res. Des.* 100: 542–553.

72 Kumar, R., Chakrabortty, S., and Pal, P. (2015). Membrane-integrated physico-chemical treatment of coke-oven wastewater: transport modelling and economic evaluation. *Environ. Sci. Pollut. Res.* 22 (8): 6010–6023.

73 Pal, P., Kumar, R., Nayak, J., and Banerjee, S. (2017). Fermentative production of gluconic acid in membrane-integrated hybrid reactor system: analysis of process intensification. *Chem. Eng. Process. Process Intensif.* 122: 258–268.

74 Shuit, S.H., Ong, Y.T., Lee, K.T. et al. (2012). Membrane technology as a promising alternative in biodiesel production: a review. *Biotechnol. Adv.* 30 (6): 1364–1380.

75 Kumar, R., Vikramachakravarthi, D., and Pal, P. (2014). Production and purification of glutamic acid: a critical review towards process intensification. *Chem. Eng. Process.* 81: 59–71.

76 Drexler, I.L. and Yeh, D.H. (2014). Membrane applications for microalgae cultivation and harvesting: a review. *Rev. Environ. Sci. Biotechnol.* 13 (4): 487–504.

77 Chmielewski, D., Zoe, Z., and Vasilios, M. (1999). Conversion targets for plug flow membrane reactors. *Chem. Eng. Sci.* 54: 2979–2984.

78 Dubé, M.A., Tremblay, A.Y., and Liu, J. (2007). Biodiesel production using a membrane reactor. *Bioresour. Technol.* 98: 639–647.

79 Xu, W., Gao, L., and Xiao, G. (2015). Biodiesel production optimization using monolithic catalyst in a fixed-bed membrane reactor. *Fuel* 159: 484–490.

80 He, H.Y., Guo, X., and Zhu, S.L. (2006). Comparison of membrane extraction with traditional extraction methods for biodiesel production. *J. Am. Oil Chem. Soc.* 83: 457–460.

81 Atadashi, I.M., Aroua, M.K., Abdul Aziz, A.R., and Sulaiman, N.M.N. (2012). High quality biodiesel obtained through membrane technology. *J. Membr. Sci.* 421–422: 154–164.

82 Amelio, A., Loise, L., Azhandeh, R. et al. (2016). Purification of biodiesel using a membrane contactor: liquid–liquid extraction. *Fuel Procss. Technol.* 142: 352–360.

83 Lauterböck, B., Moder, K., Germ, T., and Fuchs, W. (2013). Impact of characteristic membrane parameters on the transfer rate of ammonia in membrane contactor application. *Sep. Purif. Technol.* 116: 327–334.

84 Gomes, M.G., Santos, D.Q., de Morais, L.C., and Pasquini, D. (2015). Purification of biodiesel by dry washing, employing starch and cellulose as natural adsorbents. *Fuel* 155: 1–6.

85 Alves, M.J., Nascimento, S.M., Pereira, I.G. et al. (2013). Biodiesel purification using micro and ultrafiltration membranes. *Renew. Energy* 58: 15–20.

86 Torres, J.J., Rodriguez, N.E., Arana, J.T. et al. (2017). Ultrafiltration polymeric membranes for the purification of biodiesel from ethanol. *J. Clean. Prod.* 141: 641–647.

87 Saleh, J., Tremblay, A.Y., and Dubé, M.A. (2010). Glycerol removal from biodiesel using membrane separation technology. *Fuel* 89: 2260–2266.

88 Thapa, S., Indrawan, N., and Bhoi, P.R. (2018). An overview on fuel properties and prospects of Jatropha biodiesel as fuel for engines. *Environ. Technol. Innov.* 9: 210–219.

10

Janus Membranes for Water Purification and Gas Separation

Jing Deng, Sepideh Razavi, and Michele Galizia

School of Chemical, Biological, and Materials Engineering, University of Oklahoma, Norman, OK, USA

10.1 Introduction

Sustainable energy and water supply are critical for mankind survival. Especially in emerging countries, most of which are experiencing a constant population increase, producing drinking water at an affordable cost has become a priority. On a worldwide scale, chemical separations account for 10% of the global energy consumption, which corresponds to 7.5 GJ per person annually [1, 2]. The global energy consumption could be alleviated by introducing more energy-efficient separation processes, among which gas and liquid membrane-based separations are attracting special attention [1].

Since the 1960s, materials science advancement has been leading the development of polymeric and inorganic membranes exhibiting high throughput (i.e. permeability) and high separation efficiency (i.e. selectivity). Among membrane-based separations, ultrafiltration and microfiltration are exploited to remove large solutes such as macromolecules, oligomers, and micro-organisms; therefore, they require porous membranes [3–5]. Molecular transport through these porous membranes is described in terms of the pore flow models, such as the Poiseuille equation [3–5]. In contrast, forward osmosis, reverse osmosis, nanofiltration, and gas separation are used to separate small molecules or ions, Hence, they require dense membrane materials, that is, membranes that do not exhibit permanent pores [2, 6]. Small molecule transport in dense membranes is described in terms of the solution-diffusion mechanism, according to which permeating species dissolve in the upstream membrane face, diffuse through the membrane thickness down a chemical potential gradient, and, finally, desorb from the downstream membrane face [6]. In 1991, Robeson warned the community about the existence of a selectivity-permeability trade-off, which limits the performance of dense polymeric gas separation membranes to below an upper bound [7]. Evidence for a rejection-permeance trade-off was reported also for water purification membranes by Park et al. [8] in 2011.

The selectivity-permeability trade-off ignited research efforts to create advanced materials by incorporating principles and methods from complementary areas [9–11]. In the past

Sustainable Separation Engineering: Materials, Techniques and Process Development, Volume 1, First Edition. Edited by Gyorgy Szekely and Dan Zhao.
© 2022 John Wiley & Sons Ltd. Published 2022 by John Wiley & Sons Ltd.

two decades, colloid and interface science has become the cornerstone in achieving assembled functional structures, such as plasmonics, metamaterials, artificial muscles, as well as membranes, using a bottom-top approach [12–20]. This assembly route, which requires the encoding of the information about the desirable final structure into the building blocks, has been extremely successful, due to the remarkable boom in particle synthesis and surface modification [21–24]. The emergence of novel nanoparticles and colloidal building blocks with well-controlled size, shape, and surface properties has enabled the engineering of unique interaction potentials, that yield a desirable ordered structure [25, 26]. Targeted use of colloid and interface science principles allows the fabrication of membrane materials exhibiting well-defined morphology and properties, to simultaneously achieve high permeability and selectivity. This approach has been used to fabricate advanced materials for gas separation and water purification exhibiting Janus features at the macroscale. A material is defined as Janus when it exhibits a two-faced chemically anisotropic structure. For example, materials exhibiting hydrophilic features on one face and hydrophobic features on the other one fall in this category. The "Janus" feature, first reported by Casagrande et al. [27] and then highlighted by the Nobel Laureate Pierre-Gilles de Gennes in 1991 [28], has impacted several fields, including tunable stability in emulsions, foams, and polymer blends [15, 29–33], bottom-top assembly of novel functional structures using Janus colloidal building blocks [34, 35], active nanomotors [36–40], biological imaging, and sensing [41, 42] and drug delivery [43, 44], just to name a few. Since 2000, this concept has been successfully incorporated in the membrane field, starting from water purification and then rapidly spreading into other membrane applications. In this chapter, we review the state of the art of water purification Janus membranes and provide an outlook on future developments in gas separation applications. We believe that the use of Janus *leitmotif* at the nanoscale will provide exciting opportunities to engineer functional materials for membrane applications.

10.2 The Nexus Between Membrane Materials Science and Interfacial Science

The membrane area-to-volume ratio, a, spans from 10^2 to $10^4\,m^2/m^3$ [45]. For example, in the plate-and-frame configuration, typically used in microfiltration, a is about 100–400 m^2/m^3, while in the hollow fiber configuration, which is used in gas separation, it can reach 30,000 m^2/m^3 [45]. In some applications, such as ultra- and micro-filtration, the presence of permanent pores helps enhance the area-to-volume ratio. For these reasons, principles of interfacial science can be conveniently exploited to tune membrane transport properties, performance, and lifetime. For example, research has shown that membrane surface properties, including membrane-impurity affinity, roughness, and electrostatic properties impact the fouling behavior; therefore, surface modification has been successfully exploited to improve the fouling resistance [46, 47]. Despite some recent groundbreaking advances in colloid science and anisotropic materials, and the tremendous potential that the Janus character, i.e. anisotropy in surface properties, can offer to the field of membrane science, the Janus materials *leitmotif* has not been fully exploited to design membranes for large-scale separations. Principles of interfacial science not only help address issues related to

membrane fouling and lifetime, but also offer a unique opportunity to overcome the permeability (permeance)/selectivity (rejection) trade-off, in order to achieve superior separation performance. These prospective opportunities will be discussed in this review.

10.3 Janus Membrane Materials

10.3.1 Water Purification: State-of-the-Art Opportunities and Challenges

Currently, based on the membrane pore size, membrane-based water separation is categorized into microfiltration (MF), ultrafiltration (UF), nanofiltration (NF), and reverse osmosis (RO). As shown in Figure 10.1, the size of the solute to be removed and the membrane pore size decrease in the order MF > UF > NF > RO. Small molecule and ion transport through these membranes occurs by pore flow in MF and UF, and by solution-diffusion in RO. The role of the two mechanisms in NF is still a subject of debate [45], even though, as shown recently by Bye and Galizia, the solution-diffusion mechanism is sufficient to describe mass transfer in NF membranes [48].

Membranes for water purification exhibit a fouling propensity, which is caused by foreign compounds accumulated on the external membrane surface (i.e. external fouling) or inside the pores (i.e. internal fouling). Fouling introduces additional resistance to mass transfer, which, in turn, reduces the water flux [49]. Surface science plays a key role in determining the factors impacting membrane fouling propensity, which is affected by the membrane surface properties, including membrane-fouling agent affinity, roughness, and electrostatic properties [49]. To impart fouling resistance, the membrane surface contacting the feed can be chemically modified with a variety of hydrophilic species, yielding a two-faced chemically anisotropic structure also known as Janus membrane. Since 2000, the concept of Janus materials has been successfully exploited to modify the surface of

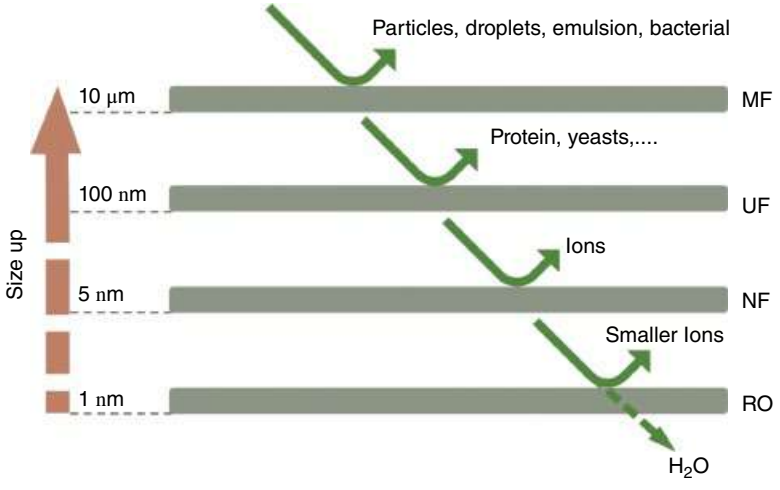

Figure 10.1 Water purification membranes vs. pore size: MF, UF, NF, and RO.

water purification membranes, with the scope of enhancing their lifetime or tune their selective transport properties.

Petroleum refining produces large volumes of wastewater that contain residual oil and refining byproducts. Each barrel of refined oil generates 3–10 barrels of wastewater [50].

10.3.1.1 Theoretical Background

For liquid separations in general, membrane surface wettability is a crucial factor. Based on the surface hydrophilicity, that is, the affinity between water and the membrane surface, membranes are classified as hydrophilic and hydrophobic. Other terms, including lyophilic/lyophobic and oleophilic/oleophobic are still commonly used in the literature to describe the wettability of solid surfaces with a certain liquid. For example, a lyophilic surface exhibits a good affinity for the liquid wetting the surface, whereas a lyophobic surface exhibits a poor affinity. Hydrophilicity and hydrophobicity of a surface can be experimentally assessed by measuring the three-phase contact angle of a water droplet on the surface. Generally, a surface is defined as "philic" to a certain liquid when the three-phase contact angle is less than 90°, and "phobic" when it is above 90°. Based on the contact angle value, θ, a surface can be classified as hydrophilic/oleophobic ($\theta_w < 90°$ and $\theta_o > 90°$), hydrophobic/oleophilic ($\theta_w > 90°$ and $\theta_o < 90°$), hydrophilic/oleophilic ($\theta_w < 90°$ and $\theta_o < 90°$), and hydrophobic/oleophobic ($\theta_w > 90°$ and $\theta_o > 90°$), where the subscripts w and o stand for water and organic liquid, respectively [51]. Hydrophilic/oleophilic and hydrophobic/oleophobic membranes are often indicated as *omniphilic* and *omniphobic*, respectively. Some examples of these surfaces are given in Figure 10.2a [52].

The contact angle can be measured experimentally, or calculated theoretically. For an ideal flat surface (Figure 10.2b), liquid contact angle on a surface in air, θ, is calculated from the Young's equation: $\cos\theta = \frac{\gamma_{SV} - \gamma_{SL}}{\gamma_{LV}}$, where γ_{SV}, γ_{SL}, and γ_{LV} are the surface tensions between the solid surface and air, solid surface and liquid, and liquid and air,

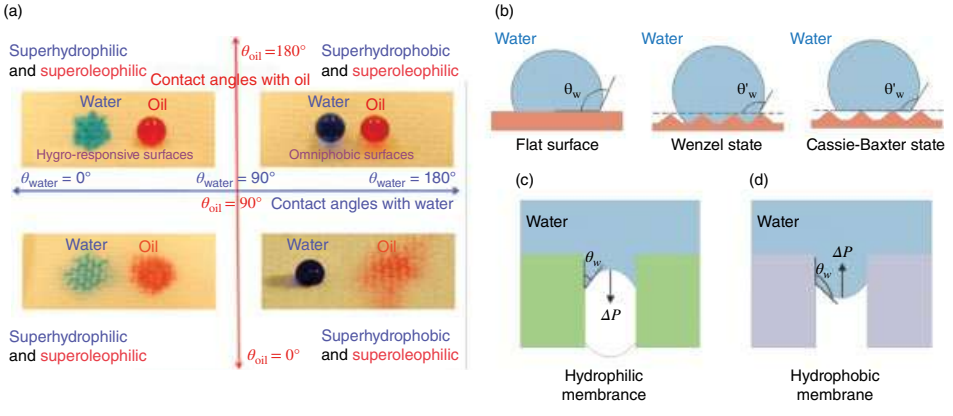

Figure 10.2 (a) Surfaces with various wettability, adapted from ref. [52] with permission of MRS Communications; (b) schematic diagrams of water droplets on a flat surface and a rough surface (under Wenzel and Cassie–Baxter hypotheses); breakthrough pressure for water penetrating through (c) hydrophilic and (d) hydrophobic membranes.

respectively [53]. This contact angle is only determined by the affinity between the solid surface material and the liquid; therefore, it is referred to as an ideal or intrinsic contact angle. However, ideal flat surfaces are rare, and real surfaces are rough or exhibit some curvature. Wenzel modified this equation for the apparent contact angle (θ') on a rough surface: $\cos\theta' = r\cos\theta$ (r is the measure of surface roughness) [54]. For ideal cases, where $r = 1$, θ' is equivalent to the intrinsic contact angle. For rough surfaces, r is larger than 1, thereby the apparent contact angle is larger than the intrinsic contact angle when $\theta > 90°$, or smaller than the intrinsic contact angle when $\theta < 90°$. Hence, the surface wettability can be tuned by engineering surface roughness, for both "philic" or "phobic" cases, which means that the surface wettability can be tuned by engineering surface roughness. However, Wenzel's equation only works if the contact between the liquid and the solid surface is homogeneous, that is, if no air bubbles are trapped between the liquid and the surface. Cassie and Baxter generalized the Wenzel model to liquid-air-solid surfaces. In the latter case, the apparent contact angle is calculated by: $\cos\theta' = f\cos\theta + f - 1$, where f is the area fraction of liquid directly contacting the surface [55]. Since f is always smaller or equal to 1, when considering Cassie–Baxter surfaces, the apparent contact angle is always greater than the intrinsic contact angle. It is worth mentioning that Cassie–Baxter equation is often used when considering "phobic" liquid surface pairs, and especially for superlyophobic surfaces ($\theta' > 150°$ [56, 57]).

In MF and UF applications, where porous membranes are used, external pressure may be needed for the liquid to penetrate the membrane pores. The minimum external pressure required, with respect to the atmospheric one, for the liquid to penetrate through a membrane pore is defined as the breakthrough, or intrusion pressure: $\Delta P = -\frac{2\gamma\cos\theta}{r_p}$, where γ is the surface tension, r_p represents the membrane average pore radius, and θ is the contact angle [58, 59].

When considering liquid water on a hydrophilic membrane surface, the breakthrough pressure is negative ($\theta_w < 90°$). Therefore, the liquid will be pulled into the membrane pores (c.f. Figure 10.2c). When water contacts a hydrophobic surface, the breakthrough pressure is positive ($\theta_w > 90°$). If the external pressure is not provided, then water will remain on the membrane surface (c.f. Figure 10.2d) [60].

10.3.1.2 Janus Membranes for Oil/Water Separation

Municipal sewage, wastewater produced by the oil and gas industry, and produced water contain large quantities of organic compounds, which are potential membrane fouling agents [5, 61]. Depending on the source, organic compounds can be petroleum fractions, hydrocarbons, and fatty acids. In laboratory experiments, vegetable oils or common solvents are used to mimic the organic phase. The size of these organic droplets spans from 0.1 to 100 μm, which is comparable to the size of the pores of MF and UF membranes. Mixtures containing droplets larger than 20 μm are thermodynamically unstable and will phase separate, giving rise to two immiscible phases: since, in general, organic liquids are lighter than water, the phase separation produces an organic-rich phase on the top and a water-rich phase on the bottom [51]. These mixtures can be easily separated using conventional technologies, such as flotation [51, 62]. However, since the driving force of sedimentation process is proportional to the volume of the dispersed phase droplet (R^3) and the density

difference between the two liquids ($\Delta\rho$) [63], this separation technique becomes ineffective as the droplet size is reduced and the Brownian motion comes into play. The interplay between convection, through gravitational force, and diffusion, by random Brownian motion, is captured in the dimensionless Peclet number $\left(\mathrm{Pe} = \frac{\Delta\rho g R^4}{k_B T}\right)$, where $Pe \gg 1$ and $Pe \ll 1$ indicate the predominance of convention and thermal fluctuations, respectively [64]. Therefore, because Pe scales as R^4, alternative separation technologies, such as membranes, are needed to separate mixtures such as microemulsions (size range 5–50 nm) and nanoemulsions (size range 20–200 nm) [65].

MF and UF membranes separate species via the size sieving mechanism, as the membrane can only reject species whose size exceeds the size of the pores (Figure 10.3a). The design strategy adopted for these membranes focuses on achieving surface superwettability coupled with small pore size. When considering superhydrophilic membranes facing oil-in-water emulsion, fast water penetration with high oil droplet rejection is easily achieved. UF and MF membranes are fabricated using cellulose, polyvinyl alcohol (PVA) and polydopamine (PDA), due to their nearly 0° water contact angle. In contrast, for oil-rich feeds (i.e. water-in-oil emulsions), superoleophilic materials, like polytetrafluoroethylene (PTFE, decane contact angle: 0° [66]) and polydimethylsiloxane (PDMS, n-hexadecane contact angle: 28° [67]) are used.

An alternative separation mechanism, which relies on the coalescence effect, has been proposed, even though several molecular details are still controversial. The idea is that dispersed droplets near the membrane surface would coalesce to form bigger droplets, which eventually demulsify the oil/water emulsion. However, depending on the membrane material properties, different scenarios may arise. In the case of oil-in-water emulsions (Figure 10.3b), it is believed that oil droplets preferentially coalesce on oleophilic rather than oleophobic surfaces [51, 68]. Therefore, researchers proposed to use oleophilic membranes where the demulsification of oily droplets and phase separation occur. Due to

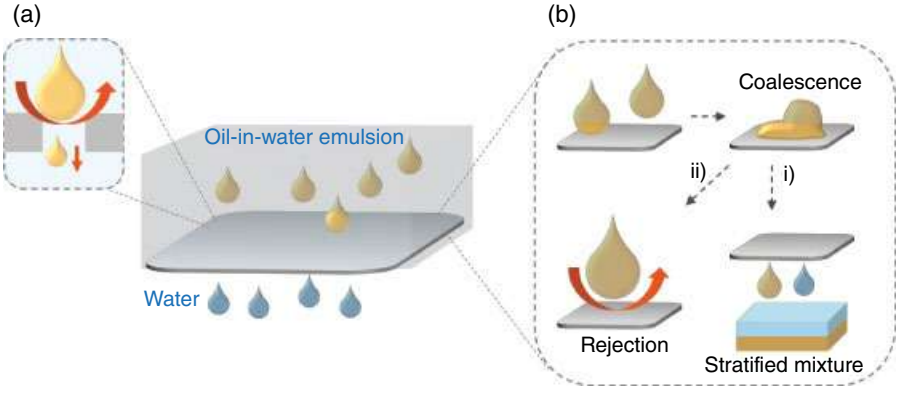

Figure 10.3 Schematic diagram of a membrane separating oil-in-water emulsion via (a) size sieving and (b) coalescence effect: i) represents an oleophilic membrane and ii) a superoleophobic membrane.

the oleophilic nature of the membrane surface and pores, the oil droplets coalesce and pass through the membrane spontaneously, and water should remain on the membrane surface since the breakthrough pressure for the continuous water phase is positive. However, when considering these oleophilic membranes, the size of the pores may exceed 5 μm. Therefore, the breakthrough pressure for water, although positive, is small [69–72]. Hence, by applying a low transmembrane pressure, such as 0.1–0.5 bar [69–73], the water phase can be pushed through the membrane pores. Therefore, the permeate is a stratified oil-water mixture, which can be separated by traditional technologies [51]. As it can be seen, the oil-water separation with this coalescence effect does not rely on the size sieving effect, that is, on the membrane pores size. Moreover, to achieve high flux, the pore size can exceed the droplet size [74]. Surface modifications to introduce functional groups acting as demulsifiers have been reported as well [75–79].

Coalescence-based separation in surfactant-free oil-in-water emulsions may also be achieved with superoleophobic membranes [62, 80, 81]. In this scenario, water preferentially permeates through the membrane and the organic compound accumulates near the membrane surface, where its local concentration rapidly increases. Since the interaction between organic droplets and a superoleophobic membrane is very weak, oil droplets tend to coalesce near the membrane surface. These big aggregates are then rejected by the membrane. However, relevant molecular aspects of this mechanism, such as the role of the size sieving effect, remain unknown [74, 82, 83].

For size sieving-based separations, the introduction of surfactants potentially reduces the size of the dispersed phase, which makes the separation very challenging. Moreover, surfactants can also change the membrane surface wettability, which may trigger faster fouling. For coalescence-based separations, surfactants stabilize dispersed droplets and prevent them from merging together on the membrane surface [83]; therefore, a higher transmembrane pressure would be needed to achieve a good separation [68].

10.3.1.2.1 Switchable Transport

Conventional membranes behave in either "water removal" (for oil-in-water emulsions) or "oil removal" (for water-in-oil emulsions) modes, via both size sieving and coalescence effects mechanisms. Recently, membranes with the ability to handle both feeds have been successfully fabricated by exploiting the Janus *leitmotif* [84]. These Janus membranes

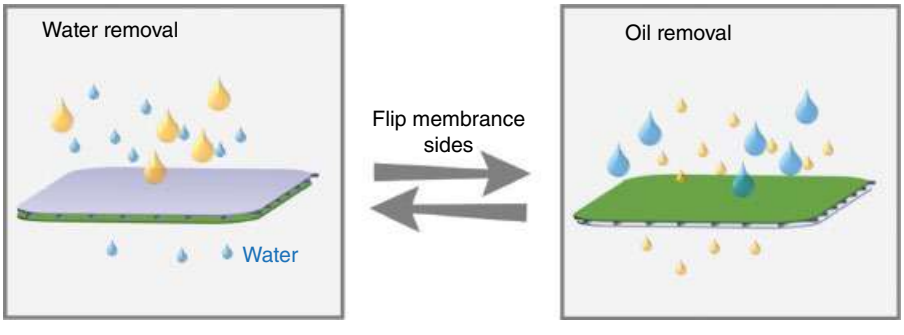

Figure 10.4 Switchable transport membranes: water-removal vs. oil-removal modes.

possess a hydrophilic face and a hydrophobic one. When the hydrophilic side faces water-rich feeds, the surface will be hydrated and reject oily compounds, by operating in the "water removal" mode, and *vice versa* (Figure 10.4). Therefore, the same membrane can be used in different scenarios, for example, to treat feeds exhibiting changing compositions, which is extremely convenient from a techno-economic standpoint.

These switchable Janus membranes can be fabricated using different approaches. "A to B"-type membranes (c.f. Figure 10.5a) are prepared by modified phase inversion, starting from a solution containing both hydrophilic and hydrophobic polymers [85, 86]. For example, Li et al. used a modified phase inversion method to prepare PVDF (polyvinylidene fluoride) + PVP-VTES (poly(vinylpyrrolidone-vinyltriethoxysilane)) Janus membranes [85], where PVDF represents the hydrophobic part of the nascent membrane, and PVP-VTES represents the hydrophilic part. First, a commercial PET (polyethylene terephthalate) nonwoven fabric was impregnated with glycerol and used as a support to cast a solution of PVDF + PVP-VTES in triethyl-phosphate as solvent. After casting the PVDF + PVP-VTES solution on the pretreated nonwoven fabric, the nascent composite membrane was soaked in water to induce phase inversion, that is, to exchange triethyl-phosphate with water. The presence of glycerol greatly slowed down the water migration from the nonwoven fabric side into the PVDF + PVP-VTES layer. In contrast, water could more easily penetrate the PVDF + PVP-VTES layer from the opposite side. This difference in solvent exchange rate causes the redistribution of polymer chains inside the nascent membrane. The final result is that the upper side of the active layer is rich in hydrophilic PVP-VTES, where a faster water exchange occurred. In contrast, the bottom side of the active layer, which contacts the nonwoven fabric directly, is rich in hydrophobic PVDF, where the water exchange occurred slowly. Therefore, a Janus membrane with a tunable wettability gradient was obtained. This membrane exhibited an underwater oleophobic PVP-VTES surface (underwater oil contact angle: 147°) and underoil superhydrophobic PVDF surface (underoil water contact angle: 170°). With this asymmetric wettability,

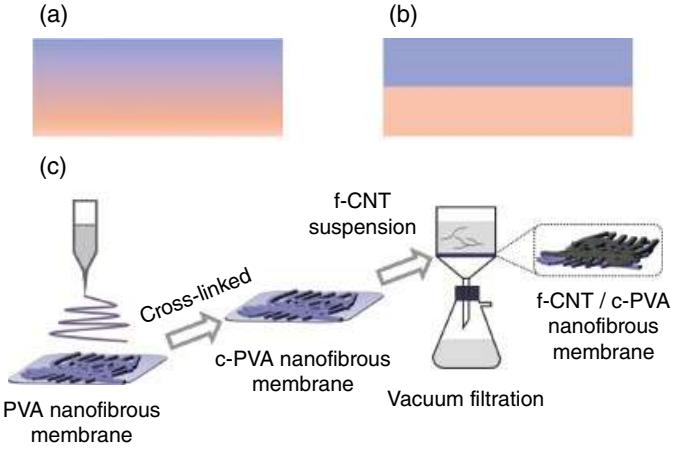

Figure 10.5 Janus membranes exhibiting switchable transport. (a) "A to B" configuration; (b) "A on B" configuration; (c) Example of "A on B" approach: f-CNT/c-PVA Janus membranes [87].

PVDF/PVP-VTES membrane can separate both oil-in-water (by PVP-VTES-rich side) and water-in-oil (using PVDF-rich surface) emulsions with rejections larger than 97.5%. In contrast, unmodified hydrophobic PVDF membranes can only separate water-in-oil emulsions. Despite applicability in a variety of scenarios, the Janus membranes prepared by Li et al. exhibited a 33% lower oil flux (water-in-toluene, 1 vol%) and around 2% lower water rejection compared to the unmodified PVDF membrane [85].

Equally important, the "A to B" protocol requires a careful selection of the two polymers. Indeed, both the hydrophilic and hydrophobic polymers must be soluble in the same solvent, which limits the number of possible polymer pairs that can be used. In the example mentioned above, to obtain a homogeneous hydrophilic plus hydrophobic polymer solution without phase separation, the hydrophilic PVP-VTES was pre-polymerized with relatively low molecular weight (e.g. ~ 2200 Dalton) inside the PVDF solution. Moreover, accurate control of the thickness and pore size is hard to achieve using the "A to B" approach.

An alternative fabrication method, referred to as "A on B," has also been proposed, which is based on the assembly of two separate layers (Figure 10.5b). The main advantage of using this approach is the possibility of modifying and engineering each layer individually, in terms of their chemical properties, roughness, pore size, and thickness. Depending on the top layer composition, vacuum filtration or spin coating can be used to cast a porous layer onto existing support [88–90]. Vacuum filtration is commonly used for inorganic fiber-like materials, while the spin coating is more suitable for polymers. Pornea et al. deposited a layer of hydrophobic fluorinated carbon nanotubes (f-CNT) on a hydrophilic cross-linked PVA (c-PVA) nanofibrous membrane via vacuum filtration, as shown in Figure 10.5c [87]. The f-CNT layer had a smaller pore size compared to c-PVA layer; therefore, the Janus membrane exhibited an enhanced rejection relative to the neat c-PVA membrane. Specifically, oil rejection (toluene-in-water, 1:30 v:v) increased from ~ 30% in neat c-PVA to ~ 99% in f-CNT/c-PVA, while water rejection (water-in-toluene, 1:114 v:v) increased from 0 in neat c-PVA to 99% in f-CNT/c-PVA. However, during pure water and oil-in-water emulsion permeation tests, water flux through the Janus membrane was 15% lower relative to the neat hydrophilic c-PVA membrane. In contrast, during water-in-oil emulsion permeation tests, the oil flux of Janus membranes was around 8000 $L/m^2/h/bar$, while the hydrophilic c-PVA membrane exhibited a negligible oil flux. This result is consistent with the analysis of breakthrough pressure in Section 10.3.1.1.

The third strategy to fabricate Janus membranes with anisotropic wettability relies on the modification of one or both sides of a pre-existing substrate. In this case, the region near the modified surfaces is relatively thin compared to the whole. For example, Ding et al. fabricated Janus ceramic membranes via a two-step modification: hydrophobization of a pristine hydrophilic Al_2O_3 membrane via grafting hexadecyltrimethoxysilane, followed by the hydrophilization of one surface via O_2/N_2 plasma treatment. The thickness of the hydrophilic region in the Janus ceramic membranes prepared only accounts for 3.5% of the whole membrane thickness [91], while for "A to B" or "A on B" type, it may be above 20%.

Commercial fabrics for MF membranes, such as PVDF, PTFE, and cellulose are the most common substrates to fabricate polymeric Janus membranes. Surface modification with bio-inspired PDA [92, 93] or treatment with O_2/N_2 plasma [94, 95] is widely used to

increase hydrophilicity, while fluorination or silylation is used to achieve hydrophobic surfaces [93, 96, 97].

Hydrophobic silica particles decorated with fluorinated or silylated oligomers have been used to enhance membrane surface hydrophobicity [95, 98, 99]. Preparation methods include spray coating, grafting, and plasma treatment [84]. Zuo et al. reported a PVDF-based Janus membrane coated with hydrophilic PDA + polyethyleneimine (PEI) on one side and hydrophobic silica nanoparticles (SiNPs) on the other side via spray coating [98]. After modification, the water contact angles of the hydrophilic and hydrophobic sides in air were ~ 10° and 170°, respectively, compared to 131° of the neat PVDF membrane. In contrast to "A to B" or "A on B" membranes, emulsion permeation experiments in Janus PVDF-PDA-PEI-SiNPs membranes showed that water and toluene flux increases relative to neat PVDF. Specifically, the Janus membrane exhibited a water flux of 2060.5 $L/m^2/h/bar$ (toluene-in-water, 1:250 v:v) and a toluene flux of 1769.0 $L/m^2/h/bar$ (water-in-toluene, 1:250 v:v), respectively. Both values were around 1385 $L/m^2/h/bar$ in neat PVDF membranes. The higher flux exhibited by the Janus PVDF membrane results from the superwettability in both surfaces, which reduces the breakthrough pressures [98]. Moreover, it is found that water flux first increases and then decreases with increasing PDA + PEI spraying density (that is, the volume of solution spread per unit membrane area). This effect results from the interplay between enhanced surface hydrophilicity and narrowed pore size. In contrast, silica particles tend to aggregate instead of covering the membrane surface homogeneously; therefore, oil flux increases monotonously with increasing silica particles spraying density [62, 100]. Equally important, these Janus PVDF membranes exhibited higher rejection for toluene (95.5%) and water droplets (99.1%) compared to neat PVDF membranes (88% for toluene and 93.5% for water).

A summary of Janus membranes for oil/water separation is shown in Table 10.1, including materials, preparation methods, flux, and separation efficiency.

10.3.1.2.2 Unidirectional Transport

According to the breakthrough pressure (Figure 10.2c), a membrane allows a lyophilic liquid (contact angle of the liquid on the solid surface < 90°) to penetrate through, and it blocks a lyophobic liquid (contact angle of the liquid on the surface > 90°) in the absence of external pressure. Recently, a reverse transport has been achieved using Janus membranes, where a fluid migrates from a lyophobic surface to a lyophilic one [107]. This behavior is referred to as unidirectional transport. For example, for an oil unidirectional membrane, oily compounds can only penetrate from the oleophobic side to the oleophilic side.

A thin lyophobic top layer is the key factor to realize this unidirectional transport. The behavior of a liquid droplet contacting a lyophobic–lyophilic Janus membrane arises from the interplay of several forces acting on the liquid along the pore: (i) the gravity force (G), which is related to the weight of the droplet, (ii) a repulsive force caused by the lyophobic surface of the layer (F_1), and (iii) an attractive force between the droplet and the lyophilic surface (F_2). These three forces are shown in Figure 10.6. F_1 and F_2 only exist when the droplet is in contact with the corresponding layers. The repulsive and attractive forces are given by the product of the pore internal surface area, which directly contacts the liquid ($2\pi Rh$, where R and h are the pore radius and the height of the liquid inside the pore,

Table 10.1 Summary of Janus membrane performance for oil/water separation.

Filtration materials	Substrate	Preparation method	Separation mixture	Flux (L/m^3 h)	Separation efficiency (–)	Ref
Form Janus membrane by one-step						
PVDF/PDA/PEI	–	non-solvent induced phase separation	O/W mixture (1:1 v:v)	W: 4500–5000; Oil: 3800–7500	–	[86]
PVDF/PVP-VTES	–	Phase separation with unidirectional segregation	Trichloromethane/W (1:99 v:v); Span 80-stabilized Water/ toluene (1:100 v:v)	O/W: 3835; W/O: 1700 -0.09 MPa	O/W: 97.5%; W/O: 97.6%	[85]
CNT	hydrophilic PAN electrospun nanofiber membrane (thickness: 13 μm)	Vacuum filtration	Surfactant-stabilized chloroform/W (1: 9 v:v) or W/ chloroform emulsion (1: 99 v:v)	80,000 L/m^{2}hbar (O/W); 12,000 L/m^{2}hbar (W/O)	99.7% (O/W); >99.2% (W/O)	[101]
Assembly of two layers						
Electrospun PVDF layer	Hydrophilic PNIPAM+ PVDF (3:1) electrospun nanofiber membrane	Subsequent electrospun	Olive oil/W (1:100 v:v)	–	> 99.5%	[102]
Hydrophobic PS membrane	Hydrophilic PAN electrospun membrane	Subsequent electrospun	SDS-stabilized Hexane/W (1:99 v:v)	227–430	–	[88]
PFOTS-coated CNT	Crosslinked PVA electrospun nanofiber mat	Vacuum filtration	Surfactant-stabilized O/W (1:30 v:v) or W/O (1:114 v:v)	0.09 MPa	–	[87]
Post-modification						
PANI-SiNP	PTFE	Immersion-spray coating	8 W/O emulsions; 4 W/O emulsions;	~ 1300 (O/W); ~ 1100 (W/O)	> 99.7% (O/W); > 99% (W/O)	[99]

(*Continued*)

Table 10.1 (Continued)

Filtration materials	Substrate	Preparation method	Separation mixture	Flux (L/m^3 h)	Separation efficiency (–)	Ref
PDA+PEI; silica nanoparticles	PVDF fabricated by thermal induced phase separation	Spray coating	toluene-in-water (1:250 v:v); surfactant-stabilized water-in-toluene (1:250 v:v)	2060.5 L/m^2 h bar (O/W); 1769.0 L/m^2 h bar (W/O); 0.2 MPa	94.0% oil rejection; 97.0% water rejection	[98]
Hydrophobic PDA-trichlorovinylsilane; Hydrophilic PDA	PVDF microfiltration membranes (pore size: 0.22 μm)	PDA coating, following silanization; UV-triggered click reaction	Immiscible O/W mixture; surfactant-stabilized O/W or W/O emulsions (1:100 v:v)	500 (O/W); 5000 (W/O); MPa	97.5% (O/W); > 98.5% (W/O)	[103]
PFTS-modified SiO_2, followed O_2/N_2 plasma-etching treated surface	PVDF	unilateral O_2/N_2 plasma-etching	surfactant-stabilized O/W or W/O emulsions (1:100 v:v)	7200 L/m^2 h bar (O/W); 9300 L/m^2 h bar (W/O);	99.8% (O/W); > 99.0% (W/O)	[95]
PDA	Hydrophobic PTFE/PET composite	Immersion polymerization and tape-peeling	Layered oil/water mixture	–	–	[93]
PS; PDMAEMA	CNT network membrane (5 μm)	Self-initiated photo-grafting and polymerization	Surfactant-stabilized O/W (1: 30 v:v) or W/O emulsion (1: 114 v:v)	4000 – 7000 L/m^{2}hbar (O/W); 7000–9000 L/m^{2}hbar (W/O); 0.09 MPa	-; > 99.8% (W/O)	[104]
PVDF with surface-coated SiO_2	PFTS	O_2/N_2 plasma	Surfactant-stabilized O/W or W/O emulsion (1: 100 v:v)	4500–7200 (O/W); 6800–9300 (W/O)	99.8% (O/W); > 99% (W/O)	[94]
Stearic acid	Cellulose	Silver mirror reaction; Single side coating	Surfactant-stabilized (0.1 wt.%) O/W or W/O (1:50 v:v)	620–685 (O/W); 295–350 (W/O)	> 96.0 % (O/W); > 95.0 % (W/O)	[105]

–	Superhydrophobic ZnO nanorod array-coated cellulose membranes	in situ growth technology and subsequent hydrophobic modification first ZnO layer, while hydrothermal for MnO_2	Surfactant-stabilized O/W (4:95.7 v:v) or W/O emulsion (4:95.7 v:v)	> 8380 L/m^2hbar (O/W); 1590 L/m^2hbar (W/O); 0.03 MPa	–; > 99.8% (O/W); > 99.4% (W/O)	[106]
PFTS	Homemade hydrophilic TiO_2-coated PPS microporous membrane	Water–oil interfacial grafting	Surfactant-free O/W or W/O emulsion (1:99 v:v)	590–650 (O/W); > 920 (W/O)	> 98.0% for O/W & W/O	[97]
–	Hydrophobic HDTMS modified ceramic (2 mm)	O_2/N_2 plasma etching (hydrophilic layer is ~ 35 um)	Surfactant-stabilized O/W (5:1000 v:v) or W/O emulsion (1:1000 or 5:1000 v:v)	–	–	[91]

O/W: oil-in-water emulsion; W/O: water-in-oil emulsion; PNIPAM: poly(N-isopropylacrylamide);
PFOTS: trichloro(1H,1H,2H,2H-perfluorooctyl)silane; PEPA: polyethylenepolyamine;
PS: polysulfone; SDS: sodium dodecyl sulfate; PPS: poly(phenylene sulfide);
PFTS: 1H,1H,2H,2H-Perfluorodecyltriethoxysilane;
PDMAEMA: poly(2-(dimethylamino)ethyl methacrylate); HDTMS: hexadecyltrimethoxysilane.

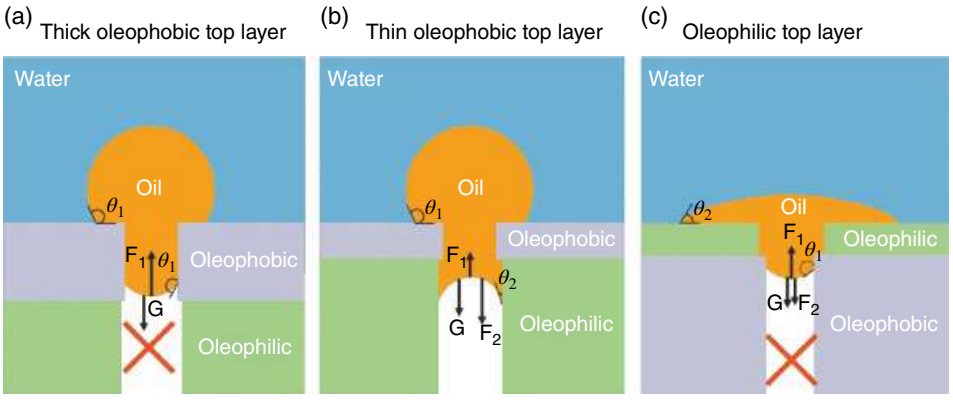

Figure 10.6 Force analysis of an oil droplet on (a) thick and (b) thin oleophobic/oleophilic, and (c) oleophilic/oleophobic Janus membranes. Subscripts 1 and 2 represent the oleophobic layer and oleophilic layer, respectively.

respectively), times the breakthrough pressure (ΔP). Due to the lyophobic and lyophilic natures of these two layers, contact angle θ_1 is always greater than 90°, while θ_2 is always smaller than 90°. When the top layer is lyophobic and thick, the droplet remains on the surface since the gravitational body force is not large enough to overcome the repulsive surface force F_1 ($=2\pi R_1 h_1 \Delta P_1 = -4\pi\gamma h_1 \cos\theta$) (c.f. Figure 10.6a). As the lyophobic layer becomes thin enough (c.f. Figure 10.6b), the droplet can contact the lyophilic layer. Hence, the total force $\Delta F = G + F_2 + F_1 = G + 4\pi\gamma h_2 \cos\theta_2 + 4\pi\gamma h_1 \cos\theta_1$ may be positive, which will push the droplet penetrating down, or negative, which will hold the droplet on the surface. Therefore, decreasing the thickness of the lyophobic layer favors a positive net force, and promotes the droplet migration from the lyophobic surface to the lyophilic region. In the opposite case, if the top layer is lyophilic, the droplet would spread on the membrane surface (Figure 10.6c). It is worth mentioning that "unidirectional transport" is achieved without an externally applied pressure gradient, and in some studies, antigravity unidirectional transport has been reported [108]. Therefore, for this type of Janus membrane, the separation mechanism relies mainly on the breakthrough forces, which are determined by the pore size, wettability, and microstructure of membrane.

As shown above, the thickness of the surface layer is crucial for unidirectional transport. Xu and coworkers investigated the influence of the oleophobic layer thickness on apparent contact angle and underwater oil transport [76, 109]. Only one side of an oleophilic polypropylene (PP) MF membrane was coated by oleophobic PDA/PDDA (poly(diallyldimethylammonium chloride)). Oil penetration from the oleophobic surface became more difficult with increasing the thickness of the PDA-PDDA layer from 0 to 27.3 μm. When the oleophobic surface layer is only 7.8 μm-thick (surface pore size = 157 nm), an oil droplet (average size ~ 34 nm) can transport through the whole membrane within seconds. In contrast, when the oleophobic surface layer is 27.3 μm thick, oil transport suddenly stops.

To obtain the thin surfaces required for unidirectional transport, Janus membranes are mostly prepared by asymmetric modification [110]. As the substrates are hydrophobic-based, such as commercial PVDF or PTFE MF membranes, the resulting membranes are

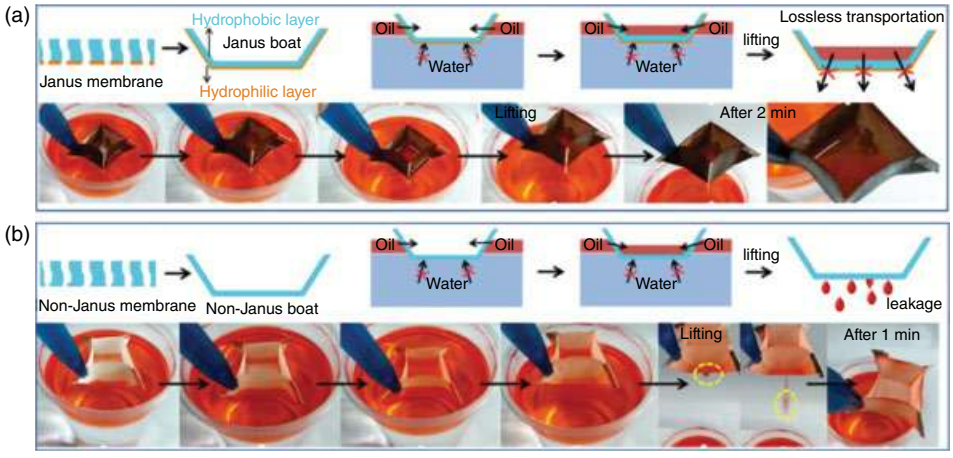

Figure 10.7 Image of oil (petroleum ether, dyed red) collection experiments using (a) Janus membrane (water pre-wetted hydrophilic PDA+PEI surface is the outer side and petroleum ether pre-wetted PTFE surface is the inner surface) and (b) surface-peeled PET/PTFE membrane. Adapted from ref. [111], with permission of the Journal of Membrane Science.

"oil-diode" after hydrophilization. Yang et al. coated PDA and PEI on one side of the hydrophobic PET/PTFE MF membrane (pore size = 0.22 μm) by floating it on a dopamine solution [111]. The hydrophilic and hydrophobic surfaces of this Janus membrane were pre-wetted by water and petroleum ether, respectively. Then the Janus membrane was folded into a small boat with the oleophobic side facing outward and placed on the surface of a petroleum ether (dyed red)/water mixture (Figure 10.7). Only petroleum ether penetrated the membrane and was collected inside the boat. When the oil-collected boats were lifted from the liquid surface, oil leakage was not observed for the Janus membrane, suggesting that the oil cannot transport from the oleophilic to the oleophobic direction. Hence, unidirectional oil transport is achieved. Furthermore, a permeation test using micrometer-sized SDS (sodium dodecyl sulfate) stabilized dichloroethane (20 vol%)-in-water emulsions was conducted, and only dichloroethane could pass through the membrane, with an oil flux over 1000 $L/m^2/h$. FTIR spectra showed that the permeate was SDS-free and water-free.

In contrast, when hydrophilic substrates are chosen, the "water-diode" membranes can be fabricated [112–116]. Yang et al. used dopamine-NH_2 reaction to selectively decorate one side of hydrophilic cotton fabric with hydrophobic octadecylamine [117]. As expected, water can only penetrate from the hydrophobic side, but not from the hydrophilic side. This Janus fabric was capable to recover small amounts of water (2 vol%) from a water-in-petroleum ether emulsion, which was stabilized by a nonionic surfactant Span® 80. The water flux was 20.8 $L/m^2/h$ with an oil rejection of 99.6%.

10.3.1.2.3 Membrane Fouling

In oil/water separations, fouling causes rapid decay of the membrane performance [118, 119]. In some UF and MF processes, fouling is so severe that the separation performance depends on the degree of fouling instead of the intrinsic membrane properties [45, 49].

Generally, fouling can be classified into inorganic-, organic-, and biofouling [46, 49, 118, 119]. The latter two may be the prevailing mechanisms in the oil/water separation.

Freeman and coworkers were among the first researchers to address the fouling issue in the UF treatment of produced water by using the Janus *leitmotif* [120, 121]. Specifically, they modified the surface of commercial membranes by casting a thin PDA layer, which enhanced hydrophilicity. Other similar molecules, such as catechol, are being inspected to achieve better control over the surface hydrophilicity and make the modification cheaper.

Ding et al. compared the antifouling performance of a surface-modified Janus ceramic membrane to the corresponding unmodified hydrophilic Al_2O_3 membrane [91]. As discussed above, Janus ceramic membranes were obtained via a two-step modification: hydrophobization of the whole membrane via grafting of hexadecyltrimethoxysilane, followed by hydrophilization of one surface via O_2/N_2 plasma treatment. When dealing with oil-in-water emulsion (oil content = 200 ppm), the oil fouled both surfaces of the unmodified Al_2O_3 membrane, causing an 84% water flux decay in 1 hour. In contrast, the Janus membrane exhibited a slower water flux decline rate (45% after 1 hour) compared to the neat hydrophilic Al_2O_3 membrane. Despite the initial water permeability of the unmodified membrane being twice that of the Janus membrane, after a short operation time (15 minutes for hexane-in-water and 2 minutes for soybean oil-in-water), the water permeability of the Janus-modified membrane exceeded that of the pristine, unmodified membrane. Equally important, the plasma-modified hexadecyltrimethoxysilane surface has higher surface energy and less fouling propensity compared to the unmodified ceramic membrane.

Membrane biofouling may be caused by bacteria deposition on the surface, followed by further growth [119]. To mitigate this issue, which is especially relevant in the treatment of drinking water, Lv et al. incorporated antibacterial silver nanoparticles into a cellulose membrane, followed by the hydrophobization of one surface [105]. Both sides of the Janus membrane exhibited a good antibacterial activity upon exposure to solutions containing *S. aureus* and *E. coli*. Moreover, the combination of the hydrophobically modified surface and the hydrophilic cellulose + silver nanoparticle bulk region yielded switchable transport properties. Therefore, a Janus membrane with both switchable transport and antibacterial properties was achieved for oil/water separation.

10.3.1.2.4 Janus Membrane Lifetime and Other Unsolved Issues

Despite their promising performance in oil/water separation, a few unresolved issues have hampered the widespread industrial use of Janus membranes. Above all, their multilayer structure provides a non-negligible mass transport resistance, which causes modest fluxes [97]. However, the impact of the layered structure, wettability, and morphology gradients on mass transport resistance is not fully understood and would benefit from further investigation. The relatively large thickness of Janus membranes also contributes to an increase in the mass transfer resistance. Therefore, fabrication protocols need to be optimized to achieve better control over the thickness of single layers. Equally important, compatibility issues between different layers have a detrimental effect on the membrane lifetime, especially during operation under chemically and thermally challenging environments, as well as at high pressures.

The stability of these Janus membranes under repeated working cycles deserves further investigation. The stability of some Janus membranes has been evaluated by running cyclic permeation tests [76, 87, 122]. For instance, a cycle of 20 oil/water separation tests was run using the aforementioned f-CNT/c-PVA membrane. Each cycle, consisting of a dead-end permeation test using a fixed amount of emulsions (110–130 mL), was followed by an ethanol wash and a 2-hour heating step to remove ethanol [87]. The separation efficiency for both water-in-toluene emulsions, using the hydrophobic f-CNT side, and toluene-in-water emulsions, using the hydrophilic c-PVA side, was constant after 20 cycles. Both water and oil fluxes decay by 10% after 20 cycles, even though this drop was within the experimental uncertainty. It is worth noting that since Janus membranes contain both hydrophilic and hydrophobic regions, the long-term contact with oil and water might induce swelling. This structural issue has been overlooked so far; therefore, its long-time effects are fairly unknown.

As mentioned previously, the oily compounds used for laboratory filtration experiments are vegetable oils or common organic solvents, such as chloroform and toluene, dispersed in water. Unfortunately, these emulsions do not necessarily mimic the complex mixtures that membranes have to face in real applications. For example, the viscosity of petroleum fractions may be higher than that of the model emulsions presented above, which means that a lower flux and more severe fouling could be encountered in real applications compared to laboratory experiments.

Another unsolved issue is the scale-up of Janus membranes for real applications. In principle, both spiral-wound and hollow-fiber configurations can be chosen for Janus membranes, depending upon the application and the structure of each layer. However, hollow fiber Janus membranes are better suited than spiral wound ones for switchable oil/water separation [82, 109].

10.3.1.3 Janus Membranes for Water Desalination

After removing large molecules via MF and UF processes, water purification proceeds with desalinization via NF or RO, where small molecules and ions are removed. Other processes, such as forward osmosis (FO) and membrane distillation (MD), have received some attention in recent years. A comparison among NF, RO, FO, and MD is presented in Table 10.2. To the best of our knowledge, the use of Janus *leitmotif* in RO has not been explored so far.

A few studies have reported the use of thin hydrophobic/thick porous hydrophilic Janus membranes for FO applications [123–125]. However, all these membranes exhibited unstable performance. For instance, Zhou et al. designed porous hydrophobic/superhydrophilic Janus membranes via coating fluorinated SiO_2 on a superhydrophilic modified PVDF support, which contained 28% wt hydrophilic additive PVP-VTES [123, 124]. In the FO tests, the hydrophobic fluorinated SiO_2 side-faced the draw solution (e.g. 1 M NaCl), and the superhydrophilic PVDF side contacted the feed (i.e. pure water). It was observed that air trapped inside the porous hydrophobic layer prevented ion transport from the draw solution to the feed side, which is known as reverse salt transport. However, these air bubbles got replaced by water shortly after the FO test started (2 hours), and thus the reverse salt flux doubled, while it should be as low as possible to keep a high driving force for the osmotic water flux. Another study used ZIF-8-coated polysulfone (PS) membranes for

Table 10.2 Comparison of NF, RO, FO, and MD processes [46, 124, 128–130].

	NF	RO	FO	MD
Membrane structures	Composite	Composite	Hydrophilic thin film composite membrane	Hydrophobic porous membrane
Representative selective materials	Polyamide	Cellulose derivatives; polyamide, poly(ether urea)	Cellulose derivatives; Polyamide	PVDF, PTFE
Driving forces	Hydraulic pressure (10–25 bar) – osmotic pressure	Hydraulic pressure (15–80 bar) – osmotic pressure	Osmotic pressure differences between feed solution and draw solution (no external pressure needed)	Water chemical potential differences between hot salty feed and cool permeate
Work pattern	Water penetrates from salty feed to penetrate side	Water penetrates from salty feed to penetrate side	Water penetrates from the less salty side (feed) to the concentrated side (draw)	Water in salty feed evaporates on membrane surface, and vapor transports through pore and then condensates on the other membrane surface
Advantages	– Mature technology	– Mature technology	– Energy efficient	– Able to deal with high-salinity water; – Low-grade heat as heat source;
Major issue	– High energy consumption – Fouling	– High energy consumption – Fouling – High retentate concentration	– Fouling – Internal concentration polarization – Lack of high performance membranes – Required further purification	– Fouling – Wetting – Pore block – Phase change required more energy
Applications	Divalent ions (Ca^{2+}, Mg^{2+}), microsolutes (MW: 500 – a few thousand Da) removal with low concentration	Monovalent ions (Na^{+}, Cl^{-}) removal	Highly saline water	Highly saline water at small-scale sites

FO [125]. However, the ZIF-8 layer was unstable upon protracted exposure to water, likely because of the hydrolysis and recrystallization into other crystalline structures [126, 127]; therefore, both water and salt fluxes were similar to those of the membranes without ZIF-8 layer after 12 hours of continuous FO operation.

10.3.1.3.1 Nanofiltration

As shown in Table 10.2, NF removes divalent ions via a mechanism that includes size sieving and electrostatic repulsive interactions between ions and the membrane surface. The selective layer of commercial NF membranes is made out of cross-linked polyamides (PAs) fabricated by the amine-acid chloride reaction, according to the procedure first reported by Cadotte [131, 132]. This fabrication protocol is also referred to as interfacial polymerization (IP) due to the fact that the monomers, namely trimesoyl chloride (TMC) and m-phenylene diamine, cannot be dissolved in the same solvent. Therefore, the reaction can only take place at the interface between the two solutions. The resulting polymer chains are confined into this thin region, which yields an ultrathin layer exhibiting extremely high throughput and high ion rejection. In recent years, enormous efforts have been devoted to optimizing the reaction conditions and the monomer selection [133, 134].

Research has indicated that incomplete IP reaction results in an excess amine and TMC accumulating on the two sides of the cross-linked PA layer, which yields surfaces exhibiting opposite electrical charge. Therefore, the resulting PA membrane can be considered as a Janus membrane. This uneven electrostatic distribution along the membrane cross-section leads to the membrane behaving like a bipolar ion-exchange polymer. Repulsive interactions between the membrane and co-ions take place, which, based on the Donnan exclusion mechanism, are expected to enhance ion rejection relative to traditional PA membranes (Figure 10.8). If the top surface is positively charged, positive ions (M^{n+}) are rejected due to the Donnan exclusion, but not negative ions. Small negative ions (M^{n-}), such as monovalent anions, may penetrate the membrane, due to thermodynamic partitioning [135]. When these negative ions migrate to the bottom side of PA layers, which is negatively charged, they should be rejected again by membranes. However, as shown in Table 10.3, these Janus membranes do not exhibit significant higher ion rejections compared to commercial membranes.

The incomplete polymerization between TMC and amine generates not only asymmetrically charged interfaces, but also a PA layer exhibiting low cross-linking density. This

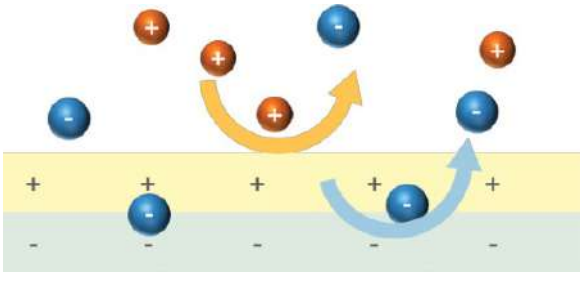

Figure 10.8 Ion rejection mechanism by a Janus polyamide (PA) membrane prepared via interfacial polymerization.

Table 10.3 Separation performance of Janus NF membranes.

Membrane	Test conditions	Pure water permeability ($L/m^2/bar/h$)	Salt rejection (%)	Ref.
Polyamide-imide hollow fiber	5 bar; 1 mM salt pH 5.75	4.9	NaCl: 85.6 $NaSO_4$: 60 $MgCl_2$: 92.2 $MgSO_4$:82.2	[136]
PA (PIP + TMC) on PVC flat-sheet	25 °C, 3.5 bar; 1000 mg/L salt (500 mg/L for NaCl)	8.7	NaCl:57.2 $NaSO_4$: 95.8 $MgCl_2$: 99.2 $MgSO_4$: 99.4 $CaCl_2$: 98.5	[137]
PA (PIP + TMC) on PVC hollow fiber, reaction at −5 °C	25 °C, 3.5 bar; 1000 mg/L salt (500 mg/L for NaCl)	16.5 15.2	$NaSO_4$: 93.2 $MgCl_2$: 97.1 $NaSO_4$: 94.3 $MgCl_2$: 98.6	[138]
PA/CNC-COOH/PES	25 °C, 8 bar; total salt: 2000 ppm with $MgCl_2$:LiCl ratio of 60:1	3.4	Li^+: 11.63 Mg^{2+}: 95.59	[139]
Janus GO	25 °C, 61 bar; 10 ppm dye	1.64×10^{-3}	100% for Ru, RB, and BB	[140]
PA (PEI + CC) on PES	10 bar; 2.0 g/L salt	3.8–10.4	$MgCl_2$: 88–94	[141]
Nadir NP030 (commercial)	40 bar	> 4	$NaSO_4$: 80–95	
GE Duracid (commercial)	15.5 bar	1.1–2.1	NaCl: 98	
GE Duracid (commercial)	25 °C,7.58 bar; 2000 ppm $MgSO_4$	1.72–1.96	$MgSO_4$: 98	[142]

PVC: poly(vinyl chloride); PIP: piperidine; CC: cyanuric chloride;
CNC-COOH: carboxylated cellulose nanocrystal; Ru: tris(2,2′-bipyridyl)dichlororuthenium(II);
RB: rhodamine B; BB: brilliant blue G

poorly cross-linked PA layer provides lower resistance to water transport, with detrimental effects on the size sieving ability. However, the charged layers enhance the repulsive interactions; therefore, the two effects seem to offset each other since, as discussed above, there is no detectable rejection change relative to commercial membranes. In contrast, water flux in all Janus membranes is up to an order of magnitude higher than in commercial membranes.

In addition to polyamide, Kim et al. reported a Janus graphene oxide (JGO)-based NF membrane, where just one side of the GO nanosheets was decorated with dodecylamine [140]. These membranes displayed almost 100% rejection for three dyes in water: tris(2,2′-bipyridyl)dichlororuthenium(II), rhodamine B, and brilliant blue G. Rejection of these

dyes was 94% in neat GO membrane [140]. Despite the great rejection, water permeance through JGO membranes reduced by 95% compared to the neat GO membrane, and it was far below that of the commercial membrane's performance (Table 10.3).

10.3.1.3.2 Membrane Distillation (MD)

In MD, a temperature gradient exists across the porous hydrophobic membrane. The feed solution contacts the hot membrane surface, where water evaporates. Following this step, water vapor diffuses through the membrane pores toward the cold permeate side, where it condenses. Species that cannot vaporize, and that can only be transported through the membrane by liquid water via the convection mechanism, such as salts, are rejected. Therefore, theoretically, only pure water can be obtained on the permeate side [130, 143–145]. The most attractive feature of MD is the ability to extract pure water from brines, which is beyond RO's range (salt concentration < 80 g/kg). Although MD has higher energy consumption than RO or NF, it only requires low-grade or waste heat, which is much cheaper than a high-grade source [130]. Hence, MD has an intrinsic advantage for treating brines in some small-scale applications, where low-grade heat is available.

To deal with these concentrated brines, which normally contain also organic compounds, MD membranes must be designed carefully. Above all, to get high water flux, low mass transport resistance and low thermal conductivity inside the membrane are needed, which requires the membrane to have high porosity and large hydrophobic pores. Therefore, porous MD membranes are generally made out of PVDF (Figure 10.9a). However, several

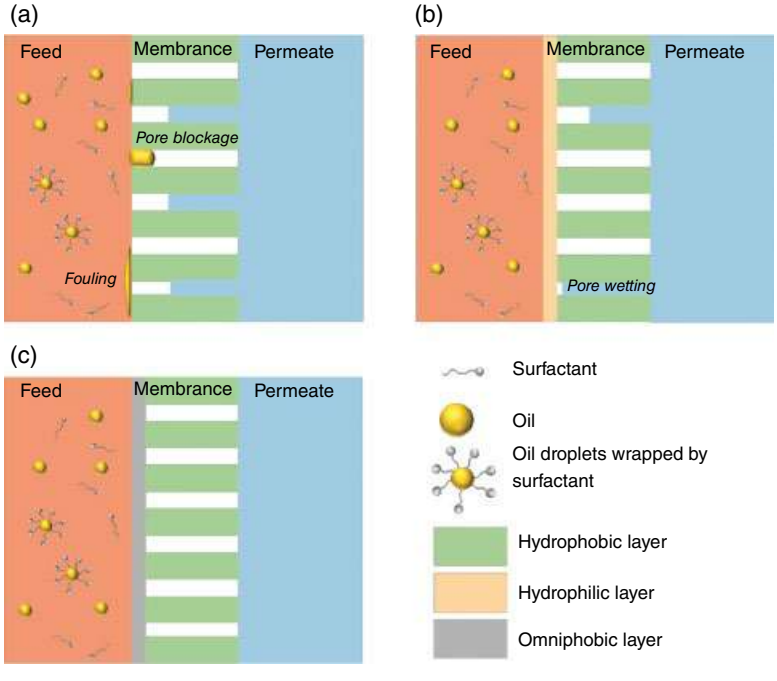

Figure 10.9 Three membranes used in MD. (a) Hydrophobic membrane, (b) Hydrophilic/hydrophobic membrane, and (c) Omniphobic/hydrophobic membrane.

major challenges have been observed in MD membranes, including fouling and pore wetting. MD membranes face liquid water on both surfaces, and pores must be free from liquid water. If the liquid water occupies the membrane pores, which is referred to as pore wetting, ions or any other solute can migrate toward the permeate side via the convection mechanism, which detriments the separation efficiency. Therefore, to mitigate the wetting issue, pores must be hydrophobic. In these conditions, however, organic compounds present in the feed are likely to create fouling issues by blocking the hydrophobic pores. Therefore, the MD membrane surface should be hydrophilic, and the pore surface should be hydrophobic. To maintain a high water flux, hydrophilic/hydrophobic Janus membranes have been fabricated (Figure 10.9b) [146, 147]. Despite their high fouling resistance, hydrophilic/hydrophobic Janus MD membranes are prone to pore wetting. More recently, to find an optimal balance between fouling and pore wetting, MD membranes exhibiting omniphobic surfaces have been considered (Figure 10.9c) [66, 143, 148, 149]. These Janus membranes have been fabricated as hollow fiber modules via phase inversion [150–155].

10.3.2 Gas Separation

Commercial gas separation membranes are fabricated by casting a nonporous active layer on porous support [156–158]; therefore, in principle, they should be considered as Janus membranes. However, asymmetric or composite membranes for gas separation exhibit Janus features at the macroscale. Conventional mixed matrix membranes (MMMs) comprising an inorganic filler embedded into a polymer matrix can also be considered as anisotropic (i.e. Janus) materials.

In the following, we will review the major issues related to conventional MMMs and discuss prospective opportunities, such as nanomembranes combining soluble-selective fillers with facilitated transport carriers.

10.3.2.1 Conventional Mixed Matrix Membranes

Analogous to water purification membranes, a selectivity-permeability trade-off constrains the performance of gas separation membranes to below an upper limit [159]. Selective permeation properties of polymer gas separation membranes are tuned by properly tailoring the membrane microstructure. Embedding porous inorganic particles in polymer matrices to fabricate MMMs is, in principle, a viable way to overcome the upper bound [2, 160, 161]. Since inorganic materials position in the upper-right side of the Robeson diagram, the resulting MMMs are expected to exhibit enhanced separation performance relative to the neat polymer. However, a major issue concerning the use of MMMs is the presence of defects at the polymer–filler interface, which adversely affects the selectivity [162, 163]. Several attempts have been made to fabricate MMMs by dispersing size-selective fillers, such as zeolites, in glassy and rubbery polymers. In most cases, the permeability enhancement was offset by a dramatic loss in selectivity due to the formation of interfacial defects. Functionalization of the zeolite surface [164], as well as the use of compatibilizers [165], while helping reduce the formation of nonselective interfacial defects, cause the zeolite's pore blockage, which thwarts the beneficial role of the filler. The use of metal–organic frameworks (MOFs) helps mitigate the

polymer/filler compatibility issue [166]. Moreover, if the organic linker is properly designed, incorporation of MOFs in polymer matrices can potentially enhance both diffusion- and sorption-selectivity. However, the high cost of MOFs makes them still commercially unattractive.

Facilitated transport is an alternative strategy to enhance the membrane selectivity via the reversible reaction between facilitated transport carriers (i.e. transition metals) and target molecules [2]. Facilitated transport membranes have been considered for CO_2 separation [167], as well as olefin-paraffin separation [168]. Although very promising, this approach suffers from several limitations, above all the instability of facilitated transport carriers, which are rapidly deactivated upon exposure to light and poisoning agents, such as H_2 and H_2S, two common natural gas contaminants. Fillers consisting of organic and inorganic compartments (i.e. Janus particles) can potentially achieve favorable polymer–filler compatibility and improve the membrane performance. However, apart from simple surface modification of the inorganic phase, altering the steric configuration of the filler can be a viable avenue to endow MMMs with a hierarchical structure and tailored transport properties.

10.3.2.2 Janus Nanomembranes for Gas Separation

In this section, we will discuss some recently reported membranes exhibiting Janus features at the nanoscale, which, in our opinion, will open a new paradigm for materials design in gas separation applications.

The recent study from Zhou et al. is one of the first attempts to exploit the Janus *leitmotif* in membrane gas separation at the nanoscale [169]. Specifically, Janus nanoparticles fabricated by chelating silver ions with dopamine were incorporated in Pebax®, a commercial block copolymer containing rigid polyamide and soft polyether segments, to fabricate MMMs for CO_2 separation. Dopamine is an organic molecule to which CO_2-facilitated transport carriers, such as silver ions, can be attached *via the chelating reaction*. The product of this reaction is Janus organic-inorganic nanoparticles, which exhibit much better compatibility with the polymer compared to neat silver nanoparticles. Remarkably, the incorporation of silver-dopamine Janus nanoparticles (20% wt) in Pebax® produced an 80% increase in CO_2/CH_4 selectivity and CO_2 permeability. However, it is not clear how silver and dopamine contribute, individually and synergistically, to CO_2-selective transport. Equally important, despite their promising performance, these materials might not be competitive from the economic point of view due to the relatively high cost of dopamine (6.6$/g).

Recently, Razavi and Galizia fabricated novel Janus nanomembranes for CO_2 separation by embedding Janus nanoparticles made of silver and Jeffamine in Pebax®. The advantage of using Jeffamine instead of dopamine comes from the fact that the former possesses ether groups, which makes Jeffamine more CO_2-phylic than dopamine. It is well known, indeed, that CO_2 interacts highly favorably with ether groups, which promotes CO_2 sorption in the membrane. Another advantage for replacing dopamine with Jeffamine is that the latter is more than one order of magnitude cheaper (0.3$/g vs. 6.6$/g). Finally, the length of Jeffamine tail (i.e. the concentration of ether groups) can be modulated, which makes the CO_2-phylicity of these materials highly and easily tailorable. As shown in Figure 10.10, MMMs containing Pebax® and 5% wt silver-Jeffamine Janus nanoparticles exhibits a CO_2

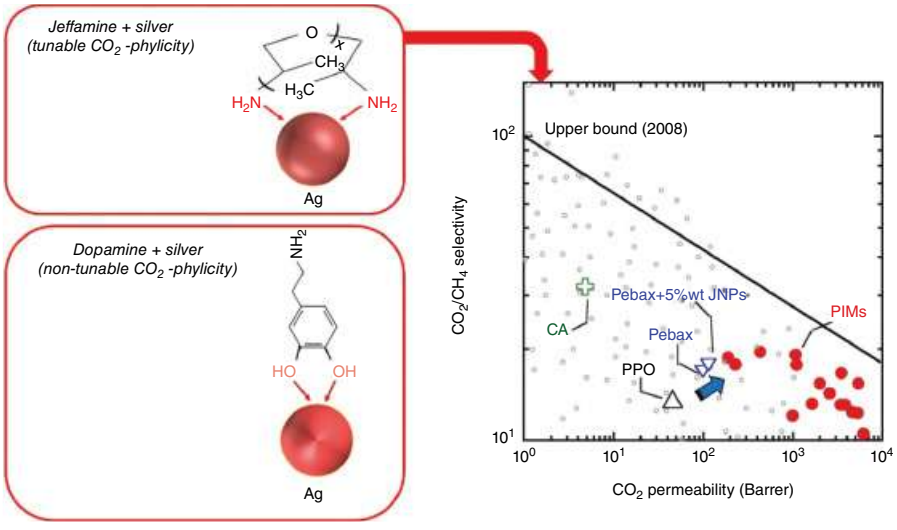

Figure 10.10 CO_2/CH_4 separation performance of Janus nanomembranes based on Pebax® and Jeffamine-silver Janus nanoparticles. Data was obtained at 10 atm and 35 °C [170].

permeability and CO_2/CH_4 selectivity exceeding by 20 and 6%, respectively, those of neat Pebax® membrane at 35 °C and 10 atm.

We believe that the approaches recently proposed by Zhou et al. and Galizia et al. to synthesize molecularly tuned Janus membranes will open the door to exciting opportunities to manipulate sorption-selectivity and diffusion-selectivity by embedding Janus-modified facilitated transport carriers in polymers. Equally important, other than CO_2 separation, such materials could also benefit other applications, such as olefin-paraffin separation, which is one of the most energy-intensive.

10.4 Conclusions

The fabrication, properties, and performance of Janus membranes for water purification and gas separation have been reviewed, and prospective opportunities were outlined. Due to their extremely high surface–to–volume ratio, performance and lifetime of membranes can be conveniently enhanced by manipulating surface properties, using principles and methods of surface science. This approach has been used to engineer porous membranes for UF and MF applications, but is still in its infancy in RO, FO, and NF applications, where nonporous membranes are used. For example, the Janus *leitmotif* has been extensively exploited to fabricate water purification membranes exhibiting enhanced water flux and ion rejection. In more recent years, the Janus approach has also been utilized to fabricate smart water purification membranes possessing sophisticated structural features and properties, such as improved fouling resistance and switchable transport properties.

Conventionally supported gas separation membranes, as well as MMMs, can also be considered as Janus membranes. However, apart from these structural features, the Janus

leitmotif has been rarely used to tailor the transport properties of gas separation membranes at the nanoscale despite some interesting results reported recently. Therefore, we believe this could be an area worth of investigation in the coming years.

Acknowledgments

Financial support from the US National Science Foundation (NSF-CBET), Grant 2005282, is gratefully acknowledged. The authors thank Mrs. Jordan Vetal and Mr. Ryan Crist for their assistance in performing experimental measurements on Pebax® and Jeffamine-silver Janus nanoparticle membranes.

References

1 Sholl, D.S. and Lively, R.P. (2016). Seven chemical separations to change the world. *Nature* 532 (7600): 435–437.
2 Galizia, M., Chi, W.S., Smith, Z.P. et al. (2017). 50th anniversary perspective: polymers and mixed matrix membranes for gas and vapor separation: a review and prospective opportunities. *Macromolecules* 50 (20): 7809–7843.
3 Geise, G.M., Lee, H.-S., Miller, D.J. et al. (2010). Water purification by membranes: the role of polymer science. *Journal of Polymer Science Part B: Polymer Physics* 48 (15): 1685–1718.
4 Werber, J.R., Osuji, C.O., and Elimelech, M. (2016). Materials for next-generation desalination and water purification membranes. *Nature Reviews Materials* 1 (5): 1–15.
5 Landsman, M.R., Sujanani, R., Brodfuehrer, S.H. et al. (2020). Water treatment: are membranes the Panacea? *Annual Review of Chemical and Biomolecular Engineering* 11 (1): 559–585.
6 Paul, D.R. (2004). Reformulation of the solution-diffusion theory of reverse osmosis. *Journal of Membrane Science* 241 (2): 371–386.
7 Robeson, L.M. (1991). Correlation of separation factor versus permeability for polymeric membranes. *Journal of Membrane Science* 62 (2): 165–185.
8 Geise, G.M., Park, H.B., Sagle, A.C. et al. (2011). Water permeability and water/salt selectivity tradeoff in polymers for desalination. *Journal of Membrane Science* 369 (1): 130–138.
9 Moon, J.D., Freeman, B.D., Hawker, C.J., and Segalman, R.A. (2020). Can self-assembly address the permeability/selectivity trade-offs in polymer membranes? *Macromolecules* 53 (14): 5649–5654.
10 Wagh, P. and Escobar, I.C. (2019). Biomimetic and bioinspired membranes for water purification: a critical review and future directions. *Environmental Progress & Sustainable Energy* 38 (3): e13215.
11 Yang, H.C., Hou, J., Chen, V., and Xu, Z.K. (2016). Janus membranes: exploring duality for advanced separation. *Angewandte Chemie International Edition English* 55 (43): 13398–13407.
12 Bouju, X., Duguet, É., Gauffre, F. et al. (2018). Nonisotropic self-assembly of nanoparticles: from compact packing to functional aggregates. *Advanced Materials* 30 (27): 1706558.

13 Furst, E.M. (2011). Directing colloidal assembly at fluid interfaces. *Proceedings of the National Academy of Sciences* 108 (52): 20853–20854.

14 Hynninen, A.-P., Thijssen, J.H.J., Vermolen, E.C.M. et al. (2007). Self-assembly route for photonic crystals with a bandgap in the visible region. *Nature Materials* 6 (3): 202–205.

15 Månsson, L.K., Peng, F., Crassous, J.J., and Schurtenberger, P. (2020). A microgel-Pickering emulsion route to colloidal molecules with temperature-tunable interaction sites. *Soft Matter* 16 (7): 1908–1921.

16 Vogel, N., Retsch, M., Fustin, C.-A. et al. (2015). Advances in colloidal assembly: the design of structure and hierarchy in two and three dimensions. *Chemical Reviews* 115 (13): 6265–6311.

17 Shah, A.A., Schultz, B., Zhang, W. et al. (2015). Actuation of shape-memory colloidal fibres of Janus ellipsoids. *Nature Materials* 14 (1): 117–124.

18 Forster, J.D., Park, J.-G., Mittal, M. et al. (2011). Assembly of optical-scale dumbbells into dense photonic crystals. *ACS Nano* 5 (8): 6695–6700.

19 Razavi, S., Hernandez, L.M., Read, A. et al. (2020). Surface tension anomaly observed for chemically-modified Janus particles at the air/water interface. *Journal of Colloid and Interface Science* 558: 95–99.

20 Razavi, S., Lin, B., Lee, K.Y.C. et al. (2019). Impact of surface amphiphilicity on the interfacial behavior of janus particle layers under compression. *Langmuir* 35 (48): 15813–15824.

21 Mirkin, C.A., Letsinger, R.L., Mucic, R.C., and Storhoff, J.J. (1996). A DNA-based method for rationally assembling nanoparticles into macroscopic materials. *Nature* 382 (6592): 607–609.

22 Glotzer, S.C. and Solomon, M.J. (2007). Anisotropy of building blocks and their assembly into complex structures. *Nature Materials* 6 (8): 557–562.

23 Pawar, A.B. and Kretzschmar, I. (2008). Patchy particles by glancing angle deposition. *Langmuir* 24 (2): 355–358.

24 Roh, K.-H., Martin, D.C., and Lahann, J. (2005). Biphasic Janus particles with nanoscale anisotropy. *Nature Materials* 4 (10): 759–763.

25 Mahynski, N.A., Rovigatti, L., Likos, C.N., and Panagiotopoulos, A.Z. (2016). Bottom-up colloidal crystal assembly with a twist. *ACS Nano* 10 (5): 5459–5467.

26 Solomon, M.J. (2018). Tools and functions of reconfigurable colloidal assembly. *Langmuir* 34 (38): 11205–11219.

27 Casagrande, C., Fabre, P., Raphaël, E., and Veyssié, M. (1989). "Janus Beads": realization and behaviour at water/oil interfaces. *Europhysics Letters (EPL)* 9 (3): 251–255.

28 De Gennes, P.-G. (1991). Soft Matter (Nobel Lecture).

29 Bradley, L.C., Stebe, K.J., and Lee, D. (2016). Clickable Janus particles. *Journal of the American Chemical Society* 138 (36): 11437–11440.

30 Hou, Y., Li, Y., Wang, L. et al. (2019). Amphiphilic Janus particles for efficient dispersion of oil contaminants in seawater. *Journal of Colloid and Interface Science* 556: 54–64.

31 Wang, H., Yang, X., Fu, Z. et al. (2017). Rheology of nanosilica-compatibilized immiscible polymer blends: formation of a "heterogeneous network" facilitated by interfacially anchored hybrid nanosilica. *Macromolecules* 50 (23): 9494–9506.

32 Yang, L., Wang, T., Yang, X. et al. (2019). Highly stabilized foam by adding amphiphilic Janus particles for drilling a high-temperature and high-calcium geothermal well. *Industrial & Engineering Chemistry Research* 58 (23): 9795–9805.

33 Yao, X., Zhao, G., Dai, C. et al. (2020). Interfacial characteristics and the stability mechanism of a dispersed particle gel (DPG) three-phase foam. *Journal of Molecular Liquids* 301: 112425.

34 Pawar, A.B. and Kretzschmar, I. (2010). Fabrication, assembly, and application of patchy particles. *Macromolecular Rapid Communications* 31 (2): 150–168.

35 Zhang, J., Grzybowski, B.A., and Granick, S. (2017). Janus particle synthesis, assembly, and application. *Langmuir* 33 (28): 6964–6977.

36 Ma, X., Hahn, K., and Sanchez, S. (2015). Catalytic mesoporous Janus nanomotors for active cargo delivery. *Journal of the American Chemical Society* 137 (15): 4976–4979.

37 Pourrahimi, A.M. and Pumera, M. (2018). Multifunctional and self-propelled spherical Janus nano/micromotors: recent advances. *Nanoscale* 10 (35): 16398–16415.

38 Jalilvand, Z., Haider, H., and Cui, J. (2020). Kretzschmar, Ilona. Pt-SiO_2 Janus particles and the water/oil interface: a competition between motility and thermodynamics. *Langmuir* 36 (25): 6880–6887.

39 Das, S., Garg, A., Campbell, A.I. et al. (2015). Boundaries can steer active Janus spheres. *Nature Communications* 6 (1): 8999.

40 Paxton, W.F., Kistler, K.C., Olmeda, C.C. et al. (2004). Catalytic nanomotors: autonomous movement of striped nanorods. *Journal of the American Chemical Society* 126 (41): 13424–13431.

41 Yi, Y., Sanchez, L., Gao, Y., and Yu, Y. (2016). Janus particles for biological imaging and sensing. *Analyst* 141 (12): 3526–3539.

42 Xing, Y., Zhou, Y., Fan, L. et al. (2019). Construction strategy for ratiometric fluorescent probe based on Janus silica nanoparticles as a platform toward intracellular pH detection. *Talanta* 205: 120021.

43 Rahmani, S., Villa, C.H., Dishman, A.F. et al. (2015). Long-circulating Janus nanoparticles made by electrohydrodynamic co-jetting for systemic drug delivery applications. *Journal of Drug Targeting* 23: 750–758.

44 Xie, H., She, Z.-G., Wang, S. et al. (2012). One-step fabrication of polymeric Janus nanoparticles for drug delivery. *Langmuir* 28 (9): 4459–4463.

45 Mulder, J. (1996). *Basic Principles of Membrane Technology*. Netherlands: Springer.

46 Nunes, S.P. (2020). Can fouling in membranes be ever defeated? *Current Opinion in Chemical Engineering* 28: 90–95.

47 Zhang, R., Liu, Y., He, M. et al. (2016). Antifouling membranes for sustainable water purification: strategies and mechanisms. *Chemical Society Reviews* 45 (21): 5888–5924.

48 Bye, K.P. and Galizia, M. (2020). Fundamental origin of flux non-linearity in organic solvent nanofiltration: formulation of a thermodynamic/diffusion framework. *Journal of Membrane Science* 603: 118020.

49 Miller, D.J., Dreyer, D.R., Bielawski, C.W. et al. (2017). Surface modification of water purification membranes. *Angewandte Chemie International Edition* 56 (17): 4662–4711.

50 Fakhru'l-Razi, A. et al. (2009). Review of technologies for oil and gas produced water treatment. *Journal of hazardous materials* 170 (2–3): 530–51.

51 Chen, C., Weng, D., Mahmood, A. et al. (2019). Separation mechanism and construction of surfaces with special wettability for oil/water separation. *ACS Applied Materials & Interfaces* 11 (11): 11006–11027.

52 Kwon, G., Post, E., and Tuteja, A. (2015). Membranes with selective wettability for the separation of oil-water mixtures. *MRS Communications* 5 (3): 475.

53 Bhushan, B. and Jung, Y.C. (2011). Natural and biomimetic artificial surfaces for superhydrophobicity, self-cleaning, low adhesion, and drag reduction. *Progress in Materials Science* 56 (1): 1–108.

54 Wenzel, R.N. (1936). Resistance of solid surfaces to wetting by water. *Industrial & Engineering Chemistry* 28 (8): 988–994.

55 Cassie, A. and Baxter, S. (1944). Wettability of porous surfaces. *Transactions of the Faraday Society* 40: 546–551.

56 Liu, M., Wang, S., and Jiang, L. (2017). Nature-inspired superwettability systems. *Nature Reviews Materials* 2 (7): 17036.

57 Drelich, J. and Chibowski, E. (2010). Superhydrophilic and superwetting surfaces: definition and mechanisms of control. *Langmuir* 26 (24): 18621–18623.

58 Mayer, R.P. and Stowe, R.A. (1965). Mercury porosimetry—breakthrough pressure for penetration between packed spheres. *Journal of Colloid Science* 20 (8): 893–911.

59 Youngblood, J.P. and McCarthy, T.J. (1999). Ultrahydrophobic polymer surfaces prepared by simultaneous ablation of polypropylene and sputtering of poly(tetrafluoroethylene) using radio frequency plasma. *Macromolecules* 32 (20): 6800–6806.

60 Rahimpour, M.R. and Esmaeilbeig, M.A. (2019). Chapter 6 - Membrane wetting in membrane distillation. In: *Current Trends and Future Developments on (Bio-) Membranes* (eds. A. Basile, E. Curcio and Inamuddin), 143–174. Elsevier.

61 Ahmad, N.A., Goh, P.S., Abdul Karim, Z., and Ismail, A.F. (2018). Thin film composite membrane for oily waste water treatment: recent advances and challenges. *Membranes* 8 (4): 86.

62 Ge, M., Cao, C., Huang, J. et al. (2018). Rational design of materials interface at nanoscale towards intelligent oil–water separation. *Nanoscale Horizons* 3 (3): 235–260.

63 Frising, T., Noïk, C., and Dalmazzone, C. (2006). The liquid/liquid sedimentation process: from droplet coalescence to technologically enhanced water/oil emulsion gravity separators: a review. *Journal of Dispersion Science and Technology* 27 (7): 1035–1057.

64 Benes, K., Tong, P., and Ackerson, B.J. (2007). Sedimentation, Péclet number, and hydrodynamic screening. *Physical Review E* 76 (5): 056302.

65 Emulsion formation, stability, and rheology. Emulsion Formation and Stability. p. 1–75.

66 Lin, S., Nejati, S., Boo, C. et al. (2014). Omniphobic membrane for robust membrane distillation. *Environmental Science & Technology Letters* 1 (11): 443–447.

67 Pan, Z., Shahsavan, H., Zhang, W. et al. (2015). Superhydro-oleophobic bio-inspired polydimethylsiloxane micropillared surface via FDTS coating/blending approaches. *Applied Surface Science* 324: 612–620.

68 Kawakatsu, T., Boom, R.M., Nabetani, H. et al. (1999). Emulsion breakdown: mechanisms and development of multilayer membrane. *AlChE Journal* 45 (5): 967–975.

69 Mino, Y., Kagawa, Y., Ishigami, T., and Matsuyama, H. (2016). Numerical simulation of coalescence phenomena of oil-in-water emulsions permeating through straight membrane pore. *Colloids and Surfaces A: Physicochemical and Engineering Aspects* 491: 70–77.

70 Agarwal, S., von Arnim, V., Stegmaier, T. et al. (2013). Effect of fibrous coalescer geometry and operating conditions on emulsion separation. *Industrial & Engineering Chemistry Research* 52 (36): 13164–13170.

71 Hu, D., Li, X., Li, L., and Yang, C. (2015). Designing high-caliber nonwoven filter mats for coalescence filtration of oil/water emulsions. *Separation and Purification Technology* 149: 65–73.

72 Hu, D., Li, L., Li, Y., and Yang, C. (2016). Fibrous coalescer for the treatment of hydrometallurgical oil dispersions. *Industrial & Engineering Chemistry Research* 55 (45): 11809–11817.

73 Kukizaki, M. and Goto, M. (2008). Demulsification of water-in-oil emulsions by permeation through Shirasu-porous-glass (SPG) membranes. *Journal of Membrane Science* 322 (1): 196–203.

74 Kocherginsky, N.M., Tan, C.L., and Lu, W.F. (2003). Demulsification of water-in-oil emulsions via filtration through a hydrophilic polymer membrane. *Journal of Membrane Science* 220 (1): 117–128.

75 Wang, Z., Wang, Y., and Liu, G. (2016). Rapid and efficient separation of oil from oil-in-water emulsions using a Janus cotton fabric. *Angewandte Chemie* 128 (4): 1313–1316.

76 Yang, J., Li, H.-N., Chen, Z.-X. et al. (2019). Janus membranes with controllable asymmetric configurations for highly efficient separation of oil-in-water emulsions. *Journal of Materials Chemistry A* 7 (13): 7907–7917.

77 An, Y.P., Yang, J., Yang, H.C. et al. (2018). Janus membranes with charged carbon nanotube coatings for deemulsification and separation of oil-in-water emulsions. *ACS Applied Materials & Interfaces* 10 (11): 9832–9840.

78 Wang, Z.J., Lehtinen, M., and Liu, G.J. (2017). Universal Janus filters for the rapid separation of oil from emulsions stabilized by ionic or nonionic surfactants. *Angewandte Chemie International Edition* 56 (42): 12892–12897.

79 Wang, Z., Song, S., Yang, J. et al. (2020). Controllable Janus porous membrane with liquids manipulation for diverse intelligent energy-free applications. *Journal of Membrane Science* 601: 117954.

80 Zhu, Y., Xie, W., Zhang, F. et al. (2017). Superhydrophilic In-Situ-cross-linked zwitterionic polyelectrolyte/PVDF-blend membrane for highly efficient oil/water emulsion separation. *ACS Applied Materials and Interfaces* 9 (11): 9603–9613.

81 Howarter, J.A. and Youngblood, J.P. (2009). Amphiphile grafted membranes for the separation of oil-in-water dispersions. *Journal of Colloid and Interface Science* 329 (1): 127–132.

82 Tirmizi, N.P., Raghuraman, B., and Wiencek, J. (1996). Demulsification of water/oil/solid emulsions by hollow-fiber membranes. *AlChE Journal* 42 (5): 1263–1276.

83 Li, Y., Cao, L., Hu, D., and Yang, C. (2017). Uncommon wetting on a special coating and its relevance to coalescence separation of emulsified water from diesel fuel. *Separation and Purification Technology* 176: 313–322.

84 Li, H.N., Yang, J., and Xu, Z.K. (2020). Asymmetric surface engineering for Janus membranes. *Advanced Materials Interfaces* 7 (7): 1902064.

85 Li, T., Liu, F., Zhang, S. et al. (2018). Janus polyvinylidene fluoride membrane with extremely opposite wetting surfaces via one single-step unidirectional segregation strategy. *ACS Applied Materials and Interfaces* 10 (29): 24947–24954.

86 Song, H.-M., Chen, C., Shui, X.-X. et al. (2019). Asymmetric Janus membranes based on in situ mussel-inspired chemistry for efficient oil/water separation. *Journal of Membrane Science* 573: 126–134.

87 Pornea, A.M., Puguan, J.M.C., Deonikar, V.G., and Kim, H. (2020). Robust Janus nanocomposite membrane with opposing surface wettability for selective oil-water separation. *Separation and Purification Technology* 236: 116297.

88 Liang, Y., Kim, S., Kallem, P., and Choi, H. (2019). Capillary effect in Janus electrospun nanofiber membrane for oil/water emulsion separation. *Chemosphere* 221: 479–485.

89 Bae, J., Kim, H., Kim, K.S., and Choi, H. (2018). Effect of asymmetric wettability in nanofiber membrane by electrospinning technique on separation of oil/water emulsion. *Chemosphere* 204: 235–242.

90 Ge, J., Zhang, J., Wang, F. et al. (2017). Superhydrophilic and underwater superoleophobic nanofibrous membrane with hierarchical structured skin for effective oil-in-water emulsion separation. *Journal of Materials Chemistry A* 5 (2): 497–502.

91 Ding, D., Mao, H., Chen, X. et al. (2018). Underwater superoleophobic-underoil superhydrophobic Janus ceramic membrane with its switchable separation in oil/water emulsions. *Journal of Membrane Science* 565: 303–310.

92 Wu, M.B., Yang, H.C., Wang, J.J. et al. (2017). Janus membranes with opposing surface wettability enabling oil-to-water and water-to-oil emulsification. *ACS Applied Materials and Interfaces* 9 (6): 5062–5066.

93 Liu, Y., Qu, R., Zhang, W. et al. (2019). Lotus- and mussel-inspired PDA-PET/PTFE Janus membrane: toward integrated separation of light and heavy oils from water. *ACS Applied Materials and Interfaces* 11 (22): 20545–20556.

94 Lin, Y., Salem, M.S., Zhang, L. et al. (2020). Development of functionalized supwerwettable Janus membrane with controllable asymmetric wettability for highly-efficient oil/water emulsions separation. *Journal of Membrane Science* 606: 118141.

95 Lin, Y., Salem, M.S., Zhang, L. et al. (2020). Development of Janus membrane with controllable asymmetric wettability for highly-efficient oil/water emulsions separation. *Journal of Membrane Science* 606: 118141.

96 Cai, Y., Chen, D., Li, N. et al. (2018). A smart membrane with antifouling capability and switchable oil wettability for high-efficiency oil/water emulsions separation. *Journal of Membrane Science* 555: 69–77.

97 Yang, C., Han, N., Han, C. et al. (2019). Design of a Janus F-TiO_2@PPS porous membrane with asymmetric wettability for switchable oil/water separation. *ACS Applied Materials and Interfaces* 11 (25): 22408–22418.

98 Zuo, J.-H., Gu, Y.-H., Wei, C. et al. (2020). Janus polyvinylidene fluoride membranes fabricated with thermally induced phase separation and spray-coating technique for the separations of both W/O and O/W emulsions. *Journal of Membrane Science* 595: 117475.

99 Zhang, W., Li, X., Qu, R. et al. (2019). Janus membrane decorated via a versatile immersion-spray route: controllable stabilized oil/water emulsion separation satisfying industrial emission and purification criteria. *Journal of Materials Chemistry A* 7 (9): 4941–4949.

100 Gupta, R.K., Dunderdale, G.J., England, M.W., and Hozumi, A. (2017). Oil/water separation techniques: a review of recent progresses and future directions. *Journal of Materials Chemistry A* 5 (31): 16025–16058.

101 Jiang, Y., Hou, J., Xu, J., and Shan, B. (2017). Switchable oil/water separation with efficient and robust Janus nanofiber membranes. *Carbon* 115: 477–485.

102 Ranganath, A.S. and Baji, A. (2018). Electrospun Janus membrane for efficient and switchable oil–water separation. *Macromolecular Materials and Engineering* 303 (11): 1800272.

103 Li, X., Zhang, W., Qu, R. et al. (2019). Asymmetric superwetting configuration of Janus membranes based on thiol–ene clickable silane nanospheres enabling on-demand and energy-efficient oil–water remediation. *Journal of Materials Chemistry A* 7 (16): 10047–10057.

104 Gu, J., Xiao, P., Chen, J. et al. (2014). Janus polymer/carbon nanotube hybrid membranes for oil/water separation. *ACS Applied Materials and Interfaces* 6 (18): 16204–16209.

105 Lv, Y., Li, Q., Hou, Y. et al. (2019). Facile preparation of an asymmetric wettability Janus cellulose membrane for switchable emulsions' separation and antibacterial property. *ACS Sustainable Chemistry & Engineering* 7 (17): 15002–15011.

106 Yue, X., Zhang, T., Yang, D. et al. (2018). Janus ZnO-cellulose/MnO_2 hybrid membranes with asymmetric wettability for highly-efficient emulsion separations. *Cellulose* 25 (10): 5951–5965.

107 Zhou, H. and Guo, Z. (2019). Superwetting Janus membranes: focusing on unidirectional transport behaviors and multiple applications. *Journal of Materials Chemistry A* 7 (21): 12921–12950.

108 Yan, L., Yang, X., Long, J. et al. (2020). Universal unilateral electro-spinning/spraying strategy to construct water-unidirectional Janus membranes with well-tuned hierarchical micro/nanostructures. *Chemical Communications* 56 (3): 478–481.

109 Li, H.-N., Yang, J., and Xu, Z.-K. (2020). Hollow fiber membranes with Janus surfaces for continuous deemulsification and separation of oil-in-water emulsions. *Journal of Membrane Science* 602: 117964.

110 Wang, H., Zhou, H., Yang, W. et al. (2015). Selective, spontaneous one-way oil-transport fabrics and their novel use for gauging liquid surface tension. *ACS Applied Materials and Interfaces* 7 (41): 22874–22880.

111 Yang, X., Wang, Z., and Shao, L. (2018). Construction of oil-unidirectional membrane for integrated oil collection with lossless transportation and oil-in-water emulsion purification. *Journal of Membrane Science* 549: 67–74.

112 Wu, J., Wang, N., Wang, L. et al. (2012). Unidirectional water-penetration composite fibrous film via electrospinning. *Soft Matter* 8 (22): 5996–5999.

113 Wang, Z., Wang, Y., and Liu, G. (2016). Rapid and efficient separation of oil from oil-in-water emulsions using a Janus cotton fabric. *Angewandte Chemie* 55 (4): 1291–1294.

114 Tian, X., Jin, H., Sainio, J. et al. (2014). Droplet and fluid gating by biomimetic Janus membranes. *Advanced Functional Materials* 24 (38): 6023–6028.

115 Yin, K., Yang, S., Dong, X. et al. (2018). Ultrafast achievement of a superhydrophilic/hydrophobic Janus foam by femtosecond laser ablation for directional water transport and efficient fog harvesting. *ACS Applied Materials and Interfaces* 10 (37): 31433–31440.

116 Cheng, Z., Wang, B., Lai, H. et al. (2017). Janus copper mesh film with unidirectional water transportation ability toward high efficiency oil/water separation. *Chemistry – An Asian Journal* 12 (16): 2085–2092.

117 Yang, X., Yan, L., Ran, F. et al. (2019). Interface-confined surface engineering constructing water-unidirectional Janus membrane. *Journal of Membrane Science* 576: 9–16.

118 Gao, Y., Qin, J., Wang, Z., and Østerhus, S.W. (2019). Backpulsing technology applied in MF and UF processes for membrane fouling mitigation: a review. *Journal of Membrane Science* 587: 117136.

119 Hilal, N., Ogunbiyi, O.O., Miles, N.J., and Nigmatullin, R. (2005). Methods employed for control of fouling in MF and UF membranes: a comprehensive review. *Separation Science and Technology* 40 (10): 1957–2005.

120 Revanur, R., McCloskey, B., Breitenkamp, K. et al. (2007). Reactive amphiphilic graft copolymer coatings applied to poly(vinylidene fluoride) ultrafiltration membranes. *Macromolecules* 40 (10): 3624–3630.

121 Kirschner, A.Y., Chang, C.-C., Kasemset, S. et al. (2017). Fouling-resistant ultrafiltration membranes prepared via co-deposition of dopamine/zwitterion composite coatings. *Journal of Membrane Science* 541: 300–311.

122 Gore, P.M. and Kandasubramanian, B. (2018). Heterogeneous wettable cotton based superhydrophobic Janus biofabric engineered with PLA/functionalized-organoclay microfibers for efficient oil–water separation. *Journal of Materials Chemistry A* 6 (17): 7457–7479.

123 Zhou, S., Xiong, Z., Liu, F. et al. (2019). Novel Janus membrane with unprecedented osmosis transport performance. *Journal of Materials Chemistry A* 7 (2): 632–638.

124 Zhou, S., Liu, F., Wang, J. et al. (2019). Janus membrane with unparalleled forward osmosis performance. *Environmental Science & Technology Letters* 6 (2): 79–85.

125 Wang, X.-p., Hou, J., Chen, F.–s., and Meng, X.–m. (2020). In-situ growth of metal-organic framework film on a polydopamine-modified flexible substrate for antibacterial and forward osmosis membranes. *Separation and Purification Technology* 236: 116239.

126 Zhang, H., Zhao, M., and Lin, Y.S. (2019). Stability of ZIF-8 in water under ambient conditions. *Microporous and Mesoporous Materials* 279: 201–210.

127 Taheri, M., Enge, T.G., and Tsuzuki, T. (2020). Water stability of cobalt doped ZIF-8: a quantitative study using optical analyses. *Materials Today Chemistry* 16: 100231.

128 Alihemati, Z., Hashemifard, S.A., Matsuura, T. et al. (2020). Current status and challenges of fabricating thin film composite forward osmosis membrane: a comprehensive roadmap. *Desalination* 491: 114557.

129 Tow, E.W., Warsinger, D.M., Trueworthy, A.M. et al. (2018). Comparison of fouling propensity between reverse osmosis, forward osmosis, and membrane distillation. *Journal of Membrane Science* 556: 352–364.

130 Deshmukh, A., Boo, C., Karanikola, V. et al. (2018). Membrane distillation at the water-energy nexus: limits, opportunities, and challenges. *Energy & Environmental Science* 11 (5): 1177–1196.

131 Cadotte, J.E. (1985). Evolution of composite reverse osmosis membranes. In: *Materials Science of Synthetic Membrances* (ed. D.R. Lloyd), 269. ACS Publications.

132 Larson, R.E., Cadotte, J.E., and Petersen, R.J. (1981). The FT-30 seawater reverse osmosis membrane--element test results. *Desalination* 38: 473–483.

133 Paul, M. and Jons, S.D. (2016). Chemistry and fabrication of polymeric nanofiltration membranes: a review. *Polymer* 103: 417–456.

134 Lau, W.-J. and Ismail, A.F. (2009). Polymeric nanofiltration membranes for textile dye wastewater treatment: preparation, performance evaluation, transport modelling, and fouling control — a review. *Desalination* 245 (1): 321–348.

135 Galizia, M., Manning, G.S., Paul, D.R., and Freeman, B.D. (2019). Ion partitioning between brines and ion exchange polymers. *Polymer* 165: 91–100.

136 Sun, S.P., Hatton, T.A., Chan, S.Y., and Chung, T.-S. (2012). Novel thin-film composite nanofiltration hollow fiber membranes with double repulsion for effective removal of emerging organic matters from water. *Journal of Membrane Science* 401-402: 152–162.

137 Wu, C., Liu, S., Wang, Z. et al. (2016). Nanofiltration membranes with dually charged composite layer exhibiting super-high multivalent-salt rejection. *Journal of Membrane Science* 517: 64–72.

138 Liu, S., Wu, C., Hung, W.-S. et al. (2017). One-step constructed ultrathin Janus polyamide nanofilms with opposite charges for highly efficient nanofiltration. *Journal of Materials Chemistry A* 5 (44): 22988–22996.

139 Guo, C., Li, N., Qian, X. et al. (2020). Ultra-thin double Janus nanofiltration membrane for separation of Li+ and Mg2+: "Drag" effect from carboxyl-containing negative interlayer. *Separation and Purification Technology* 230: 115567.

140 Akbari, M., Shariaty-Niassar, M., Matsuura, T., and Ismail, A.F. (2018). Janus graphene oxide nanosheet: a promising additive for enhancement of polymeric membranes performance prepared via phase inversion. *Journal of Colloid and Interface Science* 527: 10–24.

141 Yu, L., Zhang, Y., Xu, L. et al. (2020). One step prepared Janus acid-resistant nanofiltration membranes with opposite surface charges for acidic wastewater treatment. *Separation and Purification Technology* 250: 117245.

142 Treatment, L.W. Duracid Series - Industrial Acid Stable Nanofiltration Elements [updated 2020/10]. https://www.lenntech.com/Data-sheets/GE-Osmonics-Duracid-Series-L.pdf (accessed 20 October 2020).

143 Lu, K.J., Chen, Y., and Chung, T.-S. (2019). Design of omniphobic interfaces for membrane distillation – a review. *Water Research* 162: 64–77.

144 Wang, P. and Chung, T.-S. (2015). Recent advances in membrane distillation processes: membrane development, configuration design and application exploring. *Journal of Membrane Science* 474: 39–56.

145 Yao, M., Tijing, L.D., Naidu, G. et al. (2020). A review of membrane wettability for the treatment of saline water deploying membrane distillation. *Desalination* 479: 114312.

146 Wang, K., Hou, D., Qi, P. et al. (2019). Development of a composite membrane with underwater-oleophobic fibrous surface for robust anti-oil-fouling membrane distillation. *Journal of Colloid and Interface Science* 537: 375–383.

147 Zuo, G. and Wang, R. (2013). Novel membrane surface modification to enhance anti-oil fouling property for membrane distillation application. *Journal of Membrane Science* 447: 26–35.

148 Wu, X.-Q., Wu, X., Wang, T.-Y. et al. (2020). Omniphobic surface modification of electrospun nanofiber membrane via vapor deposition for enhanced anti-wetting property in membrane distillation. *Journal of Membrane Science* 606: 118075.

149 Wang, W., Du, X., Vahabi, H. et al. (2019). Trade-off in membrane distillation with monolithic omniphobic membranes. *Nature Communications* 10 (1): 3220.

150 Li, B. and Sirkar, K.K. (2004). Novel membrane and device for direct contact membrane distillation-based desalination process. *Industrial & Engineering Chemistry Research* 43 (17): 5300–5309.

151 Edwie, F., Teoh, M.M., and Chung, T.-S. (2012). Effects of additives on dual-layer hydrophobic–hydrophilic PVDF hollow fiber membranes for membrane distillation and continuous performance. *Chemical Engineering Science* 68 (1): 567–578.

152 Lu, K.-J., Zuo, J., and Chung, T.-S. (2016). Tri-bore PVDF hollow fibers with a super-hydrophobic coating for membrane distillation. *Journal of Membrane Science* 514: 165–175.

153 Chew, N.G.P., Zhao, S., Malde, C., and Wang, R. (2018). Polyvinylidene fluoride membrane modification via oxidant-induced dopamine polymerization for sustainable direct-contact membrane distillation. *Journal of Membrane Science* 563: 31–42.

154 Lu, K.J., Zuo, J., Chang, J. et al. (2018). Omniphobic hollow-fiber membranes for vacuum membrane distillation. *Environmental Science & Technology* 52 (7): 4472–4480.

155 Zou, L., Gusnawan, P., Zhang, G., and Yu, J. (2020). Novel Janus composite hollow fiber membrane-based direct contact membrane distillation (DCMD) process for produced water desalination. *Journal of Membrane Science* 597: 117756.

156 Dai, Z., Ansaloni, L., and Deng, L. (2016). Recent advances in multi-layer composite polymeric membranes for CO_2 separation: a review. *Green Energy & Environment* 1 (2): 102–128.

157 Baker, R.W. and Low, B.T. (2014). Gas separation membrane materials: a perspective. *Macromolecules* 47 (20): 6999–7013.

158 Baker, R.W. (2004). *Membrane Technology and Applications. mta*, 552. England: Wiley.

159 Robeson, L.M. (2008). The upper bound revisited. *Journal of Membrane Science* 320 (1): 390–400.

160 Park, H.B., Kamcev, J., Robeson, L.M. et al. (2017). Maximizing the right stuff: the trade-off between membrane permeability and selectivity. *Science* 356 (6343): eaab0530.

161 Wang, Y., Wang, X., Guan, J. et al. (2019). 110th anniversary: mixed matrix membranes with fillers of intrinsic nanopores for gas separation. *Industrial & Engineering Chemistry Research* 58 (19): 7706–7724.

162 Mahajan, R. and Koros, W.J. (2000). Factors controlling successful formation of mixed-matrix gas separation materials. *Industrial & Engineering Chemistry Research* 39 (8): 2692–2696.

163 Moore, T.T. and Koros, W.J. (2005). Non-ideal effects in organic–inorganic materials for gas separation membranes. *Journal of Molecular Structure* 739 (1): 87–98.

164 Li, Y., Guan, H.-M., Chung, T.-S., and Kulprathipanja, S. (2006). Effects of novel silane modification of zeolite surface on polymer chain rigidification and partial pore blockage in polyethersulfone (PES)–zeolite A mixed matrix membranes. *Journal of Membrane Science* 275 (1): 17–28.

165 Hudiono, Y.C., Carlisle, T.K., Bara, J.E. et al. (2010). A three-component mixed-matrix membrane with enhanced CO_2 separation properties based on zeolites and ionic liquid materials. *Journal of Membrane Science* 350 (1): 117–123.

166 Liu, G., Chernikova, V., Liu, Y. et al. (2018). Mixed matrix formulations with MOF molecular sieving for key energy-intensive separations. *Nature Materials* 17 (3): 283–289.

167 Wang, S., Li, X., Wu, H. et al. (2016). Advances in high permeability polymer-based membrane materials for CO_2 separations. *Energy & Environmental Science* 9 (6): 1863–1890.

168 Ren, Y., Liang, X., Dou, H. et al. (2020). Membrane-based olefin/paraffin separations. *Advanced Science* 7 (19): 2001398.

169 Zhou, T., Luo, L., Hu, S. et al. (2015). Janus composite nanoparticle-incorporated mixed matrix membranes for CO_2 separation. *Journal of Membrane Science* 489: 1–10.

170 Crist, R.D., Vetal, J., Razavi, S., and Galizia, M. Unpublished results.

WILEY

Edited by
Gyorgy Szekely and Dan Zhao

Sustainable Separation Engineering

Materials, Techniques and Process Development

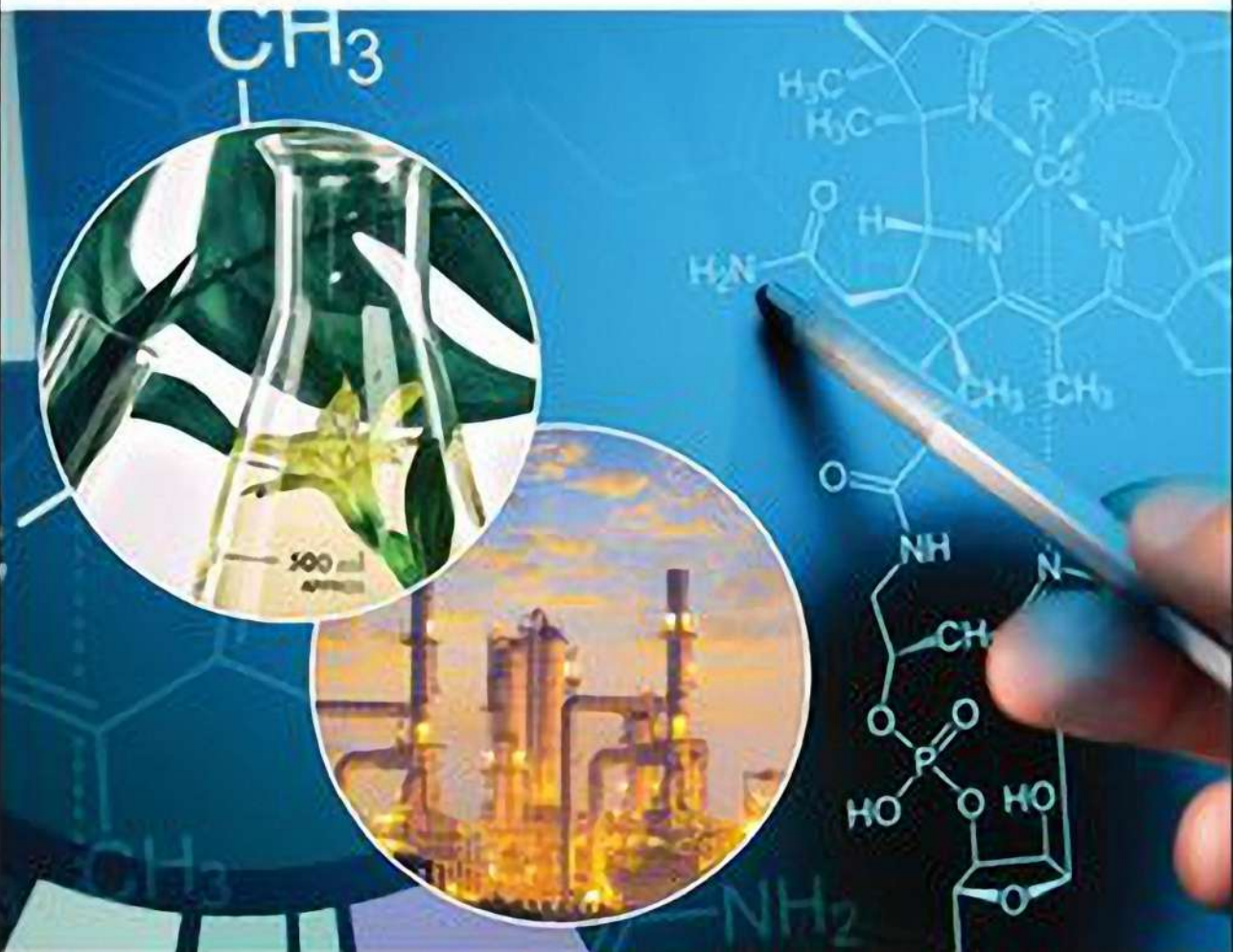

Sustainable Separation Engineering

Sustainable Separation Engineering

Materials, Techniques and Process Development

Volume 2

Edited by

Gyorgy Szekely
KAUST
Advanced Membranes and Porous Materials Center
Thuwal, Saudi Arabia

Dan Zhao
National University of Singapore
Chemical and Biomolecular Engineering
Singapore, Singapore

WILEY

This edition first published 2022
© 2022 by John Wiley & Sons Ltd. All rights reserved.

All rights reserved. No part of this publication may be reproduced, stored in a retrieval system, or transmitted, in any form or by any means, electronic, mechanical, photocopying, recording or otherwise, except as permitted by law. Advice on how to obtain permission to reuse material from this title is available at http://www.wiley.com/go/permissions.

The right of Gyorgy Szekely and Dan Zhao to be identified as the authors of this work has been asserted in accordance with law.

Registered Offices
John Wiley & Sons, Inc., 111 River Street, Hoboken, NJ 07030, USA
John Wiley & Sons Ltd, The Atrium, Southern Gate, Chichester, West Sussex, PO19 8SQ, UK

Editorial Office
The Atrium, Southern Gate, Chichester, West Sussex, PO19 8SQ, UK

For details of our global editorial offices, customer services, and more information about Wiley products visit us at www.wiley.com. Wiley also publishes its books in a variety of electronic formats and by print-on-demand. Some content that appears in standard print versions of this book may not be available in other formats.

Limit of Liability/Disclaimer of Warranty
In view of ongoing research, equipment modifications, changes in governmental regulations, and the constant flow of information relating to the use of experimental reagents, equipment, and devices, the reader is urged to review and evaluate the information provided in the package insert or instructions for each chemical, piece of equipment, reagent, or device for, among other things, any changes in the instructions or indication of usage and for added warnings and precautions. While the publisher and authors have used their best efforts in preparing this work, they make no representations or warranties with respect to the accuracy or completeness of the contents of this work and specifically disclaim all warranties, including without limitation any implied warranties of merchantability or fitness for a particular purpose. No warranty may be created or extended by sales representatives, written sales materials or promotional statements for this work. The fact that an organization, website, or product is referred to in this work as a citation and/or potential source of further information does not mean that the publisher and authors endorse the information or services the organization, website, or product may provide or recommendations it may make. This work is sold with the understanding that the publisher is not engaged in rendering professional services. The advice and strategies contained herein may not be suitable for your situation. You should consult with a specialist where appropriate. Further, readers should be aware that websites listed in this work may have changed or disappeared between when this work was written and when it is read. Neither the publisher nor authors shall be liable for any loss of profit or any other commercial damages, including but not limited to special, incidental, consequential, or other damages.

For general information on our other products and services or for technical support, please contact our Customer Care Department within the United States at (800) 762-2974, outside the United States at (317) 572-3993 or fax (317) 572-4002.

Wiley also publishes its books in a variety of electronic formats. Some content that appears in print may not be available in electronic formats. For more information about Wiley products, visit our web site at ww.wiley.com.

Library of Congress Cataloging-in-Publication Data applied for:
ISBN: 9781119740087

Cover Design: Wiley
Cover Images: © nicolas_/Getty Image RonFullHD/Getty Images Artfully79/Getty Images

Set in 9.5/12.5pt STIXTwoText by Straive, Pondicherry, India

10 9 8 7 6 5 4 3 2 1

Contents

About the Editors

Gyorgy Szekely

Gyorgy Szekely received his MSc degree in Chemical Engineering from the Technical University of Budapest, Hungary. He subsequently earned his PhD degree in Chemistry from the Technical University of Dortmund, Germany, under Marie Curie Actions. Gyorgy worked as an Early Stage Researcher in the Pharmaceutical Research and Development Centre of Hovione PharmaScience Ltd. in Portugal and as an IAESTE Fellow at the University of Tokyo, Japan. He was a visiting researcher at Biotage MIP Technologies AB in Sweden. Gyorgy was a Postdoctoral Research Associate working with Prof. Andrew Livingston in Imperial College London, UK. He was appointed as a Lecturer in Chemical Engineering at The University of Manchester, UK, between 2014 and 2019, where he received the Distinguished Visiting Fellowship of the Royal Academy of Engineering. Gyorgy also served as an Adjunct Faculty Member at Saveetha University between 2016 and 2018. He is currently an Assistant Professor in Chemical Engineering at the Advanced Membranes & Porous Materials Center at King Abdullah University of Science and Technology (KAUST), Saudi Arabia, and has been a Visiting Academic at The University of Manchester, 2019–2022. His multidisciplinary professional background covers green process engineering, green solvents and materials, continuous reactions, and membrane separations. He serves as an Academic Editor for the journals *Advances in Polymer Technology, Advanced Materials Letters*; as an Associate Editor for the Separation Processes section of *Frontiers in Chemical Engineering*; he is a member of the Editorial Advisory Board for *ACS Applied Polymer Materials*, and a member of the Early Career Editorial Board of the *Journal of Membrane Science*. He is a Member of the Royal Society of Chemistry and a Fellow of the Higher Education Academy in the UK. Gyorgy has been designing

novel materials and processes for molecular level separations, which has resulted in several articles, industrial collaborations and consultancy works, books, patents, and invited keynote lectures. To learn more about Gyorgy, follow him on Twitter @SzekelyGroup and through his group's website at www.szekelygroup.com.

Dan Zhao

Dan Zhao received his MS degree in Polymer Chemistry and Physics from Zhejiang University, China. He went on to obtain his PhD degree in Chemistry (Inorganic Division) from Texas A&M University, USA, under Prof. Hong-Cai Zhou in 2010. Following this, he worked with Dr. Di-Jia Liu at Argonne National Laboratory as a Postdoctoral Fellow between 2010 and 2012. Dan was appointed as an Assistant Professor in Chemical Engineering at the National University of Singapore between 2012 and 2018, where he received multiple local and global accolades for his outstanding academic contributions and commendable teaching dedications. He has been an Associate Professor in Chemical Engineering at the National University of Singapore since 2019. Dan is highly interested in interdisciplinary research in advanced porous materials and hybrid membranes for applications in clean energy and environmental sustainability. His work has generated multiple highly cited papers, industrial collaboration and translation, patents, book chapters, and invited presentations. He is the Clarivate Analytics' Highly Cited Researcher (Cross-Field) for 2019–2020 and was appointed as the Dean's Chair of the Faculty of Engineering at the National University of Singapore in 2021. Dan served as a Member of the Editorial Advisory Board for *Inorganic Chemistry* from 2018 to 2020. He is currently serving as the Associate Editor for *Industrial & Engineering Chemistry Research*, an Advisory Board Member of *Aggregate*, and an Early Career Advisory Board Member of *ACS Sustainable Chemistry & Engineering* and *Chemistry – An Asian Journal*. He is an Executive Committee Member of the Materials Research Society of Singapore and a Membrane of the Membrane Society of Singapore. To learn more about Dan, follow him on Twitter @ZhaoGroupNUS and through his group's website at https://blog.nus.edu.sg/dzhao/.

List of Contributors

Andrea Adamo
Zaiput Flow Technologies
Waltham, MA, USA

Elaf A. Ahmed
Research & Development Center
Saudi Aramco
Dhahran, Saudi Arabia

Faheem Hassan Akhtar
Biological and Environmental Science and Engineering Division (BESE)
Water Desalination and Reuse Center (WDRC)
King Abdullah University of Science and Technology (KAUST)
Thuwal, Saudi Arabia

Hasan A. Al Abdulgader
Research & Development Center
Saudi Aramco, Dhahran, Saudi Arabia

T. Alan Hatton
Department of Chemical Engineering
Massachusetts Institute of Technology
Cambridge, MA, USA

Sajad Razavi Bazaz
School of Biomedical Engineering
University of Technology Sydney
Sydney, Australia

Muhammad Burhan
Biological and Environmental Science and Engineering Division (BESE)
Water Desalination and Reuse Center (WDRC)
King Abdullah University of Science and Technology (KAUST)
Thuwal, Saudi Arabia

Yus Donald Chaniago
Ulsan National Institute of Science and Technology
Ulsan, South Korea

Farid Chemat
GREEN Extraction Team, INRAE
Avignon University
Avignon, France

Qian Chen
Biological and Environmental Science and Engineering Division (BESE)
Water Desalination and Reuse Center (WDRC)
King Abdullah University of Science and Technology (KAUST)
Thuwal, Saudi Arabia

Young Chul Choi
Research & Development Center
Saudi Aramco
Dhahran, Saudi Arabia

Mariana C. da Costa
School of Chemical Engineering (FEQ)
University of Campinas (UNICAMP)
Campinas, São Paulo, Brazil

André M. da Costa Lopes
CICECO – Aveiro Institute of Materials
Department of Chemistry
University of Aveiro
Aveiro, Portugal
CECOLAB – Collaborative Laboratory
Towards Circular Economy
R. Nossa Senhora da Conceição
Oliveira do Hospital
Coimbra, Portugal

Gergő Dargó
RotaChrom Technologies LLC
Dabas, Hungary

Gaurav G. Dastane
Department of Chemical Engineering
Institute of Chemical Technology
Mumbai, India

Jing Deng
School of Chemical, Biological, and
Materials Engineering
University of Oklahoma
Norman, OK, USA

Ketan S. Desai
Department of Chemical Engineering
Institute of Chemical Technology
Mumbai, India

Francesco Donsi
Department of Industrial Engineering
University of Salerno
Fisciano, Italy

Eric Falascino
William G. Lowrie Department of
Chemical and Biomolecular Engineering
The Ohio State University
Columbus, OH, USA

Liang-Shih Fan
William G. Lowrie Department of
Chemical and Biomolecular
Engineering
The Ohio State University
Columbus, OH, USA

Michele Galizia
School of Chemical, Biological, and
Materials Engineering
University of Oklahoma
Norman, OK, USA

María González-Miquel
Department of Chemical Engineering
and Analytical Sciences
The University of Manchester
Manchester, UK
Departamento de Ingeniería Química
Industrial y del Medioambiente
ETS Ingenieros Industriales
Universidad Politécnica de Madrid
Madrid, Spain

Patricia Gorgojo
Department of Chemical Engineering
and Analytical Sciences
The University of Manchester
Manchester, UK

Nanoscience and Materials Institute of
Aragón (INMA)
CSIC-Universidad de Zaragoza
Zaragoza, Spain

Chemical and Environmental Engineering
Department
Universidad de Zaragoza
Zaragoza, Spain

Benjamin S. Hsiao
Department of Chemistry
Stony Brook University
Stony Brook, NY, USA

Xiangyu Huang
Department of Chemistry
Stony Brook University
Stony Brook, NY, USA

Ananda J. Jadhav
Department of Chemical Engineering
Institute of Chemical Technology
Mumbai, India

Anet Režek Jambrak
Faculty of Food Technology and Biotechnology
University of Zagreb
Zagreb, Croatia

Muhammad Ahmad Jamil
Mechanical & Construction Engineering Department
Northumbria University
Newcastle Upon Tyne, UK

Kalyani Jangam
William G. Lowrie Department of Chemical and Biomolecular Engineering
The Ohio State University
Columbus, OH, USA

Anuj Joshi
William G. Lowrie Department of Chemical and Biomolecular Engineering
The Ohio State University
Columbus, OH, USA

Shankar B. Kausley
TCS Research
Physical Sciences Research Area
Tata Consultancy Services
Pune, India

Chetsada Khositanon
Department of Chemical Engineering
Burapha University
Muang, Chonburi, Thailand

Árpád Könczöl
RotaChrom Technologies LLC
Dabas, Hungary

Kai Fabian Kruber
Institute of Process Systems Engineering
Hamburg University of Technology
Hamburg, Germany

Ramesh Kumar
Department of Earth Resources & Environmental Engineering
Hanyang University
Seoul, Republic of Korea

M. Kumja
Biological and Environmental Science and Engineering Division (BESE)
Water Desalination and Reuse Center (WDRC)
King Abdullah University of Science and Technology (KAUST)
Thuwal, Saudi Arabia

Moonyong Lee
Yeungnam University
Gyeongsan, South Korea

Ki Min Lim
School of Chemical and Energy Engineering
Universiti Teknologi Malaysia
Johor Bahru, Malaysia

Pablo López-Porfiri
Department of Chemical Engineering and Analytical Sciences
The University of Manchester
Manchester, UK

Ali Abouei Mehrizi
Department of Life Sciences Engineering
University of Tehran, Tehran, Iran

Francesco Meneguzzo
Istituto per la Bioeconomia
CNR, Sesto Fiorentino, FI, Italy

Fateme Mirakhorli
School of Biomedical Engineering
University of Technology Sydney
Sydney, Australia
Climate Change Cluster
University of Technology Sydney
Australia

Pinak Mohapatra
William G. Lowrie Department of
Chemical and Biomolecular
Engineering
The Ohio State University
Columbus, OH, USA

Seyed Sepehr Mohseni
Department of Life Sciences
Engineering
University of Tehran
Tehran, Iran

Rattana Muangrat
Faculty of Agro-Industry
Chiang Mai University
Chiang Mai, Thailand

Trevor Murray
Zaiput Flow Technologies
Waltham, MA, USA

Kim Choon Ng
Biological and Environmental Science
and Engineering Division (BESE)
Water Desalination and Reuse
Center (WDRC)
King Abdullah University of Science and
Technology (KAUST)
Thuwal, Saudi Arabia

Marinela Nutrizio
Faculty of Food Technology and
Biotechnology
University of Zagreb
Zagreb, Croatia

Lanre M. Oshinowo
Research & Development Center
Saudi Aramco
Dhahran, Saudi Arabia

Parimal Pal
Chemical Engineering Department
National Institute of Technology
Durgapur, India

Mario Pagliaro
Istituto per lo Studio dei Materiali
Nanostrutturati
CNR, Palermo, Italy

Aniruddha B. Pandit
Department of Chemical Engineering
Institute of Chemical Technology
Mumbai, India

Rajshree A. Patil
Department of Chemical Engineering
Institute of Chemical Technology
Mumbai, India

Yuthana Phimolsiripol
Faculty of Agro-Industry
Chiang Mai University
Chiang Mai, Thailand

Peter J. Ralph
Climate Change Cluster
University of Technology Sydney
Australia

Sepideh Razavi
School of Chemical, Biological, and
Materials Engineering
University of Oklahoma
Norman, OK, USA

Thomas Rodgers
Department of Chemical Engineering
and Analytical Science
The University of Manchester
Manchester, UK

Phisit Seesuriyachan
Faculty of Agro-Industry
Chiang Mai University
Chiang Mai, Thailand

Mateus Lodi Segatto
Department of Chemistry
Federal University of São Carlos
São Paulo, Brazil

Vedant Shah
William G. Lowrie Department of
Chemical and Biomolecular Engineering
The Ohio State University
Columbus, OH, USA

Muhammad Wakil Shahzad
Mechanical & Construction Engineering
Department
Northumbria University
Newcastle Upon Tyne, UK

Priyanka R. Sharma
Department of Chemistry
Stony Brook University
Stony Brook, NY, USA

Sunil K. Sharma
Department of Chemistry
Stony Brook University
Stony Brook, NY, USA

Armando J. D. Silvestre
CICECO – Aveiro Institute of Materials
Department of Chemistry
University of Aveiro
Aveiro, Portugal

Mirko Skiborowski
Institute of Process Systems Engineering
Hamburg University of Technology
Hamburg, Germany

Filipe H. B. Sosa
School of Chemical Engineering (FEQ)
University of Campinas (UNICAMP)
Campinas, São Paulo, Brazil
CICECO – Aveiro Institute of Materials
Department of Chemistry
University of Aveiro
Aveiro, Portugal

Aylon Matheus Stahl
Department of Chemistry
Federal University of São Carlos
São Paulo, Brazil

Kai-Jher Tan
Department of Chemical Engineering
Massachusetts Institute of Technology
Cambridge, MA, USA

Thomas Waltermann
Covestro Deutschland AG
Process Technology – Digital Process
Leverkusen, Germany

Majid Ebrahimi Warkiani
School of Biomedical Engineering
University of Technology Sydney
Sydney, Australia
Institute of Molecular Medicine
Sechenov University
Moscow, Russia

Nazlee Faisal Ghazali
School of Chemical and Energy Engineering
Universiti Teknologi Malaysia
Johor Bahru, Malaysia

Nopphon Weeranoppanant
Department of Chemical Engineering
Burapha University
Muang, Chonburi, Thailand
School of Biomolecular Science and
Engineering (BSE)
Vidyasirimedhi Institute of Science and
Technology (VISTEC)
Wangchan, Rayong, Thailand

Mengying Yang
Department of Chemistry
Stony Brook University
Stony Brook, NY, USA

Doskhan Ybyraiymkul
Biological and Environmental Science and Engineering Division (BESE)
Water Desalination and Reuse Center (WDRC)
King Abdullah University of Science and Technology (KAUST)
Thuwal, Saudi Arabia

Karine Zanotti
Department of Chemistry
Federal University of São Carlos
São Paulo, Brazil

Vânia Gomes Zuin
Department of Chemistry
Federal University of São Carlos
São Paulo, Brazil
Green Chemistry Centre of Excellence
University of York, York, UK
Institute of Sustainable and Environmental Chemistry, Leuphana University
Lüneburg, Germany

Preface

Welcome to the first edition of our book *Sustainable Separation Engineering*. This is the brainchild of our academic and industrial research, as well as our university teachings on advanced separations and green engineering. You will find this two-volume book both as an engaging and exciting reference guide on the latest materials, techniques, and processes related to sustainable separations and as a textbook that builds a solid theoretical foundation for sustainable separations. Our main objective is to present an overview of the fundamentals underlying the conventional and emerging separation processes, with an emphasis on sustainability. Gone are the days when separation engineering was the exclusive domain of chemical engineers. Modern sustainable separation engineering is highly interdisciplinary, with significant contributions ranging from chemical engineering to materials and polymer sciences to renewable energy sciences. Therefore, this book is intended for a broad audience to provide a bird's-eye view of the interplay among these disciplinaries to design sustainable solutions. An up-to-date reference index is also provided for easy lookup of the most relevant literature for a more detailed description of each topic.

One of the aims of sustainability is to manufacture products in the most environmentally benign, economic, and socially beneficial way through the optimization of resource utilization and the conservation of materials, energy, and natural resources. The Sustainable Development Goals set by the United Nations crafted a blueprint through which a thriving and more sustainable future can be achieved for all. These goals target the global challenges we face, and most of them are directly or indirectly linked to material separations. During the manufacturing of products, separation steps are undesired yet unavoidable. Owing to the high energy demand and considerable waste produced during separation processes, there is a need to develop advanced materials and processes that minimize the associated environmental burden. Academic and industrial researchers are making great efforts to design greener processes and products. The authors of the 21 chapters in this book aimed to develop a holistic view of various types of separations covering microscale (chemistry, materials), mesoscale (unit operations), and macroscale (processes). Discussion is also extended to the role of sustainable separations in the chemical engineering curriculum.

This book gives a contemporary and inclusive account of the sustainability aspects of separation engineering. It will be a useful resource for students of separation engineering and experts alike, as well as prospective learners who wish to broaden their horizons and discover other topics related to their core discipline.

Gyorgy Szekely
Jeddah, Saudi Arabia
Advanced Membranes and Porous Materials Center
King Abdullah University of Science and Technology (KAUST)

Dan Zhao
Singapore
Chemical and Biomolecular Engineering
National University of Singapore (NUS)

11

Adsorption Processes for Seawater Desalination

Qian Chen[1], Muhammad Burhan[1], Faheem Hassan Akhtar[1], Doskhan Ybyraiymkul[1], M. Kumja[1], Muhammad Ahmad Jamil[2], Muhammad Wakil Shahzad[2], and Kim Choon Ng[1]

[1] *Biological and Environmental Science and Engineering Division (BESE), Water Desalination and Reuse Center (WDRC), King Abdullah University of Science and Technology (KAUST), Thuwal, Saudi Arabia*
[2] *Mechanical & Construction Engineering Department, Northumbria University, Newcastle Upon Tyne, UK*

11.1 Introduction

The ever-rising global water demand is expected to touch 6900 Bm^3 in 2030 from mere 4200 Bm^3 in 2015 [1, 2]. The prime contributors to an exponential rise in water demands include population growth, industrial expansions, and standard of living [3, 4]. To ameliorate this situation, desalination is proven to be the most viable option because ~97% of global water is saline and cannot be used without proper treatment [5]. For this, various desalination technologies are developed and being used on commercial scales globally augmenting ~95.37 Mm^3/day of desalinated water to the freshwater resources [6].

Conventionally, three major desalination processes employed at a large scale are: (i) seawater reverse osmosis (SWRO), (ii) multistage flashing (MSF) and (iii) multi-effect desalination (MED). Many other processes are proposed such as membrane distillation (MD) [7, 8], forward osmosis (FO) [9, 10], humidification-dehumidification desalination (HDH) [11, 12] and direct-contact spray desalination (DCSEC) [13–15]. The market share of major desalination systems is presented in Figure 11.1 [16–18]. Application of these processes depends on the size of the plant and feed water quality and accordingly they have some limitations. For example, SWRO, even though is famous around the world, has operational limitations in terms of feed water quality. It is leading in the overall desalination market where processes are mostly installed on brackish or river water treatment. In terms of seawater desalination, in the Gulf region, the other two desalination processes hold over 60% market. Frequent occurrences of hazardous algae bloom, red tides, and sea foams are the major hindrance of SWRO applications in most of the Gulf regions. Slight variation in seawater quality in terms of silt density index is another example of SWRO process complication and it requires large pretreatment systems. Moreover, these plants reject large

Sustainable Separation Engineering: Materials, Techniques and Process Development, Volume 2, First Edition. Edited by Gyorgy Szekely and Dan Zhao.
© 2022 John Wiley & Sons Ltd. Published 2022 by John Wiley & Sons Ltd.

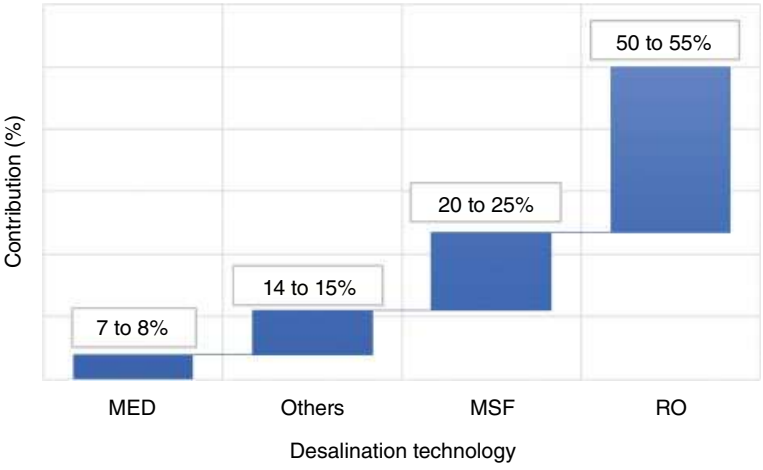

Figure 11.1 Desalination technology market shares [16–18].

quantities of chemicals into the sea and affect marine life. On the other hand, thermal desalination processes such as MSF and MED are robust and can also handle variation in feed water quality without affecting the overall plant operation. These plants are leading in the Gulf region; however, they also have limitations in terms of operational temperatures. For example, MED processes operate between 40 and 65 °C and MSF 40 and 130 °C.

One major challenge of desalination systems is high energy intensity. The equivalent energy consumption of conventional desalination systems to produce a unit volume of freshwater ranges between 3.7 and 8 kWh/m^3 for RO, 14.45 and 21.35 kWh/m^3 for MED, and 19.58 and 27.25 kWh/m^3 for MSF [19, 20]. These energy inputs are well above (~5–30 times) the minimum work of separation, i.e. 0.72 kWh/m^3 at 35 g/kg and 25 °C with an infinitesimal recovery [21, 22]. Therefore, out-of-the-box solutions are required for a quantum jump in the performance of conventional desalination systems.

Adsorption desalination is an emerging desalination method that possesses the merits of a low temperature and yet low cost. The adsorption cycle employs the high affinity of adsorbent materials (e.g. silica gel) on water molecules as the driving force. It is able to bring down the vapor saturation temperature to <5 °C. This substantial decrease in temperature allows substantial evaporation effects to be introduced, either in a standalone adsorption desalination system or in its hybridization with other desalination cycles [23, 24]. Some other salient features of the adsorption-based desalination systems include higher interstage temperature difference, low-grade energy usage, and no significant rotating equipment addition, thus reducing maintenance issues, and less corrosion or fouling susceptibility.

This chapter provides a comprehensive overview of the adsorption-based desalination systems. A universal adsorption isotherm model is firstly introduced to allow a fundamental understanding of the adsorption thermodynamics. Then various applications of the adsorption cycle are presented, including standalone adsorption desalination cycles (both temperature-swing and pressure-swing) and their integration with other water treatment systems (multi-effect distillation and evaporative crystallizer). These results will form a solid foundation for future application on adsorption-based desalination systems.

11.2 Adsorption Theory and Modeling

Various adsorbent materials have been known for centuries. However, the scientific work on their sorption properties started during the eighteenth century [25, 26]. These adsorbent materials are dominated by porous materials including natural adsorbents, e.g. silica, zeolites, and, more recently, metal-organic frameworks (MOFs). Synthesis of porous metal oxides and the development of the sol-gel process have revolutionized the field of adsorbent science and applications [27]. The pioneering work of Prof. Barrer in the field of porous materials and films has laid down the foundations of the field for various porous and dense materials [28–31]. These adsorbents including polymers as shown by Barrer have been known for many years and widely accepted for various applications.

The adsorbent surface is intricate by nature and it comprises many types of interlinking pores such as the micro-, meso-, and macropores [32] as shown schematically in Figure 11.2. For the modelling of the heterogeneous adsorbent surfaces, it can be estimated by the gathering of several quasi-static homogenous sites where each homogenous patch is assumed to have the same pattern of energy levels (ε) that are applicable to monolayer coverage of infinitesimal mass uptake $\partial\theta(\varepsilon)$. Furthermore, each homogeneous patch can be laden with many adsorption sites having the same energy level that is associated with the other forms of

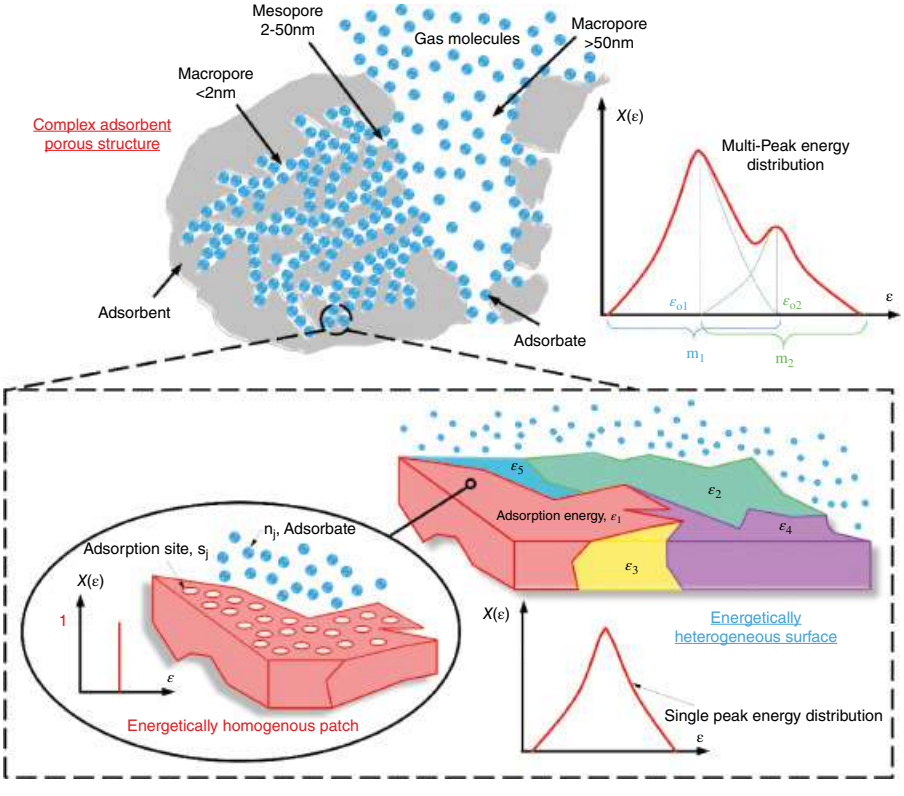

Figure 11.2 Complex heterogeneous porous surface.

energy distribution functions of adsorption sites. If there is a higher chance of occurrence of an energy site, this indicates that there will be higher localized adsorption uptake. On the other hand, this energy distribution function is different for various pores, i.e. micro-, meso-, or macropores, and extended to the multilayer development. In order to describe the fraction of the energy distribution or the uptake, a probability factor is introduced which is linked to the individual pore size or the multiple layers on the adsorbent surface [33].

If it is assumed that there is quasi-static patch approximation and there is only one molecule for every energy site of adsorption surface, the localized adsorption uptake for a homogeneous area of adsorption surface is given by:

$$\theta(\varepsilon)_j = \frac{n_j}{s_j} \tag{11.1}$$

where n_j symbolizes the number of molecules and s_j symbolizes the locally available energy sites of adsorption. Therefore, the total adsorption uptake for the available energy sites is given by:

$$\theta_t = \frac{N_a}{S_o} = \sum_{j=1}^{\infty} \theta(\varepsilon)_j \tag{11.2}$$

where S_o and N_a symbolize the number of adsorption sites and molecules adsorbed, respectively. The extension of Eq. (11.2) as a summation of all local coverage and their respective probability factors, s_j/S_o is given by:

$$\theta_t = \frac{s_1}{S_o}\theta_1 + \frac{s_2}{S_o}\theta_2 + \frac{s_3}{S_o}\theta_3 + \ldots\ldots + \frac{s_\infty}{S_o}\theta_\infty \tag{11.3}$$

The distribution function $X(\varepsilon)$ of adsorption energy sites is proportional to the probability factors, and for the entire adsorption surface, this ratio is equal to unity, i.e.

$$\frac{s_i}{S_o}(\varepsilon) = X(\varepsilon)\mathrm{d}\varepsilon \tag{11.4}$$

$$\int_0^\infty X(\varepsilon)\mathrm{d}\varepsilon = \sum_{n=1}^{\infty} \frac{s_i}{S_o}(\varepsilon) = 1 \tag{11.5}$$

By taking the integral of the coverage, the total uptake of the adsorption heterogeneous surface with quasi-static patches is given by integral Eq. (11.6).

$$\theta_t = \int_0^\infty \{\theta(\varepsilon)X(\varepsilon)\}\mathrm{d}\varepsilon \tag{11.6}$$

$\longleftarrow$ all sites

Hence, if the distribution function X(ε) of adsorption energy sites and the uptake $\theta(\varepsilon)$ of the adsorption heterogeneous surfaces are known, either by design or measurement of the

isotherms, then the total coverage is given by Eq. (11.6). If the simultaneous occurrence of adsorption and desorption rates is known, then the rate of total adsorption uptake is written as:

$$\frac{\mathrm{d}\theta(\varepsilon)}{\mathrm{d}t} = R_a - R_d$$

Where the adsorption and desorption rates of adsorbate molecules on the adsorbent surface are represented by R_a and R_d, respectively, specified through classical Absolute Rate Theory (ART) as [34, 35]:

$$\frac{\mathrm{d}\theta(\varepsilon)}{\mathrm{d}t} = K_a p(1-\theta)\exp\left(\frac{-\varepsilon_a}{RT}\right) - K_d\theta\exp\left(\frac{-\varepsilon_d}{RT}\right)$$

When there is an equilibrium, the adsorption and desorption rates come to be equal, which means the rate of change of adsorption uptake is zero, $\frac{\mathrm{d}\theta(\varepsilon)}{\mathrm{d}t} = 0$. So, by simplifying the above equation and letting $K = K_a/K_d$ and $\Delta\varepsilon = \varepsilon_d - \varepsilon_a = \varepsilon - h_{fg}$, we arrived at the Langmuir isotherm equation for the localized adsorption uptake at the homogeneous patch.

$$\theta(\varepsilon) = \frac{Kp\exp\left(\frac{\Delta\varepsilon}{RT}\right)}{\left(1 + Kp\exp\left(\frac{\Delta\varepsilon}{RT}\right)\right)} \tag{11.7}$$

where the condensation approximation is defined by the limit, ε_c

$$\varepsilon_c = -RT\ln Kp \text{ or } Kp = \exp\frac{-\varepsilon_c}{RT} \tag{11.8}$$

So, by replacing the Kp term of Eq. (11.8) into Eq. (11.7), the Langmuir isotherm becomes:

$$\theta(\varepsilon) = \frac{\exp\left(\frac{\Delta\varepsilon - \varepsilon_c}{RT}\right)}{\left(1 + \exp\left(\frac{\Delta\varepsilon - \varepsilon_c}{RT}\right)\right)} \tag{11.9}$$

The adsorption uptake $\theta(\varepsilon)$ with temperature dependence is given by the above Eq. (11.9), which becomes a step function at an extremely low temperature of $T \to 0$. Invoking the condensation approximation, we have:

$$\lim_{T\to 0}\theta(\varepsilon) = \theta_c(\varepsilon) = \begin{cases} 0 \text{ for } \Delta\varepsilon \le \varepsilon_c \\ 1 \text{ for } \Delta\varepsilon \ge \varepsilon_c \end{cases}$$

Therefore, Eq. (11.6) can be disintegrated into two parts where the first part has zero uptake and, thus,

$$\theta_t = \int_0^{\varepsilon_c} \left(0 \times X\left(\varepsilon\right)\right) \mathrm{d}\varepsilon + \int_{\varepsilon_c}^{\infty} \left(1 \times X\left(\varepsilon\right)\right) \mathrm{d}\varepsilon$$

$$\theta_t = \int_{\varepsilon_c}^{\infty} X\left(\varepsilon\right) \mathrm{d}\varepsilon \tag{11.10}$$

As depicted by Eq. (11.10), the distribution function of the adsorption energy sites is only depending upon the total adsorption uptake. The symmetrical Gaussian function is estimated here to characterize the distribution of the energy sites over the heterogeneous adsorption surface. For the fraction of the total uptake between micro- and macropores, a probability factor "α" is incorporated into the energy distribution function that gives a universal and physically meaningful representation of both single- and multi-peak energy distributions on the surfaces, i.e.

$$X\left(\varepsilon\right) = \sum_{i=1}^{n} \alpha_i \left\{ \frac{\exp\left(\dfrac{\Delta\varepsilon - \varepsilon_o}{m}\right)}{m\left[1 + \exp\left(\dfrac{\Delta\varepsilon - \varepsilon_o}{m}\right)\right]^2} \right\}_i \tag{11.11}$$

where "ε_o" denotes the adsorption energy site having a higher probability, which also shows the "*relative position*" of the energy distribution curve. The factor "m" represents the surface heterogeneity of all the energy sites, which is related to the pore size, i.e. micro- or meso-/macropores. It determines the overall spread or the variance of the energy distribution curve. It is emphasized that the summation of the probability "α_i" parameters equal to "1."

$$\sum_{i=1}^{n} \alpha_i = 1$$

Therefore, the overall adsorption uptake equation is integrated according to the energy distribution functions.

$$\theta_t = \int_{\varepsilon_c}^{\infty} \left[\sum_{i=1}^{n} \alpha_i \left\{ \frac{\exp\left(\dfrac{\Delta\varepsilon - \varepsilon_o}{m}\right)}{m\left[1 + \exp\left(\dfrac{\Delta\varepsilon - \varepsilon_o}{m}\right)\right]^2} \right\}_i \right] \mathrm{d}\varepsilon \tag{11.12}$$

By resolving the integral and permitting $\varepsilon_c = -RT\ln Kp$:

$$\theta_t = \sum_{i=1}^{n}\alpha_i\left\{\left[1+\exp\left(\frac{-RT\ln Kp-\varepsilon_o}{m}\right)\right]^{-1}\right\}_i \tag{11.13}$$

Upon generalization, and permitting the adsorption equilibrium constant $K = 1/p_s$, the universal isotherm model is derived with the pressure ratio, p/p_s

$$\theta_t = \sum_{i=1}^{n}\alpha_i\left\{\frac{\left(\frac{p}{p_s}\exp\left(\frac{\varepsilon_{oi}}{RT}\right)\right)^{\frac{RT}{mi}}}{1+\left(\frac{p}{p_s}\exp\left(\frac{\varepsilon_{oi}}{RT}\right)\right)^{\frac{RT}{mi}}}\right\}_i \tag{11.14}$$

where p_s symbolizes the saturation pressure for maximum uptake of an adsorbent. For the Type-I to Type-V isotherms, the energy distribution functions with two nominal peaks, i.e. $n = 2$, can lead to factors of α_1 and α_2:

$$\theta_t = \alpha_1\left[\frac{\left(\frac{p}{p_s}\exp\left(\frac{\varepsilon_{o1}}{RT}\right)\right)^{\frac{RT}{m1}}}{1+\left(\frac{p}{p_s}\exp\left(\frac{\varepsilon_{o1}}{RT}\right)\right)^{\frac{RT}{m1}}}\right] + \alpha_2\left[\frac{\left(\frac{p}{p_s}\exp\left(\frac{\varepsilon_{o2}}{RT}\right)\right)^{\frac{RT}{m2}}}{1+\left(\frac{p}{p_s}\exp\left(\frac{\varepsilon_{o2}}{RT}\right)\right)^{\frac{RT}{m2}}}\right] \tag{11.15}$$

where $\alpha_1 + \alpha_2 = 1$

Similarly, for Type-VI Isotherm, it has four peak energy distribution functions which can be integrated into a decomposed form as:

$$\begin{aligned}\theta_t = {} & \alpha_1\left[\frac{\left(\frac{p}{p_s}\exp\left(\frac{\varepsilon_{o1}}{RT}\right)\right)^{\frac{RT}{m1}}}{1+\left(\frac{p}{p_s}\exp\left(\frac{\varepsilon_{o1}}{RT}\right)\right)^{\frac{RT}{m1}}}\right] + \alpha_2\left[\frac{\left(\frac{p}{p_s}\exp\left(\frac{\varepsilon_{o2}}{RT}\right)\right)^{\frac{RT}{m2}}}{1+\left(\frac{p}{p_s}\exp\left(\frac{\varepsilon_{o2}}{RT}\right)\right)^{\frac{RT}{m2}}}\right] \\ & + \alpha_3\left[\frac{\left(\frac{p}{p_s}\exp\left(\frac{\varepsilon_{o3}}{RT}\right)\right)^{\frac{RT}{m3}}}{1+\left(\frac{p}{p_s}\exp\left(\frac{\varepsilon_{o3}}{RT}\right)\right)^{\frac{RT}{m3}}}\right] + \alpha_4\left[\frac{\left(\frac{p}{p_s}\exp\left(\frac{\varepsilon_{o4}}{RT}\right)\right)^{\frac{RT}{m4}}}{1+\left(\frac{p}{p_s}\exp\left(\frac{\varepsilon_{o4}}{RT}\right)\right)^{\frac{RT}{m4}}}\right]\end{aligned} \tag{11.16}$$

where $\alpha_1 + \alpha_2 + \alpha_3 + \alpha_4 = 1$. With four energy distribution function (EDF) peaks and when integrated over the energy levels (ε_c to ∞), it captures the complex thermodynamics of mass uptake [36] over the range of the pressure ratio, *P/Ps*, exerted on the adsorbed phase of

adsorbate-adsorbent. Hence, the thermodynamics of an adsorbate on the heterogeneous porous adsorbent can be precisely represented by a unified form of Eq. (11.14).

Figure 11.3 compares predicted isotherms with experimental measurements for different types of adsorbent-adsorbate pairs. As shown in the figure, the proposed model is able to predict all six types of isotherms with high accuracy. In contrast, conventional theories (Langmuir [37], Langmuir-Freundlich [LF] [38], Tóth [39], and Dubinin-Astakhov [DA] [40] models) can only fit 1–2 types of isotherms. The proposed model enables a more in-depth understanding of the adsorption thermodynamics, thus allowing the design and optimization of adsorption beds.

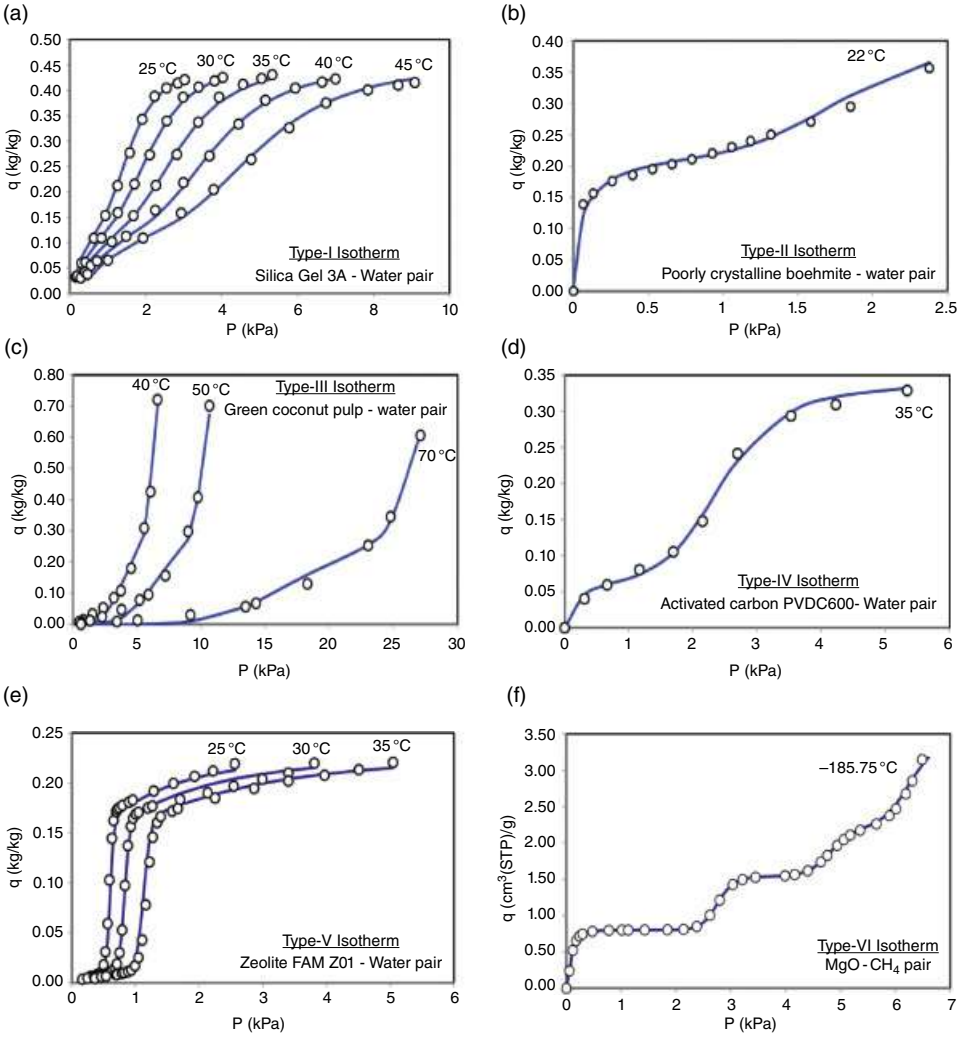

Figure 11.3 Comparison of predicted isotherms with experimental measurements for different types of isotherms [33]: (a) Type-I, (b) Type-II, (c) Type-III, (d) Type-IV, (e) Type-V and (f) Type-VI.

11.3 Application of Adsorption in Water Treatment

Adsorption has broad applications in water treatment. The adsorption cycle can be directly used for desalination and water treatment by spraying seawater/wastewater in the evaporator. It can also be integrated with the existing water treatment systems, e.g. MED and crystallizer, to achieve better productivity and energy efficiency.

11.3.1 Temperature-swing Adsorption Desalination Cycle

The adsorption cycle consists of five main components including an evaporator, adsorption-desorption reactor beds, a condenser, pumps, and a pretreatment section. The adsorption desalination (AD) cycle operates in a batch process and involves two main operations, i.e. adsorption-assisted evaporation and desorption-activated condensation. In the former process, the vapors produced in the evaporator are adsorbed by a high water vapor affinity adsorbent. It is important to mention that the evaporation process is initiated by the heat supplied (through the water at 5 to 30 °C) in the evaporator. However, the adsorbent accelerates the vapor formation by reducing the evaporator pressure. The adsorption process goes on until the adsorbent beds are saturated. In the second process, the saturated adsorbent is regenerated by circulating hot water (with a temperature of 55–85 °C) through the desorbers. Vapor is separated from the adsorbent when it reaches a high temperature, and the released vapors are condensed in a water-cooled condenser as a distillate [23]. Since the desorption process is temperature-driven, the cycle is called the temperature-swing adsorption cycle (TSAD).

Since AD is a batch process, the multi-bed arrangement is used for continuous operation, as shown in Figure 11.4a [24]. In this arrangement, two parallel pairs of adsorbent reactor beds are employed of which one undergoes adsorption process and the other one desorption process simultaneously. The switching between the role of beds (for adsorption or desorption) is controlled by an automatic controller which governs the flow of hot/cold water to the respective bed using valves. The switching between beds is accompanied by an intermittent short period known as switching time during which the vapor valves are closed and the adsorber bed is preheated whilst the desorber bed is precooled which boosts the system performance. Figure 11.4b is a pictorial view of the TSAD pilot plant located at King Abdullah University of Science and Technology (KAUST), Saudi Arabia.

Figure 11.5 shows the transient temperature profiles for the adsorber, desorber, evaporator and condenser of the TSAD system. Due to the batchwise operation of the system, the temperature profiles are in a cyclical manner. The system reaches a cyclic steady state after three half-cycles (1500 seconds). At a steady state, the temperature change is dramatic at the beginning of each cycle, and the profiles become steady afterward. This is because the adsorbent in the adsorption beds has a low uptake at the beginning, and is able to induce dramatic evaporation. Meanwhile, the desorption beds are fully saturated since they were under the adsorption process in the previous cycle, and the desorption rate is high. With the cycle going on, the adsorption beds slowly get saturated, while uptake in the desorption beds becomes lower. As a result, the driving forces for evaporation and condensation diminish, leading to a slower change of temperature profiles.

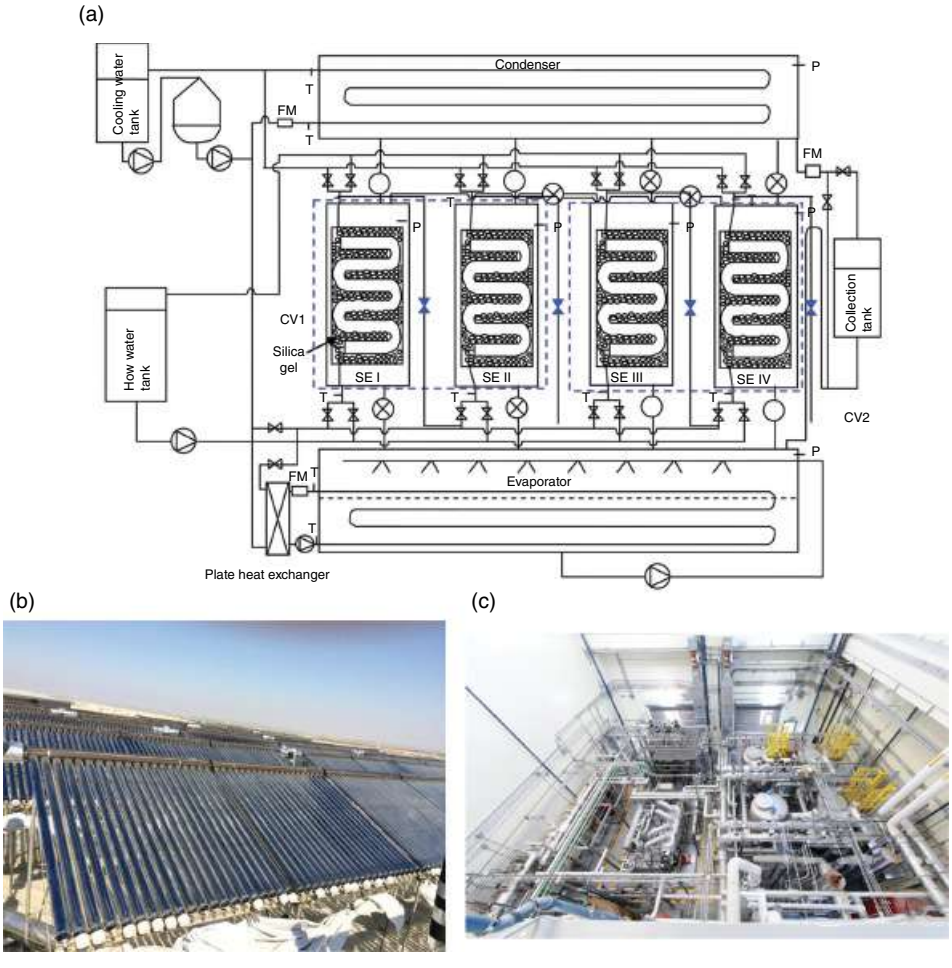

Figure 11.4 (a) The schematic of a four-bed adsorption desalination and cooling pilot plant; (b–c) pictorial views of the solar-powered adsorption desalination cum chiller plant at KAUST, SA [41].

Figure 11.6 illustrates the water production rate of the TSAD desalination cycle. The productivity also shows a cyclic manner. Its value is high at the beginning of each cycle and decreases with time due to less driving force for evaporation and condensation. The cycle-average production rate is 0.49 L/min, and during the switching period, there is no production of freshwater.

Figure 11.7 shows the specific water production under assorted heat source temperatures and cycle times. The productivity is higher under a higher heat source temperature. This is because a higher heat source temperature leads to more complete desorption, and, therefore, provides a larger driving force during the adsorption cycle. For the cycle time, productivity firstly increases with a longer cycle time, and the trend is reversed after some threshold value. The reason can be explained as follows. On the one hand, a longer cycle time enables more complete desorption and promotes water evaporation when the cycle time is short. However, a longer cycle time results in excessive heating of the beds after

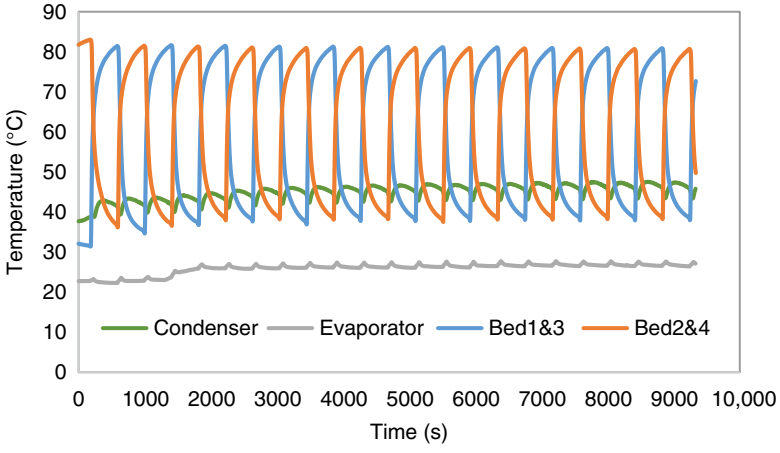

Figure 11.5 The temperature profiles of the major component of the TSAD cycle T_{hw} = 85 °C, T_{cw} = 29.8 °C, $T_{chilled}$ = 30 °C, m_{hw}/m_{cw} = 0.8 kg/s, $m_{chilled}$ = 0.8 kg/s, half cycle time = 350 seconds, and switching time = 20 seconds.

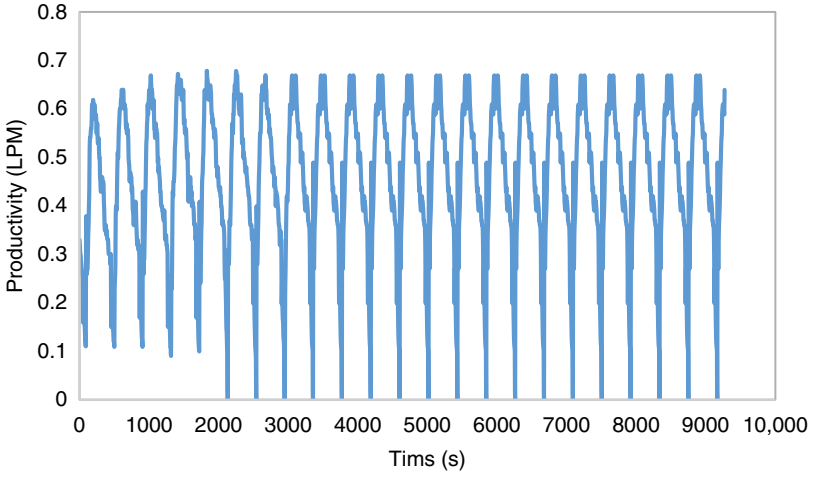

Figure 11.6 Water production rate of a 4-bed TSAD desalination plant.

desorption is completed, which damps water vapor sorption in the next cycle. The optimal cycle time is shorter with higher heat source temperature, as desorption is faster.

11.3.2 Pressure-swing Adsorption Desalination Cycle

The TSAD desalination system described above employs a low-temperature heat source for regeneration. In actual applications, heat sources may have higher temperatures. For example, exhaust steam from the power plant is >120 °C (2 bar at pressure). If employed directly for the TSAD cycle, the high exergy content in the steam is wasted. Under such situations, a pressure-swing adsorption cycle (PSAD) is preferable. The PSAD cycle uses

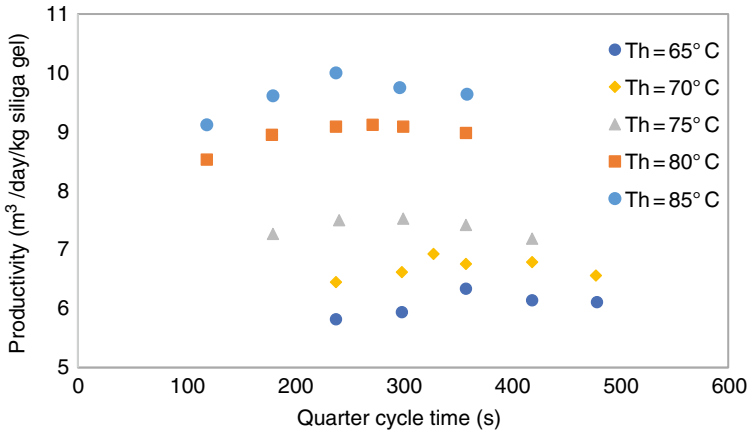

Figure 11.7 Freshwater productivity of adsorption desalination at different cycle times and heat source temperatures [42].

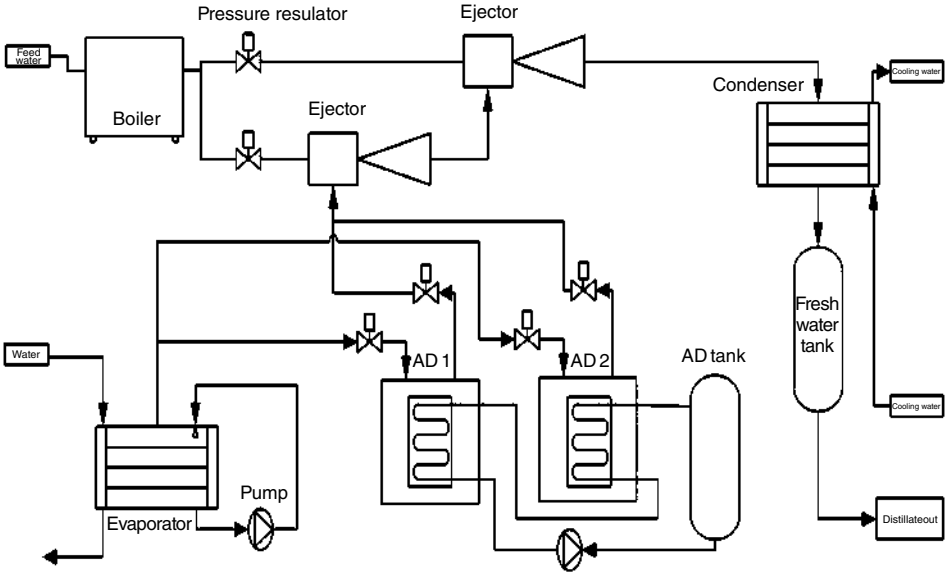

Figure 11.8 Schematic diagram of the designed TVC-AD.

the high-pressure steam to drive a thermal vapor compressor (TVC) to generate a low pressure in the desorber, and desorption is driven by pressure difference.

Figure 11.8 shows the schematic diagram of the novel PSAD system. The system consists of two AD beds, two ejectors, a boiler, a condenser, an evaporator, a distillate tank, and an AD heat-exchanging liquid tank. Similar to the TSAD cycle, a PSAD cycle operates in batch-mode. The adsorber adsorbs vapor produced from the evaporator, while the desorber is connected to the TVC to undergo desorption. At the exit of the TVC, the mixture of desorbed vapor and high-pressure steam is directed to the condenser to be condensed. Heat

transfer fluid is circulated between two beds to recover the adsorption heat from the adsorber for regeneration in the desorber.

Following the schematic of Figure 11.8, a pilot PSAD plant is commissioned in KAUST. The system components, i.e. ejectors, tanks, evaporators, and condensers are made of corrosion-resistive stainless steel. Type RD silica gel is used as the adsorbent due to its high water uptake and low cost. Evaporator pressure is measured by pressure sensors (Yokogawa) with an accuracy of ±0.125 kPa. The vapor temperature in the evaporator is measured with a 10 kΩ thermistor (±0.15 °C). Other temperatures are measured with a Pt 100 resistance thermometer (±0.15 °C).

During operation, the boiler maintains the desired steam pressure. Two electrical pressure regulators, which are installed after the boiler, control inlet pressure to ejectors (primary steam pressure). Serially connected ejectors are able to achieve up to 1 kPa in a suction line with primary steam from 2 to 5 bar. The discharge pressure of the ejector depends on primary steam and suction pressure. Discharged steam from ejectors goes to the condenser and condensed fresh water accumulates in the distillate tank. When the distillate tank is full, excess freshwater is diverted to drain by the pump.

Temperature profiles of adsorbent beds of the PS-AD are illustrated in Figure 11.9. Primary steam pressure and suction (desorption) pressure are constant at 5 bar. The temperature of silica gel changes from 19 to 31 °C during adsorption and decreases from 31 to 19 °C during desorption. The pressure profile of the adsorbent bed of the PS-AD system is imaged in Figure 11.10. AD bed pressure was increased from 0.5 to 2.5 kPa during the adsorption cycle. The distillate productivity also shows a cyclic manner, as shown in Figure 11.11. The average water production rate was around 7.3 L/hr.

The temperature profile of the evaporator of PSAD-TVC is shown in Figure 11.12. The seawater supply temperature is fixed at 26 °C, and the outlet temperature is changing from 22 to 18 °C. The low-temperature can be used in the condenser to reduce the discharge pressure, thus increasing the entrainment ratio of the TVC and reduce steam consumption. Alternatively, it can be used for cooling purpose.

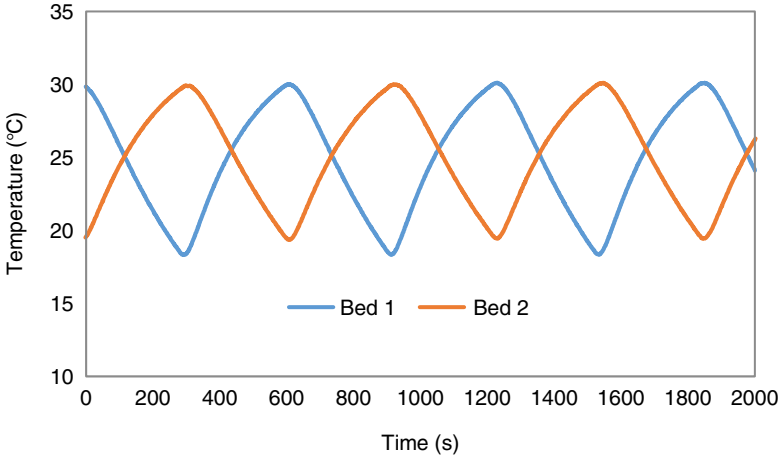

Figure 11.9 Temperature profiles of adsorbent beds in PS-AD cycle.

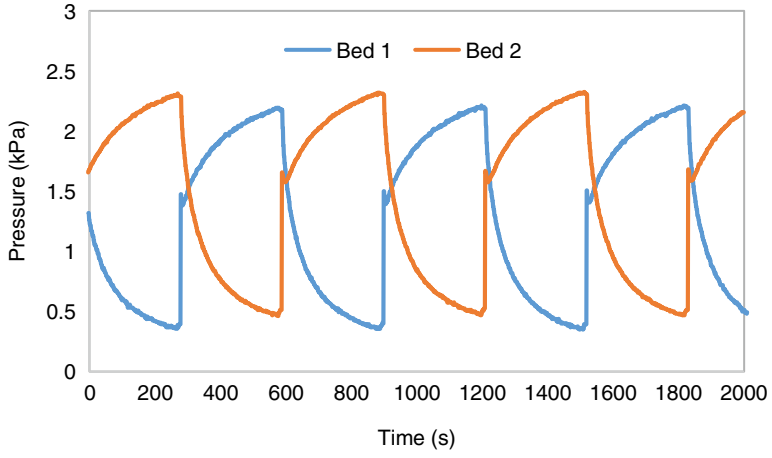

Figure 11.10 Pressure profiles of adsorbent beds in the PS-AD cycle.

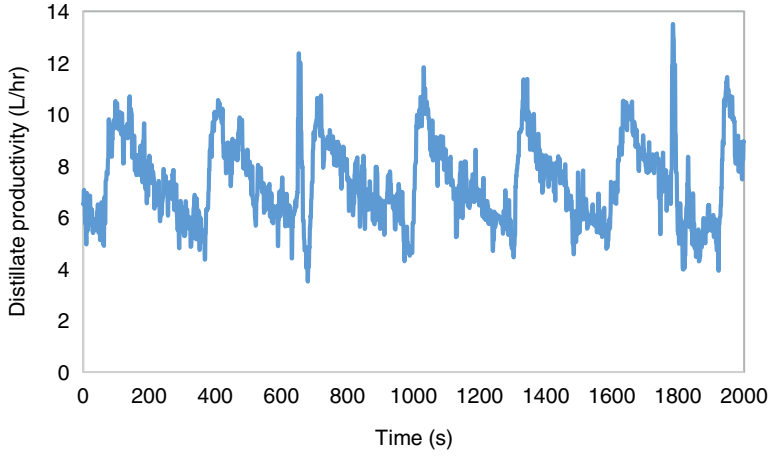

Figure 11.11 Distillate productivity in the PS-AD cycle.

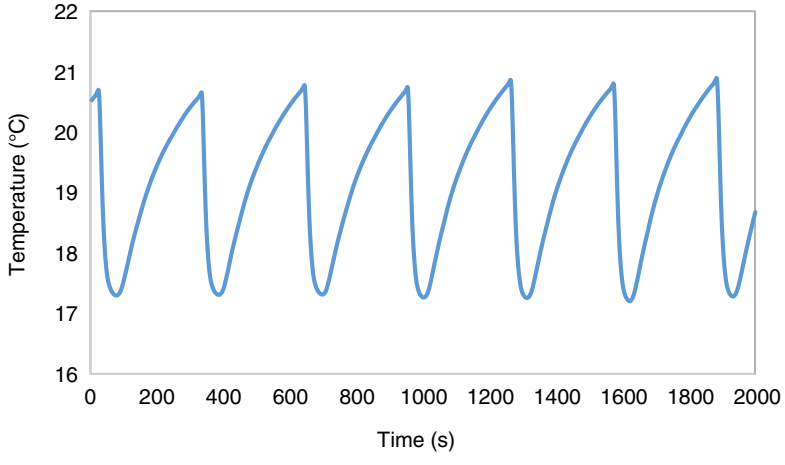

Figure 11.12 Temperature profiles of the chilled water in the evaporator.

The experimental results reveal that the PSAD-TVC system operates stably and produces potable water and cooling at the same time. The proposed system can be operated with a combined cycle gas turbine (CCGT) plant, where the extracted low-pressure steam can be more efficiently used for the production of cooling and water. It has been successfully demonstrated that 2 bar primary steam can regenerate silica gel at less than 1 kPa pressure using a properly designed TVC system. The proposed system will not only reduce the footprint, but also reduce capital and operating costs due to its robust design and easy operation than thermal-driven AD.

11.3.3 Hybrid Multi-effect Distillation and Adsorption Cycle

In addition to standalone operation, the adsorption cycle can also be integrated with existing desalination systems to achieve better performance. For example, the productivity and thermal efficiency of a conventional multi-effect distillation (MED) system is limited by the temperature difference between the heat source and the cooling. By integrating MED with the adsorption cycle, the vapor pressure in the last MED effect can be significantly reduced, thus providing a larger temperature difference for operation.

The conventional MED system consists of a steam generation facility and a number of evaporators connected in forward, parallel, or parallel cross-feed flow arrangement as shown in Figure 11.13 [43]. In the first arrangement, all the feed is sprayed in the first evaporator and the brine of each evaporator serves as a feed of forthcoming evaporators. In the second arrangement, the feed is evenly sprayed in all effects. In the third arrangement, the feed is sprayed in a parallel manner. However, the brine from each effect is introduced in the next effect at the bottom which results in additional vapor production due to flashing effects. The vapors produced in each effect serve as steam for the next effect and the vapors from the last effect are condensed in an external condenser.

The hybrid MED and adsorption desalination (MEDAD) cycle consists of a MED cycle integrated with an AD cycle, as shown in Figure 11.14 [2]. The process starts as the

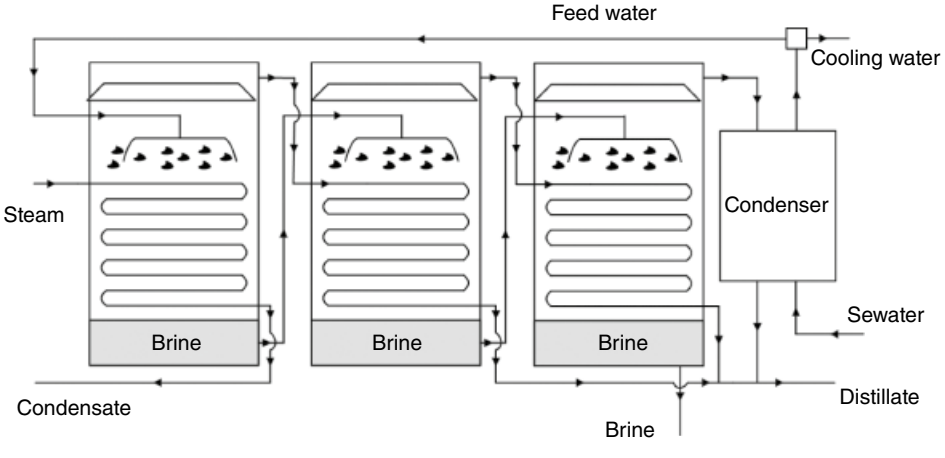

Figure 11.13 The conventional MED system [43].

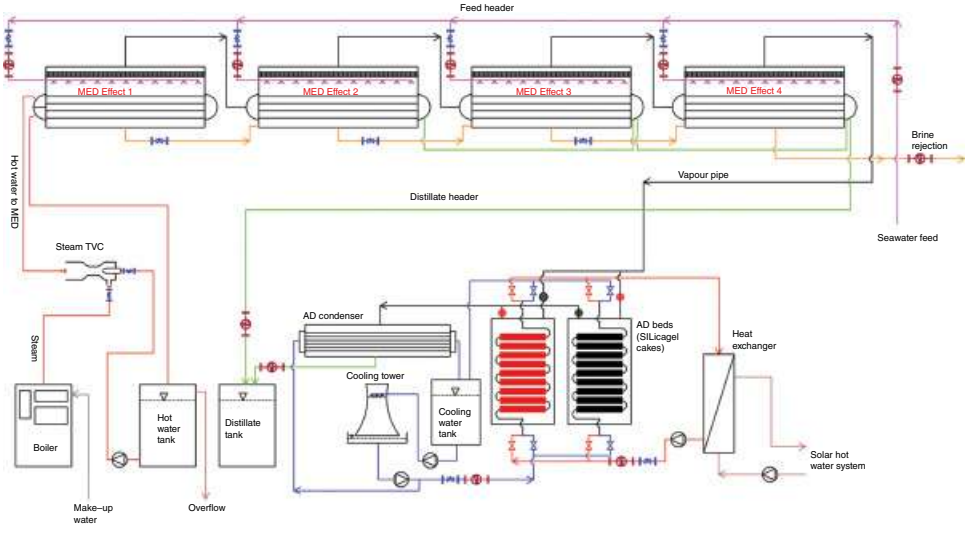

Figure 11.14 Four effect MED and AD hybrid system schematic.

preheated feedwater is sprayed through nozzles in the evaporators where it evaporates using latent heat of vapors from the previous effect flowing in the tubes of a horizontal tube falling film evaporator [44]. The condensate from all effects is collected in a distillate collection tank and the brine in a brine collection tank. The vapors from the last effect of the MED system are directed to an AD system where these are adsorbed onto an adsorbent. The high affinity of the adsorbent for water significantly reduces the temperature (below ambient) in the last effects. Then heat is supplied to desorb the vapors which are then collected as a distillate after condensing in a condenser and augment the MED distillate. The auxiliary equipment in the system includes steam jet ejectors to remove non-condensable gases for better thermal performance, a pump to maintain feed pressure and flowrate, flow meters to monitor the required flowrate, and a vacuum pump to maintain the system operating pressure.

Based on the above proposed MEDAD hybrid cycle, a pilot experimental setup with a nominal distillate capacity of $10\,m^3$/day is fabricated and installed at KAUST as shown in Figure 11.15. The system consists of four effect MED system with a heat transfer area of ~4 m^2/effect, integrated with an AD system. The AD system consists of two pairs of silica gel beds to adsorb water from the last MED effect, thus reducing the bottom brine temperature (BBT) to as low as 10 °C. Besides, an evacuated tube solar thermal collector system of $12\,m^3$ storage capacity and $352\,m^2$ area is attached with the adsorption system to harness the solar energy for adsorbent regeneration at the end of each cycle. The detailed process and geometric specifications of the pilot MEDAD system are provided in Table 11.1.

The system operates as the preheated feed from the Red Sea is sprayed in the falling film evaporators of the MED system after an initial screening. The nozzles are used to maintain the film thickness to achieve falling film evaporation. The feed in the first effect is evaporated using heat from the hot water flowing inside tubes coming from a boiler. The vapors

Figure 11.15 Pilot MEDAD hybrid plant installed at KAUST.

Table 11.1 Process and geometrical specifications of the pilot MEDAD hybrid system [45].

Parameter	Value	
Hot water flowrate, m^3/h	5	
Hot water inlet temperature, °C	25–65	
Feedwater flowrate, m^3/h	0.4–0.5	
Feedwater temperature, °C	30–33	
Feedwater salinity, ppm	35,000	
Adsorption cycle		
The total mass of adsorbent (silica gel), kg	312	
The surface area of adsorbent, m^2/kg	850	
Switching time, adsorption/desorption, s	270/30	
MED cycle	**Steam generator**	**MED stages**
Heat transfer area per effect, m^2	4	4
Number of effects	1	3
Tube outside diameter, m	0.015	0.019
Tube thickness, m	0.0005	0.0005
Tube length, m	0.635	0.635
Tube arrangement (tubes/row × number of rows)	8 × 14	8 × 14
Evaporator volume, m^3	0.650 × 0.520 × 700	0.650 × 0.500 × 700

produced in the first effect are then used to evaporate the next effect and so on. In a standalone MED operation, the vapors from the last effect are condensed as a distillate in a water-cooled condenser which also serves as a preheater in this case. While in the case of the MEDAD hybrid arrangement, the vapors are captured by the AD system in which silica gel beds undergo adsorption and desorption alternatively. In this case, the water production is an aggregate of MED and AD system vapors which is almost twice the standalone MED system.

Figure 11.16 shows the temperature trend of the MEDAD cycle. It was observed that the top brine temperature in the first effect for the standalone MED system was close to 45–50 °C which decreased by 1–1.5 °C per effect in the subsequent stages. Therefore, the BBT in the last effect was observed as 38–39 °C. This BBT cannot be lower than 35 °C because of condenser cooling water temperature constraints, thus limiting the number of stages. While a drastic change in these temperatures was observed by switching the system to the hybrid MEDAD mode as depicted in the middle section of Figure 11.16. The TBT dropped below 40–41 °C with 2–3 °C of interstage temperature differences.

It is also important to notice that in the MEAD arrangement, the last evaporation effect operated below the ambient temperature, i.e. 23–24 °C, thus allowing the addition of intermediate stages even at low temperature (50 °C) heat sources. Moreover, the effect of the AD cycle on the temperature profile is prominent in the downstream stages and diminishes toward the upstream stages. The visible kinks in the temperature profiles of stage 4 are due to the batch operation of their main driver, i.e. AD cycle and shrinks in the initial stages

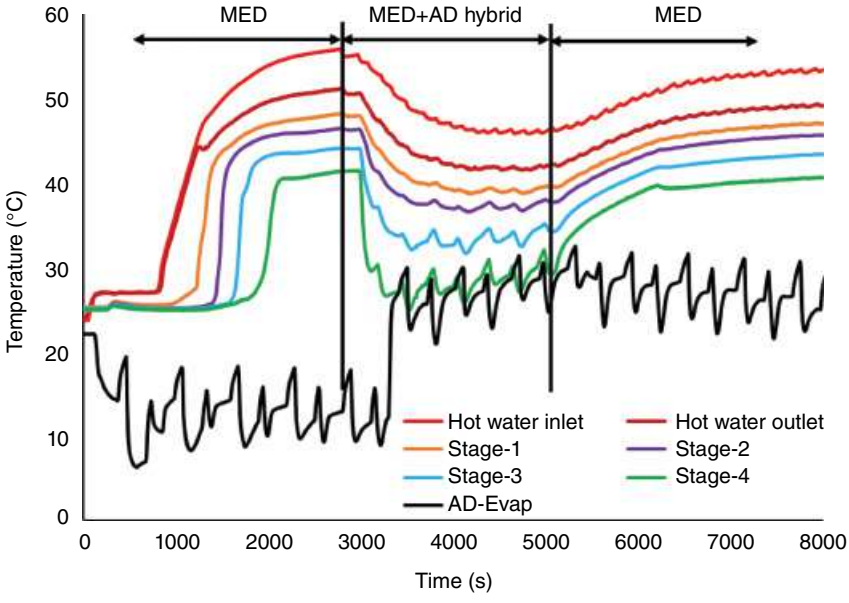

Figure 11.16 Temperature trend of MEDAD systems.

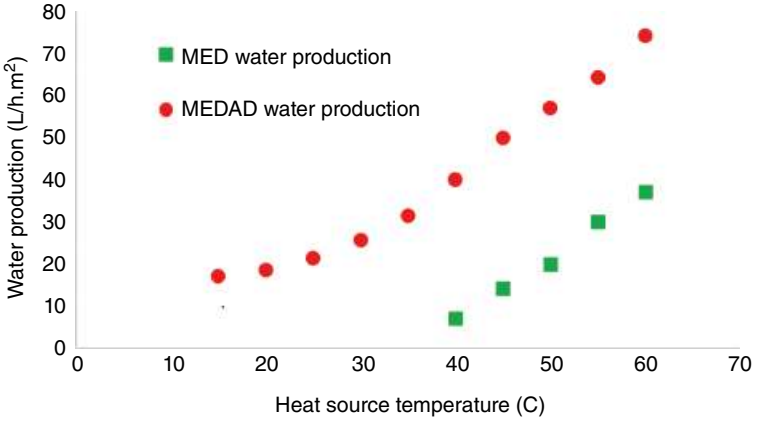

Figure 11.17 Water production at different heat source temperatures.

due to smooth operation of steam generator which controls the evaporation in these stages. Though the AD system is robust and has high system reliability, the possibility of tripping the AD system due to any endogenous or exogenous malfunctioning in MEDAD is also studied. It is observed that upon shutdown of the AD cycle, the MEDAD system was switched to a standalone MED system as shown in the third part of Figure 11.16. The system adapts the temperature trend of standalone MED without any prerequisite.

Figure 11.17 shows freshwater production rates at different heat source temperatures. It is observed that an increase in the heat source temperature increased water production due to higher heat fluxes. Moreover, the integration of the AD cycle with MED boosted the

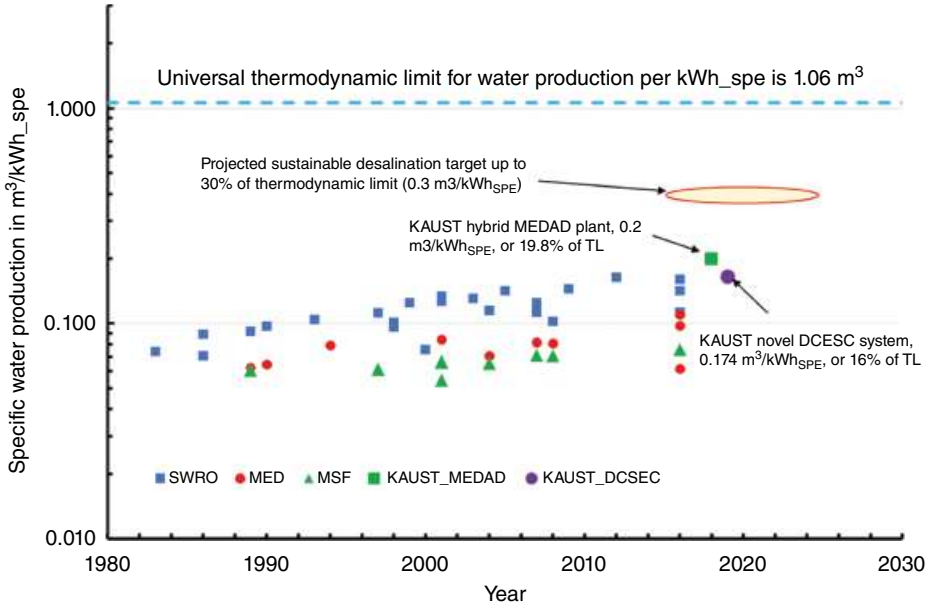

Figure 11.18 Rationale thermodynamic limit-based comparison of different desalination technologies [46–48].

distillate by two to three folds. This surge in water production is because of the AD cycle which reduces the stage saturation temperature resulting in a higher thermal gradient. Additionally, the high water vapor affinity of Silica Gel drives the hybrid systems from both ends (i.e. steam generator and adsorption beds), thus increasing the evaporation rate. Meanwhile, it is worth mentioning that the water production in a hybrid system can be further increased by incorporating additional evaporation effects due to a higher overall operational temperature gap (60–10 °C) compared to conventional MED (60–35 °C).

Figure 11.18 compares the different conventional and novel desalination system operations in terms of thermodynamic limits (TLs). It can be noticed that the conventional systems like SWRO, MED and MSF operate in 10–13% of their TLs. A novel Direct Contact Spray Evaporation and Condensation (DCSEC) tested at KAUST operates at 16% of TL. While the proposed hybrid MEDAD operates at ~20% of TL, thus showing superiority over other systems in terms of thermodynamic synergy. However, for sustainable system operation, the targeted TL is ~30% for which more such technological breakthroughs are required.

11.3.4 Zero Liquid Discharge Desalination Enhanced by Adsorption

The adsorption phenomenon can also be employed in the zero liquid discharge (ZLD) system. It can lower the vapor pressure in the crystallizer, thus promoting the evaporation rate and accelerating the crystallization process.

Figure 11.19 shows a typical ZLD system, which consists of a regular desalination unit (e.g. MED, MSF, RO, MD, etc.), a brine concentrator and a crystallizer. Seawater is firstly

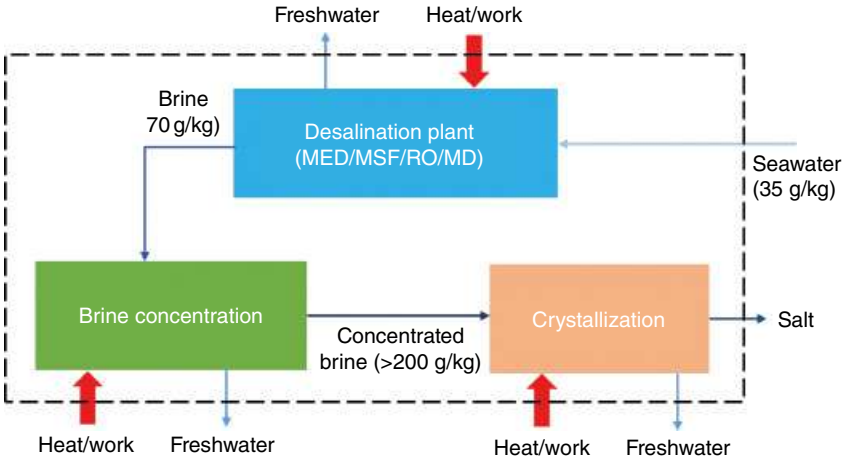

Figure 11.19 Schematic of a zero-liquid-discharge desalination system.

treated in the desalination plant to recover 40–60% of freshwater [48–50]. The remaining stream is named the brine, which has a salinity of ~70 g/kg. The brine is concentrated in the brine concentrator to further recover freshwater. A brine concentrator can be any of the existing evaporative desalination systems, but will require different construction materials and operation strategies to handle a higher feed salinity [50]. The stream leaving the brine concentrator will have a salinity of >200 g/kg. The further concentrated stream is finally directed to the crystallizer to achieve complete separation of salt and water.

Crystallization is the last step of the ZLD process. Figure 11.20 is the schematic of a typical evaporative crystallizer. Concentrated brine [1] is mixed with recirculation liquid (5b) separated from the bottom of the crystallization chamber. The mixture is heated to state [3]

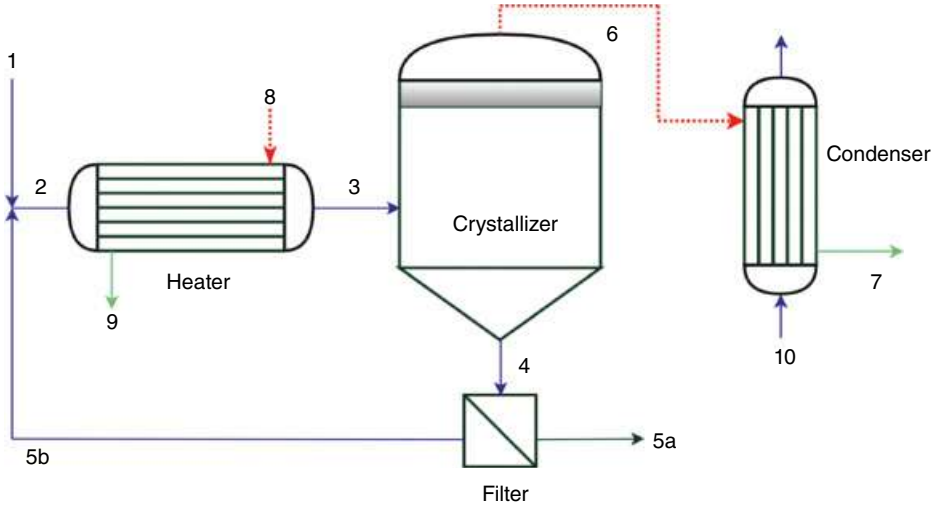

Figure 11.20 Schematic of an evaporative crystallizer.

and injected into the crystallization chamber that is under vacuum condition. In the crystallization chamber, a portion of the brine flashes off into vapor [6], and the remaining stream [4] is supersaturated (i.e. salt concentration exceeds its solubility). Salt precipitation takes place at the bottom of the crystallizer. Salt is separated from the salt–liquid mixture, while the remaining liquid is mixed with the feed brine for further evaporation and crystallization. The produced vapor is condensed in the condenser using cooling water [10]. The above-mentioned crystallization process is schematically depicted in the temperature-salinity diagram in Figure 11.21.

To achieve a ZLD status, the flash-off vapor [7] should be equal to the amount of water in the feed brine [1], and the crystallization rate (5a) has to be the same as the salt content in the feed. For example, for 1 kg/s of brine with a salinity of 250 g/kg, the corresponding evaporation and crystallization rates are 0.75 and 0.25 kg/s, respectively. However, there is no heat input to the brine inside the crystallization chamber, and the enthalpy contained in the brine itself is the only source of evaporation. Due to a high latent heat of vaporization with respect to the sensible heat, only a very small portion of brine can evaporate and the increase in salt concentration is small. As a result, the brine has to be recirculated at a high flowrate to achieve the required evaporation and crystallization rates. Table 11.2 shows the states of the brine in the evaporative crystallizer. As can be seen from the table, <3% of the brine injected into the crystallizer flashes, and the increase of salinity is only 7 g/kg. In order to treat 1 kg/s of feed brine, the required circulation flowrate is 26 kg/s. Such a high recirculation flowrate not only makes the system bulky but also consumes a significant amount of electricity for pumping.

The key to reducing the recirculation flowrate is to increase the temperature difference between the feed brine (T3) and the vapor in the chamber (T7). However, the temperature of the brine cannot exceed 75 °C due to higher scaling and fouling potential at higher temperatures, while the vapor temperature is limited by the cooling water

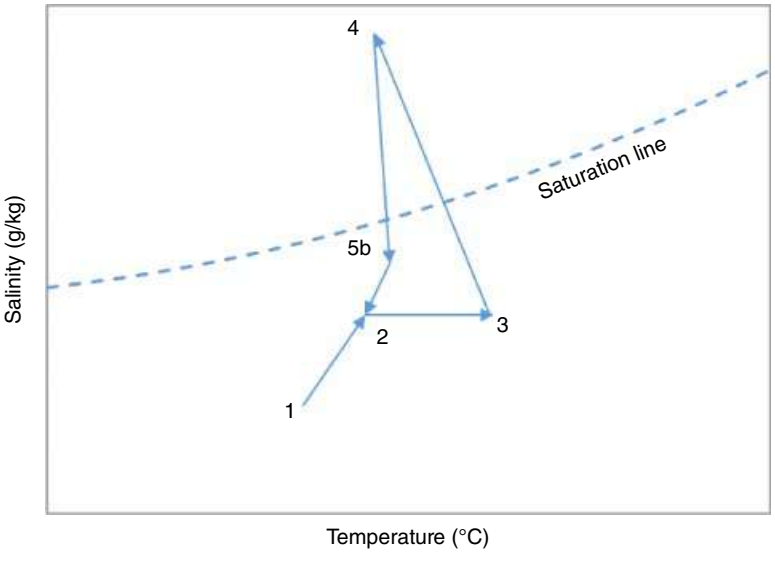

Figure 11.21 Evaporative crystallization process in the temperature-solubility diagram.

Table 11.2 States of streams for an evaporative crystallizer.

		Flowrate	Temperature	Salinity
Point	**State**	**kg/s**	**°C**	**g/kg**
1	Feed brine	1.00	40.00	250.00
2	Brine mixture	26.24	48.86	270.61
3	Heated brine	26.24	68.06	270.61
4	Brine slurry	25.49	46.01	277.06
5a	Salt crystallizer	0.25	46.13	1000.00
5b	Liquid brine	25.24	46.13	271.42
6	Vapor	0.75	40.51	0.00
7	Distillate	0.75	40.51	0.00
8	Heat source	0.74	75.00	0.00
9	Condensate	0.74	75.00	0.00
10	Cooling water inlet	92.17	30.00	35.00
11	Cooling water outlet	92.17	34.73	35.00

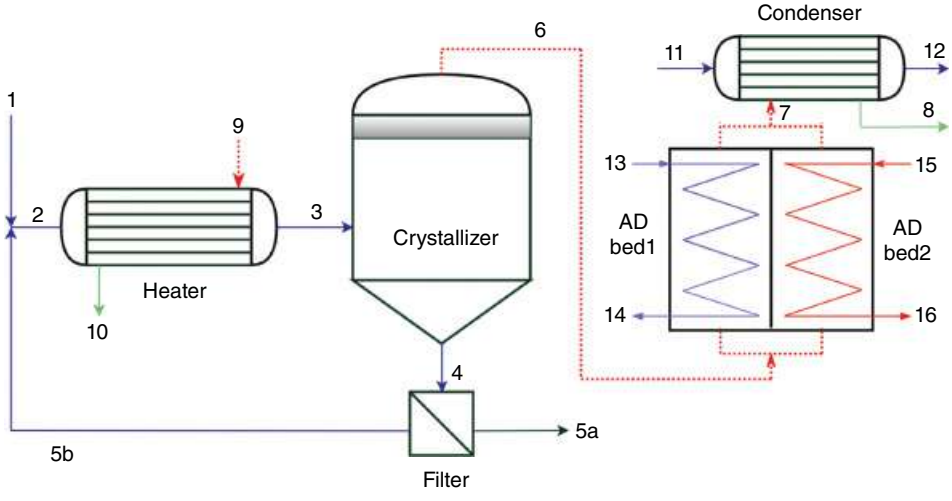

Figure 11.22 Schematic of an evaporative crystallizer integrated with adsorption cycle.

temperature (T10). These restrictions limit the temperature difference in the conventional evaporative crystallizer.

With a high affinity of adsorbents to water vapor, adsorption can effectively expand the temperature difference by inducing low vapor pressure. Figure 11.22 shows the integration of evaporative crystallizer with an adsorption cycle. Vapor [6] produced in the crystallization chamber is directed to the adsorption bed to be adsorbed. Then the adsorption bed is heated by hot water [16] to separate the vapor from the adsorbent. The vapor [7] separated

from the AD bed has a higher temperature and can be condensed using the cooling water [11]. Due to the high affinity of adsorbent materials to water molecules, the adsorption system is able to significantly lower the vapor temperature in the crystallization chamber (T6). Table 11.3 shows the states of the water and vapor streams for an evaporative crystallizer integrated with adsorption cycle. It is assumed that the average saturation vapor temperature in the crystallizer is 15 °C. Compared with a regular evaporative crystallizer operating at the same heat source and cooling water temperatures, the temperature difference between the feed brine and the vapor is almost doubled. As a result, the recirculation flowrate is reduced from 26 to 11 kg/s. Such a lower recirculation flowrate not only reduces the pumping power consumption, but also makes the system more compact. The potential benefits include a reduction in both initial and operational costs.

Figure 11.23 shows the recirculation flowrate at different saturation vapor temperatures. The recirculation flowrate increases exponentially with the increase of saturation vapor pressure in the crystallization chamber. Considering a cooling water temperature of 30 °C, the saturation vapor temperature in a regular crystallizer is usually >35 °C, and the corresponding recirculation flowrate is above 20 kg/s for 1 kg/s of feed brine. On the other hand, the saturation vapor temperature can be reduced to <25 °C by integrating the adsorption system, thus lowering the recirculation flowrate to below 13 kg/s. In practical operation, the vapor temperature will be determined by several key design and operating parameters,

Table 11.3 States of streams for an evaporative crystallizer integrated with adsorption cycle.

		Flowrate	Temperature	Salinity
Point	**State**	**kg/s**	**°C**	**g/kg**
1	Feed brine	1.00	40.00	250.00
2	Brine mixture	11.35	23.41	269.94
3	Heated brine	11.35	73.05	269.94
4	Brine slurry	10.60	20.73	289.04
5a	Salt crystallizer	0.25	21.05	1000.00
5b	Liquid brine	10.35	21.05	271.87
6	Vapor	0.75	15.07	0.00
7	Regenerated vapor	0.75	37.00	0.00
8	Distillate	0.75	35.00	0.00
9	Heat source	0.71	75.00	0.00
10	Condensate	0.71	75.00	0.00
11	Condenser cooling water inlet	92.17	30.00	40.00
12	Condenser cooling water outlet	92.17	34.73	40.00
13	AD cooling water inlet	92.17	30.00	35.00
14	AD cooling water outlet	92.17	34.73	35.00
15	AD hot water inlet	92.17	85.00	0.00
16	AD hot water outlet	92.17	75.00	0.00

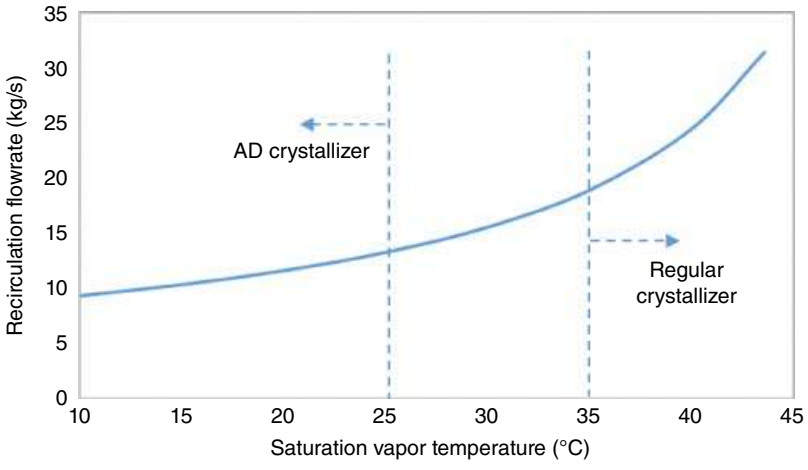

Figure 11.23 Recirculation flowrate under different vapor temperatures at a heat source temperature of 75 °C and a feed brine salinity of 250 g/kg.

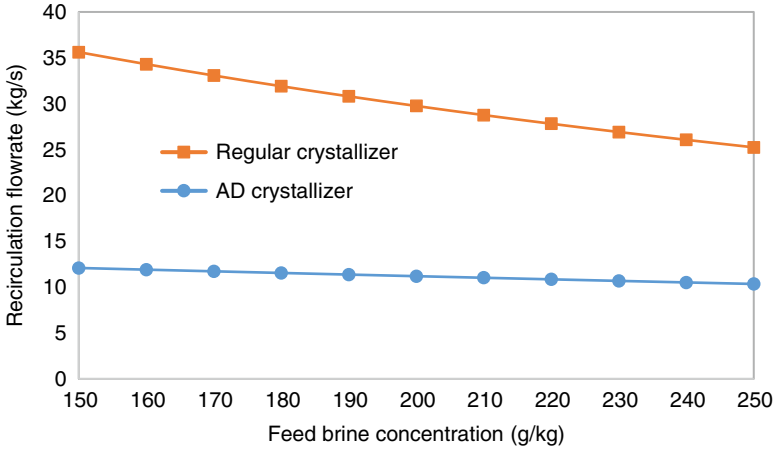

Figure 11.24 Recirculation flowrate under different feed brine salinities at a vapor temperature of 15 °C and a heat source temperature of 75 °C.

such as the type of adsorbent used, the heat transfer area, the regeneration temperature, and the cycle time.

The recirculation flowrate in a crystallizer is also impacted by the feed salinity. When the brine supplied to the crystallizer has a lower salinity, it needs a higher evaporation rate and, thus, a higher recirculation flowrate. As can be seen from Figure 11.24, the recirculation flowrate for the regular evaporative crystallizer increases from 25 to 35 kg/s when the inlet brine salinity is reduced from 250 to 150 g/kg. The change is less significant for a hybrid adsorption-crystallization system, i.e. from 10 to 12 kg/s. In other words, the hybrid system allows for a lower brine salinity from the brine concentrator. Such a feature will benefit the design and operation of the brine concentrator, as it reduces the potential of scaling and fouling.

11.4 Conclusion

This chapter summarizes the fundamental theory of adsorption and the applications of the adsorption phenomenon in the water industry. A universal adsorption isotherm model is firstly presented, which is able to describe the adsorption thermodynamics of different types of adsorbent-adsorbate pairs, thus providing a powerful tool for the design and optimization of the adsorption process. Afterward, various adsorption systems are introduced. The temperature-swing and pressure-swing adsorption cycles are capable of producing freshwater and cooling effect simultaneously using a low-grade heat source. When integrated with a multi-effect distillation system, adsorption can significantly lower the vapor pressure in the last effect, thus promoting water evaporation and reducing heat consumption. For ZLD desalination, adsorption can be integrated with an evaporative crystallizer to enhance evaporation and reduce the recirculation rate, which will lead to lower pumping power consumption and smaller component size.

Despite great success at the research level, adsorption systems have great room for further improvement, such as enhancement of heat and mass transfer in the adsorption beds, development of more advanced adsorbent materials, and optimal integration with other processes. With these advances, more energy-efficient and sustainable desalination systems based on adsorption can be expected in the near future.

References

1 UN-Water U (2020). *United Nations World Water Development Report 2020: Water and Climate Change*. Paris, France: UNESCO.

2 Ng, K.C., Thu, K., Oh, S.J. et al. (2015). Recent developments in thermally-driven seawater desalination: energy efficiency improvement by hybridization of the MED and AD cycles. *Desalination* 356: 255–270.

3 Connor, R. (2015). *The United Nations World Water Development Report 2015: Water for a Sustainable World*, vol. 1. UNESCO Publishing.

4 UNICEF (2018). *Progress on Drinking Water, Sanitation and Hygiene: Joint Monitoring Programme 2017 Update and SDG Baselines*. World Health Organization (WHO).

5 Shahzad, M.W., Burhan, M., Ybyraiymkul, D., and Ng, K.C. (2019). Desalination processes' efficiency and future roadmap. *Entropy* 21 (1): 84.

6 Al-Sahali, M. and Ettouney, H. (2007). Developments in thermal desalination processes: design, energy, and costing aspects. *Desalination* 214 (1–3): 227–240.

7 Chen, Q., Muhammad, B., Akhtar, F.H. et al. (2020). Thermo-economic analysis and optimization of a vacuum multi-effect membrane distillation system. *Desalination* 483: 114413.

8 Alkhudhiri, A., Darwish, N., and Hilal, N. (2012). Membrane distillation: a comprehensive review. *Desalination* 287: 2–18.

9 Zhao, S., Zou, L., Tang, C.Y., and Mulcahy, D. (2012). Recent developments in forward osmosis: opportunities and challenges. *Journal of Membrane Science* 396: 1–21.

10 Chung, T.-S., Zhang, S., Wang, K.Y. et al. (2012). Forward osmosis processes: yesterday, today and tomorrow. *Desalination* 287: 78–81.

11 Chen, Q., Burhan, M., Shahzad, M.W. et al. (2020). Simultaneous production of cooling and freshwater by an integrated indirect evaporative cooling and humidification-dehumidification desalination cycle. *Energy Conversion and Management* 221: 113169.
12 Lienhard, J.H. (2019). Humidification-dehumidification desalination. In: *Desalination: Water from Water* (ed. J. Kucera), 387–446. Scrivener Publishing.
13 Chen, Q., Oh, S., Li, Y., and Ja, M.K. (2020). Thermodynamic optimization of a low-temperature desalination system driven by sensible heat sources. *Energy* 192: 116633.
14 Chen, Q. and Chua, K.J. (2018). A spray assisted low-temperature desalination technology. In: *Emerging Technologies for Sustainable Desalination Handbook*, 255–284. Elsevier.
15 Qian, C., Alrowais, R., Burhan, M. et al. (2020). A self-sustainable solar desalination system using direct spray technology. *Energy* 205: 118037.
16 Malaeb, L. and Ayoub, G.M. (2011). Reverse osmosis technology for water treatment: state of the art review. *Desalination* 267 (1): 1–8.
17 Shahzad, M.W., Burhan, M., and Ng, K.C. (2017). Pushing desalination recovery to the maximum limit: membrane and thermal processes integration. *Desalination* 416: 54–64.
18 Abid, A., Jamil, M.A., Us Sabah, N. et al. (2020). Exergoeconomic optimization of a forward feed multi-effect desalination system with and without energy recovery. *Desalination* 499: 114808.
19 Al-Karaghouli, A. and Kazmerski, L.L. (2013). Energy consumption and water production cost of conventional and renewable-energy-powered desalination processes. *Renewable and Sustainable Energy Reviews* 24: 343–356.
20 Chen, Q., Ja, M.K., Li, Y., and Chua, K. (2018). Energy, economic and environmental (3E) analysis and multi-objective optimization of a spray-assisted low-temperature desalination system. *Energy* 151: 387–401.
21 Lienhard, J.H. V, Mistry, K.H., Sharqawy, M.H., and Thiel, G.P. (2017). Thermodynamics, exergy, and energy efficiency in desalination systems. In: *Desalination Sustainability: A Technical, Socioeconomic, and Environmental Approach* (ed. H.A. Arafat). Elsevier Publishing Co.
22 Chen, Q., Ja, M.K., Li, Y., and Chua, K. (2017). On the second law analysis of a multi-stage spray-assisted low-temperature desalination system. *Energy Conversion and Management* 148: 1306–1316.
23 Shahzad, M.W., Ng, K.C., Thu, K. et al. (2014). Multi effect desalination and adsorption desalination (MEDAD): a hybrid desalination method. *Applied Thermal Engineering* 72 (2): 289–297.
24 Shahzad, M.W., Thu, K., Kim, Y.-D., and Ng, K.C. (2015). An experimental investigation on MEDAD hybrid desalination cycle. *Applied Energy* 148: 273–281.
25 Lowitz, T. (1786). Chromatographic adsorption analysis: selected works. *Crell's Chem Ann* 1: 211.
26 Scheele, C.W. (1894). *Chemische Abhandlung von der Luft und dem Feuer:(1777)*. Engelmann.
27 Aristov, Y.I. (2020). *Nanocomposite Sorbents for Multiple Applications*. Singapore: Jenny Stanford Publishing Pte. Ltd.
28 Barrer, R.M. (1982). *Hydrothermal Chemistry of Zeolites*. Academic Press.
29 Barrer, R.M. (1981). Zeolites and their synthesis. *Zeolites* 1 (3): 130–140.
30 Barrer, R. and Rideal, E.K. (1939). Permeation, diffusion and solution of gases in organic polymers. *Transactions of the Faraday Society* 35: 628–643.

31 Barrer, R.M. (1941). Diffusion in and through solids: Рипол Классик.

32 Burhan, M., Shahzad, M.W., and Ng, K.C. (2018). Energy distribution function based universal adsorption isotherm model for all types of isotherm. *International Journal of Low Carbon Technologies* 13 (3): 292–297.

33 Ng, K.C., Burhan, M., Shahzad, M.W., and Ismail, A.B. (2017). A universal isotherm model to capture adsorption uptake and energy distribution of porous heterogeneous surface. *Scientific Reports* 7 (1): 1–11.

34 Rudziński, W., Borowiecki, T., Dominko, A., and Pańczyk, T. (1999). A new quantitative interpretation of temperature-programmed desorption spectra from heterogeneous solid surfaces, based on statistical rate theory of interfacial transport: the effects of simultaneous readsorption. *Langmuir* 15 (19): 6386–6394.

35 Rudzinski, W. and Panczyk, T. (2002). The Langmuirian adsorption kinetics revised: a farewell to the XXth century theories? *Adsorption* 8 (1): 23–34.

36 Burhan, M., Shahzad, M.W., and Ng, K.C. (2019). A universal theoretical framework in material characterization for tailored porous surface design. *Scientific Reports* 9 (1): 1–7.

37 Langmuir, I. (1918). The adsorption of gases on plane surfaces of glass, mica and platinum. *Journal of the American Chemical Society* 40 (9): 1361–1403.

38 Dabrowski, A. and Jaroniec, M. (1980). Effects of surface heterogeneity in adsorption from binary liquid mixtures: III. Analysis of experimental data by using Langmuir – Freundlich type equations. *Journal of Colloid and Interface Science* 73 (2): 475–482.

39 Toth, J. (1971). State equation of the solid-gas interface layers. *Models in Chemistry* 69: 311–328.

40 Dubinin, M. and Astakhov, V. (1971). Development of ideas of volume filling of micropores during adsorption of gases and vapours by microporous adsorbents. *Izvestiya Akademii Nauk SSSR, Seriya Khimicheskaya* 20: 3–7.

41 Ng, K.C., Thu, K., Chakraborty, A. et al. (2009). Solar-assisted dual-effect adsorption cycle for the production of cooling effect and potable water. *International Journal of Low Carbon Technologies* 4 (2): 61–67.

42 Aristov, Y.I., Tokarev, M., Cacciola, G., and Restuccia, G. (1996). Selective water sorbents for multiple applications, 1. CaCl 2 confined in mesopores of silica gel: sorption properties. *Reaction Kinetics and Catalysis Letters* 59 (2): 325–333.

43 Jamil, M.A. and Zubair, S.M. (2018). Effect of feed flow arrangement and number of evaporators on the performance of multi-effect mechanical vapor compression desalination systems. *Desalination* 429: 76–87.

44 Shahzad, M.W. (2013). The hybrid multi-effect desalination (MED) and the adsorption (AD) cycle for desalination. PhD thesis. National University of Singapore. https://core.ac.uk/download/pdf/48679046.pdf.

45 Son, H.S., Shahzad, M.W., Ghaffour, N., and Ng, K.C. (2020). Pilot studies on synergetic impacts of energy utilization in hybrid desalination system: multi-effect distillation and adsorption cycle (MED-AD). *Desalination* 477: 114266.

46 Chen, Q., Li, Y., and Chua, K. (2016). On the thermodynamic analysis of a novel low-grade heat driven desalination system. *Energy Conversion and Management* 128: 145–159.

47 Ng, K.C., Shahzad, M.W., Son, H.S., and Hamed, O.A. (2017). An exergy approach to efficiency evaluation of desalination. *Applied Physics Letters* 110 (18): 184101.

48 Chen, Q., Ja, M.K., Li, Y., and Chua, K. (2019). Energy, exergy and economic analysis of a hybrid spray-assisted low-temperature desalination/thermal vapor compression system. *Energy* 166: 871–885.

49 Chen, Q., Burhan, M., Shahzard, M.W. et al. (2020). A novel low-temperature thermal desalination technology using direct-contact spray method. In: *Desalination-Challenges and Opportunities*. IntechOpen.

50 Chen, Q., Burhan, M., Shahzad, M.W. et al. (2021). A zero liquid discharge system integrating multi-effect distillation and evaporative crystallization for desalination brine treatment. *Desalination* 502: 114928.

12

Sustainable Distillation Processes

Mirko Skiborowski[1], Kai Fabian Kruber[1], and Thomas Waltermann[2]

[1] *Institute of Process Systems Engineering, Hamburg University of Technology, Hamburg, Germany*
[2] *Covestro Deutschland AG, Process Technology – Digital Process, Leverkusen, Germany*

12.1 Introduction

Distillation is one of the oldest and most frequently used purification methods. In its most elementary form, a liquid mixture is heated to its saturation temperature and partially evaporated, such that the generated vapor is separated and condensed to form a product. Application of such a simple batch distillation dates back several thousand years with historical evidence indicating e.g. the preparation of solvents for the extraction of essential oils from herbs by the Sumerian around 3500 BC [1]. Today, simple batch distillation is primarily used in the laboratory for the recovery or purification of products from experiments in chemical or biochemical engineering. When operated continuously, single-stage separation by partial evaporation is also referred to as flash distillation, in which a continuous feed is partially vaporized to give a vapor richer in the more volatile components than the remaining liquid. Flash distillation can either be accomplished through lowering the pressure of a boiling liquid and exploiting the temperature dependency of the vapor pressure, or by continuously heating a boiling liquid and separating and condensing the produced vapor. The latter option is illustrated in Figure 12.1 (left), while Figure 12.1 (right) illustrates the potential separation of the feed stream with flow rate F and composition x^{F}, into the distillate (V, x^{D}), which is the condensed vapor stream, and the residue (L, x^{B}). The product compositions depend on the heat duty applied for the partial evaporation (Q_{B}), as well as the vapor-liquid equilibrium (VLE), which for binary mixtures (A,B) is oftentimes expressed on the basis of the relative volatility:

$$\alpha = \alpha_{\mathrm{AB}} = \frac{y_{\mathrm{A}} / x_{\mathrm{A}}}{y_{\mathrm{B}} / x_{\mathrm{B}}} = \frac{\gamma_{\mathrm{A}} P_{0\mathrm{A}}^{\mathrm{LV}}}{\gamma_{\mathrm{B}} P_{0\mathrm{B}}^{\mathrm{LV}}}. \tag{12.1}$$

Sustainable Separation Engineering: Materials, Techniques and Process Development, Volume 2, First Edition. Edited by Gyorgy Szekely and Dan Zhao.
© 2022 John Wiley & Sons Ltd. Published 2022 by John Wiley & Sons Ltd.

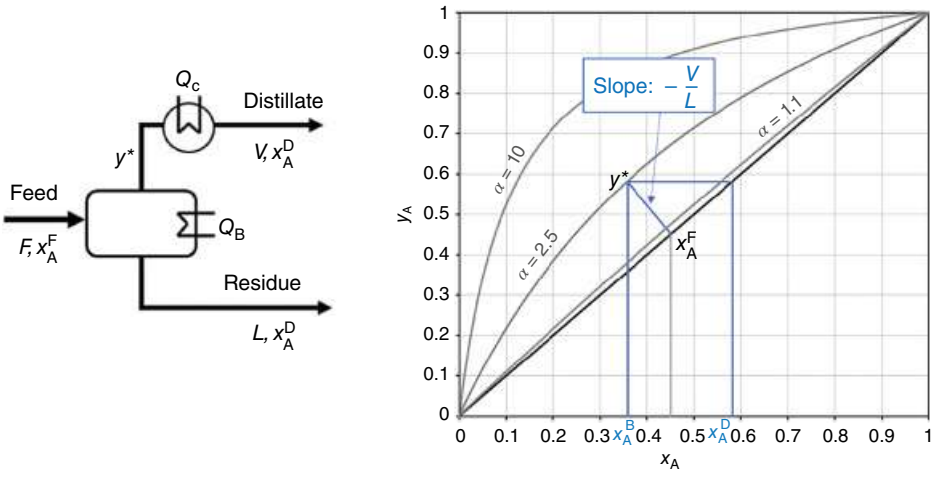

Figure 12.1 Illustration of simple flash distillation (left) and respective separation for a binary mixture with constant relative volatility $\alpha = 2.5$ (right).

For closely ideal systems, for which the activity coefficients (γ) are approximately 1, the relative volatility depends solely on the pure component vapor pressure. The indicated VLE lines in the y,x-diagram in Figure 12.1 furthermore represent the assumption of a constant relative volatility.

While simple flash distillation is able to satisfy the product purity at least for one product for very wide boiling systems ($\alpha > 10$), such as e.g. in seawater desalination, it is obviously incapable of producing two products with high purity, especially if $\alpha \to 1$. In order to overcome the limitation of a single equilibrium stage, a cascade of flash drums can be integrated countercurrently, enabling the production of two products with high purity by means of a multistage distillation (rectification). Figure 12.2 (top) illustrates such a countercurrent cascade, which can be divided in a rectifying section above the feed stage and a stripping section below the feed stage. It is important to note that high purities of both products become feasible, as long as the relative volatility $\alpha > 1$, while the required number of equilibrium stages of course depends on α, as well as the liquid that is recycled on top of the column, after the condenser, and the boil-up, which is the vapor created in the reboiler at the bottom of the column. Applying the well-known method of McCabe and Thiele [2], which has been proposed almost a century ago, the respective stage-profile, which is illustrated in Figure 12.2 (botom) can be constructed based on the specification of the desired products and the reflux ratio. We assume that the reader is familiar with these basic concepts and refer e.g. to the excellent textbooks of Mersmann et al. [3] and de Haan et al. [4].

It is well known that mass and heat transfer benefit from countercurrent configurations, with all kinds of separation processes, such as liquid–liquid extraction, absorption/desorption, and adsorption all exploiting countercurrent contacting. However, while similar countercurrent cascades with recycling have been considered e.g. for multistage membrane separations [5], the simplicity of a gravity-driven countercurrent contacting and separation of gas/vapor and liquid has made this specific configuration most prominent in distillation. In fact, the first continuously working distillation column has been patented by

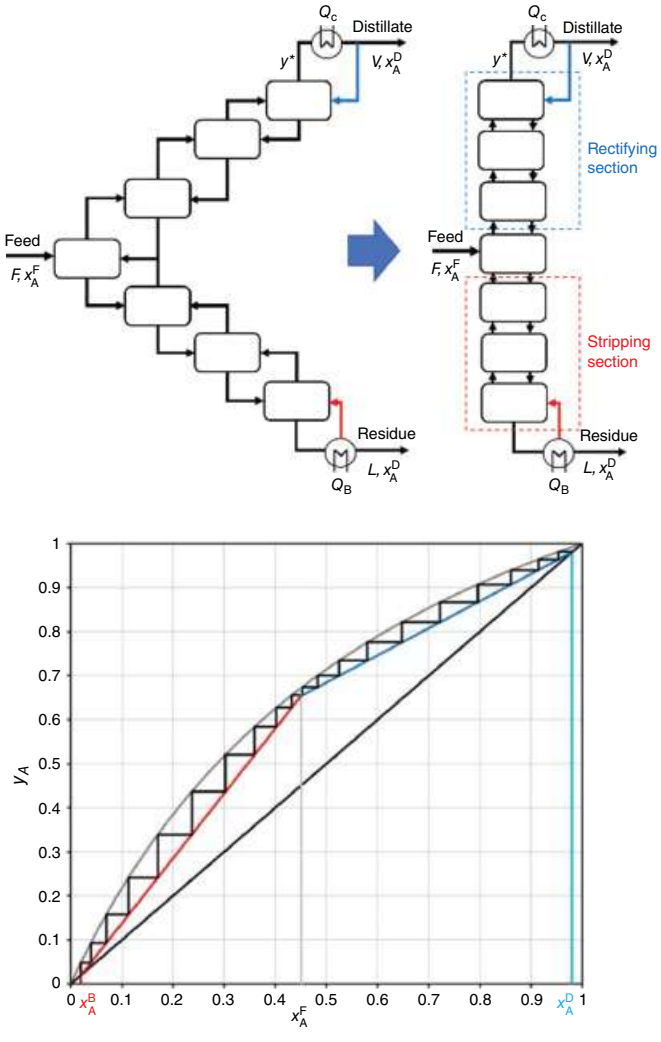

Figure 12.2 Illustration of countercurrent multistage distillation (top) and respective equilibrium stage profile for the separation of a mixture with constant relative volatility α = 2.5 (bottom).

Jean-Baptiste Cellier-Blumenthal more than 200 years ago, with constant improvements on all scales [1]. This also holds true for modeling efforts that most often build on the equilibrium-stage model, whose concept has been outlined for the distillation of alcohol almost 140 years ago by Sorel, and is nowadays supported by rate-based nonequilibrium models, as well as computational fluid dynamics for the development of advanced internals [6, 7]. Distillation columns are industrially applied at all kinds of conditions, ranging from vacuum conditions (100 mbar, sometimes even 10 mbar) to high pressure (~35 bar, exceptionally up to 100 bar) [8, 9], and temperatures ranging from cryogenic conditions up to 350 °C [10]. While distillation columns in most cases produce a light boiling top and a heavy boiling bottoms product, wide-boiling systems may be separated into three products

with sufficient purity in a single column, and refinery processes in the petrochemical industry have even implemented single towers (crude unit) that produce six different fractions from the crude oil feed. Distillation columns range from small laboratory scale, with a diameter of a few cm and variable height, to large-scale towers with a diameter of several meters and up to a hundred meters in height. While the crude unit of a refinery plant can process around 40.000 m^3/day at a diameter of 8–9 m and a height of approximately 50 m [11], for the special application of a cryogenic separation of isotropic argon with a relative volatility of just $\alpha = 1.0015$, a column of 350 m height, exceeding the Eifel tower, has been constructed below ground level in a dismissed coal mine [12]. Given this rich history and versatility, it is not surprising that distillation is considered both, the most mature and most-widely applied separation technology (cf. Figure 12.3 (top)). With approximately 40.000 distillation columns operated in the United States alone, distillation is estimated to account for 90–95% of all industrial fluid separations [13–15].

However, distillation is considered as one of the most energy-intensive separation processes, which accounts for roughly 40% of the total energy consumption in the chemical

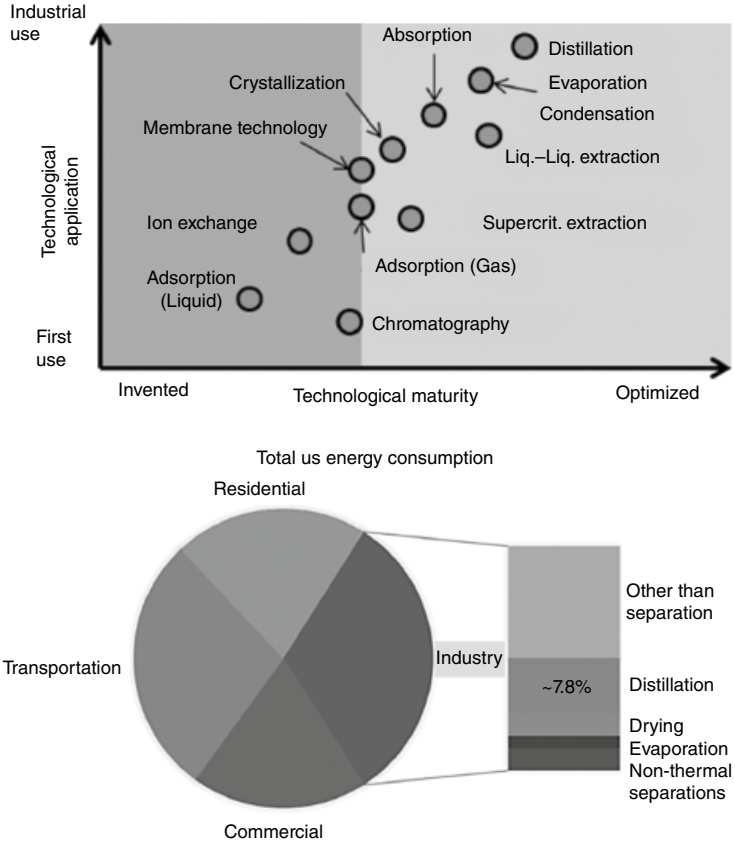

Figure 12.3 Illustration of technological maturity and application of fluid separation processes according to Goedecke [16] (top) and approximate distribution of US energy consumption according to Sholl and Lively [17] (bottom).

industry [18], amounting to approximately 8% of the total energy consumption in the United States [17] (cf. Figure 12.3 (bottom)). Since the energy supplied for distillation is mostly obtained from fossil fuels, the need to reduce greenhouse gas emissions mandates more sustainable solutions, with significantly reduced energy requirements. However, besides the environmental impact, improved energy efficiency also provides a huge economic incentive for today's industry, as distillation can make up more than 50% of the operating costs of a chemical plant [19]. The apparent exergy loss through take-up of high temperature heat in the reboiler and low temperature heat release in the condenser, as well as the reported low thermodynamic efficiency of distillation processes in the range of 5–20% [20, 21] have resulted in an increasing belief that distillation is severely inefficient and other processes, especially membrane separations, could save up to 90% of the energy used for distillation [17]. While there are of course cases which illustrate that such improvements are feasible, these are so far rare exceptions, which still require a thorough consideration of possible energy integration. In fact, analyzing the thermodynamic efficiency, defined as the free energy of unmixing divided by the minimum work and heat necessary for simplified ideal processes, Agrawal and Herron [22] illustrate that such low efficiencies are primarily related to low concentrated feed streams, while efficiencies can range from 30 to 80% for feed compositions between 0.15 and 0.75 mol/mol, depending on the relative volatility. Based on a similar analysis of ideal alternative separation processes, such as liquid–liquid extraction with a completely selective solvent and membrane processes with infinitely selective membranes, Cussler and Dutta [23] conclude that although these processes may enable high efficiencies, e.g. up to almost 100% for reverse osmosis, these efficiencies quickly drop to comparable levels of distillation once both products are required with high purity, mandating high recoveries. These results are further confirmed by Blahusiak et al. [24, 25], treating the process as a heat engine and finally suggesting to improve the efficiency of fluid separation processes by

- considering *pre-concentration or modification of the separation problem considering affinity-based separations* such as liquid–liquid extraction, extractive/azeotropic distillation, or membrane separation *in case of low concentrated feed streams*.
- considering different means for *energy integration*, such as heat integration, multi-effect distillation (MED), heat pumps, thermal coupling (TC), etc.

These efforts can dramatically reduce the energy requirements of distillation-based separations, making them the most efficient options in certain cases, and allowing for tremendous energy savings with respect to thousands of running distillation processes. **Thus, despite the existing misconceptions about the efficiency and maturity of distillation, properly designed distillation-based processes may oftentimes be the most sustainable option and one should not judge distillation solely on the heat of vaporization [15, 26]**.

This chapter provides an overview of the most prominent methods for improving the energy efficiency of distillation processes, focusing on the process configuration, the choice of operating conditions, heat and mass integration, as well as the use of mass separating agents. While this provides a portfolio of options that can foster significant improvements in the energy efficiency of certain separations, it should be noted that for the practical realization the specific choice of equipment and internals is also of vital importance. Improved

internals for classical distillation columns, such as the different generations of random and structured packings, do not only provide advantages in terms of low pressure drop and large operating ranges, but also reduced the required height equivalent to a theoretical plate (HETP) from approx. 0.5 to 1 m in the recent century to values between 0.05 and 0.15 m for recently developed high-performance wire gauze packings [1, 27, 28]. Yet, it is important to note that the HETP depends not only on the specific packing, but also on the physical properties of the chemical system, the operating conditions, and possible maldistribution [29]. Since distillation is industrially applied at various pressures and variable liquid and vapor loads, it is important to determine an appropriate internal based on the specific application [8, 9]. Further reduction of the HETP may be realized by performing the vapor–liquid contacting in a completely different type of equipment, such as a rotating packed bed (RPB), which utilizes the centrifugal force to provide a significantly extended operating range and allow for the application of ultrahigh surface area packings, such as metal foams ($a = 2500\ \mathrm{m^2/m^3}$), enabling HETP values down to 0.015 m [30]. While originally developed in the 1980s in the United Kingdom, industrial RPB implementations are today primarily found in Asia [31], whereas they are more frequently applied as standalone units for absorption and desorption. Cortes Garcia et al. [32] provide an elaborate overview of the different types of RPBs as well as a list of benefits and shortcomings that allow for a first assessment of this type of technology. Membrane distillation and cyclic distillation present further options to implement a separation by means of distillation, with certain benefits and limitations [21]. An in-depth analysis of membrane distillation is provided by Kiss and Kattan Readi [33], while Bildea et al. [34] provide a focused review on cyclic distillation columns.

The following sections of this chapter focus on the conceptual design of distillation processes, which builds on a thermodynamic analysis of the individual process configurations, without further consideration of the specific equipment that is used to implement the processes. Thus, even though we refer to distillation columns in the discussion and use illustrations of distillation columns, these may be implemented by classical tray or packed columns or any other device for vapor–liquid contacting. We start the discussion with several options for improving the energy-efficiency of single splits (binary distillation) in Section 12.2, followed by further options for multiproduct separations, which are usually conducted in a sequence of distillation columns, in Section 12.3. Section 12.4 addresses important options for the separation of close-boiling and azeotropic mixtures, which generally require the combination of distillation with an alternative separation process as well as some form of mass-separating agent. We finally close the chapter in Section 12.5 with a short summary and some remarks for further consideration.

12.2 Sustainable Distillation for Single Splits

The separation of a feed stream into two products (binary distillation) can be performed in a single distillation column. Given classical textbook procedures for the design of a binary distillation [3, 4, 35] and available rigorous models in commercial flowsheet simulation software, such as Aspen Plus or CHEMCAD, this task may seem trivial. However, the resulting conventional distillation column design is oftentimes far from optimal with

respect to energy use and process economics, since a multitude of options can reduce the energy requirement significantly [15]. These options include the use of intermediate heat-exchangers, double and MED, various types of heat pumps, as well as internally heat-integrated distillation column (HIDiC). The latter are addressed in Sections 12.2.3–12.2.4. While these options should be considered for single splits, additional options become viable in case the individual split is part of a multi-product separation (see Section 12.3).

12.2.1 Pressure Variation

While the complexity of a separation by distillation is directly linked to the VLE, any increase in relative volatility can result in a decrease of the energy requirement. Pressure variation directly affects the VLE and especially for closely ideal mixtures, for which vapor pressure is the controlling factor, the relative volatility usually decreases with increasing pressure [9]. Thus, vacuum distillation is a possible option to reduce the energy requirement for distillation. For example, the relative volatility of the prominent test system of cyclohexane and n-heptane increases from 1.42 to 1.94 (+37%), when considering a pressure decrease from 4.14 bar to 0.17 bar. This results in a possible energy reduction of ~40%, while allowing for a gentle separation at 32 °C (top vapor) to 48 °C (bottoms). Thus, vacuum distillation can considerably improve energy efficiency. Yet, this option should be carefully evaluated since pressure affects multiple physical properties in both phases, including density, viscosity, diffusivity, and surface tension, thus also affecting mass transfer [9]. The applicable pressure ranges are generally limited by the temperature limits induced by available utilities and the thermal stability of the processed media. Since overhead vapor temperatures below 30 °C mandate expensive cooling brine, column design usually aims at a reflux drum temperature of 40–50 °C [36, 37]. The bottoms temperature has to be below that causing thermal degradation and should consider availability and cost of hot utilities. Further factors that need to be considered for vacuum distillation are the increase in the volumetric vapor flow rates, caused by the decrease in vapor density, as well as the increasing importance of the pressure drop, which can become decisive for distillation at high vacuum, mandating expensive equipment, such as thin-film or wiped-wall columns. Consequently, the evaluation should not be focused exclusively on energy-efficiency of the single unit operation, but consider a case-specific assessment of the various factors, including the possible heat integration with other distillation columns (see Section 12.3.1). After all, even the relative volatility does not generally increase for vacuum distillation, and as for any heuristic rule there are certain exceptions, as e.g. a mixture of water and acetic acid [36].

12.2.2 Multi-Effect Distillation (MED)

Apart from the effect that pressure has on the VLE, the pressure-dependency of the boiling temperatures can be exploited in so-called MED, by splitting the separation among different columns. These columns are operated at different pressures in order to facilitate a direct heat transfer between the top vapor produced in a high-pressure (HP) and the liquid bottoms stream of a low-pressure (LP) column, whereas one heat exchanger acts as condenser of the HP column and reboiler of the LP column. Even for the simplest case of a double-effect distillation with two pressure levels, five alternative configurations can be evaluated,

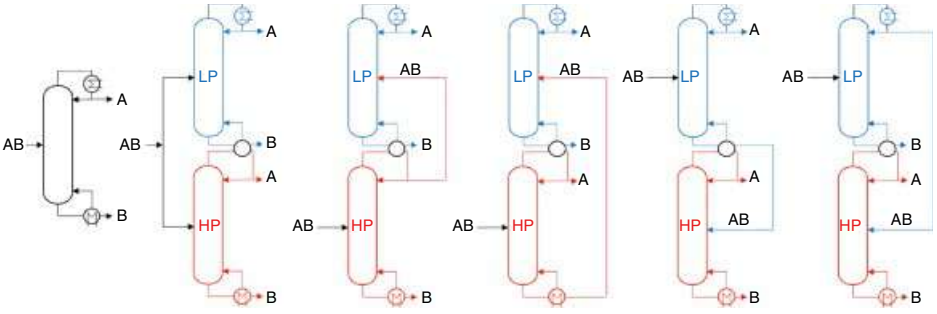

Figure 12.4 Illustration of binary distillation of low boiling component A and heavy boiling component B in a simple column (left), as well as five alternative double-effect configurations. *Source:* Modified from [38].

considering either a parallel setup in which both columns perform the same split, or a sequential setup, for which the first column (either LP or HP) purifies only one product, while processing the concentrated other product in the subsequent column [38]. The simple column and the five double-effect configurations are illustrated in Figure 12.4.

Properly designed, the double-effect configuration requires approximately 50% less energy. However, this energy reduction comes at the cost of an additional column and the increased temperature difference ($T_B(p_{HP}) - T_A(p_{LP})$), which limits the reduction of the exergy loss and may result in the need for more expensive utilities. Thus, while additional effects can further reduce the absolute energy requirements, also these limiting factors increase further. Due to the additional investment required and the decreasing potential for energy savings, applications rarely exceed double-effect configurations for distillation processes [38, 39]. Additionally, start-up and control of such heat-integrated systems is considered more complex [40, 41]. While reported industrial applications for multistage distillation are rather limited, with e.g. a triple-effect configuration as part of a five-column process for methanol distillation [42], the working principle is widely applied in evaporation processes, with 10–16 effects being applied in seawater desalination plants [43]. This effectively reduces the thermal energy requirement from the heat of evaporation of the water of 2257 MJ/m^3 to just 145–230 MJ/m^3 (6.5–10%). Yet, due to the low recovery of seawater desalination processes (~50%) and highly efficient pressure exchange systems, with net transfer efficiencies of ~97% [44], reverse osmosis plants still provide a considerable potential for energy savings, operating at less than 50% of the equivalent electricity consumption. However, this advantage and the applicability of the membrane process diminish quickly with increasing recovery [23].

12.2.3 Heat Pumps

Considering that a distillation column can be conceptualized as a heat engine that transforms the heat duty of the reboiler into separation work performed at the temperature level of the condenser [24], heat pumps build on the reversed process and are an effective option to improve the energy efficiency of binary distillation. The general concept of a heat pump builds on the pressure-dependency of the boiling point and performs an upgrade of low-quality heat through the addition of work. Thereby, the heat pump

transfers heat from a low temperature source (T_C) to a high temperature heat sink (T_H) using mechanical work (W), as illustrated in Figure 12.5. The most common example is implemented in the refrigerator that is basically present in every household. However, heat pumps are also applied in many industrial processes that provide low-quality heat sources, as e.g. hot humid air, (waste)water, geothermal or condenser heat, and heat sinks, such as dryers or reboilers [45]. Process streams are yet the most relevant heat sources and sinks in the chemical process industry, with the top vapor stream of a distillation column and the liquid bottoms stream representing an interesting locally confined combination of source and sink.

The possible improvement in energy efficiency is regularly characterized for heat pumps through the coefficient of performance (**COP**), which describes the ratio of exploitable heat delivered by the heat pump and the required mechanical work. The COP is generally limited by the COP of an ideal Carnot heat pump cycle (COP_{rev}), which only depends on the temperature lift (ΔT_{lift}) from the absolute temperature of the cold source (T_C) to the hot sink (T_H) measured in Kelvin:

$$COP = \frac{Q_H}{W} \leq \frac{T_H}{T_H - T_C} = COP_{rev}. \tag{12.2}$$

Heat pumps are mostly operated at a COP of around 4–6, leaving future room for improvement, when compared with combined heat and power plants with a COP of about 9 [45]. However, already a heat pump with a COP of 4 provides four times the thermal energy that is introduced by the mechanical work, by upgrading the low-quality energy of the source (T_C) to the temperature level of the sink (T_H). To provide a brief example, consider a heat source providing a saturated vapor stream at $T_C = 60\,°C$ and a hot heat sink with a boiling liquid at $T_H = 120\,°C$. The respective reversible Carnot cycle has a $COP_{rev} = \frac{393K}{(393-333)K} \approx 6.6$, resulting in a reasonable 60% efficiency of a real heat pump with a *COP* of 4. With this COP, the heat pump can upgrade 1 MW of low-temperature heat to about 1.33 MW of high-temperature heat, given an extra 0.33 MW of mechanical work. Thus, reducing the energy requirement by about 75%.

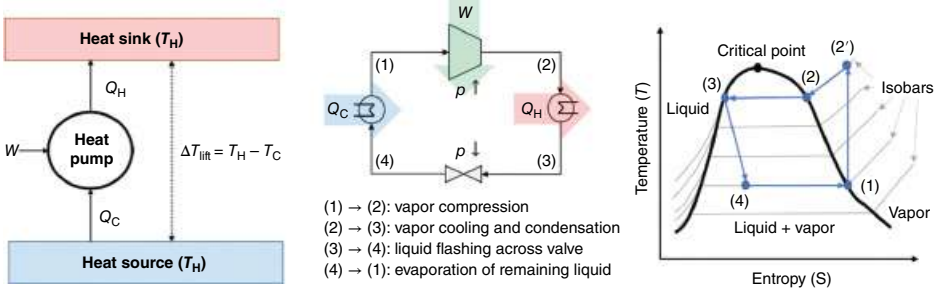

Figure 12.5 Concept of a mechanically driven heat pump (left), a vapor-compression cycle (middle), and the respective temperature-entropy (T,S) diagram (right).

Of course, it has to be considered that thermal energy and the electrical energy required to drive the compressor are not equivalent. However, with increasing provision of electrical energy from renewable sources such as wind and solar, the use of heat pumps does not only become more attractive in terms of energy efficiency and economics, but it also provides the option to significantly reduce the related greenhouse-gas emissions of thermal separations by running them on renewable energy [46]. Nevertheless, heat pumps are not free of drawbacks: the reliability of the required compressor as rotating equipment and the significant investment are still considered as critical aspects. Yet, with an increasing acceptance of carbon/energy taxes around the world, the possible energy savings and an operation based on renewable energy will further increase interest in the application of heat pumps [47].

A variety of different concepts have been proposed for heat pump-assisted distillation. Some of the most frequently applied concepts are further described in the following and illustrated in Figure 12.6. Yet, the interested reader is referred to the articles of Kiss et al. [21, 39] and Jana [47], as well as the text book of Kiss and Ferreira [45] for a more elaborate discussion. Kiss et al. [39] furthermore propose a pragmatic selection scheme for the different technologies based on the information on the boiling point difference, temperature lift, operating pressure, and relative volatility, building on an extensive literature review, which can support the initial selection of promising technologies for closer investigation.

The first three concepts illustrated in Figure 12.6 are all based on electrically driven vapor recompression, and have first gained increasing interest in the 1950s [47]. In direct or mechanical vapor recompression (**MVR**), the top vapor of the column does not enter a condenser, but is directly upgraded as working fluid by the compressor, such that one heat exchanger can be saved in addition to the energy which is transferred in the reboiler. Showing the lowest complexity in comparison to the alternative heat pump concepts MVR is considered as a state-of-the art industrial system for binary distillation [39], and probably the most popular type of heat pump [47]. The alternative bottom flashing (**BF**) configuration shows a similar complexity and represents a viable alternative, in case of light boiling products. While both configurations have the advantage that they are operated without an additional working fluid, which reduces the necessary temperature lift, the respective stream, either the distillate for the MVR or the bottoms product for the BF configuration,

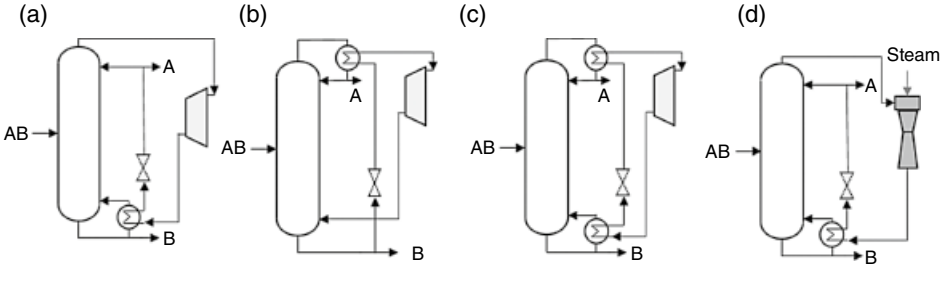

Figure 12.6 Selected major concepts for heat pump-assisted distillation: (a) direct or mechanical vapor recompression (MVR), (b) bottom flashing (BF) (c) vapor recompression (VC), and (d) thermal vapor compression (TVR). *Source:* Modified from [47].

has to meet the operational requirements and criteria for safe and economic operation of the compressor. These additional constraints pose certain limitations of the applicability of the MVR and BF configuration, except possible modification required due to the change in utilities.

Vapor compression (**VC**) is another well-established heat pump concept that is applied on industrial scale [21]. In contrast to the MVR and BF concept that represent (semi-)open cycles in which the working fluid only passes the heat pump once, an additional working fluid is applied in a closed cycle in VC. Thus, the VC configuration requires both heat exchangers and while introducing an additional compressor and flash valve, does not require any modifications of the simple distillation column. VC is generally favored over MVR or BF if the processed media are potentially corrosive or fouling [39]. While the working fluid needs to satisfy the same operational, environmental, and safety constraints for the compressor as in the MVR and BF design, the choice of working fluid represents an important additional degree of freedom, and continuous research is aiming at an increased eco-efficiency [26]. An industrial example of a VC is the ethylene–ethane separation using propylene as working fluid [48]. The lower investment for MVR and BF has to be compensated by an improved COP through an optimal choice of working fluid. Yet, the main drawback of all three configurations is the economic penalty related to the large investment for the compressor. It should further be noted that in case of a mismatch between the heat duty provided by the heat pump and required in the reboiler, an additional auxiliary condenser or reboiler might be required. Furthermore, an additional heat exchanger for superheating of the top vapor stream may be necessary in order to avoid condensation during compression, depending on the fluid properties.

By replacing the compressor with a steam ejector, the thermal vapor recompression (TVR) represents a modification of MVR that avoids the costly compressor. The steam ejector exploits the Venturi effect to generate mechanical energy from steam injection into a special variable diameter pipe [21]. TVR has been widely implemented in industry, given the reduced investment and avoidance of rotating parts. However, the steam ejector itself has a relatively low efficiency and as the steam input is mixed with the top vapor to generate the required pressure, TVR is almost exclusively of interest for systems producing water as top product. Absorption heat pumps (**AHP**), which are probably the oldest type of heat pump technology [47], are another type of thermally driven heat pump, which operates in a closed cycle, avoiding the mixing constraint of the TVR. AHP considers a thermochemical conversion, for which a mixed working fluid, either ammonia–water or water–lithium bromide, is applied, providing the heat for evaporation of the bottoms product by condensation of one of the components and exothermic absorption in two separate heat exchangers [45]. While the costly compressor is avoided, the AHP configuration is rather complex and requires overall five heat exchangers [39].

While the range of applications in which these classical configurations are economically attractive is usually limited to a temperature lift of about 30K, innovative heat pump concepts further extend the range of application, such that temperature lifts of 30–100 K are feasible, allowing for significant energy savings of up to 80% [45]. Hybrid heat pumps combine the working principles of different concepts. The compression resorption heat pump (CRHP) has a similar configuration as the VC, but exploits a two-phase working fluid similar to the AHP in combination with wet compression for increased energy efficiency and

economic performance with temperature lifts up to 124 K [49]. Heat pumps that are based on other driving forces are also available and already used in consumer goods. Solid-state heat pump technologies, such as magnetic heat pumps, which can be used to attain extremely low temperatures, or thermo-acoustic heat pumps, which consist of thermo-acoustic devices that use high-amplitude soundwaves to pump heat from one place to another, are comparably less efficient than the classical configurations, but score with long lifetimes, the absence of moving parts, and avoidance of potentially hazardous working fluids [45].

In case the distillation column is considered as stand-alone unit, the use of a heat pump is one of the most promising techniques for improved sustainability. Yet, as for MED, it is of course important to consider further options for heat integration in case the distillation column is part of a multi-product separation (cf. Section 12.3) or part of a general process flow sheet with additional heat sources and sinks [21]. For the latter classical heat integration methods, such as the well-known pinch analysis of Linnhoff [50, 51] should always be considered to evaluate alternative options. It needs to be noted that all heat pump concepts can also be applied to exchange heat between the reboiler and condenser of different columns, or between heat exchangers in the flow sheet with the reboiler or condenser of a distillation column. Consequently, the column should always be considered as part of the overall process system. However, given the locally confined heat integration offered by heat pump-assisted distillation, the above-described concepts are of particular interest.

As apparent from Eq. (12.2), the temperature levels at which heat is to be exchanged are the determining factors of the ideal Carnot heat pump cycle (COP_{rev}), which represents the upper bound for the COP of a real heat pump. Thus, variation of the temperature levels presents an immediate option to improve the energy efficiency of heat pump-assisted distillation. Therefore, a variety of modifications of the classical configurations in Figure 12.6 have been proposed in the literature, by implementing intermediate heat exchangers for the distillation column [47]. This also includes the application of multistage vapor recompression configurations [52]. The subsequent section addresses one of the most prominent concepts following this direction.

12.2.4 Heat-Integrated Distillation Columns (HIDiC)

The concept of the HIDiC represents the most radical approach to the idea of intermediate heat exchange for a heat pump-assisted distillation, resulting in a combination of internal heat integration and MVR. As illustrated in Figure 12.7, the HIDiC concepts breaks with the idea of augmenting the conventional distillation column with a heat pump, but rather separates rectifying and stripping section, in order to enable a direct heat exchange between a HP rectifier and a LP stripper. For this purpose, a compressor raises the pressure of the top vapor of the stripping section prior to entering the rectifier, such that the temperature lift in the rectifying section allows for heat transfer to the stripping section. Through direct heat transfer between both sections, a diabatic operation of the column sections is performed in which the condensing vapor creates an internal reflux in the rectifying section, that is returned to the stripper, where the heat of condensation is used to evaporate liquid along the column height of the stripper.

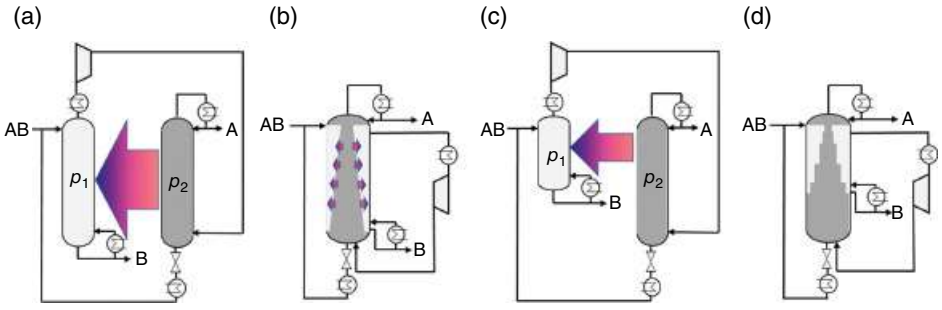

Figure 12.7 Illustration of the HIDiC concept: (a) HIDiC with separate stripping and rectifying section operated at p_1 and $p_2 > p_1$, respectively, (b) thermodynamically equivalent ideal integration in a single column shell, (c) HIDiC with separate stripping section and rectifier with different sizes, and (d) respective multi-diameter HIDiC in a single column shell. *Source:* Modified from [54].

Properly designed, the reboiler duty can be close to zero and only a small external reflux is required at the top of the rectifier in order to produce the required distillate purity [53]. While the heat pump-assisted distillation columns, as illustrated in Figure 12.6, connect a single heat source and sink, the whole rectifying section becomes the heat source in the HIDiC concept, while the stripping section acts as a heat sink. In the ideal case that the rectifying and stripping section are of equal height, both can be integrated into a single column shell (cf. Figure 12.7b), while various modifications and implementations have been proposed in case the rectifying and stripping sections are of different size (cf. Figure 12.7c–d) [54]. The illustrated gradients in the diameter of the individual column sections in Figure 12.7b and d are the result of the continuous heat transfer along the height of the column sections. The latter implies a steady decrease of the vapor load in the rectification section and a steady increase of the vapor load upward in the stripping section.

Through combination of the diabatic distillation and MVR, a reversible process can be approached [55, 56], resulting in possible energy savings of 30–50% in comparison with stand-alone MVR [39, 57]. This is a direct result of an increased COP resulting from the lower temperature lift, which can be kept low, with gliding temperatures across both column sections. Several studies report COP values around 10, e.g. for the separation of cyclohexane/n-heptane [58] or propane/propylene [55], with methanol/water even reaching a COP of 12.9 [59]. For optimal energy efficiency, the compression ratio should be minimized, which however is linked to a reduced approach temperature and driving force for heat transfer that can only be compensated by sufficiently large heat transfer areas. Thus, an optimal design seeks a tradeoff between heat transfer area and the compression ratio, simultaneously accounting for the specific structure and respective constraints [55].

Particular attention must be given to the distribution of the heat transfer area, which can seriously limit the applicability of internal heat exchangers along the height of the column [47, 55]. The successful implementation of a HIDiC design consequently depends on an appropriate hardware that accomplishes both heat and mass transfer at the same time. Furthermore, the trade-off between process design economics and process operation should be considered carefully for such a tight integration [21]. In order to enable the installation of a sufficient heat-transfer area, various configurations, such as multi-tube, multi-shell, or plate-type equipment have been proposed, which can either be considered as fractionating

heat exchangers (e.g. shell and tube, platefin) or heat-exchanging distillation columns (e.g. concentric columns, parallel columns, and partitioning-wall columns) [21, 54].

While the general concept of the HIDiC has been introduced by Mah et al. [60] in 1977 and despite the proven potential for further energy improvements, a variety of different concepts for the implementation and several pilot-scale implementations, so far no final industrial application on plant scale has been reported [58, 61]. While the energy requirement of the HIDiC may approach the thermodynamic minimum in certain cases, Shenvi et al. [62] showed that in case the temperatures profiles in both sections do not match, MVR with or without an intermediate heat exchanger can outperform the HIDiC. This is further supported by several other studies that evaluated the design of HIDiC and simplified heat pump-assisted distillation columns [63–65]. Even in case an ideal HIDiC is more energy-efficient than a simple heat pump-assisted distillation column, a simplified external combination of the rectifying and stripping section with few individual heat exchangers can provide a simpler and more economic design [64, 66, 67]. While somewhat similar arrangements are applied also in air separation [63], a discrete HIDiC with three intermediate heat exchangers, termed Super HIDiC was developed by Toyo Engineering Corp. and is continuously operated as a methyl ethyl ketone fractionator in the Chiba Factory of Maruzen Petrochemical Co. Ltd in Japan [68–70]. Figure 12.8 provides an illustration of the process flow diagram and an image of the commercial plant [69].

As numerous studies have shown that the HIDiC concept can in certain cases provide energy savings of up to 70% compared with a conventional distillation column, research and development of the practical implementation will continue. For all mechanical heat pumps, the investment for the compressor represents a major obstacle for a widespread implementation, which, however, may change in the future due to increasing energy prices or carbon taxes [47]. Besides further improvements on the practical implementation, efficient conceptual design tools will be an important asset in order to identify the most simple and effective heat pump-assisted distillation configuration, as simple heuristics may not result in the optimal choices [62].

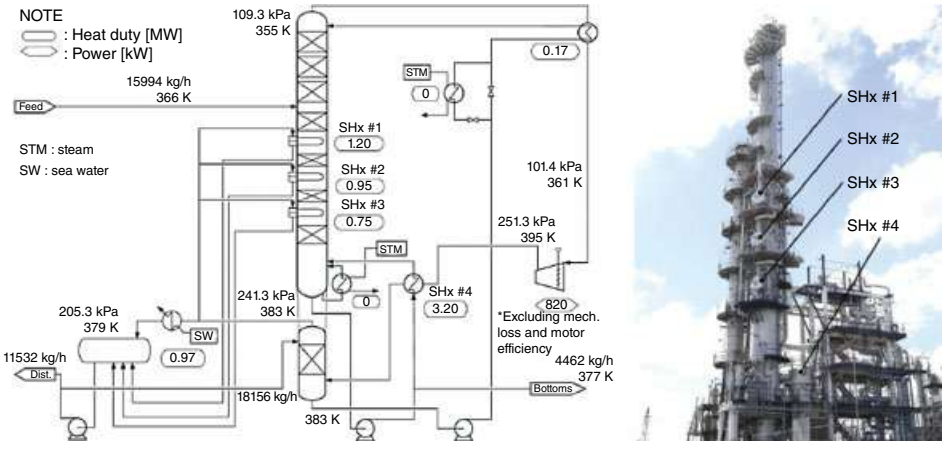

Figure 12.8 Illustration of the process flow diagram (left) and an image of the commercial Super HIDiC developed by Toyo Engineering Corp. in Japan. *Source:* Reprinted from [69], with permission from Elsevier.

12.3 Sustainable Multiproduct Distillation Processes

While each individual split for a multiproduct separation can be improved by means of MED or heat pump-assisted distillation, as described in Section 12.2, additional options become applicable if three or more products are to be separated by means of distillation. This includes heat integration between adjacent distillation columns as well as the principle of TC and DWCs as the equipment-integrated equivalent. These options can be considered as modification of basic configurations, which result from the sequence in which the individual products are to be separated. Following the definition of Agrawal [71], all configurations that separate a mixture into n_p products with n_p-1 columns are considered as basic configurations. Note, that within this section it is assumed that all products can be separated in accordance with their boiling order, which is equivalent to the assumption of a zeotropic mixture in case all products are pure components. For azeotropic mixtures, special distillation processes are required that either exploit the pressure-sensitivity of the azeotropes, the curvature of a distillation boundary, or a mass-separating agent, as further discussed in Section 12.4. Please refer to the work of Westerberg et al. [72], Doherty and Knapp [73], and Skiborowski et al. [74, 75] for further information on synthesis and design of azeotropic distillation processes.

Considering the separation of a zeotropic ternary mixture ABC into the three individual products A, B, and C (in order of decreasing volatility), the three possible basic configurations, as well as an additional side-stream column are illustrated in Figure 12.9. The first two options (a) and (b) perform a sharp separation of either the light boiling product A (direct split) or the heavy boiling product C (indirect split) first, while the intermediate boiling product is separated in the subsequent column. The number of possible sharp split sequences (sequence of n_p-1 binary distillation columns) increases exponentially with the number of products and can directly be calculated as [76]

$$N_S = \frac{\left[2\left(n_p-1\right)\right]!}{n_p!\left(n_p-1\right)!}. \tag{12.3}$$

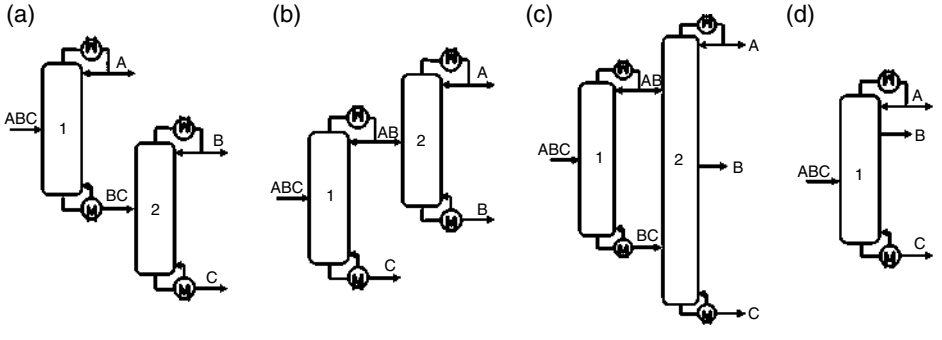

Figure 12.9 Illustration of basic distillation configurations and side-stream column for a separation of three individual products: (a) direct and (b) indirect split sequence (both sharp splits), (c) sloppy split sequence with prefractionator, and (d) side-stream column.

Thus, while only the two sharp split sequences illustrated in Figure 12.9 are feasible for a ternary separation problem, this number increases to five for a quaternary separation problem and to 132 for the separation of seven individual products. The number of basic sequences can further be increased by consideration of sloppy splits and multi-feed side-stream columns, as illustrated in Figure 12.9c. These additional configurations are of special interest for the design of thermally coupled DWCs and exploit that the sloppy split in the prefractionator is in fact the preferred separation, that is performed at minimum energy requirements with both sections being pinched [77]. Given a sufficient volatility difference between the individual products, the separation of n_p products may, however, also be performed in less than $n_p - 1$ columns. For the ternary separation, such a side-stream column is illustrated in Figure 12.9d, assuming that the intermediate product has a lower boiling temperature than the saturated feed stream. Note, that unlike the prefractionator configuration illustrated in Figure 12.9c, the side-stream column may not allow for a sufficient purification of all individual products [78, 79]. Nevertheless, as pointed out in Section 12.1, the crude unit of a petrochemical plant produces six product streams at once.

The following two sections will introduce the concepts of direct heat integration and TC, as well as the equipment integrated dividing wall column (DWC) concept. While these sections focus on the separation of three or four products, systematic methods for the synthesis of all possible configurations, including all potential DWC configurations for general multicomponent mixtures have been presented in the literature [80–82]. In combination with shortcut models and global optimization methods, these configurations can be effectively screened to identify the most energy-efficient option [83, 84]. Thus, there is no longer a need to rely on simpler heuristics, such as the ease of separation index [85]. However, more general heuristics, such as prioritization of the separation of toxic, hazardous, or corrosive components, or thermal sensitivity of the components, should always be considered in addition to the energy requirements and costs of the individual process configurations.

12.3.1 Direct Heat Integration

While MED allows for the direct heat integration between columns that perform a binary distillation (cf. Section 12.2.3), similar integration between the condenser and reboiler of two columns can be performed for a sequence of columns in multi-product distillation processes. Of course, the condensation of the top vapor from one distillation column has to be performed at a sufficient temperature above the evaporation temperature of the bottoms product of the other column. Thus, similar to MED, direct heat integration between adjacent columns in a sequence requires the modification of the operating pressure of at least one of the columns, in order to generate a sufficient temperature difference for heat integration. This is exemplarily illustrated in Figure 12.10 for the direct split sequence (cf. Figure 12.9a). The Q, T-diagram on the right side of the nonintegrated sequence (left) illustrates that operation of the first column requires the provision of a heat duty $Q_{B,1}$ at a temperature $T_{B,1}$ while a heat duty $Q_{C,1}$ is dissipated at a considerably lower temperature $T_{C,1}$. Since the bottoms product of the first columns represents the feed stream of the second column, the condensation temperature of the top product $T_{C,2}$ and the evaporation temperature of the bottoms product $T_{B,2}$ are below and above the bottoms temperature of the first column ($T_{B,1}$), when operated at the same pressure. Note that the illustration in

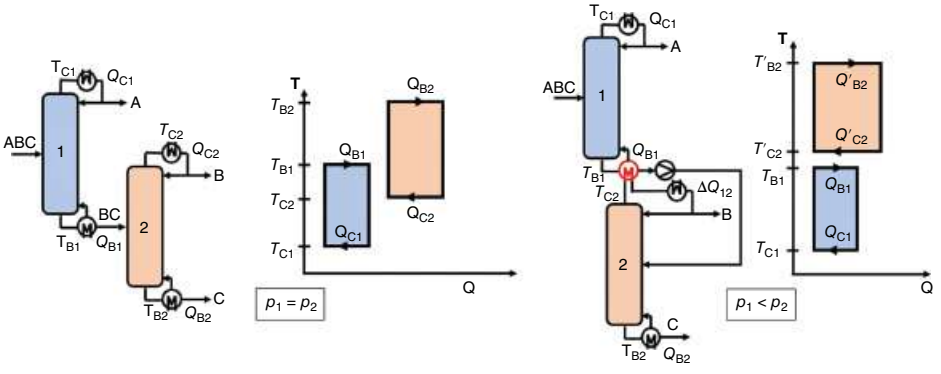

Figure 12.10 Illustration of direct split sequence without (left) and with heat integration (right), together with the indicative Q,T-diagram.

Figure 12.10 is simplified with respect to the Q,T-diagram, since at least the intermediate bottoms product of the first column will not evaporate at a single temperature, but over a temperature range depending on the VLE between the intermediate and heavy product. The same applies to the other reboiler and condenser in case the final products are not pure components.

Similar to MED, the temperature levels for condensation and evaporation can be shifted through modification of the operating pressure, allowing for direct heat integration, once the condensation temperature of the top product of the second column is sufficiently raised above the bottoms temperature of the first column. In this case, the operating pressure of the second column is increased ($p_2 > p_1$), such that the condensation temperature of the top vapor $T'_{C,2} \geq T_{B,1} + \Delta T_{min}$. The potential heat integration is illustrated in Figure 12.10 (right), for which an additional heat exchanger compensates for the difference in heat duties ($\Delta Q_{l,2} = Q'_{C,2} - Q_{B,1}$). An additional preheater prior to the second column may also be considered to upgrade the feed to saturation prior to entering the column. Not accounting for this preheater, the heat-integrated process requires only provision of the heat duty of the second column ($Q'_{B,2}$), which, however, has to be provided at an increased temperature level ($T'_{B,2} > T_{B,2}$) that may imply the necessity of a more expensive utility. Instead of raising the operating pressure of the second column, the first column of the sequence could also be operated at a lower operating pressure, which might furthermore be beneficial with respect to the VLE (cf. Section 12.2.1), but should consider the respective limits on the utility for operating the condenser. Consequently, all of the previously introduced constraints and consequences related to vacuum or HP operation (cf. Section 12.2.1 and 12.2.2) should be accounted for, when evaluating the heat-integrated configuration. This also includes the possible formation of azeotropes that may render the separation infeasible. The same possibilities and considerations for direct heat-integration hold for the indirect sequence (cf. Figure 12.9b) and can be applied for any adjacent columns in multi-column sequences.

Distillation processes with four or more products may, however, also provide additional options for direct heat integration, without the necessity of modifying the operating pressure. Two of these options are further illustrated in Figure 12.11 for the separation of a quaternary zeotropic mixture, with components A–D listed from light to heavy boiling.

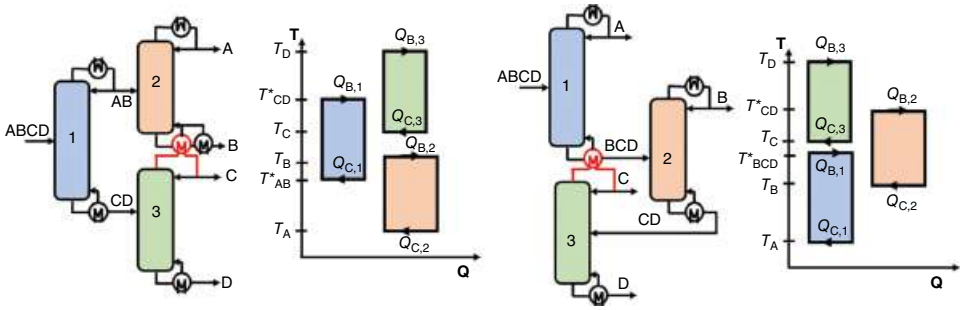

Figure 12.11 Illustration of direct heat integration options for the separation of a quaternary zeotropic mixture, together with the indicative Q,T-diagram.

In the first process configuration (left), the feed is initially separated into two fractions of the lower and heavier boiling components, which are subsequently separated in the second and third column. As the boiling point of component C is always above that of component B, direct heat integration can be applied between the second and third column, or both columns may be integrated into the basic sequence illustrated in Figure 12.9c. The second process configuration illustrated in Figure 12.11 (right) performs two direct splits and allows for direct heat integration between the first and the third column, if the ternary mixture produced as bottoms product of the first column has a lower boiling point as component C, which is produced as top product of the third column. As such, feasibility of this configuration depends on the specific mixture and feed composition. However, it is important to note that directly heat-integrated configurations like this are in certain cases more energy efficient as the fully thermally coupled configurations presented in the subsequent section. Refer to the article of Mathew et al. [86] for some specific case studies for quaternary and quinary separation problems.

When evaluating the possibility of direct heat integration for distillation processes, the evaluation should always go beyond the scope of the individual column sequence and cover as much of the surrounding background process as possible. This is best accomplished by an integration with classical pinch analysis [50], which nowadays is available as build-in option in process simulation software such as Aspen Plus (Aspen Energy Analyzer). Through combination of pinch analysis and conceptual process design methods, such as shortcut methods [87, 88] or optimization-based design methods [89–91], an optimal integration of the distillation process and the background process can be sought. Thus, the required energy for a heat-integrated process may be covered by the background process [92] or given a sufficient amount of heat is dissipated at the necessary temperature, even a nonintegrated process configuration, such as the direct split sequence in Figure 12.12 may be integrated with the background process in such a way that the required heat duties are covered by the background process and distillation can be operated without the need for any external utilities.

12.3.2 Thermal Coupling and Dividing Wall Columns (DWCs)

While direct heat integration, as presented in Section 12.3.1, is sometimes referred to as **TC** via heat transfer [86], we will only refer to TC in the sense of a combined heat and mass

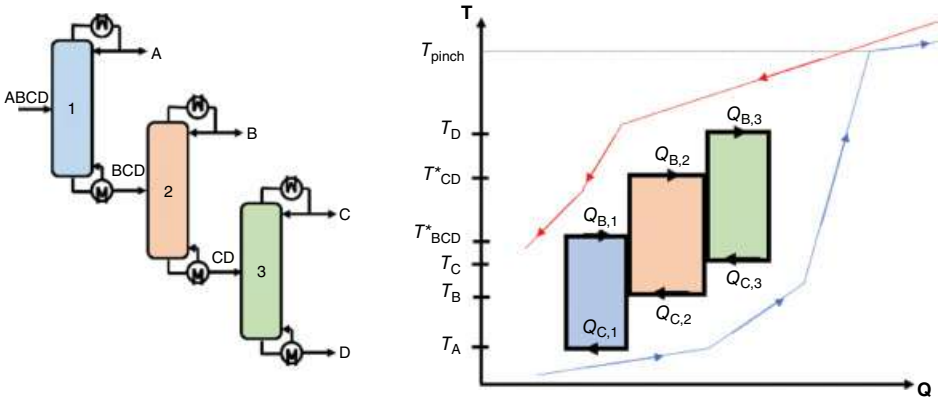

Figure 12.12 Illustration of heat integration for the direct split sequence for the separation of a quaternary mixture (left) with respect to the overall hot (red) and cold (blue) composite curves determined in the context of pinch analysis in the Q,T-diagram (right).

transfer, for which two columns, or adjacent column sections, are connected via vapor and liquid transfer streams. Any basic configuration can be converted into a TC configuration by exchanging the reboiler or condenser and the one-directional connecting stream with a bidirectional vapor and liquid transfer. All possible options for basic configurations, TC configurations and possible integration of these in terms of **DWCs**, as well as modified DWC with better controllability through the exchange of the bidirectional vapor and liquid transfer by a one-directional liquid-only transfer (LOT) [93], can be synthesized systematically, by means of an extended matrix method [80–82]. In the following, we will focus on the specific TC and DWC configurations for three and four-product separations, as these are the only configurations that have been applied in industry so far [94].

12.3.2.1 Three Product Separations

The transformation from a simple sequence to the TC and DWC equivalent is illustrated in Figure 12.13 for the sloppy split sequence. The first column acts as a prefractionator that separates the light boiler (A) and the heavy boiler (C), while distributing the intermediate boiling component (B). The subsequent columns perform the separation of the individual binary mixtures. Through optimal distribution of the intermediate boiling product, the prefractionator performs the so-called preferred split [77], which represents the minimum energy separation of the initial ternary mixture. As both subsequent columns produce the intermediate boiling product (B) at the adjacent column ends, both columns may be integrated into a side-stream column, resulting in the basic configuration that was illustrated in Figure 12.9c.

This configuration can further be converted to the so-called Petlyuk configuration [95], by exchanging the reboiler and condenser of the prefractionator by means of the bidirectional vapor and liquid transfer streams. It is termed fully thermally coupled configuration and represents the most energy-efficient configuration for a three-product separation, among all basic and thermally coupled configurations [96]. In fact, it requires only the necessary energy required for the more difficult binary separation of either the low boiling

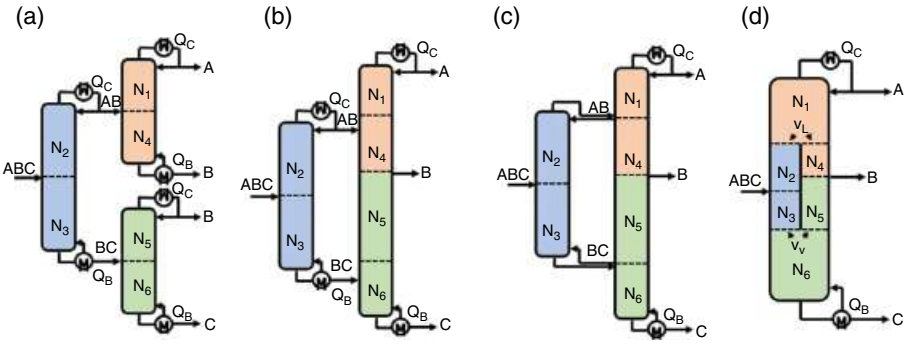

Figure 12.13 Transformation of the simple sloppy split to the corresponding fully thermally coupled process configurations. (a) Simple sloppy split sequence, (b) Sloppy split sequence with side-stream column, (c) Petlyuk column, and (d) DWC.

top product (A|BC) or the heavy boiling bottoms product (A|BC). Thus, the heat duty required by the fully thermally coupled configuration can conveniently be identified by so-called $V_{\min}$ diagrams [97, 98], which plot the required vapor-to-feed ratio over the distillate-to-feed ratio. While these diagrams are mostly generated based on Underwoods method [99], it is important to note that this method assumes constant relative volatilities and molar overflow and it should be substituted by more rigorous methods if these assumptions do not hold [74].

An exemplary $V_{\min}$ diagram for a three-product separation is illustrated in Figure 12.14. The lines in the diagram present the minimum vapor flow rate for different product recoveries depending on the D/F ratio in a simple column with an infinite number of stages. The vapor flow rate, in this regard, is representative for the minimum energy demand of the separation. Depending on the D/F ratio, the products obtained as distillate or bottoms streams change and are indicated by the respective visualizations. The peaks in the diagram illustrate the minimum vapor flow rate for the individual sharp splits (A|BC and AB|C). The higher peak in the $V_{\min}$ diagram indicates the more difficult split and corresponds to the minimum energy demand of the fully thermally coupled configuration. For the exemplary diagram shown in Figure 12.14, the sharp split AB|C presents the highest peak and thus corresponds for this case to the limiting separation within the Petlyuk column or DWC. Therefore, the additional product splits in a DWC are covered by the excess in vapor required for this separation. The results of the $V_{\min}$ diagram analysis provide an excellent basis for the initialization of a rigorous model-based design [100] and provide lower bounds for process optimization [101].

Fully thermally coupled configurations can be generated for any number of products (n_p) in a similar fashion as indicated in Figure 12.13. They generally require $n_p(n_p-1)$ column sections and transfer all individual intermediate products [82]. Note that while the overall number of basic and TC configurations increases exponentially with n_p, there is only one fully thermally coupled configuration for any number of products. However, since it is not exclusively thermodynamically optimal, other simpler configurations with a lower number of column sections are usually competitive with the fully thermally coupled configuration, depending on the separation problem. For ternary separations,

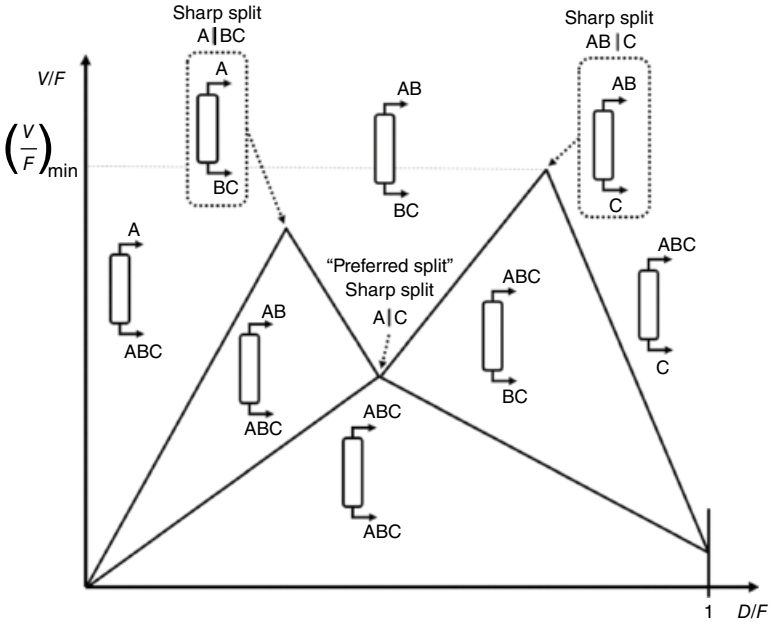

Figure 12.14 Exemplary V_{min} diagram for a ternary separation [102].

these simpler TC configurations are the side-rectifier and side-stripper configurations that result from TC of the direct and indirect sequence (cf. Figure 12.9).

The fully thermally coupled configuration enables energy savings of 25–45% in comparison to the basic sequences [21, 39, 94, 103] while additionally saving two heat exchangers. The energy savings result from reduced (re-)mixing effects of internal streams, particularly at the feed positions and the upper and lower ends of the columns [104]. The prefractionator plays a vital role as it enables additional flexibility in shifting the internal composition profile and allowing for optimal feed allocation. While the fully thermally coupled configuration is the most energy-efficient configuration among all basic and thermally coupled configurations, it is not necessarily the most thermodynamically efficient and the range of feed compositions for which it is most favorable for a specific mixture can be quite limited [105, 106]. This is primarily related to the fact that fully thermally coupled configurations require that heat is transferred at the highest possible temperature, while the top product needs to be condensed at the lowest temperature. As the pressure may not be modified for TC configurations with bidirectional vapor and liquid transfer, the operating window cannot be reduced in terms of the temperature. As for intermediate heat exchangers, the individual heat exchangers of the sloppy split sequence (Figure 12.13a) allow for heat transfer at reduced temperature levels and thus either the exploitation of lower quality steam as external utility or potentially lower value heat sources of the background process, while even if the energy requirement of the Petlyuk configuration (Figure 12.13c) is significantly lower, all heat needs to be supplied at the highest temperature level. Therefore, the energy requirement should not be the only considered factor, when evaluating alternative process configurations. Moreover, the previous quantification as most energy-efficient

distillation process explicitly does not account for external heat integration, as indicated in the previous section, or heat pumps.

However, besides the energy savings, TC also allows for an implementation as an equipment-integrated DWC (cf. Figure 12.13d). Due to reduced costs of materials, piping, foundations, and space requirements, the DWC can further reduce capital investment by up to 30% [104, 107]. As the DWC is the thermodynamic equivalent of the TC configuration, it also allows for the separation of high-purity side products in contrast to simple side-streams columns (Figure 12.9d) and is considered as attractive retrofitting option. Despite these benefits, it took almost 40 years from the introduction of the concept in 1949 by Wright [108] until the first industrial application of a DWC in 1985 [12] and published reports in 1987 [109]. The number of applications continuously increased from roughly 25 DWCs in 2002 [107] to more than 300 applications worldwide reported in 2019 [110]. Various applications, patents, and industrial implementations are listed by Kiss et al. [21, 39], Dejanović et al. [104], and Yildirim et al. [111], also covering the equipment-integrated equivalents of the side-rectifier and side-stripper that despite their dividing wall, which is either connected to the top or the bottom of the column, are oftentimes rather referred to as split shell columns. While the design of a DWC is considerably more complex as the design of the basic sequence and still lacks predefined models in most flowsheet simulators, a variety of design tools have been proposed, which effectively overcome these limitations. A comprehensive review regarding DWC design methods has been provided by Waltermann and Skiborowski [101], while more recently the first equation-based equilibrium-stage parallel column model for a DWC has been implemented in ChemSep [112].

Concerns regarding DWC controllability, as another major reason for the initial slow acceptance in industry, have also been resolved by now. Various decentralized and centralized control schemes have been proposed for DWC and good controllability of DWCs has been proven, given the selection of a suitable control scheme [113]. Generally, the distillate or reflux, the bottoms product or boil-up, as well as the side-stream flow rate and the liquid split in the column can be manipulated to control the product purities and keep the heat duty low. However, the vapor split is not adjustable during DWC operation, such that the hydraulic design of the column considering the placement of the partitioning wall and the selection of the column internals are of vital importance, since they determine the pressure drop in the adjacent column sections and thereby the split ratio of the vapor stream along the partition wall. While Kaibel [109] stated that "*no special measures are required for the distribution of vapor flow at the lower end of the partition*" and that "*distribution ratios can be varied from 2:1 to 1:2 with only minor disadvantages with respect to energy consumption and separation performance*," the importance of a careful hydraulic design is highlighted in multiple publications [114–116]. Apparently, the sensitivity depends on the specific separation task and was shown to be much higher in cases of close-boiling systems [117].

The associated malperformance risks can, however, be reduced significantly if vapor splits are avoided or externally controlled [114]. For the latter, two options for active vapor split control have been proposed so far, either building on special vapor split valves [118] or a special type of chimney tray that allows for the introduction of an additional pressure drop [119, 120]. An interesting alternative to the active control of vapor splits has been proposed by Agrawal [93], who replaced the bidirectional vapor and liquid transfer with a one-directional LOT, which requires an additional column section and heat exchanger. The modification is

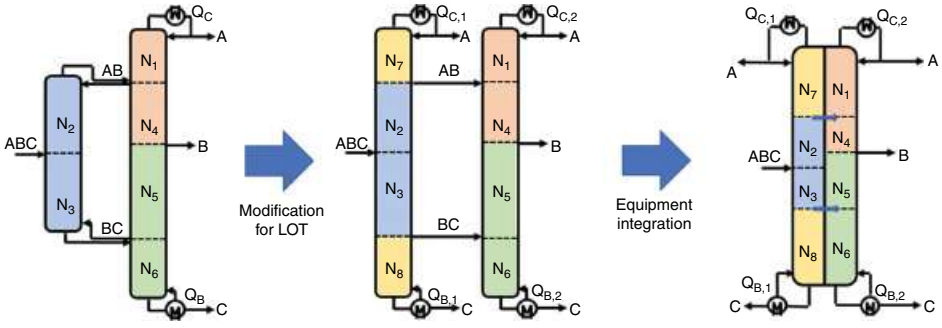

Figure 12.15 Derivation of the fully thermally coupled LOT configuration and respective DWC with enhanced controllability.

illustrated for the Petlyuk configuration in Figure 12.15. While the additional column section (N_7 and N_8) as well as the additional heat exchangers increase the necessary investment, they avoid any vapor split and enable an active control of the vapor flow rates on both sides of the dividing wall through the individual reboilers. However, unlike the sloppy split sequence with the side-stream column (cf. Figure 12.13b), the LOT configuration is thermodynamically equivalent to the fully thermally coupled Petlyuk configuration and thus preserves the respective energy savings. As the heat duties of the reboilers ($Q_{B,1} + Q_{B,2} \approx Q_B$) and condensers ($Q_{C,1} + Q_{C,2} \approx Q_C$) merely represent a distribution of the heat duties of the reboiler and condenser of the Petlyuk configuration, following the liquid and vapor split, the additionally required investment is also not that pronounced [121].

Since the temperature difference across the partitioning wall is a limiting factor, which may result in an undesired heat transfer over the partitioning wall [122], a separate column design may be advantageous. While proper insulation of the dividing wall can significantly reduce undesired heat transfer [94], the mechanical stability of the partitioning wall should be checked for large temperature differences that exceed 30 K [123].

12.3.2.2 Four-Product Separations

While the concept of a DWC has been proposed for ternary separation almost 70 years ago, further application to quaternary separations were also introduced about 30 years ago by Kaibel [109]. Several studies have indicated energy savings of 40–50% for four-product separations [121] and Dejanović et al. [114] even comment on energy saving potentials of up to 57% for the separation of a multicomponent aromatics mixture. Yet, no industrial implementations with multiple dividing walls have been reported so far [124, 125]. The only reported four-product DWC implementations are performed in a configuration with a single dividing wall [125, 126], which is oftentimes referred to as Kaibel column. The specific DWC is illustrated in Figure 12.16a, together with the fully thermally coupled Sargent configuration (b) and simplified version of the double-DWC (c). The Kaibel column is also termed 2–4 configuration, as it represents a thermally coupled configuration of a two-product and a four-product distillation column [127], comprises seven column sections, as well as a vapor and liquid split, together with a single reboiler and condenser. Representing a combination of the Petlyuk configuration and an additional side-stream column, the maximum purity of one of the side-stream products is somehow limited. However, the

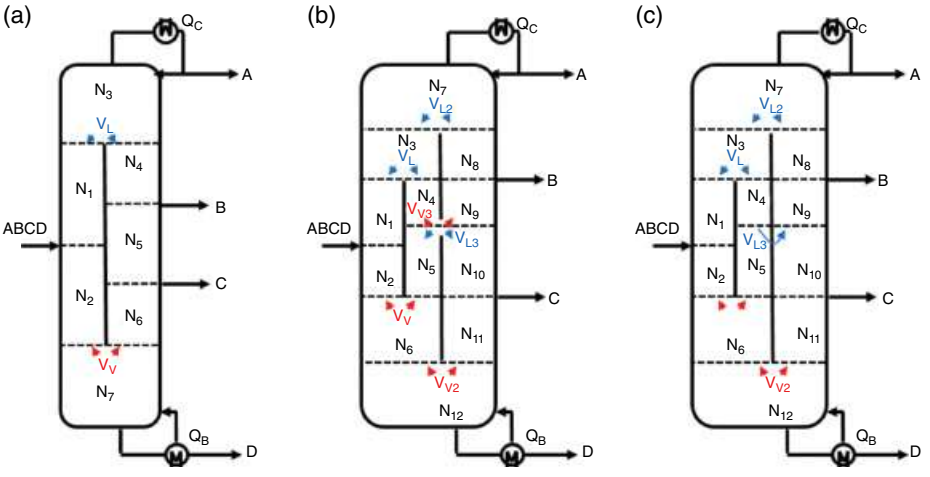

Figure 12.16 Illustration of prominent four-product DWC: (a) Kaibel or 2–4 column (left), (b) Sargent or 2–3–4 column (middle), and (c) simplified s2–3–4 column (right) [7].

design of the Kaibel column is only marginally more complex compared with the Petlyuk configuration.

On the contrary, the design of the Sargent configuration is much more complex as it represents the thermally coupled version of a two-product, a three-product, and a four-product column. Therefore, it requires the specification of twelve column sections, three liquid and three vapor splits, in addition to the aforementioned heat duties for the reboiler and condenser, as well as the side stream flow rates. Thus, overall, 22 design degrees need to be determined during conceptual process design. Based on the analysis of various simplifications, Halvorsen et al. [127] conclude that especially the s2–3–4 configuration that requires a vapor split less than the Sargent configuration, comes with similar energy requirements as the Sargent configuration for most separation problems [124, 127]. Different case studies indicate that the Sargent configuration may require 15–20% less energy than the Kaibel column [128, 129] and cost savings of about 15% [128]. However, the specific savings always depend on the separation problem and particularly the required purities of the two side-stream products [121]. In case of rather wide-boiling mixtures, the economic savings of the Sargent over the Kaibel column may not justify the added complexity of the Sargent column [121]. In the end, the most appropriate configuration should be determined by a case-specific evaluation.

While not established in industry, at least theoretically the DWC concept can be expanded to separations of more than four products. Refer to the work of Madenoor Ramapriya et al. [80, 81] for a general methodology to generate such DWC concepts for an arbitrary number of products.

12.3.3 Innovative Combinations

While especially MED, MVR, and DWC are industrially established solutions for binary and ternary distillation processes [21, 39] and DWC have also been realized for four-product separations in terms of Kaibel columns [94], also integration of the different techniques

have been proposed to further improve the energy efficiency. Since the single measures allow for energy saving potentials from 20 to 50% compared with conventional distillation [39], further improvements may be expected when combining these techniques [47]. However, each approach also comes with limitations. For nonideal mixtures, any variation of the operating pressure may result in undesired modifications of the VLE, potentially impeding a separation by means of distillation. For DWC, pressure variation is not a direct option, because all column sections in the DWC operate at approximately the same pressure, apart from the pressure drop of the specific equipment. While MED and DWC both allow for considerable energy savings, they also increase the temperature difference between the condenser and reboiler and thus heat sources and heat sinks. Therefore, a combination of the different techniques might not even be applicable at all and by any means requires a case-specific evaluation and potentially tailored design. In the following, two examples of such innovative combinations are described, which might be exploited on a broader basis.

The first example deals with a heat pump-assisted extractive DWC (see also Section 12.4.1), as proposed by Luo et al. [130] for bioethanol dehydration. An illustration of this configuration is depicted in Figure 12.17 (left). Due to the large temperature difference between the condenser and reboiler for the fully thermally coupled DWC, the proposed MVR extension does not integrate heat between the compressed top vapor stream and the heavy boiling entrainer produced as bottoms product, but with the side-product in an additional intermediate reboiler. Thereby, the required temperature lift and the workload of the compressor are reduced.

While Luo et al. [131] report merely any energy savings and only little economic savings of about 7% for the thermally coupled extractive DWC compared with the non-integrated extractive distillation process, the combination with the additional heat pump enables energy savings of about 40% and additional economic saving potential, resulting in an

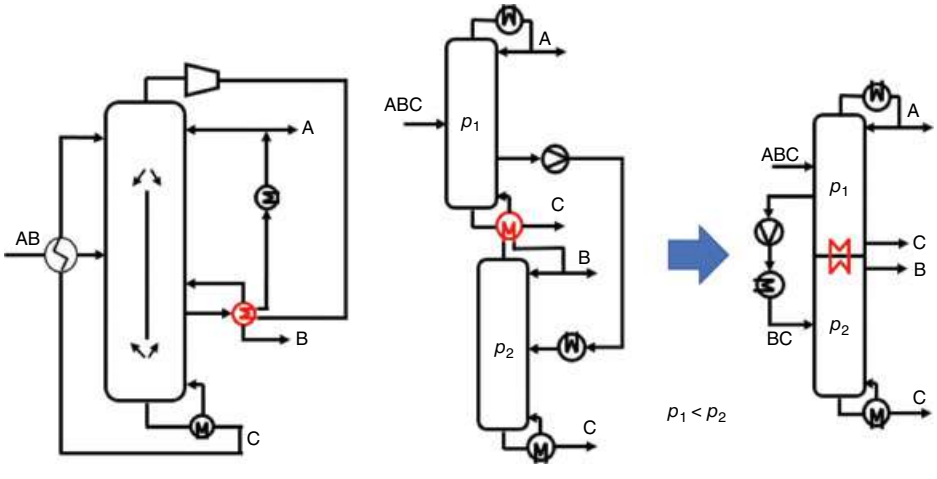

Figure 12.17 Heat pump-assisted extractive DWC with an intermediate reboiler as proposed by Luo et al. [131] (left) and heat-integrated thermally coupled LOT side-rectifier configuration following the concept of Agrawal [132] (right).

overall 24% cost reduction compared with the non-integrated extractive distillation process. Of course, the complexity of such a two-fold integrated process is considerably higher, but Luyben [133] showed at least on a model basis that such a process can be controlled given a sufficient plant-wide control structure.

Another interesting combination of direct heat integration and TC was initially proposed by Agrawal [132]. Through modification of the thermally coupled configuration and with the aforementioned LOT [93], the individual columns can be operated at different pressures. Thus, the LOT configuration does not only allow for a direct control of the vapor loads in the different columns, but also potentially enables further heat integration through appropriate pressure modification. By means of some approximate calculations based on constant relative volatilities, Agrawal [132] concluded that the heat-integrated fully thermally coupled LOT configuration allows for the largest energy savings of up to 50% as compared with the fully thermally coupled configuration without heat integration, but the possible energy savings depend largely on the specific mixture and feed composition. For many feed composition, either the respective side-rectifier or side-stripper configuration provide similar potential for energy savings, but at the same time allow for a reduced temperature lift. Therefore, Skiborowski [134] performed a more detailed investigation of the heat-integrated thermally coupled LOT side-rectifier configuration, which is illustrated in Figure 12.17(right). By evaluating the energy requirement of this configuration and comparing it with 19 alternatives, including the non-integrated basic configurations, different degrees of TC, direct heat integration, and MVR, Skiborowski [134] showed that the combination performed specifically advantageous in terms of energy requirements, when processing feed streams with larger fractions of heavy boiler in the inspected separation of a benzene–toluene–ethylbenzene mixture. While only a configuration with MVR for both columns in a direct sequence enabled higher energy savings at the expense of two compressors, the integrated concepts allowed for energy savings of up to 30% compared with the fully thermally coupled Petlyuk column. However, a more rigorous process design indicated that the 30% energy savings would be compensated by the reduced equipment costs of a fully thermally coupled DWC in case of a grassroot design. Yet, this shifts depending on the energy costs and depreciation period.

12.4 Separation of Close-Boiling and Azeotropic Mixtures

While Section 12.2 already introduced several concepts for improving the energy efficiency of binary distillation, classical heuristics suggest to rely on special distillation processes or combinations with other separation technologies in case the relative volatility drops below a threshold value of 1.1 [135]. As long as the relative volatility exceeds the lower limit of 1, such narrow-boiling systems can still be separated by distillation but only with a high number of theoretical stages and high reflux ratio, resulting in large equipment and utility costs. Azeotropic mixtures exhibit a relative volatility of 1 at a certain composition, such that according to the Greek translation, the liquid boils unchanged at this composition and, as such, cannot be separated by distillation. Apart from the possibility to exploit a pressure-sensitivity of an azeotropic composition by means of pressure-swing distillation, especially the exploitation of the effect of an additional mass separating agent (MSA) on the VLE

plays an important role in the separation of close-boiling and azeotropic mixtures. The following subsections provide a description of the most relevant distillation-based hybrid processes, which still build on the combination of distillation with another separation technology, contributing to the same separation task [136]. Figure 12.18 provides an illustration of the three most common distillation-based hybrid processes that exploit a MSA in form of a liquid entrainer.

The first two cases are generally referred to as azeotropic distillation processes. In extractive distillation (cf. Figure 12.18 (left)), the entrainer is fully miscible with the feed mixture but affects the relative volatility in such a form that it enables the separation of the azeotropic mixture in a distillation column with an additional intermediate column section. In heterogeneous azeotropic distillation (cf. Figure 12.18 (center)), the immiscibility of the entrainer with the feed mixture is exploited through a combination of distillation columns that operate outside of the miscibility gap, while the condenser and potentially subcooled top vapor is separated in two liquid phases in an additional decanter, thus combining distillation and liquid–liquid phase separation. The latter is further exploited to a larger extent in a hybrid process with liquid–liquid extraction (cf. Figure 12.18 (right)), in which distillation is used for thermal recovery of the entrainer. Note that the illustrated process concepts represent single examples of the respective type of processes. They are not only of interest for the separation of azeotropic and narrow-boiling mixtures but also in the case of strongly asymmetric feed compositions [24, 25].

All three of the aforementioned process concepts share the dependency of the MSA as an additional component that facilitates the separation by altering the thermodynamic properties of a given mixture. Therefore, it is not surprising that the selection of the MSA is considered as the key factor for a sustainable and economical design of these processes [137]. Due to a tremendous number of possible candidates and constraints that have to be considered, the selection of an appropriate MSA can be a tedious and challenging task. Selection criteria usually relate to thermodynamic properties, such as selectivity and boiling point, as well as process parameters, like the minimal entrainer-to-feed ratio [138]. Additionally, general aspects, such as low corrosivity and toxicity, low heat of vaporization, a sufficient thermal stability, and high availability at acceptable costs, are important criteria that need to be considered [73, 139]. Unless the solvent is supposed to react with one of the feed components, it should be nonreactive, while any reaction should be reversible for a reactive solvent. The "12 Principles of Green Engineering" provide further guidance for a sustainable solvent selection [140].

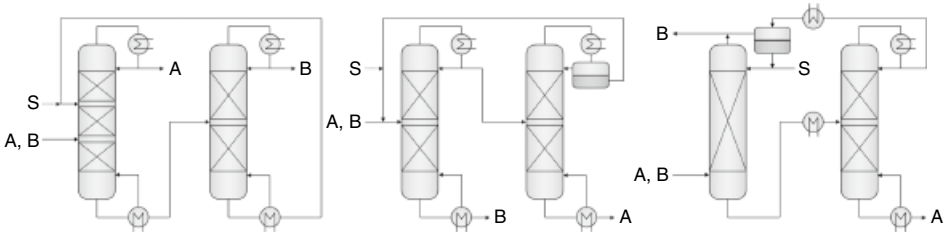

Figure 12.18 Exemplary process flow sheets for extractive distillation (left), heteroazeotropic distillation (center), and a hybrid liquid–liquid extraction–distillation process (right) for separating a mixture of A and B by adding a MSA S. *Source:* Based on [136].

While still building on expert knowledge and heuristic guidelines, systematic tools for solvent selection and computer-aided molecular design (CAMD) have been established and are gaining practical relevance [141, 142]. In CAMD, candidate molecules or mixtures are generated and screened in an algorithmic procedure evaluating specific performance criteria based on thermodynamic prediction via group contribution or quantum chemical methods [141]. The CAMD procedure can either build on a generate-and-test procedure [143] or a structural molecular optimization based on a MINLP formulation [144, 145], which may also build on an evolutionary algorithm [146]. The MSA candidates are either evaluated by simple performance indicators, such as selectivity and capacity, or process-specific shortcut methods [146, 147]. These tools are particularly valuable when integrated in a larger framework that finally pursues the design of an optimized process [138, 148, 149]. Especially, the simultaneous consideration of MSA and process design, which is referred to as computer-aided molecular and process design (CAMPD) [141, 146], can reduce the possibility to settle for suboptimal solutions [138, 150]. For comprehensive insights in CAMD and CAMPD, we refer to the review articles by Austin et al. [145], Papadopoulos et al. [151], and Gertig et al. [141].

Besides the mentioned similarities of the considered processes, there are distinct differences in the concepts and the specific criteria that need to be considered for MSA selection. These specifics are further addressed in Sections 12.4.1–12.4.3. Furthermore, Section 12.4.4 provides a brief introduction to membrane-assisted distillation processes, which introduces additional options for the exploitation of hybrid separations for narrow-boiling and azeotropic mixtures. We also refer to the review paper of Skiborowski et al. [75] for a broader overview on the conceptual design of such distillation-based hybrid processes.

12.4.1 Extractive Distillation

Extractive distillation is one of the most prominent separation techniques in industry for the separation of narrow-boiling or azeotropic mixtures [152], especially if the number and composition of the existing azeotropes are insensitive to pressure variations. In extractive distillation, a solvent is introduced as a second feed stream into a distillation column generating an extraction section between the rectifying and the stripping section. The separate feed streams distinguish extractive from homogeneous azeotropic distillation, for which a solvent is simply mixed with the feed stream to facilitate a certain separation task by exploiting curvature of distillation boundaries [73]. Consequently, extractive distillation is more versatile in separating mixtures by allowing the recovery of intermediate boiling components [152]. The presence of the MSA affects the activity coefficients of the feed components and is supposed to increase the relative volatility between the components in the feed mixture, allowing for the separation of narrow-boiling and azeotropic mixtures.

The most applied process concept, as illustrated in Figure 12.18 (left), is used to separate a mixture that forms a minimum boiling azeotrope by adding a heavy boiling MSA. The component in the feed mixture that shows higher affinity to the MSA is leaving the column as bottoms product, while the other component (in this case component A) is separated as top product. Note that the top products depend on the affinity with the MSA, not the pure component boiling temperature. The bottoms product is further separated in a subsequent simple column to recover the MSA, which is recycled back to the extractive distillation

column. The obtained purity of the solvent plays an important role as it affects the product recovery of the extractive column and the total energy consumption, especially in case of a heavy boiling solvent [152, 153]. While large boiling point differences between the MSA and the feed components are supposed to ease the separation in the solvent recovery column [138], resulting in increased interest in nonvolatile solvents, such as ionic liquids [154], thermal stability, utility availability, and costs should also be considered. While the depicted process configuration is the most prominent, a similar process concept with light boiling solvents could be as common as heavy solvents according to Laroche et al. [155] who investigated more than 400 mixtures. However, the application of light boiling MSA is reported to a much lesser extent in the literature [152], which might be related to the preference of obtaining products as distillate to avoid contamination by nonvolatile impurities. While also feasible, the use of intermediate boiling MSA is quite rare [156]. Any of the following discussions is based on the assumption of a heavy boiling MSA but can easily be transferred to the case of a light boiling MSA, for which the process flow sheet would transform from a direct to an indirect split sequence with the MSA being added below the feed and the products obtained as bottom products.

The desired modification of the relative volatility of the feed mixture is illustrated in the augmented xy-diagram in Figure 12.19 (right), while Figure 12.19 (left) illustrates the respective Gibbs triangle of the ternary system with the additional MSA. The dashed line represents the univolatility curve, for which the relative volatility α_{AB} between the feed components is 1. The solid lines represent individual residue curves and indicate that the ternary mixture does not contain a distillation boundary despite the binary azeotrope between the feed components. For this particular case, the azeotrope is the unstable node, while the MSA is the stable node, meaning that all residue curves start from the azeotrope and end in the MSA vertex. Both components of the feed mixture (A and B) are saddle points and, therefore, not suitable as high purity products via simple distillation. This specific type of feed-MSA combination dominates reports on extractive distillation with a coverage of over 90% of the conducted studies between 2000 and 2016 [152].

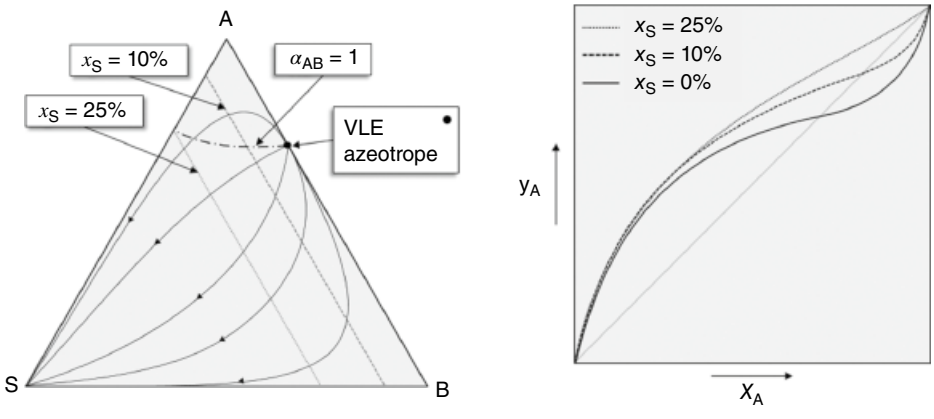

Figure 12.19 Residue curve map (left) and pseudo binary equilibrium curve (right) for an extractive distillation process with a heavy solvent (S) separating a minimum boiling azeotropic mixture (A, B).

As highlighted in Figure 12.19, the univolatility curve plays a decisive role in the design of extractive distillation processes. The intersection of the univolatility curve with the binary edge of the Gibbs triangle does not only determine which of the feed components can be separated as top product in the extractive column, but also provides an indication of the suitability of the MSA, as it separates regions with different volatility order [157, 158]. The closer the intersection of the univolatility curve and the binary edge is to the pure component vertex, the lower is the amount of MSA required to enable the separation. This becomes apparent from the comparison between the Gibbs triangle and the augmented xy-diagram in Figure 12.19, which indicates that a separation of the feed components becomes potentially feasible at a molar composition of the MSA of 25%. The separation is only potentially feasible, as depending on the amount of entrainer, additional limitations on the minimum and maximum applicable reflux ratio exists that limit the operating window of the extractive column [159]. Therefore, it is important to mention that extractive distillation is generally infeasible at total reflux and the stable operation depends heavily on the MSA-to-feed ratio.

In order to determine a suitable MSA, different performance indicators can be considered. Based on the relative volatility and the assumption of a constant ratio of the pure vapor pressures for small deviations in temperature, the selectivity S_{AB} for an extractive distillation solvent with respect to the binary feed in the presence of the MSA is defined by [138, 160]:

$$S_{AB} = \left(\frac{\gamma_A}{\gamma_B} \right)_S . \tag{12.4}$$

In general, a potential solvent should alter the relative volatility as far from unity as possible, which corresponds to a high selectivity. However, the activity coefficients and selectivity are strongly dependent on the liquid composition as well as the amount of solvent added to the system. Thus, oftentimes the selectivity at infinite dilution (∞) is considered instead:

$$S_{AB}^{\infty} = \left(\frac{\gamma_A^{\infty}}{\gamma_B^{\infty}} \right)_S , \tag{12.5}$$

which enables the comparison of MSAs by a distinct value. This represents the maximum possible selectivity as the effect of the MSA decreases with decreasing amount of MSA [138]. The capacity C_{BS}^{∞} [160] is an additional factor for MSA selection and is defined as:

$$C_{BS}^{\infty} = \left(\frac{1}{\gamma_B^{\infty}} \right)_S . \tag{12.6}$$

Here, a small activity coefficient at infinite dilution γ_{BS}^{∞} refers to strong interactions between the solvent S and the solute B, which ends up in an increased capacity [138]. Oftentimes, high selectivity MSA exhibits low capacities [160]. In general, the selected MSA should be completely miscible with the feed and not introduce additional azeotropes to the system [161]. Both are unlikely if the boiling point of the MSA differs by at least 30–50 K from the boiling points of the feed components [162]. While the selectivity and capacity provide good indication on the suitability of a MSA for extractive distillation, they do not provide any information on the effort necessary for MSA recovery. The latter requires at least the

determination of the MSA-to-feed ratio, but in the best case considers the whole integrated process of extractive distillation and MSA recovery. For an integrated molecular and process design, shortcut methods, such as the pinch-based method of Brüggemann and Marquardt [159], are providing an excellent basis to evaluate a large variety of MSA candidates, while Kossack et al. [138] proposed a hierarchical framework for the conceptual design of extractive distillation processes, combining CAMD, shortcut methods, and rigorous process optimization.

While extractive distillation is applied to a lower extent in industry than heteroazeotropic distillation [160], quite a number of processes rely on extractive distillation. One of the first industrial applications is the production of toluene and butadiene [156], which was later adapted by the petrochemical and chemical industry for versatile applications [156] with a capacity of hundreds of kilotons per year [161]. Extractive distillation is particularly used for the dehydration of aliphatic alcohols [163], as in the dehydration of (bio)ethanol with heavy solvents, such as ethylene glycol (with salts), glycerol, and tetraethylene glycol [156, 157, 161]. A few further examples are the separation of acetone and methanol with water as heavy entrainer [16], the separation of C4 hydrocarbons from crude oil with acetone, acetonitrile, or dimethylformamide (DMF) [157, 161], the separation of C5 hydrocarbons with DMF [157, 161], or the separation of methanol and methyl acetate in the methyl acetate synthesis with water [157]. For a more detailed overview, we refer to the work of Gerbaud et al. [157] and Lei et al. [161].

Similar to simple distillation sequences, the energy efficiency of extractive distillation may be improved by the techniques introduced in Sections 12.2 and 12.3. Gerbaud et al. [157] present an overview of several studies that investigated heat-integrated extractive distillation, extractive DWCs, as well as heat pump-assisted extractive distillation. They summarize that heat integration can in some cases reduce energy requirements by 20–30%, while heat pump-assisted extractive distillation may even save more than 40% of the energy requirement, while reducing costs by more than 20%. Similar to the example investigated by Luo et al. [131] and reported in Section 12.3.3, Gerbaud et al. [157] also summarize only small improvements achieved by extractive DWC. These results are also confirmed by a recent optimization-based evaluation of several MSAs and process configurations for the separation of an azeotropic mixture of acetone and methanol [164]. The results of this comparative evaluation are summarized in Figure 12.20, which indicates the optimized process performance of the different process configurations for the MSAs water, chlorobenzene, and dimethyl sulfoxide (DMSO). An important result of this study, which was recently confirmed by a more sophisticated optimization approach [165], is the difference in the screening results when limiting the investigation to the basic extractive distillation configuration. For the latter, DMSO is identified as the most suitable MSA providing the lowest total annualized costs (TAC). For this MSA choice, heat integration was not considered viable due to the limitation for utilities to resort to high-pressure steam, while MVR provided only little saving potentials, which also relates to the large temperature lift caused by the high boiling point of DMSO. On the contrary, water as naturally sustainable solvent provides considerable potential for heat integration and enables TAC savings of around 20%. Yet, process design might focus on a different candidate, when considering energy integration only as a subsequent step of process design, as proposed in the hierarchical frameworks [164, 165].

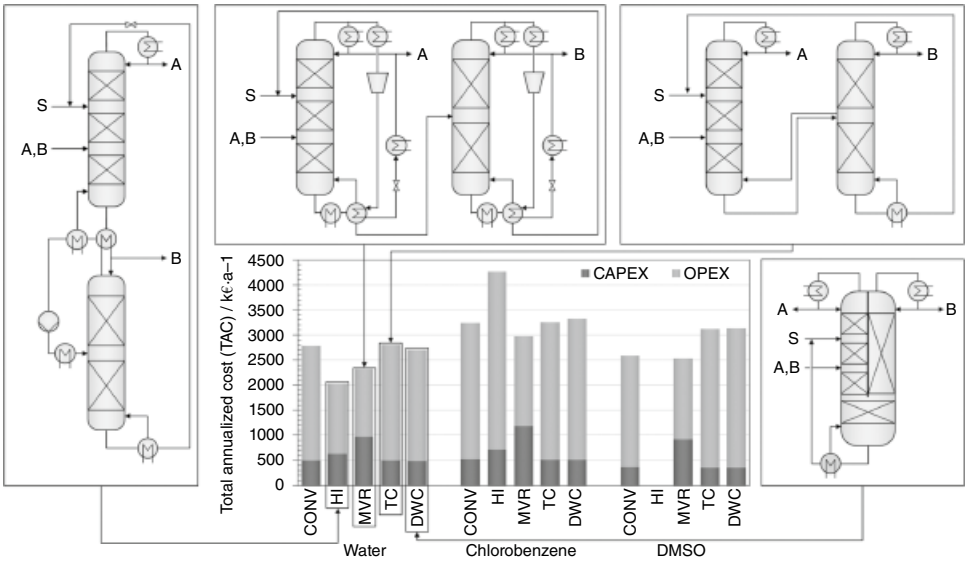

Figure 12.20 Illustration of the results of an optimization-based design of several energy-integrated extractive distillation processes for the separation of an azeotropic acetone and methanol feed using different MSA, as presented by Waltermann et al. [164].

12.4.2 Heteroazeotropic Distillation

Unlike extractive distillation, heteroazeotropic distillation or heterogeneous azeotropic distillation builds on the partial immiscibility of the MSA and the feed mixture, while specifically exploiting the presence of a heterogeneous azeotrope. The latter is generally a minimum boiling azeotrope. The feasibility of a heteroazeotropic distillation process depends on the topology of the Gibbs triangle, specifically the number and type of azeotropes as well as the size of the miscibility gap, which may further depend on the temperature. In the standard configuration illustrated in Figure 12.18 (center), the top vapor stream of one of the columns has a composition located inside the miscibility gap, representing either the minimum boiling heteroazeotrope or at least a composition inside the miscibility gap at the temperature of the decanter. The decanter performs a liquid–liquid phase split, which allows for the production of two separate liquid phases of which at least one is located in another distillation region and as such enables the combination of distillation and decantation to produce two products in separate distillation regions effectively crossing the distillation boundary. While other non-standard configurations of the distillation column and the decanter are possible [166, 167], the presented configuration is the most common variant. The process configuration is further illustrated with an exemplary Gibbs triangle diagram in Figure 12.21 illustrating the separation of a binary azeotropic mixture of components A and B with a MSA S, which forms binary azeotropes with both components (one homogeneous and one heterogeneous) as well as a ternary heterogeneous azeotrope. As a result, the Gibbs triangle is separated in three distillation regions with the ternary heteroazeotrope being the single unstable node and all pure components being stable nodes. Thus, both components can be produced as bottoms product, while the top vapor from the column may be condensed and potentially subcooled to further exploit the liquid phase split in the decanter. In this particular case, the miscibility gap occurs between the solvent and component B. Since the topology of the Gibbs triangle is considerably more complex compared with the extractive distillation case in Figure 12.19, the mass balance lines for the individual unit operations (colored lines), as well as liquid composition profiles for both columns (dashed lines) are introduced in the Gibbs triangle.

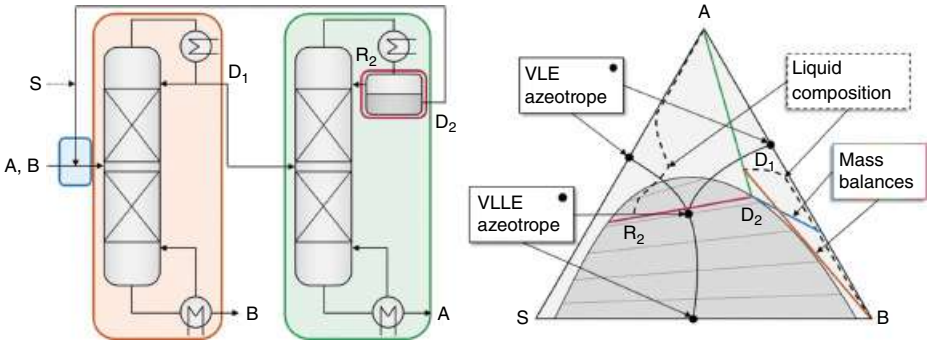

Figure 12.21 Heteroazeotropic distillation process (left) and Gibbs triangle (right) for a heteroazeotropic distillation process with a MSA (S) separating an azeotropic mixture (A, B).

In the given example, the feed stream is richer in component B than the binary azeotrope of the feed mixture. Thus, the first column produces this component as bottoms product while generating a top product close to the distillation boundary located inside the Gibbs triangle, due to the addition of the MSA agent, which is primarily recycled as top product of the heteroazeotropic distillation column. The latter effectively crosses the distillation boundary by producing component A as bottoms product, while producing a top vapor stream close to the ternary heteroazeotrope which is condensed and potentially subcooled, before it is separated in the decanter into a solvent-rich (reflux) and a solvent-lean (product) phase. It is important to note that the reflux R_2 and the top product D_2 may be equal to the individual liquid phases or may be mixed to a certain extent. As mentioned before, heteroazeotropic distillation may be performed in other process configurations depending on the specific topology of the Gibbs triangle with respect to the vapor–liquid–liquid equilibrium (VLLE) and liquid–liquid equilibrium (LLE) [73, 167, 168].

Identifying unique selection criteria for solvents in heteroazeotropic distillation processes is a complex task, because the existence and location of multiple azeotropes, as well as the form and size of the miscibility gap need to be determined and analyzed. While the feasibility and potential process configuration for new system can be conveniently designed by means of a graphical analysis of the residue curve map and the miscibility gaps [73], this approach is limited in practice to ternary systems, i.e. a binary feed mixture and a pure component MSA [169]. As a consequence of this limitation, algorithmic methods for solvent screening of suitable MSA have not been applied to heteroazeotropic distillation processes so far.

Once a suitable combination of MSA and process configuration has been identified, the specific process needs to be evaluated by means of simulation or optimization studies in order to evaluate the performance and compare it with alternatives. An important aspect that needs to be considered in the evaluation is the correct solution of the VLLE, which usually requires a special approach to quantify phase stability [170, 171]. For each equilibrium tray, either VLE or VLLE calculations need to be performed. The restriction to just VLE calculations typically results in considerable qualitative errors [172, 173]. Process simulators usually deal with this issue by starting the simulation with either VLE or VLLE computations and performing intermediate adaptions based on a separate phase stability test [174], which builds either on the Gibbs tangent plane criterion [175] or performs a global optimization of Gibbs free energy [176]. As the latter is computationally demanding, other hybrid methods based on homotopy continuation [177, 178] combine improved reliability with increased computational efficiency. An efficient integration of such a phase-stability test for the optimization-based design of heteroazeotropic distillation processes is presented by Skiborowski et al. [169], who also provide a more general overview on the different modeling and design methods. It is important to note that the possible liquid phase separation should be considered during equipment design, especially with respect to steady hold-up in e.g. the liquid distributer. However, as pointed out by Doherty and Knapp [73], mass-transfer efficiency and hydrodynamic performance are not considered much of a problem in practical applications, as de-mixing of the liquid on the plates of tray column is highly unlikely due to violent agitation by rapid bubbling of the vapor phase.

The most prominent industrial application of heteroazeotropic distillation is the dehydration of alcohols, which was first applied for ethanol dehydration in 1902 using benzene

as entrainer [179]. A batch process was later patented in 1903 by Young and a continuous process in 1915 by Kubierschky [73]. Formerly, benzene was the state-of-the-art solvent [180], which was later exchanged by cyclohexane due to its less harmful properties [181, 182]. An exemplary comparison of alternative solvents for ethanol dehydration is presented in Figure 12.22. The reported TAC are the result of an individual process optimization, considering the process configuration illustrated in Figure 12.21 and a feed stream with an ethanol composition of 6 mol% and a flow rate of 10 mol/sec [183]. While all investigated MSA have been reported as suitable candidates in the literature [180], cyclohexane and hexane provide more than 15% cost savings compared with iso-octane and toluene. Similar to extractive distillation, also heteroazeotropic distillation processes may be improved through application of the options for energy integration presented in Sections 12.2 and 12.3. According to the work of Wu et al. [184, 185], especially TC and DWC provide a considerable potential for the improvement of heteroazeotropic distillation. This is confirmed for the considered example of ethanol dehydration with cyclohexane as MSA, for which the TAC can be reduced by additional 11%, when the heteroazeotropic distillation is implemented in a DWC in terms of a split shell configuration [164]. As illustrated in Figure 12.22 (right), neither direct heat integration nor MVR allow for a reduction of the TAC, while MVR could reduce the energy requirement.

Other examples of heteroazeotropic distillation include the purification of butyl acetate, and vinyl acetate [181], or the separation of formic acid and acidic acid with chloroform [16]. Further examples and illustrations of the respective residue curve maps are provided by Doherty and Knapp [73]. Blass [160] concludes that heteroazeotropic distillation processes are applied almost four times as often in industry as extractive distillation processes.

12.4.3 Hybrid Extraction–Distillation Processes

Liquid–liquid extraction is another option to separate narrow-boiling and azeotropic mixtures by addition of a MSA that introduces a miscibility gap. However, unlike heteroazeotropic distillation, a countercurrent contacting of the solvent and the feed mixture, which is assumed to contain a low amount of dissolved product in a carrier, is performed

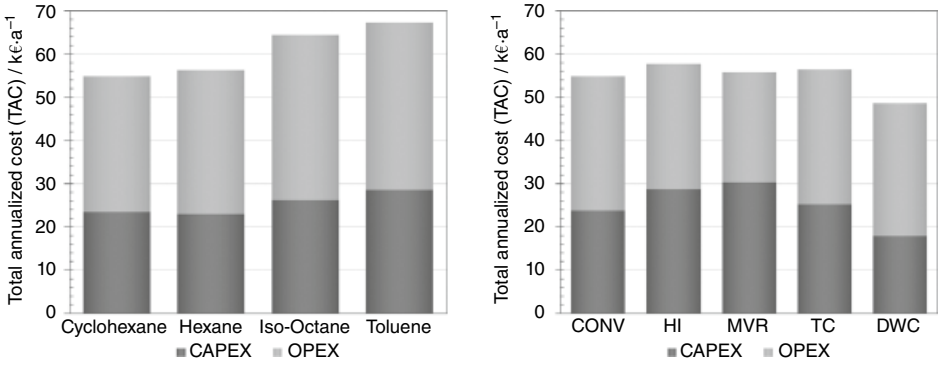

Figure 12.22 Total annualized costs (TAC) for the optimized processes for the dehydration of ethanol with different solvent candidates (left) and with different means for energy integration for cyclohexane as solvent (right) as reported by Kruber et al. [183] and Waltermann et al. [164].

in an extraction column or mixer-settler battery, producing a product-rich extract phase of the MSA and a product-lean raffinate phase of the carrier. Liquid–liquid extraction is frequently used for the separation of highly diluted solutions [186]. In order to recover the MSA, a subsequent distillation is predominantly used for thermal regeneration, while other non-thermal regeneration options, such as (reactive) back extraction with temperature- or diluent-swing [187], are used in case neither the product nor the MSA are volatile.

A classical flowsheet of an extraction–distillation hybrid process for the separation of an azeotropic mixture with a volatile MSA is depicted in Figure 12.23 together with an illustration of the according Gibbs triangle, highlighting the miscibility gap and the mass balance lines of the extraction and distillation column. The feed mixture is countercurrently contacted with the MSA, which, in the best case, is completely immiscible with the carrier, while preferentially extracting the product, leaving the extraction column on the bottom as extract stream. The lighter carrier leaves the column on top as raffinate stream. In case the MSA does not form an azeotrope with the product component, the recovery column is a simple distillation column, which depending on the operating temperature of the extraction column and a possible solubility of the carrier stream in the MSA, is followed by an additional decanter prior to the extraction column. Depending on the solubility of the MSA in the carrier stream and resulting raffinate composition, additional treatment of the raffinate might be necessary.

Suitable MSA for liquid–liquid extraction obviously need to induce a sufficient miscibility gap in the system, whereas the size and the orientation of the liquid–liquid tie-lines directly correlate with the separation performance. The larger the miscibility gap and the stronger liquid–liquid tie-lines are oriented toward the carrier, the easier the separation by liquid–liquid extraction [188]. As a quantitative measure, the solvent loss can be estimated by the inverse of the activity coefficient at infinite dilution of the solvent in the raffinate phase [188]:

$$\text{solvent loss} \approx \frac{1}{\gamma_{S,R}^{\infty}}. \tag{12.7}$$

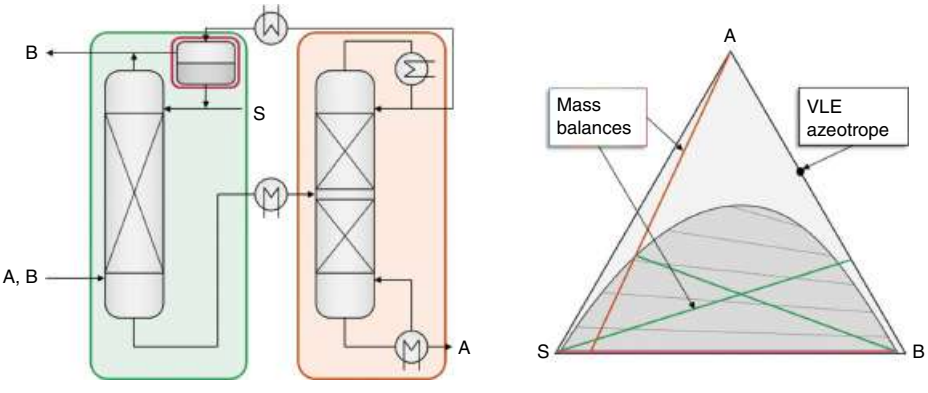

Figure 12.23 General process flow sheet of a liquid–liquid extraction–distillation hybrid process (left) and the corresponding Gibbs triangle for the separation of a azeotropic mixture (A, B) with a MSA S.

Comparable to extractive distillation, the selectivity (cf. Eq. (12.5)) and the capacity (cf. Eq. (12.6)) are good performance indicators of a solvent candidate. While a high selectivity generally benefits the separation performance, a high capacity relates to reduced amount of MSA for the separation and, therefore, the required energy demand in the subsequent MSA recovery. Besides the previously introduced definitions, the capacity and selectivity for an extraction solvent can be estimated by the distribution coefficient K_A of the solute A and the ratio of the distribution coefficients of A and the carrier B, respectively [188]:

$$K_A = \frac{\gamma_{A,R}}{\gamma_{A,E}} \approx \frac{x_{A,E}}{x_{A,R}}, \tag{12.8}$$

$$\alpha_{AB}^{ext} = \frac{K_A}{K_B}. \tag{12.9}$$

Moreover, the selection should consider the density difference of the extract and raffinate phase, which can be estimated by the difference of the solvent and the raffinate main component. A high density difference is preferred to ease phase separation, while at least a difference of 50 kg/m^3 should be realized [16]. The interfacial tension should be small to increase the mass transfer area at the risk of emulsion formation [188]. However, this effect is compensated by a high density difference as well as a low viscosity [189]. Preferentially, low viscosities similar to water should be aimed for to increase the mass transfer [16]. A comprehensive overview of the different criteria for an extraction solvent is given in [188]. While MSA selection mostly focuses on liquid–liquid extraction, the secondary separation, in this case distillation, should be considered in determining the optimal MSA choice, not only accounting for boiling points and relative volatilities, but also the energy and costs for solvent recovery.

While the amount of MSA required to accomplish the primary separation in the extraction does of course correlate with the necessary effort for solvent recovery in the secondary separation, it is important to note that it is not the only factor that needs to be taken into account since a higher affinity of the product to the MSA also results in a higher effort for MSA recovery. This is illustrated for the results of a computational screening of possible MSAs based on thermodynamically sound shortcut models by Scheffczyk et al. [147] for the purification of an aqueous γ-valerolactone (GVL) stream with a feed composition of 5 mol% of GVL and a flow rate of 100 mol/sec. Based on an initial screening of 4500 candidate molecules, more than 1400 MSA candidates are identified, which form a miscibility gap without introducing additional azeotropes. Figure 12.24 (left) illustrates the derived minimum amount of MSA (S_{min}) and the minimum energy requirement for MSA recovery (Q_{min}) using the shortcut methods of Redepenning et al. [190] and Bausa et al. [191]. While the minimum energy requirements also relate to low minimum amounts of MSA, the results indicate that low minimum amounts of MSA do not guarantee low energy requirements for solvent recovery. The results of the study further indicated the large potential of such computational MSA screening, resulting in more than 150 MSA candidates that show the potential to outperform the considered benchmark solvent butyl acetate. The large list of possible candidates can effectively be narrowed down considering additional criteria on availability, price, and health and safety criteria. Based on such considerations

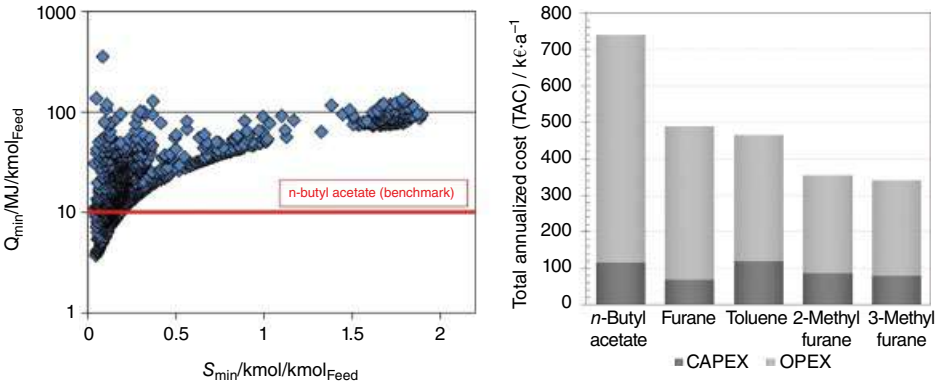

Figure 12.24: Minimum energy demand and minimum amount of solvent for 1439 valid solvent candidates (left). *Source:* Reprinted from [147]. Results for an optimization of the operational degrees of freedom for the purification of γ-valerolactone in an extraction–distillation process as reported by Kruber et al. [149] (right).

Kruber et al. [149] selected four of the promising MSA candidates and performed an optimization-based design of the processes seeking the minimal TAC. The results are summarized in Figure 12.24 (right) indicating economic savings of about 50% for the solvents 2-methyl furane and 3-methyl furane, as well as about 30% for the widely available toluene.

Anyhow, it should be considered that the detailed design of an extraction process is not a trivial task and oftentimes requires special equipment with mechanical agitation in order to provide sufficient phase contact area, accounting for the much smaller density difference between the occurring phases. For a mixer-settler setup, the phase contact is established by the impellers in the mixing step, while extraction columns are often implemented as either stirred or pulsed columns [192]. While the common approach for the design of such processes builds on a sequential selection of a suitable solvent, conceptual process design, and the design of the extraction equipment [193], current research effort aims at an integration of MSA selection and profound process models to avoid suboptimal process designs [147, 193].

Industrial application of liquid–liquid extraction in columns was firstly introduced in 1889 [160] and is predominantly used for the separation of metal ions and for the purification of temperature sensitive and/or highly diluted product streams [16]. As the latter ones oftentimes occur in the downstream processing of bio-bases processes, liquid–liquid extraction is a common technique to recover the desired product, such as carboxylic acids [186, 194]. In the area of process wastewater treatment, liquid–liquid extraction plays a key role to reduce the content of contaminants and leftovers, like phenol or aniline, with e.g. naphtha or methyl isobutyl ketone as solvents [195].

12.4.4 Membrane-Assisted Distillation Processes

Membrane separations are not limited by the presence of azeotropes or close-boiling components in multicomponent mixtures and therefore have been claimed to enable energy savings of up to 90% when compared with distillation [17]. However, this comparison

usually does not account for the possible energy savings that can be accomplished by the methods introduced in the previous sections and while the thermodynamic efficiency of especially pressure-driven membrane processes, such as nanofiltration, reverse osmosis, or gas permeation, can be extraordinarily high, the efficiency drops significantly [23] with an increasing recovery. Consequently, membrane processes are often economically unviable if sharp splits characterized by high purities and recoveries are desired, for which multistage processes with recycle streams are required [75]. Considering both aspects, Agrawal et al. [15] present an exemplary evaluation of the thermodynamic efficiency for a propylene/propane separation, comparing a heat pump-assisted distillation process with a multistage gas permeation process. For the specific case study, the heat pump-assisted distillation process was twice as efficient as the gas permeation process. It is important to note that this is not a general result but it illustrates that membrane processes should not generally be considered more energy efficient.

In order to overcome limitations of the individual technologies, hybrid processes combining a suitable membrane process with distillation provides particular potential for the separation of close-boiling and azeotropic mixtures. Particularly, hybrid processes based on a combination of distillation and pervaporation (PV) or vapor permeation (VP) have found widespread implementation. PV-assisted distillation was first proposed by Binning and James in 1958 [196] but not implemented before the late 1980s [197]. Lipnizki et al. [197, 198] and Baker [199] present elaborate overviews of various applications that focus mostly on the dehydration of organic streams, especially the concentration of alcohols with hydrophilic membranes as well as the removal of small amounts of volatile organic compounds from contaminated water by means of hydrophobic membranes. In recent years, organic–organic separations by organophilic membranes are actively investigated and have been used for solvent separations such as toluene–heptane, methanol–benzene, and methanol–toluene [13]. Another application is the separation of isomers, such as o-xylene, m-xylene, p-xylene, and ethyl benzene and dichlorobenzene isomers [200].

However, other membranes, such as organic solvent nanofiltration membranes, may also be combined with distillation in order to enable an overall improved energy efficiency of the hybrid process [201, 202]. As for the previously presented distillation-based processes, the respective process configurations depend on the mixture to be separated and the type of membrane process and its separation characteristics [203]. Since the latter depends strongly on the specific membrane and usually cannot be predicted, a tight integration between an experimental and model-based assessment enables a directed development process [204]. This evaluation should also take the presented options for energy integration into account, which may further be extended by innovative configurations, such as the heat-integrated hybrid distillation PV process presented by del Pozo Gomez et al. [205].

12.5 Summary

Due to its unique capability to produce two or more products at high purity, distillation will maintain its important role as a leading unit operation for fluid separations in downstream processing. As presented in the current chapter, a whole portfolio of options is available for improving the energy efficiency of distillation processes, making them more sustainable.

The optimal process configuration depends on the specific separation problem as well as its integration in the overall process or site, considering the integration with other unit operations and the utility system. Given the widespread implementation and considerable energy consumption of distillation processes, the various options for heat and mass integration provide an immense potential to reduce the energy consumption in the chemical industry and reduce the related greenhouse gas emissions.

As recently pointed out by Agrawal et al. [15], the consideration that distillation is the most energy-intensive unit operation for fluid separations and that distillation technology is mature are common misconceptions, which are particularly founded in the lack of detailed comparative evaluations of thermal and non-thermal separation processes, which are based on a fair comparison that considers the potential for energy-integration. As already pointed out by Cussler and Dutta [23], other separation technologies can significantly outperform distillation for certain separation tasks, but also suffer a significant drop in efficiency when targeting sharp splits that are usually addressed by distillation. Consequently, energy integration and especially heat pump-assisted distillation as well as hybrid processes are of special interest when designing energy-efficient separation processes [24, 25].

Thus, although classical distillation columns and the specific equipment can be considered a robust technology, the design of energy-efficient sustainable distillation processes has experienced significant progress in recent years [15, 21] with plenty of prospect ahead [26]. The problem in process design has shifted from simulation and optimization of a specific option to efficiently addressing the versatility that comes with the tremendous number of options that result from the different means of energy integration. Heat pump-assisted distillation allows to run the thermal separation process primarily by electrical energy, providing an enormous potential for improving the sustainability of existing processes by exploiting renewable energy sources [15]. Finally, the most sustainable and economically affordable process needs to be identified to foster the implementation of more sustainable distillation processes in the context of the overall process or even total site integration. Consequently, the separation process should be evaluated in the context of the overall available heat sources and sinks, considering classical pinch analysis [50, 51] but also extensions for heat and work integration [206]. Furthermore, controllability should be considered as additional important aspect for a practical implementation, as it is fairly true that the degree of heat integration and controllability are likely to have an inverse relation [84]. After all, distillation-based processes show a considerable potential for improvements in terms of sustainability, but still require the development of advanced methods to guide and support the process engineer in identifying the best solution from a complex and large set of alternatives.

References

1 Kockmann, N. (2014). 200 years in innovation of continuous distillation. *ChemBioEng Reviews* 1: 40–49.

2 McCabe, W.L. and Thiele, E.W. (1925). Graphical design of fractionating columns. *Ind. Eng. Chem.* 17: 605–611.

3 Mersmann, A., Kind, M., and Stichlmair, J. (2011). *Thermal Separation Technology: Principles, Methods, Process Design*. New York: Springer.

4 de Haan, A.B., Schuur, B., and Eral, H.B. (2020). *Industrial Separation Processes: Fundamentals, De Gruyter Textbook*. Berlin, Boston: De Gruyter.

5 Melin, T. and Rautenbach, R. (2007). *Membranverfahren: Grundlagen der Modul- und Anlagenauslegung*, 3e. Berlin, Heidelberg: VDI-Buch, Springer-Verlag Berlin Heidelberg.

6 Taylor, R. (2007). (Di)still modeling after all these years: a view of the state of the art - catching up with the Past. *Ind. Eng. Chem. Res.* 46: 4349–4357.

7 Waltermann, T., Schlueter, S., Benfer, R. et al. (2020). Model discrimination for multicomponent distillation – a geometrical approach for total reflux. *Chemie-Ingenieur-Technik* 92: 890–906.

8 Spiegel, L. and Duss, M. (2014). Structured packings. In: *Distillation* (eds. A. Górak and Z. Olujic), 145–181. Elsevier.

9 Olujić, Ž. (2014). Vacuum and high-pressure distillation. In: *Distillation* (eds. A. Górak and Z. Olujic), 295–318. Elsevier.

10 Luyben, W.L. (2011). Design and control of the acetone process via dehydrogenation of 2-propanol. *Ind. Eng. Chem. Res.* 50: 1206–1218.

11 Fraser, S. (2014). Distillation in refining. In: *Distillation* (eds. A. Górak and H. Schoenmakers), 155–190. Elsevier.

12 Simeone, M. (2018). The Aria project: production of depleted argon for the darkside experiment.

13 Wankat, P.C. (2012). *Separation Process Engineering: Includes Mass Transfer Analysis*, 3e. Upper Saddle River, NJ: Prentice Hall.

14 Sorensen, E. (2014). Principles of binary distillation. In: *Distillation* (eds. A. Górak and E. Sorensen), 145–185. Elsevier.

15 Agrawal, R. and Tumbalam Gooty, R. (2020). Misconceptions about efficiency and maturity of distillation. *AICHE J.* 66: e16294.

16 Goedecke, R. (2008). *Fluidverfahrenstechnik*. Hoboken: Wiley-VCH.

17 Sholl, D.S. and Lively, R.P. (2016). Seven chemical separations to change the world. *Nature* 532: 435–437.

18 Humphrey, J.L. and Siebert, A.F. (1992). Separation technologies: an opportunity for energy savings. *Chem. Eng. Prog.* 88: 32–41.

19 Taylor, R., Krishna, R., and Kooijman, H. (2003). Real-world modeling of distillation. *Chem. Eng. Prog.* 99: 28–39.

20 Koeijer, G. and Kjelstrup, S. (2000). Minimizing entropy production rate in binary tray distillation. *Int. J. Appl. Thermodyn.* 3: 105–110.

21 Kiss, A.A. (2014). Distillation technology - still young and full of breakthrough opportunities. *J. Chem. Technol. Biotechnol.* 89: 479–498.

22 Agrawal, R. and Herron, D.M. (1997). Optimal thermodynamic feed conditions for distillation of ideal binary mixtures. *AICHE J.* 43: 2984–2996.

23 Cussler, E.L. and Dutta, B.K. (2012). On separation efficiency. *AICHE J.* 58: 3825–3831.

24 Blahušiak, M., Kiss, A.A., Kersten, S.R.A., and Schuur, B. (2016). Quick assessment of binary distillation efficiency using a heat engine perspective. *Energy* 116: 20–31.

25 Blahušiak, M., Kiss, A.A., Babic, K. et al. (2018). Insights into the selection and design of fluid separation processes. *Sep. Purif. Technol.* 194: 301–318.

26 Kiss, A.A. and Smith, R. (2020). Rethinking energy use in distillation processes for a more sustainable chemical industry. *Energy* 203: 117788.

27 Schulz, R., Rietfort, T., Jansen, H., and Olujić, Ž. (2019). Hydraulics and mass transfer performance of an advanced wire gauze structured packing under deep vacuum distillation conditions. *Chem. Eng. Res. Des.* 145: 334–342.

28 Amini, Y., Karimi-Sabet, J., Nasr Esfahany, M. et al. (2019). Experimental and numerical study of mass transfer efficiency in new wire gauze with high capacity structured packing. *Sep. Sci. Technol.* 54: 2706–2717.

29 Mackowiak, J. and Mackowiak, J.F. (2014). Random packings. In: *Distillation* (eds. A. Górak and Z. Olujic), 85–144. Elsevier.

30 Ramshaw, C. (1993). The opportunities for exploiting centrifugal fields. *Heat Recovery Syst. CHP* 13: 493–513.

31 Neumann, K., Gladyszewski, K., Groß, K. et al. (2018). A guide on the industrial application of rotating packed beds. *Chem. Eng. Res. Des.* 134: 443–462.

32 Cortes Garcia, G.E., van der Schaaf, J., and Kiss, A.A. (2017). A review on process intensification in HiGee distillation. *J. Chem. Technol. Biotechnol.* 92: 1136–1156.

33 Kiss, A.A. and Kattan Readi, O.M. (2018). An industrial perspective on membrane distillation processes. *J. Chem. Technol. Biotechnol.* 93: 2047–2055.

34 Bîldea, C.S., Pătruţ, C., Jørgensen, S.B. et al. (2016). Cyclic distillation technology - a mini-review. *J. Chem. Technol. Biotechnol.* 91: 1215–1223.

35 Smith, R. (2016). *Chemical Process: Design and Integration*, 2e. Chichester, West Sussex, United Kingdom: Wiley.

36 Kiss, A.A. (2013). *Advanced Distillation Technologies: Design, Control and Applications, Advanced Distillation Technologies: Design, Control and Applications*. Hoboken: Wiley.

37 Al-Arfaj, M.A. and Luyben, W.L. (2000). Effect of number of fractionating trays on reactive distillation performance. *AICHE J.* 46: 2417–2425.

38 Cui, C., Xi, Z., Liu, S., and Sun, J. (2019). An enumeration-based synthesis framework for multi-effect distillation processes. *Chem. Eng. Res. Des.* 144: 216–227.

39 Kiss, A.A., Flores Landaeta, S.J., and Infante Ferreira, C.A. (2012). Towards energy efficient distillation technologies – making the right choice. *Energy* 47: 531–542.

40 Engelien, H.K. and Skogestad, S. (2004). Selecting appropriate control variables for a heat-integrated distillation system with prefractionator. *Comput. Chem. Eng.* 28: 683–691.

41 Wendt, M., Königseder, R., Li, P., and Wozny, G. (2003). Theoretical and experimental studies on startup strategies for a heat-integrated distillation column system. *Chem. Eng. Res. Des.* 81: 153–161.

42 Zhang, J., Liang, S., and Feng, X. (2010). A novel multi-effect methanol distillation process. *Chem. Eng. Process.* 49: 1031–1037.

43 Al-Karaghouli, A. and Kazmerski, L.L. (2013). Energy consumption and water production cost of conventional and renewable-energy-powered desalination processes. *Renew. Sust. Energ. Rev.* 24: 343–356.

44 Huang, B., Pu, K., Wu, P. et al. (2020). Design, selection and application of energy recovery device in seawater desalination: a review. *Energies* 13: 4150.

45 Kiss, A.A. and Ferreira, C.A.I. (2017). *Heat Pumps in Chemical Process Industry*. Boca Raton, London, New York: CRC Press Taylor & Francis Group.

46 Jarre, M., Noussan, M., and Simonetti, M. (2018). Primary energy consumption of heat pumps in high renewable share electricity mixes. *Energy Convers. Manag.* 171: 1339–1351.

47 Jana, A.K. (2014). Advances in heat pump assisted distillation column: a review. *Energy Convers. Manag.* 77: 287–297.

48 Zimmermann, H. and Walzl, R. (2000). Ethylene. In: *Ullmann's Encyclopedia of Industrial Chemistry* (ed. F. Ullmann). Weinheim, Germany: Wiley-VCH Verlag GmbH & Co. KGaA https://onlinelibrary.wiley.com/doi/book/10.1002/14356007.

49 van de Bor, D.M., Infante Ferreira, C.A., and Kiss, A.A. (2014). Optimal performance of compression–resorption heat pump systems. *Appl. Therm. Eng.* 65: 219–225.

50 Linnhoff, B. and Hindmarsh, E. (1983). The pinch design method for heat exchanger networks. *Chem. Eng. Sci.* 38: 745–763.

51 Linnhoff, B. (1993). Pinch analysis - a state-of-the-art overview. *TI* 71: 503–522.

52 Kumar, V., Kiran, B., Jana, A.K., and Samanta, A.N. (2013). A novel multistage vapor recompression reactive distillation system with intermediate reboilers. *AICHE J.* 59: 761–771.

53 Bruinsma, D. and Spoelstra, S. (2010). Heta pumps in distillation. *Proceedings Distillation Absorption 2010*, Eindhoven, The Netherlands (12–15 September 2010), (ed. A. de Haan, H. Kooijman, A. Górak), 21–28.

54 Kiss, A.A. and Olujić, Ž. (2014). A review on process intensification in internally heat-integrated distillation columns. *Chem. Eng. Process. Process Intensif.* 86: 125–144.

55 Olujić, Ž., Sun, L., de Rijke, A., and Jansens, P.J. (2006). Conceptual design of an internally heat integrated propylene-propane splitter. *Energy* 31: 3083–3096.

56 Rivero, R. (2001). Exergy simulation and optimization of adiabatic and diabatic binary distillation. *Energy* 26: 561–593.

57 Olujić, Ž., Jödecke, M., Shilkin, A. et al. (2009). Equipment improvement trends in distillation. *Chem. Eng. Process. Process Intensif.* 48: 1089–1104.

58 Bruinsma, O.S.L., Krikken, T., Cot, J. et al. (2012). The structured heat integrated distillation column. *Chem. Eng. Res. Des.* 90: 458–470.

59 Gadalla, M.A. (2009). Internal heat integrated distillation columns (iHIDiCs)—new systematic design methodology. *Chem. Eng. Res. Des.* 87: 1658–1666.

60 Mah, R.S.H., Nicholas, J.J., and Wodnik, R.B. (1977). Distillation with secondary reflux and vaporization: a comparative evaluation. *AICHE J.* 23: 651–658.

61 Matsuda, K., Iwakabe, K., and Nakaiwa, M. (2012). Recent advances in internally heat-integrated distillation columns (HIDiC) for sustainable development. *J. Chem. Eng. Japan / JCEJ* 45: 363–372.

62 Shenvi, A.A., Herron, D.M., and Agrawal, R. (2011). Energy efficiency limitations of the conventional heat integrated distillation column (HIDiC) configuration for binary distillation†. *Ind. Eng. Chem. Res.* 50: 119–130.

63 Suphanit, B. (2011). Optimal heat distribution in the internally heat-integrated distillation column (HIDiC). *Energy* 36: 4171–4181.

64 Harwardt, A. and Marquardt, W. (2012). Heat-integrated distillation columns: vapor recompression or internal heat integration? *AICHE J.* 58: 3740–3750.

65 Campbell, J.C., Wigal, K.R., van Brunt, V., and Kline, R.S. (2008). Comparison of energy usage for the vacuum separation of acetic acid/acetic anhydride using an internally heat integrated distillation column (HIDiC). *Sep. Sci. Technol.* 43: 2269–2297.

66 Chen, H., Huang, K., and Wang, S. (2010). A novel simplified configuration for an ideal heat-integrated distillation column (ideal HIDiC). *Sep. Purif. Technol.* 73: 230–242.

67 Wakabayashi, T. and Hasebe, S. (2015). Higher energy saving with new heat integration arrangement in heat-integrated distillation column. *AICHE J.* 61: 3479–3488.

68 Wakabayashi, T., Ferrari, A., and Hasebe, S. (2019). Design and commercial operation of a discretely heat-integrated distillation column. *Chem. Eng. Res. Des.* 147: 214–221.

69 Wakabayashi, T., Yoshitani, K., Takahashi, H., and Hasebe, S. (2019). Verification of energy conservation for discretely heat integrated distillation column through commercial operation. *Chem. Eng. Res. Des.* 142: 1–12.

70 Fang, J., Cheng, X., Li, Z. et al. (2019). A review of internally heat integrated distillation column. *Chin. J. Chem. Eng.* 27: 1272–1281.

71 Agrawal, R. (2003). Synthesis of multicomponent distillation column configurations. *AICHE J.* 49: 379–401.

72 Westerberg, A.W., Lee, J.W., and Hauan, S. (2000). Synthesis of distillation-based processes for non-ideal mixtures. *Comput. Chem. Eng.* 24: 2043–2054.

73 Doherty, M.F. and Knapp, J.P. (2003). Distillation, azeotropic, and extractive. In: *Encyclopedia of Chemical Technology* (eds. R.E. Kirk and D.F. Othmer). New York, NY: Wiley.

74 Skiborowski, M., Harwardt, A., and Marquardt, W. (2014). Conceptual design of azeotropic distillation processes. In: *Distillation* (eds. A. Górak and E. Sorensen), 305–355. Elsevier.

75 Skiborowski, M., Harwardt, A., and Marquardt, W. (2013). Conceptual design of distillation-based hybrid separation processes. *Annu. Rev. Chem. Biomol. Eng.* 4: 45–68.

76 Thompson, R.W. and King, C.J. (1972). Systematic synthesis of separation schemes. *AICHE J.* 18: 941–948.

77 Stichlmair, J., Offers, H., and Potthoff, R.W. (1993). Minimum reflux and minimum reboil in ternary distillation. *Ind. Eng. Chem. Res.* 32: 2438–2445.

78 Glinos, K.N. and Malone, M.F. (1985). Design of sidestream distillation columns. *Ind. Eng. Chem. Proc. Des. Dev.* 24: 822–828.

79 von Watzdorf, R., Bausa, J., and Marquardt, W. (1999). Shortcut methods for nonideal multicomponent distillation: 2. Complex columns. *AICHE J.* 45: 1615–1628.

80 Madenoor Ramapriya, G., Tawarmalani, M., and Agrawal, R. (2018). A systematic method to synthesize all dividing wall columns for *n* -component separation: Part II. *AICHE J.* 64: 660–672.

81 Madenoor Ramapriya, G., Tawarmalani, M., and Agrawal, R. (2018). A systematic method to synthesize all dividing wall columns for *n* -component separation-Part I. *AICHE J.* 64: 649–659.

82 Shah, V.H. and Agrawal, R. (2010). A matrix method for multicomponent distillation sequences. *AICHE J.* 56: 1759–1775.

83 Nallasivam, U., Shah, V.H., Shenvi, A.A. et al. (2016). Global optimization of multicomponent distillation configurations: 2. Enumeration based global minimization algorithm. *AICHE J.* 62: 2071–2086.

84 Nallasivam, U., Shah, V.H., Shenvi, A.A. et al. (2013). Global optimization of multicomponent distillation configurations: 1. Need for a reliable global optimization algorithm. *AICHE J.* 59: 971–981.

85 Tedder, D.W. and Rudd, D.F. (1978). Parametric studies in industrial distillation: Part I. Design comparisons. *AICHE J.* 24: 303–315.

86 Mathew, T.J., Tumbalam Gooty, R., Tawarmalani, M., and Agrawal, R. (2019). 110th anniversary: thermal coupling via heat transfer: a potential route to simple distillation configurations with lower heat duty. *Ind. Eng. Chem. Res.* 58: 21671–21678.

87 Andrecovich, M.J. and Westerberg, A.W. (1985). An MILP formulation for heat-integrated distillation sequence synthesis. *AICHE J.* 31: 1461–1474.

88 Skiborowski, M. (2018). Fast screening of energy and cost efficient intensified distillation processes. *Chem. Eng. Trans.* 69: 199–204.

89 Harwardt, A., Kraemer, K., and Marquardt, W. (eds.) (2009). Optimization based design of heat integrated distillation processes.

90 Waltermann, T. and Skiborowski, M. (2019). Efficient optimization-based design of energy-integrated distillation processes. *Comput. Chem. Eng.* 129: 106520.

91 Floudas, C.A. and Paules, G.E. (1988). A mixed-integer nonlinear programming formulation for the synthesis of heat-integrated distillation sequences. *Comput. Chem. Eng.* 12: 531–546.

92 Pyrgakis, K.A. and Kokossis, A.C. (2019). Systematic synthesis and integration of multiple-effect distillation into overall processes: the case of biorefineries. *AICHE J.* 65: e16631.

93 Agrawal, R. (2000). Thermally coupled distillation with reduced number of intercolumn vapor transfers. *AICHE J.* 46: 2198–2210.

94 Kaibel, B. (2014). Dividing-wall columns. In: *Distillation* (eds. A. Górak and Z. Olujic), 183–199. Elsevier.

95 Petlyuk, F.B., Platonov, V.M., and Slavinsk, D.M. (1965). Thermodynamically optimal method for separating multicomponent mixtures. *IEC* 5: 555–561.

96 Fidkowski, Z. and Krolikowski, L. (1986). Thermally coupled system of distillation columns: optimization procedure. *AICHE J.* 32: 537–546.

97 Halvorsen, I.J. and Skogestad, S. (2003). Minimum energy consumption in multicomponent distillation. 2. Three-product Petlyuk arrangements. *Ind. Eng. Chem. Res.* 42: 605–615.

98 Halvorsen, I.J. and Skogestad, S. (2003). Minimum energy consumption in multicomponent distillation. 1. V_{min} diagram for a two-product column. *Ind. Eng. Chem. Res.* 42: 596–604.

99 Underwood, A.J.V. (1948). Fractional distillation of multicomponent mixtures. *Chem. Eng. Prog.* 44: 603–614.

100 Ränger, L.-M., Preißinger, U., and Grützner, T. (2018). Robust initialization of rigorous process simulations of multiple dividing wall columns via Vmin diagrams. *ChemEng.* 2: 25.

101 Waltermann, T. and Skiborowski, M. (2017). Conceptual design of highly integrated processes - optimization of dividing wall columns. *Chemie Ingenieur Technik* 89: 562–581.

102 Halvorsen, I.J. and Skogestad, S. (2011). Energy efficient distillation. *J. Nat. Gas Sci. Eng.* 3: 571–580.

103 van Duc Long, N. and Lee, M. (2012). Dividing wall column structure design using response surface methodology. *Comput. Chem. Eng.* 37: 119–124.

104 Dejanović, I., Matijašević, L., and Olujić, Ž. (2010). Dividing wall column—a breakthrough towards sustainable distilling. *Chem. Eng. Process. Process Intensif.* 49: 559–580.

105 Agrawal, R. and Fidkowski, Z.T. (1998). Are thermally coupled distillation columns always thermodynamically more efficient for ternary distillations? *Ind. Eng. Chem. Res.* 37: 3444–3454.

106 Brüggemann, S. and Marquardt, W. (2004). Rapid screening of design alternatives for nonideal multiproduct distillation processes. *Comput. Chem. Eng.* 29: 165–179.

107 Schultz, M.A., Stewart, D.G., Harris, J.M. et al. (2002). Reduce cost with dividing-wall columns. *Chem. Eng. Prog.* 98: 64–71.

108 Wright, R.O. (1949). US Patent 2,471,134, Standard Oil Development Co., Elizabeth, NJ.

109 Kaibel, G. (1987). Distillation columns with vertical partitions. *Chem. Eng. Technol.* 10: 92–98.

110 Lukač, G., Halvorsen, I.J., Olujić, Ž., and Dejanović, I. (2019). On controllability of a fully thermally coupled four-product dividing wall column. *Chem. Eng. Res. Des.* 147: 367–377.

111 Yildirim, O., Kiss, A.A., and Kenig, E.Y. (2011). Dividing wall columns in chemical process industry: a review on current activities. *Sep. Purif. Technol.* 80: 403–417.

112 Zhou, J., Kooijman, H.A., and Taylor, R. (2019). Parallel column model for dividing wall column simulations. *Comput. Chem. Eng.* 125: 114–133.

113 Kiss, A. and Bildea, C. (2011). A control perspective on process intensification in dividing-wall columns. *Chem. Eng. Process.* 50: 281–292.

114 Dejanović, I., Halvorsen, I.J., Skogestad, S. et al. (2014). Hydraulic design, technical challenges and comparison of alternative configurations of a four-product dividing wall column. *Chem. Eng. Process.* 84: 71–81.

115 Gómez-Castro, F.I., Segovia-Hernández, J.G., Hernández, S. et al. (2008). Dividing wall distillation columns: optimization and control properties. *Chem. Eng. Technol.* 31: 1246–1260.

116 Hwang, K.S., Kim, B.C., and Kim, Y.H. (2011). Design and control of a fully thermally coupled distillation column modified from a conventional system. *Chem. Eng. Technol.* 34: 273–281.

117 Madenoor Ramapriya, G., Tawarmalani, M., and Agrawal, R. (2014). Thermal coupling links to liquid-only transfer streams: a path for new dividing wall columns. *AICHE J.* 60: 2949–2961.

118 Dwivedi, D., Strandberg, J.P., Halvorsen, I.J. et al. (2012). Active vapor split control for dividing-wall columns. *Ind. Eng. Chem. Res.* 51: 15176–15183.

119 Kang, K.J., Harvianto, G.R., and Lee, M. (2017). Hydraulic driven active vapor distributor for enhancing operability of a dividing wall column. *Ind. Eng. Chem. Res.* 56: 6493–6498.

120 Harvianto, G.R., Kim, K.H., Kang, K.J., and Lee, M. (2019). Optimal operation of a dividing wall column using an enhanced active vapor distributor. *Chem. Eng. Res. Des.* 144: 512–519.

121 Waltermann, T., Sibbing, S., and Skiborowski, M. (2019). Optimization-based design of dividing wall columns with extended and multiple dividing walls for three- and four-product separations. *Chem. Eng. Process. Process Intensif.* 146: 107688. https://www.sciencedirect.com/science/article/pii/S0255270119310712.

122 Ehlers, C., Schröder, M., and Fieg, G. (2015). Influence of heat transfer across the wall of dividing wall columns on energy demand. *AICHE J.* 61: 1648–1662.

123 Asprion, N. and Kaibel, G. (2010). Dividing wall columns: fundamentals and recent advances. *Chem. Eng. Process. Process Intensif.* 49: 139–146.

124 Ge, X., Liu, B., Yuan, X., and Liu, B. (2017). Simplifying and synthesizing practical four-product dividing wall column configurations. *Chem. Eng. Res. Des.* 125: 433–448.

125 Ränger, L.-M., Preißinger, U., and Grützner, T. (2019). Multiple dividing-wall columns - current status and future prospects. *Chemie Ingenieur Technik* 91: 420–428.

126 Kaibel, G., Miller, C., Stroezl, M. et al. (2004). Industrieller Einsatz von Trennwandkolonnen und thermisch gekoppelten Destillationskolonnen. *Chem. Ing. Techn.* 76: 258–263.

127 Halvorsen, I.J., Dejanović, I., Skogestad, S., and Olujić, Ž. (2013). Internal configurations for a multi-product dividing wall column. *Chem. Eng. Res. Des.* 91: 1954–1965.

128 Dejanović, I., Matijašević, L., Halvorsen, I.J. et al. (2011). Designing four-product dividing wall columns for separation of a multicomponent aromatics mixture. *Chem. Eng. Res. Des.* 89: 1155–1167.

129 Ling, H., Qiu, J., Hua, T., and Wang, Z. (2018). Remixing analysis of four-product dividing-wall columns. *Chem. Eng. Technol.* 41: 1359–1367.

130 Kiss, A.A., Luo, H., and Bildea, C.S. (2015). Energy efficient bioethanol purification by heat pump assisted extractive distillation. *Comput. Aided Chem. Eng.* 37.

131 Luo, H., Bildea, C.S., and Kiss, A.A. (2015). Novel heat-pump-assisted extractive distillation for bioethanol purification. *Ind. Eng. Chem. Res.* 54: 2208–2213.

132 Agrawal, R. (2000). Multieffect distillation for thermally coupled configurations. *AICHE J.* 46: 2211–2224.

133 Luyben, W.L. (2017). Improved plantwide control structure for extractive divided-wall columns with vapor recompression. *Chem. Eng. Res. Des.* 123: 152–164.

134 Skiborowski, M. (2020). Energy efficient distillation by combination of thermal coupling and heat integration. In: *Computer Aided Chemical Engineering 30 European Symposium on Computer Aided Process Engineering* (eds. S. Pierucci, F. Manenti, G.L. Bozzano and D. Manca), 991–996. Elsevier.

135 Barnicki, S.D. and Fair, J.R. (1990). Separation system synthesis: a knowledge-based approach. 1. Liquid mixture separations. *Ind. Eng. Chem. Res.* 29: 421–432.

136 Franke, M., Górak, A., and Strube, J. (2004). Design and optimization of hybrid separation processes. *Chem. Ing. Techn.* 76: 199–210.

137 Ng, L.Y., Chong, F.K., and Chemmangattuvalappil, N.G. (2015). Challenges and opportunities in computer-aided molecular design. *Comput. Chem. Eng.* 81: 115–129.

138 Kossack, S., Kraemer, K., Gani, R., and Marquardt, W. (2008). A systematic synthesis framework for extractive distillation processes. *Chem. Eng. Res. Des.* 86: 781–792.

139 Sattler, K. and Feindt, H.J. (1995). *Thermal Separation Processes: Principles and Design*. Weinheim, New York: VCH.

140 Anastas, P. and Zimmerman, J. (2003). Through the 12 principles of green engineering. *Environ. Sci. Technol.* 37: 94–101.

141 Gertig, C., Leonhard, K., and Bardow, A. (2020). Computer-aided molecular and processes design based on quantum chemistry: current status and future prospects. *Curr. Opin. Chem. Eng.* 27: 89–97.

142 Zhou, T., McBride, K., Linke, S. et al. (2020). Computer-aided solvent selection and design for efficient chemical processes. *Curr. Opin. Chem. Eng.* 27: 35–44.

143 Harper, P.M. and Gani, R. (2000). A multi-step and multi-level approach for computer aided molecular design. *Comput. Chem. Eng.* 24: 677–683.

144 Karunanithi, A.T., Achenie, L.E.K., and Gani, R. (2005). A new decomposition-based computer-aided molecular/mixture design methodology for the design of optimal solvents and solvent mixtures. *Ind. Eng. Chem. Res.* 44: 4785–4797.

145 Austin, N.D., Sahinidis, N.V., and Trahan, D.W. (2016). Computer-aided molecular design: an introduction and review of tools, applications, and solution techniques. *Chem. Eng. Res. Des.* 116: 2–26.

146 Scheffczyk, J., Schäfer, P., Fleitmann, L. et al. (2018). COSMO-CAMPD: a framework for integrated design of molecules and processes based on COSMO-RS. *Mol. Syst. Des. Eng.* 3: 645–657.

147 Scheffczyk, J., Redepenning, C., Jens, C.M. et al. (2016). Massive, automated solvent screening for minimum energy demand in hybrid extraction–distillation using COSMO-RS. *Chem. Eng. Res. Des.* 115: 433–442.

148 Zhou, T., Song, Z., Zhang, X. et al. (2019). Optimal solvent design for extractive distillation processes: a multiobjective optimization-based hierarchical framework. *Ind. Eng. Chem. Res.* 58 (15): 5777–5786.

149 Kruber, K.F., Scheffczyk, J., Leonhard, K. et al. (2018). A hierarchical approach for solvent selection based on successive model refinement. In: *28th European Symposium on Computer Aided Process Engineering* (eds. A. Friedl, J.J. Klemeš, S. Radl, et al.), 325–330. Amsterdam: Elsevier.

150 Papadopoulos, A.I. and Linke, P. (2006). Efficient integration of optimal solvent and process design using molecular clustering. *Chem. Eng. Sci.* 61: 6316–6336.

151 Papadopoulos, A.I., Tsivintzelis, I., Linke, P., and Seferlis, P. (2018). Computer-aided molecular design: fundamentals, methods, and applications. In: *Reference Module in Chemistry, Molecular Sciences and Chemical Engineering*. Elsevier https://www.sciencedirect.com/science/article/pii/B9780124095472143422?via%3Dihub.

152 Gerbaud, V., Rodriguez-Donis, I., Hegely, L. et al. (2019). Review of extractive distillation. Process design, operation, optimization and control. *Chem. Eng. Res. Des.* 141: 229–271.

153 You, X., Rodriguez-Donis, I., and Gerbaud, V. (2016). Low pressure design for reducing energy cost of extractive distillation for separating diisopropyl ether and isopropyl alcohol. *Chem. Eng. Res. Des.* 109: 540–552.

154 Lei, Z., Dai, C., Zhu, J., and Chen, B. (2014). Extractive distillation with ionic liquids: a review. *AICHE J.* 60: 3312–3329.

155 Laroche, L., Bekiaris, N., Andersen, H.W., and Morari, M. (1992). The curious behavior of homogeneous azeotropic distillation - implications for entrainer selection. *AICHE J.* 38: 1309–1328.

156 Gerbaud, V. and Rodriguez-Donis, I. (2014). Extractive distillation. In: *Distillation: Equipment and Processes* (eds. A. Górak and Ž. Olujić), 201–245. Academic Press Inc.

157 Gerbaud, V. and Rodriguez-Donis, I. (2019). Advances in extractive distillation. In: *Reference Module in Chemistry, Molecular Sciences and Chemical Engineering*. Elsevier https://www.sciencedirect.com/science/article/pii/B9780124095472143422?via%3Dihub.

158 Petlyuk, F., Danilov, R., and Burger, J. (2015). A novel method for the search and identification of feasible splits of extractive distillations in ternary mixtures. *Chem. Eng. Res. Des.* 99: 132–148.

159 Brüggemann, S. and Marquardt, W. (2004). Shortcut methods for nonideal multicomponent distillation: 3. Extractive distillation columns. *AICHE J.* 50: 1129–1149.

160 Blass, E. (1997). *Entwicklung verfahrenstechnischer Prozesse*. Berlin: Springer.

161 Lei, Z.G., Li, C.Y., and Chen, B.H. (2003). Extractive distillation: a review. *Sep. Purif. Rev.* 32: 121–213.

162 Perry, H.R. and Green, D.W. (eds.) (1997). *Perry's Chemical Engineers' Handbook*. McGraw-Hill.

163 Luyben, W.L. and Chien, I.-L. (2010). *Design and Control of Distillation Systems for Separating Azeotropes*. Hoboken, N.J.: John Wiley.

164 Waltermann, T., Grueters, T., Muenchrath, D., and Skiborowski, M. (2020). Efficient optimization-based design of energy-integrated azeotropic distillation processes. *Comput. Chem. Eng.* 133: 106676.

165 Kruber, K.F., Grüters, T., and Skiborowski, M. (2021). Advanced hybrid optimization methods for the design of complex separation processes. *Comput. Chem. Eng.* 147: 107257.

166 Ciric, A.R. and Gu, D. (1994). Synthesis of nonequilibrium reactive distillation processes by MINLP optimization. *AICHE J.* 40: 1479–1487.

167 Urdaneta, R.Y., Bausa, J., Brüggemann, S., and Marquardt, W. (2002). Analysis and conceptual design of ternary heterogeneous azeotropic distillation processes. *Ind. Eng. Chem. Res.* 41: 3849–3866.

168 Wasylkiewicz, S.K., Kobylka, L.C., and Castillo, F.J.L. (2003). Synthesis and design of heterogeneous separation systems with recycle streams. *Chem. Eng. J.* 92: 201–208.

169 Skiborowski, M., Harwardt, A., and Marquardt, W. (2015). Efficient optimization-based design for the separation of heterogeneous azeotropic mixtures. *Comput. Chem. Eng.* 72: 34–51.

170 Kovach, J.W. and Seider, W.D. (1987). Heterogeneous azeotropic distillation: experimental and simulation results. *AICHE J.* 33: 1300–1314.

171 Widagdo, S. and Seider, W.D. (1996). Azeotropic distillation. *AICHE J.* 42: 96–130.

172 Brüggemann, S., Oldenburg, J., and Marquardt, W. (2004). Combining conceptual and detailed methods for batch distillation process design. *Sixth International Conference on Foundations of Computer-Aided Process Design*, Princeton University, New Jersey (11–16 July 2004).

173 Cairns, B.P. and Furzer, I.A. (1990). Multicomponent three-phase azeotropic distillation. 3. Modern thermodynamic models and multiple solutions. *Ind. Eng. Chem. Res.* 29: 1383–1395.

174 Doherty, M.F. and Malone, M.F. (2001). *Conceptual Design of Distillation Systems*. Boston: McGraw-Hill.

175 Baker, L.E., Pierce, A.C., and Luks, K.D. (1982). Gibbs energy analysis of phase equilibria. *Soc. Pet. Eng. J.* 22: 731–742.

176 McDonald, C.M. and Floudas, C.A. (1995). Global optimization for the phase-stability problem. *AICHE J.* 41: 1798–1814.

177 Bausa, J. and Marquardt, W. (2000). Quick and reliable phase stability test in VLLE flash calculations by homotopy continuation. *Comput. Chem. Eng.* 24: 2447–2456.

178 Steyer, F., Flockerzi, D., and Sundmacher, K. (2005). Equilibrium and rate-based approaches to liquid-liquid phase splitting calculations. *Comput. Chem. Eng.* 30: 277–284.

179 Young, S. (1902). The preparation of absolute alcohol from strong spirit. *J. Chem. Soc. Trans.* 81: 707–717.

180 Frolkova, A.K. and Raeva, V.M. (2010). Bioethanol dehydration: state of the art. *Theor. Found. Chem. Eng.* 44: 545–556.

181 Furzer, I.A. (1994). Synthesis of entrainers in heteroazeotropic distillation systems. *Can. J. Chem. Eng.* 72: 358–364.

182 Müller, D. and Marquardt, W. (1997). Experimental verification of multiple steady states in heterogeneous azeotropic distillation. *Ind. Eng. Chem. Res.* 36: 5410–5418.

183 Kruber, K.F. and Skiborowski, M. Automatisierte Initialisierung und Optimierung von Heteroazeotrop-Rektifikationsprozessen, Dechema - Jahrestreffen der ProcessNet-Fachgruppen Fluidverfahrenstechnik und Membrantechnik, Potsdam. 28 March 2019.

184 Wu, Y.C., Lee, H.-Y., Huang, H.-P., and Chien, I.-L. (2014). Energy-saving dividing-wall column design and control for heterogeneous azeotropic distillation systems. *Ind. Eng. Chem. Res.* 53: 1537–1552.

185 Wu, Y.C., Hsu, P.H.-C., and Chien, I.-L. (2013). Critical assessment of the energy-saving potential of an extractive dividing-wall column. *Ind. Eng. Chem. Res.* 52: 5384–5399.

186 Hatti-Kaul, R. (2010). Downstream processing in industrial biotechnology. In: *Industrial Biotechnology* (eds. W. Soetaert and E.J. Vandamme), 279–321. Weinheim, Germany: Wiley-VCH Verlag GmbH & Co. KGaA.

187 Sprakel, L.M.J. and Schuur, B. (2019). Solvent developments for liquid-liquid extraction of carboxylic acids in perspective. *Sep. Purif. Technol.* 211: 935–957.

188 Gmehling, J. and Schedemann, A. (2014). Selection of solvents or solvent mixtures for liquid–liquid extraction using predictive thermodynamic models or access to the dortmund data bank. *Ind. Eng. Chem. Res.* 53: 17794–17805.

189 Hampe, M. (1978). Liquid-liquid extraction: applications and choice of solvent. *Chem. Ing. Techn.* 50: 647.

190 Redepenning, C., Recker, S., and Marquardt, W. (2017). Pinch-based shortcut method for the conceptual design of isothermal extraction columns. *AICHE J.* 63: 1236–1245.

191 Bausa, J., Watzdorf, R.V., and Marquardt, W. (1998). Shortcut methods for nonideal multicomponent distillation: 1. Simple columns. *AICHE J.* 44: 2181–2198.

192 Schmalenberg, M., Frede, T.A., Mathias, C., and Kockmann, N. (2021). Efficient shortcut method for determining the process window in stirred-pulsed extraction columns. *Chemie Ingenieur Technik* 93: 466–472.

193 Kampwerth, J., Weber, B., Rußkamp, J. et al. (2020). Towards a holistic solvent screening: on the importance of fluid dynamics in a rate-based extraction model. *Chem. Eng. Sci.* 227: 115905.

194 Claypool, J.T. and Raman, D.R. (2013). Development and validation of a technoeconomic analysis tool for early-stage evaluation of bio-based chemical production processes. *Bioresour. Technol.* 150: 486–495.

195 Sattler, K. (2012). *Thermische Trennverfahren: Grundlagen, Auslegung, Apparate*, 3. rev.e. Weinheim [u.a.]: Wiley-VCH.

196 Binning, R.C. and James, F.E. (1958). Now separate by membrane permeation. *Pet. Refiner* 37 (5): 214–215.

197 Lipnizki, F., Field, R.W., and Ten, P.K. (1999). Pervaporation-based hybrid process: a review of process design, applications and economics. *J. Membr. Sci.* 153: 183–210.

198 Lipnizki, F. and Field, R.W. (2001). Pervaporation-based hybrid processes in treating phenolic wastewater: thecnical aspects and cost engineering. *Sep. Sci. Technol.* 36: 3311–3335.

199 Baker, R.W. (2004). *Membrane Technology and Applications*. Ltd, Chichester, UK: John Wiley & Sons.

200 Basile, A., Figoli, A., and Khayet, M. (2015). *Pervaporation, Vapour Permeation and Membrane Distillation: Principles and Applications*. Cambridge, UK, op.: Elsevier, Woodhead Publishing.

201 Micovic, J., Werth, K., and Lutze, P. (2014). Hybrid separations combining distillation and organic solvent nanofiltration for separation of wide boiling mixtures. *Chem. Eng. Res. Des.* 92 (11): 2131–2147.

202 Lutze, P. and Górak, A. (2013). Reactive and membrane-assisted distillation: recent developments and perspective. *Chem. Eng. Res. Des.* 91: 1978–1997.

203 Kreis, P. and Górak, A. (2006). Process analysis of hybrid separation processes. *Chem. Eng. Res. Des.* 84: 595–600.

204 Scharzec, B. and Skiborowski, M. (2018). Improved modeling of membrane separation in integrated hybrid processes. In: *28th European Symposium on Computer Aided Process Engineering* (eds. A. Friedl, J.J. Klemeš, S. Radl, et al.), 561–562. Amsterdam: Elsevier.

205 Del Pozo Gomez, M.T., Repke, J.-U., Kim, D.-y. et al. (2009). Reduction of energy consumption in the process industry using a heat-integrated hybrid distillation pervaporation process. *Ind. Eng. Chem. Res.* 48: 4484–4494.

206 Fu, C. and Gundersen, T. (2016). Heat and work integration: fundamental insights and applications to carbon dioxide capture processes. *Energy Convers. Manag.* 121: 36–48.

13

Recovery of Solvents and Fine Chemicals

Yus Donald Chaniago[1] *and Moonyong Lee*[2]

[1] *Ulsan National Institute of Science and Technology, Ulsan, South Korea*
[2] *Yeungnam University, Gyeongsan, South Korea*

13.1 Introduction

Solvents, and dissolution in general, have been an integral part of numerous industries for hundreds of years. As early as the fifteenth century, alchemists were already searching for solvents to aid dissolution processes. In particular, they sought to find the so-called universal menstruum, a universal solvent that possessed the power to remove all seeds of disease from the human body. Throughout the century, solvents have gained increasing attention, and nowadays, they encompass our lives. From the production of life-saving drugs to the manufacturing of coffee machines, solvents play a vital role in modern society. Particularly, in the chemical industry, solvents are necessary auxiliaries in processes, and most of the manufacturing methods require various kinds of solvents [1].

The word "solvent" originates from Latin. The verb "solvo" means to loosen or untie; this corresponds to the key property of solvents, which loosens the intermolecular bonds between the solute molecules, separating them from each other. The definition of solvents is a subject of debate. The International Union of Pure and Applied Chemistry nomenclature provides the following definition for solutions, solutes, and solvents: "[A solution is] a liquid or solid phase containing more than one substance when, for convenience, one (or more) substance, which is called the solvent, is treated differently from the other substances, which are called solutes." Solid solutions (e.g. alloys or plasticizer-containing polymers) are materials in which one compound (solute) is randomly incorporated into the crystal structure of another compound or in an amorphous solid (solvent). The *Oxford Dictionary* and *Encyclopedia Britannica* give a different, more straightforward definition, which narrows down the concept of solvents by excluding solids: "[A solvent is a] liquid in which other materials dissolve to form a solution." Ignoring the solids in the definition can be justified because the dissolution phenomenon always occurs in the liquid phase, except for one particular example: at room temperature and atmospheric pressure, solid palladium can absorb and dissolve hydrogen up to 900 times its volume. An ultimate definition

Sustainable Separation Engineering: Materials, Techniques and Process Development, Volume 2, First Edition. Edited by Gyorgy Szekely and Dan Zhao.
© 2022 John Wiley & Sons Ltd. Published 2022 by John Wiley & Sons Ltd.

can be worded for this chapter as follows: Solvents are substances present in a liquid form under the conditions of their applications and in which other substances can dissolve, and from which they can be recovered unchanged upon removal of the solvent. Many substances conform to this definition, practically all those that can be liquefied under given conditions. Subsequently, the definition is not very helpful unless the word "application" is stressed, implying that the solvents and solutions in them ought to be applicable for some purpose. The essential solvent of nature is water. Life is unimaginable without water, and it can be found almost everywhere on Earth. The human race has also used it as a solvent for many applications since the dawn of mankind. The present chapter will focus on organic solvents, which are extensively used in industrial production. The synthesis and production of organic solvents have been one of the biggest successes of early chemical science. Since the Second Industrial Revolution at the end of the 1800s, organic solvents have gained importance in various industrial processes. However, during the twentieth century, their adverse effects on health and the environment saw the light of day. In parallel with the increasing emphasis on sustainability and safety, organic solvents have become a concern [1].

The chemical industry is divided into branches, with fine chemicals acting as the smallest segment; its partners are commodities and chemicals. Commodity chemicals are mass-produced on a large scale to supply global markets. They consist of general compounds that are the same from supplier to supplier. Specialty chemicals are often sold as brand-name products and are marketed for their unique qualities and abilities to perform functions that other chemicals cannot. They consist of one or more fine chemicals.

Heavy chemicals are chemicals that are used extensively in industries, which are produced in vast quantities. Fine chemicals are chemicals produced in small quantities for specific purposes to a very high degree of purity. Fine chemicals are complex, single, pure chemical substances produced in limited quantities in multipurpose plants by multistep batch chemical or biotechnological processes. They are described by exacting specifications, used for further processing within the chemical industry, and sold for more than \$10/kg (see the comparison of fine chemicals, commodities, and specialties). The class of fine chemicals is subdivided based on the added value (building blocks, advanced intermediates, or active ingredients) or the type of business transaction, namely standard or exclusive products.

Fine chemicals are produced in limited volumes (<1000 tons/year) and at relatively high prices (>\$10/kg) according to exacting specifications, mainly by the traditional organic synthesis in multipurpose chemical plants. Biotechnical processes are gaining ground. The global production value is approximately \$85 billion. Fine chemicals are used as starting materials for specialty chemicals, particularly pharmaceuticals, biopharmaceuticals, and agrochemicals. Custom manufacturing for the life science industry plays a big role; however, a significant portion of the total production volume of fine chemicals is manufactured in-house by large users. The industry is fragmented and extends from small, privately owned companies to divisions of large, diversified chemical enterprises. The term "fine chemicals" is used in distinction to "heavy chemicals," which are produced and handled in large lots and are often in a crude state.

Producing fine chemicals is specialized. Because of this, fine chemistry cannot occur on a large-scale basis. Consequently, the prices of these materials tend to be high. Some

processes that sometimes produce fine chemicals are chemical synthesis, biotechnology, extraction, and hydrolysis.

1) Chemical Synthesis: Chemical synthesis uses one or more chemical reactions that change raw materials or other chemicals into a product or multiple products. Chemical synthesis has helped chemists learn the physical and biological properties of many compounds.
2) Biotechnology: Biotechnology is the field of using organisms or their life processes to create technologies that make our health and world better. There are three areas of biotechnology. These are biocatalysts, biosynthesis, and cell culture technology.
3) Extraction: Extraction involves isolating and purifying products from animals and plants. Some of these products might be alkaloids, antibacterial, steroids, protein hormones, and polysaccharides. These are all useful in making pharmaceuticals, foods, and cosmetics.
4) Hydrolysis: Hydrolysis is a chemical process that uses water to break a chemical compound bond. It is used to produce fine chemicals to break down proteins into amino acids using heat as a catalyst.

Once fine chemicals are isolated from or synthesized using other materials, these genuine, high-quality products can be used in many different industries. They can be combined with other substances to form the ingredients of specialty chemicals. They may end up becoming food flavors, agricultural insecticides, resins, liquid crystals for TVs, and more. However, the most prevalent function of fine chemicals is as active pharmaceutical ingredients (API); that is, they make medicines effective.

The products that are obtained from the synthesis of fine chemicals are classified by the way they are sold. They may belong to either the exclusive category or the standard category. Exclusive fine chemicals are custom-manufactured for a proprietary product. Companies that commission these exclusive products are sometimes the only ones who know precisely how they are used. These tend to be the most expensive and limited in production.

Common examples of fine chemicals are ethylene, propylene, methanol, benzene, toluene, xylenes, phthalic anhydride, poly(vinyl chloride) soda, and sulfuric acid, propylene glycol methyl ether (PGME), and propylene glycol methyl ether acetate (PGMEA).

13.2 Challenge

Continuous population growth, economic development, and accelerated industrial advancements have led to increased energy demands and costs, and the need to employ efficient, sustainable processes is growing with the need to comply with stricter environmental regulations [2–8]. One of the challenges faced by the manufacturing industry is to enhance fabrication output, while reducing the production footprint related to energy expense, environmental pollution, and social issues [9]. The chemical industry is predicted to grow rapidly until 2030 [10], and solvents have already been an integral part of various industries for hundreds of years [1]. However, inefficient processes and poor solvent selection have led to concerns over environmental pollutant emissions and health and safety issues [11]. The

United States Environmental Protection Agency (US EPA) has projected that the growth of the chemical market could lead to solvent emissions equivalent to 10 million metric tons of CO_2. This quantity of chemical emissions accounted for up to 62% of the total emissions in 2017, and was consequentially associated with an increase in global warming potential (GWP) [11]. The industries identified as significant sources of chemical waste are fine chemicals [12], pharmaceuticals [12], and semiconductors [13, 14]. For example, the raw materials required to produce APIs can be up to 80–90% solvent by mass [15, 16], with typical recovery efficiencies of 50–80% [17]. Furthermore, due to purity concerns, solvents are often disposed of after one process cycle, impacting process sustainability [15, 16, 18, 19].

Many industrial processes are now being inspected to address the sustainability issue associated with solvent consumption [19–22]. The amount of waste produced in industrial processes is represented by the E-factor: a higher E-factor means more waste (water is generally excluded); therefore, a more significant environmental footprint. Ideally, the E-factor should be zero [23]. The oil refining industry (E-factor < 0.1), bulk chemicals industry (E-factor < 1–5), and fine chemical or pharmaceutical sectors (E-factor 25–100) [24, 25], are some notable examples.

In the semiconductor industry, large quantities of various solvents are utilized in processing [13] and significant quantities of waste solvents are generated [14]. Poor waste treatment is a critical issue because numerous waste solvents discharged from the process are incinerated at high temperatures [26]. Incineration of waste provides a last-resort option for environmentally acceptable disposal; however, it can discharge acidic gases and other highly persistent environmental pollutants into the atmosphere [27–29], resulting in detrimental effects on human health through respiratory exposure and food chain contamination [30]. In addition to the fact that incineration methods require sophisticated facilities [31], they are recognized alongside other solvent disposal methods to contribute negatively toward the emission footprint, producing nearly 6.7 kg CO_2 equivalent of organic carbon [11]. The options for waste discharge treatment largely depend on the environmental impact of the original solvent production. Waste incineration may be the best option if the impact is low; however, if the impact is high, solvent recovery (SR) is usually the best choice [32]. Another major concern is the economic considerations of solvent treatment on process competitiveness [33–35]. If the waste solvent is a fine chemical, or to reduce the production cost, a SR option may be preferable [36].

13.3 Waste Minimization and Solvent Recovery

The general objectives of green chemistry and engineering are to minimize the usage and production of hazardous materials, use renewable sources, promote sustainability, reduce energy consumption, and maximize process efficiency, all without sacrificing economic viability [20, 37]. Reducing the quantity of harmful organic solvents escaping into the environment can be attained by redesigning the process or product to eliminate the use of organic solvents, economically recapture and recycling at process sites, and carefully selecting solvents or their mixtures [31]. The most effective ways to reduce waste output involve solvent mitigation in chemical reactions and performing separation under neat conditions (no solvent). In both cases, reducing inputs makes processes more efficient [1, 38, 39]. One

example of such sustainable processes can be found in the production of propylene glycol monomethyl ether acetate (PGMEA), a solvent commonly used in the production of semiconductors [8]. The factors include the use of renewable sources, waste mitigation, less toxic reactants with a reduction in reactant usage, solvent-free separation, reduced CO_2 emissions, and minimized energy and cost. However, the processes used in the pharmaceutical industry to produce APIs, and semiconductor industries that require solvents or thinners (fine chemicals) for photoresist (PR) cleaning, heavily rely on solvents, making the production of waste solvents inevitable. In ideal engineering practice, chemical processes are designed with an emphasis on recovering and reusing waste solvents [40]. The recovery process is very important for achieving sustainability and environmental impact mitigation. Accordingly, it is an urgent environmental and economic concern for industrial manufacturers to retrieve processed chemicals and minimize chemical waste discharge [13]; thus, large quantities of solvents and fine chemicals must be recovered. SR, based on life cycle and environmental analysis, is capable of reducing CO_2 emissions, minimizing energy usage, and reducing the transport and disposal cost of wasted chemicals [9]. Multiple processes for SR or solvent recycling have been attempted in recent years.

In the chemical and petrochemical industries, the methods used for the separation of methanol, ketone-group solvents, cresol, and *N*-methyl-2-pyrrolidone (NMP) [9] include adsorption methods [1, 41], distillation [42–45], PV membranes [46–48], nanocomposite membranes [49], and crystallization [50].

In the pharmaceutical sector, some recovery methods have been applied, mostly based on distillation, such as distillation methods [51] and advanced and hybrid distillation [52–57], as well as other methods such as liquid–liquid extraction [58], PV membranes [59, 60], and nano-filtration membranes [61]. The SR approach in pharmaceutical manufacturing integrates a continuous end-to-end process to overcome the disadvantages of the traditional batch process [62]. The integrated process consists of dissolution and clarification (DC) of the raw material with a SR process, reactive crystallization (RC) of the pre-reaction mixture from DC, filtration, and resuspension of slurry from RC with SR following drying and separation, and extrusion-molding-coating. A process control system controls the entire process. The recovered solvent purities for integrated continuous manufacturing (ICM) in the pharmaceutical industry are > 99.9 wt% for the first solvent (solvent 1) and > 99.8 wt% for the second solvent (solvent 2); the recovery yields were 94.9 and 98.3%, respectively. From the E-factor analysis, approximately 30% less waste was generated in the ICM process than the corresponding batch process. After integrating the SR system, the E-factors for both the batch and ICM processes decreased significantly, from 1.63 to 0.29 and from 0.77 to 0.21, respectively.

The semiconductor sector utilizes the recovery of isopropyl alcohol (IPA), hydrochlorofluorocarbons, PGMEA, N-methylpyrrolidone (NMP), perfluorocarbons, and dimethyl sulfoxide. The most suitable methods are adsorption [63–65], advanced distillation [2, 3, 13, 36], and the use of gas permeation membranes [66, 67] and PV membranes [68]. Other processes that emphasize SR include SR from vegetable oil by polydimethylsiloxane [69–71], ionic liquid recovery by a flash drum in biogas upgrading [72] and SR of NMP in Li-ion battery manufacturing by adsorption and distillation [73].

A recent approach implements switchable solvents with on-demand and reversible switching of their physiochemical properties triggered by carbon dioxide (CO_2) [74]. The

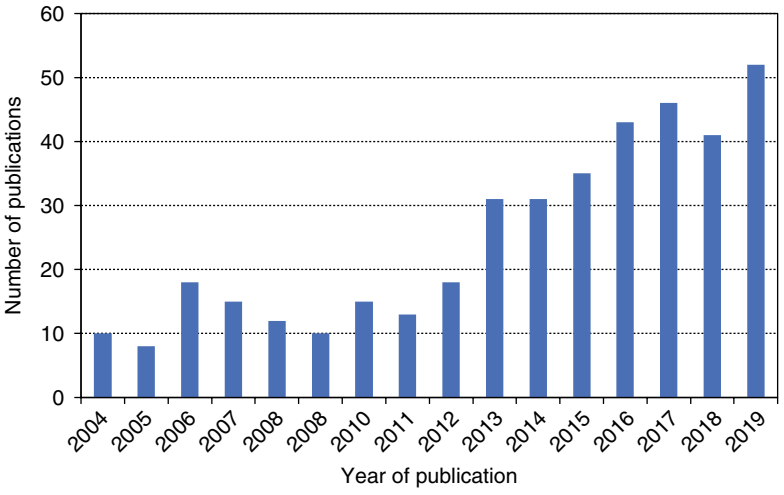

Figure 13.1 Number of articles per year with the keywords "solvent recovery" from 2004 to 2019. The data were obtained from Web of Science™. https://www.webofknowledge.com.

utilization and widespread implementation of switchable solvents can dramatically reduce environmental risks and energy requirements for solvent removal and recovery processes.

The SR process is of utmost importance; the number of articles on SR has increased dramatically, as shown in Figure 13.1.

13.4 Distillation Process for Recovery of Solvent and Fine Chemicals

Sustainability is of considerable importance in the semiconductor industry because of economic and environmental factors because valuable chemicals are discharged during manufacturing [75]. The recovery of discharged solvents from the production processes offers waste elimination and reduced chemical cost, and is an important consideration for the overall efficiency and profitability of plants. SR by distillation is a common method for the reduction of solvent waste [76].

In the distillation process, the feasibility split is an important factor. For ideal or non-azeotropic solutions, feasibility is not an issue, as the volatility order is a solid indicator. A greater difference in the relative volatility from unity indicates easier separation. The number of distillation columns in the sequence for sharp splitting can be easily determined as the number N of components in the mixture minus 1 (i.e. N−1) [3]. For batch distillation, the process is used extensively in laboratory separations and the production of fine and specialty chemicals, pharmaceuticals, polymers, and biochemical products either for purification purposes or for the recovery of valuable solvents. When a mixture exhibits azeotrope, advanced distillation is required, for example, pressure swing distillation (PSD), azeotropic distillation (AD), and extractive distillation (ED). Azeotropic distillation is

defined as "distillation that involves components that form azeotropes." Many industrially relevant liquid mixtures are strongly nonideal and exhibit azeotropic behavior. This behavior has a tremendous influence on distillation process design since the composition space is divided into regions with different volatility orders of the components. Another method to separate azeotropes is ED, which utilizes an additional solvent or entrainer. The solvent used in ED increases the relative volatility of the azeotrope mixture; thus, the mixture can be separated by a simple distillation column. The feasibility of ED depends on the entrainer flow rate (or the ratio of both feed streams) and the reflux ratio. ED is only feasible above a minimum entrainer flow rate for a given reflux ratio limited by minimum and maximum reflux ratios.

13.4.1 Reclamation of Valuable Components from Waste Solvents in the Semiconductor Industry

To investigate a feasible distillation method for SR, waste PR strippers were collected for six months from a real industrial thin flat transistor liquid-crystal display (TFT-LCD) stripping process [36]. The composition of the waste PR stripper was analyzed using a flame ionization detector (FID), gas chromatograph (GC) (Younglin Scientific Co., Model Acme 600; column HP-5), Coulometric Karl Fischer titrator (GRS Instruments, Model GRS 2000) for moisture content, an inductively coupled plasma mass spectrometer (ICP-MS) (Perkin-Elmer, Model Elan 9000), and a colorimeter (Nippon Denshouku Industris Co., OME-2000) based on the ASTM D 1209–69 method for color scale. Following are the GC-operating conditions: initial temperature = 80 °C (retention time 0 minute), and heating rate = 10 °C/min from 80 to 200 °C. Analysis using GC and Karl Fischer titration revealed that high boiling point solvents (HBS), such as methyl diglycol (MDG) and 1-(2-hydroxyethyl)piperazine (HEP), comprised more than 50 wt% of the waste strippers. Low boiling point solvents (LBPS), including monoisopropanolamine (MIPA), IPA, N-methylformamide (NMF), and H_2O, were also major components. The analysis results' composition of IPA, H_2O, MIPA, MDG, NMF, and HEP are 3, 12, 12, 33, 15, and 21 weight (wt)%, respectively. The results indicate that the retrieved solvent met all requirements for commercial use. The experimental results of HBS through distillation confirmed the feasibility of waste SR, with HEP and MDP purity $\geq$ 98 wt%, water content $\leq$ 0.07 wt%, and IPA content $\leq$ 0.05.

After a feasibility result is obtained, the distillation sequence can be designed by following distillation design heuristics [77–79]. The nonrandom two-liquid model (NRTL) thermodynamic method was applied in this study. The universal quasichemical (UNIQUAC) functional-group activity coefficient (UNIFAC) method was used to approximate the missing parameters of the NTRL system. For the preliminary design of the distillation system, the shortcut column method was applied in Aspen HYSYS V7.3 [36], with a reflux ratio specification equivalent set to 1.1 of minimum reflux. The most rigorous distillation design among the feasible designs using the heuristic, when considering the overall feasible design performance criteria, such as high-purity main target product (MDG and HEP), lowest total reboiler duty, and lowest estimated capital and operating cost, was the proposed design shown in Figure 13.2.

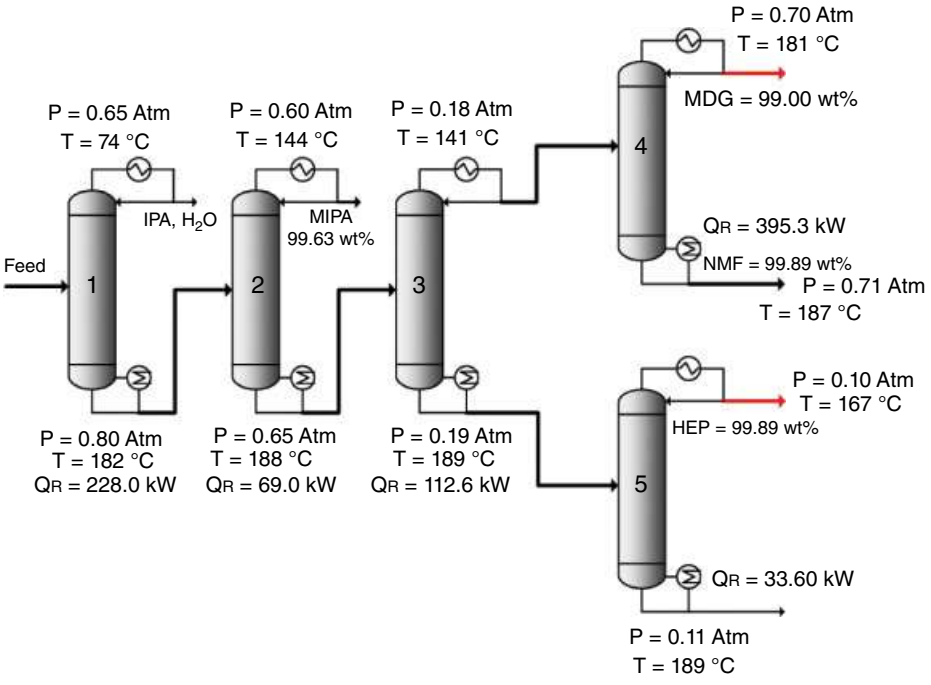

Figure 13.2 Modified direct distillation sequence of waste SR, where P is pressure, T is temperature, and Q is reboiler duty. An overall comparison of the preliminary study results shows that a modified direct distillation sequence is recommended. *Taken from* [13].

13.4.2 Advanced Design of Distillation for Waste Solvent Recovery

The recommended design from Section 13.5.1, as shown in Figure 13.8, was chosen as the basis of further study. Since maximizing the efficiency of design is a green engineering principle [37], the design was rigorously optimized to obtain detailed optimal conditions [13]. The objective function of optimization is that of a column reboiler, which can be formulated as follows:

$$\text{Min}\left(Q\right) = f\left(R, P_c, T_F, N_F, N_T\right), \tag{13.1}$$

where R is the reflux ratio, P_c is the pressure of the column (atm), T_F is the temperature of the feed (°C), N_F is the feed stage location, and N_T is the number of column stages. All five variables were only applied to the first column because the T_F variable for the subsequent column was defined by variables from the previous column. Therefore, for the columns that followed, only four variables were adjusted: R, P_c, N_F, and N_T. To optimize all sequences of the conventional columns, the Box method [80] was applied because of accessibility in Aspen HYSYS V7.3. The overall constraints of optimization for conventional distillation are presented in Table 13.1.

After the optimal conditions were obtained, some columns were intensified by thermally coupled distillation (TCD) [78, 81–83]. This intensified configuration contributes to potential energy saving compared to conventional direct sequences [84–87]. Intensifying columns 3 and 5 through TCD achieved nearly 15% energy saving compared to the same

Table 13.1 Overall constraints for optimization of conventional distillation (top pressure < bottom pressure).

Column 1	Column 2	Column 3	Column 4	Column 5
Top temperature < 80 °C	Mass Frac MIPA > 98.9%	Bottom temperature < 188.9 °C	Mass Frac MDG > 98.9%	Mass Frac HEP > 98.9%
Bottom temperature < 188.9 °C	Bottom temperature < 188.9 °C		Mass Frac NMF > 98.9%	Bottom temperature < 188.9 °C
H_2O mass flow Top > 118 kg/h			Bottom temperature < 188.9 °C	

Taken from [13].

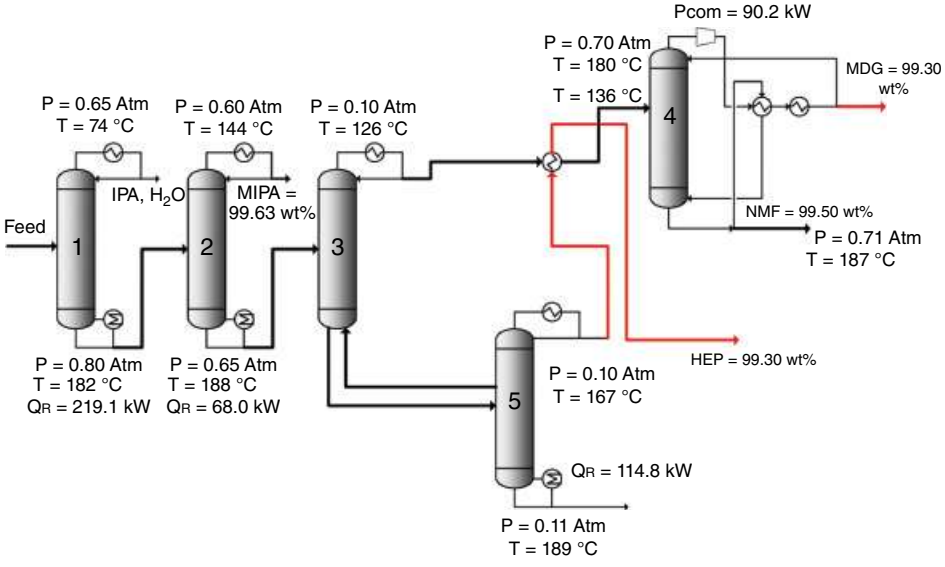

Figure 13.3 Recommended design, improved by heat integration and heat pump-assisted distillation. *Taken from* [13].

columns in the optimal conventional sequence. After the columns were intensified, the TCD was optimized using the response surface method [88]. After optimization, the energy-saving improved by 7% compared to the nonoptimal TCD 3–5 of the previously proposed design. Maximizing the process efficiency is one of the green engineering practices [37], and can be achieved by heat integration [37] and heat pump-assisted distillation [89]. The final recommended distillation configuration deployed TCD (columns 3 and 5), heat integration (the red line from the top of column 5), and heat pump-assisted distillation (column 4), as shown in Figure 13.3. The final configuration of distillation achieved a significant energy saving of 40.5% compared to that of the conventional column case.

13.4.3 Dividing Wall Column Azeotropic Distillation for Waste Azeotropic Mixture Separation

The semiconductor industry uses water and a wide range of toxic and hazardous organic and inorganic chemicals in large quantities. Therefore, this industry suffers from serious environmental impact issues. To solve the waste disposal problem, recovery and reuse of valuable chemicals and water are a favorable option, but the requirement for high purity of chemicals and water means there is a need to reprocess the recovered chemicals [90]. Waste valuable chemical recovery is an attractive option. However, the recovery process becomes more complex and challenging when components with close boiling points or azeotropes exist in the waste mixture [2]. During the manufacturing of display and semiconductor materials, a PR thinner consisting of a fine chemical, such as propylene glycol monomethyl ether (PGME) and PGMEA, is discharged alongside water as waste [2]. The waste PR thinner is generally recovered by distillation. However, PGME and PGMEA, as the target constituents, form azeotropes with water in the waste thinners, hindering the efficient recovery of the target constituents due to the inability of conventional distillation processes to attain the required purity and recover beyond the azeotropic composition [2]. Ternary mixtures of PGME, PGMEA, and water exhibit a distillation boundary (line B), two binary homogeneous azeotropes (PGME + water and PGMEA + water), and one heterogeneous azeotrope represented by the area bounded by the blue line, as shown in Figure 13.4. The direct

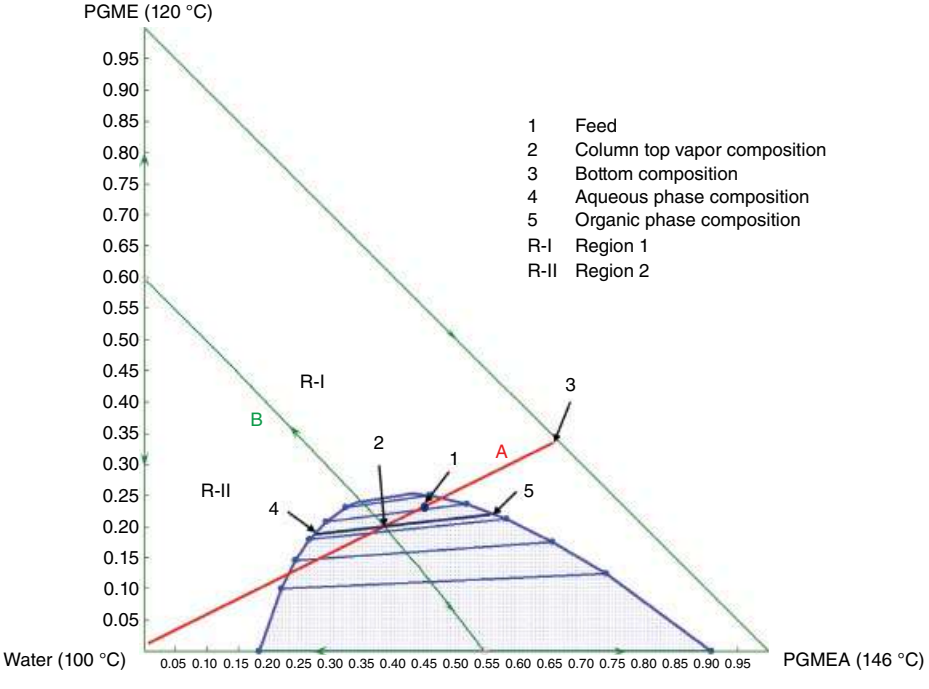

Figure 13.4 Ternary map with direct sequence line for water + PGME + PGMEA in mass fraction at 1 atm. *Taken from* [2].

Table 13.2 Binary interaction parameters of UNIQUAC-HOC used in simulation.

	UNIQUAC-HOC		
System	***bij***	***bji***	**AAD**
PGMEA + water	−494.3	59.1223	0.0185
Water + PGME	241.841	−492.419	0.0027
PGME + PGMEA	66.5676	−103.641	0.0053

Taken from [2].

sequence line (line A) represents the initial design configuration of a direct sequence of distillation.

To rigorously simulate every candidate for distillation configuration, Aspen Plus V8.6 was used with the UNIQUAC activity-coefficient models and the Hayden and O'Connell (HOC) [91] second virial coefficient model. The binary interaction parameters [2] are presented in Table 13.2.

Four distillation process candidates were investigated: conventional (base case), and heterogeneous azeotropic-dividing wall column (HA-DWC) with thermal integration (TI) for each case. The complete proposed process is shown in Figure 13.5. Table 13.3 presents the results of the energy and economic performance analysis.

The final design, by applying a combination of HA-DWC and TI, greatly reduced the total reboiler duty and TAC by 33.1 and 27.2%, respectively. The proposed HA-DWC with TI method is expected to provide an attractive option for improving waste recovery efficiency in the manufacturing of display and semiconductor materials.

13.4.4 Waste Solvent Recovery Process Design from Complex Quaternary Azeotropic Mixtures

A waste solvent consisting of an azeotropic mixture requires an advanced method for separating the constituents. In the case of ternary, or more complex quaternary azeotropic mixtures, distillation requires a complex method and numerous sequences to obtain the target constituents [92–96]. A novel computationally efficient method was developed through a residue curve map and exploiting the Fenske–Underwood–Gilliland (FUG) method, a well-known shortcut method for estimating the minimum number of stages and minimum reflux ratio for quaternary azeotropic mixtures [3]. The FUG method is widely used as a shortcut for column design separating non-azeotropic mixtures because of its simplicity and efficiency as a practical solution that allows fast pattern screening from many solutions. Although the FUG method is less accurate than other complex, rigorous methods, it is capable of efficiently determining the feasible separation of an azeotropic mixture without a complex procedure, making it extremely computationally efficient [97].

A distillation design was investigated for the waste SR process of a quaternary solvent mixture from real industrial waste comprising methyl 2-hydroxybutyrate (HBM), PGMEA, ethyl lactate (EL), and ethyl-3-ethoxy propionate (EEP). Aspen Plus V9, with the NRTL

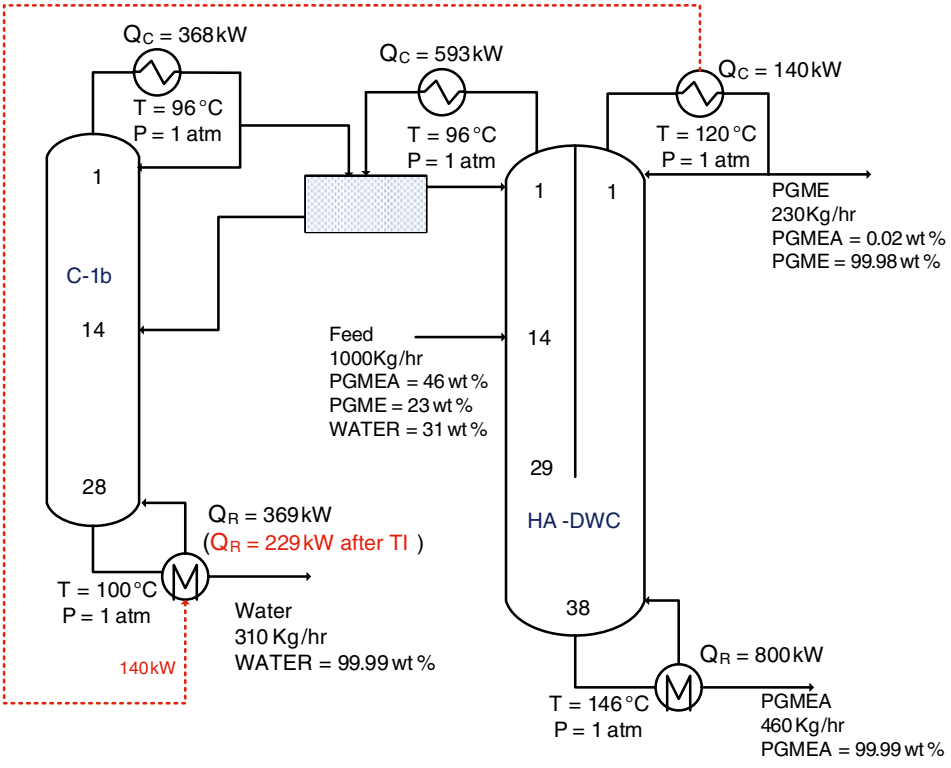

Figure 13.5 HA-DWC (with and without thermal integration). The red-dotted line corresponds to an energy transfer from a heat source. *Taken from* [2].

Table 13.3 Energy and economic performances of the process configurations studied.

	Conventional (base case)	Conventional (with TI)	HA-DWC	HA-DWC (with TI)
PGME (kg/h)	229.96	229.96	229.98	229.98
PGME (wt%)	99.98	99.98	99.98	99.98
PGMEA (kg/h)	459.96	459.96	459.97	459.97
PGMEA (wt%)	99.99	99.99	99.99	99.99
Total reb. duty (kW)	1539	1373	1169	1029
Energy saving (%)[a]	—	10.8	24.0	**33.1**
Capital cost (million US$)	1.204	1.204	0.972	0.972
Op. cost (million US$/yr)	1.399	1.253	1.128	1.005
TAC (million US$/yr)	1.579	1.433	1.273	1.149
TAC saving (%)[a]	—	9.3	19.4	**27.2**

[a] Compared with conventional direct sequence (base case).
TAC = Total Annual Cost.
Taken from [2].

activity coefficient model and HOC second virial coefficient model with association parameters, was used to predict mixture vapor-liquid equilibrium (VLE), create a graphical design approach, and simulate shortcut and rigorous columns of each distillation process. Initially, binary and ternary VLE data were investigated, binary azeotrope compositions at mass basis are HBM+PGMEA at 0.8403:0.1597 and 136.81 °C, PGMEA+ EL at 0.8455:0.1545 and 145.47 °C, and EL+EEP at 0.8002:0.1998 and 154.10 °C.

After the mixture behavior was understood, a feasible split to follow the first was determined by investigating the possibility of PSD or ED [3]. Binary azeotrope composition over pressure range, HBM+PGMEA, PGMEA+EL, and EL+EEP, show the azeotrope compositions are sensitive to pressure change, further relative volatility of HBM+PGMEA tends to increase with increasing EEP when EEP becomes a solvent for HBM+PGMEA mixture [3]. This explains PSD and ED methods are feasible.

The design objective was to produce a very high target composition of HBM, PGMEA, EL, and EEP: more than 99% by mass, 99.5% by mass, 99% by mass, and 99% by mass, respectively. Before the first component split investigation, all possible pairs of light key (LK)–heavy key (HK) were determined. The boiling point temperature is as follows: 1. HBM: (137 °C); 2. PGMEA (145 °C); 3. EL (154 °C); 4. EEP (168 °C). LK and HK represent the pair components with lower and higher boiling point temperatures, respectively. The heavier component is invalid as LK when paired with a lighter component. For example, in the HBM + PGMEA pair, HBM = LK and PGMEA = HK; in this case, PGMEA cannot be LK. There are six feasible first splits using the LK and HK pairs from the quaternary mixture. After the first splits were investigated, the next separation for each first split was projected using a feasible PSD and ED. The results show three route designs for waste SR while maintaining very high target product purity constraints. However, only one route is a simpler sequence compared to others as shown in Figure 13.6.

A shortcut column simulation was applied in Aspen Plus V9 for the initial design of the column sequence, PSD, and ED. However, the actual results of the distillation design's ability to recover valuable components from a quaternary azeotropic mixture may differ due to

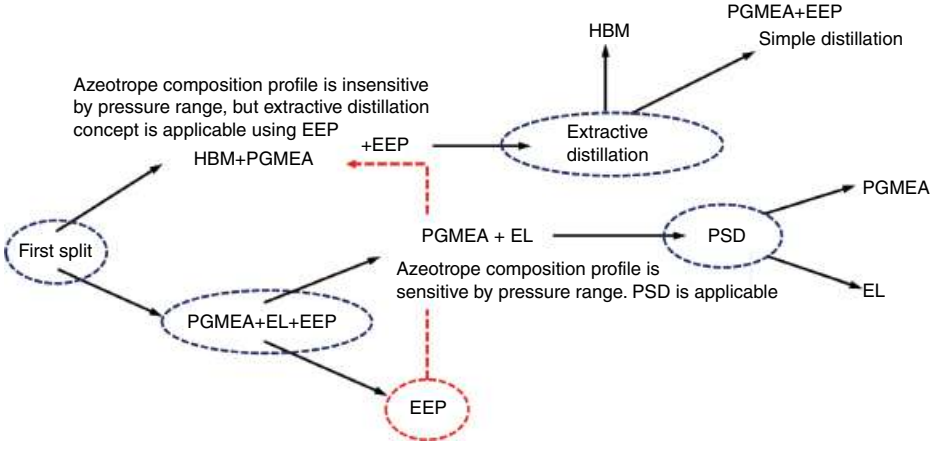

Figure 13.6 The simpler sequence for separation of quaternary mixture HBM+PGMEA+EL+EEP. *Taken from* [3].

certain design assumptions in the shortcut column approach. The complete simpler sequence is presented in Figure 13.7.

A simpler route was selected for further optimization, and the variables of optimization were the feed location, number of stages, and reflux ratio. Each column optimization, except for the last, was constrained by the product purity specification of the subsequent column due to consecutive influence in the system.

The results of optimization are listed in Table 13.4.

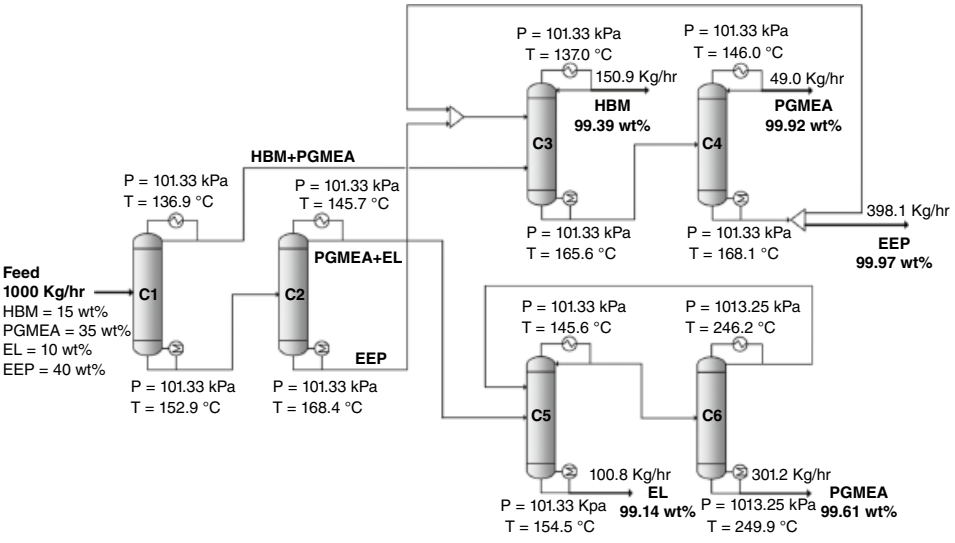

Figure 13.7 Complete sequence of rigorous columns of the simpler route. *Taken from* [3].

Table 13.4 Optimization result for a simpler route.

	C1	C2	C3	C4	C5	C6
Number of stages	62	69	70	45	53	59
Feed location	35	45	60	26	5	30
Solvent feed location			22			
Recycle location					16	
Reflux ratio (Mole)	10	3	6	20	5	7
Temperature (Top) °C	136.9	145.7	137	145.9	144.4	244.5
Temperature (Bottom) °C	152.9	168.1	165.5	168.1	154.5	250
Pressure (Top) kPa	101.33	101.33	101.33	101.33	101.33	1013.25
Pressure (Bottom) kPa	101.33	101.33	101.33	101.33	101.33	1013.25
Condenser duty (kWh)	202.5	142.2	99.9	86.6	529.7	369
Reboiler duty (kWh)	268.3	144	99.6	87	481.7	438.4

Taken from [3].

This novel approach successfully demonstrates a simpler method to design distillation columns to recover waste solvent from complex quaternary azeotropic mixtures. Despite the lower accuracy when using the shortcut method, this method offers efficient screening for feasible separation sequences because it easily identifies the separation feasibility of the two target compositions (LK and HK), owing to several assumptions compared to other more accurate methods. The combination of the shortcut method and graphical map method easily projected the available solutions into feasible complete sequences where all the target constituents of the distillation product are obtained. This novel efficient method is not only expected to be an attractive solution for designing complex waste SR processes in the display and semiconductor material-manufacturing industries, but also other processes that suffer from the issues involved with complex quaternary azeotropic mixtures.

13.4.5 Solvent Recovery in the Continuous Separation of Lignin from Organosolv Pulping Liquors

The solubility and softening behavior of lignin from acid-catalyzed ethanol/water pulping were determined in various ethanol/water solvent mixtures and a process-relevant temperature range. The operating conditions for an optimized lignin separation process were derived from the determined lignin phase behavior. A continuous lignin separation and SR process was developed on a lab-scale and was successfully scaled up to a dedicated pilot plant at Fraunhofer CBP (WO2016062676A1). Agglomeration of softened lignin particles and lignin "stickiness" were adjusted by temperature (38–44 °C at 80–120 mbar) and ethanol content of the lignin dispersion (6–9 wt%). In this manner, ethanol recovery by evaporation and lignin particle formation was facilitated simultaneously and monitored by inline infrared spectroscopy [98]. The agglomeration behavior of different lignins was monitored via inline particle size analysis. Optimal process conditions resulted in good filterability of the lignin dispersion with average filter cake resistances of 10^{11} to 10^{13} m^{-2}, and lignin yields close to 100 wt% of water-insoluble lignin. To maintain continuous operation, the ethanol content in the distillate must be higher than that in the pulping liquor. Thus, more pulping liquor must be added than distillate is removed.

13.5 Adsorption Method for Recovery of Waste Organic Solvents

13.5.1 Recovery of IPA from Waste Solvent of Manufacturing Plants

Volatile organic compounds (VOCs) are pollutant gases emitted in the atmosphere from certain liquids and solids, including a variety of chemical components. Owing to the high vapor pressure and a low boiling point at typical room temperature, VOC is easily evaporated to pollute the surrounding air. The recoverable resources of VOCs from waste solvents are recovered for environmental benefit. Although distillation and PV are widely used as separation methods for the recovery of important chemicals from waste solvents, separation and purification of VOCs by distillation and membrane require energy-intensive and complex processes, respectively [63]. The adsorption method is alternatively utilized

for the effective recovery of valuable compounds from VOCs. Furthermore, significant amounts of organic and less volatile solvents can also contaminate industrial wastewater. Adsorption is widely utilized in water treatment, and is utilized as the main method to recover less volatile solvents from industrial contaminated wastewater [1].

In the pharmaceutical industry, waste incineration is the base scenario of waste solvent treatment in the celecoxib process. In the attempt of solvent minimization using green chemistry and engineering, waste SR from active ingredient manufacturing has been studied [57]. The recovery of waste IPA is a concern in the manufacturing process of celecoxib due to the existence of an azeotropic mixture [57].

A conceptual study was conducted using a computer simulation (Aspen Plus and Microsoft Excel) to recover IPA at high concentrations. The study covers a conventional approach by distillation and a hybrid method by combining distillation with a PV membrane and molecular sieve adsorption. However, adsorption is used after the distillation column as a secondary recovery step to separate the azeotrope from distillation overhead [57]. The final analysis results show that combination distillation and molecular sieve adsorption are effective in recovering reusable waste solvent from azeotropic mixture and life cycle emission reduction from 64 to 93% in the overall emission compared with the general process [57].

In another case, a high concentration of IPA solvent is generally discharged as waste in the semiconductor-manufacturing industry [63]. Active carbon fiber (ACF) adsorption and condensation in conjunction with air stripping are utilized to recover high concentrations of IPA. The process involves condensing the IPA vapor in the gas mixture from the air-stripping column in a water-cooled side condenser. After condensation, the residual IPA in the gas mixture is adsorbed in the packed ACF column. The apparatus of the process is relatively simple, easy to operate, and inexpensive. The diagram of packed activated carbon fiber adsorption of IPA is shown in Figure 13.8.

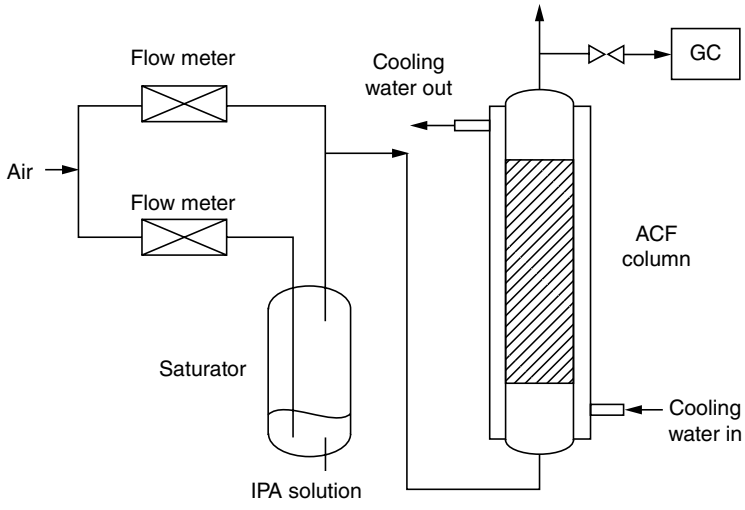

Figure 13.8 Schematic diagram of packed activated carbon fiber adsorption of IPA. *Taken from* [63].

Experimental test results show efficient IPA removal from waste solvent and a 93% recovery of IPA that was originally present in waste solvent [63].

13.5.2 Recovery of Heavy Component Solvent NMP

In the battery-manufacturing process, the cathode consists of different kinds of solids such as lithium metal oxide particles and carbon black conductive additives, and polymeric binders are initially dry mixed. Further, the dry mix is mixed with a solution of the binder dissolved in the heavy solvent NMP to form a slurry that is soluble in water [73]. Alongside the process, NMP in the cathode is evaporated in the dryer by flow of hot air for recycling and recovery. The NMP-laden hot air is first passed through an air-to-air heat exchanger and further cooled by a chilled water condenser. Liquid condensate consisting of NMP, water, and higher hydrocarbons is subsequently separated in a distillation column. A few ppm of NMP in the cooled air from the condenser is split into two streams: recycle and purge stream. The zeolite wheel adsorbs most of the NMP from the purge stream. This NMP recovery process based on a battery-manufacturing plant producing 100,000 battery packs per year for 10 kWh plug-in hybrid electric vehicle (PHEV) batteries, where each pack costs approximately $3100 ($310 per kWh) is depicted in Figure 13.9 [73]. The recovery of NMP in battery manufacturing significantly saves costs and generates environmental benefits.

13.5.3 Valorization of Agricultural Waste with an Adsorption/ Nanofiltration Hybrid Process

Downstream processing is considered a bottleneck in pharmaceutical manufacturing because its development has not kept pace with upstream production. In some cases, the lack of efficient downstream processing capacity can seriously affect both the sustainability and profitability of a pharmaceutical product and result in its failure. Minimizing solvent and raw material consumption, as well as utilizing waste, can make a significant difference toward environmentally benign and economically viable chemical production. Waste utilization in agriculture has gained increasing attention because it is ranked as the second highest contributor to global greenhouse gas emissions. Imprinted polymers were developed for the selective scavenging of oleuropein (OR) from olive leaf extracts using green solvents. The mild temperature-swing (25–43 °C) process allows the continuous isolation of OR at 1.75 g product per kg of adsorbent per hour with an unprecedented 99.7% purity. In situ SR was realized with a solvent-resistant nanofiltration (NF) membrane allowing 97.5% solvent recycling and 44.5% total carbon footprint reduction while concentrating both the product stream for crystallization and the waste stream for disposal [99]. A schematic process scheme for the continuous isolation of OR from an olive leaf extract is shown in Figure 13.10.

13.6 Membrane Technology in Solvent Recovery

High energy and capital costs, poor recovery yield, and process safety issues present multiple challenges in solvent waste treatment [9]. Currently, membrane technology has been gradually extended in SR because of its efficiency improvement, low energy cost, and

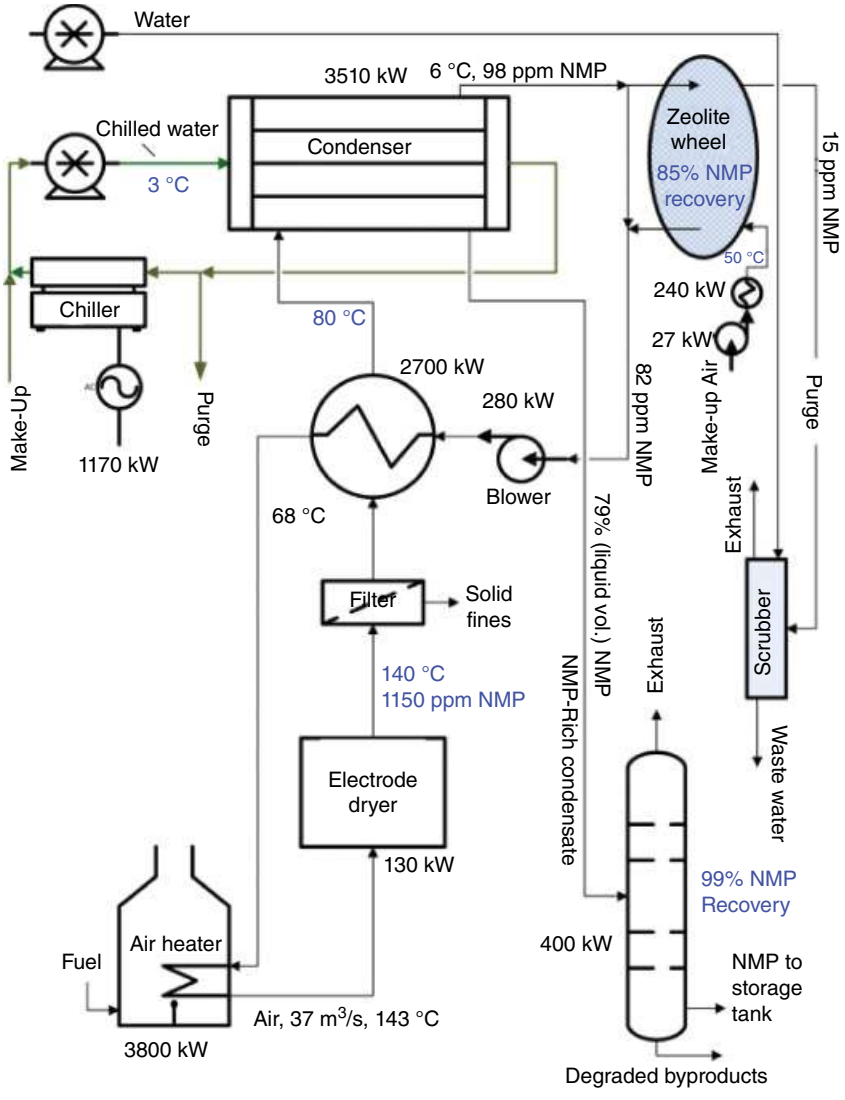

Figure 13.9 Process schematic for the drying and recovery of the cathode solvent NMP in a battery-manufacturing plant. *Taken from* [73].

capability to overcome the existence of azeotrope in the liquid effluent [100]. In the SR process, the membrane is fabricated from either organic or inorganic materials.

13.6.1 Pervaporation (PV) Membrane for Solvent Recovery

Pervaporation (PV) separation has proved to be an efficient and reliable method due to its ability to exceed conventional distillation limitations in azeotropic mixture separation, low energy demand and low device volume requirement, constant performance in handling

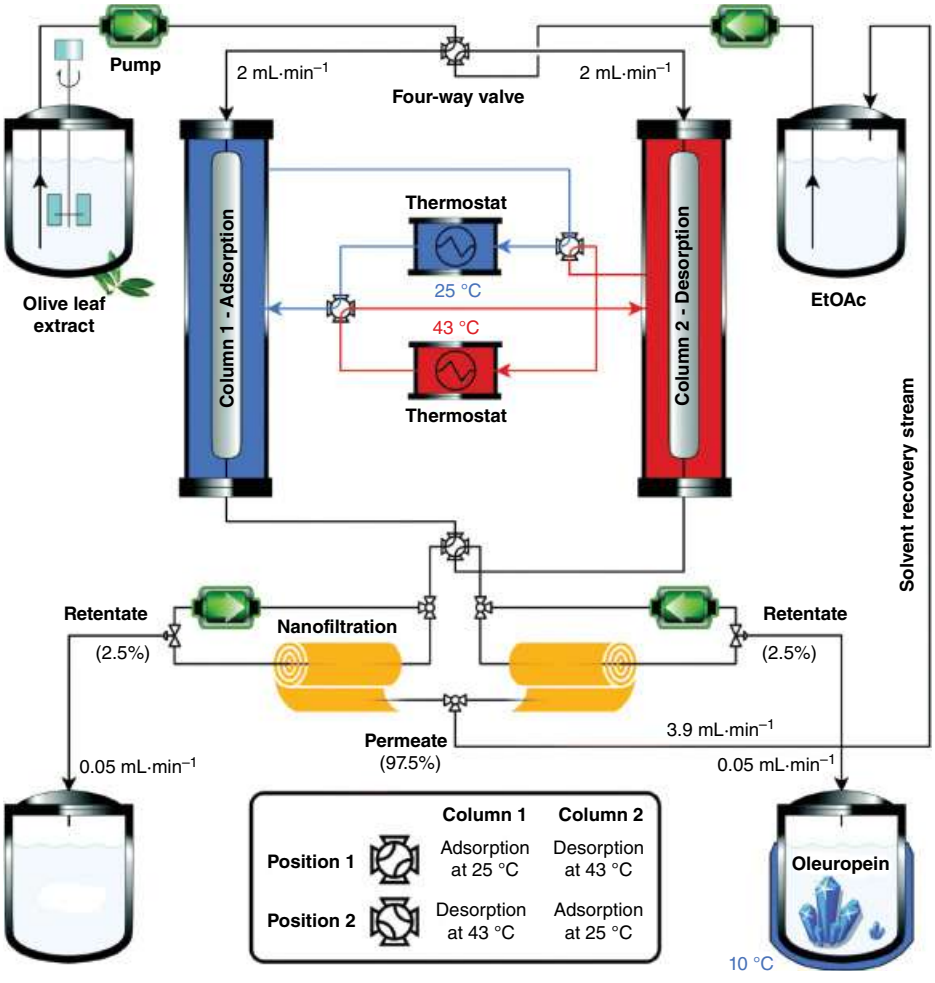

Figure 13.10 Schematic process scheme for the continuous isolation of OR from an olive leaf extract. The two columns are packed with imprinted polymers scavenging the OR, and the subsequent NF units concentrate both the waste and product streams while the solvent is being recovered in situ. The compact design resulted in approximately a 2 m^2 footprint for the whole unit. *Taken from* [99].

mixtures of aqueous organic, and no requirement for the use of additional chemicals [101, 102]. A hydrophilic-based-PV membrane is utilized for water removal or solvent dehydration from high concentrations of organic solvents, and hydrophobic based-PV membranes are applied for organic solvent removal or solvent reclamation from aqueous solution [9]. PV accounts for approximately 3.6% of the total number of membrane applications in the chemical and petrochemical industries [102] and can potentially revolutionize the separation process in a variety of industrial sectors [101].

In the chemical industry, Alcohol-based solvents are the most common organic solvents used in numerous chemical productions. Ceramic PV membranes have gained attention in

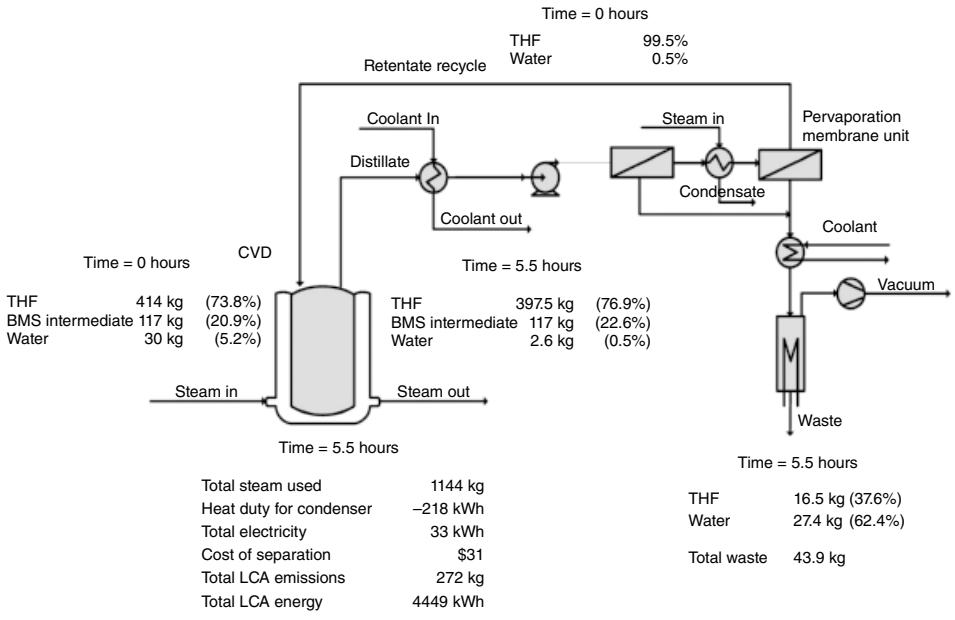

Figure 13.11 Process of THF recovery through CVD-PV. *Taken from* [60].

a wide range of industrial applications, with an increasing trend in the last two decades, and are currently commercially available for the dehydration of alcohol in the fermentation process [9]. Ceramic PV membranes are also used in fermentation and dehydration for bioethanol production [103]. Further, it is applied for the SR process in concentrated and diluted bioethanol [104]. In the petrochemical industry, main aromatic compounds and water-insoluble organic solvents are frequently utilized as solvents during the refinery process of crude oil [105]. Among the main aromatic compounds, the recovery of xylene through the PV membrane is an important application because xylene is frequently used in various chemical processes. In the synthesis of pharmaceutical ingredients, the recovery of tetrahydrofuran (THF) is a process in which PV is considered a green drying process and is widely used for THF SR [55, 60, 106]. The PV membrane process for the recovery of THF at a 68-kg pilot-scale operation with constant-volume distillation (CVD) [60] is presented in Figure 13.11. Another separation process of THF from water is demonstrated by a ceramic PV membrane, which indicates that the ceramic PV membrane is suitable for THF dehydration from a mixture with water [9]. Another process for recovery of IPA is demonstrated with good performance by various PV membranes [107–109].

13.6.2 Solvent Recovery Through Organic Solvent Forward Osmosis

API synthesis involves various organic solvents. Among various membrane technologies, organic solvent nanofiltration (OSN) is typically utilized for the pharmaceutical concentration recovery of organic solvents. However, the pressure-driven method remains a great concern because the high-pressure process of an OSN may increase the operating

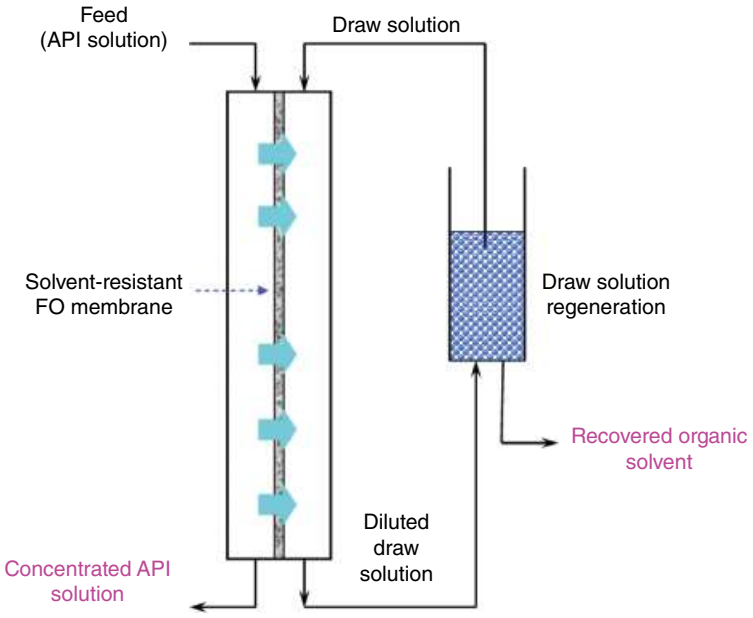

Figure 13.12 OSFO process for organic SR and product concentration. *Taken from* [110].

cost. Accordingly, there is a need for more cost-effective and sustainable processes [110]. Recently, forward osmosis (FO) membranes have gained considerable attention owing to their capability to transport water between two sides of the concentration gradient, from low to high concentration side [111, 112] and take advantage of the lack of external pressure compared to other pressure-driven membrane processes such as reverse osmosis (RO) and NF. With a relatively lower pressure than the high pressure of pressure-driven RO and NF, the flux is comparatively higher than the direct filtration process [113–115], which may depreciate the total cost [114]. The processes of organic solvent FO (OSFO) for the simultaneous organic SR and pharmaceutical product concentration are depicted in Figure 13.12.

Alcohol-based solvents such as ethanol are a common solvent used in the pharmaceutical process; however, the pharmaceutical industry utilizes a variety of organic solvents. Thus, the practical performance of the OSFO was evaluated by [110]. The process of OSFO is applicable to various pure systems of ethanol, IPA, and hexane and is potentially applicable to other systems of solvents. For the simultaneous process of product concentration and recovery of organic solvent, an active ingredient solution consisting of 2000 ppm tetracycline ($M_w = 444.4$ g/mol) in ethanol and a 2 M lithium chloride (LiCl) ethanol solution were employed as the feed and draw solutions, respectively. The results show that tetracycline rejection was above 99%. Different solvent systems of tetracycline and IPA, including triglycerides and hexane, were also employed as feed-in OSFO. When rejection is above 99%, the result shows a promising starting point of OSFO application, and further development is required to increase the flux of solvent [110]

13.6.3 Organic Solvent Nanofiltration

OSN is considered a sustainable alternative to conventional separation techniques with an evolving range of applications around the recovery of products, catalysts, and solvents. Recent developments in the field have provided membranes with long-sought-after properties of stability in harsh environments, including polar aprotic solvents and extreme pH, high flux, and low molecular weight cutoff (MWCO). Nine solvents with polarity indices ranging from 0.1 to 5.8 (hexane to acetonitrile) were used as treatment and process solvents on commercial Borsig GMT-oNF-2, Evonik Duramem 300, and emerging tailor-made polybenzimidazole (PBI) membranes. TGA-GCMS, HS-GC-FID, and NMR techniques were employed to better understand the effect of solvent treatment on the polymer matrix of membranes. Apart from the direct effect of solvent treatment on membrane performance, a subsequent indirect effect on the ultimate separation process was observed in this study. Consequently, a pharmaceutical case study employing chlorhexidine disinfectant and antiseptic was used to demonstrate the effect of solvent treatment on NF-based purification. It was shown that treatment of PBI membranes with acetone resulted in a 25% increase in product recovery at 99% impurity removal. The cost of process intensification is negligible in terms of solvent consumption, mass intensity, and processing time [116].

13.6.4 In Situ Solvent Recovery by Organic Solvent Nanofiltration [117]

Reducing solvent consumption in chemical industries is increasingly becoming a topic of interest. The field of OSN has markedly evolved in the past decade, and effective membranes are now available to withstand aggressive solvents while completely rejecting small solutes at the lower end of the NF range (100–2000 g/mol). With such membranes in hand and the advantages of membrane modularity, it is now possible to design innovative configurations to drastically reduce solvent consumption and enhance the sustainability of downstream processes. OSN membranes can withstand aggressive solvents and sufficiently retain small solutes. Such features make OSN a good candidate for SR in the fine chemical industries, where impurities are usually small with MW < 400 g/mol. Current state-of-the-art OSN membranes have been screened, which showed it is now possible to implement an SR unit down to a range of 100 g/mol with appropriate configurations and operation protocols. Hence, a continuous and control-free in situ SR configuration has been implemented to recycle the waste solvent consumed during a membrane diafiltration process. The effect of impurity rejection by the membrane on the maximum achievable purity was assessed and validated in a pharmaceutical case study, which gave almost quantitative product yield and 98% impurity removal with no additional fresh solvent. The product purity can be further improved by simply repeating the process without loss of yield. The operability and carbon footprint of the proposed membrane-based SR is advantageous compared to adsorptive- and distillation-based SR. The main advantages of membrane-based SR, apart from its simplicity, are low solid waste generation and low energy consumption. It has been shown and emphasized that the modularity of the membrane processes allows convenient operation, and the overall operability of the process can be significantly simplified.

13.6.5 Continuous and Simultaneous Isolation of Antioxidants: An Upcycling Approach for Olive Leaf Waste

The isolation of individual pharmaceutical-grade bioactive compounds from complex plant extracts is still a sustainability challenge. Process intensification improves manufacturing design to achieve significant benefits in process efficiency and operation, product quality, and waste management. A process optimization and intensification methodology for the simultaneous isolation of biophenols from agricultural waste using imprinted materials and NF membranes is reported herein [118]. Schematic piping and instrumentation diagram for the continuous and simultaneous isolation and fractionation of OR (OR), luteolin (LU), and pinoresinol (PN) from olive leaf extracts is shown in Figure 13.13.

First, temperature-swing molecular imprinting technology was used to selectively extract individual biophenols from olive leaf extracts. Second, solvent-resistant NF was used to concentrate the product and waste streams and recover the solvent. The predictive mathematical models for the adsorption dynamics and membrane separation resulted in a significant reduction in the carbon footprint, E factor, and economic sustainability. This process was designed for easy operation with multiway valves to aid safety and reduce operating costs. The proposed process intensification methodology can be generally adapted for waste upcycling through the sustainable isolation of multiple high-value products from complex mixtures.

Mathematical models for the adsorption dynamics and membrane separation were developed to assist with process optimization, reducing the need for excessive experimentation. The optimized process resulted in a 61 and 49% reduction in the ecological and carbon footprints, respectively. Novel metrics for the assessment of the economic sustainability of waste and emitted CO_2 have been introduced.

Economic sustainability for waste (left columns) and emitted CO_2 (right columns) estimations are shown in Figure 13.14.

13.6.6 Solvent Recycle with Imperfect Membranes

For the separation of a two-component mixture, a three-stage OSN process is presented, which comprises a two-stage membrane cascade for separation with a third membrane stage added for integrated SR, that is, solvent recycling. The two-stage cascade allows for increased separation selectivity, while the integrated SR stage mitigates the otherwise large solvent consumption of the purification [119]. This operation attains purity of 98.7% through the semicontinuous operation with two washes of the SR stage, even when imperfect membranes are used in a closed-loop setup. Such results contrast favorably with the 83.0% maximum purity achievable in a similar setup with a single continuous run. The process achieved a slightly lower (−0.7%) yield of approximately 98.2% compared to a continuously operated process without SR but consumed approximately 85% less solvent (theoretical analysis suggests up to 96% reduction is possible). Nine different membranes, both commercial (GMT, Novamem, and SolSep) and in-house fabricated, are screened and tested on a separation challenge associated with the synthesis of macrocycles. Among the membrane materials are polyimide (PI), PBI, and polyetheretherketone (PEEK).

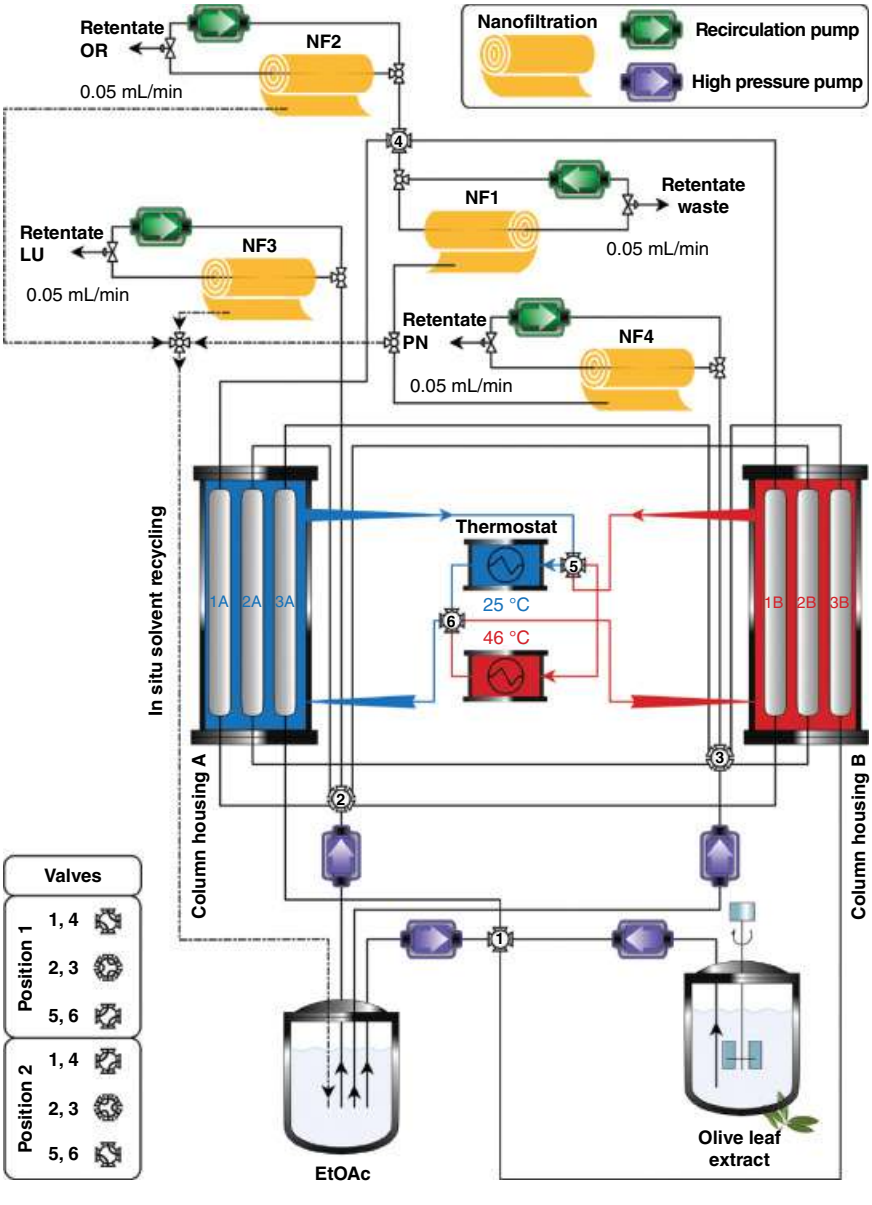

Figure 13.13 Schematic piping and instrumentation diagram for the continuous and simultaneous isolation and fractionation of oleuropein (OR), luteolin (LU), and pinoresinol (PN) from olive leaf extracts. The two sets of three columns are equipped with imprinted materials selective to OR [1], LU [2], and PN [3]. Both the waste and biophenol streams are concentrated by the membrane units, while ethyl acetate is in-line recycled. *Taken from* [118].

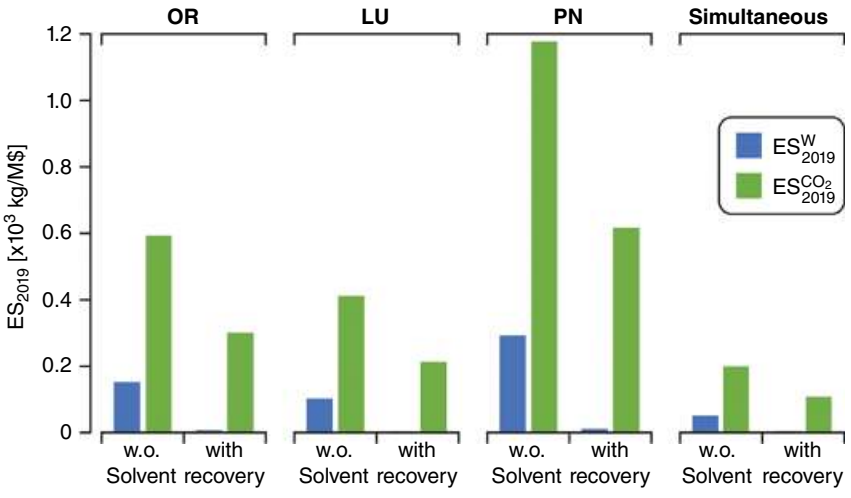

Figure 13.14 Economic sustainability for waste (left columns) and emitted CO_2 (right columns) estimations for single biophenol isolation, without (left clusters) and with (right clusters) in-line solvent recycle, and for the simultaneous isolation process. *Taken from* [118].

13.6.7 Increasing the Sustainability of Membrane Processes Through Cascade Approach and Solvent Recovery

Membrane processes suffer from limitations such as low product yield and high solvent consumption, hindering their widespread application in the pharmaceutical and fine chemical industries. The process has been validated for the purification of APIs from genotoxic impurities (GTIs) using OSN. The model system selected for this study comprised roxithromycin macrolide antibiotic (Roxi) with 4-dimethylaminopyridine (DMAP) and ethyl tosylate (EtTS) as API and GTIs, respectively. By implementing a two-stage cascade configuration for membrane diafiltration, the process yield was increased from 58 to 95% while maintaining less than 5 ppm GTI in the final solution. Through this yield enhancement, the membrane process has been "revamped" from an unfeasible process to a highly competitive unit operation compared to other traditional processes. The advantage of size exclusion membranes over other separation techniques has been illustrated by the simultaneous removal of two GTIs from different chemical classes. In addition, an SR step has been assessed using charcoal as a nonselective adsorbent. It has been shown that pure solvent can be recovered from the permeate. When considering the costs of solvent, charcoal, and waste disposal, it was concluded that 70% SR is the cost-optimum point. Conventional single-stage diafiltration (SSD) and two-stage diafiltration (TSD) configurations were compared in terms of green metrics such as cost, mass and solvent intensity, and energy consumption. It was calculated that implementation of TSD, depending on the batch scale, can achieve up to 92% cost savings while reducing the mass and solvent intensity up to 73%. In addition, the advantage of adsorptive SR has been assessed, revealing up to 96% energy reduction compared to distillation and a 70% reduction in CO_2 footprint [120].

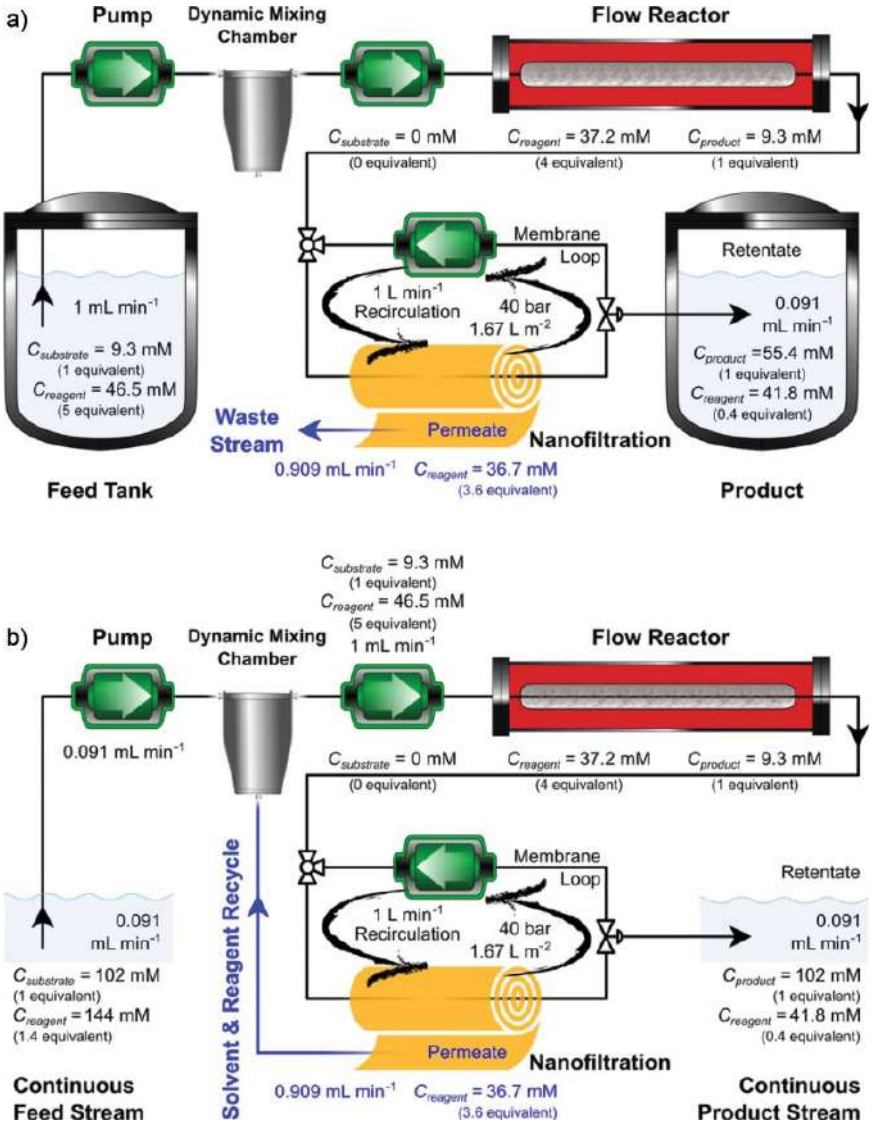

Figure 13.15 Process configuration and conditions for the start-up (a) and continuous steady-state (b) operation of the hybrid process. The jacketed flow reactor operated at 50 °C allowing 100% conversion of the substrate. The NF unit was operated continuously at 40 bar, splitting the crude mixture into a concentrated, product-rich retentate stream, and a reagent-rich permeate stream. Initially, the permeate stream was discarded (a) and once a steady state was reached, recycling of the permeate stream was commenced (b), and the feed concentration and flow rate were adjusted. *Taken from* [121].

13.6.8 Nanofiltration-enabled in situ Solvent and Reagent Recycle for Sustainable Continuous-flow Synthesis

Solvent usage in the pharmaceutical sector accounts for 90% of the overall mass during manufacturing processes. Consequently, solvent consumption poses high costs and an environmental burden. Continuous processing, in particular continuous-flow reactors, has great potential for the sustainable production of pharmaceuticals, but subsequent downstream processing remains challenging. Separation processes for concentrating and purifying chemicals account for 80% of the total manufacturing costs. An NF unit was coupled to a continuous-flow reactor for in situ solvent and reagent recycling; the NF unit is straightforward to implement and simple to control during continuous operation. The hybrid process operated continuously over six weeks, recycling approximately 90% of the solvent and reagent. Consequently, the e-factor and the carbon footprint were reduced by 91 and 19%, respectively [121]. Moreover, the NF unit led to a solution of the product being eleven times more concentrated than the reaction mixture and increased the purity from 52.4 to 91.5%. The boundaries for process conditions were investigated to facilitate the implementation of the methodology by the pharmaceutical sector. Process configuration is shown in Figure 13.15.

13.6.9 Artificial Intelligence in the Nanofiltration Membrane Process

There is an urgent need to develop predictive methodologies that will fast-track the industrial implementation of OSN. However, the performance prediction of OSN membranes has been a daunting and challenging task, owing to the high number of possible solvents and the complex relationship between solvent–membrane, solute–solvent, and solute–membrane interactions. Therefore, instead of developing fundamental mathematical equations, we have broken away from conventions by compiling a large dataset and building artificial intelligence (AI)-based predictive models for both rejection and permeance, based on a collected dataset containing 38,430 data points with more than 18 dimensions (parameters). To elucidate the important parameters that affect membrane performance, we carried out a thorough principal component analysis (PCA), which revealed that the factors affecting both permeance and rejection are surprisingly similar. We trained three different AI models (artificial neural network, support vector machine, and random forest) that predicted membrane performance with unprecedented accuracy, as high as 98% (permeance) and 91% (rejection). This findings pave the way toward appropriate data standardization not only for performance prediction but also for better membrane design and development [122].

References

1 Cseri, L., Razali, M., Pogany, P., and Szekely, G. (2018). *Chapter 3.15 – Organic Solvents in Sustainable Synthesis and Engineering* (eds. B. Török and T.B.T.-G.C. Dransfield), 513–553. Elsevier http://www.sciencedirect.com/science/article/pii/B9780128092705000200.

2 Chaniago, Y.D., Harvianto, G.R., Bahadori, A., and Lee, M. (2016). Enhanced recovery of PGME and PGMEA from waste photoresistor thinners by heterogeneous azeotropic dividing-wall column. *Process Saf Environ Prot* 103: 413–423. https://www.sciencedirect.com/science/article/pii/S0957582016300714.

3 Chaniago, Y.D. and Lee, M. (2018). Distillation design and optimization of quaternary azeotropic mixtures for waste solvent recovery. *J Ind Eng Chem* 67: 255–265. https://www.sciencedirect.com/science/article/pii/S1226086X18303277.

4 Zou, C., Zhao, Q., Zhang, G., and Xiong, B. (2016). Energy revolution: from a fossil energy era to a new energy era. *Nat Gas Ind B* 3 (1): 1–11. https://www.sciencedirect.com/science/article/pii/S2352854016300109#fig2.

5 Duflou, J.R., Sutherland, J.W., Dornfeld, D. et al. (2012). Towards energy and resource efficient manufacturing: a processes and systems approach. *CIRP Ann* 61 (2): 587–609. http://www.sciencedirect.com/science/article/pii/S0007850612002016.

6 Tula, A.K., Befort, B., Garg, N. et al. (2017). Sustainable process design & analysis of hybrid separations. *Comput Chem Eng* 105: 96–104. http://www.sciencedirect.com/science/article/pii/S0098135416303799.

7 Vooradi, R., Bertran, M.-O., Frauzem, R. et al. (2018). Sustainable chemical processing and energy-carbon dioxide management: review of challenges and opportunities. *Chem Eng Res Des* 131: 440–464. https://www.sciencedirect.com/science/article/pii/S0263876217306925.

8 Chaniago, Y.D., Hussain, A., Andika, R., and Lee, M. (2019). Reactive pressure-swing distillation toward sustainable process of novel continuous ultra-high-purity electronic-grade propylene glycol monomethyl ether acetate manufacture. *ACS Sustain Chem Eng* https://doi.org/10.1021/acssuschemeng.9b05251.

9 Saw, E.T., Ang, K.L., He, W. et al. (2019). Molecular sieve ceramic pervaporation membranes in solvent recovery: a comprehensive review. *J Environ Chem Eng* 7 (5): 103367. https://www.sciencedirect.com/science/article/pii/S2213343719304907#bib0155.

10 United Nations Environment Programme (2019). Global Chemicals Outlook II – From Legacies to Innovative Solutions – Synthesis Report. https://www.unenvironment.org/resources/report/global-chemicals-outlook-ii-legacies-innovative-solutions.

11 Chea, J.D., Lehr, A.L., Stengel, J.P. et al. (2020). Evaluation of solvent recovery options for economic feasibility through a superstructure-based optimization framework. *Ind Eng Chem Res* 59 (13): 5931–5944. https://doi.org/10.1021/acs.iecr.9b06725.

12 Abou-Shehada, S., Clark, J.H., Paggiola, G., and Sherwood, J. (2016). Tunable solvents: shades of green. *Chem Eng Process Process Intensif* 99: 88–96. http://www.sciencedirect.com/science/article/pii/S025527011530057X.

13 Chaniago, Y.D., Minh, L.Q., Khan, M.S. et al. (2015). Optimal design of advanced distillation configuration for enhanced energy efficiency of waste solvent recovery process in semiconductor industry. *Energy Convers Manag* 102: 92–103. https://www.sciencedirect.com/science/article/pii/S019689041500312X.

14 Gilles, D.G. and Loehr, R.C. (1994). Waste generation and minimization in semiconductor industry. *J Environ Eng* 120 (1) 10.1061/(ASCE)0733-9372(1994)120:1(72).

15 Raymond, M.J., Slater, C.S., and Savelski, M.J. (2010). LCA approach to the analysis of solvent waste issues in the pharmaceutical industry. *Green Chem* 12 (10): 1826–1834. http://dx.doi.org/10.1039/C003666H.

16 Henderson, R.K., Jiménez-González, C., Constable, D.J.C. et al. (2011). Expanding GSK{'}s solvent selection guide – embedding sustainability into solvent selection starting at medicinal chemistry. *Green Chem* 13 (4): 854–862. http://dx.doi.org/10.1039/C0GC00918K.

17 Sheldon, R.A. (2005). Green solvents for sustainable organic synthesis: state of the art. *Green Chem* 7 (5): 267–278. http://dx.doi.org/10.1039/B418069K.

18 Jimenez-Gonzalez, C., Ponder, C.S., Broxterman, Q.B., and Manley, J.B. (2011). Using the right green yardstick: why process mass intensity is used in the pharmaceutical industry to drive more sustainable processes. *Org Process Res Dev* 15 (4): 912–917. https://doi.org/10.1021/op200097d.

19 Constable, D.J.C., Jimenez-Gonzalez, C., and Henderson, R.K. (2007). Perspective on solvent use in the pharmaceutical industry. *Org Process Res Dev* 11 (1): 133–137. https://doi.org/10.1021/op060170h.

20 Clarke, C.J., Tu, W.-C., Levers, O. et al. (2018). Green and sustainable solvents in chemical processes. *Chem Rev* 118 (2): 747–800. https://doi.org/10.1021/acs.chemrev.7b00571.

21 Savelski, M.J., Slater, C.S., Tozzi, P.V., and Wisniewski, C.M. (2017). On the simulation, economic analysis, and life cycle assessment of batch-mode organic solvent recovery alternatives for the pharmaceutical industry. *Clean Techn Environ Policy* 19 (10): 2467–2477. https://doi.org/10.1007/s10098-017-1444-8.

22 Alder, C.M., Hayler, J.D., Henderson, R.K. et al. (2016). Updating and further expanding GSK{'}s solvent sustainability guide. *Green Chem* 18 (13): 3879–3890. http://dx.doi.org/10.1039/C6GC00611F.

23 Sheldon, R. (2010). Introduction to green chemistry, organic synthesis and pharmaceuticals. In: *Green Chemistry in the Pharmaceutical Industry*, 1–20. (Wiley Online Books). 10.1002/9783527629688.ch1.

24 Sheldon, R.A. (2007). The E factor: fifteen years on. *Green Chem* 9 (12): 1273–1283. http://dx.doi.org/10.1039/B713736M.

25 Sheldon, R.A. (2017). The E factor 25 years on: the rise of green chemistry and sustainability. *Green Chem* 19 (1): 18–43. http://dx.doi.org/10.1039/C6GC02157C.

26 Chaniago, Y.D., Khan, M.S., Choi, B., and Lee, M. (2014). Energy efficient optimal design of waste solvent recovery process in semiconductor industry using enhanced vacuum distillation. *Energy Procedia* 61: 1451–1454. http://www.sciencedirect.com/science/article/pii/S1876610214031749.

27 Slater, C.S., Savelski, M.J., Carole, W.A., and Constable, D.J.C. (2010). Solvent use and waste issues. In: *Green Chemistry in the Pharmaceutical Industry*, 49–82. Wiley https://onlinelibrary.wiley.com/doi/abs/10.1002/9783527629688.ch3.

28 Tyrer, M. (2013). 12 – municipal solid waste incinerator (MSWI) concrete. In: *Woodhead Publishing Series in Civil and Structural Engineering* (eds. F. Pacheco-Torgal, S. Jalali, J. Labrincha and V.M.B.T.-E.-E.C. John), 273–310. Woodhead Publishing http://www.sciencedirect.com/science/article/pii/B9780857094247500128.

29 Allsopp, M., Costner, P., and Johnston, P. (2001). Incineration and human health. *Environ Sci Pollut Res* 8 (2): 141–145. https://doi.org/10.1007/BF02987308.

30 Sharma, R., Sharma, M., Sharma, R., and Sharma, V. (2013). The impact of incinerators on human health and environment. *Rev Environ Health* 28 (1): 67–72. https://www.degruyter.com/view/journals/reveh/28/1/article-p67.xml.

31 Smallwood, I.M. (2002). *Solvent Recovery Handbook*, 2e, 1. Wiley-Blackwell.

32 Amelio, A., Genduso, G., Vreysen, S. et al. (2014). Guidelines based on life cycle assessment for solvent selection during the process design and evaluation of treatment alternatives. *Green Chem* 16 (6): 3045–3063. http://dx.doi.org/10.1039/C3GC42513D.

33 George, A., Brandt, A., Tran, K. et al. (2015). Design of low-cost ionic liquids for lignocellulosic biomass pretreatment. *Green Chem* 17 (3): 1728–1734. http://dx.doi.org/10.1039/C4GC01208A.

34 Chen, L., Sharifzadeh, M., Mac Dowell, N. et al. (2014). Inexpensive ionic liquids: [HSO4]—-based solvent production at bulk scale. *Green Chem* 16 (6): 3098–3106. http://dx.doi.org/10.1039/C4GC00016A.

35 Brandt-Talbot, A., Gschwend, F.J.V., Fennell, P.S. et al. (2017). An economically viable ionic liquid for the fractionation of lignocellulosic biomass. *Green Chem* 19 (13): 3078–3102. http://dx.doi.org/10.1039/C7GC00705A.

36 Chaniago, Y.D., Kim, J.-K., Park, M.-J. et al. (2016). Design and modeling of optimal distillation sequence for recovery of valuable components from a waste photoresist stripper. *J Mater Cycles Waste Manag* 18 (2): 366–376. 10.1007/s10163-014-0339-6.

37 Anastas, P.T. and Zimmerman, J.B. (2003). Peer reviewed: design through the 12 principles of green engineering. *Environ Sci Technol* 37 (5): 94A–101A. 10.1021/es032373g.

38 Clark, J., Macquarrie, D., Gronnow, M., and Budarin, V. (2013). *Green Chemistry Principles. Process Intensification for Green Chemistry*, 33–58. (Wiley Online Books). 10.1002/9781118498521.ch2.

39 Rosenfeld, P.E. and Feng, L.G.H. (2011). 22 – strategies for the future – waste reduction and recycling, treatment technologies, and green chemistry. In: (eds. P.E. Rosenfeld and Feng LGHBT-R of HW), 269–284. Boston: William Andrew Publishing. http://www.sciencedirect.com/science/article/pii/B9781437778427000222.

40 Clark, J.H. and Tavener, S.J. (2007). Alternative solvents: shades of green. *Org Process Res Dev* 11 (1): 149–155. 10.1021/op060160g.

41 Cooney, D.O., Nagerl, A., and Hines, A.L. (1983). Solvent regeneration of activated carbon. *Water Res* 17 (4): 403–410. http://www.sciencedirect.com/science/article/pii/0043135483901367.

42 Seyler, C., Capello, C., Hellweg, S. et al. (2006). Waste-solvent management as an element of green chemistry: a comprehensive study on the swiss chemical industry. *Ind Eng Chem Res* 45 (22): 7700–7709. 10.1021/ie060525l.

43 Capello, C., Hellweg, S., Badertscher, B., and Hungerbühler, K. (2005). Life-cycle inventory of waste solvent distillation: statistical analysis of empirical data. *Environ Sci Technol* 39 (15): 5885–5892. https://doi.org/10.1021/es048114o.

44 Mendez-Alvarez, C., Plesu, V., Bonet Ruiz, A.E. et al. (2016). Distillation energy assessment for solvent recovery from carbon dioxide absorption. In: *26 European Symposium on Computer Aided Process Engineering* (eds. Z. Kravanja and M.B.T.-C.A.C.E. Bogataj), 1917–1922. Elsevier http://www.sciencedirect.com/science/article/pii/B9780444634283503246.

45 Davies, A., James, B, and Sherman, P. (1967). Method of solvent recovery in refining hydrocarbon mixtures with n-methyl-2-pyrrolidone. US Patent 3476681A. https://patents.google.com/patent/US3476681A/en.

46 García, V., Pongrácz, E., Phillips, P.S., and Keiski, R.L. (2013). From waste treatment to resource efficiency in the chemical industry: recovery of organic solvents from waters containing electrolytes by pervaporation. *J Clean Prod* 39: 146–153. https://www.sciencedirect.com/science/article/pii/S0959652612004428.

47 Sharif Rohani, A., Mehrani, P., and Thibault, J. (2015). Comparison of in-situ recovery methods of gas stripping, pervaporation, and vacuum separation by multi-objective

optimization for producing biobutanol via fermentation process. *Can J Chem Eng* 93 (6): 986–997. https://onlinelibrary.wiley.com/doi/abs/10.1002/cjce.22186.

48 Slater, C.S. (1997). Recovery of ethyl acetate from process effluents using pervaporation technology. *J Environ Sci Health A Environ Sci Eng Toxicol* 32 (5): 1339–1352. https://doi.org/10.1080/10934529709376613.

49 Namvar-Mahboub, M., Pakizeh, M., and Davari, S. (2014). Preparation and characterization of UZM-5/polyamide thin film nanocomposite membrane for dewaxing solvent recovery. *J Membr Sci* 459: 22–32. http://www.sciencedirect.com/science/article/pii/S0376738814001203.

50 Lee, H.S., Lee, N.R., and Yang, D.R. (2013). A new method of amine solvent recovery with acid addition for energy reduction in the CO2 absorption process. *Chem Eng Res Des* 91 (12): 2630–2638. http://www.sciencedirect.com/science/article/pii/S0263876213002414.

51 Antonova, Z.A., Kruk, V.S., Kursevich, V.N. et al. (2012). On separating mixtures containing methanol, tetrahydrofuran, and water by distillation. *Russ J Appl Chem* 85 (9): 1447–1453. https://doi.org/10.1134/S1070427212090248.

52 Sugiyama, H., Morikawa, Y., Matsuura, M., and Xu, M. (2019). Relevance of regulatory constraints in designing pharmaceutical manufacturing processes: a case study on waste solvent recovery. *Sustain Prod Consum* 17: 136–147. https://www.sciencedirect.com/science/article/pii/S2352550918301040.

53 Wang, Y., Cui, P., and Zhang, Z. (2014). Heat-integrated pressure-swing-distillation process for separation of tetrahydrofuran/methanol with different feed compositions. *Ind Eng Chem Res* 53 (17): 7186–7194. https://doi.org/10.1021/ie500235f.

54 Szanyi, A., Mizsey, P., and Fonyo, Z. (2004). Novel hybrid separation processes for solvent recovery based on positioning the extractive heterogeneous-azeotropic distillation. *Chem Eng Process Process Intensif* 43 (3): 327–338. https://www.sciencedirect.com/science/article/pii/S0255270103001326#BIB7.

55 Luis, P., Amelio, A., Vreysen, S. et al. (2014). Simulation and environmental evaluation of process design: distillation vs. hybrid distillation–pervaporation for methanol/tetrahydrofuran separation. *Appl Energy* 113: 565–575. https://www.sciencedirect.com/science/article/pii/S0306261913005473.

56 Genduso, G., Amelio, A., Luis, P. et al. (2014). Separation of methanol-tetrahydrofuran mixtures by heteroazeotropic distillation and pervaporation. *AIChE J* 60 (7): 2584–2595. https://aiche.onlinelibrary.wiley.com/doi/abs/10.1002/aic.14432.

57 Slater, C.S., Savelski, M., Hounsell, G. et al. (2012). Green design alternatives for isopropanol recovery in the celecoxib process. *Clean Techn Environ Policy* 14 (4): 687–698. https://doi.org/10.1007/s10098-011-0433-6.

58 Yi, C.-C., Shen, W., and Chien, I.-L. (2018). Design and control of an energy-efficient alternative process for the separation of methanol/toluene/water ternary azeotropic mixture. *Sep Purif Technol* 207: 489–497. http://www.sciencedirect.com/science/article/pii/S1383586618313753.

59 Koczka, K., Manczinger, J., Mizsey, P., and Fonyo, Z. (2007). Novel hybrid separation processes based on pervaporation for THF recovery. *Chem Eng Process Process Intensif* 46 (3): 239–246. https://www.sciencedirect.com/science/article/pii/S0255270106001644.

60 Slater, C.S., Savelski, M.J., Moroz, T.M., and Raymond, M.J. (2012). Pervaporation as a green drying process for tetrahydrofuran recovery in pharmaceutical synthesis. *Green Chem Lett Rev* 5 (1): 55–64. https://doi.org/10.1080/17518253.2011.578590.

61 Sereewatthanawut, I., Lim, F.W., Bhole, Y.S. et al. (2010). Demonstration of molecular purification in polar aprotic solvents by organic solvent nanofiltration. *Org Process Res Dev* 14 (3): 600–611. https://doi.org/10.1021/op100028p.

62 Shores, B.T., Sieg, P.E., Nicosia, A.T. et al. (2020). Design of a continuous solvent recovery system for end-to-end integrated continuous manufacturing of pharmaceuticals. *Org Process Res Dev* 24 (10): 1996–2003. https://doi.org/10.1021/acs.oprd.0c00092.

63 Lin, S.H. and Wang, C.S. (2004). Recovery of isopropyl alcohol from waste solvent of a semiconductor plant. *J Hazard Mater* 106 (2–3): 161–168. https://www.sciencedirect.com/science/article/pii/S0304389403004151.

64 Tsai, W.-T., Chang, C.-Y., Ho, C.-Y., and Chen, L.-Y. (2000). Adsorption properties and breakthrough model of 1,1-dichloro-1-fluoroethane on granular activated carbon and activated carbon fiber. *Sep Sci Technol* 35 (10): 1635–1650. https://doi.org/10.1081/SS-100100245.

65 Tsai, W.-T. (2002). A review of environmental hazards and adsorption recovery of cleaning solvent hydrochlorofluorocarbons (HCFCs). *J Loss Prev Process Ind* 15 (2): 147–157. http://www.sciencedirect.com/science/article/pii/S0950423001000237.

66 Hirayama, Y., Tanihara, N., Kusuki, Y. et al. (1999). Permeation properties to hydrocarbons, perfluorocarbons and chlorofluorocarbons of cross-linked membranes of polymethacrylates with poly(ethylene oxide) and perfluorononyl moieties. *J Membr Sci* 163 (2): 373–381. http://www.sciencedirect.com/science/article/pii/S0376738899001775.

67 Tsai, W.-T., Chen, H.-P., and Hsien, W.-Y. (2002). A review of uses, environmental hazards and recovery/recycle technologies of perfluorocarbons (PFCs) emissions from the semiconductor manufacturing processes. *J Loss Prev Process Ind* 15 (2): 65–75. http://www.sciencedirect.com/science/article/pii/S0950423001000675.

68 Hosseini, M. and Ameri, E. (2017). Pervaporation characteristics of a PDMS/PMHS membrane for removal of dimethyl sulfoxide from aqueous solutions. *Vacuum* 141: 288–295. http://www.sciencedirect.com/science/article/pii/S0042207X17300283.

69 Shi, G.M., Davood Abadi Farahani, M.H., Liu, J.Y., and Chung, T.-S. (2019). Separation of vegetable oil compounds and solvent recovery using commercial organic solvent nanofiltration membranes. *J Membr Sci* 588: 117202. https://www.sciencedirect.com/science/article/pii/S0376738818335944.

70 Cai, W., Sun, Y., Piao, X. et al. (2011). Solvent recovery from soybean oil/hexane miscella by PDMS composite membrane. *Chin J Chem Eng* 19 (4): 575–580. https://www.sciencedirect.com/science/article/pii/S1004954111600244.

71 Firman, L.R., Ochoa, N.A., Marchese, J., and Pagliero, C.L. (2013). Deacidification and solvent recovery of soybean oil by nanofiltration membranes. *J Membr Sci* 431: 187–196. https://www.sciencedirect.com/science/article/pii/S0376738813000057.

72 Haider, J., Qyyum, M.A., Kazmi, B. et al. (2019). Simulation study of biomethane liquefaction followed by biogas upgrading using an imidazolium-based cationic ionic liquid. *J Clean Prod* 231: 953–962. https://www.sciencedirect.com/science/article/pii/S0959652619317883.

73 Ahmed, S., Nelson, P.A., Gallagher, K.G., and Dees, D.W. (2016). Energy impact of cathode drying and solvent recovery during lithium-ion battery manufacturing. *J Power Sources* 322: 169–178. http://www.sciencedirect.com/science/article/pii/S037877531630475X.

74 Han, S., Raghuvanshi, K., and Abolhasani, M. (2020). Accelerated material-efficient investigation of switchable hydrophilicity solvents for energy-efficient solvent recovery. *ACS Sustain Chem Eng* 8 (8): 3347–3356. https://doi.org/10.1021/acssuschemeng.9b07304.

75 Shen, C., Tran, P., and Minh, L.P. (2018). Chemical waste management in the U.S. semiconductor industry. *Sustain For* 10 (5): 1545. http://www.mdpi.com/2071-1050/10/5/1545.

76 Welton, T. (2015). Solvents and sustainable chemistry. *Proc R Soc A Math Phys Eng Sci* 471 (2183): 20150502. https://royalsocietypublishing.org/doi/10.1098/rspa.2015.0502.

77 Seider, W.D. (2003). *Product and Process Design Principles Synthesis, Analysis, and Evaluation*, 2e, 251–253. New York, NY: Wiley.

78 Smith, R. (2005). *Chemical Process Design and Integration*, 2e, 211–217. New York, NY: Wiley.

79 Biegler, L.T. and Grossman, I.E.W.A. (1997). *Systematic Methods of Chemical Process Design*, 110–141. New Jersey: Prentice Hall Inc.

80 Box, M.J. (1965). A new method of constrained optimization and a comparison with other methods. *Comput J* 8 (1): 42–52. https://doi.org/10.1093/comjnl/8.1.42.

81 Amminudin, K.A., Smith, R., Thong, D.Y.-C., and Towler, G.P. (2001). Design and optimization of fully thermally coupled distillation columns: part 1: preliminary design and optimization methodology. *Chem Eng Res Des* 79 (7): 701–715. http://www.sciencedirect.com/science/article/pii/S0263876201721016.

82 Glinos, K.N., Nikolaides, I.P., and Malone, M.F. (1986). New complex column arrangements for ideal distillation. *Ind Eng Chem Process Des Dev* 25 (3): 694–699. https://doi.org/10.1021/i200034a016.

83 Jiménez, A., Ramírez, N., Castro, A., and Hernández, S. (2003). Design and energy performance of alternative schemes to the Petlyuk distillation system. *Chem Eng Res Des* 81 (5): 518–524. http://www.sciencedirect.com/science/article/pii/S0263876203723375.

84 Alatiqi, I.M. and Luyben, W.L. (1985). Alternative distillation configurations for separating ternary mixtures with small concentrations of intermediate in the feed. *Ind Eng Chem Process Des Dev* 24 (2): 500–506. https://doi.org/10.1021/i200029a047.

85 Agrawal, R. (1999). More operable fully thermally coupled distillation column configurations for multicomponent distillation. *Chem Eng Res Des* 77 (6): 543–553. http://www.sciencedirect.com/science/article/pii/S026387629971823X.

86 Fidkowski, Z. and Królikowski, L. (1987). Minimum energy requirements of thermally coupled distillation systems. *AIChE J* 33 (4): 643–653. https://doi.org/10.1002/aic.690330412.

87 Khan, M.S., Chaniago, Y.D., Getu, M., and Lee, M. (2014). Energy saving opportunities in integrated NGL/LNG schemes exploiting: thermal-coupling common-utilities and process knowledge. *Chem Eng Process Process Intensif* 82: 54–64. https://www.sciencedirect.com/science/article/pii/S0255270114001184.

88 Van Duc, L.N. and Lee, M. (2012). Dividing wall column structure design using response surface methodology. *Comput Chem Eng* 37: 119–124. http://www.sciencedirect.com/science/article/pii/S0098135411002092.

89 Long, N.V.D., Kwon, Y., and Lee, M. (2013). Design and optimization of thermally coupled distillation schemes for the trichlorosilane purification process. *Appl Therm Eng* 59 (1): 200–210. http://www.sciencedirect.com/science/article/pii/S1359431113003980.

90 Doble, M. and Kumar, A. (2005). *Chapter 14 – Semiconductor Waste Treatment* (eds. M. Doble and Kumar ABT-B of IE), 157–168. Burlington: Butterworth-Heinemann http://www.sciencedirect.com/science/article/pii/B9780750678384500154.

91 Hayden, J.G. and O'Connell, J.P. (1975). A generalized method for predicting second virial coefficients. *Ind Eng Chem Process Des Dev* 14 (3): 209–216. https://doi.org/10.1021/i260055a003.

92 Levy, S.G., Van Dongen, D.B., and Doherty, M.F. (1985). Design and synthesis of homogeneous azeotropic distillations. 2. Minimum reflux calculations for nonideal and azeotropic columns. *Ind Eng Chem Fundam* 24 (4): 463–474. https://doi.org/10.1021/i100020a011.

93 Thong, D.Y.-C., Castillo, F.J.L., and Towler, G.P. (2000). Distillation design and retrofit using stage-composition lines. *Chem Eng Sci* 55 (3): 625–640. http://www.sciencedirect.com/science/article/pii/S0009250998004965.

94 Bausa, J., Watzdorf, R.V., and Marquardt, W. (1998). Shortcut methods for nonideal multicomponent distillation: I. Simple columns. *AIChE J* 44 (10): 2181–2198. https://doi.org/10.1002/aic.690441008.

95 Rooks, R.E., Julka, V., Doherty, M.F., and Malone, M.F. (1998). Structure of distillation regions for multicomponent azeotropic mixtures. *AIChE J* 44 (6): 1382–1391. https://doi.org/10.1002/aic.690440616.

96 Thong, D.Y.-C. and Jobson, M. (2001). Multicomponent homogeneous azeotropic distillation 1. Assessing product feasibility. *Chem Eng Sci* 56 (14): 4369–4391. http://www.sciencedirect.com/science/article/pii/S0009250901000550.

97 Liu, G., Jobson, M., Smith, R., and Wahnschafft, O.M. (2004). Shortcut design method for columns separating azeotropic mixtures. *Ind Eng Chem Res* 43 (14): 3908–3923. https://doi.org/10.1021/ie030678y.

98 Schulze, P., Leschinsky, M., Seidel-Morgenstern, A., and Lorenz, H. (2019). Continuous separation of lignin from organosolv pulping liquors: combined lignin particle formation and solvent recovery. *Ind Eng Chem Res* 58 (9): 3797–3810. https://doi.org/10.1021/acs.iecr.8b04736.

99 Didaskalou, C., Buyuktiryaki, S., Kecili, R. et al. (2017). Valorisation of agricultural waste with an adsorption/nanofiltration hybrid process: from materials to sustainable process design. *Green Chem* 19 (13): 3116–3125. http://dx.doi.org/10.1039/C7GC00912G.

100 Ruthusree, S., Sundarrajan, S., and Ramakrishna, S. (2019). Progress and perspectives on ceramic membranes for solvent recovery. *Membranes (Basel)* 9 (10): 128. https://www.mdpi.com/2077-0375/9/10/128.

101 Rajawat, A., Subramanian, S., and Ramakrishna, S. (2020). Progress on silica pervaporation membranes in solvent dehydration and solvent recovery processes. *Materials (Basel)* 13 (15): 3354. https://www.mdpi.com/1996-1944/13/15/3354.

102 Mahdi, T., Ahmad, A., Nasef, M.M., and Ripin, A. (2015). State-of-the-art technologies for separation of azeotropic mixtures. *Sep Purif Rev* 44 (4): 308–330. https://doi.org/10.1080/15422119.2014.963607.

103 Saha, K., Uma, R., Sikder, J. et al. (2017). Membranes as a tool to support biorefineries: applications in enzymatic hydrolysis, fermentation and dehydration for bioethanol production. *Renew Sust Energ Rev* 74: 873–890. http://www.sciencedirect.com/science/article/pii/S1364032117303301.

104 Singh, A. and Rangaiah, G.P. (2017). Review of technological advances in bioethanol recovery and dehydration. *Ind Eng Chem Res* 56 (18): 5147–5163. https://doi.org/10.1021/acs.iecr.7b00273.

105 Takht Ravanchi, M., Kaghazchi, T., and Kargari, A. (2009). Application of membrane separation processes in petrochemical industry: a review. *Desalination* 235 (1): 199–244. http://www.sciencedirect.com/science/article/pii/S0011916408005961.

106 McGinness, C.A., Slater, C.S., and Savelski, M.J. (2008). Pervaporation study for the dehydration of tetrahydrofuran-water mixtures by polymeric and ceramic membranes. *J Environ Sci Health Part A* 43 (14): 1673–1684. https://doi.org/10.1080/10934520802330107.

107 Zhang, Q.G., Liu, Q.L., Chen, Y., and Chen, J.H. (2007). Dehydration of isopropanol by novel poly(vinyl alcohol)—silicone hybrid membranes. *Ind Eng Chem Res* 46 (3): 913–920. https://doi.org/10.1021/ie0609719.

108 Klinov, A.V., Akberov, R.R., Fazlyev, A.R., and Farakhov, M.I. (2017). Experimental investigation and modeling through using the solution-diffusion concept of pervaporation dehydration of ethanol and isopropanol by ceramic membranes HybSi. *J Membr Sci* 524: 321–333. http://www.sciencedirect.com/science/article/pii/S0376738816310079.

109 Shirazi, Y., Ghadimi, A., and Mohammadi, T. (2012). Recovery of alcohols from water using polydimethylsiloxane–silica nanocomposite membranes: characterization and pervaporation performance. *J Appl Polym Sci* 124 (4): 2871–2882. https://doi.org/10.1002/app.35313.

110 Cui, Y. and Chung, T.-S. (2018). Pharmaceutical concentration using organic solvent forward osmosis for solvent recovery. *Nat Commun* 9 (1): 1426. https://doi.org/10.1038/s41467-018-03612-2.

111 Huang, L., Bui, N.-N., Meyering, M.T. et al. (2013). Novel hydrophilic nylon 6,6 microfiltration membrane supported thin film composite membranes for engineered osmosis. *J Membr Sci* 437: 141–149. http://www.sciencedirect.com/science/article/pii/S0376738813000835.

112 Shen, L., Zhang, X., Zuo, J., and Wang, Y. (2017). Performance enhancement of TFC FO membranes with polyethyleneimine modification and post-treatment. *J Membr Sci* 534: 46–58. http://www.sciencedirect.com/science/article/pii/S0376738817302612.

113 Valladares Linares, R., Li, Z., Sarp, S. et al. (2014). Forward osmosis niches in seawater desalination and wastewater reuse. *Water Res* 66: 122–139. http://www.sciencedirect.com/science/article/pii/S0043135414005880.

114 Valladares Linares, R., Li, Z., Yangali-Quintanilla, V. et al. (2016). Life cycle cost of a hybrid forward osmosis – low pressure reverse osmosis system for seawater desalination and wastewater recovery. *Water Res* 88: 225–234. http://www.sciencedirect.com/science/article/pii/S0043135415302815.

115 Li, Z.-Y., Yangali-Quintanilla, V., Valladares-Linares, R. et al. (2012). Flux patterns and membrane fouling propensity during desalination of seawater by forward osmosis. *Water Res* 46 (1): 195–204. http://www.sciencedirect.com/science/article/pii/S004313541100649X.

116 Razali, M., Didaskalou, C., Kim, J.F. et al. (2017). Exploring and exploiting the effect of solvent treatment in membrane separations. *ACS Appl Mater Interfaces* 9 (12): 11279–11289. https://doi.org/10.1021/acsami.7b01879.

117 Kim, J.F., Szekely, G., Schaepertoens, M. et al. (2014). In situ solvent recovery by organic solvent nanofiltration. *ACS Sustain Chem Eng* 2 (10): 2371–2379. https://doi.org/10.1021/sc5004083.

118 Voros, V., Drioli, E., Fonte, C., and Szekely, G. (2019). Process intensification via continuous and simultaneous isolation of antioxidants: an upcycling approach for olive leaf waste. *ACS Sustain Chem Eng* 7 (22): 18444–18452. https://doi.org/10.1021/acssuschemeng.9b04245.

119 Schaepertoens, M., Didaskalou, C., Kim, J.F. et al. (2016). Solvent recycle with imperfect membranes: a semi-continuous workaround for diafiltration. *J Membr Sci* 514: 646–558. https://www.sciencedirect.com/science/article/pii/S0376738816302940.

120 Kim, J.F., Székely, G., Valtcheva, I.B., and Livingston, A.G. (2014). Increasing the sustainability of membrane processes through cascade approach and solvent recovery – pharmaceutical purification case study. *Green Chem* 16 (1): 133–145. http://dx.doi.org/10.1039/C3GC41402G.

121 Fodi, T., Didaskalou, C., Kupai, J. et al. (2017). Nanofiltration-enabled in situ solvent and reagent recycle for sustainable continuous-flow synthesis. *ChemSusChem* 10 (17): 3435–3444. https://doi.org/10.1002/cssc.201701120.

122 Hu, J., Kim, C., Halasz, P. et al. (2021). Artificial intelligence for performance prediction of organic solvent nanofiltration membranes. *J Membr Sci* 619: 118513. https://www.sciencedirect.com/science/article/pii/S0376738820310905.

14

Toward Green Extraction Processes

Marinela Nutrizio[1], Farid Chemat[2], Rattana Muangrat[3], Phisit Seesuriyachan[3], Yuthana Phimolsiripol[3], Francesco Donsi[4], and Anet Režek Jambrak[1]

[1] *Faculty of Food Technology and Biotechnology, University of Zagreb, Zagreb, Croatia*
[2] *GREEN Extraction Team, INRAE, Avignon University, Avignon, France*
[3] *Faculty of Agro-Industry, Chiang Mai University, Chiang Mai, Thailand*
[4] *Department of Industrial Engineering, University of Salerno, Fisciano, Italy*

14.1 Introduction

Sustainability has gained much attention with Agenda 2030 issued by the United Nations in 2015. The idea is to reach the sustainable wealth-being and coexistence of humans, technology, and environment through 17 sustainable development goals (SDGs). In the last 10 years, more than 8500 research papers were published about sustainable extraction processes (Scopus search). The objective of extraction is to recover valuable soluble components from raw materials. It is well known that conventional thermal extractions, such as Soxhlet extraction or maceration, are used in extraction processes. However, many research studies and review papers are dealing with nonthermal and/or advanced thermal processing in extractions. Energy consumption is very low in the nonthermal processing of food as compared with thermal processing. The food quality and safety can be assured using nonthermal technologies. To meet the market demand for safe, functional, and quality food products, various companies and research institutes are extensively involved in the innovational programs to develop advanced and cost-effective nonthermal and advanced processing technologies. The nonthermal processing market for food, based on technology, is divided into high-pressure processing, pulsed electric field, ultrasonic, cold plasma, irradiation, and others. The high-pressure processing segment is projected to grow at the highest compound annual growth rate among all nonthermal processing technologies from 2017 to 2022 [1]. It is a consumer-driven request to preserve the freshness of food products as well as aids in extending their shelf life, as well as their demand for natural, fresh, and minimally processed foods, as no preservatives or additives are added to the products. Due to these factors, the market is projected to grow at a significant rate in the future. Several

Sustainable Separation Engineering: Materials, Techniques and Process Development, Volume 2, First Edition. Edited by Gyorgy Szekely and Dan Zhao.
© 2022 John Wiley & Sons Ltd. Published 2022 by John Wiley & Sons Ltd.

research studies reported the usage of nonthermal processing in ultrasound-assisted extraction (UAE) from plants [2, 3], fruits [4] and waste materials (by-products) [5], high-pressure extraction [6], cold plasma extraction [7, 8], pulsed electric field [9], and other nonthermal technologies. It is also important to mention advanced thermal processing extraction such as microwave extraction [10, 11] and ohmic heating [12]. For all above-mentioned processing techniques, there is mentioning that they can be considered as sustainable, eco-friendly, low emission, lower impact on the environment, fast, clean, and green extraction processing techniques. However, there is no concrete overview and recommendation in what is needed to claim that one process for the extraction of bioactive compounds, nutraceuticals, fibers, and other natural compounds can be considered as green sustainable processes. There is concern about energy consumption, environmental impact, social impact, and economical consideration of novel proposed techniques in different processes.

The conventional approach of assessing a chemical process through the measurement of reaction efficiencies in terms of yield gives a good indication of process economics but does not present a likewise good indication of the process sustainability [13]. A different approach can be considered, such as computerized solvent selection using Conductor-like Screening Model for Real Solvents (COSMO-RS) or HANSEN software [14]. Nowadays, green chemistry metrics have been developed for assessment of sustainability, which can be applied to green extraction processes. Life cycle assessment (LCA) is a more expensive and time-consuming method that can be implemented for sustainability determination [15, 16]. Different types of green solvents can be used in green sustainable extraction processes such as limonene, pinene, environmentally derived, eco-friendly solvents. Also, there are natural-based deep eutectic solvents (NaDES) that are specially designed to be used in extraction processes [17]. Also, an important parameter is solvent recycling for multiple use and processing with less waste [15].

Therefore, this chapter aims to provide insight into the approach for solvent selection, giving an overview of sustainable green parameters in determining the sustainability of extraction processes, and providing recommendations on the approach to be followed for claiming that one intensified process of extraction could be considered as green. This can be a good way in achieving SDGs regarding extraction processes. In this chapter, nonthermal and advanced thermal processing extraction techniques are overviewed in terms of sustainability. Detailed analysis of past and present literature confirms explicitly the usefulness of these green extraction techniques and solvents. It is hoped that this chapter will widen the scope of laboratory and commercial success for the potential applications of green extraction as sustainable techniques for producing food and natural extracts and products. Several case studies are given to justify the mentioned aim, i.e. green extraction processes based on high-pressure homogenization (HPH), as a technique to cause complete cell disruption, significantly enhancing the release in water as extraction medium of both soluble compounds (e.g. proteins, polysaccharides) and water-insoluble molecules (e.g. lycopene, polyphenols), as recently shown for tomato peels [18]. Another example is the extraction from spent coffee grounds [19, 20] and microalgae [21]. Different extraction techniques such as sustainable green extractions including supercritical carbon dioxide (CO_2) extraction, subcritical solvent extraction, ultrasonication, and HPH for various materials are given.

14.2 Green Extraction Processes

14.2.1 Extractions and Sustainability

Nowadays, green chemistry has become the foundation of many chemical processes, driving the development of completely novel products and processes, rather than pursuing the improvement of existing ones [15]. In the food industry, green food processing is generally considered to be at the basis of the development of innovative processes, which specifically enables (i) the reduction of resource consumption, and in particular energy and water, (ii) the recycling of secondary products through the integration in a wider biorefinery approach, and (iii) the production of safer and higher quality products [11].

Green extraction processes were introduced in the 2000s in research laboratories [22, 23]. There are many reviews and research that are proposing and reporting improvement in advanced thermal and nonthermal extractions. The commonly used thermal methods used such as Soxhlet extraction was even improved, i.e. in combination with ultrasound [24], to accelerate the extraction process. The idea is to use green solvents, reduce extraction time, improve existing processes, invent some new process, reduce solvent consumption, use low emission techniques and use less energy, and consequently, to impact less on the environment (Figure 14.1). This approach is driven by Agenda 2030, issued by the United Nations and 17 SDGs. The idea is to set processes and procedures to be sustainable in each life

Figure 14.1 A great example is given in overview in the JRC report "*Mapping the role of Raw Materials in Sustainable Development Goals. A preliminary analysis of links, monitoring indicators and related policy initiatives*" [25].

point. Sustainable development and sustainability is defined with responsible action toward the economy, environment, and society. Efforts of industry, governments, producers, scientists, and every human being are to improve and act according to 17 SDGs. Green processing can be defined also in line with Agenda 2030 and SDGs.

A great example is given in overview by Mancini et al. [25] where there is direct impact of extractions with a positive contribution to SDG 6, 8, 9, 13, and 15, and indirect impact to SDGs 1, 2, 3, 4, 7, and 17; adverse impact to SDGs 3, 5, 6, 8, 11, 13, 14, and 15, and indirect impact to SDGs 1, 2, 7, 10, and 16 [25]. Mancini et al. [25] defined extractions for the industrial activities of mining and forestry and that approach could be considered in the separation of compounds based on their partitioning in nonmiscible liquid and liquid/solid phases. The approach is realized as needed as a root for green extraction procedures. There is necessity of this green approach to industry and there are many applications and improvements in existing extraction processes.

14.2.2 Green Principles

Anastas and Warner introduced 12 principles of green chemistry in 1998 (listed in Figure 14.2) [26]. Among those 12, 6 of those are important for green extractions. These principles should be viewed for industry and scientists as a direction to establish an innovative and green label, zero waste, clean processing, the zero-emission standard for modern conventional advanced thermal, or nonthermal-assisted green extraction method.

Six principles are of great importance for extraction and separation of compounds. Principle 1 is dealing with innovation by selection of varieties and use of renewable plant resources. The idea is to select plant resources, without pesticides residues and metals in final products [27]. Principle 2 is about use of alternative solvents and principally water or agri-solvents. The idea is to use solvent selection tools by applying modern computer methodologies such as softwares COSMO-RS and HANSEN [28, 29]. Principle 3 is about reducing energy consumption by energy recovery and using innovative technologies. The consideration should be focused toward usage of nonthermal processing technologies such as power UAE [30] and low power ultrasound, high-pressure processing [31], supercritical fluids extraction [32], instantaneous controlled pressure drop [33], high-voltage electrical discharge [34], pulsed electric field [8], accelerated solvent extraction [35], cavitation-based extraction methods include already mentioned UAE, negative pressure cavitation extraction, and hydrodynamic cavitation extraction. Another approach is hot water extraction (HWE) (subcritical water extraction) [36]. The most commonly used method is enzyme-assisted extractions and there is also a great green and zero-energy consuming procedure based on solar energy using solar hydrodistillation. Also, there are innovative advanced thermal processing extraction techniques such as microwave-assisted extraction and ohmic heating, but there should be more combinations of advanced thermal and nonthermal extraction techniques to use all their advantages for efficient green sustainable extraction. The mechanism of action, advantages of each technique, disadvantages, and sustainable aspects are discussed is several review papers [3, 37–39].

Principle 4 is about production of coproducts instead of waste to include the bio- and agro-refining industry: use of waste (by-products) products from the agri-food industry and extraction of bioactive compounds [36, 40, 41]. There is a huge amount of by-product

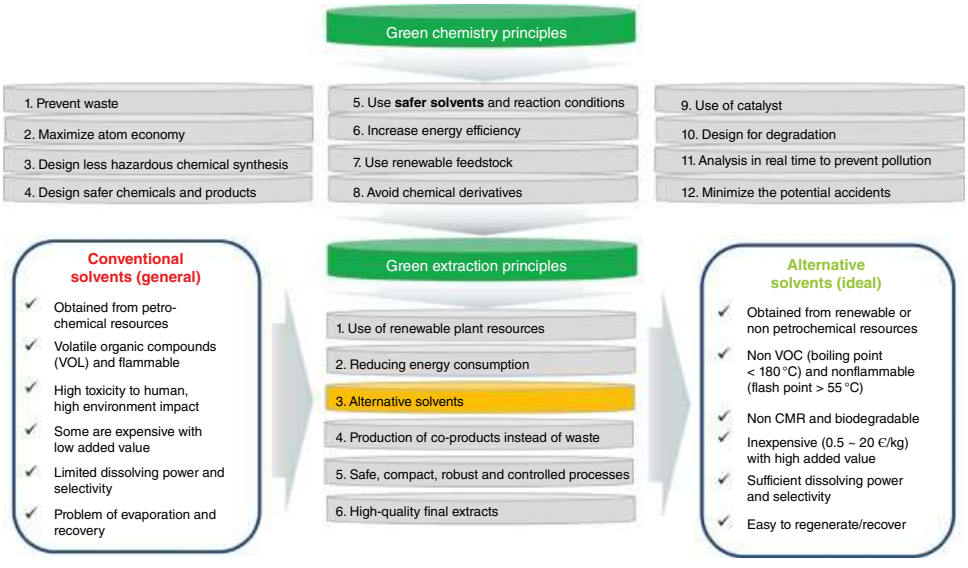

Figure 14.2 Development from conventional to alternative solvents based on green principles.

(waste) in agri-food industries that can be used to obtain bioactive compounds [42] by nonthermal green extraction; to obtain pectin [43] from residues; to obtain pigments and antioxidants, and to use extracted essential oils and biopesticides [44–46], or to obtain fibers [47] by green extraction methods. Principle 5 is how to reduce unit operations and favor safe, robust, and controlled processes: there are new improved equipment units, many producers of extraction technique equipment. There should be also more reporting of energy consumption, carbon emission of novel equipment with emphasized advantages over previously used equipment. In the future, there will also be smarter sensors used for monitoring extraction processes, renewable energy usage (sun), use of artificial intelligence, with the aim of process control and monitoring [34]. There is also a strong implementation need of the elements of Industry 4.0 in processing, such as machine learning, big data processing, artificial intelligence, and additive technologies. Industry 4.0 is a strategic initiative that supports development of the industrial sector (fourth industrial revolution) with the main idea to exploit the potential of new technologies and concepts [48]. In currently ongoing project GREENVOLTEX, funded by Croatian Science Foundation (GREENVOLTEX), there is the use of additive technologies (3D printing) to design, optimize, and produce edible gels with incorporated extracted bioactive compounds from Mediterranean herbs. There is also research aim to develop an encapsulated product with extracts that are going to be used in food products (i.e. olive oil enriched with microcapsules with extracts from rosemary, olive leaves extract, sage, oregano, and thyme) with the aim of a fast or slow dissolution of capsules; microcapsules or nanocapsules are going to be used in nonalcoholic beverages to have the rapid dissolution of capsules in beverages (data not shown, in preparation for publishing).

Principle 6 has an aim to provide a non-denatured and biodegradable extract without contaminants. This is the basis of modern sustainable processes with respect to REACH (Registration, Evaluation, Authorization and Restriction of Chemicals) directive concerning chemical substances, either as such, or entering into products or manufactured objects, while Integrated Pollution Prevention Control is aimed at reducing the contribution of the industry to non-sustainable development. There is the need to obtain extracts, in which compounds will maintain their antioxidant, bioactive properties, and that the extract will be efficiently solubilized in the solvent (predicted by computer softwares) and biodegradable. When using different techniques (where there are electrodes, tips, probes, wires, plates ultrasound, pulsed electric fields, or high-voltage electrical discharge – plasma), it is important to have in mind abrasion of electrodes, probes tips, and the residues of those materials in extracts that we would like to obtain. There are not so many research articles that are reporting this potential obstacle and hazard, but this should be taken care of with percussing. Some research articles are reporting the abrasion of electrodes and metal residues after nonthermal processing [27, 34, 49].

In order to say that we have green processing, we need to assure lower CO_2 emission than conventional extraction processing [5, 50, 51]. There is also a need to have a complete overview of LCA [52] of complete processes of obtaining extracts by the green process. There are research articles that are reporting the impact of nonthermal processing on the environment [53–55] and circular economy strategies [25, 56]. The aim of applying green processing should be in the focus of Agenda 2030 and in line with SDGs.

14.2.3 Evaluating Sustainability in Green Extraction Processes

The sustainability of novel food production processes, including extractions, especially in the phase of translation from lab-scale to industrial scale, should be carefully assessed, taking into account the wider picture of the overall impact on the sustainability. As a general principle, all the resources involved in the production should be used at a sustainable rate, which means that they can be replaced naturally as they are used, and, at the same time, waste generation should take place at a slower pace than its remediation, when considering its capability to be readily assimilated by the natural environment [57, 58].

Within this picture, it must be remarked that, despite many scientific articles claim that the proposed alternatives to existing processes represent a greener approach [59], based on their compliance with one or more of the sustainability principles, very often, when assessed with a larger production context, taking into account the factors related to scalability, economics, and regulatory constraints, they turn out to be less sustainable [60]. Therefore, a more holistic approach is needed for the development of novel technologies of interest for the food industry, which should be multidisciplinary and possibly start already at the technology development stage, evaluating the inherent interconnections with sustainability [61].

In particular, the integration of green chemistry into a biorefinery, coupled with the use of low environmental impact technologies, is considered to be a suitable route toward the development of truly sustainable green extraction processes [62]. Therefore, it is clear that extraction processes should minimize the resource demand, especially for energy, safer processes should be preferred, the use of hazardous chemicals should be avoided, with a preference toward totally environmentally benign processes, including also the required purification step, the residues of extraction should be kept at a minimum, and possibly be also easily recyclable.

The question is, therefore, within this holistic approach, which metrics are suitable for the evaluation of process sustainability, with specific reference to green extraction processes. The conventional approach of assessing a chemical process through the measurement of reaction efficiencies in terms of yield gives a good indication of process economics but does not present a likewise good indication of the process sustainability [13]. Nowadays, several green chemistry metrics have been developed to provide a holistic assessment of sustainability, which can be applied also to green extraction processes. They are summarized in Table 14.1.

Mass-efficiency metrics are considered to be at the foundation of the green process design because they pertain to 5 of the 12 principles summarized in the previous sections (numbers 1, 2, 5, 8, and 9) of green chemistry [58]. The different mass-efficiency metrics are presented in detail, with advantages and disadvantages, especially when referred to extraction processes, reported in Table 14.1. They can be classified in metrics related to mass efficiency (theoretical, such as for Atom Economy), or real and depending on process optimization, such as (Reaction Mass Efficiency, Mass Productivity, Effective Mass Yield, and Carbon Economy) and in metrics conceptually equivalent to the E-factor.

Atom Economy describes the inherent by-product formation in a chemical reaction, through molecular weights and stoichiometric ratios. Atom Economy-equivalent indicators take into account the mass of the product, in comparison with the total mass of

Table 14.1 Metrics of interest for green extraction processes.

Metric indicator	Descriptor	Purpose and scope	Limitations	References
Mass-efficiency metrics				
Atom Economy	Molecular weight of product/Sum of molecular weights of starting materials	Simple calculation based on the stoichiometry of the reaction, without taking into account solvents, reagents, reaction yield, and reactant molar excess. Theoretical definition that can be applied without the need for experimentation. The solvents are excluded from calculations	Not suitable for extraction processes but processes including chemical reactions, and applied to individual process steps	[70]
Reaction Mass Efficiency	Mass of product/Total mass of reactants	Useful to identify specific parts of an industrial process that contribute the most negatively/positively to the process, and to help to reduce waste. It provides also an economic indicator of the process	Not sufficient to measure the greenness and sustainability of processes	[13]
Mass Productivity	Mass of product/Total mass (including solvents)	The reagents here may include any used reactant, solvent, or catalyst. When most reagents are benign, effective mass efficiency can be greater than 100%. It provides also an economic indicator of the process	Very general definition, which does not take into account the wastes and greenness of the processes	[58]
Effective Mass Yield	Mass of product/Mass of non-benign reagents	Useful to assess the mass of the product as compared with the mass of hazardous and toxic reagents, ignoring benign solvents (e.g. water). Specifically suitable for extraction processes	Problem of the definition of non-benign reagent and levels of acceptable toxicology	[71]

Carbon Economy	Mass of carbon in the product/ Total mass of carbon in the reactants	Simple calculation, useful to estimate the percentage of carbon in the reagents used in organic synthesis that remain in the final desired product. Specifically suggested for the evaluation of the greenness of organic synthesis based solely on carbon accounting	Not suitable for extraction processes	[13]
E-factor	Mass waste/Mass product	It can easily be applied to a multistep process for its holistic assessment. Suitable for extraction processes. Lower E-factors can be correlated with reduced manufacturing costs. Water and solvents can be accounted for in the waste	Not sufficient to measure the greenness and sustainability of processes	[58]
Mass Intensity	Total mass in process (excluding H_2O)/Mass of product. [MI = E-factor + 1]	Useful for accounting reaction efficiency, stoichiometry, amount of solvents, all reagents and auxiliary substances used in synthesis. An ideal synthesis, in which the total mass of input is equal to the mass of the product, has a MI = 1. Easily adapted to several processes	Mass intensities not directly additive in multistep processes. Not sufficient to measure the greenness and sustainability of processes	[13]
Process Mass Intensity	Total mass in process (including H_2O)/Mass of product	Useful for assessing the reagents, solvents, and stoichiometry for the synthesis of a given product. Adopted for pharmaceutical productions, with large water consumptions	The impact of the waste produced from the process is not accounted for. Focus on reducing the costs of the raw materials input rather than waste production	[72]
Waste Water Intensity	Mass of process water/Mass of product	Focused on water use, it is especially suitable for integrated, multistep processes	Not specifically suitable for extraction processes	[58]
Solvent Intensity	Mass of solvents/Mass of product	Focused on water use, it is especially suitable for extraction processes	It does not take into account process economics and solvent unfriendliness	[58]

(*Continued*)

Table 14.1 (Continued)

Metric indicator	Descriptor	Purpose and scope	Limitations	References
Material Recovery Parameter	Mass of recovered or recycled reagents/Total mass of reagents	Introduction of the concepts of recovery and recycle of products used during the reaction including purification and workup. If all solvents, catalysts, and non-product reagents are recovered, Material Recovery Parameter = 1. It is of interest to the pharmaceutical industry	It neglects process yields and economic considerations	[73]
C-factor	Total mass of CO_2 emitted/Mass of product	Useful for comparing biomass-based vs. fossil resource-based processes	Less useful for extraction processes	[74]
Energy-efficiency metrics				
Cumulative Energy Demand	Total amount of primary energy potential used during the production cycle	It correlates well with LCA. A large fraction of the environmental impacts of extraction processes can be linked to energy and resource use	It is a purely resource-oriented method	[75]
Global Warming Potential, also known as Carbon Footprint	CO_2 generated in the burning of fuels and the manufacture of chemical products	It is calculated in CO_2 equivalents, meaning that the greenhouse potential of emission is given in relation to CO_2. Useful for assessing the use of biomass-derived and renewable solvents	Strong variations between the different data sources	[75]
Environmental-impact metrics				
Q-factor	E-factor multiplied by an environmental quotient	It takes into account the unfriendliness of reagents and solvents. It may derive from a score sheet based on safety, health, and environment (SHE) hazards	Arbitrariness of the environmental quotient	[58]

Life cycle assessment (LCA)	Environmental impact of a product, in all stages of its life, from raw materials acquisition through production and use to end-of-life treatment and disposal or recycling	Methodology useful for assessing environmental impacts associated with all the stages of the life cycle of the process (but also suitable for a commercial product, or a service). Adding a life-cycle perspective to green extraction processes may enlarge their scope and enhances their environmental benefits	Not easy to use and based on arbitrary parameters	[58]
Eco-Footprint	Simplified LCA, based on carbon footprint, water footprint, aqueous waste valorization, used solvents valorization, energy consumption	Combination of manufacturing footprint and an eco-design to cover the supply chain from the supplier's gate to the product leaving the plant	Not easy to use and based on arbitrary parameters	[65]
"Green" Motion	Simplified LCA, based on raw material, solvents, hazard/toxicity of reagents, reaction yields, process energy requirements, hazard/toxicity of products, waste generation	Assessment of the health, safety, and environmental impacts of the different manufacturing industries. Suitable for extraction processes	Based on arbitrary parameters	[66]
Sustainability metrics				
Eco-efficiency Analysis	Quantification of the sustainability of products and processes over the whole life cycle (cradle-to-grave) taking into account economic and ecological aspects (Raw materials consumption, Energy consumption, Resulting emissions, Toxicity potential, Abuse and risk potential, Land use)	Combination of economic and ecological aspects, which are given equal weights	Societal impact is still neglected, and must be separately assessed	[76]
GREENSCOPE	Simplified LCA, based on environment, energy, efficiency, and economics	Combination of mass and energy efficiency, economic and environmental indicators. Useful for sustainability assessment to assist in the design of chemical processes	Not specifically suitable for extraction processes	[77]

starting materials. Both Atom Economy and E-factor and equivalent indicators take instead into account the mass of waste produced during processing per mass of the product, with the possibility of accounting also for water and solvents in the waste stream. These metrics are easy to use, measure, and implement, but they suffer from the major disadvantage that all types of wastes have the same impact [58].

Both Atom Economy and E-factor, which describe the theoretical and real waste production rates of the chemical reactions involved, can be related to the economic effectiveness of processes (indicating the operating costs of the required raw materials), and therefore they provide an indirect indication of long-term sustainability, which can be applied to green chemistry. The fact that an economic component is not implicitly included in the green chemistry approach, has been considered as a major disadvantage by industry, which, therefore, adopted preferentially the more inclusive concept of sustainable development [58].

Energy-efficiency metrics have been developed to cope with energy-intensive processes, as the extraction process from plant matrices frequently can be. However, these metrics, also described in Table 14.1, are resource-oriented and therefore, limited in their outreach, especially when large waste streams are generated.

However, most green chemistry metrics do not take into adequate account the upstream and downstream processes, which are often determining the success of a sustainable process. More specialized metrics have been, hence, developed to integrate economic and environmental factors [63, 64]. A more holistic approach is represented by environmental-impact metrics, based on LCA approaches, which are characterized by a complex evaluation of all the stages of the production. Data acquired from secondary sources, such as databases, literature references, and simulations, are required to assess the entire life of the products and raw materials.

They become, however, increasingly difficult to use, as more details are added, and inherently uncertain as arbitrary parameters are needed, especially when including emerging technologies that are not supported by sufficient data, making the assessments increasingly complicated and costly. Moreover, if lab-scale reactions are not adequately optimized, these metrics may suggest exceedingly poor ratings [15].

Simplified approaches have been adopted by different industries (e.g. pharmaceutics, cosmetics) to better fit their processes [65, 66]. They are based on narrowing the LCA boundaries, such as in the gate-to-gate or cradle-to-gate approaches [67], to enable the assessment also of processes under development, as all the required data for a full LCA become available only after the product reaches the market. LCAs, or simplified LCAs, can also help in solvent selection, to pursue an optimal balance between production, application, and disposal, while considering the environmental impact [68].

To take into account the environmental aspects, yet maintaining a simple metric indicator, the E-factor was modified through a so-called environmental quotient to give the Q-factor, which accounts for the unfriendliness of reagents and solvents [58], enabling a more exhaustive comparison of different process alternatives.

Nonetheless, sustainability is a wider anthropocentric concept, which is based on human judgment of the balance among different social, environmental, and economic factors [69]. If a technology is not perceived to have potential societal benefits, it is difficult that it can be considered sustainable. However, societal benefits are hard to quantify, as they are very subjective and may significantly vary with company policy, market segment involved, and

the geographical location [58]. For example, in a hypothetical desert country, where agricultural land is scarce but fossil resources are abundant, it is likely that importing bio-based solvents for extractions from other countries at a high cost and with the burden of high CO_2 emissions of transportation, or diverting significant parts of the limited agricultural capacity from food production to bio-based solvent production for the extraction, reducing food supplies for the population, is less sustainable than using fossil-based solvent from the local resources. In general, it is true that avoiding the use of toxic reactants and preventing any safety hazard process operation will contribute to achieving important societal objectives, related to the protection of workers and consumers. Furthermore, the inclusion in the metrics of environmental-impact factors implicitly contributes to the pursue of societal benefits. Some metrics have, therefore, tried to pursue wider-scope process assessment, as described in Table 14.1.

14.2.4 Energy Optimization

Another important issue to be considered in the development of green extraction processes is energy optimization. Energy-efficient technologies must be employed to extract the compounds of interest from biomass. For example, the use of supercritical CO_2, which is recognized as a green solvent because it is safe (nonflammable and nontoxic), it is available as an industrial by-product (e.g. from the combustion of fossil resources such as oil, natural gas, or coal) and does not produce solvent residue, has substantial energy requirements, which may significantly reduce any environmental benefits of the replacement of organic solvents. As a consequence, the use of supercritical CO_2 may be best suited to locations where renewable energy sources are available [62].

Another example, where energy considerations are discriminant in process adoption, is represented by microwave- and UAE processes, which exhibit great potential as greener and energy-efficient alternatives to conventional extraction processes at laboratory scale. However, in some processes, microwaves are used to selectively heating the solid matrix (e.g. to evaporate the moisture content of plant cells and promote extraction processes). In these cases, for example, if microwaves are coupled to the use of ethanol, which is highly microwave-absorbing, the process might be not energetically convenient at large scale, whereas the use of supercritical water, which is almost completely transparent to microwaves, is more suitable. Similarly, despite on a certain scale, neither ultrasounds nor supercritical CO_2 might be convenient, their combination has been reported to result in significant improvement in extraction rate and yields, potentially improving both energy efficiency and economics of supercritical processes [62].

14.2.5 Economic Considerations

As stated by Welton, a truly sustainable chemical product should be supplied at a price that makes it accessible by its users while remaining commercially viable for its producers [78]. The impact of solvent cost on process competitiveness represents, in fact, a major concern, together with application-specific technical factors, such as performance, in the selection of alternative green solvents [79]. While the vast majority of scientific studies have addressed the performance criteria, industrial uptake is much

more dependent on the economic viability of solvent, along with ancillary considerations related to its availability, disposal, as well as corrosiveness, thermal stability, or toxicity [15]. Only a full process techno-economic model or LCA can contribute to estimating the cost of bulk-scale production of chemicals, including the use of novel solvents [80, 81].

The evolution from a traditional linear economy to a circular economy adds complexity to the picture of sustainable production [82]. In particular, recovery and regeneration of resources represents a key element of the design of green extraction processes, which should include the economic burden of recirculation for the recovery and reuse of materials/solvents, to minimize the impact on ecology and health [83]. In a bigger picture, however, the circular economy within the European Union is expected to contribute to saving over $340 billion in material costs by recycling resources and $520 billion annually with the implementation of green economy processes [84].

It must be added that economic analysis of process viability is also significantly dependent on geographical location. The cost of raw materials, equipment, and labor can vary tremendously from location to location, which should be taken into account when comparing different green technologies and green solvents [58].

14.3 Green Solvents: Selection and Application in Extractions

14.3.1 Development of Green Solvents

Solvents are extensively used in various industries as reaction media, as diluents or additives, in synthesis and extraction, or for cleaning of equipment. It is impossible to imagine food, cosmetic, pharmaceutical, or biofuel industries without solvent usage. Therefore, solvents can play a key role in the impact on health, safety, and environment [85].

With nowadays growing consumer demands and growing production, both society and industries created clear needs for sustainable production and high-quality products. At the same time, environmental directives and legislation have addressed the reduction of solvent emissions (Clean Air Act of 1990 and the European Union Solvents Emission Directive 1999/13/EC) or the reduction of the use of potentially harmful or environmentally damaging chemical substances (REACH) [86].

The development of alternative (green) solvents first started with principles of green chemistry [26] where the use of safer solvents and reaction conditions was introduced. Moreover, the green extraction principles were presented by Chemat et al. [22] to replace organic solvents with green solvents, obtained from renewable (non-petrochemical) resources produced from biomasses such as wood, starch, vegetable oils, or fruits at reasonable prices. The ideal alternative solvents suitable for green chemistry are nonvolatile organic compounds, have a high solvent power, low toxicity, low environmental impact, and are being easily biodegradable (Figure 14.2). For sure, there is no perfect green solvent that can satisfy all abovementioned requirements and apply to all situations and reactions. Therefore, the decision for the most favorable solvent in each reaction is a challenge for researchers to overcome for each experiment [87].

14.3.2 An Overview of Green Solvents and Their Usage

Water is widely used as a solvent since it is the cheapest and most available solvent for green extractions. Its polar nature is suitable for the extraction of natural water-soluble products such as proteins, sugars, and different organic and inorganic substances. The only problem with water is that it is a highly evaporative solvent and consequently, has high energy consumption and CO_2 emissions and finally not unfavorable environmental impact. It is recommended to either limit the evaporation during extractions with water or to find different ways to concentrate or separate extracts from aqueous solutions. The innovative promising application of water as green solvent is pressurized HWE or subcritical water. The subcritical region for water is between boiling point (100 °C) and critical point (374 °C) and was shown to be efficient in the extraction of both polar and moderately polar compounds. The polarity changes mostly depend on the temperature, rather than the pressure. For example, subcritical water at 250 °C and a pressure just over 4 MPa have a value of the dielectric constant of 27, which is close to ethanol and is, therefore, suitable for extraction of low-polarity compounds. Accordingly, this is considered an efficient, economical, and promising method for resource recovery without significant influence to the quality of the extracted products [22, 87, 88]. Additionally, some cosolvents, such as hydrotropes or surfactants, can significantly adjust water properties. As a consequence, different structures or aggregates are formed, which affect the solubility and the extractive potential of aqueous solutions [89].

Another commonly used green solvent is bioethanol, or ethanol from natural origins, obtained by fermentation of materials rich in sugar, by enzymatic hydrolysis of starch or from lignocellulosic raw materials. It is easily available in high purity, cheap, and completely biodegradable. The production of bioethanol significantly reduces the greenhouse gas emissions characteristic for conventional fuel combustion. Since ethanol is a well-known solvent for various extractions, bioethanol can be used instead [34, 90].

Like bioethanol, some agro- or bio-based solvents can also be used in extractions, organic synthesis, or other applications. Bio-based solvents are obtained from at least one renewable raw material produced from biomasses such as wood, starch, vegetable oils, or fruits [91]. In this category, some terpenes can be found, i.e. α-pinene extracted from pine or D-limonene extracted from citrus fruit skin. These solvents are biodegradable, usually nonflammable, have low polarity, and very high solvent power for extractions of natural compounds such as bioactive molecules or fats and oils [14].

Even some vegetable oils (sunflower, soya, cocoa, and rapeseed) are considered as green solvents. Vegetable oils are nonpolar lipophilic systems with a variable composition according to their origin, quality, and obtaining method. Besides their usual use, they could be used in extractions of bioactive compounds from natural sources, such as carotenoids or aromas [92, 93].

Many other green solvents were proposed and researched, such as organic acid esters (ethyl lactate, ethyl acetate), fatty acid esters (Diester), synthetic bio-based solvents (2-methyltetrahydrofuran), and solvents obtained from chemical synthesis (dimethyl carbonate). Recently, the most researched solvents are supercritical CO_2 and ionic liquids.

The extraction with supercritical CO_2 has been introduced in the 1970s and has been quite developed until today. The extraction technique with supercritical CO_2 uses

compressed gas at a pressure of up to 300 MPa at a moderate temperature (30–40 °C) when it acts as a solvent and can replace organic solvents, such as hexane. The advantages of this method are that there is no denaturation of thermolabile compounds at moderate temperatures, it is nonflammable odorless gas that is completely eliminated as a gas by the return to atmospheric pressure at the end of extraction so no traces of solvent are presented in the final extract [94]. It is being applied in many different industries including the food, pharmaceutical, and cosmetic industry, and is used for extraction of molecules with low polarity and low molecular weight, i.e. pigments, aromas, triglycerides, or in decaffeination process [95, 96].

On the other side, ion liquids gain a huge interest recently. The term ionic liquids stands for a wide range of solvents that are salts in the liquid state at low-to-moderate temperatures. In terms of green solvents, ionic liquids have a negligible vapor pressure and for that reason do not contribute to the volatile organic compounds' problems [97]. An important type of ionic liquids is represented by eutectic solvents, which are a mixture of compounds that form a eutectic with a much lower melting point than its components taking individually. The newest class is represented by NaDES inspired by the way that metabolites are dissolved in the plant cell, by eutectic combinations of sugars and nitrogen compounds. NaDESs generally consist of biological compounds, such as sugars, organic acid, and choline chloride and represent a great alternative for organic hazardous solvents [98–100].

It can be concluded that future sustainable solvents need to be characterized by diverse chemical compositions and a broad range of physicochemical properties to meet the diversified needs of the process industry. However, it can be expected that they all share the common feature of renewability. Currently, bio-based solvents from renewable sources offer the possibility of direct replacement of many nonrenewable conventional solvents and, it can be expected in the near future that even more green, bio-based renewable solvents will be available, with tailored properties.

14.3.3 Solvent Sustainability and Selectivity Prediction Models

The proper solvent selection that is suitable for the desired extraction procedure is the most important step of the reaction. The experimental laboratory procedures for solvent selection are precise and reliable, but usually require high solvent and time consumption, which is consequently expensive and not sustainable due to high energy consumption [101]. As a result of the tendency to reduce solvent consumption and screening, its economic costs and tendency toward greener solvents, theoretical and computational methods and models were developed for the prediction of solubility parameters of new solvents and solutes. Also, there is a limitation in the user's knowledge and experience with these new and daily growing number of solvents. Therefore, computational methods may play a key role in guiding the selection and design of solvents in various applications [102].

It is well known that solvent effects are related to certain or set of solvent properties. That is the reason why it is important to find reliable property prediction models. Most of them are predicted using the physical properties of solvents like Kauri-butanol index, Kamlet–Taft scale, Hildebrand solubility parameters, or Hansen solubility parameters, while some are more powerful, such as COSMO-RS which allows the prediction of electrostatic interaction between a solute and a solvent including also thermodynamic properties [91].

A Kauri-butanol index is a standardized value to measure solvent power for a hydrocarbon solvent ruled by American Society for Testing and Materials (ASTM) designation ASTM D1133 and is based on the titration of a solution of Kauri resin and n-butyl alcohol with a solvent up to the defined degree of turbidity. This index indicates a maximum amount of solvent that can be added to a solution of Kauri gum in 1-butanol without causing cloudiness. Kauri-butanol values range from 10 (very mild) to over 200 (very strong). However, it is not suitable for oils and fats and some experimental experiences showed inconsistency with theoretical results [103].

There is also a Kamlet–Taft scale whose parameters measure separately the hydrogen bond donor (α), hydrogen bond acceptor (β), and dipolarity/polarizability (π*) properties of solvents as contributing to overall solvent polarity. For example, this method was used to assess the potential of volatile methyl siloxanes as greener solvents for chemical synthesis to replace organic solvents. The polarities of volatile methylsiloxanes and as miscibility with other liquids were found to be similar to those of alkane solvents and the results showed that volatile methylsiloxanes provide environmentally more sustainable alternatives to replace nonpolar solvents [104]. Recent research by Duereh et al. [105] used generalized preferential solvation model and Wilson solvation model for estimating Kamlet–Taft dipolarity/polarizability (π*) and results showed that application of the models makes it possible to identify favorable compositions of ternary (heptane-ethyl acetate-ethanol) solvents being used in replacements of dichloromethane, for example in chromatography [105].

The Hildebrand solubility parameters (δ) provide a numerical estimate of interaction degree between chemicals and can be a good indication of solubility, especially for nonpolar or slightly polar systems without hydrogen bonding. The Hildebrand solubility is defined as the square root of the cohesive energy density, the energy required to break interactions between molecules (ΔU) per molar volume (V) which is consequently equal to the square root of the difference of heat of vaporization (ΔH) and ideal gas constant (R) timing with temperature (T) per molar volume (V) (Eq. 14.1) [106].

$$\delta = \sqrt{\frac{\Delta U}{V}} = \sqrt{\frac{\Delta H - RT}{V}} \tag{14.1}$$

The Hildebrand solubility parameters can be evaluated by various methods: heat vaporization (temperature data), group contributions, solubility measurement, swelling, osmotic pressure, and intrinsic viscosity. It is especially used in polymer–solvent interactions where it gives useful predictions of solubility and swelling of polymers by solvents [106, 107]. More recent research was focused on assessing the solubility of ionic liquids as environmentally friendly molten salts with high polarities, low melting points, non-volatility, and designability, which have an increasing interest in industries as solvents, catalysts, and electrically conducting fluids [106, 108–110].

An extension of Hildebrand parameters by division into a three-component system leads to the development of Hansen solubility parameters. Both models are based on "like dissolves like" rule meaning that a liquid is a good solvent for a solute if their solubility parameters are close to each other. The extension is that Hansen solubility parameters divide the total Hildebrand value into three components: a dispersion force (δ_d), a hydrogen bonding (δ_h), and a polar force (δ_p). Hansen solubility parameters (δ_{total}) are

based on the concept that the total cohesive energy density is characterized by the sum of the energy densities (Eq. 14.2):

$$\delta_{\text{total}}^2 = \delta_d^2 + \delta_p^2 + \delta_h^2 \tag{14.2}$$

Solvent solubility can be presented through a three-dimensional graph with axes δ_d, δ_p, and δ_h, which can be easily made using Hansen solubility parameters programming. Based on experimental determinations, the program proposes also a sphere around the parameters of a considered solute, with the parameters of potentially good solvents inside and poor solvents outside. The radius of the Hansen solubility sphere (R_o) presents the probable maximum difference in the parameters of the solute and of different solvents, to find the ideal solvent which is the closest to the sphere center. In order to optimize Hansen solubility parameters results, a simple composite affinity parameter was developed, a relative energy difference (RED) number. RED is presenting the solubility between solvents and solutes and is calculated according to Eq. 14.3:

$$\text{RED} = \frac{R_a}{R_o}, \tag{14.3}$$

where R_a is the distance of a solvent from the center of the Hansen solubility sphere, and is calculated as presented in Eq. 14.4:

$$R_a^2 = 4\left(\delta_d A - \delta_d B\right)^2 + \left(\delta_p A - \delta_p B\right)^2 + \left(\delta_h A + \delta_h B\right)^2, \tag{14.4}$$

where A refers to the solute and B refers to the solvent. The factor 4 is based on Prigogine's Corresponding States Theory, as it has proved to effectively expand the dimensions in order to give spherical plots. The better affinity between solutes and solvents is presented with smaller R_a value. Accordingly, when RED = 0, no energy difference is found which means it is a "perfect solvent," RED < 1 presents a high affinity, i.e. a potentially good solvent; if the RED value is between 1 and 3, then the solvent has a medium solubility for the solute, and RED > 3 indicates low affinity, i.e. a poor solvent [14, 111, 112].

The use of Hansen solubility parameters as a tool to evaluate the solubility of different analytes, especially from natural sources in various green solvents, has increased in last years. That is the reason why some green solvents such as ethanol, D-limonene, vegetable oils, CO_2, and ionic liquids are already included in the Hansen software database. Recent applications included the prediction of solubility of various high-added compounds including carotenoids [113, 114], triacylglycerides and fatty acids, food aromas [14], and polyphenols [29, 115] in green solvents, and these results were successfully compared with experimental data with many different green emerging technologies. Nevertheless, the physicochemical properties of some green solvents, for example ionic liquids and NaDES, have been insufficiently investigated and, therefore, their application is still limited [111].

The more accurate computational method for solvent selectivity is COSMO, which was applied in a wide range of industrial applications since its first introduction. During the application, some limitations were presented, such as the inability to distinguish two solvents with essentially identical dielectric constants but quite different solvent properties. This problem led to the development of a perfectly innovative concept, a COSMO for "real

solvents" (COSMO-RS), a statistical thermodynamic method for molecular description and solvent screening based on a quantum-chemical approach. It combines quantum chemical considerations (COSMO) and statistical thermodynamics (RS) to determine and predict thermodynamic properties.

The COSMO-RS enables the transfer from the solutes' molecular state, which is considered to be embedded in a cavity with a virtual surrounding conductor to real solvents. The calculations are performed in two steps at different scales: a microscopic scale step and a macroscopic scale step. In the microscopic step, the COSMO is used to apply a virtual conductor environment for the molecule, inducing a polarization charge density on its surface (σ-surface). The σ-surface represents the repartition of charge density on the molecular surface that is segmented and reduced to a histogram called σ-profile. This σ-profile provides information about the molecular polarity distribution and is accordingly integrated to calculate the chemical potential of the surface (σ-potential). The σ-profiles and σ-potentials, together with other thermodynamic parameters, can assure prescreening and classification of various solvents together with the multivariate statistical analyses to select adequate solvents for different applications. All calculation steps are summarized in Figure 14.3 [87, 91, 116].

The research and literature data regarding the use of COSMO-RS is increasing every day. Moreover, it has been successfully applied in extractions with the screening of alternative solvents for the replacement of conventionally used solvents. Until today, the COSMO-RS has been shown as the most accurate method for solvent solubility screening of green solvents. This approach has already been used in different fields, such as the selection of an excipient for pharmaceutical development in early discovery [117], for separation of long-chain fatty acids [118], for predicting the solubility of sulfur to investigate novel electrolytes for lithium-sulfur batteries [119], or in the cosmetic industry [120, 121]. However, most studies presented COSMO-RS with successful application in extractions of natural compounds for the replacement of conventional solvents with green solvents [14, 29, 50, 122].

Finally, before the implementation of the selected green solvents in industries or other processes, the environmental impact of solvents should also be assessed. For that reason, a LCA should be performed, mainly for primary life cycle stages of solvent usage: manufacture, distribution, usage, and disposal. Many alternative solvents are produced from renewable sources, in which water and CO_2 require purification or condensation instead of manufacture processing; ionic liquids require multistage syntheses; choline as a NaDES solvent has a high boiling point, so it requires high energy for processing. Thereby, scientists and technologists should pay attention to the whole life cycle of the solvent and take into account all stages of solvent preparation. For that reason, LCA is the best tool to analyze carefully all disadvantages compared with their benefits. The greenest option is still a solvent-free process, but this is not always possible, so it is important to highlight that the development of computational methods, such as Hansen solubility parameters or COSMO-RS with large databases and in combination with LCA, leads to great discoveries about green solvents and their application in research, laboratories, and industries [87].

Recently, a 10-step method was proposed, encompassing a hierarchy of assessments and tests designed to help to select bio-based alternatives to organic solvents [16]. Initially, solvent properties are compared using the Kamlet–Abboud–Taft solvatochromic parameters and Hansen solubility parameters, for identification of the required solvent types and the

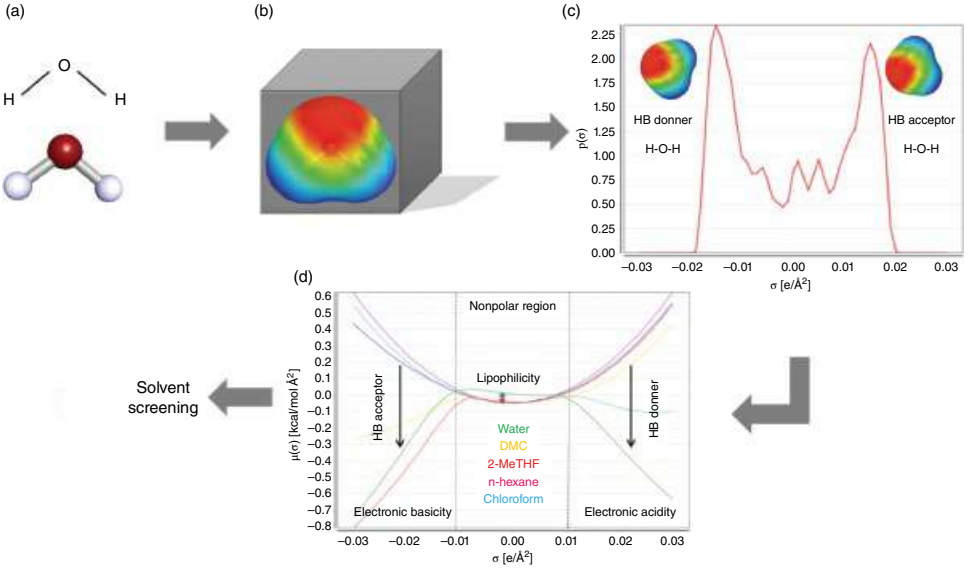

Figure 14.3 The COSMO-RS schematic diagram: (a) the transformation of the 2D molecular structure with (b) σ-surfaces, (c) conversion into σ-profile, and (d) σ-potentials of five representative solvents: nonpolar (n-hexane), highly polar hydrogen bonding (HB) acceptor and donor (water), HB acceptor (2-methyltetrahydrofuran, dimethyl carbonate), and HB donor (chloroform).

screening of new solvents. Intermediate steps of the 10-step method require the optimization of solvent synthetic pathways, using green chemistry principles. Subsequently, the solvent physical properties are determined or tested, together with simple toxicological testing (e.g. Ames test) for finer screening. Finally, more expensive and time-consuming LCA studies are implemented for sustainability determination [15, 16].

14.3.4 The Role of Solvent Recycling in Extractions

As discussed in the previous sections, many efforts have been devoted by the scientific community to explore novel and greener technologies for the extraction from plant materials, characterized by higher process efficiency for the recovery of high value-added compounds. However, despite the introduction of innovative technologies, organic solvents and their aqueous solutions are still heavily used to increase the selectivity toward the desired extracts [123], but also to enhance process control, safety, and handling [124]. As a consequence, a high amount of toxic waste is generated, consisting of the residues of the extraction process contaminated with the organic solvents, with a negative impact on health, safety, and the environment [125], and consequently, worse green chemistry metrics. It is hence clear why the interest to pursue the reduction of solvent consumption and the use of greener solvents has exponentially grown in recent years [126, 127].

According to Welton, solvent use in chemical processes becomes more sustainable, if the solvent has dual roles (e.g. as extractant and as reagent), or if it contributes to producing higher quality products, reducing the number of synthetic steps, reducing by-product formation, or improving product separation [78]. For example, neoteric solvents, which include ionic liquids, deep eutectic solvents, liquid polymers, supercritical CO_2, gas expanded solvents, and switchable solvents, have gathered an increasing industrial interest, because they provide significant advantages over conventional organic or aqueous, solvents, typically by improving product separation [15]. However, the replacement of a conventional solvent with a greener alternative should always be assessed according to the sustainability criteria, discussed in Table 14.1, possibly taking into account the entire life cycle of a chemical process and the solvents, auxiliaries, reagents, products, as well as following solvent isolation and purifications phases for reuse [15]. In fact, despite a wide number of tools are available for solvent selection as a function of its degree of greenness and applicability, determining the environmental impacts of new solvents are made difficult by the possible lack of data required for assessment [128], and classification of the greenness is still a subject of much debate [129, 130].

It must be highlighted that an important parameter, which is often neglected, during solvent selection, is the scale of manufacturing processes. The solvent impact depends on the volume used in a process. For this reason, solvent recovery and recycling have an important role for greener extractions. Although the number of scientific papers about solvent recycling is rapidly growing every day, more than half of waste related to chemicals, which is mostly concerning production solvents, does still not recycle. Solvent recycling in industries is not only recommended to meet regulations and preserve the environment, but also may increase their profit [131]. Since waste solvents produce a high carbon footprint, it is recommended to recycle solvents on-site. Most often used technologies for solvent recovery are distillation, adsorption, and membrane processes such as organophilic

pervaporation and solvent-resistant nanofiltration. Some rarely used techniques include cocurrent or countercurrent extraction and steam/gas stripping [132].

Großeheilmann et al. [133] studied switchable-hydrophilicity solvents for easy product/catalyst separation as well as catalyst recycling. These solvents have a possibility to switch between a water-miscible state and a state that forms a biphasic mixture with water. The catalyst recycling experiment showed that it is possible to isolate the product with high purity (>98%) without further purification steps. The catalyst was reused without any loss of activity for four times [133]. Great examples for recycling are given with olive leaves research. Olive leaves are an agricultural waste, and waste utilization in agriculture is the second highest global greenhouse gas emission contributor [134]. Didaskalou et al. [134] developed a model of a continuous adsorption process with in situ solvent (ethyl acetate) recovery for the isolation of oleuropein from olive leaves. The model demonstrated to be an advantageous tool for the in silico design and optimization of the process, reducing the need for excessive experimentation. On the other side, a process optimization and intensification via continuous and simultaneous isolation of biophenols from olive leaves was performed. Firstly, a temperature-swing molecular imprinting technology was used for extraction of individual biophenols from olive leaves extracts. Secondly, concentration of the product and waste streams was performed using solvent-resistant nanofiltration, as well as for solvent recovery. Results showed that the predictive mathematical models for the adsorption dynamics and the membrane separation had a significant reduction of the carbon footprint, E-factor, and economic sustainability. This process is easy for operation with multiway valves to aid safety and reduce operating costs [135].

The main disadvantage with solvent recycling, are low volatile solvents such as ionic liquids, deep eutectic solvents, or bio-based terpenoids. For example, it is a problem during distillation since it requires handling volatile liquids, all nonvolatile and low-volatile liquids remain in the still bottoms during the process. Since their boiling points are so high, it makes the distillation process too energy-costly. Kralisch et al. [136] published a paper where recycling of ionic liquids was performed using a rotary evaporator filled with a water-bath, with pressure decay adjusted to the boiling point of the solvent [136]. Another possible method of ionic liquids recycling is with protonated cations. For example, they can be switched off by deprotonation resulting with neutral carbene molecules (i.e. amine) that are stable and can be further recycled by distillation [137].

Despite solvent recycling is important, not always it is operationally or economically viable. For this reason, it is recommended for companies not to implement solvent recovery and recycling in the early stages of process development. Once the process is well-established, solvent recovery could be one of the key upgrades considered to improve profit margins [15].

14.3.5 Solvent Selection Guides

The basis of green food processing includes not only reduction of energy and water consumption, recycle by-products through bio-refinery approaches, and higher quality products [11], but also ameliorated process safety. A truly sustainable green extraction process should employ low environmental damaging technologies based on environmentally friendly solvents [62], characterized by adequate environmental, health, and safety

properties (EHS). Understanding solvent properties is, therefore, a necessary part of sustainable development. Many solvents of interest for conventional and green extraction processes have already been ranked by their EHS characteristics [129], making a vital part of the solvent selection practice. Several pharmaceutical companies have published their guides to the green solvent selection, based on their EHS ranking and compliance with company policy [15].

Several solvent selection guides for general purpose have now been published with purpose to reduce use of the most hazardous solvents, but these have mostly been arranged according to each company usage policy [123]. For example, researchers from Rowan University developed a guide with comparison between the different solvent options available for a process. It is available for everyone and is easy to use. An index with 12 environmental parameters was developed for each solvent and it includes also occupational health considerations such as biodegradation and global warming potential. A summation of all parameters results with a score from 0 to 10, where lower score presents greener solvent [138]. Another example comes from Pfizer company. They developed a simple, color-coded hierarchical solvent selection guide. This guide lists solvents as "preferred," "usable," or "undesirable." Even though the guide has limitations, a useful substitution guide is provided for solvents presented as "undesirable" due to their issues such as carcinogenicity, emissions, and reproductive toxicity. After introducing this guide, Pfizer reported a significant (50%) reduction in chlorinated solvents use over 2 years, and 97% reduction of undesirable ethers [139].

Solvent selection guides by GlaxoSmithKline (GSK) were developed for medicinal chemistry laboratories in 1999. The methodology for solvent assessment was more miscellaneous compared with Pfizer tool, including detailed distribution of scores for different EHS categories. Recently, versions of GSK guides included LCA impact, expanded the number of solvents, and provided a customizable version for posting in different business areas. GSK guides include multiple health, environment, safety, and waste categories that combined can reach a single composite score and color assignment [140, 141].

More recently, Sanofi has developed selection guides to help chemists in early development to select greener solvents that will be accepted in all production sites. Guides take into account data from safety, health, environmental impact, quality, and industrial constraints. Each solvent has an ID that indicated the overall ranking which is divided in four colored categories: green (recommended solvent), yellow (substitution advisable), red (substitution requested), and brown (banned solvent). The residual solvent limits for pharmaceuticals according to the International Conference on Harmonisation are also included, as well as physical properties, cost, and substitution advice for solvents. The Sanofi solvent selection guide consists of much more solvents compared with Pfizer and GSK guides [142].

According to Pfizer, Sanofi, and GSK selection guides, the greenest solvents are water and mostly alcohols and esters, such as n-propyl acetate, i-propyl acetate, 1-butanol, and 2-butanol. This is also in line with Rowan University tools. These guides are user friendly for users to promote awareness of greener alternatives, and accordingly, large reductions in undesirable solvents have been reported upon guides' implementation. However, these guides often lack valuable information about the performance of solvents and their economics. For that reason, future solvent selection will require a greater sophistication and more data, especially for new solvents [123].

14.4 Case Studies Related to Zero Waste, Low Carbon Emission, Clean Label, and Other Sustainable Values

Recent studies have applied several techniques for the extraction of bioactive compounds, such as UAE, microwave-assisted extraction, supercritical fluid extraction, and subcritical solvent extraction. UAE is often inexpensive and simple. It could increase the yield of extracted components, decrease the extraction time, and use lower temperatures. Therefore, it is usually used for the extraction of thermolabile and unstable compounds [143]. Subcritical and supercritical fluids are an alternative media of solvents. The subcritical fluid is at temperatures above its normal boiling point and below its critical point. After extraction, the solvent is removed at a low temperature under a vacuum condition. The supercritical fluid is considered to be in its critical state when it is both heated and pressurized above its critical temperature and critical pressure, respectively. The properties of supercritical fluids can be adjusted by pressure and/or temperature above their critical points which causes a change of solvent selectivity toward required compounds. It is a particularly interesting method in the case of the extraction procedure. Supercritical fluids have properties between those of a liquid and a gas. Its density is close to liquid and its viscosity is close to gases. Meanwhile, its diffusivity is between liquid and gas leading to enhanced mass transfer between the target solute and the supercritical fluids. Therefore, subcritical and supercritical fluid extraction technology has attracted many researchers for its applications as a green alternative process than conventional solvent extraction. The subcritical and supercritical CO_2 extraction has been widely used for the extraction of oil from agro-industrial residues and plant materials [144] and bioactive compounds from herbs, vegetables, and fruits. Another treatment that has been successfully applied to green extraction processes is based on HPH, as a technique to cause complete cell disruption, significantly enhancing the release in water as extraction medium of both soluble compounds (e.g. proteins, polysaccharides) and water-insoluble molecules (e.g. lycopene, polyphenols), as recently shown for tomato peels [18], spent coffee grounds [19, 20], and microalgae [21]. This section describes the example and case studies of sustainable green extractions including supercritical CO_2 extraction, subcritical solvent extraction, ultrasonication, and HPH for various materials.

14.4.1 Extraction of Assam Tea Seed (*Camellia Sinensis* var. *Assamica*) Oil Using Supercritical CO_2, Subcritical Solvent, and Soxhlet Extraction Methods

Assam tea seed oil could be extracted by supercritical CO_2 extraction, subcritical solvent extraction, and Soxhlet extraction methods. Hexane, petroleum ether, and isopropanol were used as solvents in subcritical solvent extraction and Soxhlet extraction methods. The extraction conditions for subcritical solvent extraction methods using hexane, petroleum ether, and isopropanol were 75 °C for 15 minutes, 75 °C for 15 minutes, and 105 °C for 15 minutes, respectively, to achieve the high-percentage oil yields which are compared with those for supercritical CO_2 extraction (at 50 °C under 220 bar for 4 hours) and Soxhlet extraction for 6 hours as shown in Figure 14.4. It can be seen that the percentage oil yield and the percentage oil recovery obtained for subcritical solvent extraction and Soxhlet extraction methods using hexane, petroleum ether, and isopropanol were in the range of

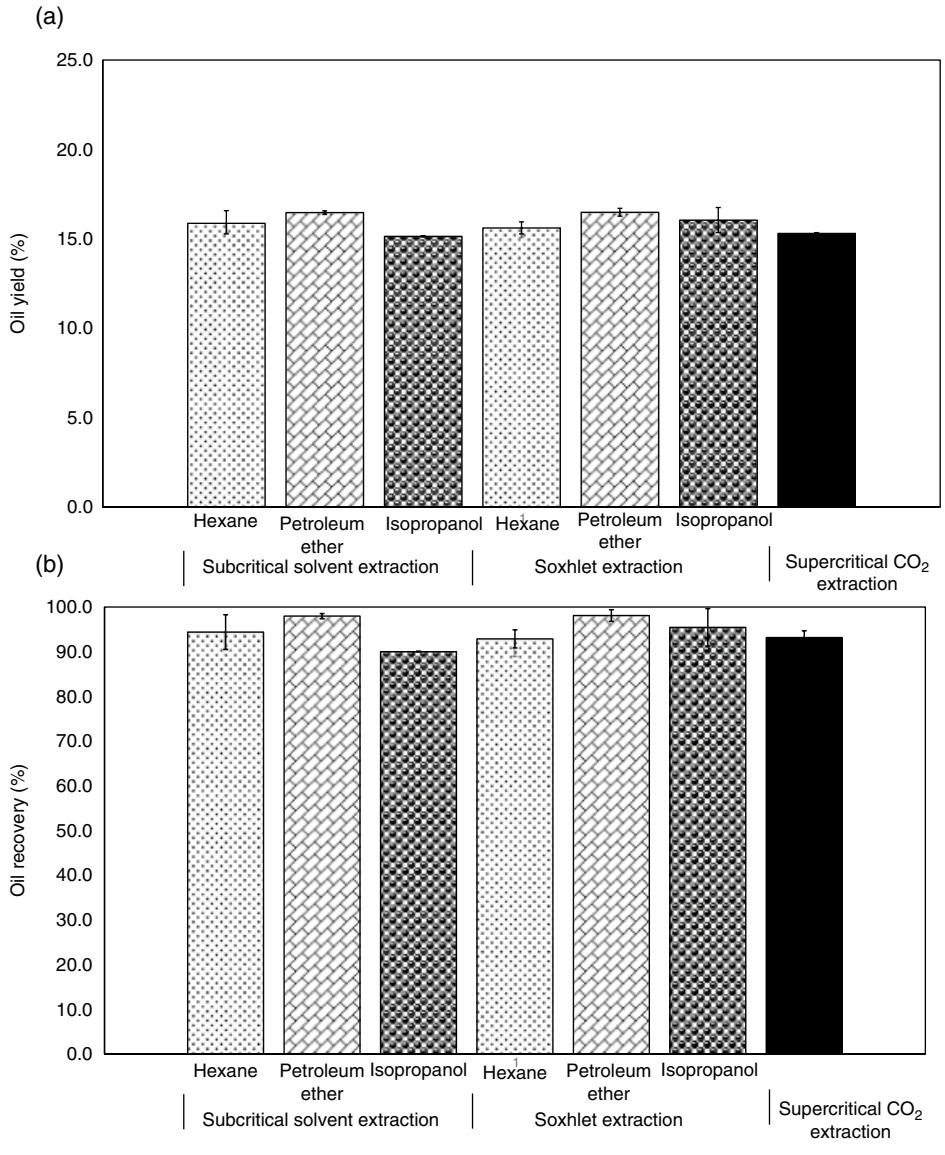

Figure 14.4 Comparison of the percentage oil yield and percentage oil recovery using subcritical solvent extraction, Soxhlet extraction, and supercritical CO_2 extraction methods.

approximately 15.61–15.87%, 16.47–16.49%, and 15.14–16.05%, respectively, and 92.86–94.39%, 97.97–98.10%, and 90.03–95.46%, respectively. Meanwhile, the percentage oil yields and the percentage oil recovery by using supercritical CO_2 extraction were 15.30 and 93.15%, respectively [145].

It was observed that the percentage oil yield and percentage oil recovery obtained by subcritical isopropanol extraction was lower than that obtained by Soxhlet extraction and supercritical CO_2 extraction. Additionally, for each extraction method, the type of

extraction solvent had affected the percentage oil yield and percentage oil recovery. Therefore, as seen in Figure 14.4, supercritical CO_2 extraction method can potentially be used to recover oil from Assam tea seeds (*Camellia sinensis* var. *assamica*) and further developed for large industrial-scale extraction system.

14.4.2 Comparison of Soxhlet Extraction, Accelerated Solvent Extraction, and Supercritical CO_2 Extraction Techniques for Recovery of Spent Coffee Grounds Oil

Several extraction techniques have been utilized for recovery of essential oils and antioxidant phenolic compounds from valuable natural sources: for example, solid–liquid extraction with organic solvents, microwave or UAE, subcritical or supercritical fluids extraction, and high-pressure extraction processes [146–148]. Among these techniques, supercritical CO_2 has been widely used as an excellent extraction solvent for the extraction of oil from agro-industrial residues and plant materials [144, 149]. Muangrat and Pongsirikul [150] investigated the effect of solvent used in the extraction techniques on the recovery of oil obtained from the spent coffee [150]. Soxhlet and accelerated solvent extraction methods for extraction of oil from spent coffee grounds were carried out using propanol as the solvent, and the results were compared with supercritical CO_2 fluid extraction. Comparing these extraction techniques as shown in Table 14.2, accelerated solvent extraction (using propanol as the solvent at extraction temperature of 120 °C under constant extraction pressure of 1500 psi for 5 minutes) had a higher average oil yield (14.02%) compared with the Soxhlet extraction (13.75%) (using propanol for extraction time of 6 hours) and supercritical CO_2 extraction (12.11%) (at extraction temperature of 50 °C under extraction pressure of 200 bar for 2 hours). However, there was no statistically significant difference in the crude oil yields extracted by the different methods ($p > 0.05$). Accelerated propanol and supercritical CO_2 extraction methods can potentially be used to recover oil from spent coffee grounds oil and also provide a high oil yield [150].

In addition, Soxhlet extraction has several disadvantages such as long extraction time, usage of a large volume of solvent, losses, and degradation of volatile organic compounds, and operation at high extraction temperature leading to undesirable off-flavor compounds [151]. Meanwhile, accelerated solvent extraction and supercritical CO_2 extraction methods have several advantages over the conventional Soxhlet extraction method; for instance, low operating temperature leading to reduce thermal degradation of volatile

Table 14.2 Crude oil yield obtained from Soxhlet extraction, accelerated solvent extraction, and supercritical CO_2 extraction methods.

Extraction method	Solvent	% Crude oils
Soxhlet extraction (6 h)	Propanol	13.75 ± 0.35
Accelerated solvent extraction (120 °C, 1500 psi for 5 min)	Propanol	14.02 ± 0.31
Supercritical CO_2 extraction (50 °C, 200 bar for 2 h)	CO_2	12.11 ± 1.33

ns: not significant.

compounds, a shorter extraction time, and an increasing selectivity in oil and bioactive compound extraction.

14.4.3 Subcritical Water Extraction of Brazilin Compounds from *Caesalpinia Sappan* L. Heartwood

The yield of crude extract and brazilin obtained by using subcritical solvent extraction were compared with those obtained by maceration with ethanol and ultrasonic bath extraction using ethanol and water as solvents as shown in Table 14.3. Ethanol and water were used as solvents in the subcritical solvent extraction method. The results showed that subcritical ethanol and water extraction were at extraction temperature of 100 °C for 30 minutes, which gave the higher yield of crude extract and brazilin. In comparison to other techniques, subcritical ethanol and subcritical water extraction were found to be more effective than maceration and ultrasonic bath extraction. Therefore, subcritical ethanol and subcritical water were a possible green extraction technique to extract brazilin from heartwood.

14.4.4 Ultrasonication Extraction for Ceylon Spinach

Ceylon spinach (*Basella alba*) is a popular local vegetable in Thailand. This plant is high in vitamin A, vitamin C, vitamin B_9 (folic acid), calcium, magnesium, phenolic compounds, and several other antioxidants. It is low in calories (by volume) and high in protein [152]. *Basella alba* has a long history of use as a medicinal plant species to treat and manage various human ailments. It can also be used as a natural source of food additives for food

Table 14.3 Crude extract (%) and brazilin content obtained using maceration, ultrasonic bath, and subcritical solvent extraction methods.

Extraction conditions	Crude extract (%)	mg Brazilin/g dry heartwood
Maceration Heartwood:ethanol ratio of 1:3 (w/w) at 25 °C for 24 h	1.48 ± 0.01^{c}	9.13 ± 0.00^{c}
Ultrasonic bath extraction Heartwood:ethanol ratio of 1:3 (w/w) at 80 °C for 30 min	1.72 ± 0.02^{e}	5.91 ± 0.01^{e}
Ultrasonic bath extraction Heartwood:water ratio of 1:3 (w/w) at 80 °C for 30 min	1.19 ± 0.00^{d}	7.20 ± 0.01^{d}
Subcritical ethanol extraction Heartwood:ethanol ratio of 1:3 (w/w) at 100 °C for 30 min	5.4 ± 0.05^{a}	44.36 ± 0.01^{a}
Subcritical water extraction Heartwood:water ratio of 1:3 (w/w) at 100 °C for 30 min	3.2 ± 0.00^{b}	28.73 ± 0.01^{b}

Means with different letters (a, b, c, d, e) in the same column are significantly different ($p \leq 0.05$).

preservation and health promotion [153]. Ultrasound is a green technology that is cost-effective, adaptable, efficient, and effective for extracting natural food ingredients. It is likely to be used more in the future [154]. Ultrasound has the potential to not only mitigate the extraction times and improve yields, but also to avoid high temperatures that destroy active ingredients [155]. UAE is based on the principle of acoustic cavitation which facilitates solvent penetration into and out of the cells through damaged cell walls [156]. Buadoktoom [157] found that the Ceylon spinach (*Basella alba*) extracts (CE) were sonicated at different amplitudes (60–100%) for 10–40 minutes in an ultrasonic bath (40 kHz, 150 W). The increase in sonication time also resulted in the rise of antioxidant activities. The antimicrobial activities of the CE were measured as the minimum inhibitory concentration and minimum bactericidal concentration against *Staphylococcus aureus*, *Escherichia coli*, *Salmonella* Typhimurium, and *Pseudomonas aeruginosa*. At 100 mg/mL, all sonicated extracts inhibited and inactivated *S. aureus* and *E. coli*. The sonicated extracts at 60% amplitude for 10, 25, and 40 minutes could also inhibit *P. aeruginosa* and *S.* Typhimurium whereas the elevated amplitudes of 80 and 100% showed corresponding minimum inhibitory concentration and minimum bactericidal concentration values with *P. aeruginosa* and *S.* Typhimurium of 50 mg/mL. The 80% amplitude for 40 minutes was thus chosen as the optimal condition for greater antioxidative and antimicrobial activities. Therefore, the sonicated polysaccharide provided better antioxidative and antimicrobial properties when compared with conventional methods. The sonicated extracts at 100 and 120 mg/mL without additive (control) were selected and used for shelf-life testing. The thiobarbituric acid reactive substances values of fresh pork treated with sonicated extracts were lower than those of controls. Fresh pork coated with 120 mg/mL sonicated extract could be kept for six days at 4 °C, two days longer than the control [157].

14.4.5 Hot Water and Ultrasonication Extraction for Polysaccharides

Polysaccharides have been used for their several biological properties including inhibiting free radicals, and antimicrobial and immunological activities [158, 159]. The biological effects of polysaccharides depend on their chemical composition, molecular weight, and structure [160]. Many studies emphasized that the water-soluble polysaccharides, because they are negatively charged such as hydroxyl groups and oxygen atoms, can be free radical scavengers and metal chelators, leading to inhibition of lipid peroxidation [161]. The UAE extracted polysaccharides from white button mushroom (*Agaricus bisporus*) showed that the UAE gave a higher yield than the HWE and the microwave-assisted extraction, with the UAE showing relative increases of 155 and 28%, respectively [162]. Ultrasonication has also been used to degrade polysaccharides to enhance antioxidant properties. Surin et al. [158] found that the yield of purple glutinous rice bran polysaccharide (PP) extracted by UAE was significantly higher than that obtained from the HWE. The antioxidant activities of UAE-PP were lower than HWE-PP because of the 197 μM Fe^{2+}/g. The UAE process is a promising method to decrease the processing time and enhance extracted yields by four times. In addition, Surin et al. [159] found that the application of green solvent as HWE at 90 °C for 2 hours for PP was good enough for further sulphation. Immunomodulatory activity of sulphated-PP, including inducing cytokine production (iNOS, TNF-α, IL-1β, and IL-10) via upregulated mRNA expression, was significantly increased by 10–86% when

compared with the crude polysaccharides. It can be concluded that the ultrasonication provided greater polysaccharide yield but conventional process with hot water treatment provided higher immunomodulatory activity.

14.4.6 Ultrasonication Extraction for Oligosaccharides Production

Carbohydrates have their molecules with different shapes, sizes, and structures resulting in food with a wide range of applications. Particularly, polysaccharides in foods have several properties in the matrix leading to increasing water retention, gel formation with the thickening property, stabilization of foam, emulsion, reducing the formation of ice crystals, and also interacting with other molecules. Nondigestible polysaccharides and oligosaccharides such as fructooligosaccharides, galactooligosaccharide, inulin, mannanooligosaccharides, raffinose oligosaccharides, xylooligosacharides, and others are considered as prebiotics and useful for health [163–165].

Cavitation, acoustic and hydrodynamic cavitation are the important mechanisms during ultrasonic extraction for physical and chemical transformations. The disruption of cell walls, particle size reduction, increasing of mass transfer, and diffusion of the solvent into the cell structure are developed during the process [156, 166]. Ultrasonication is reported to attack plant cell walls to enhance yields of extraction, releasing of extractives, especially polysaccharides in a shorter time of operation at lower temperatures [167–169]. Natural oligosaccharides (1-kestose (GF2), nystose (GF3), 1F-β-fructofuranosylnystose (GF4), raffinose, and stachyose) from blueberry, nectarine, raspberry, watermelon, garlic, Jerusalem artichoke, leek, scallion, spring garlic, and white onion were extracted using ultrasonication and the yields increased 2–4 fold compared with conventional extraction [170]. The Response Surface Methodology via Box–Behnken was used to optimize both the extraction yield and molecular weight of extracted β-glucans from barley. Under the optimal condition, the yield of extraction using the ultrasonic process (up to 44.3%) depended on the amplitude and especially on time; nevertheless, molecular weight decreases with time to produce oligosaccharides [171]. With another application for the synthesis reaction, Rico-Rodríguez (2018) reported the production of galactooligosaccharides using a combination of a multi-enzymatic system with commercial β-galactosidase (β-gal) from *Kluyveromyces lactis* and glucose oxidase and ultrasound resulting in the high yield of galactooligosaccharides (49%) after 2 hours of reaction.

The sonocatalytic–Fenton reaction, a combination of sonocatalytic reaction and Fenton reaction, gave a higher yield of extraction and lignin removal that was better than the separation of sonocatalytic and Fenton reactions. Ninomiya et al. [172] firstly introduced the sonocatalytic–Fenton reaction for synergistically enhanced hydroxyl (OH) radical generation and then degradation of lignin. The reaction was also applied to the pretreatment of cellulosic biomass to enhance enzymatic saccharification [172]. With the strategy of sonocatalytic–Fenton reaction, Kawee-Ai [173] demonstrated a two-step pretreatment process consisting of the alkali treatment by 2% KOH pretreatment within 1 hour (pretreatment) and sonocatalytic–synergistic Fenton process for 4 hours (post-treatment) and then subsequent enzymatic hydrolysis for 48 hours that could enhance the release of lignin concentration and xylooligosaccharides with 157.12 mg/g substrate of corncob. Under the optimal condition, 20.76 mg/g corncob for xylopentaose, 31.69 mg/g corncob for xylotretaose,

37.63 mg/g corncob for xylotriose, and 67.04 mg/g corncob for xylobiose were produced. It was noticed that sonocatalytic and Fenton reaction decreased alkali concentration used in the process of delinification [173].

The ultrasonic technique is simple, fast, and green chemical extraction that is highly suitable for applications in the food and medicinal industries. In a recent study, the ultrasonic-microwave synergistic process has been optimized for prebiotic oligosaccharides from sweet potatoes (*Ipomoea batatas* L.). The optimal conditions were an extraction time of 100 seconds, ultrasonic power of 300 W, and microwave power of 200 W [143]. The ultrasound–microwave-assisted extraction is a new process technology; the heat activated by microwave induces the migration of dissolved molecules. Simultaneously, the ultrasound enhances mass transfer and yield of oligosaccharides. The new technique for the extraction of prebiotic oligosaccharides promotes a cost-effective and innovative process that can be used on the industrial scale. Green techniques of ultrasonication in the process of extraction under mild conditions were alternatively combined with other methods to enhance the efficiency of extraction, reduce harmful chemicals released into the environment, speed up the reaction, and also increase the yield of the products.

14.4.7 Waste Minimization Through High-Pressure Homogenization Cell Disruption

HPH treatments have been applied to the extraction of different compounds, such as proteins, carbohydrates, polyphenols, and carotenoids, from different plant, microbial, or microalgal matrices. In a recent work, it was demonstrated that HPH treatment of tomato peel suspensions (10% wt.) at pressures of 100 MPa and for 5–10 passes was able to completely disrupt the tomato peel cells (as shown in Figure 14.5), unlocking all the valuable

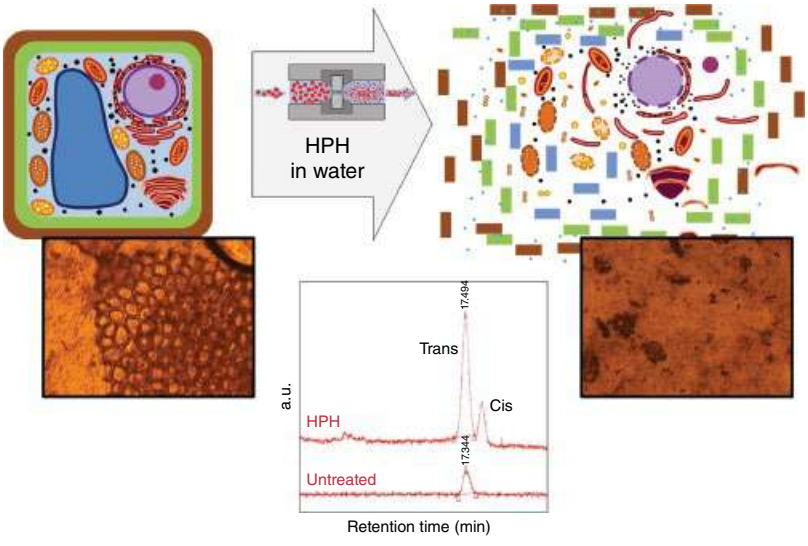

Figure 14.5 Schematic representation of the HPH treatment of tomato peel suspensions in water (10% wt.) showing the micrographs of tomato peel cell disruption and the increased lycopene release, upon treatment at 100 MPa, 25 °C for 5 passes, in comparison with untreated suspension.

intracellular components that, otherwise, would have been extracted with the use of high temperatures, organic solvents, or enzymes. More specifically, in comparison with a high-shear mixing treatment, which was able to disaggregate cells but not to disrupt them, HPH treatment resulted in a significant increase in the aqueous phase of proteins (+70%), sugars (+10%), polyphenols (+32.2%), and water-insoluble lycopene. Remarkably, up to 56.1% of the initial peel content of lycopene was recovered, which is higher than the values reported by scientific literature for organic solvents or supercritical CO_2 [18].

With the same approach, HPH treatment of *Chlorella vulgaris* microalgae enabled to significantly increase the release of carbohydrates and proteins. In particular, in comparison with a pulsed electric field treatment (electric field strengths of 10–30 kV/cm and total specific energy input of 20–100 kJ/kg), HPH caused a 1.1-fold and a 10.3-fold increase in yields of carbohydrates and protein, respectively [21]. Interestingly, the most significant increase was observed for larger molecules (proteins vs. carbohydrates or sugars) and water-insoluble molecules (e.g. lycopene).

The considerable advantages in terms of increased yields of extraction in the water of intracellular compounds are counterbalanced by the complete lack of selectivity of the HPH treatment, which contradicts one of the pillars of the green extraction processes. However, it must be said that HPH processing offers other considerable advantages.

First of all, HPH processing is based on the use of water as an extraction solvent, which is intrinsically environmentally benign and prevents the need for organic solvents, also for the recovery of water-insoluble compounds, such as lycopene. More specifically, HPH enables to obtain high yields of all the intracellular compounds in water. Subsequently, the plant material or microalgal suspension can be used as a food ingredient, where the molecules of interest are highly bioaccessible as already released from the cells (for example, with high antioxidant activity [18]) or the aqueous phase can be separated by centrifugation, carrying a significant concentration of the desired compounds. In the case of tomato peels, 39.2% of the initial content of lycopene was transferred, as a complex with sugars, in the aqueous phase. The pellet (exhaust material), which has been processed only through a physical process, can be disposed of exactly as the initial residue, adding significant benefit to the proposed technology [174]. In the case where, for example, pure lycopene is desired, it can be subjected to solvent or supercritical extraction applied directly on the aqueous supernatant, drastically reducing the exhaust material to be treated [18].

In another work, the same authors have demonstrated that the residue of the aqueous extraction of HPH-treated tomato peels or spent coffee grounds can find advantageous use in the food industry as oil structurant. In detail, the HPH-treated and micronized agri-food residues were suspended at 25% vol in peanut oil [19, 20]. Upon the addition of water as a secondary immiscible fluid, the formation of a 3-D network, termed capillary suspension [175], was induced, through the formation of capillary bridges because water preferentially wets the particle surface. Remarkably, the strength of the capillary bridges resulted to depend on the surface properties of the particles, and in particular their hydrophilicity, and the mean particle size of the residues. As a result, the capillary suspensions prepared with HPH-treated residues (70 MPa, 3 passes) exhibited a very strong structuring ability, with apparent yield stress more than one order of magnitude higher than that measured in capillary suspensions prepared with high-shear mixed residues (> 100 Pa vs. < 10 Pa).

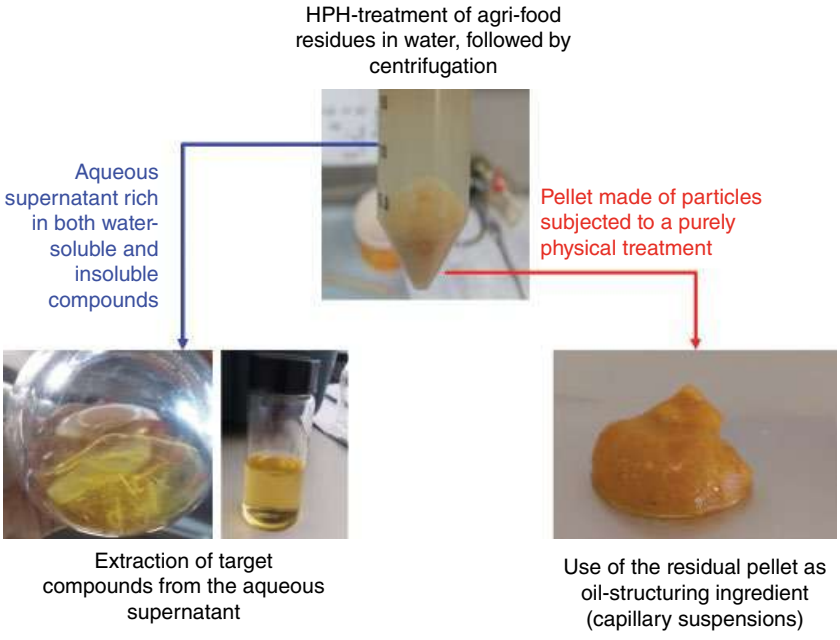

Figure 14.6 Schematics of the total use of HPH-treated agri-food residues.

It must be remarked that this application is made possible by the purely physical treatment carried out through HPH, which leaves the residual pellet with the same food-grade as the original by-product. Therefore, it is possible to hypothesize an HPH-assisted extraction process, which abides by the zero-waste principle, as shown in Figure 14.6. HPH-treated aqueous suspensions of agri-food residues can be separated in two fractions by centrifugation or sieving: the aqueous supernatant, containing the intracellular components released during the HPH treatment, and the residual solid pellet, consisting of the plant cell debris and hence mainly fibers and proteins, micronized by purely physical high-shearing, high-pressure fluid-mechanical stresses. The aqueous supernatant can be sent for further purification/separation to eventually isolate the compounds of interest (e.g. lycopene), minimizing the residue contaminated by the solvents used and to be disposed of, or can be used as a total extract containing highly bioaccessible proteins and polyphenols. The pellets can be used as food ingredients, for example in vegetable oil structuring, to support the development of novel food ingredients or replacement of existing ones (e.g. margarine, spreads, and creams), with the additional advantage that a fraction of the lipids are replaced by dietary fibers [20].

14.5 Conclusion and Future Trends

One of the great success stories of modern chemistry and engineering has been the evolution of a system that is increasingly more efficient at directly translating knowledge into technology and commercial products. The utilization of green extraction of food and

natural is such a system that has evolved to keep the wheel of development rolling. Green extraction techniques make use of physical and chemical phenomena that are fundamentally different compared with those applied in conventional extraction techniques. It is such some novel processes that can produce extracts in concentrate form, free from any residual solvents, contaminants, or artifacts. The innovative techniques developed to date indicate that green extraction offers net advantages in terms of yield and selectivity, with better extraction time, extract's composition, and environmentally friendly. Understanding, on the molecular and macro scale, of processes relevant to green extraction techniques has not yet reached the degree of maturity of other topics in chemistry and engineering. Such a challenge is somewhat ambitious and requires a special approach.

Acknowledgments

Authors would like to thank Croatian Science Foundation for funding the project "High voltage discharges for green solvent extraction of bioactive compounds from Mediterranean herbs (IP-2016-06-1913)." Marinela Nutrizio and Anet Režek Jambrak would like to thank "Young researchers' career development project – training of doctoral students" of the Croatian Science Foundation funded by the European Union from the European Social Fund.

References

1 Non-thermal processing market for food by food type, technology, region - 2022 | Markets and Markets [Internet]. [cited 2020 May 22]. https://www.marketsandmarkets.com/Market-Reports/food-non-thermal-processing-market-158213636.html (accessed 8 June 2020).
2 Singanusong, R., Nipornram, S., Tochampa, W., and Rattanatraiwong, P. (2015). Low power ultrasound-assisted extraction of phenolic compounds from mandarin (Citrus reticulata Blanco cv. Sainampueng) and lime (Citrus aurantifolia) peels and the antioxidant. *Food Anal. Methods* 8 (5): 1112–1123.
3 Giacometti, J., Bursać Kovačević, D., Putnik, P. et al. (2018). Extraction of bioactive compounds and essential oils from mediterranean herbs by conventional and green innovative techniques: a review. *Food Res. Int.* 113: 245–262.
4 Picot-Allain, M.C.N., Ramasawmy, B., and Emmambux, M.N. (2020). Extraction, characterisation, and application of pectin from tropical and sub-tropical fruits: a review. *Food Rev. Int.* 3: 1–31. https://doi.org/10.1080/87559129.2020.1733008.
5 Chemat, F., Rombaut, N., Sicaire, A.G. et al. (2017). Ultrasound assisted extraction of food and natural products. Mechanisms, techniques, combinations, protocols and applications. A review. *Ultrason. Sonochem.* 34: 540–560.
6 Alexandre, E.M.C., Araújo, P., Duarte, M.F. et al. (2017). Experimental design, modeling, and optimization of high-pressure-assisted extraction of bioactive compounds from pomegranate peel. *Food Bioprocess Technol.* 10 (5): 886–900.
7 Paixão, L.M.N., Fonteles, T.V., Oliveira, V.S. et al. (2019). Cold plasma effects on functional compounds of siriguela juice. *Food Bioprocess Technol.* 12 (1): 110–121.

8 Misra, N.N., Martynenko, A., Chemat, F. et al. (2017). Thermodynamics, transport phenomena, and electrochemistry of external field-assisted nonthermal food technologies. Critical Reviews in Food Science and Nutrition.

9 Barba, F.J., Parniakov, O., Pereira, S.A. et al. (2015). Current applications and new opportunities for the use of pulsed electric fields in food science and industry. *Food Res. Int.* 77: 773–798.

10 Hock, T.K., Chala, G.T., and Cheng, H.H. (2020). An innovative hybrid steam-microwave sterilization of palm oil fruits at atmospheric pressure. *Innov. Food Sci. Emerg. Technol.* 60: 102289.

11 Chemat, F., Rombaut, N., Meullemiestre, A. et al. (2017). Review of green food processing techniques. Preservation, transformation, and extraction. *Innov. Food Sci. Emerg. Technol.* 41: 357–377.

12 Hashemi, S.M.B., Nikmaram, N., Esteghlal, S. et al. (2017). Efficiency of ohmic assisted hydrodistillation for the extraction of essential oil from oregano (Origanum vulgare subsp. viride) spices. *Innov. Food Sci. Emerg. Technol.* 41: 172–178.

13 Constable, D.J.C., Curzons, A.D., and Cunningham, V.L. (2002). Metrics to "green" chemistry - Which are the best? *Green Chem.* 4 (6): 521–527.

14 Aissou, M., Chemat-Djenni, Z., Yara-Varón, E. et al. (2017). Limonene as an agro-chemical building block for the synthesis and extraction of bioactive compounds. *Comptes. Rendus Chim.* 20 (4): 346–358.

15 Clarke, C.J., Tu, W.-C., Levers, O. et al. (2018). Green and sustainable solvents in chemical processes. *Chem. Rev.* 118 (2): 747–800.

16 Jin, S., Byrne, F., McElroy, C.R. et al. (2017). Challenges in the development of bio-based solvents: a case study on methyl(2,2-dimethyl-1,3-dioxolan-4-yl)methyl carbonate as an alternative aprotic solvent. *Faraday Discuss.* 202: 157–173.

17 Bakirtzi, C., Triantafyllidou, K., and Makris, D.P. (2016). Novel lactic acid-based natural deep eutectic solvents: efficiency in the ultrasound-assisted extraction of antioxidant polyphenols from common native Greek medicinal plants. *J. Appl. Res. Med. Aromat. Plants.* 3 (3): 120–127.

18 Jurić, S., Ferrari, G., Velikov, K.P., and Donsì, F. (2019). High-pressure homogenization treatment to recover bioactive compounds from tomato peels. *J. Food Eng.* 262: 170–180.

19 Ferrari, G., Mustafa, W., and Donsì, F. (2017). Use of agri-food residues for oil structuring and functionalization. *Chem. Eng. Trans.* 57: 1831–1836.

20 Mustafa, W., Pataro, G., Ferrari, G., and Donsì, F. (2018). Novel approaches to oil structuring via the addition of high-pressure homogenized agri-food residues and water forming capillary bridges. *J. Food Eng.* 236: 9–18.

21 Carullo, D., Abera, B.D., Casazza, A.A. et al. (2018). Effect of pulsed electric fields and high pressure homogenization on the aqueous extraction of intracellular compounds from the microalgae Chlorella vulgaris. *Algal Res.* 31: 60–69.

22 Chemat, F., Vian, M.A., and Cravotto, G. (2012). Green extraction of natural products: concept and principles. *Int. J. Mol. Sci.* 13 (7): 8615–8627.

23 Ferhat, M.A., Meklati, B.Y., and Chemat, F. (2007). Comparison of different isolation methods of essential oil from citrus fruits: cold pressing, hydrodistillation and microwave "dry" distillation. *Flavour Fragr. J.* 22 (6): 494–504.

24 Jambrak, A.R. (2013). Application of high power ultrasound and microwave in food processing: extraction. *J. Food Process. Technol.* 4: 1. https://doi.org/10.4172/2157-7110.1000e113.

25 Mancini, L., Vidal-Legaz, B., Vizzarri, M. et al. (2019). *Mapping The Role of Raw Materials in Sustainable Development Goals*. Publications Office of the European Union.

26 Anastas, P.T. and Warner, J.C. (1998). *Green Chemistry: Theory and Practice: Paperback: Paul Anastas - Oxford University Press*, 148. Oxford [England] ;;New York: Oxford University Press.

27 Žuntar, I., Putnik, P., Bursać Kovačević, D. et al. (2019). Phenolic and antioxidant analysis of olive leaves extracts (Olea europaea L.) obtained by high voltage electrical discharges (HVED). *Foods (Basel, Switzerland)* 8 (7): 248. https://doi.org/10.3390/foods8070248.

28 Breil, C., Abert Vian, M., Zemb, T. et al. (2017). "Bligh and Dyer" and Folch methods for solid–liquid–liquid extraction of lipids from microorganisms. Comprehension of solvatation mechanisms and towards substitution with alternative solvents. *Int. J. Mol. Sci.* 18 (4): 708. https://doi.org/10.3390/ijms18040708.

29 Bundeesomchok, K., Filly, A., Rakotomanomana, N. et al. (2016). Extraction of α-mangostin from Garcinia mangostana L. using alternative solvents: computational predictive and experimental studies. *LWT - Food Sci. Technol.* 65: 297–303.

30 Kujundžić, D., Jambrak, A.R., Vukušić, T. et al. (2017). Near-infrared spectroscopic characterization of steviol glycosides extracted from Stevia rebaudiana Bertoni using high-power ultrasound and gas-phase plasma. *J. Food Nutr. Res.* 56 (2): 109–120. 12p.

31 Putnik, P., Lorenzo, J., Barba, F. et al. (2018). Novel food processing and extraction technologies of high-added value compounds from plant materials. *Foods* 7 (7): 106.

32 Andrade, K.S., Poncelet, D., and Ferreira, S.R.S. (2017). Sustainable extraction and encapsulation of pink pepper oil. *J. Food Eng.* 204: 38–45.

33 Chemat, F., Fabiano-Tixier, A.S., Vian, M.A. et al. (2015). Solvent-free extraction of food and natural products. *TrAC - Trends Anal. Chem.* 71: 157–168.

34 Nutrizio, M., Gajdoš Kljusurić, J., Badanjak Sabolović, M. et al. (2020). Valorization of sage extracts (Salvia officinalis L.) obtained by high voltage electrical discharges: process control and antioxidant properties. *Innov. Food Sci. Emerg. Technol.* 60: 102284.

35 Nayak, B., Dahmoune, F., Moussi, K. et al. (2015). Comparison of microwave, ultrasound and accelerated-assisted solvent extraction for recovery of polyphenols from citrus sinensis peels. *Food Chem.* 187: 507–516.

36 Ameer, K., Shahbaz, H.M., and Kwon, J.H. (2017). Green extraction methods for polyphenols from plant matrices and their byproducts: a review. *Compr. Rev. Food Sci. Food Saf.* 16: 295–315. Blackwell Publishing Inc.

37 Jambrak, A.R., Donsì, F., Paniwnyk, L., and Djekic, I. (2019). Impact of novel nonthermal processing on food quality: sustainability, modelling, and negative aspects. *J. Food Qual.* 2019: 2171375.

38 Jambrak, A.R. (2019). Non-thermal and innovative processing technologies. In: *Encyclopedia of Food Security and Sustainability* (eds. P. Ferranti, E. Berry and A. Jock), 477–483. Elsevier.

39 Rombaut, N., Tixier, A.S., Bily, A., and Chemat, F. (2014). Green extraction processes of natural products as tools for biorefinery. *Biofuels Bioprod. Biorefin.* 8 (4): 530–544.

40 Saini, A., Panesar, P.S., and Bera, M.B. (2019). Valorization of fruits and vegetables waste through green extraction of bioactive compounds and their nanoemulsions-based delivery

system. *Bioresour. Bioprocess.* 6: Article number: 26. https://doi.org/10.1186/s40643-019-0261-9.

41 El-Hadary, A.E. and Taha, M. (2020). Pomegranate peel methanolic-extract improves the shelf-life of edible-oils under accelerated oxidation conditions. *Food Sci. Nutr.* https://doi.org/10.1002/fsn3.1391.

42 Žugčić, T., Abdelkebir, R., Alcantara, C. et al. (2019). From extraction of valuable compounds to health promoting benefits of olive leaves through bioaccessibility, bioavailability and impact on gut microbiota. *Trends Food Sci. Technol.* 83: 63–77.

43 Satari, B., Palhed, J., Karimi, K. et al. (2017). Process optimization for citrus waste biorefinery via simultaneous pectin extraction and pretreatment. *Bioresources* 12 (1): 1706–1722.

44 Drosou, C., Kyriakopoulou, K., Bimpilas, A. et al. (2015). A comparative study on different extraction techniques to recover red grape pomace polyphenols from vinification byproducts. *Ind. Crop. Prod.* 75: 141–149.

45 Wiktor, A., Sledz, M., Nowacka, M. et al. (2015). The impact of pulsed electric field treatment on selected bioactive compound content and color of plant tissue. *Innov. Food Sci. Emerg. Technol.* 30: 69–78.

46 Pavela, R. and Benelli, G. (2016). Essential oils as ecofriendly biopesticides? Challenges and constraints. *Trends Plant Sci.* 21 (12): 1000–1007.

47 Mariño, M., Da Silva, L.L., Durán, N., and Tasic, L. (2015). Enhanced materials from nature: nanocellulose from citrus waste. *Molecules* 20 (4): 5908–5923.

48 Rojko, A. (2017). Industry 4.0 concept: background and overview. *Int. J. Interact Mob. Technol.* 11 (5): 77.

49 Neves, R.C.F., Moraes, P.M., Saleh, M.D. et al. (2009). FAAS determination of metal nutrients in fish feed after ultrasound extraction. *Food Chem.* 113 (2): 679–683.

50 Filly, A., Fabiano-Tixier, A.S., Louis, C. et al. (2016). Water as a green solvent combined with different techniques for extraction of essential oil from lavender flowers. *Comptes Rendus Chimie. Elsevier Masson SAS* 19: 707–717.

51 Vian, M.A., Fernandez, X., Visinoni, F., and Chemat, F. (2008). Microwave hydrodiffusion and gravity, a new technique for extraction of essential oils. *J. Chromatogr. A* 1190 (1–2): 14–17.

52 Rodríguez-Meizoso, I., Castro-Puyana, M., Börjesson, P. et al. (2012). Life cycle assessment of green pilot-scale extraction processes to obtain potent antioxidants from rosemary leaves. *J. Supercrit. Fluids* 72: 205–212.

53 Bousbia, N., Abert Vian, M., Ferhat, M.A. et al. (2009). Comparison of two isolation methods for essential oil from rosemary leaves: hydrodistillation and microwave hydrodiffusion and gravity. *Food Chem.* 114 (1): 355–362.

54 Barba, F.J., Orlien, V., Mota, M.J. et al. (2016). Implementation of emerging technologies. In: *Innovation Strategies in the Food Industry: Tools for Implementation*, 1e (ed. C. Galanakis), 117–148. Academic Press https://doi.org/10.1016/B978-0-12-803751-5.00007-6.

55 Lupacchini, M., Mascitti, A., Giachi, G. et al. (2017). Sonochemistry in non-conventional, green solvents or solvent-free reactions. *Tetrahedron* 73 (6): 609–653.

56 Haas, W., Krausmann, F., Wiedenhofer, D., and Heinz, M. (2015). How circular is the global economy?: an assessment of material flows, waste production, and recycling in the European union and the world in 2005. *J. Ind. Ecol.* 19 (5): 765–777.

57 Cséfalvay, E., Akien, G.R., Qi, L., and Horváth, I.T. (2015). Definition and application of ethanol equivalent: sustainability performance metrics for biomass conversion to carbon-based fuels and chemicals. *Catal. Today* 239: 50–55.

58 Sheldon, R.A. (2018). Metrics of green chemistry and sustainability: past, present, and future. *ACS Sustainable Chem. Eng.* 6: 32–48. American Chemical Society.

59 Fegade, S.L. and Trembly, J.P. (2015). Dispute over designating an ionic liquid as a green solvent. *Chem. Eng. J.* 273: 668.

60 Winterton, N. (2016). Green chemistry: deliverance or distraction? *Clean Techn. Environ. Policy* 18 (4): 991–1001.

61 Sáez-Martínez, F.J., Lefebvre, G., Hernández, J.J., and Clark, J.H. (2016). Drivers of sustainable cleaner production and sustainable energy options. *J. Clean. Prod.* 138 (Part 1): 1–7.

62 Clark, J.H., Deswarte, F.E.I., and Farmer, T.J. (2009). The integration of green chemistry into future biorefineries. *Biofuels Bioprod. Biorefin.* 3 (1): 72–90.

63 Van Aken, K., Strekowski, L., and Patiny, L. (2006). EcoScale, a semi-quantitative tool to select an organic preparation based on economical and ecological parameters. *Beilstein J. Org. Chem.* 2 (1): 3. https://doi.org/10.1186/1860-5397-2-3.

64 Hoffmann, V.H., Hungerbühler, K., and McRae, G.J. (2001). Multiobjective screening and evaluation of chemical process technologies. *Ind. Eng. Chem. Res.* 40 (21): 4513–4524.

65 Leseurre, L., Merea, C., Duprat De Paule, S., and Pinchart, A. (2014). Eco-footprint: a new tool for the "made in Chimex" considered approach. *Green Chem.* 16 (3): 1139–1148.

66 Phan, T.V.T., Gallardo, C., and Mane, J. (2015). GREEN MOTION: a new and easy to use green chemistry metric from laboratories to industry. *Green Chem.* 17 (5): 2846–2852.

67 Klöpffer, W. (2005). Life cycle assessment as part of sustainability assessment for chemicals. *Environ. Sci. Pollut. Res.* 12 (3): 173–177.

68 Kralisch, D., Ott, D., and Gericke, D. (2015). Rules and benefits of life cycle assessment in green chemical process and synthesis design: a tutorial review. *Green Chem.* 17 (1): 123–145.

69 Isoni, V., Wong, L.L., Khoo, H.H. et al. (2016). Q-SA√ESS: a methodology to help solvent selection for pharmaceutical manufacture at the early process development stage. *Green Chem.* 18 (24): 6564–6572.

70 Trost, B.M. (1991). The atom economy - a search for synthetic efficiency. *Science* 254 (5037): 1471–1477.

71 Hudlicky, T., Frey, D.A., Koroniak, L. et al. (1999). Toward a "reagent-free" synthesis: Tandem enzymatic and electrochemical methods for increased effective mass yield (EMY). *Green Chem.* 1 (2): 57–59.

72 Jimenez-Gonzalez, C., Ponder, C.S., Broxterman, Q.B., and Manley, J.B. (2011). Using the right green yardstick: why process mass intensity is used in the pharmaceutical industry to drive more sustainable processes. *Org. Process. Res. Dev.* 15 (4): 912–917.

73 Andraos, J. (2005). Unification of reaction metrics for green chemistry: applications to reaction analysis. *Org. Process. Res. Dev.* 9 (2): 149–163.

74 Voss, B., Andersen, S.I., Taarning, E., and Christensen, C.H. (2009). Cfactors pinpoint resource utilization in chemical industrial processes. *ChemSusChem.* 2 (12): 1152–1162.

75 Wernet, G., Papadokonstantakis, S., Hellweg, S., and Hungerbühler, K. (2009). Bridging data gaps in environmental assessments: modeling impacts of fine and basic chemical production. *Green Chem.* 11 (11): 1826–1831.

76 Saling, P., Kicherer, A., Dittrich-Krämer, B. et al. (2002). Eco-efficiency analysis by BASF: the method. *Int. J. Life Cycle Assess* 7 (4): 203–218.

77 Gonzalez, M.A. and Smith, R.L. (2003). A methodology to evaluate process sustainability. *Environ. Prog.* 22 (4): 269–276.

78 Welton, T. (2015). Solvents and sustainable chemistry. *Proc. R. Soc. A Math Phys. Eng. Sci.* 471 (2183): 20150502. https://doi.org/10.1098/rspa.2015.0502.

79 Chen, L., Sharifzadeh, M., Mac Dowell, N. et al. (2014). Inexpensive ionic liquids: $[HSO_4]^-$-based solvent production at bulk scale. *Green Chem.* 16 (6): 3098–3106.

80 Zhang, Y., Bakshi, B.R., and Demessie, E.S. (2008). Life cycle assessment of an ionic liquid versus molecular solvents and their applications. *Environ. Sci. Technol.* 42 (5): 1724–1730.

81 Sherwood, J., Clark, J.H., Farmer, T.J. et al. (2017). Recirculation: a new concept to drive innovation in sustainable product design for bio-based products. *Molecules* 22 (1): 48. https://doi.org/10.3390/molecules22010048.

82 Sheldon, R.A. (2016). Green chemistry and resource efficiency: towards a green economy. *Green Chem.* 18 (11): 3180–3183.

83 Clark, J.H., Farmer, T.J., Herrero-Davila, L., and Sherwood, J. (2016). Circular economy design considerations for research and process development in the chemical sciences. *Green Chem.* 18 (14): 3914–3934.

84 Zuin, V.G. (2016). Circularity in green chemical products, processes and services: innovative routes based on integrated eco-design and solution systems. *Curr. Opin. Green Sustain. Chem.* 2: 40–44.

85 Yim, K.H., Stambouli, M., and Pareau, D. (2014). Alternative solvents for natural products extraction. *Green Chem. Sustain. Technol.*: 221–235.

86 Kerton, F. and Marriott, R. (2013). Green solvents - legislation and certification. In: *RSC Green Chemistry*, 31–50 p. The Royal Society of Chemistry.

87 Li, Y., Kunz, W., and Chemat, F. (2019). *From Petroleum to Bio-Based Solvents: From Academia to Industry*, 51–87. Singapore: Springer.

88 Essien, S.O., Young, B., and Baroutian, S. (2020). Recent advances in subcritical water and supercritical carbon dioxide extraction of bioactive compounds from plant materials. *Trends Food Sci. Technol.* 97: 156–169. Elsevier Ltd.

89 Fairchild, E.H., Komor, J.A., Petro, A.J., and Baird, G.T. (1999). Industrial applications of surfactants IV. In: *Industrial Applications of Surfactants IV* (ed. D.R. Karsa), 50–62. Woodhead Publishing.

90 Chemat, F., Abert-Vian, M., Fabiano-Tixier, A.S. et al. (2019). Green extraction of natural products. Origins, current status, and future challenges. *TrAC Trends Anal. Chem.* 118: 248–263.

91 Sicaire, A.-G., Filly, A., Vian, M. et al. (2018). Cosmo-RS-assisted solvent screening for Green extraction of natural products. In: *Handbook of Green Chemistry*, 117–138. Weinheim, Germany: Wiley-VCH Verlag GmbH & Co. KGaA.

92 Li, Y., Fabiano-Tixier, A.S., Tomao, V. et al. (2013). Green ultrasound-assisted extraction of carotenoids based on the bio-refinery concept using sunflower oil as an alternative solvent. *Ultrason. Sonochem.* 20 (1): 12–18.

93 Li, Y., Fabiano-Tixier, A.S., Ginies, C., and Chemat, F. (2014). Direct green extraction of volatile aroma compounds using vegetable oils as solvents: theoretical and experimental solubility study. *LWT Food Sci. Technol.* 59 (2P1): 724–731.

94 Jesus, S.P. and Meireles, M.A.A. (2014). *Supercritical Fluid Extraction: A Global Perspective of the Fundamental Concepts of this Eco-Friendly Extraction Technique*, 39–72. Berlin, Heidelberg: Springer.

95 Chemat, F., Abert Vian, M., Fabiano-Tixier, A.-S. et al. (2020). A review of sustainable and intensified techniques for extraction of food and natural products. *Green Chem.* 22: 2325–2353.

96 De Marco, I., Riemma, S., and Iannone, R. (2018). Life cycle assessment of supercritical CO_2 extraction of caffeine from coffee beans. *J. Supercrit. Fluids* 133: 393–400.

97 Baskar, G., Kalavathy, G., Aiswarya, R., and Abarnaebenezer Selvakumari, I. (2019). Advances in bio-oil extraction from nonedible oil seeds and algal biomass. In: *Advances in Eco-Fuels for a Sustainable Environment* (ed. A.K. Azad), 187–210. Sawston: Woodhead Publishing https://doi.org/10.1016/B978-0-08-102728-8.00007-3.

98 Wu, Y.C., Wu, P., Li, Y.B. et al. (2018). Natural deep eutectic solvents as new green solvents to extract anthraquinones from: Rheum palmatum L. *RSC Adv.* 8 (27): 15069–15077.

99 Fernández, M.d.l.Á., Boiteux, J., Espino, M. et al. (2018). Natural deep eutectic solvents-mediated extractions: the way forward for sustainable analytical developments. *Anal. Chim. Acta* 1038: 1–10. Elsevier B.V.

100 Cui, Q., Liu, J.-Z., Wang, L.-T. et al. (2018). Sustainable deep eutectic solvents preparation and their efficiency in extraction and enrichment of main bioactive flavonoids from sea buckthorn leaves. *J. Clean. Prod.* 184: 826–835.

101 Klamt, A., Eckert, F., and Arlt, W. (2010). COSMO-RS: an alternative to simulation for calculating thermodynamic properties of liquid mixtures. *Annu. Rev. Chem. Biomol. Eng.* 1 (1): 101–122.

102 Zhou, T., McBride, K., Linke, S. et al. (2020). Computer-aided solvent selection and design for efficient chemical processes. *Curr. Opin. Chem. Eng.* 27: 35–44. Elsevier Ltd.

103 Lucia, A. and Finger, E.J. (2004). Co-solvent selection and recovery. *Adv. Environ. Res.* 8 (2): 197–211.

104 Ab Rani, M.A., Borduas, N., Colquhoun, V. et al. (2014). The potential of methylsiloxanes as solvents for synthetic chemistry applications. *Green Chem.* 16 (3): 1282–1296.

105 Duereh, A., Guo, H., Sato, Y., and Inomata, H. (2020). Local composition models for predicting Kamlet-Taft dipolarity/polarizability of nonaqueous binary and ternary mixtures. *J. Mol. Liq.* 304: 112691.

106 Weerachanchai, P., Chen, Z., Leong, S.S.J. et al. (2012). Hildebrand solubility parameters of ionic liquids: effects of ionic liquid type, temperature and DMA fraction in ionic liquid. *Chem. Eng. J.* 213: 356–362.

107 Lee, S.H. and Lee, S.B. (2005). The Hildebrand solubility parameters, cohesive energy densities and internal energies of 1-alkyl-3-methylimidazolium-based room temperature ionic liquids. *Chem. Commun.* 27: 3469–3471.

108 Sistla, Y.S., Jain, L., and Khanna, A. (2012). Validation and prediction of solubility parameters of ionic liquids for CO_2 capture. *Sep. Purif. Technol.* 97: 51–64.

109 Alavianmehr, M.M., Hosseini, S.M., Mohsenipour, A.A., and Moghadasi, J. (2016). Further property of ionic liquids: hildebrand solubility parameter from new molecular thermodynamic model. *J. Mol. Liq.* 218: 332–341.

110 Dębski, B., Hänel, A., Aranowski, R. et al. (2019). Thermodynamic interpretation and prediction of CO_2 solubility in imidazolium ionic liquids based on regular solution theory. *J. Mol. Liq.* 291: 110477.

111 Sánchez-Camargo, A.d.P., Bueno, M., Parada-Alfonso, F. et al. (2019). Hansen solubility parameters for selection of green extraction solvents. *TrAC - Trends Analyt. Chem.* 118: 227–237. Elsevier B.V.

112 Hansen, C.M. (2007). Methods of characterization - surfaces. In: *Hansen Solubility Parameters: A Users Handbook*, 2e (ed. C.M. Hansen), 113–123. CRC Press, Inc.

113 del Pilar Sánchez-Camargo, A., Pleite, N., Herrero, M. et al. (2017). New approaches for the selective extraction of bioactive compounds employing bio-based solvents and pressurized green processes. *J. Supercrit. Fluids* 128: 112–120.

114 Yara-Varón, E., Fabiano-Tixier, A.S., Balcells, M. et al. (2016). Is it possible to substitute hexane with green solvents for extraction of carotenoids? A theoretical versus experimental solubility study. *RSC Adv.* 6 (33): 27750–27759.

115 El Kantar, S., Rajha, H.N., Boussetta, N. et al. (2019). Green extraction of polyphenols from grapefruit peels using high voltage electrical discharges, deep eutectic solvents and aqueous glycerol. *Food Chem.* 295: 165–171.

116 Moity, L., Durand, M., Benazzouz, A. et al. (2012). Panorama of sustainable solvents using the COSMO-RS approach. *Green Chem.* 14 (4): 1132–1145.

117 Pozarska, A., Da Costa Mathews, C., Wong, M., and Pencheva, K. (2013). Application of COSMO-RS as an excipient ranking tool in early formulation development. *Eur. J. Pharm. Sci.* 49 (4): 505–511.

118 Xing, H., Zhang, X., Yang, Q. et al. (2014). Separation of long chain fatty acids with different number of unsaturated bonds by fractional extraction: experimental and COSMO-RS study. *Food Chem.* 143: 411–417.

119 Jeschke, S. and Johansson, P. (2017). Predicting the solubility of sulfur: a COSMO-RS-based approach to investigate electrolytes for Li–S batteries. *Chem - A Eur. J.* 23 (38): 9130–9136.

120 Goussard, V., Duprat, F., Ploix, J.-L. et al. (2020). A new machine-learning tool for fast estimation of liquid viscosity. Application to cosmetic oils. *J. Chem. Inf. Model.* https://doi.org/10.1021/acs.jcim.0c00083.

121 Goussard, V., Duprat, F., Gerbaud, V. et al. (2017). Predicting the surface tension of liquids: comparison of four modeling approaches and application to cosmetic oils. *J. Chem. Inf. Model.* 57 (12): 2986–2995.

122 Sicaire, A.-G., Vian, M.A., Fine, F. et al. (2015). Experimental approach versus COSMO-RS assisted solvent screening for predicting the solubility of rapeseed oil. *OCL* 22 (4): D404.

123 Byrne, F.P., Jin, S., Paggiola, G. et al. (2016). Tools and techniques for solvent selection: green solvent selection guides. *Sustain. Chem. Process.* 4 (1): 7.

124 Buncel, E., Stairs, R.A., Robert, A., and Wilson, H. (2003). *The Role of the Solvent in Chemical Reactions*, 159. Oxford University Press.

125 Vian, M., Breil, C., Vernes, L. et al. (2017). Green solvents for sample preparation in analytical chemistry. *Curr. Opin. Green Sustain. Chem.* 5: 44–48.

126 Tomé, L.I.N., Baião, V., da Silva, W., and Brett, C.M.A. (2018). Deep eutectic solvents for the production and application of new materials. *Appl. Mater. Today* 10: 30–50.

127 Cvjetko Bubalo, M., Vidović, S., Radojčić Redovniković, I., and Jokić, S. (2018). New perspective in extraction of plant biologically active compounds by green solvents. *Food Bioprod. Process.* 109: 52–73.

128 Reinhardt, D., Ilgen, F., Kralisch, D. et al. (2008). Evaluating the greenness of alternative reaction media. *Green Chem.* 10 (11): 1170–1181.

129 Capello, C., Fischer, U., and Hungerbühler, K. (2007). What is a green solvent? A comprehensive framework for the environmental assessment of solvents. *Green Chem.* 9 (9): 927–934.

130 Clark, J.H. and Tavener, S.J. (2007). Alternative solvents: shades of green. *Org. Process. Res. Dev.* 11 (1): 149–155.

131 Cseri, L., Razali, M., Pogany, P., and Szekely, G. (2018). Organic solvents in sustainable synthesis and engineering. In: *Green Chemistry: An Inclusive Approach* (eds. B. Torok and T. Dransfield), 513–553. Elsevier Inc.

132 Smallwood, I.M. (2002). *Solvent Recovery Handbook*, 2e, 424. Florida, USA: Blackwell Science.

133 Großeheilmann, J., Vanderveen, J.R., Jessop, P.G., and Kragl, U. (2016). Switchable-hydrophilicity solvents for product isolation and catalyst recycling in organocatalysis. *ChemSusChem* 9 (7): 696–702.

134 Didaskalou, C., Buyuktiryaki, S., Kecili, R. et al. (2017). Valorisation of agricultural waste with an adsorption/nanofiltration hybrid process: from materials to sustainable process design. *Green Chem.* 19 (13): 3116–3125.

135 Voros, V., Drioli, E., Fonte, C., and Szekely, G. (2019). Process intensification via continuous and simultaneous isolation of antioxidants: an upcycling approach for olive leaf waste. *ACS Sustain. Chem. Eng.* 7 (22): 18444–18452.

136 Kralisch, D., Reinhardt, D., and Kreisel, G. (2007). Implementing objectives of sustainability into ionic liquids research and development. *Green Chem.* 9 (12): 1308–1318.

137 Lu, J., He, A., Li, S. et al. (2015). Synthesis, purification and recycling of ionic liquid. *Mini. Rev. Org. Chem.* 12 (5): 435–448.

138 Slater, C.S. and Savelski, M. (2007). A method to characterize the greenness of solvents used in pharmaceutical manufacture. *J. Environ. Sci. Heal - Part A Toxic/Hazardous Subst. Environ. Eng.* 42 (11): 1595–1605.

139 Alfonsi, K., Colberg, J., Dunn, P.J. et al. (2008). Green chemistry tools to influence a medicinal chemistry and research chemistry based organisation. *Green Chem.* 10 (1): 31–36.

140 Henderson, R.K., Jiménez-González, C., Constable, D.J.C. et al. (2011). Expanding GSK's solvent selection guide – embedding sustainability into solvent selection starting at medicinal chemistry. *Green Chem.* 13 (4): 854–862.

141 Alder, C.M., Hayler, J.D., Henderson, R.K. et al. (2016). Updating and further expanding GSK's solvent sustainability guide. *Green Chem.* 18 (13): 3879–3890.

142 Prat, D., Pardigon, O., Flemming, H.W. et al. (2013). Sanofi's solvent selection guide: a step toward more sustainable processes. *Org. Process. Res. Dev.* 17 (12): 1517–1525.

143 Guo, Z., Zhao, B., Li, H. et al. (2019). Optimization of ultrasound-microwave synergistic extraction of prebiotic oligosaccharides from sweet potatoes (Ipomoea batatas L.). *Innov. Food Sci. Emerg. Technol.* 54: 51–63.

144 Karmee, S.K., Niemeijer, B., Casiraghi, L. et al. (2014). Facile biocatalytic synthesis of a macrocyclic lactone in sub- and supercritical solvents. *Biocatal. Biotransfor.* 32 (2): 125–131.

145 Uoonlue, N. and Muangrat, R. (2019). Effect of different solvents on subcritical solvent extraction of oil from Assam tea seeds (Camellia sinensis var. assamica): optimization of oil extraction and physicochemical analysis. *J. Food Process Eng.* 42 (2): e12960.

146 Cortazar, E., Bartolomé, L., Delgado, A. et al. (2005). Optimisation of microwave-assisted extraction for the determination of nonylphenols and phthalate esters in sediment samples and comparison with pressurised solvent extraction. *Anal. Chim. Acta* 534 (2): 247–254.

147 Markom, M., Hasan, M., Daud, W.R.W. et al. (2007). Extraction of hydrolysable tannins from Phyllanthus niruri Linn.: effects of solvents and extraction methods. *Sep. Purif. Technol.* 52 (3): 487–496.

148 Martins, S., Aguilar, C.N., de la Garza-Rodriguez, I. et al. (2010). Kinetic study of nordihydroguaiaretic acid recovery from Larrea tridentata by microwave-assisted extraction. *J. Chem. Technol. Biotechnol.* 85 (8): 1142–1147.

149 Araújo, J.M.A. and Sandi, D. (2007). Extraction of coffee diterpenes and coffee oil using supercritical carbon dioxide. *Food Chem.* 101 (3): 1087–1094.

150 Muangrat, R. and Pongsirikul, I. (2019). Recovery of spent coffee grounds oil using supercritical CO_2: extraction optimisation and physicochemical properties of oil. *CyTA – J. Food* 17 (1): 334–346.

151 Grigonis, D., Venskutonis, P.R., Sivik, B. et al. (2005). Comparison of different extraction techniques for isolation of antioxidants from sweet grass (Hierochloë odorata). *J. Supercrit. Fluids* 33 (3): 223–233.

152 Oyewole, O. and Kalejaiye, O.A. (2012). The antimicrobial activities of Ethanolic extracts of Basella alba on selected microorganisms. *Sci. J. Microbiol.* 1: 113–118.

153 Adhikari, R., Kumar, H.N.N., and Shruthi, S.D. (2012). A review on medicinal importance of Basella alba L. *Int. J. Pharm. Sci. Drug Res.* 4 (2): 110–114.

154 Ogutu, F.O. (2015). Ultrasonic modification of selected polysaccharides-review. *J. Food Process Technol.* 6: 5. https://doi.org/10.4172/2157-7110.1000446.

155 Liu, Y., Luo, X., Lan, Z. et al. (2017). Ultrasonic-assisted extraction and antioxidant capacities of flavonoids from Camellia fascicularis leaves. *CyTA – J. Food* 16 (1): 105–112.

156 Tiwari, B.K. (2015). Ultrasound: a clean, green extraction technology. *TrAC - Trends in Analytical Chemistry* 71: 100–109. Elsevier B.V.

157 Buadoktoom, S. (2019). Extraction of ceylon spinach mucilage for shelf-life extension of fresh pork. Master Thesis. Agro-Industrial Product Development, Chiang Mai University, Thailand.

158 Surin, S., Seesuriyachan, P., Thakeow, P., and You, S.G. (2018). Antioxidant and antimicrobial properties of polysaccharides from rice brans. *Chiang Mai J. Sci.* 45 (3): 1372–1382.

159 Surin, S., Surayot, U., Seesuriyachan, P. et al. (2018). Antioxidant and immunomodulatory activities of sulphated polysaccharides from purple glutinous rice bran (*Oryza sativa* L.). *Int. J. Food Sci. Technol.* 53 (4): 994–1004.

160 Xiong, Q., Li, X., Zhou, R. et al. (2014). Extraction, characterization and antioxidant activities of polysaccharides from E. corneum gigeriae galli. *Carbohydr. Polym.* 108 (1): 247–256.

161 Wang, H., Peng, J., Xie, C. et al. (2015). Fruit quality evaluation using spectroscopy technology: a review. *Sensors (Switzerland)* 15: 11889–11927. MDPI AG.

162 Tian, Y., Zeng, H., Xu, Z. et al. (2012). Ultrasonic-assisted extraction and antioxidant activity of polysaccharides recovered from white button mushroom (Agaricus bisporus). *Carbohydr. Polym.* 88 (2): 522–529.

163 Mohanty, D., Misra, S., Mohapatra, S., and Sahu, P.S. (2018). Prebiotics and synbiotics: recent concepts in nutrition. *Food Biosci.* 26: 152–160. Elsevier Ltd.

164 Moreno, F.J., Corzo, N., Montilla, A. et al. (2017). Current state and latest advances in the concept, production and functionality of prebiotic oligosaccharides. *Curr. Opin. Food Sci.* 13: 50–55. Elsevier Ltd.

165 Wang, S., Xiao, Y., Tian, F. et al. (2020). Rational use of prebiotics for gut microbiota alterations: specific bacterial phylotypes and related mechanisms. *J. Funct. Foods* 66: 103838. Elsevier Ltd.

166 Fu, X., Belwal, T., Cravotto, G., and Luo, Z. (2020). Sono-physical and sono-chemical effects of ultrasound: primary applications in extraction and freezing operations and influence on food components. *Ultrason. Sonochem.* 60: 104726. Elsevier B.V.

167 Fu, C., Tian, H., Li, Q. et al. (2006). Ultrasound-assisted extraction of xyloglucan from apple pomace. *Ultrason. Sonochem.* 13 (6): 511–516.

168 Hromádková, Z., Košťálová, Z., and Ebringerová, A. (2008). Comparison of conventional and ultrasound-assisted extraction of phenolics-rich heteroxylans from wheat bran. *Ultrason. Sonochem.* 15 (6): 1062–1068.

169 Subhedar, P.B. and Gogate, P.R. (2014). Alkaline and ultrasound assisted alkaline pretreatment for intensification of delignification process from sustainable raw-material. *Ultrason. Sonochem.* 21 (1): 216–225.

170 Jovanovic-Malinovska, R., Kuzmanova, S., and Winkelhausen, E. (2015). Application of ultrasound for enhanced extraction of prebiotic oligosaccharides from selected fruits and vegetables. *Ultrason. Sonochem.* 22: 446–453.

171 Benito-Román, Ó., Alonso, E., and Cocero, M.J. (2013). Ultrasound-assisted extraction of β-glucans from barley. *LWT Food Sci. Technol.* 50 (1): 57–63.

172 Ninomiya, K., Takamatsu, H., Onishi, A. et al. (2013). Sonocatalytic-Fenton reaction for enhanced OH radical generation and its application to lignin degradation. *Ultrason. Sonochem.* 20 (4): 1092–1097.

173 Kawee-Ai, A., Srisuwun, A., Tantiwa, N. et al. (2016). Eco-friendly processing in enzymatic xylooligosaccharides production from corncob: influence of pretreatment with sonocatalytic-synergistic Fenton reaction and its antioxidant potentials. *Ultrason. Sonochem.* 31: 184–192.

174 Naviglio, D., Pizzolongo, F., Ferrara, L. et al. (2008). Extraction of pure lycopene from industrial tomato by-products in water using a new high-pressure process. *J. Sci. Food Agric.* 88 (14): 2414–2420.

175 Koos, E. (2014). Capillary suspensions: particle networks formed through the capillary force. *Curr. Opin. Colloid Interface Sci.* 19: 575–584.

15

Cellulose Nanofibers for Sustainable Separations

Priyanka R. Sharma, Xiangyu Huang, Mengying Yang, Sunil K. Sharma, and Benjamin S. Hsiao

Department of Chemistry, Stony Brook University, Stony Brook, NY, USA

15.1 Introduction

Scarcity of clean drinking water and lack of low-cost purification methods to treat contaminated water remain to be major global water challenges. Although conventional filtration/adsorption technologies can offer reliable solutions to remove unwanted contaminants, these technologies are not able to deal with all aspects of societal needs [1]. To reduce cost, enhance efficiency, and ensure the sustainability of any water purification solutions, one promising direction is through the development of new sustainable nanomaterials by taking advantage of their large surface area, vast active functionality through adsorption, flocculation, or filtration processes [2].

Cellulose nanofiber (CNF), an abundant and renewable nanomaterial, is of great interest for water purification because of its high hydrophilicity, water stability, abundant functionality, and high specific surface areas, some properties are superior to synthetic polymers [3, 4]. For example, the abundant hydroxyl groups at the C2, C3, and C6 positions of the cellulosic repeating unit on the nanocellulose surface can render the material as an effective adsorbent to attract a variety of charged organic (e.g. dye and protein molecules) and inorganic (e.g. toxic metal ions) contaminants [5, 6], or a low-fouling barrier layer on filtration membrane with improved biofouling resistance [7, 8] and bacteria removal capability [9]. From the perspective of surface charge, nanocellulose can be differentiated into two types: negatively charged (anionic) nanocellulose and positively charged (cationic) nanocellulose, which are described as follows.

15.1.1 Negatively Charged (Anionic) Nanocellulose

The negative charge functionality on nanocellulose can be obtained directly by varying chemical reaction-facilitated defibrillation processes, such as acid hydrolysis (sulfuric acid), (2,2,6,6-tetramethylpiperidin-1-yl)oxidanyl (TEMPO)-oxidation [10], carboxymethylation,

Sustainable Separation Engineering: Materials, Techniques and Process Development, Volume 2, First Edition. Edited by Gyorgy Szekely and Dan Zhao.
© 2022 John Wiley & Sons Ltd. Published 2022 by John Wiley & Sons Ltd.

enzymatic hydrolysis [11, 12], combined sodium chlorite-alkaline [13], and ultrasonication [14], as well as the newly developed nitro-oxidation process (NOP) [15–19]. In this section, we will highlight some recent advances in using nitro-oxidized nanocellulose as an adsorbent for the removal of different metal ions and TEMPO-oxidized cellulose nanofibers (TEMPO-CNF) as a thin-film nanofibrous composite (TFNC) membrane with biofouling resistance. Our rationale is as follows. TEMPO oxidation remains to be the most energy-efficient way to produce carboxycellulose nanofibers with a high aspect ratio, where the resulting TEMPO-CNF was found to be particularly suited for use as the membrane barrier layer. NOP has recently been found to be very effective to extract CNF from raw nonwoody plant biomass with significantly reduced consumption of energy, water and chemicals, as the process offers both functions of pulping and cellulose oxidation. As a result, nitro-oxidized cellulose nanofibers (NOCNF) may complement activated carbon and serve as a cost-effective adsorbent. Some brief descriptions of NO, TEMPO-oxidation and carboxymethylation are as follows.

i) Nitro-oxidation process. Recently, Sharma et al. has demonstrated the use of NOP to directly extract carboxycellulose nanofibers from untreated (raw) biomass, ranging from wood to agriculture residues with significantly reduced consumption of chemicals, water and energy [15–19]. The NOP involves the use of nitric acid and sodium nitrite mixtures, where nitric acid acts as a pretreatment agent that can remove lignin and hemicellulose components, while the reaction product between nitric acid and sodium nitrite-nitrosonium ion – can act as a primary oxidant that is responsible for the selective conversion of the hydroxyl group at the C6 position in the anhydroglucose unit to a carboxylic acid group. In this chapter, nanocellulose obtained using the NOP is abbreviated as NOCNF. The maximum charge density obtained for NOCNF was found to be about 1.28 mmol/g, where the extracted NOCNF has a possibility to possess a trace amount of lignin and hemicellulose. Additionally, the effluent from the NOP treatment can be easily recycled to nitrogen-rich salts and used as plant fertilizers.
ii) TEMPO-oxidation: TEMPO-oxidation is a well-known method to generate the carboxycellulose nanofibers from the biomass pulp, i.e. cellulose (after removal of lignin and hemicellulose) [20]. This method has been well documented in the application of cellulose from different biomass sources, including plant, algae, and bacterial cellulose. This method is a mild oxidation approach that can generate a wide range of charged nanocellulose. Here, nanocellulose extracted from TEMPO-oxidation is abbreviated as TEMPO-CNF, which rarely possesses any lignin and hemicellulose residues. Various chemical pathways such as sodium hypochlorite (NaClO)/sodium bromide (NaBr)/TEMPO [21]; TEMPO/NaClO/sodium chlorite ($NaClO_2$) [22]; and TEMPO/Laccase/oxygen (O_2) [23] have been reported, all can oxidize and defibrillate cellulose microfibers to carboxycellulose nanofibers. TEMPO-oxidation also selectively oxidizes hydroxyl group at the C6 position in the anhydroglucose unit into the carboxyl group.
iii) Carboxymethylation: Carboxymethylation is another method that can produce negatively charged nanocellulose. The preparation of carboxymethylated nanocellulose includes alcohol-containing cellulose fibers reacting with monochloroacetic acid in an

alkaline medium [24, 25]. Like the TEMPO-oxidation method, carboxymethylation has also been reported on the modification of pretreated biomass (i.e. cellulose). Carboxymethylated nanocellulose possesses a high negative charge, as the method non-selectively oxidizes all hydroxyl groups (at C2, C3, and C6 positions) in the anhydroglucose unit. Hence, the degree of substitution (DS) is an important term used for carboxymethylated cellulose that indicates the number of substituted hydroxyl groups with the carboxymethylated group in the anhydroglucose unit. It is known that morphological, chemical, and rheological properties of carboxymethylated cellulose vary with DS. However, we will not discuss this nanocellulose material for separation applications in this chapter.

15.1.1.1 Applications of Negatively Charged Nanocellulose in Water Purification

The negatively charged nanocellulose has been well suited as an adsorbent or membrane barrier layer to attract positively charged contaminants, such as heavy metal ions and cationic dye molecules [17, 26–31]. In most of the adsorption studies, the adsorption mechanism involved only electrostatic interactions between the charged species [32], but in some cases, the mineralization process was also observed [17, 26, 27, 30]. In the case of using CNF as a barrier layer material, surface charge density becomes essential in influencing its fouling behavior during UF [33–35]. It was found that the negatively charged nanocellulose layer could repel negatively charged pollutants and reduce the fouling tendency. Specifically, the increase in charge density (or degree of oxidation [DO]) could positively decrease the degree of fouling in TFNC membranes based on TEMPO-CNF-coating layer. The CNF surface charge is directly related to the zeta potential, and hydrophilicity of the membranes could also be adjusted by the coating layer thickness. Generally, the filtration property (e.g. flux) and fouling behavior of TFNC membranes containing the CNF barrier layer are much better than commercial poly(vinylidene fluoride) (PVDF) UF membrane in wastewater treatments.

15.1.2 Positively Charged (Cationic) Nanocellulose

The positively charged (cationic) nanocellulose can be prepared by several different routes. Here, we describe a two-step method, involving the conversion of cellulose to 2,3-Dialdehyde cellulose (DAC) through periodate oxidation and then the functionalization of DAC to cationic DAC (c-DAC) prepared using Girard's reagent T (GT).

Periodate oxidation of cellulose is a popular approach to modify cellulose by introducing aldehyde groups into the chain, facilitating further chemical modifications. Specifically, periodate oxidation can effectively cleave the C2–C3 bonds between the two vicinal hydroxyl groups in the glucose unit, forming two adjacent aldehyde groups without causing significant side reactions [36, 37]. The resulting product is usually referred to as DAC. The possible forms of the DAC structure include the free aldehyde form (-CHO), hydrated form (-$CH(OH)_2$), 2,3-hemialdal form (-CH(OH)-O-CH(OH)-), and both intramolecular and intermolecular 2,6- or 3,6-hemiacetal forms (-CH(OH)-O-CH_2-). The appearance of the varying DAC form corresponds with the addition of one molecule of water on per aldehyde group (the hydrated form), the addition of one molecule of water on per two aldehyde groups (the hemialdal form) or the rearrangement between the alcohol

group on the cellulose unit and one of the aldehyde groups (the hemiacetal form) [38]. The presence of these forms is pH-dependent, as the double-bonded carbonyl group is base-sensitive and relatively stable under the acidic environment, while the "protected" carbonyl forms (hydrated and hemiacetal) are quite stable in the basic media [39]. Therefore, under appropriate conditions, all forms of the DAC structure could react as free aldehydes. Periodate oxidation of cellulose could be performed under mild conditions (in darkness at room temperature or slightly elevated temperatures) in an aqueous system and can be stopped by adding ethylene glycol [40]. The morphology and structure of DAC products can be adjusted by the reaction conditions, such as reaction time, temperature, amount of sodium periodate, etc. [41, 42]

15.1.2.1 Applications of Positively Charged Nanocellulose in Water Purification

Due to the relatively straightforward route to prepare DAC, which has become a popular intermediate for further modification to make functional nanocellulose for water purification. For example, the aldehyde groups in DAC can be converted to carboxylic groups [43, 44], primary alcohols [45], or imines with primary amines through the Schiff base reaction [46–49]. The amine modification will result in positively charged nanocellulose (e.g. c-DAC), which will be discussed later. The functionalized DAC materials can be used as coagulants for activated sludge [50] or adsorbents for removal of heavy metals [43, 46, 51], dyes [52–54], and proteins [55, 56]. Cellulose modification can also be done by grafting poly(methyl methacrylate) [57], and by making a composite with polylactic(acid) [58, 59].

In the following, we describe several example studies using two different nonwoody plant sources (sugarcane bagasse and raw jute) to prepare nanocellulose using different extraction methods: TEMPO-oxidation and NOP to prepare anionic nanocellulose, as well as periodate oxidation/Girard's reagent T to prepare cationic nanocellulose. The resulting nanocellulose materials have shown to be very efficient for water purification such as adsorbent and membrane barrier layer materials.

15.2 Synthesis, Properties, and Application of NOCNF

The synthesis of NOCNF included the grinding of 10 g of untreated biomass and placed in a 3000 mL three-neck round-bottom flask with 210 mL (22.2 mmol) of nitric acid. The sample in the flask could completely soak before adding 14.4 g of sodium nitrite (14 mmol). The addition of sodium nitrite forms red gases inside the flask, so the mouths of the round bottom flask were sealed with stoppers and parafilm. The reaction was performed at 50 °C for 12 hours and was then quenched by adding 1 L deionized (DI) water. The supernatant liquid was discarded to remove excess acid and decantation with 80% (70% ethanol [EtOH]) and 20% DI water was performed 4–5 times depending on the suspension of the fibers in water. The nanofiber suspension was then transferred to a dialysis bag (Spectral/Por, molecular weight cut-off [MWCO]: 6–8 kDA) and equilibrated until the conductivity of the water reached below 5 μS. The fibers were subsequently treated with 8% sodium bicarbonate until pH reached 7.5 to generate the hydrophilic carboxylate functional groups with ionic charge. The carboxylate content of NOCNF was determined using the conductometric titration method.

15.2.1 Remediation Experiments Using NOCNF

Metal salt stock solutions (i.e. lead ions (Pb^{2+} or Pb(II)), cadmium ions (Cd^{2+} or Cd(II)), uranyl ions (UO_2^{2+})) with various ion concentrations ranging from 50 to 5000 ppm were prepared for this study. The adsorption study was carried out as follows. 2 mL of the metal salt solution was mixed with 2 or 5 mL of a ~0.23 wt% NOCNF suspension. The clear water above the settled gel floc/precipitant was removed from the test tubes and diluted by a factor of 100. The resulting solution was analyzed using inductively coupled plasma mass spectrometry (ICP-MS) (SQ-ICP-MS, Thermo Fisher Scientific) with required dilution in the range of ppb. Based on the adsorption rates at various concentrations of metal ions (pH = 7), an isotherm curve was generated. The maximum adsorption capacity of NOCNF against different metal ions was determined using the Langmuir model of the adsorption data.

15.2.2 Properties of NOCNF

NOCNF was analyzed using the Fourier transform infrared spectroscopy (FTIR) and conductometric titration methods to determine the functionality of NOCNF, where the results are shown in Figure 15.1(a). The FTIR spectrum of NOCNF showed the main characteristic peaks at 3400 cm^{-1} for hydroxyl (-OH) stretching, 2900 cm^{-1} for C-H symmetrical stretching, 1232 cm^{-1} for C-OH bending at C6 position and 1204 cm^{-1} for C-O-C symmetric stretching; along with COO^- stretching peak at 1594 cm^{-1} confirming the presence of carboxylate group in NOCNF. While the spectrum of the jute fibers exhibited other relevant peaks at 1515 cm^{-1} due to C = C aromatic symmetrical stretching in the lignin; 1739, 1460, 1240, and 810 cm^{-1} representing xylan and glucomannan of hemicellulose. Notably, the intensity of these peaks at 1739, 1460, 1240, 810, and 1515 cm^{-1} was significantly reduced or completely disappeared in NOCNF, indicating that the treatment of NOP was effective in removing other biomass components, such as hemicellulose and lignin present in jute fibers.

Morphological analysis of NOCNF was performed by transmission electron microscopy (TEM) analysis, where the results are shown in Figure 15.1(b) and (c). It was shown that the average length of NOCNF fibers extracted from jute fibers was in the range of 290 ± 40 nm and the average width was in the range of 4.47 ± 0.5 nm. In contrast, the TEM image of NOCNF extracted from spinifex fibers indicated that the average length was 190 ± 90 nm and the average width was in the range of 4.0 ± 1.5 nm. The charge on the extracted NOCNF was measured using the conductometric titration method [60]. Figure 15.1(d) showed the conductometric titration curve for NOCNF extracted from jute fibers where this curve represented the amount of NaOH added and the change in conductivity of NOCNF. The difference between the end points of the titration curve was used to determine the carboxylate content of NOCNF using Eq. 15.1. The results indicated that the carboxylate content of NOCNF extracted from jute fibers was 1.15 mmol/g, while the carboxylate content of NOCNF extracted from spinifex fibers was 0.78 mmol/g.

$$\text{Carboxylate content}\left(\text{mmol}/\text{g}\right) = N \times \left(V_2 - V_1\right) / W \times 100 \tag{15.1}$$

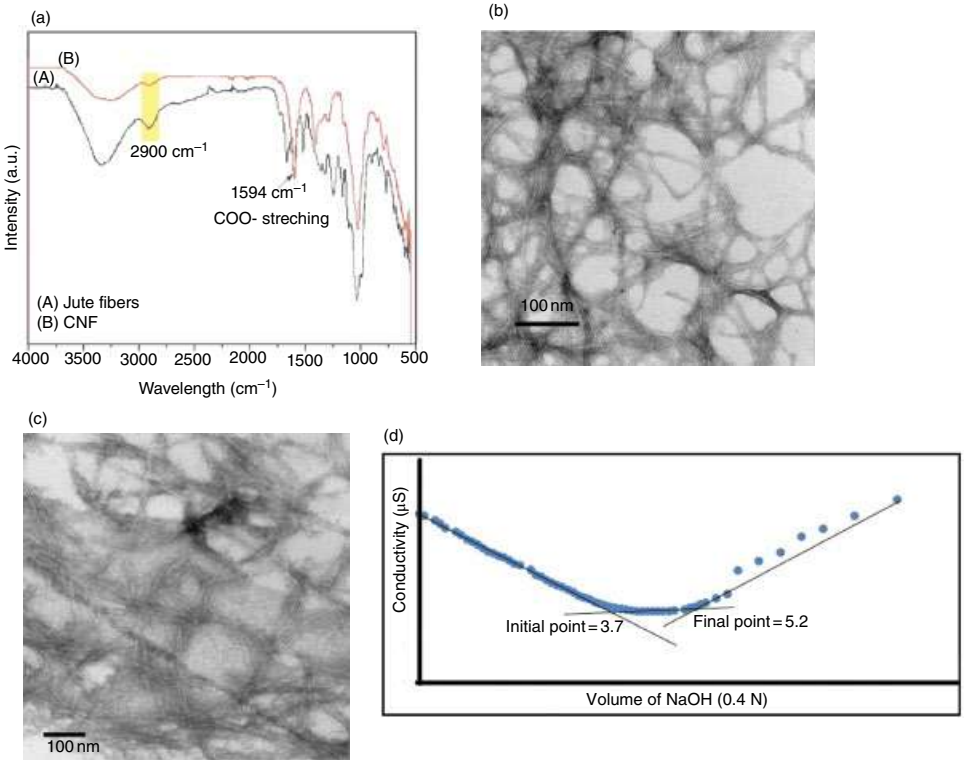

Figure 15.1 (a) FTIR of untreated jute fibers and extracted NOCNF (Copyright 2017, American Chemical Society). (b) TEM of NOCNF extracted from jute fibers [15] (Copyright 2017, American Chemical Society). (c) TEM of NOCNF extracted from spinifex fibers [26] (Copyright 2018, American Chemical Society). (d) Conductometric titration curve for NOCNF extracted from jute fibers.

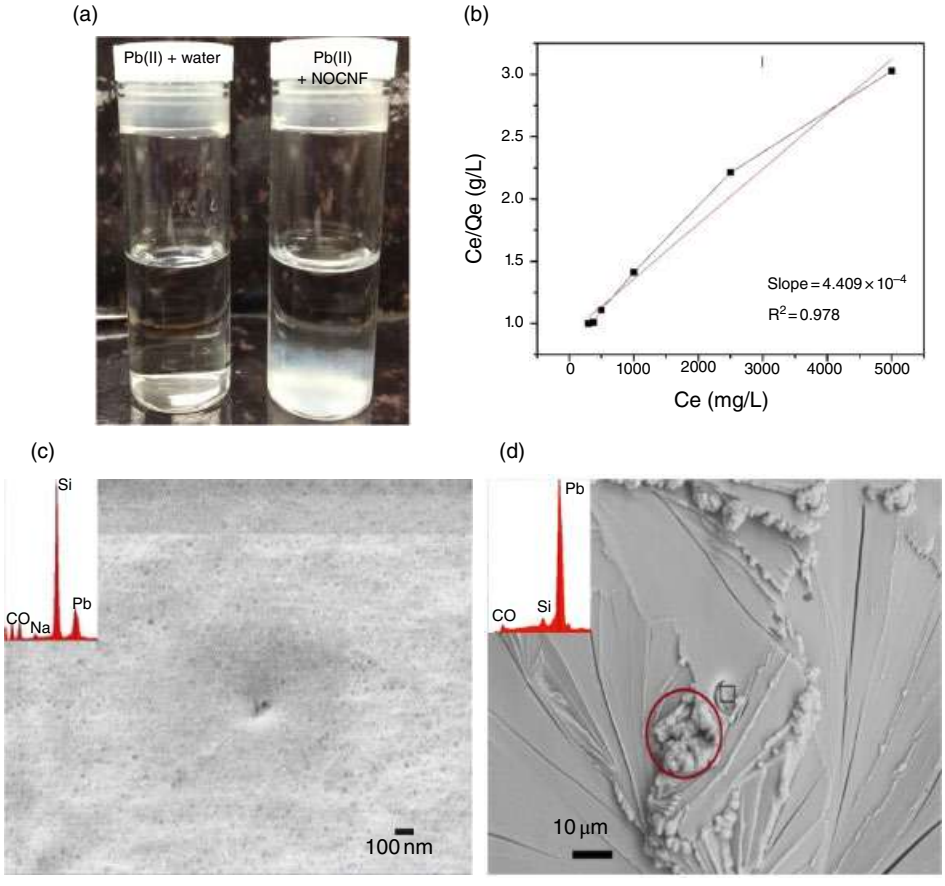

Figure 15.2 (a) Photograph showing the pure lead acetate solution (109,000 ppm) (left), and the mixture of NOCNF (11.5 mg) and lead acetate solution (109,000 ppm) (right); (b) the Langmuir isotherm fitting curve of Pb(II) adsorption data, (c) SEM images of the floc formed from the mixture of NOCNF and Pb(II) solution at 750 ppm (< 1000 ppm) of (inset left: EDS spectrum), and (d) SEM image of the floc formed from the mixture of NOCNF and Pb(II) solution at 1200 ppm (> 1000 ppm) (red circle presents the formation of lead crystals) (inset left: EDS spectrum). Copyright 2018, Springer Nature [17].

where N is the normality of NaOH, V_2 and V_1 is the final and initial volume in L of NaOH, W is the weight of the NOCNF dried fibers added in g.

15.2.3 Lead Removal by NOCNF

NOCNF extracted from untreated jute fibers using the NOP possessed high carboxylate content (1.15 mmol/g) and high surface charge (−70 mV), making them an excellent adsorbent for Pb(II) ion removal from water. Figure 15.2(a) shows the picture of two bottles, one containing 5 g distilled water and 1 g (109,000 ppm) of lead acetate, and another containing 5 g of 0.23 wt% NOCNF suspension and 1 g (109,000 ppm) of lead acetate, respectively. Because of the high concentration of lead acetate, the solution was slightly

cloudy but homogeneous. However, in the presence of NOCNF, a thick and white gel-like precipitant formed at the bottom of the bottle. This photograph clearly showed the efficiency of NOCNF in capturing the Pb(II) ions, which acted as ionic cross-linkers for appositively charged nanocellulose. The remediation of Pb(II) by NOCNF was found to be so fast that it happened in a few minutes. The remediation experiments were performed on a wide range of Pb(II) concentration in between 50 and 5000 ppm. The data obtained from the ICP-MS measurement were fitted by the Langmuir isotherm model. Based on the Langmuir model (Figure 15.2(b), the value of C_e/Q_e was plotted against C_e, where the data could be fitted by a straight line (i.e. least squares regression line, LSRL) with the excellent R^2 value of 0.978. This indicated that the Pb(II) adsorption results of NOCNF followed the Langmuir isotherm model that supported the monolayer adsorption mechanism. Based on this approach, the inverse of the slope against C_e/Q_e versus C_e provided the adsorbent's maximum adsorption capacity (Q_m), which was found about 2270 mg/g (the slope of LSRL was 4.409×10^{-4}) for NOCNF. The mechanism of removal of Pb(II) ions was examined using the scanning electron microscopy (SEM)/energy dispersive X-ray spectroscopy (EDS) techniques in Figure 15.2(c) and (d). The study showed that the high removal efficiency of NOCNF was due to the combined effects of adsorption which was dominated at the concentration of Pb(II) ≤ 1000 ppm; and mineralization of lead crystals (in hydrolyzed form $Pb(OH)_2$) which was effective at high Pb(II) concentration (> 1000 ppm) as shown in Figure 15.2(c) and (d). At low concentrations of Pb(II) ≤ 1000 ppm, the image showed the aggregation of NOCNF in a very homogeneous fashion. However, on the addition of a high concentration of Pb(II) (≥ 1000 ppm), the flower-like aggregate structure (in red circle) appeared, indicating the formation of lead crystals during the remediation process. Their corresponding EDS spectra from SEM images (Figure 15.2(c) and (d), shown in inset left of corresponding images) also confirmed the adsorption and mineralization processes of Pb(II) in the presence of NOCNF. It was seen that the NOCNF floc formed with > 1000 ppm Pb(II) ion concentration revealed the electron dispersive X-ray (EDX) peaks for carbon (C), oxygen (O), sodium (Na, from carboxylate groups), and the Pb peak comparatively the same as C and O while the EDX spectrum of the NOCNF floc formed at high Pb(II) concentrations (≥ 1000 ppm) showed the larger Pb peak as compared to C, O, and Na. This further indicated that the adsorbed Pb(II) ions in the NOCNF scaffold behaved as nuclei when at high Pb(II) concentration, resulting in lead crystallization.

15.2.4 Cadmium Removal by NOCNF

NOCNF with high charge (−68 mV) and relatively high carboxylate content (0.78 mmol/g) were prepared from dry spinifex grass using the NOP. The extracted NOCNFs were studied for cadmium (Cd(II)) removal from water. It was found that a low concentration of NOCNF (0.20 wt%) was effective in removing a wide range of Cd^{2+} (cadmium ions) impurities from 50–5000 ppm in a short time interval of ≤ 5 minutes. A photograph showing the Cd(II) solution (conc. ~ 5000 ppm) in water and Cd(II) (conc. ~ 5000 ppm) in NOCNF suspension is illustrated in Figure 15.3(a). The figure showed that the Cd(II) solution was clear and transparent. However, the addition of NOCNF (0.20 wt%; 10 mg in 5 mL) into the Cd(II) solution caused the appearance of white precipitation at the bottom of the bottle in a few minutes

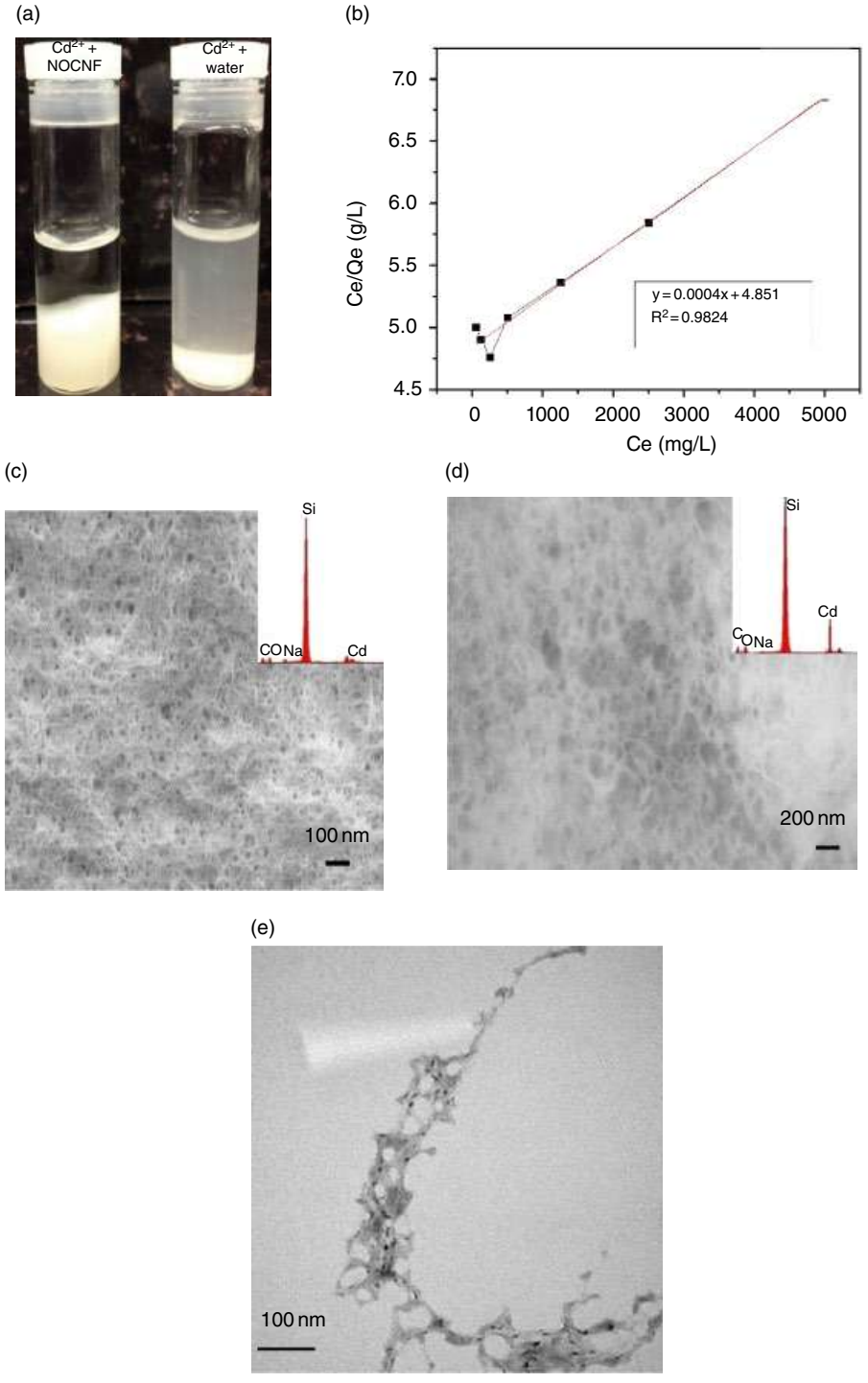

Figure 15.3 (a) Photographs of two samples, left: solution of cadmium nitrate (~5000 ppm), right: a mixture of NOCNF suspension (0.20 wt%) with cadmium nitrate solution (~5000 ppm) at pH 7; (b) Langmuir isotherm fitting; (c) SEM of floc from solution with Cd(II) ions (500 ppm), corresponding EDS spectra on inset left; (d) SEM of floc formed from solution with Cd(II) ions (1000 ppm), corresponding EDS spectra on inset left; (e) TEM image of floc consists of NOCNF with Cd(II) ions. The black dots on NOCNF indicate the formation of cadmium nanocrystals in the scaffold of CNFs. Copyright 2018, American Chemical Society [26].

(< 2 minutes). This indicates that the negative charges on NOCNF were effective in capturing the oppositely charged metal ions through electrostatic interactions leading to high adsorption capability. The remediation data were analyzed using the ICP-MS method and the results were fitted into the Langmuir isotherm model based on the monolayer adsorption mechanism. The data showed that the adsorption data fitted by the Langmuir model yielded a good R^2 value of 0.986. Based on the Langmuir isotherm model, the coefficient of the LSRL of the C_e against C_e/Q_e plot was 3.910×10^{-4} which is the reciprocal of the adsorption capacity (Figure 15.3(b)). Thus, the maximum adsorption capacity (Q_m) obtained for NOCNF against Cd(II) adsorption was 2550 mg/g. A similar combined mechanism including both adsorption and mineralization, observed in Pb (II) adsorption using NOCNF, was also found in the Cd(II) adsorption using NOCNF. Such a mechanism was further confirmed by SEM/EDS spectra, showing the appearance of pure adsorption when the Cd(II) concentration was below 500 ppm and additional mineralization when the Cd(II) concentration was above 500 ppm. The SEM image of the floc containing NOCNF and Cd(II) ions (Figure 15.3(c) and (d)) at low concentrations (below 500 ppm) showed the appearance of nanofiber aggregates induced by the cross-linking of Cd(II) ions. In contrast, the SEM image (Figure 15.3(d)) of the floc formed at high Cd(II) concentrations (1000 ppm) exhibited large aggregates substantially thicker than the nanofiber aggregates observed in Figure 15.3(c). The corresponding EDS spectra (inset graphs) showed that in both cases, the peaks of carbon (C), oxygen (O), and sodium (Na) were present which indicated the existence of NOCNF; while the peak of Cd was more prominent when the Cd(II) was at a higher concentration (1000 ppm). The presence of the intense Cd peak in EDS (Figure 15.3(d)) was due to the mineralization of cadmium. Most probably, the adsorbed Cd(II) ions on the NOCNF surface acted as nuclei, responsible for crystal growth in the presence of high Cd(II) concentration. A similar study was observed when the lead sulfate solution was added to polyethyleneimine polyelectrolyte to produce lead crystals [61]. TEM of the floc formed at high Cd(II) concentration (≥ 1000 ppm) confirmed the existence of cadmium nanocrystals (the black dots in Figure 15.3(e)) formed in the NOCNF scaffold. At low Cd(II) concentrations (< 500 ppm), the dominant adsorption mechanism is the electrostatic interaction between Cd(II) ions and NOCNF, whereas at high Cd(II) concentrations (≥ 1000 ppm), the mineralization process took place that greatly enhanced the adsorption capacity of NOCNF.

15.2.5 Uranyl Removal by NOCNF

NOCNF extracted from jute fibers with high surface charge (−70 mV) and high carboxylate content (1.15 mmol/g) prepared using the NOP were also studied for removal of a broad range (25–1250 ppm) of UO_2^{2+} ion impurities from water. Photographs of adsorption experiments are shown in Figure 15.4(a). In this figure, the left bottle illustrated the UO_2^{2+} solution (2120 ppm), while the right bottle illustrated the mixture of 5 mL UO_2^{2+} solution with 5 mL NOCNF suspension (0.23 wt%, 11.5 mg). Notably, the UO_2^{2+} solution was slightly yellow in color but completely transparent. However, the mixture containing NOCNF and UO_2^{2+} impurities exhibited a yellow-colored precipitate settled at the bottom of the bottle. The precipitation occurred in a very short time (less than 2 minutes of mixing). This experiment indicated the excellent efficacy of NOCNF to remove the UO_2^{2+} impurities from water.

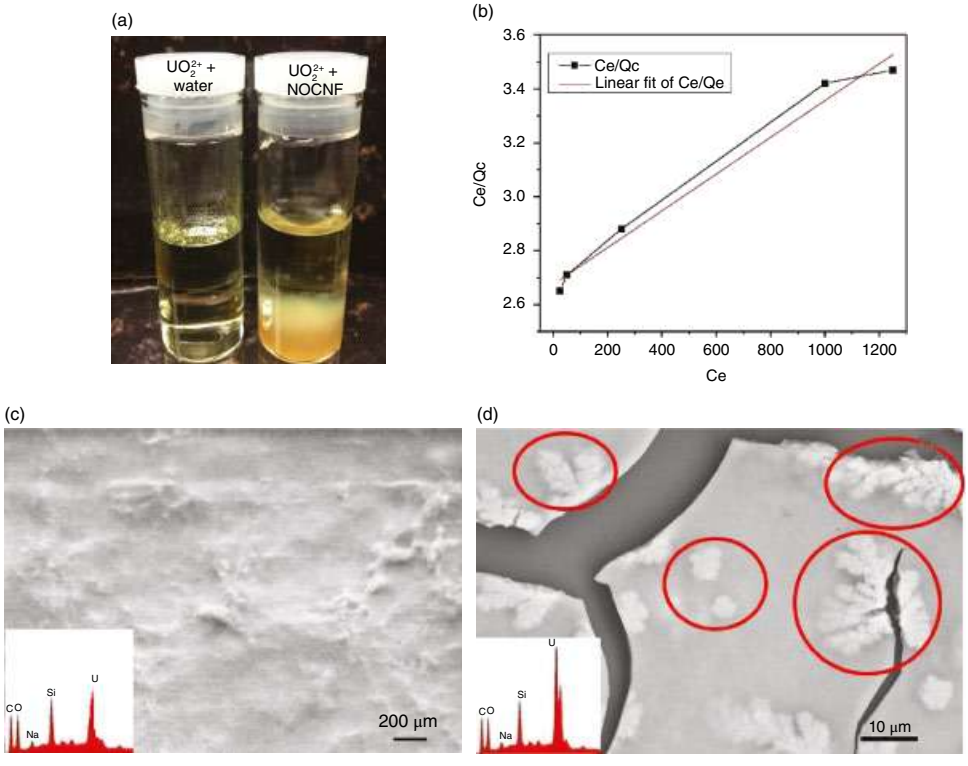

Figure 15.4 (a) Photographs of a 0.02 wt% uranyl acetate solution (2120 ppm), left; a mixture of uranyl acetate solution (2120 ppm) and 5 mL NOCNF suspension (0.23 wt%) at pH 7, right; (b) the Langmuir isotherm fitting result of the UO_2^{2+} adsorption data; (c) SEM image of the floc formed from mixing of UO_2^{2+} (500 ppm) and NOCNF (0.23 wt%), the corresponding EDS spectrum is on inset left; (d) SEM image of the floc formed from mixing of UO_2^{2+} (1250 ppm) and NOCNF (0.23 wt%), the corresponding EDS spectrum is on inset left (red circles indicating the mineralized UO_2 nanocrystals). Copyright 2017, American Chemical Society [27].

It was found that NOCNF exhibited excellent efficiency between 80 and 87% when the UO_2^{2+} ion concentration was below 1000 ppm. In contrast, NOCNF showed a decrease in efficiency to about 60%, when UO_2^{2+} ion concentration was around 1250 ppm. The reason for this decrease was due to the saturation (neutralization) of the negative charges on the NOCNF surface. The data obtained from ICP-MS was fitted by the Langmuir isotherm model to obtain the maximum adsorption efficiency of NOCNF for the UO_2^{2+} ion removal. It was found that NOCNF exhibited the maximum adsorption capacity (Q_m) of 1470 mg/g, based on the Langmuir model (Figure 15.4(b)). The mechanism of removal of UO_2^{2+} by NOCNF also involved both adsorption and mineralization processes, as indicated by the SEM/EDX results (Figure 15.4(c) and (d)). It was seen that the SEM image of the floc obtained by interactions of low concentration of UO_2^{2+} (500 ppm) and NOCNF exhibited nanofiber aggregates. However, the SEM image of the floc based on the high concentration of UO_2^{2+} ions (1250 ppm) exhibited large cloud-like aggregates that covered the entire NOCNF surface. The aggregates appeared especially at the edge of the fractured layer, clearly indicating the crystallization of U crystals. This was further confirmed by the TEM image of the floc containing the uranyl acetate solution (1250 ppm) and (0.23 wt%) NOCNF as shown in Figure 15.4(e). It was found that small black dots of UO_2 crystals were evenly distributed on the NOCNF surface. Notably, to preserve the original morphology of the floc, no staining agent was used during the preparation of TEM samples.

The EDS spectra of the respective SEM images showed the corresponding population of different elements present on the specimen. The EDS spectrum of the SEM image in Figure 15.4(c) exhibited the peaks of carbon (C), oxygen (O), and sodium (Na) from NOCNF along with a distinct U peak that was comparatively similar to the peaks of C, O, and Na, corresponding to NOCNF. This indicated that the interactions between UO_2^{2+} and NOCNF occurred at about the same mass ratio at low UO_2^{2+} concentration (500 ppm). However, the EDS spectrum of the SEM image in Figure 15.4(d) indicated that when high UO_2^{2+} concentration ($\geq$1000 ppm) was used, the results showed that the U peak was significantly larger than those of C, O, and Na peaks (i.e. NOCNF), confirming the presence of a high mass of uranium impurities due to mineralization. Hence, the results verified that the mechanism of UO_2^{2+} removal by NOCNF included both adsorption and mineralization processes. At low concentrations of UO_2^{2+} ($\leq$500 ppm), the adsorption process was dominant; at high concentrations of UO_2^{2+} ($\geq$1250 ppm), the mineralization process became the predominant effect. Figure 15.5(a) shows the TEM of the floc containing the NOCNF and UO_2^{2+} impurities where UO_2 nanocrystals appeared as black dots. In Figure 15.5(b), simple gravity-driven microfiltration was used to remove the floc of UO_2^{2+} and NOCNF.

15.3 Preparation, Characterization, and Application of Nanocellulose-derived TFNC Membrane

15.3.1 Preparation of TEMPO-CNF with Different Degrees of Oxidation

CNFs were prepared from bleached jute following TEMPO-mediated oxidation method reported before. [20, 62] Briefly, 0.2 g NaBr and 0.03 g TEMPO reagent were firstly added to 200 g suspension of 1 wt% dispersed delignified jute fibers. The oxidation process was initiated by dosing a predetermined amount of NaClO solution (6, 10, and 20 mmol NaClO per

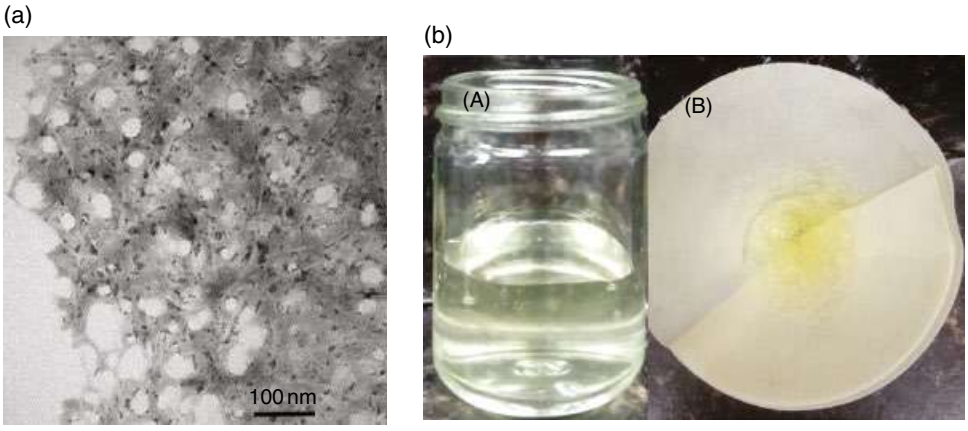

Figure 15.5 (a) TEM image of the floc formed between the interactions of NOCNF with UO_2^{2+} ions (1250 ppm). The black dots on NOCNF show the aggregation of UO_2 nanocrystals (nucleating sites); (b) gravity-driven microfiltration; pictures show (A) the floc formed between the mixture of NOCNF and UO_2^{2+} ions (500 ppm); (B) the floc obtained by the filtration of (A) using a filter paper (average pore size: 40 μm). Copyright 2017, American Chemical Society [27].

gram of dry cellulose for 0.85, 1.35, and 1.80 DO, respectively) and then maintained stirring for 24 hours with a controlled pH value (pH = 10). Finally, the oxidized fibers were centrifuged and washed several times with DI water until the pH value of supernatant reached 7.0 after terminating the reaction with 5 mL ethanol. Ultimately, a high-pressure homogenizer was used to defibrillate the microfibers into nanofibers. The final CNFs were dispersed in aqueous suspensions of 0.2 wt% for TFNC membrane preparation.

15.3.2 Preparation of Hierarchical TFNC Membranes

To maintain the high flux of TFNC membranes, a highly porous electrospun polyacrylonitrile (ePAN) substrate (porosity > 80%) was selected to support a thin coating of CNFs. First, the ePAN substrate was soaked in hydrochloric acid solution (pH = 2) for 10 minutes to fill all the pores with an acid solution. Then, the extra acid solution inside the substrate was removed by rolling a glass rod on the surface of the ePAN substrate (fixated on a flat glass plate). Subsequently, different amounts of the 0.05 wt% TEMPO-CNF suspension were applied evenly on the substrate surface to create TEMPO-CNF barrier layers of different thicknesses. Varying membrane surface charge was obtained by utilizing TEMPO-CNF of difference DO. During the barrier layer formation, a transparent TEMPO-CNF gel layer was formed on top of the substrate surface because of the acidic environment, which prevents TEMPO-CNF to penetrate the pores of the ePAN substrate. Finally, all TFNC membranes were thermo-treated at 115 °C for 20 minutes before testing.

15.3.3 Characteristics of the TFNC Membrane

The surface charge values of varying TFNC membranes were evaluated by the zeta potential measurement, where the results (Figure 15.6(a)) were used to demonstrate their essential impact on the antifouling properties of nanocellulose membranes. Because of

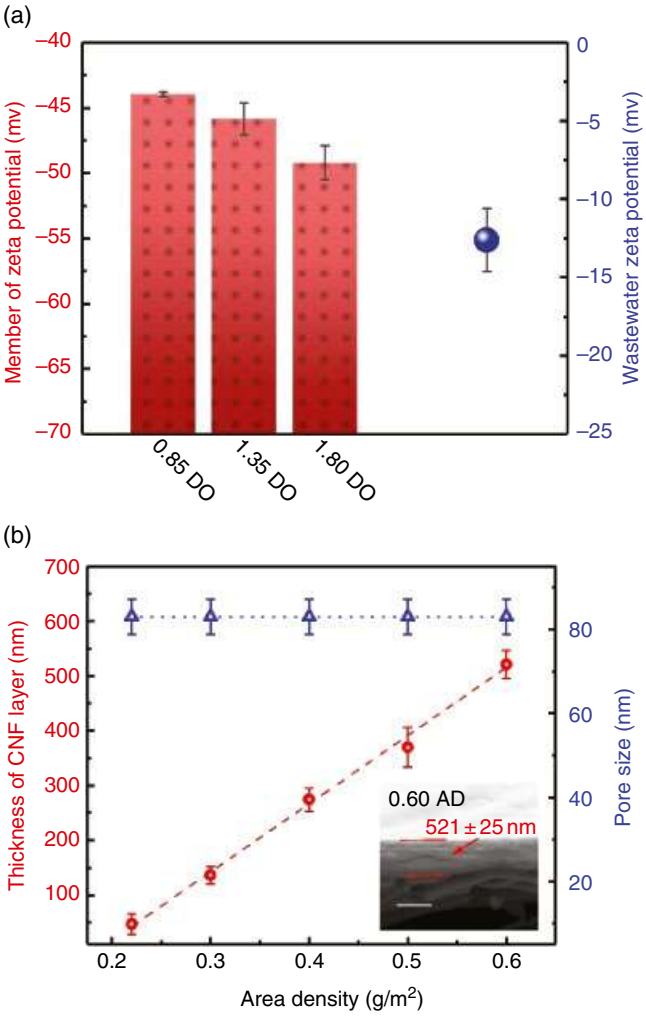

Figure 15.6 (a) Membrane zeta potential values of the 0.85 DO, 1.35 DO, and 1.80 DO CNF-TFNC membranes with 0.60 AD under a fixed ionic strength (1 mM KCl) using the same wastewater (zeta potential = −12.6 ± 2.0 mV) at neutral pH; (b) barrier layer thickness and pore size of the TFNC membranes with different CNF AD (the inset is the cross sectional SEM image of the 0.6 AD CNF-TFNC membrane) [66].

the abundant carboxylate groups on TEMPO-CNF, the surface charge of all tested membranes was negative at neutral pH. Furthermore, the membrane zeta potential became lower (i.e. more negatively charged) as DO of TEMPO-CNF elevated. This trend could be attributed to the greater amount of carboxylate group exposed on the TEMPO-CNF membrane surface with a higher DO of CNF. Meanwhile, the lower membrane zeta potential value resulted in more intensive electrostatic repulsion between the membrane surface and the foulants (the wastewater zeta potential was -12.6 ± 2.0 mV), decreasing the adhesion of the foulant to the membrane and enhancing the antifouling properties of TEMPO-CNF membranes [63–65].

As shown in Figure 15.6(b), the thickness of the CNF barrier layer exhibited a linear relationship with the TEMPO-CNF area density (AD) while the pore size of the CNF-TFNC membrane remained similar regardless of the increasing CNF's AD. The representative cross sectional SEM image (the inset in Figure 15.6(b)) of the CNF-TFNC membrane

(0.60 g/m^2 AD) depicted the two-layer hierarchical structure, where the TEMPO-CNF barrier layer was uniformly formed on top of the ePAN substrate. According to the MWCO test using dextran molecules, the mean pore size of all the membranes was 83 ± 4 nm, irrespective of DO and AD (barrier layer thickness). This observation indicated that CNF was randomly stacked in the barrier layer, where the pore formation process was determined by the interfibrillar interactions (e.g. physical-hydrophobic aggregation and chemical crosslinking) during drying and thermal treatment [67, 68]. Although the increase in TEMPO-CNF content could build up the barrier layer thickness, the final pore structure in the nanofiber network remained unchanged.

15.3.4 Separation Performance and Fouling Behavior of Nanocellulose-TFNC Membranes

Membrane fouling is a major issue in wastewater treatment. In this demonstration, a unique class of low-fouling nanocellulose-enabled TFNC UF membranes was fabricated by coating negatively charged TEMPO-CNF on the porous ePAN substrate. Our laboratory was the first group to demonstrate that hydrophilic and charged TEMPO-CNF, containing abundant hydroxyl and carboxylated groups, can be used as a barrier layer material to develop high-flux and low-fouling UF membranes. This is because the surface of oxidized CNF via TEMPO-oxidation contains negatively charged carboxylated groups, which can enhance electrostatic repulsion between the CNF barrier layer and negatively charged foulants, as in wastewater. The diameter of the CNF also plays a role in tailoring the mechanical properties [69].

Figure 15.7 illustrates the fouling ratio (*J/Jo*, where *J* represents the current flux value and *Jo* represents the initial flux value) and flux recovery behavior of TEMPO-oxidized CNF-TFNC versus those of a conventional PVDF UF membrane for wastewater filtration. It was observed that both TFNC membranes (with a barrier layer of CNF having different DO) exhibited less fouling tendency and greater flux recovery ratio than those of the PVDF membrane. During the filtration process, the rejection ratio for all tested membranes was higher than 99.5% in terms of turbidity. It was interesting to note that the CNF-TFNC membrane with a higher negative charge (using CNF of higher DO) resulted in higher water flux after each wastewater run and more effective flux recovery after hydraulic cleaning.

The above results could be attributed to the lower zeta potential of the TEMPO-CNF barrier layer, which led to stronger repulsion between the TFNC membrane and negatively charged foulants in wastewater, thus weakening the adhesion of foulants on the surface of the CNF barrier layer. In contrast, the commercial PVDF membrane suffered severe fouling (fouling decay: 53 ± 5%) upon contacting the wastewater and displayed the lowest flux recovery ratio (33 ± 3%) after hydraulic washing. This is because the relatively high hydrophobic surface and the lack of charged functional groups of PVDF membrane made it vulnerable to both reversible fouling (i.e. the cake layer formed on top of the membrane) and irreversible fouling (i.e. the pore blocking occurred inside the membrane tunnel) [7]. We believe that the characteristics of NOCNF and TEMPO-CNF are very similar, in which both can enhance the antifouling property of the membrane by surface coating.

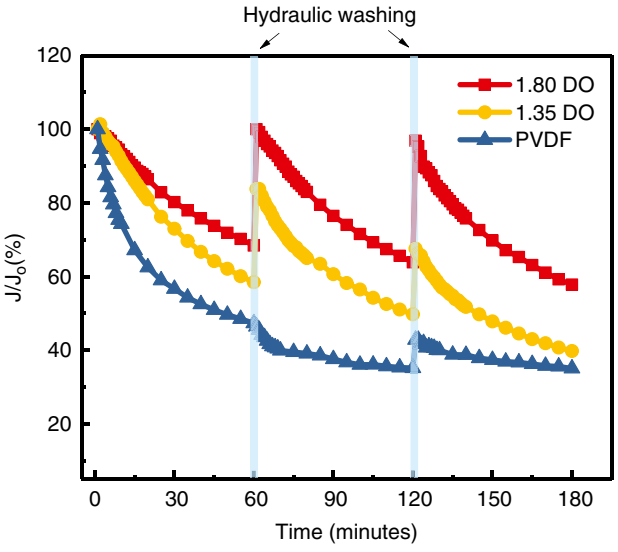

Figure 15.7 Fouling and flux recovery behavior of a commercial PVDF membrane and CNF-TFNC membranes with the same barrier layer thickness (0.40 AD) but different DO values (1.80 and 1.35) during wastewater filtration [66].

15.4 Preparation, Characterization, and Applications of Cationic Dialdehyde Cellulose (c-DAC)

Preparation steps for positively charged nanocellulose were performed using the untreated sugarcane bagasse and involved the following steps:

15.4.1 Pretreatment of Sugarcane Bagasse

Raw sugarcane bagasse samples were cut into small pieces with a length between 2 and 4 cm, where these chopped samples were subsequently immersed in 1 M NaOH solution overnight under continuous stirring. After washing the alkali-treated bagasse with water, the fibers were soaked in 1.8 w/v% $NaClO_2$ buffer solution (acetic acid and sodium acetate buffer solution, pH at around 4.5) and stirred at 70 °C for 2 hours. The $NaClO_2$ delignification procedure was repeated 3–5 times to ensure the complete removal of lignin and hemicellulose. Afterward, the delignified sugarcane cellulose pulp (Delig_SC) was washed thoroughly using water and stored in the never-dried state in the refrigerator for future use [70].

15.4.2 Periodate Oxidation

DAC was prepared by adding 2.2 g sodium metaperiodate into 400 g of 1.25 wt% Delig_SC suspension (2 mmol/g sodium periodate [$NaIO_4$]/dried cellulose ratio) under dark conditions to prevent chemical degradation, followed by continuous stirring at 55 °C. After 24 hours, 10 mL ethylene glycol was added to terminate the reaction. Afterward, the recovered DAC fibers were washed with water by vacuum filtration until the conductivity of the filtrate was below 5 μS/cm. The resulting samples were stored in the suspension form. The formed iodate in the periodate oxidation was regenerated back to periodate using 1.25 M hypochlorite solution under the alkaline condition, according to a method reported by Liimatainen et al. [71]

15.4.3 Preparation of c-DAC Adsorbent

c-DAC was prepared by functionalizing the DAC samples with Girard's reagent T (GT). In brief, GT was added into the DAC suspensions with a GT/anhydroglucose unit (mole ratio of 3/1), where the pH value of the reaction mixture was adjusted to 4.5. The mixture was stirred continuously at room temperature for 72 hours. The resulting c-DAC sample was washed with water by centrifugation to remove the unreacted GT (the procedure was repeated several times until the conductivity of the supernatant was below 5 μS/cm). Finally, the washed c-DAC fibers were re-dispersed in water for further characterization.

15.4.4 Degree of Oxidation in DAC and Degree of Substitution in c-DAC

The aldehyde content in the DAC sample was obtained using the titration method [72]. Specifically, a DAC suspension (equals to 0.1 g of dry DAC) was added into 40 mL of 0.25 M hydroxylamine hydrochloride solution (pH = 4.5), where the mixture was stirred at room temperature for 24 hours. Subsequently, the released hydrochloric acid (HCl) from the Schiff's base reaction was titrated with 0.05 M NaOH until the pH value of the solution was back to 4.5. The GT groups grafted onto the c-DAC sample were determined using the CHNS elemental analysis technique (Thermo Scientific, EA1112).

15.4.5 Hexavalent Chromium (Cr(VI)) Adsorption Test

The efficiency of c-DAC adsorbent on the Cr(VI) removal was investigated by adding c-DAC suspension (equivalent to 7.5 mg of dry c-DAC) into 15 mL of dichromate solutions (initial concentration C_0 = 10–300 mg/L, pH = 6). The effect of the initial pH value on the Cr(VI) removal efficiency was investigated by adding c-DAC suspension into a fixed concentration of Cr(VI) solution (100 mg/L) at different pH values (2–10). All the tests were conducted in triplicate at room temperature (25 ± 1 °C) and shaken at 250 rpm for 24 hours.

The initial and final concentrations of the dichromate solutions were determined by a UV-VIS spectrophotometer (Thermo Scientific, Genesys 10S) using 1,5 diphenylcarbazide as an indicator at the wavelength of 540 nm [73]. The amount of Cr(VI) adsorbed per unit weight of c-DAC Q_e (mg/g) was determined according to Equation 15.2:

$$Q_e = \frac{(C_0 - C_e)V}{m} \tag{15.2}$$

where C_0 and C_e (mg/L) are the initial and final dichromate concentrations, respectively, V (L) is the solution volume, and m (g) is the quantity of c-DAC on a dry sample basis added to the solution.

The synthesis of c-DAC adsorbent/coagulant is schematically illustrated in Figure 15.8. In this figure, the cationic DAC-derivative adsorbents/coagulants were prepared through two consecutive reactions: periodate oxidation and DAC cationization. According to the titration result, the DO of DAC was 18.91% and it contained 2.33 mmol/g aldehyde content. To modify the DAC samples into a cationic adsorbent for the removal of anionic contaminants, GT was grafted onto DAC and formed c-DAC. Table 15.1 summarizes the CHNS elemental analysis results of Delig_SC and c-DAC samples. It confirmed the successful

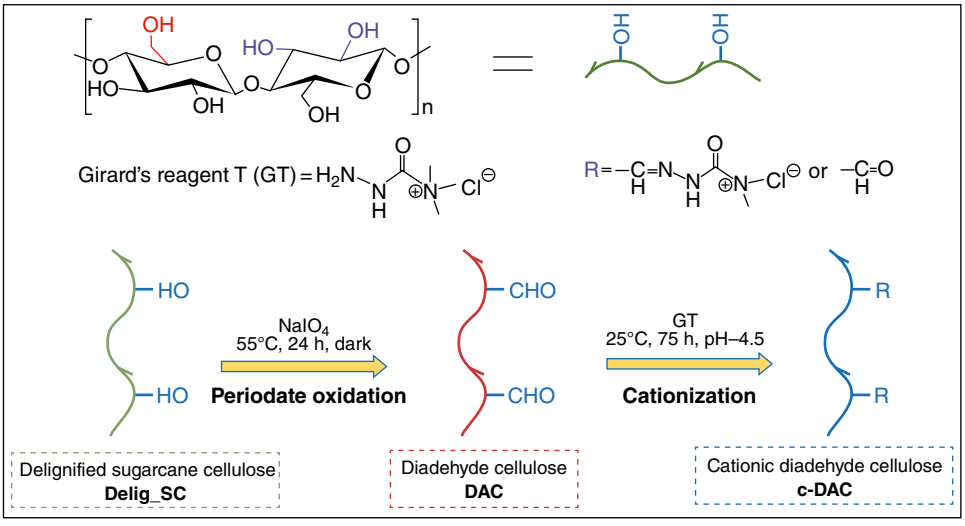

Figure 15.8 Schematic illustration for the synthesis of c-DAC adsorbent/coagulant.

Table 15.1 CHNS elemental analysis result of Delig_SC and c-DAC [46].

	Average % (w/w)				
Sample	**N**	**C**	**H**	**GT content (mmol/g)**	**DS[a]%**
Delig_SC	0.0 ± 0.0	41.0 ± 0.6	6.7 ± 2.0	0.00	0
c-DAC	2.4 ± 1.0	41.0 ± 1.1	7.2 ± 1.1	0.57	10.87

[a] DS denotes the degree of GT substitution.

introduction of GT onto the cellulose materials as the nitrogen element (this was not observed in the pristine cellulose) took place in the c-DAC sample (2.4%).

Figure 15.9 illustrates the SEM and TEM images of the original c-DAC sample and the sample after the Cr(VI) adsorption (c-DAC_Cr). It was found that the GT cationization significantly changed the morphology of the cellulose fibers, as the fibers were defibrillated into nanofibers with a relatively homogeneous fiber size distribution (18.3 ± 6.0 nm). This could be attributed to the combined effect of (i) opening of glucose rings by periodate oxidation and (ii) grafting of positively charged groups that caused the partial destruction of crystalline regions in cellulose [46]. It was also observed from the EDX-mapping measurements (Figure 15.9(b) and (e)) that the chloride ions attached to the GT disappeared after the adsorption process where the chromium ions became noticeable. This observation was consistent with the TEM images of the c-DAC_Cr sample (Figure 15.9(f)), which exhibited some dark spots. These dark spots indicated the formation (mineralization) of chromium-based nanocrystals in the c-DAC scaffold after the adsorption process.

The chemical structure changes of sugarcane fibers after periodate oxidation and GT cationization were characterized by the FTIR technique, as the results are shown in

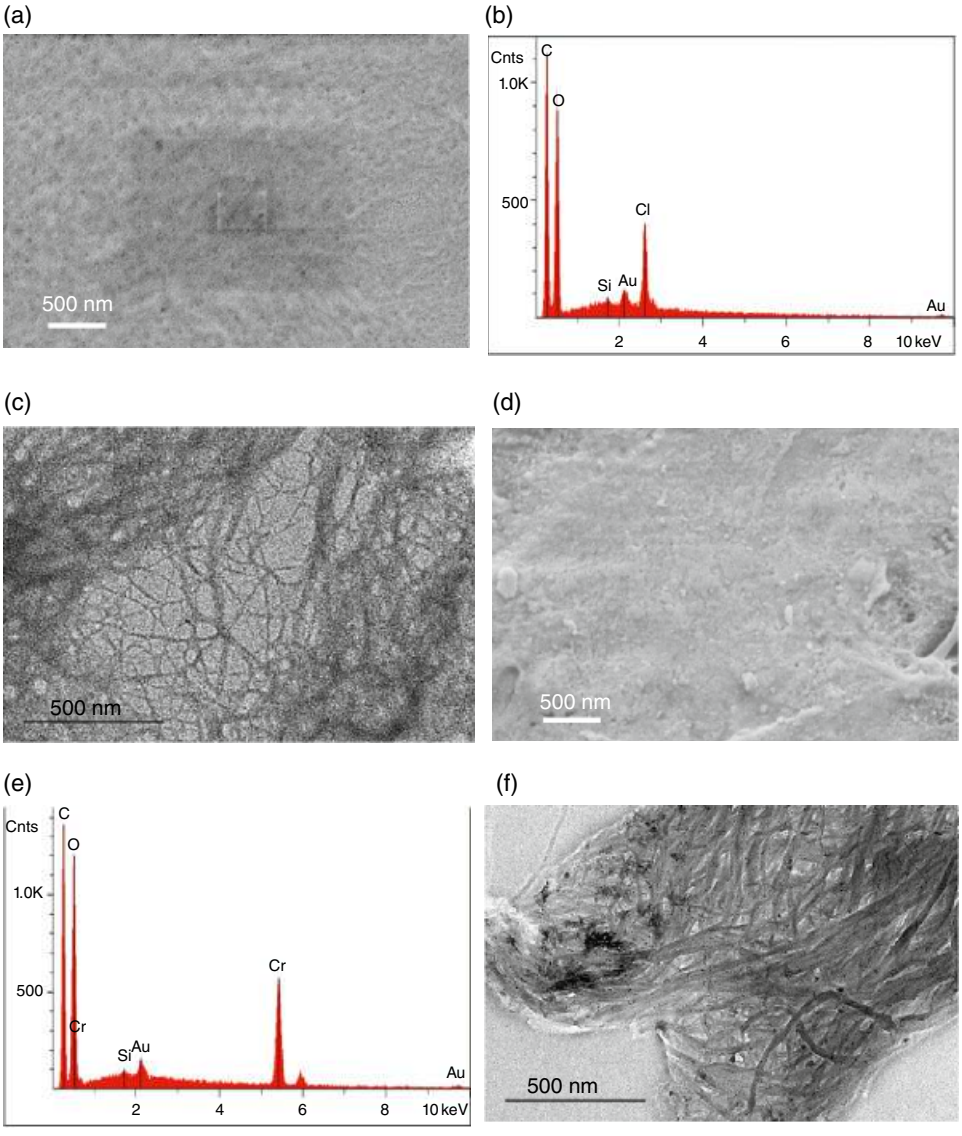

Figure 15.9 SEM images, corresponding EDX spectra and TEM images of c-DAC adsorbent before and after Cr(VI) adsorption: (a, b, c) c-DAC and (d, e, f) c-DAC_Cr.

Figure 15.10. It was found that all three samples exhibited typical characteristic peaks for cellulose materials. In comparison, the spectrum of the DAC sample showed two additional characteristic peaks at 1730 and 887 cm^{-1}, which could be attributed to the carbonyl group stretching and hemiacetal linkage formed from periodate oxidation, respectively [74]. After cationization, several new peaks were observed at 1689, 1559, and 926 cm^{-1} in the spectrum of c-DAC, which could be assigned to the carbonyl group on the hydrazide structure of the GT, imine bond formed between the aldehyde group on DAC and the GT reagent, and the N–N bonds in the GT, respectively [46].

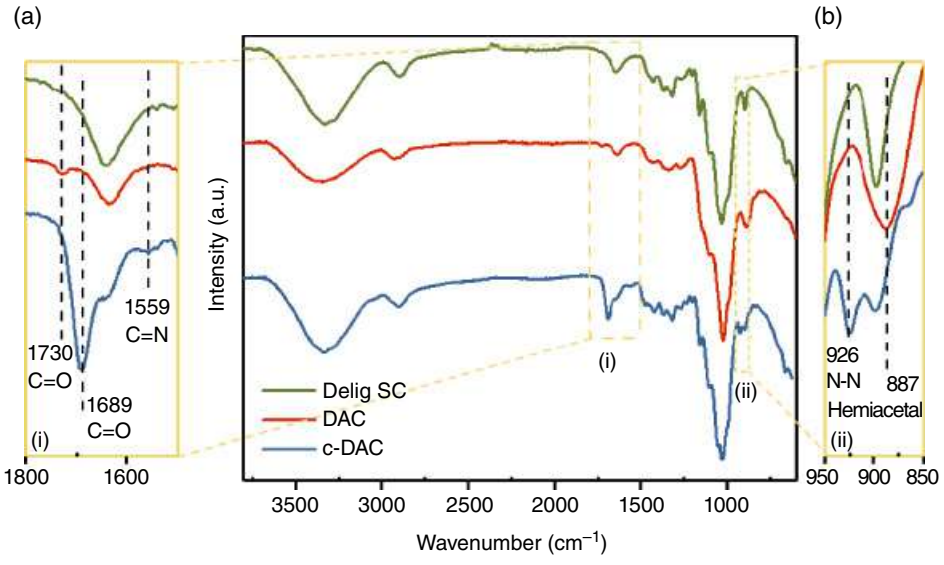

Figure 15.10 FTIR spectra of Delig_SC, DAC, and c-DAC and the enlarged regions of interest: (a) 1800–1500 cm^{-1} and (b) 950–850 cm^{-1}.

15.4.6 Chromium Cr(VI) Adsorption by c-DAC

To investigate c-DAC adsorbent's efficiency in removing anionic contaminants from wastewater, the negatively charged dichromate was chosen as a representative adsorbate for the demonstration. The equilibrium adsorption isotherm of Cr(VI) onto the c-DAC adsorbent was measured and fitted by both Langmuir and Freundlich isotherm models. The relevant calculated parameters of the two models and the adsorption curves are summarized in Table 15.2 and Figure 15.11. It was found that the adsorption curve using the Langmuir model could fit the experimental data well with an excellent R^2 coefficient value (0.9956). That indicates that the adsorption of Cr(VI) ions on c-DAC followed the monolayer adsorption mechanism. This agrees with the predicted mechanism that the electrostatic interactions between the negatively charged dichromate and positively charged quaternary ammonium functional groups on the c-DAC surface are mainly responsible for the adsorption process. According to the Langmuir isotherm analysis, the calculated maximum adsorption capacity (Q_m) was 80.45 mg/g, which confirmed that this DAC-derivative adsorbent is a competitive and promising adsorbent for the removal of negatively charged contaminants when comparing to the study [46].

Table 15.2 Calculated Langmuir and Freundlich isotherm model parameters estimated from the Cr(VI) adsorption results using c-DAC adsorbent [46].

Langmuir isotherm				Freundlich isotherm		
α_L (L/mg)	q_{max} (mg/g)	R_L[a]	R^2	K_F (L/g)	n	R^2
0.1122	80.45	0.0289	0.9956	23.9144	4.2648	0.8803

[a] R_L value is calculated using $C_0 = 300$ mg/L.

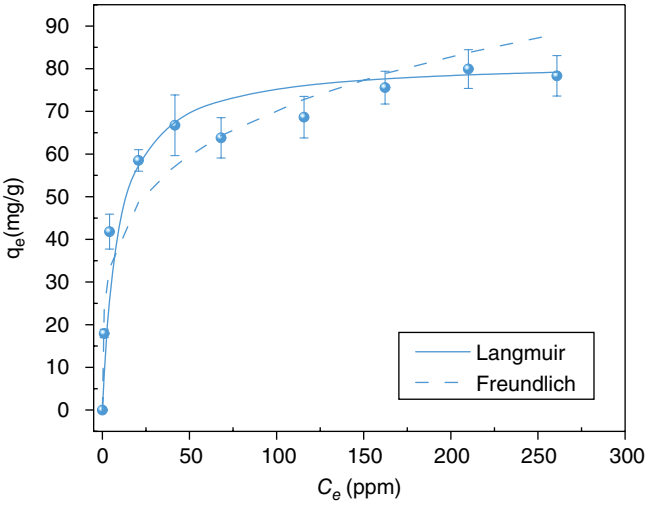

Figure 15.11 Cr(VI) isotherm adsorption by c-DAC adsorbent and the correlation of isotherm models (Langmuir and Freundlich).

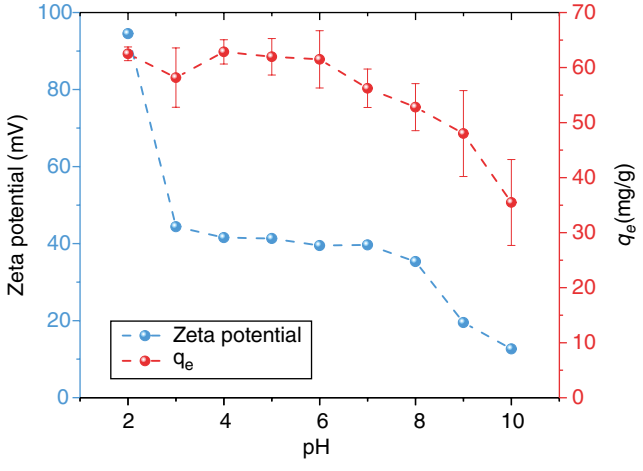

Figure 15.12 The effect of the zeta potential on the adsorption of Cr(VI) as a function of pH for the c-DAC adsorbent.

Figure 15.12 shows that the zeta potential values of c-DAC sample decrease with the pH value of the environment increases. The highly positive charge at lower pH levels is attributed to the protonation of -OH and -NH_2 groups on the c-DAC surface in the acidic environment. When the pH values increase, the protonation effect is less significant and abundant OH^- ions in the aqueous surroundings would attach onto the surface of the c-DAC, therefore causing the zeta potential value to decrease. However, it is worthwhile to mention that the c-DAC material could maintain its positive surface charge in the wide pH range from 2 to 10. This is benefited from the grafted quaternary ammonium groups ($N^+(CH_3)_3$) on the c-DAC surface, which cannot be deprotonated even under an extreme basic environment. The pH effects on the adsorption efficiency of Cr(VI) correspond with the zeta potential measurement result: the adsorption capacity did not change significantly at the pH levels between 2 and 6, afterward it shows a slowly

decreasing trend with pH level increases from 7 to 10. This is due to both the change of existing chromium speciation forms and adsorbent surface charge in response to the pH environment [46].

15.5 Conclusion

In conclusion, this chapter describes several selective methods to prepare CNFs with varying functionalities: (i) anionic, (ii) cationic, and their applications in separation technologies as adsorbent and membrane materials. The use of CNFs as adsorbents can effectively remove a wide range of charged metal ions with excellent adsorption capability. In this application, the adsorbed ions can behave as ionic cross-linkers for CNF scaffolds and render the floc formation between CNF/metal ion. The resulting floc with a large effective dimension and relatively high density can be easily separated by low-energy microfiltration (e.g. by gravity) or sedimentation. The use of CNFs as the barrier layer of the membranes based on the TFNC format has led to a new class of low-fouling and high-flux UF filters. The nature of hydrophilicity and negative surface charge of CNF has resulted in low-fouling tendency, easy-cleaning characteristics, and long sustainability of the CNF-TFNC membranes. This study can be further expanded to include other types of modified nanocellulose, such as phosphorylated, sulfonated, and alkylated nanocellulose. In addition, the formation of organic/inorganic hybrid nanocomposite scaffolds created by nanocellulose-metal ion charge interactions can be another pathway to generate effective media for the removal of suitable contaminants from water.

Acknowledgment

The financial support for this work was provided by a grant from the Polymer Program of the Division of Materials Science in the National Science Foundation (DMR-1808690). The authors further thank Dr. Chung-Chueh Chang at the Advanced Energy Research and Technology Center in Stony Brook University for his assistance of the SEM and TEM measurements, and Ms. Katie Wooton at the Facility for Isotope Research and Student Training in Stony Brook University for her help with the ICP-MS study.

References

1 Li, X., Mo, Y., Li, J. et al. (2017). In-situ monitoring techniques for membrane fouling and local filtration characteristics in hollow fiber membrane processes: a critical review. *Journal of Membrane Science* 528: 187–200.
2 Voisin, H., Bergström, L., Liu, P., and Mathew, A.P. (2017). Nanocellulose-based materials for water purification. *Nanomaterials* 7 (3): 57.
3 Mondal, S. (2017). Preparation, properties and applications of nanocellulosic materials. *Carbohydrate Polymers* 163: 301–316.

4 Su, Y., Burger, C., Hsiao, B.S., and Chu, B. (2014). Characterization of TEMPO-oxidized cellulose nanofibers in aqueous suspension by small-angle X-ray scattering. *Journal of Applied Crystallography* 47 (2): 788–798.

5 Ma, H., Burger, C., Hsiao, B.S., and Chu, B. (2012). Highly permeable polymer membranes containing directed channels for water purification. *ACS Macro Letters* 1 (6): 723–726.

6 Karim, Z., Claudpierre, S., Grahn, M. et al. (2016). Nanocellulose based functional membranes for water cleaning: tailoring of mechanical properties, porosity and metal ion capture. *Journal of Membrane Science* 514: 418–428.

7 Hadi, P., Yang, M., Ma, H. et al. (2019). Biofouling-resistant nanocellulose layer in hierarchical polymeric membranes: synthesis, characterization and performance. *Journal of Membrane Science* 579: 162–171.

8 Li, N., Zheng, J., Hadi, P. et al. (2019). Synthesis and characterization of a high flux nanocellulose–cellulose acetate nanocomposite membrane. *Membranes* 9 (6): 70.

9 Hassan, M., Abou-Zeid, R., Hassan, E. et al. (2017). Membranes based on cellulose nanofibers and activated carbon for removal of Escherichia coli bacteria from water. *Polymers* 9 (8): 335.

10 Isogai, A. and Bergström, L. (2018). Preparation of cellulose nanofibers using green and sustainable chemistry. *Current Opinion in Green and Sustainable Chemistry* 12: 15–21.

11 Koskela, S., Wang, S., Xu, D. et al. (2019). Lytic polysaccharide monooxygenase (LPMO) mediated production of ultra-fine cellulose nanofibres from delignified softwood fibres. *Green Chemistry* 21 (21): 5924–5933.

12 Henriksson, M., Henriksson, G., Berglund, L.A., and Lindström, T. (2007). An environmentally friendly method for enzyme-assisted preparation of microfibrillated cellulose (MFC) nanofibers. *European Polymer Journal* 43 (8): 3434–3441.

13 Tanpichai, S., Biswas, S.K., Witayakran, S., and Yano, H. (2019). Water hyacinth: a sustainable lignin-poor cellulose source for the production of cellulose nanofibers. *ACS Sustainable Chemistry & Engineering* 7 (23): 18884–18893.

14 Shahi, N., Min, B., Sapkota, B., and VKJS, R. (2020). Eco-friendly cellulose nanofiber extraction from sugarcane bagasse and film fabrication. *Sustainability* 12 (15): 6015.

15 Sharma, P.R., Joshi, R., Sharma, S.K., and Hsiao, B.S. (2017). A simple approach to prepare carboxycellulose nanofibers from untreated biomass. *Biomacromolecules* 18 (8): 2333–2342.

16 Hsiao, B.S., Chu, B., and Sharma, P.R., inventors; The Research Foundation for the State University of New York (Albany, NY, US), assignee. Production of carboxylated nanocelluloses. United States patent U.S. Patent 20180086851. 2018. 29.

17 Sharma, P.R., Chattopadhyay, A., Zhan, C. et al. (2018). Lead removal from water using carboxycellulose nanofibers prepared by nitro-oxidation method. *Cellulose* 25 (3): 1961–1973.

18 Sharma, P.R., Zheng, B., Sharma, S.K. et al. (2018). High aspect ratio carboxycellulose nanofibers prepared by nitro-oxidation method and their nanopaper properties. *ACS Applied Nano Materials* 1 (8): 3969–3680.

19 Kumar, R., Kumari, S., Rai, B. et al. (2020). A facile chemical approach to isolate cellulose nanofibers from jute fibers. *Journal of Polymers and the Environment* 28: 2761–2770.

20 Isogai, A., Saito, T., and Fukuzumi, H. (2011). TEMPO-oxidized cellulose nanofibers. *Nanoscale* 3 (1): 71–85.

21 Tang, Z., Li, W., Lin, X. et al. (2017). TEMPO-oxidized cellulose with high degree of oxidation. *Polymers* 9 (9): 421.

22 Isogai, A., Hänninen, T., Fujisawa, S., and Saito, T. (2018). Review: catalytic oxidation of cellulose with nitroxyl radicals under aqueous conditions. *Progress in Polymer Science* 86: 122–148.

23 Jiang, J., Ye, W., Liu, L. et al. (2017). Cellulose nanofibers prepared using the TEMPO/Laccase/O_2 system. *Biomacromolecules* 18 (1): 288–294.

24 Naderi, A., Lindström, T., and Sundström, J. (2014). Carboxymethylated nanofibrillated cellulose: rheological studies. *Cellulose* 21 (3): 1561–1571.

25 Naderi, A., Lindström, T., and Sundström, J. (2015). Repeated homogenization, a route for decreasing the energy consumption in the manufacturing process of carboxymethylated nanofibrillated cellulose? *Cellulose* 22 (2): 1147–1157.

26 Sharma, P.R., Chattopadhyay, A., Sharma, S.K. et al. (2018). Nanocellulose from spinifex as an effective adsorbent to remove cadmium(II) from water. *ACS Sustainable Chemistry & Engineering* 6 (3): 3279–3290.

27 Sharma, P.R., Chattopadhyay, A., Sharma, S.K., and Hsiao, B.S. (2017). Efficient removal of UO_2^{2+} from water using carboxycellulose nanofibers prepared by the nitro-oxidation method. *Industrial & Engineering Chemistry Research* 56 (46): 13885–13893.

28 Sharma, P.R., Sharma, S.K., Antoine, R., and Hsiao, B.S. (2019). Efficient removal of arsenic using zinc oxide nanocrystal-decorated regenerated microfibrillated cellulose scaffolds. *ACS Sustainable Chemistry & Engineering* 7 (6): 6140–6151.

29 Chen, H., Sharma, S.K., Sharma, P.R. et al. (2019). Arsenic(III) removal by nanostructured dialdehyde cellulose–cysteine microscale and nanoscale fibers. *ACS Omega* 4 (26): 22008–22020.

30 Sharma, P.R., Sharma, S.K., Lindström, T., and Hsiao, B.S. (2020). Nanocellulose-enabled membranes for water purification: perspectives. *Advanced Sustainable Systems* 4 (5): 1900114.

31 Zhan, C., Li, Y., Sharma, P.R. et al. (2019). A study of TiO_2 nanocrystal growth and environmental remediation capability of TiO_2/CNC nanocomposites. *RSC Advances* 9 (69): 40565–40576.

32 Al-Ahmed, Z.A., Hassan, A.A., El-Khouly, S.M., and El-Shafey, S.E. (2019). TEMPO-oxidized cellulose nanofibers/TiO_2 nanocomposite as new adsorbent for Brilliant Blue dye removal. *Polymer Bulletin* 77: 6213–6226.

33 Wu, J., Wei, W., Li, S. et al. (2018). The effect of membrane surface charges on demulsification and fouling resistance during emulsion separation. *Journal of Membrane Science* 563: 126–133.

34 Ahmad, A., Abdulkarim, A., Shafie, Z.M., and Ooi, B. (2017). Fouling evaluation of PES/ZnO mixed matrix hollow fiber membrane. *Desalination* 403: 53–63.

35 Yu, W., Liu, T., Crawshaw, J. et al. (2018). Ultrafiltration and nanofiltration membrane fouling by natural organic matter: mechanisms and mitigation by pre-ozonation and pH. *Water Research* 139: 353–362.

36 Bruneel, D. and Schacht, E. (1993). Chemical modification of pullulan: 1. Periodate oxidation. *Polymer* 34 (12): 2628–2632.

37 Kim, U.-J., Kuga, S., Wada, M. et al. (2000). Periodate oxidation of crystalline cellulose. *Biomacromolecules* 1 (3): 488–492.

38 Maekawa, E. and Koshijima, T. (1991). Preparation and structural consideration of nitrogen-containing derivatives obtained from dialdehyde celluloses. *Journal of Applied Polymer Science* 42 (1): 169–178.

39 Potthast, A., Rosenau, T., Kosma, P. et al. (2005). On the nature of carbonyl groups in cellulosic pulps. *Cellulose* 12 (1): 43–50.

40 Vicini, S., Princi, E., Luciano, G. et al. (2004). Thermal analysis and characterisation of cellulose oxidised with sodium methaperiodate. *Thermochimica Acta* 418 (1-2): 123–130.

41 Kim, U.J., Lee, Y.R., Kang, T.H. et al. (2017). Protein adsorption of dialdehyde cellulose-crosslinked chitosan with high amino group contents. *Carbohydrate Polymers* 163: 34–42.

42 Lindh, J., Carlsson, D.O., Stromme, M., and Mihranyan, A. (2014). Convenient one-pot formation of 2,3-dialdehyde cellulose beads via periodate oxidation of cellulose in water. *Biomacromolecules* 15 (5): 1928–1932.

43 Abou-Zeid, R.E., Dacrory, S., Ali, K.A., and Kamel, S. (2018). Novel method of preparation of tricarboxylic cellulose nanofiber for efficient removal of heavy metal ions from aqueous solution. *International Journal of Biological Macromolecules* 119: 207–214.

44 Coseri, S., Biliuta, G., Zemljič, L.F. et al. (2015). One-shot carboxylation of microcrystalline cellulose in the presence of nitroxyl radicals and sodium periodate. *RSC Advances* 5 (104): 85889–82897.

45 Kasai, W., Morooka, T., and Ek, M. (2013). Mechanical properties of films made from dialcohol cellulose prepared by homogeneous periodate oxidation. *Cellulose* 21 (1): 769–776.

46 Huang, X., Dognani, G., Hadi, P. et al. (2020). Cationic dialdehyde nanocellulose from sugarcane bagasse for efficient chromium (VI) removal. *ACS Sustainable Chemistry & Engineering* 8 (12): 4734–4744.

47 Liimatainen, H., Sirvio, J., Sundman, O. et al. (2011). Flocculation performance of a cationic biopolymer derived from a cellulosic source in mild aqueous solution. *Bioresource Technology* 102 (20): 9626–9632.

48 Sirviö, J.A., Anttila, A.-K., Pirttilä, A.M. et al. (2014). Cationic wood cellulose films with high strength and bacterial anti-adhesive properties. *Cellulose* 21 (5): 3573–3583.

49 Zhu, W., Liu, L., Liao, Q. et al. (2016). Functionalization of cellulose with hyperbranched polyethylenimine for selective dye adsorption and separation. *Cellulose* 23 (6): 3785–3797.

50 Suopajärvi, T., Sirviö, J.A., and Liimatainen, H. (2017). Cationic nanocelluloses in dewatering of municipal activated sludge. *Journal of Environmental Chemical Engineering* 5 (1): 86–92.

51 Yao, M., Wang, Z., Liu, Y. et al. (2019). Preparation of dialdehyde cellulose graftead graphene oxide composite and its adsorption behavior for heavy metals from aqueous solution. *Carbohydrate Polymers* 212: 345–351.

52 Kim, U.J., Kimura, S., and Wada, M. (2019). Highly enhanced adsorption of Congo red onto dialdehyde cellulose-crosslinked cellulose-chitosan foam. *Carbohydrate Polymers* 214: 294–302.

53 Zheng, X., Li, X., Li, J. et al. (2018). Efficient removal of anionic dye (Congo red) by dialdehyde microfibrillated cellulose/chitosan composite film with significantly improved stability in dye solution. *International Journal of Biological Macromolecules* 107 (Pt A): 283–289.

54 Tian, X., Hua, F., Lou, C., and Jiang, X. (2018). Cationic cellulose nanocrystals (CCNCs) and chitosan nanocomposite films filled with CCNCs for removal of reactive dyes from aqueous solutions. *Cellulose* 25 (7): 3927–3939.

55 Liu, Y., Huang, H., Huo, P., and Gu, J. (2017). Exploration of zwitterionic cellulose acetate antifouling ultrafiltration membrane for bovine serum albumin (BSA) separation. *Carbohydrate Polymers* 165: 266–275.

56 Kim, U.-J., Lee, Y.R., Kang, T.H. et al. (2017). Protein adsorption of dialdehyde cellulose-crosslinked chitosan with high amino group contents. *Carbohydrate Polymers* 163: 34–42.

57 Yang, X., Ku, T.-H., Biswas, S.K. et al. (2019). UV grafting: surface modification of cellulose nanofibers without the use of organic solvents. *Green Chemistry* 21 (17): 4619–4624.

58 Li, M.Z., Li, D.G., Deng, Q.Y. et al. (2012). Fabrication and properties of green cellulose nanofibers/polylactic acid composites. *Applied Mechanics and Materials* 174-177: 885–892.

59 Takagi, H. (2014). Fabrication and evaluation of cellulose-nanofiber-reinforced green composites. In: *Cellulose Based Composites* (eds. J.P. Hinestroza and A.N. Netravali), 27–42. Weinheim, Germany: Wiley-VCH.

60 Saito, T. and Isogai, A. (2004). TEMPO-mediated oxidation of native cellulose. The effect of oxidation conditions on chemical and crystal structures of the water-insoluble fractions. *Biomacromolecules* 5 (5): 1983–1989.

61 Hirasawa, I., Mikami, T., Katayama, A., and Sakuma, T. (2006). Strategy to obtain nm size crystals through precipitation in the presence of polyelectrolyte. *Chemical Engineering & Technology* 29 (2): 212–214.

62 Jabbar, A., Militký, J., Ali, A., and Usman, J.M. (2017). Mechanical behavior of nanocellulose coated jute/green epoxy composites. *IOP Conference Series: Materials Science and Engineering* 254: 042015.

63 Dong, H., Wu, L., Zhang, L. et al. (2015). Clay nanosheets as charged filler materials for high-performance and fouling-resistant thin film nanocomposite membranes. *Journal of Membrane Science* 494: 92–103.

64 Kumar, R. and Ismail, A. (2015). Fouling control on microfiltration/ultrafiltration membranes: effects of morphology, hydrophilicity, and charge. *Journal of Applied Polymer Science* 132 (21): 42042–42062.

65 Zhang, M., Liao, B.-q., Zhou, X. et al. (2015). Effects of hydrophilicity/hydrophobicity of membrane on membrane fouling in a submerged membrane bioreactor. *Bioresource Technology* 175: 59–67.

66 Yang, M., Hadi, P., Yin, X. et al. (2021). Antifouling nanocellulose membranes: how subtle adjustment of surface charge lead to self-cleaning property. *Journal of Membrane Science* 618: 118739.

67 Hu, L., Zheng, G., Yao, J. et al. (2013). Transparent and conductive paper from nanocellulose fibers. *Energy & Environmental Science* 6 (2): 513–518.

68 Ma, H., Burger, C., Hsiao, B.S., and Chu, B. (2014). Fabrication and characterization of cellulose nanofiber based thin-film nanofibrous composite membranes. *Journal of Membrane Science* 454: 272–282.

69 Zhang, T., Zhang, X., Chen, Y. et al. (2018). Green fabrication of regenerated cellulose/graphene films with simultaneous improvement of strength and toughness by tailoring the nanofiber diameter. *ACS Sustainable Chemistry & Engineering* 6 (1): 1271–1278.

70 Su, Y., Burger, C., Ma, H. et al. (2015). Exploring the nature of cellulose microfibrils. *Biomacromolecules* 16 (4): 1201–1209.

71 Liimatainen, H., Sirviö, J., Pajari, H. et al. (2013). Regeneration and recycling of aqueous periodate solution in dialdehyde cellulose production. *Journal of Wood Chemistry and Technology* 33 (4): 258–266.

72 Veelaert, S., De Wit, D., Gotlieb, K., and Verhé, R. (1997). Chemical and physical transitions of periodate oxidized potato starch in water. *Carbohydrate Polymers* 33 (2-3): 153–162.

73 Zakaria, Z.A., Zakaria, Z., Surif, S., and Ahmad, W.A. (2007). Hexavalent chromium reduction by acinetobacter haemolyticus isolated from heavy-metal contaminated wastewater. *Journal of Hazardous Materials* 146 (1–2): 30–38.

74 Yang, H. and van de Ven, T.G.M. (2016). Preparation of hairy cationic nanocrystalline cellulose. *Cellulose* 23 (3): 1791–1801.

16

Recycling of Lithium Batteries

Mario Pagliaro[1] *and Francesco Meneguzzo*[2]

[1] *Istituto per lo Studio dei Materiali Nanostrutturati, CNR, Palermo, Italy*
[2] *Istituto per la Bioeconomia, CNR, Sesto Fiorentino, FI, Italy*

16.1 Introduction

With several million battery electric vehicles (BEVs) manufactured and sold since the mid-2010s, the Li-ion battery (LIB) is the key new energy technology, which is enabling the transition from internal combustion engine vehicles (cars, buses, and trucks) to BEVs [1]. Today manufactured through advanced continuous manufacturing processes, battery cells comprised a graphite anode, a Li-containing cathode, electrolyte, and separator. The cells are assembled in modules, and the latter are further assembled into battery packs whose typical capacity in a small BEV as of mid-2020 averaged 30 kWh. Following the first main LIBs on the market in the 2005–2014 decade based on lithium cobalt oxide ($LiCoO_2$, LCO) cathode, layered cathodes were commercialized. They include lithium nickel manganese cobalt oxide ($LiNi_xMn_yCo_zO_2$, NMC), lithium manganese oxide ($LiMn_2O_4$, LMO), lithium iron phosphate ($LiFePO_4$, LFP), and lithium nickel cobalt aluminum oxide ($LiNi_{0.8}Co_{0.15}Al_{0.05}O_2$, NCA) [2].

Likewise to any battery, the cathode and anode of LIBs are electronically insulated, but connected by an electrolyte and a separator. The cathodes and anodes of LIBs are comprised of active materials that can reversibly intercalate lithium ions. The anode is generally made of a copper anode coated with graphite, while the cathode uses an aluminum foil coated with one of the aforementioned "intercalating" lithium-metal oxides.

A typical EV LIB pack has a useful first life of 250,000 km [3], even though increasingly adopted fast-charging (at power values > 50 kW) reduces the battery pack duration since battery degradation rapidly accelerates with charging current [4].

The reduced ability to store and deliver electricity is chiefly due to a solid product formation during the charge and discharge cycles due to the reaction of the lithiated anode with the alkyl carbonate comprising the electrolyte solution mainly consisting of stable (such as Li_2CO_3) and metastable components (polymers, $ROCO_2Li$, $(CH_2OCO_2Li)_2$, and ROLi) [5].

Sustainable Separation Engineering: Materials, Techniques and Process Development, Volume 2, First Edition. Edited by Gyorgy Szekely and Dan Zhao.
© 2022 John Wiley & Sons Ltd. Published 2022 by John Wiley & Sons Ltd.

Prone to decompose exothermically at temperatures > 90 °C, releasing flammable gases and oxygen that may easily ignite [6], the latter products progressively deposit on the anode surface forming a passivating film. This film limits the electrochemical reaction by making graphite sites inaccessible for Li^+ to intercalate, thus leading to an increase in internal ohmic resistance.

When the automotive battery pack loses 20% (15% for certain EV models) of its initial capacity, it becomes unfit for traction as the lower capacity of the battery affects the acceleration, range, and regeneration capabilities of the electric vehicle. The battery pack then is ready for stationary applications, which demand lower current densities.

Hence, modules of spent batteries retaining between 80–85% of their original capacity are collected, sorted out, and reassembled in new "repurposed" battery packs, ready for stationary usage [7], such as utility-scale grid applications as well as to power buildings coupled to rooftop photovoltaic arrays, and telecommunication towers.

After several years of service in stationary applications, the batteries are ready for recycling. According to Melin [8], a leading expert in the lithium battery recycling market, by 2025 about 75% of spent EV batteries will be reused in second-life solutions after retirement from vehicles, after which they will be sent to recycling to recover all the valued components.

In 2019, we published a circular economy insight on LIB reuse and recycling [9], forecasting that the first-generation LIB recycling processes, generally based on the first-generation recovery technologies in which a pyrometallurgical process to obtain different streams of raw materials is followed by a leaching process to extract metals [10], would be increasingly replaced by green chemistry processes producing highly pure ("battery-grade") lithium, cobalt, and manganese compounds along with graphite, copper, and aluminum.

Aiming to offer a practical analysis of the situation, rather than an academic review, this chapter focuses on the LIB recycling industry whose ultimate goal is to use the battery-grade chemicals recovered from spent batteries to produce new battery cathodes rather than selling the highly pure chemicals recovered.

The technical details of LIB recycling technologies are presented and discussed in comprehensive recent books [11, 12], reviews [9, 10], and book chapters [13]. In this account, we offer a critical analysis of a large industry which only in 2019 processed over 100,000 tonnes of spent LIBs generating revenues exceeding $1.5 billion [14], whose role in the key new energy technology goes beyond the role played by recyclers in any other segment of the global material recycling industry.

Two important research policies emerge from the present analysis, which are of direct relevance to policymakers in all industrialized countries, urgently called to establish the national LIB industries to end reliance on foreign countries for a technology whose importance goes beyond that of the internal combustion engine, which formed the basis of the wealth of all industrialized nations in the twentieth century.

16.2 The Lithium Battery Recycling Industry

Recycling of LIBs is carried out on a large industrial scale chiefly in China and South Korea with China recycling around 67,000 tonnes of LIBs in 2018 (69% of all the stock available for recycling worldwide, and 18,000 tonnes being recycled in South Korea [15].

Rather than being "limited" or "antieconomic" as claimed in several reports regularly published in scientific journals citing data going back to 2010 [16], the LIB industry by mid-2020 included already over 90 LIB recyclers, out of which 35 were in China, 20 in Europe, 15 in the United States of America and Canada, 8 in South Korea, 6 in Japan, and 9 in other countries [17].

Aiming to maximize revenues, the early LIB recycling companies initially focused on recovering highly valued Co and Ni from layered oxides due to their high cobalt and nickel content. According to reputed industry's analysts, the $1.5 billion LIB industry in 2019 will increase almost tenfold by 2025, when it should reach $12.2 billion (and $18.1 billion by 2030) growing at a compound growth annual rate of 8.2% between 2025 and 2030 [14].

The first BEV industrially significant production and uptake started in China in the mid-2010s [1] led to a first large increase in the price of lithium, cobalt, and graphite. For example, the price of 99% lithium carbonate went from slightly more than $5,000/tonne as of January 2016 to $15,000/tonne as of September 2018 [18]. The price of 99% cobalt sulfate went from about $24,000/tonne as of January 2016 to $80,000/tonne as of January 2018 [19].

Since then, prices have significantly decreased. In 2019, for example, the price of battery-grade lithium carbonate averaged $13,000/tonne [20]. In any case, the recovery of valued minerals and graphite from spent LIBs became and remains a profitable economic activity. Using different technologies, all LIB recycling companies manufacture only battery-grade minerals. Indeed, it is the "lengthy processing and purification processes of the raw materials to reach battery-grade" which determines the true cost to manufacture [21] LIBs.

16.3 Toward Zero-Emission Lithium Battery Recycling

In May 2020, citizens of Endicott, a village in the State of New York, continuing their protests against the project of a LIB recycling plant (Figure 16.1) created a group to organize opposition to the project [22]. Noting that the proposed site is adjacent to three baseball fields, a swimming pool, community green, and homes, protestors objected that the plant was permitted to release in the air human carcinogens such as 2,3,7,8-tetrachlorodibenzo-*p*-dioxin, chromium(VI), nickel, and formaldehyde (though within emission limits, control requirements, or compliance-monitoring conditions) [23].

This happens because the first-generation approach to LIB recycling uses incineration to convert all the metals in the battery into a metal-rich ore from which valued metals are subsequently extracted ("leached") and precipitated via straightforward wet chemistry processes [10].

Incineration of plastics in the presence of metals such as copper catalyzes the formation of dioxins, which add to toxic micro- and nanoparticulate inevitably formed during combustion of plastics and other waste in incinerators. To mitigate pollution, waste-to-energy plants are equipped with filters and other pollution control devices [24].

Replacing the aforementioned pyrometallurgical approach to LIB recycling, hydrometallurgy is an environmentally friendly technology by which all the valued substances in spent LIBs (including costly and strategically important pure graphite) are recovered and made available as battery-grade materials, with virtually zero emissions in air, water, and soil.

Figure 16.1 Citizens of Endicott, State of New York, protesting against a new LIB recycling plant on May 16, 2020. [Photo by Jared Smolinsky, reproduced from noburnbroome.com].

In brief, batteries are pretreated using physical processes such as shredding and sieving followed by wet chemical processes involving the combination of metal dissolution and chemical precipitation.

For instance, a company based in Wendeburg, Germany, uses one such industrial process developed during three research projects funded by the German government through its Ministry of the Environment including LithoRec I and LithoRec II between 2009 and 2015 [25].

In brief (Scheme 16.1), the spent batteries are first discharged feeding the residual electrical energy into the grid through which the company is able to cover 50% of its first plant energy needs. Following disassembly of the battery packs, the batteries are crushed with a 20 mm rotary shear crusher under a nitrogen atmosphere at 100–140 °C. The solvent in the electrolyte recovered from the crushed material by means of vacuum distillation, thereby preventing the formation of toxic gases, is sent to the chemical industry for further processing [25].

Unfortunately, from the green chemistry viewpoint, electrolytes used in LIBs are Li-salts of halogen-containing complex anions such as BF_4^- and PF_6^- dissolved along with flame retardants and thermal runaway inhibitors for improving thermal stability in an organic aprotic solvent such as ethylene carbonate (EC), ethyl methyl carbonate (EMC), and dimethyl carbonate (DMC). These fluoride-containing salts are toxic and potentially highly polluting. Hence, intense researches are aimed to replace them, for example, with new

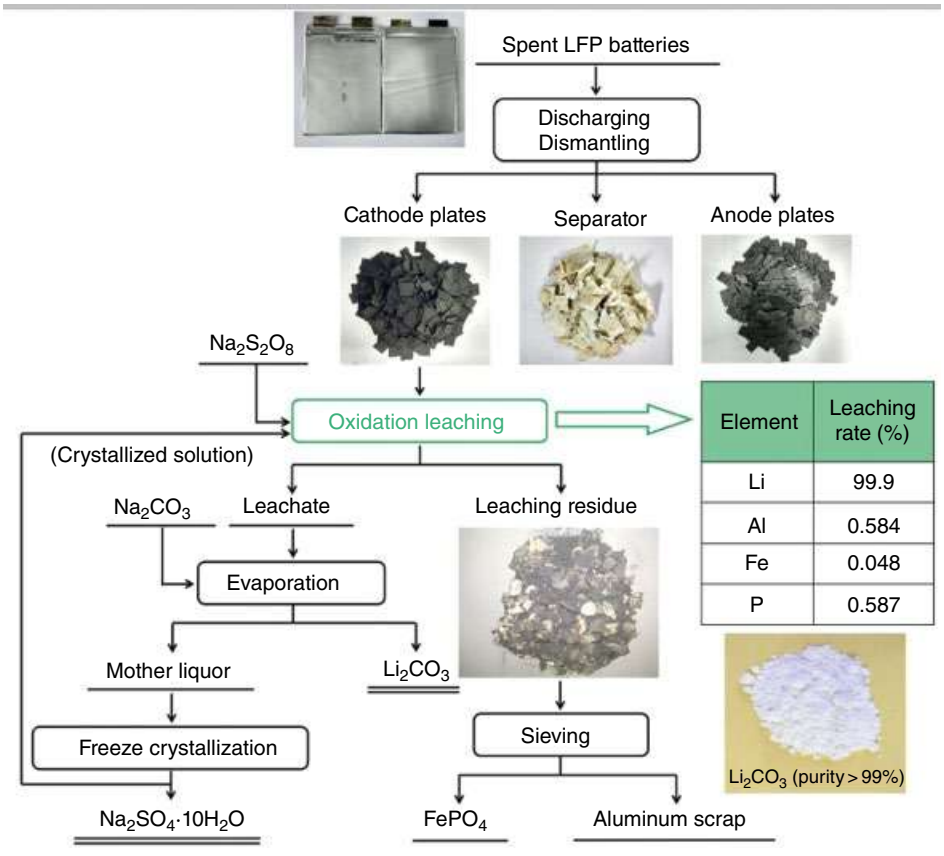

Scheme 16.1 Material recovery with the Duesenfeld recycling process. [Reproduced from Zhang J; Hu J; Liu Y; Jing Q; Yang C; Chen Y; Wang C (2019) Sustainable and Facile Method for the Selective Recovery of Lithium from Cathode Scrap of Spent LiFePO4 Batteries. ACS Sustainable Chemistry & Engineering 7:5626-5631. with kind permission, Copyright American Chemical Society. DOI-https://doi.org/10.1021/acssuschemeng.9b00404].

electrolytic salts such as safe, halogen-free LiB_4H_{13} and LiB_5H16 which are as conducting as existing $LiBF_4$ and $LiPF_6$ [26].

The company is not able to recover only two components: the ethyl carbonate electrolyte (5%) and the separator (4%).

The dried crushed material is separated into different material fractions on the basis of physical characteristics such as particle size, density as well as magnetic and electrical properties; these then undergo further metallurgical processing. The iron, copper, and aluminum fractions are recovered and sold for standard recycling.

The "black mass," which contains the electrode-active materials and the conducting fluorine-containing salt, is initially processed to completely remove fluoride prior to leaching, in order to prevent the formation of toxic hydrofluoric acid. Once all fluoride has been removed, Co, Li, Ni, and Mn are subsequently leached and precipitated in the mineral form preferred by the LIB industry to produce new cathodes, whereas graphite is recovered and sent for material purification prior to reuse.

It is relevant to learn that the company is the outcome of over 10 years of developmental research funded by the German Ministry of the Environment with the aim to develop a new industrial green recycling process at the onset of which some 30 researchers and engineers worked for five years on the basic engineering and chemistry aspects during the aforementioned three different research projects [27].

By weight percentage (g material/g battery), a typical LIB based on layered oxides (and thus not referring to the cathodes in olivine LFP) comprises about: 7% Co, 7% Li (expressed as lithium carbonate equivalent (LCE), 1 g of lithium = 5.17 g LCE), 4% Ni, 5% Mn, 10% Cu, 15% Al, 16% graphite, and 36% other materials [28].

Based on their higher energy density, most EV market experts concur that EV LIBs will soon be dominated by cobalt-containing cathodes such as lithium-nickel, manganese, cobalt (NMC) and lithium-nickel, cobalt, aluminum oxide (NCA). On the other hand, in 2019, we forecasted that intrinsically safe and long-life LFP cathode technology was going to dominate the EV market for decades to come [1]. The forecast was based on the large potential for improvement in terms of the energy density of LFP-based cells and batteries.

In early 2020, the world's second-largest LIB and world's leading EV manufacturer announced the mass production of a new LFP cathode LIB in which the re-engineered electrochemical cells, acting also as structural elements, afford a 50% increase in the space utilization of the battery pack when compared to conventional lithium iron phosphate block batteries, retaining the excellent safety profile of said batteries [29]. The new electric sedan equipped with such a battery produced by the same company has 605 km autonomy on a single charge.

The intrinsic safety of LFP cathodes is due to the strong P–O covalent bond of phosphate which prevents oxygen release, while the olivine crystal structure of the oxide is retained upon prolonged charge–discharge cycles making the cathode directly recyclable.

This means that cobalt-free and intrinsically safe batteries based on the LFP cathode technology will regain expansion to passenger electric vehicles beyond the electric bus market segment where they largely dominate [30]. Indeed, the world's first LIB manufacturer announced in February 2020 the launch of new lithium iron phosphate batteries, "which use no cobalt, the most expensive metal in EV batteries" with the company having "developed a simpler and less expensive way of packaging battery cells, called cell-to-pack, that eliminates the middle step of bundling cells" [29].

Under these circumstances, the discovery of Wang and coworkers [31] at Beijing Key Laboratory of Green Recycling and Extraction of Metals, enabling direct cathode recycling by simply stirring at room temperature for 20 minutes, a suspension of powdered cathode plates in aqueous sodium persulfate (Eq. 16.1) assumes strategic relevance:

$$LiFePO_4 + Na_2S_2O_8 \rightarrow FePO_4 \downarrow + Li_2SO_4 + Na_2SO_4 \tag{16.1}$$

The orthorhombic $FePO_4$ leaching residue obtained adding 1.05 times the stoichiometric amount of persulfate to extract 99.8% of Li can be used as such to produce new LFP cathodes. Being recovered as battery-grade Li_2CO_3 (>99% pure) by the addition of Na_2CO_3 to the leachate followed by evaporation (Scheme 16.2), recovered lithium is ready to be processed for the same purpose.

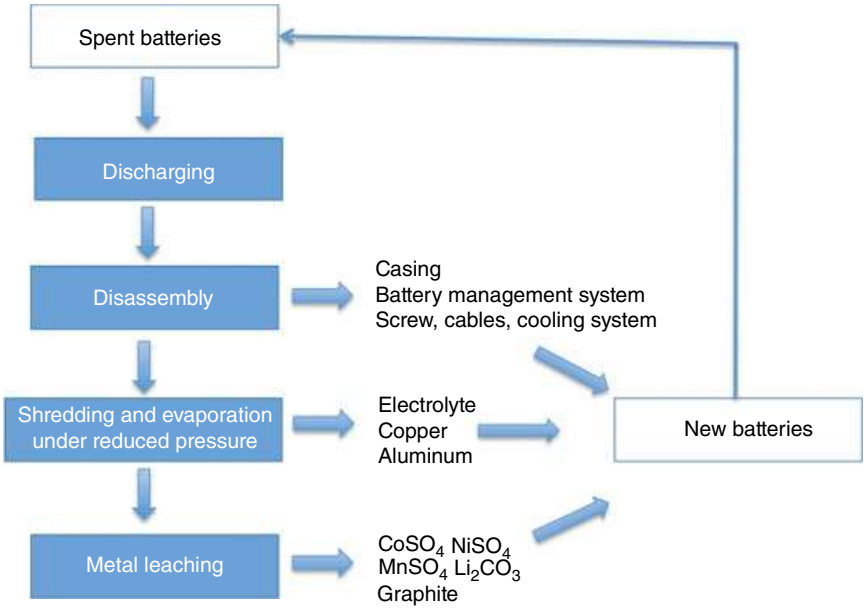

Scheme 16.2 Flowsheet of the process for treating entire spent $LiFePO_4$ batteries using aqueous sodium sulfate under neutral conditions for Li leaching and subsequent precipitation as battery-grade lithium carbonate. [Reproduced from Ref.[31], with kind permission, Copyright American Chemical Society].

The battery is first discharged and then dismantled recovering both the separator and the anode. The cathode plates cut into small pieces are then subjected to extraction with the persulfate aqueous solution. No acid or alkali is employed and no prior separation of cathode active material and the Al foil (the most demanding procedure in the present recycling process of spent LIBs) is required due to the strong oxidative environment, with the rapid formation of a thin layer of Al_2O_3 and extremely low leaching of Al. The solid residue is sieved, recovering the aluminum scrap and the powdered $FePO_4$, whereas the mother liquor is freeze-dried to isolate pure $Na_2SO_4{\cdot}10H_2O$.

Allowing to also recover copper and aluminum (18% and 32% in weight of the LFP cell) [32], this green chemistry route is ideally suited for LFP cells also because it fixes the main problem with recycling LIBs based on LFP cathodes, namely the low content (0.6 wt%) of lithium in these cells [32].

Indeed, by taking into account the revenues generated by selling lithium carbonate, iron phosphate in olivine form, aluminum scrap and sodium sulfate, the team calculated [31] that revenues exceeding $510 per tonne of spent LFP battery can be generated (Table 16.1). Remarkably, no wastewater or air treatment costs would be borne by any company uptaking this simple, safe, and highly efficient technology.

Similarly, efficient and rapid metal recovery processes now exist even for the most complex quaternary cathode materials. For example, all metals can be readily and conveniently leached from a $LiNi_{0.5}Co_{0.2}Mn_{0.3}O_2$ cathode with excellent leaching efficiency (100% Li, 93.38% Ni, 91.63% Co, and 92.00% Mn) using an environmentally friendly leachant mixture

Table 16.1 Economic analysis for recycling 1 tonne of spent LFP batteries in China (Reproduced from Ref. [31].

Product	**Weight (kg)**	**Value ($/kg)**	**Revenues ($)**
Li_2CO_3	76.7	11.5	882.1
$FePO_4$	293.8	1	293.8
Al scrap	76.1	0.3	22.8
$Na_2SO_4 \cdot 10H_2O$	639.1	0.115	73.5
	Total		1272.2
Reagent	**Weight (kg)**	**Value ($/kg)**	**Cost ($)**
$Na_2S_2O_8$	236.2	1.05	248
Na_2CO_3	115.4	0.24	28.7
Energy	**Consumption (kWh)**	**Value ($/kWh)**	**Cost ($)**
	1667.5	0.15	250.1
Other costs	**Water consumption (tonne)**	**Value ($/t)**	**Cost ($)**
Water	1.5	0.36	0.5
Labor			150
Equipment depreciation			70
Maintenance			15
	Net value		510.8

of 0.2 M phosphoric acid and 0.4 M citric acid at 90 °C with a solid–to–liquid ratio of 20 g/L with no need for reductant because citric acid acts both as leachant and reductant [33] promoting the reduction of Co^{3+}, Mn^{4+} and Ni^{3+}, to Co^{2+}, Mn^{2+}, and Ni^{2+} while being entirely oxidized to CO_2 and H_2O.

A widely employed organic acid, citric acid is produced in over 2 million tonnes per year amount via molasses fermentation [34]. Its abundance and affordable cost ($290/tonne was the average price in 2019) would, therefore, enable to carry out the green extraction of Li, Co, Mn, and Ni from widely used NMC cathodes at the economically viable cost of $2055 per tonne of cathode processed [33].

16.4 Outlook and Perspectives

Besides their widespread use in BEVs, LIBs are now massively used in energy storage systems (ESS) in conjunction with large photovoltaic and wind plants to make electricity obtained from non-programmable weather-dependent renewable energy sources of even higher quality and reliability when compared to power generated from fossil fuels [35].

These systems are ideally suited to reuse dismissed EV batteries, and will likely absorb most batteries dismissed from electric cars and buses since a large ESS system with state-of-charge limits in a 65–15% to minimize cycle aging, extends the project life to over 16 years allowing EV manufacturers to sell second-life batteries for <60% of their original price to

developers of highly profitable solar-plus-storage projects [36]. After that, and typically when a LIB reaches its end-of-life at 60% of its original capacity, the battery is ready for recycling making available highly pure lithium carbonate and other minerals to produce new LIBs.

Besides being economically profitable, lithium battery recycling is also needed from the lithium supply viewpoint. Lithium is abundant and most of the world's Li natural sources remain unexploited [37].

What is in high and increasing demand is "battery quality," namely lithium carbonate and lithium hydroxide of high purity (>99.5%) whose production and supply from existing refiners have not scaled up with demand, with the largest suppliers having struggled to bring new capacity online in recent years.

To understand the origins of today's insufficient supply, one needs to understand that since 2017, when the demand of battery quality lithium exceeded 50% of the market for the first time, the lithium industry had to evolve from an extractive to a chemical industry, which required substantial investment in refining plants typical of the chemical industry.

For example, commenting projections issued by LIB market experts, who were reporting 103 battery plants planned or under construction with a total capacity of 2028 GWh by 2028, one of the world's most reputed lithium market experts (Lowry) noted how:

> All these planned factories will not be built on a timely basis. The total capacity would require 1.6 million tonnes of battery quality LCE, which the industry is not in a position to do by 2028 given the lack of investment and the fact current BQ capacity is less than 250,000 tonnes. I continue to be surprised that OEMs and battery producers are blindly expecting a lithium supply miracle while many lithium mining projects can't move forward due to lack of financing [38].

Under these circumstances, the price of LIBs fell below $100/kWh in 2019 due to much more rapidly increasing production [39] to eventually drive the inevitable massive uptake of BEVs well beyond China. The LIB recycling industry will switch to green chemistry routes for the recovery of all battery components.

The low capital and operational costs of said hydrometallurgical routes already enable new companies to enter the LIB recycling industry, with distributed recycling minimizing transportation of hazardous spent LIBs. Cutting transportation cost, this will increase the competitiveness of a network of small recyclers in place of large, energy-intensive recycling plants using pyrometallurgical processes requiring expensive treatment of noxious emissions.

Substantiating these conclusions and supporting the present forecasts, by mid-2020, a Canada-based company founded in 2016 in less than 4 years became the largest LIB recycler in North America, with one plant in Kingston, Ontario, and another with a 10,000-tonne/year capacity under construction in the New York State [40]. Both these plants use a two-step process involving safe crushing of the spent LIBs followed by green chemistry extraction routes to recover nickel, cobalt, copper, aluminum, and lithium in the form of highly pure chemicals, leaching them one at a time in a series of conical bottom tanks under agitation, along with plastics, electrolytes, and graphite, without noxious gases to treat and no solid waste to manage [28]. The innovative idea here was to carry out the shredding process in water so as to prevent ignition, followed by separating the size-reduced feed stream into a magnetic product stream and a nonmagnetic feed stream [28].

Beyond the prices for cobalt sulfate and lithium carbonate, the key financial drives of the latter technology are plant operational expenses [41]. Proving once again the need to increase sustainability a team of scholars with education in economic and management topics discovered in a feedback process between the chemical testing work and techno-economic analysis that minimization of the operating expenses (OPEX) required optimization of acid and sodium hydroxide reagent consumption required for leaching and neutralization since the latter were identified as key OPEX drivers [42].

In closer detail, the optimized method developed to separate the copper and aluminum foils from the cathode and anode powders prior to leaching reduced the Al precipitated as aluminum hydroxide, resulting in a 15% reduction in total OPEX due to a 30% reduction in acid consumption and a similar reduction in NaOH consumption for neutralization [41].

The same scholars turned into entrepreneurs of LIB recycling would discover that greater economy comes from a flow rather than scale [43]. Hence, they would create a continuous recycling process whose cost is not just the aggregation of unit costs, but rather the outcome of smooth and economically sound integration of the parts in the final assembly, to provide customers with battery grade metal salts produced at the rate of customer demand [43].

Remarkably, both first- and new-generation LIB recycling plants make use of conveyors in continuous processes whose overall economy is enhanced thanks to the aforementioned smooth integration of the unit steps.

It is thanks to such enhanced profitability due to economies of flow, and not to economies of scale, that first-generation technologies for the recycling of LIBs based on preliminary incineration ("pyrometallurgical" processes) will be progressively replaced by new-generation recycling routes based on emission-free green chemistry technologies including those mentioned in this account.

Eventually, LIB recycling plants extracting economic value from spent batteries through a distributed network of recycling companies in which collection and transportation costs are minimized will become ubiquitous.

Author ORCID information

Mario Pagliaro: 0000-0002-5096-329X
Francesco Meneguzzo: 0000-0002-5952-9166

Conflict of Interest

The authors declare no conflict of interest.

References

1 Pagliaro, M. and Meneguzzo, F. (2019). The driving power of the electron. *Journal of Physics: Energy* 1: 011001.

2 Yoshino, A. (2014). Development of the lithium-ion battery and recent technological trends. In: *Lithium-Ion Batteries* (ed. G. Pistoia). Amsterdam: Elsevier.

3 Gao, Y., Jiang, J., Zhang, C. et al. (2017). Lithium-ion battery aging mechanisms and life model under different charging stresses. *Journal of Power Sources* 356: 103–114.
4 Saxena, S., Le Floch, C., MacDonald, J., and Moura, S. (2015). Quantifying EV battery end-of-life through analysis of travel needs with vehicle powertrain models. *Journal of Power Sources* 282: 265–276.
5 Vetter, J., Novak, P., Wagner, M.R. et al. (2005). Ageing mechanisms in lithium-ion batteries. *Journal of Power Sources* 147: 269–281.
6 Liu, K., Liu, Y., Lin, D. et al. (2018). Materials for lithium-ion battery safety. *Science Advances* 4: eaas9820.
7 Sanghai, B., Sharma, D., Baidya, K., and Raja, M. (2019). Refurbished and repower: second life of batteries from electric vehicles for stationary application. *SAE Technical Paper 2019-26-0156*.
8 Melin, H. (2017). *E- Circular Opportunities in the Lithium-Ion Industry*. London: Creation Inn.
9 Pagliaro, M. and Meneguzzo, F. (2019). Lithium battery reusing and recycling: a circular economy insight. *Heliyon* 5: e01866.
10 Lv, W., Wang, Z., Cao, H. et al. (2018). Critical review and analysis on the recycling of spent lithium-ion batteries. *ACS Sustainable Chemistry & Engineering* 6: 1504–1521.
11 An, L. (ed.) (2019). *Recycling of Spent Lithium-Ion Batteries*. Berlin: Springer.
12 Zhao, G. (2017). *Reuse and Recycling of Lithium-Ion Power Batteries*. New York: Wiley.
13 Elwert, T., Römer, F., Schneider, K. et al. (2018). Recycling of batteries from electric vehicles. In: *Behaviour of Lithium-Ion Batteries in Electric Vehicles* (eds. G. Pistoia and B. Liaw). Berlin: Springer.
14 MarketsandMarkets (2020). Lithium-ion battery recycling market by battery chemistry, industry and region - global forecast to 2030, Pune.
15 Melin, H.E. (2018). (Circular Energy Storage) cited in: Deign J. How China Is Cornering the Lithium-Ion Cell Recycling Market, greentechmedia.com. www.greentechmedia.com/articles/read/how-china-is-cornering-the-lithium-ion-cell-recycling-market/ (accessed 19 July 2020).
16 Nature Energy (2019). Recycle spent batteries. *Nature Energy* 4: 253.
17 Circular Energy Storage (2020). *Database*. London. https://circularenergystorage.com/subscription/ (accessed 19 May 2020).
18 Benchmark Mineral Intelligence cit. in Els F. The lithium price bulls were right. *Mining*, 30 November 2018. www.mining.com/lithium-price-bulls-right (accessed 19 May 2020).
19 Nelson, E. (2018). Price of cobalt. *Quartz*. www.theatlas.com/charts/r1VKbCcwG (accessed 19 July 2020).
20 Statista (2020). Average lithium carbonate price from 2010 to 2019 (in U.S. dollars per tonne). www.statista.com/statistics/606350/battery-grade-lithium-carbonate-price/ (accessed 19 July 2020).
21 Battery University (2019). BU-705a: battery recycling as a business. https://batteryuniversity.com/learn/article/battery_recycling_as_a_business/ (accessed 19 July 2020).
22 No Burn Broom 2020. https://noburnbroome.com/ (accessed 19 May 2020).
23 New York State, Department of Environmental Conservation, Permit under the Environmental Conservation Law (ECL). Facility DEC ID: 7034600218, Albany: NY, 2020.

http://fluoridealert.org/wp-content/uploads/endicott.air-permit.3-30-20.pdf (accessed 19 July 2020).

24 Pagliaro, M. (2020). Waste-to-wealth: the economic reasons for replacing waste-to-energy with the circular economy of municipal solid waste. *Visions for Sustainability* https://doi.org/10.13135/2384-8677/4421.

25 Hanisch, C., Diekmann, J., Stieger, A. et al. (2015). Recycling of lithium-ion batteries. In: *Handbook of Clean Energy Systems* (ed. J. Yan). Boston: Wiley.

26 Srivastava, A.K. and Misra, N. (2016). Designing new electrolytes for lithium ion batteries using superhalogen anions. *Polyhedron* 117: 422–426.

27 Leon, H. (2019). Startup develops eco-friendly process to recycle lithium-ion EV batteries. *The Observer*. https://observer.com/2019/12/duesenfeld-lithium-ion-battery-recycling-eco-friendly/ (accessed 19 July 2020).

28 Kochhar, A. and Johnston T.G. (2018). A process, apparatus, and system for recovering materials from batteries. WO2018218358A1.

29 BYD (2020). BYD's New Blade Battery Set to Redefine EV Safety Standards, Shenzhen.

30 Pagliaro, M. and Meneguzzo, F. (2019). Electric bus: a critical overview on the dawn of its widespread uptake. *Advanced Sustainable Systems* 3: 1800151.

31 Zhang, J., Hu, J., Liu, Y. et al. (2019). Sustainable and facile method for the selective recovery of lithium from cathode scrap of spent $LiFePO_4$ batteries. *ACS Sustainable Chemistry & Engineering* 7: 5626–5631.

32 Elwert, T., Hua, Q., and Schneider, K. (2019). Recycling of lithium Iron phosphate batteries: future prospects and research needs. *Materials Science Forum* 959: 9–68.

33 Zhuang, L., Sun, C., Zhou, T. et al. (2019). Recovery of valuable metals from $LiNi_{0.5}Co_{0.2}Mn_{0.3}O_2$ cathode materials of spent Li-ion batteries using mild mixed acid as leachant. *Waste Management* 85: 175–185.

34 Ciriminna, R., Meneguzzo, F., Delisi, R., and Pagliaro, M. (2017). Citric acid: emerging applications of key biotechnology industrial product. *Chemistry Central Journal* 11: 22.

35 Pagliaro, M. (2019). Renewable energy systems: enhanced resilience, lower costs. *Energy Technology* 7: 1900791.

36 Mathews, I., Xu, B., He, W. et al. (2020). Technoeconomic model of second-life batteries for utility-scale solar considering calendar and cycle aging. *Applied Energy* 269: 115127.

37 Narins, T.P. (2017). The battery business: lithium availability and the growth of the global electric car industry. *The Extractive Industries and Society* 4: 321–328.

38 Lowry, J. (2020). cit. In Palandrani P (2019) Joe Lowry (aka "Mr. Lithium") on the state of the lithium industry. *Global X*, 6 December. www.globalxetfs.com/joe-lowry-aka-mr-lithium-on-the-state-of-the-lithium-industry/ (accessed 19 July 2020).

39 Benchmark Mineral Intelligence cit. In: Written Testimony of Simon Moores, Managing Director, Benchmark Mineral Intelligence, US Senate Committee on Energy and Natural Resources Committee, 5 February 2019. https://www.energy.senate.gov/public/index.cfm/files/serve?File_id=9BAC3577-C7A4-4D6D-A5AA-33ACDB97C233 (accessed 19 July 2020).

40 BNN Bloomberg. Power Shift: Li-Cycle looks to improve battery materials recycling rate, 19 February 2020. https://www.bnnbloomberg.ca/commodities/power-shift/power-shift-li-cycle-looks-to-improve-battery-materials-recycling-rate~1904004/ (accessed 19 July 2020).

41 Davis, B., Watson, K., Roy, A. et al. (2019). Li-cycle - a case study. In: *REWAS 2019. The Minerals, Metals & Materials Series* (eds. G. Gaustad, C. Fleuriault, M. Gökelma, et al.), 247–260. Cham: Springer.

42 Ciriminna, R., Pecoraino, M., Meneguzzo, F., and Pagliaro, M. (2016). Reshaping the education of energy managers. *Energy Research & Social Science* 21: 44–48.

43 Seddon, J. and Caulkin, S. (2007). Systems thinking, lean production and action learning. *Action Learning: Research and Practice* 4: 9–24.

17

Deep Eutectic Solvents for Sustainable Separation Processes

Filipe H. B. Sosa[1,2], Mariana C. da Costa[1], Armando J. D. Silvestre[2], and André M. da Costa Lopes[2,3]

[1] *School of Chemical Engineering (FEQ), University of Campinas (UNICAMP), Campinas, São Paulo, Brazil*
[2] *CICECO – Aveiro Institute of Materials, Department of Chemistry, University of Aveiro, Aveiro, Portugal*
[3] *CECOLAB – Collaborative Laboratory Towards Circular Economy, R. Nossa Senhora da Conceição, Oliveira do Hospital, Coimbra, Portugal*

17.1 Introduction

Throughout the decades, the excessive dependence on nonrenewable fossil resources coupled with the increasing carbon dioxide (CO_2) levels in the atmosphere have led to unprecedented worldwide climate change events with negative impact on the planet ecosystems and environment, putting in risk the current and future generation thrive. This global issue has stimulated the development of more sustainable approaches envisaging the society growth with simultaneous protection of biodiversity and surrounding environment [1]. Today, the development of novel technologies needs to address both economic and environmental high standards, including high technological efficiency, high selectivity, and low energy consumption aligned with factual benefits to the environment and public health. The scientific progress notably in domains such as biotechnology, chemical engineering, applied chemistry, biology, and physics has been enabling the rise of emerging technologies to produce energy, fuels, materials, and chemicals with potential to reduce the negative impact of the current industrial activity. In this context, the traditional processes that have been in use during the last few decades of the last century, which often do not address concerns to minimize the energy demand, the overexploitation of nonrenewable resources, the production and disposing of a wide range of toxic wastes in the landfill, are losing their place in the coming era. Bioeconomy approaches, circularity of resources, and process efficiency are the main strategies to push forward an economic growth independent of resource consumption. This new paradigm is expected to help society accomplishing a sustainable future [2, 3].

The sustainability of industrial plants has been thus pursued and one of the most critical and important steps that crosses many industrial sectors, as for instance oil industry, pharmaceuticals, and metallurgy, is to replace or substantially modify the current extraction

Sustainable Separation Engineering: Materials, Techniques and Process Development, Volume 2, First Edition. Edited by Gyorgy Szekely and Dan Zhao.
© 2022 John Wiley & Sons Ltd. Published 2022 by John Wiley & Sons Ltd.

and separation processes/steps by more sustainable ones. A myriad of scientific and technological challenges have been settled for the advancement of new extraction and separation strategies to meet sustainability guidelines. This includes which solvents and technical apparatus must be used to extract, separate, and purify chemical and biological compounds with lower carbon footprint than conventional processes, reduced or no toxicity, higher recyclability as well as maintaining or overcoming their separation efficiency [4]. In this sense, the application of green chemistry principles, proposed by Paul Anastas and John Warner [5], may stand as a useful tool. Green chemistry aims at designing more environmentally benign chemical processes and methodologies, allowing the elimination or reduction of hazardous or toxic chemicals at any stage of laboratory or industrial production [6]. It contemplates 12 good practices as depicted in Figure 17.1 to achieve low impact on the environment and health, increasing the sustainability in chemical processing [5].

The importance of applying these principles is transversal in the design of new chemical processes and some of them can be applied in the development of extraction, separation,

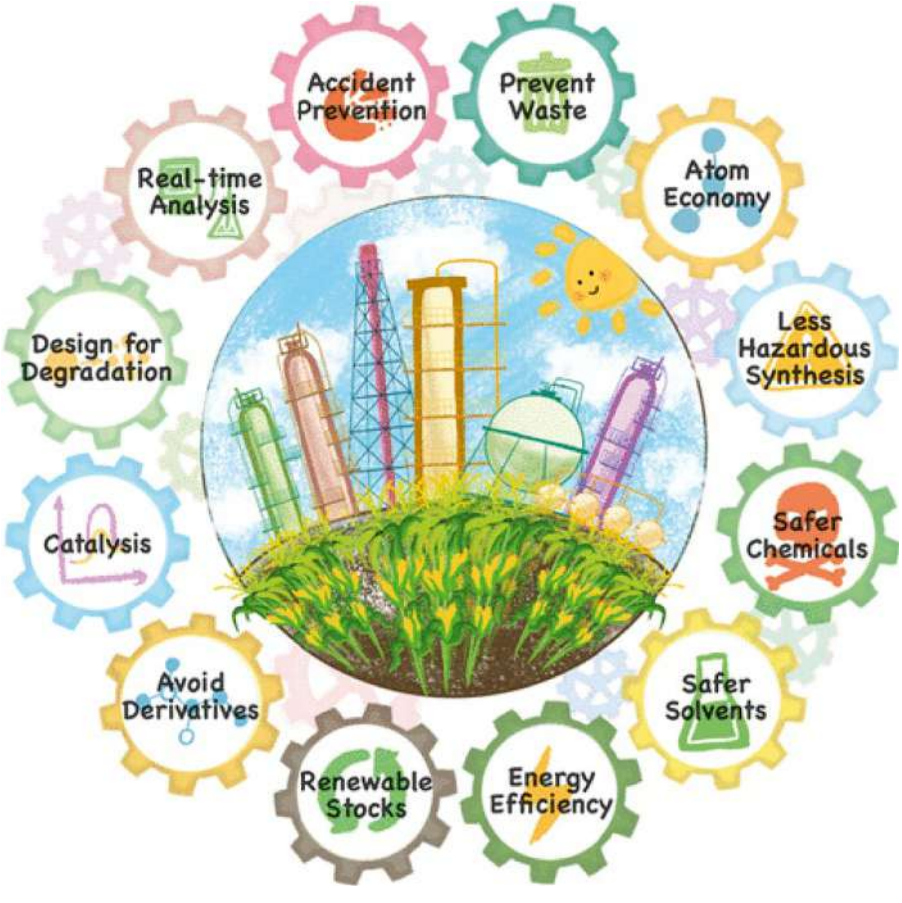

Figure 17.1 The 12 principles of Green Chemistry proposed by Paul Anastas and John Warner. *Source:* Reprinted with permission from [7].

and purification technologies, such as the prevention of waste production, the enhancement of atom economy, the improvement of energy efficiency of proposed processes, and the use of safer chemicals and solvents as well. On the basis of the last two principles, researchers have been working on the efficient extraction and separation processes by replacing conventional organic solvents with the so-quoted "green solvents" to build up sustainable technologies [4]. Most of the organic solvents being used nowadays in chemical processes rely on volatile, toxic, and polluting solvents that must be avoided. In this context, green solvents rise as key tool in the extraction, separation, and purification steps, where ionic liquids (ILs) and deep eutectic solvents (DES) could be major players [4].

ILs are organic salts composed of an asymmetric organic cation coupled with an inorganic or organic anion. By definition, their melting point should be below 100 °C, otherwise being considered as regular salts. The fact that they possess low melting point allows some of them to be liquid at room temperature, and thus can be used as solvents for a plethora of applications. ILs possess a wide range of physicochemical properties, in which the high thermal stability, low vapor pressure and wide polarity, acidity, and basicity stand out as important features to classify them as green solvents. Their application in several separation and purification technologies has been deeply explored in the last two decades, including oil/water mixture separation [8], desulfurization of fuels [9], biomass extraction and fractionation [10], protein separation and purification [11], biotechnological broth stream separation [12], among others. However, their use in industrial processes is still limited. This is not related to their performance, which in most cases is significantly better, but the costs to implement an IL-based technology are, in many cases, preventing industrial stakeholders to bet on these solvents. Nevertheless, the increasing research of their applications together with efforts to achieve an efficient recycling of these solvents can be a real opportunity in the future. Nevertheless, other classes of green solvents are emerging as less-expensive alternatives to ILs. DES are one of the most promising examples and they have been drawing attention of researchers in the last decade, due to their easy (and inexpensive) preparation and by sharing similar physicochemical properties with ILs [13].

17.2 Deep Eutectic Solvents (DES)

DES are by definition systems composed of at least two compounds, a hydrogen bond acceptor (HBA) and a hydrogen bond donor (HBD), which self-associate to form an eutectic mixture characterized by a melting point (the eutectic point) lower than that of the ideal liquid mixture [14]. Figure 17.2 shows a representative phase diagram of two solids as a function of melting temperature demonstrating the eutectic point. The decreasing of the melting temperature is mostly a result of the hydrogen bonding interactions taking place between HBA and HBD components. Nevertheless, van der Waals interactions and electrostatic forces can also occur [15].

In 2004, Abbott et al. [16] were the first to introduce the potential of DES by demonstrating the formation of a liquid phase after mixing a variety of quaternary ammonium salts and carboxylic acids [16]. The depression in melting temperature makes most eutectic solvents liquid at temperatures lower than 70 °C and some of them are liquid at room

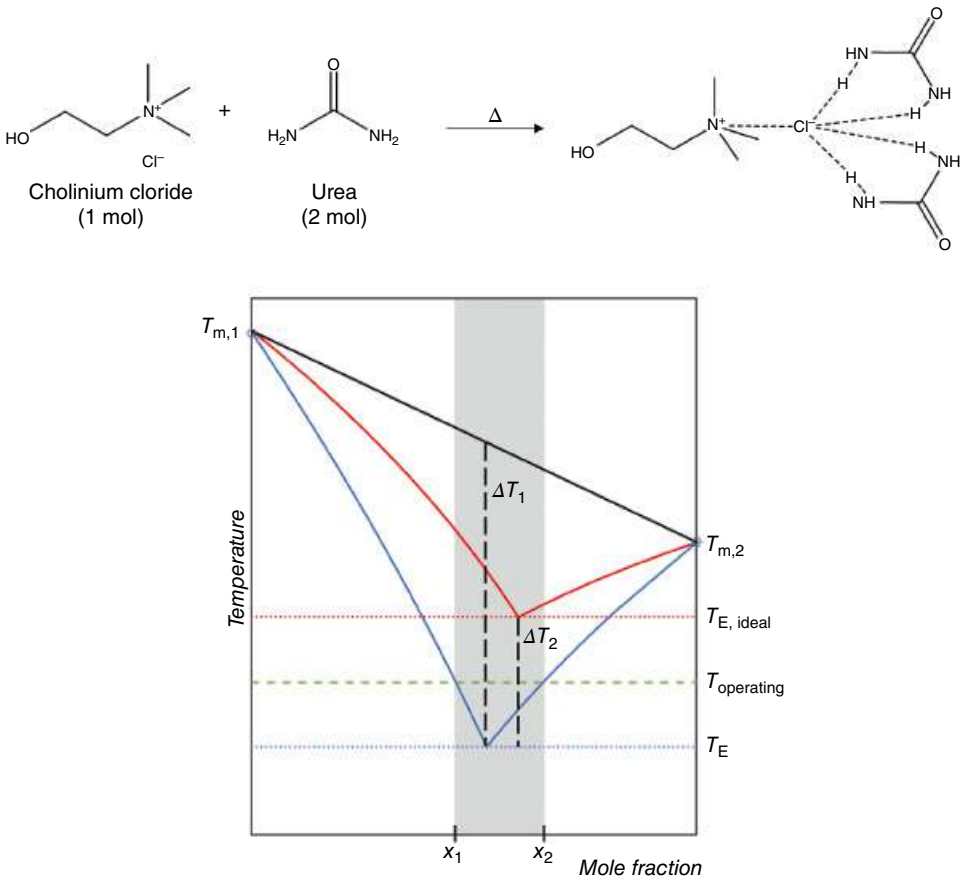

Figure 17.2 Schematic representation of deep eutectic solvent formation. An example with cholinium chloride and urea is illustrated at the top, while a phase diagram is represented at the bottom (Tm: melting temperature). *Source:* Reprinted with permission from [14].

temperature [17]. DES can be prepared by mixing abundant and often inexpensive compounds, which act as HBAs or HBDs, in a simple heating step [15].

The heating and stirring method is the most used methodology for the preparation of DES. The components are placed in a recipient with stirring bar, heated in water bath (50–90 °C) and kept under agitation until a clear liquid is formed. On the other hand, components can be first dissolved in water and afterward the solvent is evaporated through a rotatory evaporator at 50 °C (30–90 minutes). The obtained liquid is then placed in a desiccator under vacuum to remove residual water content. Another option to remove water in one step is freeze-drying (2–24 hours). In addition, water can be replaced by other solvent, as long as components are still soluble and the solvent is easily distillable. Recently, Gomez et al. [18] introduced the preparation of DES by microwave irradiation. The authors argued environmental advantages by using this method, since it enables decreasing the preparation time from 60 minutes (conventional heating method) to 20 seconds, equivalent to 650 time reduction of energy consumption [18]. Therefore, DES are easy to be prepared and it is a relevant advantage over IL synthesis, which needs more steps, including purification.

DES reported to date are classified into four main types (I, II, III, and IV) [19, 20] depending on their constituents as follows [19]:

Type I – quaternary ammonium salt + metal chloride;
Type II – quaternary ammonium salt + metal chloride hydrate;
Type III – quaternary ammonium salt + hydrogen bond donor;
Type IV – metal chloride hydrate + hydrogen bond donor.

More recently, Abranches et al. [21] demonstrated that nonionic DES can be formed. In this case, phenolic compounds establishing phenolic hydrogen bonding with other molecular species (as hydrogen bond acceptors) are also able to promote higher temperature melting depression than that of an ideal mixture. The mixture menthol:thymol was given as a main example of type V DES [21]. Among those classifications, type III DES are the most common, in which cholinium chloride:urea ([Ch]Cl:U) or cholinium chloride:lactic acid [Ch]Cl:LA are some examples. However, a wide number of possible combinations of HBA and HBD can be performed and some of them are portrayed in Figure 17.3.

Additionally, the application of so-called natural deep eutectic solvents (NADES) has been rising in the last few years. In this case, the HBA and the HBD constituting DES are naturally occurring molecules, such as [Ch]Cl, organic acids, amino acids, and sugars, combined in a specific molar ratio that form a liquid at ambient temperature. In fact, some of these combinations do exist in nature and seem to play an important role in living organisms [22]. Therefore, in addition to their potential as solvent alternatives to replace conventional organic solvents in many research areas, they might also bear interesting

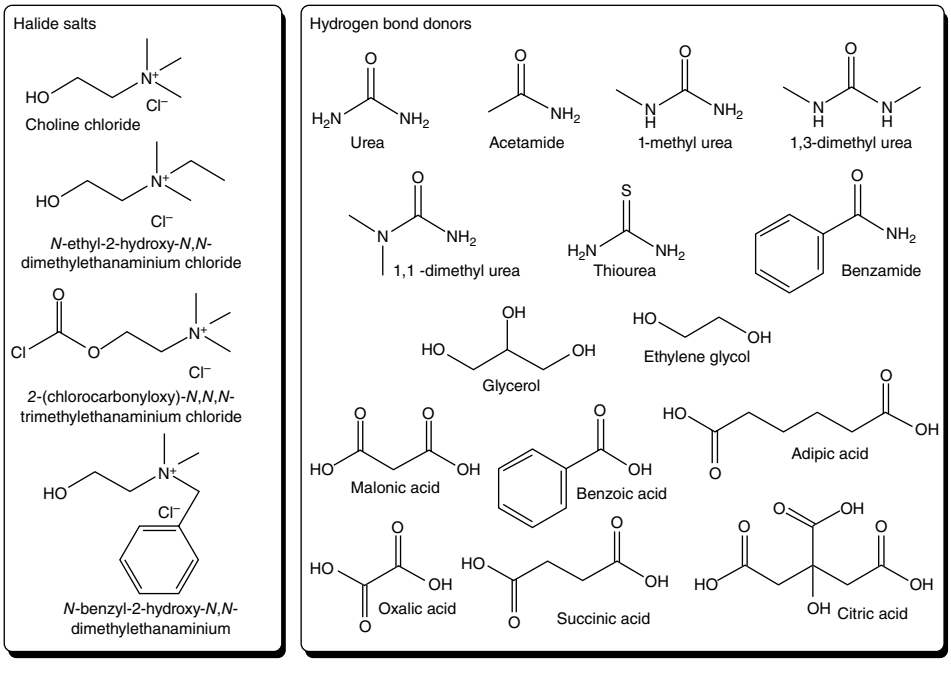

Figure 17.3 Structure of some HBA (e.g. halide salts) and HBD used in the preparation of DES. *Source:* Reprinted with permission from [19].

biological properties [23]. One of the most promising applications is the extraction of bioactive compounds from biomass sources with NADES. The produced extracts with biological activity can be further applied in new product formulations without further purification, due to the nontoxic character of the solvent [24].

In general, DES are nonreactive with water and most often show low or non-toxicity and biodegradability. Some physicochemical properties of DES, including melting point, density, viscosity, surface tension, conductivity [25], biocompatibility, acidity, basicity, and polarity [26], can be tailored by changing the type and molar composition of HBAs and HBDs. This feature turns DES into designer solvents, which is relevant for their application in tailored technologies.

Viscosity is an important property for the selection of DES, since it directly affects the mass transfer and heat transfer in physical and chemical processes using these solvents. The nature of HBA and HBD, including the alkyl chain size or type of functional groups, the HBA:HBD molar ratio, and the water content, are crucial factors influencing DES viscosity. For instance, the presence of a carboxylic or hydroxyl group in HBA and/or HBD structure allows establishing strong hydrogen bonds, resulting in increased viscosity. As an example, glycerol (Gly) contains three hydroxyl groups, which provide strong hydrogen bonding network and consequent low mobility of free species within DES [16, 27]. In this sense, Gly-based DES exhibit higher viscosity (700–900 mPa·s) than its ethylene glycol (EG) counterparts (110 mPa·s) [28].

Moreover, the chemical nature of HBA or HBD has a direct impact on the pH exhibited by DES. For instance, [Ch]Cl:Gly (1:2) and [Ch]Cl:EG (1: 2) showed pH values between 4.08 and 4.40, while DES composed of organic acids disclose pH range from 1.20 to 2.74 [29–31]. The acidity, neutrality, and basicity of DES are important properties to bear in mind in the extraction and separation processes with these solvents in different applications. On the other hand, a wide polarity range is attributed to DES. The polarities of most DES are similar to those of methanol (0.76) and greater than acetonitrile (0.49) and dimethyl sulfoxide (DMSO) (0.46) and strongly depend on the nature of HBD. For example, the polarity values for DES [Ch]Cl:EG (0.82), [Ch]Cl:Gly (0.84) are higher than short-chain alcohols (ethanol [0.66] and methanol [0.76]) [32, 33]. The higher polarities of these DES can be attributed to their high capacity for donating hydrogen bonds [34]. Moreover, DES can be also divided between their hydrophilicity and hydrophobicity, which are also vital properties influencing their choice for certain applications. For instance, the extraction of several substances (e.g. metal ions, polycyclic aromatic hydrocarbons, pesticides, phytocannabinoids, and dyes) from aqueous solutions has been studied with hydrophobic DES [35–37].

Up to date, DES have been used in a myriad of chemical and physical processes, but in the beginning, their applications were limited to the pharmaceutical field [38] and to materials science in electroplating processes [39]. However, the biocompatibility and environmentally friendly features of DES and NADES, in particular, have drawn attention to use them in other applications, as, for example, in biocatalysis [40] and extraction [41] processes. This opened the window to apply them as solvents in the extraction, separation, and purification technologies, as they offer a sustainable solution to accomplish greener processes [25].

17.3 Scope of the Chapter

This chapter specifically addresses the potential of DES to solve three distinct and emerging challenges in the current extraction and separation fields: (i) separation of aromatic compounds from aliphatic hydrocarbons; (ii) extraction of bioactive compounds from biomass; and (iii) extraction and separation of metals from metallurgic and electronic wastes, which today are of utmost relevance from industrial and economic perspective. Distillation, acid–base neutralization, liquid–liquid and solid–liquid separation technologies with volatile and toxic solvents have been used in these separations providing some disadvantages, such as energy-intensive processes, azeotrope formation (distillation), large amount of alkali and acid waste streams, large amount of wastewater with toxic and pollutant species, volatilization of organic solvents, and serious equipment corrosion. The high cost and lack of sustainability of these processes must be overcome. In this view, the application of DES as extraction and separation solvents may improve those separations to achieve high technical efficiency, high selectivity, low energy consumption, and low impact on the environment and public health. The DES' ability to perform such separations will be scrutinized in this chapter and main factors governing their performance will be discussed as well. A series of innovative methodological approaches will also be described as possible technologies to be implemented in industry.

17.4 Extraction and Separation of Aromatic Compounds from Aliphatic Hydrocarbons

The separation of phenolic, non-phenolic, nitrogen-, and sulfur-based aromatic compounds from oil mixtures is imperative to avoid technical hurdles in downstream processing and to achieve more sustainable and less pollutant oils and fuels, as well as to recover those compounds for further valorization to achieve improved circularity of resources. However, these separations have revealed challenges due to the physicochemical affinity of aromatic contaminants from the predominantly hydrocarbon-like composition of fossil oils.

17.4.1 Toluene and Benzene

The separation of aromatic compounds, such as toluene and benzene, from aliphatic hydrocarbons is generally made by distillation processes. However, this strategy is energy-intensive, while the compounds to distil present similar volatilities and leads to azeotrope formation between the aromatic compounds and other hydrocarbons [42]. An alternative separation that has been explored over the past years is the liquid–liquid separation due to easy handling and low-cost operation. The typical solvents that have shown good performance on this specific separation are sulfolane (Sulf), Dimethyl sulfoxide (DMSO), *N*-methylpyrrolidone (NMP), and *N*-formylmorpholine (NFM), although they are not considered as green solvents due to their volatility, toxicity, flammability as well as they are difficult to recover [43]. In this context, the use of green solvents, including DES, as benign

alternative in the liquid–liquid separation of aromatic compounds, such as toluene and benzene, from aliphatic hydrocarbons has been addressed.

Recently, a study demonstrated the [Ch]Cl:phenol ability to extract toluene from both *n*-hexane and *n*-heptane as model systems at 30 °C and 85 kPa by liquid–liquid extraction [44]. The authors studied two molar ratios of [Ch]Cl:phenol (1:3 and 1:4) and observed that molar ratio 1:4 enabled higher toluene distribution coefficients (0.186–0.355) than 1:3 (0.121–0.160). This means that toluene extraction from the aliphatic hydrocarbons was favored by higher phenol molarity in DES composition. On the other hand, a molar ratio of 1:3 allowed higher selectivity at low concentrations of toluene [44]. The application of [Ch]Cl:phenol as extraction solvent of toluene from aliphatic hydrocarbons was recommended by authors, especially at low toluene concentrations, since they presented better results than other solvents like Sulf, ethyl triphenylphosphonium iodide ([ETPP]I):Sulf (1:4), 1,3-dimethyl-2-imidazolidinone (DMI), and ILs as well [44]. The approach of liquid–liquid separation using [Ch]Cl:phenol can be a good solution in the separation of aromatic and aliphatic hydrocarbons at an aromatic content lower than 20% of the total mixture, which is one of the bottlenecks in this separation [45].

In another work, liquid–liquid extractions of benzene from cyclohexane as well as toluene from *n*-heptane were evaluated using two DES formed by *N*-ethylpyridinium bromide ([NEP]Br) as HBA, and NFM or levulinic acid (LevA) as HBD at a molar ratio of 1:3 [46]. The choice of these DES was based on specific characteristics, such as the aromatic structure of the HBA to enable π–π interactions with toluene and benzene, the high solubility of aromatic compounds in NFM, and the favorable interaction between the C=O bond of LevA with aromatic rings. In terms of selectivity and distribution coefficient, both DES showed reasonable separation results, although [NEP]Br:NFM showed the best performance. For instance, this DES enabled a selectivity and distribution coefficient of 23.8 and 1.733, respectively, in the separation of benzene from cyclohexane. The separation was more effective at low temperature (20 °C) and as much as DES amount was added into the system [46].

In 2016, Gouveia et al. conducted a study upon the separation of toluene from *n*-heptane via liquid−liquid extraction at 25 °C using DES formed by LevA (HBD) and ammonium salts, such as [Ch]Cl, benzylcholinium chloride ([BzCh]Cl) and tetrabutylammonium chloride ([TBA]Cl), as HBAs in the molar ratio of 1:2 (HBD:HBA) [47]. The ternary phase diagrams showed that [Ch]Cl:LevA and [BzCh]Cl:LevA are practically immiscible in *n*-heptane and both demonstrated miscibility with toluene. This miscibility is slightly higher for [BzCh]Cl:LevA, as a consequence of favored interactions between toluene and the aromatic ring of [BzCh]Cl as shown in Figure 17.4. On the other hand, the use of [TBA]Cl as HBA resulted in increased miscibility of DES ([TBA]Cl:LevA) in both toluene and *n*-heptane, probably due to the higher hydrophobicity character of [TBA]Cl [47].

The distribution coefficients of toluene in *n*-heptane liquid–liquid equilibrium ranged from 0.095 to 0.127 with [Ch]Cl:LevA, from 0.158 to 0.337 with [BzCh]Cl:LevA, and from 0.480 to 0.742 with [TBA]Cl:LevA, while the selectivity values were found from 9.47 to 23.90, from 12.31 to 39.11, and from 0.60 to 13.41, for each ternary system, respectively. Therefore, [BzCh]Cl:LevA presented better selectivity than [Ch]Cl:LevA and [TBA]Cl:LevA, and also higher distribution coefficients when compared with [Ch]Cl:LevA. Nonetheless, the results show that the distribution coefficient is influenced by the hydrophobicity of [TBA]Cl, since it increased for ternary systems formed by *n*-heptane + toluene + [TBA]Cl:LevA.

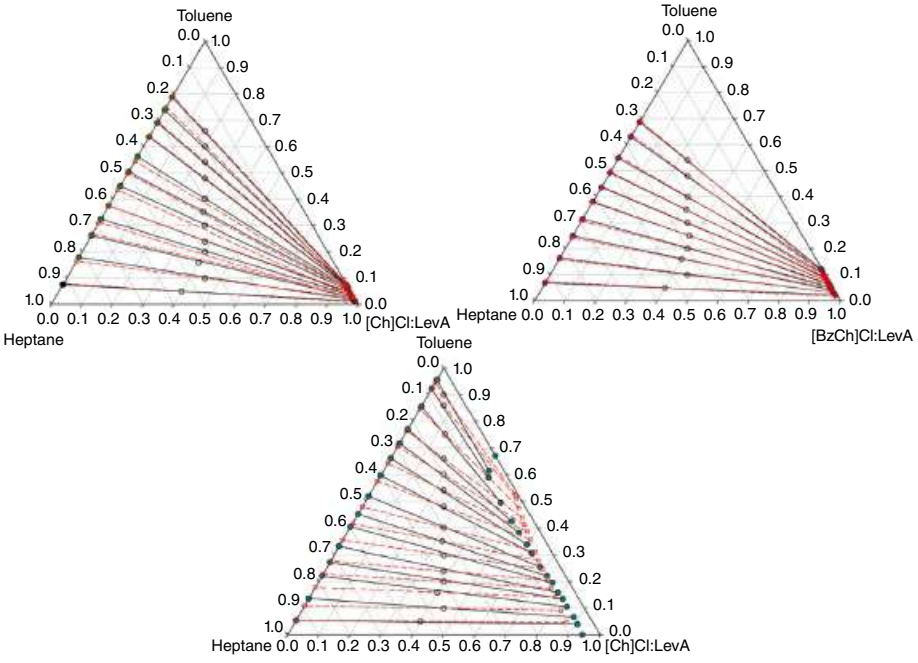

Figure 17.4 Tie-lines for ternary mixtures of: (a) *n*-heptane + toluene + [Ch]Cl:LevA, (b) heptane + toluene + [BzCh]Cl:LevA, and (c) *n*-heptane + toluene + [TBA]Cl:LevA at 25 °C and 0.1 MPa. Symbols: (circles, –), experimental data; (squares, - - -), COSMO-RS. *Source:* Reprinted with permission from [47].

Therefore, [TBA]Cl (the most hydrophobic HBA) improved the distribution coefficient of toluene separation, while the aromaticity of [BzCh]Cl enhanced both distribution coefficient and selectivity. The authors stated that distribution coefficients can be related to the operation costs, while selectivity can be associated with the number of required extraction stages [47]. In this sense, a balance between those parameters is desired for a successful extraction process, which [BzCh]Cl:LevA seems to provide rather than other examined DES. This DES disclosed the highest selectivity (40.0) and a very low solubility in the *n*-heptane-rich phase, which minimize the loss of DES and, consequently, the contamination of the refined aliphatic stream.

Hundreds of HBA and HBD combinations can be used in separation processes, but what kind of DES exhibit ability to extract a specific aromatic compound from aliphatic hydrocarbons? A more detailed study regarding toluene extraction from *n*-heptane with several DES was performed by Wang et al. [48]. By taking into account the freezing point, the hydrophilicity, viscosity, and corrosion properties, 24 potential DES were selected to separate toluene from *n*-heptane. Their performance was evaluated in terms of selectivity and distribution ratios. A summary of the obtained data is depicted in Figure 17.5, where the influence of different variables concerning the HBA and HBD structures were exploited on this separation [48].

First, the influence of the HBA on the separation performance was studied [48]. The selectivity for toluene extraction was greatly influenced by the alkyl chain length of HBA (in combination with lactic acid as HBD) and according to Figure 17.5Ia, it decreases in the

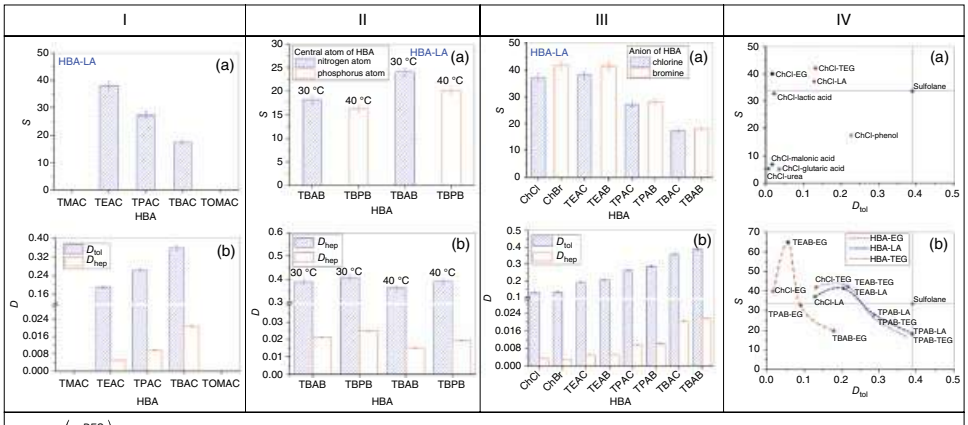

$$D_i = \left(\frac{x_i^{DES}}{x_i^{Oil}} \right) \text{ where i is toluene or } n\text{-heptane; } S = \frac{D_{toluene}}{D_{n-heptane}}$$

Figure 17.5 Influence on (a) selectivity S and (b) distribution ratio (D) for the ternary system of toluene + *n*-heptane + DES: (I) effect of the alkyl chain length of HBA; (II) effect of the central atom of HBA; (III) effect of the anion of HBA; (IV) effect of selected HBDs and different HBAs on S and D ratios of toluene; separation conditions for all: toluene content, 30 wt%; nLA: nHBA = 4:1; nHBA: ntol = 1:1; T = 30 °C. *Source:* Adapted with permission from [48].

following order: [TEA]Cl > tetrapropylammonium chloride ([TPA]Cl) > [TBA]Cl > tetramethylammonium ([TMA]Cl) = trioctylmethylammonium ([TOMA]Cl). In Figure 17.5Ib, it is possible to note that alkyl chain of the HBA cation has more affinity for *n*-heptane than toluene, meaning that aliphatic/aliphatic interactions are favored over aromatic/aliphatic ones [48]. Furthermore, when using a HBA cation with a large central atom, such as phosphonium cations, the selectivity increases in comparison with the ammonium ones as seen in Figure 17.5IIa, while the distribution ratio of toluene shows the opposite order (Figure 17.5IIb). HBA's phosphonium cations strongly interact with *n*-heptane molecules and simultaneously hamper the interaction with toluene molecules, due to steric hindrance, resulting in high selectivity. Concerning the HBA anion, the selectivity was higher for bromide-based quaternary ammonium salts than for the chloride counterparts, which indicates that large anions like Br^- are more likely to interact with toluene than *n*-heptane molecules (Figure 17.5IIIa and b) [48].

The influence of HBD on the selectivity of toluene extraction from *n*-heptane is shown in Figure 17.5IVa. In combination with [Ch]Cl, the best results were achieved with the following HBDs: EG, lactic acid (LA), and triethylene glycol (TriEgly). Afterward, these HBDs were combined with selected HBAs (Figure 17.5IVb) and the obtained selectivity increased with longer HBA's side chain up to a maximum point and then decreased sharply. Concluding, as the side chains of [Ch] is very short, the interaction with toluene and *n*-heptane is weak and consequently the distribution rate is small. The increase of the side chain length of HBA, to [TEA], for example, makes easier the interaction with *n*-heptane [48].

Larriba et al. demonstrated a step forward by applying DES in the extraction of benzene and toluene from reformer and pyrolysis gasoline models [49]. Six cholinium chloride ([Ch]Cl)-based DES pairing with EG, glycerol (Gly), levulinic acid (LevA), phenylacetic acid (PheAc), malonic acid (MaloA), and urea (U) as HBDs were applied in this study. Among the examined DES, the best performance was achieved with [Ch]Cl:LevA at a molar ratio of 1:3 mainly due to its extractive ability. Moreover, its suitable viscosity, density, and thermal stability favored the pumping of the solvent into the extractor, enabled fast phase separation, and efficient solvent recovery. This DES was able to extract benzene almost completely and removed significant amounts of toluene from reformer and pyrolysis gasolines. After generating liquid–liquid equilibrium data and performing simulation and optimization, the authors proposed a novel process for the separation of aromatic compounds from aliphatic hydrocarbons with DES and their subsequent recovery as shown in Figure 17.6. Computational simulations showed that optimal conditions of flash distillation should be at 90 °C and 5 kPa to separate extracted aromatic compounds from residual aliphatic hydrocarbon content and to regenerate the solvent. At these optimal conditions, the recovery yields of aliphatic and aromatics between the vapor stream and feed stream for reformer gasoline were 98 and 78.9%, respectively, while 98.8 and 88.4% were achieved for pyrolysis gasoline, correspondingly. The solvent recovery was estimated to 99.2% in the end of the process [49]. In this scenario, the high separation efficiency exhibited by DES allows this technology to attend the regulations over the benzene content in commercial gasoline [50].

In conclusion, the liquid–liquid separation of aromatic compounds, like toluene and benzene, from aliphatic hydrocarbons with DES seems promising, especially at low

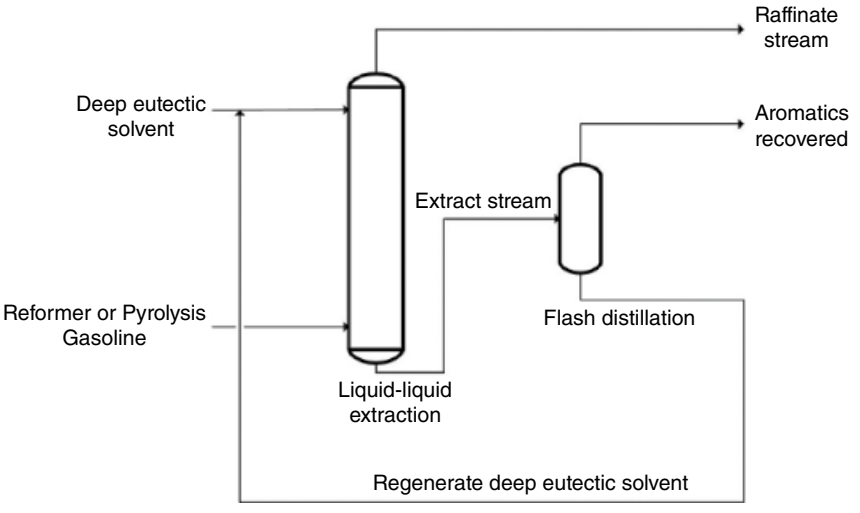

Figure 17.6 Flow diagram of the proposed dearomatization process of reformer or pyrolysis gasoline using DES. *Source:* Reprinted with permission from [49].

aromatic content. The results have shown that tuning the structure and properties of DES allows enhancing the selectivity of aromatic compound extraction to DES phase. Furthermore, DES seem to maintain their intermolecular structure arrangement, i.e. no dissociation of DES components is exhibited in these specific separations [47]. This is an advantage over aqueous systems, where DES components generally tend to dissociate in water [51, 52], losing for instance their extraction and separation performances at certain water contents.

17.4.2 Phenol and Derivatives

The presence of phenol and its derivatives in various hydrocarbonaceous streams, like coal liquefaction oil, coal tar, and petroleum, but also renewable biomass pyrolysis oil, is a major bottleneck in the processing of these oil raw materials to produce fuels and chemical commodities in the modern society. The high reactivity of phenols during oil processing causes degradation and formation of undesired resinous and solid products, leading to severe technical and operational problems in downstream processing [53, 54]. Therefore, the removal of phenol and its derivatives from oily streams is of utmost importance in the efficiency of oil processing.

The current separation of phenol and its derivatives from oil is mostly addressed by acid–base reactions using strong alkaline (e.g. NaOH) and acidic (e.g. H_2SO_4 and H_2CO_3) solutions. In alkaline solutions, phenol react with the oxides or hydroxides resulting in the formation of aqueous soluble phenoxide salts, thus allowing their removal from the oil mixture, and latter could be recovered by neutralization under acidic conditions. However, the use of these chemicals can bring serious environmental and technical damage [55]. The production of excessive volumes of wastewater containing phenol and derivatives, which are harmful to the environment and live organisms as well as the severe corrosion of the

technical equipment are two main disadvantages [56]. An alternative to conventional phenol extraction processes that use the acid–base neutralization is the liquid–liquid extraction with organic solvents [57, 58]. Liquid–liquid extraction processes disclose advantages over the traditional alkali and acid methods mentioned above, such as low cost and ease of operation. However, the use of volatile organic compounds as separation agents, such as benzene and chloroform, which are highly volatile, flammable, and toxic solvents, is also a disadvantage to bear in mind. Therefore, their replacement by other less polluting and safer solvents is demanding [59]. In this perspective, DES have been suggested as green and sustainable substitutes to perform this complex separation.

In this sense, Jiao et al. [60] used DES to separate phenol from coal tar. Extraction efficiencies greater than 90% were obtained with [Ch]Cl:trifluoroacetic acid (TFA). In addition, this DES was recycled by back-extraction with excellent recycling properties, maintaining the phenol extraction efficiency above 90% after 4 cycles without significant mass loss [60]. In this work, the authors revealed that HBD and HBA had significant influences on the extraction process, related to the electron attraction capacity of HBA and the acidity of HBD. An HBA with high electron capacity ([Ch]Cl) combined with a strong acid HBD (TFA) presented the highest phenol extraction. However, other factors may govern DES ability to extract phenol. In another study, Yi et al. [61] evaluated the interaction between phenol derivative compounds and DES through quantum chemical calculations and spectral experiments to explore the possibility of extracting phenol from coal-based liquid oil using a [Ch]Cl:Gly. The computational results showed that hydrogen bonds between DES and phenol derivative compounds are the main driving force of this separation process. In addition, extraction experiments were performed and demonstrated that [Ch]Cl:Gly (1:1) is able to extract 98.3% of the phenol derivative compounds with only 4.2% of neutral oil entrained [61].

These last studies described the application of DES in the extraction of phenol from model oil and real oil samples within a normal liquid–liquid separation approach. The DES is prior prepared, by mixing HBA and HBD in suitable molar ratios, and it is subsequently applied in the separation step. However, in another perspective, phenol separation from oil mixtures through the *in situ* formation of DES has been demonstrated as a more disruptive strategy [62, 63]. The concept relies on adding an organic salt to the phenol/oil solution that leads the formation of a eutectic mixture between the organic salt (HBA) and phenol (HBD). The *in situ* formed phenol-based DES is immiscible with the oil-rich phase creating a biphasic mixture enabling the nonaqueous separation of phenol from oil [62, 63]. For example, Pang et al. [62] added a known amount of [Ch]Cl into a model oil solution containing toluene, *p*-xylene, hexane, and phenol. The resulting solution was heated, stirred, and after reaching equilibrium, two liquid phases were formed as a consequence of the polar eutectic mixture induced by the strong interaction between [Ch]Cl (HBA) and phenol (HBD). No [Ch]Cl was found in the upper oil phase (hexane) in equilibrium with *in situ* formed DES, while a phenol removal efficiency of 92% was achieved [62]. After the separation of the *in situ* formed DES from the oil phase, diethyl ether was added to extract phenol from [Ch]Cl and the latter can be reused without mass and efficiency loss. This methodology is highlighted in Figure 17.7 and shows sustainable advantages over the conventional separation methods. Nevertheless, a more benign alternative to diethyl ether to precipitate [Ch]Cl would be recommended.

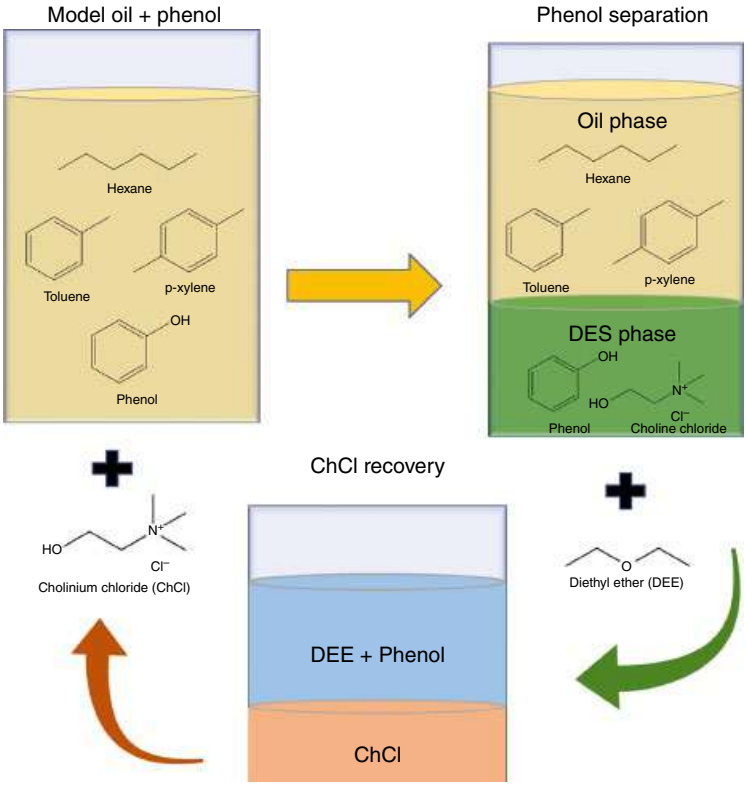

Figure 17.7 Separation of phenol from model oil by *in situ* DES formation ([Ch]Cl + phenol). *Source:* Adapted from [65].

Besides [Ch]Cl, a variety of quaternary ammonium salts, such as ammonium chloride ([NH_4]Cl), [Ch]Br, [TMA]Cl, [TMA]Br, ([TEA]Cl), [TEA]Br, methyltriethylammonium chloride ([MTEA]Cl), [TPA]Cl, and [TBA]Cl were studied to separate phenol from model oils (hexane, toluene, and *p*-xylene) and the effects of cations and anions on phenol removal were inspected [62, 63]. For instance, Guo et al. [63] reported a phenol removal efficiency of 96% using [TMA]Cl, while [MTEA]Cl exhibited 99.9% efficiency. This means that increasing the alkyl chain length of the HBA cation favors the ability to form *in situ* DES and subsequently enhances the extraction of phenol from oil. The authors also highlighted that chloride-based quaternary ammonium salts are more efficient to remove phenol when compared with bromide counterparts. For example, the phenol removal efficiency was 95.4% using [Ch]Cl, whereas 90.4% was obtained for [Ch]Br. The higher electronegativity and stronger interaction of the chloride ion with the phenol OH group than bromide may explain the observed results [63]. It was later revealed that imidazole and amide compounds can also strongly interact with phenol and cresols to form *in situ* DES immiscible with oil. These DES enabled phenol separation with an extraction efficiency of more than 90% [60, 64].

The separation of phenol from non-phenolic aromatic compounds is also an issue that requires research and technology development. In this context, the use of DES for the

separation of phenol from toluene was studied by Byrne et al. [66]. The efficacy of [Ch]Cl and trialkyl-2,3-dihydroxypropylammonium chloride salts as HBA for the *in situ* formation of DES when mixed with phenol was evaluated. The improvement in the separation performance was achieved by the incorporation of butyl groups in the dihydroxypropylammonium cation ($[Bu_3NCH_2CH(OH)CH_2OH]Cl$), which allowed a simultaneous good association with phenol and increased immiscibility with toluene. Furthermore, as shown in Figure 17.8, the extraction efficiency of phenol at low concentrations (0.1 M) in toluene with $[Bu_3NCH_2CH(OH)CH_2OH]Cl$ was substantially higher than that found with [Ch]Cl and two other salt counterparts containing methyl and ethyl as alkyl chains ($[Me_3NCH_2CH(OH)CH_2OH]Cl$ and $[Et_3NCH_2CH(OH)CH_2OH]Cl$) [66]. Therefore, the size of the alkyl chain in ammonium cations seems crucial to improve the separation of phenols from non-phenolic aromatic compounds like toluene. These results show that separation can be tuned by the inclusion of lipophobic/hydrophilic groups, overcoming the co-miscibility of longer chain functionalized ammonium salts with aromatic-rich feeds. This allows for successful extraction of phenol by *in situ* DES formation, while simultaneously hindering miscibility of quaternary ammonium salts with non-phenolic aromatics.

Recently, Yao et al. [67] discovered that two types of zwitterionic alkaloids, betaine (Bet) and L-carnitine (Carn), can also form DES with phenol allowing its separation from toluene. The authors studied the phase equilibrium of the two ternary systems: toluene + phenol + Bet and toluene + phenol + Carn (at 25, 45, and 65 °C under atmospheric pressure). The experiments showed three types of phase regions: liquid, liquid–liquid, and liquid–liquid–solid, in which the separation of phenol from oil mixtures is promoted in the last two phase regions. Among the studied zwitterionic alkaloids, Carn performed better separation of phenol from oils than Bet. For example, at the same temperature (65 °C) and same molar ratio (0.4) of zwitterionic alkaloids to phenol, the selectivity of Carn was six-fold higher than that of Bet (184.7 and 29.8, respectively). On the other hand, the authors have

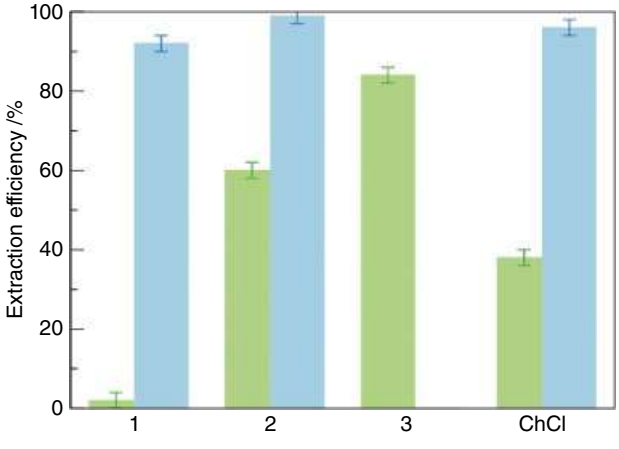

Figure 17.8 Phenol extraction efficiencies by *in situ* DES formation with [Ch]Cl (or $[Me_3NCH_2CH_2OH]Cl$), (1) $[Me_3NCH_2CH(OH)CH_2OH]Cl$, (2) $[Et_3NCH_2CH(OH)CH_2OH]Cl$, and (3) $[Bu_3NCH_2CH(OH)CH_2OH]Cl$, using 0.1 M (green) and 2 M (blue) phenol concentration in toluene feed solutions (salt:phenol ratio 1:1, 30 °C, 30 minutes contact). *Source:* Reprinted with permission from [66].

shown that temperature increase did not favor the separation, decreasing the distribution coefficient and selectivity, while small amounts of toluene were dragged into the DES phase as well [67].

17.4.3 Sulfur- and Nitrogen-based Aromatic Compounds

Sulfur and nitrogen-based aromatic compounds are contaminants in oil feedstocks and fuels that must be removed to avoid undesired emissions of polluting sulfur and nitrogen oxides produced during fuel combustion. For instance, sulfur dioxide is the main combustion product of sulfur-based compounds and it has been recognized as a precursor of acid rain and air pollution. Since sulfur and nitrogen oxides emissions are a serious problem to the environment, many countries are implementing tight regulations concerning their emission to the atmosphere [68].

Although hydrodesulfurization is a widely used technique to remove sulfur from refined petroleum, it is not efficient to remove sulfur-based aromatic contaminants, such as thiophene, benzothiophene, and dibenzothiophene, from oil mixtures. High pressure and temperature are often needed to increase the separation efficiency, but it drives in high operation cost and low effectiveness to attend the regulations [69]. Therefore, solvents that bring better interaction with those compounds, and thus higher removal efficiency, are highly pursued to facilitate this separation. DES could be used as solvent to comply with the most restrictive regulations concerning sulfur- and nitrogen-based aromatic compounds content in oil feedstocks and fuels, benefiting from their unique physicochemical properties toward an efficient separation.

Li et al. reported the efficiency of DES on the extractive desulfurization of a model fuel (*n*-octane), accessing the removal of benzothiophene [69]. [Ch]Cl, [TMA]Cl, and [TBA]Cl were chosen as HBA, while propionic acid (PA), MaloA, Gly, tetraethylene glycerol (TEG), EG, and polyethylene glycol (PEG) were selected as HBD. Among examined solvents, [TBA]Cl-based DES showed the highest removal efficiency, whereas [TBA]Cl:PEG at a molar ratio of 1:2 enabled the best result by removing 82.8% on one cycle and 99.5% after five extraction cycles. This means a sulfur content reduction to less than 8.5 ppm after a five-cycle process [69], which complies with the requirements specified by DIRECTIVE 2009/30/EC to achieve less than 10 ppm concentration of such compound [50].

In another work, 16 different DES were used as extraction media for the removal of thiophene and dibenzothiophene from *n*-heptane as model fuel [70]. Gly, EG, TriEgly, and PEG with different molecular weights (200, 300, 400, and 600 molar mass) were examined as HBD, while ammonium-based salts ([Ch]Cl, [TBP]Br, [TBA]Cl, [TBA]Br, [TEA]Br), [TPA]Br, and [THA]Br) were tested as HBA. The extraction procedure comprehended the mixture of DES and *n*-heptane containing small amounts of thiophene and dibenzothiophene, followed by stirring for 15 minutes at 25 °C and kept in equilibrium for 12 hours. A biphasic mixture was formed and the fuel-rich phase at the top was collected and analyzed by UV-VIS. The results showed that all DES successfully extracted the target compounds from *n*-heptane, yet [TBA]Cl:PEG400 revealed the best extraction efficiency (85.0%) [70]. The obtained data demonstrated that the HBD has greater influence than HBA on the desulfurization of *n*-heptane, following the order: EG < TEG < PEG200 < PEG300 < PEG400≈PEG600. Concerning the effect of HBA on desulfurization process, the authors

concluded that the longer the alkyl chains of the quaternary ammonium salts, the greater the extraction efficiency is, especially for dibenzothiophene extraction. Moreover, [TBA]Cl:PEG400 can be totally recovered after a regeneration step and further reused without substantially losing its extraction capacity [70].

The benefits of computational tools to better predict/understand the interactions responsible for the extraction of sulfur-based aromatic compounds with DES were demonstrated by Wagle et al. [71]. The researchers investigated through quantum chemical calculations the advantages to oxidize benzothiophene and dibenzothiophene present in fuels prior to their extraction with [Ch]Cl:U and [Ch]Cl:EG, both at a molar ratio of 1:2. The obtained data showed that sulfur-based compounds may interact with HBD and cholinium cation from HBA through multiple weak noncovalent interactions, while no interaction with HBA's chloride anion was predicted. The chloride anion remains linked to the cholinium cation and HBD species through strong hydrogen bonds. However, the authors revealed that the respective sulfoxide and sulfone oxidation derivatives establish stronger interactions with DES, as the additional oxygen atoms act as an additional electron donor for hydrogen bonding with both HBA's cholinium cation and HBD, which may enhance the partition of these oxidized sulfur-based compounds from liquid fuel to the DES phase [71]. However, these results were not validated by experimental data.

The oxidation of sulfur-based compounds to favor their extraction was experimentally tested by Jiang et al. [72]. The researchers reported the application of a ternary DES formed of [Ch]Cl, PEG, and boric acid (BA) in the extraction and oxidative desulfurization of diesel fuel. After optimizing the molar ratio of the ternary [Ch]Cl:PEG:BA (1:1:1.5), desulfurization of diesel fuel up to 99.2% was achieved. In this case, a synergy between PEG and BA was proposed for enhanced fuel desulfurization. BA was referred to participate in the catalytic oxidation of sulfur-based aromatic compounds, while PEG enables the extraction of oxidized compounds from diesel fuel [72].

Denitrogenation of oil mixtures with DES was evaluated too. Warrag et al. studied the influence of the hydrocarbon chain size of model oils on the pyridine removal with DES [73]. For such study, methyltriphenylphosphonium bromide ([MTPP]Br):EG binary DES at a molar ratio of 1:4 and [MTPP]Br:Gly:EG ternary DES at a molar ratio of 1:2:2 were tentatively applied for the extraction of pyridine from three different fuel models, namely *n*-hexane, *n*-heptane, and *n*-octane. Liquid–liquid equilibrium data were determined for the ternary systems formed by n-alkane + pyridine + DES at 25 °C and 1.01 bar. The pyridine distribution coefficient was lower for Gly-based DES, while the extraction selectivity was higher. Nevertheless, selectivity decreased sharply for higher pyridine concentration in the model oil. Regarding the chain length of the model fuel, no effect on the distribution coefficient of pyridine was observed, while the selectivity for pyridine extraction in DES-rich phase was higher when using longer chain hydrocarbons (*n*-octane). Between the two examined systems, the ternary DES (MTPPBr:Gly:EG) showed moderate viscosity ($\eta = 455$ mPa.s), lower than the binary MTPPBr:Gly ($\eta = 1894$ mPa.s), higher distribution coefficients (>3), and higher selectivity (>1150), characteristics that make it a good candidate for denitrogenation [73].

A different strategy was studied by Hizaddin et al. [74], who have shown a computational evaluation of the capacity of 94 DES for nitrogen-based aromatic compounds' removal from model diesel fuel by COSMO-RS thermodynamical model [74]. The first step of such

study was checking the accuracy of COSMO-RS results for nitrogen systems by comparing the ternary LLE data predicted by the COSMO-RS method to those reported in the literature for the systems pyridine + n-heptane + 1-ethyl-3-methylimidazolium thiocyanate and pyridine + n-heptane + 1-butyl-3-methylimidazolium trifluoromethanesulfonate. The root mean square deviation (RMSD) result between calculated and experimental tie lines of the mentioned systems was equal to 2.08 and 4.98%. Similarly, the calculation method was validated to DES systems comparing COSMO-RS results and LLE experimental data of toluene + n-heptane + [TBP]Br:EG (1:2) ternary system at 40 °C. The RMSD was equal to 4.91% and, according to the authors, proved that COSMO-RS prediction is good for systems containing nitrogen compounds and DES. With the validation of COSMO-RS calculation, the authors started the second step that was the activity coefficient calculation at infinite dilution followed by the prediction of the selectivity, capacity, and performance index of the following compounds: pyrrole, indole, indoline, carbazole, and benzocarbazole (nonbasic compounds) and pyridine, quinoline, and benzoquinoline (basic compounds) [74]. The equation and definitions are presented in Table 17.1.

The authors observed that the heterocyclic structure of nitrogen-based compounds influenced the selectivity and capacity values, whereas basic compounds exhibited higher values for both parameters than nonbasic compounds. Moreover, the selectivity and capacity values decreased with the number of aromatic rings in the compound structure [74]. This study demonstrated that computational tools could be relevant to better understand the interactions between components that are not always easy to comprehend only with experimental data.

The application of DES in the integrated desulfurization and denitrogenation process was also examined and an illustrative concept is presented in Figure 17.9 [75]. Different DES were prepared, including [TBA]Cl, [TBA]Br, or [TBP]Br as pairing HBAs and PEG400 or Sulf as HBDs, to remove simultaneously sulfur-based aromatic compounds, represented by thiophene and dibenzothiophene, and nitrogen-based aromatic compounds, such as pyridine and carbazole, from *n*-heptane and simulated fuels [75].

Table 17.1 Equation of selectivity, capacity, and performance index at infinite dilution and definition of them [74].

Equation	Definition
$S_{12,\max} = S_{12}^{\infty} = \left(\frac{\gamma_2^{\infty}}{\gamma_1^{\infty}}\right)_{\text{DES phase}}$	The maximum selectivity, $S_{12,\max}$, can be defined as the ratio between the activity coefficients at infinite dilution for diesel (2) to that of nitrogen-based compound (1) in DES.
$C_1^{\infty} = \left(\frac{1}{\gamma_1^{\infty}}\right)_{\text{DES phase}}$	Capacity is an estimation of DES amount needed for removing the nitrogen-based compounds. Operationally, it defines the maximum amount of nitrogen-based compounds that can be dissolved in the DES.
$PI = S_{12}^{\infty} \times C_1^{\infty} = \left(\frac{\gamma_2^{\infty}}{\left(\gamma_1^{\infty}\right)^2}\right)_{\text{DES phase}}$	It is the product of maximum selectivity and maximum capacity.

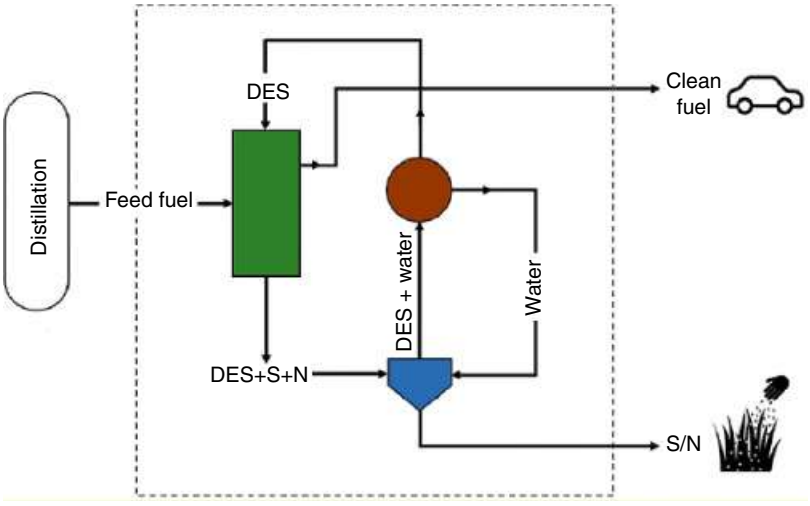

Figure 17.9 Integrated desulfurization and denitrogenation process using DES. *Source:* Reprinted with permission from [75].

In a first step, the authors made a screening with four DES ([TBA]Cl:PEG400, [TBA]Cl:Sulf, [TBA]Br:Sulf, and [TBP]Cl:Sulf) to remove single nitrogen- or sulfur-based aromatic compounds from *n*-heptane [75]. Sulfur-based aromatic compounds were the hardest to be removed, with thiophene exhibiting the lowest removal efficiency (≈65%) in [TBA]Cl:Sulf, while approximately 90% was obtained for pyridine extraction using the same DES. Due to the low polarity of the sulfur-based compounds, their interaction with tested DES is not strong, which explains their low extraction yields in DES-rich phase. Nevertheless, [TBP]Br:Sulf (1:4) presented simultaneously good capacities for the removal of both sulfur- and nitrogen-based aromatic compounds. Moreover, this DES exhibited the lowest viscosity and the highest density among all studied DES, showing the most attractive properties to carry out a liquid–liquid extraction.

These beneficial features allowed [TBP]Br:Sulf (1:4) to be selected as extracting solvent for the removal of a mixture of thiophene, dibenzothiophene, pyridine, and carbazole as the following step [75]. These nitrogen- and sulfur-based compounds were dissolved in *n*-heptane to observe competition during the removal, and afterward, different hydrocarbons were added to *n*-heptane to simulate gasoline and diesel. Figure 17.10 shows the extraction efficiencies of each model compound from different fuel matrices in comparison to single extractions from *n*-heptane. It is possible to note that the removal of nitrogen-based compounds was favored in the presence of those constituted by sulfur, increasing from 99 and 97 to 100% for both pyridine and carbazole, respectively. On the other hand, the extraction of thiophene and dibenzothiophene slightly decreased from 67 and 88 to 63 and 86%, when comparing simultaneous and single extractions in *n*-heptane, respectively. This means that extraction of sulfur-based aromatic compounds with [TBP]Br:Sulf (1:4) were impaired by the presence of those containing nitrogen. Yet, the extraction efficiencies of target compounds in simulated gasoline and diesel were not affected by nitrogen-based compounds, while it slightly improved for thiophene in simulated gasoline and suffered small reduction for both sulfur-based compounds in simulated diesel [75].

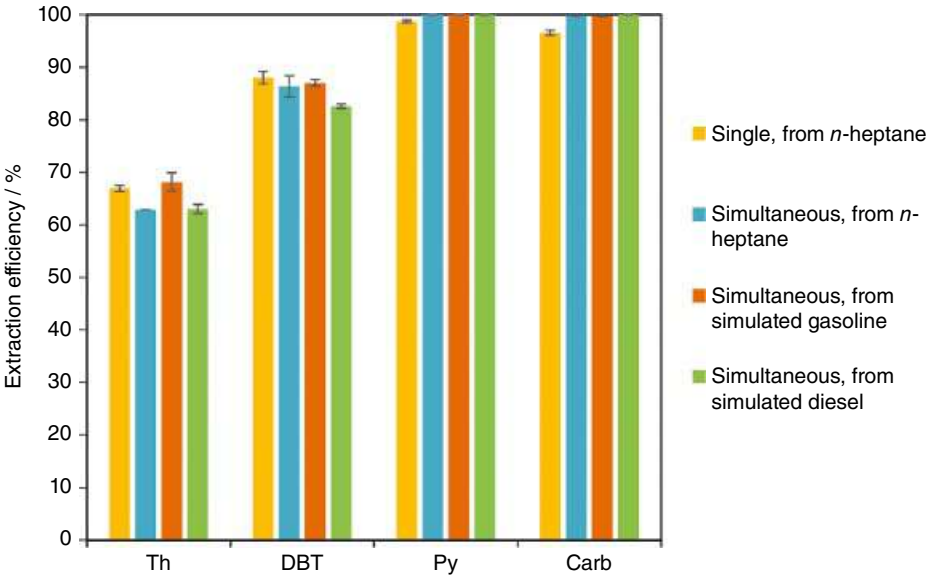

Figure 17.10 Comparison between single and simultaneous removal of thiophene (Th), dibenzothiophene (DBT), pyridine (Py), and carbazole (Carb) from *n*-heptane or simulated gasoline and diesel by the solvent [TBP]Br:Sulf (1:4). *Source:* Reprinted with permission from [75].

The number of extraction cycles that are required to bring the target compound's concentration to a desired level according to environmental regulations were also investigated by the same research team [75]. The authors observed that nitrogen-based aromatic compounds can be removed to the desired levels in a single extraction cycle, while for sulfur-based aromatic compounds, four extraction cycles were required to achieve less than 10 ppm concentration [75]. However, after five cycles of reuse, [TBP]Br:Sulf (1:4) lost 78 and 44% of its capacity to extract thiophene and dibenzothiophene, correspondingly, and maintained almost the same extraction capacity for nitrogen-based compounds as illustrated in Figure 17.11. Nevertheless, [TBP]Br:Sulf (1:4) can be regenerated by water addition, causing the precipitation of dibenzothiophene and carbazole and the formation of a second liquid phase rich in thiophene that can also be separated. [TBP]Br:Sulf (1:4) can then be dried and reused, recovering its total extraction capacity for sulfur-based aromatic compounds as shown in Figure 17.11 [75].

In another study, [Ch]Cl:Gly at 1:1.5, 1:2, and 1:3 molar ratios were tested for denitrogenation and desulfurization of a model gasoline sample composed of three aliphatic hydrocarbons (*n*-hexane, *n*-heptane, and isooctane) [76]. Pyridine and thiophene were used as representatives of nitrogen- and sulfur-based aromatic compounds, and toluene as non-phenolic aromatic compound. The results showed that [Ch]Cl:Gly was more efficient to extract pyridine than thiophene and toluene. After one extraction step, a denitrogenation efficiency of 58.0% was achieved, while an efficiency of 99.6% was achieved after five extraction steps. After five steps, a removal efficiency of 90.0 and 29.7% for thiophene and toluene was also achieved, respectively. Furthermore, the removal efficiency showed to be independent of the HBA:HBD molar ratio [76].

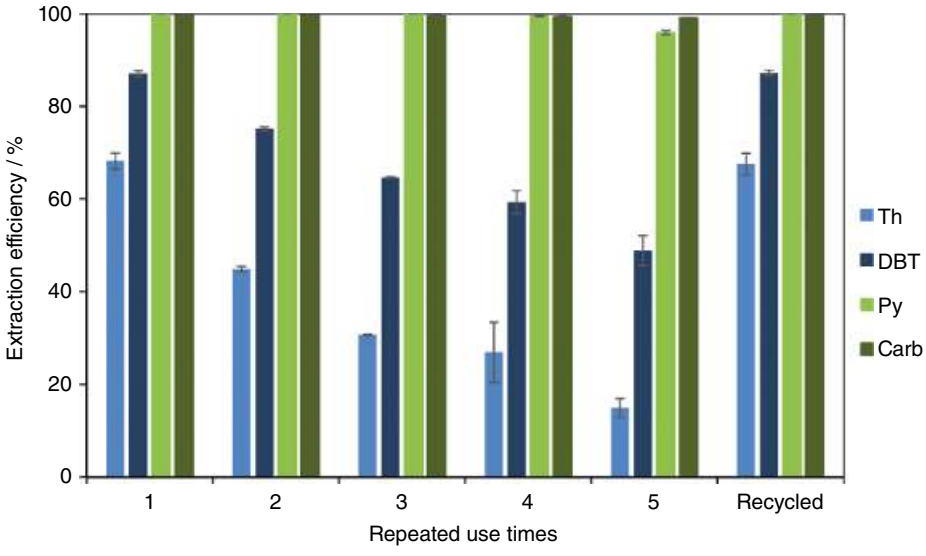

Figure 17.11 Reusability of [TBP]Br:Sulf (1:4) in the extraction of thiophene (Th), dibenzothiophene (DBT), pyridine (Py), and carbazole (Carb) at the same time from the simulated gasoline, without regeneration for five cycles and after regeneration. *Source:* Reprinted with permission from [75].

In another study, liquid–liquid equilibrium data at 25 °C and atmospheric pressure were determined for pseudo-ternary systems composed of hydrocarbons (*n*-hexane, *n*-heptane, isooctane, or toluene), pyridine, or thiophene, and DES formed of betaine:propylene glycol (Bet:PG) at a molar ratio of 1:4 or 1:5 [77]. It was observed that Bet:PG is highly selective for pyridine and thiophene at both ratios, since the amount of hydrocarbons in the DES-rich phase was negligible. However, solute distribution ratios indicated that Bet:PG in both ratios is more efficient to remove nitrogen-based compounds than the sulfur-based ones. The distribution ratios for pyridine ranged from 1.8 to 4.4, while for thiophene, the ratios were lower than 0.6 [77].

17.5 Extraction and Separation of Bioactive Compounds

Bioactive compounds are defined as secondary plant metabolites eliciting pharmacological or toxicological effects in human and animals [78]. They can be found in different organisms, i.e. plants, microorganisms, algae, and fungi [38]. Mbous and coworkers stated that these compounds are necessary for several vital mechanisms, such as stress-response and natural defense mechanisms [38]. Many studies point out that such compounds can reduce the risk of diabetes, cancer, inflammation, neurodegenerative and cardiovascular diseases, among many others [79–82]. In this sense, bioactive compounds have a prominent place at pharmaceutical, cosmetic, agrochemical, and chemical industries [83]. Moreover, some bioactive compounds are necessary for food industry, to manufacture biologically active substances, additives, surfactants, nutritional supplements, flavor enhancers, coloring,

among others. They are also used as antioxidants to enhance the properties of foods for nutritional purposes or preservation [84].

There are different families and classes of bioactive compounds existing in nature. An interesting classification distributes them into three major groups: phenolic compounds, terpenes, and alkaloids [85]. Inside these groups, an incredible variety of molecules can be found, more than two hundred thousand [86], to which are accredited many health benefits. Unfortunately, they are not free compounds and need to be extracted for further use in different applications. The huge number of identified bioactive compounds, their structural diversity, and polarity, make evident that the methods necessary to extract them are specific to each and every type [87].

The traditional techniques employed at lab scale for the extraction of bioactive compounds are solvent extraction either with Soxhlet or by maceration and hydrodistillation. Water and simple alcohols have been intensively used in these extractions, but they lack selectivity for target compounds. [85, 88]. Moreover, many hydrophobic compounds are of extreme interest in this research field, where water and alcohols exhibit poor extraction efficiency. In this context, non-environmentally friendly organic solvents are often used for this purpose, which should be avoided due to its negative impact on both health and environment.

In this regard, the application of DES as selective solvents could be a solid alternative and solution to accomplish green extracts with enriched target bioactive compounds. Furthermore, the application of DES and mostly NADES toward the extraction of bioactive compounds has been addressed as an advantage in contrast to other water and ethanol not only because of the higher extraction yields accomplished with these solvents, but also due to their ability to extract both nonpolar and polar compounds. In addition, the fact that NADES are composed of primary metabolites, their separation from extracted bioactive compounds could be unnecessary in the formulation of new products [24].

DES have many of the desired properties for the extraction of target bioactive compounds, but one of the most critical features of these solvents is their viscosity. In general, this makes difficult the mass transfer of bioactive compounds from intricate matrices to the extraction media, while it is also a problem in downstream processing, such as decantation, dissolution, and filtration steps. Nevertheless, the viscosity can be tuned by choosing appropriate HBAs and HBDs or by adding water or another benign solvent, such as ethanol [88].

17.5.1 Phenolic Compounds

As an example, vanillin is one of the most tracked phenolic compounds for commercialization as flavoring agent in the formulation of food and cosmetic products [89]. In this regard, González et al. attempted its extraction from vanilla pods with 14 different NADES [90]. The researchers showed evidences that some NADES, such as CitA (citric acid):Fru:Glucose (Glu), Fru:Glu, malic acid (MalA):Glu, and MalA:Fru:Glu, performed better (7.6, 10.1, 16.7, and 16.3 $mg/g_{biomass}$, respectively) than ethanol (4.4 $mg/g_{biomass}$) in the extraction of vanillin from pods. The authors have mentioned that this is a clear advantage since this type of NADES are safe in high doses and have received GRAS certification. Therefore, the extract containing vanillin and NADES can be included directly in food products [90].

On the other hand, flavonoids are a specific family of phenolic compounds with high market value, due to their bioactive properties, including antioxidant, antimicrobial, and antifungal activities [88]. Flavonoids can be found in several biomass sources and their extraction with DES has been tackled intensively over the past few years [91]. In this path, Bi et al. [92] examined the capacity of alcohol-based DES for the extraction of two specific flavonoids, myricetin and amentoflavone, from *Chamaecyparis obtusa* leaves. In general, the extracted amount of amentoflavone was higher than that of myricetin in all cases. The authors have shown that the fact that amentoflavone has a larger molecular size and greater hydrophobicity than myricetin favored its extraction in these alcohol-based DES. [Ch]Cl:1,4-butanediol at 1:5 ratio was found to be the best alcohol-based DES in this extraction, reaching maximum yields of 0.031 and 0.518 mg/g of myricetin and amentoflavone, respectively, after optimal conditions of water content, solid/liquid ratio, temperature, and time determined by response surface methodology (RSM). These extraction yields of these flavonoids were similar to that obtained with conventional methanol extraction [92].

In another study, Zhuang et al. [93] evaluated the capacity of 12 NADES composed by different HBAs, namely [Ch]Cl, Bet, and L-proline (Pro), and HBDs (carboxylic acid, alcohols, amides, and sugars) for the extraction of flavonoid glycosides (myricitrin and quercetin) and aglycones (amentoflavone and hinokiflavone, both less polar) from dried leaves of Cupressus tree (*Platycladi Cacumen).* All DES were more efficient to extract flavonoid glycosides from than water, methanol, or a mixture of both. Besides, some DES, like [Ch]Cl:LA, also showed better results on the extraction of the corresponding aglycones than methanol [93]. In fact, among all the examined DES, [Ch]Cl:LA presented the best performance for simultaneous extraction of flavonoids in both glucoside and aglycone forms. At the end, flavonoids were recovered from DES by microporous resin LX-38 with yields ranging from 77.4 to 98.9%. Regarding the difference extraction performances disclosed by DES, the authors stated that the polarity of applied solvents revealed a higher influence on flavonoid extraction rather than the extraction time or solid/liquid ratio [93]. This means that the choice for HBA and HBD in DES composition is of extreme importance in flavonoid extraction.

Similar findings were reported in the extraction of phenolic compounds with different polarities from mulberry leaves with the same kind of solvents [94]. DES based on [Ch]Cl, Bet, and Pro as HBA and amides, alcohols, and carboxylic acid as HBDs (U, EG, Gly, CitA, MalA, LevA, and LA) were examined. A total of 13 phenolic compounds were identified in a screening approach and the best yields were obtained with [Ch]Cl-based DES (Figure 17.12). Among them, [Ch]Cl:CitA enabled the extraction of phenolic compounds with a broadest range of polarity and allowed better extraction (22.66 mg/$g_{biomass}$) than conventional methanol extraction system (15.29 mg/$g_{biomass}$) [94].

The higher efficiency of [Ch]Cl:CitA when compared with methanol and water was also correlated with ability to disrupt the morphology of mulberry leaves, as demonstrated by scanning electron microscopy (Figure 17.13). The authors noticed that [Ch]Cl:CitA was able to disrupt the cell wall structure in mulberry leaves at great extent, while water maintained its integrity and methanol caused only a slight disruption [94]. A similar behavior was observed in catechin extraction from green tea powder using Bet:Gly:Glu [95].

In another work, 20 NADES were applied in the extraction of isoflavones (ononin, sissotrin, formononetin, and biochanin A) from chickpea sprouts (*Cicer arietinum* L.) [96].

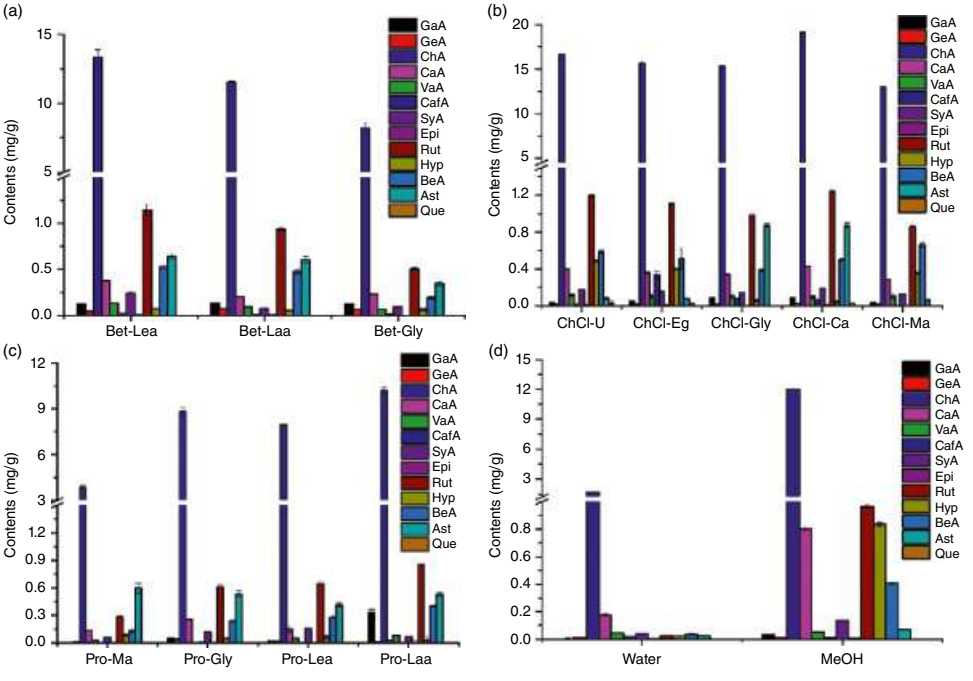

Figure 17.12 Total extraction of phenolic compounds with: (a) Bet-based DES; (b) [Ch]Cl-based DES; (c) Pro-based DES; (d) water and methanol. 13 phenolic compounds were identified: gallic acid (GaA), gentisic acid (GeA), chlorogenic acid (ChA), catechinic acid (CaA), vanillic acid (VaA), caffeic acid (CafA), syringic acid (SyA), epicatechin (Epi), rutin (Rut), hyperin (Hyp), benzoic acid (BeA), astragalin (Ast), and quercetin (Que). *Source:* Reprinted with permission from [94].

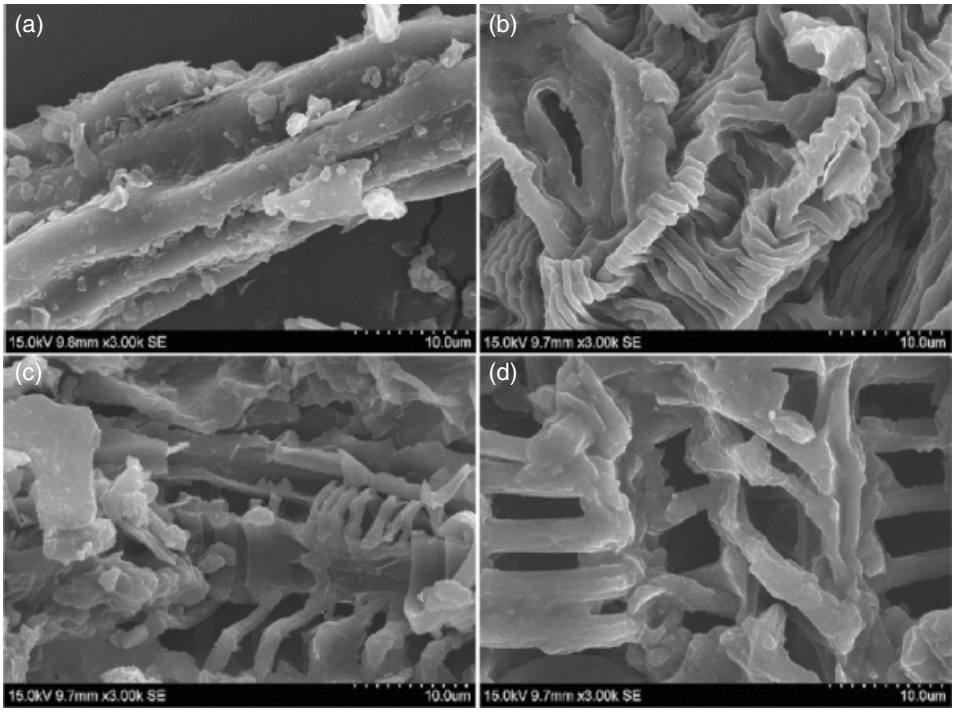

Figure 17.13 Scanning electron micrographs of mulberry leaves before (a) and after treatment with: water (b); methanol (c); and [Ch]Cl: CitA (d). *Source:* Reprinted with permission from [94].

The best extraction yield was obtained with [Ch]Cl:PG at a molar ratio of 1:1, reaching an optimal extraction of 8.24 $mg/g_{biomass}$ total flavonoid content, from which 0.58, 1.53, 1.64, and 2.44 $mg/g_{biomass}$ yields were achieved in the extraction of ononin, sissotrin, formononetin, and biochanin A, respectively. [Ch]Cl:PG was the less polar among the examined DES. Furthermore, authors tested the antioxidant activity of the extracts measured by 2,2-diphenyl-1-picrylhydrazyl (DPPH) and 20-azinobis-(3-ethylbenzthiazoline-6-sulfonate) (ABTS) free radical scavenging methods and they confirmed the highest antioxidant capacity of this extract in contrast to those obtained with other DES [96].

Indeed, the antioxidant capacity and other bioactive properties of extracts produced with DES treatment is imperative for food, cosmetic, and pharmaceutical applications. However, the toxicity and biocompatibility of DES is equally or more important in the formulation of new bioactive products. By bearing this in mind, Li et al. [95] evaluated the extraction of a epigallocatechin-3-gallate (EGCG), a potent antioxidant catechin derivative, from green tea (*Camellia sinensis*) with different binary and also ternary NADES compatible to cosmetic formulations. Among the examined solvents, the ternary system Bet:Gly:Glu (4:20:1) disclosed the best performance allowing an extraction yield of EGCG up to 81% at room temperature for 6.5 minutes (ultrasound-assisted extraction). Not only the EGCG yields were higher than conventional methods involving high temperature and prolonged extraction, but also EGCG stability increased in the presence of this ternary NADES when compared with methanol [95].

Disrupting the intricate biomass matrix is one of the keys to improve the extractability of phenolic compounds. As mentioned before, some DES are able to achieve a high degree of cell wall disruption and some of them allowed better extraction yields of these compounds when compared with water and methanol in conventional heating processes. This behavior can be further enhanced when assisted with alternative heating methods, such as microwave- and ultrasound-assisted technologies, enabling higher extraction yields, or at least reaching the same yields but reducing significantly the time of extraction. In this regard, a microwave extraction of phenolic compounds with [Ch]Cl:maltose (Malt) was performed by Wei et al. [97]. Good extraction and recovery yields of fourteen different phenolic compounds from *Cajanus cajan* were achieved at 60 °C. These extraction trials produced phenolic recovery yields that surpassed 90.0% and the isolation of those compounds was achieved through chromatographic separation using a silica gel column with yields higher than 97.0% [97].

Another study reported quercetin extraction with 127.0 $mg/g_{biomass}$ yield from *Flos sophorae* at ambient temperature assisted with ultrasound and using Pro:Gly as the extracting solvent [98]. Water was then applied as an anti-solvent allowing to isolate 92.0% of the extracted quercetin [98].

Another important aspect to take into account in the extraction of phenolic compounds is the presence of water. In some cases, one of the disadvantages in using DES and/or NADES as extraction solvents is their inherent viscosity. In order to circumvent this technical limitation that has direct impact in the extraction step as well as in the further downstream processing (separation and purification), water can be added to reduce the viscosity exhibited by a high number of DES. Nevertheless, a rational addition of water must be carried out to avoid a loss of extraction performance. For instance, the extraction of anthocyanins forms wine lees revealed that the addition of water to NADES at certain levels improved the extraction efficiencies, by reducing the viscosity of the solvent and subsequently allowing better mass-transfer rates [99]. However, more than 50% water content was unfavorable, possibly due to the weakening of the interactions between NADES and the target compounds. Furthermore, the water content that provided optimal extraction of anthocyanins was significantly different between examined NADES. Among studied NADES, ChCl:MalA at 35.4 wt% water content exhibited the highest anthocyanin extraction from wine lees (6.55 $mg/g_{biomass}$) [99].

In this context, other studies demonstrated that DES aqueous solutions may favor the extraction of phenolic compounds from biomass. A study showed the extraction of hydroxysafflor yellow A, cartormin, and carthamin from *Carthamus tinctorius L.* using Pro:MalA and [Ch]Cl:Suc aqueous solutions at 40 °C [100]. The effect of water was more pronounced in the extraction with the highly viscous [Ch]Cl:Suc, in which 25 wt% water content triggered the extraction yield of those phenolic compounds. Higher amount of water did not favor the extraction of the less polar carthamin. After extraction, the phenolic compounds were recovered through a chromatography column of silica gel reaching 90.0% recovery of both hydroxysafflor yellow A and cartormin, while the less polar compound carthamin was recovered in the range of 75.0–84.0% yield [100]. Giving the importance of water in the extraction of phenolic compounds with DES, other researchers attempted optimization of phenolic compound extraction placing water content as variable. Xia et al. [101] used ultrasonic extraction technique and employed [Ch]Cl:EG aqueous solutions as solvent to extract

rosmarinic acid and salviaflaside from *Prunella vulgaris*. Maximum extraction yields were obtained for rosmarinic acid (3.7 $mg/g_{biomass}$) and salviaflaside (1.0 $mg/g_{biomass}$) at water/DES ratio of 36 and 30% (v/v), correspondingly [101].

Adding water to DES may influence the molecular arrangement of HBA and HBD as well as the physicochemical properties of DES affecting their capacity for the extraction of target compounds. On the one hand, the addition of water can improve the extraction performance of DES, especially at low water contents, by reducing the viscosity and increasing the polarity of the solvent as well as improving the thermodynamic performance to some extent. However, water can disrupt interactions between DES constituents, competing for interactions between DES and target compounds. Dai et al. [102] demonstrated through FTIR and ^{1}H NMR analyses that intensive H-bonding interactions exist between the DES components and dilution with water gradually weakens those interactions up to a certain point (around 50% [v/v] water content), where HBA and HBD are totally solvated by water molecules. The authors also found out that a small amount of water could reduce the viscosity of DES to the range of water and increase the conductivity by up to 100 times for some DES [102], reason to enhance the extraction performance for polar compounds. In another work, a synergy between microwave irradiation and DES aqueous solution in anthraquinone extraction from *Rheum palmatum* was found [103]. It was observed that heating rates of most of the examined DES decreased under microwave irradiation with increasing water content as a consequence of increased heat capacity. This behavior allowed high-efficiency extraction for thermally sensitive compounds, such as anthraquinones. Among different aqueous solutions of [Ch]Cl-based DES combined with different HBDs (e.g. alcohols, amides, and carboxylic acids), [Ch]Cl:CitA aqueous solution was the most efficient to extract these phenolic compounds from biomass. At 20% water content in DES, HBA:HBD molar ratio of 1:1 and 16 minutes of residence time, maximum yields of 2.29, 2.32, 35.44, and 20.80 $mg/g_{biomass}$ of aloe-emodin, emodin, chrysophanol, and physcion were achieved, respectively [103].

17.5.2 Terpenic Compounds

Terpenoids (e.g. linalool, α-terpineol, and terpinyl acetate) and terpenes (e.g. limonene) are natural organic molecules found in several biomass materials [104]. Both terpenes and terpenoids are broadly explored in the pharmaceutical, cosmetic, and food industries, and therefore present a high commercial value similar to phenolic compounds [104]. In general, these compounds are hydrophobic and their extraction with conventional solvents, like water and alcohols, are often inefficient. The reference technique for the extraction of terpenic compounds is hydrodestillation, in which steam allows the formation of azeotrope between terpenic compounds and water and subsequent extraction of those compounds from plant matrices. However, alternatives to this energy-intensive process have been studied, including the application of DES. For instance, a study reported the extraction of three terpenoids, linalool (2.0 ng/mL), α-terpineol (3.2 ng/mL), and terpinyl acetate (2.1 ng/mL), from *Chamaecyparis obtusa* leaves using headspace-solvent microextraction with [Ch]Cl:EG at 100 °C for 30 minutes [105]. Product recoveries ranging from 79.4 to 100.0% were reported [105]. In another study, conducted by Ozturk et al. [104], favorable yields in the extraction of limonene and linalool from essential oils with a liquid–liquid separation

using [Ch]Cl:Gly as the extraction solvent were demonstrated [104]. The pure DES presented better yields as opposed to DES aqueous solutions, which can be associated with the nonpolar character of the major fraction of terpenic compounds. Nevertheless, the presence of water increased DES polarity and subsequent selectivity for linalool extraction [104].

In a comprehensive work, Duan and coworkers evaluated the ultrasound-assisted extraction of several bioactive molecules, including triterpenic saponins (Ginsenoside RG1, ginsenoside RB1, and notoginsenoside R1) from five Chinese herbal medicines, namely *Berberidis Radix, Epimedii Folium, Notoginseng Radix et Rhizoma, Rhei Rhizoma et Radix,* and *Salviae Miltiorrhizae Radix et Rhizoma*, using DES as extracting solvents [106]. In this case, these compounds are amphiphilic, which means they present hydrophobic and hydrophilic parts. A screening of 43 DES using different HBA ([Ch]Cl, Bet, and Pro) and HBD constituents (amides, carboxylic acids, alcohols, and sugars) at different molar ratios was approached. The combination of HBAs and HBDs produced DES with a large spectrum of physical properties, including viscosity and polarity, and consequently different extraction abilities were achieved [106]. Interestingly, the best result for saponin extraction was achieved with amide-based DES, while the worst was found to carboxylic acid-based DES. This clearly shows that DES can be fine-tuned toward the selective extraction of specific compounds from biomass to the detriment of others, which are simultaneously extracted when using conventional polar solvents like water and methanol [106].

A different methodological approach was attempted by Cai et al. [107], who applied aqueous biphasic systems formed by ethanol and DES for the salting-out extraction, preconcentration, and preliminary purification of ursolic acid from *Cynomorium songaricum* Rupr. DES acted as adjuvants in ethanol extraction of the triterpenic acid assisted by ultrasound and allowed the formation of a biphasic system toward ursolic acid separation as depicted in Figure 17.14. [Ch]Cl as HBA and 10 different HBDs were used in DES preparation, and their action in the extraction and separation of ursolic acid were evaluated. Among the studied DES, [Ch]Cl:OxaA presented the best result allowing the higher triterpene extraction and enabling the separation of the ursolic acid at the top phase of the biphasic system by nearly 99% yield. The top phase was separated, ethanol was evaporated, and 96.6% ursolic acid was precipitated with water reaching a total purity of 73.6% [107].

17.5.3 Alkaloids

Another class of compounds possessing bioactive properties and a high value for pharmaceutical industry are alkaloids. Similar to phenolic compounds and terpenes, their extraction from different biomass sources has also been attempted with DES [106, 108].

Jiang et al. [108] studied the application of DES in the extraction of five alkaloids, including morphinane, protoberberine, bisbenzylisoquinoline, indole, and quinolizidine, from different herbal medicines (*Caulis sinomenii*, *Coptis chinensis*, *Stephania tetrandra*, *Tetradium ruticarpum*, and *Sophora flavescens*). Binary and ternary DES possessing different polarity, viscosity, and pH were screened for alkaloid extraction [108]. Interestingly, [Ch]Cl:LA showed high extraction performance for almost all studied alkaloids with the exception of bisbenzylisoquinoline (no extraction). In addition, authors demonstrated that the pH of DES influences the extraction of alkaloids. DES containing acidic HBDs (LA or LevA) allowed better alkaloid extraction than neutral-based DES (amides and sugars). This

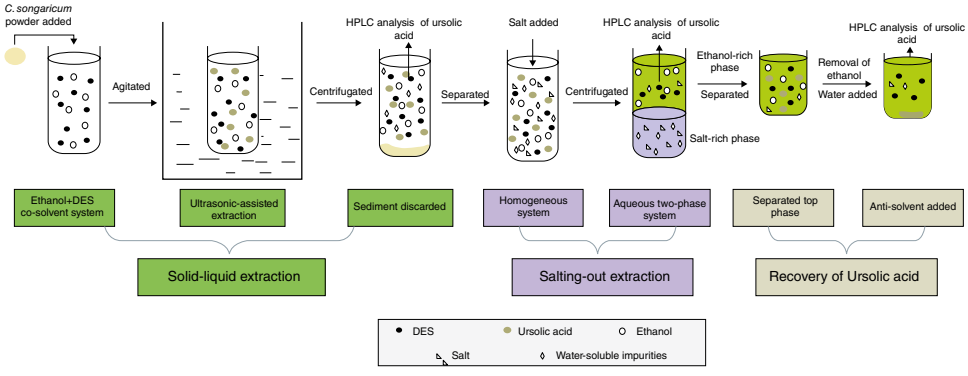

Figure 17.14 A proposed process for ursolic acid extraction, separation, and purification using DES as both extraction adjuvant and phase separation agent. *Source:* Reprinted with permission from [107].

behavior was not surprising, since it is widely known that under acidic conditions, alkaloids are predominantly in the cationic/salt form enabling higher solubilities. Yet again, viscosity and polarity also influenced the alkaloid extraction yield, where the more polar and less viscous DES, such as [Ch]Cl:LA, enhance this extraction [108].

Several alkaloids, including jatrorrhizine hydrochloride, berberine hydrochloride, and palmatine hydrochloride, were favorably extracted with carboxylic-based DES. The best extraction yields were achieved with [Ch]Cl:LA as well. The results with acidic DES were better than that with methanol, which again can be associated with cationic/salt form of alkaloid structure at low pH [106].

17.6 Extraction and Separation of Metals

17.6.1 Metals from Metallurgic Wastes

Metals are finite commodities and represent an important source of economic value [109]. The extraction of metals from ores is usually energy intensive and requires either high temperature melting (pyrometallurgy) or leaching, or the consumption of large amounts of strong acids and bases. These processes usually produce wastes, in gaseous, liquid (aqueous), or solid form, which require extensive and expensive treatments before being disposed of in a landfill, where they still present considerable environmental risks. Aside from that, the treatment of these wastes also needs high consumption of energy and/or hazardous chemicals [110, 111]. Therefore, the development of sustainable processes for metal production with minimal waste and/or selective metal extraction technologies for waste valorization is thus necessary for the implementation of a global circular economy [112, 113].

Hydrometallurgy is one of the most used techniques involving the separation of metals from mines and wastes using aqueous solutions. It is often preferred due to its ability to recover metals from a variety of sources, allowing the use of low process temperatures, the recycling of used reagents during the separation process, and low energy consumption [114]. A crucial step of any hydrometallurgical process is solvent extraction, in which metals are selectively divided into immiscible liquid phases, usually consisting of an acidic aqueous solution and an organic solvent [115]. However, this process still causes mining and metal processing industry to accumulate large amounts of metal-based wastes. Therefore, new technologies for the extraction and separation of metals have been proposed.

An alternative is the solvometallurgy, a division of extractive metallurgy that uses nonaqueous solvents, such as molecular organic solvents, ILs, or DES, instead of aqueous solutions [116]. Solvometallurgy has the advantage of being less energy-intensive than pyrometallurgy and has shown better selectivity than hydrometallurgy in the recovery of other wastes, including those from zinc industry [117–120]. Notable advances in the development of metal extraction systems have been made from traditional solvent extraction with common organic solvents, to the most recent developments based on the separation of metals mediated by green solvents, including ILs and DES [4, 115, 121].

An example was proposed by Rodriguez et al. [122] by using DES in the selective leaching of zinc from the goethite residue, a generated by-product from industrial zinc production. The study showed that carboxylic acid-based DES can leach more metal content than

those composed of polyol and amide. For instance, the leaching efficiency of zinc increased in the following order [Ch]Cl:U < [Ch]Cl:EG < [Ch]Cl:LevA. In addition, for DES composed of the same HBD (LevA), the leaching efficiency of zinc and iron increased with the size of the central atom of the HBA quaternary salt. For example, the iron leaching efficiency for [Ch]Cl:LevA was 2.2%, while around 20.0% efficiency was achieved with [TBP]Cl:LevA. Since the phosphonium cation ([TBP]) exhibits lower electronegativity than nitrogen counterpart ([Ch]), weaker intramolecular interactions are provided between DES components, making both [TBP]Cl and LevA more available for interaction with metals. Nevertheless, the authors recommended the use of [Ch]Cl:LevA, since the best compromise between efficiency and selectivity of zinc leaching against iron was achieved as depicted in Figure 17.15 [122, 123].

In another work, a ternary DES, [Ch]Cl:U:EG (2:4:1), was applied for zinc recovery from zinc oxide (ZnO) dust, a by-product from metallurgic industry [124]. The best result laid on 85.2% recovery of total ZnO from the initial residue (containing iron, calcium, aluminum, and silica as contaminants) when using slurry concentration of 50 g/L, 80 °C, and 600 rpm as main conditions. The researchers reported that DES acts as a complexing and solvent agent during leaching of ZnO dust. Electrospray ionization (ESI) mass spectra showed the formation of $[ZnO{\cdot}ureaCl]^-$ complexes and were referred to improve the zinc extraction. Bearing this in mind and since the role of EG was not reported in this study, a marginal effect of EG on zinc extraction can be inferred. After extraction, metal zinc can be electrodeposited directly from leach solutions through electrowinning. The $[ZnO{\cdot}ureaCl]^-$ complexes can be electro-reduced at electrowinning apparatus cathode generating metal zinc and releasing O^{2-} ions. Approximately, 82.6% of extracted ZnO was obtained as metal zinc after this process. No further purification of metal zinc was needed, while DES can be recycled in new extraction steps [124].

In a later study, Zürner et al. [125] investigated the leaching behavior of three DES, namely [Ch]Cl:EG (1:2), [Ch]Cl:U (1:2), and [Ch]Cl:OxaA (1:1), to selectively separate indium and tin from a pyrometallurgical residue, the flue dust (containing also iron, zinc, lead, and copper) from zinc smelters. DES composed of [Ch]Cl and OxaA were considered the most efficient by attaining extraction yields of 83% for iron, 88% for zinc, 93% for lead, 76% for copper, but most importantly 92 and 88% for indium and tin, respectively. The authors also proposed a two-stage precipitation procedure to separate target metals (indium and tin) from other metal components (iron, zinc, lead, and copper). In this procedure, the

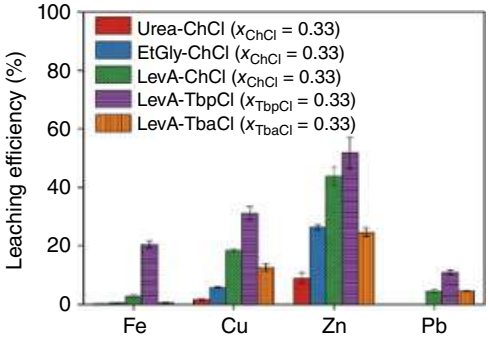

Figure 17.15 Leaching efficiency of the goethite residue using different DES as lixiviant. The experimental conditions were: Liquid/Solid = 10; T= 40 °C; and t = 24 hours. *Source:* Reprinted with permission from [122].

DES leachate was diluted with water, resulting in the formation of a precipitate mostly composed of $ZnC_2O_4{\cdot}2H_2O$ and PbC_2O_4. A second step allowed the precipitation of iron by photoinduced reduction. In this step, iron (III) oxalate complexes, formed in the DES leachate, are reduced and subsequently precipitated as $FeC_2O_4{\cdot}{}_2H_2O$. Both indium and tin were not detected in any of the precipitates, remaining in the DES aqueous solution. The advantage of this process relies on the high chloride concentration provided by [Ch]Cl:OxaA that improves the stability of the indium and tin in solution, probably due to the formation of stable complexes, which inhibit coprecipitation with iron [125].

In another approach, NADES formed by the combination of [Ch]Cl with fructose (Fru), sucrose (Suc), Gly, or EG were used to extract lead from soils contaminated by mining activities [126]. A natural biodegradable surfactant saponin, extracted from the pericarp of the soap nut fruit, was mixed with DES to promote metal's solubilization through a micellar mechanism. The obtained results showed that metal removal improves as the concentration of DES and saponin increases. A lead extraction above 72.7% was achieved using 40 wt% of [Ch]Cl:Fru and 1 wt% saponin mixture [126]. Moreover, the comparison of XRD spectra and SEM images between lead-contaminated soil and soils treated with DES or mixture of DES/saponin (Figure 17.16) demonstrated no relevant changes in soil composition and texture, i.e. the soil minerals did not suffer corrosion or mining changes after DES treatment [126]. Therefore, DES can be used safely in lead extraction without affecting soil properties.

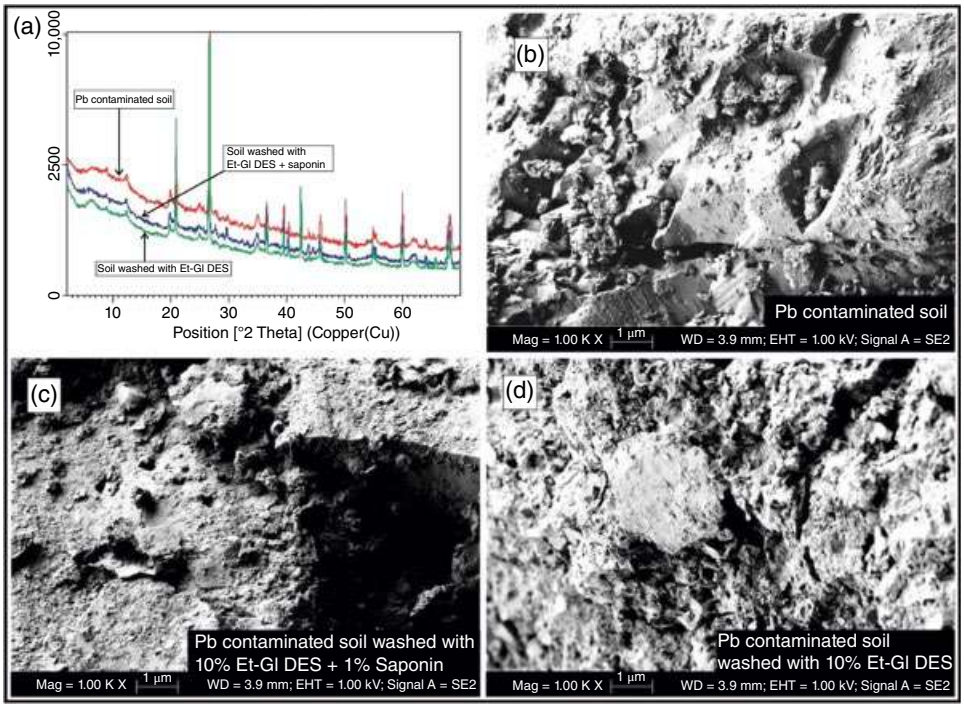

Figure 17.16 (a) XRD spectra and (b–d) SEM imagery of soil before and after washing with DES ([Ch]Cl:EG) and DES/saponin mixture. *Source:* Reprinted with permission from [126].

17.6.2 Recovery of Metals from Electronic Waste

Electronic and electrical equipment wastes are now becoming a major concern in developed and developing countries. The primary sources are printed circuit boards, cathode ray tubes, magnets, all types of batteries, discharge lamps, liquid crystal displays, computer and peripherals, wind turbines, among others. On the one hand, these wastes are hazardous to environment due to toxic composition, and, on the other, they contain many useful and valuable materials, including metals [127]. Thus, a green and sustainable recovery approach of metals from electronic wastes is of utmost importance to recycle and reuse these materials.

As an example, the common use of lithium-ion batteries (LIB) in portable electronic devices and electric vehicles drives to an exponential growth in battery consumption and discard. Among recycling technologies, processes that use mild conditions and provide high recycling efficiencies are gaining increasing interest. In this sense, the process of solvometallurgy using DES to recover cobalt and lithium from batteries has been studied [128–130]. Peeters et al. [128] observed that DES composed of [Ch]Cl and carboxylic acids (CitA, MaliA) at a molar ratio of 1:1 with 20 wt% water content can be considered an effective leacher solution for lithium cobalt oxide ($LiCoO_2$) in the presence of metallic aluminum and copper. The use of DES takes advantage over the conventional leaching with hydrochloric acid as reducing agent, by avoiding toxic chlorine gas formation. With [Ch]Cl:CitA at mild leaching conditions (60 °C, 900 rpm, 20 wt% water), a cobalt recovery over 80%, in the form of oxalate, was achieved after addition of an oxalic acid aqueous solution, and approximately 95% of aluminum (III) and lithium (I) remained in the DES solution, which could be recovered via nonaqueous solvent extraction and/or precipitation [128].

Roldán-Ruiz et al. [129] studied [Ch]Cl:p-toluene sulfonic acid (pTSA) and their aqueous solutions to recover cobalt from the cathode part of LIBs ($LiCoO_2$). In comparison with organic acids, this DES offered a significant reduction in the ratio of solute to solvent required for the complete dissolution of cobalt. The recovery efficiencies of cobalt from spent LIB were up to 94%. Afterward, cobalt was recovered from DES solutions using sodium carbonate and ammonium carbonate as precipitating agents. A final calcination of precipitates was performed to obtain Co_3O_4 to be used in new batteries.

In another work, an illustrative example was given by Tran et al. [131] as depicted in Figure 17.17. The authors proposed a previous disassembly of spent LIB, whereas the cathode waste (major fraction) is impregnated and heated in DES. At this step, cobalt and lithium are extracted from other cathode components, like aluminum foil, binder, and conductive carbon. The leachate is filtered and extracted cobalt can be separated from lithium through precipitation and/or electrodeposition. With this method, authors have shown that [Ch]Cl:EG can efficiently extract metals (cobalt and lithium) from these batteries, reaching extraction efficiencies up to 99% after heating at 180 °C for 24 hours [131]. However, the recovery of remaining lithium from DES solution was not covered in this study, which is also a bottleneck.

In addition, Wang et al. [130] stated that although DES have shown ability to dissolve a wide range of metal oxides through coordination, their weak reducing power requires raising the temperature and extending the duration of the process to allow an effective metal extraction, which in authors' opinion is not efficient. The researchers mentioned that

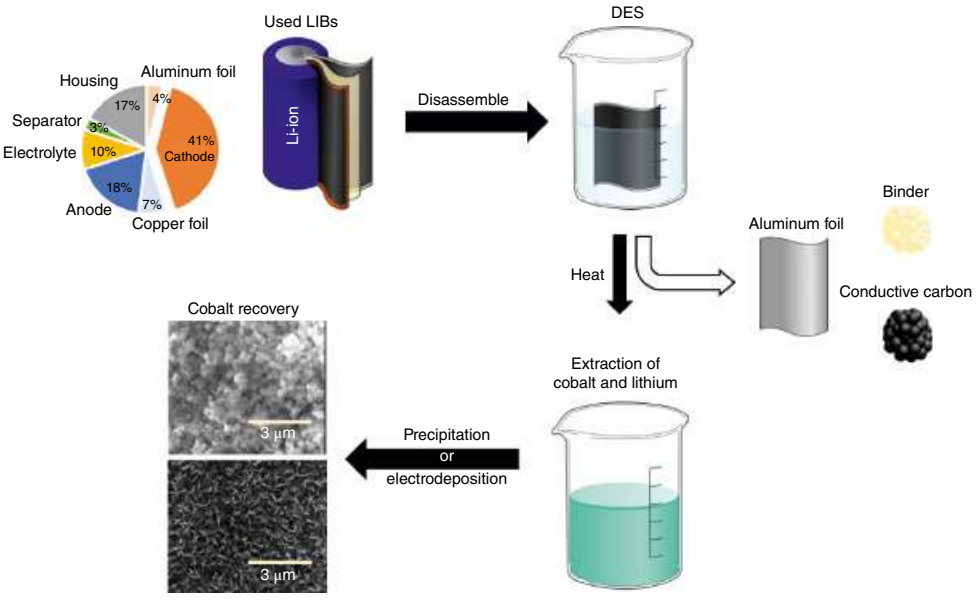

Figure 17.17 A proposed process for spent LIB recycling with DES. *Source:* Reprinted with permission from [131].

lithium and cobalt can be dissolved in DES not only by coordination, but also mediated by chemical reduction, particularly the reduction of Co(III) to Co(II) to enable higher dissolution of this metal in DES without high temperature and prolonged treatment. In this sense, a simple and robust experimental method based on electrochemical principles (cyclic voltammetry) was performed to quickly determine the reducing power of examined DES. The reduction potential of the [Ch]Cl:U was determined as more negative than that of the [Ch]Cl:EG, which indicated stronger reducibility of metal exhibited by [Ch]Cl:U than [Ch]Cl:EG under the same extraction conditions. In experimental extractions of Li and Co from LIBs with those DES, the extraction efficiency of both metals by [Ch]Cl:U was much higher than that of the [Ch]Cl:EG. The [Ch]Cl:U was found to extract lithium and cobalt up to 95% efficiency from spent LIBs at 180 °C for 12 hours as optimal conditions [130]. The DES containing leached cobalt was recovered by cobalt precipitation with consecutive additions of Na_2CO_3, oxalic acid, and NaOH solutions.

17.6.3 Hydrophobic DES: An Alternative Tool for Metal Separation

The concept of hydrophobic DES (HDES) was introduced by van Osch and colleagues [132] in 2015 when they combined several quaternary ammonium salts with decanoic acid and obtained a water-immiscible solvent. This type of DES was applied to extract water-insoluble volatile organic compounds exhibiting high yield and extraction efficiency [132]. Since then, progressive research on the application of HDES has been performed in a wide range of scientific fields, whereas promising results have been particularly achieved in the separation of metals, mainly from aqueous streams.

In 2016, HDES were used for the first time to remove metal ions from non-buffered water [36]. In this study, HDES composed of decanoic acid (DecA) and lidocaine (Lid) were used in several molar ratios (2:1, 3:1, and 4:1) and the distribution coefficients of the ions composing the metal chloride salts were determined for cobalt chloride ($CoCl_2$), iron chloride ($FeCl_2$), nickel chloride ($NiCl_2$), manganese chloride ($MnCl_2$), copper chloride ($CuCl_2$), zinc chloride ($ZnCl_2$), sodium chloride (NaCl), potassium chloride (KCl), and lithium chloride (LiCl). The obtained results are highlighted in Table 17.2, which show different selectivity of DecA:Lid at different molar ratios on the distribution of metal cations and chloride anions between DES and water phases. High distribution coefficients were achieved as a consequence of possible ion-exchange extraction mechanism, in which the positively charged metal ion is most likely exchanged for positively charged lidocaine. It can be seen that metal cations are selectively extracted to the DES phase to the detriment of chloride anion. On the other hand, transition metals (Co, Ni, Zn, and Cu) are favorably extracted to DES phase rather than alkali metals (Li, K, and Na) [36].

The use of a hydrophobic DES capable of removing metal ions from aqueous media seems promising application in various industrial processes. For instance, in pulp and paper industry, hydrophobic DES may remove transition metal ions such as Mn(II) and Fe(II) from fiber

Table 17.2 Distribution coefficients (D) of metal cations and chloride anions over the hydrophobic DES and water phases. For D = 0, the ion remains in the aqueous phase, while the ion is completely extracted to DES phase when D = 1.

		Distribution coefficients (D)		
Entry		**DecA:Lid (2:1)**	**DecA:Lid (3:1)**	**DecA:Lid (4:1)**
Exp. 1	**Co**	>0.996 ± 0.001	>0.996 ± 0.001	0.983 ± 0.002
	Cl	0.113 ± 0.002	0.078 ± 0.008	0.101 ± 0.059
Exp. 2	**Fe**	>0.992 ± 0.001	>0.991 ± 0.001	>0.991 ± 0.001
	Cl	0.197 ± 0.003	0.080 ± 0.001	0.113 ± 0.007
Exp. 3	**Mn**	>0.992 ± 0.001	0.3991 ± 0.001	0.983 ± 0.004
	Cl	0.086 ± 0.002	0.081 ± 0.027	0.065 ± 0.011
Exp. 4	**K**	0.457 ± 0.001	0.397 ± 0.011	0.457 ± 0.001
	Cl	0.141 ± 0.001	0.078 ± 0.031	0.072 ± 0.001
Exp. 5	**Co**	0.990 ± 0.001	0.946 ± 0.012	0.777 ± 0.008
	Ni	>0.996 ± 0.001	0.983 ± 0.001	0.880 ± 0.004
	Zn	>0.995 ± 0.001	>0.995 ± 0.001	>0.995 ± 0.001
	Cu	>0.996 ± 0.001	>0.996 ± 0.001	>0.996 ± 0.001
	Na	0.195 ± 0.001	0.140 ± 0.009	0.127 ± 0.040
	K	0.211 ± 0.028	0.161 ± 0.018	0.134 ± 0.005
	Li	0.266 ± 0.015	0.166 ± 0.001	0.128 ± 0.036

Source: Reprinted with permission from [36].

suspensions before bleaching with hydrogen peroxide, replacing ethylenediaminetetraacetic acid and other non-benign chemicals often used for that purpose [133].

HDES were also used for the recovery of indium and transition metals from chloride media [36, 134] as well as Cu(II) separation from other transition metals, such as Co(II) and Ni(II) [135]. In this last study, Schaeffer et al. [135] evaluated the extraction of Cu (II) from aqueous solution and its separation from other transition metals Co (II) and Ni (II) using HDES based on terpenes, menthol, or thymol, combined with long-chain carboxylic acids (Figure 17.18). The authors discovered that the efficiency of these DES in the extraction of Cu (II) from aqueous solution is correlated with the alkyl chain length of the carboxylic acid. The increase of the alkyl chain length decreased the extraction efficiency. The results also revealed that a higher carboxylic acid content in DES composition did not favor the extraction yield, suggesting that only a fraction of the acid is involved in the extraction of Cu (II) [135]. Although the mechanism of metal extraction from aqueous solution with these HDES was not covered in this study, the researchers reported an important role of the carboxylic acid in this process, since thymol and menthol, without carboxylic acid, were unable to extract Cu (II) from aqueous solution.

The capacity of quaternary ammonium-based HDES for the extraction of Au(III) chloride present in hydrochloric acid solution ($AuCl_4^-$ form) has been also reported in the literature [136]. This study showed that [TMA]Br, [TEA]Br, [TPA]Br, [TBA]Br, and [TOMA]Br combined with n-hexanoic acid can be used for that purpose. Their low viscosity was highlighted as an advantage for this type of extraction. Among the examined DES, [TOMA]Br:n-hexanoic acid showed the best gold extraction capacity (96.8%). The mechanism of gold removal was based on an anion exchange mechanism as illustrated in Figure 17.19. The anion exchange mechanism lied on strong hydrogen bonding between Br^- and n-hexanoic acid forming $[C_5H_{13}\text{-}COOH\cdots\cdots Br]^-$ complex, enabling higher ionic interaction between HBA cation (e.g. $[TOMA]^+$) and $AuCl_4^-$. In addition, Au (III) extracted in the DES phase can be easily recovered by stripping with sodium borohydride ($NaBH_4$) solution, while DES can be reused up to 5 times without losing efficiency [136].

All these studies expand the potential of HDES for integrated extraction–separation stages of various metal ions. The hydrophobicity and good interaction with desired

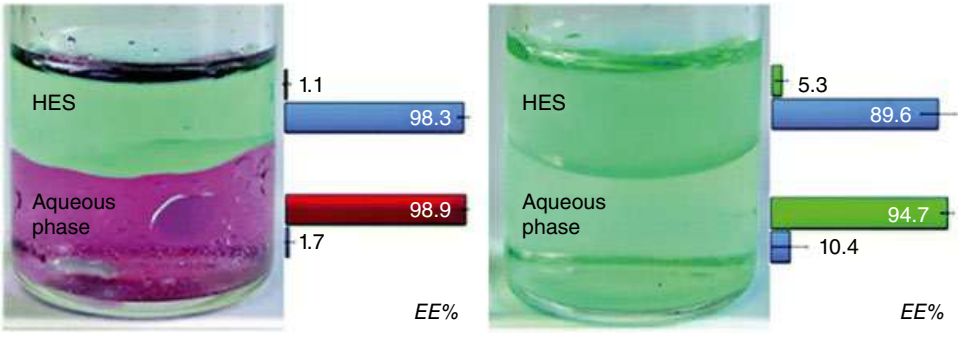

Figure 17.18 Separation of Cu(II) (0.01 M, blue) from 0.1 M solution of Co(II) (red) and Ni(II) (green), respectively, in the thymol:capric acid HES ($x_{capric\ acid}$ = 0.7, T = 20 °C, pH = 4.9). *Source:* Reprinted with permission from [135].

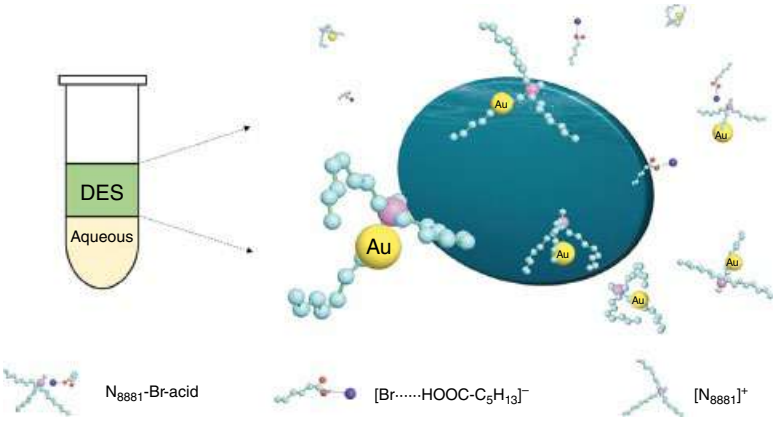

Figure 17.19 The representation of gold extraction process with HDES based on an anion exchange mechanism. [N8881] ([TOMA] in this chapter) is visualized as a claw grabbing Au(III) in the aqueous phase. *Source:* Reprinted with permission from [136].

metals exhibited by this type of DES are suitable properties for the recovery of these valuable compounds from acidic aqueous solutions generally used in metal extraction processes.

17.7 Conclusions

It is unavoidable that the current separation technologies face new challenges to achieve sustainable performances. The application of the so-rated green DES (and NADES) toward the selective extraction and separation of valuable compounds from a myriad of liquid streams and solid matrices can be foreseen as an alternative solution. In this sense, some of the most promising separation approaches with DES and latest results were herein reported and discussed to open new windows of opportunity in both research and industry fields.

The separation of aromatic compounds from aliphatic hydrocarbons with DES revealed to be an advance toward green separation. This technology allows remarkable solvent loss prevention during the extraction process, since in some cases, DES are not detected in the hydrocarbon-rich layer. The new methodological approach of *in situ* formation of DES to recover phenol from oil mixtures appears as one of the most exciting technologies to follow up. Furthermore, according to Warrag and coworkers "desulfurization of fuels using DES will provide a promising green and inexpensive option with a potential for industrial application" [42]. On the other hand, the extraction of added-value bioactive compounds (e.g. phenolic, terpenes, and alkaloid compounds) from biomass matrices with DES disclosed high selectivity and, in some cases, best performances than conventional extraction processes using water and methanol as solvents. Particularly, the application of NADES for the extraction seems quite auspicious, since no intensive downstream processing (separation and purification steps) of obtained extracts might be needed, due to nontoxic character of these solvents. In fact, most of the compounds composing NADES are certified Generally Recognized as Safe (GRAS). At last and not the least, the separation of metals from

metallurgic and electronic wastes is today a big challenge and once more DES arise as multifunctional tools capable of performing selective interaction with particular types of metals. Among the distinct alternatives, hydrophobic DES stand as thrilling technology that enables easier separation of metals from aqueous streams.

This chapter reviewed some of the best DES performing extraction and separation of aromatic compounds, metals, and bioactive compounds. However, despite all the advantages offered by DES in these key separation technologies, there is still room for testing, learning, and improvement. One must also bear in mind a good choice of DES components that respect environment and sustainability. For instance, there were studies revised in this chapter that use phenol to make up DES, which is questionable, since it is considered a toxic substance. At scientific point of view, it could be relevant to use all types of DES to understand the chemistry behind separation, but at industrial application perspective, DES that do not fulfill the environmental standards must be avoided.

The multiple combinations of HBD and HBA as well as the wide range of HBD/HBA molar ratios allow designing new tailored solvents with tuned physicochemical properties, such as viscosity, polarity, acidity, basicity, and reactivity, to achieve a maximal separation performance (efficiency *versus* selectivity). The viscosity is one of the major bottlenecks of DES application that not only influences the extraction and separation efficiencies, but also present high impact on downstream processing, creating technological barriers during filtration and purification steps, for example. The addition of water or other benign solvents like ethanol allows reducing DES viscosity and fine-tune their extraction and separation abilities. There were cases reviewed in this chapter that co-solvent substantially aided DES separation efficiency.

Furthermore, more efforts should be made in the recovery of target compounds from DES and subsequent recycling of the solvent, which are equally or far more important than extraction and separations steps, to increase the sustainability of the whole process. Only few studies have tackled the recovery and reuse of DES. Back-extraction, flash distillation, and precipitation (e.g. [Ch]Cl) were some examples of developed recovery processes, but there is still low amount of data regarding these stages of the process to consider DES as good recyclable solvents. In this sense, it is a hot topic research that must be addressed in the future.

Abbreviations

Ammonium chloride	$[NH_4]Cl$
Benzothiophene	BTh
Benzylcholinium	BzCh
Betaine	Bet
Bromide	Br
Carbazole	Carb
Carbon dioxide	CO_2
Chloride	Cl
Cholinium	Ch

Citric acid	CitA
Decanoic acid	DecA
Deep eutectic solvents	DES
Dibenzothiophene	DBTh
Dimethyl sulfoxide	DMSO
Ethylene glycol	EG
Ethyltriphenylphosphonium	ETPP
Fructose	Fru
Glycerol	Gly
Glucose	Glu
Hydrogen bond acceptor	HBA
Hydrogen bond donor	HBD
Iodide	I
Ionic liquids	ILs
L-carnitine	Carn
L-proline	Pro
Lactic acid	LA
Levulinic acid	LevA
Lidocaine	Lid
Lithium-ion batteries	LIB
Malonic acid	MaloA
Maltose	Malt
Methyltriethylammonium	MTEA
Methyltriphenylphosphonium	MTPP
N,N′-dimethylurea	DMU
N-methylpyrrolidone	NMP
N-formylmorpholine	NFM
Natural deep eutectic solvents	NADES
Oxalic acid	OxaA
Phenylacetic acid	PheA
Polyethylene glycol	PEG
Propionic acid	PA
Propylene glycol	PG
p-Toluenesulfonic acid	pTSA
Pyridine	Py
Sucrose	Suc
Sulfolane	Sulf
Tetrabutylammonium	TBA
Tetrabutylphosphonium	TBP
Tetraethylammonium	TEA
Tetraethylene glycerol	TEG
Tetrapropylammonium	TPA
Tetrahexylammonium	THA
Thiophene	Th
Triethylene glycol	TriEgly

Trifluoroacetic acid	TFA
Tetrapropylammonium	TPA
Tetramethylammonium	TMA
Trioctylmethylammonium	TOMA
Urea	U

Acknowledgments

This work was developed within the scope of the project CICECO-Aveiro Institute of Materials, FCT Ref. UIDB/50011/2020 & UIDP/50011/2020, financed by national funds through the FCT/MCTES. The authors would like to thank the Coordenação de Aperfeiçoamento de Pessoal de Nível Superior – Brasil (CAPES) – Finance Code 001, FAPESP [2014/21252-0], CNPq [169459/2017-9, 200627/2018-0, 310272/2017-3, 306666/2020-0], Banco Santander S. A., PROCAD (88887.200617/2018-00), CAPES/PRINT(88881.310551/2018-01). André M. da Costa Lopes thanks his research contract funded by Fundação para a Ciência e Tecnologia (FCT) and project CENTRO-04-3559-FSE-000095 - Centro Portugal Regional Operational Programme (Centro2020), under the PORTUGAL 2020 Partnership Agreement, through the European Regional Development Fund (ERDF).

References

1 Colin, R. and BjØrn, K. (2006). *Basic Biotechnology*, 3e, 1–666. New York: Cambridge University Press.
2 D'Amato, D., Droste, N., Allen, B. et al. (2017). Green, circular, bio economy: a comparative analysis of sustainability avenues. *J Clean Prod* 168: 716–734.
3 Maina, S., Kachrimanidou, V., and Koutinas, A. (2017). A roadmap towards a circular and sustainable bioeconomy through waste valorization. *Curr Opin Green Sustain Chem* 8: 18–23.
4 Clarke, C.J., Tu, W.-C., Levers, O. et al. (2018). Green and sustainable solvents in chemical processes. *Chem Rev* 118 (2): 747–800.
5 Anastas, P.T. and Warner, J.C. (1998). *Green Chemistry: Theory and Practice*. New York: Oxford University Press.
6 Khandelwal, S., Tailor, Y.K., and Kumar, M. (2016). Deep eutectic solvents (DESs) as eco-friendly and sustainable solvent/catalyst systems in organic transformations. *J Mol Liq* 215: 345–386.
7 Whiteker, G.T. (2019). Applications of the 12 Principles of green chemistry in the crop protection industry. *Org Process Res Dev* 23: 2109–2121.
8 Pei, X., Xiong, D., Pei, Y. et al. (2018). Switchable oil-water phase separation of ionic liquid-based microemulsions by CO2. *Green Chem* https://doi.org/10.1039/C8GC00801A.
9 Ibrahim, M.H., Hayyan, M., Hashim, M.A., and Hayyan, A. (2017). The role of ionic liquids in desulfurization of fuels: a review. *Renew Sust Energ Rev* 76: 1534–1549.
10 Da Costa Lopes, A.M., Lins, R.M.G., Rebelo, R.A., and Łukasik, R.M. (2018). Biorefinery approach for lignocellulosic biomass valorisation with an acidic ionic liquid. *Green Chem* 20 (17): 4043–4057.

11 Vicente, F.A., Bairos, J., Roque, M. et al. (2019). Use of ionic liquids as cosurfactants in mixed aqueous micellar two-phase systems to improve the simultaneous separation of immunoglobulin G and human serum albumin from expired human plasma. *ACS Sustain Chem Eng* 7 (17): 15102–15113.

12 Yu, H., Cui, K., Li, T. et al. (2019). Recovery of butanol from ABE fermentation broth with hydrophobic functionalized ionic liquids as extractants. *ACS Sustain Chem Eng* 7 (10): 9318–9329.

13 Liu, X., Xu, D., Diao, B. et al. (2018). Separation of dimethyl carbonate and methanol by deep eutectic solvents: liquid–liquid equilibrium measurements and thermodynamic modeling. *J Chem Eng Data* 63 (5): 1234–1239.

14 Martins, M.A.R., Pinho, S.P., and Coutinho, J.A.P. (2019). Insights into the nature of eutectic and deep eutectic mixtures. *J Solut Chem* 48 (7): 962–982.

15 Zdanowicz, M., Wilpiszewska, K., and Spychaj, T. (2018). Deep eutectic solvents for polysaccharides processing. a review. *Carbohydr Polym* 200: 361–380.

16 Abbott, A.P., Boothby, D., Capper, G. et al. (2004). Deep eutectic solvents formed between choline chloride and carboxylic acids: versatile alternatives to ionic liquids. *J Am Chem Soc* 126 (29): 9142–9147.

17 Zhang, Q., De Oliveira, V.K., Royer, S., and Jérôme, F. (2012). Deep eutectic solvents: syntheses, properties and applications. *Chem Soc Rev* 41 (21): 7108–7146.

18 Gomez, F.J.V., Espino, M., Fernández, M.A., and Silva, M.F. (2018). A greener approach to prepare natural deep eutectic solvents. *ChemistrySelect* 3 (22): 6122–6125.

19 Smith, E.L., Abbott, A.P., and Ryder, K.S. (2014). Deep eutectic solvents (DESs) and their applications. *Chem Rev* 114 (21): 11060–11082.

20 Abbott, A.P., Al-Barzinjy, A.A., Abbott, P.D. et al. (2014). Speciation{,} physical and electrolytic properties of eutectic mixtures based on CrCl3·6H2O and urea. *Physiol Chem Phys* 16 (19): 9047–9055.

21 Abranches, D.O., Martins, M.A.R., Silva, L.P. et al. (2019). Phenolic hydrogen bond donors in the formation of non-ionic deep eutectic solvents: the quest for type v des. *Chem Commun* 55 (69): 10253–10256.

22 Kumar, A.K., Parikh, B.S., and Pravakar, M. (2016). Natural deep eutectic solvent mediated pretreatment of rice straw: bioanalytical characterization of lignin extract and enzymatic hydrolysis of pretreated biomass residue. *Environ Sci Pollut Res Int* 23 (10): 9265–9275. http://dx.doi.org/10.1007/s11356-015-4780-4.

23 Vanda, H., Dai, Y., Wilson, E.G. et al. (2018). Green solvents from ionic liquids and deep eutectic solvents to natural deep eutectic solvents. *CR Chim* 21 (6): 628–638.

24 Paiva, A., Craveiro, R., Aroso, I. et al. (2014). Natural deep eutectic solvents – solvents for the 21st century. *ACS Sustain Chem Eng* 2: 1063–1071.

25 Satlewal, A., Agrawal, R., Bhagia, S. et al. (2018). Natural deep eutectic solvents for lignocellulosic biomass pretreatment: recent developments, challenges and novel opportunities. *Biotechnol Adv* 36 (8): 2032–2050.

26 Liu, Y., Friesen, J.B., McAlpine, J.B. et al. (2018). Natural deep eutectic solvents: properties, applications, and perspectives. *J Nat Prod* 81 (3): 679–690.

27 Shahbaz, K., Mjalli, F.S., Hashim, M.A. et al. (2007). Eutectic-based ionic liquids with metal-containing anions and cations. *Fluid Phase Equilib* 199 (1–2): 6495–6501.

28 Sarmad, S., Xie, Y., Mikkola, J.-P., and Ji, X. (2017). Screening of deep eutectic solvents (DESs) as green CO2 sorbents: from solubility to viscosity. *New J Chem* 41 (1): 290–301.

29 Qin, H., Hu, X., Wang, J. et al. (2019). Overview of acidic deep eutectic solvents on synthesis, properties and applications. *Green Energy Environ* 5 (1): 8–21.

30 Pateli, I.M., Thompson, D., Alabdullah, S.S.M. et al. (2020). The effect of pH and hydrogen bond donor on the dissolution of metal oxides in deep eutectic solvents. *Green Chem* 22 (16): 5476–5486.

31 Skulcova, A., Russ, A., Jablonsky, M., and Sima, J. (2018). Peer reviewed brief communication the pH behavior of seventeen deep eutectic solvents. *Bioresources* 3: 5042–5051.

32 Pandey, A., Rai, R., Pal, M., and Pandey, S. (2014). How polar are choline chloride-based deep eutectic solvents? *Physiol Chem Phys* 16 (16): 1559–1568.

33 Tang, W. and Row, K.H. (2020). Design and evaluation of polarity controlled and recyclable deep eutectic solvent based biphasic system for the polarity driven extraction and separation of compounds. *J Clean Prod* 268: 122306.

34 Farooq, M.Q., Abbasi, N.M., and Anderson, J.L. (1633). Deep eutectic solvents in separations: methods of preparation, polarity, and applications in extractions and capillary electrochromatography. *J Chromatogr A* 2020: 461613.

35 Xu, K., Xu, P., and Wang, Y. (2020). Aqueous biphasic systems formed by hydrophilic and hydrophobic deep eutectic solvents for the partitioning of dyes. *Talanta* 213: 120839.

36 Van Osch, D.J.G.P., Parmentier, D., Dietz, C.H.J.T. et al. (2016). Removal of alkali and transition metal ions from water with hydrophobic deep eutectic solvents. *Chem Commun* 52 (80): 11987–11990.

37 Mako, P., Przyjazny, A., and Boczkaj, G. (2018). Hydrophobic deep eutectic solvents as "green" extraction media for polycyclic aromatic hydrocarbons in aqueous samples. *J Chromatogr A* 1570: 28–37.

38 Mbous, Y.P., Hayyan, M., Hayyan, A. et al. (2017). Applications of deep eutectic solvents in biotechnology and bioengineering – promises and challenges. *Biotechnol Adv* 35 (2): 105–134.

39 Loow, Y.L., New, E.K., Yang, G.H. et al. (2017). Potential use of deep eutectic solvents to facilitate lignocellulosic biomass utilization and conversion. *Cellulose* 24 (9): 3591–3618.

40 Yang, T.-X., Zhao, L.-Q., Wang, J. et al. (2017). Improving whole-cell biocatalysis by addition of deep eutectic solvents and natural deep eutectic solvents. *ACS Sustain Chem Eng* 5 (7): 5713–5722.

41 Xu, K., Wang, Y., Huang, Y. et al. (2015). A green deep eutectic solvent-based aqueous two-phase system for protein extracting. *Anal Chim Acta* 864: 9–20.

42 Warrag, S.E.E., Peters, C.J., and Kroon, M.C. (2017). Deep eutectic solvents for highly efficient separations in oil and gas industries. *Curr Opin Green Sustain Chem* 5: 55–60.

43 Sarwono, M.M., Hadj-Kali, M.K.O., and Alnashef, I.M. (2013). Application of deep eutectic solvents for the separation of aliphatics and aromatics. 2013 International Conference on Technology, Informatics, Management, Engineering and Environment, 48–53.

44 Hosseini, A., Haghbakhsh, R., and Raeissi, S. (2019). Experimental investigation of liquid-liquid extraction of toluene + heptane or toluene + hexane using deep eutectic solvents. *J Chem Eng Data* 64 (9): 3811–3820.

45 Hadj-Kali, M.K., Salleh, Z., Ali, E. et al. (2017). Separation of aromatic and aliphatic hydrocarbons using deep eutectic solvents: a critical review. *Fluid Phase Equilib* 448: 152–167.

46 Feng, S., Sun, J., Ren, Z. et al. (2019). Effective separation of aromatic hydrocarbons by pyridine-based deep eutectic solvents. *Can J Chem Eng* 97 (12): 3138–3147.

47 Gouveia, A.S.L., Oliveira, F.S., Kurnia, K.A., and Marrucho, I.M. (2016). Deep eutectic solvents as azeotrope breakers: liquid-liquid extraction and COSMO-RS prediction. *ACS Sustain Chem Eng* 4 (10): 5640–5650.

48 Wang, Y., Hou, Y., Wu, W. et al. (2016). Roles of a hydrogen bond donor and a hydrogen bond acceptor in the extraction of toluene from: N-heptane using deep eutectic solvents. *Green Chem* 18 (10): 3089–3097.

49 Larriba, M., Ayuso, M., Navarro, P. et al. (2018). Choline chloride-based deep eutectic solvents in the dearomatization of gasolines. *ACS Sustain Chem Eng* 6 (1): 1039–1047.

50 Parliament THEE, Union P (2009). European Parliament Directive 2009/30/EC. Off J Eur Union. L140/88-L140/113.

51 Shang, X., Dou, Y., Zhang, Y. et al. (2019). Tailoring properties of natural deep eutectic solvents with water to facilitate their applications. *Food Chem* 187 (August): 111724.

52 Esquembre, R., Sanz, J.M., Wall, J.G. et al. (2013). Thermal unfolding and refolding of lysozyme in deep eutectic solvents and their aqueous dilutions. *Physiol Chem Phys* 15 (27): 11248–11256.

53 Elliott, M.A. *Chemistry of Coal Utilization. Second Supplementary Volume*, 1e. New York, NY: Wiley.

54 Schobert, H.H. and Song, C. (2002). Chemicals and materials from coal in the 21st century. *Fuel* 81 (1): 15–32.

55 Richard Henry, S. and Charles, G.S. (1981). Removal of phenols from phenol-containing streams. US4256568, 3–17.

56 Jiao, T., Gong, M., Zhuang, X. et al. (2015). A new separation method for phenolic compounds from low-temperature coal tar with urea by complex formation. *J Ind Eng Chem* 29: 344–348.

57 Amen-Chen, C., Pakdel, H., and Roy, C. (1997). Separation of phenols from Eucalyptus wood tar. *Biomass Bioenergy* 13 (1): 25–37.

58 Venter, D.L. and Nieuwoudt, I. (1998). Separation of m-cresol from neutral oils with liquid—liquid extraction. *Ind Eng Chem Res* 37 (10): 4099–4106.

59 Fan, Y., Li, Y., Dong, X. et al. (2014). Extraction of phenols from water with functionalized ionic liquids. *Ind Eng Chem Res* 53 (51): 20024–20031.

60 Jiao, T., Qin, X., Zhang, H. et al. (2019). Separation of phenol and pyridine from coal tar via liquid–liquid extraction using deep eutectic solvents. *Chem Eng Res Des* 145: 112–121.

61 Yi, L., Feng, J., Li, W., and Luo, Z. (2019). High-performance separation of phenolic compounds from coal-based liquid oil by deep eutectic solvents. *ACS Sustain Chem Eng* 7 (8): 7777–7783.

62 Pang, K., Hou, Y., Wu, W. et al. (2012). Efficient separation of phenols from oils via forming deep eutectic solvents. *Green Chem* 14 (9): 2398–2401.

63 Guo, W., Hou, Y., Wu, W. et al. (2013). Separation of phenol from model oils with quaternary ammonium salts via forming deep eutectic solvents. *Green Chem* 15 (1): 226–229.

64 Jiao, T., Li, C., Zhuang, X. et al. (2015). The new liquid-liquid extraction method for separation of phenolic compounds from coal tar. *Chem Eng J* 266: 148–155.

65 Soltanmohammadi, F., Jouyban, A., and Shayanfar, A. (2020). New aspects of deep eutectic solvents: extraction, pharmaceutical applications, as catalyst and gas capture. *Chem Pap* https://doi.org/10.1007/s11696-020-01316-w.

66 Byrne, E.L. and Holbrey, J.D. (2020). Phenol recovery from aromatic solvents by formation of eutectic liquids with trialkyl-2,3-dihydroxypropylammonium Chloride Salts. *Sustain Chem* 1 (1): 49–61.

67 Yao, C., Hou, Y., Ren, S. et al. (2017). Efficient separation of phenol from model oils using environmentally benign quaternary ammonium-based zwitterions via forming deep eutectic solvents. *Chem Eng J* 326: 620–626.

68 Demirbas, A., Alidrisi, H., and Balubaid, M.A. (2015). API gravity, sulfur content, and desulfurization of crude oil. *Pet Sci Technol* 33 (1): 93–101.

69 Li, C., Li, D., Zou, S. et al. (2013). Extraction desulfurization process of fuels with ammonium-based deep eutectic solvents. *Green Chem* 15 (10): 2793–2799.

70 Lima, F., Gouvenaux, J., Branco, L.C. et al. (2018). Towards a sulfur clean fuel: deep extraction of thiophene and dibenzothiophene using polyethylene glycol-based deep eutectic solvents. *Fuel* 234 (February): 414–421.

71 Wagle, D.V., Zhao, H., Deakyne, C.A., and Baker, G.A. (2018). Quantum chemical evaluation of deep eutectic solvents for the extractive desulfurization of fuel. *ACS Sustain Chem Eng* 6 (6): 7525–7531.

72 Jiang, W., Jia, H., Li, H. et al. (2019). Boric acid-based ternary deep eutectic solvent for extraction and oxidative desulfurization of diesel fuel. *Green Chem* 21 (11): 3074–3080.

73 Warrag, S.E.E., Darwish, A.S., Adeyemi, I.A. et al. (2020). Extraction of pyridine from n-alkane mixtures using methyltriphenylphosphonium bromide-based deep eutectic solvents as extractive denitrogenation agents. *Fluid Phase Equilib* 517: 112622.

74 Hizaddin, H.F., Ramalingam, A., Hashim, M.A., and Hadj-Kali, M.K.O. (2014). Evaluating the performance of deep eutectic solvents for use in extractive denitrification of liquid fuels by the conductor-like screening model for real solvents. *J Chem Eng Data* 59 (11): 3470–3487.

75 Lima, F., Dave, M., Silvestre, A.J.D. et al. (2019). Concurrent desulfurization and denitrogenation of fuels using deep eutectic solvents. *ACS Sustain Chem Eng* 7 (13): 11341–11349.

76 Zagajski Kučan, K. and Rogošić, M. (2019). Purification of motor fuels by means of extraction using deep eutectic solvent based on choline chloride and glycerol. *J Chem Technol Biotechnol* 94 (4): 1282–1293.

77 Rogošić, M., Krišto, A., and Kučan, K.Z. (2019). Deep eutectic solvents based on betaine and propylene glycol as potential denitrification agents: a liquid-liquid equilibrium study. *Braz J Chem Eng* 36 (4): 1703–1716.

78 Bernhoft, A. (2010). *Bioactive compounds in plants – benefits and risks for man and animals*, vol. 88 (ed. A. Bernhoft), 821–825. Laeknabladid, Oslo: The Norwegian Academy of Science and Letters.

79 Kris-Etherton, P.M., Hecker, K.D., Bonanome, A. et al. (2002). Bioactive compounds in foods: their role in the prevention of cardiovascular disease and cancer. *Am J Med* 113 (9 SUPPL. 2): 71–88.

80 Dima, C., Assadpour, E., Dima, S., and Jafari, S.M. (2020). Nutraceutical nanodelivery; an insight into the bioaccessibility/bioavailability of different bioactive compounds loaded within nanocarriers. *Crit Rev Food Sci Nutr*: 1–35. https://doi.org/10.1080/10408398.2020.1792409.

81 Comim, S.R.R., Franceschi, E., Borges, G.R. et al. (2010). Phase equilibrium measurements and modelling of ternary system (carbon dioxide plus ethanol plus palmitic acid). *J Chem Thermodyn* 42 (3): 348–354.

82 Ferreira, I.C.F.R., Martins, N., and Barros, L. (2017). Phenolic compounds and its bioavailability: in vitro bioactive compounds or health promoters? *Adv Food Nutr Res* 82: 1–44.

83 Joana Gil-Chávez, G., Villa, J.A., Fernando Ayala-Zavala, J. et al. (2013). Technologies for extraction and production of bioactive compounds to be used as nutraceuticals and food ingredients: an overview. *Compr Rev Food Sci Food Saf* 12 (1): 5–23.

84 Rice-Evans, C.A., Miller, N.J., and Paganga, G. (1997). Antioxidant properties of phenolic compounds. *Trends Plant Sci* 2 (4): 152–159.

85 Azmir, J., Zaidul, I.S.M., Rahman, M.M. et al. (2013). Techniques for extraction of bioactive compounds from plant materials: a review. *J Food Eng* 117 (4): 426–436.

86 Vuolo, M.M., Lima, V.S., and Maróstica Junior, M.R. (2018). *Phenolic Compounds: Structure, Classification, and Antioxidant Power. Bioactive Compounds: Health Benefits and Potential Applications*, 33–50. Elsevier Inc.

87 Agostini-costa, T.S., Vieira, R.F., Bizzo, H.R. et al. (2012). Secondary metabolites. In: *Chromatography and Its Applications* (ed. S. Dhanarasu). IntechOpen https://doi.org/10.5772/35705.

88 Zainal-Abidin, M.H., Hayyan, M., Hayyan, A., and Jayakumar, N.S. (2017). New horizons in the extraction of bioactive compounds using deep eutectic solvents: a review. *Anal Chim Acta* 979: 1–23.

89 Araújo, J.D.P., Grande, C.A., and Rodrigues, A.E. (2010). Vanillin production from lignin oxidation in a batch reactor. *Chem Eng Res Des* 88 (8): 1024–1032.

90 González, C.G., Mustafa, N.R., Wilson, E.G. et al. (2018). Application of natural deep eutectic solvents for the "green" extraction of vanillin from vanilla pods. *Flavour Fragr J* 33 (1): 91–96.

91 Skarpalezos, D. and Detsi, A. (2019). Deep eutectic solvents as extraction media for valuable flavonoids from natural sources. *Appl Sci* 9 (19): 4169.

92 Bi, W., Tian, M., and Row, K.H. (2013). Evaluation of alcohol-based deep eutectic solvent in extraction and determination of flavonoids with response surface methodology optimization. *J Chromatogr A* 1285: 22–30.

93 Zhuang, B., Dou, L.L., Li, P., and Liu, E.H. (2017). Deep eutectic solvents as green media for extraction of flavonoid glycosides and aglycones from Platycladi Cacumen. *J Pharm Biomed Anal* 134: 214–219.

94 Zhou, P., Wang, X., Liu, P. et al. (2018). Enhanced phenolic compounds extraction from Morus alba L. leaves by deep eutectic solvents combined with ultrasonic-assisted extraction. *Ind Crop Prod* 120 (May): 147–154.

95 Jeong, K.M., Ko, J., Zhao, J. et al. (2017). Multi-functioning deep eutectic solvents as extraction and storage media for bioactive natural products that are readily applicable to cosmetic products. *J Clean Prod* 151: 87–95.

96 Shang, X., Dou, Y., Zhang, Y. et al. (2019). Tailor-made natural deep eutectic solvents for green extraction of isoflavones from chickpea (Cicer arietinum L.) sprouts. *Ind Crop Prod* 140 (August): 111724.

97 Wei, Z., Qi, X., Li, T. et al. (2015). Application of natural deep eutectic solvents for extraction and determination of phenolics in Cajanus cajan leaves by ultra performance liquid chromatography. *Sep Purif Technol* 149: 237–244.

98 Nam, M.W., Zhao, J., Lee, M.S. et al. (2015). Enhanced extraction of bioactive natural products using tailor-made deep eutectic solvents: application to flavonoid extraction from Flos sophorae. *Green Chem* 17 (3): 1718–1727.

99 Bosiljkov, T., Dujmić, F., Cvjetko Bubalo, M. et al. (2017). Natural deep eutectic solvents and ultrasound-assisted extraction: green approaches for extraction of wine lees anthocyanins. *Food Bioprod Process* 102: 195–203.

100 Dai, Y., Witkamp, G.J., Verpoorte, R., and Choi, Y.H. (2013). Natural deep eutectic solvents as a new extraction media for phenolic metabolites in carthamus tinctorius L. *Anal Chem* 85 (13): 6272–6278.

101 Xia, B., Yan, D., Bai, Y. et al. (2015). Determination of phenolic acids in Prunella vulgaris L.: a safe and green extraction method using alcohol-based deep eutectic solvents. *Anal Methods* 7 (21): 9354–9364.

102 Dai, Y., Witkamp, G.J., Verpoorte, R., and Choi, Y.H. (2015). Tailoring properties of natural deep eutectic solvents with water to facilitate their applications. *Food Chem* 187: 14–19.

103 Wang, J., Jing, W., Tian, H. et al. (2020). Investigation of deep eutectic solvent-based microwave-assisted extraction and efficient recovery of natural products. *ACS Sustain Chem Eng* 8 (32): 12080–12088.

104 Ozturk, B., Esteban, J., and Gonzalez-Miquel, M. (2018). Deterpenation of citrus essential oils using glycerol-based deep eutectic solvents. *J Chem Eng Data* 63 (7): 2384–2393.

105 Tang, B., Bi, W., Zhang, H., and Row, K.H. (2014). Deep eutectic solvent-based HS-SME coupled with GC for the analysis of bioactive terpenoids in Chamaecyparis obtusa leaves. *Chromatographia* 77 (3–4): 373–377.

106 Duan, L., Dou, L.L., Guo, L. et al. (2016). Comprehensive evaluation of deep eutectic solvents in extraction of bioactive natural products. *ACS Sustain Chem Eng* 4 (4): 2405–2411.

107 Cai, C., Wu, S., Wang, C. et al. (2019). Deep eutectic solvents used as adjuvants for improving the salting-out extraction of ursolic acid from Cynomorium songaricum Rupr. in aqueous two-phase system. *Sep Purif Technol* 209 (July 2018): 112–118.

108 Jiang, Z.M., Wang, L.J., Gao, Z. et al. (2019). Green and efficient extraction of different types of bioactive alkaloids using deep eutectic solvents. *Microchem J* 145 (October 2018): 345–353.

109 Ongondo, F.O., Williams, I.D., and Cherrett, T.J. (2011). How are WEEE doing? A global review of the management of electrical and electronic wastes. *Waste Manag* 31 (4): 714–730.

110 Jenkin, G.R.T.T., Al-Bassam, A.Z.M.M., Harris, R.C. et al. (2016). The application of deep eutectic solvent ionic liquids for environmentally-friendly dissolution and recovery of precious metals. *Miner Eng* 87: 18–24.

111 Fu, F. and Wang, Q. (2011). Removal of heavy metal ions from wastewaters: a review. *J Environ Manag* 92 (3): 407–418.

112 Moreau, V., Sahakian, M., van Griethuysen, P., and Vuille, F. (2017). Coming full circle: why social and institutional dimensions matter for the circular economy. *J Ind Ecol* 21 (3): 497–506.

113 European Commission (2017). *Circular Economy Research and Innovation: Connecting Economic & Environmental Gains*. Luxembourg: Publications Office of the European Union https://doi.org/10.2777/688203.

114 Liu, T., Chen, J., Li, H. et al. (2019). Further improvement for separation of heavy rare earths by mixtures of acidic organophosphorus extractants. *Hydrometallurgy* 188: 73–80.

115 Wilson, A.M., Bailey, P.J., Tasker, P.A. et al. (2014). Solvent extraction: the coordination chemistry behind extractive metallurgy. *Chem Soc Rev* 43 (1): 123–134.

116 Binnemans, K. and Jones, P.T. (2017). Solvometallurgy: an emerging branch of extractive metallurgy. *J Sustain Metall* 3 (3): 570–600.

117 Palden, T., Onghena, B., Regadío, M., and Binnemans, K. (2019). Methanesulfonic acid: a sustainable acidic solvent for recovering metals from the jarosite residue of the zinc industry. *Green Chem* 21 (19): 5394–5404.

118 Forte, F., Horckmans, L., Broos, K. et al. (2017). Closed-loop solvometallurgical process for recovery of lead from iron-rich secondary lead smelter residues. *RSC Adv* 7 (79): 49999–50005.

119 Gijsemans, L., Forte, F., Onghena, B., and Binnemans, K. (2018). Recovery of rare earths from the green lamp phosphor LaPO4:Ce3+{,}Tb3+ (LAP) by dissolution in concentrated methanesulphonic acid. *RSC Adv* 8 (46): 26349–26355.

120 Riaño, S., Petranikova, M., Onghena, B. et al. (2017). Separation of rare earths and other valuable metals from deep-eutectic solvents: a new alternative for the recycling of used NdFeB magnets. *RSC Adv* 7 (51): 32100–32113.

121 Pena-Pereira, F. and Namieśnik, J. (2014). Ionic liquids and deep eutectic mixtures: sustainable solvents for extraction processes. *ChemSusChem* 7 (7): 1784–1800.

122 Rodriguez Rodriguez, N., Machiels, L., Onghena, B. et al. (2020). Selective recovery of zinc from goethite residue in the zinc industry using deep-eutectic solvents. *RSC Adv* 10 (12): 7328–7335.

123 Rodriguez Rodriguez, N., MacHiels, L., and Binnemans, K. (2019). P-toluenesulfonic acid-based deep-eutectic solvents for solubilizing metal oxides. *ACS Sustain Chem Eng* 7 (4): 3940–3948.

124 Zhu, X.L., Xu, C.Y., Tang, J. et al. (2019). Selective recovery of zinc from zinc oxide dust using choline chloride based deep eutectic solvents. *Trans Nonferrous Met Soc China* 29 (10): 2222–2228.

125 Zürner, P. and Frisch, G. (2019). Leaching and selective extraction of indium and tin from zinc flue dust using an oxalic acid-based deep eutectic solvent. *ACS Sustain Chem Eng* 7 (5): 5300–5308.

126 Mukhopadhyay, S., Mukherjee, S., Adnan, N.F. et al. (2016). Ammonium-based deep eutectic solvents as novel soil washing agent for lead removal. *Chem Eng J* 294: 316–322.

127 Swain, N. and Mishra, S. (2019). A review on the recovery and separation of rare earths and transition metals from secondary resources. *J Clean Prod* 220: 884–898.

128 Peeters, N., Binnemans, K., and Riaño, S. (2020). Solvometallurgical recovery of cobalt from lithium-ion battery cathode materials using deep-eutectic solvents. *Green Chem* 22 (13): 4210–4221.

129 Roldán-Ruiz, M.J., Ferrer, M.L., Gutiérrez, M.C., and Del Monte, F. (2020). Highly efficient p-toluenesulfonic acid-based deep-eutectic solvents for cathode recycling of Li-ion batteries. *ACS Sustain Chem Eng* 8 (14): 5437–5445.

130 Wang, S., Zhang, Z., Lu, Z., and Xu, Z. (2020). A novel method for screening deep eutectic solvent to recycle the cathode of Li-ion batteries. *Green Chem* 22 (14): 4473–4482.

131 Tran, M.K., Rodrigues, M.T.F., Kato, K. et al. (2019). Deep eutectic solvents for cathode recycling of Li-ion batteries. *Nat Energy* 4 (4): 339–345.

132 van Osch, D.J.G.P., Zubeir, L.F., van den Bruinhorst, A. et al. (2015). Hydrophobic deep eutectic solvents as water-immiscible extractants. *Green Chem* 17 (9): 4518–4521.

133 Susilo, R. and Chandraghatgi, R.E.P. (2005). Partitioning of iron, manganese, copper between fibres and liquor and the role of water chemistry. Pulp Pap Canada.

134 Tereshatov, E.E., Boltoeva, M.Y., and Folden, C.M. (2016). First evidence of metal transfer into hydrophobic deep eutectic and low-transition-temperature mixtures: indium extraction from hydrochloric and oxalic acids. *Green Chem* 18 (17): 4616–4622.

135 Schaeffer, N., Martins, M.A.R., Neves, C.M.S.S. et al. (2018). Sustainable hydrophobic terpene-based eutectic solvents for the extraction and separation of metals. *Chem Commun* 54 (58): 8104–8107.

136 Geng, Y., Xiang, Z., Lv, C. et al. (2019). Recovery of gold from hydrochloric medium by deep eutectic solvents based on quaternary ammonium salts. *Hydrometallurgy* 188 (March): 264–271.

18

Microfluidic Platforms for Cell Sorting

Fateme Mirakhorli[1,2], Seyed Sepehr Mohseni[3], Sajad Razavi Bazaz[1], Ali Abouei Mehrizi[3], Peter J. Ralph[2], and Majid Ebrahimi Warkiani[1,4]

[1] *School of Biomedical Engineering, University of Technology Sydney, Sydney, Australia*
[2] *Climate Change Cluster, University of Technology Sydney, Australia*
[3] *Department of Life Sciences Engineering, University of Tehran, Tehran, Iran*
[4] *Institute of Molecular Medicine, Sechenov University, Moscow, Russia*

18.1 Introduction

Isolation and separation of cells and particles are essential for many chemical, biomedical, and industrial applications. In these applications, the target cell should be separated from a sample containing different cells and particles and then used for further investigations. Although it depends on the particular application, the number of these target cells is relatively low compared with the sample size [1]. For instance, circulating tumor cells (CTCs) are a low proportion of the total cell population existing in the blood of cancer patients. Traditionally, some lab-based techniques have been developed for separating, sorting, or isolating these target particles or cells. These traditional sorting techniques have been comparatively successful. However, they require a large amount of sample and expensive reagents, are prone to human error, suffer from batch-to-batch different results, and have long processing times [2].

Since the introduction of microfluidic devices, many techniques have been developed to separate cells or particles from bulk samples. These techniques can be either active or passive. Active techniques make use of an external field for particle separation. This field can be acoustic, magnetic, electric, or optic. In active techniques, the separation resolution is often high; however, the throughput of these systems is usually low since a specific amount of time must be provided for the external field to affect particles. On the other hand, passive techniques do not require an external field for particle sorting, and they rely solely on microchannel physical structure or particle–particle or particle–fluid interactions. Passive techniques include pinched flow fractionation (PFF), deterministic lateral displacement (DLD), inertial and Dean force, and microfiltration techniques. These methods are attractive since they are simple and low cost [3, 4]. In this chapter, we briefly review each of these techniques, followed by some examples of developed devices.

Sustainable Separation Engineering: Materials, Techniques and Process Development, Volume 2, First Edition. Edited by Gyorgy Szekely and Dan Zhao.
© 2022 John Wiley & Sons Ltd. Published 2022 by John Wiley & Sons Ltd.

18.2 Passive Microfluidic Cell Sorting Systems

18.2.1 Pinched Flow Fractionation

PFF, first introduced by Yamada [5], is a method that uses laminar flow to sort particles based on their size. Channels that work with the concept of PFF are usually T- or Y-junction. In this technique, usually, one stream has a diluted sample of particles, while the other one is without particle. The PFF channels contain a pinched segment (a narrow channel) that enters an expanded segment. The width of the expanded segment is significantly larger than the pinched segment. By adjusting the flow rate ratio between the two inlets, the sheath flow pushes all particles toward the pinched segment wall. Since particles of different sizes have different center of mass, they are placed in different positions relative to the wall. Due to the parabolic nature of the velocity profile in Poiseuille flow, this spacing amplifies where particles pass through the expanded section and follow different streamlines. Therefore, a slight difference in the position of particles in the pinched segment is boosted in the expanded section, and particles or cells of different sizes can be collected from their assigned outlets (Figure 18.1a). The boundary angle, total flow rate, flow rate ratio of two inlets, and the width and roughness of the pinched section can affect the device performance. It has been shown that the PFF technique is unable to isolate particles that have a size similar or less compared with the roughness wall [6].

PFF technique was first used to separate 15 μm from 30 μm particles [5]. The channel they used in their study was symmetric; therefore, the hydraulic resistance and flow rate of all outlets were similar. This becomes an issue for the separation of particles that are significantly smaller than channel width in the pinched segment, and all particles migrated to one outlet. To address this issue, the asymmetric arrangement of outlets has been proposed where one outlet (drain channel) is wider or shorter than other outlets to break the symmetry of hydraulic resistance of outlets and change the streamline of the channels (Figure 18.1b). This method can increase the resolution of particle separation where the capability of the device for the separation of 1 μm from 2.1 μm particle with 80% efficiency at 20 μL/h flow rate has been demonstrated [7]. In addition, the versatility of the method for the separation of emulsion droplets has been showcased [8]. Using a valve at outlets can also change the flow rate that guides particles of different sizes toward different outlets [9]. Geometrical modification of the channel can also enhance the separation efficiency in PFF devices. For instance, Vig has used a snakelike structure at the enlarged segment of the PFF layout to increase the spacing between particles, leading to a more efficient separation (Figure 18.1c) [10].

Besides the methods used to increase the efficiency of the PFF method, the combination of this technique with other approaches can increase the separation efficiency. For example, the gap between particles can be amplified using dielectrophoretic or optical forces [11, 12]. Additionally, PFF and sedimentation techniques can be coupled to sort particles based on their size and density [13]. Based on Figure 18.1d, at first, particles are separated from each other on the pinched segment at the horizontal part. Once they enter the vertical curved channel, the sedimental effect separates particles that have similar sizes but different densities. A centrifugal force can also be added to the systems to enhance the separation efficiency [13]. To increase the throughput, Lu and Xuan combined inertial lift forces

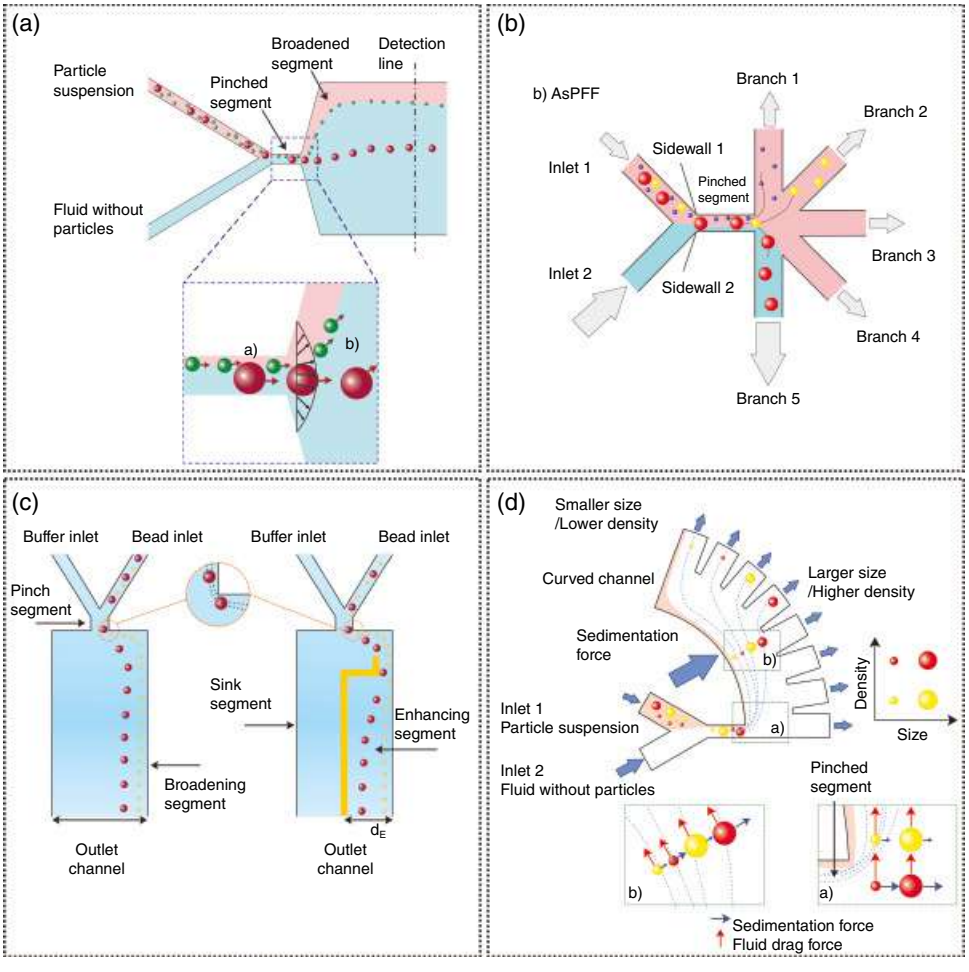

Figure 18.1 (a) First, PFF design is depicted. Depending on the size, particles are pushed toward the wall and positioned in different streamlines. By increasing the distance between streamlines in the broadened segment, particles with different sizes are separated. (b) Asymmetric PFF, (c) PFF with snakelike segment added to increase the distance between the particles, and (d) sedimentation PFF used for size- and density-based separation of particles.

with PFF by increasing the length of the pinched segment [14]. Later, they expand this concept by proposing a device using the concept of elasto-inertial PFF for shape-based separation of particles [15]. In total, PFF devices are simple and have relatively high separation efficiency. Nevertheless, their throughput is usually low, and they require at least one sheath flow to operate the system.

18.2.2 Deterministic Lateral Displacement

DLD is a well-known method for its ability to separate cells and particles based on their size. This device consists of regular rows of micropillar obstacles that each row is shifted to

the right by a specific amount of Δλ. This micropillar pattern will create multiple stagnation points on the way of fluid flow toward the outlet, leading to separate streamlines with inclination angle θ. Consequently, particles of a specific size will strike each pillar and move in θ direction (Figure 18.2a). The smaller particles, however, will not experience the interaction and move directly toward the other outlet [3]. This phenomenon was firstly discovered by Huang et al. [16] as DNA diffused in the arrays of obstacles and has been employed for various purposes such as DNA fragments separation [16], separation of tumor cells [17] or parasite [18] from blood, and exosome separation [19].

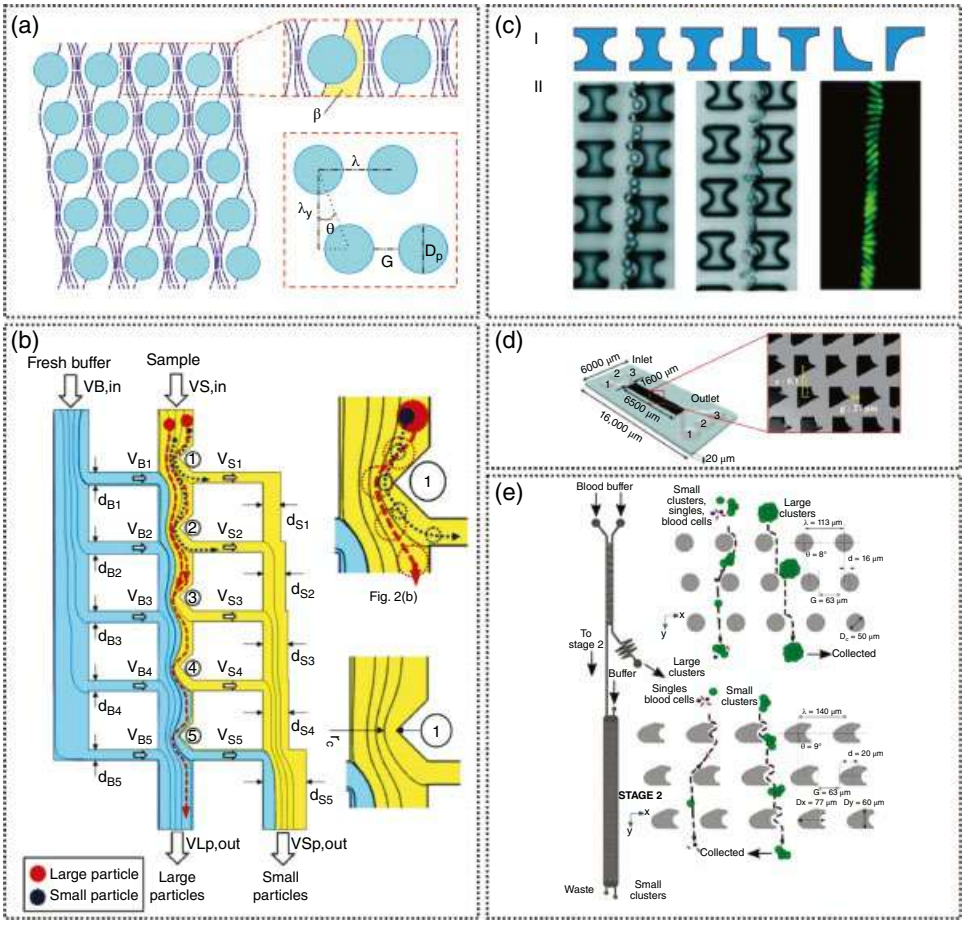

Figure 18.2 (a) Different parameters important for DLD design. Lateral shifting of the rows indicated by angle θ will determine D_c and particle displacement. (b) Single-column DLD device consists of two buffer (blue) and sample (yellow) inlets. Small particles (blue circles) move along with the sample fluid (blue dashed-line) and the larger particles (red circles) that are bigger than the critical diameter remain in the central column (their trajectory is shown by red dashed-line) exit from the large particle outlet [38]. (c) I) DLD posts designed with different shapes, and II) application of I-shaped post to separate RBCs and rod-shaped bacteria [40]. (d) Optimized DLD model with 15.2% increase in efficiency [41]. (e) Separation of clusters of CTCs using a two-stage DLD device [32].

The critical diameter (D_c) is defined as a particle diameter in which the DLD can be operated as a clog-free device. The particle size of smaller and bigger than critical size can be controlled and separated through DLD. D_c is typically smaller than the gap, G, leading to a hasty conversion of the particle migration path [20]. The concept, design, and fabrication of DLD have been thoroughly investigated for more than a decade and adapted for different applications [21]. The working principle of DLD is essentially influenced by three parameters, namely laminar flow, diffusion, and fluidic resistance. At small scales (micro- and nanoscale), the amount of viscous forces surpasses the forces generated by fluid momentum (inertial forces). Therefore, laminar fluid flow is the dominant fluid regime. The fluid behavior can be predicted via the Navier–Stokes equation, in which the nonlinear terms of velocity are neglected.

As the fluid flow is laminar, the streamlines can only mix through diffusion. To investigate the role of diffusion in the particle migration path, the Peclet number (Pe), defined as the ratio of convection to diffusion rate, is given as follows:

$$\mathrm{Pe} = vw / D \tag{18.1}$$

In Eq. (18.1) [22, 23], v, w, and D are delegated to the velocity, the width of microchannel, and the diffusion coefficient, respectively. Using Stokes–Einstein relation, D can be defined as [24]:

$$D = kT / 6\pi\eta a \tag{18.2}$$

where k, T, a, and η refer to Boltzmann constant, absolute temperature, particle hydrodynamic radius, and viscosity. By increasing the Pe number and decreasing the Re number, the mixing time will increase. This phenomenon allows researchers to predict fluid behavior more precisely. For instance, the Pe number for a protein with an approximate size of 5 nm and diffusivity and velocity of 40 $\mu m^2/s$ and 100 $\mu m/s$ traveling through a 100 μm wide channel is 250. It means that this protein requires 25 seconds to diffuse 10 μm across the width of the microchannel [20].

The fluidic resistance is the third dominant force influencing the DLD function, defined as the force generated by the friction between microchannel walls and fluid. An increase in fluidic resistance by reducing the volume to surface area ratio can be considered an essential factor in the flow rate (Q) limitations of DLD. This relationship between the resistance of the microchannels and flow rate is described as follows for a pressure-driven flow:

$$Q = \Delta P / R \tag{18.3}$$

where ΔP is the pressure difference through the length of microchannel, and Q and R are the flow rate and channel resistance, respectively. The resistance R is calculated for a rectangular channel with width, height, and length of w, h, and l, respectively, using Eq. (18.4).

$$R = \frac{12\eta l}{wh^3}\left[1 - \frac{h}{w}\left(\frac{192}{\pi^5}\sum_{n=1,3,5}^{\infty}\frac{1}{n^5}\tan h\left(\frac{n\pi w}{2h}\right)\right)\right]^{-1} \tag{18.4}$$

Eq. (18.4) can be simplified and rewritten for microchannels with a high aspect ratio as Eq. (18.5).

$$R = \frac{12\eta l}{wh^3} \tag{18.5}$$

By employing the abovementioned equations, it can be interpreted that how any change in DLD dimensions can lead to a change in operational flow rate and possible particle sorting time.

Huang et al. [16] and Inglis et al. [25] have investigated the DLD principles for the first time and determined that each lateral displacement of posts can create distinct streamlines, thereby facilitating particle separation. As shown in Figure 18.2a, the streamline right next to the post is the widest streamline (β) due to the no-slip boundary condition and lower velocity. Generally, particles smaller than D_c have a hydrodynamic center inside the first streamline, meaning that they move within the width of the streamline. However, particles with a diameter larger than D_c are inclined to dislocate from one streamline to the next one with an inclination angle, as their hydrodynamic center is outside the first streamline. This inclination angle is denoted by θ, which is the result of rows' lateral displacement. The number of flow lanes between two posts is defined by the number of rows (N) periodically displaced for a certain amount of $\Delta\lambda$. That is, $N+1$ is in a same position as the first row of posts, and N can be described as Eq. (18.6).

$$N = \frac{\lambda}{\Delta\lambda} \tag{18.6}$$

where λ is the center-to-center distance between the obstacles; accordingly, row shift fraction (ε) as presented in Eq. (18.7) is defined as the inverse form of Eq. (18.6).

$$\varepsilon = \frac{\Delta\lambda}{\lambda} = \frac{1}{N} \tag{18.7}$$

In 2016, Zeming et al. [26] have modified the abovementioned equation for the devices in which the lateral displacement (λ) and vertical distance between the posts (λ_y) are of unequal size.

$$\varepsilon' = \frac{\lambda_y}{\lambda}\tan\theta \tag{18.8}$$

This formula depicted the role of downstream gap size in D_c calculations of asymmetrical DLD devices. Therefore, the D_c can be written as:

$$D_c = 2\alpha G\varepsilon' \tag{18.9}$$

where α is dimensionless factor demonstrated by Beech for nonuniform flow in a DLD [24].

In addition to the aforementioned parameters that can affect the critical diameter, there are other factors such as post shape and size [20], device depth [24], fluid properties [27], and cyclicity required to be taken into account for D_c estimation. For instance, by decreasing the depth or obstacle diameter, while other factors are unchanged, D_c will decrease [24].

The theories that have been established for DLD mostly used a small range of particle properties, including rigid spherical particles. However, in reality, particles processed with DLD are mostly cells with the ability to deform and change their shape in response to shear

forces. In this regard, an effective size is introduced for different cells and particles as a substitute for actual size. This effective size is influenced by various factors such as particle–particle and particle–post interaction, mechanical properties, operational flow rate, particle positioning, and shear stress. In DLD systems, it has been shown that at small gaps and high shear stress, cells are inclined to move within the streamlines with their smallest dimension as the critical dimension. This alteration in dimension and repositioning of the particles due to shear rate can be regulated by applying constrictions such as device depth reduction [18, 28]. Particle concentration is another factor that can impact particle–particle and particle–post interaction, fluid flow disturbance, and particle deformation. Although DLD systems rely on the interaction between particles and posts, particle–particle interaction caused by increased concentration decreases separation efficiency [29].

DLD devices were mainly used for particle separation based on their size disparity. However, it has been revealed that DLD has the potential to be used for the separation of particles based on other features such as deformability and electrical properties. One well-known application of DLD is the separation of blood components such as white blood cells [30] and platelets [31] with relatively low cost. CTCs are other components that can be effectively isolated using DLD. For example, Au et al. reported a 99% recovery with 87% viability of CTC clusters using a two-stage DLD device [32]. In addition to the separation of microscale particles, a limited number of documents have reported the DLD potentials as a tool for the separation of nanoscale particles, including DNA molecules, exosomes, and proteins [33, 34]. Using chemical treatments [26], external forces [35, 36], and nanofabrication technique, DLD can be effectively employed as a nanoparticle isolation platform. For example, polyethylene glycol (PEG) is used to pack the genomic DNA molecules down to reduce the size and increase the shear modulus [37]. Wunsch et al. also developed a nanofabrication process to downscale DLD for the purpose of exosome sorting [19]. To increase the throughput, Liang et al. have also introduced a new DLD design with the ability to separate 4.8 μm from 9.9 μm particles at tenfold flow rates (Figure 18.2b) [38]. In another study, Hyun et al. presented an optimized DLD in which the gap between the posts increased without reducing the efficiency. As a result of the gap increase, the probability of the clog formation decreased, and the device was able to maintain high separation efficiency for a long period of time. Despite all the advances in the field of nanofabrication, there are still complexities in fabrication and drawbacks such as low throughput in DLD devices [39].

To separate nonspherical particles, researchers have designed and examined DLD systems with different obstacles' shape and arrangement. In 2014, Ranjan et al. have investigated the role of different shapes of posts in the separation efficiency of nonspherical particles. They designed I-shape, L-shape, inverted L-shape, and anvil shape obstacles and assessed their role in separating particles with different shapes (Figure 18.2cI). Their results revealed that protrusions and grooves could create different pathways, thereby controlling and restricting particle trajectories and orientations (Figure 18.2cII) [40]. In 2018, Bech et al. also revealed that particles with different lengths could be separated using an optimized DLD design (Figure 18.2d) [41].

As DLD systems are mainly utilized for biological samples, the deformability of the cells is of irrefutable importance in the estimation of critical diameter and separation efficiency. Flow rate, fluid properties such as viscosity, pathways dimensions, and shear rate are proved to be influential on the separation efficiency of deformable bio-particles [42–44]. As

it was proved that stiffer particles are more inclined to displace between the posts [45], Kruger et al. showed that diseased red blood cells could be isolated from healthy red blood cells in malaria patients [46]. Also, Au et al. developed a two-staged DLD device consisting of a conventional DLD with circular posts and an optimized DLD for CTCs separation. Large CTC clusters were separated from other blood components in the first DLD stage, and the remaining smaller ones were separated in the second stage of the DLD device (Figure 18.2e) [32].

18.2.3 Microfiltration

Microfiltration is a well-known technique for the separation of particles and cells based on their size. This approach can be divided into three groups of membranes, pillars, and weirs (Figure 18.3a–c). Based on the flow direction also, this method can be classified into the two groups of cross-flow and dead-end filters (Figure 18.3d and e). In the cross-flow filters,

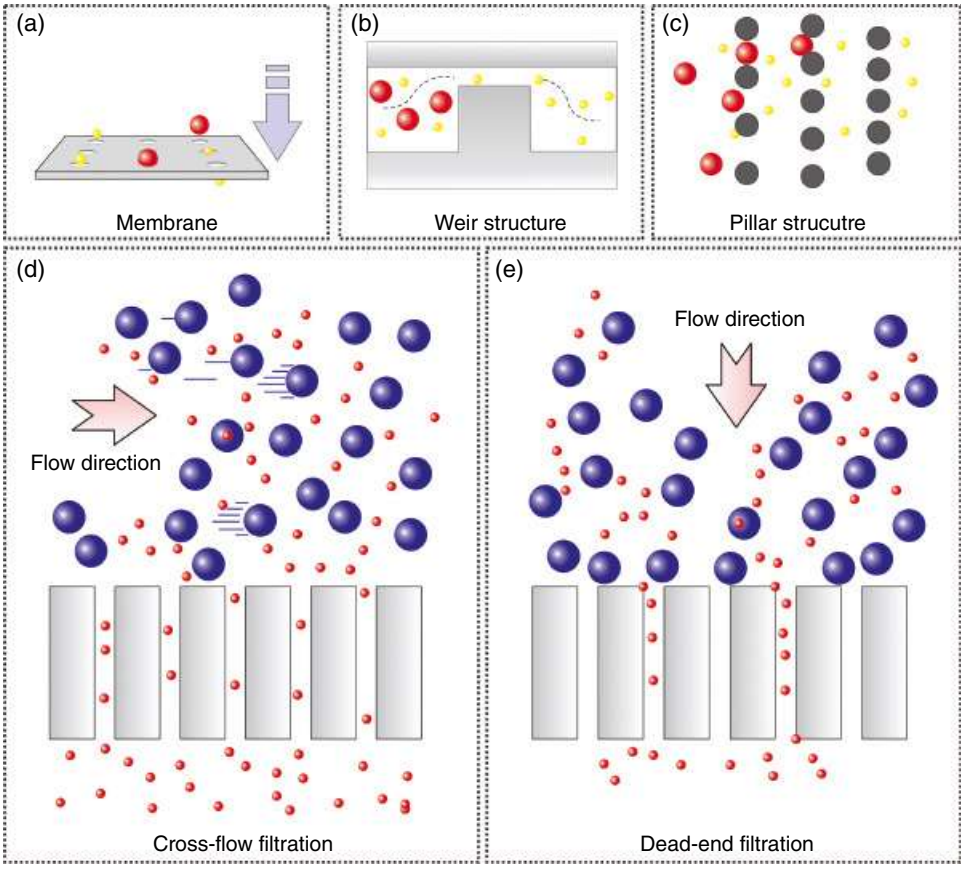

Figure 18.3 Schematic illustration of (a) membrane-based, (b) weir-based, and (c) pillar-based as three categories of microfiltration methods. Microfilters also classified into the two modes of separations which are (d) cross-flow filtration and (e) dead-end filtration. Dead-end filtration is more efficient for the separation of large particles at the risk of clogging.

the main stream is parallel to the filter surface, while in the dead-end filters, the streamlines are perpendicular to the filter direction. For capturing large particles, dead-end filters are more efficient; however, they suffer from clogging issues. Cross-flow filters can address this issue by washing large particles from the filer.

The first membrane filters have been used in the late 1980s for the separation of particles up to 50 nm size [47, 48]. First attempts at designing the membrane filters were mainly utilized as dead-end filtration type [47]. Nevertheless, recently, more attention has been devoted to the design of cross-flow membrane filters. For instance, Aran et al. developed a membrane-based cross-flow filtration device for the continuous separation of plasma from whole blood [49]. The device was fabricated using two PDMS layers and a 200 nm polycarbonate porous membrane. Blood components cannot pass through the membrane, and pure plasma and proteins can be extracted from the device. Through parallelization, this device can separate 2.5 mL of pure plasma from whole blood in 4 hours.

Pillar and weir filters, similar to membrane-based microfilters, have been extensively used to separate wide ranges of cells and particle in both modes of cross-flow and dead-end filtrations. As an example, Wilding and colleagues have used micropillars and weir filters for the separation of WBCs and RBCs [50]. For small cells and particles, this gap must be adjusted in a way to eliminate the clogging issue. As a result, the flow rate in these types of devices is usually low. Benefiting from this concept, Wu and colleagues have proposed a weir filter for the blood plasma separation [51].

All examples mentioned so far are based on the assumption that cells are rigid. Nonetheless, in reality, cells are not rigid, and their stiffness impact upon the device performance. This has been the subject of many studies for the separation of cells [52, 53]. For instance, straight channels with ridges have been used to separate live Jurkat cells from dead ones based on the stiffness difference between them [54].

18.2.4 Inertial and Dean Drag Forces

Inertial microfluidics defines the positioning of randomly dispersed particles toward certain equilibrium positions. This phenomenon was first observed by Segre and Silberg [55], but in the last decade, it gained a significant amount of attention and progressed massively [56, 57]. The effect of inertial force on particles in straight channels is usually described by channel Reynolds number (Re_c) (Eq. (18.10)) as the ratio of inertial and viscous force and particle Reynolds number (Re_p) (Eq. (18.11)) [58].

$$\mathrm{Re}_c = \frac{U_m D_h}{\nu} \tag{18.10}$$

$$\mathrm{Re}_p = \mathrm{Re}_c \frac{a^2}{{D_h}^2} \tag{18.11}$$

Here, D_h is the hydraulic diameter of the channel that can be calculated by $4A/P$ (A is the area channel cross-section and P is the wetted perimeter of the channel cross-section), U_m is the maximum fluid velocity, ν is the kinematic viscosity, and a is particle diameter. In a straight channel, inertial lift force has two components, shear gradient and wall-induced lift force. Shear gradient lift forces generate due to the velocity difference between the

middle and wall of the channel and push particles toward the channel wall. On the other hand, when particles move toward the wall, wall-induced lift forces repel particles from the wall. The balancing of these two forces defines the equilibrium position of particles [59]. The magnitude of inertial lift force, F_L, applied on a particle can be calculated using Eq. (18.12).

$$F_L = \rho\left(\frac{U_m}{D_h}\right)C_L a^4 \tag{18.12}$$

where C_L is dimensionless lift coefficient number and depends on the initial position of particles and channel Reynolds number. These cases are for rigid particles. Deformable particles experience another lift force that pushes them away from the particle wall. The balance of deformability-induced and inertial lift forces defines their equilibrium position. In straight channels with circular cross-sections, particles migrate to an annulus ~ 0.6 times the radius (Figure 18.4a). Changing the channel cross-section to square (aspect ratio of 1) reduces particle focusing positions to four points at the center of each wall (Figure 18.4b). In rectangular channels as the most widely used channel cross-section, however, particles show two-stage migration, and the focusing positions reduce to two points at the center of long walls (Figure 18.4c) [59]. In straight channels, the migration velocity of particles and focusing length can be calculated by Eqs. (18.13) and (18.14), respectively.

$$U_L = \frac{\rho_f U^2 a^3}{6\pi\mu H^2} \tag{18.13}$$

$$L_{\min} = \frac{3\pi\mu H^3}{\rho_f U a^3} \tag{18.14}$$

Straight channels have been considered as the fundamental channel for most inertial studies and are used for various applications [60]. For instance, the focusing principles in straight channels have been used to generate new flow cytometry devices with the capability of counting and differentiating different cells [61]. Bhagat and colleagues show the potential of continuous particle filtration and extraction within a straight rectangular channel [62].

A change in the channel shape from straight to curve, serpentine, curvilinear, or contraction and expansion arrays of microchannels leads to the generation of additional force called Dean drag force. For a curve channel, Dean drag force can be calculated by Eq. (18.15).

$$F_D = 5.4\times10^{-4}\pi\mu \mathrm{De}^{1.63}a,\ \mathrm{De} = \mathrm{Re}\sqrt{D_h/2R} \tag{18.15}$$

where R is the curvature radius and De is the Dean number and defines the distribution and strength of Dean force. The secondary velocity generated within the channel can be approximated by $1.8\times10^{-4}\times{F_D}^{1.63}$. In spiral channels, Dean number, channel aspect ratio, and the ratio of channel dimensions to curvature radius significantly affect the distribution of secondary flows and, as a result, particle focusing [63, 64]. In inertial microfluidics, spiral microchannels have been investigated significantly. Most of the particle sorting and

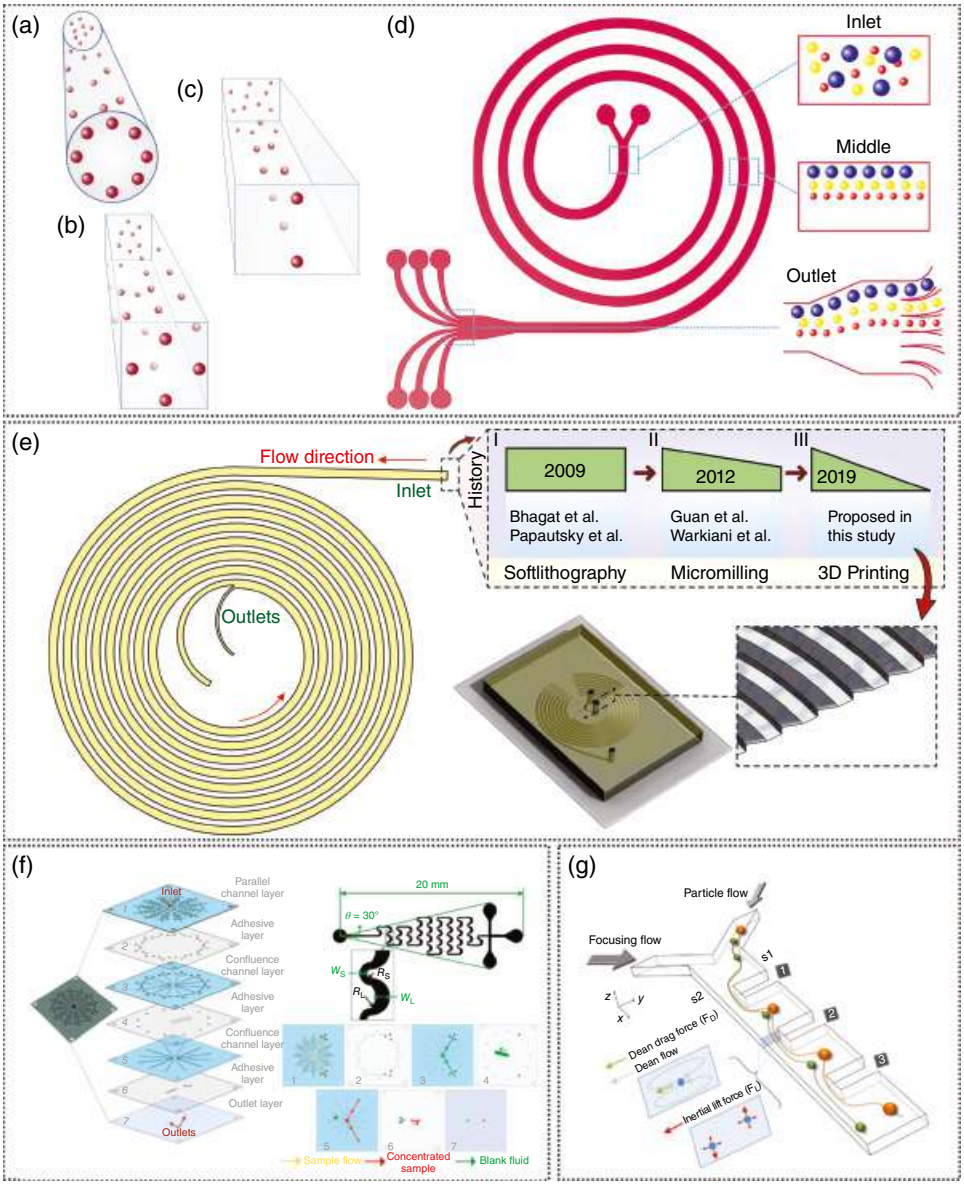

Figure 18.4 Inertial migration of particles in (a) straight circular, (b) square, (c) rectangular, and (d) spiral microchannel. (e) Fabrication of spiral inertial microfluidic channel with right-angled triangular cross-section using additive manufacturing method [72]. (f) A polymeric multilayer inertial microfluidic device for algae dewatering [77]. (g) Inertial microfluidic phenomena in contraction–expansion arrays of microchannels [79].

separations are applied with spiral channels. One of the most significant benefits of spiral channels is their capability to run with high throughput. Based on the principles of particle focusing in spiral channels, Bhagat et al. proposed a sheathless flow cytometry system capable of processing 2100 particle/s [65].

Based on Eqs. (18.12) and (18.15), the force that is imposed on each particle is related to the particle diameter ($F_L \propto a^4$, $F_D \propto a$), indicating that particles with different sizes occupy various focusing positions in the channel cross-section and can be collected from their assigned outlet (Figure 18.4d). Hence, particle and cell sorting become one of the main applications of spiral microfluidics. Kuntaegowdanahalli et al. demonstrated the potential of spiral microfluidics for simultaneous separation of 10, 15, and 20 μm particles with > 90% separation efficiency using a spiral channel with a rectangular cross-section. Sun et al. proposed a double spiral microchannel that can isolate cancer cells from blood [66]. They claim that the double spiral device can improve the separation efficiency and works better for smaller particles. Xiang et al. employed a spiral microchannel with five loops with rectangular cross-section of 50 μm height and 150 μm width. They showcased the application of the channel for high-throughput blood cell focusing and plasma isolation [67]. Changing the channel cross-section from rectangular to trapezoidal can further increase the separation resolution. Rzhevskiy et al. demonstrate the use of a trapezoidal spiral microchannel with a width of 600 μm, the inner wall of 90 μm, and the outer wall of 140 μm for prostate cancer cell separation from the urine of patients [68]. Also, Condina and colleagues proposed a trapezoidal spiral channel for efficient and high-throughput separation of yeast cells from beer spoilage microorganisms to improve the limit of detection of beer spoilage bacteria in beer samples [69]. Recently, with the massive improvement of additive manufacturing and its combination to microfluidics, spiral with cross-sections rather than rectangular and trapezoidal has been proposed [70, 71]. For instance, Razavi Bazaz et al. have fabricated a novel spiral microchannel with a right-angled triangular cross-section using DLP 3D printing method (Figure 18.4e). The channel has the capability of focusing particle along the side of the triangle, appropriate for flow cytometry and sample dewatering [72]. Apart from straight and spiral channels, serpentine and curvilinear channels have been used frequently for various applications. These channels gain significant attention as they have enhanced particle focusing ability, small footprint, and huge parallelization potential. In these channels, the alternating direction of the curvature leads to unsteady secondary flow generation in an intricate behavior. Usually, three focusing patterns are observed in these channels. By increasing the flow rate, modes of particle focusing changes from double side focusing to transition and then single line focusing. This focusing pattern depends on the particles' size and can be used for separation of particles with different sizes where one is in the double line focusing mode while the other one is in the single line focusing mode [73].

Di Carlo et al. was the first who investigated particle focusing in an asymmetric curvilinear channel and reveal that the focusing of particles reduces to one position within these channels [74]. Later, Zhang et al. investigated the complete mechanism of particle focusing in curvilinear channels [75]. Inertial focusing in these channels can successfully order cells and particles with well-defined particle focusing, appropriate for such applications as particle concentrating, flow cytometry, and single-cell stretching. Square wave microchannels have also been used for inertial particle focusing. Zhang and colleagues showed blood plasma extraction with a purity of > 99% at a flow rate of 350 μL/min. The system was further parallelized to reach the flow rate of 2.8 mL/min and throughput of 7×10^8 cells/min [76]. Recently, Xiang et al. reported a novel multilayer inertial microfluidic device consisting of asymmetric curvilinear channels with the throughput of 8 mL/min for concentrating Algae cells (Figure 18.4f) [77].

Channels with contraction–expansion arrays are indeed straight channels with adding or subtracting a specific geometry. These channels can be asymmetric or symmetric if the contraction–expansion arrays are all on one side or both sides of the channel. These channels are capable of separating particles with different sizes due to the prolonged impact of Dean drag and inertial forces. Also, these systems can be operated with or without sheath flow [58]. Using symmetric contraction–expansion arrays of microchannels, the isolation of Malaria parasites from blood has been demonstrated [78]. Lee et al. have been used asymmetric contraction expansion arrays of microchannels for blood plasma separation and various cancer cells. They showed that the aspect ratio less than 1 is ideal for these systems [79]. Using the same concept, Kim and colleagues proposed a microfluidic channel for the separation of microalgae using a contraction–expansion array microchannel. They showed that they could successfully separate *Chlorella vulgaris* from *Haematococcus pluvialis* with more than 95% purity [80].

18.3 Active Microfluidic Cell Sorting Systems

18.3.1 Acoustic-Based Separation

Acoustic separation within microfluidic devices is a method in which particles are manipulated via acoustic forces. These forces are generated by acoustic waves. In general, acoustic waves are divided into two varieties of surface acoustic waves (SAWs), including traveling surface acoustic waves (TSAWs) plus standing surface acoustic waves (SSAWs), and bulk acoustic waves (BAWs) [81]. The SAWs that scatter in one direction and spread away from the acoustic sources are denominated TSAWs, illustrated in Figure 18.5a. Two opposite TSAWs interfering or reflecting TSAWs, which create fixed nodes and antinodes in an unclosed or bounded domain, generate SSAWs, as displayed in Figure 18.5b [82]. Propagation of the acoustic standing waves in a microfluidic channel induces primary acoustic forces exerted on particles, which can be actively employed for particle manipulation. In acoustic separation based on employing SAWs, ultrasonic standing waves can be formed with two opposing sound sources or using a single transducer fronting a sound reflector. Generally, piezoceramic elements are used as the ultrasonic sources, and they can be coupled directly or through a coupling layer into the liquid [83]. Acoustic waves, formed within a piezoelectric element, such as interdigital transducers (IDTs) patterned on a piezoelectric substrate, through the transduction of electric fields, scatter within and onward to the material boundaries [84, 85]. In contrast to SAWs that spread along the surface of a material, BAWs propagate inside the resonant chamber of the microchannel within the bulk of a material, as shown in Figure 18.5c [86]. Therefore, to obtain similar acoustic effects within microfluidic devices, a higher level of energy is required. In this manner, piezoelectric transducers are tied to the microchannels and operated with an AC power supply to generate BAWs inside the microfluidic devices [87]. Although SAW systems have more precision in terms of particle positioning, BAW devices are able to create a faster movement of particles [88, 89]. Moreover, since BAWs can easily propagate within the channels made of hard materials such as silicon, BAW-based acoustophoresis has gained more attention [86].

Generally, suspended particles are affected by induced Stokes drag force (F_{drag}) in a streaming flow. At low Reynolds numbers, F_{drag} acting on a suspended particle is calculated

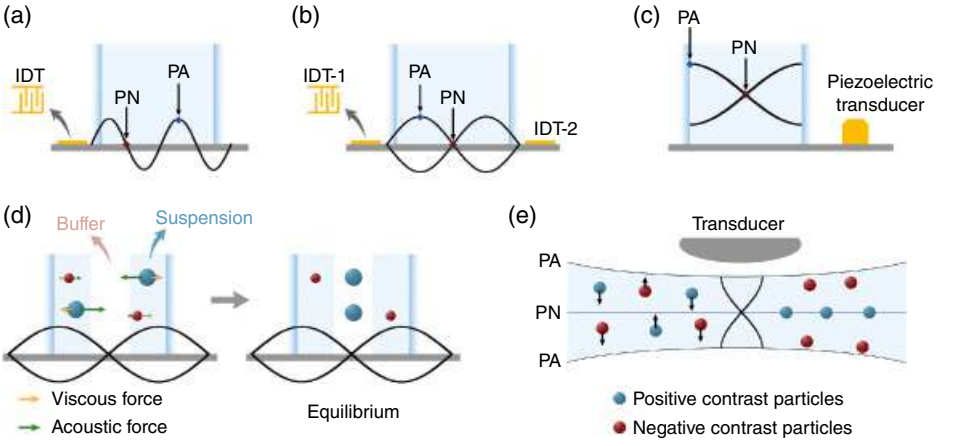

Figure 18.5 (a) Schematic illustration of traveling surface acoustic waves (TSAWs) propagation in a microfluidic channel cross-section [81], (b) schematic illustration of standing surface acoustic waves (SSAWs) propagation in a microfluidic channel cross-section [81], (c) schematic illustration of bulk acoustic waves (BAWs) propagation in a microfluidic channel cross-section [81], (d) positioning the particles by the acoustic and drag forces, where the larger particles are shifted to the center, and the smaller ones are moved to the edges [93], and (e) separation of particles based on their acoustic contrast factor in a BAW-based device, where positive contrast particles are positioned in pressure node, and negative contrast particles are shifted to the pressure antinodes [92]. PN intimates the pressure node, and the PA indicates pressure antinode.

by Eq. (18.16), in which μ is the fluid viscosity, R_p is the radius of the particle, and v donates the relative velocity between fluid and particles.

$$F_{\text{drag}} = -6\pi\mu R_p \upsilon \tag{18.16}$$

In the acoustic-based separation methods, employing the acoustic wave makes it possible to spatially control the positioning of particles in continuously streaming microfluidic channels. Acoustic waves propagating through the liquid generate a pressure gradient that produces the acoustic force, including an axial and a transverse component. The axial acoustic force, F_{axial}, pushes the particle to the node or antinode of the acoustic field. Commonly, F_{axial} is observed in the SSAW-based separation methods, along with the propagating direction of the acoustic waves, which can be calculated by Eq. (18.17) [81, 90].

$$F_{\text{axial}} = -\left(\frac{\pi P_0 V_p \beta_{c_m}}{2\lambda}\right) \varnothing\left(\beta_c, \rho\right) \sin\left(2kx\right) \tag{18.17}$$

$$\varnothing = \frac{5\rho_p - 2\rho_m}{2\rho_p + \rho_m} - \frac{\beta_{c_p}}{\beta_{c_m}} \tag{18.18}$$

where P_0, V_p, λ, k, x, ρ, and β_c correspond to the pressure amplitude, particle volume, wavelength, wave vector, distance from the maximum pressure amplitude to the minimum pressure amplitude, density, and compressibility, respectively. Also, ϕ indicates the acoustic contrast factor, which can be calculated by Eq. (18.18). The p and m subscripts symbolize

particles and medium, respectively. Balancing the acoustic and viscous force determines the positioning of the particles, as illustrated in Figure 18.5d. When the particle moves to the position of the pressure node, the axial component of acoustic force is negligible, and the transverse component (F_{trn}), calculated by Eq. (18.19), pushes the particles close to each other in the nodal plane [81, 91]. As identified by Eq. (18.19), F_{trn} is directly dependent on the gradient of the acoustic energy ($\nabla\langle E_{ac}\rangle$).

$$F_{trn} = 3d_p^3 \frac{\rho_p - \rho_m}{2\rho_p + \rho_m} \nabla\left(E_{ac}\right) \tag{18.19}$$

Regularly, BAW-based devices work at a low frequency and a long wavelength, which is beneficial for the handling of larger particles. In this method, smaller particles are shifted by the induced drag force, while the larger particles are manipulated by the acoustic force. However, smaller particles can be directly manipulated by scaling down the device size and scaling up the frequency. In this case, BAW-based separation systems are usually used to isolate particles based on their size differences [86]. Moreover, Fornell et al. demonstrated the possibility of separating various particles with different acoustic contrast factors within a water-in-oil droplet. They proved that in BAW-based microfluidic devices, positive acoustic contrast particles are shifted to the pressure node, and negative acoustic contrast particles are directed to the pressure antinodes, as shown in Figure 18.5e [92]. Furthermore, the mechanical vibrations of the walls in BAW-based separation devices excite waves in microfluidic channels at geometrically determined resonant frequencies. These waves generate higher pressure amplitudes compared with SAW-based devices. Hence, BAW-based microfluidic devices supply a faster acoustophoretic movement of particles than SAW-based systems [89].

By considering the mentioned details about each method employed for acoustic separation of the particles within microfluidic channels, it has been noticed that the SAW-based microfluidic separation method has the following advantages compared with the BAW-based microfluidic devices. The first is the ability to control excitation frequencies in a wide range so that utilizing higher excitation frequencies make it possible to precisely control particles and their medium. Also, channels made of materials with high acoustic reflection are not required, which allows the fabrication of microfluidic devices with a wide range of polymers. Due to the convenient fabrication of SAW-based microfluidic separation devices through standard micro and nanofabrication processes, these systems are more versatile for mass production. Moreover, since SAWs propagate on the surface instead of the bulk of the device substrate, they need a lower amount of power supply to have the same effect as BAWs have [94].

Based on Eq. (18.18), the differences in physical properties, such as compressibility and density, between the particles and their surrounding medium causes the transformation of particles by generated acoustic wave forces [83]. Moreover, numerical studies are widely suggested for improving the separation efficiency of acoustic-based separation in microfluidic devices. For example, Shamloo et al. numerically simulated the influence of varying the amplitude of the acoustic field as a result of the applied voltage on the performance of the blood component separation [95]. Also, by considering Eqs. (18.17) and (18.19), the particle properties, including the particle size, compressibility, acoustic properties, and

density, determine the positioning of them in the microchannel [96, 97]. It was proved that displacing particles to distinct size-dependent streamlines make it possible to differentiate multiple types of particles, such as vesicles, by their size profile. It is caused by various acoustic forces, which are proportional to the volume of particles. Nam et al. presented a density-based acoustic separation in the microchannel, which confirmed that beads with a similar size but different densities are focused in the center of microchannels through hydrodynamic forces [90]. In their study, however, as SSAWs propagate, monodisperse particles are separated and shifted toward the sidewalls due to their density. Based on the proposed method, they successfully separated alginate beads with equal size but different in the number of encapsulated cells.

Employing acoustic waves offers contact-free manipulation of the particles from different sizes and densities. The separation occurs within microfluidic channels by tuning the frequency and the magnitude of acoustic waves beside the induced drag force of the fluid flow [98]. Based on the specified advantage, the potential for sample contamination reduces. It is noteworthy that in acoustic-based microfluidic separation devices, acoustic waves in the range of ultrasonic power intensity and frequency are employed. Ultrasonic waves are widely used in biomedical applications, such as ultrasonic imaging [94]. As ultrasonic waves hardly damage biological tissues, using this range of acoustic waves emerged as a safe and biocompatible method for particle manipulation [99]. Moreover, utilizing acoustic waves for acoustic focusing eliminates the requirement of the sheath flows in particle manipulation. Hence, focused bioparticles can remain in their native fluids and are not diluted, which can minimize the shocks from the buffer and eliminate the concentrating step [100].

Functionalities of acoustic-based separation devices, such as high biocompatibility and ease of preparation and test procedure, provide the possibility toward cellular and subcellular particles manipulation. For instance, a compact microfluidic system was designed to integrate size-based acoustic separation with biomarker expression-based immunolabeling for cell analysis toward whole blood investigations [101]. The proposed device offered integration of complete hematological separation of about 100% trapping efficiency of spiked polystyrene beads plus MCF-7 cells and on-chip immunofluorescent labeling. Additionally, a plastic-based acoustofluidic device was used to separate the platelet sample from undiluted human whole blood, which established a sample throughput of 20 mL/min, an RBC and WBC removal rate of 88.9%, and a platelet recovery rate of 87.3% [102]. Evaluating the platelet activation level, hypotonic shock response (HSR), platelet aggregation activity, and morphology in the cited research presented a better quality for the isolated platelets than those separated using the gold standard methods, such as centrifugation. Furthermore, acoustic-based devices have been recognized as reliable and high-throughput systems for the isolation and separation of rare cells, such as CTCs. Zheng et al. developed a multistage acoustic microfluidic device to separate CTCs from blood cells, as presented in Figure 18.6a, containing a pair of straight IDTs and focused interdigital transducers (FIDTs) [103]. Based on the proposed method, they were able to separate $90 \pm 2.4\%$ of U87 glioma cells from RBCs. Due to the size variations between blood cells and bacteria, acoustofluidic devices emerged as a reliable option toward the separation and identification of pathogenic bacteria for sepsis diagnosis. For example, a study on the isolation of E. coli from human blood samples using a tilted-angle standing surface acoustic wave (taSSAW) field, as shown in

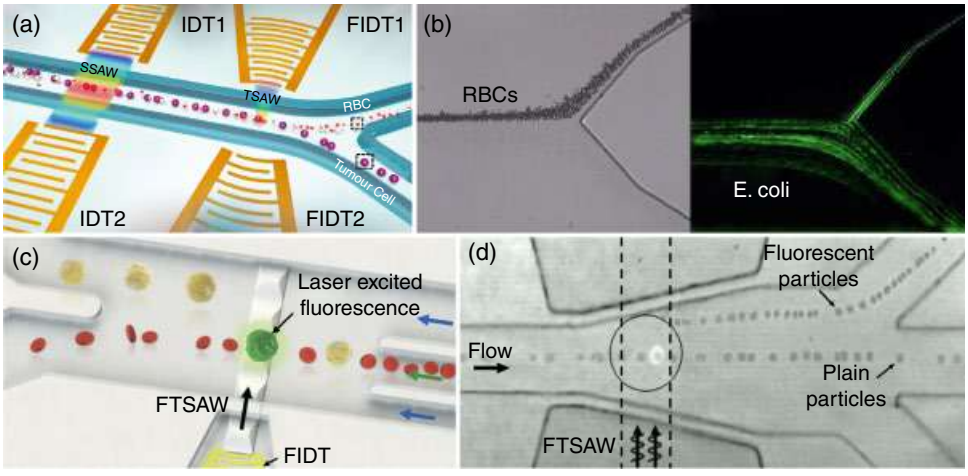

Figure 18.6 (a) Utilizing a multistage acoustic microfluidic device for CTCs separation, containing a pair of straight interdigital transducers (IDTs) and focused interdigital transducers (FIDTs) [103], (b) E. coli isolation using a tilted-angle standing surface acoustic wave (taSSAW), left is the bright-field and right is the fluorescence image representing RBCs and E. coli following taSSAW apply [104], (c) sorting of fluorescently labeled micron-sized particles and biological cells by applying focused traveling surface acoustic wave in an A-FACS device [110], (d) a sheathless A-FACS system taking advantage of elasto-inertial cell focusing and traveling surface acoustic wave (FTSAW) for cell separation [111].

Figure 18.6b, demonstrated the purity of more than 96%, enabling more sensitive and specific detection of pathogens from biofluids in the detection unit [104].

It is worth mentioning that acoustofluidic separation technology has the capability of submicron scale isolation. For example, a developed acoustic-based microfluidic system is used for label-free and continuous filtration of microvesicles [105]. Wu et al. produced an acoustofluidic chip for label-free and contact-free isolation of exosomes in a single chip integrated with two acoustofluidic modules [106]. In their stated device, exosomes, which are nanoscale extracellular vesicles (EVs) approximately 30 to 150 nm in diameter, separated from whole blood with a blood cell removal rate of over 99.999%. Following that, Wu et al. designed an acoustofluidic system for the label-free and biocompatible separation of EVs plus lipoprotein subgroups [107]. In their proposed device, isolation happened based on vesicles and lipoprotein acoustic properties, which exhibit negative contrast as oppose to positive contrast. A novel approach called diffractive-acoustic surface acoustic waves (DASAW) was proposed for continuous particle focusing at the micron and submicron size. This method allows for continuous focusing on a variety of channel shapes. Moreover, in the DASAW method, particles above an acoustic-contrast-factor-dependent size migrate to channel edges, where the acoustic radiation force is dominant. Due to the no-slip boundary condition, particles near the channel edges experience a lower flow velocity, which maximizes their time exposed to the acoustic field [108].

Integrating acoustic wave with fluorescence-activated cell sorting (FACS) systems, instead of electrical-based forces as declared for the E-FACS systems, enables higher throughput, optimal sorting purity, and reliable cell viability in cell separation. In the last

decades, acoustic-based fluorescence-activated cell sorters (A-FACS) have been proposed by using the piezoelectric substrates for acoustic wave generation [109]. In the A-FACS method, sorting does not require magnetic or dielectric labeling of cells. Also, it is independent of the electrolytic buffer utilized to suspend the cells, which simplifies the manipulation of cells and biohazardous materials. For instance, Schmid et al. produced a versatile SAW-actuated microfluidic sorter based on the A-FACS technique with sorting rates as high as several kHz (3000 cells/s) [109]. Their study proved the biocompatibility of the stated method as only low shear forces were needed for cell sorting, while fluid volumes had switched instead of applying forces directly to the desired cells. Also, it was demonstrated that in the A-FACS method, by employing SAW, cells can be directly sorted from the medium without prior encapsulation into drops. Lately, Ma et al. fabricated a benchtop scale A-FACS system, as displayed in Figure 18.6c, which facilitated the sorting of micron-sized particles and biological cells, such as cancer cells, using about 50 μm focused traveling surface acoustic wave (FTSAW) [110]. Also, they numerically investigated the isolation and sorting mechanism of micron-size particles and cells, which were exposed to a focused traveling acoustic field. By employing the A-FACS method, they attained to separate fluorescently labeled breast cancer cells from diluted whole blood samples with a purity of higher than 86% without generating aerosols. Recently, Li et al. proposed a sheathless A-FACS system, as shown in Figure 18.6d, which took advantage of elasto-inertial cell focusing and highly (about 50 μm wide) FTSAW for cell separation without sample dilution [111]. Through the fabricated A-FACS system, sorting of cells with both purity and recovery rate of about 90% were achieved besides maintaining high cell viability, only 3–4% lower than using a commercial FACS machine.

In summary, acoustic-based microfluidic devices have been successfully employed for the separation of blood cells, cancer cells, bacteria, and submicron EVs. In these devices, by controlling acoustic and drag forces, particles can be separated based on their size, density, compressibility, and acoustic properties. Advantages of this method include being contact-free, label-free, biocompatible, highly controllable, high-throughput, and versatile, which made these systems a reliable option for biological research and clinical usages.

18.3.2 Electric-Based Separation

Electrical separation within microfluidic devices is a noninvasive and label-free method in which particles are manipulated using the electrokinetic effects of an electrical field [112]. In this method, particles suspended in a fluid are carried by an electrical effect, which enables their selective manipulation and separation. The separation process in this method can be divided into electrophoresis (EP), dielectrophoresis (DEP), and electric-based fluorescence-activated cell sorting (E-FACS), which will be discussed in the following paragraphs.

The separation of particles in EP occurs using uniform direct current (DC) voltage applied to two electrodes. In an EP-based microfluidic device, the particle trajectory is determined by hydrodynamic drag and electrophoretic forces. Hydrodynamic drag force is induced by the applied pressure-driven and electroosmotic flow, which is in parallel and opposite directions of the electrophoretic force [113]. The electric field, E, at a point between anode and cathode, is equivalent to the electric force (F_e, also known as

electrostatic force or Coulomb force) per unit charge (q) (Eq. (18.20)). The electric force F_e is also known as the electrostatic force or Coulomb force [114].

$$E = \frac{F_e}{q} \tag{18.20}$$

F_e is a force that a particle in the electric field experiences. q is a scalar quantity that has either positive or negative magnitude without any direction. However, the electric force F_e and E are vectors. In this case, if q has a positive charge, F_e will act in the same direction as E, but if q has a negative charge, F_e and E will be in opposite directions. In devices based on EP, particles are isolated due to the magnitude of their charges and the electrical field, as shown in Figure 18.7a [114].

In contrast to the EP method with a fixed electric charge, the separation in the DEP technique depends on the generation of induced surface charges related to the intrinsic dielectric properties of the particle and its surrounding medium [115]. Also, both DC and alternating current (AC) fields can be employed, but the field applied must be nonuniform [114]. Applying an electric field on a polarizable particle suspended in a conductive medium causes a redistribution of charges on the particle surface and its surrounding medium, which induces a dipole on the particle. In a nonuniform electric field, the particle experiences a net force inducing translational motion of the particle called dielectrophoretic force [112]. DEP devices can contain embedded electrodes or be electrodeless. Electrodes are created by lithographic processes, and the device can include numerous planar electrode configurations. In this manner, electrodes enable the high electric fields and field gradient creation with a relatively low applied potential. Also, they are compatible

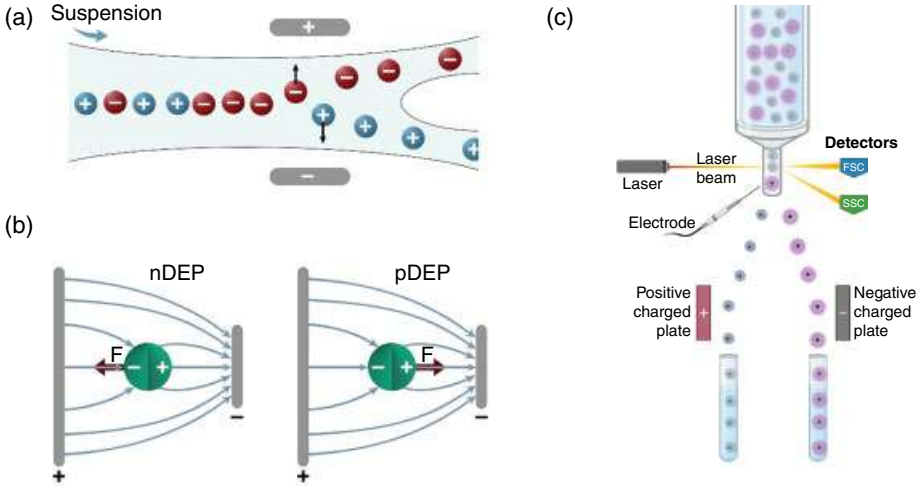

Figure 18.7 (a) Electrophoresis-based separation of particles based on their charges and the magnitude of a uniform DC electrical field, (b) In negative DEP, the dielectrophoretic force moves the polarized particles toward the lower electric field (on the left), and in positive DEP, the dielectrophoretic force pushes the polarized particles in the higher electric field direction (on the right) [119], and (c) Schematic illustration of E-FACS method. Droplets containing targeted cells are deflected by an electric field, after identifying in a flow cytometer system.

with the high-frequency operation of about 10^4 Hz. In electrodeless or insulative DEP, electrodes are placed in external reservoirs. It provides DEP devices' actuation with both AC and DC electric fields, also at low frequencies [116].

Generally, particles in the DEP method are affected by F_{DEP} (Eq. (18.21)), where ε_m is the absolute permittivity of the surrounding medium, R determines the particle radius, E denotes the amplitude of the electric field, and ∇ represents the gradient operator. Also, CM implies the Clausius–Mossotti factor related to the effective polarizability of the particle, which was precisely discussed in reference [117] and refers to the real component of the Clausius–Mossotti factor calculated by Eq. (18.22) [118]:

$$F_{\mathrm{DEP}} = 2\pi\varepsilon_m R^3 \mathrm{CM}\left(\nabla E^2\right) \tag{18.21}$$

$$\mathrm{CM} = \frac{\varepsilon_p^* - \varepsilon_m^*}{\varepsilon_p^* + 2\varepsilon_m^*} \tag{18.22}$$

where ε_p^* and ε_m^* indicate the complex permittivity of the particle and the medium, respectively. Furthermore, the complex dielectric constant can be calculated by Eq. (18.23) [119], where j is $\sqrt{-1}$, ε refers to the dielectric constant, σ indicates conductivity, and ω means the angular frequency of the applied electric field.

$$\varepsilon^* = \varepsilon - \frac{j\sigma}{\omega} \tag{18.23}$$

DEP can be categorized into positive and negative modes, which pushes particles toward strong or weak field regions, based on the CM factor sign, as presented in Figure 18.7b [120]. In the positive DEP, particles migrate to a region of the stronger electric field, closed by the electrodes, while they have a higher permeability than the surrounding fluid, $\mathrm{CM} > 0$. Conversely, in negative DEP, particles having lower permeability than the surrounding fluid, $\mathrm{CM} < 0$, are shifted far from the greater electric field [121].

Since the dielectrophoretic force scales with the radius of the particles (Eq. (18.21)), it is approved as a suitable method for the size fractionation of cells and particles. Zhou et al. numerically investigated the particle electrophoretic motion due to the effect of DEP force employing a time-dependent arbitrary Lagrangian–Eulerian finite element numerical model [122]. It revealed that in both Newtonian and viscoelastic fluids, particles with different sizes own different trajectories, which can be used for continuous manipulation of the biological particle within the microchannel. For instance, Jones et al. demonstrated a microfluidic device with an efficiency of more than 92% integrated with dielectrophoretic mechanisms for size-based sorting of 1.0, 10.2, 19.5, and 48.5 kbp dsDNA analytes [123]. The channel performance was tunable based on applied potential and frequency. Recently, Dabighi et al. designed and computationally simulated a microfluidic device to diagnose, count, and separate cancer cells from the blood sample [124]. The study evaluated the effects of EP and DEP forces within an electrical field on CTCs. Under the same condition applied for manipulating spherical particles in the presented device, it was proved that particles of different sizes experienced various electrokinetic forces, which can be used as a basis for cancer cell separation.

Based on Eq. (18.23), altering the frequency of the applied voltage makes it possible to induce a dipole moment in a particle, which causes the particle to undergo a movement [119]. Hence, particles in different sizes can be sorted by manipulating the frequency of the applied voltage. Modarres et al. introduced a new concept termed frequency hopping DEP to provide a modulating force field for cell and particle isolation [125]. As displayed in Figure 18.8a, two frequencies were used for capturing and releasing polarizable polystyrene microspheres in a nonuniform electric field. Within the designed device, a mixture of particles was withdrawn into the microfluidic system at a flow rate at which the negative dielectrophoretic force catches all incoming particles. The capture frequency for all particle sizes was set at 1 MHz to produce the maximum negative dielectrophoretic force. Then, the frequency was decreased from 1 MHz till desired particles started escaping the dielectrophoretic traps. Based on this method, the isolation of 3, 5, and 10 μm particles, with purities of 98.7% and cells with separation efficiency of 82.2% were achieved. Also, repetitive DEP trapping and release in a flow system demonstrated a high-resolution separation of particles. Particles in the proposed method are refocused in every trapping step. Thus, the efficiency of the multistep DEP trapping-based separation method increases and is a direct function of the number of trap-and-release steps [126].

Employing the DEP method offers manipulation of the particles based on their polarizability. For instance, Zhang et al. demonstrated particle separation by utilizing the induced charge electroosmotic flows. In their proposed method, a region of circulating flows, formed by applying a DC electric field on a pair of metal plates embedded on the side channel walls, provided the particle trajectories depending on their sizes and polarizabilities [127].

Combining forces induced by channel structure with electrically induced forces provide further precise manipulation of particles in microfluidic devices. As presented in Figure 18.8b, Jia et al. used vaulted obstacles to facilitate the separation by hydrodynamically focusing particles in regions strongly affected by AC DEP [128]. Also, by utilizing 3D electrodes, a spatially nonuniform electric field in various heights of the main channel can be generated, which increases the throughput of the proposed microfluidic devices compared with the ones embedded with planar electrodes. Moreover, Calero et al. demonstrated tunable micro and nanoparticle separation system by joining electric fields within a DLD separation device. In their device, the separation of particles smaller than the critical diameter of the DLD device improved by applying DC and AC orthogonal electric fields [129]. Likewise, Ho et al. presented an integrated DLD device with electrokinetics (eDLD), as shown in Figure 18.8c, to sort particles based on their sizes and zeta potential (electrokinetic charge indicator). They were successfully able to show a tunable separation of micro and nanoparticles, such as liposomes and EVs, having different sizes and surface charges. In the introduced device, electrokinetic wall force fields around the pillars adjust the particle trajectories [130].

E-FACS is an electrical separation method in which fluorescence-labeled particles are isolated using an electric field. To understand the concept of E-FACS, it is worth mentioning the flow cytometry technique. Flow cytometry measures the properties of cells in a flow system by analyzing light-scattering properties of the cells [118]. Figure 18.7c illustrates the mechanism of the flow cytometer and the E-FACS system. Primarily, cells flow one at a time through a fluorescence measurement site by utilizing a hydraulic system. As the cell passes through the laser beam, light is scattered in all directions approaching the detectors.

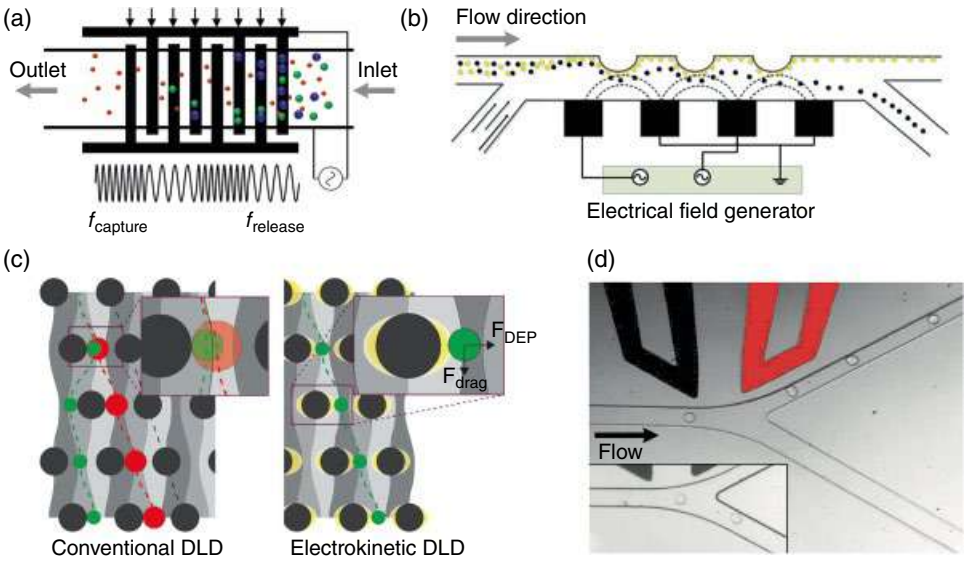

Figure 18.8 (a) Using two frequencies for capturing and releasing polarizable microspheres in an applied nonuniform electric field in which red particles were allowed to pass the capture zone, but blue and green particles were trapped [125], (b) hydrodynamically focusing particles in regions, which are strongly affected by AC DEP by utilizing vaulted obstacles on a channel wall [128], and (c) a conventional DLD device (on the left) and an integrated DLD device with electrokinetics to manipulate particles based on their size and zeta potential (on the right). In an eDLD device, electrokinetic wall force fields around the pillars (F DEP) shift the particles away from the pillars [130], (d) trajectories of droplets stream in a fluorescence-activated droplet sorter (FADS). By applying an AC electric field, the droplets were deflected toward the positive arm [138].

The sensing system contains two types of forwarding and side detectors. The size of the cells and cell count can be obtained through the forwarding detector, while reflected light at 90° (right-angled, side) is analyzed in the side detectors for measuring the properties of cells. A computer system that collects data recognized the properties of the cells, which can be used for sorting them [119, 131]. In E-FACS systems, to accurately identify different cell types within a heterogeneous population, the desired cells are conjugated with specific fluorescence-labeled antibodies or dyes. Then, cells were encapsulated in droplets individually. Droplets containing the desired labeled cells can be specifically charged according to the derived properties from the flow cytometer and later deflected by an electric field into an appropriate reservoir [132].

Due to the high sensitivity and throughput of the FACS system, it has become one of the most applicable methods of cell counting and sorting. The commercially flow cytometry systems were capable of sorting cells with high purity at rates from 25,000 to 60,000 cell/s [133]. As mentioned, cells must flow one by one through a fluorescence measurement site. In conventional FACS systems, hydrodynamic focusing of cells occurred using sheath fluid flow. Integrating the FACS system within microfluidic devices make it possible to take advantage of the laminar flow in microchannels, which focuses particles toward the center line [134]. Early attempts regarding uniting E-FACS systems with microfluidic devices date back to the 1990s [135, 136]. The development of microfabricated

fluorescence-activated cell sorters (μFACS) provides higher sensitivity, no cross-contamination, and lower cost [136].

Advantages to microfluidic-based E-FACS systems include the benefits of microfluidic devices, such as being smaller, portable, and low cost, besides the precise isolation available in the E-FACS method. Moreover, microfluidic-based E-FACS is feasible for precisely handling single cells in the laminar microflow [137]. Furthermore, employing the E-FACS method within microchannels allows the performance of micro actuators, which are merely powerful enough to cause micrometer cell flow deflection [137]. For instance, Baret et al. demonstrated a microfluidic sorting system, as presented in Figure 18.8d, based on fluorescence-activated droplet sorter (FADS) by combining the advantages of microtiter-plate screening and E-FACS [138]. Contrary to the declared E-FACS method, in the fabricated device, they applied the AC electric field (like the field used in the DEP method), and the deflection of droplets into the positive arm was observed. By operating the FADS device, single cells, which are compartmentalized in emulsion droplets, separated using the E-FACS technique, based on DEP, at rates up to 2000 droplet/s. Recently, Zhu et al. developed a high-throughput screening system based on droplet microfluidic sorting employing FACS [139]. In this system, encapsulated cells in water-in-oil-in-water (W/O/W) droplets, with a volume of about 12 picoliters, were used as picoliter-reactors for lactic acid fermentation. After fermentation, the FACS system was utilized with an analysis rate of 500–1000 event/s and a sorting rate of 100–500 event/s. By integrating microfluidics, the application of the FACS technique emerged as an ultrahigh-throughput, highly sensitive, and practical method due to the little reagent consumption (picoliter level) for flow cytometry and cell separation.

In brief, electrical separation within microfluidic devices can be carried out in EP, DEP, and E-FACS manners. In the EP-based devices, separation of particles in various sizes occurred only by charge density of the particle in a uniform electric field [1]. However, in DEP-based devices, by controlling the frequency of the applied voltage or polarizing the particle in a nonuniform electric field, the separation of particles in different sizes is possible [1]. Advantages of this method include being highly controllable, sensitive, and high throughput, which made these systems a versatile alternative for biomedical and clinical research.

18.3.3 Magnetic-Based Separation

Magnetophoresis within microfluidic devices is a method in which particles and cells are manipulated using magnetic forces. In continuous-flow microfluidic devices, magnetic force deflects different particles into various trajectories toward the outlets based on their size, shape, density, and magnetic properties [140]. The magnetic flux source applied in microfluidic devices can be adjusted by employing electromagnets, soft magnets, and permanent magnets. These flux sources have both pros and cons. For example, utilizing electromagnets and soft magnets, opposed to permanent magnets, enables on/off switching, but require extra pieces of equipment. Also, Joule heating is another highlighted shortcoming of electromagnets-based devices.

Based on the magnetic property of the particle and its surrounding medium, magnetophoresis is categorized into positive and negative manners. In the positive magnetophoresis,

microparticles with a greater magnetization than their surrounding medium, for example, magnetic microparticles suspended in the diamagnetic surrounding medium, move toward the field maxima, near the external magnetic source, as shown in Figure 18.9a and b [140, 141]. Positive magnetophoresis is suitable for separating magnetic microparticles or biological entities with intrinsic magnetic properties. Similarly, labeling diamagnetic cells enables the functionality of the positive method. However, since bounding cells with the magnetic particles is a laborious and time-consuming technique [142], alternatively, magnetic separation of diamagnetic microparticles can be done by employing the label-free negative magnetophoresis method [140]. Under the magnetic field, diamagnetic particles suspended in a paramagnetic fluid represent negative magnetophoresis, which leads to the migration of particles in the direction of a weaker magnetic field of the magnetic domain, as illustrated in Figure 18.9c [143].

To shed light upon the magnetic separation strategy, the forces and the parameters causing the magnetic manipulation of microparticles within microfluidic devices are discussed in the following. Magnetic forces generated by the interaction between magnetism and fluid flow on the microscale can actively actuate and manipulate particles within microfluidic devices [144]. Magnetic particles suspended in a continuous flow are deflected by the applied magnetic field and the viscous drag force. The velocity of deflection of the magnetic particles (u_{def}), as shown in Eq. (18.24), is defined as the summation of two vectors of the magnetically induced flow velocity on the particle (u_{mag}) and the velocity of the hydrodynamic flow (u_{hyd}) [145]. U_{mag}, presented in Eq. (18.25), is defined as the ratio of the magnetic force exerted on the particle by the magnetic field to the viscous drag force [145].

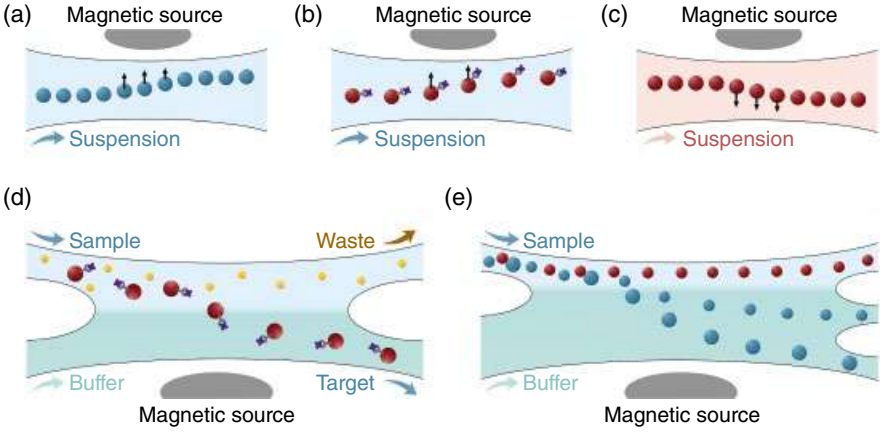

Figure 18.9 (a) Positive magnetophoresis manipulation of particles with intrinsic magnetic properties suspended in the diamagnetic surrounding medium, where particles migrate to the stronger magnetic field, (b) positive magnetophoresis manipulation of magnetically labeled diamagnetic particles suspended in the diamagnetic surrounding medium, where tagged particles move closer to the magnetic source, (c) negative magnetophoresis manipulation of diamagnetic particles suspended in a paramagnetic fluid, where particles are shifted to the weaker magnetic field, distant from the magnetic source, (d) separation of targeted magnetically labeled cells within the H-like channel magnetophoresis device, and (e) possibility of parallel magnetic separation based on various particle size and their magnetic properties.

$$u_{\text{def}} = u_{\text{mag}} + u_{\text{hyd}} \tag{18.24}$$

$$u_{\text{mag}} = \frac{F_{\text{mag}}}{F_{\text{drag}}} = \frac{F_{\text{mag}}}{6\pi\mu r} \tag{18.25}$$

where μ is the viscosity of the medium, and r the particle radius. Also, the magnetic force is defined as Eq. (18.26), in which B, V_p, ΔX, and μ_0 are the magnetic flux density, the particle volume, the difference in magnetic susceptibility between the particle (X_P) and the medium (X_m), and the permeability of a vacuum, respectively [146].

$$F_{\text{mag}} = \frac{\nabla X \cdot V_p}{\mu_0} \cdot \left(\nabla \cdot B\right) \cdot B \tag{18.26}$$

To intensify the separation efficiency, the magnetic field gradient can be amplified by employing powerful superconducting magnets to enhance the magnetic force strength. This method is appropriate for the separation of several cell types, such as red blood cells due to their high concentration of Fe ions [147]. Alternatively, the magnetic force strength can effortlessly increase by adjusting the magnetic susceptibility of the medium (X_m) [148]. A report on the label-free magnetophoretic microparticles separation method, including biological cells, using paramagnetic salts proved this approach [148]. In their study, biocompatible Gd–DTPA paramagnetic solutions were used to enhance the magnetic susceptibility of the medium, which led to an increase in the magnetic force acting on the cells.

Another option to increase the efficiency of magnetic cell separation is by improving the magnetic susceptibility of the particles (X_P). Magnetic labeling of cells by magnetic beads with the recognition molecule, like antibodies, is a way that has been frequently used. In this method, by employing a gradient magnetic field, the magnetic beads will be isolated, which in turn picked out the labeled cells [1]. As stated, in positive magnetophoresis, toward a nonuniform magnetic field, particles are deflected to the region of maximum magnetic field strength as a result of the magnetic force acting on the labeled cells with greater magnetic susceptibility than that of the surrounding medium [149]. This strategy is also commercially available, called magnetic activated cell sorting (MACS) and CELLSEARCH. Drawbacks of the MACS method includes prolonged processing time and the possibility of low sorting efficiency due to the nonspecific binding of antibodies [150]. Besides, these systems require a large number of samples, cell-specific antibodies, and magnetic particles for isolating the labeled cells with high throughput (10^9–10^{10} cells/h), high purity, and high recovery rate for functionality [151]. To address these problems, microfluidic-based magnetically actuated cell sorters (μMACS) have been developed to increase the efficiency of cell separation and reduce sample consumption [150]. μMACS systems are normally designed using electromagnets, permanent magnets, or self-assembled magnets [151]. μMAC systems are usually provided with H-like channels, as shown in Figure 18.9d, containing two inlets for the mixture sample plus sheath flow (buffer) and two outlets for cell separation. Furthermore, the number of outlets can be increased to separate tagged cells with variously sized magnetic particles, presented in Figure 18.9e, which experience different magnetic forces [152]. In these microfluidic devices, a mixture of labeled and unlabeled cells introduced into one inlet, and the sheath

flow enters into the other one. In the presence of magnetic force, labeled cells cross the distinct laminar streams and are gathering by the target outlet [151].

As discussed in a review regarding applications of magnetic force-based microfluidic devices in cellular and tissue bioengineering, μMACS systems enable cell manipulation with low conflict within cell function, cell viability, and the cellular environment [153]. Besides, μMACS systems allow low cost eliciting various cells simultaneously [1]. Even though magnetic separation is identified as a biocompatible method, higher magnetic field strength can endanger the cell viability due to the Joule heating [154]. To solve this issue, embedded cooling channels are employed. It was proved, by using cooling channels, a biocompatible temperature condition of approximately 37 °C can be provided [155].

However, the critical limitations of μMACS systems are their low precision in separating micrometer-sized biological molecules such as bacteria in the blood sample, due to the high viscosity [156], the challenge of removing the antigen and label from separated cells, and necessitating the expertise of biologists in selecting the appropriate antibodies [150]. In the following, suggested solutions for drawbacks observed in microfluidic-based magnetic separation systems are discussed.

Optimizing the forces causing particle separation is one of the main challenges in magnetic separation systems. The forces must be strong enough to enhance the separation purity and reduce the number of particles that leave the channel through the undesired outlet. However, the balancing of forces is required to prevent particles from sticking on the wall closer to the magnet. Integrating the functionalities of viscoelastic fluids in the magnetic separation method, reviewed in the following, makes it feasible to precisely manipulate the particles in the flow streamlines for effective separation. For instance, a study reported a deflection of magnetic particles with an efficiency of up to 96% by focusing the magnetic beads along a single streamline via using a viscoelastic fluid as a suspending medium before magnetic separation, as displayed in Figure 18.10a [157]. Similarly, it has been reported that particles of different sizes can be easily separated in a two-step operation, including a focusing module, which concentrated the particles of different sizes at the center of a narrow channel by the elastic force and separating them by a differential migration depends on their sizes using the magnetophoretic repulsion force [158]. As it was stated, due to the high viscosity of samples, separation of cells and micrometer-sized biological molecules is facing a challenge. In high viscose samples, the reduction of magnetic flux density gradients occurs as the distance from the magnetic source increases. In this case, a study on the separation of E. coli represented that by patterning the obstacle arrays on the channel, generated rotational flows shift the magnetic nanoparticles to the high augmented magnetic force area, improving the efficiency to more than 91.68% [156].

The demand for accurate and noninvasive cancer cell separation induces scientists to employ magnetophoresis [159]. For instance, a platform was introduced that integrates a DLD structure with a magnetic-based separator for antigen-independent isolation of CTCs. In the suggested strategy, most red blood cells and platelets were removed in DLD structures, and the labeled white blood cells were isolated using a magnetic-based separator [160].

To enhance the accuracy of magnetophoresis separation, multistage separation of particles has been proposed. For example, a report on negative magnetophoresis for size-dependent separation of brain cancer cells demonstrated a method regarding a two-step separation of cells with dual-neodymium magnets microfluidic device [161]. In the proposed device, the

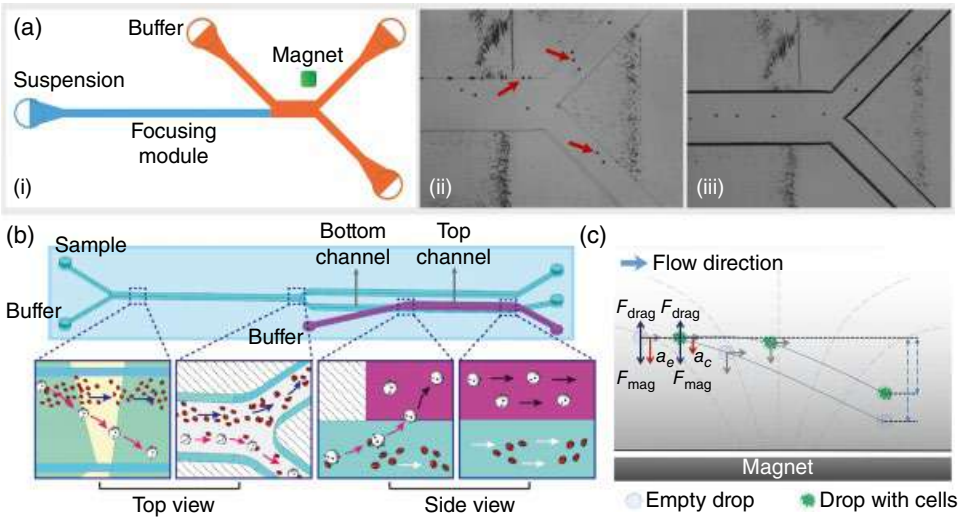

Figure 18.10 (a) i: Using a long channel as a viscoelastic flow-focusing module in a magnetophoresis device, ii: low efficiency of particle separation by applying a magnetic field without focusing the magnetic beads along a single streamline, iii: high efficiency of particle separation up to 96% by applying a magnetic field after focusing the magnetic beads along a single streamline using a flow-focusing module [157], (b) two-stage magnetic separation in a continuous flow using a flyover-style microfluidic chip, which enables the isolation of particles laterally and vertically [162], and (c) the effect of density in separating magnetic drops with equal size. Drops containing cells undergo the same force as empty drops but based on the higher density, they experience a lower acceleration (a_c), which consequently decreases the lateral displacement comparing with the empty droplets with an acceleration of (a_e) [163].

separation occurred in two steps after focusing the microparticles to the center of the channel in non-Newtonian viscoelastic poly (ethylene oxide) solution. Furthermore, as presented in Figure 18.10b, a flyover-style microfluidic chip for separating and purifying WBCs from whole blood was developed by two-stage magnetic separation in a continuous flow [162]. In this device, at the first stage, in the lateral magnetic sorting region, the WBCs cross the interface of the sample mixture to the buffer stream. In the following, to obtain a higher purity of WBCs, they were vertically separated within a flyover-style microchannel.

It has been also demonstrated that under the same condition in the microparticle diameters and magnetic property, the particle density can be used for particle separation. For instance, utilizing the magnetophoretic sorting method provided a promising platform for isolating microdroplets with different microalgal cell densities, as displayed in Figure 18.10c [163]. The magnetic microdroplets used in the mentioned study were performed using dextran-coated magnetic nanoparticles to exhibit magnetic properties when an inhomogeneous magnetic field is applied. Since the magnetic microdroplets had the same magnetic properties, they were influenced by an equal net force. By considering Newton's second law, the mass of the microdroplet determined by the quantity of encapsulated cells can define the lateral displacement of the droplet.

In summary, magnetophoresis within microfluidic devices is an active method of separation, which can isolate biological particles, such as cells, using their magnetic nature or by

labeling them with magnetic markers. The separation efficiency within magnetic-based microfluidic separation devices is influenced by magnetic nanoparticle concentration, the flow rate, viscosity of the medium, the lateral or vertical location of the magnet, and diameter plus density of the microparticles. The proposed magnetic devices proved to be adaptable for biological applications due to their biocompatibility, being accurate and high-throughput, and the ability to separate different particles simultaneously.

18.3.4 Optic-Based Separation

Integrating a focused beam of light within microfluidic devices makes it possible to directly manipulate particles of different sizes using optical radiation force [164, 165]. This promising platform can preserve the cell function, carry out accurate spatial control in three dimensions, and manipulate small particles [166]. Moreover, optical manipulation systems enable online reconfiguration due to the possibility of dynamic regulation of optical forces in time and space [164]. A focused laser beam can trap particles via generated optical scattering and gradient forces caused by the mismatch in the refractive index between the cell and its surrounding fluid [164]. Within optical microfluidic devices, besides the drag force that controls the velocity change, particles experience gradient and scattering forces. Scattering forces (F_s) push particles away from the source of light in the direction of light propagation. In contrast, the gradient forces (F_g) focus particles to the highest intensity point generated by the light [167]. To shed more light on the optical-based microfluidic sorting systems, particles are redirecting until scattering forces in the direction of light propagation exceed the gradient forces, where particles are optically trapped (Figure 18.11a and b) [167]. Employing Rayleigh theory, the optical forces on particles smaller than the wavelength can be calculated by Eq. (18.27) [168, 169] and Eq. (18.28) [170].

$$F_g(r) = 2\pi n_{\text{med}}^2 \varepsilon a^3 \left(\frac{m^2-1}{m^2+1}\right) \nabla \left|E^2(r)\right| \tag{18.27}$$

$$F_s(r) = \frac{n_{\text{med}}}{c} \frac{128\pi^5 a^6}{3\lambda^4} \left(\frac{m^2-1}{m^2+2}\right)^2 I(r) \tag{18.28}$$

where r indicates the position vector, ε denotes the electric constant in the vacuum, and m shows the ratio between the refractive index, n, of the particle with a radius of a and its surrounding medium n_{med}. Also, c, λ, E, and I imply speed of light, wavelength, optical field, and beam intensity, respectively.

The trapping of cells and particles in optical fields by precisely controlling a focused laser beam is called optical tweezers [119], which can be used in a microfluidic device to isolate the target population from a sample, as presented in Figure 18.11c [167, 171]. As derived from Eqs. (18.27) and (18.28), the manipulation of particles within optic-based microfluidic devices is obtainable owing to the objects' size differences and the refractive index of particles plus their surrounding medium. Also, trapping and separating targeted particles can be provided using optical polarizing within the optical fields [1]. Acceleration of freely suspended micron-sized particles in liquids and gas by the forces of radiation pressure from

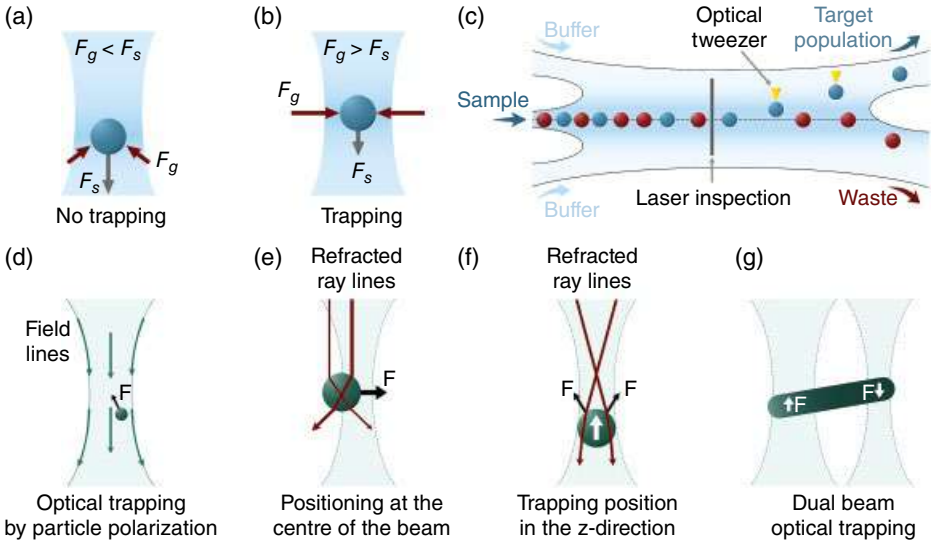

Figure 18.11 (a) Particles are deflected if scattering forces exceed gradient forces from a focused laser beam [167], (b) particles are optically trapped if gradient forces exceed scattering forces from a focused laser beam [167], (c) detection of targeted cells using laser inspection and isolating them by optical tweezers [167, 171], (d) optically trapping particles (smaller than the laser trapping wavelength) by polarizing them within the electric field of the light [174], and (e) the focused light is refracted through the particle (larger than the laser trapping wavelength). The induced force transfers the particle until it reaches an equilibrium position at the symmetric beam center [174], (f) manipulating and predicting the optical trapping position of the particles in the z-direction [174], and (g) optical trapping of an elongated particle using multiple beams [176].

a continuous-wave (CW) visible laser light was primary observed in 1969 [172]. Following that, for the first time in 1986, Ashkin and colleagues introduced the optical trapping of dielectric particles by a single-beam gradient force trap [170]. The generated forces in their study shift particles with a high refractive index to the center of the beam and relocate them in the propagation direction. The proposed platform could trap dielectric particles ranging from 25 nm to about 10 µm, using two propagating beams. In this method, the axial stability was provided using a single strongly focused beam with a considerable axial gradient force. Later, the forces of optical tweezers on micron-sized dielectric spheres in the ray optics regime was calculated by the same group [173], which can explain laser trapping and manipulation of living cells and organelles within cells.

In the Rayleigh regime (in which particles are much smaller than the laser trapping wavelength), the electric field of the light generates an induced dipole in the particles and shift them toward the center of the beam, where their energy is minimized, as illustrated in Figure 18.11d. In this regime, particles are aligned based on their polarizability. However, in the Mie regime (where particles are larger than the laser trapping wavelength), as shown in Figure 18.11e and f, particles are separated due to their transparency. In the Mie regime, the reflection and refraction of light generate the scattering plus gradient forces [174, 175]. Besides, the particle shape and the light field contour alter the orientation of a nonspherical particle within a beam. The orientation of certain particles, such as rod-shaped bacteria,

can be regulated by applying multiple beams (Figure 18.11g) sculpted light fields or changing beams dynamically. Lenton et al. demonstrated the advantage of using annular beams to trap nonspherical particles or cells. They dynamically adjusted the beams' potential to move motive E. coli bacteria toward the desired orientation. Also, they declared that utilizing annular beams can reduce back reflection and consequently improve the axial optical trap depth [176].

Although optical tweezers allow the manipulation of a single nanoparticle in a steady liquid medium, challenges arise in dealing with the group of nanoparticles in a flowing system. The issue is adjusting the additional Stokes forces by the fast velocity of streams and dispersed nanoparticles in the medium. Wu et al. proposed a microfluidic device, as presented in Figure 18.12a, in which, by employing opposite impinging streams, Stokes force was reduced. Also, nanoparticles were focused in a narrow stream to be separated by a moderate power laser beam [177].

The development of optical tweezers opens a broad spectrum of opportunities in studies of manipulating, trapping, and sorting target particles, typically in the nano to microscale range. Recently, optical fiber tweezers have been used as a versatile tool for non-contact and damage-free optical trapping and manipulation of biological cells. This is due to their flexible manipulation, ease of fabrication, and compact structure [178]. Also, optical

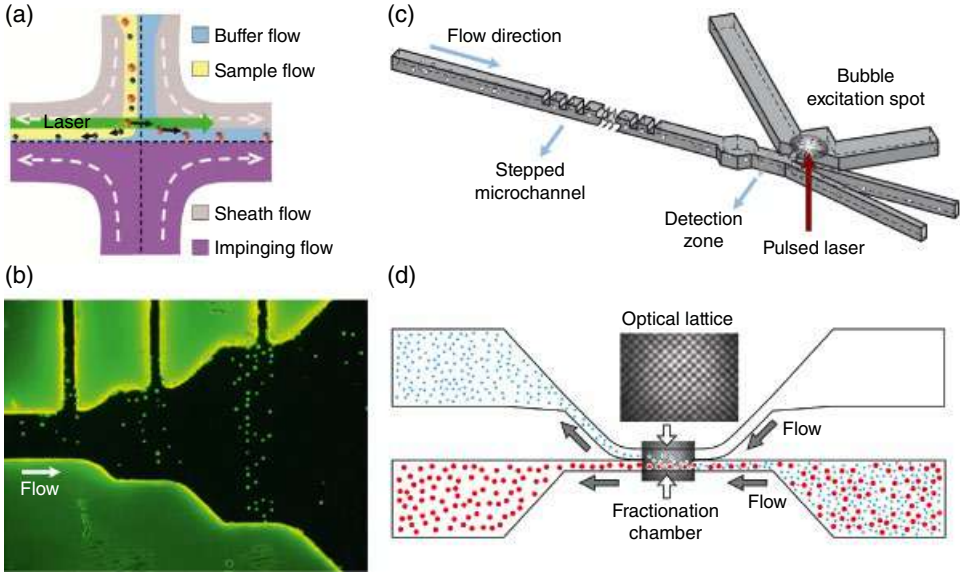

Figure 18.12 (a) Using opposite impinging streams for reducing Stokes force to enhance the nanoparticle separation purity by a moderate power laser beam [177], (b) an ODEP-based microfluidic system for continuous isolation and purification of CTCs using four optical light-based virtual cell filters within optimal flow velocity [182], and (c) particle separation based on pulsed laser activated cell sorter (PLACS). After identifying the desired particle in the detection zone, a laser pulse makes a cavitation bubble in the bubble excitation spot, which generates a liquid jet for deflecting the targeted particle toward the objective outlet [186], (d) Separation of two-component cell mixture in a continuous flow by employing a 3D optical lattice. Laser beams were utilized to create flow paths similar to a DLD system without physical obstacles [191].

tweezers were reported as a noninvasive method for the study of cells, such as red blood cells [179]. The precise trapping of cells can be achieved in a label-free manner, only based on their different sizes and shapes. For instance, Liu et al. recently integrated optical fiber tweezers into a T-type microfluidic channel, which enabled selective trapping of Escherichia coli in human blood solution [180]. In their system, once the laser was applied, the Escherichia coli cells were trapped, whereas RBCs were collected from the waste outlet.

As mentioned earlier, a light beam can polarize particles of various sizes. The polarization is caused by the generation of a nonuniform electric field near the surface of the light-patterned areas. Hence, particles of different sizes experience different negative DEP forces toward the center of the light beam. The induced force is called optically induced-dielectrophoresis (ODEP), which can be used to sort particles in their medium [181]. For example, Chou et al. proposed an ODEP-based microfluidic system for continuous isolation and purification of CTCs based on their size [182]. The separation of CTCs in the designed microfluidic device, as shown in Figure 18.12b, has occurred baseD on four optical light-based virtual cell filters within optimal flow velocity. Results revealed the capacity of the device in isolating cancer cells from the surrounding leukocytes, with purity as high as $94.9 \pm 0.3\%$. The ODEP force imposed on the particle does not grow linearly with the particle volume. Zhang et al. confirmed that the existing nonlinear relationship between the particle volume and the dielectrophoretic force relies on the distribution of the nonuniform electric field and the field gradient in the optoelectronic tweezers systems [183]. They calculated the variation of forces on biological cells and polystyrene microbeads over different sizes by integrating the simulated and experimentally measured ∇E^2 over the particle volume. Predicting the induced forces in optoelectronic tweezers provides intuition of microfluidic devices designing for manipulating dielectric microparticles and biological samples in various sizes.

Similar to the E-FACS and A-FACS methods (electric-based and acoustic-based separation sections), a laser beam can increase sorting efficiency, recognizing as the optical switch. In this regard, Wang et al. designed a microfluidic device based on optical switching for controlling and sorting mammalian cells with the rapidity of 2–4 ms [184]. They presented that the planar nature of most microfluidic chip designs allows the integration of optical switching controls at any desired position, which enables a rapid active manipulation of cell routing on a microfluidic chip. Recently, Chiou et al. invented a pulsed-laser triggered microfluidic switching mechanism with the same sorting manner, which achieved a switching time of 70 μs [185]. Furthermore, as illustrated in Figure 18.12c, Chen et al. proposed a method called pulsed laser activated cell sorter (PLACS) in which by employing a laser pulse, the target particle is indirectly separated [186]. In this device, after identifying the desired particle in the detection zone, a laser pulse is triggered to excite a cavitation bubble at a proper delay time. The bubble produces a liquid jet through the nozzle, deflecting the targeted particle toward the target outlet.

The optical forces acting on particles much smaller than the wavelength (smaller than 100 nm) become weak and less efficient. This limitation is due to the dependency of gradient force on the third power of particle radius (Eq. (18.27)). Using evanescent waves paved the way for optical trapping and manipulation by generating sufficient gradient force [187]. A waveguide is a dielectric structure that guides energy at a wavelength, which minimizes the energy loss by restricting the transmission of it in one direction [188]. For instance,

Kim et al. presented a microfluidic chip, which facilitates free-space optical trapping and manipulation. The device takes advantage of a trench to form a trapping channel and manipulate the particles to an arbitrary position, among the waveguides, with a resolution of lower than 100 nm [189]. Furthermore, Applegate Jr. and colleagues produced an integrated optical waveguide network within a microfluidic device in which the particle's fluorescence characteristics were identified with a waveguide and sorted using a diode laser bar. It was proved that waveguide allows particle detection and trajectory tracking due to its ability to regulate fluorescence excitation localization [190]. While most optical systems use focused beams directly for particle sorting, MacDonald et al. proposed a 3D optical lattice, as presented in Figure 18.12d, to fractionate a two-component cell mixture in a continuous flow [191]. The separation mechanism was based on a DLD system produced by interfering laser beams. The strong optical interactions selectively generate separate flow paths in the absence of physical obstacles, which enabled the deflection of selected particles from their original trajectories without clogging.

In brief, by integrating a focused beam of light within microfluidic devices, particles can be manipulated and separated due to their size, shape, refractive index, transparency, and polarizability. A focused beam of light can be directly used in optical tweezers and optical switching devices for a mixture component fractionation. However, PLACS systems and optical lattices have been proposed to isolate targeted particles indirectly. Advantages to this method include being highly controllable in three dimensions, precise in desired particle selection, high throughput, noninvasive, and biocompatible, besides online reconfiguration of the system.

18.4 Conclusion

In this chapter, we have presented different microfluidic systems used for cell separation and sorting. These platforms are divided into two general groups of active and passive based on their operating principles and energy intake. Active microfluidic systems are dependent on an external source of energy to be operated. On the other hand, passive platforms are able to function with hydrodynamic forces that result from specific features of channel geometry. Microfluidic platforms possess several advantages that make them a favorable device for clinical and biomedical trials and applications. First and foremost, these devices are cost-effective in terms of sample and reagent consumption. This will result in a reduction in costs and invasion of sample collection from patients. Additionally, the time needed for sample preparation, processing, and analysis is shorter than conventional methods. As microfluidic devices are fabricated with highly accurate instruments with high spatial resolution, users are able to precisely control and manipulate samples with minimum human intervention. Accordingly, human errors and contaminations can be eliminated in these systems. Finally, due to the portability of these platforms and their simple operation procedure, all laboratories will be allowed to benefit from these platforms to conduct their experiments with the minimum requirement for equipment and apparatus. However, to improve the efficiency of these platforms in terms of cell viability and throughput, further investigation is required.

Despite the fact that microfluidics technology is yet to be fully commercialized, these platforms have proved to be able to reproduce experimental results of cell and particle separation, thereby demonstrating the great potential of these devices for being marketed. Another approach to expand the application of microfluidics technology is developing integrated systems that will allow researchers to manipulate and handle a small volume of biological samples for different purposes in addition to separation. These integrated devices can ultimately be an inseparable part of all laboratories as an affordable, versatile device for scientific assays and diagnostic purposes.

Acknowledgment

M.E.W. would like to acknowledge the support of the Australian Research Council through Discovery Project Grants (DP170103704 and DP180103003) and the National Health and Medical Research Council through the Career Development Fellowship (APP1143377).

References

1 Bhagat, A.A.S., Bow, H., Hou, H.W. et al. (2010). Microfluidics for cell separation. *Medical & Biological Engineering & Computing* **48** (10): 999–1014.
2 Dalili, A., Samiei, E., and Hoorfar, M. (2019). A review of sorting, separation and isolation of cells and microbeads for biomedical applications: microfluidic approaches. *Analyst* **144** (1): 87–113.
3 Gossett, D.R., Weaver, W.M., Mach, A.J. et al. (2010). Label-free cell separation and sorting in microfluidic systems. *Analytical and Bioanalytical Chemistry* **397** (8): 3249–3267.
4 Warkiani, M.E., Wu, L., Tay, A.K.P., and Han, J. (2015). Large-volume microfluidic cell sorting for biomedical applications. *Annual Review of Biomedical Engineering* **17** (1): 1–34.
5 Yamada, M., Nakashima, M., and Seki, M. (2004). Pinched flow fractionation: continuous size separation of particles utilizing a laminar flow profile in a pinched microchannel. *Analytical Chemistry* **76** (18): 5465–5471.
6 Jain, A. and Posner, J.D. (2008). Particle dispersion and separation resolution of pinched flow fractionation. *Analytical Chemistry* **80** (5): 1641–1648.
7 Takagi, J., Yamada, M., Yasuda, M., and Seki, M. (2005). Continuous particle separation in a microchannel having asymmetrically arranged multiple branches. *Lab on a Chip* **5** (7): 778–784.
8 Maenaka, H., Yamada, M., Yasuda, M., and Seki, M. (2008). Continuous and size-dependent sorting of emulsion droplets using hydrodynamics in pinched microchannels. *Langmuir* **24** (8): 4405–4410.
9 Sai, Y., Yamada, M., Yasuda, M., and Seki, M. (2006). Continuous separation of particles using a microfluidic device equipped with flow rate control valves. *Journal of Chromatography A* **1127** (1): 214–220.
10 Vig, A.L. and Kristensen, A. (2008). Separation enhancement in pinched flow fractionation. *Applied Physics Letters* **93** (20): 203507.

11 Lee, K.H., Kim, S.B., Lee, K.S., and Sung, H.J. (2011). Enhancement by optical force of separation in pinched flow fractionation. *Lab on a Chip* **11** (2): 354–357.

12 Khashei, H., Latifi, H., Seresht, M.J., and Ghasemi, A.H.B. (2016). Microparticles manipulation and enhancement of their separation in pinched flow fractionation by insulator-based dielectrophoresis. *ELECTROPHORESIS* **37** (5-6): 775–785.

13 Morijiri, T., Sunahiro, S., Senaha, M. et al. (2011). Sedimentation pinched-flow fractionation for size- and density-based particle sorting in microchannels. *Microfluidics and Nanofluidics* **11** (1): 105–110.

14 Lu, X. and Xuan, X. (2015). Continuous microfluidic particle separation via elasto-inertial pinched flow fractionation. *Analytical Chemistry* **87** (12): 6389–6396.

15 Lu, X. and Xuan, X. (2015). Elasto-inertial pinched flow fractionation for continuous shape-based particle separation. *Analytical Chemistry* **87** (22): 11523–11530.

16 Huang, L.R., Cox, E.C., Austin, R.H., and Sturm, J.C. (2004). Continuous particle separation through deterministic lateral displacement. *Science* **304** (5673): 987.

17 Loutherback, K., D'Silva, J., Liu, L. et al. (2012). Deterministic separation of cancer cells from blood at 10 mL/min. *AIP Advances* **2** (4): 042107.

18 Holm, S.H., Beech, J.P., Barrett, M.P., and Tegenfeldt, J.O. (2011). Separation of parasites from human blood using deterministic lateral displacement. *Lab on a Chip* **11** (7): 1326–1332.

19 Wunsch, B.H., Smith, J.T., Gifford, S.M. et al. (2016). Nanoscale lateral displacement arrays for the separation of exosomes and colloids down to 20 nm. *Nature Nanotechnology* **11** (11): 936–940.

20 McGrath, J., Jimenez, M., and Bridle, H. (2014). Deterministic lateral displacement for particle separation: a review. *Lab on a Chip* **14** (21): 4139–4158.

21 Salafi, T., Zhang, Y., and Zhang, Y. (2019). A review on deterministic lateral displacement for particle separation and detection. *Nano-Micro Letters* 11 (1): 1–33.

22 Squires, T.M. and Quake, S.R.J.R.o.m.p. (2005). Microfluidics: fluid physics at the nanoliter scale. *Reviews of Modern Physics* **77** (3): 977.

23 Razavi Bazaz, S., Amiri, H.A., Vasilescu, S. et al. (2020). Obstacle-free planar hybrid micromixer with low pressure drop. *Microfluidics and Nanofluidics* **24** (8): 61.

24 Beech, J. (2011). *Microfluidics Separation and Analysis of Biological Particles*. Lund University.

25 Inglis, D.W., Davis, J.A., Austin, R.H., and Sturm, J.C. (2006). Critical particle size for fractionation by deterministic lateral displacement. *Lab on a Chip* **6** (5): 655–658.

26 Zeming, K.K., Salafi, T., Chen, C.-H., and Zhang, Y. (2016). Asymmetrical deterministic lateral displacement gaps for dual functions of enhanced separation and throughput of red blood cells. *Scientific Reports* **6** (1): 22934.

27 D'Avino, G.J.R.A. (2013). Non-Newtonian deterministic lateral displacement separator: theory and simulations. *Rheologica Acta* **52** (3): 221–236.

28 Adolfsson, K. (2011). *Deformability-Based Separation of Erythrocytes with Deterministic Lateral Displacement*. Department of Solid State Physics, Lund Institute of Technology.

29 Lubbersen, Y.S., Schutyser, M.A.I., and Boom, R.M. (2012). Suspension separation with deterministic ratchets at moderate Reynolds numbers. *Chemical Engineering Science* **73**: 314–320.

30 Civin, C.I., Ward, T., Skelley, A.M. et al. (2016). Automated leukocyte processing by microfluidic deterministic lateral displacement. *Cytometry Part A* **89** (12): 1073–1083.

31 Campos-González, R., Skelley, A.M., Gandhi, K. et al. (2018). Deterministic lateral displacement: the next-generation CAR T-cell processing? *SLAS TECHNOLOGY: Translating Life Sciences Innovation* **23** (4): 338–351.

32 Au, S.H., Edd, J., Stoddard, A.E. et al. (2017). Microfluidic isolation of circulating tumor cell clusters by size and asymmetry. *Scientific Reports* **7** (1): 2433.

33 Laki, A.J., Botzheim, L., Iván, K. et al. (2015). Separation of microvesicles from serological samples using deterministic lateral displacement effect. *BioNanoScience* **5** (1): 48–54.

34 Santana, S.M., Antonyak, M.A., Cerione, R.A., and Kirby, B.J. (2014). Microfluidic isolation of cancer-cell-derived microvesicles from hetergeneous extracellular shed vesicle populations. *Biomedical Microdevices* **16** (6): 869–877.

35 Beech, J.P., Jönsson, P., and Tegenfeldt, J.O. (2009). Tipping the balance of deterministic lateral displacement devices using dielectrophoresis. *Lab on a Chip* **9** (18): 2698–2706.

36 Jiang, M., Mazzeo, A.D., and Drazer, G. (2016). Centrifuge-based deterministic lateral displacement separation. *Microfluidics and Nanofluidics* **20** (1): 17.

37 Chen, Y., Abrams, E.S., Boles, T.C. et al. (2015). Concentrating genomic length DNA in a microfabricated array. *Physical Review Letters* **114** (19): 198303.

38 Liang, W., Austin, R.H., and Sturm, J.C. (2020). Scaling of deterministic lateral displacement devices to a single column of bumping obstacles. *Lab on a Chip* **20** (18): 3461–3467.

39 Hochstetter, A., Vernekar, R., Austin, R.H. et al. (2020). Deterministic lateral displacement: challenges and perspectives. *ACS Nano* **14** (9): 10784–10795.

40 Ranjan, S., Zeming, K.K., Jureen, R. et al. (2014). DLD pillar shape design for efficient separation of spherical and non-spherical bioparticles. *Lab on a Chip* **14** (21): 4250–4262.

41 Hyun, J.-c., Hyun, J., Wang, S. et al. (2017). Improved pillar shape for deterministic lateral displacement separation method to maintain separation efficiency over a long period of time. *Separation and Purification Technology* **172**: 258–267.

42 Zhang, Z., Henry, E., Gompper, G., and Fedosov, D.A. (2015). Behavior of rigid and deformable particles in deterministic lateral displacement devices with different post shapes. *The Journal of Chemical Physics* **143** (24): 243145.

43 Ye, S., Shao, X., Yu, Z., and Yu, W. (2014). Effects of the particle deformability on the critical separation diameter in the deterministic lateral displacement device. *Journal of Fluid Mechanics* **743**: 60–74.

44 Kabacaoğlu, G. and Biros, G. (2019). Sorting same-size red blood cells in deep deterministic lateral displacement devices. *Journal of Fluid Mechanics* **859**: 433–475.

45 Holmes, D., Whyte, G., Bailey, J. et al. (2014). Separation of blood cells with differing deformability using deterministic lateral displacement†. *Interface Focus* **4** (6): 20140011.

46 Krüger, T., Holmes, D., and Coveney, P.V. (2014). Deformability-based red blood cell separation in deterministic lateral displacement devices—a simulation study. *Biomicrofluidics* **8** (5): 054114.

47 Stemme, G. and Kittilsland, G. (1988). New fluid filter structure in silicon fabricated using a self-aligning technique. *Applied Physics Letters* **53** (16): 1566–1568.

48 Kittilsland, G., Stemme, G., and Nordén, B. (1990). A sub-micron particle filter in silicon. *Sensors and Actuators A: Physical* **23** (1): 904–907.

49 Aran, K., Fok, A., Sasso, L.A. et al. (2011). Microfiltration platform for continuous blood plasma protein extraction from whole blood during cardiac surgery. *Lab on a Chip* **11** (17): 2858–2868.

50 Wilding, P., Kricka, L.J., Cheng, J. et al. (1998). Integrated cell isolation and polymerase chain reaction analysis using silicon microfilter chambers. *Analytical Biochemistry* **257** (2): 95–100.

51 Wu, C.-C., Hong, L.-Z., and Ou, C.-T. (2012). Blood cell-free plasma separated from blood samples with a cascading weir-type microfilter using dead-end filtration. *Journal of Medical and Biological Engineering* **32** (3): 163–168.

52 Wang, G., Crawford, K., Turbyfield, C. et al. (2015). Microfluidic cellular enrichment and separation through differences in viscoelastic deformation. *Lab on a Chip* **15** (2): 532–540.

53 Arata, J.P. and Alexeev, A. (2009). Designing microfluidic channel that separates elastic particles upon stiffness. *Soft Matter* **5** (14): 2721–2724.

54 Islam, M., Brink, H., Blanche, S. et al. (2017). Microfluidic sorting of cells by viability based on differences in cell stiffness. *Scientific Reports* **7** (1): 1997.

55 Segre, G. and Silberberg, A. (1961). Radial particle displacements in Poiseuille flow of suspensions. *Nature* **189** (4760): 209.

56 Raoufi, M.A., Bazaz, S.R., Niazmand, H. et al. (2020). Fabrication of unconventional inertial microfluidic channels using wax 3D printing. *Soft Matter* **16** (10): 2448–2459.

57 Xiang, N., Wang, J., Li, Q. et al. (2019). Precise size-based cell separation via the coupling of inertial microfluidics and deterministic lateral displacement. *Analytical Chemistry* **91** (15): 10328–10334.

58 Zhang, J., Yan, S., Yuan, D. et al. (2016). Fundamentals and applications of inertial microfluidics: a review. *Lab on a Chip* **16** (1): 10–34.

59 Razavi Bazaz, S., Mashhadian, A., Ehsani, A. et al. (2020). Computational inertial microfluidics: a review. *Lab on a Chip* **20** (6): 1023–1048.

60 Di Carlo, D. (2009). Inertial microfluidics. *Lab on a Chip* **9** (21): 3038–3046.

61 Tang, W., Tang, D., Ni, Z. et al. (2017). Microfluidic impedance cytometer with inertial focusing and liquid electrodes for high-throughput cell counting and discrimination. *Analytical Chemistry* **89** (5): 3154–3161.

62 Bhagat, A.A.S., Kuntaegowdanahalli, S.S., and Papautsky, I. (2009). Inertial microfluidics for continuous particle filtration and extraction. *Microfluidics and Nanofluidics* **7** (2): 217–226.

63 Bayareh, M. (2020). An updated review on particle separation in passive microfluidic devices. *Chemical Engineering and Processing - Process Intensification* **153**: 107984.

64 Vasilescu, S.A., Khorsandi, S., Ding, L. et al. (2021). A microfluidic approach to rapid sperm recovery from heterogeneous cell suspensions. *Scientific Reports* **11** (1): 7917.

65 Bhagat, A.A.S., Kuntaegowdanahalli, S.S., Kaval, N. et al. (2010). Inertial microfluidics for sheath-less high-throughput flow cytometry. *Biomedical Microdevices* **12** (2): 187–195.

66 Sun, J., Li, M., Liu, C. et al. (2012). Double spiral microchannel for label-free tumor cell separation and enrichment. *Lab on a Chip* **12** (20): 3952–3960.

67 Xiang, N. and Ni, Z. (2015). High-throughput blood cell focusing and plasma isolation using spiral inertial microfluidic devices. *Biomedical Microdevices* **17** (6): 110.

68 Rzhevskiy, A.S., Bazaz, S.R., Ding, L. et al. (2019). Rapid and label-free isolation of tumour cells from the urine of patients with localised prostate cancer using inertial microfluidics. *Cancers* **12** (1): 81.

69 Condina, M.R., Dilmetz, B.A., Bazaz, S.R. et al. (2019). Rapid separation and identification of beer spoilage bacteria by inertial microfluidics and MALDI-TOF mass spectrometry. *Lab on a Chip* **19** (11): 1961–1970.

70 Mihandoust, A., Bazaz, S.R., Maleki-Jirsaraei, N. et al. (2020). High-throughput particle concentration using complex cross-section microchannels. *Micromachines* **11** (4): 440.

71 Razavi Bazaz, S., Kashaninejad, N., Azadi, S. et al. (2019). Rapid softlithography using 3D-printed molds. *Advanced Materials Technologies* **4** (10): 1900425.

72 Razavi Bazaz, S., Rouhi, O., Raoufi, M.A. et al. (2020). 3D printing of inertial microfluidic devices. *Scientific Reports* **10** (1): 5929.

73 Jiang, D., Tang, W., Xiang, N., and Ni, Z. (2016). Numerical simulation of particle focusing in a symmetrical serpentine microchannel. *RSC Advances* **6** (62): 57647–57657.

74 Di Carlo, D., Irimia, D., Tompkins, R.G., and Toner, M. (2007). Continuous inertial focusing, ordering, and separation of particles in microchannels. *Proceedings of the National Academy of Sciences* **104** (48): 18892–18897.

75 Zhang, J., Yuan, D., Zhao, Q. et al. (2019). Fundamentals of differential particle inertial focusing in symmetric sinusoidal microchannels. *Analytical Chemistry* **91** (6): 4077–4084.

76 Zhang, J., Yan, S., Li, W. et al. (2014). High throughput extraction of plasma using a secondary flow-aided inertial microfluidic device. *RSC Advances* **4** (63): 33149–33159.

77 Xiang, N., Zhang, R., Han, Y., and Ni, Z. (2019). A multilayer polymer-film inertial microfluidic device for high-throughput cell concentration. *Analytical Chemistry* **91** (8): 5461–5468.

78 Warkiani, M.E., Tay, A.K.P., Khoo, B.L. et al. (2015). Malaria detection using inertial microfluidics. *Lab on a Chip* **15** (4): 1101–1109.

79 Lee, M.G., Choi, S., Kim, H.-J. et al. (2011). Inertial blood plasma separation in a contraction–expansion array microchannel. *Applied Physics Letters* **98** (25): 253702.

80 Kim, G.-Y., Son, J., Han, J.-I., and Park, J.-K. (2021). Inertial microfluidics-based separation of microalgae using a contraction–expansion array microchannel. *Micromachines* **12** (1): 97.

81 Gao, Y., Wu, M., Lin, Y., and Xu, J. (2020). Acoustic microfluidic separation techniques and bioapplications: a review. *Micromachines* **11** (10): 921.

82 Destgeer, G. and Sung, H.J. (2015). Recent advances in microfluidic actuation and micro-object manipulation via surface acoustic waves. *Lab on a Chip* **15** (13): 2722–2738.

83 Laurell, T., Petersson, F., and Nilsson, A. (2007). Chip integrated strategies for acoustic separation and manipulation of cells and particles. *Chemical Society Reviews* **36** (3): 492–506.

84 Yeo, L.Y. and Friend, J.R. (2014). Surface acoustic wave microfluidics. *Annual Review of Fluid Mechanics* **46**: 379–406.

85 Talebjedi, B., Tasnim, N., Hoorfar, M. et al. (2020). Exploiting microfluidics for extracellular vesicle isolation and characterization: potential use for standardized embryo quality assessment. *Frontiers in Veterinary Science* **7**: 1139.

86 Leibacher, I., Reichert, P., and Dual, J. (2015). Microfluidic droplet handling by bulk acoustic wave (BAW) acoustophoresis. *Lab on a Chip* **15** (13): 2896–2905.

87 Gautam, G.P., Burger, T., Wilcox, A. et al. (2018). Simple and inexpensive micromachined aluminum microfluidic devices for acoustic focusing of particles and cells. *Analytical and Bioanalytical Chemistry* **410** (14): 3385–3394.

88 Lin, S.-C.S., Mao, X., and Huang, T.J. (2012). Surface acoustic wave (SAW) acoustophoresis: now and beyond. *Lab on a Chip* **12** (16): 2766–2770.

89 Shields, C.W.t., Cruz, D.F., Ohiri, K.A. et al. (2016). Fabrication and operation of acoustofluidic devices supporting bulk acoustic standing waves for sheathless focusing of particles. *Journal of Visualized Experiments: JoVE* (109): 53861.

90 Nam, J., Lim, H., Kim, C. et al. (2012). Density-dependent separation of encapsulated cells in a microfluidic channel by using a standing surface acoustic wave. *Biomicrofluidics* **6** (2): 024120.

91 Whitworth, G., Grundy, M., and Coakley, W. (1991). Transport and harvesting of suspended particles using modulated ultrasound. *Ultrasonics* **29** (6): 439–444.

92 Fornell, A., Cushing, K., Nilsson, J., and Tenje, M. (2018). Binary particle separation in droplet microfluidics using acoustophoresis. *Applied Physics Letters* **112** (6): 063701.

93 Shi, J., Huang, H., Stratton, Z. et al. (2009). Continuous particle separation in a microfluidic channel via standing surface acoustic waves (SSAW). *Lab on a Chip* **9** (23): 3354–3359.

94 Ding, X., Li, P., Lin, S.-C.S. et al. (2013). Surface acoustic wave microfluidics. *Lab on a Chip* **13** (18): 3626–3649.

95 Shamloo, A. and Boodaghi, M. (2018). Design and simulation of a microfluidic device for acoustic cell separation. *Ultrasonics* **84**: 234–243.

96 Zhang, T., Hong, Z.-Y., Tang, S.-Y. et al. (2020). Focusing of sub-micrometer particles in microfluidic devices. *Lab on a Chip* **20** (1): 35–53.

97 Baasch, T., Reichert, P., Lakämper, S. et al. (2018). Acoustic compressibility of caenorhabditis elegans. *Biophysical Journal* **115** (9): 1817–1825.

98 Yang, F., Liao, X., Tian, Y., and Li, G. (2017). Exosome separation using microfluidic systems: size-based, immunoaffinity-based and dynamic methodologies. *Biotechnology Journal* **12** (4): 1600699.

99 Miller, D.L., Smith, N.B., Bailey, M.R. et al. (2012). Overview of therapeutic ultrasound applications and safety considerations. *Journal of Ultrasound in Medicine* **31** (4): 623–634.

100 Zhang, C., Huang, K.-C., Rajwa, B. et al. (2017). Stimulated Raman scattering flow cytometry for label-free single-particle analysis. *Optica* **4** (1): 103–109.

101 Garg, N., Westerhof, T.M., Liu, V. et al. (2018). Whole-blood sorting, enrichment and in situ immunolabeling of cellular subsets using acoustic microstreaming. *Microsystems & Nanoengineering* **4** (1): 1–9.

102 Gu, Y., Chen, C., Wang, Z. et al. (2019). Plastic-based acoustofluidic devices for high-throughput, biocompatible platelet separation. *Lab on a Chip* **19** (3): 394–402.

103 Wang, K., Zhou, W., Lin, Z. et al. (2018). Sorting of tumour cells in a microfluidic device by multi-stage surface acoustic waves. *Sensors and Actuators B: Chemical* **258**: 1174–1183.

104 Li, S., Ma, F., Bachman, H. et al. (2016). Acoustofluidic bacteria separation. *Journal of Micromechanics and Microengineering* **27** (1): 015031.

105 Lee, K., Shao, H., Weissleder, R., and Lee, H. (2015). Acoustic purification of extracellular microvesicles. *ACS Nano* **9** (3): 2321–2327.

106 Wu, M., Ouyang, Y., Wang, Z. et al. (2017). Isolation of exosomes from whole blood by integrating acoustics and microfluidics. *Proceedings of the National Academy of Sciences* **114** (40): 10584–10589.

107 Wu, M., Chen, C., Wang, Z. et al. (2019). Separating extracellular vesicles and lipoproteins via acoustofluidics. *Lab on a Chip* **19** (7): 1174–1182.

108 Devendran, C., Choi, K., Han, J. et al. (2020). Diffraction-based acoustic manipulation in microchannels enables continuous particle and bacteria focusing. *Lab on a Chip* **20** (15): 2674–2688.

109 Schmid, L., Weitz, D.A., and Franke, T. (2014). Sorting drops and cells with acoustics: acoustic microfluidic fluorescence-activated cell sorter. *Lab on a Chip* **14** (19): 3710–3718.

110 Ma, Z., Zhou, Y., Collins, D.J., and Ai, Y. (2017). Fluorescence activated cell sorting via a focused traveling surface acoustic beam. *Lab on a Chip* **17** (18): 3176–3185.

111 Li, P., Liang, M., Lu, X. et al. (2019). Sheathless acoustic fluorescence activated cell sorting (aFACS) with high cell viability. *Analytical Chemistry* **91** (24): 15425–15435.

112 Waheed, W., Sharaf, O.Z., Alazzam, A., and Abu-Nada, E. (2020). Dielectrophoresis-field flow fractionation for separation of particles: a critical review. *Journal of Chromatography A* 1637: 461799.

113 Jeon, H., Kim, Y., and Lim, G. (2016). Continuous particle separation using pressure-driven flow-induced miniaturizing free-flow electrophoresis (PDF-induced μ-FFE). *Scientific Reports* **6**: 19911.

114 Pethig, R.R. (2017). *Dielectrophoresis: Theory, Methodology and Biological Applications*. John Wiley & Sons.

115 Pohl, H.A. (1951). *The motion and precipitation of suspensoids in divergent electric fields*. *Journal of Applied Physics* **22** (7): 869–871.

116 Hawkins, B.G., Smith, A.E., Syed, Y.A., and Kirby, B.J. (2007). Continuous-flow particle separation by 3D insulative dielectrophoresis using coherently shaped, dc-biased, ac electric fields. *Analytical Chemistry* **79** (19): 7291–7300.

117 Pethig, R. (2010). Review article-dielectrophoresis: status of the theory, technology, and applications. *Biomicrofluidics* **4** (2): 022811.

118 Picot, J., Guerin, C.L., Le Van Kim, C., and Boulanger, C.M. (2012). Flow cytometry: retrospective, fundamentals and recent instrumentation. *Cytotechnology* 64 (2): 109–130.

119 Lenshof, A. and Laurell, T. (2010). Continuous separation of cells and particles in microfluidic systems. *Chemical Society Reviews* **39** (3): 1203–1217.

120 Gascoyne, P.R. and Vykoukal, J. (2002). Particle separation by dielectrophoresis. *Electrophoresis* **23** (13): 1973.

121 Fiedler, S., Shirley, S.G., Schnelle, T., and Fuhr, G. (1998). Dielectrophoretic sorting of particles and cells in a microsystem. *Analytical Chemistry* **70** (9): 1909–1915.

122 Zhou, T., Deng, Y., Zhao, H. et al. (2018). The mechanism of size-based particle separation by dielectrophoresis in the viscoelastic flows. *Journal of Fluids Engineering* **140** (9): 091302. (6 pages).

123 Jones, P.V., Salmon, G.L., and Ros, A. (2017). Continuous separation of DNA molecules by size using insulator-based dielectrophoresis. *Analytical Chemistry* **89** (3): 1531–1539.

124 Dabighi, A. and Toghraie, D. (2020). A new microfluidic device for separating circulating tumor cells based on their physical properties by using electrophoresis and dielectrophoresis forces within an electrical field. *Computer Methods and Programs in Biomedicine* **185**: 105147.

125 Modarres, P. and Tabrizian, M. (2019). Frequency hopping dielectrophoresis as a new approach for microscale particle and cell enrichment. *Sensors and Actuators B: Chemical* **286**: 493–500.

126 Aldaeus, F., Lin, Y., Amberg, G., and Roeraade, J. (2006). Multi-step dielectrophoresis for separation of particles. *Journal of Chromatography A* **1131** (1-2): 261–266.

127 Zhang, F. and Li, D. (2014). A novel particle separation method based on induced-charge electro-osmotic flow and polarizability of dielectric particles. *Electrophoresis* **35** (20): 2922–2929.

128 Jia, Y., Ren, Y., and Jiang, H. (2015). Continuous dielectrophoretic particle separation using a microfluidic device with 3D electrodes and vaulted obstacles. *Electrophoresis* **36** (15): 1744–1753.

129 Calero, V., Garcia-Sanchez, P., Ramos, A., and Morgan, H. (2019). Combining DC and AC electric fields with deterministic lateral displacement for micro-and nano-particle separation. *Biomicrofluidics* **13** (5): 054110.

130 Ho, B.D., Beech, J.P., and Tegenfeldt, J.O. (2020). Charge-based separation of micro-and nanoparticles. *Micromachines* **11** (11): 1014.

131 Macey, M.G. and Macey, M.G. (2007). *Flow Cytometry*. Springer.

132 Bonner, W., Hulett, H., Sweet, R., and Herzenberg, L. (1972). Fluorescence activated cell sorting. *Review of Scientific Instruments* **43** (3): 404–409.

133 Ashcroft, R.G. and Lopez, P.A. (2000). Commercial high speed machines open new opportunities in high throughput flow cytometry (HTFC). *Journal of Immunological Methods* **243** (1-2): 13–24.

134 Telleman, P., Larsen, U.D., Philip, J. et al. (1998). Cell sorting in microfluidic systems. In: *Micro Total Analysis Systems' 98* (eds. D.J. Harrison and A. van den Berg). Springer.

135 Krüger, J., Singh, K., O'Neill, A. et al. (2002). Development of a microfluidic device for fluorescence activated cell sorting. *Journal of Micromechanics and Microengineering* **12** (4): 486.

136 Fu, A.Y., Spence, C., Scherer, A. et al. (1999). A microfabricated fluorescence-activated cell sorter. *Nature Biotechnology* **17** (11): 1109–1111.

137 Liu, C. (2018). Microfluidic FACS becoming real. *Cytometry Part A* **93** (6): 589–591.

138 Baret, J.-C., Miller, O.J., Taly, V. et al. (2009). Fluorescence-activated droplet sorting (FADS): efficient microfluidic cell sorting based on enzymatic activity. *Lab on a Chip* **9** (13): 1850–1858.

139 Zhu, X.-D., Shi, X., Wang, S.-W. et al. (2019). High-throughput screening of high lactic acid-producing Bacillus coagulans by droplet microfluidic based flow cytometry with fluorescence activated cell sorting. *RSC Advances* **9** (8): 4507–4513.

140 Alnaimat, F., Dagher, S., Mathew, B. et al. (2018). Microfluidics based magnetophoresis: a review. *The Chemical Record* **18** (11): 1596–1612.

141 Hejazian, M. and Nguyen, N.-T. (2016). Magnetofluidic concentration and separation of non-magnetic particles using two magnet arrays. *Biomicrofluidics* **10** (4): 044103.

142 Robert, D., Pamme, N., Conjeaud, H. et al. (2011). Cell sorting by endocytotic capacity in a microfluidic magnetophoresis device. *Lab on a Chip* **11** (11): 1902–1910.

143 Rosensweig, R.E. (2013). *Ferrohydrodynamics*. Courier Corporation.

144 Nguyen, N.-T. (2012). Micro-magnetofluidics: interactions between magnetism and fluid flow on the microscale. *Microfluidics and Nanofluidics* **12** (1-4): 1–16.

145 Pamme, N. and Manz, A. (2004). On-chip free-flow magnetophoresis: continuous flow separation of magnetic particles and agglomerates. *Analytical Chemistry* **76** (24): 7250–7256.

146 Hatch, G.P. and Stelter, R.E. (2001). Magnetic design considerations for devices and particles used for biological high-gradient magnetic separation (HGMS) systems. *Journal of Magnetism and Magnetic Materials* **225** (1-2): 262–276.

147 Zborowski, M., Ostera, G.R., Moore, L.R. et al. (2003). Red blood cell magnetophoresis. *Biophysical Journal* **84** (4): 2638–2645.

148 Shen, F., Hwang, H., Hahn, Y.K., and Park, J.-K. (2012). Label-free cell separation using a tunable magnetophoretic repulsion force. *Analytical Chemistry* **84** (7): 3075–3081.

149 Zhu, T., Cheng, R., Liu, Y. et al. (2014). Combining positive and negative magnetophoreses to separate particles of different magnetic properties. *Microfluidics and Nanofluidics* **17** (6): 973–982.

150 Sivaramakrishnan, M., Kothandan, R., Govindarajan, D.K. et al. (2020). Active microfluidic systems for cell sorting and separation. *Current Opinion in Biomedical Engineering* **13**: 60–68.

151 Yousuff, C.M., Ho, E.T.W., Ismail Hussain, K., and Hamid, N.H.B. (2017). Microfluidic platform for cell isolation and manipulation based on cell properties. *Micromachines* **8** (1): 15.

152 Adams, J.D., Kim, U., and Soh, H.T. (2008). Multitarget magnetic activated cell sorter. *Proceedings of the National Academy of Sciences* **105** (47): 18165–18170.

153 Yaman, S., Anil-Inevi, M., Ozcivici, E., and Tekin, H.C. (2018). Magnetic force-based microfluidic techniques for cellular and tissue bioengineering. *Frontiers in Bioengineering and Biotechnology* **6**: 192.

154 Miralles, V., Huerre, A., Malloggi, F., and Jullien, M.-C. (2013). A review of heating and temperature control in microfluidic systems: techniques and applications. *Diagnostics* **3** (1): 33.

155 Song, S.-H., Kwak, B.-S., and Jung, H.-I. (2009). Analysis and utilization of Joule heating in an electromagnet integrated microfluidic device for biological applications. *Current Applied Physics* **9** (4): e287–e290.

156 Jung, S.H. (2019). Improved continuous magnetic separation assisted with advection flows in microfluidic channels.

157 Del Giudice, F., Madadi, H., Villone, M.M. et al. (2015). Magnetophoresis 'meets' viscoelasticity: deterministic separation of magnetic particles in a modular microfluidic device. *Lab on a Chip* **15** (8): 1912–1922.

158 Kim, M.J., Lee, D.J., Youn, J.R., and Song, Y.S. (2016). Two step label free particle separation in a microfluidic system using elasto-inertial focusing and magnetophoresis. *RSC Advances* **6** (38): 32090–32097.

159 Liang, W., Liu, J., Yang, X. et al. (2020). Microfluidic-based cancer cell separation using active and passive mechanisms. *Microfluidics and Nanofluidics* **24** (4): 1–19.

160 Wang, X., Sun, L., Zhang, H. et al. (2019). Microfluidic chip combined with magnetic-activated cell sorting technology for tumor antigen-independent sorting of circulating hepatocellular carcinoma cells. *PeerJ* **7**: e6681.

161 Kye, H.G., Park, B.S., Lee, J.M. et al. (2019). Dual-neodymium magnet-based microfluidic separation device. *Scientific Reports* **9** (1): 1–10.

162 Lin, S., Zhi, X., Chen, D. et al. (2019). A flyover style microfluidic chip for highly purified magnetic cell separation. *Biosensors and Bioelectronics* **129**: 175–181.

163 Sung, Y.J., Kim, J.Y.H., Choi, H.I. et al. (2017). Magnetophoretic sorting of microdroplets with different microalgal cell densities for rapid isolation of fast growing strains. *Scientific Reports* **7** (1): 1–11.

164 Tsutsui, H. and Ho, C.-M. (2009). Cell separation by non-inertial force fields in microfluidic systems. *Mechanics Research Communications* **36** (1): 92–103.

165 Jonáš, A. and Zemanek, P. (2008). Light at work: the use of optical forces for particle manipulation, sorting, and analysis. *Electrophoresis* **29** (24): 4813–4851.

166 Neuman, K.C. and Nagy, A. (2008). Single-molecule force spectroscopy: optical tweezers, magnetic tweezers and atomic force microscopy. *Nature Methods* **5** (6): 491–505.

167 Shields, C.W. IV, Reyes, C.D., and López, G.P. (2015). Microfluidic cell sorting: a review of the advances in the separation of cells from debulking to rare cell isolation. *Lab on a Chip* **15** (5): 1230–1249.

168 Yang, Y., Y. Shi, L. Chin et al. (2013). Optofluidic nanoparticles sorting by hydrodynamic optical force. *International Conference on Solid State Sensors and Actuators (TRANSDUCERS)*, Barcelona, Spain (16–20 June 2013).

169 Ng, L.N., Luff, B.J., Zervas, M.N., and Wilkinson, J.S. (2000). Forces on a Rayleigh particle in the cover region of a planar waveguide. *Journal of Lightwave Technology* **18** (3): 388–400.

170 Ashkin, A., Dziedzic, J.M., Bjorkholm, J.E., and Chu, S. (1986). Observation of a single-beam gradient force optical trap for dielectric particles. *Optics Letters* **11** (5): 288–290.

171 Wang, X., Chen, S., Kong, M. et al. (2011). Enhanced cell sorting and manipulation with combined optical tweezer and microfluidic chip technologies. *Lab on a Chip* **11** (21): 3656–3662.

172 Ashkin, A. (1970). Acceleration and trapping of particles by radiation pressure. *Physical Review Letters* **24** (4): 156.

173 Ashkin, A. (1992). Forces of a single-beam gradient laser trap on a dielectric sphere in the ray optics regime. *Biophysical Journal* **61** (2): 569–582.

174 Dholakia, K., Reece, P., and Gu, M. (2008). Optical Micromanipulation. *Chemical Society Reviews* **37** (1): 42–55.

175 Dholakia, K. and Reece, P. (2006). Optical micromanipulation takes hold. *Nano Today* **1** (1): 18–27.

176 Lenton, I.C., Armstrong, D.J., Stilgoe, A.B. et al. (2020). Orientation of swimming cells with annular beam optical tweezers. *Optics Communications* **459**: 124864.

177 Wu, W., Zhu, X., Zuo, Y. et al. (2016). Precise sorting of gold nanoparticles in a flowing system. *ACS Photonics* **3** (12): 2497–2504.

178 Zhao, X., Zhao, N., Shi, Y. et al. (2020). Optical fiber tweezers: a versatile tool for optical trapping and manipulation. *Micromachines* **11** (2): 114.

179 Zhu, R., Avsievich, T., Popov, A., and Meglinski, I. (2020). Optical tweezers in studies of red blood cells. *Cells* **9** (3): 545.

180 Liu, S., Li, Z., and Weng, Z. (2019). Miniaturized optical fiber tweezers for cell separation by optical force. *Optics Letters* **44** (7): 1868–1871.

181 Lin, W.-Y., Lin, Y.-H., and Lee, G.-B. (2010). Separation of micro-particles utilizing spatial difference of optically induced dielectrophoretic forces. *Microfluidics and Nanofluidics* **8** (2): 217–229.

182 Chou, W.-P., Wang, H.-M., Chang, J.-H. et al. (2017). The uti l ization of optically-induced-dielectrophoresis (ODEP)-based virtual cell filters in a microfluidic system for continuous isolation and purification of circulating tumour cells (CTCs) based on their size characteristics. *Sensors and Actuators B: Chemical* **241**: 245–254.

183 Zhang, S., Li, W., Elsayed, M. et al. (2019). Size-scaling effects for microparticles and cells manipulated by optoelectronic tweezers. *Optics Letters* **44** (17): 4171–4174.

184 Wang, M.M., Tu, E., Raymond, D.E. et al. (2005). Microfluidic sorting of mammalian cells by optical force switching. *Nature Biotechnology* **23** (1): 83–87.

185 Chiou, P.-Y.E., Wu, T.-H.S., and Teitell, M.A. (2019). Pulsed laser triggered high speed microfluidic switch and applications in fluorescent activated cell sorting. Google Patents.

186 Chen, Y., Chung, A.J., Wu, T.H. et al. (2014). Pulsed laser activated cell sorting with three dimensional sheathless inertial focusing. *Small* **10** (9): 1746–1751.

187 Paiè, P., Zandrini, T., Vázquez, R.M. et al. (2018). Particle manipulation by optical forces in microfluidic devices. *Micromachines* **9** (5): 200.

188 Snyder, A.W. and Love, J. (2012). *Optical Waveguide Theory*. Springer Science & Business Media.

189 Kim, J. and Shin, J.H. (2016). Stable, free-space optical trapping and manipulation of sub-micron particles in an integrated microfluidic chip. *Scientific Reports* **6**: 33842.

190 Applegate, R.W. Jr., Squier, J., Vestad, T. et al. (2006). Microfluidic sorting system based on optical waveguide integration and diode laser bar trapping. *Lab on a Chip* **6** (3): 422–426.

191 MacDonald, M.P., Spalding, G.C., and Dholakia, K. (2003). Microfluidic sorting in an optical lattice. *Nature* **426** (6965): 421–424.

19

Sustainable Separations Using Organic Solvent Nanofiltration

Nazlee Faisal Ghazali and Ki Min Lim

School of Chemical and Energy Engineering, Universiti Teknologi Malaysia, Johor Bahru, Malaysia

19.1 Introduction to Organic Solvent Nanofiltration

In the early days, filtration of liquids can be performed by using sands and gravels, where gravels can sieve all the large solute particles, and small solute particles can be trapped by the layer of sands. The fundamental theory of filtration with a dense layer and a porous layer was then transformed into membrane filtration in the present day. The basis of filtration depends on the solute molecular size, where it determines the molecular weight cut-off (MWCO) of a membrane. The MWCO of a membrane can be determined by plotting the data of solute rejection against molecular weight, obtained through experimental filtration of feed solution containing solutes with different molecular weights. The minimum molecular weight of solute that is rejected above 90% indicates the MWCO of a particular membrane, for example, MWCO of 400 Da for the data obtained in Figure 19.1b. In membrane filtration, different sizes of solutes can be rejected by the membrane of different MWCO, namely microfiltration (>100 kDa), ultrafiltration (100 to 2 kDa), and reverse osmosis for solutes less than (200 Da) [1].

Nanofiltration involves the filtration of solutes in the range between ultrafiltration and reverse osmosis. Typically, the nanofiltration membrane separates solutes of 200–1000 Da from the target feed solution (Figure 19.1). The nanofiltration process can be carried out in two modes, dead-end or cross-flow. Normally, the dead-end mode of the nanofiltration process can be performed by connecting the outlet of a pressuring gas cylinder (usually nitrogen gas) to a filtration cell. The liquid pressurized by the nitrogen gas will flow perpendicular to the surface of the membrane, to the permeate side. A schematic representation of a dead-end cell is shown in Figure 19.2.

On the other hand, in cross-flow mode, the liquid will flow parallel to the surface of the membrane. The feed solution pressure of the cross-flow mode of filtration can be generated by using either a peristaltic pump, diaphragm pump, or centrifugal pump, depending on the magnitude of pressure required. A schematic representation of a cross-flow cell is shown in Figure 19.3.

Sustainable Separation Engineering: Materials, Techniques and Process Development, Volume 2, First Edition. Edited by Gyorgy Szekely and Dan Zhao.
© 2022 John Wiley & Sons Ltd. Published 2022 by John Wiley & Sons Ltd.

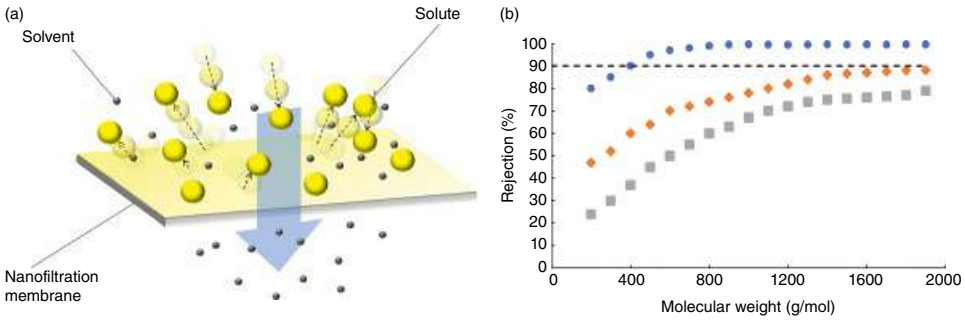

Figure 19.1 Filtration process by using a nanofiltration membrane. (a) Illustration of a nanofiltration process. (b) Typical MWCO curve.

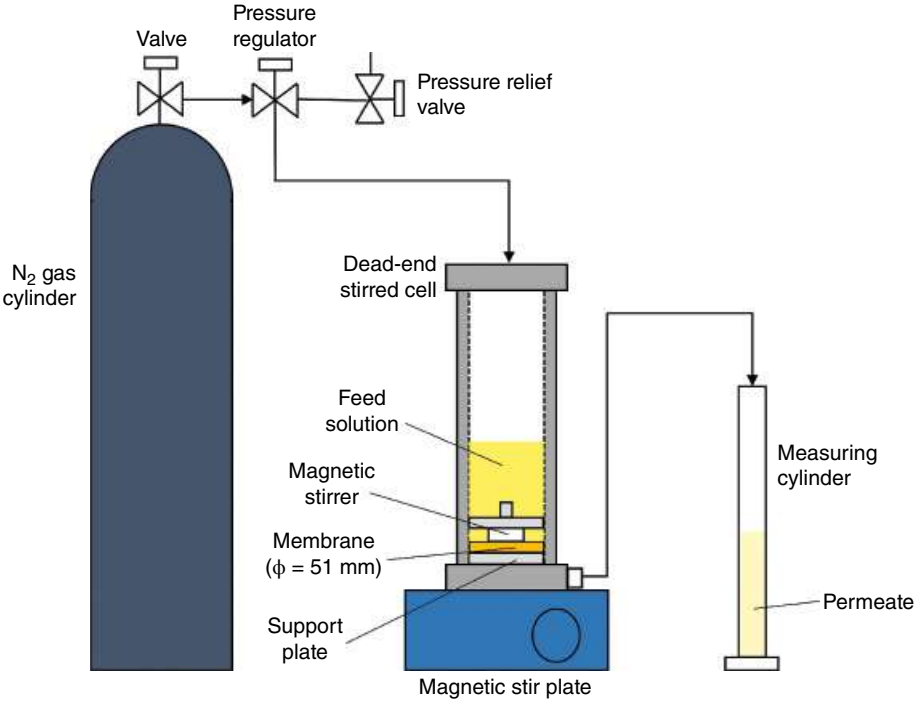

Figure 19.2 Schematic showing the typical configuration of a dead-end cell.

The pressure difference between the feed side of the membrane and permeate side of the membrane will result in the transport of solute/solvent across the membrane. Solute or solvent transport in the membrane can occur by diffusion or convection. In diffusion, the solute or solvent particles move toward the feed interface of the membrane, travels through the membrane matrix, and then detach from the membrane. Diffusion can be driven by concentration or pressure gradient across the membrane.

During nanofiltration, concentration polarization may occur on the membrane, especially for concentrated feed solution. Concentration polarization is the gradual accumulation of

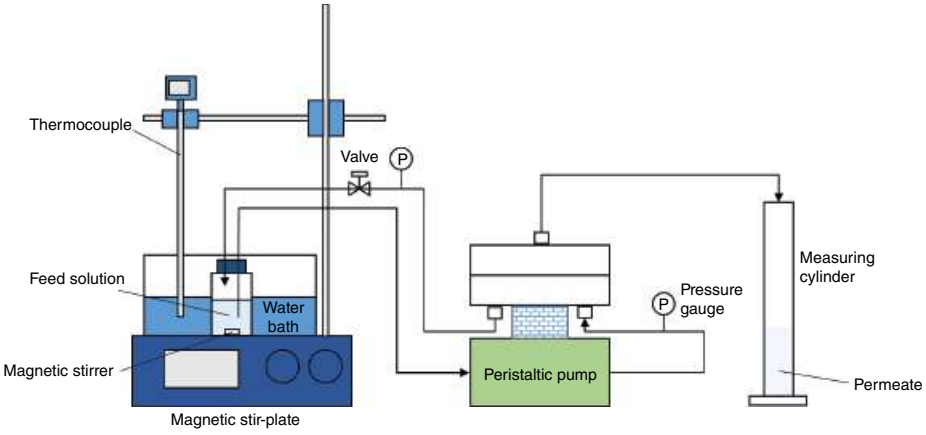

Figure 19.3 Schematic showing the configuration of a cross-flow cell.

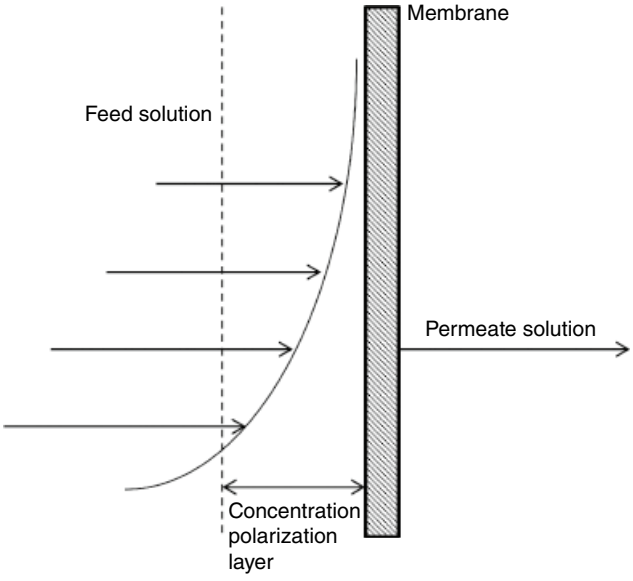

Figure 19.4 Schematic showing concentration polarization during a filtration process.

solutes on the feed side of the membrane, forming a polarizing layer (Figure 19.4). The concentration polarization layer will cause a decrease in solvent permeation rate and increases the rejection of solutes. As concentration polarization is a reversible process, its effect can be reduced. Therefore, in a typical dead-end cell, a magnetic stirrer operated by a magnetic stirring plate can be employed to reduce the thickness of the polarizing layer. On the other hand, in the cross-flow mode of filtration, the cross-flow velocity can be increased to reduce the thickness of the polarizing layer. Membrane fouling occurs when the thickness concentration polarization layer can no longer be reduced, which results in cake formation.

When performing a nanofiltration experiment, the membrane separation performance can be observed by its permeation flux and solute rejection. The permeation flux can be obtained by measuring the mass or volume of the permeate against time. The flux can be calculated by the following formula:

$$J = \frac{1}{A}\frac{\Delta V}{\Delta t} \tag{19.1}$$

where ΔV is the permeate volume accumulated during the operation time, Δt and A is the surface area of the membrane.

The solute rejections are typically obtained by employing the following formula:

$$R_0 = \left(1 - \frac{C_P}{C_R}\right) \times 100\% \tag{19.2}$$

where C_P and C_R are the final concentrations in the permeate and retentate, respectively.

In an aqueous nanofiltration process, the membrane separation performances are mostly impacted by the concentration polarization, membrane fouling, and solute-membrane affinity when a certain membrane is employed at an acceptable operating pressure and temperature of membrane. Despite some of the difficulties and drawbacks, membrane technology has been successfully employed in various water treatment facilities around the world. The application of membrane separation technique in water purification industries have motivated researchers to explore the possibilities of implementing the technology in other fields, such as in the purification of pharmaceuticals [2], purification of oleochemicals [3], catalyst recovery [4], organic solvent recovery [5], chiral compound separations [6], heavy metal removal [7], and virus removal [8]. Organic solvent nanofiltration (OSN) is a pressure-driven process by which solutes dissolved in a solvent are filtered using solvent-resistant nanofiltration membrane. As of current, ExxonMobil's Beaumont refinery manages to deploy OSN membrane units for the purification of 11,500 m^3 of lubrication oil a day, which ultimately reduces 20% of the total energy consumption in their processes [9].

Despite that, the effects of different solvents on the membrane material and structure need to be considered for a wider application of OSN. The membrane material can be made of ceramic/inorganic or polymers/organic. Ceramic membranes generally have better resistance toward harsh organic solvents and operating conditions. Hosseinabadi et al. [10] have investigated Grignard functionalized ceramic nanofiltration membrane for OSN applications. In their study, it was found that their modified ceramic membrane was able to reject mixtures of polystyrenes in acetone, comparable to the commercial DuraMem 300 membrane with an acceptable flux. In another research by Xia et al. [11], a ceramic-supported thin-film composite (TFC) was fabricated for OSN. Their membrane was able to reject methyl orange (327 Da) and acid fuchsin (585 Da) at 30.6 and 90.2%, respectively, with methanol permeance of 26.3 LMH/bar. Although the rejection of solutes was not remarkable as compared with other researches, the permeate flux of methanol in their modified ceramic membrane was substantially higher in comparison.

However, the costly material of ceramic membranes and its sensitivity toward vibrations or physical impacts makes it a difficult material to be developed for various industrial applications. On the other hand, the ease of manufacture and the wider pore size availability of polymeric membranes is a better choice for further modification, improvement, and development. However, as organic solvents can be ranged from mild to harsh, the polymer materials in the membrane can be greatly affected, in which the polymers could be subjected to plasticization. Membrane plasticization or also known as membrane swelling [12] often leads to the loss of mechanical strength of the membrane. The swelling is caused by the sorption of solvent within the polymer matrix which increases the fractional free volume of the membrane. As the mechanical strength decreases, it causes an increase in solvent permeability with low selectivity. Further plasticization will then lead to total membrane failure as the polymer support structure collapses.

Therefore, solvent-resistant polymer materials were often used to fabricate a mechanically and chemically stable membrane. This in turn requires aggressive solvents and high temperatures to dissolve the polymers. In the previous decade, See Toh et al. [13] have discovered the fabrication of solvent-resistant membranes with impressive separation capability. Their membranes were successfully fabricated at room temperature by using polyimide P84 in solvent dimethylformamide (DMF) and 1,4-dioxane. Their work is already advantageous as compared with other polymeric membrane fabrication in terms of temperature requirements. Nevertheless, in recent years, there are rising concerns about their impact on the environment as organic solvents such as 1,4-dioxane and DMF are difficult to be removed from water due to their high boiling point (HBP) [14]. Besides that, studies by Szekely et al. [14] show that the mass intensity and solvent intensity (which is related to green metrics) resulting from membrane preparation in large-scale processes is lower than small or lab scale. This indicates that the solvent waste generated from lab-scale membrane fabrication processes should be either diluted with a huge amount of water before disposal. Nevertheless, membrane fabrication solvent plays an important role in determining the membrane morphology and membrane performance. Therefore, replacing the solvent with a greener alternative should not only dissolve the polymer, but the membrane should also have a good performance in terms of selectivity and permeation flux.

In a recently reported survey of OSN research [15], best recommendation solutions or practices in the OSN field were listed based on a critical assessment of 177 journal articles published from 2015 to 2019. From the listed solutions, about 60% of the solutions have been published in the literature. Besides that, Nguyen Thi et al. [16] have reviewed some of the most recent advances in sustainable OSN membrane fabrications. From the review, it can be known that the fabrication of OSN membranes by using sustainable materials and solvents has been achieved with excellent results, comparable to the traditional OSN fabrications. However, toxic solvents such as DMF, DMAc, and N-Methyl-2-pyrrolidone (NMP) are still widely used in membrane fabrication processes over the past six years [17]. Aside from that, it has been said that the widely used NIPS and TIPS in membrane fabrication processes are unlikely to be replaced [17]. Therefore, a greener solvent and material alternatives for the fabrication of solvent-resistant membrane without compromising its separation performance should be advocated for a sustainable purification process.

19.2 Green Membrane Materials for Organic Solvent Nanofiltration

As the OSN separation technology has become a popular consideration to substitute various conventional chemical separation processes, strategies are needed to ensure that this technology is sustainable in a long run. Various points have been highlighted in the recent reviews on sustainable membrane fabrication and applications (Figure 19.5) [14, 18].

In the "substitution" approach, it is desired to replace conventional solvents used for dissolving the polymer, with greener or low toxicity chemicals. In the recent review [16], a list of chemicals ranging from undesirable to preferred solvents was listed. The preferred solvents are environmentally safe solvents such as water, ethanol, and ionic liquids, while undesirable solvents are toxic solvents such as hexane, NMP, chloroform, and DMF. The use of green solvents has been increasingly adopted by researchers in the OSN field, where some of the latest inventions were listed and discussed in a recent review [19]. Besides that, by replacing the OSN membrane material with renewable resources, such as cellulose and other naturally occurring materials [20], the separation technology can be sustained without the expense of the environment.

In the "reduce" approach, it is recommended to reduce the number of steps in producing the membrane. Through the reduction in the number of steps, the toxic waste resulting from the membrane fabrication during the solvent exchange or polymerization steps can be minimized. Additionally, the costs and energy required for the operations also will be lowered if the number of steps is reduced. The recovery of the solvents or catalysts used is also advantageous, where it can further minimize the cost of the materials, as well as the waste generated from the separation process.

Although it is widely known that the implementation of membrane technology can significantly decrease the energy consumption for a separation process, the use of green

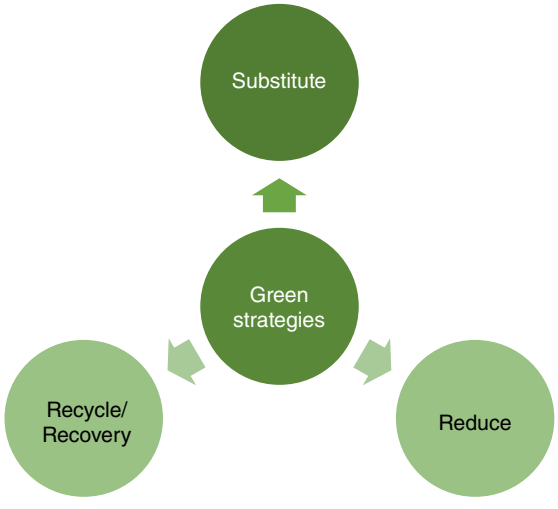

Figure 19.5 Three main green strategies to achieve a sustainable OSN membrane fabrication process.

materials and solvents is rarely highlighted. Therefore, some of the latest inventions that use green strategies will be discussed in this chapter. Two main types of membranes can be fabricated, which are TFC membranes and integrally skinned asymmetric (ISA) membranes (Table 19.1, Figure 19.6) [21].

19.2.1 Thin-film Composite Membranes

TFC membranes are membranes having a porous substrate as the support layer and an active top thin membrane. The porous substrate is an ultrafiltration or nanofiltration grade of ISA membrane that is created through the phase inversion (PI) technique. On the other hand, the selective thin layer is usually produced by interfacial polymerization or dip-coating method. In the filtration process involving TFC, the membrane separation performance mainly depends on the thin selective layer.

To achieve excellent selectivity of TFC membranes for the OSN processes, various materials and techniques have been experimented with by the researchers. In a study by Zhang et al. [32], they reported the fabrication of TFC membranes through the use of beta-cyclodextrin and polydopamine as the materials for the thin selective layer. The porous substrate layer was fabricated by using P84 polyimide which was prepared in solvent DMF/dioxane. Subsequently, the porous substrate was coated in a dip-coating solution (dopamine and beta-cyclodextrin in Tris buffer solution). The prepared membrane was found to be able to reject methyl blue at the rate of 97.6, 95.5, and 98.2% in ethanol, acetone, and water, respectively, with the permeate flux of 8–12 LMH/bar. In another study by Yao et al., they have fabricated a TFC membrane with a cross-linked porous substrate and an ultrathin selective film. The cross-linked porous substrate was constructed by using P84 polyimide cross-linked in an HDA/IPA bath. An interlayer of tannic acid (TA)–copper (Cu) was then constructed on the cross-linked substrate by pouring tannic acid on the PI substrate surface and immersing it in a copper chloride solution. The cross-linked substrate with TA–Cu interlayer was then subjected to interfacial polymerization, whereby m-phenylenediamine (MPD) in DI water and trimesoyl chloride (TMC) in n-hexane was used. The resultant TFC membrane was found to reject 97.72% of Rhodamine B (479 Da) in ethanol, with a permeation flux of 6.027 LMH/bar. The presence of TA–Cu interlayer was found to improve the hydrophilicity of the polyimide (PI) substrate.

In an effort to produce green TFC OSN membranes that can replace the conventional membranes with toxic solvents as part of the materials in the fabrication process, other green solvents and materials have been explored. A cellulose-based membrane was fabricated by Abdellah and his coworkers [36]. Their membrane was made of cellulose porous sublayer with catechin as the thin separating layer. The cellulose porous layer was constructed by using 1-ethyl-3-methylimidazolium acetate (EMIM Ac) as the polymer-solvent and polyethylene as the support. It was found that their membrane was able to reject 92% of Amido-black (617 Da) with 1.4 LMH/bar in DMF.

In another study by Puspasari et al. [37], they have discovered a unique way of fabricating a cellulose-polyethyleneimine (PEI) TFC membrane. Their method uses trimethylsilyl as a precursor for their membrane fabrication, which subsequently undergoes hydrolysis for cellulose regeneration. Their membrane was found to have the MWCO of 450 Da with methanol as the solvent. Their membrane also exhibited a considerably high permeation

Table 19.1 Some of the commonly used chemicals and materials in OSN membrane fabrications and their performances.

Material	Fabrication solvent	Crosslinker	Conditioning solvent	Coating	Thin film	Additives	Type	Mode	Solute-process	Solvent-process	Rejection	Flux (LMH/bar)	Ref
PI P84 support	NMP	HDA/IPA	—	[SiO1.5 (C3H6NH3+ Cl-)]8 POSS-NH3+Cl-	—	—	TFC	Dead-end	Rose Bengal (1017 Da)	Ethanol	99%	1.26	[22]
PI P84/PE support	PEG400 DMF	HDA/IPA	DMF	—	M-phenylenediamine (MPD) in DI water Trimesoyl chloride (TMC) in n-hexane	COFs	TFN	Cross-flow	Rhodamine B (479 Da)	Ethanol	99.40%	7.98	[23]
sPPSU	DMF, THF	0.3 wt% HPEI	—	1 wt% HPEI in ethanol	—	—	TFC	Dead-end	Rose Bengal (1017 Da)	Ethanol	99.9%	1.47	[24]
PMIA/PI support	LiCl DMAc	—	Acetone	—	β-CD-AMA (adamantylamine)/ AMmA (adamantane-methylamine)	—	TFC	Cross-flow	Rose Bengal (1017 Da)	Methanol	98.20%	4.83	[25]
PI P84/PE support	PEG400 DMF	HDA/IPA	DMF	—	M-phenylenediamine (MPD) in DI water Trimesoyl chloride (TMC) in n-hexane	Graphene quantum dots (GQDs)	TFN	Cross-flow	Rhodamine B (479 Da)	Ethanol	98.70%	4.03	[26]
sPPSU	NMP	—	—	PEI coated	—	—	TFC	Dead-end	Eosin Y (645 Da)	Ethanol	100%	10	[27]
		Glutaraldehyde (GTA)		PEI coated					Methyl orange (326 Da)	Ethanol	66.8%	10	
				PEI coated + 0.1 wt% GTA					Methyl orange (327 Da)	Ethanol	89.6%	1.40	

PS/PE support	NMP	—	—	—	Poly-trimethylsilyl-propyne (PTMSP)	—	TFC	Dead-end	Rose Bengal (1017 Da)	Methanol	93%	11	[28]
					PTMSP – Porous Aromatic Framework (PAF-1)	—	TFC	Dead-end	Rose Bengal (1017 Da)	Methanol	94%	17	
					PTMSP – poly-dichloro-xylene (p-DCX)	—	TFC	Dead-end	Rose Bengal (1017 Da)	Methanol	95%	20	
PI P84/PE support	PEG400 DMF	HDA/IPA	DMF	—	M-phenylenediamine (MPD) in DI water Trimesoyl chloride (TMC) in n-hexane	Nanosized amine-modified zeolitic imidazolate framework−8 (mZIF-8)	TFN	Cross-flow	Rhodamine B (479 Da)	Ethanol	99.10%	2.76	[29]
PI P84/PE support	PEG400 DMF	HDA/IPA	DMF	—	Amino-functionalized graphene quantum dots (aGQDs)+ M-phenylenediamine (MPD) in DI water 1,2,4,5-Benzenetetracarboxylic acyl chloride (BTAC) in n-hexane	—	TFN	Cross-flow	Rhodamine B (479 Da)	Ethanol	98%	3.21	[30]
									Rose Bengal (1017 Da)	DMF	99.6%	1.42	
PI P84/PE support	PEG400 DMF	HDA/IPA	DMF	Tannic acid (TA) $CuCl_2$ aqueous solution	M-phenylenediamine (MPD) in DI water Trimesoyl chloride (TMC) in n-hexane	—	TFC	Cross-flow	Rhodamine B (479 Da)	Ethanol	97.72%	6.03	[31]
PI P84	DMF/ Dioxane	—	—	Dopamine (DA) and β-CD in Tris buffer solution	—	—	TFC	Dead-end	Methyl blue (800 Da)	Ethanol	97.6%	13.0	[32]
									Methyl blue (800 Da)	Acetone	95.5%	9.62	
									Methyl blue (800 Da)	Water	98.2%	8.06	

(*Continued*)

Table 19.1 (Continued)

Material	Fabrication solvent	Crosslinker	Conditioning solvent	Coating	Thin film	Additives	Type	Mode	Solute-process	Solvent-process	Rejection	Flux (LMH/bar)	Ref
PAN/PE support	—	—	—	—	Trimesoyl chloride (TMC)/4,4'-(5H-cyclopenta[1,2-b:5,4-b'] dipyridine-5,5-diyl) diphenol (mBHPF)	—	TFC	Dead-end	Methylene blue (320 Da)	Methanol	21.54%	14.5	[33]
									Crystal violet (408 Da)	Methanol	36.3%	14.5	
									Victoria blue (506 Da)	Methanol	47.85%	14.5	
									Methyl blue (800 Da)	Methanol	98.14%	14.5	
									Rose Bengal (1017 Da)	Methanol	98.19%	14.5	
									Alcian blue (1299 Da)	Methanol	99.42%	14.5	
PBI-sPPSU/PP support	DMAc, 1,4-Dioxane cosolvent	DBI-DBX sPPSU-HPEI	—	—	—	—	ISA	Dead-end	Tetracycline (444 Da)	Methanol	84%	6.43	[34]
										Ethanol	83%	4.24	
										Acetone	81%	11.79	
										DMF	66%	10.49	
										Water	66%	7.02	
PI Matrimid 5218	NMP, DEG, THF	HDA/IPA	PEG400/IPA	—	—	—	ISA	Dead-end	Rose Bengal (1017 Da)	IPA	99.64%	5.91	[35]
										THF	98.52%	23.8	
sPPSU	DMF, THF	0.3 wt% HPEI	—	—	—	—	ISA	Dead-end	Rose Bengal (1017 Da)	Ethanol	51%	7.96	[24]

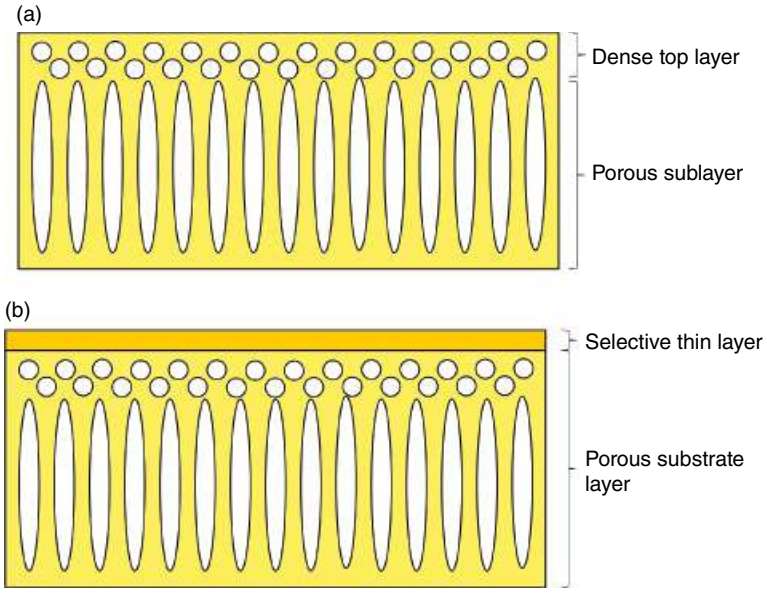

Figure 19.6 Schematic showing the structure of (a) ISA membrane and (b) TFC membrane.

flux, at 35.6 LMH/bar. Puspasari et al. [38] had performed another study by using cellulose-polydimethylsiloxane (PDMS) TFC membrane. They have found that their membrane was able to perform relatively well by using acetone as the solvent, whereby 10 LMH/bar and MWCO of 750 Da was achieved. Their studies had proven the feasibility of employing cellulose-based membrane for the separation of solutes in the organic solvent.

Most recently, Aburabie et al. [39] have discovered a biopolymer TFC membrane for OSN. Their membrane was made of a thin layer consisting of sodium alginate and the porous layer with polyacrylonitrile (PAN) or cross-linked PAN as the main polymeric material. Sodium alginate is a naturally available polysaccharide that can be obtained from brown seaweed. Their cross-linked PAN membrane was produced by using an ionic cross-linking bath (CaCl2/water). Their membranes performed well in methanol and DMF solvents where 98% rejection of Vitamin B12 with an acceptable permeate flux was achieved (Table 19.2).

19.2.2 Integrally Skinned Asymmetric Membranes

ISA are membranes having a dense top layer and a porous bottom layer which enable the separation of solutes and solvents through diffusion and/or convection. ISA membranes can be made through the phase separation (PS) process or PI process, developed by Loeb and Sourirajan [49]. There are four techniques to induce the PS or PI process, namely, evaporation-induced (EIPS), vapor-induced (VIPS), temperature-induced (TIPS), or non-solvent-induced (NIPS) [21]. In TIPS, the process is based on solvent or diluent that dissolves polymer at the temperature close to the melting point of the polymer but performs as non-solvent at lower temperatures. In VIPS, the PI process occurs through the

Table 19.2 The latest research on green TFC and TFN membrane fabrications for OSN applications.

Material	Solvent-membrane	Crosslinker	Conditioning	Coating	Thin film	Additives	Type	Mode	Solute-process	Solvent-process	Rejection	Flux (LMH/bar)	Ref
sPPSU support	NMP	Epichlorohydrin (ECH)	—	PEI-pyrocatechol	—	—	TFC	Dead-end		Ethanol	93% MW > 645 g/mol	11.9	[40]
Remarks: One-step coating.													
PP support	—	Glutaraldehyde (GTA)	PEG	—	GO nanosheets-polyelectrolytes (HPE-1)	—	TFC	Dead-end	Alcian blue (1299 Da)	Ethanol	95%	14.9	[41]
					GO nanosheets-polyelectrolytes (PSS)	—	TFC	Dead-end	Rose Bengal (1017 Da)	Ethanol	97%	3.10	
Remarks: Water-based fabrication.													
PI P84 PP support	DMSO	HDA/IPA	PE/PEG	—	M-phenylenediamine (MPD) in DI water	ZIF-8	TFN	Dead-end	Sunset Yellow (452 Da)	Methanol	95.2%	8.50	[42]
					Trimesoyl chloride (TMC) in n-hexane	ZIF-93	TFN	Dead-end	Sunset Yellow (452 Da)	Methanol	93.1%	11	
						UiO-66	TFN	Dead-end	Sunset Yellow (452 Da)	Methanol	97.9%	11	
Remarks: Green solvent fabrication.													

PAN/PP support	DMF	Hydrazine hydrate in DI water	—	Tannic acid (TA) in phosphate buffer pH7	Terephtaloyl chloride (TPC) in cyclohexane	—	TFC	Dead-end	Rose Bengal (1017 Da)	NMP	93%	0.08	[43]
									Brilliant blue (826 Da)	NMP	93%	0.08	
									Congo red (696 Da)	NMP	93%	0.09	
Remarks: Tannic acid – naturally available material for thin-film fabrication.													
PI Matrimid 5218/PE support	NMP/THF/DEG	HDA/water	IPA/n--hexane	VPC- 1,4-Bis (3-aminopropyl) piperazine (BAPP)	—	UiO-66-NH_2	TFN	Cross-flow	Tetracycline (444 Da)	IPA	90%	1.28	[44]
Remarks: Less waste production by using amine vapor (VPC) for thin-film fabrication.													
PI Matrimid	NMP/ THF cosolvent DEG non-solvent	HDA/IPA	—	VPC- tris (3-aminopropyl) amine (TAPA)	—	UiO-66-NH_2	TFN	Dead-end	Rose Bengal (1017 Da)	IPA	95%	0.40	[45]
Remarks: Less waste production by using amine vapor (VPC) for thin-film fabrication.													
PAN support Cross-linked PAN (XPAN) support Alumina support	—	$CaCl_2$/water	—	—	NaAlg/water	—	TFC	Dead-end	Vitamin B12 (1355 Da)	DMF	Cross-linked Alg/ alumina 70%	0.25	[39]
									Vitamin B12 (1355 Da)	DMF	Cross-linked Alg/XPAN 98%	0.21	

(*Continued*)

Table 19.2 (Continued)

Material	Solvent-membrane	Crosslinker	Conditioning	Coating	Thin film	Additives	Type	Mode	Solute-process	Solvent-process	Rejection	Flux (LMH/bar)	Ref
									Vitamin B12 (1355 Da)	Methanol	Cross-linked Alg/alumina 90%	1.60	
									Vitamin B12 (1355 Da)	Methanol	Cross-linked Alg/PAN 98%	1.27	
Remarks: Polymer solution prepared at room temperature, fabrication solvent used is water, the polymer is biodegradable, cheap, and nontoxic, Cross-linking bath is an aqueous salt solution (nontoxic), Post drying at room temperature.													
Cellulose (Avicel PH101)/PE support	1-ethyl-3-methylimidazolium acetate (EMIM Ac, purity 97%)	—	—	—	Catechin in NaOH/terephethaloyl chloride (TPC) in alpha-pinene	—	TFC	Dead-end	Amido-black (617 Da)	DMF	92%	1.40	[36]
Remarks: Cellulose – green polymer material, and an environmentally friendly ionic liquid as fabrication solvent, hydrocarbon-based solvent for the interfacial polymerization were replaced by bio-derived alpha-pinene.													
PAN support	—	—	—	—	Polyethyleneimine (PEI) + trimesoyl-chloride (TMC)/decanoic acid	—	TFC	Dead-end	Congo red (697 Da)	Methanol	99%	14.7	[46]
									Rose Bengal (1018 Da)	Methanol	99%	13.7	
Remarks: Decanoic acid – green organic phase solvent for TMC (green interfacial polymerization).													
PET support	—	—	—	—	Priamine + Tannic acid/p-cymene + water	—	TFC	Cross-flow	Styrene dimer (235 Da)	Acetone	90%	13.7	[47]
Remarks: Plant-based monomers (Priamine, tannic acid) and green solvents (p-cymene, water) (green interfacial polymerization).													
ODPA, HAB, ODA (1:0.5:0.5) Nanofibrous sheet	DMSO	Cross-linked in a convection oven (180 °C)	—	Sulfonated poly(arylene ether sulfone)	—	—	TFC	Cross-flow	Polystyrene oligomers (400 Da)	DMF	70%	0.37	[48]
Remarks: Plant-based monomers (Priamine, tannic acid) and green solvents (p-cymene, water) (green interfacial polymerization).													

adsorption of non-solvent from a vapor phase (which contains nitrogen or other gases), which subsequently precipitates the casted polymer solution. In EIPS, the precipitation occurs through the evaporation of solvent from the polymer solution. Finally, in NIPS, the polymer solution prepared from dissolving the polymer in a solvent is cast on a nonwoven fabric or glass plate. The casted polymer solution, along with a glass plate or nonwoven fabric, is then immersed in a non-solvent bath to induce polymer precipitation. During PI, the dense top layer is formed through a rapid solvent exchange, while the lower solvent exchange rate forms the porous sublayer. Currently, most of the ISA membranes are fabricated through a combination of techniques [18].

From the previous decades, membranes made of various polymers have been tested for their viability in organic solvent filtration. As organic solvent can be harsh, commonly used membranes in water filtration such as cellulose acetate membranes are not suitable for use. The organic solvent used for the filtration process can easily dissolve the membrane structure, thus making the membrane unusable. From the abundant studies made by researchers on OSN [18, 50], several polymers have been found useful in terms of their resistivity toward organic chemicals. These polymers are PI, PAN, PDMS, polybenzimidazole (PBI), and polyphenylsulfone (PPSU) (Table 19.3). The solvents that are commonly used for dissolving these polymers are DMF, Dioxane, and NMP.

Livingston and See Toh have patented an article [51] that detailed the fabrication of polyimide P84 membrane, which is not only chemical-resistant but also has great performance in terms of rejection and permeation flux of organic solvents. Besides that, they also described the different solvent/cosolvent compositions [52] which produce membrane with different macro-void level. The membranes with macro-voids can be optimized to separate molecules of different sizes or can be employed as a support layer [52, 53].

The mechanical and chemical strength of the polymeric membrane can be fortified through polymeric chain cross-linking. The cross-linking of polymeric membranes, especially PI, was initially constructed to reduce the effect of membrane plasticization during gas or chemical separations [54, 55]. The cross-linking process has since been employed for the fabrication of membranes to resist a wide range of organic chemicals in OSN [56]. Some of the common crosslinkers are 1,2-ethylenediamine (EDA), 1,3-propanediamine (DAP), 1,6-hexanediamine (HDA), and 1,8-octanediamine (ODA) [57]. In 2015, Valtcheva et al. [58] had performed the investigation of different crosslinker parameters on the performance of the membrane, namely, reaction time, temperature, the concentration of crosslinker, and reaction solvent. It was found that the reaction time has the most significant influence on membrane performance. Although cross-linking greatly improves the membrane structure, polymer cross-linking can cause a decrease in permeation flux, which makes some of the cross-linked membranes unapplicable for industrial processes. More importantly, the presence of these hazardous crosslinkers in wastewater will cause detrimental effects to human health [59]. Recently, Farahani et al. [60] have developed a novel cross-linking technique for PBI polymer. The new cross-linking method utilizes TMC which has lower toxicity [60] and 2-Methyl tetrahydrofuran (2-MeTHF) which is a greener solvent [61]. Their studies have revealed that the PBI membrane produced through the new cross-linking method was able to reject tetracycline (444 Da) in ethanol with a rejection rate of 90.4%, with acceptable permeance of 13.8 LMH/bar.

Table 19.3 Chemical structures of commonly used polymers for OSN membrane fabrication.

Polymer	Structure
Polyimide (PI) P84	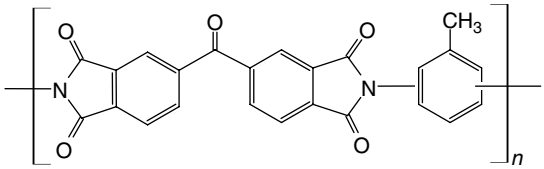 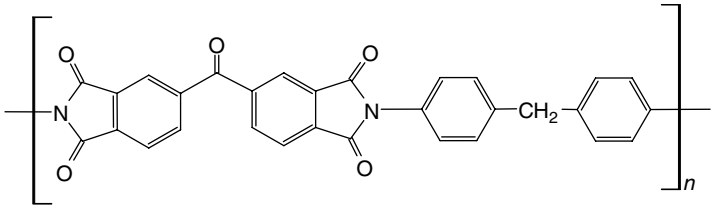
Polyimide (PI) Matrimid	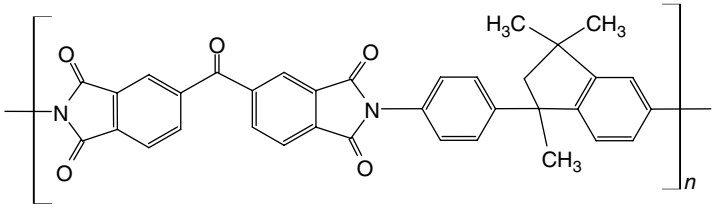
Polyacrylonitrile (PAN)	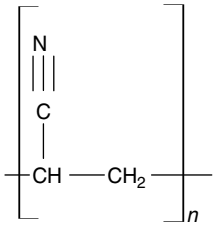
Polydimethylsiloxane (PDMS)	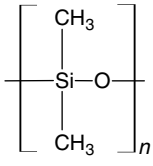
Polybenzimidazole (PBI)	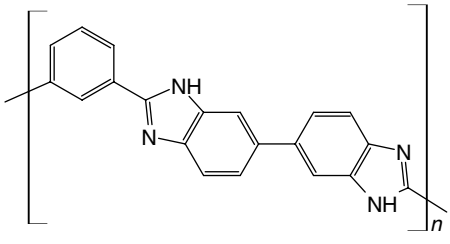
Polyphenylsulfone (PPSU)	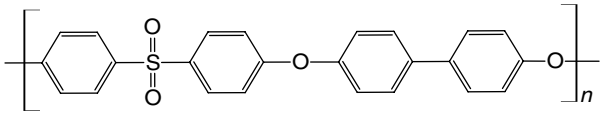

In another study, Tham and Chung [62] have incorporated biophenol (tannic acid) in fabricating their membrane. Their membrane was cross-linked through a single-step cross-linking process, whereby their membrane was immersed in the cross-linking bath containing tannic acid and hydrazine in a certain ratio. Their membrane was able to have a stable performance of 1.2 LMH/bar of methanol with 100% rejection of Evans blue (980 g/mol). Yao et al. [31] have also employed tannic acid for the construction of thin film on a PI substrate. Their membrane has the capability of rejecting 98.7% of Rose Bengal with 15 LMH/bar using DMF as the solvent. Fei et al. [63] have performed an in-depth investigation on different biophenols, namely, dopamine, tannic acid, vanillyl alcohol, eugenol, morin, and quercetin, for the construction of coatings on different solvent-resistant membrane supports. From their results, the membranes after coating with the different biophenols exhibited different ranges of MWCO (mostly between 200 and 1000 g/mol). Their study concluded that the presence of dopamine in the membrane coating enhances the resistance of the PAN and PVDF membranes toward polar aprotic solvent Cyrene. Zhao and his coworkers [64] have fabricated an interpenetrating polymer network (IPN)-based membrane, through the incorporation of polydopamine (PDA) and PBI. Their membrane was successfully developed and was found to have excellent resistance against organic solvent. The presence of PDA was found to improve the permeance of different organic solvents (such as DMF, DMSO, NMP, and Cyrene) in PBI membranes significantly. However, a longer PDA polymerization duration resulted in lower permeance of the membranes, due to the increase in hydrophobicity and decrease in pore size [64]. In a similar study, Xu et al. [22] have fabricated a mussel-inspired catechol and octaammonium polyhedral oligomeric silsesquioxane onto PI substrate. Their membrane was found to have ethanol permeance of 1.26 LMH/bar with 99% rejection of Rose Bengal, which is higher rejection than polydopamine/PI membrane at 2.03 LMH/bar and 55% rejection of Rose Bengal. These studies showed that the membranes fabricated through the use of biophenols have excellent resistance toward organic solvent. Furthermore, the presence of biophenols in some of the investigations showed an improvement in the permeation flux without compromising its MWCO. Therefore, the inclusion of biophenols in membrane fabrication is an excellent green method to tweak the performance of the membrane as compared with the traditional cross-linking which uses toxic chemicals [16].

During the membrane formation process, usually through NIPS, solvent exchange occurs, whereby solvent from the polymer solution will be exchanged with the non-solvent (usually water) bath [21, 51]. The resultant waste solvent bath will then be discarded as chemical waste. The generation of chemical waste from the membrane fabrication process has been a concern by the researchers, which questions the sustainability of the separation process.

Recently, various efforts have been made to replace the solvent for dissolving the polymers with a greener solvent. In a notable study by Soroko et al. [65], they have found that dimethyl sulfoxide (DMSO) can be used as a solvent for dissolving the sturdy P84 polyimide polymer. In their study, DMSO along with acetone as the cosolvent was used to prepare polyimide P84 dope solution. According to the U.S. Food and Drug Administration (FDA), both DMSO and acetone belong to class 3 [66], which can be defined as the solvents with low toxic potential to humans and no health-based exposure limit is needed. They have concluded that the performance of OSN membranes prepared from DMSO/acetone is the

same as the ones prepared from DMF/1,4-dioxane, with DMF as the process solvent. In another research, Hanafia et al. [67] have discovered a novel porous membrane that was made of a bio-based polymer. The bio-based polymer solution can be prepared by dissolving and stirring 20 wt% of hydroxypropylcellulose powder in preheated distilled water (60 °C). Then, the polymer solution was left overnight for degassing. After degassing, 0.5 wt% of crosslinker (glutaraldehyde) was added to the polymer solution and HCl was added before casting, to initiate polymer cross-linking. Their cross-linked bio-based membrane was found to be stable in DMSO, THF, methanol, and chloroform as no re-solubilization was observed in these solvents.

Besides that, Szekely and his coworkers [68] have introduced the use of bamboo fiber as the material for membrane porous substrate or membrane backing construction. In their study, bamboo fiber and polylactic acid were dissolved in dimethyl carbonate and subsequently cast on a glass plate at room temperature. Then, a dope solution of PBI in DMAc was prepared and cast on the bamboo fiber-based porous substrate. The PBI membrane with bamboo fiber backing was then tested with various solvents for its stability. The fabricated membrane was found to be stable in organic solvents such as DMF, NMP, DMSO, acetone, and other solvents [68]. The results from the research show that the commonly used petroleum-based nonwoven membrane backing (polypropylene and polyethylene) can be replaced by a green and biodegradable membrane backing or porous substrate.

In another study by Yuan et al. [69], they have discovered that Kevlar nanofibers can be used as the polymer for membrane construction. Furthermore, the Kevlar nanofibrous membrane was fabricated by using DMSO as the solvent. The Kevlar OSN membrane was able to perform excellently in solvents ethanol, methanol, and isopropanol with the permeances of 2.9, 7.6, and 3.1 LMH/bar while rejecting 95.40% of Rose Bengal (1017 Da). Recently, different ionic liquids were also considered to replace toxic solvents during membrane fabrication [70]. In the investigation by Sukma and Çulfaz-Emecen [70], they have employed a naturally available polymer, cellulose with ionic liquid, 1-ethyl-3-methylimidazolium acetate (EMIM Ac), and acetone as the solvent for the polymer dope preparation. They have found that the fabricated membrane was able to reject 87% of bromothymol blue (624 Da) with 1.5 LMH/bar permeation flux in ethanol solution. As cellulose is a renewable source of material, its availability and biodegradability make it a green and sustainable membrane that should be further investigated and developed.

In the development of ISA membranes, various modifications (Table 19.4) have been attempted which leads to a new class of membrane, mixed matrix membrane. Mixed matrix membranes or composite organic–inorganic/organic–organic membranes have the same fabrication procedure as ISA membranes; however, the inorganic/organic materials (nanoparticles) were mixed with the polymer dope solution before the fabrication process. The introduction of the organic/inorganic materials demonstrated a significant boost in robustness, selectivity, and overall performance of the membrane. From a comprehensive review by Cheng et al. [71], various materials have been studied as the potential fillers for the fabrication of MMMs, which are namely zeolites, metal oxides, activated carbon, carbon molecular sieves, and carbon nanotubes. In a study by Soroko and Livingston [72], titanium dioxide/P84 polyimide MMM and titanium dioxide/cross-linked P84 polyimide were fabricated. It was found that the presence of titanium dioxide prevented the collapse of the

Table 19.4 The latest research on green MMM and ISA membrane fabrications for OSN.

Material	Fabrication solvent	Crosslinker	Conditioning	Additives	Type	Mode	Solute-process	Solvent-process	Rejection	Flux (LMH/bar)	Ref
PEI/PE/PP support	DMSO	—	—	Aramid nanofibers (ANFs) ZIF-8	MMM	Dead-end	Rose Bengal (1017 Da)	IPA	98.2%	1.8	[74]
							Erythrosin (836 Da)	IPA	93.8%	1.8	
Remarks: Green fabrication solvent.											
Celazole® S26 polybenzimidazole (PBI)/PP support	DMAc	TMC in 2-MeTHF	PEG400/IPA	—	ISA	Dead-end	Fast green FCF (809 Da)	MeCN	99.9%	40.7	[60]
							Remazol brilliant blue R (627 Da)	Acetone	99.6%	29	
							Tetracycline (444 Da)	Ethanol	90.4%	13.8	
							Safranin O (351 Da)	IPA	69.8%	5.8	
							L-α-lecithin (758 Da)	Hexane	92%	80.8	
Remarks: Green cross-linking method.											
Kevlar 69	DMSO-KOH/water	—	—	—	ISA	Cross-flow	Rose Bengal (1017 Da)	Ethanol	95.40%	2.9	[69]
								Methanol	95.40%	7.6	
								IPA	95.40%	3.1	
Remarks: Green fabrication solvent.											
Cellulose	Ionic liquid, 1-ethyl-3-methylimidazolium acetate (EMIM Ac)/acetone cosolvent	—	Ethanol	—	ISA	Dead-end	Bromothymol blue (624 Da)	Ethanol	87%	1.5	[70]
Remarks: Green fabrication solvent and cosolvent. Naturally available polymer.											

(*Continued*)

Table 19.4 (Continued)

Material	Fabrication solvent	Crosslinker	Conditioning	Additives	Type	Mode	Solute-process	Solvent-process	Rejection	Flux (LMH/bar)	Ref
Polybenzimidazole (PBI)	Ionic liquid, 1-ethyl-3-methylimidazolium acetate (EMIM Ac)	1,2,7,8-diepoxyoctane (DEO)	Thermal annealing -Ethylene glycol/LiCl	—	ISA	Dead-end	Remazol brilliant blue R (626 Da)	Ethanol	99%	1.02	[75]
PE support							Remazol brilliant blue R (626 Da)	Ethyl acetate	90%	1.37	
							Remazol brilliant blue R (626 Da)	DMSO	90%	0.31	
Polybenzimidazole (PBI)	Ionic liquid, 1-ethyl-3-methylimidazolium acetate (EMIM Ac)	Glutaraldehyde (GA)	Thermal annealing -Ethylene glycol/LiCl	—	ISA	Dead-end	Remazol brilliant blue R (626 Da)	Ethanol	99%	4.16	
PE support							Remazol brilliant blue R (626 Da)	Ethyl acetate	90%	6.57	

Remarks: Green fabrication solvent.

membrane porous structure. Besides that, the presence of titanium dioxide improved the mechanical strength and hydrophilicity of the membranes. In another study, Farahani et al. [73] had fabricated amine-functionalized multi-walled carbon nanotubes (NH2-MWCNT) cross-linked P84 polyimide MMM. It was found that the lower loadings of NH2-MWCNT improved the membrane porosity and permeability with a slight decline in rejection to small solutes. Higher NH2-MWCNT loading caused agglomeration and reduced the membrane separation performance.

19.3 Green Organic Solvent Nanofiltration Processes

In a conventional purification process, the large volume of chemical waste generated from chemical reactions, and waste process water from process equipment cleaning, have been a concern, particularly on its impact on human health and the environment. Since the past century, the chemical effluents from industrial processes were the major contributor to environmental pollution particularly in aquatic ecosystems [76]. Therefore, to reduce the amount of chemical waste generated, various ways and methods have been investigated to recover organic chemicals and catalysts from industrial processes.

19.3.1 Catalyst Recovery

Organic synthesis usually involves the use of homogeneous catalysts, such as organometallic compounds. In the review by Priske et al. [77], homogenous catalysts are typically used in metathesis, hydroformylation, Suzuki coupling, telomerization, and palladium-catalyzed cross-coupling to reduce the substantial amount of energy required for the reactions. Theoretically, the catalysts are not consumed during the chemical reactions, therefore can be recovered for further usage. Thus, the homogeneous catalysts in the post-reaction mixture commonly undergo heterogenization where the homogeneous catalysts were modified to allow separations and recovery [78]. However, the heterogenization process often resulted in a decrease in the performance of the catalysts [77]. Moreover, conventional post-reaction processing techniques involve multiple mass and energy-intensive stages, such as solvent extraction and evaporation, to obtain a purified product. Therefore, OSN was proposed by the researchers as it can provide separations with minimal or no changes to the performance of the catalysts.

In the earlier studies, Tsoukala et al. [79] had proposed the recovery of palladium catalyst after Heck coupling reaction by using polyimide P84 membrane (MWCO of 200 Da). It was reported that their method was able to recover 100% of the palladium catalyst ($[Pd^0(PPh_3)_2OAc]^-$, MW = 690.04 Da) with the solvent acetone permeation flux of 40 LMH with 40 bar operating pressure in 40 minutes. In another study by Wong et al., the catalysts after the Suzuki reaction were recovered by using OSN [80]. In their study, the post-reaction mixture with tris(dibenzylidenacetone)dipalladium catalysts was diluted by using ethyl acetate. The catalysts were then separated from the mixture by using STARMEM 122 membrane (a PI-based membrane). It was reported that they were able to recover 75 to 85% of palladium catalyst from the ionic reaction mixture. In a similar study, Xaba and his coworkers [81] have investigated the recovery of palladium catalysts in a Heck coupling

reaction mixture. The separation was performed by using a dead-end type of filtration cell with different commercial NF/RO membranes supplied by Dow/FilmTec companies. It was found that all of the investigated membranes (XLE, NF90, and BW30) were able to reject more than 99% of bis(triphenylphosphine)palladium (II) chloride catalysts in 2-propanol at 20 bar operating pressure. However, the membranes performed poorly in the recovery of palladium acetate catalysts, whereby the rejections were less than 30% in all the investigated membranes. The lower rejection of palladium acetate catalysts was due to their smaller size (224 g/mol) as compared with bis(triphenylphosphine)palladium (II) chloride catalysts (701.91 g/mol). Nonetheless, the investigations have proven that the recovery of palladium catalysts (701.91 g/mol) was possible given the high rate of rejection. In the recent study by Shen et al. [82], they had performed the investigations of palladium acetate catalysts recovery by using PuraMem S600 and DuraMem 500 membranes. It was found that Duramem 500 membrane was able to reject more than 90% of the palladium acetate catalysts in isopropanol, butanol/water, and methanol. PuraMem S600, on the other hand, performs poorer, whereby the rejection in toluene, isopropanol, and methanol are about 60, 75, and 75%, respectively. However, after agglomeration by using 1,2-Bis (diphenylphosphino) benzene (dppBz) complex, the PuraMem S600 membrane was able to recover 99.5% of the palladium acetate catalysts in toluene and isopropanol and about 90% in methanol.

In a study by Ormerod et al. [83], they have investigated the recovery of palladium catalyst by OSN. They have proposed the use of N-heterocyclic carbenes (NHC) to functionalize palladium catalyst, thus enabling the formation of tailed Pd NHC complexes. The introduction of NHC not only improves the membrane rejection through size exclusion and affinity but also improves the catalyst's resistance toward cluster formation. Their investigations showed that there was a significant improvement in the product recovery, whereby 67% of the tailed catalyst were recovered as compared with the untailed catalyst, 20%. Further process intensification yielded a greater rejection of the tailed catalyst at >90% retention of the catalysts. Bayrakdar et al. [84] have introduced OSN for the recovery of gold catalysts. The model reaction employed in their study was the hydration of diphenylacetylene to produce phenylacetophenone. Their investigation yielded an excellent result, whereby 98.2% of gold catalyst was recovered, with 47% of the product rejected with Me-THF permeance of 10.33 LMH/bar by using a ceramic membrane, Borsig oNF-1. Van der Gryp et al. [85] have also employed OSN to recover Grubbs-type precatalysts after metathesis reaction. It was revealed that STARMEM 228 membrane was able to recover more than 99% of the different catalysts in olefins.

In a recent study by Kisszekelyi et al. [86], they have introduced the use of cyclodextrin to form inclusion complexes with cinchona-based organocatalysts. The formation of the complexes had improved the recovery of the catalyst, whereby 100% of the catalysts were recovered with 98% product purity at 80 g/L/h. In another interesting study by Kisszekelyi et al. [87], OSN membrane was employed for the recovery of catalysts used in an environmentally friendly organic electrosynthesis. In the study, 2,2,6,6-tetramethylpiperidinyl-N-oxyl (TEMPO) catalyst was used in the reaction to convert 5-hydroxymethylfurfural (HMF) into 2,5-diformylfuran (DFF), which is a useful derivative of HMF in pharmaceutical, organic conductors, fungicides, and other applications [87]. The HMF which can be obtained from fructose has undergone electrocatalysis by using green solvents such as

acetonitrile. Before the OSN process, the TEMPO catalysts were anchored to small trifunctional hubs for size enlargement (to form Hub-TEMPO), so that they can be easily separated from other reaction components [88]. Their OSN process yielded a good result, whereby OSN membrane, particularly DuraMem300, was able to reject Hub-TEMPO catalyst at 90–100% rejection, with a lower rejection of other solutes (10–20%) in acetonitrile at 0.73 LMH/bar. The high selectivity of the OSN process enables the recycling of the high-value catalysts for further usage.

19.3.2 Solvent Recovery

Researchers have introduced membrane technology for the recovery of chemical solvents in the recent decade. Kimmerle et al. [89] had introduced the use of polydimethylsilicone-polysulfone composite membrane for the recovery of organic solvent from the air. They have tested the membrane with an acetone–air system. It was found that the membrane was able to recover about 10% of the feed solvent (with 1 wt% of solvent acetone in the air) while about 25% of the feed solvent (with 10% of solvent acetone in the air). On the other hand, White and Nitsch [90] had performed the recovery of solvents from lube oil filtrates by using a PI membrane. The PI membrane was found to successfully recover methyl-ethyl-ketone (MEK)/toluene solvents with more than 99% purity.

Cui and Chung [91] have demonstrated solvent recovery through a pressure-assisted osmosis OSN for pharmaceutical processing. A TFC membrane with MPD/TMC thin layer and polyimide Matrimid 5218 as the substrate was used as the OSN membrane. In their investigation of the tetracycline/IPA system, they were able to recover IPA at the flux of 2.58 LMH/bar with 99% of the tetracycline rejected. They had also performed the investigation of triglyceride/hexane system, whereby 99% of triglyceride were rejected with 5 LMH/bar permeate flux. In another study, Li et al. [92] have prepared a graphene oxide-deposited composite membrane for the pharmaceutical concentration and solvent recovery. Their study revealed that the prepared membrane was able to reject Roxithromycin and Vitamin B12 at the rejection of 92.21 and 95.34%, respectively, with the pure IPA permeation rate of 0.53 LMH/bar. As the use of viscous green solvents such as IPA in OSN often resulted in a low permeation flux, Jang et al. [93] have discovered improved nanofiltration of IPA, whereby a turbostratic nanoporous carbon sheet (TNCS) membrane was used. The TNCS membrane showed incredible solvent permeance of 12900 LMH/bar for acetone (0.33 cP), 1600 LMH/bar for 1-butanol (3 cP). Besides that, the permeation flux of isopropanol (2.4 cP) was achieved at 1840 LMH/bar. The TNCS membrane also showed a high rejection toward solutes larger than 600 Da, such as Congo red, methyl blue, and Evans blue, with more than 99% rejection. Their discovery provides a significant breakthrough in OSN development, as viscous solvents such as IPA are widely used in industries.

Recently, Goh et al. [92] have fabricated a polyamide TFC hollow fiber membrane for the recovery of acetonitrile. Astonishingly, their membrane was able to reject 98.2% of Levofloxacin with acetonitrile permeate flux of 10.58 LMH/bar, in which the solvent permeate flux is considerably high as compared with other works in the literature.

Besides that, various studies have been conducted to recover solvents from vegetable oil in recent years. In a conventional vegetable oil purification process, solvent hexane that was used in the extraction process was commonly evaporated, to obtain crude vegetable oil

for further use. The evaporation of a large quantity of solvent hexane undeniably possesses the risk of explosion, fire, and also chemical pollution to the environment. Recently, Shi et al. [94] had performed investigations on vegetable oil compounds and solvent separations by using commercially available OSN membranes. In their study, it was found that the PuraMem280 polyimide membrane by Evonik was able to obtain solvent acetone at a high permeation rate. Werth et al. [3] also demonstrated the potential of OSN membrane in separating vegetable oil and recovering solvent in the oleochemical industry. In their investigation, a theoretical case study was studied, whereby a series of purification units were modeled by Aspen Custom Modeler (ACM). The process modeling was performed by using experimental data obtained from their previous work [95]. The final result of the process modeling revealed that the model with OSN membranes can achieve more than 70% energy savings as compared with the conventional process. In an investigation by Darvishmanesh et al. [96], they have performed a study on the solvent recovery from different pharmaceutical/solvent mixtures by using PI-based membranes. They have discovered that more than 90% rejection was achieved for DuraMem150 in all tested solvents (methanol, ethanol, isopropanol, and ethyl acetate). Through process modeling by ACM, a comparison between the traditional evaporator and solvent recovery through OSN was performed. It was found that a considerable reduction of energy consumption (>90% reduction) was obtained when OSN was used, with a similar amount of product recovered and similar permeation flux as compared with the traditional evaporator unit. Through simulations, their study has proven the advantages of OSN in terms of energy consumption, as well as recovered solvent over the traditional evaporator process.

Szekely and his coworkers [97] have developed a continuous adsorption process with in-situ solvent recovery. The model of study is based on the solvent used for the extraction of bioactive compounds such as biophenols, as it has been widely extracted for various industrial usage. Ethyl acetate was found to be the most preferable solvent for the process, as it is ranked the highest in the list of GSK solvent recommendations [98]. In the measure of the greenness of a process, the E factor (environmental factor) has been introduced by researchers, which is defined as the ratio of the mass of waste per mass of product. The use of ethyl acetate coupled with OSN has significantly lowered the E factor by 96.4%, as the recycling of 97.5% of ethyl acetate and 44.5% reduction of the carbon footprint was achieved. Besides that, the high selectivity of the membrane yielded a high recovery of oleuropein (99.7% purity). Furthermore, process intensification [99] can improve the recovery of the desired product which subsequently lowered the E factor of the process. In another study by Fodi et al. [100], in-situ solvent recovery in flow reactors coupled with nanofiltration of a pharmaceutical process was investigated. Their model of the study was based on the use of Trialkylamine base catalyst for the Michael addition process. From their investigation, it was found that 90% of the solvent was recovered, with 91% and 19% reduction of E factor and carbon footprint, respectively. Their proposed nanofiltration unit was successful in concentrating the product by 11 times with a purity of 91.5%. The studies demonstrated that OSN membrane is still the best alternative in recovering organic solvents, especially when the E factor is involved.

19.3.3 Fractionation

In a solution mixture of more than two solutes or solvents, fractionation can be used to improve the separations. Fractionation is where the solution mixtures are separated by a

series of separation units, resulting in purified streams of solutes or solvents. Traditionally, the feed liquid solution mixtures were treated by using distillation columns, which yielded purified distillates and bottoms. However, distillation requires a huge amount of energy, especially for multiple distillation units. With the invention of membrane separation units, appropriate arrangements of the separation units will allow the high recoveries of both solutes and solvents with minimal energy requirements. In the membrane separation process, the fractionation of solutes and solvents can be performed through membrane cascades or diafiltration.

In the investigations by Chun-Te Lin and Livingston [101], they have reported a countercurrent membrane cascade for the solvent exchange of methanol with tetraoctylammonium bromide (TOABr)/toluene solution. In their study, the feed solution containing the HBP toluene solvent was replaced by low boiling point (LBP) methanol solvent through a solvent exchange process. The constructed membrane cascade consists of three stages of solvent exchange processes, which aimed to yield purified TOABr/methanol and toluene in the retentate stream and permeate stream, respectively. The final retentate from their study yielded 75.3 wt% of methanol and 0.135 wt% of TOABr. In another study, Kim et al. [102] had constructed a process that consisted of a single-stage diafiltration and two-stage cascade diafiltration. The feed solution in their experiment consisted of PEG-400 and PEG-2000 in acetonitrile. In their two-stage cascade experiment, the solution mixture was fed into a membrane cell (first), in which the permeate stream was connected in series to another membrane cell (second), and the retentate streams from both the membrane cells were recycled back to the feed tank. The final product was collected from the permeate stream of the second membrane cell. To replenish solvents in the retentate stream, a fresh acetonitrile solvent stream was connected to the feed tank, which resulted in a diafiltration process stage. Their work reported a successful application of membrane cascade, where the rejection of PEG-2000 was improved from the initial 59 to 94%.

Siew et al. [103] had proposed an alternative to diafiltration in their OSN experiments. Their alternative incorporated the McCabe–Thiele approach, which was developed into a series of membrane cascades with recycle streams, yielding purified solute and solvent. From their theoretical study, it was found that the constructed membrane cascade design was able to decrease solvent usage significantly and improve separation with a minimal number of stages. In a study by Firman et al. [104], they have designed a seven-stage membrane filtration process without recycling stream. In their study, they have compared the solvent recovery of n-hexane, and soybean oil concentration of their designed process with the conventional process. From their calculations, their designed process was able to save around 50% of energy requirements and 60% of steam and cooling water. Besides that, from the initial feed of 5000 kg/h of n-hexane (containing 25 wt% oil), 4074.94 kg/h of n-hexane (containing 9.5 wt% oil) can be recovered. In another theoretical study by Scharzec et al. [105], they have designed a three-stage process where the permeates from the first and third stages were collected as the purified permeate stream, and retentates from the second and third stages were collected as the purified retentate stream. Before the theoretical study, they performed the filtration of feed containing methanol, water, and catalyst by using various commercially available membranes. From the membrane screening process, DuraMem 150 was selected as the membrane for their subsequent study. After their calculations, a single filtration process wasted 3.522 kg/h of methanol in the retentate stream, considering 10 kg/h of feed solution. By using their process configuration, 9.3 kg/h of

methanol (0 wt% catalyst, 4 wt% water) can be recovered from the 10 kg/h of methanol (0.95 wt% catalyst, 3.8 wt% water). This shows a promising result where more than 90% of the solvents and 99.9% of the catalyst can be recovered.

In the field of bioprocessing, the use of OSN has been recently proposed to fractionate biomass. In a study by Livingston and his coworkers [106], they have introduced the use of OSN membrane to purify catalytic upstream biorefining (CUB) liquor. In their study, isopropanol was employed as the solvent to extract lignin from the liquor. The use of solvent-resistant membranes was able to achieve purity of 97.3% for species more than 1 kDa with 5 LMH/bar. In another study [107], OSN membrane was used to recover extracted biofuels (n-butanol) from an aqueous fermentation system. As high toxicity might affect the microbial metabolism in fermentation, the extractant used to extract biofuels was carefully considered. In their study, 2-ethyl-1-hexanol was chosen as the extractant. It was found that the overall energy consumption of n-butanol (3.9 MJ/kg) was substantially lower than other recovery processes (17–29.4 MJ/kg) with the n-butanol recovery of more than 99.5% purity. In a different investigation by Dubreuil et al. [108], they have performed biomass valorization toward bio-aromatics. Commercial polyamide-based and ceramic membranes were screened in their experiments. It was found that the fractionation of lignin derivatives with lower than 300 g/mol was possible by using Desal-5DK membrane.

In recent years, Renouard et al. [109] had performed simulations on different membrane cascade configurations. They had constructed one configuration where the recycle streams from the second filtration stages are combined with the feed stream of the first filtration stage. In the second configuration, the recycle streams from the second stages are combined with their purified streams, respectively, where the permeate from the enriching cascade is combined with the feed of stripping cascade and vice versa. According to their case studies, different configurations can be chosen based on specific criteria for the separation process.

The fractionation of solutes was proven to be attainable through careful considerations during the construction of membrane cascades and diafiltration in a membrane process design.

19.4 Conclusions and Future Outlook

Various types of membranes have been explored for their capabilities in separating and recovering essential products without altering or degrading the original properties of the compounds. However, environmental concerns of OSN during membrane fabrication and its processes have instigated the research on the sustainability of OSN separations. Recently, various researches have been carried out to improve the green aspects of the current OSN processes. These include the use of greener solvents to replace toxic solvents during membrane fabrication processes, the use of greener or naturally available resources as the membrane materials, reduction in the number of steps during cross-linking, and the reduction in chemical usage and waste generation. The researchers have obtained promising results in their pursue of greener OSN membrane and processes. Some of the latest green membranes produced even have better performance than the ones produced by using toxic

chemicals. Besides that, the currently proposed fractionation method was able to recover products of high purity without high solvent consumption. Some of the currently proposed membrane performance can also be modified or improved through ionic cross-linking instead of toxic organic chemicals. All these efforts showed a major improvement in OSN technology, as compared with the previous decade. Despite this, there is still plenty of research needed, especially in scale-up process development. As of current, there is still insufficient literature on the simultaneous optimization in material, process, and fabrication for scale-up OSN processes as were highlighted by Szekely et al. [14]. The use of efficient investigation techniques such as the design of experiments (DOE), artificial neural networks (ANN) in consideration of material, process, and fabrication are still scarce. Therefore, more research should be done on the scale-up processes to obtain sufficient data for the implementation of green OSN in the industry.

References

1 Federation, W.E. (2005). *Membrane Systems for Wastewater Treatment*. McGraw-Hill Education.

2 Buonomenna, M. and Bae, J. (2015). Organic solvent nanofiltration in pharmaceutical industry. *Separation and Purification Reviews* 44 (2): 157–182.

3 Werth, K., Kaupenjohann, P., and Skiborowski, M. (2017). The potential of organic solvent nanofiltration processes for oleochemical industry. *Separation and Purification Technology* 182: 185–196.

4 Peddie, W.L., Van Rensburg, J.N., Vosloo, H.C., and Van der Gryp, P. (2017). Technological evaluation of organic solvent nanofiltration for the recovery of homogeneous hydroformylation catalysts. *Chemical Engineering Research and Design* 121: 219–232.

5 Rundquist, E.M., Pink, C.J., and Livingston, A.G. (2012). Organic solvent nanofiltration: a potential alternative to distillation for solvent recovery from crystallisation mother liquors. *Green Chemistry* 14 (8): 2197–2205.

6 Ghazali, N.F., Ferreira, F.C., White, A.J., and Livingston, A.G. (2006). Chiral separation by enantioselective inclusion complexation-organic solvent nanofiltration. *Desalination* 199 (1–3): 398–400.

7 Chaudhari, L.B. and Murthy, Z. (2010). Treatment of landfill leachates by nanofiltration. *Journal of Environmental Management* 91 (5): 1209–1217.

8 Kim, J.P., Kim, J.H., Kim, J. et al. (2016). A nanofilter composed of carbon nanotube-silver composites for virus removal and antibacterial activity improvement. *Journal of Environmental Sciences* 42: 275–283.

9 Lively, R.P. and Sholl, D.S. (2017). From water to organics in membrane separations. *Nature Materials* 16 (3): 276–279.

10 Hosseinabadi, S.R., Wyns, K., Meynen, V. et al. (2014). Organic solvent nanofiltration with Grignard functionalised ceramic nanofiltration membranes. *Journal of Membrane Science* 454: 496–504.

11 Xia, L., Ren, J., Weyd, M., and McCutcheon, J.R. (2018). Ceramic-supported thin film composite membrane for organic solvent nanofiltration. *Journal of Membrane Science* 563: 857–863.

12 Gugliuzza, A. (2015). Membrane swelling. In: *Encyclopedia of Membranes* (eds. E. Drioli and L. Giorno), 1–2. Berlin, Heidelberg: Springer.

13 Toh, Y.S., Lim, F., and Livingston, A. (2007). Polymeric membranes for nanofiltration in polar aprotic solvents. *Journal of Membrane Science* 301 (1–2): 3–10.

14 Szekely, G., Jimenez-Solomon, M.F., Marchetti, P. et al. (2014). Sustainability assessment of organic solvent nanofiltration: from fabrication to application. *Green Chemistry* 16 (10): 4440–4473.

15 Le Phuong, H.A., Blanford, C.F., and Szekely, G. (2020). Reporting the unreported: the reliability and comparability of the literature on organic solvent nanofiltration. *Green Chemistry* 22 (11): 3397–3409.

16 Nguyen Thi, H.Y., Nguyen, B.T.D., and Kim, J.F. (2021). Sustainable fabrication of organic solvent nanofiltration membranes. *Membranes* 11 (1): 19.

17 Kim, J. (2020). Recent progress on improving the sustainability of membrane fabrication. *Journal of Membrane Science and Research* 6 (3): 241–250.

18 Marchetti, P., Jimenez Solomon, M.F., Szekely, G., and Livingston, A.G. (2014). Molecular separation with organic solvent nanofiltration: a critical review. *Chemical Reviews* 114 (21): 10735–10806.

19 Kim, D. and Nunes, S.P. (2020). Green solvents for membrane manufacture: recent trends and perspectives. *Current Opinion in Green and Sustainable Chemistry* 28: 100427.

20 Xie, W., Li, T., Tiraferri, A. et al. (2020). *Toward the Next Generation of Sustainable Membranes from Green Chemistry Principles*. ACS Sustainable Chemistry & Engineering.

21 Hilal, N., Ismail, A.F., and Wright, C. (2015). *Membrane Fabrication*. CRC Press.

22 Xu, Y.C., Tang, Y.P., Liu, L.F. et al. (2017). Nanocomposite organic solvent nanofiltration membranes by a highly-efficient mussel-inspired co-deposition strategy. *Journal of Membrane Science* 526: 32–42.

23 Li, C., Li, S., Tian, L. et al. (2019). Covalent organic frameworks (COFs)-incorporated thin film nanocomposite (TFN) membranes for high-flux organic solvent nanofiltration (OSN). *Journal of Membrane Science* 572: 520–531.

24 Tashvigh, A.A., Luo, L., Chung, T.-S. et al. (2018). A novel ionically cross-linked sulfonated polyphenylsulfone (sPPSU) membrane for organic solvent nanofiltration (OSN). *Journal of Membrane Science* 545: 221–228.

25 Xu, S.-J., Shen, Q., Xu, Z.-L., and Dong, Z.-Q. (2019). Novel designed TFC membrane based on host-guest interaction for organic solvent nanofiltration (OSN). *Journal of Membrane Science* 588: 117227.

26 Liang, Y., Li, C., Li, S. et al. (2020). Graphene quantum dots (GQDs)-polyethyleneimine as interlayer for the fabrication of high performance organic solvent nanofiltration (OSN) membranes. *Chemical Engineering Journal* 380: 122462.

27 Feng, Y., Weber, M., Maletzko, C., and Chung, T.-S. (2018). Facile fabrication of sulfonated polyphenylenesulfone (sPPSU) membranes with high separation performance for organic solvent nanofiltration. *Journal of Membrane Science* 549: 550–558.

28 Liu, Q., Smith, S.J., Konstas, K. et al. (2021). Construction of ultrathin PTMSP/Porous nanoadditives membranes for highly efficient organic solvent nanofiltration (OSN). *Journal of Membrane Science* 620: 118911.

29 Yang, S., Li, H., Zhang, X. et al. (2020). Amine-functionalized ZIF-8 nanoparticles as interlayer for the improvement of the separation performance of organic solvent nanofiltration (OSN) membrane. *Journal of Membrane Science* 614: 118433.

30 Li, S., Li, C., Su, B. et al. (2019). Amino-functionalized graphene quantum dots (aGQDs)-embedded thin film nanocomposites for solvent resistant nanofiltration (SRNF) membranes based on covalence interactions. *Journal of Membrane Science* 588: 117212.

31 Yao, Q., Li, S., Zhang, R. et al. (2021). High-throughput thin-film composite membrane via interfacial polymerization using monomers of ultra-low concentration on tannic acid–Copper interlayer for organic solvent nanofiltration. *Separation and Purification Technology* 258: 118027.

32 Zhang, Y., Sun, H., Sadam, H. et al. (2019). Supramolecular chemistry assisted construction of ultra-stable solvent-resistant membranes for angstrom-sized molecular separation. *Chemical Engineering Journal* 371: 535–543.

33 Ren, D., Li, Y.-H., Ren, S.-P. et al. (2020). Microporous polyarylate membrane with nitrogen-containing heterocycles to enhance separation performance for organic solvent nanofiltration. *Journal of Membrane Science* 610: 118295.

34 Tashvigh, A.A., Luo, L., Chung, T.-S. et al. (2018). Performance enhancement in organic solvent nanofiltration by double crosslinking technique using sulfonated polyphenylsulfone (sPPSU) and polybenzimidazole (PBI). *Journal of Membrane Science* 551: 204–213.

35 Gao, Z.F., Shi, G.M., Cui, Y., and Chung, T.-S. (2018). Organic solvent nanofiltration (OSN) membranes made from plasma grafting of polyethylene glycol on cross-linked polyimide ultrafiltration substrates. *Journal of Membrane Science* 565: 169–178.

36 Abdellah, M.H., Pérez-Manríquez, L., Puspasari, T. et al. (2018). A catechin/cellulose composite membrane for organic solvent nanofiltration. *Journal of Membrane Science* 567: 139–145.

37 Puspasari, T., Huang, T., Sutisna, B., and Peinemann, K.-V. (2018). Cellulose-polyethyleneimine blend membranes with anomalous nanofiltration performance. *Journal of Membrane Science* 564: 97–105.

38 Puspasari, T., Chakrabarty, T., Genduso, G., and Peinemann, K.-V. (2018). Unique cellulose/polydimethylsiloxane blends as an advanced hybrid material for organic solvent nanofiltration and pervaporation membranes. *Journal of Materials Chemistry A* 6 (28): 13685–13695.

39 Aburabie, J.H., Puspasari, T., and Peinemann, K.-V. (2020). Alginate-based membranes: paving the way for green organic solvent nanofiltration. *Journal of Membrane Science* 596: 117615.

40 Feng, Y., Weber, M., Maletzko, C., and Chung, T.-S. (2019). Fabrication of organic solvent nanofiltration membranes via facile bioinspired one-step modification. *Chemical Engineering Science* 198: 74–84.

41 Hua, D. and Chung, T.-S. (2017). Polyelectrolyte functionalized lamellar graphene oxide membranes on polypropylene support for organic solvent nanofiltration. *Carbon* 122: 604–613.

42 Paseta, L., Navarro, M., Coronas, J., and Téllez, C. (2019). Greener processes in the preparation of thin film nanocomposite membranes with diverse metal-organic frameworks for organic solvent nanofiltration. *Journal of Industrial and Engineering Chemistry* 77: 344–354.

43 Pérez-Manríquez, L., Neelakanda, P., and Peinemann, K.-V. (2017). Tannin-based thin-film composite membranes for solvent nanofiltration. *Journal of Membrane Science* 541: 137–142.

44 Gao, Z.F., Naderi, A., Wei, W., and Chung, T.-S. (2020). Selection of crosslinkers and control of microstructure of vapor-phase crosslinked composite membranes for organic solvent nanofiltration. *Journal of Membrane Science* 616: 118582.

45 Gao, Z.F., Feng, Y., Ma, D., and Chung, T.-S. (2019). Vapor-phase crosslinked mixed matrix membranes with UiO-66-NH2 for organic solvent nanofiltration. *Journal of Membrane Science* 574: 124–135.

46 Ong, C., Falca, G., Huang, T. et al. (2020). Green synthesis of thin-film composite membranes for organic solvent nanofiltration. *ACS Sustainable Chemistry & Engineering* 8 (31): 11541–11548.

47 Park, S.-H., Alammar, A., Fulop, Z. et al. (2021). Hydrophobic thin film composite nanofiltration membranes derived solely from sustainable sources. *Green Chemistry* 23: 1175–1184.

48 Kim, J.H., Cook, M., Park, S.H. et al. (2018). A compact and scalable fabrication method for robust thin film composite membranes. *Green Chemistry* 20 (8): 1887–1898.

49 Loeb, S. and Sourirajan, S. (1964). UCLA Engineering Report 60-60 (1960). US Patents 3(3,133,137), 196.

50 Lee, S., Kang, T., Lee, J.Y. et al. (2021). Thin-film composite nanofiltration membranes for non-polar solvents. *Membranes* 11 (3): 184.

51 Livingston, A.G. and See-Toh, Y.H. (2014). Asymmetric membranes for use in nanofiltration. Google Patents.

52 See-Toh, Y.H., Silva, M., and Livingston, A. (2008). Controlling molecular weight cut-off curves for highly solvent stable organic solvent nanofiltration (OSN) membranes. *Journal of Membrane Science* 324 (1–2): 220–232.

53 Tan, X. and Rodrigue, D. (2019). A review on porous polymeric membrane preparation. Part I: production techniques with polysulfone and poly (vinylidene fluoride). *Polymers* 11 (7): 1160.

54 Wind, J.D., Staudt-Bickel, C., Paul, D.R., and Koros, W.J. (2002). The effects of crosslinking chemistry on CO2 plasticization of polyimide gas separation membranes. *Industrial & Engineering Chemistry Research* 41 (24): 6139–6148.

55 Galizia, M. and Bye, K.P. (2018). Advances in organic solvent nanofiltration rely on physical chemistry and polymer chemistry. *Frontiers in Chemistry* 6: 511.

56 Asadi Tashvigh, A., Feng, Y., Weber, M. et al. (2019). 110th anniversary: selection of cross-linkers and cross-linking procedures for the fabrication of solvent-resistant nanofiltration membranes: a review. *Industrial & Engineering Chemistry Research* 58 (25): 10678–10691.

57 Vanherck, K., Koeckelberghs, G., and Vankelecom, I.F. (2013). Crosslinking polyimides for membrane applications: a review. *Progress in Polymer Science* 38 (6): 874–896.

58 Valtcheva, I.B., Marchetti, P., and Livingston, A.G. (2015). Crosslinked polybenzimidazole membranes for organic solvent nanofiltration (OSN): analysis of crosslinking reaction mechanism and effects of reaction parameters. *Journal of Membrane Science* 493: 568–579.

59 Sweet, D.V., Anderson, V.P., and Fang, J.C. (1999). An overview of the registry of toxic effects of chemical substances (RTECS): critical information on chemical hazards. *Chemical Health & Safety* 6 (6): 12–16.

60 Farahani, M.H.D.A. and Chung, T.-S. (2019). A novel crosslinking technique towards the fabrication of high-flux polybenzimidazole (PBI) membranes for organic solvent nanofiltration (OSN). *Separation and Purification Technology* 209: 182–192.

61 Clarke, C.J., Tu, W.-C., Levers, O. et al. (2018). Green and sustainable solvents in chemical processes. *Chemical Reviews* 118 (2): 747–800.

62 Tham, H.M. and Chung, T.-S. (2020). One-step cross-linking and tannic acid modification of polyacrylonitrile hollow fibers for organic solvent nanofiltration. *Journal of Membrane Science* 610: 118294.

63 Fei, F., Le Phuong, H.A., Blanford, C.F., and Szekely, G. (2019). Tailoring the performance of organic solvent nanofiltration membranes with biophenol coatings. *ACS Applied Polymer Materials* 1 (3): 452–460.

64 Zhao, D., Kim, J.F., Ignacz, G. et al. (2019). Bio-inspired robust membranes nanoengineered from interpenetrating polymer networks of polybenzimidazole/polydopamine. *ACS Nano* 13 (1): 125–133.

65 Soroko, I., Bhole, Y., and Livingston, A.G. (2011). Environmentally friendly route for the preparation of solvent resistant polyimide nanofiltration membranes. *Green Chemistry* 13 (1): 162–168.

66 Reid, G.L. (2020). Residual solvents. In: *Specification of Drug Substances and Products* (eds. C.M. Riley, T.W. Rosanske and G. Reid), 345–365. Elsevier.

67 Hanafia, A., Faur, C., Deratani, A. et al. (2017). Fabrication of novel porous membrane from biobased water-soluble polymer (hydroxypropylcellulose). *Journal of Membrane Science* 526: 212–220.

68 Le Phuong, H.A., Izzati Ayob, N.A., Blanford, C.F. et al. (2019). Nonwoven membrane supports from renewable resources: bamboo fiber reinforced poly (lactic acid) composites. *ACS Sustainable Chemistry & Engineering* 7 (13): 11885–11893.

69 Yuan, S., Swartenbroekx, J., Li, Y. et al. (2019). Facile synthesis of Kevlar nanofibrous membranes via regeneration of hydrogen bonds for organic solvent nanofiltration. *Journal of Membrane Science* 573: 612–620.

70 Sukma, F.M. and Çulfaz-Emecen, P.Z. (2018). Cellulose membranes for organic solvent nanofiltration. *Journal of Membrane Science* 545: 329–336.

71 Cheng, Y., Ying, Y., Japip, S. et al. (2018). Advanced porous materials in mixed matrix membranes. *Advanced Materials* 30 (47): 1802401.

72 Soroko, I. and Livingston, A. (2009). Impact of TiO2 nanoparticles on morphology and performance of crosslinked polyimide organic solvent nanofiltration (OSN) membranes. *Journal of Membrane Science* 343 (1–2): 189–198.

73 Farahani, M.H.D.A., Hua, D., and Chung, T.-S. (2018). Cross-linked mixed matrix membranes (MMMs) consisting of amine-functionalized multi-walled carbon nanotubes and P84 polyimide for organic solvent nanofiltration (OSN) with enhanced flux. *Journal of Membrane Science* 548: 319–331.

74 Li, Y., Li, J., Soria, R.B. et al. (2020). Aramid nanofiber and modified ZIF-8 constructed porous nanocomposite membrane for organic solvent nanofiltration. *Journal of Membrane Science* 603: 118002.

75 Xing, D.Y., Chan, S.Y., and Chung, T.-S. (2014). The ionic liquid [EMIM] OAc as a solvent to fabricate stable polybenzimidazole membranes for organic solvent nanofiltration. *Green Chemistry* 16 (3): 1383–1392.

76 Wexler, P. (2014). *Encyclopedia of Toxicology*. Elsevier Science.

77 Priske, M., Lazar, M., Schnitzer, C., and Baumgarten, G. (2016). Recent applications of organic solvent nanofiltration. *Chemie Ingenieur Technik* 88 (1–2): 39–49.

78 Collis, A.E. and Horvath, I.T. (2011). Heterogenization of homogeneous catalytic systems. *Catalysis Science & Technology* 1 (6): 912–919.

79 Tsoukala, A., Peeva, L., Livingston, A.G., and Bjørsvik, H.R. (2012). Separation of reaction product and palladium catalyst after a Heck coupling reaction by means of organic solvent nanofiltration. *ChemSusChem* 5 (1): 188–193.

80 Wong, H.-T., Pink, C.J., Ferreira, F.C., and Livingston, A.G. (2006). Recovery and reuse of ionic liquids and palladium catalyst for Suzuki reactions using organic solvent nanofiltration. *Green Chemistry* 8 (4): 373–379.

81 Xaba, B.M., Modise, S.J., Okoli, B.J. et al. (2020). Characterization of selected polymeric membranes used in the separation and recovery of palladium-based catalyst systems. *Membranes* 10 (8): 166.

82 Shen, J., Beale, K., Amura, I., and Emanuelsson, E.A. (2020). Ligand and solvent selection for enhanced separation of palladium catalysts by organic solvent nanofiltration. *Frontiers in Chemistry* 8: 375.

83 Ormerod, D., Dorbec, M., Merkul, E. et al. (2018). Synthesis of Pd complexes containing tailed NHC ligands and their use in a semicontinuous membrane-assisted Suzuki cross-coupling process. *Organic Process Research & Development* 22 (11): 1509–1517.

84 Bayrakdar, T.A., Nahra, F., Zugazua, O. et al. (2020). Improving process efficiency of gold-catalyzed hydration of alkynes: merging catalysis with membrane separation. *Green Chemistry* 22 (8): 2598–2604.

85 Van der Gryp, P., Barnard, A., Cronje, J.-P. et al. (2010). Separation of different metathesis Grubbs-type catalysts using organic solvent nanofiltration. *Journal of Membrane Science* 353 (1–2): 70–77.

86 Kisszekelyi, P., Alammar, A., Kupai, J. et al. (2019). Asymmetric synthesis with cinchona-decorated cyclodextrin in a continuous-flow membrane reactor. *Journal of Catalysis* 371: 255–261.

87 Kisszekelyi, P., Hardian, R., Vovusha, H. et al. (2020). Selective electrocatalytic oxidation of biomass-derived 5-hydroxymethylfurfural to 2, 5-diformylfuran: from mechanistic investigations to catalyst recovery. *ChemSusChem* 13 (12): 3127.

88 Cseri, L., Fodi, T., Kupai, J. et al. (2017). Membrane-assisted catalysis in organic media. *Advanced Materials Letters* 8 (12): 1094–1124.

89 Kimmerle, K., Bell, C., Gudernatsch, W., and Chmiel, H. (1988). Solvent recovery from air. *Journal of Membrane Science* 36: 477–488.

90 White, L.S. and Nitsch, A.R. (2000). Solvent recovery from lube oil filtrates with a polyimide membrane. *Journal of Membrane Science* 179 (1–2): 267–274.

91 Cui, Y. and Chung, T.-S. (2019). Solvent recovery via organic solvent pressure assisted osmosis. *Industrial & Engineering Chemistry Research* 58 (12): 4970–4978.

92 Goh, K.S., Chen, Y., Chong, J.Y. et al. (2021). Thin film composite hollow fibre membrane for pharmaceutical concentration and solvent recovery. *Journal of Membrane Science* 621: 119008.

93 Jang, J., Nam, Y.T., Kim, D. et al. (2020). Turbostratic nanoporous carbon sheet membrane for ultrafast and selective nanofiltration in viscous green solvents. *Journal of Materials Chemistry A* 8 (17): 8292–8299.

94 Shi, G.M., Farahani, M.H.D.A., Liu, J.Y., and Chung, T.-S. (2019). Separation of vegetable oil compounds and solvent recovery using commercial organic solvent nanofiltration membranes. *Journal of Membrane Science* 588: 117202.

95 Werth, K., Kaupenjohann, P., Knierbein, M., and Skiborowski, M. (2017). Solvent recovery and deacidification by organic solvent nanofiltration: experimental investigation and mass transfer modeling. *Journal of Membrane Science* 528: 369–380.

96 Darvishmanesh, S., Firoozpour, L., Vanneste, J. et al. (2011). Performance of solvent resistant nanofiltration membranes for purification of residual solvent in the pharmaceutical industry: experiments and simulation. *Green Chemistry* 13 (12): 3476–3483.

97 Didaskalou, C., Buyuktiryaki, S., Kecili, R. et al. (2017). Valorisation of agricultural waste with an adsorption/nanofiltration hybrid process: from materials to sustainable process design. *Green Chemistry* 19 (13): 3116–3125.

98 Henderson, R.K., Jiménez-González, C., Constable, D.J. et al. (2011). Expanding GSK's solvent selection guide–embedding sustainability into solvent selection starting at medicinal chemistry. *Green Chemistry* 13 (4): 854–862.

99 Voros, V., Drioli, E., Fonte, C., and Szekely, G. (2019). Process intensification via continuous and simultaneous isolation of antioxidants: an upcycling approach for olive leaf waste. *ACS Sustainable Chemistry & Engineering* 7 (22): 18444–18452.

100 Fodi, T., Didaskalou, C., Kupai, J. et al. (2017). Nanofiltration-enabled in situ solvent and reagent recycle for sustainable continuous-flow synthesis. *ChemSusChem* 10 (17): 3435.

101 Chun-Te Lin, J. and Livingston, A.G. (2007). Nanofiltration membrane cascade for continuous solvent exchange. *Chemical Engineering Science* 62 (10): 2728–2736.

102 Kim, J.F., da Silva, A.M.F., Valtcheva, I.B., and Livingston, A.G. (2013). When the membrane is not enough: a simplified membrane cascade using organic solvent nanofiltration (OSN). *Separation and Purification Technology* 116: 277–286.

103 Siew, W.E., Livingston, A.G., Ates, C., and Merschaert, A. (2013). Continuous solute fractionation with membrane cascades–a high productivity alternative to diafiltration. *Separation and Purification Technology* 102: 1–14.

104 Firman, L.R., Ochoa, N.A., Marchese, J., and Pagliero, C. (2020). Designing of spiral wound nanofiltration multistage process for oil concentration and solvent recovery from soybean oil/n-hexane miscella. *Chemical Engineering Research and Design* 164: 46–58.

105 Scharzec, B., Holtkötter, J., Bianga, J. et al. (2020). Conceptual study of co-product separation from catalyst-rich recycle streams in thermomorphic multiphase systems by OSN. *Chemical Engineering Research and Design* 157: 65–76.

106 Sultan, Z., Graça, I., Li, Y. et al. (2019). Membrane fractionation of liquors from lignin-first biorefining. *ChemSusChem* 12 (6): 1203–1212.

107 Kim, J.H., Cook, M., Peeva, L. et al. (2020). Low energy intensity production of fuel-grade bio-butanol enabled by membrane-based extraction. *Energy & Environmental Science* 13 (12): 4862–4871.

108 Dubreuil, M.F., Servaes, K., Ormerod, D. et al. (2017). Selective membrane separation technology for biomass valorization towards bio-aromatics. *Separation and Purification Technology* 178: 56–65.

109 Renouard, T., Lejeune, A., and Rabiller-Baudry, M. (2018). Separation of solutes with an organic solvent nanofiltration cascade: designs, simulations and systematic study of all configurations. *Separation and Purification Technology* 194: 111–122.

20

Sustainable Separations in the Chemical Engineering Curriculum

Thomas Rodgers

Department of Chemical Engineering and Analytical Science, The University of Manchester, Manchester, UK

20.1 Introduction

Separations are a very diverse area, as seen from the previous chapters. In addition to the basic science underlying the separation mechanism, there are factors such as industry preference, cost, competing methods, scale-up/staging, separation factor needed, and corporate social responsibility/sustainability.

This chapter will limit some of this scope by only considering separations within the Chemical Engineering sector, i.e. industrial chemical separations, and thus ignore those found within analytical chemistry, mechanical engineering, etc. From Figure 20.1, it can be seen that over the last 25 years, the number of articles published on both sustainability and separations have been increasing – in this case the filter of chemical engineering has been used, which is likely to have removed a large proportion of articles; however, this also means that sustainability not related to the chemical industry has not been included, e.g. sustainable buildings. A small proportion of the published articles also include the key word education; however, these are also increasing demonstrating the increasing importance of teaching both separations and sustainability.

Separations are key within industrial processes accounting for 40–70% of both capital and operating expenses [2]. They also present opportunities for more efficient use of energy and raw materials as well as opportunities for waste reduction. Not only are new developments in sustainable separations, as given in the previous chapters, critical for continued competitive productivity but also the teaching of sustainability within separations is needed. This chapter will examine some of the current approaches used for teaching separations and will also make some comments on future directions.

Sustainable Separation Engineering: Materials, Techniques and Process Development, Volume 2, First Edition. Edited by Gyorgy Szekely and Dan Zhao.
© 2022 John Wiley & Sons Ltd. Published 2022 by John Wiley & Sons Ltd.

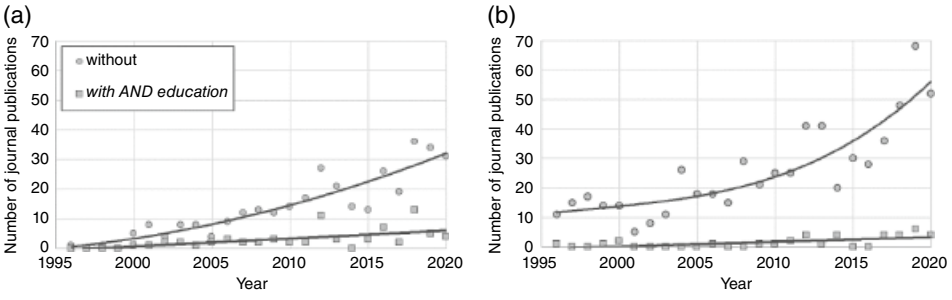

Figure 20.1 Search for "Chemical Engineering" articles through Web of Science [1] with and without the additional search keyword of education. (a) is for variants of the key word sustainability (with AND sustainab*) and (b) is for variants of the key word separation (with AND separat*). Lines are not a fit and just used to guide the eye.

20.2 Current Approaches to Teaching Separations

In order to discuss what the current approach to teaching separations on degree courses are, it is important to be able to classify them. Table 20.1 provides this classification by the general method, though it is not uncommon to classify by separation property or similarity in design analysis [3].

From Table 20.1, it is clear that there are a large number of potential separations (and that is not an exhaustive list); therefore, to teach all of these, a large amount of time would need to be allocated. This separations-oriented Chemical Engineering curriculum would have to use separations as the unifying theme; however, this does not fit into current or future trends in curriculum development [4–6]. With overcrowded curriculums, separation methods receive a small section of the time and thus, courses have chosen which separations to include. Figure 20.2 provides the key separations taught across representative chemical engineering courses.

Table 20.1 Some Separations as classified by the general method.

Method	Examples
Phase addition/creation	Condensation, vapourization, continuous/batch distillation, extractive distillation, absorption, stripping, liquid–liquid extraction, drying, evaporation, solution/melt crystallization, leaching, coagulation/flocculation, molecular distillation, reactive distillation
Barrier	Osmosis, reverse osmosis, dialysis, filtration, micro-/ultra-filtration, gas permeation, pervaporation
Solid agents	Adsorption, chromatography, ion exchange
External field/gradient	Gravity settling, flotation, centrifugation, (hydro)cyclone, electrolysis, electrodialysis, field-flow fractionation, magnetic

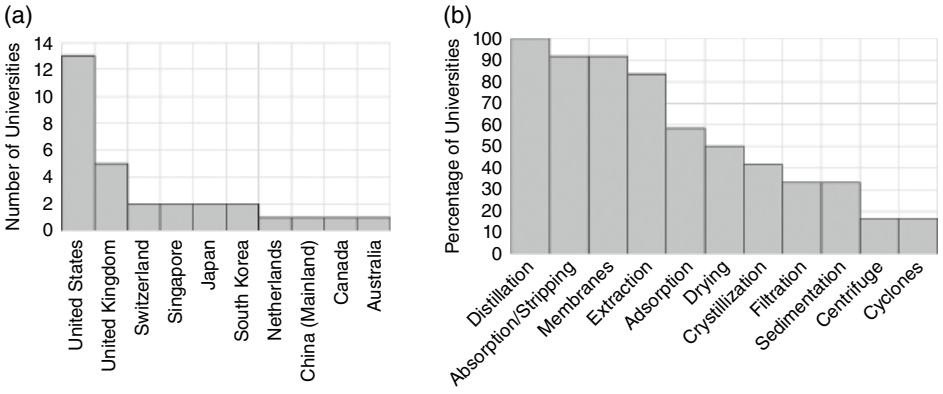

Figure 20.2 Summary of named separation techniques listed by name in courses on the top 30 Chemical Engineering degrees as ranked by the QS World University Rankings 2019 [7]. (a) is the breakdown of location of the top 30 degrees and (b) is the percentage of degrees which name the separation techniques. It should be noted that some separations may be taught that are not listed here, but this is due to them not being directly named in unit specifications.

Distillation is a named separation topic on all courses, this is likely due to its wide use in industry (in the late 1990s, it was estimated that 90–95% of all separations in the chemical process industry were distillation [2]) and that it can be typically well modeled using process simulators [8]. Absorption and stripping are likewise named on almost all courses, due to the similar design methods and staging as distillation columns.

Membrane separation processes are also commonly named, likely due to their current success in water treatment and medical applications. Although commonly named, quite a number of the modules with this listed are optional. Due to its usefulness for cases where distillation does not work, extraction is also commonly named as an examined separation technique.

Just over half of the degree courses had adsorption as a listed separation technique, and many of these within optional units at the higher end of the courses. This is likely due to a perceived difficulty of the topic and the rate-based analysis method needed; membranes are probably the easiest of the rate-based separations to teach due to typical operation at steady state. Drying and crystallization is similarly placed, although critically important in many industry areas, these have not always been considered core chemical engineering areas. Interestingly, mechanical separations such as filtration, settling, centrifugation, and cyclones are widely ignored on most degrees although fundamental in many areas.

The classical method of teaching separations was to start with equilibrium-stage separations, typically one stage, e.g. evaporation, and then extend this to multistage, e.g. distillation, and then potentially to the addition of a mass separating agent, e.g. extraction. To do this, graphical methods were heavily utilized, including McCabe–Thiele, Ponchon Savarit, and Hunter–Nash (on triangular diagrams). These taught sessions were often accompanied

Figure 20.3 Approx. 4 m pilot-scale absorption column based within the Department of Chemical Engineering at the University of Manchester.

by laboratory sessions with operation of distillation, adsorption, and extraction equipment, ideally at a large scale, see for example Figure 20.3. As computers became more widely used and available, the graphical approaches were supplemented with the use of software, initially with students writing their own programs, but then progressing to use dedicated programs like ChemSep and Aspen Hysys as these become more widely available at universities.

Current chemical engineering practice tends to focus on the use of commercial process simulators such as AspenPlus, ChemCad, Hysys, and Pro II. This to make sure that students are prepared for commercial practice [9]; simulating and designing equilibrium-staged separations using a commercial simulator [10, 11]. Unfortunately, students often treat these simulators as black-boxes and tend to believe the results they obtain without further checking [12].

A current area of educational development is in simulation-based educations tools with the aim to offer a rich and dynamic learning experience by allowing the user to interact with a model of a physical system via adjusting parameters and watching the corresponding response. The aim is to try to address the black-box issue.

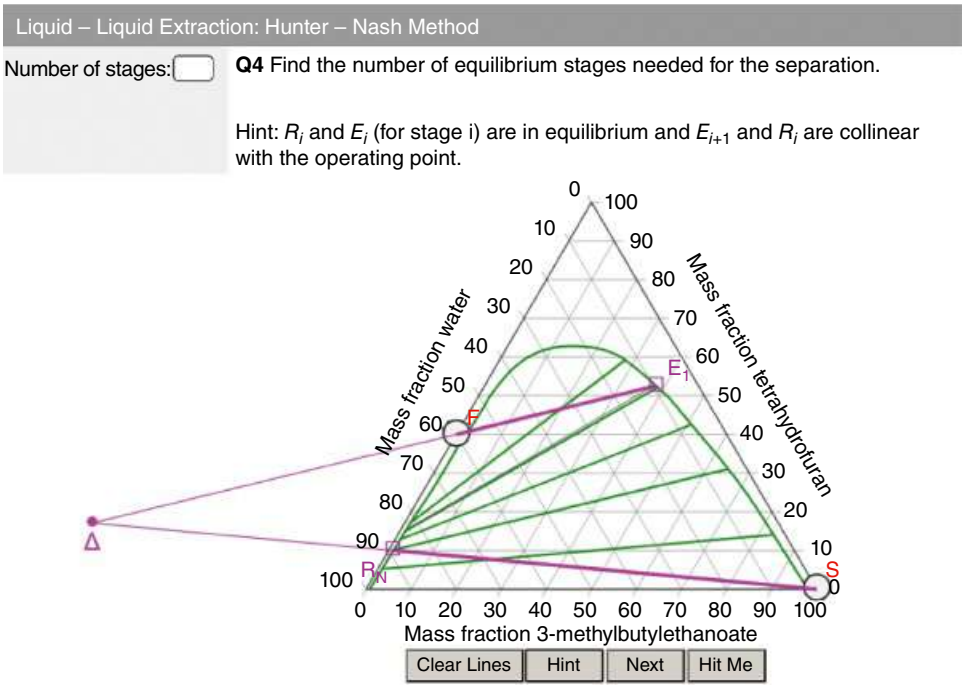

Figure 20.4 Screenshot of LLTernary web-app on which graphic methods can be undertaken digitally [21].

Mathematica-based Wolfram Demonstrations Project [13–15] and R-based Shiny [16] packages have been widely used to produce high-quality teaching materials. These applications lack the ability for students to practice problems, they simply allow students to manipulate variables to only see change, not calculate these changes. Therefore, these do not facilitate enhanced engagement enabling through visual/kinaesthetic interactions as traditional graphic plotting could achieve. Typically, improvements have been made over these more passive simulations by linking to multiple choice questions [17].

It is also typical to examine stage-by-stage calculations using excel [18, 19]. This acts an intermediate between a full simulation and undertaking calculations/plotting by hand. This increases student interaction, but does not give the same approach as would be achieved with pen and paper. For extraction, a web–app was introduced to have a strong free-hand feel allowing students to retain the enhanced visual and kinaesthetic engagement with the material, while giving students the opportunity of practicing on a large number of randomly generated exercises [20], an example is shown in Figure 20.4. The apps also give students the option of skipping to the sections they wish to practice, e.g. if they want to practice calculation of the separation they can get a generated equilibrium curve instead of having to plot this first. Moreover, incorporating graphic student input along with numeric answers into demonstration-based tools is important for student learning as this allows them to practice and apply knowledge they have learnt.

20.3 Current Approaches to Teaching Sustainability

In the last couple of decades, significant progress has been made in recognizing the issues in sustainability and its inclusion in the chemical engineering curriculum. The same universities in Figure 20.2 were examined for courses listed to do with sustainability or environmental. Around 75% of the degree programs had at least one course (around 18% with two or more courses); however, there was a clear focus on energy and environmental chemistry with a small number offering process analysis topics, e.g. life cycle assessment (LCA).

The importance of educating engineers in sustainable development principles has been highlighted in the literature [22, 23]. Professional institutions, such as the Royal Academy of Engineering and the Institution of Chemical Engineers, have introduced a number of initiatives/statements to encourage the integration of sustainability into HE as well as its industrial application [24]. This is emphasized by the requirement of the provision of guiding principles on engineering for sustainable development within the curriculum to achieve accreditation [25, 26].

Many original courses on sustainability were focused on green chemistry principles, with a current trend toward measuring sustainability with tools like LCA including ecological, social, and economic considerations. Several implementations have been used for sustainability teaching within courses, these tend to vary from more traditional lecture courses with some problem-based learning activities [27], implementing with experimental activities [28] and games [29], and within the capstone design project.

20.4 Perspective, Future Directions, and Conclusions

The future direction of separations teaching would be simple if nearly all graduates went into a single industry, the needs of that industry could then guide the topics. Industries can be classified by the separations they use. For example, the petroleum and petrochemicals industries are heavy users of distillation plus absorption, extraction, gravity separation of liquid phases, plus to a lesser extent membrane separations and adsorption. While the pharmaceutical and food industries much more rely on centrifugation, filtration, membrane separators, extraction, solution crystallization, precipitation, chromatography, and drying. Table 20.2 provides a breakdown of the chemical sales in 2018 by the EU-28 countries; this shows that there is no longer a dominant chemicals area and the table excludes large industries requiring separations such as food production, water treatment, and the core petroleum industry.

It is clear that the mix of jobs taken by graduates of most chemical engineering programs is much too large to choose what to teach based solely on the hiring industry. Therefore, what should happen?

Distillation (including absorption and stripping) will remain a major player in industry and thus should remain a major part of chemical engineering curriculum. Focus here can be used with process simulators, though making sure the students understand what is

Table 20.2 Sectoral breakdown of EU-28 chemical sales in 2018. Base, specialty, and consumer chemicals (€565 billion) from [30] and pharmaceuticals (€170 billion) from [31].

Sector	Subsectors
Base chemicals (46%)	Petrochemicals
	Plastics and synthetic rubber
	Man-made fibers
	Basic inorganics (e.g. acids and bases)
	Industrial gases
	Fertilizers
Pharmaceuticals (23%)	Products and preparations
Specialty chemicals (21%)	Paints & inks
	Crop protection
	Dyes & pigments
	Auxiliaries for industry (e.g. glues, essential oils, and gelatine)
Consumer chemicals (10%)	Perfumes
	Cosmetics
	Personal care (e.g. soaps, shampoos)
	Home care (e.g. detergents, cleaners)

happening in the "black-box" with links to graphic methods. Extraction should then be included to examine more complex graphic techniques, but it is important to make sure that unique extraction design issues are covered.

Membrane and adsorption separation processes will likely continue to increase in industrial applications and thus should be continued to be taught within chemical engineering degrees. These need rate-based analysis to design and thus allow students sensible examples of this more complex analysis. It is likely that mechanical separations and crystallization will continue to not be included in many chemical engineering degrees but as these are core separation techniques in many industrial areas, these should be looked at where they can be included, especially in universities that want to have focus on pharmaceutical and consumer industries.

Clearly coupled with these separations, the need to deliver a sustainable chemical industry is a continuing driver of the future. While the objectives of courses may need to be changed to factor this in, it does not imply an in-depth rebuild of the curriculum. Activities such as lab work with molecules from renewable sources, design projects where sustainable chemistry constraints are taken into account, and worked examples of sustainable chemical industry processes [32]. A taught unit to introduce the basics, for example, energy analysis, metrics like LCA, and environmental impact though greenhouse gases balances, would however be needed. The application of the 12 principles of green engineering [33] and analysis tools such as LCA built into the capstone design project should be a key area[1] [34, 35]. It is vital to embed the content within the curriculum, rather than using a "bolt-on" approach [36, 37].

Note

1 This is an activity undertaken at the University of Manchester which has led to six wins of the IChemE's Macnab Lacey Prize for best sustainable student design project between 2021 and the inception of the award in 2011.

References

1 Clarivate Analytics. Web of Science. https://apps.webofknowledge.com/ (accessed 23 December 2020).
2 Humphrey, J.L. and Keller, G.E. II (1997). *Separation Process Technology*. New York, NY: McGraw-Hill.
3 Wankat, P.C. (2001). Teaching separations: why, what, when, and how? *Chemical Engineering Education* 35: 168–171.
4 Cussler, E.L., Savage, D.W., Middelberg, A.P.J., and Kind, M. (2002). Refocusing Chemical Engineering. *Chemical Engineering Progress* 98: 26S.
5 Varma, A. and Grossmann, I.E. (2014). Evolving trends in chemical engineering education. *AIChE Journal* 60 (11): 3692–3700.
6 Armstrong, R.C. (2006). A vision of the chemical engineering curriculum of the future. *Chemical Engineering Education* 40 (2): 104–109.
7 QS World University Rankings (2019). Subject 2019: Engineering - Chemical. https://www.topuniversities.com/university-rankings/university-subject-rankings/2019/engineering-chemical (accessed 23 December 2020).
8 Adler, S., Beaver, E., Biyan, P. et al. (1998). *Vision 2020: 1998 Separations Roadmap*. New York: Center for Waste Reduction Technologies of AIChE.
9 Wankat, P.C. (2002). Integrating the use of commercial simulators into lecture courses. *Journal of Engineering Education* 91: 19–23.
10 Roman, C. and García-Morales, M. (2019). Achieving a better understanding of binary azeotropic mixtures distillation through Aspen Plus process simulations. *Computer Applications in Engineering Education* 27: 1453–1464.
11 Calvo, L. and Prieto, C. (2016). The teaching of enhanced distillation processes using a commercial simulator and a project-based learning approach. *Education for Chemical Engineers* 17: 65–74.
12 Roman, C., Delgado, M.A., and García-Morales, M. (2020). Using process simulators in chemical engineering education: is it possible to minimize the "black box" effect? *Computer Applications in Engineering Education* 28: 1369–1385.
13 Wolfram Research Inc. Wolfram Demonstrations Project. https://demonstrations.wolfram.com/ (accessed 26 December 2020).
14 Binous, H. (2006). Liquid-lLiquid equilibrium and extraction using mathematica®. *Computers in Education Journal* 16: 78–81.
15 Maguire, M.E., and Baumann, R.L. (2014). Ternary Phase Diagram with Phase Envelope. https://demonstrations.wolfram.com/TernaryPhaseDiagramWithPhaseEnvelope/ (accessed 26 December 2020).

16 RStudio Inc. Shiny. https://shiny.rstudio.com/ (accessed 26 December 2020).
17 Falconer, J. and Nicodemus, G. (2014). Interactive mathematica simulations in chemical engineering courses. *Chemical Engineering Education* 48: 165–174.
18 Teppaitoon, W. (2016). Solving LL extraction problems with Excel spreadsheet. *Chemical Engineering Education* 50: 169–175.
19 Briones, L., Morales, V., Iglesias, J. et al. (2019). Application of the microsoft excel solver tool in the optimization of distillation sequences problems. *Computer Applications in Engineering Education* 28: 304–313.
20 Bánsági, T. Jr. and Rodgers, T.L. (2018). Graphic web–apps for teaching ternary diagrams and liquid–liquid extraction. *Education for Chemical Engineers* 22: 27–34.
21 Bánsági Jr., T., and Rodgers, T.L. LL Ternary. https://www.ceas.manchester.ac.uk/teaching-resources/lle/ (accessed 26 December 2020).
22 Mulder, K. (2006). *Sustainable Development for Engineers: A Handbook and Resource Guide*. Greenleaf Publishing Ltd.
23 Gallego-Schmid, A., Schmidt Rivera, X.C., and Stamford, L. (2018). Introduction of life cycle assessment and sustainability concepts in chemical engineering curricula. *International Journal of Sustainability in Higher Education* 19: 442–458.
24 IChemE (2020). IChemE position on Climate Change.
25 IChemE (2020). Accreditation of chemical engineering programmes.
26 Mitchell, C. (2000). Integrating sustainability in chemical engineering practice and education: concentricity and its consequences. *Process Safety and Environmental Protection* 78: 237–242.
27 Gilmore, K.R. (2016). Teaching life cycle assessment in environmental engineering: a disinfection case study for students. *The International Journal of Life Cycle Assessment* 21: 1706–1718.
28 Farrell, S. and Cavanagh, E. (2014). An introduction to life cycle assessment with hands-on experiments for biodiesel production and use. *Education for Chemical Engineers* 9: 67–76.
29 Bevilacqua, M., Ciarapica, F.E., Mazzuto, G., and Paciarotti, C. (2015). "Cook & Teach": learning by playing. *Journal of Cleaner Production* 106: 259–271.
30 European Chemical Industry Council 2020 Facts and figures of the European chemical industry. 2020.
31 The European Federation of Pharmaceutical Industries and Associations (2018). The pharmaceutical industry in figures.
32 Favre, E., Falk, V., Roizard, C., and Schaer, E. (2008). Trends in chemical engineering education: process, product and sustainable chemical engineering challenges. *Education for Chemical Engineers* 3 (1): e22–e27.
33 McDonough, W., Braungart, M., Anastas, P.T., and Zimmerman, J.B. (2003). Applying the principles of green engineering to cradle-to-cradle design. *Environmental Science & Technology* 37 (23): 434A–441A.
34 Tuzun, U. (2020). Introduction to systems engineering and sustainability PART I: student-centred learning for chemical and biological engineers. *Education for Chemical Engineers* 31: 85–93.
35 Tuzun, U. (2020). Introduction to systems engineering and sustainability part II: interactive teaching of sustainability modeling by systems integration design for chemical and biological engineers. *Education for Chemical Engineers* 31: 94–104.

36 Tomkinson, B. and Engel, C. (2008). The use of a Delphi consultation to explore the curriculum for sustainable development in engineering. *International Journal of Sustainable Engineering* 1: 298–303.

37 Glassey, J. and Haile, S. (2012). Sustainability in chemical engineering curriculum. *International Journal of Sustainability in Higher Education* 13 (4): 354–364.

Index

Sustainable Separation Engineering: Materials, Techniques and Process Development, First Edition. Edited by Gyorgy Szekely and Dan Zhao.
© 2022 John Wiley & Sons Ltd. Published 2022 by John Wiley & Sons Ltd.

b

C

d

e

f

g

h

i

j

k

l

m

p

q

r

S

t

u

Z